

Chapter 8: Carbon Capture and Storage (CCS)

1. IPCC Report: Climate Change 2014: Synthesis Report (2014)
2. Energie und Klimaschutz: Einige grundsätzliche Betrachtungen (2016)
3. Der Grundriss für ein neues Klimaregime (2016)
4. IPCC Special Report: Carbon Dioxide Capture and Storage (2005)
5. Snatching Carbon Dioxide from Mid-Air (2017)
6. ZEP: The Post-2020 Cost-Competitiveness of CCS (2011)
7. ZEP: The Costs of CO₂ Capture, Transport and Storage (2011)
8. How to Cut Emissions (2007)
9. Carbon Capture Journal (2019/20)

Oxyfuel-Process

10. Design Concept for a Large Output Graz Cycle Gas Turbine (2006)
11. Characteristics of Cycle Components for CO₂ Capture (2006)
12. Qualitative and Quantitative Comparison of Two Promising Oxy-Fuel Power Cycles for CO₂ Capture (2007)
13. Evaluation of Design Performance of the Semi-Closed Oxy-Fuel Combustion Combined Cycle (2012)
14. Zero CO₂ emission SOLRGT power system (2012)
15. Adapting the zero-emission Graz Cycle for hydrogen combustion and investigation of its part load behavior (2018)
16. Thermodynamic Analysis of Zero-Atmospheric Emissions Power Plant (2004)
17. Optimization of Thermodynamically Efficient Nominal 40 MW Zero Emission Pilot and Demonstration Power Plant in Norway (2005)
18. Demonstration of the Allam Cycle: An update on the development status of a high efficiency supercritical carbon dioxide power process employing full carbon capture (2017)
19. A modified Allam cycle without compressors realizing efficient power generation with peak load shifting and CO₂ capture (2019)
20. Thermodynamic optimization and equipment development for a high efficient fossil fuel power plant with zero emissions (2019)
21. Advanced Zero Emissions Gas Turbine Power Plant (2005)
22. Proposal and Analysis of a Novel Zero CO₂ Emission Cycle With Liquid Natural Gas Cryogenic Exergy Utilization (2006)
23. A technical evaluation, performance analysis and risk assessment of multiple novel oxy-turbine power cycles with complete CO₂ capture (2016)
24. Chemical Looping Combustion – Analysis of Natural Gas Fired Power Cycles With Inherent CO₂ Capture (2004)
25. Vattenfall's 30 MW_{th} Oxyfuel Power Plant Project + First Operating Experiences (2009)

Post-Combustion Capture

- 26. CO₂ capture from power plants Part I. A parametric study of the technical performance based on monoethanolamine (2007)
- 27. CO₂ capture from power plants Part II. A parametric study of the economical performance based on mono-ethanolamine (2007)
- 28. Performance and Cost Analysis of a Novel Gas Turbine Cycle With CO₂ Capture (2007)
- 29. Energy and exergy analyses for the carbon capture with the Chilled Ammonia Process (CAP) (2009)
- 30. Quantitative evaluation of the chilled-ammonia process for CO₂ capture using thermodynamic analysis and process simulation (2010)
- 31. Techno-economic evaluation of the evaporative gas turbine cycle with different CO₂ capture options (2012)

Pre-Combustion Capture

- 32. Analysis of Gas-Steam Combined Cycles With Natural Gas Reforming and CO₂ Capture (2005)

IGCC

- 33. CO₂ Emission Abatement in IGCC Power Plants by Semiclosed Cycles: Part A – With Oxygen Blown Combustion (1999)
- 34. CO₂ Emission Abatement in IGCC Power Plants by Semiclosed Cycles: Part B – With Air Blown Combustion and CO₂ Physical Absorption (1999)
- 35. Thermodynamic Performance of IGCC with Oxy-Combustion CO₂ Capture (2009)
- 36. RWE's 450 MW IGCC/CCS Project – Status and Outlook (2008)
- 37. Overall environmental impacts of CCS technologies—A life cycle approach (2012)
- 38. Ökobilanz und externe Kosten zukünftiger fossiler Stromerzeugungstechnologien mit CO₂-Abscheidung und Speicherung

CLIMATE CHANGE 2014

Synthesis Report

Summary for Policymakers

Edited by

The Core Writing Team
Synthesis Report
IPCC

Rajendra K. Pachauri
Chairman
IPCC

Leo Meyer
Head, Technical Support Unit
IPCC

Core Writing Team

R.K. Pachauri (Chair); Myles R. Allen (United Kingdom), Vicente Ricardo Barros (Argentina), John Broome (United Kingdom), Wolfgang Cramer (Germany/France), Renate Christ (Austria/WMO), John A. Church (Australia), Leon Clarke (USA), Qin Dahe (China), Purnamita Dasgupta (India), Navroz K. Dubash (India), Ottmar Edenhofer (Germany), Ismail Elgizouli (Sudan), Christopher B. Field (USA), Piers Forster (United Kingdom), Pierre Friedlingstein (United Kingdom/Belgium), Jan Fuglestad (Norway), Luis Gomez-Echeverri (Colombia), Stephane Hallegatte (France/World Bank), Gabriele Hegerl (United Kingdom/Germany), Mark Howden (Australia), Kejun Jiang (China), Blanca Jimenez Cisneros (Mexico/UNESCO), Vladimir Kattsov (Russian Federation), Hoesung Lee (Republic of Korea), Katharine J. Mach (USA), Jochem Marotzke (Germany), Michael D. Mastrandrea (USA), Leo Meyer (The Netherlands), Jan Minx (Germany), Yacob Mulugetta (Ethiopia), Karen O'Brien (Norway), Michael Oppenheimer (USA), Joy J. Pereira (Malaysia), Ramón Pichs-Madruga (Cuba), Gian-Kasper Plattner (Switzerland), Hans-Otto Pörtner (Germany), Scott B. Power (Australia), Benjamin Preston (USA), N.H. Ravindranath (India), Andy Reisinger (New Zealand), Keywan Riahi (Austria), Matilde Rusticucci (Argentina), Robert Scholes (South Africa), Kristin Seyboth (USA), Youba Sokona (Mali), Robert Stavins (USA), Thomas F. Stocker (Switzerland), Petra Tschakert (USA), Detlef van Vuuren (The Netherlands), Jean-Pascal van Ypersele (Belgium)

Technical Support Unit for the Synthesis Report

Leo Meyer, Sander Brinkman, Line van Kesteren, Noemie Leprince-Ringuet, Fijke van Boxmeer

NOTE: subject to final copy-edit and layout prior to its final publication

Contents

Summary for Policymakers	1
<i>SPM 1. Observed Changes and their Causes</i>	<i>1</i>
<i>SPM 2. Future Climate Changes, Risks and Impacts</i>	<i>8</i>
<i>SPM 3. Future Pathways for Adaptation, Mitigation and Sustainable Development</i>	<i>17</i>
<i>SPM 4. Adaptation and Mitigation.....</i>	<i>29</i>

Summary for Policymakers

SPM Introduction

This Synthesis Report is based on the reports of the three Working Groups of the Intergovernmental Panel on Climate Change (IPCC), including relevant Special Reports. It provides an integrated view of climate change as the final part of the IPCC's Fifth Assessment Report (AR5).

This summary follows the structure of the longer report, which addresses the following topics: Observed changes and their causes; Future climate change, risks and impacts; Future pathways for adaptation, mitigation and sustainable development; Adaptation and mitigation.

In the Synthesis Report, the certainty in key assessment findings is communicated as in the Working Group Reports and Special Reports. It is based on the author teams' evaluations of underlying scientific understanding and is expressed as a qualitative level of confidence (from *very low* to *very high*) and, when possible, probabilistically with a quantified likelihood (from *exceptionally unlikely* to *virtually certain*)¹. Where appropriate, findings are also formulated as statements of fact without using uncertainty qualifiers.

This report includes information relevant to Article 2 of the United Nations Framework Convention on Climate Change (UNFCCC).

SPM 1. Observed Changes and their Causes

Human influence on the climate system is clear, and recent anthropogenic emissions of greenhouse gases are the highest in history. Recent climate changes have had widespread impacts on human and natural systems. {1}

SPM 1.1 Observed changes in the climate system

Warming of the climate system is unequivocal, and since the 1950s, many of the observed changes are unprecedented over decades to millennia. The atmosphere and ocean have warmed, the amounts of snow and ice have diminished, and sea level has risen. {1.1}

Each of the last three decades has been successively warmer at the Earth's surface than any preceding decade since 1850. The period from 1983 to 2012 was *likely* the warmest 30-year period of the last 1400 years in the Northern Hemisphere, where such assessment is possible (*medium confidence*). The globally averaged combined land and ocean surface temperature data as calculated by a linear trend, show a warming of 0.85 [0.65 to 1.06] °C² over the period 1880 to 2012, when multiple independently produced datasets exist (Figure SPM.1a). {1.1.1, Figure 1.1}

In addition to robust multi-decadal warming, the globally averaged surface temperature exhibits substantial decadal and interannual variability (Figure SPM.1a). Due to this natural variability, trends based on short records are very sensitive to the beginning and end dates and do not in general reflect long-term climate trends. As one example, the rate of warming over the past 15 years (1998–2012; 0.05 [–0.05 to 0.15] °C per

¹ Each finding is grounded in an evaluation of underlying evidence and agreement. In many cases, a synthesis of evidence and agreement supports an assignment of confidence. The summary terms for evidence are: limited, medium, or robust. For agreement, they are low, medium, or high. A level of confidence is expressed using five qualifiers: very low, low, medium, high, and very high, and typeset in italics, e.g., *medium confidence*. The following terms have been used to indicate the assessed likelihood of an outcome or a result: virtually certain 99–100% probability, very likely 90–100%, likely 66–100%, about as likely as not 33–66%, unlikely 0–33%, very unlikely 0–10%, exceptionally unlikely 0–1%. Additional terms (extremely likely: 95–100%, more likely than not >50–100%, more unlikely than likely 0–<50% and extremely unlikely 0–5%) may also be used when appropriate. Assessed likelihood is typeset in italics, e.g., *very likely* (see Guidance Note on Uncertainties, 2010, IPCC for more details).

² Ranges in square brackets or following “±” are expected to have a 90% likelihood of including the value that is being estimated, unless otherwise stated.

decade), which begins with a strong El Niño, is smaller than the rate calculated since 1951 (1951–2012; 0.12 [0.08 to 0.14] °C per decade). {1.1.1, Box 1.1}

Ocean warming dominates the increase in energy stored in the climate system, accounting for more than 90% of the energy accumulated between 1971 and 2010 (*high confidence*), with only about 1% stored in the atmosphere. On a global scale, the ocean warming is largest near the surface, and the upper 75 m warmed by 0.11 [0.09 to 0.13] °C per decade over the period 1971 to 2010. It is *virtually certain* that the upper ocean (0–700 m) warmed from 1971 to 2010, and it *likely* warmed between the 1870s and 1971. {1.1.2, Figure 1.2}

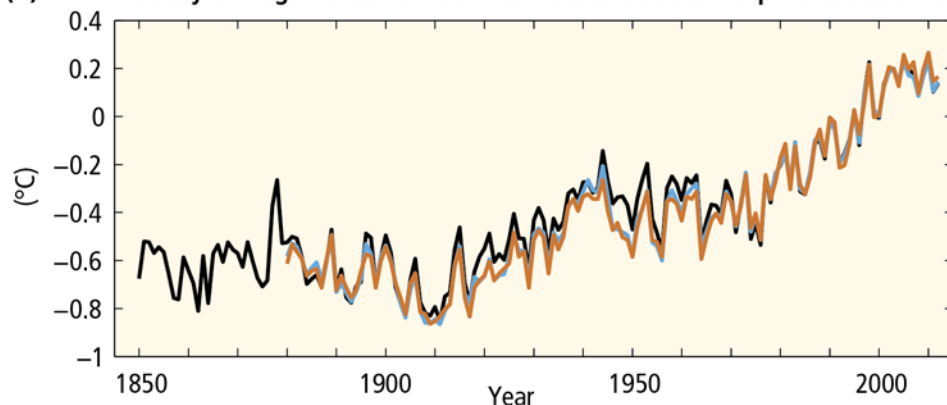
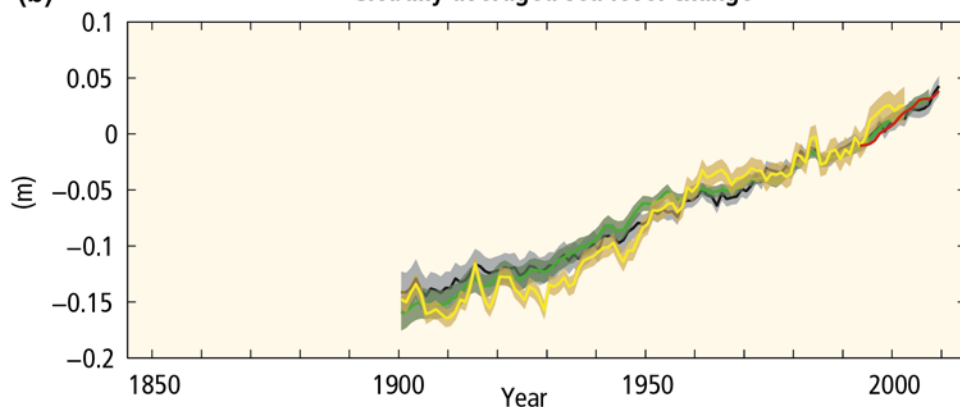
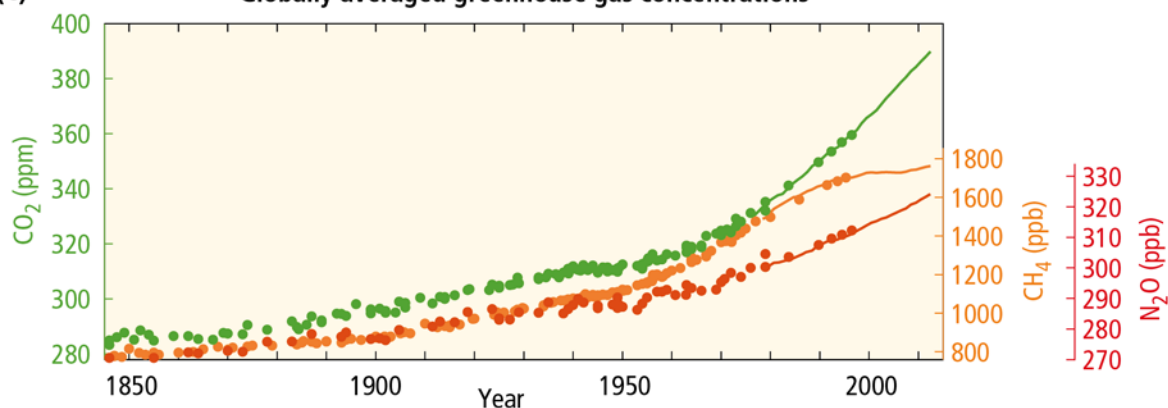
Averaged over the mid-latitude land areas of the Northern Hemisphere, precipitation has increased since 1901 (*medium confidence* before and *high confidence* after 1951). For other latitudes, area-averaged long-term positive or negative trends have *low confidence*. Observations of changes in ocean surface salinity also provide indirect evidence for changes in the global water cycle over the ocean (*medium confidence*). It is *very likely* that regions of high salinity, where evaporation dominates, have become more saline, while regions of low salinity, where precipitation dominates, have become fresher since the 1950s. {1.1.1, 1.1.2}

Since the beginning of the industrial era, oceanic uptake of CO₂ has resulted in acidification of the ocean; the pH of ocean surface water has decreased by 0.1 (*high confidence*), corresponding to a 26% increase in acidity, measured as hydrogen ion concentration. {1.1.2}

Over the period 1992 to 2011, the Greenland and Antarctic ice sheets have been losing mass (*high confidence*), *likely* at a larger rate over 2002 to 2011. Glaciers have continued to shrink almost worldwide (*high confidence*). Northern Hemisphere spring snow cover has continued to decrease in extent (*high confidence*). There is *high confidence* that permafrost temperatures have increased in most regions since the early 1980s in response to increased surface temperature and changing snow cover. {1.1.3}

The annual mean Arctic sea-ice extent decreased over the period 1979 to 2012, with a rate that was *very likely* in the range 3.5 to 4.1% per decade. Arctic sea-ice extent has decreased in every season and in every successive decade since 1979, with the most rapid decrease in decadal mean extent in summer (*high confidence*). It is *very likely* that the annual mean Antarctic sea-ice extent increased in the range of 1.2 to 1.8% per decade between 1979 and 2012. However, there is *high confidence* that there are strong regional differences in Antarctica, with extent increasing in some regions and decreasing in others. {1.1.3, Figure 1.1}

Over the period 1901 to 2010, global mean sea level rose by 0.19 [0.17 to 0.21] m (Figure SPM.1.b). The rate of sea-level rise since the mid-19th century has been larger than the mean rate during the previous two millennia (*high confidence*). {1.1.4, Figure 1.1}

(a) Globally averaged combined land and ocean surface temperature anomaly**(b) Globally averaged sea level change****(c) Globally averaged greenhouse gas concentrations****(d) Global anthropogenic CO₂ emissions**

Quantitative information of CH₄ and N₂O emission time series from 1850 to 1970 is limited

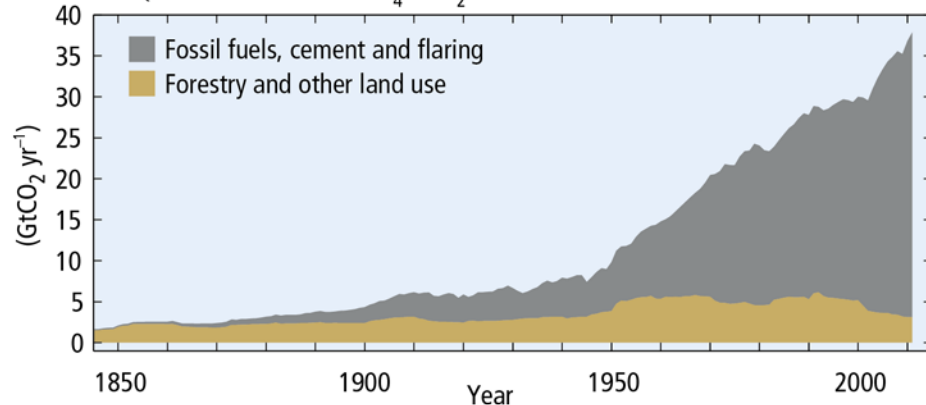
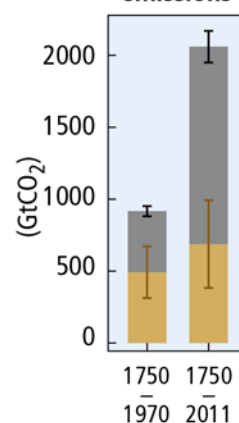
**Cumulative CO₂ emissions**

Figure SPM.1: The complex relationship between the observations (panels a, b, c, yellow background) and the emissions (panel d, light blue background) is addressed in Section 1.2 and topic 1. Observations and other indicators of a changing global climate system. Observations: (a) Annually and globally averaged combined land and ocean surface temperature anomalies relative to the average over the period 1986 to 2005. Colours indicate different data sets. (b) Annually and globally averaged sea-level change relative to the average over the period 1986 to 2005 in the longest-running dataset. Colours indicate different data sets. All datasets are aligned to have the same value in 1993, the first year of satellite altimetry data (red). Where assessed, uncertainties are indicated by coloured shading. (c) Atmospheric concentrations of the greenhouse gases carbon dioxide (CO₂, green), methane (CH₄, orange), and nitrous oxide (N₂O, red) determined from ice core data (dots) and from direct atmospheric measurements (lines). Indicators: (d) Global anthropogenic CO₂ emissions from forestry and other land use as well as from burning of fossil fuel, cement production, and flaring. Cumulative emissions of CO₂ from these sources and their uncertainties are shown as bars and whiskers, respectively, on the right hand side. The global effects of the accumulation of CH₄ and N₂O emissions are shown in panel c). Greenhouse gas emission data from 1970 to 2010 are shown in Figure SPM.2. {Figures 1.1, 1.3, 1.5}

SPM 1.2 Causes of climate change

Anthropogenic greenhouse gas emissions have increased since the pre-industrial era, driven largely by economic and population growth, and are now higher than ever. This has led to atmospheric concentrations of carbon dioxide, methane and nitrous oxide that are unprecedented in at least the last 800,000 years. Their effects, together with those of other anthropogenic drivers, have been detected throughout the climate system and are *extremely likely* to have been the dominant cause of the observed warming since the mid-20th century. {1.2, 1.3.1}

Anthropogenic greenhouse gas (GHG) emissions since the pre-industrial era have driven large increases in the atmospheric concentrations of CO₂, CH₄ and N₂O (Figure SPM.1c). Between 1750 and 2011, cumulative anthropogenic CO₂ emissions to the atmosphere were 2040 ± 310 GtCO₂. About 40% of these emissions have remained in the atmosphere (880 ± 35 GtCO₂); the rest was removed from the atmosphere and stored on land (in plants and soils) and in the ocean. The ocean has absorbed about 30% of the emitted anthropogenic CO₂, causing ocean acidification. About half of the anthropogenic CO₂ emissions between 1750 and 2011 have occurred in the last 40 years (*high confidence*) (Figure SPM.1d). {1.2.1, 1.2.2}

Total anthropogenic greenhouse gas emissions have continued to increase over 1970 to 2010 with larger absolute increases between 2000 and 2010, despite a growing number of climate change mitigation policies. Anthropogenic greenhouse gas emissions in 2010 have reached 49 ± 4.5 GtCO₂ eq/yr.³ Emissions of CO₂ from fossil fuel combustion and industrial processes contributed about 78% of the total greenhouse gas emissions increase from 1970 to 2010, with a similar percentage contribution for the increase during the period 2000 to 2010 (*high confidence*) (Figure SPM.2). Globally, economic and population growth continued to be the most important drivers of increases in CO₂ emissions from fossil fuel combustion. The contribution of population growth between 2000 and 2010 remained roughly identical to the previous three decades, while the contribution of economic growth has risen sharply. Increased use of coal has reversed the long-standing trend of gradual decarbonization (i.e., reducing the carbon intensity of energy) of the world's energy supply (*high confidence*). {1.2.2}

³ Greenhouse gas emissions are quantified as CO₂-equivalent (GtCO₂-eq) emissions using weightings based on the 100 year Global Warming Potentials, using IPCC Second Assessment Report values unless otherwise stated. {Box 3.2}

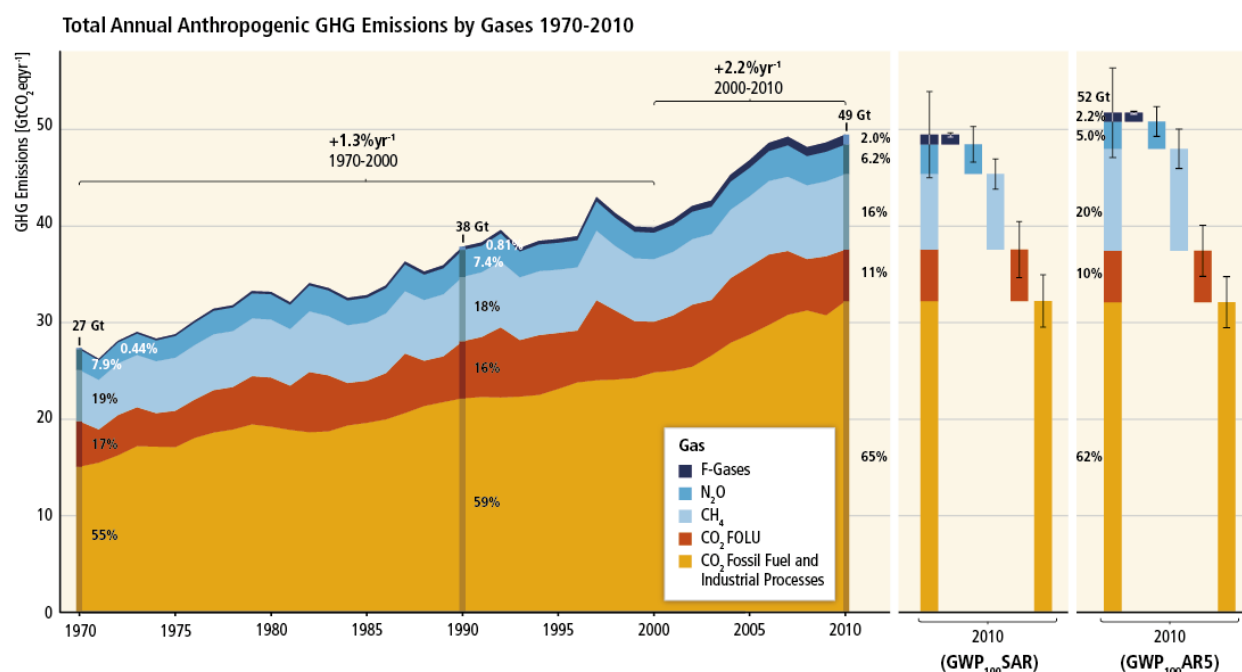


Figure SPM.2: Total annual anthropogenic greenhouse gas (GHG) emissions (gigatonne of CO₂-equivalent per year, GtCO₂-eq/yr) for the period 1970 to 2010 by gases: CO₂ from fossil fuel combustion and industrial processes; CO₂ from Forestry and Other Land Use (FOLU); methane (CH₄); nitrous oxide (N₂O); fluorinated gases covered under the Kyoto Protocol (F-gases). Right hand side shows 2010 emissions, using alternatively CO₂-equivalent emission weightings based on Second Assessment Report (SAR) and AR5 values. Unless otherwise stated, CO₂-equivalent emissions in this report include the basket of Kyoto gases (CO₂, CH₄, N₂O as well as F-gases) calculated based on 100-year Global Warming Potential (GWP₁₀₀) values from the SAR (see Glossary). Using the most recent 100-year Global Warming Potential values from the AR5 (right-hand bars) would result in higher total annual greenhouse gas emissions (52 GtCO₂-eq/yr) from an increased contribution of methane, but does not change the long-term trend significantly. {Figure 1.6, Box 3.2}

The evidence for human influence on the climate system has grown since the Fourth Assessment Report (AR4). It is *extremely likely* that more than half of the observed increase in global average surface temperature from 1951 to 2010 was caused by the anthropogenic increase in greenhouse gas concentrations and other anthropogenic forcings together. The best estimate of the human-induced contribution to warming is similar to the observed warming over this period (Figure SPM.3). Anthropogenic forcings have *likely* made a substantial contribution to surface temperature increases since the mid-20th century over every continental region except Antarctica⁴. Anthropogenic influences have *likely* affected the global water cycle since 1960 and contributed to the retreat of glaciers since the 1960s and to the increased surface melting of the Greenland ice sheet since 1993. Anthropogenic influences have *very likely* contributed to Arctic sea-ice loss since 1979 and have *very likely* made a substantial contribution to increases in global upper ocean heat content (0–700 m) and to global mean sea-level rise observed since the 1970s. {1.3, Figure 1.10}

⁴ For Antarctica, large observational uncertainties result in *low confidence* that anthropogenic forcings have contributed to the observed warming averaged over available stations.

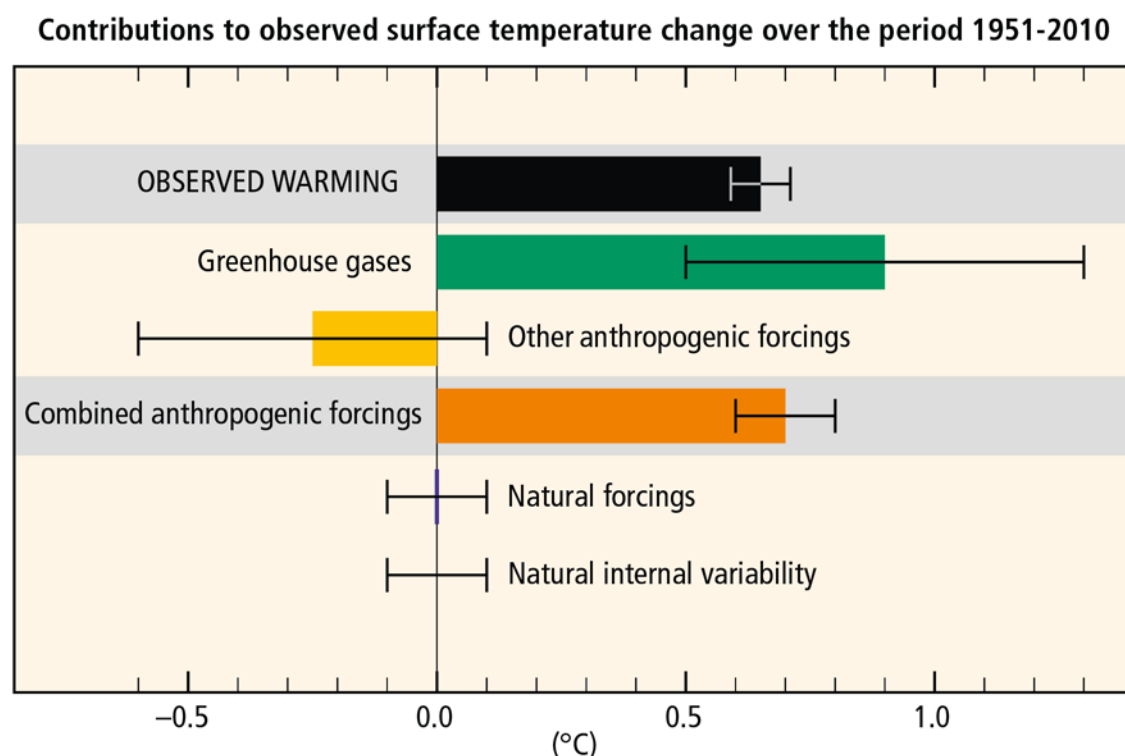


Figure SPM.3: Assessed *likely* ranges (whiskers) and their mid-points (bars) for warming trends over the 1951–2010 period from well-mixed greenhouse gases, other anthropogenic forcings (including the cooling effect of aerosols and the effect of land-use change), combined anthropogenic forcings, natural forcings, and natural internal climate variability (which is the element of climate variability that arises spontaneously within the climate system even in the absence of forcings). The observed surface temperature change is shown in black, with the 5–95% uncertainty range due to observational uncertainty. The attributed warming ranges (colours) are based on observations combined with climate model simulations, in order to estimate the contribution of an individual external forcing to the observed warming. The contribution from the combined anthropogenic forcings can be estimated with less uncertainty than the contributions from greenhouse gases and from other anthropogenic forcings separately. This is because these two contributions partially compensate, resulting in a combined signal that is better constrained by observations. {Figure 1.9}

SPM 1.3 Impacts of climate change

In recent decades, changes in climate have caused impacts on natural and human systems on all continents and across the oceans. Impacts are due to observed climate change, irrespective of its cause, indicating the sensitivity of natural and human systems to changing climate. {1.3.2}

Evidence of observed climate-change impacts is strongest and most comprehensive for natural systems. In many regions, changing precipitation or melting snow and ice are altering hydrological systems, affecting water resources in terms of quantity and quality (*medium confidence*). Many terrestrial, freshwater, and marine species have shifted their geographic ranges, seasonal activities, migration patterns, abundances, and species interactions in response to ongoing climate change (*high confidence*). Some impacts on human systems have also been attributed to climate change, with a major or minor contribution of climate change distinguishable from other influences (Figure SPM.4). Assessment of many studies covering a wide range of regions and crops shows that negative impacts of climate change on crop yields have been more common than positive impacts (*high confidence*). Some impacts of ocean acidification on marine organisms have been attributed to human influence (*medium confidence*). {1.3.2}

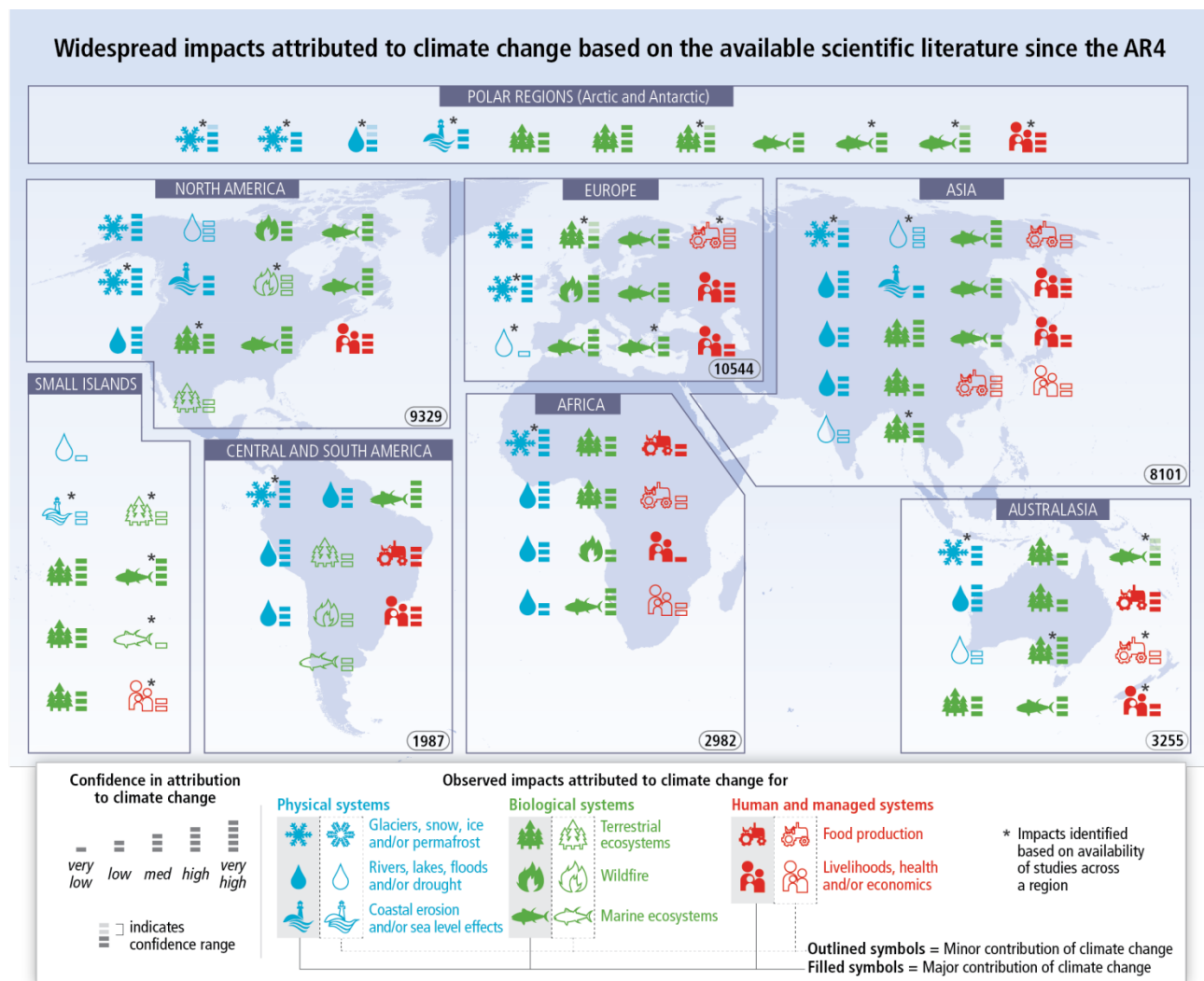


Figure SPM.4: Based on the available scientific literature since the AR4, there are substantially more impacts in recent decades now attributed to climate change. Attribution requires defined scientific evidence on the role of climate change. Absence from the map of additional impacts attributed to climate change does not imply that such impacts have not occurred. The publications supporting attributed impacts reflect a growing knowledge base, but publications are still limited for many regions, systems and processes, highlighting gaps in data and studies. Symbols indicate categories of attributed impacts, the relative contribution of climate change (major or minor) to the observed impact, and confidence in attribution. Each symbol refers to one or more entries in WGII Table SPM.A1, grouping related regional-scale impacts. Numbers in ovals indicate regional totals of climate change publications from 2001 to 2010, based on the Scopus bibliographic database for publications in English with individual countries mentioned in title, abstract or key words (as of July 2011). These numbers provide an overall measure of the available scientific literature on climate change across regions; they do not indicate the number of publications supporting attribution of climate change impacts in each region. The inclusion of publications for assessment of attribution followed IPCC scientific evidence criteria defined in WGII Chapter 18. Studies for polar regions and small islands are grouped with neighboring continental regions. Publications considered in the attribution analyses come from a broader range of literature assessed in the WGII AR5. See WGII Table SPM.A1 for descriptions of the attributed impacts. {Figure 1.11}

SPM 1.4 Extreme events

Changes in many extreme weather and climate events have been observed since about 1950. Some of these changes have been linked to human influences, including a decrease in cold temperature extremes, an increase in warm temperature extremes, an increase in extreme high sea levels and an increase in the number of heavy precipitation events in a number of regions. {1.4}

It is *very likely* that the number of cold days and nights has decreased and the number of warm days and nights has increased on the global scale. It is *likely* that the frequency of heat waves has increased in large parts of Europe, Asia and Australia. It is *very likely* that human influence has contributed to the observed

global scale changes in the frequency and intensity of daily temperature extremes since the mid-20th century. It is *likely* that human influence has more than doubled the probability of occurrence of heat waves in some locations. There is *medium confidence* that the observed warming has increased heat-related human mortality and decreased cold-related human mortality in some regions. {1.4}

There are *likely* more land regions where the number of heavy precipitation events has increased than where it has decreased. Recent detection of increasing trends in extreme precipitation and discharge in some catchments imply greater risks of flooding at regional scale (*medium confidence*). It is *likely* that extreme sea levels (for example, as experienced in storm surges) have increased since 1970, being mainly a result of rising mean sea level. {1.4}

Impacts from recent climate-related extremes, such as heat waves, droughts, floods, cyclones, and wildfires, reveal significant vulnerability and exposure of some ecosystems and many human systems to current climate variability (*very high confidence*). {1.4}

SPM 2. Future Climate Changes, Risks and Impacts

Continued emission of greenhouse gases will cause further warming and long-lasting changes in all components of the climate system, increasing the likelihood of severe, pervasive and irreversible impacts for people and ecosystems. Limiting climate change would require substantial and sustained reductions in greenhouse gas emissions which, together with adaptation, can limit climate change risks. {2}

SPM 2.1 Key drivers of future climate

Cumulative emissions of CO₂ largely determine global mean surface warming by the late 21st century and beyond. Projections of greenhouse gas emissions vary over a wide range, depending on both socio-economic development and climate policy. {2.1}

Anthropogenic greenhouse gas emissions are mainly driven by population size, economic activity, lifestyle, energy use, land-use patterns, technology and climate policy. The “Representative Concentration Pathways” (RCPs) which are used for making projections based on these factors describe four different 21st century pathways of greenhouse gas emissions and atmospheric concentrations, air pollutant emissions and land-use. The RCPs include a stringent mitigation scenario (RCP2.6), two intermediate scenarios (RCP4.5 and RCP6.0), and one scenario with very high greenhouse gas emissions (RCP8.5). Scenarios without additional efforts to constrain emissions (“baseline scenarios”) lead to pathways ranging between RCP6.0 and RCP8.5. RCP2.6 is representative of a scenario that aims to keep global warming *likely* below 2°C above pre-industrial temperatures (Figure SPM.5.a). The RCPs are consistent with the wide range of scenarios in the literature as assessed by WGIII⁵. {2.1, Box 2.2, 4.3}

⁵ Roughly 300 baseline scenarios and 900 mitigation scenarios are categorized by CO₂-equivalent concentration (CO₂-eq) by 2100. The CO₂-eq includes the forcing due to all GHGs (including halogenated gases and tropospheric ozone), aerosols and albedo change.

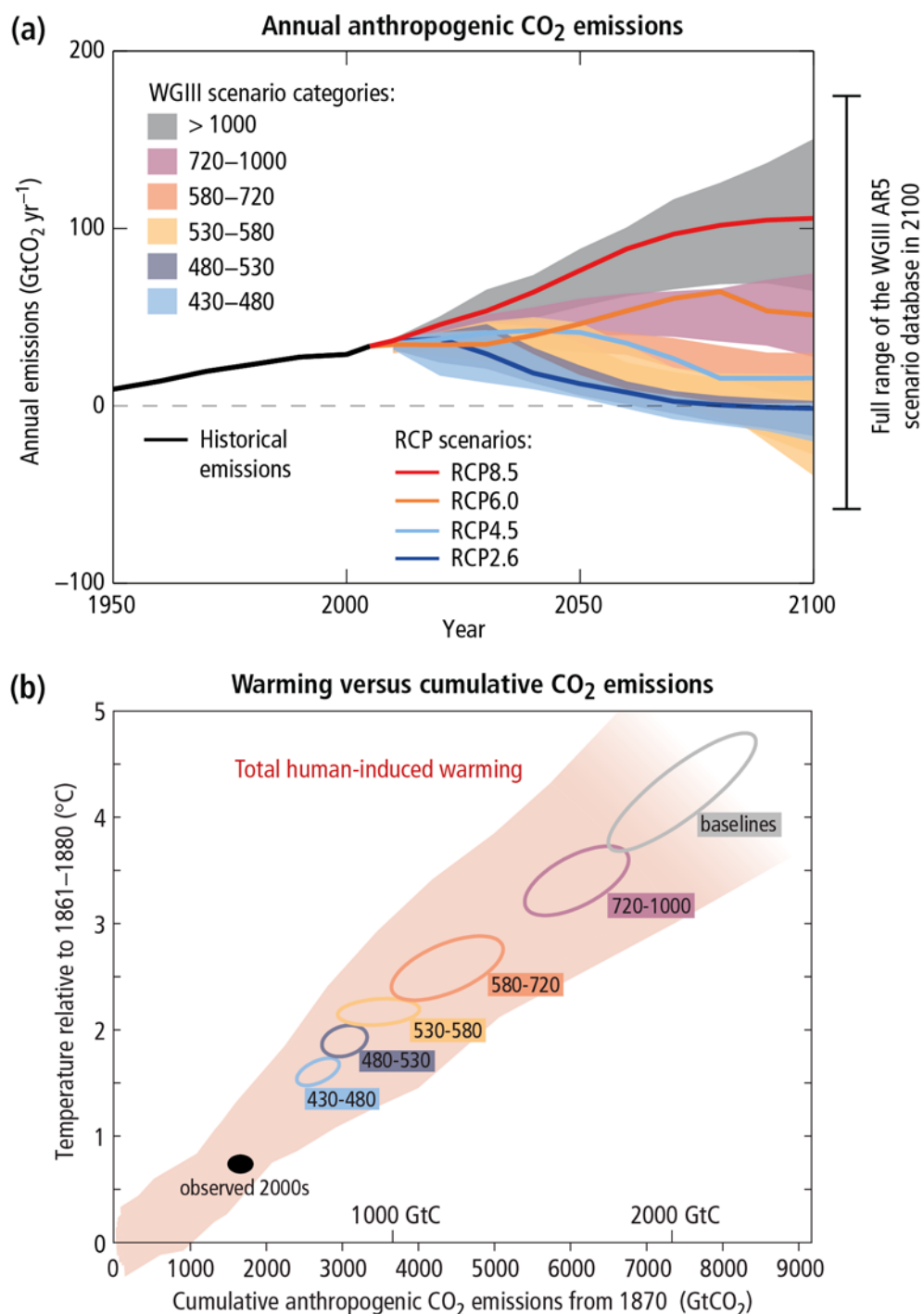


Figure SPM.5: (a) Emissions of CO₂ alone in the Representative Concentration Pathways (lines) and the associated scenario categories used in WGIII (coloured areas show 5–95% range). The WGIII scenario categories summarize the wide range of emission scenarios published in the scientific literature and are defined on the basis of CO₂-eq concentration levels (in ppm) in 2100. The time series of other greenhouse gas emissions are shown in Box 2.2, Figure 1. (b) Global mean surface temperature increase at the time global CO₂ emissions reach a given net cumulative total, plotted as a function of that total, from various lines of evidence. Coloured plume shows the spread of past and future projections from a hierarchy of climate-carbon cycle models driven by historical emissions and the four RCPs over all times out to 2100, and fades with the decreasing number of available models. Ellipses show total anthropogenic warming in 2100 versus cumulative CO₂ emissions from 1870 to 2100 from a simple climate model (median climate response) under the scenario categories used in WGIII. The width of the ellipses in terms of temperature is caused by the impact of different scenarios for non-CO₂ climate drivers. The filled black ellipse shows observed emissions to 2005 and observed temperatures in the decade 2000–2009 with associated uncertainties. {Box 2.2, Figure 1, Figure 2.3}

Multiple lines of evidence indicate a strong, consistent, almost linear relationship between cumulative CO₂ emissions and projected global temperature change to the year 2100 in both the RCPs and the wider set of mitigation scenarios analysed in WGIII (Figure SPM.5.b). Any given level of warming is associated with a range of cumulative CO₂ emissions⁶, and therefore, e.g., higher emissions in earlier decades imply lower emissions later. {2.2.5, Table 2.2}

Multi-model results show that limiting total human-induced warming to less than 2°C relative to the period 1861-1880 with a probability of >66%⁷ would require cumulative CO₂ emissions from all anthropogenic sources since 1870 to remain below about 2900 GtCO₂ (with a range of 2550-3150 GtCO₂ depending on non-CO₂ drivers). About 1900 GtCO₂⁸ had already been emitted by 2011. For additional context see Table 2.2. {2.2.5}

SPM 2.2 Projected changes in the climate system

The projected changes in Section SPM 2.2 are for 2081-2100 relative to 1986-2005, unless otherwise indicated.

Surface temperature is projected to rise over the 21st century under all assessed emission scenarios. It is very likely that heat waves will occur more often and last longer, and that extreme precipitation events will become more intense and frequent in many regions. The ocean will continue to warm and acidify, and global mean sea level to rise. {2.2}

Future climate will depend on committed warming caused by past anthropogenic emissions, as well as future anthropogenic emissions and natural climate variability. The global mean surface temperature change for the period 2016-2035 relative to 1986-2005 is similar for the four RCPs and will *likely* be in the range 0.3°C–0.7°C (*medium confidence*). This assumes that there will be no major volcanic eruptions or changes in some natural sources (e.g., CH₄ and N₂O), or unexpected changes in total solar irradiance. By mid-21st century, the magnitude of the projected climate change is substantially affected by the choice of emissions scenario. {2.2.1, Table 2.1}

Relative to 1850-1900, global surface temperature change for the end of the 21st century (2081-2100) is projected to *likely* exceed 1.5°C for RCP4.5, RCP6.0 and RCP8.5 (*high confidence*). Warming is *likely* to exceed 2°C for RCP6.0 and RCP8.5 (*high confidence*), *more likely than not* to exceed 2°C for RCP4.5 (*medium confidence*), but *unlikely* to exceed 2°C for RCP2.6 (*medium confidence*). {2.2.1}

The increase of global mean surface temperature by the end of the 21st century (2081-2100) relative to 1986-2005 is *likely* to be 0.3°C–1.7°C under RCP2.6, 1.1°C–2.6°C under RCP4.5, 1.4°C–3.1°C under RCP6.0, and 2.6°C–4.8°C under RCP8.5⁹. The Arctic region will continue to warm more rapidly than the global mean (Figure SPM.6.a, Figure SPM.7.a). {2.2.1, Figure 2.1, Figure 2.2, Table 2.1}

It is *virtually certain* that there will be more frequent hot and fewer cold temperature extremes over most land areas on daily and seasonal timescales, as global mean surface temperature increases. It is *very likely* that heat waves will occur with a higher frequency and longer duration. Occasional cold winter extremes will continue to occur. {2.2.1}

⁶ Quantification of this range of CO₂ emissions requires taking into account non-CO₂ drivers.

⁷ Corresponding figures for limiting warming to 2°C with a probability of >50% and >33% are 3000 GtCO₂ (range of 2900-3200 GtCO₂) and 3300 GtCO₂ (range of 2950-3800 GtCO₂) respectively. Higher or lower temperature limits would imply larger or lower cumulative emissions respectively.

⁸ This corresponds to about two thirds of the 2900 GtCO₂ that would limit warming to less than 2°C with a probability of >66%; to about 63% of the total amount of 3000 GtCO₂ that would limit warming to less than 2°C with a probability of >50%; and to about 58% of the total amount of 3300 GtCO₂ that would limit warming to less than 2°C with a probability of >33%.

⁹ The period 1986-2005 is approximately 0.61 [0.55 to 0.67] °C warmer than 1850-1900. {2.2.1}

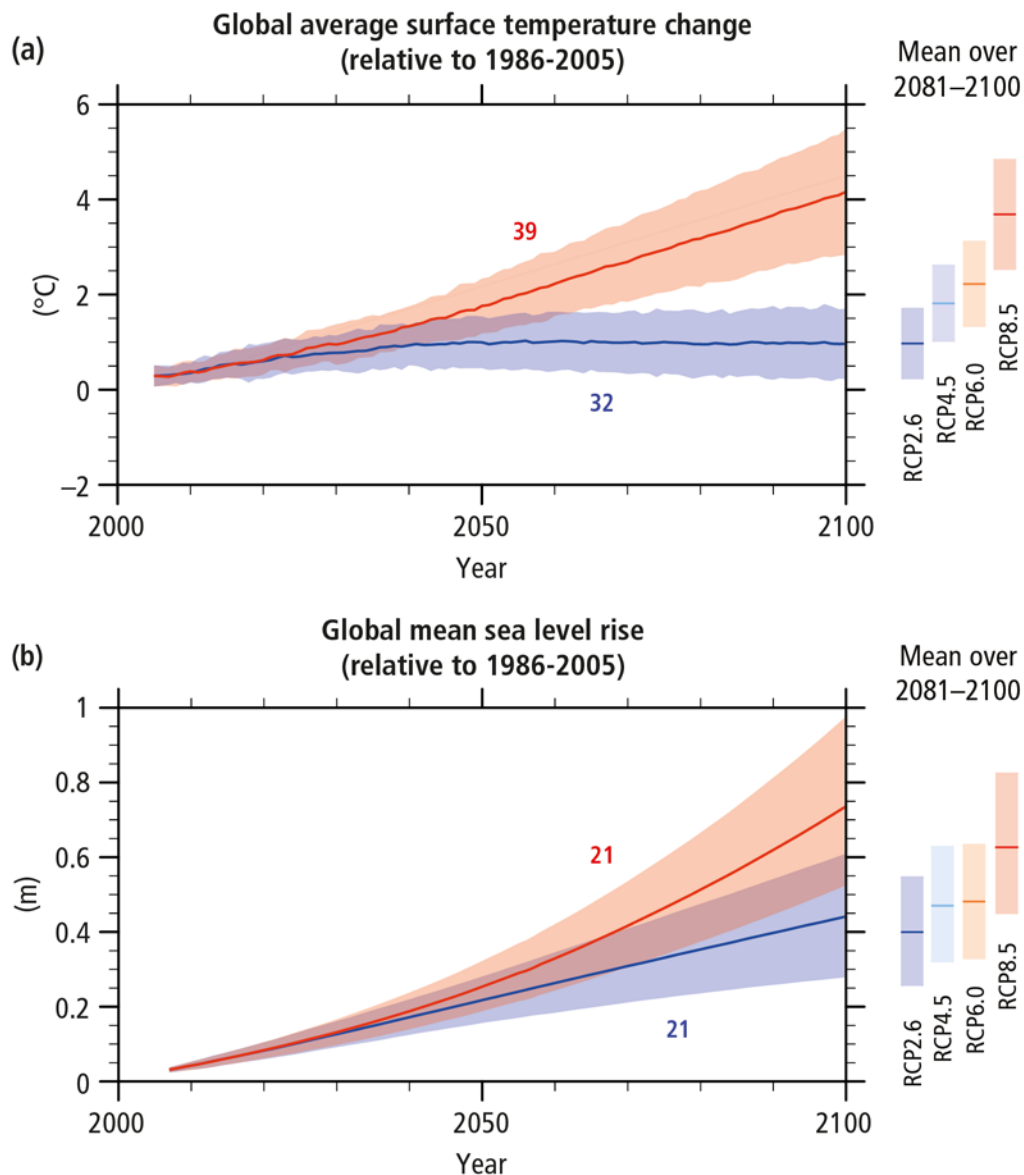


Figure SPM.6: Global average surface temperature change **(a)** and global mean sea-level rise¹⁰ **(b)** from 2006 to 2100 as determined by multi-model simulations. All changes are relative to 1986–2005. Time series of projections and a measure of uncertainty (shading) are shown for scenarios RCP2.6 (blue) and RCP8.5 (red). The mean and associated uncertainties averaged over 2081–2100 are given for all RCP scenarios as coloured vertical bars at the right hand side of each panel. The number of Coupled Model Intercomparison Project Phase 5 (CMIP5) models used to calculate the multi-model mean is indicated. {2.2, Figure 2.1}

¹⁰ Based on current understanding (from observations, physical understanding and modelling), only the collapse of marine-based sectors of the Antarctic ice sheet, if initiated, could cause global mean sea level to rise substantially above the *likely* range during the 21st century. There is *medium confidence* that this additional contribution would not exceed several tenths of a meter of sea-level rise during the 21st century.

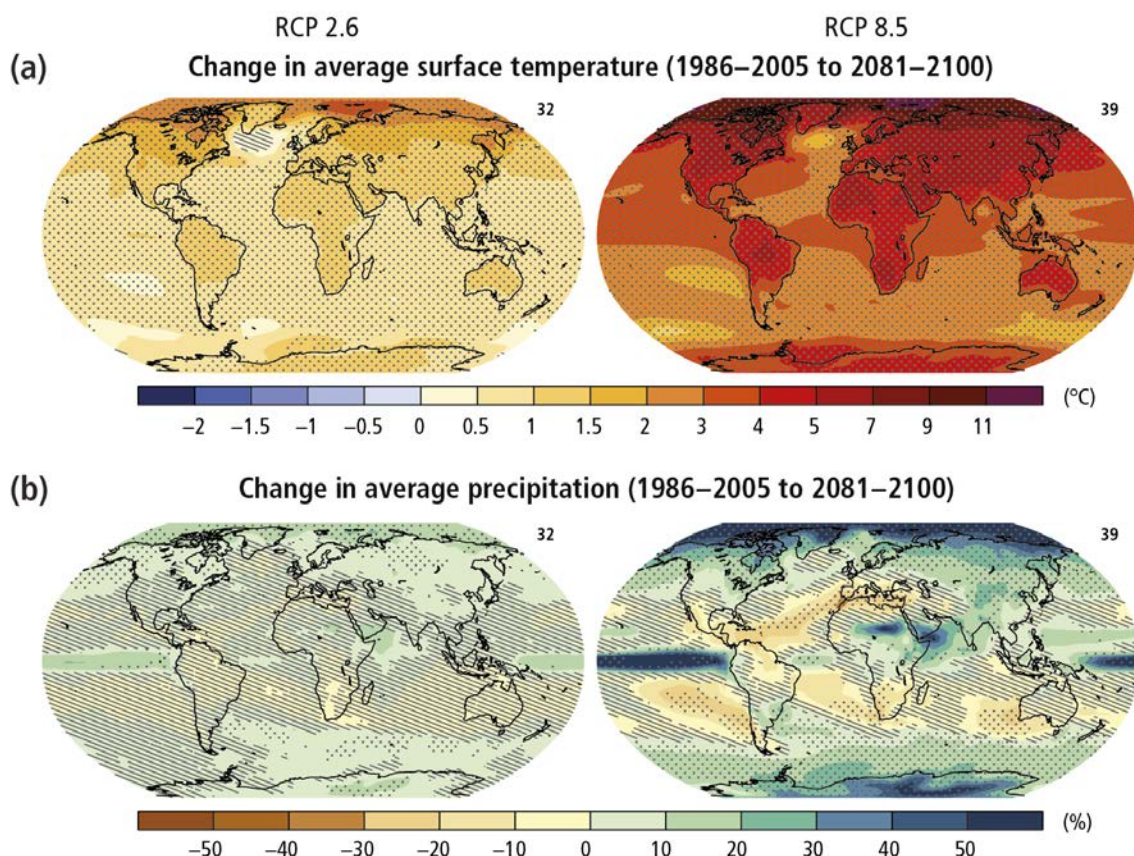


Figure SPM.7: Change in average surface temperature **(a)** and change in average precipitation **(b)** based on multi-model mean projections for 2081–2100 relative to 1986–2005 under the RCP2.6 (left) and RCP8.5 (right) scenarios. The number of models used to calculate the multi-model mean is indicated in the upper right corner of each panel. Stippling (i.e., dots) shows regions where the projected change is large compared to natural internal variability, and where at least 90% of models agree on the sign of change. Hatching (i.e., diagonal lines) shows regions where the projected change is less than one standard deviation of the natural internal variability. {2.2, Figure 2.2}

Changes in precipitation will not be uniform. The high-latitudes and the equatorial Pacific are *likely* to experience an increase in annual mean precipitation under the RCP8.5 scenario. In many mid-latitude and subtropical dry regions, mean precipitation will *likely* decrease, while in many mid-latitude wet regions, mean precipitation will *likely* increase under the RCP8.5 scenario (Figure SPM.7.b). Extreme precipitation events over most of the mid-latitude land masses and over wet tropical regions will *very likely* become more intense and more frequent. {2.2.2, Figure 2.2}

The global ocean will continue to warm during the 21st century, with the strongest warming projected for the surface in tropical and Northern Hemisphere subtropical regions (Figure SPM.7.a). {2.2.3, Figure 2.2}

Earth System Models project a global increase in ocean acidification for all RCP scenarios by the end of the 21st century, with a slow recovery after mid-century under RCP2.6. The decrease in surface ocean pH is in the range of 0.06 to 0.07 (15–17% increase in acidity) for RCP2.6, 0.14 to 0.15 (38–41%) for RCP4.5, 0.20 to 0.21 (58–62%) for RCP6.0, and 0.30 to 0.32 (100–109%) for RCP8.5. {2.2.4, Figure 2.1}

Year-round reductions in Arctic sea ice are projected for all RCP scenarios. A nearly ice-free¹¹ Arctic Ocean in the summer sea-ice minimum in September before mid-century is *likely* for RCP8.5¹² (*medium confidence*). {2.2.3, Figure 2.1}

¹¹ When sea-ice extent is less than one million km² for at least five consecutive years.

¹² Based on an assessment of the subset of models that most closely reproduce the climatological mean state and 1979–2012 trend of the Arctic sea-ice extent.

It is *virtually certain* that near-surface permafrost extent at high northern latitudes will be reduced as global mean surface temperature increases, with the area of permafrost near the surface (upper 3.5 m) projected to decrease by 37% (RCP2.6) to 81% (RCP8.5) for the multi-model average (*medium confidence*). {2.2.3}

The global glacier volume, excluding glaciers on the periphery of Antarctica (and excluding the Greenland and Antarctic ice sheets), is projected to decrease by 15 to 55% for RCP2.6, and by 35 to 85% for RCP8.5 (*medium confidence*). {2.2.3}

There has been significant improvement in understanding and projection of sea-level change since the AR4. Global mean sea-level rise will continue during the 21st century, *very likely* at a faster rate than observed from 1971 to 2010. For the period 2081-2100 relative to 1986-2005, the rise will *likely* be in the ranges of 0.26 to 0.55 m for RCP2.6, and of 0.45 to 0.82 m for RCP8.5 (*medium confidence*)¹⁰ (Figure SPM.6.b). Sea-level rise will not be uniform across regions. By the end of the 21st century, it is *very likely* that sea level will rise in more than about 95% of the ocean area. About 70% of the coastlines worldwide are projected to experience a sea-level change within $\pm 20\%$ of the global mean. {2.2.3}

SPM 2.3 Future risks and impacts caused by a changing climate

Climate change will amplify existing risks and create new risks for natural and human systems. Risks are unevenly distributed and are generally greater for disadvantaged people and communities in countries at all levels of development. {2.3}

Risk of climate-related impacts results from the interaction of climate-related hazards (including hazardous events and trends) with the vulnerability and exposure of human and natural systems, including their ability to adapt. Rising rates and magnitudes of warming and other changes in the climate system, accompanied by ocean acidification, increase the risk of severe, pervasive, and in some cases irreversible detrimental impacts. Some risks are particularly relevant for individual regions (Figure SPM.8), while others are global. The overall risks of future climate change impacts can be reduced by limiting the rate and magnitude of climate change, including ocean acidification. The precise levels of climate change sufficient to trigger abrupt and irreversible change remain uncertain, but the risk associated with crossing such thresholds increases with rising temperature (*medium confidence*). For risk assessment, it is important to evaluate the widest possible range of impacts, including low-probability outcomes with large consequences. {1.5, 2.3, 2.4, 3.3, Box Introduction 1, Box 2.3, Box 2.4}

A large fraction of species faces increased extinction risk due to climate change during and beyond the 21st century, especially as climate change interacts with other stressors (*high confidence*). Most plant species cannot naturally shift their geographical ranges sufficiently fast to keep up with current and high projected rates of climate change in most landscapes; most small mammals and freshwater molluscs will not be able to keep up at the rates projected under RCP4.5 and above in flat landscapes in this century (*high confidence*). Future risk is indicated to be high by the observation that natural global climate change at rates lower than current anthropogenic climate change caused significant ecosystem shifts and species extinctions during the past millions of years. Marine organisms will face progressively lower oxygen levels and high rates and magnitudes of ocean acidification (*high confidence*), with associated risks exacerbated by rising ocean temperature extremes (*medium confidence*). Coral reefs and polar ecosystems are highly vulnerable. Coastal systems and low-lying areas are at risk from sea-level rise, which will continue for centuries even if the global mean temperature is stabilized (*high confidence*). {2.3, 2.4, Figure 2.5}

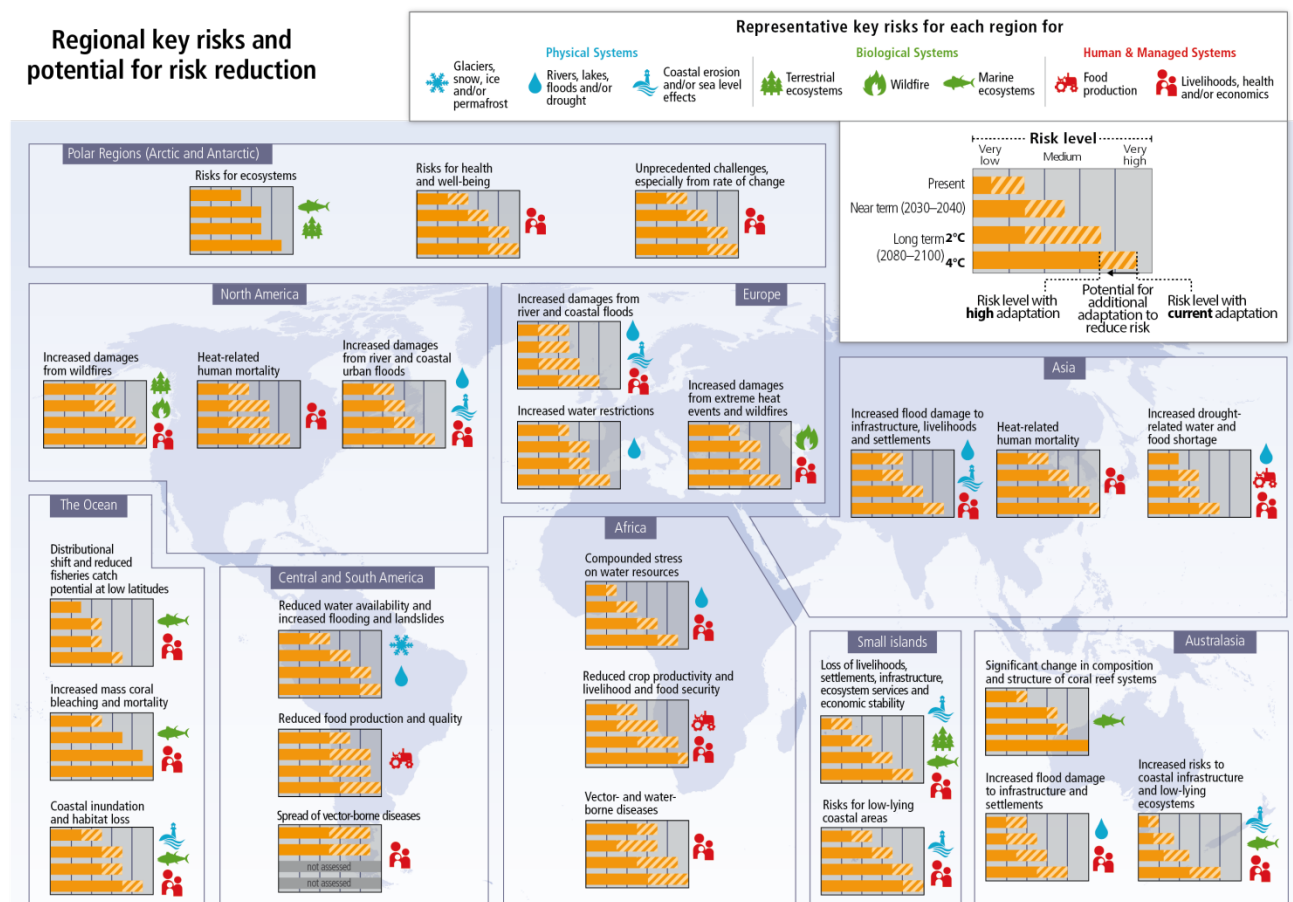


Figure SPM.8: Representative key risks¹³ for each region, including the potential for risk reduction through adaptation and mitigation, as well as limits to adaptation. Each key risk is assessed as very low, low, medium, high, or very high. Risk levels are presented for three time frames: present, near term (here, for 2030–2040), and long term (here, for 2080–2100). In the near term, projected levels of global mean temperature increase do not diverge substantially across different emission scenarios. For the long term, risk levels are presented for two possible futures (2°C and 4°C global mean temperature increase above pre-industrial levels). For each timeframe, risk levels are indicated for a continuation of current adaptation and assuming high levels of current or future adaptation. Risk levels are not necessarily comparable, especially across regions. {Figure 2.4}

Climate change is projected to undermine food security (Figure SPM.9). Due to projected climate change by the mid-21st century and beyond, global marine species redistribution and marine biodiversity reduction in sensitive regions will challenge the sustained provision of fisheries productivity and other ecosystem services (*high confidence*). For wheat, rice, and maize in tropical and temperate regions, climate change without adaptation is projected to negatively impact production for local temperature increases of 2°C or more above late-20th century levels, although individual locations may benefit (*medium confidence*). Global temperature increases of ~4°C or more¹⁴ above late-20th century levels, combined with increasing food demand, would pose large risks to food security globally (*high confidence*). Climate change is projected to reduce renewable surface water and groundwater resources in most dry subtropical regions (*robust evidence, high agreement*), intensifying competition for water among sectors (*limited evidence, medium agreement*). {2.3.1, 2.3.2}

¹³ Identification of key risks was based on expert judgment using the following specific criteria: large magnitude, high probability, or irreversibility of impacts; timing of impacts; persistent vulnerability or exposure contributing to risks; or limited potential to reduce risks through adaptation or mitigation.

¹⁴ Projected warming averaged over land is larger than global average warming for all RCP scenarios for the period 2081–2100 relative to 1986–2005. For regional projections, see Figure SPM.7. {2.2}

Climate change poses risks for food production

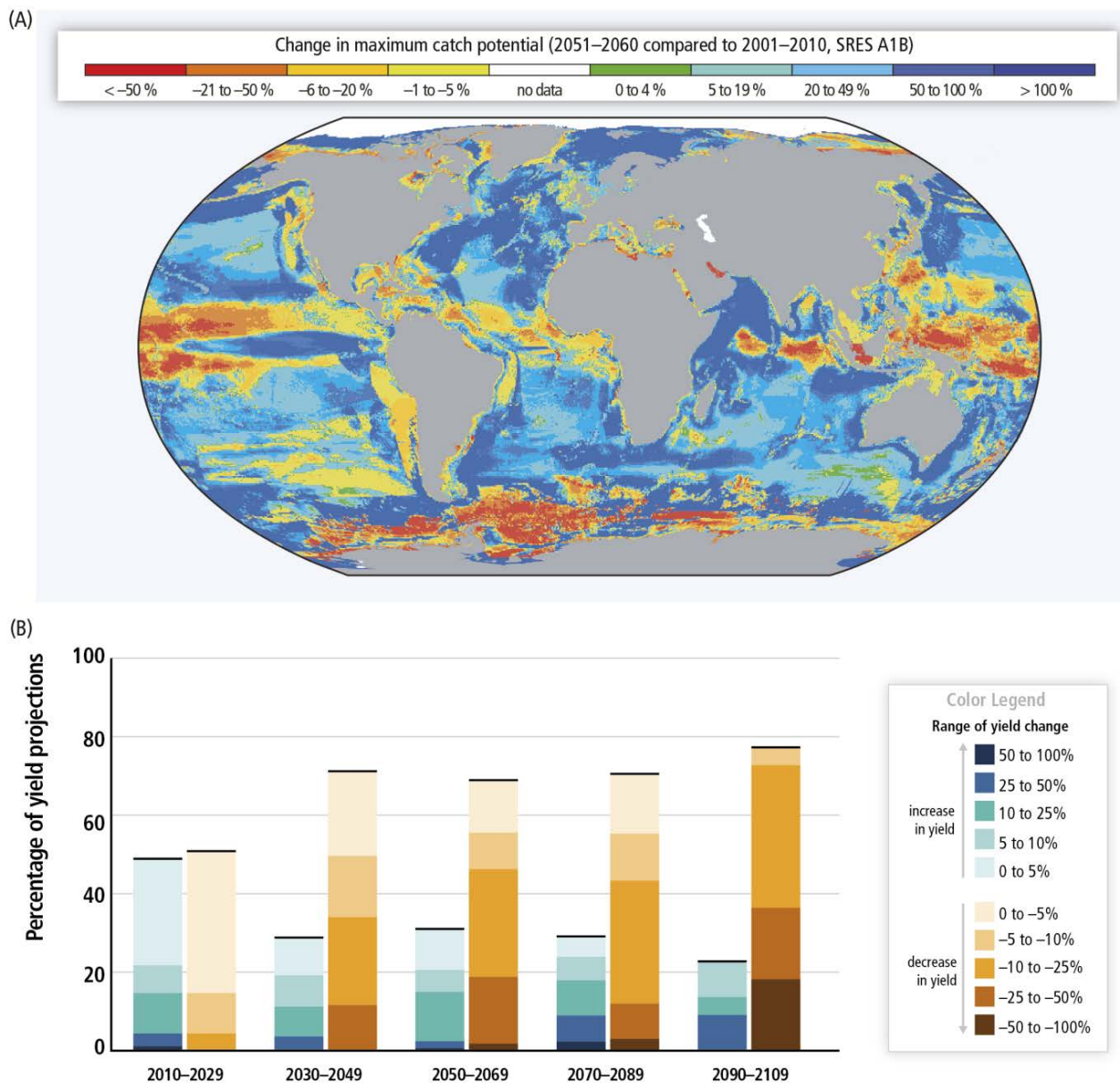


Figure SPM.9: (A) Projected global redistribution of maximum catch potential of ~1000 exploited marine fish and invertebrate species. Projections compare the 10-year averages 2001–2010 and 2051–2060 using ocean conditions based on a single climate model under a moderate to high warming scenario, without analysis of potential impacts of overfishing or ocean acidification. (B) Summary of projected changes in crop yields (mostly wheat, maize, rice, and soy), due to climate change over the 21st century. Data for each timeframe sum to 100%, indicating the percentage of projections showing yield increases versus decreases. The figure includes projections (based on 1090 data points) for different emission scenarios, for tropical and temperate regions, and for adaptation and no-adaptation cases combined. Changes in crop yields are relative to late-20th century levels. {Figure 2.6.a, Figure 2.7}

Until mid-century, projected climate change will impact human health mainly by exacerbating health problems that already exist (*very high confidence*). Throughout the 21st century, climate change is expected to lead to increases in ill-health in many regions and especially in developing countries with low income, as compared to a baseline without climate change (*high confidence*). By 2100 for RCP8.5, the combination of high temperature and humidity in some areas for parts of the year is expected to compromise common human activities, including growing food and working outdoors (*high confidence*). {2.3.2}

In urban areas, climate change is projected to increase risks for people, assets, economies and ecosystems, including risks from heat stress, storms and extreme precipitation, inland and coastal flooding, landslides, air

pollution, drought, water scarcity, sea-level rise, and storm surges (*very high confidence*). These risks are amplified for those lacking essential infrastructure and services or living in exposed areas. {2.3.2}

Rural areas are expected to experience major impacts on water availability and supply, food security, infrastructure, and agricultural incomes, including shifts in the production areas of food and non-food crops around the world (*high confidence*). {2.3.2}

Aggregate economic losses accelerate with increasing temperature (*limited evidence, high agreement*) but global economic impacts from climate change are currently difficult to estimate. From a poverty perspective, climate change impacts are projected to slow down economic growth, make poverty reduction more difficult, further erode food security, and prolong existing and create new poverty traps, the latter particularly in urban areas and emerging hotspots of hunger (*medium confidence*). International dimensions such as trade and relations among states are also important for understanding the risks of climate change at regional scales. {2.3.2}

Climate change is projected to increase displacement of people (*medium evidence, high agreement*). Populations that lack the resources for planned migration experience higher exposure to extreme weather events, particularly in developing countries with low income. Climate change can indirectly increase risks of violent conflicts by amplifying well-documented drivers of these conflicts such as poverty and economic shocks (*medium confidence*). {2.3.2}

SPM 2.4 Climate change beyond 2100, irreversibility and abrupt changes

Many aspects of climate change and associated impacts will continue for centuries, even if anthropogenic emissions of greenhouse gases are stopped. The risks of abrupt or irreversible changes increase as the magnitude of the warming increases. {2.4}

Warming will continue beyond 2100 under all RCP scenarios except RCP2.6. Surface temperatures will remain approximately constant at elevated levels for many centuries after a complete cessation of net anthropogenic CO₂ emissions. A large fraction of anthropogenic climate change resulting from CO₂ emissions is irreversible on a multi-century to millennial time scale, except in the case of a large net removal of CO₂ from the atmosphere over a sustained period. {2.4, Figure 2.8}

stabilization of global average surface temperature does not imply stabilization for all aspects of the climate system. Shifting biomes, soil carbon, ice sheets, ocean temperatures and associated sea-level rise all have their own intrinsic long timescales which will result in changes lasting hundreds to thousands of years after global surface temperature is stabilized. {2.1, 2.4}

There is *high confidence* that ocean acidification will increase for centuries if CO₂ emissions continue, and will strongly affect marine ecosystems. {2.4}

It is *virtually certain* that global mean sea-level rise will continue for many centuries beyond 2100, with the amount of rise dependent on future emissions. The threshold for the loss of the Greenland ice sheet over a millennium or more, and an associated sea-level rise of up to 7 m, is greater than about 1°C (*low confidence*) but less than about 4°C (*medium confidence*) of global warming with respect to pre-industrial temperatures. Abrupt and irreversible ice loss from the Antarctic ice sheet is possible, but current evidence and understanding is insufficient to make a quantitative assessment. {2.4}

Magnitudes and rates of climate change associated with medium- to high-emission scenarios pose an increased risk of abrupt and irreversible regional-scale change in the composition, structure, and function of marine, terrestrial and freshwater ecosystems, including wetlands (*medium confidence*). A reduction in permafrost extent is *virtually certain* with continued rise in global temperatures. {2.4}

SPM 3. Future Pathways for Adaptation, Mitigation and Sustainable Development

Adaptation and mitigation are complementary strategies for reducing and managing the risks of climate change. Substantial emissions reductions over the next few decades can reduce climate risks in the 21st century and beyond, increase prospects for effective adaptation, reduce the costs and challenges of mitigation in the longer term, and contribute to climate-resilient pathways for sustainable development. {3.2, 3.3, 3.4}

SPM 3.1 Foundations of decision-making about climate change

Effective decision making to limit climate change and its effects can be informed by a wide range of analytical approaches for evaluating expected risks and benefits, recognizing the importance of governance, ethical dimensions, equity, value judgments, economic assessments and diverse perceptions and responses to risk and uncertainty. {3.1}

Sustainable development and equity provide a basis for assessing climate policies. Limiting the effects of climate change is necessary to achieve sustainable development and equity, including poverty eradication. Countries' past and future contributions to the accumulation of GHGs in the atmosphere are different, and countries also face varying challenges and circumstances and have different capacities to address mitigation and adaptation. Mitigation and adaptation raise issues of equity, justice, and fairness. Many of those most vulnerable to climate change have contributed and contribute little to GHG emissions. Delaying mitigation shifts burdens from the present to the future, and insufficient adaptation responses to emerging impacts are already eroding the basis for sustainable development. Comprehensive strategies in response to climate change that are consistent with sustainable development take into account the co-benefits, adverse side-effects and risks that may arise from both adaptation and mitigation options. {3.1, 3.5, Box 3.4}

The design of climate policy is influenced by how individuals and organizations perceive risks and uncertainties and take them into account. Methods of valuation from economic, social and ethical analysis are available to assist decision making. These methods can take account of a wide range of possible impacts, including low-probability outcomes with large consequences. But they cannot identify a single best balance between mitigation, adaptation and residual climate impacts. {3.1}

Climate change has the characteristics of a collective action problem at the global scale, because most greenhouse gases accumulate over time and mix globally, and emissions by any agent (e.g., individual, community, company, country) affect other agents. Effective mitigation will not be achieved if individual agents advance their own interests independently. Cooperative responses, including international cooperation, are therefore required to effectively mitigate GHG emissions and address other climate change issues. The effectiveness of adaptation can be enhanced through complementary actions across levels, including international cooperation. The evidence suggests that outcomes seen as equitable can lead to more effective cooperation. {3.1}

SPM 3.2 Climate change risks reduced by mitigation and adaptation

Without additional mitigation efforts beyond those in place today, and even with adaptation, warming by the end of the 21st century will lead to high to very high risk of severe, widespread, and irreversible impacts globally (*high confidence*). Mitigation involves some level of co-benefits and of risks due to adverse side-effects, but these risks do not involve the same possibility of severe, widespread, and irreversible impacts as risks from climate change, increasing the benefits from near-term mitigation efforts. {3.2, 3.4}

Mitigation and adaptation are complementary approaches for reducing risks of climate change impacts over different time scales (*high confidence*). Mitigation, in the near-term and through the century, can substantially reduce climate change impacts in the latter decades of the 21st century and beyond. Benefits from adaptation can already be realized in addressing current risks, and can be realized in the future for addressing emerging risks. {3.2, 4.5}

Five "Reasons For Concern" (RFCs) aggregate climate change risks and illustrate the implications of warming and of adaptation limits for people, economies, and ecosystems across sectors and regions. The Five RFCs are associated with: (1) Unique and threatened systems, (2) Extreme weather events, (3) Distribution of impacts, (4) Global aggregate impacts, and (5) Large-scale singular events. In this report, the RFCs provide information relevant to Article 2 of UNFCCC. {Box 2.4}

Without additional mitigation efforts beyond those in place today, and even with adaptation, warming by the end of the 21st century will lead to high to very high risk of severe, widespread, and irreversible impacts globally (*high confidence*) (Figure SPM.10). In most scenarios without additional mitigation efforts (those with 2100 atmospheric concentrations >1000ppm CO₂-eq), warming is *more likely than not* to exceed 4°C above pre-industrial levels by 2100. The risks associated with temperatures at or above 4°C include substantial species extinction, global and regional food insecurity, consequential constraints on common human activities, and limited potential for adaptation in some cases (*high confidence*). Some risks of climate change, such as risks to unique and threatened systems and risks associated with extreme weather events, are moderate to high at temperatures 1°C to 2°C above pre-industrial levels. {2.3, Figure 2.5, 3.2, 3.4, Box 2.4, Table SPM.1}

Substantial cuts in greenhouse gas emissions over the next few decades can substantially reduce risks of climate change by limiting warming in the second half of the 21st century and beyond. Cumulative emissions of CO₂ largely determine global mean surface warming by the late 21st century and beyond. Limiting risks across RFCs would imply a limit for cumulative emissions of CO₂. Such a limit would require that global net emissions of CO₂ eventually decrease to zero and would constrain annual emissions over the next few decades (Figure SPM.10) (*high confidence*). But some risks from climate damages are unavoidable, even with mitigation and adaptation. {2.2.5, 3.2, 3.4}

Mitigation involves some level of co-benefits and risks, but these risks do not involve the same possibility of severe, widespread, and irreversible impacts as risks from climate change. Inertia in the economic and climate system and the possibility of irreversible impacts from climate change increase the benefits from near-term mitigation efforts (*high confidence*). Delays in additional mitigation or constraints on technological options increase the longer-term mitigation costs to hold climate change risks at a given level (Table SPM.2). {3.2, 3.4}

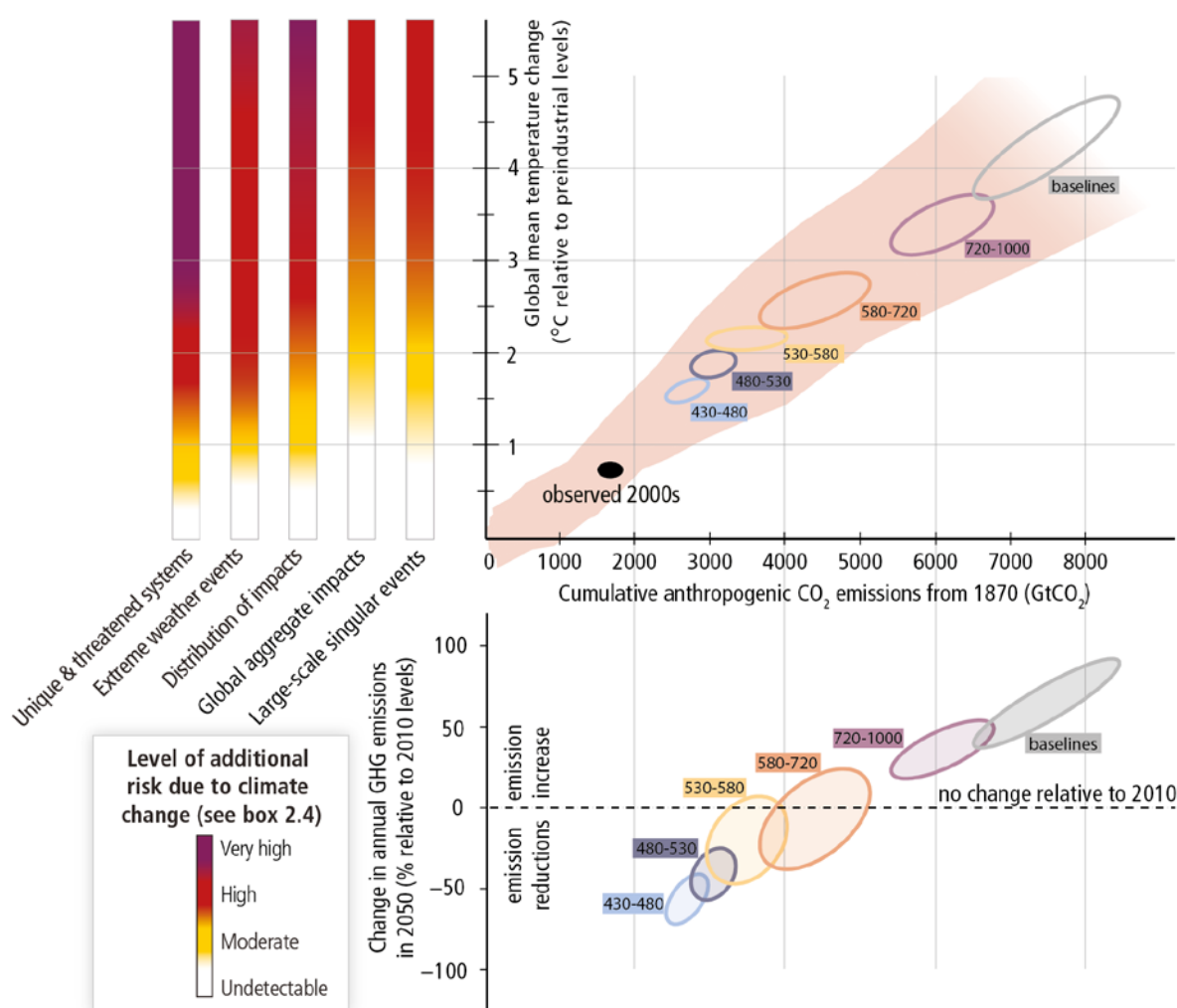
(A) Risks from climate change... (B) ...depend on cumulative CO₂ emissions...**(C) ...which in turn depend on annual GHG emissions over the next decades**

Figure SPM.10: The relationship between risks from climate change, temperature change, cumulative CO₂ emissions, and changes in annual GHG emissions by 2050. Limiting risks across Reasons For Concern (panel A) would imply a limit for cumulative emissions of CO₂ (panel B), which would constrain annual GHG emissions over the next few decades (panel C). (A) reproduces the five Reasons For Concern {Box 2.4}. (B) links temperature changes to cumulative CO₂ emissions (in GtCO₂) from 1870. They are based on CMIP5 simulations (pink plume) and on a simple climate model (median climate response in 2100), for the baselines and five mitigation scenario categories (six ellipses). Details are provided in Figure SPM.5. (C) shows the relationship between the cumulative CO₂ emissions (in GtCO₂) of the scenario categories and their associated change in annual GHG emissions by 2050, expressed in percentage change (in percent GtCO₂-eq per year) relative to 2010. The ellipses correspond to the same scenario categories as in Panel B, and are built with a similar method (see details in Figure SPM.5). {Figure 3.1}

SPM 3.3 Characteristics of adaptation pathways

Adaptation can reduce the risks of climate change impacts, but there are limits to its effectiveness, especially with greater magnitudes and rates of climate change. Taking a longer-term perspective, in the context of sustainable development, increases the likelihood that more immediate adaptation actions will also enhance future options and preparedness. {3.3}

Adaptation can contribute to the well-being of populations, the security of assets, and the maintenance of ecosystem goods, functions and services now and in the future. Adaptation is place- and context-specific (*high confidence*). A first step towards adaptation to future climate change is reducing vulnerability and

exposure to present climate variability (*high confidence*). Integration of adaptation into planning, including policy design, and decision making can promote synergies with development and disaster risk reduction. Building adaptive capacity is crucial for effective selection and implementation of adaptation options (*robust evidence, high agreement*). {3.3}

Adaptation planning and implementation can be enhanced through complementary actions across levels, from individuals to governments (*high confidence*). National governments can coordinate adaptation efforts of local and subnational governments, for example by protecting vulnerable groups, by supporting economic diversification, and by providing information, policy and legal frameworks, and financial support (*robust evidence, high agreement*). Local government and the private sector are increasingly recognized as critical to progress in adaptation, given their roles in scaling up adaptation of communities, households, and civil society and in managing risk information and financing (*medium evidence, high agreement*). {3.3}

Adaptation planning and implementation at all levels of governance are contingent on societal values, objectives, and risk perceptions (*high confidence*). Recognition of diverse interests, circumstances, social-cultural contexts, and expectations can benefit decision-making processes. Indigenous, local, and traditional knowledge systems and practices, including indigenous peoples' holistic view of community and environment, are a major resource for adapting to climate change, but these have not been used consistently in existing adaptation efforts. Integrating such forms of knowledge with existing practices increases the effectiveness of adaptation. {3.3}

Constraints can interact to impede adaptation planning and implementation (*high confidence*). Common constraints on implementation arise from the following: limited financial and human resources; limited integration or coordination of governance; uncertainties about projected impacts; different perceptions of risks; competing values; absence of key adaptation leaders and advocates; and limited tools to monitor adaptation effectiveness. Another constraint includes insufficient research, monitoring, and observation and the finance to maintain them. {3.3}

Greater rates and magnitude of climate change increase the likelihood of exceeding adaptation limits (*high confidence*). Limits to adaptation emerge from the interaction among climate change and biophysical and/or socioeconomic constraints. Further, poor planning or implementation, overemphasizing short-term outcomes, or failing to sufficiently anticipate consequences, can result in maladaptation, increasing the vulnerability or exposure of the target group in the future or the vulnerability of other people, places, or sectors (*medium evidence, high agreement*). Underestimating the complexity of adaptation as a social process can create unrealistic expectations about achieving intended adaptation outcomes. {3.3}

Significant co-benefits, synergies, and trade-offs exist between mitigation and adaptation and among different adaptation responses; interactions occur both within and across regions (*very high confidence*). Increasing efforts to mitigate and adapt to climate change imply an increasing complexity of interactions, particularly at the intersections among water, energy, land use, and biodiversity, but tools to understand and manage these interactions remain limited. Examples of actions with co-benefits include (i) improved energy efficiency and cleaner energy sources, leading to reduced emissions of health-damaging climate-altering air pollutants; (ii) reduced energy and water consumption in urban areas through greening cities and recycling water; (iii) sustainable agriculture and forestry; and (iv) protection of ecosystems for carbon storage and other ecosystem services. {3.3}

Transformations in economic, social, technological, and political decisions and actions can enhance adaptation and promote sustainable development (*high confidence*). At the national level, transformation is considered most effective when it reflects a country's own visions and approaches to achieving sustainable development in accordance with its national circumstances and priorities. Restricting adaptation responses to incremental changes to existing systems and structures, without considering transformational change, may increase costs and losses, and miss opportunities. Planning and implementation of transformational adaptation could reflect strengthened, altered or aligned paradigms and may place new and increased demands on governance structures to reconcile different goals and visions for the future and to address possible equity and ethical implications. Adaptation pathways are enhanced by iterative learning, deliberative processes, and innovation. {3.3}

SPM 3.4 Characteristics of mitigation pathways

There are multiple mitigation pathways that are *likely* to limit warming to below 2°C relative to pre-industrial levels. These pathways would require substantial emissions reductions over the next few decades and near zero emissions of CO₂ and other long-lived GHGs by the end of the century. Implementing such reductions poses substantial technological, economic, social, and institutional challenges, which increase with delays in additional mitigation and if key technologies are not available. Limiting warming to lower or higher levels involves similar challenges, but on different timescales. {3.4}

Without additional efforts to reduce GHG emissions beyond those in place today, global emissions growth is expected to persist, driven by growth in global population and economic activities. Global mean surface temperature increases in 2100 in baseline scenarios – those without additional mitigation – range from 3.7 to 4.8°C above the average for 1850-1900 for a median climate response. They range from 2.5°C to 7.8°C when including climate uncertainty (5th to 95th percentile range). (*high confidence*) {3.4}

Emissions scenarios leading to GHG concentrations in 2100 of about 450 ppm CO₂-eq or lower are *likely* to maintain warming below 2°C over the 21st century relative to pre-industrial levels.¹⁵ These scenarios are characterized by 40% to 70% global anthropogenic GHG emissions reductions by 2050 compared to 2010¹⁶, and emissions levels near zero or below in 2100. Mitigation scenarios reaching concentration levels of about 500 ppm CO₂-eq by 2100 are *more likely than not* to limit temperature change to less than 2°C, unless they temporarily overshoot concentration levels of roughly 530 ppm CO₂-eq before 2100, in which case they are *about as likely as not* to achieve that goal. In these 500 ppm CO₂-eq scenarios, global 2050 emissions levels are 25-55% lower than in 2010. Scenarios with higher emissions in 2050 are characterized by a greater reliance on Carbon Dioxide Removal (CDR) technologies beyond mid-century (and vice versa). Trajectories that are *likely* to limit warming to 3°C relative to pre-industrial levels reduce emissions less rapidly than those limiting warming to 2°C. A limited number of studies provide scenarios that are *more likely than not* to limit warming to 1.5°C by 2100; these scenarios are characterized by concentrations below 430 ppm CO₂-eq by 2100 and 2050 emission reduction between 70% and 95% below 2010. For a comprehensive overview of the characteristics of emissions scenarios, their GHG concentrations and their likelihood to keep warming to below a range of temperature levels, see Table SPM.1.{*Figure SPM.11, 3.4, Table SPM.1*}.

¹⁵ For comparison, the CO₂-eq concentration in 2011 is estimated to be 430 ppm (uncertainty range 340 ppm – 520 ppm).

¹⁶ This range differs from the range provided for a similar concentration category in AR4 (50% – 85% lower than 2000 for CO₂ only). Reasons for this difference include that this report has assessed a substantially larger number of scenarios than in AR4 and looks at all GHGs. In addition, a large proportion of the new scenarios include Carbon Dioxide Removal (CDR) technologies (see below). Other factors include the use of 2100 concentration levels instead of stabilization levels and the shift in reference year from 2000 to 2010.

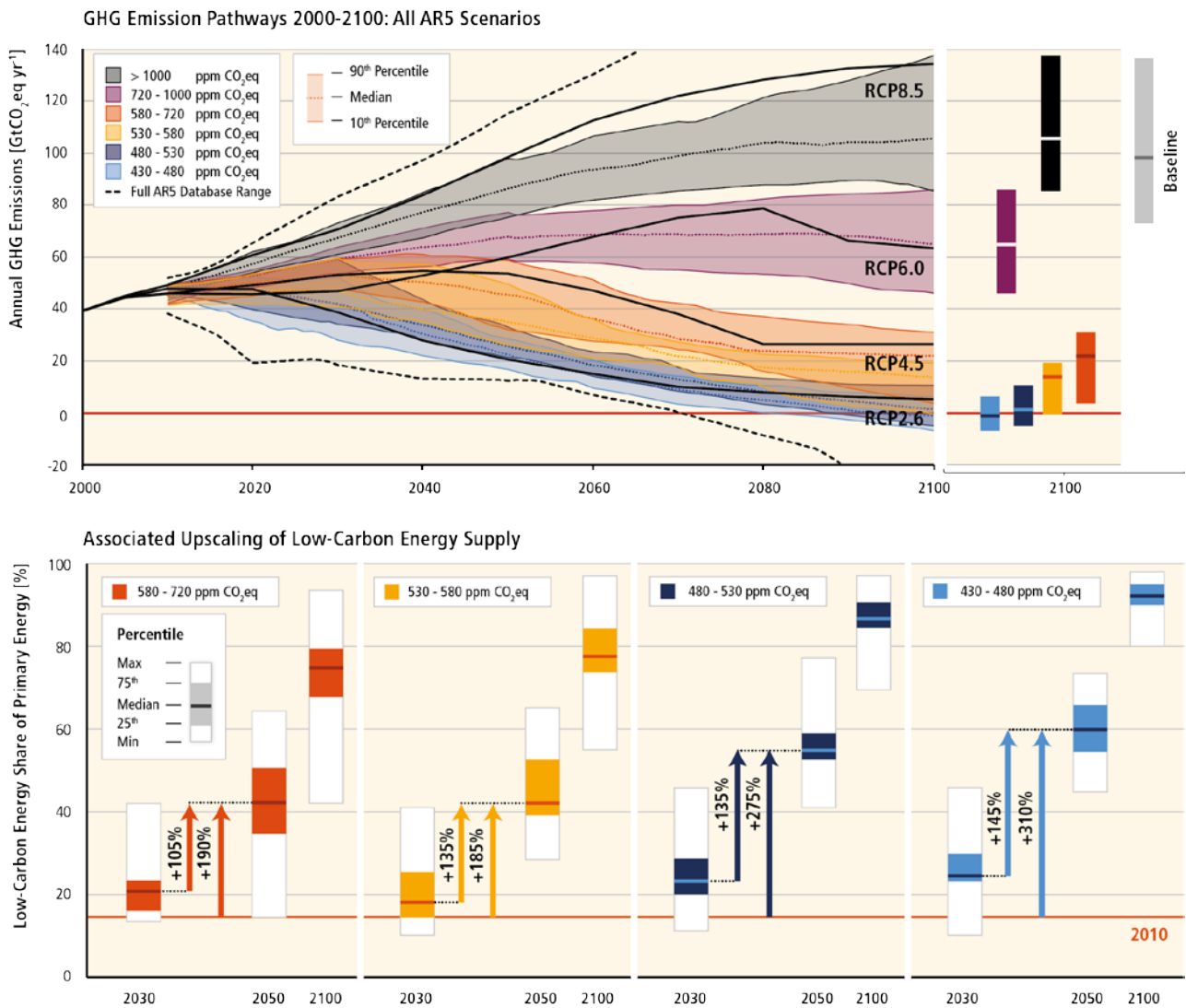


Figure SPM.11: Global GHG emissions (GtCO₂-eq/yr) in baseline and mitigation scenarios for different long-term concentration levels (upper panel) and associated upscaling requirements of low-carbon energy (% of primary energy) for 2030, 2050 and 2100 compared to 2010 levels in mitigation scenarios (lower panel). {Figure 3.2}

Table SPM.1: Key characteristics of the scenarios collected and assessed for WGIII AR5. For all parameters, the 10th to 90th percentile of the scenarios is shown.^{15,16} {Table 3.1}

CO ₂ -eq Concentrations in 2100 (CO ₂ -eq) ⁶	Subcategories	Relative position of the RCPs ⁴	Change in CO ₂ -eq emissions compared to 2010 (in %) ³		Likelihood of staying below a specific temperature level over the 21st century (relative to 1850-1900) ^{4,5}			
Category label (conc. range)			2050	2100	1.5°C	2°C	3°C	4°C
< 430	Only a limited number of individual model studies have explored levels below 430 ppm CO ₂ -eq ¹⁰							
450 (430 – 480)	Total range ^{1,7}	RCP2.6	-72 to -41	-118 to -78	More unlikely than likely	Likely	Likely	Likely
500 (480 – 530)	No overshoot of 530 ppm CO ₂ -eq		-57 to -42	-107 to -73	Unlikely	More likely than not		
	Overshoot of 530 ppm CO ₂ -eq		-55 to -25	-114 to -90		About as likely as not		
550 (530 – 580)	No overshoot of 580 ppm CO ₂ -eq		-47 to -19	-81 to -59		More unlikely than likely ⁹		
	Overshoot of 580 ppm CO ₂ -eq		-16 to 7	-183 to -86				
(580 – 650)	Total range	RCP4.5	-38 to 24	-134 to -50		Unlikely	More likely than not	
(650 – 720)	Total range		-11 to 17	-54 to -21			More unlikely than likely	
(720 – 1000) ²	Total range	RCP6.0	18 to 54	-7 to 72	Unlikely ⁸	Unlikely ⁸	Unlikely	
>1000 ²	Total range	RCP8.5	52 to 95	74 to 178		Unlikely ⁸	Unlikely	More unlikely than likely

¹ The 'total range' for the 430 ppm to 480 ppm CO₂-eq concentrations scenarios corresponds to the range of the 10th-90th percentile of the subcategory of these scenarios shown in Table 6.3 of the Working Group III report.

² Baseline scenarios fall into the >1000 and 720 ppm – 1000 ppm CO₂-eq categories. The latter category includes also mitigation scenarios. The baseline scenarios in the latter category reach a temperature change of 2.5–5.8°C above the average for 1850-1900 in 2100. Together with the baseline scenarios in the >1000 ppm CO₂-eq category, this leads to an overall 2100 temperature range of 2.5–7.8°C (range based on median climate response: 3.7–4.8°C) for baseline scenarios across both concentration categories.

³ The global 2010 emissions are 31% above the 1990 emissions (consistent with the historic GHG emission estimates presented in this report). CO₂-eq emissions include the basket of Kyoto gases (CO₂, CH₄, N₂O as well as F-gases).

⁴ The assessment here involves a large number of scenarios published in the scientific literature and is thus not limited to the RCPs. To evaluate the CO₂-eq concentration and climate implications of these scenarios, the MAGICC model was used in a probabilistic mode. For a comparison between MAGICC model results and the outcomes of the models used in WGI, see Section WGI 12.4.1.2 and WGI 12.4.8 and 6.3.2.6.

⁵ The assessment in this table is based on the probabilities calculated for the full ensemble of scenarios in WGIII using MAGICC and the assessment in WGI of the uncertainty of the temperature projections not covered by climate models. The statements are therefore consistent with the statements in WGI, which are based on the CMIP5 runs of the RCPs and the assessed uncertainties. Hence, the likelihood statements reflect different lines of evidence from both WGs. This WGI method was also applied for scenarios with intermediate concentration levels where no CMIP5 runs are available. The likelihood statements are indicative only {WGIII 6.3} and follow broadly the terms used by the WGI SPM for

temperature projections: *likely* 66-100%, *more likely than not* >50-100%, *about as likely as not* 33-66%, and *unlikely* 0-33%. In addition the term *more unlikely than likely* 0-<50% is used.

⁶ The CO₂-equivalent *concentration* (see Glossary) is calculated on the basis of the total forcing from a simple carbon cycle/climate model, MAGICC. The CO₂ equivalent concentration in 2011 is estimated to be 430 ppm (uncertainty range 340 ppm – 520 ppm). This is based on the assessment of total anthropogenic radiative forcing for 2011 relative to 1750 in WGI, i. e. 2.3 W m⁻², uncertainty range 1.1 to 3.3 W m⁻².

⁷ The vast majority of scenarios in this category overshoot the category boundary of 480 ppm CO₂-eq concentration.

⁸ For scenarios in this category, no CMIP5 run or MAGICC realization stays below the respective temperature level. Still, an ‘*unlikely*’ assignment is given to reflect uncertainties that may not be reflected by the current climate models.

⁹ Scenarios in the 580 ppm – 650 ppm CO₂-eq category include both overshoot scenarios and scenarios that do not exceed the concentration level at the high end of the category (e.g. RCP4.5). The latter type of scenarios, in general, have an assessed probability of *more unlikely than likely* to stay below the 2°C temperature level, while the former are mostly assessed to have an *unlikely* probability of staying below this level.

¹⁰ In these scenarios, global CO₂-eq emissions in 2050 are between 70–95% below 2010 emissions, and they are between 110–120% below 2010 emissions in 2100.

Mitigation scenarios reaching about 450 ppm CO₂-eq in 2100 (consistent with a *likely* chance to keep warming below 2°C relative to pre-industrial levels) typically involve temporary overshoot¹⁷ of atmospheric concentrations, as do many scenarios reaching about 500 ppm CO₂-eq to about 550 ppm CO₂-eq in 2100 (Table SPM.1). Depending on the level of overshoot, overshoot scenarios typically rely on the availability and widespread deployment of bioenergy with carbon dioxide capture and storage (BECCS) and afforestation in the second half of the century. The availability and scale of these and other Carbon Dioxide Removal (CDR) technologies and methods are uncertain and CDR technologies are, to varying degrees, associated with challenges and risks.¹⁸ CDR is also prevalent in many scenarios without overshoot to compensate for residual emissions from sectors where mitigation is more expensive (*high confidence*). {3.4, Box 3.3}

Reducing emissions of non-CO₂ agents can be an important element of mitigation strategies. All current GHG emissions and other forcing agents affect the rate and magnitude of climate change over the next few decades, although long-term warming is mainly driven by CO₂ emissions. Emissions of non-CO₂ forcers are often expressed as “CO₂-equivalent emissions”, but the choice of metric to calculate these emissions, and the implications for the emphasis and timing of abatement of the various climate forcers, depend on application, policy context, and contains value judgments. {3.4, Box 3.2}

Delaying additional mitigation to 2030 will substantially increase the challenges associated with limiting warming over the 21st century to below 2°C relative to pre-industrial levels. It will require substantially higher rates of emissions reductions from 2030 to 2050; a much more rapid scale-up of low-carbon energy over this period; a larger reliance on CDR in the long term; and higher transitional and long-term economic impacts. Estimated global emissions levels in 2020 based on the Cancún Pledges are not consistent with cost-effective mitigation trajectories that are at least *about as likely as not* to limit warming to below 2°C relative to pre-industrial levels, but they do not preclude the option to meet this goal (*high confidence*) (Figure SPM.12, Table SPM.2). {3.4}

¹⁷ In concentration “overshoot” scenarios, concentrations peak during the century and then decline.

¹⁸ CDR methods have biogeochemical and technological limitations to their potential on the global scale. There is insufficient knowledge to quantify how much CO₂ emissions could be partially offset by CDR on a century timescale. CDR methods may carry side-effects and long-term consequences on a global scale.

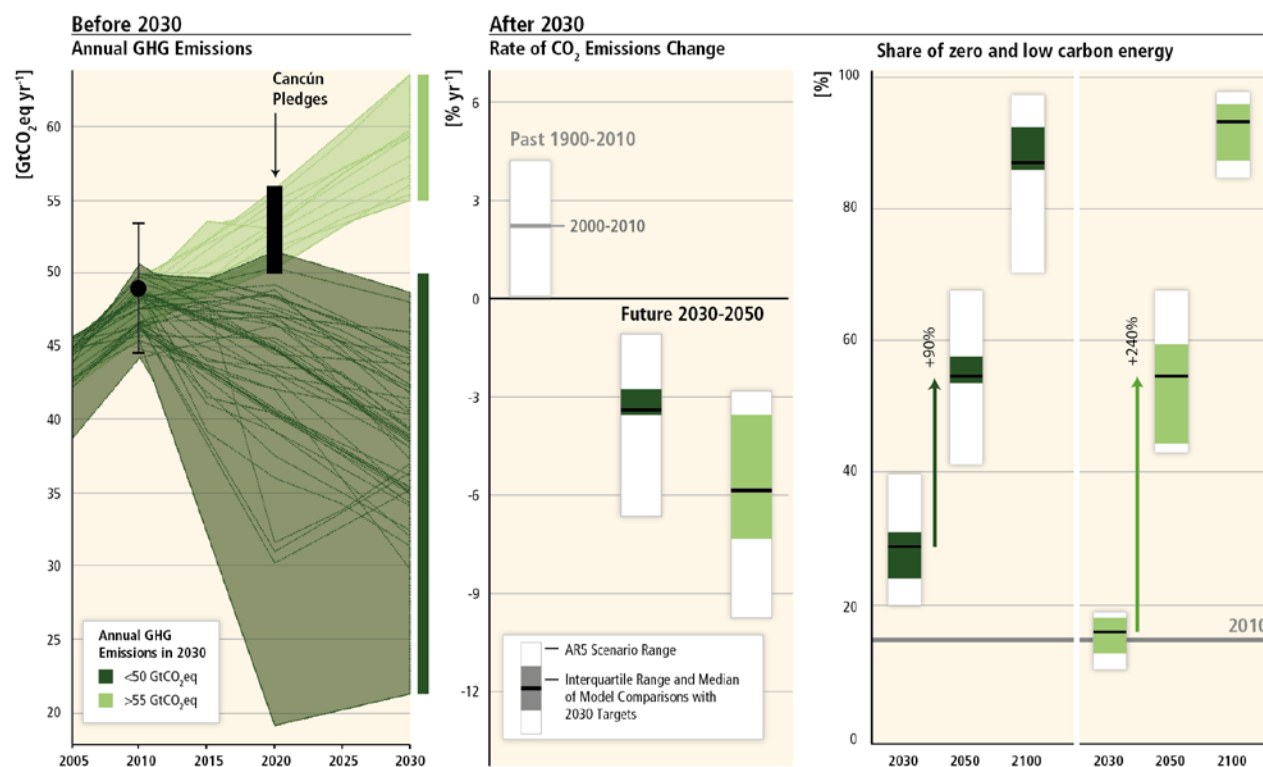


Figure SPM.12: The implications of different 2030 GHG emissions levels for the rate of CO₂ emissions reductions and low-carbon energy upscaling in mitigation scenarios that are at least *about as likely as not* to keep warming throughout the 21st century below 2°C relative to pre-industrial levels (2100 GHG concentrations of 430 ppm CO₂-eq - 530 ppm CO₂-eq). The scenarios are grouped according to different emissions levels by 2030 (coloured in different shades of green). The left panel shows the pathways of GHG emissions (GtCO₂-eq/yr) leading to these 2030 levels. Black dot with whiskers gives historic GHG emission levels and associated uncertainties in 2010 as reported in Figure SPM.2. The black bar shows the estimated uncertainty range of GHG emissions implied by the Cancún Pledges. The middle panel denotes the average annual CO₂ emissions reduction rates for the period 2030–2050. It compares the median and interquartile range across scenarios from recent inter-model comparisons with explicit 2030 interim goals to the range of scenarios in the Scenario Database for WGIII AR5. Annual rates of historical emissions change (sustained over a period of 20 years) and the average annual CO₂ emission change between 2000 and 2010 are shown as well. The arrows in the right panel show the magnitude of zero and low-carbon energy supply up-scaling from 2030 to 2050 subject to different 2030 GHG emissions levels. Zero- and low-carbon energy supply includes renewables, nuclear energy, and fossil energy with carbon dioxide capture and storage (CCS), or bioenergy with CCS (BECCS). [Note: Only scenarios that apply the full, unconstrained mitigation technology portfolio of the underlying models (default technology assumption) are shown. Scenarios with large net negative global emissions (>20 GtCO₂-eq/yr), scenarios with exogenous carbon price assumptions, and scenarios with 2010 emissions significantly outside the historical range are excluded.] [Figure 3.4]

Estimates of the aggregate economic costs of mitigation vary widely depending on methodologies and assumptions, but increase with the stringency of mitigation. Scenarios in which all countries of the world begin mitigation immediately, in which there is a single global carbon price, and in which all key technologies are available, have been used as a cost-effective benchmark for estimating macro-economic mitigation costs (Figure SPM.13). Under these assumptions mitigation scenarios that are *likely* to limit warming to below 2°C through the 21st century relative to pre-industrial levels entail losses in global consumption — not including benefits of reduced climate change as well as co-benefits and adverse side-effects of mitigation — of 1% to 4% (median: 1.7%) in 2030 and 2% to 6% (median: 3.4%) in 2050, and 3% to 11% (median: 4.8%) in 2100 relative to consumption in baseline scenarios that grows anywhere from 300% to more than 900% over the century (Figure SPM.13). These numbers correspond to an annualized reduction of consumption growth by 0.04 to 0.14

(median: 0.06) percentage points over the century relative to annualized consumption growth in the baseline that is between 1.6% and 3% per year (*high confidence*). {3.4}

Global Mitigation Costs and Consumption Growth in Baseline Scenarios

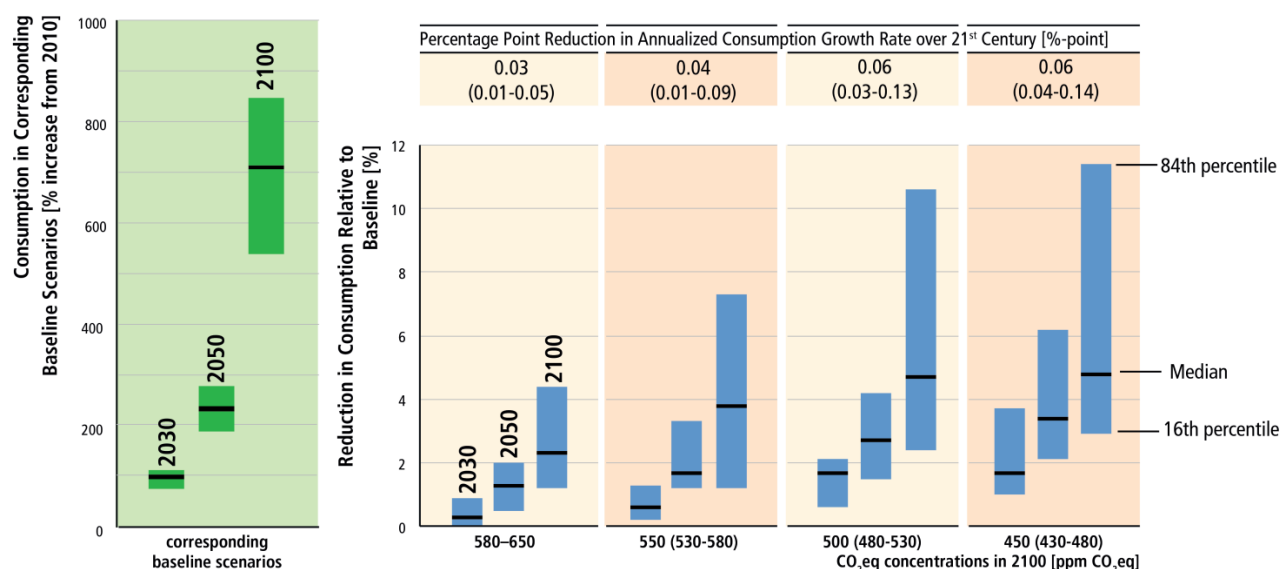


Figure SPM.13: Global mitigation costs in cost-effective scenarios at different atmospheric concentrations levels in 2100. Cost-effective scenarios assume immediate mitigation in all countries and a single global carbon price, and impose no additional limitations on technology relative to the models' default technology assumptions. Consumption losses are shown relative to a baseline development without climate policy (left panel). The table at the top shows percentage points of annualized consumption growth reductions relative to consumption growth in the baseline of 1.6% to 3% per year (e.g., if the reduction is 0.06 percentage points per year due to mitigation, and baseline growth is 2.0% per year, then the growth rate with mitigation would be 1.94% per year). Cost estimates shown in this table do not consider the benefits of reduced climate change or co-benefits and adverse side-effects of mitigation. Estimates at the high end of these cost ranges are from models that are relatively inflexible to achieve the deep emissions reductions required in the long run to meet these goals and/or include assumptions about market imperfections that would raise costs. {Figure 3.3}

In the absence or under limited availability of mitigation technologies (such as bioenergy, CCS and their combination BECCS, nuclear, wind/solar), mitigation costs can increase substantially depending on the technology considered. Delaying additional mitigation increases mitigation costs in the medium- to long-term. Many models could not limit *likely* warming to below 2°C over the 21st century relative to pre-industrial levels if additional mitigation is considerably delayed. Many models could not limit *likely* warming to below 2°C if bioenergy, CCS, and their combination (BECCS) are limited (*high confidence*) (Table SPM.2).





Mitigation scenarios reaching about 450 or 500 ppm CO₂ equivalent by 2100 show reduced costs for achieving air quality and energy security objectives, with significant co-benefits for human health, ecosystem impacts, and sufficiency of resources and resilience of the energy system. {4.4.2.2}

Mitigation policy could devalue fossil fuel assets and reduce revenues for fossil fuel exporters, but differences between regions and fuels exist (*high confidence*). Most mitigation scenarios are associated with reduced revenues from coal and oil trade for major exporters (*high confidence*). The availability of CCS would reduce the adverse effects of mitigation on the value of fossil fuel assets (*medium confidence*). {4.4.2.2}

Table SPM.2: Increase in global mitigation costs due to either limited availability of specific technologies or delays in additional mitigation¹ relative to cost-effective scenarios.² The increase in costs is given for the median estimate and the 16th to 84th percentile range of the scenarios (in parentheses).³ In addition, the sample size of each scenario set is provided in the coloured symbols. The colours of the symbols indicate the fraction of models from systematic model comparison exercises that could successfully reach the targeted concentration level. {Table 3.2}

2100 concentrations (ppm CO ₂ -eq)	Mitigation cost increases in scenarios with limited availability of technologies ⁴ [%increase in total discounted ⁵ mitigation costs (2015-2100) relative to default technology assumptions]				Mitigation cost increases due to delayed additional mitigation until 2030 [% increase in mitigation costs relative to immediate mitigation]	
	no CCS	nuclear phase out	limited solar/wind	limited bioenergy	medium term costs (2030-2050)	long term costs (2050-2100)
450 (430-480)	138 % (29-297%)	7 % (4-18%)	6 % (2-29%)	64 % (44-78%)	44 % (2-78%)	37 % (16-82%)
500 (480-530)	N/A	N/A	N/A	N/A		
550 (530-580)	39 % (18-78%)	13 % (2-23%)	8 % (5-15%)	18 % (4-66%)	15 % (3-32%)	16 % (5-24%)
580-650	N/A	N/A	N/A	N/A		

Symbol legend – fraction of models successful in producing scenarios (numbers indicate the number of successful models)

 : all models successful
 : between 50 and 80% of models successful
 : between 80 and 100% of models successful
 : less than 50% of models successful

¹ Delayed mitigation scenarios are associated with GHG emission of more than 55 GtCO₂-eq in 2030, and the increase in mitigation costs is measured relative to cost-effective mitigation scenarios for the same long-term concentration level.

² Cost-effective scenarios assume immediate mitigation in all countries and a single global carbon price, and impose no additional limitations on technology relative to the models' default technology assumptions.

³ The range is determined by the central scenarios encompassing the 16th to 84th percentile range of the scenario set. Only scenarios with a time horizon until 2100 are included. Some models that are included in the cost ranges for concentration levels above 530 ppm CO₂-eq in 2100 could not produce associated scenarios for concentration levels below 530 ppm CO₂-eq in 2100 with assumptions about limited availability of technologies and/or delayed additional mitigation.

⁴ No CCS: CCS is not included in these scenarios. Nuclear phase out: No addition of nuclear power plants beyond those under construction, and operation of existing plants until the end of their lifetime. Limited Solar/Wind: a maximum of 20% global electricity generation from solar and wind power in any year of these scenarios. Limited Bioenergy: a maximum of 100 EJ/yr modern bioenergy supply globally (modern bioenergy used for heat, power, combinations, and industry was around 18 EJ/yr in 2008).

⁵ Percentage increase of net present value of consumption losses in percent of baseline consumption (for scenarios from general equilibrium models) and abatement costs in percent of baseline GDP (for scenarios from partial equilibrium models) for the period 2015–2100, discounted at 5% per year.

Solar Radiation Management (SRM) involves large-scale methods that seek to reduce the amount of absorbed solar energy in the climate system. SRM is untested and is not included in any of the mitigation scenarios. If it were deployed, SRM would entail numerous uncertainties, side-effects, risks, shortcomings and has particular governance and ethical implications. SRM would not reduce ocean acidification. If it were terminated, there is *high confidence* that surface temperatures would rise very rapidly impacting ecosystems susceptible to rapid rates of change. {Box 3.3}

SPM 4. Adaptation and Mitigation

Many adaptation and mitigation options can help address climate change, but no single option is sufficient by itself. Effective implementation depends on policies and cooperation at all scales, and can be enhanced through integrated responses that link adaptation and mitigation with other societal objectives. {4}

SPM 4.1 Common enabling factors and constraints for adaptation and mitigation responses

Adaptation and mitigation responses are underpinned by common enabling factors. These include effective institutions and governance, innovation and investments in environmentally sound technologies and infrastructure, sustainable livelihoods, and behavioural and lifestyle choices. {4.1}

Inertia in many aspects of the socio-economic system constrains adaptation and mitigation options (*high agreement, medium evidence*). Innovation and investments in environmentally sound infrastructure and technologies can reduce greenhouse gas emissions and enhance resilience to climate change (*very high confidence*). {4.1}

Vulnerability to climate change, GHG emissions, and the capacity for adaptation and mitigation are strongly influenced by livelihoods, lifestyles, behaviour and culture (*medium evidence, medium agreement*). Also, the social acceptability and/or effectiveness of climate policies are influenced by the extent to which they incentivise or depend on regionally appropriate changes in lifestyles or behaviours. {4.1}

For many regions and sectors, enhanced capacities to mitigate and adapt are part of the foundation essential for managing climate change risks (*high confidence*). Improving institutions as well as coordination and cooperation in governance can help overcome regional constraints associated with mitigation, adaptation, and disaster risk reduction (*very high confidence*). {4.1}

SPM 4.2 Response options for adaptation

Adaptation options exist in all sectors, but their context for implementation and potential to reduce climate-related risks differs across sectors and regions. Some adaptation responses involve significant co-benefits, synergies and trade-offs. Increasing climate change will increase challenges for many adaptation options. {4.2}

Adaptation experience is accumulating across regions in the public and private sectors and within communities. There is increasing recognition of the value of social (including local and indigenous), institutional, and ecosystem-based measures and of the extent of constraints to adaptation. Adaptation is becoming embedded in some planning processes, with more limited implementation of responses (*high confidence*). {1.7, 4.2, 4.4.2.1}

The need for adaptation along with associated challenges are expected to increase with climate change (*very high confidence*). Adaptation options exist in all sectors and regions, with diverse potential and approaches depending on their context in vulnerability reduction, disaster risk management or proactive adaptation planning (Table SPM.3). Effective strategies and actions consider the potential for co-benefits and opportunities within wider strategic goals and development plans. {4.2}

Table SPM.3: Approaches for managing the risks of climate change through adaptation. These approaches should be considered overlapping rather than discrete, and they are often pursued simultaneously. Examples are presented in no specific order and can be relevant to more than one category. {Table 4.2}

Overlapping Approaches	Category	Examples
Vulnerability & Exposure Reduction through development, planning, & practices including many low-regrets measures	Human development	Improved access to education, nutrition, health facilities, energy, safe housing & settlement structures, & social support structures; Reduced gender inequality & marginalization in other forms.
	Poverty alleviation	Improved access to & control of local resources; Land tenure; Disaster risk reduction; Social safety nets & social protection; Insurance schemes.
	Livelihood security	Income, asset, & livelihood diversification; Improved infrastructure; Access to technology & decision-making fora; Increased decision-making power; Changed cropping, livestock, & aquaculture practices; Reliance on social networks.
	Disaster risk management	Early warning systems; Hazard & vulnerability mapping; Diversifying water resources; Improved drainage; Flood & cyclone shelters; Building codes & practices; Storm & wastewater management; Transport & road infrastructure improvements.
	Ecosystem management	Maintaining wetlands & urban green spaces; Coastal afforestation; Watershed & reservoir management; Reduction of other stressors on ecosystems & of habitat fragmentation; Maintenance of genetic diversity; Manipulation of disturbance regimes; Community-based natural resource management.
	Spatial or land-use planning	Provisioning of adequate housing, infrastructure, & services; Managing development in flood prone & other high risk areas; Urban planning & upgrading programs; Land zoning laws; Easements; Protected areas.
	Structural/physical	Engineered & built-environment options: Sea walls & coastal protection structures; Flood levees; Water storage; Improved drainage; Flood & cyclone shelters; Building codes & practices; Storm & wastewater management; Transport & road infrastructure improvements; Floating houses; Power plant & electricity grid adjustments.
		Technological options: New crop & animal varieties; Indigenous, traditional, & local knowledge, technologies, & methods; Efficient irrigation; Water-saving technologies; Desalinization; Conservation agriculture; Food storage & preservation facilities; Hazard & vulnerability mapping & monitoring; Early warning systems; Building insulation; Mechanical & passive cooling; Technology development, transfer, & diffusion.
		Ecosystem-based options: Ecological restoration; Soil conservation; Afforestation & reforestation; Mangrove conservation & replanting; Green infrastructure (e.g., shade trees, green roofs); Controlling overfishing; Fisheries co-management; Assisted species migration & dispersal; Ecological corridors; Seed banks, gene banks, & other <i>ex situ</i> conservation; Community-based natural resource management.
		Services: Social safety nets & social protection; Food banks & distribution of food surplus; Municipal services including water & sanitation; Vaccination programs; Essential public health services; Enhanced emergency medical services.
	Institutional	Economic options: Financial incentives; Insurance; Catastrophe bonds; Payments for ecosystem services; Pricing water to encourage universal provision and careful use; Microfinance; Disaster contingency funds; Cash transfers; Public-private partnerships.
		Laws & regulations: Land zoning laws; Building standards & practices; Easements; Water regulations & agreements; Laws to support disaster risk reduction; Laws to encourage insurance purchasing; Defined property rights & land tenure security; Protected areas; Fishing quotas; Patent pools & technology transfer.
		National & government policies & programs: National & regional adaptation plans including mainstreaming; Sub-national & local adaptation plans; Economic diversification; Urban upgrading programs; Municipal water management programs; Disaster planning & preparedness; Integrated water resource management; Integrated coastal zone management; Ecosystem-based management; Community-based adaptation.
	Social	Educational options: Awareness raising & integrating into education; Gender equity in education; Extension services; Sharing indigenous, traditional, & local knowledge; Participatory action research & social learning; Knowledge-sharing & learning platforms.
		Informational options: Hazard & vulnerability mapping; Early warning & response systems; Systematic monitoring & remote sensing; Climate services; Use of indigenous climate observations; Participatory scenario development; Integrated assessments.
		Behavioral options: Household preparation & evacuation planning; Migration; Soil & water conservation; Storm drain clearance; Livelihood diversification; Changed cropping, livestock, & aquaculture practices; Reliance on social networks.
Transformation including incremental & transformational adjustments	Spheres of change	Practical: Social & technical innovations, behavioral shifts, or institutional & managerial changes that produce substantial shifts in outcomes.
		Political: Political, social, cultural, & ecological decisions & actions consistent with reducing vulnerability & risk & supporting adaptation, mitigation, & sustainable development.
		Personal: Individual & collective assumptions, beliefs, values, & worldviews influencing climate-change responses.

SPM 4.3 Response options for mitigation

Mitigation options are available in every major sector. Mitigation can be more cost-effective if using an integrated approach that combines measures to reduce energy use and the GHG intensity of end-use sectors, decarbonize energy supply, reduce net emissions and enhance carbon sinks in land-based sectors. {4.3}

Well-designed systemic and cross-sectoral mitigation strategies are more cost-effective in cutting emissions than a focus on individual technologies and sectors, with efforts in one sector affecting the need for mitigation in others (*medium confidence*). Mitigation measures intersect with other societal goals creating the possibility of co-benefits or adverse side effects. These intersections, if well-managed, can strengthen the basis for undertaking climate action. {4.3}

Emissions ranges for baseline scenarios and mitigation scenarios that limit greenhouse gas concentrations to low levels (about 450 ppm CO₂-eq, *likely* to limit warming to 2°C above pre-industrial levels) are shown for different sectors and gases in Figure SPM.14. Key measures to achieve such mitigation goals include decarbonizing (i.e., reducing the carbon intensity of) electricity generation (*medium evidence, high agreement*) as well as efficiency enhancements and behavioural changes, in order to reduce energy demand compared to baseline scenarios without compromising development (*robust evidence, high agreement*). In scenarios reaching 450 ppm CO₂-eq concentrations by 2100, global CO₂ emissions from the energy supply sector are projected to decline over the next decade and are characterized by reductions of 90% or more below 2010 levels between 2040 and 2070. In the majority of low-concentration stabilization scenarios (about 450 to about 500 ppm CO₂-eq, at least *as likely as not* to limit warming to 2°C above pre-industrial levels), the share of low-carbon electricity supply (comprising renewable energy (RE), nuclear and CCS, including BECCS) increases from the current share of approximately 30% to more than 80% by 2050, and fossil fuel power generation without CCS is phased out almost entirely by 2100. {4.3}

Near-term reductions in energy demand are an important element of cost-effective mitigation strategies, provide more flexibility for reducing carbon intensity in the energy supply sector, hedge against related supply-side risks, avoid lock-in to carbon-intensive infrastructures, and are associated with important co-benefits. The most cost-effective mitigation options in forestry are afforestation, sustainable forest management and reducing deforestation, with large differences in their relative importance across regions; and in agriculture, cropland management, grazing land management, and restoration of organic soils (*medium evidence, high agreement*). {4.3, Figures 4.1, 4.2, Table 4.3}

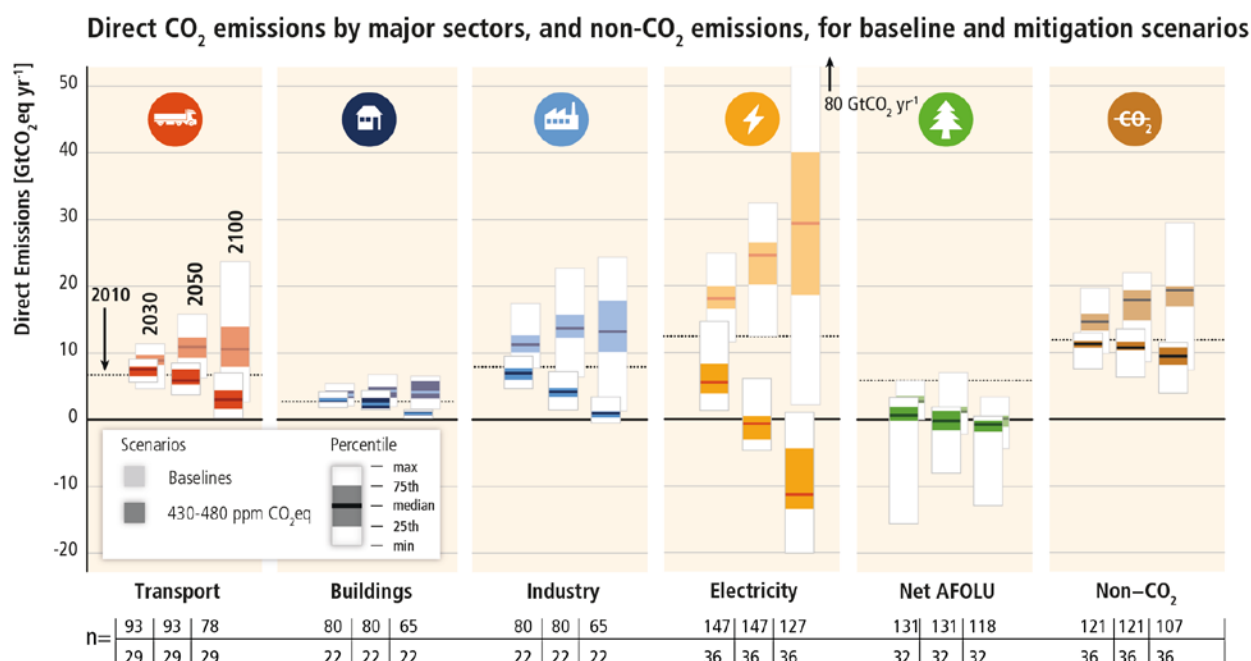


Figure SPM.14: CO₂ emissions by sector and total non-CO₂ GHGs (Kyoto gases) across sectors in baseline (faded bars) and mitigation scenarios (solid colour bars) that reach about 450 (430–480) ppm CO₂-eq concentrations in 2100 (*likely* to limit warming to 2°C above pre-industrial levels). Mitigation in the end-use sectors leads also to indirect emissions reductions in the upstream energy supply sector. Direct emissions of the end-use sectors thus do not include the emission reduction potential at the supply-side due to, e.g., reduced electricity demand. The numbers at the bottom of the graphs refer to the number of scenarios included in the range (upper row: baseline scenarios; lower row: mitigation scenarios), which differs across sectors and time due to different sectoral resolution and time horizon of models. Emissions ranges for mitigation scenarios include the full portfolio of mitigation options; many models cannot reach 450 ppm CO₂-eq concentration by 2100 in the absence of CCS. Negative emissions in the electricity sector are due to the application of BECCS. ‘Net’ AFOLU emissions consider afforestation, reforestation as well as deforestation activities. {4.3, Figure 4.1}

Behaviour, lifestyle and culture have a considerable influence on energy use and associated emissions, with high mitigation potential in some sectors, in particular when complementing technological and structural change (*medium evidence, medium agreement*). Emissions can be substantially lowered through changes in consumption patterns, adoption of energy savings measures, dietary change and reduction in food wastes. {4.1, 4.3}

SPM 4.4 Policy approaches for adaptation and mitigation, technology and finance

Effective adaptation and mitigation responses will depend on policies and measures across multiple scales: international, regional, national and sub-national. Policies across all scales supporting technology development, diffusion and transfer, as well as finance for responses to climate change, can complement and enhance the effectiveness of policies that directly promote adaptation and mitigation. {4.4}

International cooperation is critical for effective mitigation, even though mitigation can also have local co-benefits. Adaptation focuses primarily on local to national scale outcomes, but its effectiveness can be enhanced through coordination across governance scales, including international cooperation. {3.1, 4.4.1}

- The United Nations Framework Convention on Climate Change (UNFCCC) is the main multilateral forum focused on addressing climate change, with nearly universal participation.

Other institutions organized at different levels of governance have resulted in diversifying international climate change cooperation. {4.4.1}

- The Kyoto Protocol offers lessons towards achieving the ultimate objective of the UNFCCC, particularly with respect to participation, implementation, flexibility mechanisms, and environmental effectiveness (*medium evidence, low agreement*). {4.4.1}
- Policy linkages among regional, national, and sub-national climate policies offer potential climate change mitigation benefits (*medium evidence, medium agreement*). Potential advantages include lower mitigation costs, decreased emission leakage, and increased market liquidity. {4.4.1}
- International cooperation for supporting adaptation planning and implementation has received less attention historically than mitigation but is increasing, and has assisted in the creation of adaptation strategies, plans, and actions at the national, sub-national, and local level (*high confidence*). {4.4.1}

There has been a considerable increase in national and sub-national plans and strategies on both adaptation and mitigation since the AR4, with an increased focus on policies designed to integrate multiple objectives, increase co-benefits and reduce adverse side-effects (*high confidence*). {4.4.2.1, 4.4.2.2}

- National governments play key roles in adaptation planning and implementation (*high agreement, robust evidence*) through coordinating actions and providing frameworks and support. While local government and the private sector have different functions, which vary regionally, they are increasingly recognized as critical to progress in adaptation, given their roles in scaling up adaptation of communities, households, and civil society and in managing risk information and financing (*medium evidence, high agreement*). {4.4.2.1}
- Institutional dimensions of adaptation governance, including the integration of adaptation into planning and decision making, play a key role in promoting the transition from planning to implementation of adaptation (*high agreement, robust evidence*). Examples of institutional approaches to adaptation involving multiple actors include economic options (e.g., insurance, public-private partnerships), laws and regulations (e.g., land zoning laws), and national and government policies and programs (e.g., economic diversification). {4.2, 4.4.2.1, Table SPM.3}
- In principle, mechanisms that set a carbon price, including cap and trade systems and carbon taxes, can achieve mitigation in a cost-effective way, but have been implemented with diverse effects due in part to national circumstances as well as policy design. The short-run effects of cap and trade systems have been limited as a result of loose caps or caps that have not proved to be constraining (*limited evidence, medium agreement*). In some countries, tax-based policies specifically aimed at reducing GHG emissions – alongside technology and other policies – have helped to weaken the link between GHG emissions and GDP (*high confidence*). In addition, in a large group of countries, fuel taxes (although not necessarily designed for the purpose of mitigation) have had effects that are akin to sectoral carbon taxes. {4.4.2.2}
- Regulatory approaches and information measures are widely used and are often environmentally effective (*medium evidence, medium agreement*). Examples of regulatory approaches include energy efficiency standards; examples of information programmes include labelling programs that can help consumers make better-informed decisions. {4.4.2.2}
- Sector-specific mitigation policies have been more widely used than economy-wide policies (*medium evidence, high agreement*). Sector-specific policies may be better suited to address sector-specific barriers or market failures and may be bundled in packages of complementary policies. Although theoretically more cost-effective, administrative and political barriers may make economy wide policies harder to implement. Interactions between or among mitigation policies may be synergistic or may have no additive effect on reducing emissions. {4.4.2.2}
- Economic instruments in the form of subsidies may be applied across sectors, and include a variety of policy designs, such as tax rebates or exemptions, grants, loans and credit lines. An

increasing number and variety of renewable energy (RE) policies including subsidies – motivated by many factors – have driven escalated growth of RE technologies in recent years. At the same time, reducing subsidies for GHG-related activities in various sectors can achieve emission reductions, depending on the social and economic context (*high confidence*). {4.4.2.2}

Co-benefits and adverse side-effects of mitigation could affect achievement of other objectives such as those related to human health, food security, biodiversity, local environmental quality, energy access, livelihoods, and equitable sustainable development. The potential for co-benefits for energy end-use measures outweighs the potential for adverse side-effects whereas the evidence suggests this may not be the case for all energy supply and AFOLU measures. Some mitigation policies raise the prices for some energy services and could hamper the ability of societies to expand access to modern energy services to underserved populations (*low confidence*). These potential adverse side-effects on energy access can be avoided with the adoption of complementary policies such as income tax rebates or other benefit transfer mechanisms (*medium confidence*). Whether or not side-effects materialize, and to what extent side-effects materialize, will be case- and site-specific, and depend on local circumstances and the scale, scope, and pace of implementation. Many co-benefits and adverse side-effects have not been well-quantified. {4.3, 4.4.2.2, Box 3.4}

Technology policy (development, diffusion and transfer) complements other mitigation policies across all scales, from international to sub-national; many adaptation efforts also critically rely on diffusion and transfer of technologies and management practices (*high confidence*). Policies exist to address market failures in R&D, but the effective use of technologies can also depend on capacities to adopt technologies appropriate to local circumstances. {4.4.3}

Substantial reductions in emissions would require large changes in investment patterns (*high confidence*). For mitigation scenarios that stabilize concentrations (without overshoot) in the range of 430-530 ppm CO₂-eq by 2100¹⁹, annual investments in low carbon electricity supply and energy efficiency in key sectors (transport, industry and buildings) are projected in the scenarios to rise by several hundred billion dollars per year before 2030. Within appropriate enabling environments, the private sector, along with the public sector, can play important roles in financing mitigation and adaptation (*medium evidence, high agreement*). {4.4.4}

Financial resources for adaptation have become available more slowly than for mitigation in both developed and developing countries. Limited evidence indicates that there is a gap between global adaptation needs and the funds available for adaptation (*medium confidence*). There is a need for better assessment of global adaptation costs, funding and investment. Potential synergies between international finance for disaster risk management and adaptation have not yet been fully realized (*high confidence*). {4.4.4}

SPM 4.5 Trade-offs, synergies and interactions with sustainable development

Climate change is a threat to sustainable development. Nonetheless, there are many opportunities to link mitigation, adaptation and the pursuit of other societal objectives through integrated responses (*high confidence*). Successful implementation relies on relevant tools, suitable governance structures and enhanced capacity to respond (*medium confidence*). {3.5, 4.5}

Climate change exacerbates other threats to social and natural systems, placing additional burdens particularly on the poor (*high confidence*). Aligning climate policy with sustainable development requires attention to both adaptation and mitigation (*high confidence*). Delaying global mitigation

¹⁹ This range comprises scenarios that reach 430-480 ppm CO₂-eq by 2100 (*likely* to limit warming to 2°C above pre-industrial levels) and scenarios that reach 480-530 ppm CO₂-eq by 2100 (without overshoot: *more likely than not* to limit warming to 2°C above pre-industrial levels).

actions may reduce options for climate-resilient pathways and adaptation in the future. Opportunities to take advantage of positive synergies between adaptation and mitigation may decrease with time, particularly if limits to adaptation are exceeded. Increasing efforts to mitigate and adapt to climate change imply an increasing complexity of interactions, encompassing connections among human health, water, energy, land use, and biodiversity (*medium evidence, high agreement*). {3.1, 3.5, 4.5}

Strategies and actions can be pursued now which will move towards climate-resilient pathways for sustainable development, while at the same time helping to improve livelihoods, social and economic well-being, and effective environmental management. In some cases, economic diversification can be an important element of such strategies. The effectiveness of integrated responses can be enhanced by relevant tools, suitable governance structures, and adequate institutional and human capacity (*medium confidence*). Integrated responses are especially relevant to energy planning and implementation; interactions among water, food, energy and biological carbon sequestration; and urban planning, which provides substantial opportunities for enhanced resilience, reduced emissions and more sustainable development (*medium confidence*). {3.5, 4.4, 4.5}

Energie und Klimaschutz: Einige grundsätzliche Betrachtungen

Andreas Veigl

DI Andreas Veigl, Untere Weißgerberstraße 10, 1030 Wien. Tel: +43 650 501 54 65.

E-Mail: info@andreasveigl.at; Web: www.andreasveigl.at

Kurzfassung: In diesem Beitrag werden einige grundsätzliche Überlegungen angestellt, welche Pfade bei Energiewende und Klimaschutz in Österreich eingeschlagen werden können, um einen fairen Beitrag zur Begrenzung der globalen Klimaerwärmung im Sinne des Paris Agreements zu leisten. Die Analyse zeigt, dass historisch das Wirtschaftswachstum den deutlichste Treiber der steigenden Energieverbräuche und CO₂-Emissionen darstellt, die durch Verbesserungen der Energie- und Kohlenstoffintensitäten bei weitem nicht kompensiert werden können. Legte man die höchsten in einem Fünfjahreszeitraum seit 1970 erzielten Verbesserungsraten an, blieben notwendige Emissionsziele bis 2050 selbst bei mäßigem BIP-Wachstum unerreichbar. Das liefert Argumente dafür, die Konzentration auf Wachstum zu hinterfragen und Energiewende sowie Klimaschutz nicht ausschließlich als technische Aufgabe zu begreifen.

Keywords: Klimaschutz; Kaya-Dekomposition; Energieintensität; Kohlenstoffintensität

1 Einleitung

Zur Begrenzung der negativen Folgen des globalen Klimawandels müssen die Emissionen von Treibhausgasen (THG) dramatisch gesenkt werden. Laut Empfehlung des IPCC müssen Industriestaaten ihre Emissionen von Treibhausgasen (THG) bis 2050 gegenüber 1990 um 80 bis 95 Prozent senken. Das ist in etwa gleichbedeutend mit der im *Paris Agreement* formulierten Übereinkunft zur Dekarbonisierung bis Mitte des 21. Jahrhunderts.

In diesem Beitrag werden einige grundsätzliche Überlegungen angestellt, welche Pfade bei Energiewende und Klimaschutz in Österreich eingeschlagen werden können, um das Energiesystem bis 2050 zu dekarbonisieren und damit einen fairen Beitrag zur Begrenzung des Klimawandels zu leisten und nicht zuletzt die international eingegangene Verpflichtung des *Paris Agreements* zu erfüllen.

Den mit Abstand größten Anteil an den THG-Emissionen Österreichs machen energiebezogene CO₂-Emissionen aus, 2013 beträgt ihr Anteil 85 % (Umweltbundesamt 2015). Damit entspricht die Reduktion dieser Emissionen auf null eine Reduktion der gesamten THG-Emissionen auf rund 15 % des Niveaus von 1990.

Im Folgenden werden historische Trends seit 1970 bzw. 1990 bis 2013 analysiert, um Hinweise für mögliche Entwicklungen bis 2050 abzuleiten.

2 Analyse historischer Trends

Im ersten Schritt werden, einer Analyse von Handrich et al. (2015) folgend, die Trajektorien dieser CO₂-Emissionen, des Bruttoinlandsverbrauchs von Primärenergie (BIV) und des fossilen Primärenergieverbrauchs in Bezug auf die Wirtschaftsentwicklung der letzten 25 Jahre aufgezeichnet, siehe Abbildung 1.

Wie in allen folgenden Betrachtungen werden die Energieverbrauchswerte der Energiebilanz 2015 entnommen (Statistik Austria 2015a), die Emissionen aus Umweltbundesamt (2015) und die Wirtschaftsentwicklung aus Zeitreihen der Statistik Austria und des WIFO (zitiert nach WKO 2015). Als Bevölkerungsstatistik wird Statistik Austria (2015c) herangezogen.

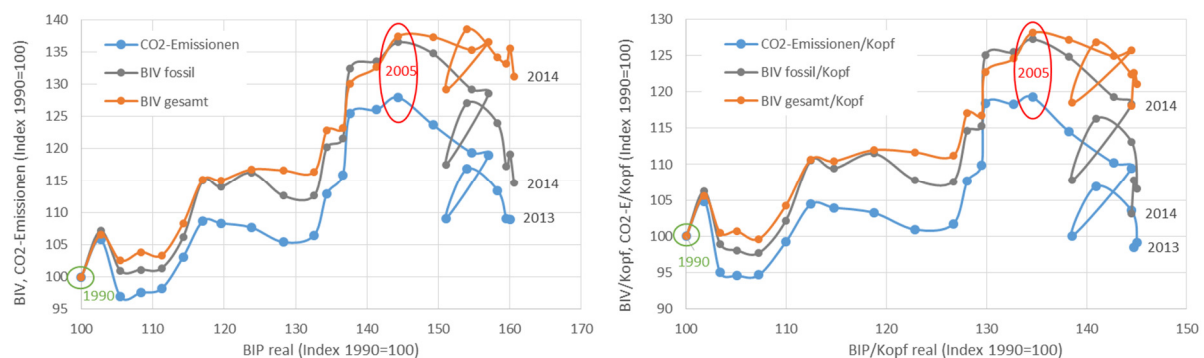


Abbildung 1: Trajektorien des Bruttoinlandsverbrauchs (BIV gesamt), des Bruttoinlandsverbrauchs an fossiler Energie (BIV fossil) und der CO₂-Emissionen in Österreich gegenüber dem realen BIP, 1990-2014. Links: Entwicklung der absoluten Werte. Rechts: Entwicklung der Pro-Kopf-Werte. Quelle: Eigene Darstellung

Es ist offensichtlich, dass der Primärenergieverbrauch und die CO₂-Emissionen bis 2005 stark ansteigen. Erst ab dann findet eine gewisse Entkopplung statt, die im Wesentlichen auf den verstärkten Einsatz erneuerbarer Energien zurückgeht, der gesamte Primärenergiebedarf sinkt nur leicht, während sein fossiler Anteil deutlich abnimmt.

2.1 Dekomposition der energiebedingten CO₂-Emissionen

Die Dekomposition der energiebedingten CO₂-Emissionen gemäß der Kaya-Dekomposition ist eine in der Literatur häufige angewendete Methode (vgl. Raupach et al. 2007, Blanco et al. 2014 oder Sussams et al. 2015). Dabei werden die Veränderungen der Emissionen in die Effekte der Entwicklungen von Bevölkerungszahl, Pro-Kopf-BIP, Energieintensität des BIP und die CO₂-Intensität des Energieverbrauchs zerlegt. Die Kaya-Identität ist eine spezielle Formulierung der allgemeinen IPAT-Identität (Ehrlich & Holdren 1971), die beschrieben wird als

$$I = P \times A \times T$$

Sie drückt aus, dass sich die Auswirkungen anthropogenen Handelns auf die natürliche Umwelt (*Impact*, I) aus einer Multiplikation der Größe der Bevölkerung (*Population*, P), ihres Wohlstands (*Affluence*, A) und der eingesetzten Technologien (*Technology*, T) errechnet. Das bedeutet, dass etwa ein Sinken eines der drei Terme P, A oder T, ceteris paribus, ein proportionales Sinken des Impacts I zur Folge hat.

- I steht dabei für eine Umweltauswirkung. Inhaltlich ist I nicht festgelegt, beliebige „Pressures“ können damit ausgedrückt werden, seien es Entnahmen von Rohstoffen oder Emissionen in die natürliche Umwelt.

- P steht in der Regel für die Größe der Bevölkerung.
- A kann je nach Anwendungsfall sehr unterschiedlich repräsentiert sein, meist wird er als BIP/Kopf ausgedrückt.
- Der Term T kann eine Vielfalt von von Triebkräften ausdrücken. Generell beschreibt er, wie stark der Einfluss menschlichen Handelns auf die natürliche Umwelt pro Kopf und Geldeinheit ist, beschreibt also die Art und Weise, wie die Gesellschaft konsumiert bzw. produziert.

In der Ausformulierung von IPAT als Kaya- Identität werden als Impact I die energiebezogenen CO₂-Emissionen modelliert in Abhängigkeit der Bevölkerungszahl P und des Pro-Kopf-BIP als Affluence A. Der Technologie-Term T wird in eine Komponente der Energieintensität des BIP und eine CO₂-Intensität des Energieverbrauchs aufgespalten:

$$CO_2Emissionen = Bevölkerungszahl \times \frac{BIP}{Bevölkerungszahl} \times \frac{BIV}{BIP} \times \frac{CO_2Emissionen}{BIV}$$

Bzw., abgekürzt:

$$CE = P \times A \times EI \times CI$$

Darin ist

CE	Energiebezogene CO ₂ -Emissionen in t pro Jahr
P	Bevölkerungszahl in Mio.
A	Pro-Kopf-BIP in EUR/Kopf
EI	Primärenergieintensität des BIP in MJ/EUR
CI	Kohlenstoffintensität des Primärenergieverbrauchs in t CO ₂ / TJ

Die Dekomposition wird nach der Logarithmic Mean Divisia Index Methode (LMDI) durchgeführt. Sie hat den Vorteil, dass kein unerklärter Residualterm verbleibt (vgl. Ang & Liu 2001 bzw. Ang 2005). Die Differenz zwischen den CO₂-Emissionen zum Zeitpunkt T und dem Startpunkt 0 kann in der additiven LMDI-Dekomposition angesetzt werden als Summe von

$$\Delta CE_{gesamt} = CE_T - CE_0 = \Delta CE_P + \Delta CE_A + \Delta CE_{EI} + \Delta CE_{CI}$$

mit den Summanden

$\Delta CE_P = \frac{CE_T - CE_0}{\ln CE_T - \ln CE_0} \times \ln \left(\frac{P_T}{P_0} \right)$	Effekt der Befölkerungsänderung
$\Delta CE_A = \frac{CE_T - CE_0}{\ln CE_T - \ln CE_0} \times \ln \left(\frac{A_T}{A_0} \right)$	Effekt der Veränderung des Pro-Kopf-BIP
$\Delta CE_{EI} = \frac{CE_T - CE_0}{\ln CE_T - \ln CE_0} \times \ln \left(\frac{EI_T}{EI_0} \right)$	Effekt der Veränderung der Energieintensität
$\Delta CE_{CI} = \frac{CE_T - CE_0}{\ln CE_T - \ln CE_0} \times \ln \left(\frac{CI_T}{CI_0} \right)$	Effekt der Veränderung der CO ₂ -Intensität

Die Dekomposition erfolgt dabei jeweils für die Phasen 1990-2005 und 2005-2013, da sich diese Phasen wie beschrieben deutlich voneinander unterscheiden.

Das Ergebnis in Abbildung 2 zeigt, dass das Pro-Kopf-BIP mit einem Anstieg von 42 % im Zeitraum 1990-2013 den höchsten Beitrag zum Anstieg der CO₂-Emissionen liefert, die Bevölkerungszunahme weitere 12 %; diese Effekte können durch die Verbesserung der

gesamtwirtschaftlichen Energieintensität und der Reduktion der CO₂-Emissionen des Primärenergiebedarfs nicht kompensiert werden. Dabei unterscheiden sich die beiden Phasen deutlich:

- 1990-2005 steigen die Emissionen aufgrund des BIP-Wachstums um fast 34 %, durch die wachsende Bevölkerung um weitere 8 %, jeweils bezogen auf 1990. Diese Effekte können durch die Verbesserung der Primärenergieintensität des BIP und die Kohlenstoffintensität des Primärenergieverbrauchs bei weitem nicht kompensiert werden, die Emissionen steigen um 28 %.
- 2005-2013 erfolgt eine gewisse Trendwende: Die Emissionen sinken, erreichen jedoch 2013 ein Niveau das 9 % über jenem von 1990 liegt. Die beschleunigte Substitution fossiler mit erneuerbaren Energieträgern führt zu einer Senkung der CO₂-Emissionen um 17 % relativ zu 2005, während die Energieintensität des BIP eine Reduktion um knapp 14 % bewirkt. Die Effekte der deutlich niedrigeren BIP-Wachstumsraten in diesem Zeitraum und der wachsenden Bevölkerung können damit deutlich überkompensiert werden.
- Während seit dem Jahr 2005, dem „all-time-high“ der CO₂-Emissionen eine absolute Entkopplung vom BIP nachgewiesen werden kann, ist die für den längere Zeitraum seit 1970 nicht möglich.

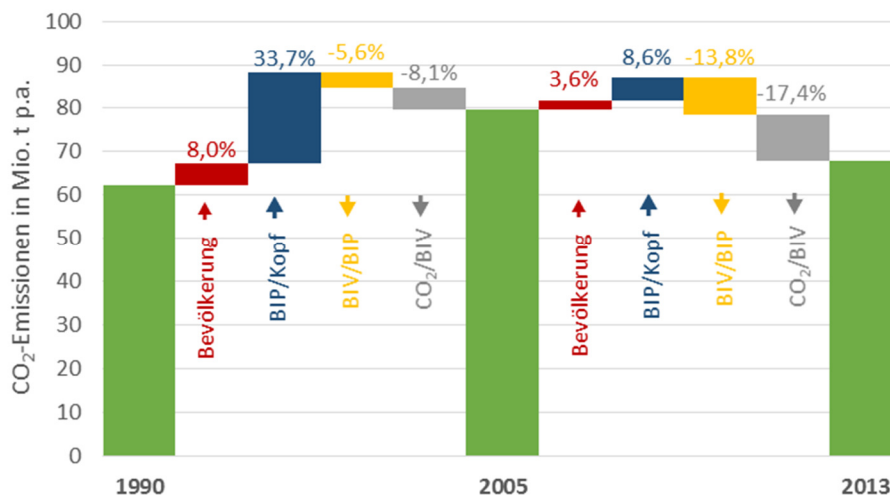


Abbildung 2: Kaya-Dekomposition der CO₂-Emissionen 1990-2005 und 2005-2013 in Effekte der Faktoren Bevölkerung, reales Pro-Kopf-BIP (BIP/Kopf), Primärenergieintensität des BIP (BIV/BIP) und CO₂-Intensität des Primärenergieverbrauchs (CO₂/BIV). Prozentsätze bezogen auf 1990. Quelle: Eigene Darstellung.

2.2 Historisch beobachtete Veränderungsraten

Im nächsten Schritt werden die historischen Veränderungsraten der einzelnen Komponenten der Kaya-Identität analysiert. Besonderes Augenmerk wird dabei auf die Veränderung des Pro-Kopf-BIP und die technischen Faktoren der Primärenergieintensität des BIP und die CO₂-

Intensität des Primärenergieverbrauchs gelegt. Außerdem wird der Beobachtungszeitraum auf 1970 bis 2013 ausgeweitet¹. Abbildung 3 zeigt die Entwicklungen.

Für die einzelnen Komponenten werden jeweils die Maxima und Minima, die Mittelwerte und die maximalen und minimalen 5-Jahres-Mittelwerte gebildet. Letztere deswegen, da für längerfristige Trends in der folgenden Szenariobildung weniger die maximal beobachtete Veränderungen einer Komponente in einem einzelnen Jahr aussagekräftig ist, sondern Veränderungsraten, die für einen etwas längeren Zeitraum aufrechterhalten werden können.

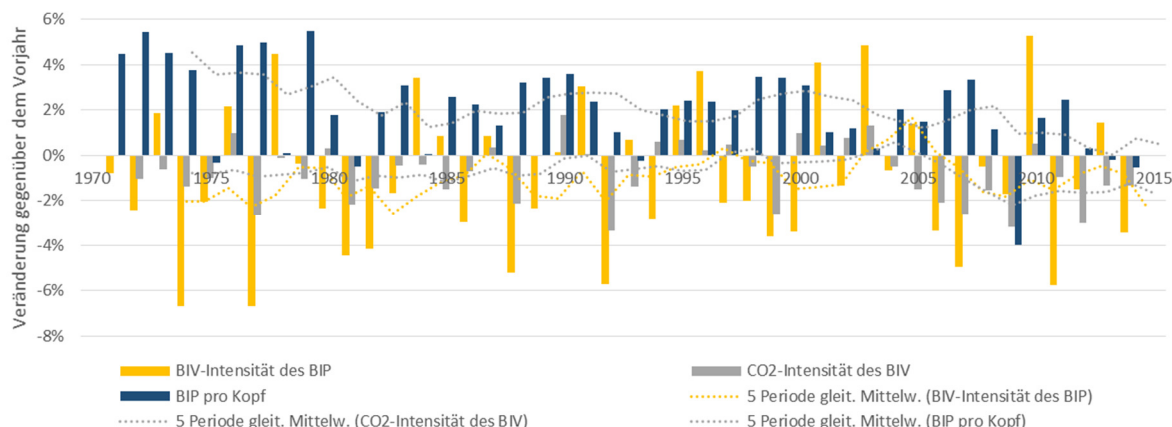


Abbildung 3: Jährliche Veränderungen der Primärenergieintensität des BIP, der CO₂-Intensität des Primärenergieverbrauchs und des Pro-Kopf-BIP, 1970-2013. Quelle: Eigene Darstellung

Die Ergebnisse sind in Tabelle 1 dargestellt: Es zeigt sich, dass im langjährigen Schnitt Verbesserungen der Energieintensität (PEV/BIP) von nur -1,0 % p.a. erreicht wurden – die beste in einem Fünfjahreszeitraum erreichte Intensitätsreduktion liegt bei -2,2 % p.a. Ähnlich das Bild für die CO₂-Emissionsintensität des Primärenergieverbrauchs (CO₂/PEV): im Mittel sinkt sie um -0,8 % p.a. mit dem besten 5-Jahres-Mittel bei -2,6 % p.a.

Tabelle 1: Veränderungsraten in % pro Jahr der einzelnen Parameter im Zeitraum 1970-2013. Quelle: Eigene Berechnungen

	BIP/Kopf	PEV/BIP	CO ₂ /PEV	CO ₂
Max	5,5%	5,3%	1,8%	7,9%
Min	-4,0%	-6,7%	-3,4%	-8,5%
Mittelwert	2,1%	-1,0%	-0,8%	0,6%
Max. 5-Jahres-Mittel	3,6%	1,7%	0,6%	3,5%
Min. 5-Jahres-Mittel	0,0%	-2,6%	-2,2%	-2,6%

¹ Die CO₂-Emissionen für die Jahre vor 1990 werden abgeschätzt anhand der Primärenergieverbräuche (Statistik Austria 2015a) und mittleren Emissionsfaktoren, abgeleitet aus Umweltbundesamt (2014).

3 Szenarien für die Zukunft

Im letzten Schritt werden einige Szenarien für die Entwicklung der energiebedingten CO₂-Emissionen bis 2050 betrachtet. Dazu werden Annahmen zu unterschiedlichen Entwicklungen für die Komponenten der Kaya-Identität angenommen bzw. kalkuliert, die einen Fächer möglicher Entwicklungen aufspannen.

Auf Basis aktueller Zahlen würde die Erreichung des Ziels einer Senkung der THG-Emissionen um 80 bis 95 % bis 2050 bedeuten, dass die CO₂-Emissionen auf Null reduziert und das Energiesystem damit de facto vollständig dekarbonisiert werden müsste, da 2013 die Emissionen von CH₄ und N₂O in der Landwirtschaft² und die Emissionen von F-Gasen über 10 Mio. t_{CO₂-eq} und damit über 13 % der THG-Emissionen bezogen auf 1990 ausmachen. Nur in dem Ausmaß, in dem auch Emissionen anderer THG als CO₂ reduziert werden, könnten daher 2050 energiebezogene CO₂-Emissionen im System verbleiben.

3.1 Annahmen

Die Annahmen für die Szenarien sind in Tabelle 2 dargestellt und setzen sich wie folgt zusammen:

- Die Szenarien 1 bis 4 sind explorative Szenarien: Unter der Annahme, wie sich einzelne Komponenten bzw. Treiber entwickeln, werden Pfade der CO₂-Emissionen bis 2050 abgeschätzt.
- Szenario 5 und 6 sind Zielszenarien: Hier werden die Intensitätsentwicklungen³ so weit verändert, dass sich die energiebedingten CO₂-Emissionen auf ein Minimum reduzieren. Dabei wird angenommen, dass 2050 die energiebedingten Emissionen bis auf einen Rest von 2 Mio. t CO₂ abnehmen, der auf die energetische Nutzung nicht-erneuerbarer Abfälle zurückgeht (vgl. Veigl 2015).
- Allen Szenarien gemeinsam ist die angenommene Bevölkerungsentwicklung. Gemäß der Hauptvariante der Bevölkerungsprognose 2015 der Statistik Austria wird davon ausgegangen, dass die österreichische Wohnbevölkerung von 8,45 Mio. im Jahr 2013 auf 9,63 Mio. im Jahr 2050 steigt (Statistik Austria 2015b); das entspricht einer durchschnittlichen jährlichen Wachstumsrate von 0,35 % p.a.
- Für das Bruttoinlandsprodukt wird einerseits in Szenario 1 und 2 ein Wachstum des pro-Kopf-BIP in der Höhe des Durchschnitts der Jahre 1970-2013 angenommen, das sind 1,62 % pro Jahr; das entspricht einer durchschnittlichen BIP-Wachstumsrate von knapp 2 % pro Jahr; andererseits wird das Pro-Kopf-BIP in Szenario 3 und 4 bis 2050 konstant gehalten, das BIP steigt also im Ausmaß der Bevölkerungszuwachses.
- Für die Primärenergieintensität werden ebenfalls zwei Varianten betrachtet: In Szenario 1 und 2 wird von einer Veränderung von -0,72 % p.a. ausgegangen, das entspricht dem Mittelwert der Verbesserung im Zeitraum 1990-2013. Szenario 3 und 4

² Zuzüglich „Sonstige“, siehe Statistik Austria (2015)

³ In den Szenarien 5 und 6 werden Energie- und CO₂-Intensität zusammengefasst, d.h. nicht zwischen den Möglichkeiten Energieeffizienz und CO₂-ärmeren Energieträgern differenziert, weil die Verfügbarkeit erneuerbarer Energiepotenziale nicht berücksichtigt wird. Dies erfolgt erst im nächsten Schritt.

bilden eine Intensitätsverbesserung von -2,2 % p.a. ab, das ist die günstigste 1970-2013 beobachtete Rate über einen Fünfjahreszeitraum.

- Die Reduktion der Kohlenstoff-Intensität des Primärenergieverbrauchs orientiert sich ebenfalls an den historischen Werten: Szenario 1 und 2 enthalten wieder den historischen Durchschnitt 1990-2013 von -0,95 % p.a., die Szenarien 3 und 4 die maximalen in einem Fünfjahreszeitraum von 1970-2013 erreichten Reduktionsraten von 2,6 % p.a.

Tabelle 2: Veränderungsraten der Komponenten der Kaya-Identität in den Szenarien bis 2050 in Prozenten pro Jahr. Quelle: Eigene Berechnungen

Szenario	Bev. % p.a.	BIP/Kopf % p.a.	BIV/BIP % p.a.	CO ₂ /BIV % p.a.	CO ₂ % p.a.	CO ₂
1	0,35%	1,62%	-0,72%	-0,95%	0,29%	
2	0,35%	0,00%	-0,72%	-0,95%	-1,31%	
3	0,35%	1,62%	-2,20%	-2,60%	-2,86%	
4	0,35%	0,00%	-2,20%	-2,60%	-4,41%	
5	0,35%	1,62%	-10,85%		-9,08%	
6	0,35%	0,00%	-9,40%		-9,08%	
	Mio.	EUR/Kopf	MJ/EUR	t/TJ	Mio. t	gg. 1990
1	9,63	65.661	3,57	33,42	75,42	+21%
2	9,63	36.226	3,57	33,42	41,61	-33%
3	9,63	65.661	2,05	17,93	23,20	-63%
4	9,63	36.226	2,05	17,93	12,80	-79%
5	9,63	65.661	-10,85%		2,00	-97%
6	9,63	36.226	-9,40%		2,00	-97%

3.2 Ergebnisse

Mit den beschriebenen Annahmen ergeben sich in den Szenarien folgende Entwicklungen, die in Tabelle 2 und Abbildung 4 dargestellt sind:

- In Szenario 1, in dem sämtliche Trends des Zeitraums 1990-2013 bis 2050 fortgeschrieben werden, ergeben sich steigende CO₂-Emissionen um +21 % gegenüber 1990.
- Szenario 2 unterscheidet sich von Szenario 1 durch das verringerte Wirtschaftswachstum. Das Ergebnis zeigt zwar sinkende CO₂-Emissionen, jedoch nehmen sie bis 2050 nur um 33 % gegenüber 1990 ab.
- Mit der historischen BIP-Wachstumsrate aber deutlich höheren Verbesserungsraten der Intensitäten ergeben sich in Szenario 3 deutlich sinkende Emissionen; insgesamt nehmen sie um 63 % gegenüber 1990 ab.
- Demgegenüber sinken die Emissionen in Szenario 4 mit niedriger BIP-Wachstumsrate um 79 % gegenüber 1990, das Ziel wird dennoch deutlich nicht erreicht.
- In den Zielszenarien 5 und 6, in denen die Emissionen annahmegemäß bis 2050 auf 2 Mio. t CO₂ sinken, müsste diese 2013 bis 2050 im Jahresschnitt um über 9 % sinken. Die Verbesserungsraten der Intensitäten müssten – zusammengekommen – jährlich durchschnittlich -10,85 % bzw. -9,40 % betragen, je nach angenommener

Wirtschaftsentwicklung. Beides sind Werte, die im Zeitraum 1970 bis 2013 in keinem einzigen Jahr – geschweige denn über einen längeren Zeitraum – erreicht wurden.

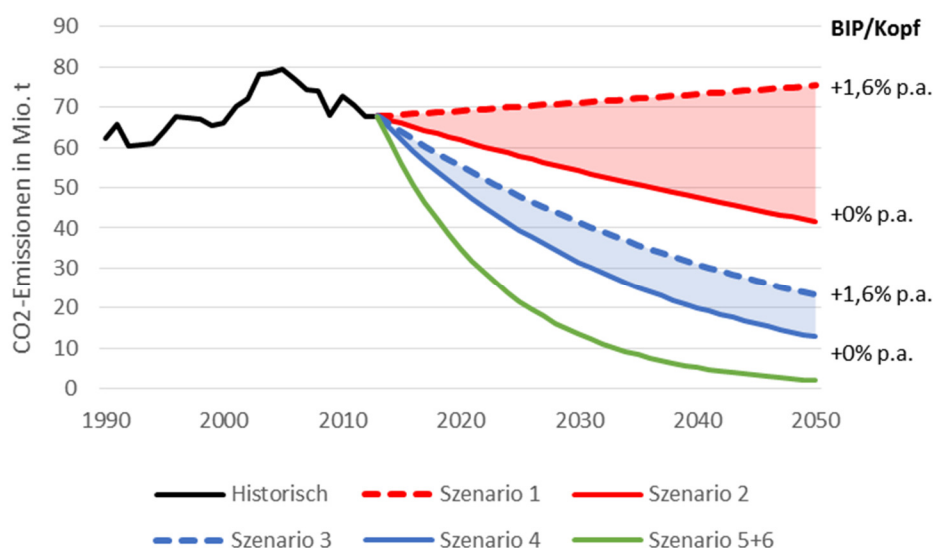


Abbildung 4: Szenarien für die Entwicklung der energiebedingten CO₂-Emissionen. Rot: dargestellt mit historischen Mittelwerten der Intensitätsverbesserungsraten, blau mit den maximal beobachteten 5-Jahres-Durchschnitten. Grün: Entwicklung in den Zielszenarien. Farbig unterlegt ist der Bereich eines Wachstums des Pro-Kopf-BIP zwischen 0 % p.a. und dem historischen Durchschnitt von 1,62 % p.a. Quelle: Eigene Darstellung.

Anhand der Szenarienergebnisse ist bereits ersichtlich, dass in den nächsten 35 Jahren jedenfalls deutlich höhere Raten für die Senkung der Energieintensität des BIP (= Entkopplung) und der Umstellung der Energieversorgung von fossilen auf erneuerbare Energieträger (= Substitution) erzielt werden müssen, als über längere Zeiträume in der Vergangenheit seit 1970.

3.3 Entkopplung und Substitution

Versucht man diese beiden Effekte zu separieren, so muss eine Annahme über die verfügbare erneuerbare Primärenergie in Österreich im Jahr 2050 getroffen werden. Zur Abschätzung dieser Größe werden Szenariostudien von Bliem et al. (2011), Christian et al. (2011) und Streicher et al. (2010) herangezogen, die auch im Österreichischen Sachstandsbericht Klimawandel (vgl. Stagl et al. 2014) analysiert wurden. Zusätzlich wird auf Veigl (2015) zurückgegriffen, wo auf Basis eben dieser Studien Abschätzungen für die ökologisch nachhaltigen Primärenergiepotenziale getroffen werden. Alle diese Studien gehen davon aus, dass der Energiebedarf Österreichs 2050 de facto vollständig auf Basis erneuerbarer Energieträger gedeckt werden und dieser Jahresbedarf an erneuerbarer Primärenergie bilanziell in Österreich aufgebracht werden kann. Dabei stellen die Studien im Wesentlichen energetische Mengen-, jedoch keine Leistungsbilanzen auf.

Der Quervergleich zwischen diesen Arbeiten zeigt, dass technische Potenziale für erneuerbare Primärenergie von bis zu 1.300 PJ gesehen werden, 2050 als nutzbar werden erneuerbare Primärenergieträger in der Größenordnung von max. 700 bis 950 PJ gehalten. Die verglichenen Szenarienergebnisse weisen dabei eine Häufung der Obergrenze zwischen

700 und 800 PJ auf und ergeben sich nicht zuletzt auch aufgrund verschiedener technologischer Pfade in der Energieaufbringung⁴.

Um 2050 das Ziel von nur mehr 2 Mio. t energiebedingter CO₂-Emissionen zu erreichen, muss nun der Primärnergieverbrauch so weit gesenkt werden, dass er mit den verfügbaren erneuerbaren Primärenergien und den restlichen im System verbleibenden nicht-erneuerbaren Abfällen, gedeckt werden kann. Tabelle 3 zeigt die Mengenverhältnisse, die Zeile „BIV gesamt“ enthält dabei die maximal verfügbare Primärenergie 2050 und damit auch den Zielwert des Bruttoinlandsverbrauchs.

Tabelle 3: Varianten von Primärenergieaufbringung und -verbrauch 2050 und der daraus resultierenden durchschnittlichen Veränderungsraten. Quelle: Eigene Berechnungen

		2013	2050	2050	2050	2050
BIV erneuerbar	PJ	417	700	800	900	1.000
BIV fossil	PJ	964	30	30	30	30
BIV gesamt	PJ	1381	730	830	930	1030
Veränderung 2013-2050 erneuerbar	% p.a.		1,4%	1,8%	2,1%	2,4%
Veränderung 2013-2050 fossil	% p.a.		-9,0%	-9,0%	-9,0%	-9,0%
Veränderung 2013-2050 gesamt	% p.a.		-1,7%	-1,4%	-1,1%	-0,8%

Damit ergeben sich in Abhängigkeit der BIP-Entwicklung und des 2050 abdeckbaren Bruttoinlandsverbrauch die in Tabelle 4 dargestellten notwendigen Reduktionsraten der Primärenergieintensität und der Kohlenstoffintensität:

- Bei einer Wachstumsrate des Pro-Kopf-BIP von 1,62 % p.a. (Szenario 5) müsste die CO₂-Intensität des BIP jährlich um knapp 11 % gesenkt werden.
 - Je nach verfügbarer erneuerbarer Primärenergiemenge – und damit maximal möglichem Bruttoinlandsverbrauch – liegt die notwendige Reduktion der Primärenergieintensität zwischen 2,8 und 3,7 % pro Jahr. Zum Vergleich: Die 1970-2013 in einem 5-Jahres-Zeitraum maximal beobachtete Rate beträgt 2,6 % p.a. Es müsste also in den nächsten 35 Jahren eine durchschnittliche Effizienzsteigerung erreicht werden, wie sie in den vergangenen 45 Jahren durch keinen 5-Jahreszeitraum hindurch beobachtet werden kann.
 - Selbiges zeigt sich punkto Senkung der Kohlenstoffintensität der Primärenergie: Die notwendigen jährlichen Raten zwischen 7,4 und 8,3 % p.a. liegen sogar mehr als doppelt so hoch wie die im besten Einzeljahr zwischen 1970 und 2013 erreichte.
- Unter der Annahme, dass das Pro-Kopf-BIP im Zeitraum 2013 bis 2050 konstant bleibt (Szenario 6) wäre eine Reduktion der CO₂-Intensität des BIP um 9,4 % p.a. erforderlich.
 - Die Primärenergieintensität des BIP müsste zwischen 1,2 und 2,1 % jährlich abnehmen. Diese Werte liegen innerhalb der Bandbreite zwischen dem

⁴ Die Werte stimmen in ihrer Höhe auch gut mit den Ergebnissen aus Haas et al. (2008) überein, wo ökonomische Analysen und Szenarien zur künftigen Bedeutung verschiedener nachhaltiger Energietechnologielinien entwickelt werden, die Technologie-Interaktionen, Lerneffekte und exogene Einflussgrößen mit berücksichtigen.

beobachteten Mittelwert 1970-2013 und dem besten Wert in einem 5-Jahres-Zeitraum innerhalb dieses Intervalls. Damit scheint dieses Erfordernis wesentlich einfacher realisierbar.

- Die Dekarbonisierung des Primärenergieverbrauchs müsste jedoch mit den gleich hohen Raten erfolgen wie in der oberen Variante.

Tabelle 4: Notwendige Verbesserungsraten der Energie- und CO₂-Intensität zur Reduktion der energiebedingten CO₂-Emissionen auf 2 Mio. t im Jahr 2050. Variiert wird dabei die Wachstumsrate des Pro-Kopf-BIP und die 2050 nutzbare erneuerbare Primärenergie.

Szenario	BIP/Kopf	BIV erneuerb.	BIV/BIP	CO ₂ /BIV	CO ₂ /BIP
	% p.a.	PJ	% p.a.	% p.a.	% p.a.
5	1,62%	700	-3,70%	-7,42%	-10,85%
		800	-3,37%	-7,74%	
		900	-3,07%	-8,03%	
		1000	-2,80%	-8,28%	
6	0,00%	700	-2,14%	-7,42%	-9,40%
		800	-1,80%	-7,74%	
		900	-1,50%	-8,03%	
		1000	-1,23%	-8,28%	

4 Schlussfolgerungen

In diesem Beitrag wird versucht, anhand der Analyse historischer Daten prinzipiell mögliche Pfade für die Dekarbonisierung des österreichischen Energiesystems bis 2050 auszuloten.

Es kann gezeigt werden, dass der Zeitraum 1990 bis 2013 in zwei Phasen zerfällt: 1990 bis 2005 ist durch ein Ansteigen sowohl des Bruttoinlandsverbrauchs von Primärenergie als auch der energiebedingten CO₂-Emissionen gekennzeichnet. Die Kaya-Dekomposition zeigt dass die in diesem Zeitraum gewachsene Bevölkerung mit einem Anstieg von 8 %, das gewachsene BIP mit fast 34 % zum Anstieg der Emissionen beitragen, jeweils bezogen auf 1990. Diese Effekte können durch die Verbesserung der Primärenergieintensität des BIP und die Kohlenstoffintensität des Primärenergieverbrauchs bei weitem nicht kompensiert werden, die Emissionen steigen um 28 %. In der Phase ab 2005 erfolgt eine gewisse Trendwende: Die Emissionen sinken, erreichen jedoch 2013 ein Niveau das 9 % über jenem von 1990 liegt. Die beschleunigte Substitution fossiler mit erneuerbaren Energieträgern führt zu einer Senkung der CO₂-Emissionen um 17 % relativ zu 1990, während die die Energieintensität des BIP eine Reduktion um knapp 14 % bewirkt. Die Effekte der deutlich niedrigeren BIP-Wachstumsraten in diesem Zeitraum und der wachsenden Bevölkerung können damit deutlich überkompensiert werden. Während also seit dem Jahr 2005, dem „all-time-high“ der CO₂-Emissionen eine absolute Entkopplung vom BIP nachgewiesen werden kann, ist dies für den längere Zeitraum seit 1970 nicht möglich.

Werden anhand historisch beobachteter Veränderungsdaten von Pro-Kopf-BIP, Primärenergieintensität (BIV/BIP) und Kohlenstoffintensität (CO₂/BIV) zusammen mit dem prognostizierten Bevölkerungszuwachs Szenarien für die Entwicklung der CO₂-Emissionen bis 2050 gebildet, so können folgende Schlüsse gezogen werden:

- Selbst in Szenarien mit konstantem Pro-Kopf-BIP ist eine de-facto-Dekarbonisierung des BIV nur dann erreichbar, wenn die technischen Faktoren – also die Energie- und Kohlenstoffintensität – ceteris paribus kontinuierlich und deutlich über das historisch erzielte Maß hinaus verbessert werden können.
- Wird der Bruttoinlandsverbrauch 2050 mit dem nachhaltig verfügbaren Angebot an erneuerbarer Primärenergie (zuzüglich einer kleinen Menge verbleibender fossiler Abfälle) begrenzt, können diese Effekte in einen Effekt der Entkopplung und einen der Substitution dekomponiert werden.
- Es zeigt sich – neben dem Erfordernis hoher Ausbauraten für erneuerbare Energien und hohen Substitutionsraten fossiler Energien – das Erfordernis der massiven Senkung der Energieintensität des BIP, das umso höher ausfällt, je höher die angenommenen BIP-Wachstumsraten liegen.
- Damit erschwert ein weiteres Wachstum des Pro-Kopf-BIP die notwendige Dekarbonisierung des Energiesystems, da es Intensitätsverbesserungsraten erforderlich macht, die teilweise deutlich über die seit 1970 erreichten Werte hinausgehen müssen. Damit müssen sie auch über die während der beiden Ölkrisen der 1970 Jahre und die Hochpreisphase ab 2004 bzw. ab 2011 hinausgehen.

Daraus kann gefolgert werden, dass Energiewende und Klimaschutz nicht lediglich als technisch bzw. techno-ökonomisch zu lösendes Problem gesehen werden sollte. Selbst wenn die Energieeffizienz deutlich angehoben werden kann verbleibt die Gefahr von Reboundeffekten, die erreichte Effizienzsteigerungen durch höheres Wirtschaftswachstum und Energiemehrverbrauch wieder zunichtemachen. Das Paradigma notwendigen BIP-Wachstums stellt damit die notwendige Dekarbonisierung infrage.

Literatur und Datenquellen

Ang BM (2005). *The LMDI approach to decomposition analysis: a practical guide*. Energy Policy 33 (2005) 867–871

Ang BW, Liu FL (2001). *A new energy decomposition method: perfect in decomposition and consistent in aggregation*. Energy 26 (2001) 537–548

Blanco G, Gerlagh R, Suh S, Barrett J, de Coninck HC, Diaz Morejon CF, Mathur R, Nakicenovic N, Ofosu Ahenkora A, Pan J, Pathak H, Rice J, Richels R, Smith SJ, Stern DI, Toth FL, Zhou P (2014). *Drivers, Trends and Mitigation*. In: *Climate Change 2014: Mitigation of Climate Change. Contribution of Working Group III to the Fifth Assessment Report of the Intergovernmental Panel on Climate Change* [Edenhofer O et al. (eds.)]. Cambridge University Press, Cambridge, United Kingdom and New York, NY, USA.

Bliem M, Friedl B, Balabanov T, Zielinska I, (2011). *Energie [R]evolution Österreich 2050* (Projektbericht; Studie im Auftrag von EVN, Greenpeace Zentral- und Osteuropa und Gewerkschaft vida). Institut für Höhere Studien (IHS), Wien.

Christian R, Feichtinger R, Christian R, Bolz R, Windsperger A, Hummel P, Weish P, Pfnier E, (2011). *Zukunftsfähige Energieversorgung für Österreich*. Berichte aus Energie- und Umweltforschung Nr. 13/2011, Bundesministerium für Verkehr, Innovation und Technologie, Wien.

Eurostat (2015). *Eurostat Datenbank*. Unter <http://ec.europa.eu/eurostat/de/data/database> [30.11.2015]

Haas R, Kranzl L, Müller A, Corradini R, Zotz M, Frankl P, Menichetti E (2008). *Szenarien der gesamtwirtschaftlichen Marktchancen verschiedener Technologielinien im Energiebereich*. Wien

Handrich L, Kemfert C, Mattes A, Pavel F, Traber T (2015). *Turning Point: Decoupling Greenhouse Gas Emissions from Economic Growth*. Published by Heinrich-Böll-Stiftung, Berlin.

Raupach MR, Marland G, Ciais P, Le Quéré C, Canadell JG, Klepper G, Field CB (2007). *Global and regional drivers of accelerating CO₂ emissions*. Proceedings of the National Academy of Sciences 104, 10288–10293

Stagl S, Schulz N, Kratena K, Mechler R, Pirgmaier E, Radunsky K, Rezai A, Köppl A (2014). *Transformationspfade*. In: *Österreichischer Sachstandsbericht Klimawandel 2014 (AAR14)*. Austrian Panel on Climate Change (APCC), Verlag der Österreichischen Akademie der Wissenschaften, Wien, Österreich, S. 1025–1076.

Statistik Austria (2015a). *Energiebilanzen Österreich 1970-2014*, Wien.

Statistik Austria (2015b). *Pressemitteilung: 11.159-219/15*. Unter http://www.statistik.at/web_de/presse/105677.html [30.11.2015]

Statistik Austria (2015c): *Jahresdurchschnittsbevölkerung seit 1952 nach Bundesland. Statistik des Bevölkerungsstandes*. Erstellt am 11.06.2015. Wien

Streicher W, Haas R, Hausberger S, Oblasser S, Schnitzer H, Steininger KW, Tatzber F, Titz M, Heimrath R, Kalt G, Damm A, Wetz I (2010). *Energieautarkie für Österreich 2050*

(Feasibility Study, Endbericht No. B068644, abgewickelt über den Klima- und Energiefonds.).
im Auftrag des österreichischen Bundesministerium für Land- und Forstwirtschaft, Umwelt und
Wasserwirtschaft (Lebensministerium), Wien.

Sussams L, Leaton J, Drew T (2015). *Lost in Transition: How the energy sector is missing
potential demand destruction*. Carbon Tracker Initiative, London

Umweltbundesamt (2014). Austria's National Inventory Report – Submission under the United
Nations Framework Convention on Climate Change and the Kyoto Protocol

Umweltbundesamt (2015). *Emissionstrends 1990–2013 – Ein Überblick über die Verursacher
von Luftschadstoffen in Österreich (Datenstand 2015)*. Report REP-0543, Wien

Veigl A (2015). *Energiezukunft Österreich. Szenario für 2030 und 2050*. Im Auftrag von
GLOBAL 2000, Greenpeace und WWF

WKO (2015). *BIP und Wirtschaftswachstum*. Aktualisierung: August 2015

schonung sowie Industrie, Gewerbe, Handel und Dienstleistungen. Derzeit liegt der Schwerpunkt beim Klimaschutzplan 2050 auf einem breiten und transparenten Dialog- und Beteiligungsprozess. Noch vor der Sommerpause 2016 soll der Klimaschutzplan 2050 vom Kabinett beschlossen werden.

Zentraler Bezugspunkt für die nationalen Planungen bleibt die europäische Klimaschutzpolitik.

Mit dem Pariser Abkommen im Rücken muss nun das Ziel sein, die klimapolitischen Beschlüsse der Europäischen Union im Detail umzusetzen. Die Weltgemeinschaft erwartet, dass Europa zu seinen Zusagen steht. Viele Eckpunkte für die europäische Klima- und Energiepolitik bis zum Jahr 2030 wurden bereits von den Staats- und Regierungschefs im Oktober 2014 festgelegt. Die Details müssen nun geklärt werden, vor allem die Aufteilung des Klimaziels zwischen den 28 EU-Mitgliedstaaten und der Beitrag des EU-Emissionshandels.

Dann müssen wir uns aber auch die Frage stellen, ob Europa nicht auch über seine bisherigen Zusagen hinausgehen kann. Das Paris-Abkommen sieht die regelmäßige Überprüfung der Klimaschutzbeiträge der Staaten und ihre kontinuierliche Anhebung vor. Wir wissen, dass die bisherigen Beiträge noch nicht ausreichen, um die Erderwärmung auf 1,5 bis 2°C zu begrenzen. Deshalb bin ich überzeugt: Die EU sollte dazu beitragen, dass die internationalen Anstrengungen ehrgeiziger werden. Das Klimaziel der EU für das Jahr 2030 ist als Mindestziel formuliert und lässt damit ausdrücklich die Möglichkeit offen, mehr zu machen. Im Pariser Abkommen hat sich die Staatengemeinschaft geeinigt, bis 2020 die nationalen Beiträge neu vorzulegen oder zu aktualisieren. Diesen Prozess müssen wir nutzen und gestalten. Er eröffnet uns die Möglichkeit, die wir benötigen um so schnell wie möglich den Gipfel der weltweiten Emissionen zu erreichen und möglichst kostengünstig auf einen Emissionspfad zu gelangen, der die Erderwärmung auf ein beherrschbares Maß beschränkt.

Mit dem Pariser Abkommen ist das Fundament für erfolgreichen internationalen Klimaschutz gelegt. Auf dieser Grundlage haben wir gemeinsam mit allen großen Emittenten eine bessere Zukunft vor Augen. Ohne Frage eine bessere Zukunft, als wir sie mit 3 oder 4°C Erderwärmung erwarten würden, aber auch eine bessere Zukunft als unsere Gegenwart. Die Transformation der Weltwirtschaft eröffnet große Chancen, das Pariser Abkommen bietet die Sicherheit, die der private Sektor benötigt um diese Möglichkeiten zu nutzen. Wenn wir es nicht falsch anpacken, dann wird das Pariser Abkommen funktionieren. Ich bin davon überzeugt: Das wird gelingen!



Ottmar Edenhofer*



Christian Flachsland**



Ulrike Kornek***

Der Grundriss für ein neues Klimaregime

Das Abkommen von Paris ist ein diplomatischer Erfolg – ein klimapolitischer Durchbruch ist es noch nicht. Die Staatengemeinschaft hat sich nach dem Scheitern der Klimakonferenz von Kopenhagen im Jahr 2009 auf ein globales Klimaschutzziel und den institutionellen Grundriss eines neuen Klimaregimes einigen können. Ein Scheitern von Paris hätte das Ende der multilateralen Klimapolitik bedeutet. In Paris wurde aber statt verbindlicher nationalstaatlicher Emissionsziele wie im Kyoto-Protokoll nur ein System aus freiwilligen Selbstverpflichtungen vereinbart. In den nächsten Jahren muss die institutionelle Statik des Regimes so weiter entwickelt werden, dass die fragile Kooperation zwischen den Staaten schrittweise stabilisiert und ausgeweitet werden kann.

Das Pariser Abkommen ruht auf drei Säulen. Zentral ist das ambitionierte Langfristziel zur Klimastabilisierung von 2°C über dem vorindustriellen Niveau sowie das Versprechen, Anstrengungen zu unternehmen, um ein noch ambitionierteres 1,5°C-Ziel zu verfolgen.

Zweitens haben sich anders als im Kyoto-Protokoll *alle* Vertragsstaaten darauf verpflichtet, bis 2020 selbst bestimmte nationale klimapolitische Pläne vorzulegen (»Nationally Determined Contributions«, NDCs). Diese Pläne basieren allerdings nicht auf einer gemeinsamen Aufteilung des beim 2°C-Ziel zulässigen globalen Kohlenstoffbudgets auf die einzelnen Staaten. Stattdessen legt jedes Land seine eigenen Vermeidungsziele fest, und es bleibt unklar, wer zur

* Prof. Dr. Ottmar Edenhofer ist Direktor des Mercator Research Institute on Global Commons and Climate Change (MCC), Berlin, Professor für die Ökonomie des Klimawandels an der Technischen Universität Berlin sowie stellvertretender Direktor und Chefökonom des Potsdam-Instituts für Klimafolgenforschung (PIK).

** Prof. Dr. Christian Flachsland leitet die Arbeitsgruppe Governance am Mercator Research Institute on Global Commons and Climate Change (MCC), Berlin und ist Assistant Professor for Climate & Energy Governance an der Hertie School of Governance.

*** Dr. Ulrike Kornek ist wissenschaftliche Mitarbeiterin am Mercator Research Institute on Global Commons and Climate Change (MCC), Berlin.

Verantwortung gezogen wird, wenn das globale Ziel nicht erreicht wird. Vor Paris haben die Staaten bereits erste Pläne vorgelegt (»Intended Nationally Determined Contributions«, INDCs). Ab 2018 wird basierend auf den INDCs über die ersten formalen NDCs verhandelt werden, deren Ambitionsniveau dann schrittweise erhöht werden soll. Grundlage für diesen anvisierten »ratcheting-up«-Mechanismus sind dabei der »global stocktake« sowie die noch festzulegenden Regeln über die Vergleichbarkeit und Überprüfbarkeit der NDCs. Im »global stocktake« werden die geplanten Anstrengungen der NDCs aufaddiert und mit den globalen Zielen verglichen. Durch transparente Berichterstattung und regelmäßige Überprüfung der Einhaltung der NDCs soll zwischenstaatliches Vertrauen aufgebaut werden.

Wenn Länder wenig ambitionierte NDCs vorlegen oder ihre Versprechen nicht umsetzen, verbleibt als einziger Sanktionsmechanismus aber nur informelles »naming & shaming« – formale Sanktionen waren in Paris nicht durchsetzbar.

Als dritte Säule wurden in Paris eine Reihe multilateraler klimapolitischer Instrumente vereinbart. Die potenziell wichtigsten Instrumente sind ein globaler Lastenausgleich durch Klimafinanzierung von jährlich mindestens 100 Mrd. US-Dollar sowie flexible Mechanismen wie etwa ein internationaler Emissionshandel zur Reduktion der Vermeidungskosten. Die genaue Ausgestaltung dieser multilateralen Instrumente ist aber noch weitgehend offen.

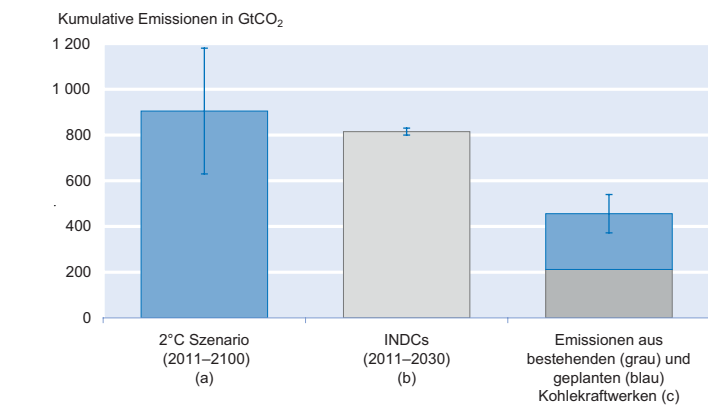
Paris hat den Grundriss für ein neues Klimaregime vorgelegt – eine tragfähige statische Konzeption wurde aber noch nicht vereinbart. Darauf aufbauend muss jetzt eine institutionelle Struktur entwickelt werden, mit der die Kooperationsbereitschaft von Paris trotz des großen Angebots billiger fossiler Ressourcen, Sorgen über nationale Wettbewerbsfähigkeit und Anreize zum Trittbrettfahren gesichert und vertieft wird. Wie kann die Konsistenz und Vergleichbarkeit der INDCs verbessert werden, damit sie eine glaubwürdige Grundlage für gegenseitige Verpflichtungen bilden und dadurch Kooperation stabilisieren? Und wie sollte insbesondere die multilaterale Klimafinanzierung ausgestaltet werden, um wirksame Anreize zur Erhöhung der Ambitionen nationaler Klimapolitiken zu setzen?

INDCs zwischen 2°C-Ziel und der Renaissance der Kohle

An der Glaubwürdigkeit der bisher vorgelegten INDCs gibt es erhebliche Zweifel: Erstens verschieben sie die Hauptlast der für das 2°C-Ziel erforderlichen Emissionsreduktionen auf

Abb. 1

Kumulative CO₂-Emissionen



Die Unsicherheitsbereiche werden durch die blauen Intervalle angezeigt.

Quelle: (a) Die bis 2100 erlaubten globalen kumulierten CO₂-Emissionen beim 2°C-Ziel (Edenhofer et al. 2014). (b) Kumulierte Emissionen aus den INDCs bis 2030 (Minx et al. 2016). (c) Kumulierte Emissionen aus bereits existierenden (ab 2012, Davis und Sokolow 2014) und geplanten Kohlekraftwerken (ab 2015, Global Coal Plant Tracker 2015) über ihre gesamte Laufzeit.

die Zeit nach 2030. Zweitens sind INDCs Versprechungen auf internationalem Parkett, die in den nationalen wirtschaftspolitischen Strategien der Regierungen bisher noch nicht überzeugend abgebildet sind. Drittens lassen sich die derzeitigen INDCs noch nicht transparent überprüfen und vergleichen.

Das 2°C-Ziel erlaubt bis zum Jahr 2100 noch 630–1180 GtCO₂ netto in der Atmosphäre zu deponieren (vgl. Abb. 1, Balken 1). Beim 1,5°C-Ziel schrumpft dieser Spielraum auf 90–310 GtCO₂ zusammen – hier wären massive negative Emissionen etwa durch die großskalige Kombination von Biomasse und CCS Technologien erforderlich (vgl. Edenhofer et al. 2014). Dagegen führt die Summe aller INDCs schon zu ca. 815 GtCO₂ kumulierten Emissionen bis zum Jahr 2030 (vgl. Abb. 1, Balken 2). Bleiben die INDCs bis 2030 unverändert, werden danach also drastische Emissionsreduktionen und negative Emissionen nötig sein, um das 2°C-Ziel noch zu erreichen. Technologisch ist dies prinzipiell möglich. Die ökonomischen Kosten sowie die gesellschaftlichen und politischen Herausforderungen der erforderlichen Emissionsreduktionen lassen aber daran zweifeln, dass künftige Regierungen und Gesellschaften diese Last auch schultern werden.

Derzeit ist aber noch nicht einmal gewährleistet, dass die Regierungen die vorgelegten INDCs in der nationalen Energiepolitik auch umsetzen. Nach wie vor setzen sie auf den Ausbau der Kohlekraft (vgl. Steckel et al. 2015). Kohle ist reichlich vorhanden und trotz aller klimapolitischen Anstrengungen und Kostensenkungen der Erneuerbaren in den meisten Regionen auf absehbare Zeit die billigste Form der Stromerzeugung. Sie spielt daher in den energiepolitischen Planungen der Wirtschaftsminister eine wichtige Rolle. Allein die im Jahr 2015 weltweit vorhandenen und geplanten Kohlekraftwerke führen zu kumulativ ca. 450 GtCO₂ – damit

wäre bereits die Hälfte des 2°C-Budgets verbraucht (vgl. Abb. 1, Balken 3). Dabei ist zu beachten, dass die INDCs (Balken 2) und die Kohleausbaupläne (Balken 3) in Abbildung 1 unterschiedliche Zeiträume betrachten. Erste detailliertere Analysen auf nationaler Ebene zeigen allerdings, dass bei den gegenwärtigen expansiven Kohleausbauplänen in zahlreichen Ländern zur Einhaltung der INDCs erhebliche Vermeidungsanstrengungen außerhalb des Stromsektors erforderlich wären (vgl. Edenhofer et al. 2016). Im Transportsektor oder im Gebäudesektor sind die Vermeidungskosten aber deutlich höher als im Stromsektor. Offenbar planen diese Regierungen entweder, ihre Vermeidungsanstrengungen unter hohen Kosten zu erbringen, oder ihre freiwilligen Selbstverpflichtungen sind nicht glaubwürdig. Die INDCs sind daher in vielen Ländern offenbar noch nicht mit den nationalen energiepolitischen Plänen konsistent: Die Regierungen haben nicht mehr viel Zeit, ihre Ausbaupläne für die Kohlekraft zu revidieren.

Für eine erfolgreiche internationale Kooperation ist die Vergleichbarkeit und Überprüfbarkeit der künftigen NDCs entscheidend. Die Nationalstaaten werden nur dann ambitionierte Politiken vorlegen, wenn sie darauf vertrauen können, dass andere Staaten ebenfalls akzeptable Anstrengungen unternehmen (vgl. Aldy et al. 2016). Die derzeitigen INDCs sind allerdings kaum miteinander vergleichbar. China und Indien etwa haben eine Reduktion der CO₂-Intensität ihrer Wirtschaft (CO₂/BIP) versprochen. Ihr absoluter Beitrag zur globalen Emissionsminderung kann daher nur mit Hilfe von unsicheren und umstrittenen Annahmen über das künftige Wachstum ihrer Wirtschaft und Emissionen ermittelt werden. Damit bleibt unklar, was China und Indien tatsächlich zum Erreichen des globalen Ziels beitragen.

Einstieg in eine konsistente Klimapolitik: Koordinierte CO₂-Preise

Internationale Kooperation erfordert gegenseitige Verpflichtungen und stabile Anreizstrukturen – und genau daran droht das Pariser System der freiwilligen Selbstverpflichtungen zu scheitern. Beobachten nämlich die Länder, dass ihre eigenen Anstrengungen nicht durch entsprechende Klimapolitik in anderen Ländern erwidert werden, könnte das erhoffte »ratcheting-up« der NDCs sich auch zu einem »ratcheting-down« entwickeln. Einsichten aus der experimentellen Spieltheorie zeigen, dass für ein erfolgreiches »ratcheting-up« gegenseitige Verpflichtungen mit wirksamen Sanktionen erforderlich sind (vgl. Ostrom und Walker 2005).

Ein ausreichend hoher und langfristig steigender nationaler CO₂-Preis ist hier ein sinnvolles klimapolitisches Instrument (vgl. McKay et al. 2015): Erstens sind CO₂-Preise relativ transparent und einfach miteinander vergleichbar. Sie zeigen wenigstens näherungsweise das klimapolitische Ambitions-

niveau und die Vermeidungskosten der Länder. Die energiepolitische Umsetzung von CO₂-Preisen ist klar: Emissionshandelssysteme, CO₂-Steuern oder fossile Energiesteuern, aber auch Hybridinstrumente, die Elemente der Mengensteuerung mit denen Preissteuerung verbinden, sind Möglichkeiten der Implementierung. In Emissionshandelssystemen ist dann ein steigender Mindestpreis sinnvoll, um glaubwürdige internationale Versprechen eingehen zu können (vgl. Edenhofer und Ockenfels 2015).

Zweitens werden durch einen CO₂-Preis die Kosten der Kohle und anderer fossiler Energieträger erhöht, und es kann ein glaubwürdiger und kosteneffizienter Dekarbonisierungspfad eingeleitet werden. Erneuerbare Energien wie Wind- und Solarkraftwerke werden wettbewerbsfähig und Investitionen in Entwicklung und Aufbau emissionsarmer Technologien und Infrastrukturen ermöglicht. Die historischen und gegenwärtigen Schwankungen des Ölpreises illustrieren eindrucksvoll die transformative Kraft von Energiepreisen.

Am Rande der Pariser Konferenz war immer wieder zu hören, die Klimarahmenkonvention sei nicht das richtige Forum, um über CO₂-Preise zu verhandeln. Das Abkommen von Paris ermöglicht jedoch, dass diese Verhandlungen auch in anderen Foren wie etwa der G 20 geführt werden (Art. 6). Eine Möglichkeit der Koordination von CO₂-Preisen ist die Verknüpfung nationaler Emissionshandelssysteme. Noch einfacher wäre die Abstimmung nationaler CO₂-Steuern oder Mindestpreise in Emissionshandelssystemen. Mit dieser Strategie könnten Befürchtungen über Wettbewerbsnachteile durch CO₂-Bepreisung entkräftet werden. Durch konditionale nationale CO₂-Preise könnte zudem ein wirksamer Sanktionsmechanismus etabliert werden: Länder würden nur dann hohe Preise implementieren, wenn andere Staaten dies ebenfalls tun. Mit Blick auf das Erreichen des 2°C-Ziels müssten dann regelmäßig die durch CO₂-Preise erreichten Emissionsreduktionen mit dem Langfristziel verglichen und die Preise entsprechend angepasst werden.

Die Einführung nationaler CO₂-Preise hat einen weiteren Vorteil: Sie ist eine neue Quelle für Staatseinnahmen. So können Einnahmen durch versteigerte Zertifikate in Emissionshandelssystemen oder CO₂-Steuern für Finanzminister auch unabhängig von klimapolitischen Erwägungen attraktiv sein (vgl. Franks et al. 2015). Die zusätzlichen Gelder könnten für öffentliche Investitionen in Infrastrukturen zum Erreichen der Sustainable Development Goals (SDGs), zur Reduktion bestehender Steuern oder direkten Kompensation ärmerer Bevölkerungsgruppen verwendet werden (vgl. Jakob et al. 2015). Bei global 36 Gt CO₂-Emissionen im Jahr 2015 und einem hypothetischen Preis von 50 US-Dollar pro Tonne wären das jährlich immerhin 1,8 Billionen US-Dollar oder 2,3% des globalen BIP. Demgegenüber werden die jährlichen Kosten der Bereitstellung eines universalen Zugangs zu saube-

rem Wasser, Sanitäranlagen und Elektrizität auf insgesamt knapp 1 Billion US-Dollar geschätzt (vgl. Jakob et al. 2015).

Klimafinanzierung zur Stabilisierung der Kooperation

Zu einer Anhebung und Koordination der regionalen CO₂-Preise wird es angesichts der großen Unterschiede zwischen Ländern nur dann kommen können, wenn ein Lastenausgleich zwischen Arm und Reich erfolgt. Die Transferzahlungen sollten an ärmere Länder allerdings unter der Bedingung gezahlt werden, dass sie einen Mindestpreis für Emissionen akzeptieren (vgl. Cramton et al. 2015). Staatseinnahmen aus CO₂-Preisen sollten in den jeweiligen Ländern verbleiben. Vorstellbar wäre auch ein System von zunächst je nach Ländergruppen differenzierten, aber ansteigenden und mittelfristig konvergierenden Mindestpreisen. Wenn die in Paris vereinbarte Klimafinanzierung in Richtung solcher konditionaler Transferzahlungen weiterentwickelt würde, könnte sie zu einem tragenden Stützpfeiler der internationalen Klimapolitik werden (vgl. Kornek und Edenhofer 2016).

Entwicklungsländern fehlt oft die Kapazität und Expertise zur Einführung von CO₂-Steuern. Ein Teil der versprochenen 100 Mrd. US-Dollar ließen sich zunächst dazu nutzen, diese Kapazitäten aufzubauen. Sorgen über regressive Wirkungen von CO₂-Steuern kann durch die Entwicklung von sozial verträglichen Steuermodellen begegnet werden. Der Green Climate Fund könnte Steuererleichterungen und Kompensationszahlungen für ärmere Bevölkerungsgruppen bei der Einführung von CO₂-Preisen vorfinanzieren, um regressive Effekte zu vermeiden und die soziale Akzeptanz zu erhöhen (vgl. Steckel et al. 2016).

Entscheidend ist jedoch die konditionale Verknüpfung der Transferzahlungen mit der Einführung eines Mindestpreises für Emissionen. Derzeit wird ein solcher strategischer Einsatz der Klimafinanzierung allerdings noch kaum diskutiert. Zudem ist das Volumen der Klimafinanzierung aus öffentlichen Geldern unklar: Für die kommenden Jahre sind nur 10 Mrd. US-Dollar für den Green Climate Fund zugesagt, 6 Mrd. US-Dollar sind bislang freigegeben. Es besteht zudem die Gefahr, dass die Industrieländer durch kreative Buchführung ihren zusätzlichen Beitrag zur Klimafinanzierung sehr viel höher erscheinen lassen, als er ist: Bereits bestehende Verpflichtungen aus der Entwicklungshilfe werden umetikettiert oder private Investitionen, die ohnehin getätigt würden, werden als internationale Klimafinanzierung angerechnet.

Fazit

Das Pariser Abkommen bietet einen Grundriss für den Aufbau eines effektiven Klimaregimes. Eine tragfähige institu-

tionelle Statik hat dieses Regime aber noch nicht. Die unverminderte Renaissance der Kohle lässt nicht mehr viel Zeit für die Verhandlungen – denn sind die Kohlekraftwerke einmal gebaut, sinken die Chancen auf eine ambitionierte Klimapolitik. Es kommt nun darauf an, die Diskussion über koordinierte CO₂-Mindestpreise und konditionale Klimafinanzierung so voranzutreiben, dass die Chancen internationaler Kooperation steigen. Sonst drohen die billige Kohle, die Sorgen über nationale Wettbewerbsfähigkeit und Anreize zum Trittbrettfahren das fragile Gebäude der multilateralen Klimakooperation wieder unter sich zu begraben.

Die G 20 sind im Hinblick auf diesen Prozess ein vielversprechendes Verhandlungsforum, immerhin repräsentieren sie 76% der gegenwärtigen globalen Emissionen. Einige G-20-Länder haben bereits CO₂-Preise eingeführt oder prüfen Möglichkeiten zu ihrer Einführung. Innerhalb der G 20 wurde bereits ein Prozess zur Abschaffung fossiler Subventionen (negativer CO₂-Preise) initiiert. Die kommenden G-20-Präsidentschaften von China und Deutschland könnten nun die Verhandlungen über koordinierte CO₂-Preise in Verbindung mit einem globalen Klimafinanzausgleich vorantreiben.

Literatur

- Aldy, J., W. Pizer und K. Akimoto (2016), »Comparing emissions mitigation efforts across countries«, *Climate Policy*, im Erscheinen.
- Cramton, P., A. Ockenfels und S. Stoft (2015), »An International Carbon-Price Commitment Promotes Cooperation«, *Economics of Energy & Environmental Policy* 4(2), 51–64.
- Davis, S.J. und R.H. Sokolow (2014), »Commitment accounting of CO₂ emissions«, *Environmental Research Letters*, verfügbar unter: <http://iopscience.iop.org/article/10.1088/1748-9326/9/8/084018/meta>.
- Edenhofer O. et al. (2014), *Technical Summary*, in: Climate Change 2014: Mitigation of Climate Change, Contribution of Working Group III to the Fifth Assessment Report of the Intergovernmental Panel on Climate Change, verfügbar unter: <http://www.ipcc.ch/report/ar5/wg3/>.
- Edenhofer, O. und A. Ockenfels (2015), »Ein Ausweg aus der Klima-Sackgasse«, *Frankfurter Allgemeine Zeitung*, 26. Oktober.
- Edenhofer, O., J.C. Steckel, M. Jakob und C. Bertram (2016), »Reading the Writing on the Wall: Coal and the Paris Agreement«, Working Paper.
- Franks, M., O. Edenhofer und K. Lessmann (2016), »Why Finance Ministers Favor Carbon Taxes, Even if They Do Not Take Climate Change into Account«, *Environmental & Resource Economics*, im Erscheinen.
- Global Coal Plant Tracker (2015), verfügbar unter: <http://endcoal.org/global-coal-plant-tracker/>.
- Jakob, M., C. Chen, S. Fuss, A. Marxen, N. Rao und O. Edenhofer (2016), »Using carbon pricing revenues to finance infrastructure access«, *World Development*, im Erscheinen.
- Kornek, U. und O. Edenhofer (2016), »The strategic dimension of financing global public goods«, Working Paper.
- Minx, J.C., F. Creutzig und O. Edenhofer (2016), »Climate goals require fast learning in negative emission technologies«, Working Paper.
- McKay, D., P. Cramton, A. Ockenfels und S. Stoft (2015), »Price carbon — I will if you will«, *Nature* 526, 315–316.

IPCC Special Report

Carbon Dioxide Capture and Storage

Technical Summary

Coordinating Lead Authors

Edward Rubin (United States), Leo Meyer (Netherlands), Heleen de Coninck (Netherlands)

Lead Authors

Juan Carlos Abanades (Spain), Makoto Akai (Japan), Sally Benson (United States), Ken Caldeira (United States), Peter Cook (Australia), Ogunlade Davidson (Sierra Leone), Richard Doctor (United States), James Dooley (United States), Paul Freund (United Kingdom), John Gale (United Kingdom), Wolfgang Heidug (Germany), Howard Herzog (United States), David Keith (Canada), Marco Mazzotti (Italy and Switzerland), Bert Metz (Netherlands), Balgis Osman-Elasha (Sudan), Andrew Palmer (United Kingdom), Riitta Pipatti (Finland), Koen Smekens (Belgium), Mohammad Soltanieh (Iran), Kelly (Kailai) Thambimuthu (Australia and Canada), Bob van der Zwaan (Netherlands)

Review Editor

Ismail El Gizouli (Sudan)

Contents

1. Introduction and framework of this report19

2. Sources of CO₂22

3. Capture of CO₂24

4. Transport of CO₂29

5. Geological storage31

6. Ocean storage37

7. Mineral carbonation and industrial uses 39

8. Costs and economic potential 41

9. Emission inventories and accounting46

10. Gaps in knowledge48

1. Introduction and framework of this report

Carbon dioxide capture and storage (CCS), the subject of this Special Report, is considered as one of the options for reducing atmospheric emissions of CO₂ from human activities. The purpose of this Special Report is to assess the current state of knowledge regarding the technical, scientific, environmental, economic and societal dimensions of CCS and to place CCS in the context of other options in the portfolio of potential climate change mitigation measures.

The structure of this Technical Summary follows that of the Special Report. This introductory section presents the general framework for the assessment together with a brief overview of CCS systems. Section 2 then describes the major sources of CO₂, a step needed to assess the feasibility of CCS on a global scale. Technological options for CO₂ capture are then discussed in Section 3, while Section 4 focuses on methods of CO₂ transport. Following this, each of the storage options is addressed. Section 5 focuses on geological storage, Section 6 on ocean storage, and Section 7 on mineral carbonation and industrial uses of CO₂. The overall costs and economic potential of CCS are then discussed in Section 8, followed by an examination in Section 9 of the implications of CCS for greenhouse gas emissions inventories and accounting. The Technical Summary concludes with a discussion of gaps in knowledge, especially those critical for policy considerations.

Overview of CO₂ capture and storage

CO₂ is emitted principally from the burning of fossil fuels, both in large combustion units such as those used for electric power generation and in smaller, distributed sources such as automobile engines and furnaces used in residential and commercial buildings. CO₂ emissions also result from some industrial and resource extraction processes, as well as from the burning of forests during land clearance. CCS would most likely be applied to large point sources of CO₂, such as power plants or large industrial processes. Some of these sources could supply decarbonized fuel such as hydrogen to the transportation, industrial and building sectors, and thus reduce emissions from those distributed sources.

CCS involves the use of technology, first to collect and concentrate the CO₂ produced in industrial and energy-related sources, transport it to a suitable storage location, and then store it away from the atmosphere for a long period of time. CCS would thus allow fossil fuels to be used with low emissions of greenhouse gases. Application of CCS to biomass energy sources could result in the net removal of CO₂ from the atmosphere (often referred to as ‘negative

emissions’) by capturing and storing the atmospheric CO₂ taken up by the biomass, provided the biomass is not harvested at an unsustainable rate.

Figure TS.1 illustrates the three main components of the CCS process: capture, transport and storage. All three components are found in industrial operations today, although mostly not for the purpose of CO₂ storage. The capture step involves separating CO₂ from other gaseous products. For fuel-burning processes such as those in power plants, separation technologies can be used to capture CO₂ after combustion or to decarbonize the fuel before combustion. The transport step may be required to carry captured CO₂ to a suitable storage site located at a distance from the CO₂ source. To facilitate both transport and storage, the captured CO₂ gas is typically compressed to a high density at the capture facility. Potential storage methods include injection into underground geological formations, injection into the deep ocean, or industrial fixation in inorganic carbonates. Some industrial processes also might utilize and store small amounts of captured CO₂ in manufactured products.

The technical maturity of specific CCS system components varies greatly. Some technologies are extensively deployed in mature markets, primarily in the oil and gas industry, while others are still in the research, development or demonstration phase. Table TS.1 provides an overview of the current status of all CCS components. As of mid-2005, there have been three commercial projects linking CO₂ capture and geological storage: the offshore Sleipner natural gas processing project in Norway, the Weyburn Enhanced Oil Recovery (EOR)¹ project in Canada (which stores CO₂ captured in the United States) and the In Salah natural gas project in Algeria. Each captures and stores 1–2 MtCO₂ per year. It should be noted, however, that CCS has not yet been applied at a large (e.g., 500 MW) fossil-fuel power plant, and that the overall system may not be as mature as some of its components.

¹ In this report, EOR means enhanced oil recovery using CO₂

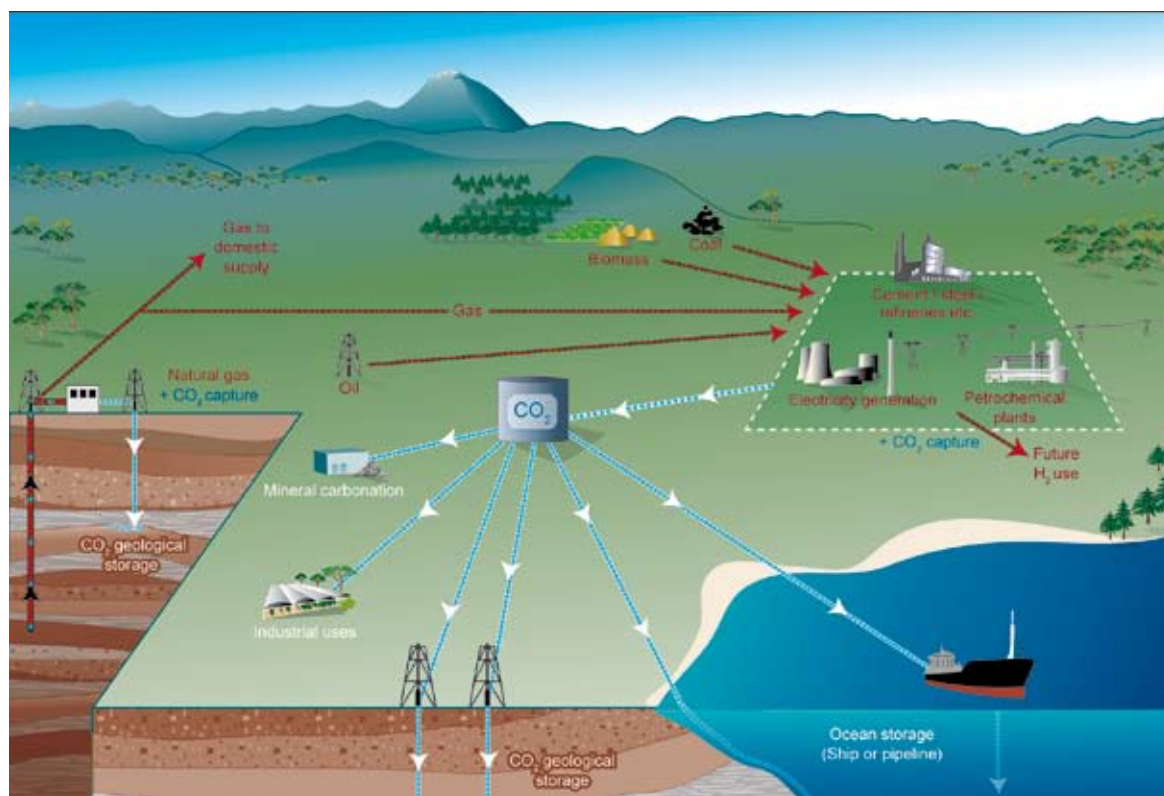


Figure TS.1. Schematic diagram of possible CCS systems. It shows the sources for which CCS might be relevant, as well as CO₂ transport and storage options (Courtesy CO2CRC).

Why the interest in CO₂ capture and storage?

In 1992, international concern about climate change led to the United Nations Framework Convention on Climate Change (UNFCCC). The ultimate objective of that Convention is the “stabilization of greenhouse gas concentrations in the atmosphere at a level that prevents dangerous anthropogenic interference with the climate system”. From this perspective, the context for considering CCS (and other mitigation options) is that of a world constrained in CO₂ emissions, consistent with the international goal of stabilizing atmospheric greenhouse gas concentrations. Most scenarios for global energy use project a substantial increase of CO₂ emissions throughout this century in the absence of specific actions to mitigate climate change. They also suggest that the supply of primary energy will continue to be dominated by fossil fuels until at least the middle of the century (see Section 8). The magnitude of the emissions reduction needed to stabilize the atmospheric concentration of CO₂ will depend on both the level of future emissions (the baseline) and the

desired target for long-term CO₂ concentration: the lower the stabilization target and the higher the baseline emissions, the larger the required reduction in CO₂ emissions. IPCC’s Third Assessment Report (TAR) states that, depending on the scenario considered, cumulative emissions of hundreds or even thousands of gigatonnes of CO₂ would need to be prevented during this century to stabilize the CO₂ concentration at 450 to 750 ppmv². The TAR also finds that, “most model results indicate that known technological options³ could achieve a broad range of atmospheric CO₂ stabilization levels”, but that “no single technology option will provide all of the emissions reductions needed”. Rather, a combination of mitigation measures will be needed to achieve stabilization. These known technological options are available for stabilization, although the TAR cautions that, “implementation would require associated socio-economic and institutional changes”.

² ppmv is parts per million by volume.

³ “Known technological options” refer to technologies that are currently at the operation or pilot-plant stages, as referred to in the mitigation scenarios discussed in IPCC’s Third Assessment Report. The term does not include any new technologies that will require drastic technological breakthroughs. It can be considered to represent a conservative estimate given the length of the scenario period.

Table TS.1. Current maturity of CCS system components. An X indicates the highest level of maturity for each component. There are also less mature technologies for most components.

CCS component	CCS technology	Research phase ^a	Demonstration phase ^b	Economically feasible under specific conditions ^c	Mature market ^d
Capture	Post-combustion			X	
	Pre-combustion			X	
	Oxyfuel combustion		X		
	Industrial separation (natural gas processing, ammonia production)				X
Transportation	Pipeline				X
	Shipping			X	
Geological storage	Enhanced Oil Recovery (EOR)				X ^e
	Gas or oil fields			X	
	Saline formations			X	
	Enhanced Coal Bed Methane recovery (ECBM) ^f		X		
Ocean storage	Direct injection (dissolution type)	X			
	Direct injection (lake type)	X			
Mineral carbonation	Natural silicate minerals	X			
	Waste materials		X		
Industrial uses of CO ₂					X

^a Research phase means that the basic science is understood, but the technology is currently in the stage of conceptual design or testing at the laboratory or bench scale, and has not been demonstrated in a pilot plant.

^b Demonstration phase means that the technology has been built and operated at the scale of a pilot plant, but further development is required before the technology is ready for the design and construction of a full-scale system.

^c Economically feasible under specific conditions means that the technology is well understood and used in selected commercial applications, for instance if there is a favourable tax regime or a niche market, or processing on in the order of 0.1 MtCO₂ yr⁻¹, with few (less than 5) replications of the technology.

^d Mature market means that the technology is now in operation with multiple replications of the technology worldwide.

^e CO₂ injection for EOR is a mature market technology, but when used for CO₂ storage, it is only economically feasible under specific conditions.

^f ECBM is the use of CO₂ to enhance the recovery of the methane present in unminable coal beds through the preferential adsorption of CO₂ on coal. Unminable coal beds are unlikely to ever be mined, because they are too deep or too thin. If subsequently mined, the stored CO₂ would be released.

In this context, the availability of CCS in the portfolio of options for reducing greenhouse gas emissions could facilitate the achievement of stabilization goals. Other technological options, which have been examined more extensively in previous IPCC assessments, include: (1) reducing energy demand by increasing the efficiency of energy conversion and/or utilization devices; (2) decarbonizing energy supplies (either by switching to less carbon-intensive fuels (coal to natural gas, for example), and/or by increasing the use of renewable energy sources and/or nuclear energy (each of which, on balance, emit little or no CO₂); (3) sequestering CO₂ through the enhancement of natural sinks by biological fixation; and (4) reducing non-CO₂ greenhouse gases.

Model results presented later in this report suggest that use of CCS in conjunction with other measures could significantly reduce the cost of achieving stabilization and would increase flexibility in achieving these reductions. The heavy worldwide reliance on fossil fuels today (approximately 80% of global energy use), the potential for CCS to reduce CO₂ emissions over the next century, and the compatibility of CCS systems with current energy infrastructures explain the interest in this technology.

Major issues for this assessment

There are a number of issues that need to be addressed in trying to understand the role that CCS could play in mitigating climate change. Questions that arise, and that are addressed in different sections of this Technical Summary, include the following:

- What is the current status of CCS technology?
- What is the potential for capturing and storing CO₂?
- What are the costs of implementation?
- How long should CO₂ be stored in order to achieve significant climate change mitigation?
- What are the health, safety and environment risks of CCS?
- What can be said about the public perception of CCS?
- What are the legal issues for implementing CO₂ storage?
- What are the implications for emission inventories and accounting?
- What is the potential for the diffusion and transfer of CCS technology?

When analyzing CCS as an option for climate change mitigation, it is of central importance that all resulting emissions from the system, especially emissions of CO₂, be identified and assessed in a transparent way. The importance of taking a “systems” view of CCS is therefore stressed, as the selection of an appropriate system boundary is essential for proper analysis. Given the energy requirements associated with capture and some storage and utilization options, and the possibility of leaking storage reservoirs, it is vital to assess the CCS chain as a whole.

From the perspectives of both atmospheric stabilization and long-term sustainable development, CO₂ storage must extend over time scales that are long enough to contribute significantly to climate change mitigation. This report expresses the duration of CO₂ storage in terms of the ‘fraction retained’, defined as the fraction of the cumulative mass of CO₂ injected that is retained in a storage reservoir over a specified period of time. Estimates of such fractions for different time periods and storage options are presented later. Questions arise not only about how long CO₂ will remain stored, but also what constitutes acceptable amounts of slow, continuous leakage⁴ from storage. Different approaches to this question are discussed in Section 8.

CCS would be an option for countries that have significant sources of CO₂ suitable for capture, that have access to storage sites and experience with oil or gas operations, and that need to satisfy their development aspirations in a carbon-constrained environment. Literature assessed in the IPCC Special Report ‘Methodological and Technological Issues and Technology

Transfer’ indicates that there are many potential barriers that could inhibit deployment in developing countries, even of technologies that are mature in industrialized countries. Addressing these barriers and creating conditions that would facilitate diffusion of the technology to developing countries would be a major issue for the adoption of CCS worldwide.

2. Sources of CO₂

This section describes the major current anthropogenic sources of CO₂ emissions and their relation to potential storage sites. As noted earlier, CO₂ emissions from human activity arise from a number of different sources, mainly from the combustion of fossil fuels used in power generation, transportation, industrial processes, and residential and commercial buildings. CO₂ is also emitted during certain industrial processes like cement manufacture or hydrogen production and during the combustion of biomass. Future emissions are also discussed in this section.

Current CO₂ sources and characteristics

To assess the potential of CCS as an option for reducing global CO₂ emissions, the current global geographical relationship between large stationary CO₂ emission sources and their proximity to potential storage sites has been examined. CO₂ emissions in the residential, commercial and transportation sectors have not been considered in this analysis because these emission sources are individually small and often mobile, and therefore unsuitable for capture and storage. The discussion here also includes an analysis of potential future sources of CO₂ based on several scenarios of future global energy use and emissions over the next century.

Globally, emissions of CO₂ from fossil-fuel use in the year 2000 totalled about 23.5 GtCO₂ yr⁻¹ (6 GtC yr⁻¹). Of this, close to 60% was attributed to large (>0.1 MtCO₂ yr⁻¹) stationary emission sources (see Table TS.2). However, not all of these sources are amenable to CO₂ capture. Although the sources evaluated are distributed throughout the world, the database reveals four particular clusters of emissions: North America (midwest and eastern USA), Europe (northwest region), East Asia (eastern coast of China) and South Asia (Indian subcontinent). By contrast, large-scale biomass sources are much smaller in number and less globally distributed.

Currently, the vast majority of large emission sources have CO₂ concentrations of less than 15% (in some cases, substantially less). However, a small portion (less than 2%) of the fossil fuel-based industrial sources have CO₂ concentrations in excess of 95%. The high-concentration sources are potential candidates for the early implementation

⁴ With respect to CO₂ storage, leakage is defined as the escape of injected fluid from storage. This is the most common meaning used in this Summary. If used in the context of trading of carbon dioxide emission reductions, it may signify the change in anthropogenic emissions by sources or removals by sinks which occurs outside the project boundary.

Table TS.2. Profile by process or industrial activity of worldwide large stationary CO₂ sources with emissions of more than 0.1 MtCO₂ per year.

Process	Number of sources	Emissions (MtCO ₂ yr ⁻¹)
Fossil fuels		
Power	4,942	10,539
Cement production	1,175	932
Refineries	638	798
Iron and steel industry	269	646
Petrochemical industry	470	379
Oil and gas processing	N/A	50
Other sources	90	33
Biomass		
Bioethanol and bioenergy	303	91
Total	7,887	13,466

of CCS because only dehydration and compression would be required at the capture stage (see Section 3). An analysis of these high-purity sources that are within 50 km of storage formations and that have the potential to generate revenues (via the use of CO₂ for enhanced hydrocarbon production through ECBM or EOR) indicates that such sources currently emit approximately 360 MtCO₂ per year. Some biomass sources like bioethanol production also generate high-concentration CO₂ sources which could also be used in similar applications.

The distance between an emission location and a storage site can have a significant bearing on whether or not CCS can play a significant role in reducing CO₂ emissions. Figure

TS.2a depicts the major CO₂ emission sources (indicated by dots), and Figure TS.2b shows the sedimentary basins with geological storage prospectivity (shown in different shades of grey). In broad terms, these figures indicate that there is potentially good correlation between major sources and prospective sedimentary basins, with many sources lying either directly above, or within reasonable distances (less than 300 km) from areas with potential for geological storage. The basins shown in Figure TS.2b have not been identified or evaluated as suitable storage reservoirs; more detailed geological analysis on a regional level is required to confirm the suitability of these potential storage sites.



Figure TS.2a. Global distribution of large stationary sources of CO₂ (based on a compilation of publicly available information on global emission sources, IEA GHG 2002)

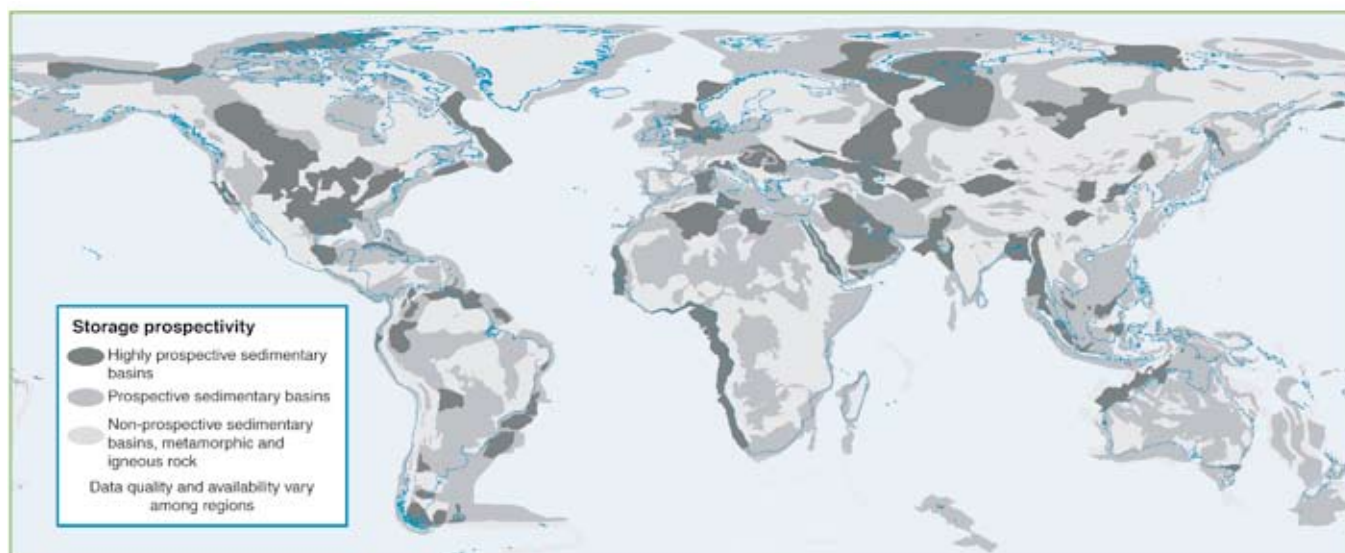


Figure TS.2b. Prospective areas in sedimentary basins where suitable saline formations, oil or gas fields, or coal beds may be found. Locations for storage in coal beds are only partly included. Prospectivity is a qualitative assessment of the likelihood that a suitable storage location is present in a given area based on the available information. This figure should be taken as a guide only, because it is based on partial data, the quality of which may vary from region to region, and which may change over time and with new information (Courtesy of Geoscience Australia).

Future emission sources

In the IPCC Special Report on Emission Scenarios (SRES), the future emissions of CO₂ are projected on the basis of six illustrative scenarios in which global CO₂ emissions range from 29 to 44 GtCO₂ (8–12 GtC) per year in 2020, and from 23 to 84 GtCO₂ (6–23 GtC) per year in 2050. It is projected that the number of CO₂ emission sources from the electric power and industrial sectors will increase significantly until 2050, mainly in South and East Asia. By contrast, the number of such sources in Europe may decrease slightly. The proportion of sources with high and low CO₂ content will be a function of the size and rate of introduction of plants employing gasification or liquefaction of fossil fuels to produce hydrogen, or other liquid and gaseous products. The greater the number of these plants, the greater the number of sources with high CO₂ concentrations technically suitable for capture.

The projected potential of CO₂ capture associated with the above emission ranges has been estimated at an annual 2.6 to 4.9 GtCO₂ by 2020 (0.7–1.3 GtC) and 4.7 to 37.5 GtCO₂ by 2050 (1.3–10 GtC). These numbers correspond to 9–12%, and 21–45% of global CO₂ emissions in 2020 and 2050, respectively. The emission and capture ranges reflect the inherent uncertainties of scenario and modelling analyses, and the technical limitations of applying CCS. These scenarios only take into account CO₂ capture from fossil fuels, and not from biomass sources. However, emissions from large-

scale biomass conversion facilities could also be technically suitable for capture.

The potential development of low-carbon energy carriers is relevant to the future number and size of large, stationary CO₂ sources with high concentrations. Scenarios also suggest that large-scale production of low-carbon energy carriers such as electricity or hydrogen could, within several decades, begin displacing the fossil fuels currently used by small, distributed sources in residential and commercial buildings and in the transportation sector (see Section 8). These energy carriers could be produced from fossil fuels and/or biomass in large plants that would generate large point sources of CO₂ (power plants or plants similar to current plants producing hydrogen from natural gas). These sources would be suitable for CO₂ capture. Such applications of CCS could reduce dispersed CO₂ emissions from transport and from distributed energy supply systems. At present, however, it is difficult to project the likely number, size, or geographical distribution of the sources associated with such developments.

3. Capture of CO₂

This section examines CCS capture technology. As shown in Section 2, power plants and other large-scale industrial processes are the primary candidates for capture and the main focus of this section.

Capture technology options and applications

The purpose of CO₂ capture is to produce a concentrated stream of CO₂ at high pressure that can readily be transported to a storage site. Although, in principle, the entire gas stream containing low concentrations of CO₂ could be transported and injected underground, energy costs and other associated costs generally make this approach impractical. It is therefore necessary to produce a nearly pure CO₂ stream for transport and storage. Applications separating CO₂ in large industrial plants, including natural gas treatment plants and ammonia production facilities, are already in operation today. Currently, CO₂ is typically removed to purify other industrial gas streams. Removal has been used for storage purposes in only a few cases; in most cases, the CO₂ is emitted to the atmosphere. Capture processes also have been used to obtain commercially useful amounts of CO₂ from flue gas streams generated by the combustion of coal or natural gas. To date, however, there have been no applications of CO₂ capture at large (e.g., 500 MW) power plants.

Depending on the process or power plant application in question, there are three main approaches to capturing the CO₂ generated from a primary fossil fuel (coal, natural gas or oil), biomass, or mixtures of these fuels:

Post-combustion systems separate CO₂ from the flue gases produced by the combustion of the primary fuel in air. These systems normally use a liquid solvent to capture the small fraction of CO₂ (typically 3–15% by volume) present in a flue gas stream in which the main constituent is nitrogen (from air). For a modern pulverized coal (PC) power plant or a natural gas combined cycle (NGCC) power plant, current post-combustion capture systems would typically employ an organic solvent such as monoethanolamine (MEA).

Pre-combustion systems process the primary fuel in a reactor with steam and air or oxygen to produce a mixture consisting mainly of carbon monoxide and hydrogen (“synthesis gas”). Additional hydrogen, together with CO₂, is produced by reacting the carbon monoxide with steam in a second reactor (a “shift reactor”). The resulting mixture of hydrogen and CO₂ can then be separated into a CO₂ gas stream, and a stream of hydrogen. If the CO₂ is stored, the hydrogen is a carbon-free energy carrier that can be combusted to generate power and/or heat. Although the initial fuel conversion steps are more elaborate and costly than in post-combustion systems, the high concentrations of CO₂ produced by the shift reactor (typically 15 to 60% by volume on a dry basis) and the high pressures often encountered in these applications are more favourable for CO₂ separation. Pre-combustion would be used at power plants that employ integrated gasification combined cycle (IGCC) technology.

Oxyfuel combustion systems use oxygen instead of air for combustion of the primary fuel to produce a flue gas that is mainly water vapour and CO₂. This results in a flue gas with

high CO₂ concentrations (greater than 80% by volume). The water vapour is then removed by cooling and compressing the gas stream. Oxyfuel combustion requires the upstream separation of oxygen from air, with a purity of 95–99% oxygen assumed in most current designs. Further treatment of the flue gas may be needed to remove air pollutants and non-condensed gases (such as nitrogen) from the flue gas before the CO₂ is sent to storage. As a method of CO₂ capture in boilers, oxyfuel combustion systems are in the demonstration phase (see Table TS.1). Oxyfuel systems are also being studied in gas turbine systems, but conceptual designs for such applications are still in the research phase.

Figure TS.3 shows a schematic diagram of the main capture processes and systems. All require a step involving the separation of CO₂, H₂ or O₂ from a bulk gas stream (such as flue gas, synthesis gas, air or raw natural gas). These separation steps can be accomplished by means of physical or chemical solvents, membranes, solid sorbents, or by cryogenic separation. The choice of a specific capture technology is determined largely by the process conditions under which it must operate. Current post-combustion and pre-combustion systems for power plants could capture 85–95% of the CO₂ that is produced. Higher capture efficiencies are possible, although separation devices become considerably larger, more energy intensive and more costly. Capture and compression need roughly 10–40% more energy than the equivalent plant without capture, depending on the type of system. Due to the associated CO₂ emissions, the net amount of CO₂ captured is approximately 80–90%. Oxyfuel combustion systems are, in principle, able to capture nearly all of the CO₂ produced. However, the need for additional gas treatment systems to remove pollutants such as sulphur and nitrogen oxides lowers the level of CO₂ captured to slightly more than 90%.

As noted in Section 1, CO₂ capture is already used in several industrial applications (see Figure TS.4). The same technologies as would be used for pre-combustion capture are employed for the large-scale production of hydrogen (which is used mainly for ammonia and fertilizer manufacture, and for petroleum refinery operations). The separation of CO₂ from raw natural gas (which typically contains significant amounts of CO₂) is also practised on a large scale, using technologies similar to those used for post-combustion capture. Although commercial systems are also available for large-scale oxygen separation, oxyfuel combustion for CO₂ capture is currently in the demonstration phase. In addition, research is being conducted to achieve higher levels of system integration, increased efficiency and reduced cost for all types of capture systems.

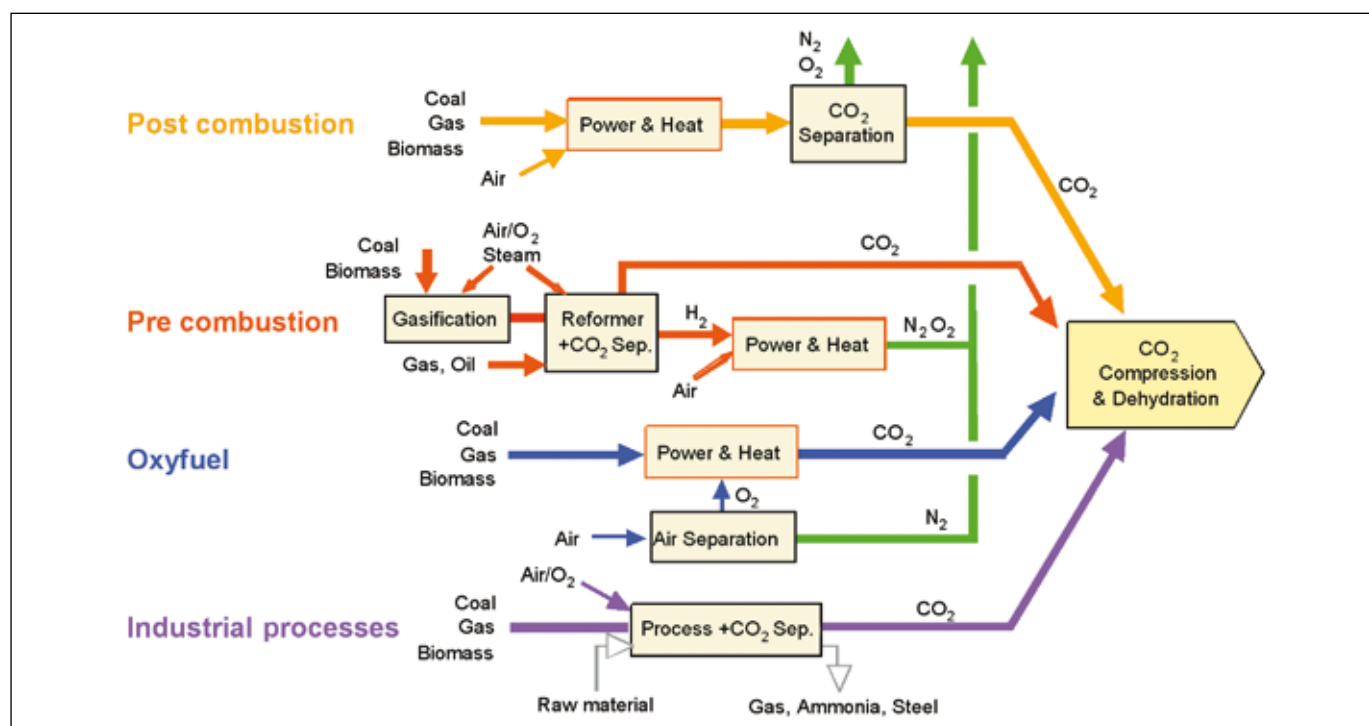


Figure TS.3. Overview of CO₂ capture processes and systems.



Figure TS.4. (a) CO₂ post-combustion capture at a plant in Malaysia. This plant employs a chemical absorption process to separate 0.2 MtCO₂ per year from the flue gas stream of a gas-fired power plant for urea production (Courtesy of Mitsubishi Heavy Industries). (b) CO₂ pre-combustion capture at a coal gasification plant in North Dakota, USA. This plant employs a physical solvent process to separate 3.3 MtCO₂ per year from a gas stream to produce synthetic natural gas. Part of the captured CO₂ is used for an EOR project in Canada.

CO₂ capture: risks, energy and the environment

The monitoring, risk and legal implications of CO₂ capture systems do not appear to present fundamentally new challenges, as they are all elements of regular health, safety and environmental control practices in industry. However, CO₂ capture systems require significant amounts of energy for their operation. This reduces net plant efficiency, so power plants require more fuel to generate each kilowatt-hour of electricity produced. Based on a review of the literature, the increase in fuel consumption per kWh for plants capturing 90% CO₂ using best current technology ranges from 24–40% for new supercritical PC plants, 11–22% for NGCC plants, and 14–25% for coal-based IGCC systems compared to similar plants without CCS. The increased fuel requirement results in an increase in most other environmental emissions per kWh generated relative to new state-of-the-art plants without CO₂ capture and, in the case of coal, proportionally larger amounts of solid wastes. In addition, there is an increase in the consumption of chemicals such as ammonia and limestone used by PC plants for nitrogen oxide and sulphur dioxide emissions control. Advanced plant designs that further reduce CCS energy requirements will also reduce overall environmental impacts as well as cost. Compared to many older existing plants, more efficient new or rebuilt plants with CCS may actually yield net reductions in plant-level environmental emissions.

Costs of CO₂ capture

The estimated costs of CO₂ capture at large power plants are based on engineering design studies of technologies in commercial use today (though often in different applications and/or at smaller scales than those assumed in the literature), as well as on design studies for concepts currently in the research and development (R&D) stage. Table TS.3 summarizes the results for new supercritical PC, NGCC and IGCC plants based on current technology with and without CO₂ capture. Capture systems for all three designs reduce CO₂ emissions per kWh by approximately 80–90%, taking into account the energy requirements for capture. All data for PC and IGCC plants in Table TS.3 are for bituminous coals only. The capture costs include the cost of compressing CO₂ (typically to about 11–14 MPa) but do not include the additional costs of CO₂ transport and storage (see Sections 4–7).

The cost ranges for each of the three systems reflect differences in the technical, economic and operating assumptions employed in different studies. While some differences in reported costs can be attributed to differences in the design of CO₂ capture systems, the major sources of

variability are differences in the assumed design, operation and financing of the reference plant to which the capture technology is applied (factors such as plant size, location, efficiency, fuel type, fuel cost, capacity factor and cost of capital). No single set of assumptions applies to all situations or all parts of the world, so a range of costs is given.

For the studies listed in Table TS.3, CO₂ capture increases the cost of electricity production⁵ by 35–70% (0.01 to 0.02 US\$/kWh) for an NGCC plant, 40–85% (0.02 to 0.03 US\$/kWh) for a supercritical PC plant, and 20–55% (0.01 to 0.02 US\$/kWh) for an IGCC plant. Overall, the electricity production costs for fossil fuel plants with capture (excluding CO₂ transport and storage costs) ranges from 0.04–0.09 US\$/kWh, as compared to 0.03–0.06 US\$/kWh for similar plants without capture. In most studies to date, NGCC systems have typically been found to have lower electricity production costs than new PC and IGCC plants (with or without capture) in the case of large base-load plants with high capacity factors (75% or more) and natural gas prices between 2.6 and 4.4 US\$ GJ⁻¹ over the life of the plant. However, in the case of higher gas prices and/or lower capacity factors, NGCC plants often have higher electricity production costs than coal-based plants, with or without capture. Recent studies also found that IGCC plants were on average slightly more costly without capture and slightly less costly with capture than similarly-sized PC plants. However, the difference in cost between PC and IGCC plants with or without CO₂ capture can vary significantly according to coal type and other local factors, such as the cost of capital for each plant type. Since full-scale NGCC, PC and IGCC systems have not yet been built with CCS, the absolute or relative costs of these systems cannot be stated with a high degree of confidence at this time.

The costs of retrofitting existing power plants with CO₂ capture have not been extensively studied. A limited number of reports indicate that retrofitting an amine scrubber to an existing plant results in greater efficiency loss and higher costs than those shown in Table TS.3. Limited studies also indicate that a more cost-effective option is to combine a capture system retrofit with rebuilding the boiler and turbine to increase plant efficiency and output. For some existing plants, studies indicate that similar benefits could be achieved by repowering with an IGCC system that includes CO₂ capture technology. The feasibility and cost of all these options is highly dependent on site-specific factors, including the size, age and efficiency of the plant, and the availability of additional space.

⁵ The cost of electricity production should not be confused with the price of electricity to customers.

Table TS.3. Summary of CO₂ capture costs for new power plants based on current technology. Because these costs do not include the costs (or credits) for CO₂ transport and storage, this table should not be used to assess or compare total plant costs for different systems with capture. The full costs of CCS plants are reported in Section 8.

Performance and cost measures	New NGCC plant			New PC plant			New IGCC plant		
	Range		Rep. value	Range		Rep. value	Range		Rep. value
	Low	High		Low	High		Low	High	
Emission rate without capture (kgCO ₂ /kWh)	0.344	- 0.379	0.367	0.736	- 0.811	0.762	0.682	- 0.846	0.773
Emission rate with capture (kgCO ₂ /kWh)	0.040	- 0.066	0.052	0.092	- 0.145	0.112	0.065	- 0.152	0.108
Percentage CO ₂ reduction per kWh (%)	83	- 88	86	81	- 88	85	81	- 91	86
Plant efficiency with capture, LHV basis (%)	47	- 50	48	30	- 35	33	31	- 40	35
Capture energy requirement (% increase input/kWh)	11	- 22	16	24	- 40	31	14	- 25	19
Total capital requirement without capture (US\$/kW)	515	- 724	568	1161	- 1486	1286	1169	- 1565	1326
Total capital requirement with capture (US\$/kW)	909	- 1261	998	1894	- 2578	2096	1414	- 2270	1825
Percent increase in capital cost with capture (%)	64	- 100	76	44	- 74	63	19	- 66	37
COE without capture (US\$/kWh)	0.031	- 0.050	0.037	0.043	- 0.052	0.046	0.041	- 0.061	0.047
COE with capture only (US\$/kWh)	0.043	- 0.072	0.054	0.062	- 0.086	0.073	0.054	- 0.079	0.062
Increase in COE with capture (US\$/kWh)	0.012	- 0.024	0.017	0.018	- 0.034	0.027	0.009	- 0.022	0.016
Percent increase in COE with capture (%)	37	- 69	46	42	- 66	57	20	- 55	33
Cost of net CO ₂ captured (US\$/tCO ₂)	37	- 74	53	29	- 51	41	13	- 37	23
Capture cost confidence level (see Table 3.6)	moderate			moderate			moderate		

Abbreviations: Representative value is based on the average of the values in the different studies. COE=cost of electricity production; LHV=lower heating value. See Section 3.6.1 for calculation of energy requirement for capture plants.

Notes: Ranges and representative values are based on data from Special Report Tables 3.7, 3.9 and 3.10. All PC and IGCC data are for bituminous coals only at costs of 1.0–1.5 US\$ GJ⁻¹ (LHV); all PC plants are supercritical units. NGCC data based on natural gas prices of 2.8–4.4 US\$ GJ⁻¹ (LHV basis). Cost are stated in constant US\$2002. Power plant sizes range from approximately 400–800 MW without capture and 300–700 MW with capture. Capacity factors vary from 65–85% for coal plants and 50–95% for gas plants (average for each=80%). Fixed charge factors vary from 11–16%. All costs include CO₂ compression but not additional CO₂ transport and storage costs.

Table TS.4 illustrates the cost of CO₂ capture in the production of hydrogen. Here, the cost of CO₂ capture is mainly due to the cost of CO₂ drying and compression, since CO₂ separation is already carried out as part of the hydrogen production process. The cost of CO₂ capture adds approximately 5% to 30% to the cost of the hydrogen produced.

CCS also can be applied to systems that use biomass fuels or feedstock, either alone or in combination with fossil fuels. A limited number of studies have looked at the costs of such systems combining capture, transport and storage. The capturing of 0.19 MtCO₂ yr⁻¹ in a 24 MWe biomass IGCC plant is estimated to be about 80 US\$/tCO₂ net captured (300

US\$/tC), which corresponds to an increase in electricity production costs of about 0.08 US\$/kWh. There are relatively few studies of CO₂ capture for other industrial processes using fossil fuels and they are typically limited to capture costs reported only as a cost per tonne of CO₂ captured or avoided. In general, the CO₂ produced in different processes varies widely in pressure and concentration (see Section 2). As a result, the cost of capture in different processes (cement and steel plants, refineries), ranges widely from about 25–115 US\$/tCO₂ net captured. The unit cost of capture is generally lower for processes where a relatively pure CO₂ stream is produced (e.g. natural gas processing, hydrogen production and ammonia production), as seen for the hydrogen plants

Table TS.4. Summary of CO₂ capture costs for new hydrogen plants based on current technology

Performance and cost measures	New hydrogen plant			
	Range		Representative value	
	Low	High		
Emission rate without capture (kgCO ₂ GJ ⁻¹)	78	- 174		137
Emission rate with capture (kgCO ₂ GJ ⁻¹)	7	- 28		17
Percent CO ₂ reduction per GJ (%)	72	- 96		86
Plant efficiency with capture, LHV basis (%)	52	- 68		60
Capture energy requirement (% more input GJ ⁻¹)	4	- 22		8
Cost of hydrogen without capture (US\$ GJ ⁻¹)	6.5	- 10.0		7.8
Cost of hydrogen with capture (US\$ GJ ⁻¹)	7.5	- 13.3		9.1
Increase in H ₂ cost with capture (US\$ GJ ⁻¹)	0.3	- 3.3		1.3
Percent increase in H ₂ cost with capture (%)	5	- 33		15
Cost of net CO ₂ captured (US\$/tCO ₂)	2	- 56		15
Capture cost confidence level	moderate to high			

Notes: Ranges and representative values are based on data from Table 3.11. All costs in this table are for capture only and do not include the costs of CO₂ transport and storage. Costs are in constant US\$2002. Hydrogen plant feedstocks are natural gas (4.7-5.3 US\$ GJ⁻¹) or coal (0.9-1.3 US\$ GJ⁻¹); some plants in dataset produce electricity in addition to hydrogen. Fixed charge factors vary from 13-20%. All costs include CO₂ compression but not additional CO₂ transport and storage costs (see Section 8 for full CCS costs).

in Table TS.4, where costs vary from 2–56 US\$/tCO₂ net captured.

New or improved methods of CO₂ capture, combined with advanced power systems and industrial process designs, could reduce CO₂ capture costs and energy requirements. While costs for first-of-a-kind commercial plants often exceed initial cost estimates, the cost of subsequent plants typically declines as a result of learning-by-doing and other factors. Although there is considerable uncertainty about the magnitude and timing of future cost reductions, the literature suggests that, provided R&D efforts are sustained, improvements to commercial technologies can reduce current CO₂ capture costs by at least 20–30% over approximately the next ten years, while new technologies under development could achieve more substantial cost reductions. Future cost reductions will depend on the deployment and adoption of commercial technologies in the marketplace as well as sustained R&D.

4. Transport of CO₂

Except when plants are located directly above a geological storage site, captured CO₂ must be transported from the point of capture to a storage site. This section reviews the principal

methods of CO₂ transport and assesses the health, safety and environment aspects, and costs.

Methods of CO₂ transport

Pipelines today operate as a mature market technology and are the most common method for transporting CO₂. Gaseous CO₂ is typically compressed to a pressure above 8 MPa in order to avoid two-phase flow regimes and increase the density of the CO₂, thereby making it easier and less costly to transport. CO₂ also can be transported as a liquid in ships, road or rail tankers that carry CO₂ in insulated tanks at a temperature well below ambient, and at much lower pressures.

The first long-distance CO₂ pipeline came into operation in the early 1970s. In the United States, over 2,500 km of pipeline transports more than 40 MtCO₂ per year from natural and anthropogenic sources, mainly to sites in Texas, where the CO₂ is used for EOR. These pipelines operate in the ‘dense phase’ mode (in which there is a continuous progression from gas to liquid, without a distinct phase change), and at ambient temperature and high pressure. In most of these pipelines, the flow is driven by compressors at the upstream end, although some pipelines have intermediate (booster) compressor stations.

In some situations or locations, transport of CO₂ by ship may be economically more attractive, particularly when the CO₂ has to be moved over large distances or overseas. Liquefied petroleum gases (LPG, principally propane and butane) are transported on a large commercial scale by marine tankers. CO₂ can be transported by ship in much the same way (typically at 0.7 MPa pressure), but this currently takes place on a small scale because of limited demand. The properties of liquefied CO₂ are similar to those of LPG, and the technology could be scaled up to large CO₂ carriers if a demand for such systems were to materialize.

Road and rail tankers also are technically feasible options. These systems transport CO₂ at a temperature of -20°C and at 2 MPa pressure. However, they are uneconomical compared to pipelines and ships, except on a very small scale, and are unlikely to be relevant to large-scale CCS.

Environment, safety and risk aspects

Just as there are standards for natural gas admitted to pipelines, so minimum standards for 'pipeline quality' CO₂ should emerge as the CO₂ pipeline infrastructure develops further. Current standards, developed largely in the context of EOR applications, are not necessarily identical to what would be required for CCS. A low-nitrogen content is important for EOR, but would not be so significant for CCS. However, a CO₂ pipeline through populated areas might need a lower specified maximum H₂S content. Pipeline transport of CO₂ through populated areas also requires detailed route selection, over-pressure protection, leak detection and other design factors. However, no major obstacles to pipeline design for CCS are foreseen.

CO₂ could leak to the atmosphere during transport, although leakage losses from pipelines are very small. Dry (moisture-free) CO₂ is not corrosive to the carbon-manganese steels customarily used for pipelines, even if the CO₂ contains contaminants such as oxygen, hydrogen sulphide, and sulphur or nitrogen oxides. Moisture-laden CO₂, on the other hand, is highly corrosive, so a CO₂ pipeline in this case would have to be made from a corrosion-resistant alloy, or be internally clad with an alloy or a continuous polymer coating. Some pipelines are made from corrosion-resistant alloys, although the cost of materials is several times larger than carbon-manganese steels. For ships, the total loss to the atmosphere is between 3 and 4% per 1000 km, counting both boil-off and the exhaust from ship engines. Boil-off could be reduced by capture and liquefaction, and recapture would reduce the loss to 1 to 2% per 1000 km.

Accidents can also occur. In the case of existing CO₂ pipelines, which are mostly in areas of low population density, there have been fewer than one reported incident per year (0.0003 per km-year) and no injuries or fatalities. This is consistent with experience with hydrocarbon pipelines,

and the impact would probably not be more severe than for natural gas accidents. In marine transportation, hydrocarbon gas tankers are potentially dangerous, but the recognized hazard has led to standards for design, construction and operation, and serious incidents are rare.

Cost of CO₂ transport

Costs have been estimated for both pipeline and marine transportation of CO₂. In every case the costs depend strongly on the distance and the quantity transported. In the case of pipelines, the costs depend on whether the pipeline is onshore or offshore, whether the area is heavily congested, and whether there are mountains, large rivers, or frozen ground on the route. All these factors could double the cost per unit length, with even larger increases for pipelines in populated areas. Any additional costs for recompression (booster pump stations) that may be needed for longer pipelines would be counted as part of transport costs. Such costs are relatively small and not included in the estimates presented here.

Figure TS.5 shows the cost of pipeline transport for a nominal distance of 250 km. This is typically 1–8 US\$/tCO₂ (4–30 US\$/tC). The figure also shows how pipeline cost depends on the CO₂ mass flow rate. Steel cost accounts for a significant fraction of the cost of a pipeline, so fluctuations in such cost (such as the doubling in the years from 2003 to 2005) could affect overall pipeline economics.

In ship transport, the tanker volume and the characteristics of the loading and unloading systems are some of the key factors determining the overall transport cost.

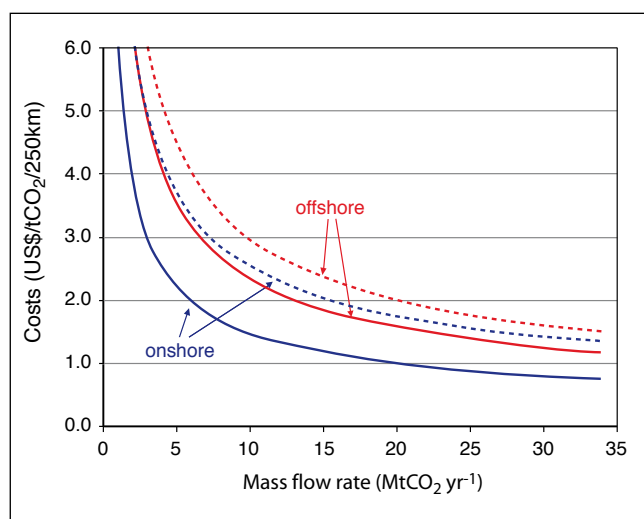


Figure TS.5. Transport costs for onshore pipelines and offshore pipelines, in US\$ per tCO₂ per 250 km as a function of the CO₂ mass flow rate. The graph shows high estimates (dotted lines) and low estimates (solid lines).

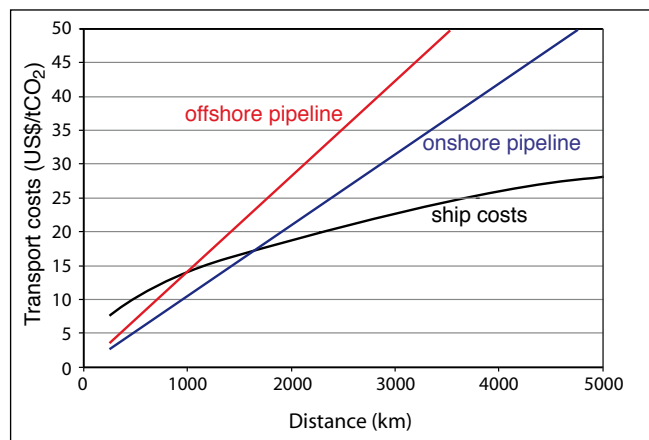


Figure TS.6. Costs, plotted as US\$/tCO₂ transported against distance, for onshore pipelines, offshore pipelines and ship transport. Pipeline costs are given for a mass flow of 6 MtCO₂ yr⁻¹. Ship costs include intermediate storage facilities, harbour fees, fuel costs, and loading and unloading activities. Costs include also additional costs for liquefaction compared to compression.

The costs associated with CO₂ compression and liquefaction are accounted for in the capture costs presented earlier. Figure TS.6 compares pipeline and marine transportation costs, and shows the break-even distance. If the marine option is available, it is typically cheaper than pipelines for distances greater than approximately 1000 km and for amounts smaller than a few million tonnes of CO₂ per year. In ocean storage the most suitable transport system depends on the injection method: from a stationary floating vessel, a moving ship, or a pipeline from shore.

5. Geological storage

This section examines three types of geological formations that have received extensive consideration for the geological storage of CO₂: oil and gas reservoirs, deep saline formations and unminable coal beds (Figure TS.7). In each case, geological storage of CO₂ is accomplished by injecting it in dense form into a rock formation below the earth's surface. Porous rock formations that hold or (as in the case of depleted oil and gas reservoirs) have previously held fluids, such as natural gas, oil or brines, are potential candidates for CO₂ storage. Suitable storage formations can occur in both onshore and offshore sedimentary basins (natural large-scale depressions in the earth's crust that are filled with sediments). Coal beds also may be used for storage of CO₂ (see Figure TS.7) where it is unlikely that the coal will later be mined and provided that permeability is sufficient. The option of storing CO₂ in coal beds and enhancing methane production is still in the demonstration phase (see Table TS.1).

Existing CO₂ storage projects

Geological storage of CO₂ is ongoing in three industrial-scale projects (projects in the order of 1 MtCO₂ yr⁻¹ or more): the Sleipner project in the North Sea, the Weyburn project in Canada and the In Salah project in Algeria. About 3–4 MtCO₂ that would otherwise be released to the atmosphere is captured and stored annually in geological formations. Additional projects are listed in Table TS.5.

In addition to the CCS projects currently in place, 30 MtCO₂ is injected annually for EOR, mostly in Texas, USA, where EOR commenced in the early 1970s. Most of this CO₂ is obtained from natural CO₂ reservoirs found in western regions of the US, with some coming from anthropogenic sources such as natural gas processing. Much of the CO₂ injected for EOR is produced with the oil, from which it is separated and then reinjected. At the end of the oil recovery, the CO₂ can be retained for the purpose of climate change mitigation, rather than vented to the atmosphere. This is planned for the Weyburn project.

Storage technology and mechanisms

The injection of CO₂ in deep geological formations involves many of the same technologies that have been developed in the oil and gas exploration and production industry. Well-drilling technology, injection technology, computer simulation of storage reservoir dynamics and monitoring methods from existing applications are being developed further for design and operation of geological storage. Other underground injection practices also provide relevant operational experience. In particular, natural gas storage, the deep injection of liquid wastes, and acid gas disposal (mixtures of CO₂ and H₂S) have been conducted in Canada and the U.S. since 1990, also at the megatonne scale.

CO₂ storage in hydrocarbon reservoirs or deep saline formations is generally expected to take place at depths below 800 m, where the ambient pressures and temperatures will usually result in CO₂ being in a liquid or supercritical state. Under these conditions, the density of CO₂ will range from 50 to 80% of the density of water. This is close to the density of some crude oils, resulting in buoyant forces that tend to drive CO₂ upwards. Consequently, a well-sealed cap rock over the selected storage reservoir is important to ensure that CO₂ remains trapped underground. When injected underground, the CO₂ compresses and fills the pore space by partially displacing the fluids that are already present (the 'in situ fluids'). In oil and gas reservoirs, the displacement of in situ fluids by injected CO₂ can result in most of the pore volume being available for CO₂ storage. In saline formations, estimates of potential storage volume are lower, ranging from as low as a few percent to over 30% of the total rock volume.

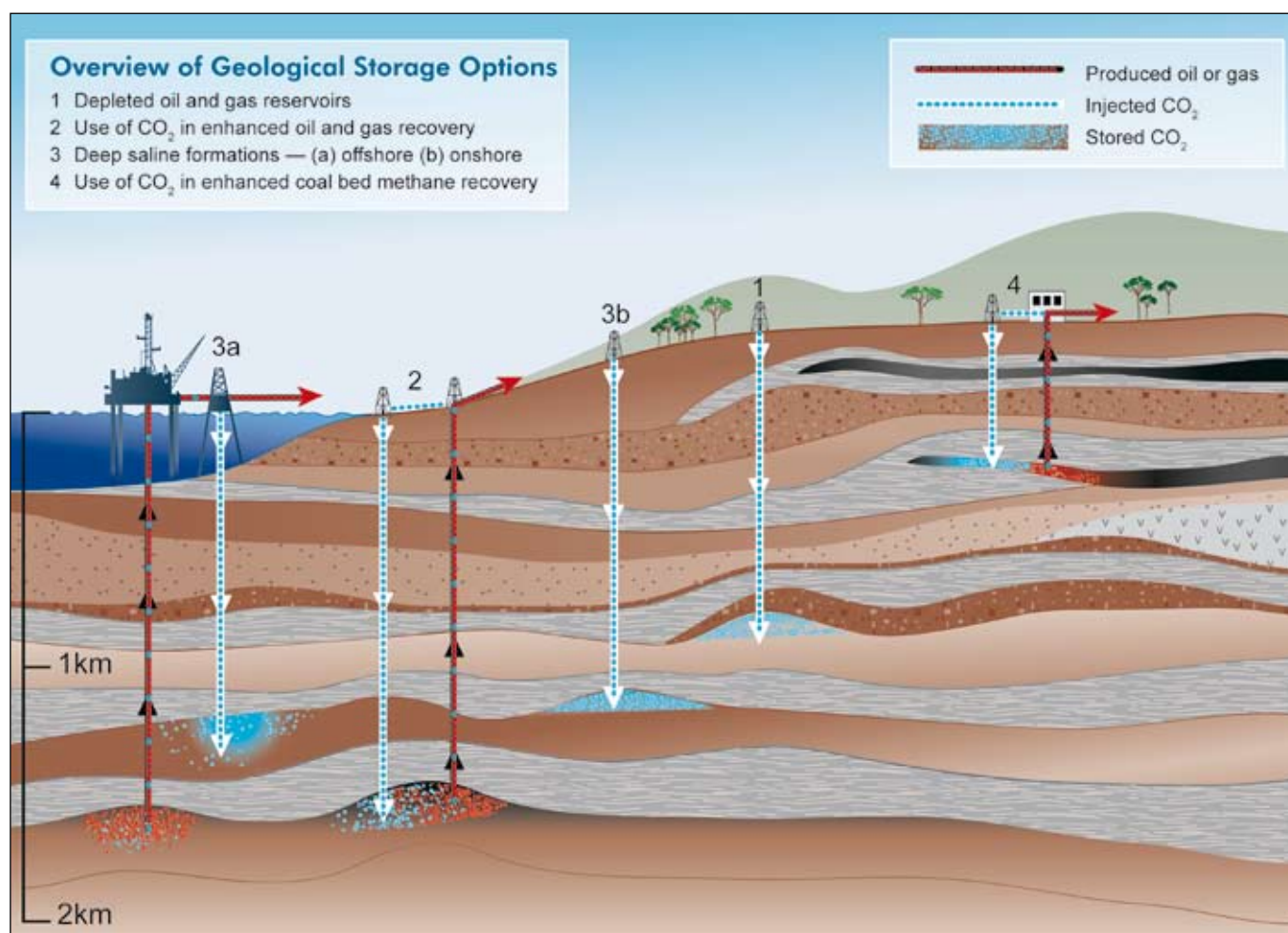


Figure TS.7. Methods for storing CO₂ in deep underground geological formations. Two methods may be combined with the recovery of hydrocarbons: EOR (2) and ECBM (4). See text for explanation of these methods (Courtesy CO2CRC).

Once injected into the storage formation, the fraction retained depends on a combination of physical and geochemical trapping mechanisms. Physical trapping to block upward migration of CO₂ is provided by a layer of shale and clay rock above the storage formation. This impermeable layer is known as the “cap rock”. Additional physical trapping can be provided by capillary forces that retain CO₂ in the pore spaces of the formation. In many cases, however, one or more sides of the formation remain open, allowing for lateral migration of CO₂ beneath the cap rock. In these cases, additional mechanisms are important for the long-term entrapment of the injected CO₂.

The mechanism known as geochemical trapping occurs as the CO₂ reacts with the in situ fluids and host rock. First, CO₂ dissolves in the in situ water. Once this occurs (over time scales of hundreds of years to thousands of years), the CO₂-laden water becomes more dense and therefore sinks down into the formation (rather than rising toward the surface).

Next, chemical reactions between the dissolved CO₂ and rock minerals form ionic species, so that a fraction of the injected CO₂ will be converted to solid carbonate minerals over millions of years.

Yet another type of trapping occurs when CO₂ is preferentially adsorbed onto coal or organic-rich shales replacing gases such as methane. In these cases, CO₂ will remain trapped as long as pressures and temperatures remain stable. These processes would normally take place at shallower depths than CO₂ storage in hydrocarbon reservoirs and saline formations.

Geographical distribution and capacity of storage sites

As shown earlier in Section 2 (Figure TS.2b), regions with sedimentary basins that are potentially suitable for CO₂ storage exist around the globe, both onshore and offshore. This report focuses on oil and gas reservoirs, deep saline

Table TS.5. Sites where CO₂ storage has been done, is currently in progress or is planned, varying from small pilots to large-scale commercial applications.

Project name	Country	Injection start (year)	Approximate average daily injection rate (tCO ₂ day ⁻¹)	Total (planned) storage (tCO ₂)	Storage reservoir type
Weyburn	Canada	2000	3,000-5,000	20,000,000	EOR
In Salah	Algeria	2004	3,000-4,000	17,000,000	Gas field
Sleipner	Norway	1996	3,000	20,000,000	Saline formation
K12B	Netherlands	2004	100 (1,000 planned for 2006+)	8,000,000	Enhanced gas recovery
Frio	U.S.A	2004	177	1600	Saline formation
Fenn Big Valley	Canada	1998	50	200	ECBM
Qinshui Basin	China	2003	30	150	ECBM
Yubari	Japan	2004	10	200	ECBM
Recopol	Poland	2003	1	10	ECBM
Gorgon (planned)	Australia	~2009	10,000	unknown	Saline formation
Snøhvit (planned)	Norway	2006	2,000	unknown	Saline formation

formations and unminable coal beds. Other possible geological formations or structures (such as basalts, oil or gas shales, salt caverns and abandoned mines) represent niche opportunities, or have been insufficiently studied at this time to assess their potential.

The estimates of the technical potential⁶ for different geological storage options are summarized in Table TS.6. The estimates and levels of confidence are based on an assessment of the literature, both of regional bottom-up, and global top-down estimates. No probabilistic approach to assessing capacity estimates exists in the literature, and this would be required to quantify levels of uncertainty reliably. Overall estimates, particularly of the upper limit of the potential, vary widely and involve a high degree of uncertainty, reflecting conflicting methodologies in the literature and the fact that our knowledge of saline formations is quite limited in most parts of the world. For oil and gas reservoirs, better estimates are available which are based on the replacement of hydrocarbon volumes with CO₂ volumes. It should be noted that, with the exception of EOR, these reservoirs will not be available for CO₂ storage until the hydrocarbons are depleted, and that pressure changes and geomechanical effects due to hydrocarbon production in the reservoir may reduce actual capacity.

Another way of looking at storage potential, however, is to ask whether it is likely to be adequate for the amounts of CO₂ that would need to be avoided using CCS under different

greenhouse gas stabilization scenarios and assumptions about the deployment of other mitigation options. As discussed later in Section 8, the estimated range of economic potential⁷ for CCS over the next century is roughly 200 to 2,000 GtCO₂. The lower limits in Table TS.6 suggest that, worldwide, it is virtually certain⁸ that there is 200 GtCO₂ of geological storage capacity, and likely⁹ that there is at least about 2,000 GtCO₂.

Site selection criteria and methods

Site characterization, selection and performance prediction are crucial for successful geological storage. Before selecting a site, the geological setting must be characterized to determine if the overlying cap rock will provide an effective seal, if there is a sufficiently voluminous and permeable storage formation, and whether any abandoned or active wells will compromise the integrity of the seal.

Techniques developed for the exploration of oil and gas reservoirs, natural gas storage sites and liquid waste disposal sites are suitable for characterizing geological storage sites for CO₂. Examples include seismic imaging, pumping tests for evaluating storage formations and seals, and cement integrity logs. Computer programmes that model underground CO₂ movement are used to support site characterization and selection activities. These programmes were initially developed for applications such as oil and

⁶ Technical potential is the amount by which it is possible to reduce greenhouse gas emissions by implementing a technology or practice that already has been demonstrated.

⁷ Economic potential is the amount of greenhouse gas emissions reductions from a specific option that could be achieved cost-effectively, given prevailing circumstances (the price of CO₂ reductions and costs of other options).

⁸ "Virtually certain" is a probability of 99% or more.

⁹ "Likely" is a probability of 66 to 90%.

Table TS.6. Storage capacity for several geological storage options. The storage capacity includes storage options that are not economical.

Reservoir type	Lower estimate of storage capacity (GtCO ₂)	Upper estimate of storage capacity (GtCO ₂)
Oil and gas fields	675 ^a	900 ^a
Unminable coal seams (ECBM)	3-15	200
Deep saline formations	1,000	Uncertain, but possibly 10 ⁴

^a These numbers would increase by 25% if ‘undiscovered’ oil and gas fields were included in this assessment.

gas reservoir engineering and groundwater resources investigations. Although they include many of the physical, chemical and geomechanical processes needed to predict both short-term and long-term performance of CO₂ storage, more experience is needed to establish confidence in their effectiveness in predicting long-term performance when adapted for CO₂ storage. Moreover, the availability of good site characterization data is critical for the reliability of models.

Risk assessment and environmental impact

The risks due to leakage from storage of CO₂ in geological reservoirs fall into two broad categories: global risks and local risks. Global risks involve the release of CO₂ that may contribute significantly to climate change if some fraction leaks from the storage formation to the atmosphere. In addition, if CO₂ leaks out of a storage formation, local hazards may exist for humans, ecosystems and groundwater. These are the local risks.

With regard to global risks, based on observations and analysis of current CO₂ storage sites, natural systems, engineering systems and models, the fraction retained in appropriately selected and managed reservoirs is very likely¹⁰ to exceed 99% over 100 years, and is likely to exceed 99% over 1000 years. Similar fractions retained are likely for even longer periods of time, as the risk of leakage is expected to decrease over time as other mechanisms provide additional trapping. The question of whether these fractions retained would be sufficient to make impermanent storage valuable for climate change mitigation is discussed in Section 8.

With regard to local risks, there are two types of scenarios in which leakage may occur. In the first case, injection well failures or leakage up abandoned wells could create a sudden and rapid release of CO₂. This type of release is likely to be detected quickly and stopped using techniques that are available today for containing well blow-outs. Hazards associated with this type of release primarily affect workers in the vicinity of the release at the time it occurs, or those called in to control the blow-out. A concentration of CO₂ greater

than 7–10% in air would cause immediate dangers to human life and health. Containing these kinds of releases may take hours to days and the overall amount of CO₂ released is likely to be very small compared to the total amount injected. These types of hazards are managed effectively on a regular basis in the oil and gas industry using engineering and administrative controls.

In the second scenario, leakage could occur through undetected faults, fractures or through leaking wells where the release to the surface is more gradual and diffuse. In this case, hazards primarily affect drinking-water aquifers and ecosystems where CO₂ accumulates in the zone between the surface and the top of the water table. Groundwater can be affected both by CO₂ leaking directly into an aquifer and by brines that enter the aquifer as a result of being displaced by CO₂ during the injection process. There may also be acidification of soils and displacement of oxygen in soils in this scenario. Additionally, if leakage to the atmosphere were to occur in low-lying areas with little wind, or in swamps and basements overlying these diffuse leaks, humans and animals would be harmed if a leak were to go undetected. Humans would be less affected by leakage from offshore storage locations than from onshore storage locations. Leakage routes can be identified by several techniques and by characterization of the reservoir. Figure TS.8 shows some of the potential leakage paths for a saline formation. When the potential leakage routes are known, the monitoring and remediation strategy can be adapted to address the potential leakage.

Careful storage system design and siting, together with methods for early detection of leakage (preferably long before CO₂ reaches the land surface), are effective ways of reducing hazards associated with diffuse leakage. The available monitoring methods are promising, but more experience is needed to establish detection levels and resolution. Once leakages are detected, some remediation techniques are available to stop or control them. Depending on the type of leakage, these techniques could involve standard well repair techniques, or the extraction of CO₂ by intercepting its leak into a shallow groundwater aquifer (see Figure TS.8).

¹⁰ “Very likely” is a probability of 90 to 99%.

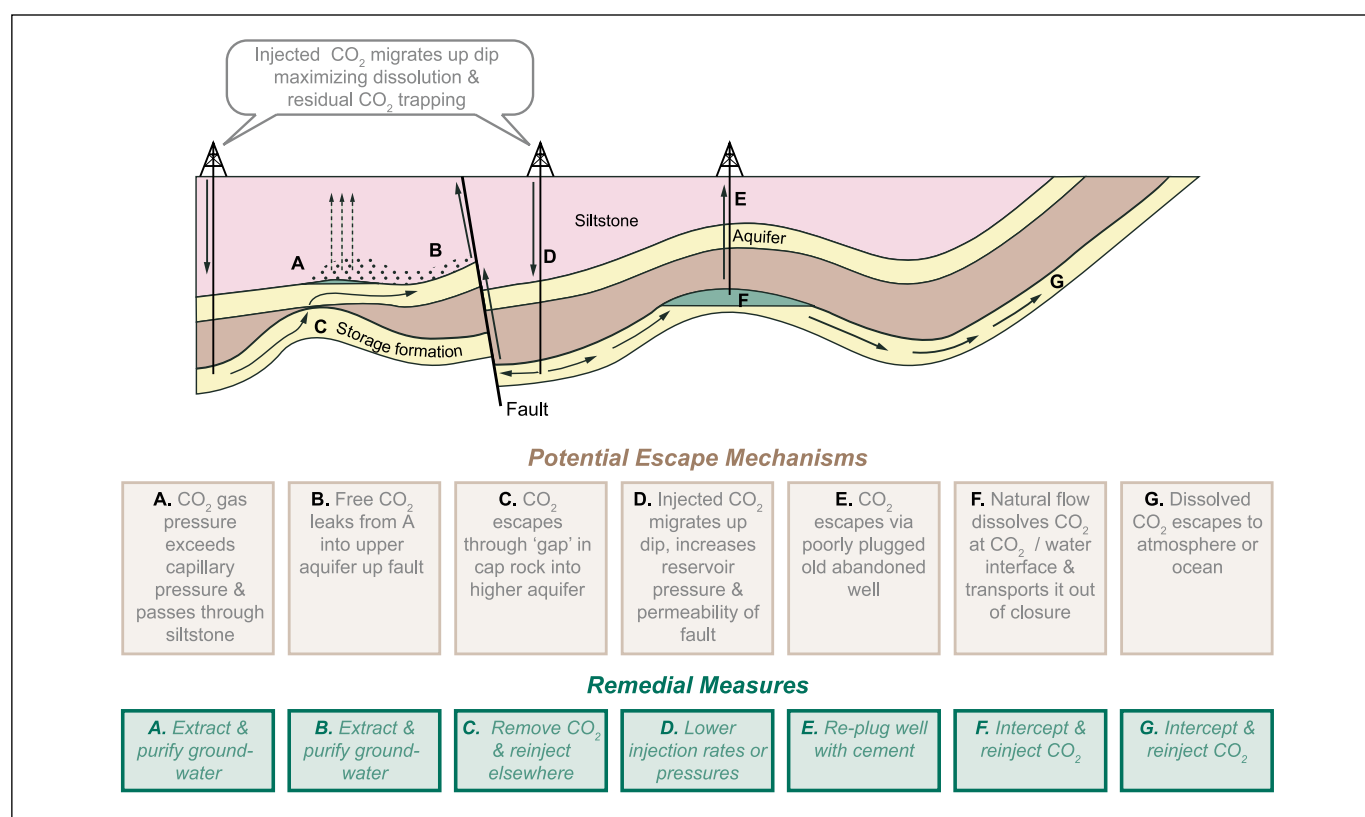


Figure TS.8. Potential leakage routes and remediation techniques for CO₂ injected into saline formations. The remediation technique would depend on the potential leakage routes identified in a reservoir (Courtesy CO₂CRC).

Techniques to remove CO₂ from soils and groundwater are also available, but they are likely to be costly. Experience will be needed to demonstrate the effectiveness, and ascertain the costs, of these techniques for use in CO₂ storage.

Monitoring and verification

Monitoring is a very important part of the overall risk management strategy for geological storage projects. Standard procedures or protocols have not been developed yet but they are expected to evolve as technology improves, depending on local risks and regulations. However, it is expected that some parameters such as injection rate and injection well pressure will be measured routinely. Repeated seismic surveys have been shown to be useful for tracking the underground migration of CO₂. Newer techniques such as gravity and electrical measurements may also be useful. The sampling of groundwater and the soil between the surface and water table may be useful for directly detecting CO₂ leakage. CO₂ sensors with alarms can be located at the injection wells for ensuring worker safety and to detect leakage. Surface-based techniques may also be used for detecting and quantifying surface releases. High-quality baseline data improve the

reliability and resolution of all measurements and will be essential for detecting small rates of leakage.

Since all of these monitoring techniques have been adapted from other applications, they need to be tested and assessed with regard to reliability, resolution and sensitivity in the context of geological storage. All of the existing industrial-scale projects and pilot projects have programmes to develop and test these and other monitoring techniques. Methods also may be necessary or desirable to monitor the amount of CO₂ stored underground in the context of emission reporting and monitoring requirements in the UNFCCC (see Section 9). Given the long-term nature of CO₂ storage, site monitoring may be required for very long periods.

Legal issues

At present, few countries have specifically developed legal and regulatory frameworks for onshore CO₂ storage. Relevant legislation include petroleum-related legislation, drinking-water legislation and mining regulations. In many cases, there are laws applying to some, if not most, of the issues related to CO₂ storage. Specifically, long-term liability issues, such as global issues associated with the

leakage of CO₂ to the atmosphere, as well as local concerns about environmental impact, have not yet been addressed. Monitoring and verification regimes and risks of leakage may play an important role in determining liability, and vice-versa. There are also considerations such as the longevity of institutions, ongoing monitoring and transferability of institutional knowledge. The long-term perspective is essential to a legal framework for CCS as storage times extend over many generations as does the climate change problem. In some countries, notably the US, the property rights of all those affected must be considered in legal terms as pore space is owned by surface property owners.

According to the general principles of customary international law, States can exercise their sovereignty in their territories and could therefore engage in activities such as the storage of CO₂ (both geological and ocean) in those areas under their jurisdiction. However, if storage has a transboundary impact, States have the responsibility to ensure that activities within their jurisdiction or control do not cause damage to the environment of other States or of areas beyond the limits of national jurisdiction.

Currently, there are several treaties (notably the UN Convention on the Law of the Sea, and the London¹¹ and OSPAR¹² Conventions) that could apply to the offshore injection of CO₂ into marine environments (both into the ocean and the geological sub-seabed). All these treaties have been drafted without specific consideration of CO₂ storage. An assessment undertaken by the Jurists and Linguists Group to the OSPAR Convention (relating to the northeast Atlantic region), for example, found that, depending on the method and purpose of injection, CO₂ injection into the geological sub-seabed and the ocean could be compatible with the treaty in some cases, such as when the CO₂ is transported via a pipeline from land. A similar assessment is now being conducted by Parties to the London Convention. Furthermore, papers by legal commentators have concluded that CO₂ captured from an oil or natural gas extraction operation and stored offshore in a geological formation (like the Sleipner operation) would not be considered ‘dumping’ under, and would not therefore be prohibited by, the London Convention.

Public perception

Assessing public perception of CCS is challenging because of the relatively technical and “remote” nature of this issue at the present time. Results of the very few studies conducted to date about the public perception of CCS indicate that the public is generally not well informed about CCS. If

information is given alongside information about other climate change mitigation options, the handful of studies carried out so far indicate that CCS is generally regarded as less favourable than other options, such as improvements in energy efficiency and the use of non-fossil energy sources. Acceptance of CCS, where it occurs, is characterized as “reluctant” rather than “enthusiastic”. In some cases, this reflects the perception that CCS might be required because of a failure to reduce CO₂ emissions in other ways. There are indications that geological storage could be viewed favourably if it is adopted in conjunction with more desirable measures. Although public perception is likely to change in the future, the limited research to date indicates that at least two conditions may have to be met before CO₂ capture and storage is considered by the public as a credible technology, alongside other better known options: (1) anthropogenic global climate change has to be regarded as a relatively serious problem; (2) there must be acceptance of the need for large reductions in CO₂ emissions to reduce the threat of global climate change.

Cost of geological storage

The technologies and equipment used for geological storage are widely used in the oil and gas industries so cost estimates for this option have a relatively high degree of confidence for storage capacity in the lower range of technical potential. However, there is a significant range and variability of costs due to site-specific factors such as onshore versus offshore, reservoir depth and geological characteristics of the storage formation (e.g., permeability and formation thickness).

Representative estimates of the cost for storage in saline formations and depleted oil and gas fields are typically between 0.5–8 US\$/tCO₂ injected. Monitoring costs of 0.1–0.3 US\$/tCO₂ are additional. The lowest storage costs are for onshore, shallow, high permeability reservoirs, and/or storage sites where wells and infrastructure from existing oil and gas fields may be re-used.

When storage is combined with EOR, ECBM or (potentially) Enhanced Gas Recovery (EGR), the economic value of CO₂ can reduce the total cost of CCS. Based on data and oil prices prior to 2003, enhanced oil production for onshore EOR with CO₂ storage could yield net benefits of 10–16 US\$/tCO₂ (37–59 US\$/tC) (including the costs of geological storage). For EGR and ECBM, which are still under development, there is no reliable cost information based on actual experience. In all cases, however, the economic benefit of enhanced production

¹¹ Convention on the Prevention of Marine Pollution by Dumping of Wastes and Other Matter (1972), and its London Protocol (1996), which has not yet entered into force.

¹² Convention for the Protection of the Marine Environment of the North-East Atlantic, which was adopted in Paris (1992). OSPAR is an abbreviation of Oslo-Paris.

depends strongly on oil and gas prices. In this regard, the literature basis for this report does not take into account the rise in world oil and gas prices since 2003 and assumes oil prices of 15–20 US\$ per barrel. Should higher prices be sustained over the life of a CCS project, the economic value of CO₂ could be higher than that reported here.

6. Ocean storage

A potential CO₂ storage option is to inject captured CO₂ directly into the deep ocean (at depths greater than 1,000 m), where most of it would be isolated from the atmosphere for centuries. This can be achieved by transporting CO₂ via pipelines or ships to an ocean storage site, where it is injected into the water column of the ocean or at the sea floor. The dissolved and dispersed CO₂ would subsequently become part of the global carbon cycle. Figure TS.9 shows some of the main methods that could be employed. Ocean storage has not yet been deployed or demonstrated at a pilot scale, and is still in the research phase. However, there have been small-scale field experiments and 25 years of theoretical, laboratory and modelling studies of intentional ocean storage of CO₂.

Storage mechanisms and technology

Oceans cover over 70% of the earth's surface and their average depth is 3,800 m. Because carbon dioxide is soluble in water, there are natural exchanges of CO₂ between the atmosphere and waters at the ocean surface that occur until equilibrium is reached. If the atmospheric concentration of CO₂ increases, the ocean gradually takes up additional CO₂. In this way, the oceans have taken up about 500 GtCO₂ (140 GtC) of the total 1,300 GtCO₂ (350 GtC) of anthropogenic emissions released to the atmosphere over the past 200 years. As a result of the increased atmospheric CO₂ concentrations from human activities relative to pre-industrial levels, the oceans are currently taking up CO₂ at a rate of about 7 GtCO₂ yr⁻¹ (2 GtC yr⁻¹).

Most of this carbon dioxide now resides in the upper ocean and thus far has resulted in a decrease in pH of about 0.1 at the ocean surface because of the acidic nature of CO₂ in water. To date, however, there has been virtually no change in pH in the deep ocean. Models predict that over the next several centuries the oceans will eventually take up most of the CO₂ released to the atmosphere as CO₂ is dissolved at the ocean surface and subsequently mixed with deep ocean waters.

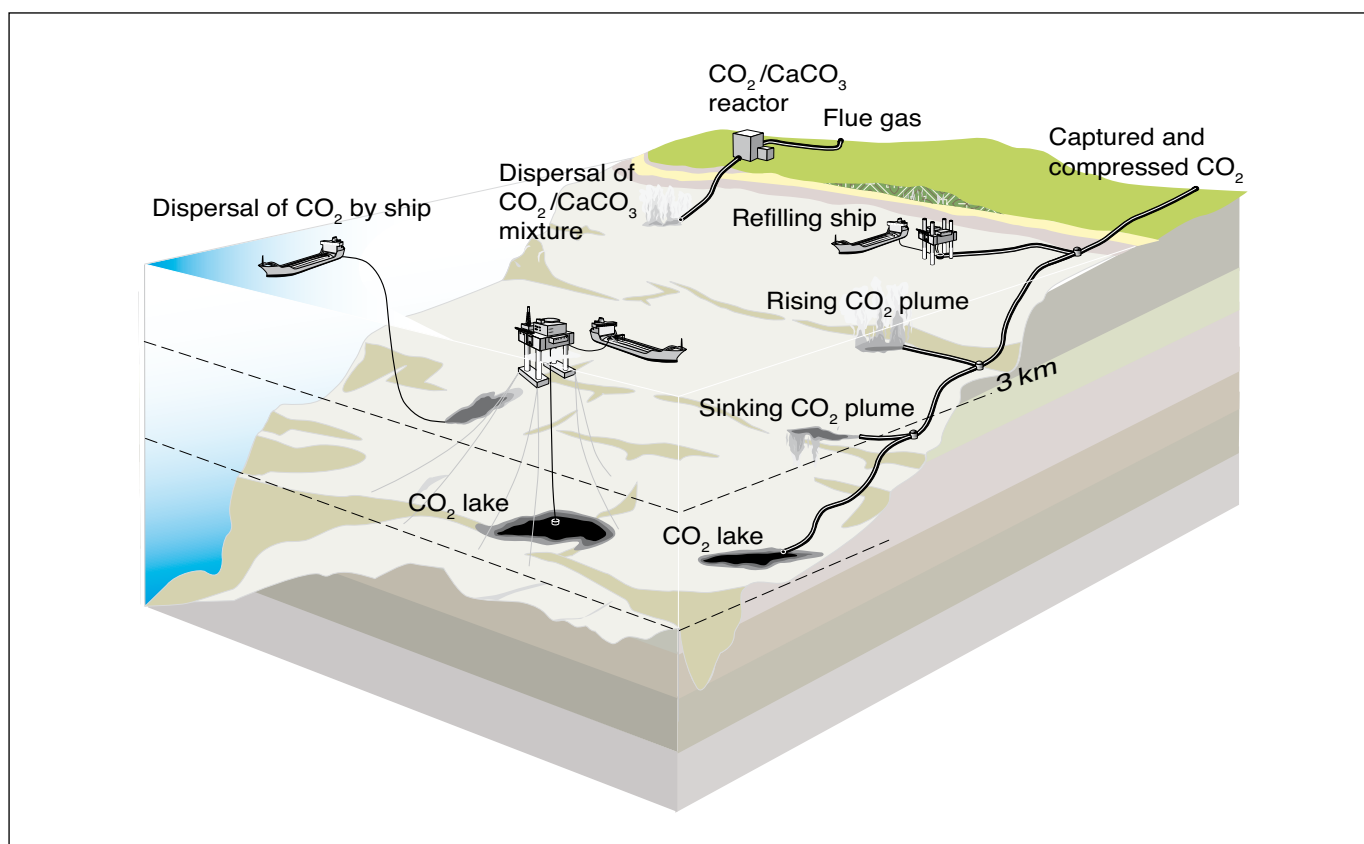


Figure TS.9. Methods of ocean storage.

There is no practical physical limit to the amount of anthropogenic CO₂ that could be stored in the ocean. However, on a millennial time scale, the amount stored will depend on oceanic equilibration with the atmosphere. Stabilizing atmospheric CO₂ concentrations between 350 ppmv and 1000 ppmv would imply that between 2,000 and 12,000 GtCO₂ would eventually reside in the ocean if there is no intentional CO₂ injection. This range therefore represents the upper limit for the capacity of the ocean to store CO₂ through active injection. The capacity would also be affected by environmental factors, such as a maximum allowable pH change.

Analysis of ocean observations and models both indicate that injected CO₂ will be isolated from the atmosphere for at least several hundreds of years, and that the fraction retained tends to be higher with deeper injection (see Table TS.7). Ideas for increasing the fraction retained include forming solid CO₂ hydrates and/or liquid CO₂ lakes on the sea floor, and dissolving alkaline minerals such as limestone to neutralize the acidic CO₂. Dissolving mineral carbonates, if practical, could extend the storage time scale to roughly 10,000 years, while minimizing changes in ocean pH and CO₂ partial pressure. However, large amounts of limestone and energy for materials handling would be required for this approach (roughly the same order of magnitude as the amounts per tonne of CO₂ injected that are needed for mineral carbonation; see Section 7).

Ecological and environmental impacts and risks

The injection of a few GtCO₂ would produce a measurable change in ocean chemistry in the region of injection, whereas the injection of hundreds of GtCO₂ would produce larger changes in the region of injection and eventually produce measurable changes over the entire ocean volume. Model simulations that assume a release from seven locations at 3,000 m depth and ocean storage providing 10% of the mitigation effort for stabilization at 550 ppmv CO₂ projected acidity changes (pH changes) of more than 0.4 over approximately 1% of the ocean volume. By comparison, in

a 550 ppmv stabilization case without ocean storage, a pH change of more than 0.25 at the ocean surface was estimated due to equilibration with the elevated CO₂ concentrations in the atmosphere. In either case, a pH change of 0.2 to 0.4 is significantly greater than pre-industrial variations in ocean acidity. Over centuries, ocean mixing will result in the loss of isolation of injected CO₂. As more CO₂ reaches the ocean surface waters, releases into the atmosphere would occur gradually from large regions of the ocean. There are no known mechanisms for sudden or catastrophic release of injected CO₂ from the ocean into the atmosphere.

Experiments show that adding CO₂ can harm marine organisms. Effects of elevated CO₂ levels have mostly been studied on time scales up to several months in individual organisms that live near the ocean surface. Observed phenomena include reduced rates of calcification, reproduction, growth, circulatory oxygen supply and mobility, as well as increased mortality over time. In some organisms these effects are seen in response to small additions of CO₂. Immediate mortality is expected close to injection points or CO₂ lakes. The chronic effects of direct CO₂ injection into the ocean on ocean organisms or ecosystems over large ocean areas and long time scales have not yet been studied.

No controlled ecosystem experiments have been performed in the deep ocean, so only a preliminary assessment of potential ecosystem effects can be given. It is expected that ecosystem consequences will increase with increasing CO₂ concentrations and decreasing pH, but the nature of such consequences is currently not understood, and no environmental criteria have as yet been identified to avoid adverse effects. At present, it is also unclear how or whether species and ecosystems would adapt to the sustained chemical changes.

Costs of ocean storage

Although there is no experience with ocean storage, some attempts have been made to estimate the costs of CO₂ storage projects that release CO₂ on the sea floor or in the deep ocean. The costs of CO₂ capture and transport to the shoreline (e.g

Table TS.7. Fraction of CO₂ retained for ocean storage as simulated by seven ocean models for 100 years of continuous injection at three different depths starting in the year 2000.

Year	Injection depth		
	800 m	1500 m	3000 m
2100	0.78 ± 0.06	0.91 ± 0.05	0.99 ± 0.01
2200	0.50 ± 0.06	0.74 ± 0.07	0.94 ± 0.06
2300	0.36 ± 0.06	0.60 ± 0.08	0.87 ± 0.10
2400	0.28 ± 0.07	0.49 ± 0.09	0.79 ± 0.12
2500	0.23 ± 0.07	0.42 ± 0.09	0.71 ± 0.14

Table TS.8. Costs for ocean storage at depths deeper than 3,000 m.

Ocean storage method	Costs (US\$/tCO ₂ net injected)	
	100 km offshore	500 km offshore
Fixed pipeline	6	31
Moving ship/platform ^a	12-14	13-16

^a The costs for the moving ship option are for injection depths of 2,000-2,500 m.

via pipelines) are not included in the cost of ocean storage. However, the costs of offshore pipelines or ships, plus any additional energy costs, are included in the ocean storage cost. The costs of ocean storage are summarized in Table TS.8. These numbers indicate that, for short distances, the fixed pipeline option would be cheaper. For larger distances, either the moving ship or the transport by ship to a platform with subsequent injection would be more attractive.

Legal aspects and public perception

The global and regional treaties on the law of the sea and marine environment, such as the OSPAR and the London Convention discussed earlier in Section 5 for geological storage sites, also affect ocean storage, as they concern the ‘maritime area’. Both Conventions distinguish between the storage method employed and the purpose of storage to determine the legal status of ocean storage of CO₂. As yet, however, no decision has been made about the legal status of intentional ocean storage.

The very small number of public perception studies that have looked at the ocean storage of CO₂ indicate that there is very little public awareness or knowledge of this subject. In the few studies conducted thus far, however, the public has expressed greater reservations about ocean storage than geological storage. These studies also indicate that the perception of ocean storage changed when more information was provided; in one study this led to increased acceptance of ocean storage, while in another study it led to less acceptance. The literature also notes that ‘significant opposition’ developed around a proposed CO₂ release experiment in the Pacific Ocean.

7. Mineral carbonation and industrial uses

This section deals with two rather different options for CO₂ storage. The first is mineral carbonation, which involves converting CO₂ to solid inorganic carbonates using chemical reactions. The second option is the industrial use of CO₂, either directly or as feedstock for production of various carbon-containing chemicals.

Mineral carbonation: technology, impacts and costs

Mineral carbonation refers to the fixation of CO₂ using alkaline and alkaline-earth oxides, such as magnesium oxide (MgO) and calcium oxide (CaO), which are present in naturally occurring silicate rocks such as serpentine and olivine. Chemical reactions between these materials and CO₂ produces compounds such as magnesium carbonate (MgCO₃) and calcium carbonate (CaCO₃, commonly known as limestone). The quantity of metal oxides in the silicate rocks that can be found in the earth’s crust exceeds the amounts needed to fix all the CO₂ that would be produced by the combustion of all available fossil fuel reserves. These oxides are also present in small quantities in some industrial wastes, such as stainless steel slags and ashes. Mineral carbonation produces silica and carbonates that are stable over long time scales and can therefore be disposed of in areas such as silicate mines, or re-used for construction purposes (see Figure TS.10), although such re-use is likely to be small relative to the amounts produced. After carbonation, CO₂ would not be released to the atmosphere. As a consequence, there would be little need to monitor the disposal sites and the associated risks would be very low. The storage potential is difficult to estimate at this early phase of development. It would be limited by the fraction of silicate reserves that can be technically exploited, by environmental issues such as the volume of product disposal, and by legal and societal constraints at the storage location.

The process of mineral carbonation occurs naturally, where it is known as ‘weathering’. In nature, the process occurs very slowly; it must therefore be accelerated considerably to be a viable storage method for CO₂ captured from anthropogenic sources. Research in the field of mineral carbonation therefore focuses on finding process routes that can achieve reaction rates viable for industrial purposes and make the reaction more energy-efficient. Mineral carbonation technology using natural silicates is in the research phase but some processes using industrial wastes are in the demonstration phase.

A commercial process would require mining, crushing and milling of the mineral-bearing ores and their transport to a processing plant receiving a concentrated CO₂ stream from a capture plant (see Figure TS.10). The carbonation process

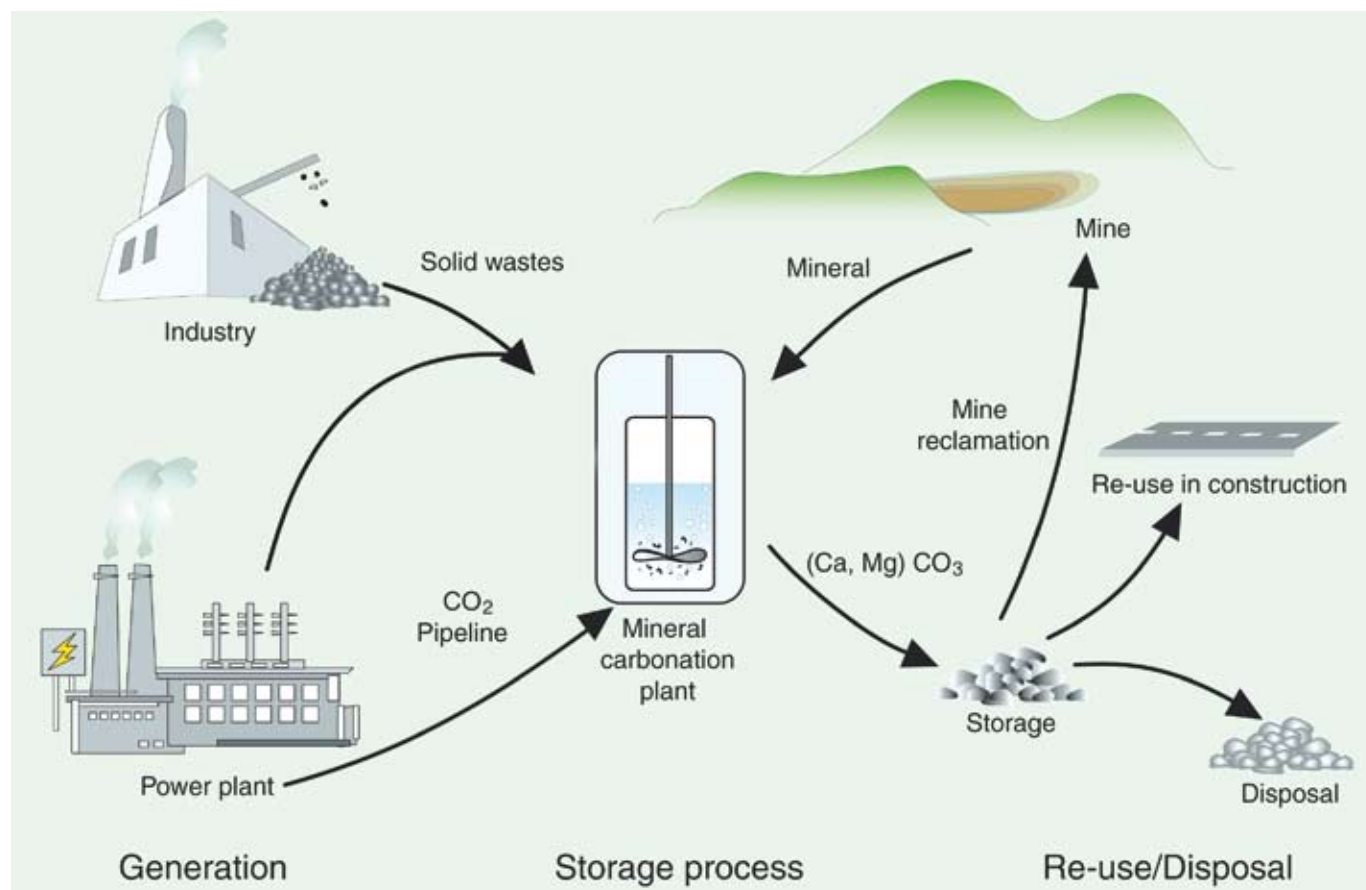


Figure TS.10. Material fluxes and process steps associated with the mineral carbonation of silicate rocks or industrial residues (Courtesy ECN).

energy required would be 30 to 50% of the capture plant output. Considering the additional energy requirements for the capture of CO₂, a CCS system with mineral carbonation would require 60 to 180% more energy input per kilowatt-hour than a reference electricity plant without capture or mineral carbonation. These energy requirements raise the cost per tonne of CO₂ avoided for the overall system significantly (see Section 8). The best case studied so far is the wet carbonation of natural silicate olivine. The estimated cost of this process is approximately 50–100 US\$/tCO₂ net mineralized (in addition to CO₂ capture and transport costs, but taking into account the additional energy requirements). The mineral carbonation process would require 1.6 to 3.7 tonnes of silicates per tonne of CO₂ to be mined, and produce 2.6 to 4.7 tonnes of materials to be disposed per tonne of CO₂ stored as carbonates. This would therefore be a large operation, with an environmental impact similar to that of current large-scale surface mining operations. Serpentine also often contains chrysotile, a natural form of asbestos. Its presence therefore demands monitoring and mitigation measures of the kind available in the mining industry. On the other hand, the products of mineral carbonation are chrysotile-

free, since this is the most reactive component of the rock and therefore the first substance converted to carbonates.

A number of issues still need to be clarified before any estimates of the storage potential of mineral carbonation can be given. The issues include assessments of the technical feasibility and corresponding energy requirements at large scales, but also the fraction of silicate reserves that can be technically and economically exploited for CO₂ storage. The environmental impact of mining, waste disposal and product storage could also limit potential. The extent to which mineral carbonation may be used cannot be determined at this time, since it depends on the unknown amount of silicate reserves that can be technically exploited, and environmental issues such as those noted above.

Industrial uses

Industrial uses of CO₂ include chemical and biological processes where CO₂ is a reactant, such as those used in urea and methanol production, as well as various technological applications that use CO₂ directly, for example in the horticulture industry, refrigeration, food packaging, welding,

beverages and fire extinguishers. Currently, CO₂ is used at a rate of approximately 120 MtCO₂ per year (30 MtC yr⁻¹) worldwide, excluding use for EOR (discussed in Section 5). Most (two thirds of the total) is used to produce urea, which is used in the manufacture of fertilizers and other products. Some of the CO₂ is extracted from natural wells, and some originates from industrial sources—mainly high-concentration sources such as ammonia and hydrogen production plants—that capture CO₂ as part of the production process.

Industrial uses of CO₂ can, in principle, contribute to keeping CO₂ out of the atmosphere by storing it in the “carbon chemical pool” (i.e., the stock of carbon-bearing manufactured products). However, as a measure for mitigating climate change, this option is meaningful only if the quantity and duration of CO₂ stored are significant, and if there is a real net reduction of CO₂ emissions. The typical lifetime of most of the CO₂ currently used by industrial processes has storage times of only days to months. The stored carbon is then degraded to CO₂ and again emitted to the atmosphere. Such short time scales do not contribute meaningfully to climate change mitigation. In addition, the total industrial use figure of 120 MtCO₂ yr⁻¹ is small compared to emissions from major anthropogenic sources (see Table TS.2). While some industrial processes store a small proportion of CO₂ (totalling roughly 20 MtCO₂ yr⁻¹) for up to several decades, the total amount of long-term (century-scale) storage is presently in the order of 1 MtCO₂ yr⁻¹ or less, with no prospects for major increases.

Another important question is whether industrial uses of CO₂ can result in an overall net reduction of CO₂ emissions by substitution for other industrial processes or products. This can be evaluated correctly only by considering proper system boundaries for the energy and material balances of the CO₂ utilization processes, and by carrying out a detailed life-cycle analysis of the proposed use of CO₂. The literature in this area is limited but it shows that precise figures are difficult to estimate and that in many cases industrial uses could lead to an increase in overall emissions rather than a net reduction. In view of the low fraction of CO₂ retained, the small volumes used and the possibility that substitution may lead to increases in CO₂ emissions, it can be concluded that the contribution of industrial uses of captured CO₂ to climate change mitigation is expected to be small.

8. Costs and economic potential

The stringency of future requirements for the control of greenhouse gas emissions and the expected costs of CCS systems will determine, to a large extent, the future deployment of CCS technologies relative to other greenhouse gas mitigation options. This section first summarizes the overall cost of CCS for the main options and process applications considered in previous sections. As used in this summary

and the report, “costs” refer only to market prices but do not include external costs such as environmental damages and broader societal costs that may be associated with the use of CCS. To date, little has been done to assess and quantify such external costs. Finally CCS is examined in the context of alternative options for global greenhouse gas reductions.

Cost of CCS systems

As noted earlier, there is still relatively little experience with the combination of CO₂ capture, transport and storage in a fully integrated CCS system. And while some CCS components are already deployed in mature markets for certain industrial applications, CCS has still not been used in large-scale power plants (the application with most potential).

The literature reports a fairly wide range of costs for CCS components (see Sections 3–7). The range is due primarily to the variability of site-specific factors, especially the design, operating and financing characteristics of the power plants or industrial facilities in which CCS is used; the type and costs of fuel used; the required distances, terrains and quantities involved in CO₂ transport; and the type and characteristics of the CO₂ storage. In addition, uncertainty still remains about the performance and cost of current and future CCS technology components and integrated systems. The literature reflects a widely-held belief, however, that the cost of building and operating CO₂ capture systems will decline over time as a result of learning-by-doing (from technology deployment) and sustained R&D. Historical evidence also suggests that costs for first-of-a-kind capture plants could exceed current estimates before costs subsequently decline. In most CCS systems, the cost of capture (including compression) is the largest cost component. Costs of electricity and fuel vary considerably from country to country, and these factors also influence the economic viability of CCS options.

Table TS.9 summarizes the costs of CO₂ capture, transport and storage reported in Sections 3 to 7. Monitoring costs are also reflected. In Table TS.10, the component costs are combined to show the total costs of CCS and electricity generation for three power systems with pipeline transport and two geological storage options.

For the plants with geological storage and no EOR credit, the cost of CCS ranges from 0.02–0.05 US\$/kWh for PC plants and 0.01–0.03 US\$/kWh for NGCC plants (both employing post-combustion capture). For IGCC plants (using pre-combustion capture), the CCS cost ranges from 0.01–0.03 US\$/kWh relative to a similar plant without CCS. For all electricity systems, the cost of CCS can be reduced by about 0.01–0.02 US\$/kWh when using EOR with CO₂ storage because the EOR revenues partly compensate for the CCS costs. The largest cost reductions are seen for coal-based plants, which capture the largest amounts of CO₂. In a few cases, the low end of the CCS cost range can be negative,

Table TS.9. 2002 Cost ranges for the components of a CCS system as applied to a given type of power plant or industrial source. The costs of the separate components cannot simply be summed to calculate the costs of the whole CCS system in US\$/CO₂ avoided. All numbers are representative of the costs for large-scale, new installations, with natural gas prices assumed to be 2.8–4.4 US\$ GJ⁻¹ and coal prices 1–1.5 US\$ GJ⁻¹.

CCS system components	Cost range	Remarks
Capture from a coal- or gas-fired power plant	15–75 US\$/tCO ₂ net captured	Net costs of captured CO ₂ , compared to the same plant without capture.
Capture from hydrogen and ammonia production or gas processing	5–55 US\$/tCO ₂ net captured	Applies to high-purity sources requiring simple drying and compression.
Capture from other industrial sources	25–115 US\$/tCO ₂ net captured	Range reflects use of a number of different technologies and fuels.
Transportation	1–8 US\$/tCO ₂ transported	Per 250 km pipeline or shipping for mass flow rates of 5 (high end) to 40 (low end) MtCO ₂ yr ⁻¹ .
Geological storage ^a	0.5–8 US\$/tCO ₂ net injected	Excluding potential revenues from EOR or ECBM.
Geological storage: monitoring and verification	0.1–0.3 US\$/tCO ₂ injected	This covers pre-injection, injection, and post-injection monitoring, and depends on the regulatory requirements.
Ocean storage	5–30 US\$/tCO ₂ net injected	Including offshore transportation of 100–500 km, excluding monitoring and verification.
Mineral carbonation	50–100 US\$/tCO ₂ net mineralized	Range for the best case studied. Includes additional energy use for carbonation.

^a Over the long term, there may be additional costs for remediation and liabilities.

indicating that the assumed credit for EOR over the life of the plant is greater than the lowest reported cost of CO₂ capture for that system. This might also apply in a few instances of low-cost capture from industrial processes.

In addition to fossil fuel-based energy conversion processes, CO₂ could also be captured in power plants fueled with biomass, or fossil-fuel plants with biomass co-firing. At present, biomass plants are small in scale (less than 100 MW). This means that the resulting costs of production with and without CCS are relatively high compared to fossil alternatives. Full CCS costs for biomass could amount to 110 US\$/tCO₂ avoided. Applying CCS to biomass-fuelled or co-fired conversion facilities would lead to lower or negative¹³ CO₂ emissions, which could reduce the costs for this option, depending on the market value of CO₂ emission reductions. Similarly, CO₂ could be captured in biomass-fueled H₂ plants. The cost is reported to be 22–25 US\$/tCO₂ (80–92 US\$/tC) avoided in a plant producing 1 million Nm³ day⁻¹ of H₂, and corresponds to an increase in the H₂ product costs of about 2.7 US\$ GJ⁻¹. Significantly larger biomass plants could potentially benefit from economies of scale, bringing down costs of the CCS systems to levels broadly similar to coal plants. However, to date, there has been little experience with large-scale biomass plants, so their feasibility has not been proven yet, and costs and potential are difficult to estimate.

The cost of CCS has not been studied in the same depth for non-power applications. Because these sources are very diverse in terms of CO₂ concentration and gas stream pressure, the available cost studies show a very broad range. The lowest costs were found for processes that already separate CO₂ as part of the production process, such as hydrogen production (the cost of capture for hydrogen production was reported earlier in Table TS.4). The full CCS cost, including transport and storage, raises the cost of hydrogen production by 0.4 to 4.4 US\$ GJ⁻¹ in the case of geological storage, and by -2.0 to 2.8 US\$ GJ⁻¹ in the case of EOR, based on the same cost assumptions as for Table TS.10.

Cost of CO₂ avoided

Table TS.10 also shows the ranges of costs for 'CO₂ avoided'. CCS energy requirements push up the amount of fuel input (and therefore CO₂ emissions) per unit of net power output. As a result, the amount of CO₂ produced per unit of product (a kWh of electricity) is greater for the power plant with CCS than the reference plant, as shown in Figure TS.11. To determine the CO₂ reductions one can attribute to CCS, one needs to compare CO₂ emissions per kWh of the plant with capture to that of a reference plant without capture. The difference is referred to as the 'avoided emissions'.

¹³ If for example the biomass is harvested at an unsustainable rate (that is, faster than the annual re-growth), the net CO₂ emissions of the activity might not be negative.

Table TS.10. Range of total costs for CO₂ capture, transport and geological storage based on current technology for new power plants using bituminous coal or natural gas

Power plant performance and cost parameters ^a	Pulverized coal power plant	Natural gas combined cycle power plant	Integrated coal gasification combined cycle power plant
Reference plant without CCS			
Cost of electricity (US\$/kWh)	0.043-0.052	0.031-0.050	0.041-0.061
Power plant with capture			
Increased fuel requirement (%)	24-40	11-22	14-25
CO ₂ captured (kg/kWh)	0.82-0.97	0.36-0.41	0.67-0.94
CO ₂ avoided (kg/kWh)	0.62-0.70	0.30-0.32	0.59-0.73
% CO ₂ avoided	81-88	83-88	81-91
Power plant with capture and geological storage^b			
Cost of electricity (US\$/kWh)	0.063-0.099	0.043-0.077	0.055-0.091
Cost of CCS (US\$/kWh)	0.019-0.047	0.012-0.029	0.010-0.032
% increase in cost of electricity	43-91	37-85	21-78
Mitigation cost (US\$/tCO ₂ avoided)	30-71	38-91	14-53
(US\$/tC avoided)	110-260	140-330	51-200
Power plant with capture and enhanced oil recovery^c			
Cost of electricity (US\$/kWh)	0.049-0.081	0.037-0.070	0.040-0.075
Cost of CCS (US\$/kWh)	0.005-0.029	0.006-0.022	(-0.005)-0.019
% increase in cost of electricity	12-57	19-63	(-10)-46
Mitigation cost (US\$/tCO ₂ avoided)	9-44	19-68	(-7)-31
(US\$/tC avoided)	31-160	71-250	(-25)-120

^a All changes are relative to a similar (reference) plant without CCS. See Table TS.3 for details of assumptions underlying reported cost ranges.

^b Capture costs based on ranges from Table TS.3; transport costs range from 0-5 US\$/tCO₂; geological storage cost ranges from 0.6-8.3 US\$/tCO₂.

^c Same capture and transport costs as above; Net storage costs for EOR range from -10 to -16 US\$/tCO₂ (based on pre-2003 oil prices of 15-20 US\$ per barrel).

Introducing CCS to power plants may influence the decision about which type of plant to install and which fuel to use. In some situations therefore, it can be useful to calculate a cost per tonne of CO₂ avoided based on a reference plant different from the CCS plant. Table TS.10 displays the cost and emission factors for the three reference plants and the corresponding CCS plants for the case of geological storage. Table TS.11 summarizes the range of estimated costs for different combinations of CCS plants and the lowest-cost reference plants of potential interest. It shows, for instance, that where a PC plant is planned initially, using CCS in that plant may lead to a higher CO₂ avoidance cost than if an NGCC plant with CCS is selected, provided natural gas is available. Another option with lower avoidance cost could be to build an IGCC plant with capture instead of equipping a PC plant with capture.

Economic potential of CCS for climate change mitigation

Assessments of the economic potential of CCS are based on energy and economic models that study future CCS deployment and costs in the context of scenarios that achieve economically efficient, least-cost paths to the stabilization of atmospheric CO₂ concentrations.

While there are significant uncertainties in the quantitative results from these models (see discussion below), all models indicate that CCS systems are unlikely to be deployed on a large scale in the absence of an explicit policy that substantially limits greenhouse gas emissions to the atmosphere. With greenhouse gas emission limits imposed, many integrated assessments foresee the deployment of CCS systems on a large scale within a few decades from the start of any significant climate change mitigation regime. Energy and economic models indicate that CCS systems

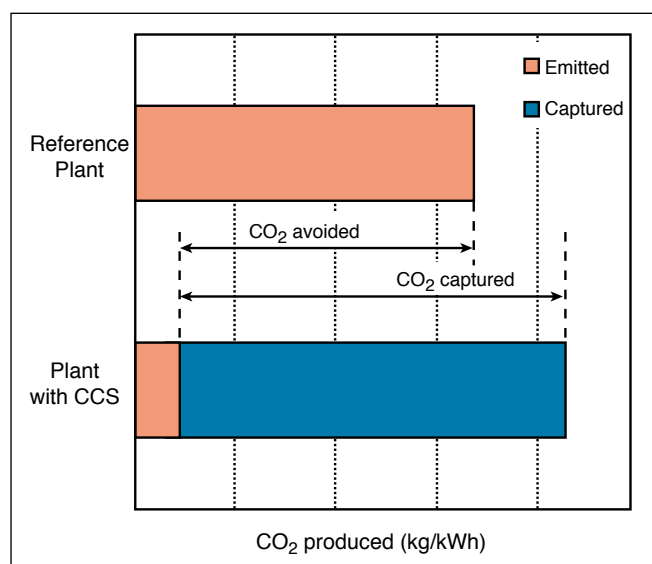


Figure TS.11. CO₂ capture and storage from power plants. The increased CO₂ production resulting from loss in overall efficiency of power plants due to the additional energy required for capture, transport and storage, and any leakage from transport result in a larger amount of “CO₂ produced per unit of product” (lower bar) relative to the reference plant (upper bar) without capture.

are unlikely to contribute significantly to the mitigation of climate change unless deployed in the power sector. For this

to happen, the price of carbon dioxide reductions would have to exceed 25–30 US\$/tCO₂, or an equivalent limit on CO₂ emissions would have to be mandated. The literature and current industrial experience indicate that, in the absence of measures for limiting CO₂ emissions, there are only small, niche opportunities for CCS technologies to deploy. These early opportunities involve CO₂ captured from a high-purity, low-cost source, the transport of CO₂ over distances of less than 50 km, coupled with CO₂ storage in a value-added application such as EOR. The potential of such niche options is about 360 MtCO₂ per year (see Section 2).

Models also indicate that CCS systems will be competitive with other large-scale mitigation options such as nuclear power and renewable energy technologies. These studies show that including CCS in a mitigation portfolio could reduce the cost of stabilizing CO₂ concentrations by 30% or more. One aspect of the cost competitiveness of CCS technologies is that they are compatible with most current energy infrastructures.

In most scenarios, emissions abatement becomes progressively more constraining over time. Most analyses indicate that notwithstanding significant penetration of CCS systems by 2050, the majority of CCS deployment will occur in the second half of this century. The earliest CCS deployments are typically foreseen in the industrialized nations, with deployment eventually spreading worldwide. While results for different scenarios and models differ (often

Table TS.11. Mitigation cost ranges for different combinations of reference and CCS plants based on current technology for new power plants. Currently, in many regions, common practice would be either a PC plant or an NGCC plant¹⁴. EOR benefits are based on oil prices of 15 - 20 US\$ per barrel. Gas prices are assumed to be 2.8 -4.4 US\$/GJ⁻¹, coal prices 1-1.5 US\$/GJ⁻¹ (based on Table 8.3a).

CCS plant type	NGCC reference plant	PC reference plant
	US\$/tCO ₂ avoided (US\$/tC avoided)	US\$/tCO ₂ avoided (US\$/tC avoided)
Power plant with capture and geological storage		
NGCC	40 - 90 (140 - 330)	20 - 60 (80 - 220)
PC	70 - 270 (260 - 980)	30 - 70 (110 - 260)
IGCC	40 - 220 (150 - 790)	20 - 70 (80 - 260)
Power plant with capture and EOR		
NGCC	20 - 70 (70 - 250)	0 - 30 (0 - 120)
PC	50 - 240 (180 - 890)	10 - 40 (30 - 160)
IGCC	20 - 190 (80 - 710)	0 - 40 (0 - 160)

¹⁴ IGCC is not included as a reference power plant that would be built today since this technology is not yet widely deployed in the electricity sector and is usually slightly more costly than a PC plant.

significantly) in the specific mix and quantities of different measures needed to achieve a particular emissions constraint (see Figure TS.12), the consensus of the literature shows that CCS could be an important component of the broad portfolio of energy technologies and emission reduction approaches.

The actual use of CCS is likely to be lower than the estimates of economic potential indicated by these energy and economic models. As noted earlier, the results are typically based on an optimized least-cost analysis that does

not adequately account for real-world barriers to technology development and deployment, such as environmental impact, lack of a clear legal or regulatory framework, the perceived investment risks of different technologies, and uncertainty as to how quickly the cost of CCS will be reduced through R&D and learning-by-doing. Models typically employ simplified assumptions regarding the costs of CCS for different applications and the rates at which future costs will be reduced.

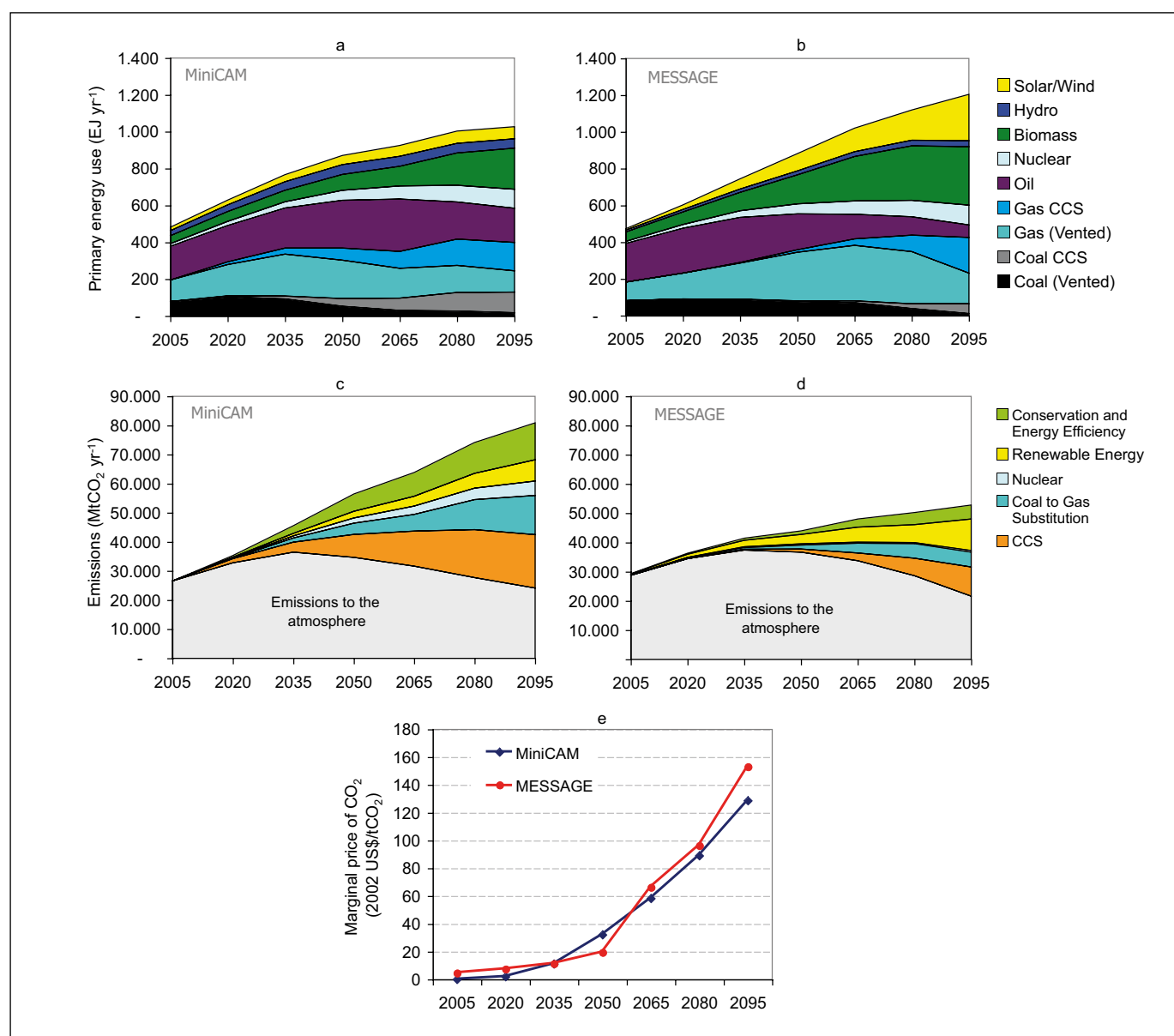


Figure TS.12. These figures are an illustrative example of the global potential contribution of CCS as part of a mitigation portfolio. They are based on two alternative integrated assessment models (MESSAGE and MiniCAM) adopting the same assumptions for the main emissions drivers. The results would vary considerably on regional scales. This example is based on a single scenario and therefore does not convey the full range of uncertainties. Panels a) and b) show global primary energy use, including the deployment of CCS. Panels c) and d) show the global CO₂ emissions in grey and corresponding contributions of main emissions reduction measures in colour. Panel e) shows the calculated marginal price of CO₂ reductions.

For CO₂ stabilization scenarios between 450 and 750 ppmv, published estimates of the cumulative amount of CO₂ potentially stored globally over the course of this century (in geological formations and/or the oceans) span a wide range, from very small contributions to thousands of gigatonnes of CO₂. To a large extent, this wide range is due to the uncertainty of long-term socio-economic, demographic and, in particular, technological changes, which are the main drivers of future CO₂ emissions. However, it is important to note that the majority of results for stabilization scenarios of 450–750 ppmv CO₂ tend to cluster in a range of 220–2,200 GtCO₂ (60–600 GtC) for the cumulative deployment of CCS. For CCS to achieve this economic potential, several hundreds or thousands of CCS systems would be required worldwide over the next century, each capturing some 1–5 MtCO₂ per year. As indicated in Section 5, it is likely that the technical potential for geological storage alone is sufficient to cover the high end of the economic potential range for CCS.

Perspectives on CO₂ leakage from storage

The policy implications of slow leakage from storage depend on assumptions in the analysis. Studies conducted to address the question of how to deal with impermanent storage are based on different approaches: the value of delaying emissions, cost minimization of a specified mitigation scenario, or allowable future emissions in the context of an assumed stabilization of atmospheric greenhouse gas concentrations. Some of these studies allow future releases to be compensated by additional reductions in emissions; the results depend on assumptions regarding the future cost of reductions, discount rates, the amount of CO₂ stored, and the assumed level of stabilization for atmospheric concentrations. In other studies, compensation is not seen as an option because of political and institutional uncertainties and the analysis focuses on limitations set by the assumed stabilization level and the amount stored.

While specific results of the range of studies vary with the methods and assumptions made, the outcomes suggest that a fraction retained on the order of 90–99% for 100 years or 60–95% for 500 years could still make such impermanent storage valuable for the mitigation of climate change. All studies imply that, if CCS is to be acceptable as a mitigation measure, there must be an upper limit to the amount of leakage that can take place.

9. Emission inventories and accounting

An important aspect of CO₂ capture and storage is the development and application of methods to estimate and report the quantities in which emissions of CO₂ (and associated emissions of methane or nitrous oxides) are reduced, avoided, or removed from the atmosphere. The two elements involved here are (1) the actual estimation and reporting of emissions for national greenhouse gas inventories, and (2) accounting for CCS under international agreements to limit net emissions.¹⁵

Current framework

Under the UNFCCC, national greenhouse gas emission inventories have traditionally reported emissions for a specific year, and have been prepared on an annual basis or another periodic basis. The IPCC Guidelines (IPCC 1996) and Good Practice Guidance Reports (IPCC 2000; 2003) describe detailed approaches for preparing national inventories that are complete, transparent, documented, assessed for uncertainties, consistent over time, and comparable across countries. The IPCC documents now in use do not specifically include CO₂ capture and storage options. However, the IPCC Guidelines are currently undergoing revisions that should provide some guidance when the revisions are published in 2006. The framework that already has been accepted could be applied to CCS systems, although some issues might need revision or expansion.

Issues relevant to accounting and reporting

In the absence of prevailing international agreements, it is not clear whether the various forms of CO₂ capture and storage will be treated as reductions in emissions or as removals from the atmosphere. In either case, CCS results in new pools of CO₂ that may be subject to physical leakage at some time in the future. Currently, there are no methods available within the UNFCCC framework for monitoring, measuring or accounting for physical leakage from storage sites. However, leakage from well-managed geological storage sites is likely to be small in magnitude and distant in time.

Consideration may be given to the creation of a specific category for CCS in the emissions reporting framework but this is not strictly necessary since the quantities of CO₂ captured and stored could be reflected in the sector in which the CO₂ was produced. CO₂ storage in a given location could include CO₂ from many different source categories, and even from sources in many different countries. Fugitive

¹⁵ In this context, “estimation” is the process of calculating greenhouse gas emissions and “reporting” is the process of providing the estimates to the UNFCCC. “Accounting” refers to the rules for comparing emissions and removals as reported with commitments (IPCC 2003).

emissions from the capture, transport and injection of CO₂ to storage can largely be estimated within the existing reporting methods, and emissions associated with the added energy required to operate the CCS systems can be measured and reported within the existing inventory frameworks. Specific consideration may also be required for CCS applied to biomass systems as that application would result in reporting negative emissions, for which there is currently no provision in the reporting framework.

Issues relevant to international agreements

Quantified commitments to limit greenhouse gas emissions and the use of emissions trading, Joint Implementation (JI) or the Clean Development Mechanism (CDM) require clear rules and methods to account for emissions and removals. Because CCS has the potential to move CO₂ across traditional accounting boundaries (e.g. CO₂ might be captured in one country and stored in another, or captured in one year and partly released from storage in a later year), the rules and methods for accounting may be different than those used in traditional emissions inventories.

To date, most of the scientific, technical and political discussions on accounting for stored CO₂ have focused on sequestration in the terrestrial biosphere. The history of these negotiations may provide some guidance for the development of accounting methods for CCS. Recognizing the potential

impermanence of CO₂ stored in the terrestrial biosphere, the UNFCCC accepted the idea that net emissions can be reduced through biological sinks, but has imposed complex rules for such accounting. CCS is markedly different in many ways from CO₂ sequestration in the terrestrial biosphere (see Table TS.12), and the different forms of CCS are markedly different from one another. However, the main goal of accounting is to ensure that CCS activities produce real and quantifiable reductions in net emissions. One tonne of CO₂ permanently stored has the same benefit in terms of atmospheric CO₂ concentrations as one tonne of CO₂ not emitted, but one tonne of CO₂ temporarily stored has less benefit. It is generally accepted that this difference should be reflected in any system of accounting for reductions in net greenhouse gas emissions.

The IPCC Guidelines (IPCC 1996) and Good Practice Guidance Reports (IPCC 2000; 2003) also contain guidelines for monitoring greenhouse gas emissions. It is not known whether the revised guidelines of the IPCC for CCS can be satisfied by using monitoring techniques, particularly for geological and ocean storage. Several techniques are available for the monitoring and verification of CO₂ emissions from geological storage, but they vary in applicability, detection limits and uncertainties. Currently, monitoring for geological storage can take place quantitatively at injection and qualitatively in the reservoir and by measuring surface fluxes of CO₂. Ocean storage monitoring can take place by

Table TS.12. Differences in the forms of CCS and biological sinks that might influence the way accounting is conducted.

Property	Terrestrial biosphere	Deep ocean	Geological reservoirs
CO ₂ sequestered or stored	Stock changes can be monitored over time.	Injected carbon can be measured.	Injected carbon can be measured.
Ownership	Stocks will have a discrete location and can be associated with an identifiable owner.	Stocks will be mobile and may reside in international waters.	Stocks may reside in reservoirs that cross national or property boundaries and differ from surface boundaries.
Management decisions	Storage will be subject to continuing decisions about land-use priorities.	Once injected there are no further human decisions about maintenance once injection has taken place.	Once injection has taken place, human decisions about continued storage involve minimal maintenance, unless storage interferes with resource recovery.
Monitoring	Changes in stocks can be monitored.	Changes in stocks will be modelled.	Release of CO ₂ can be detected by physical monitoring.
Expected retention time	Decades, depending on management decisions.	Centuries, depending on depth and location of injection.	Essentially permanent, barring physical disruption of the reservoir.
Physical leakage	Losses might occur due to disturbance, climate change, or land-use decisions.	Losses will assuredly occur as an eventual consequence of marine circulation and equilibration with the atmosphere.	Losses are unlikely except in the case of disruption of the reservoir or the existence of initially undetected leakage pathways.
Liability	A discrete land-owner can be identified with the stock of sequestered carbon.	Multiple parties may contribute to the same stock of stored CO ₂ and the CO ₂ may reside in international waters.	Multiple parties may contribute to the same stock of stored CO ₂ that may lie under multiple countries.

detecting the CO₂ plume, but not by measuring ocean surface release to the atmosphere. Experiences from monitoring existing CCS projects are still too limited to serve as a basis for conclusions about the physical leakage rates and associated uncertainties.

The Kyoto Protocol creates different units of accounting for greenhouse gas emissions, emissions reductions, and emissions sequestered under different compliance mechanisms. ‘Assigned amount units’ (AAUs) describe emissions commitments and apply to emissions trading, ‘certified emission reductions’ (CERs) are used under the CDM, and ‘emission reduction units’ (ERUs) are employed under JI. To date, international negotiations have provided little guidance about methods for calculating and accounting for project-related CO₂ reductions from CCS systems (only CERs or ERUs), and it is therefore uncertain how such reductions will be accommodated under the Kyoto Protocol. Some guidance may be given by the methodologies for biological-sink rules. Moreover, current agreements do not deal with cross-border CCS projects. This is particularly important when dealing with cross-border projects involving CO₂ capture in an ‘Annex B’ country that is party to the Kyoto Protocol but stored in a country that is not in Annex B or is not bound by the Protocol.

Although methods currently available for national emissions inventories can either accommodate CCS systems or be revised to do so, accounting for stored CO₂ raises questions about the acceptance and transfer of responsibility for stored emissions. Such issues may be addressed through national and international political processes.

10. Gaps in knowledge

This summary of the gaps in knowledge covers aspects of CCS where increasing knowledge, experience and reducing uncertainty would be important to facilitate decision-making about the large-scale deployment of CCS.

Technologies for capture and storage

Technologies for the capture of CO₂ are relatively well understood today based on industrial experience in a variety of applications. Similarly, there are no major technical or knowledge barriers to the adoption of pipeline transport, or to the adoption of geological storage of captured CO₂. However, the integration of capture, transport and storage in full-scale projects is needed to gain the knowledge and experience required for a more widespread deployment of CCS technologies. R&D is also needed to improve knowledge of emerging concepts and enabling technologies for CO₂ capture that have the potential to significantly reduce the costs of capture for new and existing facilities. More specifically, there are knowledge gaps relating to large coal-

based and natural gas-based power plants with CO₂ capture on the order of several hundred megawatts (or several MtCO₂). Demonstration of CO₂ capture on this scale is needed to establish the reliability and environmental performance of different types of power systems with capture, to reduce the costs of CCS, and to improve confidence in the cost estimates. In addition, large-scale implementation is needed to obtain better estimates of the costs and performance of CCS in industrial processes, such as the cement and steel industries, that are significant sources of CO₂ but have little or no experience with CO₂ capture.

With regard to mineral carbonation technology, a major question is how to exploit the reaction heat in practical designs that can reduce costs and net energy requirements. Experimental facilities at pilot scales are needed to address these gaps.

With regard to industrial uses of captured CO₂, further study of the net energy and CO₂ balance of industrial processes that use the captured CO₂ could help to establish a more complete picture of the potential of this option.

Geographical relationship between the sources and storage opportunities of CO₂

An improved picture of the proximity of major CO₂ sources to suitable storage sites (of all types), and the establishment of cost curves for the capture, transport and storage of CO₂, would facilitate decision-making about large-scale deployment of CCS. In this context, detailed regional assessments are required to evaluate how well large CO₂ emission sources (both current and future) match suitable storage options that can store the volumes required.

Geological storage capacity and effectiveness

There is a need for improved storage capacity estimates at the global, regional and local levels, and for a better understanding of long-term storage, migration and leakage processes. Addressing the latter issue will require an enhanced ability to monitor and verify the behaviour of geologically stored CO₂. The implementation of more pilot and demonstration storage projects in a range of geological, geographical and economic settings would be important to improve our understanding of these issues.

Impacts of ocean storage

Major knowledge gaps that should be filled before the risks and potential for ocean storage can be assessed concern the ecological impact of CO₂ in the deep ocean. Studies are needed of the response of biological systems in the deep sea to added CO₂, including studies that are longer in duration and larger in scale than those that have been performed until

now. Coupled with this is a need to develop techniques and sensors to detect and monitor CO₂ plumes and their biological and geochemical consequences.

Legal and regulatory issues

Current knowledge about the legal and regulatory requirements for implementing CCS on a larger scale is still inadequate. There is no appropriate framework to facilitate the implementation of geological storage and take into account the associated long-term liabilities. Clarification is needed regarding potential legal constraints on storage in the marine environment (ocean or sub-seabed geological storage). Other key knowledge gaps are related to the methodologies for emissions inventories and accounting.

Global contribution of CCS to mitigating climate change

There are several other issues that would help future decision-making about CCS by further improving our understanding of the potential contribution of CCS to the long-term global mitigation and stabilization of greenhouse gas concentrations. These include the potential for transfer and diffusion of CCS technologies, including opportunities for developing countries to exploit CCS, its application to biomass sources of CO₂, and the potential interaction between investment in CCS and other mitigation options. Further investigation is warranted into the question of how long CO₂ would need to be stored. This issue is related to stabilization pathways and intergenerational aspects.

SNATCHING CARBON DIOXIDE FROM MID-AIR

CARBON DIOXIDE BUBBLES beverages, fuels greenhouse-grown plants, spews out of fire extinguishers, and even decaffeinated coffee. Typically, it's obtained as a byproduct of ammonia, hydrogen, or ethanol production, but now several companies have developed equipment that extracts it directly from the air.

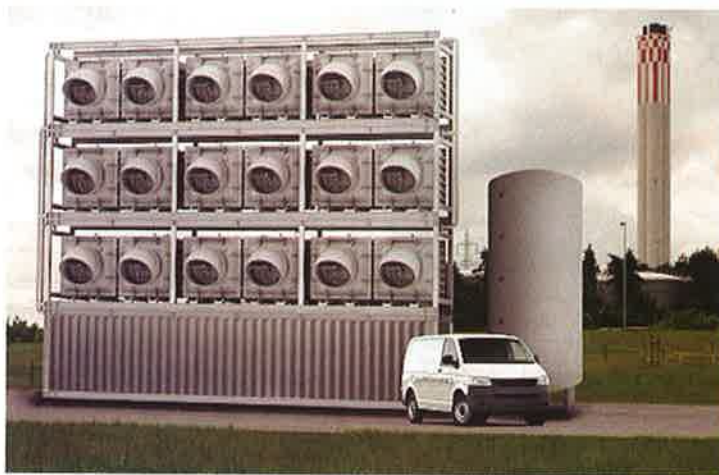
Today's commercial market uses 10-15 million metric tons of carbon dioxide. An additional 120 million tons goes for synthetic renewable fuels, said Dominique Kronenberg, COO of Climeworks, one of the companies that has developed these new CO₂-grabbing technologies, which are known as "direct air capture" of CO₂.

That might be enough to keep a few small companies afloat, and it could even be the beginning of a new industry. But it's a drop in the bucket compared to the 40 billion tons of CO₂ emitted annually.

Still, if the companies making CO₂-grabbing technology can one day achieve sufficient scale, it could contribute to offsetting global CO₂ emissions.

"The only way to prevent catastrophic climate change is to remove the CO₂ directly from the air," said Graciela Chichilnisky, a lead author of the United Nations Intergovernmental Panel on Climate Change's Fifth Assessment report. Climeworks, a seven-year-old startup based in Zurich, Switzerland, is building the first commercial carbon-dioxide-capture plant. The plant, which is being built at the Hinwil waste incineration plant just outside Zurich, should be operational early in 2017.

To remove the CO₂, Climeworks uses a solid sorbent material, and it uses low-grade heat to release the carbon dioxide. Climeworks developed the process and the filter material in collaboration with ETH Zurich and the Swiss Federal Laboratories for Materials Science and Technology. They hope to sell their carbon-capture machines, which



Six Climeworks CO₂ collectors fit in a standard 40-foot container. Each module captures 35 kg of CO₂ per hour, or 300 metric tons per year.

are modular, to other companies. These companies would then install them to obtain a free, local, and continual supply of carbon dioxide.

For the Swiss project, Climeworks' machines will capture 900 tons of CO₂ annually, and feed it to a nearby greenhouse that grows tomatoes, cucumbers and lettuce. The growers expect to see a 20 percent increase in growth, Kronen-

berg said. The Swiss Federal Office of Energy is paying for the project.

Ultimately, Climeworks is looking to produce synthetic low-carbon fuels from the carbon dioxide they capture.

Chichilnisky also leads a company, New York City-based Global Thermostat, that aims to combine direct-air capture of carbon dioxide with production of carbon-fiber composites. Global Thermostat has built a pilot-scale demonstration system on the campus of SRI International in Silicon Valley that consists of an air-handling chamber with an exchanger coated with a proprietary sorbent material with an affinity for CO₂. The units are designed to remove 50 percent of the

CO₂ from the air passing through. Global Thermostat releases the CO₂ by heating the sorbent to 85 °C, which also regenerates the sorbent.

A Canadian company called Carbon Engineering is also using captured carbon to produce synthetic low-carbon fuels. Their technology draws streams of air and CO₂ through a high-surface-area exchanger containing corrugated plastic sheets that are coated with a liquid absorbent. They collect CO₂ in the form of a liquid carbonate

solution, then release it as needed.

As direct-air-capture devices continue to become cost-effective and energy-efficient, large numbers of them could be deployed, perhaps as public-works projects to capture carbon and sequester it underground, Chichilnisky said. **ME**

R.P. SIEGEL is a technology writer based in Rochester, N.Y.

The post-2020 Cost-Competitiveness of CCS

Dr. Lars Stromberg
Co-Chair Taskforce Technology, ZEP
& Senior Advisor, Vattenfall AB



Why is this Work Ground-Breaking?

**Publicly
available cost
data on CCS**

...remains scarce

**Reliable base
for ZEP
estimations**

new, in-house data
provided **exclusively**
by 15 ZEP member
organisations

**Over 100
contributors
and 2 years
of work...**

**Complete CCS
value chains;
individual
reports
analyse costs**

- CO₂ Capture
- CO₂ Transport
- CO₂ Storage

**Focus on new-
build coal- and
gas-fired
power plants**

located at a generic
site in Northern
Europe from the
early 2020s

**The study
features a
BASE
and an
OPTIMISED
case**

**Reference
point for costs
of CCS**, based
on a “snapshot”
in time
(investment costs
referenced to Q2
2009)

Key Conclusions

CCS is applicable to both coal- and gas-fired power plants

- CCS can technically be applied to both coal- and gas-fired power plants
- Relative economics mainly depend on power plant cost levels, and fuel prices
- In the 2020s all CCS equipped power plants will operate in base-load since the variable generation cost of a CCS equipped plant will be considerably lower than the variable cost for a corresponding conventional plant.
- It is too early to distinguish a technology winner, due to that uncertainties are still large and differences small

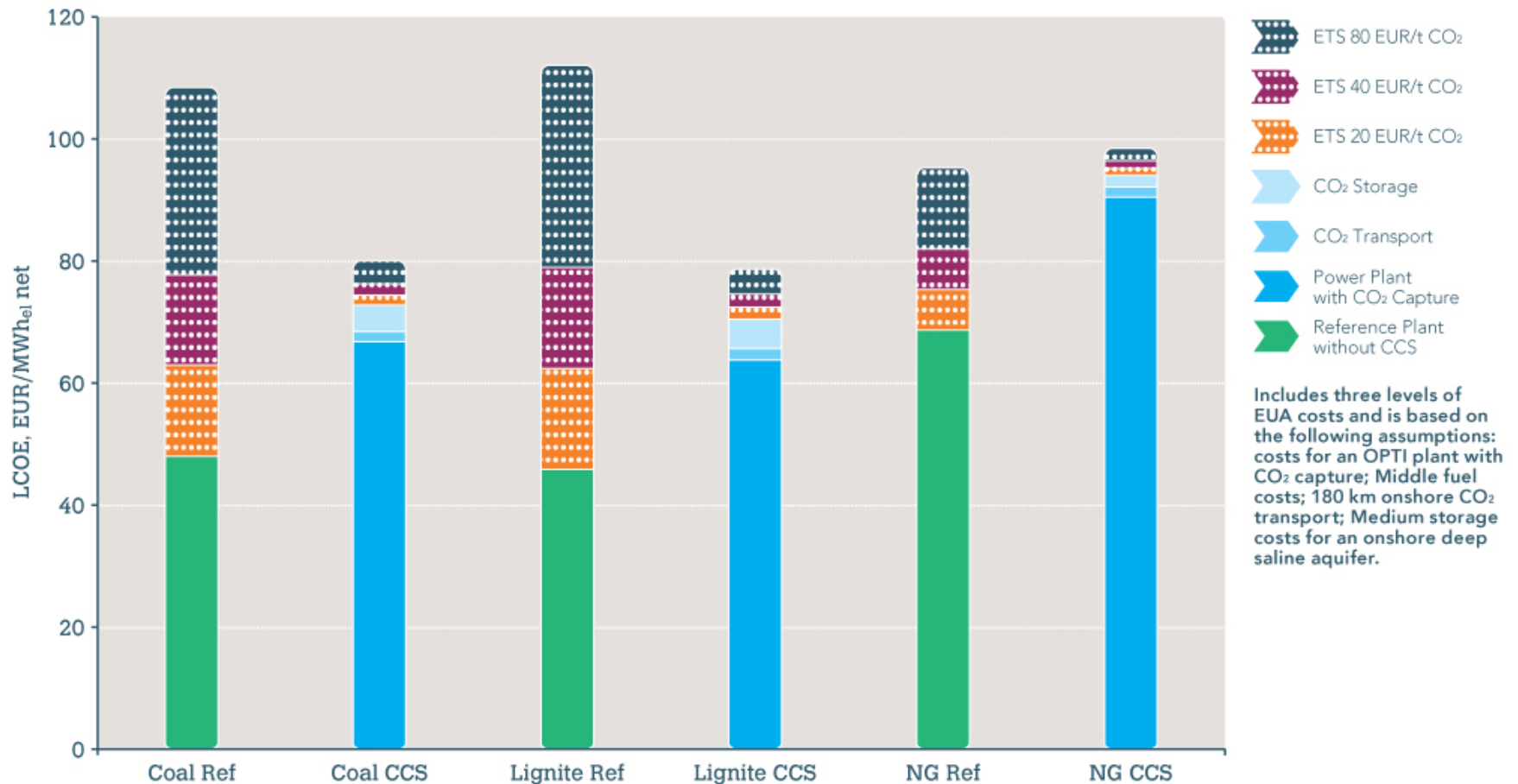
Key Conclusions

CCS will be cost-competitive with other low-carbon power technologies

- EU CCS demonstration programme will validate and prove the costs of CCS technologies and form the basis for future cost reductions (introduction of 2nd- and 3rd-gen. technologies)
- **Results of the reports indicate post-demonstration CCS will be cost-competitive with any other low-carbon energy technology (on-/offshore wind, solar power & nuclear), but also will form a reliable low-carbon power source**
- CCS is on track to become one of the key technologies for combating climate change
- ZEP will undertake a complementary study on the costs of CCS in the context of other low-carbon energy technologies

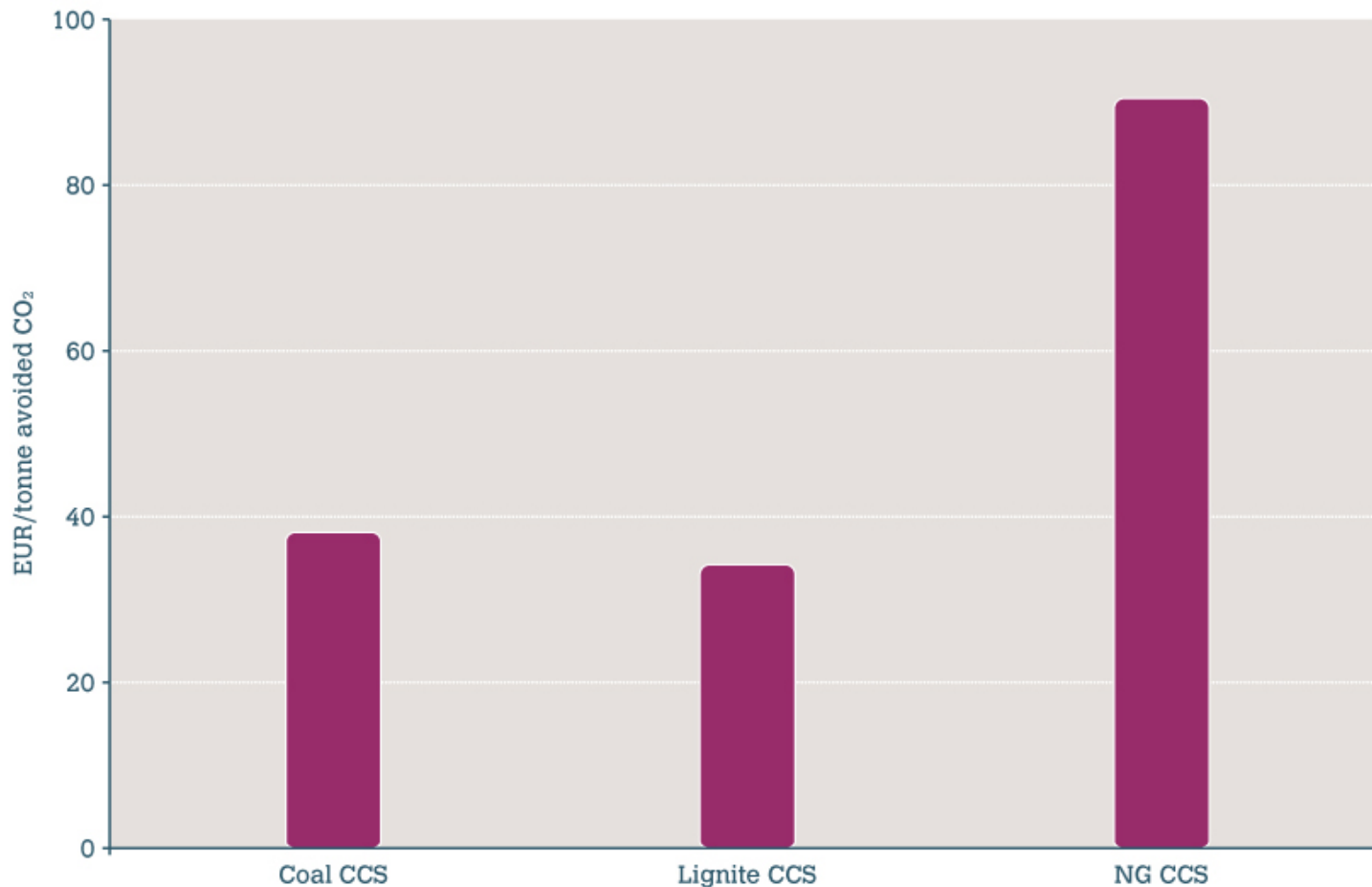
Levelized Cost of Electricity (LCOE) for Integrated CCS projects (coal and gas)

The Levelised Cost of Electricity (LCOE) of integrated CCS projects (blue bars) compared to the reference plants without CCS (green bars)



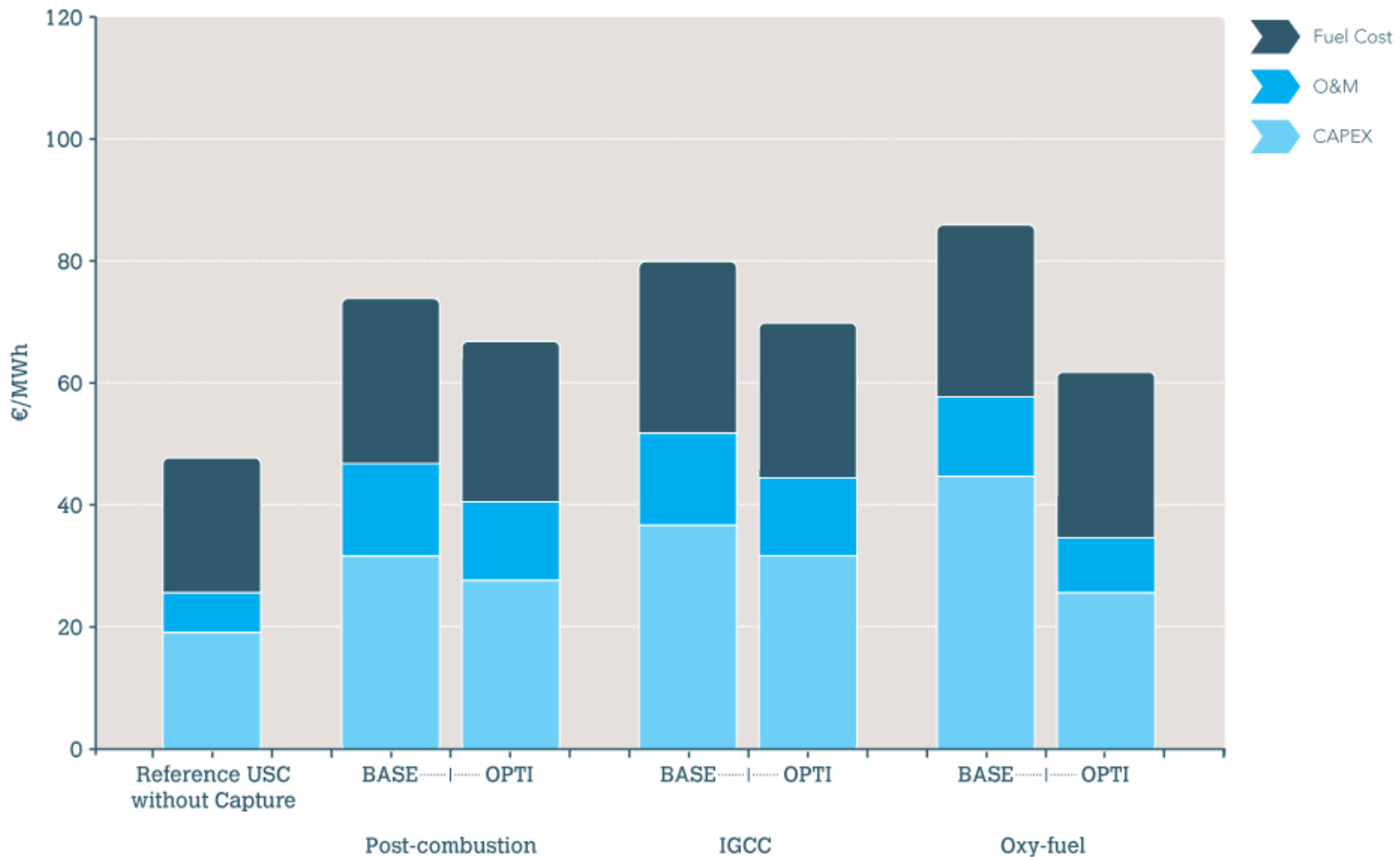
CO₂ Avoidance Costs – Price of EUAs to Justify Building CCS Projects vs. Plant w/o CCS

CO₂ avoidance costs for possible plants commissioned in the mid 2020s – the price of EUAs required to justify building CCS projects vs. a plant without CCS from a purely economic point of view (calculated on the same basis as previous graph)



LCOE for Hard Coal Plants w/CO₂ Capture (capture costs only)

The LCOE for hard coal-fired power plants with CO₂ capture (using Middle fuel costs)



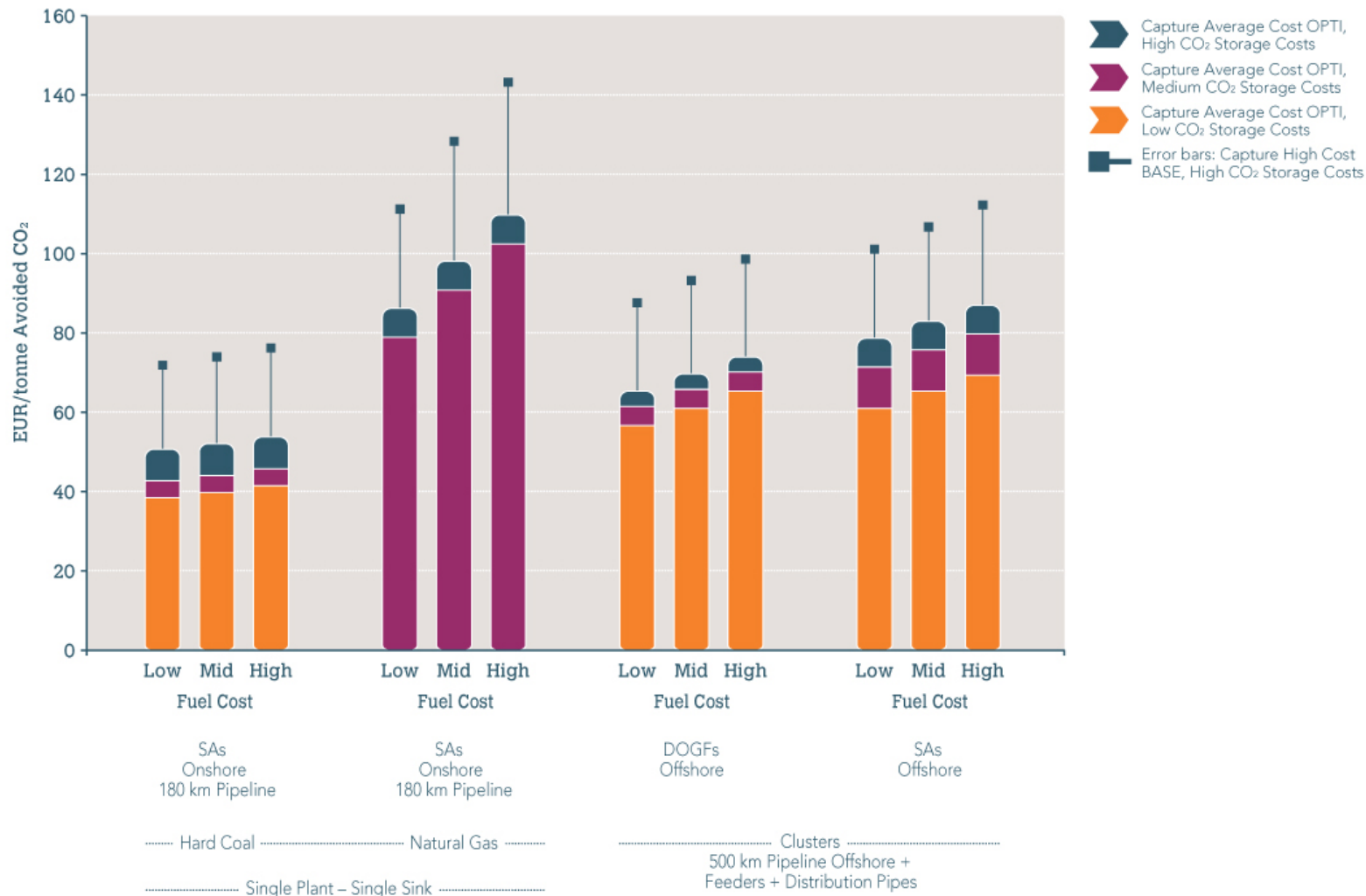
Key Conclusions

All three CO₂ capture technologies could be competitive once successfully demonstrated

- Currently no clear difference between capture technologies & all could be competitive once successfully demonstrated (using agreed assumptions & LCOE as main quantitative value)
- Fuel/investment costs are main factors influencing total costs
- Reports include the three main capture technologies (post-combustion, pre-combustion and oxy-fuel)...
- ...but exclude second-generation technologies (e.g. chemical looping, advanced gas turbine cycles)
- The LCOE and CO₂ avoidance costs calculated are higher than those of previous European capture cost studies, but tend to be slightly lower than majority of recent international studies

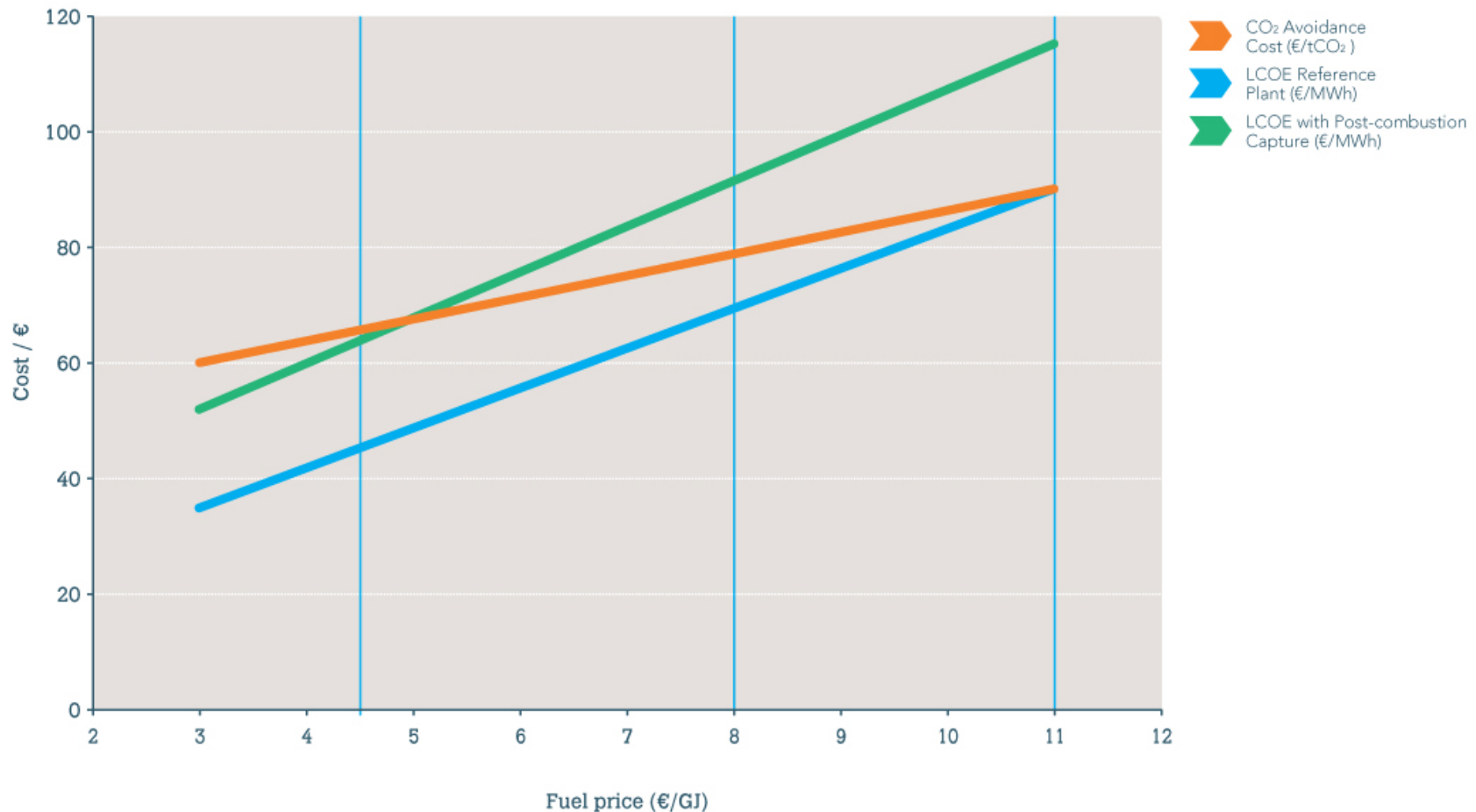
Total CO₂ Avoidance Costs for Integrated CCS Projects

Total CO₂ avoidance costs for integrated CCS projects – the price of EUAs required to justify building CCS projects vs. a plant without CCS from a purely economic point of view.



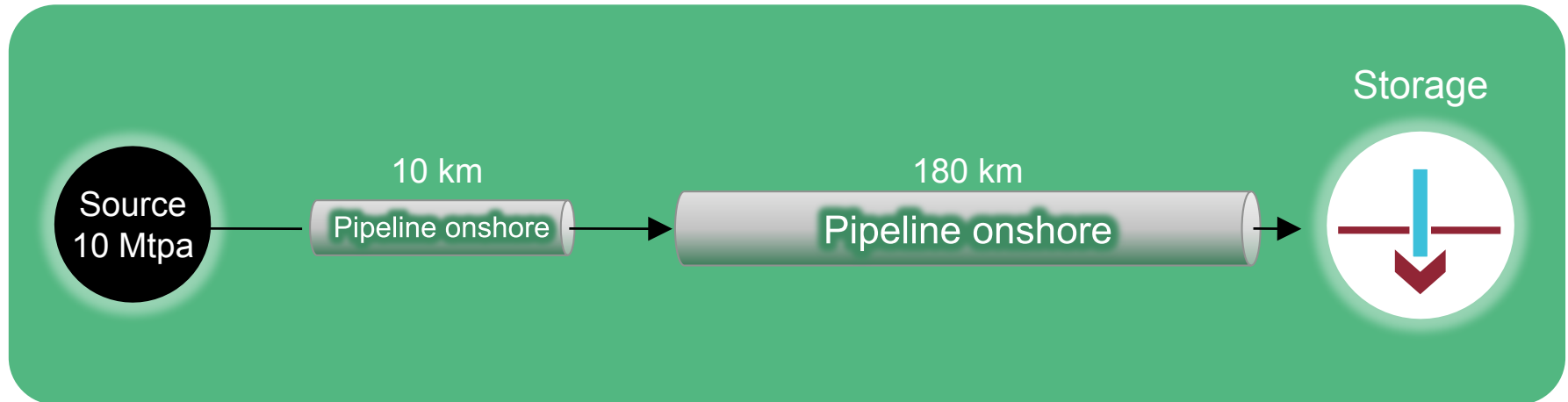
LCOE for Natural Gas Plants w/CO₂ Capture (capture costs only)

LCOE and CO₂ avoidance costs for natural gas-fired power plants with CO₂ capture are heavily dependent on the fuel cost. The vertical blue lines for €4.5, €8 and €11/GJ represent the Low, Middle and High cases used for gas fuel cost.

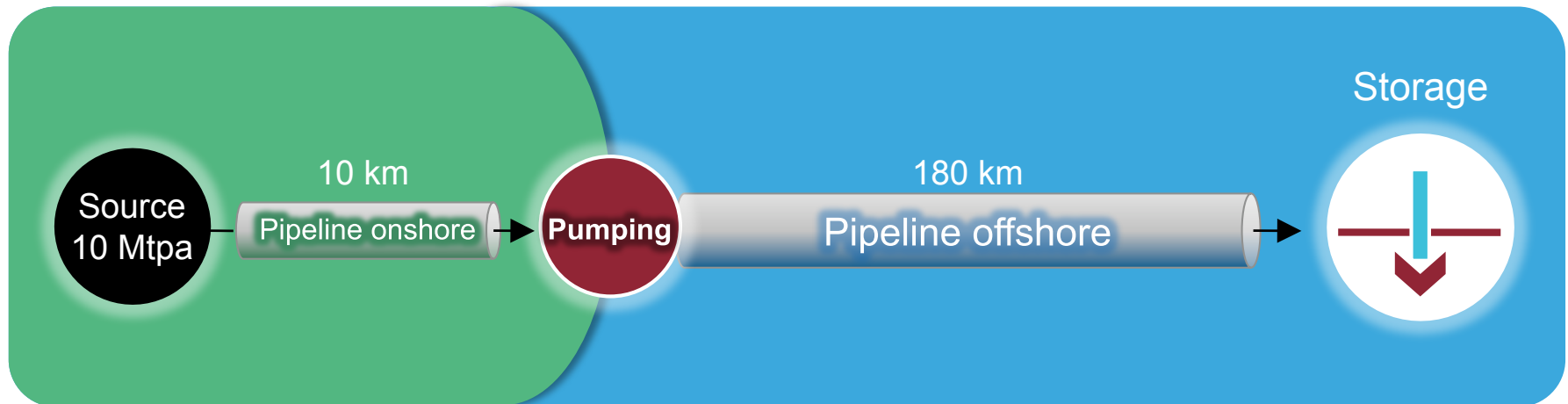


CO₂ Transport from Point-to-Point ...

Onshore spine

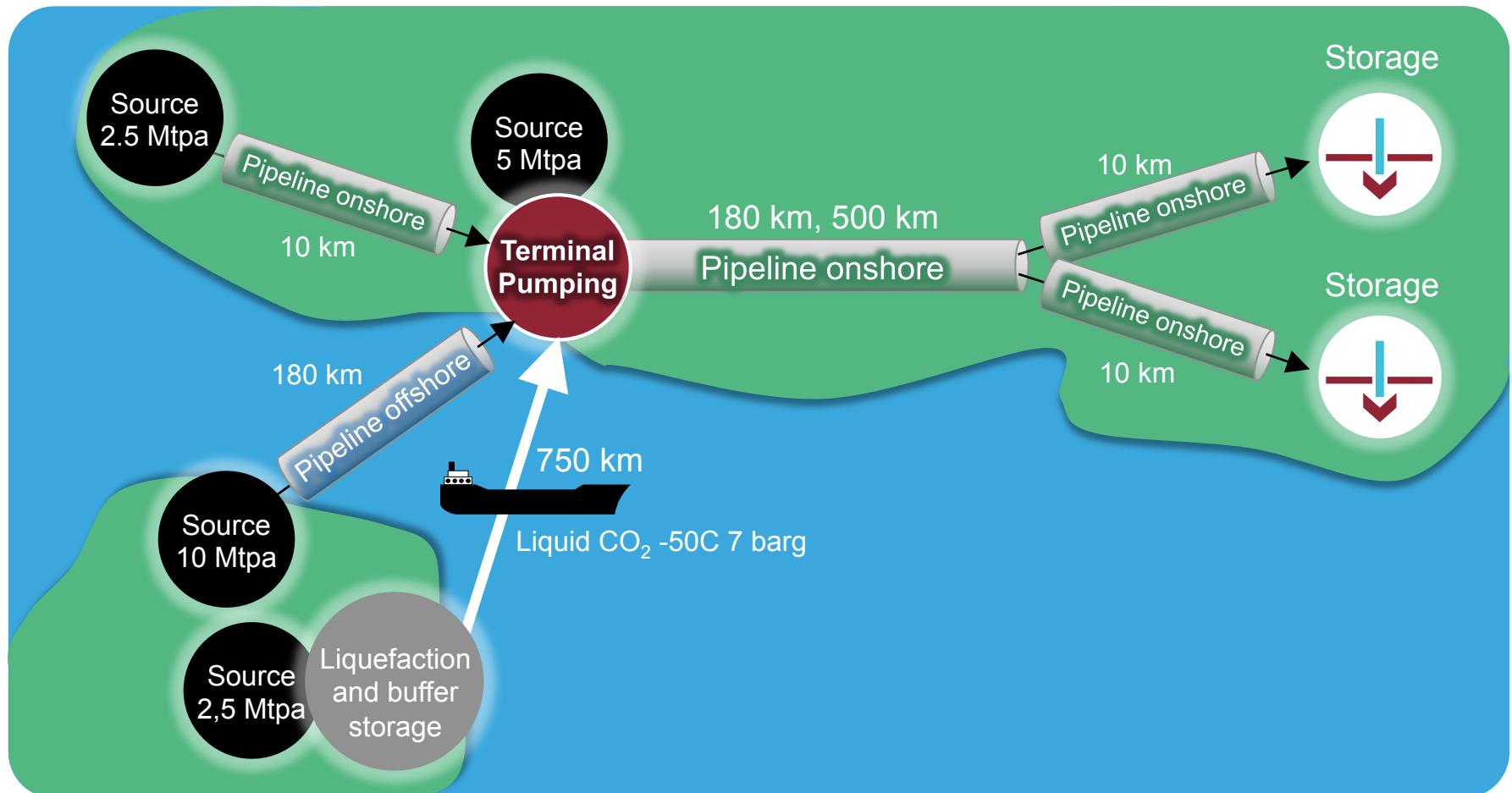


Offshore spine



... to Complex Networks

Complex networks with onshore pipeline spine of 180 km and 500 km



CO₂ Transport – Onshore vs. Offshore Pipelines

Short distance (180 km) pipeline;
SMALL volume transported
(2.5 MT CO₂ per year)



5.4 €/
tonne CO₂



onshore

9.3 €/
tonne CO₂



offshore

Short distance (180 km) pipeline;
LARGE volume transported
(20 MT CO₂ per year)



1.5 €/
tonne CO₂



onshore

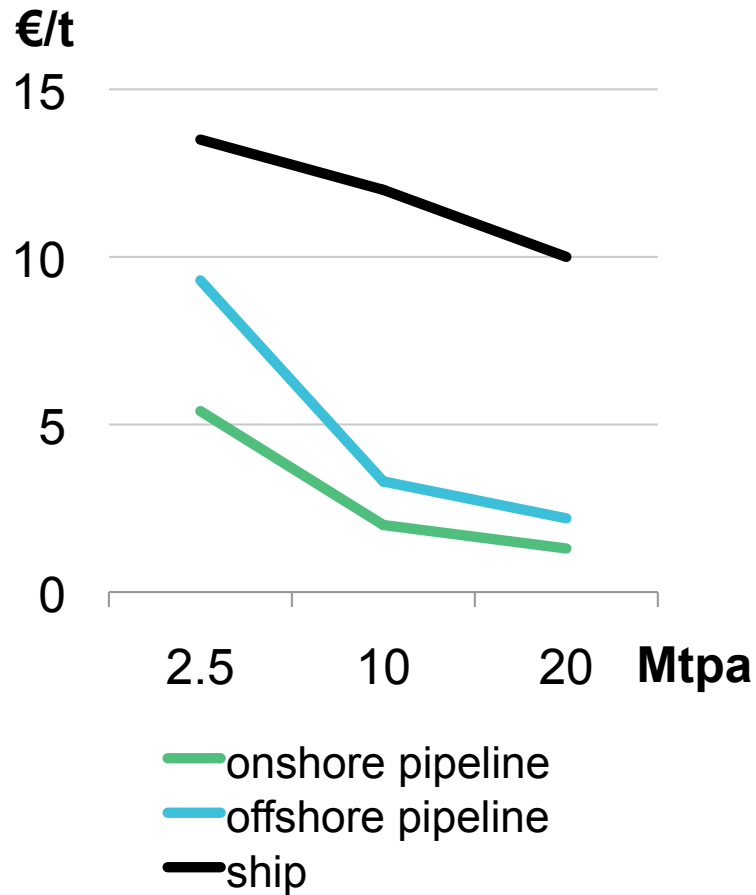
3.4 €/
tonne CO₂



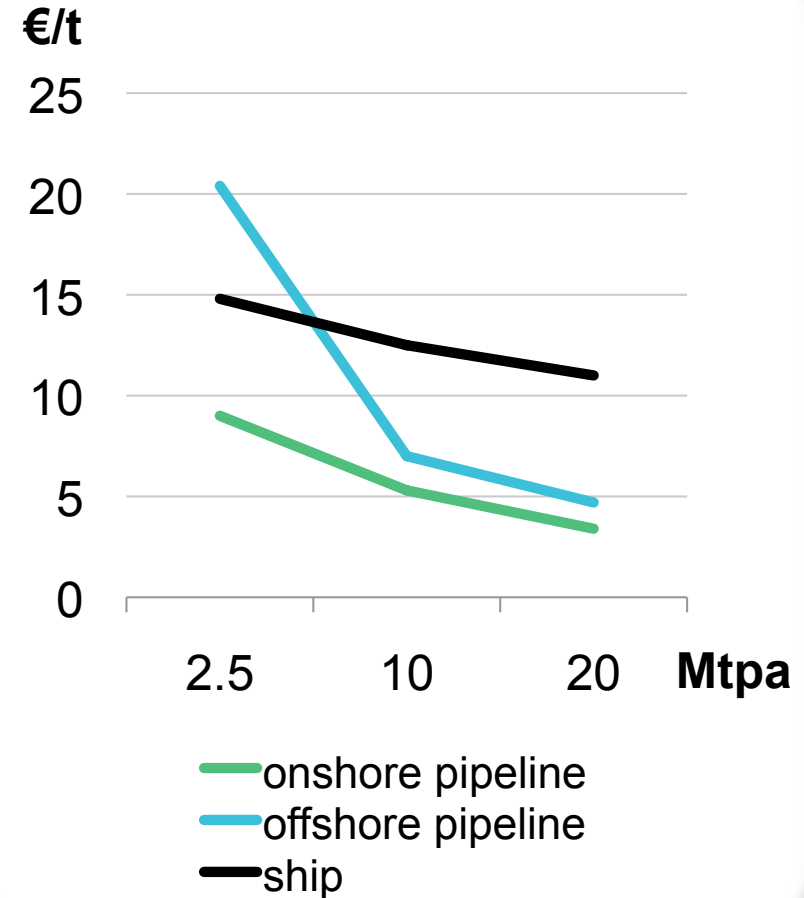
offshore

Total Cost Euro Per Tonne

Point-to-Point **180 km**



Point-to-Point **500 km**



Key Conclusions

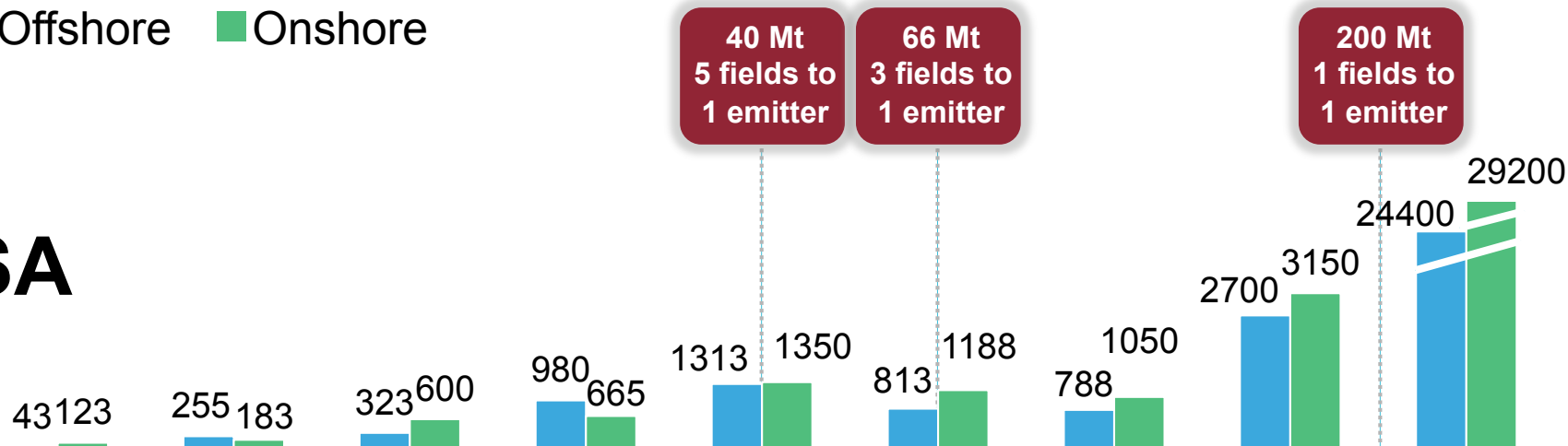
Early strategic planning of large-scale CO₂ transport infrastructure is vital to reduce costs

- Clustering plants to a transport network can achieve significant economies of scale – in both CO₂ transport/storage in larger reservoirs (on- and offshore)
- Large-scale CCS requires the development of a transport infrastructure equivalent to the current hydrocarbon infrastructure
- Greatly reduced long-term costs can be ensured with early strategic planning – including the development of clusters and over-sized pipelines – and the removal of cross-border restrictions

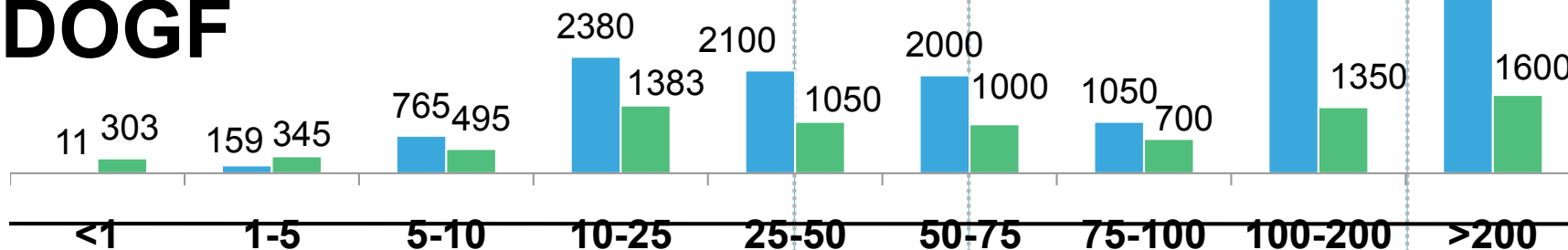
Storage Capacity Estimates

■ Offshore ■ Onshore

SA



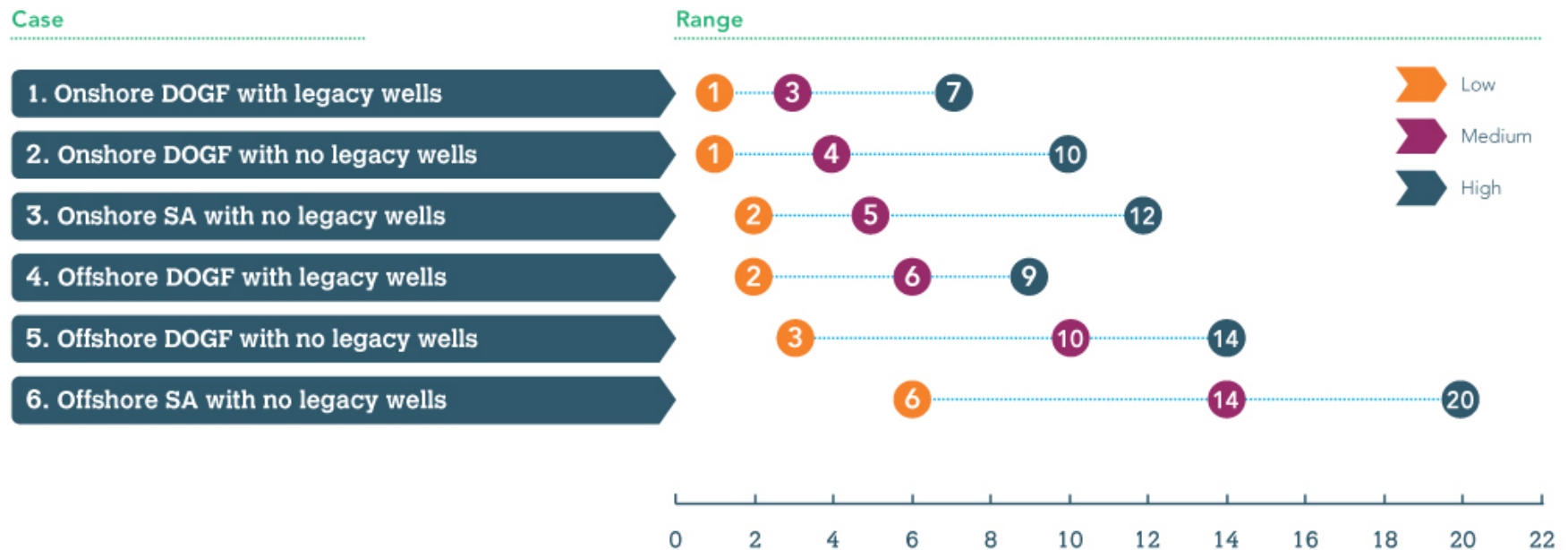
DOGF



CO₂ Storage Cost Ranges

Storage cost per case, with uncertainty ranges; purple dots correspond to base assumptions

€/tonne CO₂ stored



Ranges are driven by setting field capacity, well injection rate and liability transfer costs to Low, Medium and High cost scenarios

Key Conclusions

A risk-reward mechanism is needed to realise the significant aquifer potential for CO₂ storage

- **1 €/tonne CO₂ - 20 €/tonne CO₂ = CO₂ storage cost range**
- Location and type of storage site, reservoir capacity and quality are the main determinants for the costs of CO₂ storage
- Onshore is cheaper than offshore
- Depleted oil and gas fields are cheaper than deep saline aquifers
- Larger reservoirs are cheaper than smaller ones
- High injectivity is cheaper than poor injectivity
- Risk-reward mechanism required for large variation in storage costs (up to a factor 10) & risk of investing in saline aquifer exploration
- Such a mechanism will aid realisation of saline aquifer potential and ensure sufficient storage capacity

General Conclusions from the Study

CCS requires a secure environment for long-term investment

- Price of Emission Unit Allowances (EUAs) will not, initially, be a sufficient driver for investment after the first generation of CCS demonstration projects is built (2015 - 2020)
- Enabling policies required in the intermediate period – after the technology is commercially proven, but before the EUA price has increased sufficiently to allow full commercial operation

The goal:

to make new build power generation *with* CCS more attractive to investors than without it



What's Next?

- ZEP acknowledges costs of CCS will be inherently uncertain until further projects come on stream
- Cost reports don't provide a forecast of cost development but...
- ...will be updated every two years in line with technological developments and the progress of the EU CCS demo programme
- Future updates will also refer to co-firing with biomass, combined heat and power plants, and the role of industrial applications
- ZEP aims to undertake further work on costs to put the cost of CCS in perspective with other low carbon energy technology options

Executive summary

A complete analysis of CCS costs in the EU post 2020

Costs for different CO₂ capture, transport and storage options were first determined using data for the three main capture technologies (post-combustion, pre-combustion and oxy-fuel) applied to hard coal, lignite and natural gas-fired power plants; the two main transport options (pipelines and ships); and the two main storage options (depleted oil and gas fields, and deep saline aquifers), both on- and offshore.

The results were then combined in order to identify:

- 1. Total costs for full-scale, commercial CCS projects in the EU post 2020*
- 2. Key trends and issues for various deployment scenarios*
- 3. The impact of fuel prices, economies of scale and other factors, e.g. economic.*

Utilising new, in-house data provided by ZEP member organisations

Publicly available cost data on CCS are scarce. In order to obtain a reliable base for the estimations, it was therefore decided to use new, in-house data provided exclusively by ZEP member organisations – 15 in total. This included five independent power companies and manufacturers of power plant equipment for CO₂ capture.

individual numbers. To this end, one person per area was assigned to collect the information, align it, create mean values and render it anonymous. However, all contributors to the study, including those who provided detailed economic data, are named in Annex II. (In future updates ZEP intends to improve the transparency of data provision, without breaching confidentiality.)

In order to access the data, all basic cost information was kept confidential, regarding both source and

Power plants with CO₂ capture – from demonstration towards maturity

CO₂ capture comprises the majority of CCS costs. It is an emerging technology and historical experience with comparable processes shows that significant improvements are achievable – traditionally referred to as learning curves. While this study does not provide a forecast of how costs will develop over time, the following notations have been applied:

- A **base ("BASE") power plant** with CO₂ capture represents today's technology choices and full economic risk, margins, redundancies and proven components – as the very first units to be built following the demonstration phase. This constitutes a conservative cost level in the early 2020s.

- An **optimised ("OPTI") power plant** with CO₂ capture represents those units commissioned *after* the first full-size CCS plants have been in operation (~2025), including technology improvements, refined solutions, improved integration, but still using the three main capture technologies. These represent optimised cost estimations, based on first commercial experience.

In short, BASE and OPTI represent normal technology refinement and development following a successful demonstration (but not a mature technology, which will only be available in the longer term).

Taking fuel cost variations into account

The fuel costs used in this study are the best estimation of a representative fuel cost in 2020. Due to the considerable uncertainty – especially in the case of natural gas, where there is a wide difference of opinion on the impact of shale gas on future prices – it was decided to use Low, Middle and High values for both natural gas and hard coal.

The ranges were selected during Q4 2010 and are consistent with detailed reviews such as the EC Second Strategic Energy Review of November 2008⁶ for the year 2020 (assuming the Base Case of Average Oil Scenarios) and the UK Electricity Generation Cost Update, June 2010.⁷

For details of all major assumptions, see pages 10-14.

MAJOR RESULTS

a) Integrated CCS projects

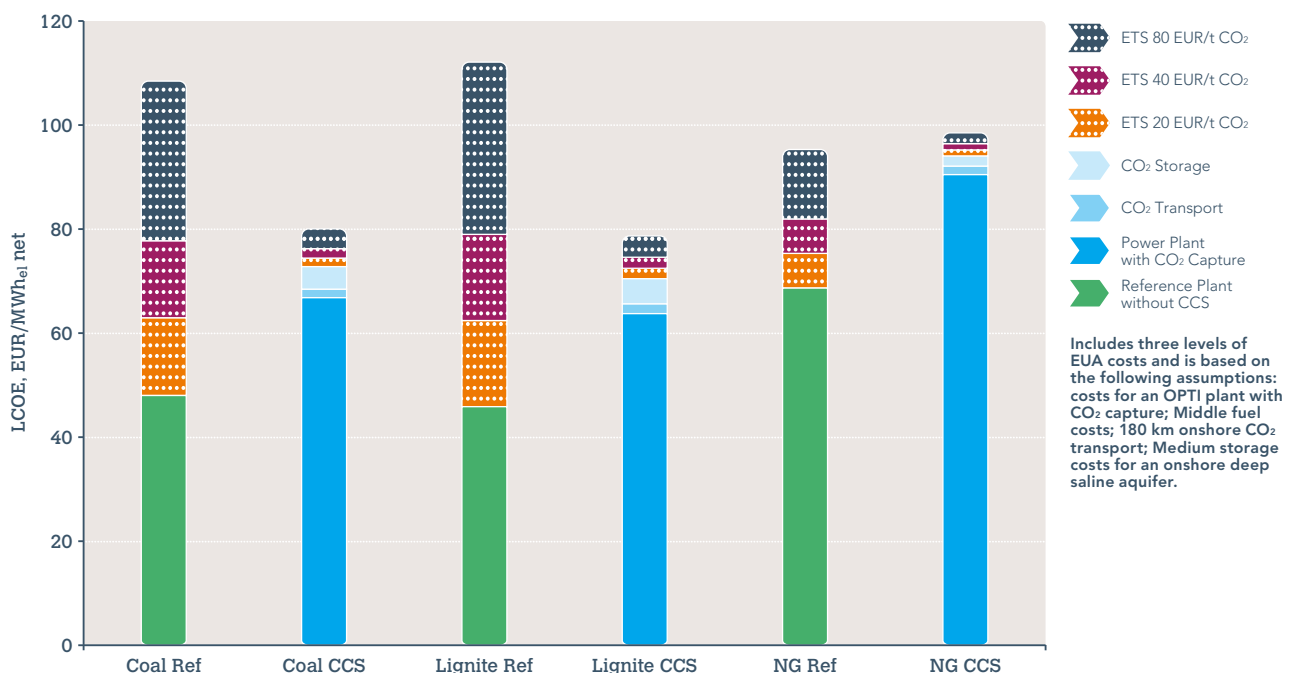
As each part of the CCS value chain includes multiple variants, the results provide a probable (but not complete) set of combinations. This includes a single plant to a single “sink” (storage site) and a cluster of plants to a cluster of sinks, with a sensitivity analysis provided per combination. In order to calculate CO₂ capture and avoidance costs, reference power plants *without* CO₂ capture were also established:

- A **natural gas-fired** single-shaft F-class Combined Cycle Gas Turbine producing 420 MW_{el} net, at an efficiency of 58-60% (LHV) for BASE and OPTI

plants respectively at €45-90/MWh depending on the fuel cost.

- For **hard coal**, a 736 MW_{el} net pulverised fuel (PF) ultra supercritical power plant at €40-50/MWh; for lignite, a PF-fired 989 MW_{el} net ultra supercritical plant and a lignite-fired 920 MW_{el} net PF ultra supercritical power plant with pre-drying of the lignite. All have steam conditions 280 bar 600/620°C live steam data.

Figure 1: The Levelised Cost of Electricity (LCOE) of integrated CCS projects (blue bars) compared to the reference plants without CCS (green bars)

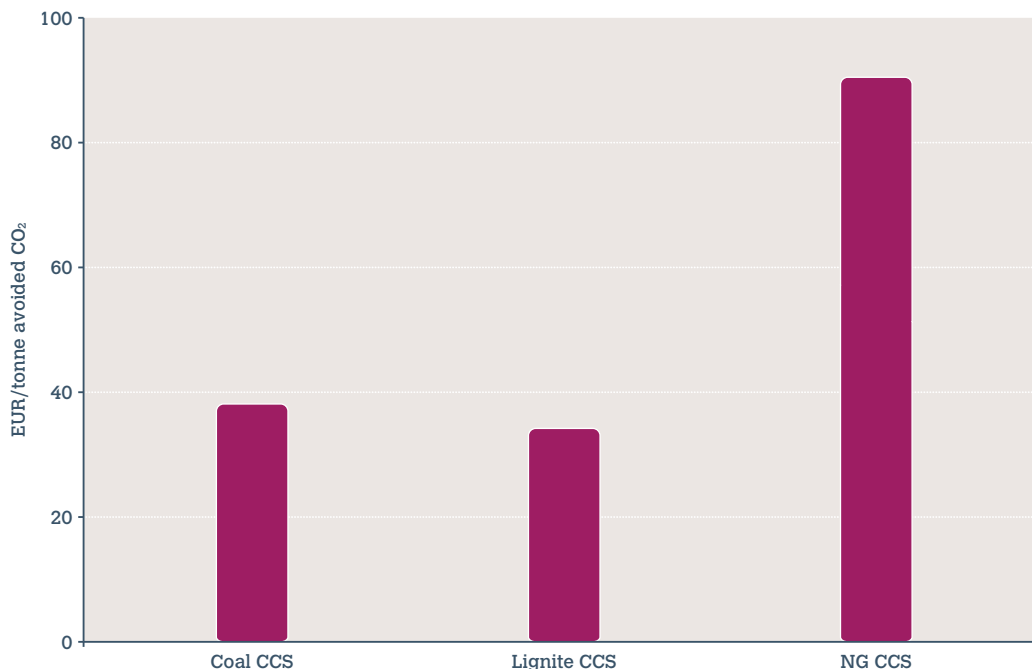


⁶ http://ec.europa.eu/energy/strategies/2008/2008_11_ser2_en.htm

⁷ www.decc.gov.uk/assets/decc/statistics/projections/71-uk-electricity-generation-costs-update-.pdf

- Following the demonstration phase, the application of CCS to fossil fuel power plants will result in higher electricity generating costs (e.g. increasing from ~€50/MWh up to ~€70/MWh for hard coal, excluding EUA costs). Corresponding CO₂ avoidance costs, compared to the reference plants with the same fuel, are shown in Figure 2 below.
- The two coal cases are similar in cost (~€70/MWh excluding EUA costs), while the gas case shows a higher cost (~€95/MWh excluding EUA costs). At lower EUA prices, the coal cases with CCS also come out more favourably than the gas case when compared to the reference plants. However, depending on different assumptions, the competitiveness of the technologies changes, with gas CCS becoming competitive at gas prices <€6/GJ. Gas CCS plants also produce less than half the amount of CO₂ to be captured per MWh than coal, resulting in lower transport and storage costs per MWh.
- The blue bars show that the combined cost of the power plant with capture comprises 80-90% of the total LCOE (~75% of the additional LCOE for CCS vs. the reference plants). However, CO₂ transport and storage to a large extent determine the location and decision to proceed with a project. Posing substantial development and scale-up challenges, costs are dominated by upfront investments, while any reward depends on volume streams, suitability of the storage site, utilisation and the development of an infrastructure (see below). While capture technology will be chosen based on a calculable economy, transport and storage costs therefore depend on the suitability of the chosen solution.

Figure 2: CO₂ avoidance costs for possible plants commissioned in the mid 2020s – the price of EUAs required to justify building CCS projects vs. a plant without CCS from a purely economic point of view (calculated on the same basis as Figure 1)



⁸ This is in accordance with EU estimates of EUA prices for 2025: http://ec.europa.eu/clima/documentation/roadmap/docs/sec_2011_288_en.pdf

- Figure 2 shows that the associated EUA break-even cost corresponds to a price of €37/tonne of CO₂ for hard coal; ~€34/tonne of CO₂ for lignite; and ~€90/tonne of CO₂ for gas. At an EUA price of €35/tonne of CO₂,⁸ these full-size, coal-fired CCS power plants are therefore close to becoming commercially viable, while the gas case is not. However, unabated gas power plants remain a commercial option, as shown in Figure 1.

N.B. Costs for OPTI plants assume a completely successful demonstration of the technology and/or that the first full-size CCS plants (following the EU CCS demonstration programme) have already been in operation. All reported costs exclude the exceptional development and other costs associated with the demonstration programme itself.

Post 2020, CCS will be cost-competitive with other low-carbon energy technologies.

For detailed results on integrated CCS projects, see pages 15-26.

b) CO₂ Capture

Capture costs were determined for first-generation capture technologies which will probably be ready for deployment in the early 2020s: post-combustion, IGCC with pre-combustion and oxy-fuel. All three were applied to hard coal and lignite-fired power plants, while post-combustion was applied to natural gas.

- On an LCOE basis, there is no significant difference between the three capture technologies for coal (within the available accuracy): hard coal-fired power plants without capture have an LCOE of ~€48/MWh (excluding EUA costs), rising to €65-70/MWh⁹ with capture for an OPTI plant. However, complexity differs considerably between the three options and none will become fully commercial until several large-scale plants have been operating following the demonstration phase. Achieving high plant availability is therefore key to keeping costs competitive.
- Natural gas-fired power plants without capture have an LCOE of ~€70/MWh, rising to ~€90/MWh with capture.⁹ However, as they have a different cost structure to coal-fired CCS plants – with a lower capital cost and higher fuel costs – the LCOE is competitive with coal⁹ if the gas price is low. At an

EUA price of ~€35/tonne of CO₂, unabated gas (at €5/GJ) is also competitive with coal with CCS.⁹

- CO₂ avoidance costs against a reference plant with the same fuel *calculated at the fence of the plants* therefore give <€30/tonne of CO₂ avoided for lignite; just over €30/tonne for hard coal; and ~€80/tonne for natural gas. (All figures exclude transport and storage costs.)
- On a unit basis, small power plants are more expensive than large; BASE plants are more expensive than OPTI plants. As the less expensive option will always be chosen during the first 10 years of deployment, the lower figures in this study are the most likely to represent CCS plants commissioned in the early 2020s. During this period, the three main capture options will also develop considerably, in parallel with second- and third-generation technologies.

All three CO₂ capture technologies could be competitive once successfully demonstrated.

For detailed results on CO₂ capture, see pages 27-31 and the underlying report: www.zeroemissionsplatform.eu/library/publication/166-zep-cost-report-capture.html

⁹ At Middle fuel prices

c) CO₂ Transport

The study presents detailed cost elements and key cost drivers for the two main methods of CO₂ transportation: pipelines and ships. These can be combined in a variety of ways – from a single source to a single sink, developing into qualified systems with several sources, networks and several storage sites over time. Several likely transport networks of varying distances are therefore presented, with total annual costs and a cost per tonne of CO₂ transported. The cost models operate with three legs of transport: feeders, spines and distribution, each of which may comprise on-/offshore pipelines or ships.

- The results show that pipeline costs are roughly proportional to distance, while shipping costs are fairly stable over distance, but have “step-in” costs, including (in this study) a stand-alone liquefaction unit potentially remote from the power plant. Pipelines also benefit significantly from scale, whereas the scale effects on ship transport costs are less significant.
- Typical costs for a short onshore pipeline (180 km) and a small volume of CO₂ (2.5 Mtpa) are just over €5/tonne of CO₂. This reduces to ~€1.5/tonne of CO₂ for a large system (20 Mtpa). Offshore pipelines are more expensive at ~€9.5 and €3.5/tonne of CO₂ respectively, for the same conditions. If length is increased to 500 km, an onshore pipeline costs €3.7/tonne of CO₂ and an offshore pipeline ~€6/tonne of CO₂.

- For ships, the cost is less dependent on distance: for a large transport volume of CO₂ (20 Mtpa) costs are ~€11/tonne for 180 km; €12/tonne for 500 km; and ~€16/tonne for very long distances (1,500 km), including liquefaction. For a smaller volume of CO₂ (2.5 Mtpa), costs for 500 km are just below €15/tonne, including liquefaction.
- For short to medium distances and large volumes, pipelines are therefore by far the most cost-effective solution, but require strong central coordination. Since high upfront costs, CAPEX and risk are barriers to rapid CCS deployment, combining ship and pipeline transport via the development of clusters could provide cost-effective solutions, especially for volume ramp-up scenarios. However, this entails the development of an infrastructure – including start-up costs, central planning and the removal of any cross-border restrictions. Technology and final costs therefore appear to be less of an issue than the development of a rational system for transport.

Early strategic planning of large-scale CO₂ transport infrastructure is vital to reduce costs.

For more detailed results on CO₂ transport, see pages 32-34 and the underlying report: www.zeroemissionsplatform.eu/library/publication/167-zep-cost-report-transport.html

d) CO₂ Storage

Publicly available data on CO₂ storage costs barely exists. A “bottom-up” approach was therefore taken, using cost components provided by ZEP members with an in-depth knowledge of closely linked activities and consolidated into a robust, consistent model. In order to cover the range of potential storage configurations and still provide reliable cost estimates, storage was divided into six main “typical” cases, according to major differentiating elements: depleted oil and gas fields (DOGF) vs. deep saline

aquifers (SA); offshore vs. onshore; and whether existing (“legacy”) wells were re-usable.

- The cost range is large – from €1 to €20/tonne of CO₂. On the assumption that the cheaper available storage sites will be developed first, and the more expensive when capacity is required, it could be argued that storage costs for the early commercial phase will be at the low/medium levels of the defined ranges for onshore SA at €2-12/tonne;

¹⁰ In the commercial phase

onshore DOGF at €1-7/tonne; offshore SA (with the largest capacities) at €6-20/tonne; and offshore DOGF at €2-14/tonne. In other words:

- onshore is cheaper than offshore
 - DOGF are cheaper than SA (particularly if they have re-usable legacy wells)
 - offshore SA show the highest costs and the widest cost range
 - sensitivity is dominated by field capacity, injection rate and depth.
- The availability and capacity of suitable storage sites developed into a key consideration. In terms of numbers, the majority of suitable sites are below the estimated capacity of 25-50 Mt, which corresponds to the need for more than five reservoirs to store 5 Mtpa¹⁰ of CO₂ for 40 years; the majority of estimated capacity is found in very large DOGF and SA (>200 Mt capacity).

- In conclusion, CO₂ storage capacity is available in Europe. However, the best known storage sites are also the smallest and not sufficient for a larger system. Offshore – followed by onshore – SA have the largest potential, but also the highest costs. If the best options can be used, costs could be as low as a few €/tonne, rising to tens of €/tonne if the larger and more remote SA have to be used. Developers of these more efficient, but less known, storage sites must therefore be rewarded for taking on the risk and upfront costs required for their exploration and development.

Given the large variation in storage costs and the risk of investing in the exploration of deep saline aquifers that are ultimately found to be unsuitable, a risk-reward mechanism is needed to realise their significant potential.

For more detailed results on CO₂ storage, see pages 35-37 and the underlying report: www.zeroemissionsplatform.eu/library/publication/168-zep-cost-report-storage.html.

Sensitivities

A sensitivity analysis of the cost results was calculated for a supercritical OPTI hard coal-fired power plant, with post-combustion capture and storage in an onshore SA. This shows that fewer running hours result in a much higher cost (€19/MWh higher LCOE when plant load factor reduces from 7,500 to 5,000 hours per year). CAPEX and WACC also give relatively large variations, which is to be expected given that capital costs dominate for a coal-fired power plant: +/- 25% CAPEX leads to LCOE changes of +/- €8/MWh; +/-2% points from the 8% WACC leads to LCOE changes of +€6/–€5/MWh).

Plant life, however, shows a low sensitivity since the cost calculation is based on the net present value of the investment. Storage costs also make

a small contribution to overall costs. Due to the relatively cheap fuel, the efficiency of the capture (absorption–desorption) process is also less important, while fuel costs as such have a larger impact. (Changing the Middle fuel cost from €2.4/GJ to a Low €2/GJ and a High €2.9/GJ leads to LCOE changes of –€4/+€5/MWh.)

Due to the cost structure for a natural gas-fired CCS power plant – with substantially lower investment costs, somewhat lower O&M costs and almost three times higher fuel costs – the total sensitivity is the reverse, i.e. much more influenced by fuel cost and less by capital.

Methodology

A complete analysis of CCS costs in the EU post 2020

The ZEP cost study presents best current estimates for full-scale commercial CCS in the power sector in Europe post 2020, based on new, in-house data provided by member organisations. The final results assume that all elements of the value chain have been successfully demonstrated in the EU CCS demonstration programme and other demonstration initiatives worldwide.

Three Working Groups within ZEP's Taskforce Technology first analysed the costs related to CO₂ capture, CO₂ transport and CO₂ storage respectively. The results of these three individual reports¹¹ were then combined to give total costs for integrated CCS projects

a) Utilising new, in-house data from ZEP member organisations

It is theoretically possible to obtain basic data on CCS technologies from several sources. However, most public reports have either used budget offers from manufacturers, quoted other studies, or calculated equipment costs from academic models. Several ZEP members have had difficulties obtaining relevant information for their specific situation and therefore undertaken a considerable amount of work themselves. Costs also differ significantly between different regions, such as the USA, Asia and Europe; and vary in time, as several public cost indices illustrate.

As reliable external cost data proved scarce, it was therefore decided to utilise the technical and economical knowledge of ZEP members who either manufacture, or have substantial research and experimental experience in CCS – 15 organisations in total. (This included five independent power companies and manufacturers of power plant equipment for CO₂ capture.) Indeed, many are already undertaking detailed engineering studies for CCS demonstration projects, encompassing the entire value chain. Power companies regularly cooperate with several manufacturers and are even now building plants of the kind described here (currently without CCS). The oil and gas industry also has decades of experience with natural gas

analogues for the majority of the transport and storage chain.

Thanks to the diverse representation within ZEP, data covering all aspects of the costs and technology performance were therefore assembled, with important CAPEX figures (and appropriate contingencies) for the coal-fired CO₂ capture cases provided by the power companies and equipment suppliers from engineering studies completed to date.

In order to access the data, all basic cost information was kept confidential, regarding both source and individual numbers. To this end, one person per area (the co-author of the underlying report) was assigned to collect the information; compare and adjust it if large discrepancies were apparent; create mean values; and render it anonymous. However, all contributors to the study, including those who provided detailed economic data, are named in Annex II. In future updates, ZEP intends to improve the transparency of data provision, without breaching confidentiality.

N.B. Data for this report were collected in spring 2010, but in order to align them, all sources were recalculated by indices to the second quarter of 2009.

¹¹ www.zeroemissionsplatform.eu/library/publication/166-zep-cost-report-capture.html;
www.zeroemissionsplatform.eu/library/publication/167-zep-cost-report-transport.html;
www.zeroemissionsplatform.eu/library/publication/168-zep-cost-report-storage.html

b) Power plants with CO₂ capture – from demonstration towards maturity

Contributors of basic data were also asked if they could illustrate the development of both costs and technical solutions over time. Since the answers were not totally consistent – and included other considerations besides pure technology development – the results are not presented in the context of traditional learning curves. However, the following notations were applied:

- **A base (“BASE”) power plant with CO₂ capture** represents today’s technology choices – including full economic risk, margins, redundancies and proven components – as the very first units to be built following the demonstration phase. This constitutes a conservative cost level in the early 2020s.
- **An optimised (“OPTI”) power plant with CO₂ capture** represents those units commissioned after the first full-size CCS plants have been

in operation (~2025), including technology improvements, but not a completely new technology, e.g. improved steam data of the plant; improved energy utilisation in conventional equipment; higher level of plant integration; lower risk margins etc. In short, normal product development based on first commercial experience.

In short, BASE and OPTI represent normal technology refinement and development following a successful demonstration (but not a mature technology, which will only be available in the longer term).

See page 17 for a more detailed description of BASE and OPTI methodologies.

c) The application of CCS to carbon-intensive industrial sectors

This study focuses on CCS for power generation, but it could also potentially reduce CO₂ emissions from the steel, cement, refineries/petrochemical and other industries. Some of the applied processes in these industries have higher concentrations of CO₂ in some of their off-gases (natural gas processing, cement, steel, hydrogen manufacturing for refineries, ammonia production etc.) which could lead to comparable or lower capture costs than those for coal.

However, the variety, uniqueness and scale of industrial production processes will lead to a wide range of capture costs and less generic solutions which are not easy to compare. ZEP will therefore seek cooperation with relevant industries in order to reference the costs of industrial CCS applications – including biomass-based applications – in future updates of the ZEP cost report.

d) Major assumptions

For consistency, a number of common assumptions were established and applied across all three Working Groups. These are presented below in order to allow full transparency and comparisons with specific projects. The sensitivity of changes to these basic assumptions were also analysed and the results are given below.

Economic assumptions

Volatility in plant and equipment costs, short- and long-term costs and currency developments have

been addressed by indexing all estimates to one specific period – the second quarter of 2009. Any user of the cost data in this report is therefore advised to estimate and adjust for developments after this period. The cost basis is European and all reported costs are in euros; currency exchange rates representative of the actual date of original studies have been used.

A real (without inflation) cost of capital for investments, here designated as WACC (Weighted

Average Cost of Capital), is assumed to be 8% (with sensitivity evaluated for 6% and 10%). The chosen real WACC reflects required return on equity and interest rates on loans and it is assumed that the inflation rate is equal for all costs and incomes during the project life. The required CAPEX has been annualised and discounted back to the present using the WACC.

The fuel costs used in this study are the best estimation of a representative fuel cost in 2020. Owing to the considerable uncertainty – especially

in the case of natural gas, where there is a wide difference of opinion on the impact of shale gas on future prices – it was decided to use Low, Middle and High values for both natural gas and hard coal. The ranges were selected during Q4 2010 and are consistent with detailed reviews such as the EC Second Strategic Energy Review of November 2008¹² for the year 2020 (assuming the Base Case of Average Oil Scenarios), and the current UK Electricity Generation Cost Update.¹³

The following fuel costs were selected for the study:

Fuel Costs	Low	Middle	High
Hard coal - €/GJ	2.0	2.4	2.9
Lignite - €/GJ	1.4	1.4	1.4
Natural gas - €/GJ	4.5	8.0	11.0

For electricity consumptions for CO₂ transport and storage operations (beyond the power plants), an electricity purchase price of €0.11/kWh was found to be representative. The agreed CCS project lifetime is 40 years for commercial hard coal-based and lignite-based projects; 25 years for natural gas turbine-based projects.

Technical assumptions

Due to the inherently high investments for thermal power plants with CO₂ capture, it is assumed that all power plants will operate in base load, operating for 7,500 hours equivalent full load each year. This is also consistent with the fact that a CCS plant, if realised, will have a lower variable operations cost than a corresponding plant without CCS (when including the EUA price) and thus always be dispatched before any other fossil fuel power plant, including gas. The only reason why a CCS plant would not work in base load mode is either because there is more prioritised power (e.g. Wind) available than is needed, or if the technical availability is lower.

Power plant concepts with CO₂ capture

The technologies studied are first-generation capture technologies: post-combustion CO₂ capture; IGCC with pre-combustion capture; and oxy-fuel, adapted

to hard coal, lignite and natural gas, as applicable. For each technology, a range of costs was developed for BASE and OPTI power plants (see above).

For hard coal-fired and lignite-fired power plants, the following power plant concepts were used:

- PF ultra supercritical (280 bar 600/620°C steam cycle) power plant with post-combustion capture based on advanced amines.
- Oxygen-blown IGCC with full quench design, sour shift and CO₂ capture with F-class Gas Turbine (diffusion burners with syngas saturation and dilution).
- Oxy-fired PF power plant with ultra supercritical steam conditions (280 bar 600/620°C steam cycle).

For the integrated CCS projects, average expected values have been used for OPTI plants with capture, since the costs for the plant concepts are similar. For hard coal-fired power plants, average sizes and quantities of captured CO₂ for one power plant block are:

- Net electric capacity: ~700 MW_e
- Captured CO₂: 0.85 t/MWh_e net, ~4.5 Mt/year.

¹² http://ec.europa.eu/energy/strategies/2008/2008_11_ser2_en.htm

¹³ www.decc.gov.uk/assets/decc/statistics/projections/71-uk-electricity-generation-costs-update-.pdf

For lignite-fired power plants, average sizes and quantities of captured CO₂ for one power plant block are:

- Net electric capacity: ~800 MW_{el}
- Captured CO₂: 0.95 t/MWh_{el} net, ~5.5 Mt /year.

For natural gas-fired Combined Cycle Gas Turbines (CCGT) power plants for the integrated CCS projects with OPTI post-combustion CO₂ capture (based on an advanced amine), the sizes and quantities of captured CO₂ for one power block (consisting of one single-shaft F-class CCGT) are:

- Net electric capacity: ~350 MW_{el}
- Captured CO₂: 0.33 t/MWh_{el} net, ~1 Mt/year.

Reference power plants concepts without CO₂ capture

The corresponding reference power plants without CO₂ capture used in this study are:

- Natural gas-fired single-shaft F-class Combined Cycle Gas Turbine producing 420 MW_{el} net at an efficiency of 58% (LHV and BASE) or 60% (LHV and OPTI).
- Hard coal 736 MW_{el} net pulverised fuel (PF) ultra supercritical (280 bar 600/620°C steam cycle) power plant.
- Lignite-fired 989 MW_{el} net PF ultra supercritical (280 bar 600/620°C steam cycle) power plant and a lignite-fired 920 MW_{el} net PF ultra supercritical (280 bar 600/620°C steam cycle) power plant with pre-drying of the lignite.

A key assumption for the design of the entire CCS chain concerns production volumes and profiles. Based on the power plant concepts with CO₂ capture, three different annual CO₂ volumes have been considered:

- 2.5 million tonnes per annum (Mtpa) representing a commercial natural gas-fired plant with CCS (a plant with two power blocks), or a coal-based demonstration project.
- 10 Mtpa representing a full-scale commercial coal-fired power plant with CCS (a plant with two power blocks).

- 20 Mtpa representing a typical full-scale, mature CCS cluster.

The production profile is assumed to be linear, with equal hourly production rates of 333, 1,330 and 2,660 tonnes CO₂/hour respectively during the 7,500 hours per year. In reality, a wide variety of volumes will be present, but the three categories illustrate the possible modus operandi for the systems.

Boundary conditions

Boundaries between the three elements of capture, transport and storage have been defined as follows:

- *Compression/liquefying/processing of the captured CO₂ to meet the requirements of the initial transport process* are included in the design and cost of the power plants with CO₂ capture. The assumed delivery conditions for CO₂ from the capture plant are:
 - 110 bar and ambient temperature (max. 30°C) for *pipeline as initial transport*, with CO₂ quality requirements that should permit the use of cost-effective carbon steel materials in CO₂ pipelines and meet health and safety requirements.
 - 7 bar and -55°C for *ship as initial transport*, with CO₂ quality as above for pipelines, but with a water content low enough to allow carbon steel for the logistic system.
- *The transport process is assumed to deliver the CO₂ to the storage process at the well-head* in the following condition:
 - Temperature offshore: ambient seawater temperature, from 4°C to 15°C
 - Temperature onshore: ambient ground temperature ~10°C
 - Pressure: minimum 60 bar
 - Cost estimates for onshore pipelines assume that the pipeline terminates in a valve and a metering station, which constitute the interface to the storage process onshore.
 - Both offshore pipeline and ship transport cost estimates include the cost of a sub-sea well-head template, whereas manifold costs are assumed to be included in storage costs with the drilling of injection wells. The boundary towards storage is therefore at the sea bottom surface, below this template. For ship transport,

Figure 6: Costs per tonne of CO₂ captured for integrated CCS projects (hard coal and natural gas) calculated with Low, Middle and High Fuel costs. Transport and Storage costs are also added (Single Source – Single Sink)

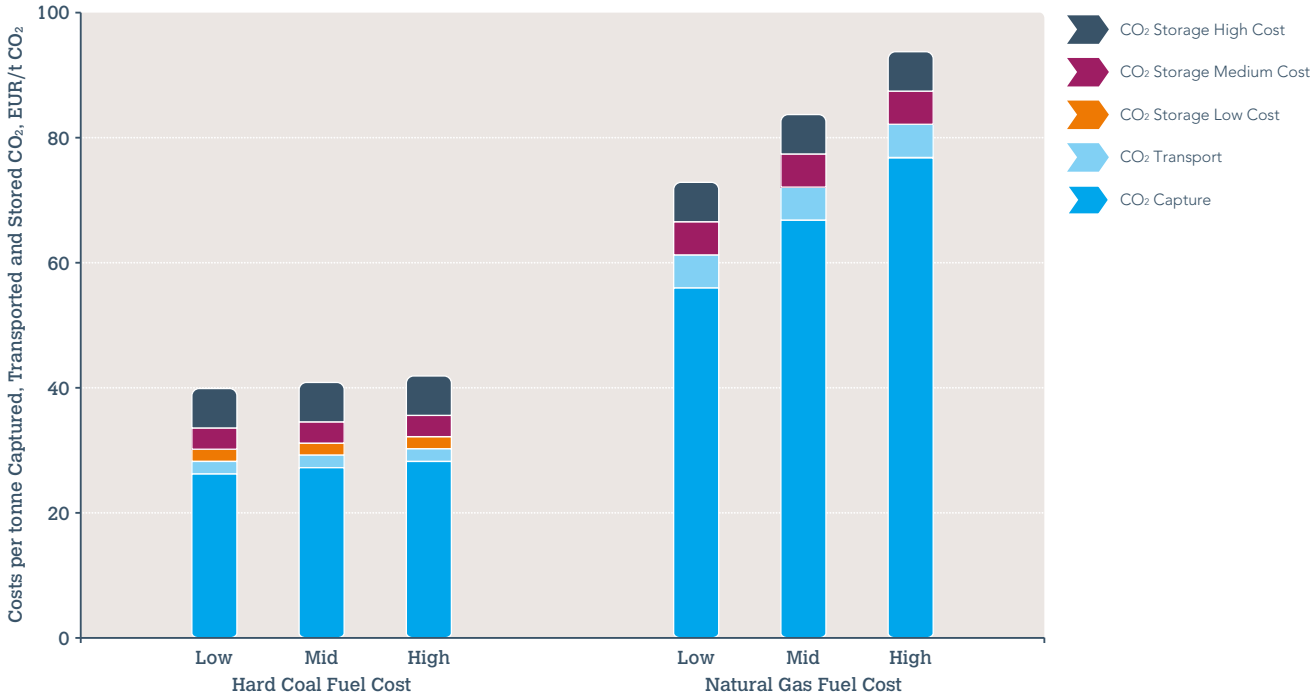


Figure 7: Additional LCOE for integrated CCS projects (hard coal and natural gas) vs. reference plants without CCS (Single Plant – Single Sink). Calculations are made for Low, Middle and High fuel costs (excluding any saved costs for EUAs)

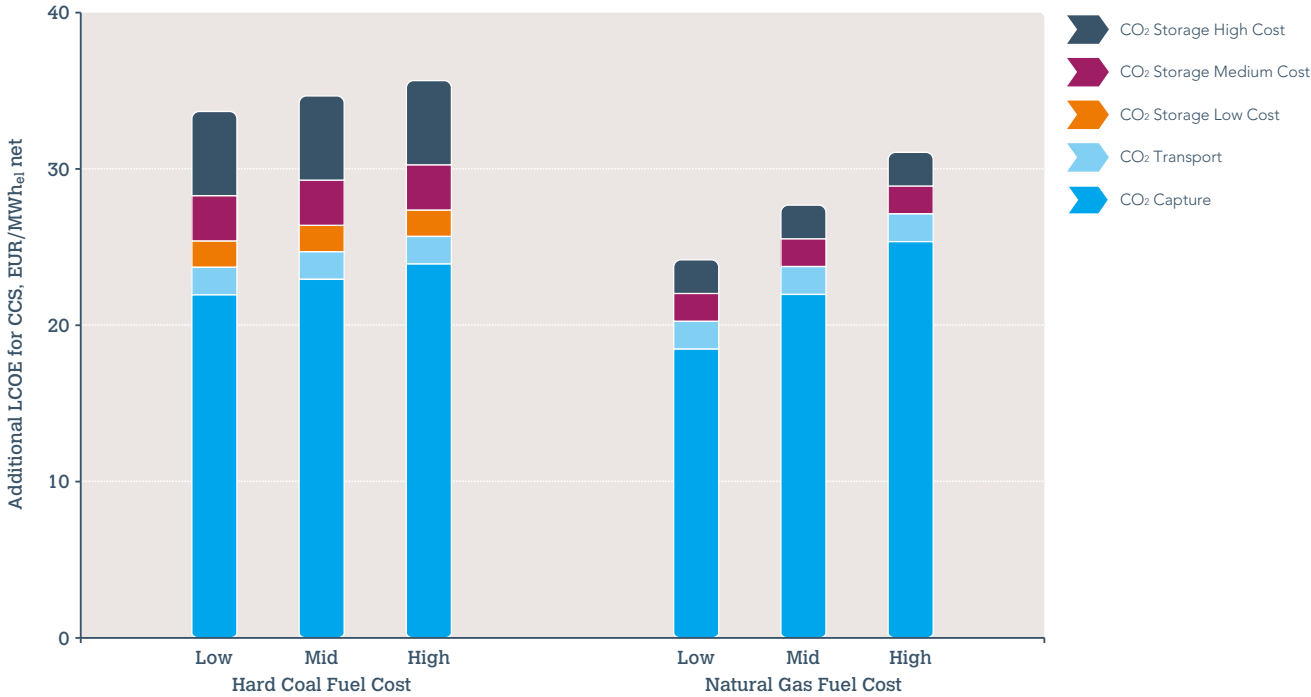


Figure 8: Calculated costs per tonne of CO₂ captured for transport and storage for integrated projects. For the Clusters, the use of SA and DOGF are highlighted

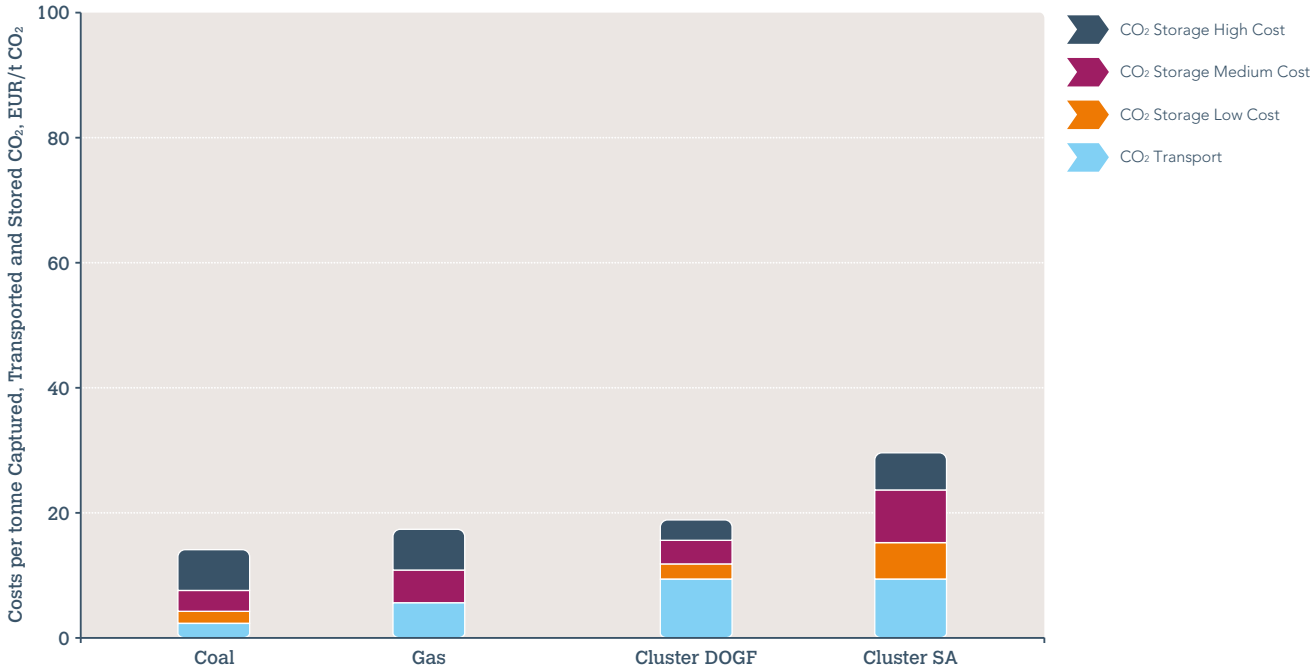


Figure 9: Calculated costs as LCOE for transport and storage for integrated projects. For the Clusters, the use of SA and DOGF are highlighted.

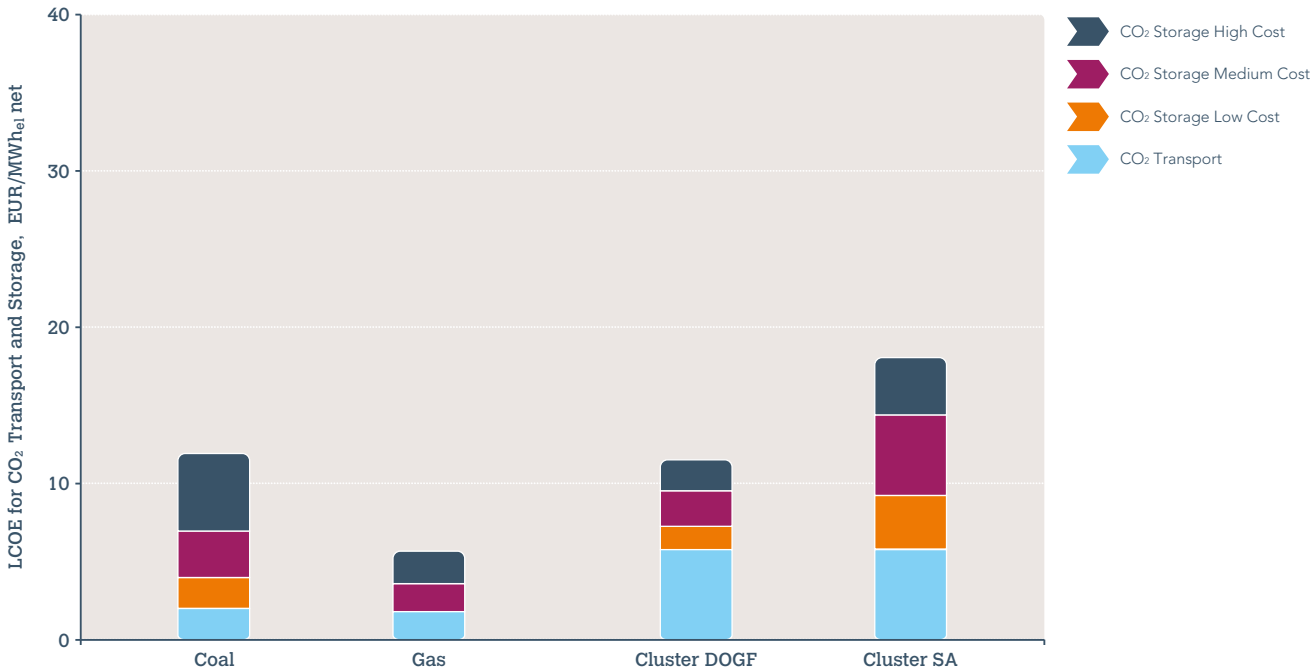
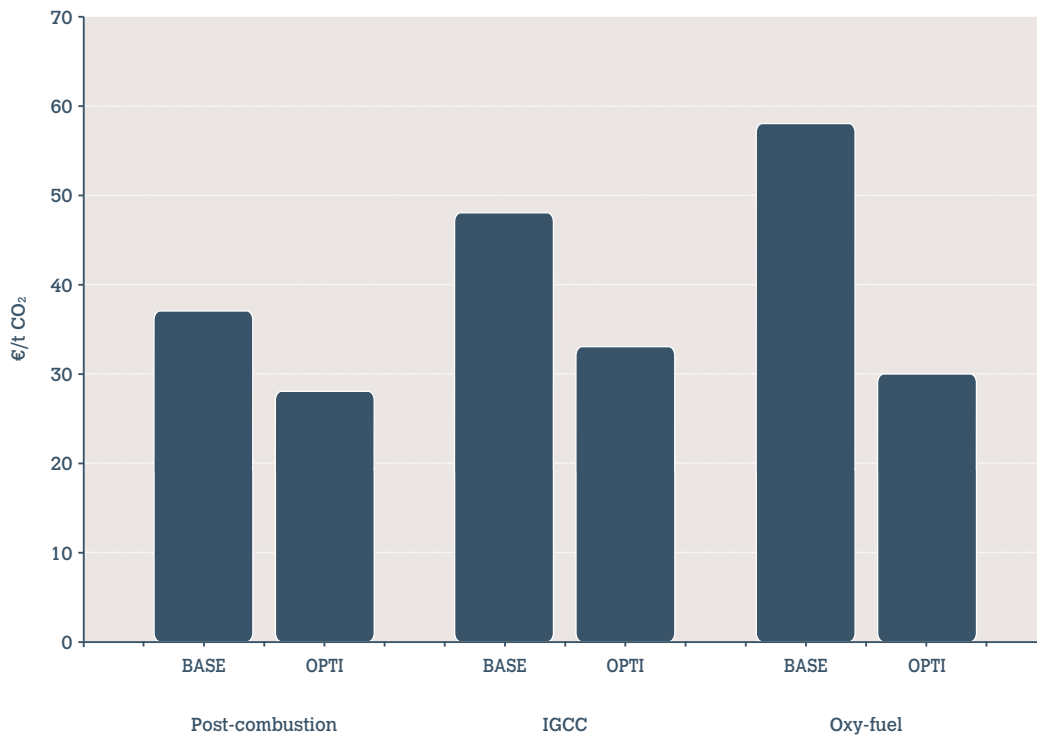


Figure 15: CO₂ avoidance costs for hard coal-fired power plants with CO₂ capture



Studies have also been undertaken for lignite-fired power plants with CO₂ capture that imply that a CO₂ avoidance cost in the range of €30/t CO₂ is possible for an OPTI advanced power plant with CO₂ capture and pre-drying of the lignite.

As anticipated, an analysis of *natural gas* CCGT power plants with post-combustion capture shows a heavy dependence of fuel costs on the final result, as can be observed in Figure 16 for an OPTI power plant.

At the lower end of the cost range of natural gas, CO₂ avoidance costs are still more than double those of a hard coal-fired power plant, but due in part to the lower quantities of CO₂ to be captured, the LCOE is competitive with other fuel sources, being ~€65/MWh for a natural gas price slightly under €5/GJ (see Figure 16).

Availability may slightly differ for the different capture technologies and the development

of renewable power may also limit the plant's operational time in the future. However, the achievement of high plant availability must be a key objective of the EU CCS demonstration programme so that costs remain competitive. This is especially important for pre-combustion capture, as the IGCC power plant design contains a considerably larger number of components and is not a common technology within the power industry.

Nevertheless, a CCS plant will always be dispatched before any other fossil-fuelled power plant, due to the lower variable operating costs (when EUA prices are taken into account). An unabated plant, on the other hand, will suffer from the cost of EUAs.

In order to illustrate the impact of availability for hard coal-fired power plants with CO₂ capture, a calculation of the generation costs has been made as a function of equivalent operating hours (Figure 17, pages 29-30).

Figure 16: LCOE and CO₂ avoidance costs for natural gas-fired power plants with CO₂ capture are heavily dependent on the fuel cost. The vertical blue lines for €4.5, €8 and €11/GJ represent the Low, Middle and High cases used for gas fuel cost.

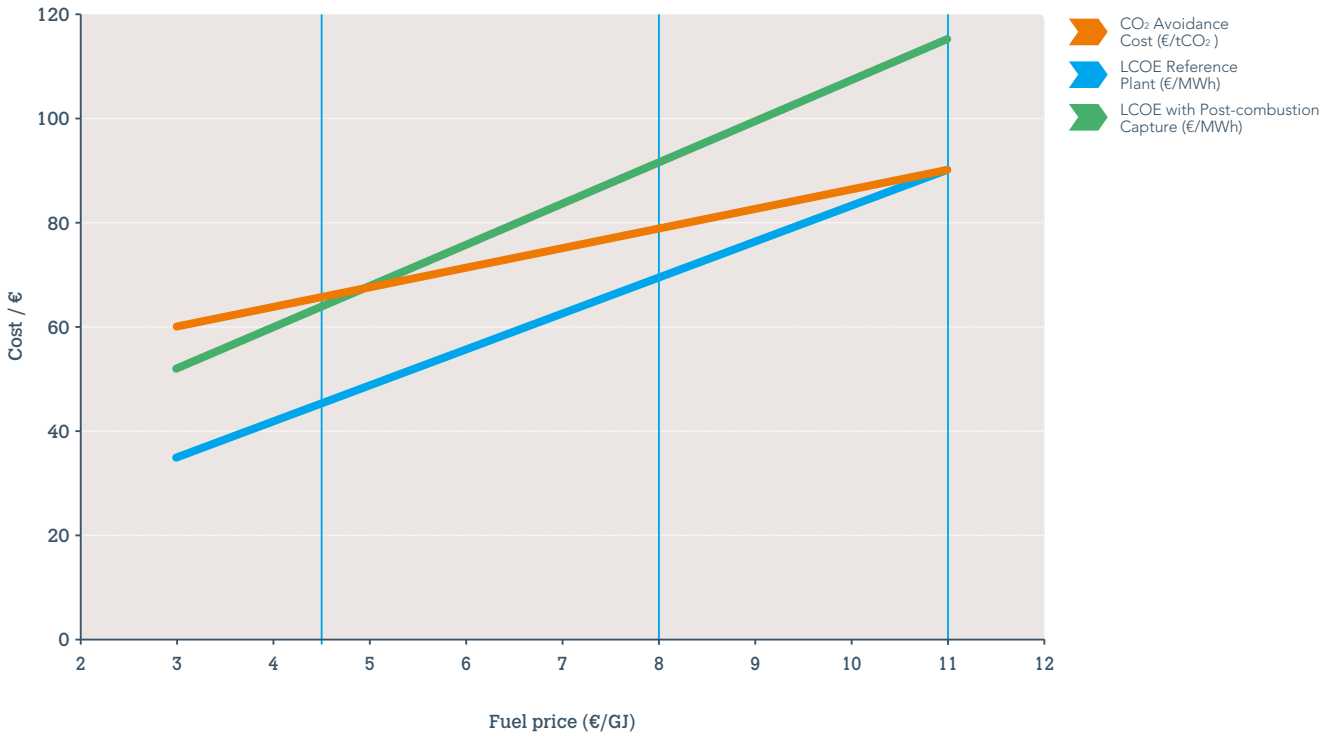
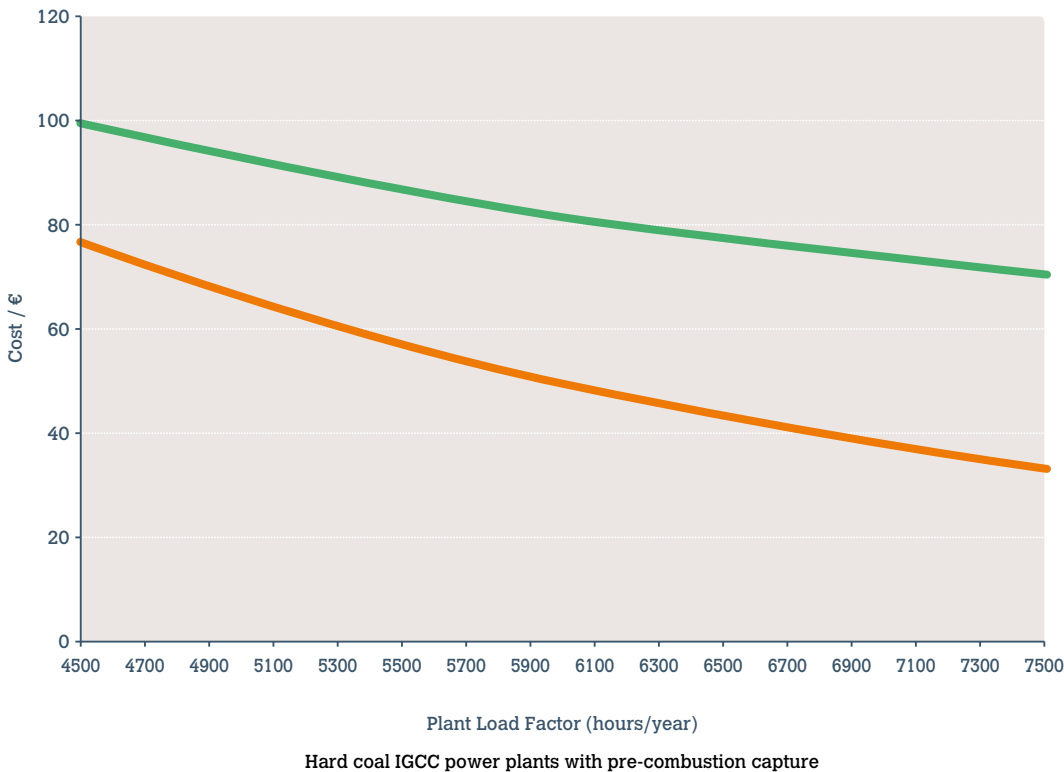
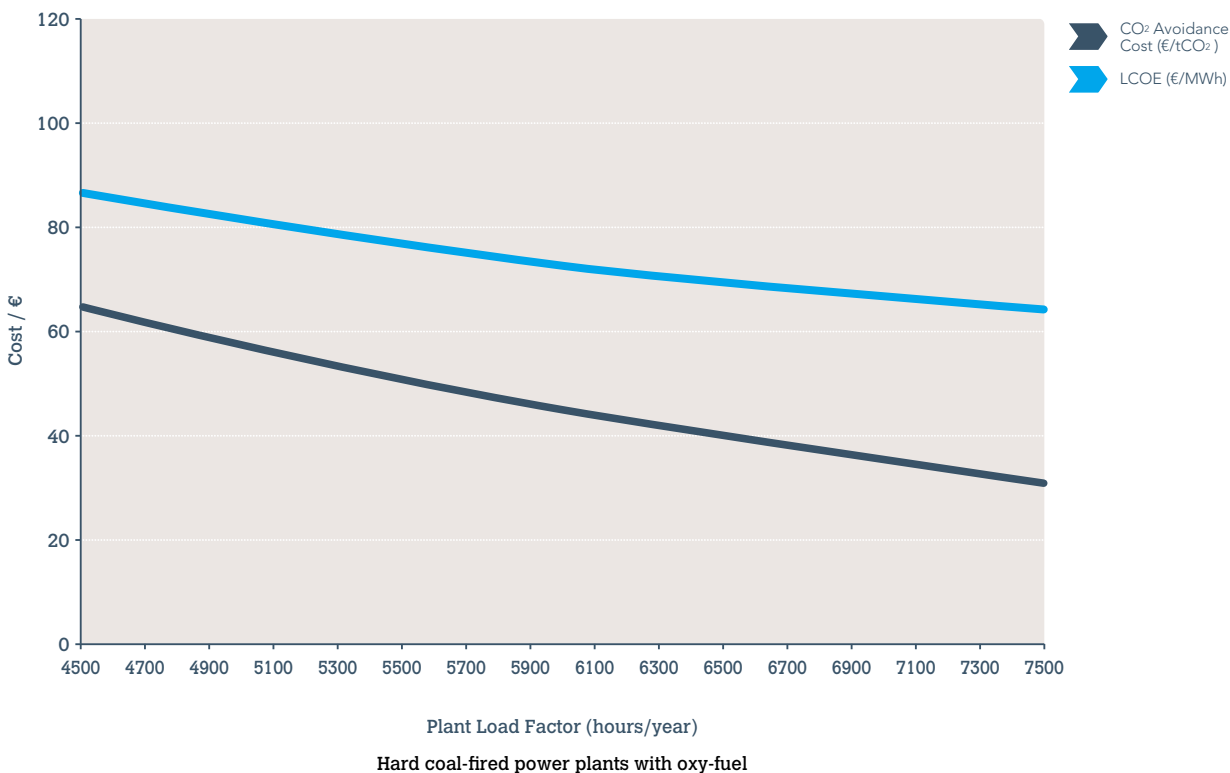
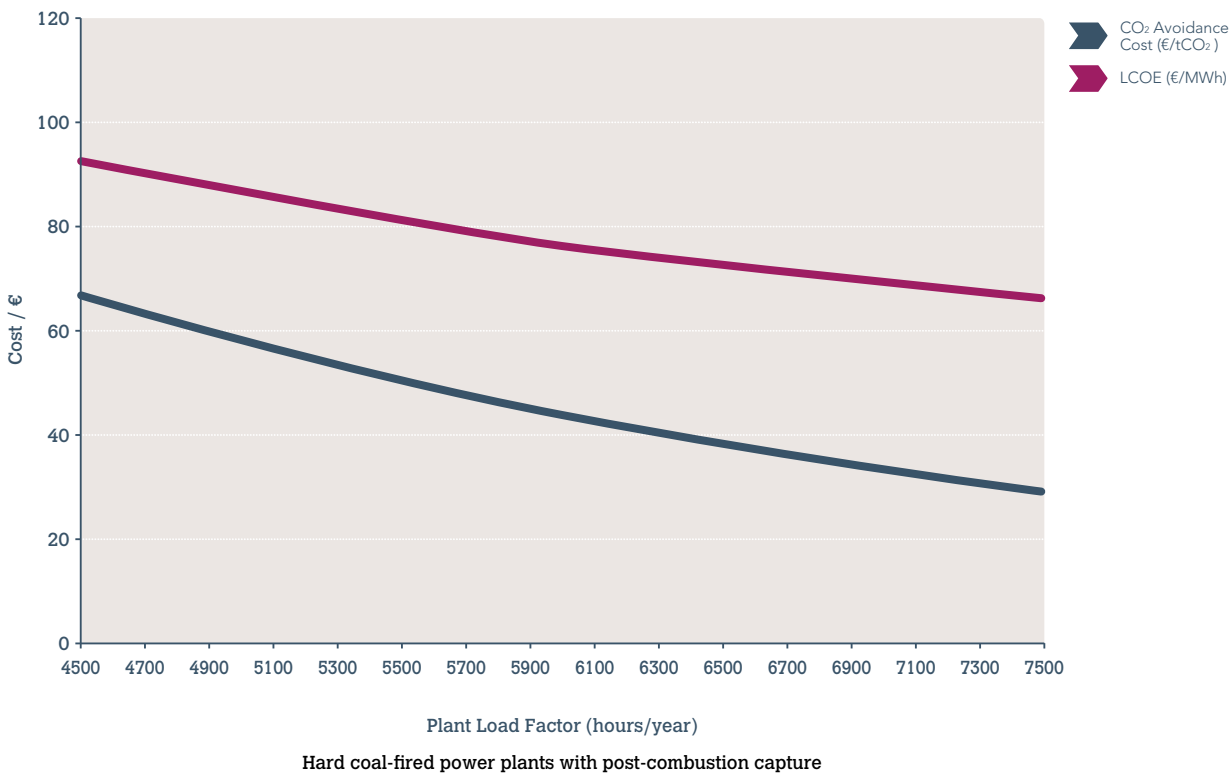


Figure 17: Dependence on Plant Load Factor for all three coal technologies, based on OPTI plants. Reference power plant load is kept at 7,500 hours per year for the calculation of CO₂ avoidance costs. Achieving high plant availability is key to keeping costs competitive.



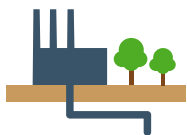
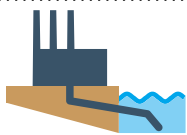




CO₂ Transport

This study describes the two major methods of transportation – pipelines (on- and offshore) and ships (including utilities) – and for each of these presents detailed cost elements and key cost drivers. These may be combined in a variety of ways – from a single source to a single sink, developing into qualified systems with several sources, networks and several storage sites over time.

Several likely transport networks of varying distances are therefore presented, including total annual costs and a cost per tonne of CO₂ transported. The cost models operate with three legs of transport: feeders, spines and distribution, each of which may comprise on- or offshore pipelines or ships. For some pipeline cases, CAPEX per tonne per km is also presented, providing a tool for comparison.

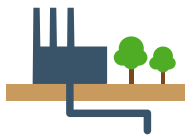
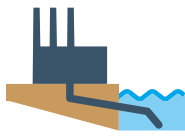

Table 1: Cost estimates (in €/t CO₂) for commercial natural gas-fired power plants with CCS or coal-based CCS demonstration projects with a transported volume of 2.5 Mtpa

Distance km	180	500	750	1500
 Onshore pipeline	5.4	n. a.	n. a.	n. a.
 Offshore pipeline	9.3	20.4	28.7	51.7
 Ship	8.2	9.5	10.6	14.5
 Liquefaction (for ship transport)	5.3	5.3	5.3	5.3

For commercial natural gas-fired power plants with CCS, or coal-based CCS demonstration projects, a typical capacity of 2.5 Mtpa and “point-to-point” connections are assumed. Table 1 shows the unit transportation cost (€/tonne) for such projects, depending on transport method and distance:

- Pipeline costs are roughly proportional to distance, while shipping costs are only marginally influenced by distance. Pipeline costs consist mainly (normally over 90%) of CAPEX, while for shipping, CAPEX is normally under 50% of total annual costs.
- If the technical and commercial risks are also considered, the construction of a “point-to-point” offshore pipeline for a single demonstration project is obviously less attractive than ship transportation for distances also below 500 km. (Pipeline costs here exclude any compression costs at the capture site, while the liquefaction cost required for ship transportation is specified.)

Table 2: Cost estimates for large-scale networks of 20 Mtpa (€/tonne CO₂). In addition to the spine distance, networks also include 10 km-long feeders (2*10 Mtpa) and distribution pipelines (2*10 Mtpa)

Spine Distance km	180	500	750	1500
 Onshore pipeline	1.5	3.7	5.3	n. a.
 Offshore pipeline	3.4	6.0	8.2	16.3
 Ship (including liquefaction)	11.1	12.2	13.2	16.1

Once CCS is a commercially driven reality, it is assumed that typical volumes are in the range of 10 Mtpa serving one full-scale coal-fired power plant, or 20 Mtpa serving a cluster of CO₂ sources. The unit transportation cost for such a network with double feeders and double distribution pipelines is estimated in Table 2.

- Pipelines benefit significantly from scale when comparing costs with the 2.5 Mtpa point-to-point solutions in Table 1, whereas the scale effects on ship transport costs are less significant. (Shipping costs here include the costs for a stand-alone liquefaction unit, i.e. remote from the power plant.)
- Ship investments are further assumed to have a residual value for hydrocarbon transportation, as well as being able to serve other CO₂ projects, which will be considered in any evaluation of project risks. All cost estimates are based on

custom design and new investment, i.e. no re-use of existing pipelines or existing semi-refrigerated LPG tonnage.

These figures assume full capacity utilisation from day one, which will probably be unrealistic for a cluster scenario. If, for example, volumes are assumed to be linearly ramped up over the first 10 years, this increases the unit cost of pipeline networks by 35-50% depending on maximum flows. For ships, ramp-up is achieved by adding ships and utilities when required, resulting in only marginal unit cost increases. To illustrate this, a calculation of the sensitivity of four key factors on pipeline transport was performed (Figure 18).

Annexes

Annex 1: Basic data for integrated CCS projects

Table 4: Total LCOE for integrated CCS projects vs. reference plants without CCS (including various assumed costs for EUAs) using Low and High Fuel costs

	Single Plant - Single Sink Hard Coal		Single Plant - Single Sink Natural Gas	
	Ref	With CCS	Ref	With CCS
Power Plant and CO₂ Capture				
• Power production (MWh _{el} net)	2 x 736	2 x 700	2 x 420	2 x 360
• LCOE (€/MWh _{el} net) (Averages for OPTI plants) for Low - High fuel prices	43 - 51	65 - 75	46 - 90	64 - 115
• LCOE Average All Plants (€/MWh _{el} net) for Low - High fuel prices	43 - 51	65 - 75	46 - 90	64 - 115
CO₂ Transport				
• CO ₂ volumes (Mtpa)	-	10	-	2.5
• Distance (km)	-	180 + Feeder	-	180
• LCOE (€/MWh _{el} net)	-	1.8	-	1.8
CO₂ Storage				
• Type of storage	SAs Onshore			SAs Onshore
• Cost scenario	-	Low	Mid	High
• CO ₂ stored over 40 years (Number of reservoirs)x(Mt per reservoir)	-	2x200	6x66	10x40
• LCOE (€/MWh _{el} net)	-	1.7	4.6	9.9
TOTAL LCOE (€/MWh_{el} net) (Excluding Emission Unit Allowances) for Low - High fuel prices				
	43-51	69-79	72-82	77-87
			46-90	68-119 70-121
Emission Unit Allowances within EU ETS Contribution to LCOE (€/MWh_{el} net)				
• For ETS 20 €/tonne CO ₂	15	2	7	1
• For ETS 40 €/tonne CO ₂	30	4	13	2
• For ETS 80 €/tonne CO ₂	61	7	27	4

Cluster			
Ref		With CCS	
Hard Coal	Nat Gas	Hard Coal	Nat Gas

3 x 736	2 x 420	3 x 700	2 x 360
43 - 51	46 - 90	65 - 75	64 - 115
	44 - 69		64 - 94

-	20		
-	500 + Feeders + Distribution Pipelines		
-	5.8		

DOGFs Offshore			
-	Low	Mid	High
-	4x200	12x66	20x40
-	1.5	3.8	5.7

44-69	71-101	74-104	75-105
-------	--------	--------	--------

11	2
23	3
45	6

Cluster			
Ref		With CCS	
Hard Coal	Nat Gas	Hard Coal	Nat Gas

3 x 736	2 x 420	3 x 700	2 x 360
43 - 51	46 - 90	65 - 75	64 - 115
	44 - 69		64 - 94

-	20		
-	500 + Feeders + Distribution Pipelines		
-	5.8		

SAs Offshore			
-	Low	Mid	High
-	4x200	12x66	20x40
-	3.5	8.7	12.4

44-69	73-103	78-108	82-112
-------	--------	--------	--------

11	2
23	3
45	6

Table 5: CAPEX for integrated CCS projects vs. reference plants without CCS

	Single Plant - Single Sink Hard Coal		Single Plant - Single Sink Natural Gas	
	Ref	With CCS	Ref	With CCS
Power Plant and CO₂ Capture				
• Power production (MWh _{el} net)	2 x 736	2 x 700	2 x 420	2 x 360
• CAPEX (€/KW _{el} net) (Averages for OPTI plants)	1600	2660	786	1511
• CAPEX (M€)	2355	3916	660	1100
• CAPEX All Plants (M€)	2355	3916	660	1100
CO₂ Transport				
• CO ₂ volumes (Mtpa)	-	10	-	2.5
• Distance (km)	-	180 + Feeder	-	180
• CAPEX (M€)	-	240	-	150
CO₂ Storage				
• Type of storage	SAs Onshore			SAs Onshore
• Cost scenario	-	Low	Mid	High
• CO ₂ stored over 40 years (Number of reservoirs)x(Mt per reservoir)	-	2x200	6x66	10x40
• CAPEX (M€ per reservoir)	-	69.5	69.5	89.1
• CAPEX (M€)	-	139	417	891
TOTAL CAPEX (M€)	2355	4295	4573	5047
			660	1354
				1473

- Table 5 shows that the capital intensity of fossil power plants will increase significantly with the addition of CCS. The overall CAPEX for gas power with CCS remains lower than for coal.
- As long as electricity market prices match the LCOEs (shown in Figure 5 for the Middle fuel costs), annual incomes will be sufficient to cover the annual costs for fuels, EUAs, O&M costs, as well as return the CAPEX (at the required interest rate) during the project lifetime. (For detailed data on annual costs for fuels, O&M and CAPEX, see the individual cost reports for CO₂ capture, transport and storage.)

Cluster			
Ref		With CCS	
Hard Coal	Nat Gas	Hard Coal	Nat Gas

3 x 736	2 x 420	3 x 700	2 x 360
1600	786	2660	1511
3533	660	5873	1100
	4193		6973

-	20		
-	500 + Feeders + Distribution Pipelines		
-	1710		

	DOGFs Offshore		
	Low	Mid	High
-			
-	4x200	12x66	20x40
-	55.5	47.8	44.1
-	222	574	882

4193	8905	9257	9565
------	------	------	------

Cluster			
Ref		With CCS	
Hard Coal	Nat Gas	Hard Coal	Nat Gas

3 x 736	2 x 420	3 x 700	2 x 360
1600	786	2660	1511
3533	660	5873	1100
	4193		6973

-	20		
-	500 + Feeders + Distribution Pipelines		
-	1710		

	SAs Offshore		
	Low	Mid	High
-			
-	4x200	12x66	20x40
-	237.6	198.6	169.3
-	950	2383	3386

4193	9634	11066	12069
------	------	-------	-------

Table 6: Overview of data for Integrated CCS cases – costs for power plants and CO₂ capture calculated for Middle fuel costs

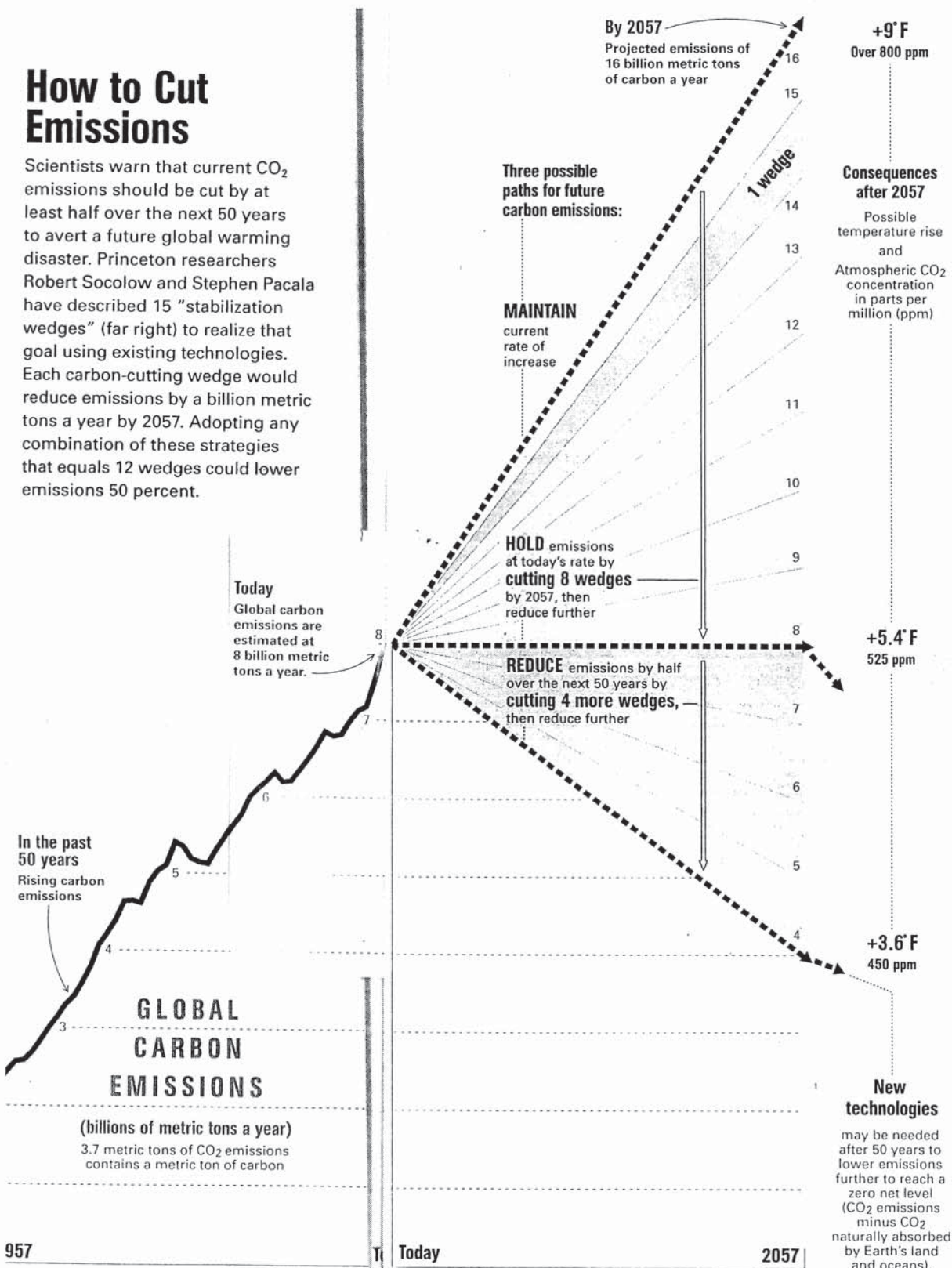
Power Plants with Capture and CO ₂ Compression/Conditioning										Transportation												
Reference plant	Capacity	Additional	Captured CO ₂			Avoided CO ₂		Blocks	Network	Volume	Source/s/	Transport					Store/s/	Cost		Accumulated		
Power Cost without Capture (EUR/MWh _{el} net)	One Block with Capture (MWh _{el} net)	Power Cost for Capture (EUR/MWh _{el})	(t/MWh _{el})	(Mt CO ₂ pa)	Cost (EUR/t)	(t/MWh _{el})	Cost (EUR/t)	Nr of		(Mtpa)	(#*Mtpa)	Feeder/s/ (km)	Type	Spine (km)	Type	Distribution (km)	Type	(#)	(EUR/t)	EUR/MWh _{el}	Mt CO ₂ (40 years)	
Commercial hard coal										Single Plant - Single Sink cases Demonstration and commercial CCS projects												
Short transport distance onshore																						
Hard coal-fired plant	46	~ 700	23	0.85	~ 4.5	27	0.67	34	2	1 a	10	1*10	10	Onshore	180	Onshore	0	–	1	2.1	1.8	400
Similar costs for the capture technologies. Average values for OPTI plants with capture according to ZEP CO ₂ capture cost report.																						
Commercial natural gas. In terms of CO ₂ quantity, also demonstration hard coal/lignite with the same transport and storage costs per tonne CO ₂ .										Short transport distance onshore												
Natural gas combined cycle	69	~ 350	22	0.33	~ 1	67	0.28	79	~ 2		2.5	1*2.5			180	Onshore		1	5.4	1.8	100	
1 gas turbine as in ZEP capture cost report. However, many other studies assume 2 gas turbines. Post-combustion capture, OPTI, according to ZEP CO ₂ capture cost report.																						
Natural gas combined cycle	69	~ 350	22	0.33	~ 1	67	0.28	79	~ 2	8 b	20	{ 2.5 2.5 5 10	10	Onshore	500	Offshore	2*10	Offshore	2	9.5	5.8	800
Natural gas combined cycle	69	~ 350	22	0.33	~ 1	67	0.28	79	~ 2				750	Ship								
Hard coal-fired plant	46	~ 700	23	0.85	~ 4.5	27	0.67	34	2				–	–								
Hard coal-fired plant	46	~ 700	23	0.85	~ 4.5	27	0.67	34	2*2				180	Offshore								
Weighted average:	57		23	0.61		37	0.49	46														

Table 6: Overview of data for Integrated CCS cases – costs for power plants and CO₂ capture calculated for Middle fuel costs

Storage																INTEGRATED CCS CASE COSTS							
Location	Type	Data quality	Legacy	Low Cost Scenario				Medium Cost Scenario				High Cost Scenario				Low Storage Cost Scenario		Medium Storage Cost Scenario		High Storage Cost Scenario			
				Field capacity	Fields	Cost		Field capacity	Fields	Cost		Field capacity	Fields	Cost		For CCS		For CCS		For CCS			
				Wells	Mt CO ₂	Nr of	€/t CO ₂	€/MWh _{el}	Mt CO ₂	Nr of	€/t CO ₂	€/MWh _{el}	Mt CO ₂	Nr of	€/t CO ₂	€/MWh _{el}	€/t CO ₂	€/MWh _{el}	€/t CO ₂	€/MWh _{el}	€/t CO ₂	€/MWh _{el}	
Single Plant - Single Sink																							
Hard coal-fired plant	Onshore	Aquifer	Data-Poor	No	200	2.0	2.0	1.7	66	6.1	5.4	4.6	40	10	11.7	9.9	~ 31.2	~ 27	~ 34.6	~ 29	~ 40.9	~ 35	
Natural gas combined cycle	Onshore	Aquifer	Data-Poor	No					66	1.5	5.4	1.8	40	2.5	11.7	3.9			~ 77	~ 26	~ 84	~ 28	
Clusters																							
Natural gas combined cycle	}	Offshore	DOGF	Data-Rich	Yes	200	4.0	2.4	1.5	66	12.1	6.2	3.8	40	20	9.4	5.7	~ 49	~ 30	~ 53	~ 32	~ 56	~ 34
Natural gas combined cycle		Offshore	Aquifer	Data-Rich	No	200	4.0	5.8	3.5	66	12.1	14.3	8.7	40	20	20.3	12.4	~ 52	~ 32	~ 61	~ 37	~ 67	~ 41
Hard coal-fired plant																							
Hard coal-fired plant																							
Weighted average:																							

How to Cut Emissions

Scientists warn that current CO₂ emissions should be cut by at least half over the next 50 years to avert a future global warming disaster. Princeton researchers Robert Socolow and Stephen Pacala have described 15 "stabilization wedges" (far right) to realize that goal using existing technologies. Each carbon-cutting wedge would reduce emissions by a billion metric tons a year by 2057. Adopting any combination of these strategies that equals 12 wedges could lower emissions 50 percent.



SOURCES: ROBERT H. SOCOLOW AND STEPHEN W. PACALA, PRINCETON UNIVERSITY (UPDATED REPORT); OAK RIDGE NATIONAL LABORATORY (GLOBAL CARBON EMISSIONS DATA); ICONS BY JONATHAN AVERY; GRAPHIC BY JUAN VELASCO, NGM ART

Carbon Capture Journal

CCUS in the UK

CCSA London forum – CCS ready
for investment?

Hydrogen: enabling the UK to
reach net-zero emissions

Urgent action needed to
progress UK CCUS

Jan / Feb 2020

Issue 73



Your reliability shines

MAN Energy Solutions
Future in the making

**Energy & Storage
solutions expertise**

Securing energy supplies

Ensuring a reliable power supply is one of the key factors for progress and prosperity. Our expertise covers solutions for hybrid power, LNG to power, energy storage, power-to-X, thermal power plants, and CHP.

www.man-es.com

CO₂ capture could be big business: up to 10 gigatonnes CO₂ a year could be stored according to study

Capturing carbon dioxide and turning it into commercial products, such as fuels or construction materials, could become a new global industry, according to a study by researchers from UCLA, the University of Oxford and five other institutions, published in *Nature*.

The research is the most comprehensive study to date investigating the potential future scale and cost of 10 different ways to use carbon dioxide, including in fuels and chemicals, plastics, building materials, soil management and forestry.

The study considered processes using carbon dioxide captured from waste gases that are produced by burning fossil fuels or from the atmosphere by an industrial process.

And in a step beyond most previous research on the subject, the authors also considered processes that use carbon dioxide captured biologically by photosynthesis.

The research found that on average each utilization pathway could use around 0.5 gigatonnes of carbon dioxide per year that would otherwise escape into the atmosphere. (A tonne, or metric ton, is equivalent to 1,000 kilograms, and a gigatonne is 1 billion tonnes, or about 1.1 billion U.S. tons.)

A top-end scenario could see more than 10 gigatonnes of carbon dioxide a year used, at a theoretical cost of under \$100 per tonne of carbon dioxide. The researchers noted, however, that the potential scales and costs of using carbon dioxide varied substantially across sectors.

“The analysis we presented makes clear that carbon dioxide utilization can be part of the solution to combat climate change, but only if those with the power to make decisions at every level of government and finance commit to changing policies and providing market incentives across multiple sectors,” said Emily Carter, a distinguished professor of chemical and biomolecular engineering at the UCLA Samueli School of Engineering and a co-author of the paper.

“The urgency is huge and we have little time

left to effect change.”

According to the Intergovernmental Panel on Climate Change, keeping global warming to 1.5 degrees Celsius over the rest of the 21st century will require the removal of carbon dioxide from the atmosphere on the order of 100 to 1,000 gigatonnes of carbon dioxide. Currently, fossil carbon dioxide emissions are increasing by over 1% annually, reaching a record high of 37 gigatonnes of carbon dioxide in 2018.

“Greenhouse gas removal is essential to achieve net zero carbon emissions and stabilise the climate,” said Cameron Hepburn, one of the study’s lead authors, director of Oxford’s Smith School of Enterprise and Environment. “We haven’t reduced our emissions fast enough, so now we also need to start pulling carbon dioxide out of the atmosphere. Governments and corporations are moving on this, but not quickly enough.

“The promise of carbon dioxide utilization is that it could act as an incentive for carbon dioxide removal and could reduce emissions by displacing fossil fuels.”

Critical to the success of these new technologies as mitigation strategies will be a careful analysis of their overall impact on the climate. Some are likely to be adopted quickly simply because of their attractive business models.

For example, in certain kinds of plastic production, using carbon dioxide as a feedstock is a more profitable and environmentally cleaner production process than using conventional hydrocarbons, and it can displace up to three times as much carbon dioxide as it uses.

Biological uses might also present opportunities to reap co-benefits. In other areas, utilization could provide a “better choice” alternative during the global decarbonization pro-

cess. One example might be the use of fuels derived from carbon dioxide, which could find a role in sectors that are harder to decarbonize, such as aviation.

The authors stressed that there is no “magic bullet” approach.

“I would start by incentivizing the most obvious solutions — most of which already exist — that can act at the gigatonne scale in agriculture, forestry and construction,” said Carter, who also is UCLA’s executive vice chancellor and provost, and the Gerhard R. Andlinger Professor in Energy and Environment Emeritus at Princeton University.

“At the same time, I would aggressively invest in R&D across academia, industry and government labs — much more so than is being done in the U.S., especially compared to China — in higher-tech solutions to capture and convert carbon dioxide to useful products that can be developed alongside solutions that already exist in agriculture, forestry and construction.”

In addition to the researchers from UCLA and Oxford, the study’s other authors are from the Mercator Research Institute on Global Commons and Climate Change in Berlin, Humboldt University in Berlin, Imperial College London’s Centre for Environmental Policy, University of Leeds’ School of Earth and Environment, and the Institute of Biological and Environmental Sciences at the University of Aberdeen in Scotland.

C

More information

samueli.ucla.edu

www.nature.com

Carbon Capture Journal

Jan / Feb 2020

Issue 73

Carbon Capture Journal

United House, North Road, London N7 9DP
www.carboncapturejournal.com
 Tel +44 (0)208 150 5295

Editor

Keith Forward
editor@carboncapturejournal.com

Publisher

Future Energy Publishing
Karl Jeffery
jeffery@d-e-j.com

Subscriptions

subs@carboncapturejournal.com

Advertising & Sponsorship

David Jeffries
 Tel +44 (0)208 150 5293
djeffries@onlymedia.co.uk

Carbon Capture Journal is your one stop information source for new technical developments, opinion, regulatory and research activity with carbon capture, transport and storage.

Carbon Capture Journal is delivered on print and pdf version to a total of 6000 people, all of whom have requested to receive it, including employees of power companies, oil and gas companies, government, engineering companies, consultants, educators, students, and suppliers.

Subscriptions: £250 a year for 6 issues. To subscribe, please contact Karl Jeffery on subs@carboncapturejournal.com Alternatively you can subscribe online at www.d-e-j.com/store

Back cover:

The "CATO Meets the Projects 2019" forum in Utrecht on November 26 showed big strides with CCS in the Netherlands (pg. 14)



Leaders - Review of 2019 and CCUS in the UK

Global Status of CCS shows growing momentum but urgent action needed
 The Global CCS Institute's flagship report finds that the deployment of CCS has continued to gather pace, with the pipeline of CCS projects continuing to grow the second year in a row, up 37 per cent since 2017 2

CCSA London forum – CCS ready for investment?

The Carbon Capture and Storage Association held a London forum on November 6 called "Capturing the Clean Growth Opportunities" – showing how UK CCS is on a path towards investability. By Karl Jeffery 4

Offshore energy integration key to UK net zero target

Innovative partnering between oil and gas, renewables, hydrogen and carbon capture can accelerate energy transition says UK Oil and Gas Authority report 8

Urgent action and investment needed to progress UK CCS

A comprehensive report from OGUK into the changing energy landscape has called for urgent action to progress low carbon technologies critical to the UK and Scottish Government's net zero ambitions 9

Hydrogen: enabling the UK to reach net-zero emissions

Element Energy has produced four 'Hy-Impact' reports for Equinor that outline the opportunity for hydrogen and CCS in the UK net-zero transition 10

North Sea technology could play leading role in energy transition

The North Sea has the potential to become a global showcase for the energy transition as a number of low carbon solutions grow in prominence says a report from PwC and Oil and Gas UK 11

A long, hard look underground is required to reach net zero says report

Advances and investment in geothermal energy, carbon capture and storage and bioenergy with carbon capture and storage (BECCS) are "critical" to moving the UK towards its target, according to a new report published in Petroleum Geoscience 12

Projects and policy

Oil and Gas Climate Initiative launches CCUS Kickstarter Initiative

OGCI has launched a new initiative to unlock large-scale investment in carbon capture, use and storage 12

CATO event – big strides in Dutch CCS

The "CATO Meets the Projects 2019" forum in Utrecht on November 26 showed big strides with CCS in the Netherlands – including an update on Dutch subsidies, an operating, commercial CCS project on a waste incinerator, and a gas turbine to be converted to hydrogen. By Karl Jeffery 14

Capture and utilisation

Effective carbon capture for hydrogen production

Decarbonising natural gas is essential to reach net zero targets. Adrian Finn, Process Technology Manager, Costain reviews a method that is gaining increasing recognition, that of reforming natural gas to hydrogen 17

Additive manufacturing of 3D ceramic structures for CO2 sorption

The 3D-CAPS project focusses on the application of 3D-printing of silica and hydrotalcites to make improved 3D-structures for the sorption of CO2 from industrial (off-)gases. By Hans Willemsen, 3D-CAT, and Robert de Boer, TNO 20

Transport and storage

Study shows world has sufficient CO2 storage capacity

The study concludes there is easily enough space in the world's nearshore continental margins to meet the IPCC's goal of storing 6 to 7 gigatons of CO2 a year by 2050 25

Global Status of CCS shows growing momentum but urgent action needed

The Global CCS Institute's flagship report launched at the UN climate change conference COP25 finds that the deployment of CCS has continued to gather pace, with the pipeline of CCS projects continuing to grow the second year in a row, up 37 per cent since 2017.

"Global Status of CCS 2019 Report: Targeting Climate Change" finds there are now 51 large-scale CCS facilities in operation or under development globally in a variety of industries and sectors. These include 19 facilities in operation, four under construction, and 28 in various stages of development. Of all the facilities in operation, 17 are in the industrial sector, and two are power projects.

"This has been one of the worst years on record for climate," said Global CCS Institute CEO Brad Page. "The clock is ticking, the world must act. Global emissions continue to rise, and climate impacts are expected to increase and have very dangerous implications. Bold climate action is needed to keep global warming to 1.5°C. CCS needs to be part of the climate solutions toolbox to tackle this challenge head on".

The United States is currently leading the way in CCS development and deployment with 24 large-scale facilities, followed by 12 facilities both in Europe and the Asia Pacific region, and three in the Middle East.

"Despite this increased momentum and progress in CCS deployment, the number of facilities needs to increase 100-fold by 2040, and scaling efforts are just not happening fast enough", warns Mr. Page. "Now is the time to rally for greater policy support and for capital to be allocated to build on the positive CCS progress of the past two years", Mr. Page adds.

Speaking at the report launch at COP25 in Madrid, Dr Julio Friedmann, Senior Research Scholar at the Center for Global Energy Policy at Columbia University, said: "The urgency of climate change and the harsh arithmetic of emissions demand CCUS deployment without delay. Policies that provide clean and durable alignment with markets and support continued innovation, especially expansion into new applications like heavy industry, hydrogen, and CO₂

The need for and benefit from urgent action

The IEA's World Energy Outlook 2019 describes the measures necessary to deliver its Sustainable Development Scenario (SDS), a future where the United Nations energy related sustainable development goals for emissions, energy access and air quality are met. This scenario is consistent with a 66 per cent probability of limiting global temperature rise to 1.8 degrees Celsius without relying on large scale negative emissions. Under this scenario:

- Carbon capture utilisation and storage (CCUS)i provides 9 per cent of the cumulative emissions reduction between now and 2050
- The average mass of CO₂ captured and permanently stored each year between 2019 and 2050 is 1.5 billion tonnes per annum
- The mass of CO₂ captured and permanently stored in 2050 reaches 2.8 billion tonnes per annum
- The mass of CO₂ captured is split almost equally between the power sector and industry sectors including iron and steel production, cement production, refineries and upstream oil and gas production.

The deployment of CCS is not happening quickly enough for it to play its role in meeting emissions reductions targets at the lowest possible cost. The IEA's 'Tracking Clean Energy' progress indicator, provides a status snapshot of 39 critical energy technologies needed to meet a less than 2°C target under its Sustainable Development Scenario (SDS). Only seven of the technologies assessed are "on-track". Critically CCS in power, and in industry and transformation, are "off-track".

To achieve the levels outlined in the SDS, the number of industrial scale facilities needs to increase a hundredfold, from 19 in operation now to more than 2,000 by 2040. To rapidly scale up the technology in a smooth and steady way, urgent action is required. Governments have a pivotal role to play, by providing a clear, stable and supportive policy framework for CCS.

The good news is that CCS provides a wealth of benefits in addition to its primary role in reducing emissions. It enables a just transition to new low emissions industries for communities currently reliant on emissions intense employment. It can protect people from the severe economic and social disruption that otherwise results from closing local industries. On top of this, CCS:

- supports high paying jobs;
- reduces total system costs of electricity supply by providing reliable, dispatchable generation capacity when fitted on flexible fossil fuel power plants;
- can utilise existing infrastructure that would otherwise be decommissioned, helping to defer shut-down costs;
- provides knowledge spillovers that can support innovation based economic growth.

The time available to limit temperature rises to 1.5°C is running out. Widespread use of CCS technology is critical to meeting these goals. We need to scale up deployment now.

removal, will make or break our future.”

The report shines light on the next wave of CCS projects globally, while also highlighting the flexibility, applicability and increasingly positive economics of applying CCS to a range of emission sources. The next wave of projects is expected to focus on large-scale abatement, through development of hubs and clusters. These capture CO₂ from multiple industrial installations and use shared infrastructure for the subsequent CO₂ transportation and storage to drive down costs.

Commenting on the report, Grantham Institute Chair, Lord Nicholas Stern, said, “We need to change the way we think about climate change as a global challenge, and start to regard it as an opportunity for innovation and growth. Against this backdrop, CCS becomes an ever more vital part of the process for reaching net-zero emissions”.

At the same time, hydrogen is also receiving policy attention not seen for decades around the globe. CCS, as a means to produce clean hydrogen on a large-scale, has gained momentum as part of this renewed interest in hydrogen as a clean energy vector of the future.

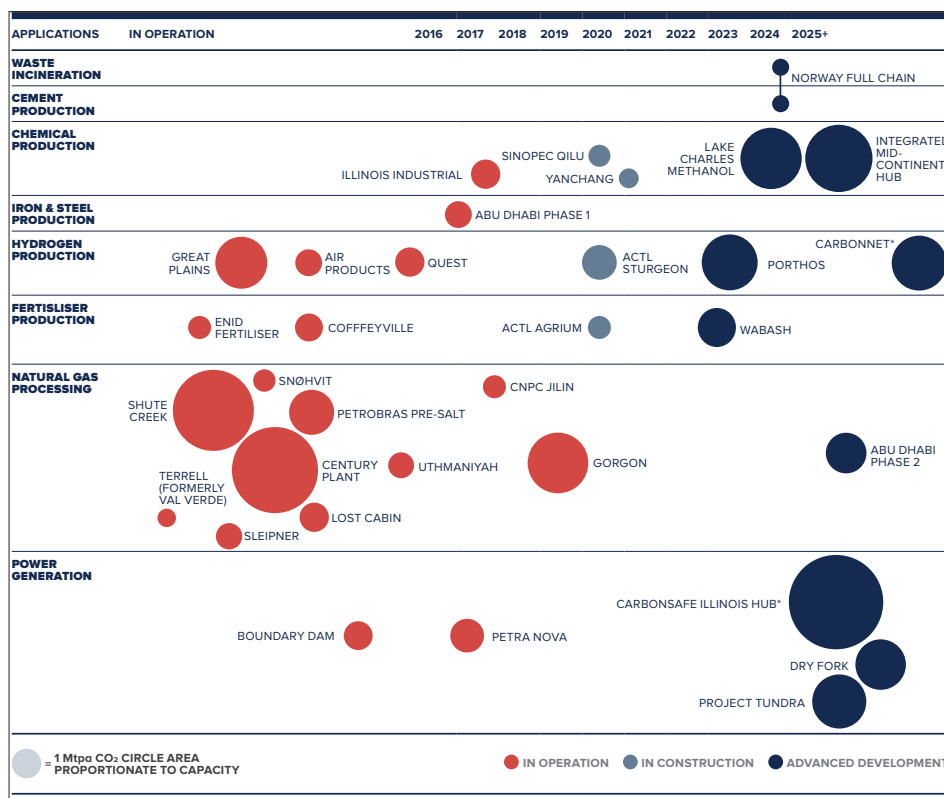
“Perhaps the most compelling development in the last 12 months though is that increasingly, CCS is a stand-out technology to genuinely deliver a just transition for many fossil fuel-based communities,” said Mr. Page.

The report features commentary and contributions from a wide range of leaders and influencers who draw on their expertise from across climate change, energy, academia, polar exploration, finance and CCS in voicing their support for the technology.

Next wave of CCS hubs and clusters

“Next wave” facilities based around CCS hubs and clusters have featured in 2019. Added to the Global CCS Institute's database in 2016, these facilities take advantage of the fact that many emissions intensive facilities (both power and industrial) tend to be concentrated in the same areas.

Hubs and clusters significantly reduce the unit cost of CO₂ storage through economies of scale, and offer commercial synergies that reduce the risk of investment. They can play a strategically important role in climate change mitigation.



Power and industrial applications of large-scale CCS facilities in operation, under construction and in advanced development (Size of the circle is proportional to the capture capacity of the facility). Source: Global Status of CCS 2019

The way CCS projects are planned in Europe has changed considerably during the last decade. The focus used to be on building full chain solutions where one source of emissions would build their own transportation pipeline to their storage site. Now, most projects are planned as hubs and clusters.

Capturing CO₂ from clusters of industrial installations, instead of single sources, and using shared infrastructure for the subsequent CO₂ transportation and storage network, will drive down unit costs across the CCS value chain. Keeping a network open for third party CO₂ deliveries, increases economies of scale.

Using a mix of transportation including pipelines and ships – but also trains and trucks – offers flexibility and accessibility to a wider range of CO₂ sources around the industrial clusters. Several major industrial regions are planning CCS cluster development:

- Netherlands – Port of Rotterdam and Port of Amsterdam
- Belgium – Port of Antwerp
- UK – Humber and Teesside.

The Ruhr industrial cluster in Germany is expected to benefit from the CCS projects developed across the border in the Netherlands. A dedicated multi-partner ALIGN-CCUS project aims to contribute to the transformation of six European industrial regions into economically robust, low-carbon centres by 2025.

The project will create blueprints for developing low-emission industry clusters through CCUS and assess commercial models for CO₂ cluster developments, including public-private partnerships.

The regulatory barrier of non-pipeline CO₂ transport under EU ETS will need to be addressed in the next couple of years for Europe to fully benefit from the economies of scale offered by hubs and clusters. The legislation as it currently stands poses a regulatory barrier to those projects that wish to transport CO₂ through different means (e.g. trains and barges).

More information

Download the full report:

www.globalccsinstitute.com

Study shows world has sufficient CO₂ storage capacity

The study concludes there is easily enough space in the world's nearshore continental margins to meet the IPCC's goal of storing 6 to 7 gigatons of carbon dioxide a year by 2050.

The study - from The University of Texas at Austin, the Norwegian University of Science and Technology and the Equinor Research Centre - looks at the amount of geological space available in formations that is likely suitable to hold greenhouse gas emissions, keeping them from the atmosphere. It also calculates the number of wells needed worldwide to reach the IPCC's 2050 goal.

The United Nation's Intergovernmental Panel on Climate Change (IPCC) has stated that CCS needs to achieve 13% of the world's necessary emission reductions by 2050. Some policy-makers, industry representatives and non-government organizations are dubious that CCS can meet its portion of the goal, but the new study published in *Nature Scientific Reports* shows that CCS could achieve its targets.

"With this paper, we provide an actionable, detailed pathway for CCS to meet the goals," said coauthor Tip Meckel of UT's Bureau of Economic Geology. "This is a really big hammer that we can deploy right now to put a dent in our emissions profile."

It concludes there is easily enough space in the world's nearshore continental margins to meet the IPCC's goal of storing 6 to 7 gigatons of carbon dioxide a year by 2050, and that the goal could be achieved by installing 10,000 to 14,000 injection wells worldwide in the next 30 years.

"The great thing about this study is that we have inverted the decarbonization challenge by working out how many wells are needed to achieve emissions cuts under the 2-degree (Celsius) scenario," said lead author Philip Ringrose, an adjunct professor at the Norwegian University of Science and Technology.

"It turns out to be only a fraction of the historical petroleum industry - or around 12,000 wells globally. Shared among 5-7 continental CCS hubs - that is only about 2,000 wells per region. Very doable! But we need to get cracking as soon as possible."

Pressure, not volume, the deciding factor

The authors first looked at continental shelves worldwide to get a sense of how much capacity there would be to store carbon dioxide.

Previous studies of how much storage would be available offshore have mainly looked at estimated volumes in different rock formations on the continental shelf. The authors argue, however, that the ability of the rock formation to handle pressure is more important in figuring out where CO₂ can be safely stored.

That's because injecting CO₂ into a rock formation will increase the pressure in the formation. If the pressures exceed what the formation can safely handle, it could develop cracks that would require early closure of projects.

Given that assumption, the researchers developed a way to classify different storage formations according to their ability to store CO₂. Under this approach, Class A formations are those without significant pressure limits, and thus the easiest to use, while Class B formations are those where CO₂ can be injected into the system up to a certain limit, and Class C formations are those where pressures will have to be actively managed to allow the CO₂ to be injected.

"We argue that this transition from early use of CO₂ injection into aquifers without significant pressure limits (Class A), through to CO₂ storage in pressure-limited aquifers (Class B) and eventually to pressure management at the basin scale (Class C), represents a global technology development strategy for storage which is analogous to the historic oil and gas production strategy," the researchers wrote.

Essentially, the authors say, as experience with injecting CO₂ into offshore formations grows, the ability to use the Class B and C areas will improve, much as geologists and petroleum engineers have gotten better over the decades at extracting hydrocarbons from more and more challenging offshore formations.

Can we drill fast enough?

It's one thing to have enough space to store CO₂ — you also have to inject it into the storage formations fast enough to meet the IPCC estimates of 6 to 7 gigatons of carbon dioxide a year by 2050.

By comparison, "Four existing large-scale projects inject 4 million tonnes CO₂ per year. If all 19 large-scale CCS facilities in operation together with a further 4 under construction are considered, they will have an installed capture capacity of 36 million tonnes per year," the researchers wrote. This is clearly not enough, since a gigatonne is 1,000 million tonnes. *ic way of going after this.*"

Nevertheless, the history of the oil and gas industry suggests that ramping up the technology and infrastructure required to reach the IPCC target by 2050 is very doable, the researchers wrote. Assuming an average injection rate per well, they calculated that more than 10,000 CO₂ wells would need to be operating worldwide by 2050.

While this may seem like an enormous number, it's equivalent to what has been developed in the Gulf of Mexico over the last 70 years, or five times what has been developed by Norwegians in the North Sea.

"Using this analysis, it is clear that the required well rate for realizing global CCS in the 2020–2050 timeframe is a manageable fraction of the historical well rate deployed from historic petroleum exploitation activities," the researchers wrote.

"With this paper, we provide an actionable, detailed pathway for CCS to meet the goals," Meckel said. "This is a really big hammer that we can deploy right now to put a dent in our emissions profile."

More information

norwegianscitechnews.com



Drilling complete at Otway low cost CO2 monitoring project

A 59-day drilling program has been successfully completed at CO2CRC's Otway National CCS Research Centre, located at Nirranda South in south-west Victoria.

On 18 September the last of four new 1600-metre-deep monitoring wells was drilled and cased with each well equipped with the latest technologies in fibre optics sensing and sub-surface gauges. Pressure communication between wells has been confirmed and the seismic imaging system is functioning on all wells as designed.

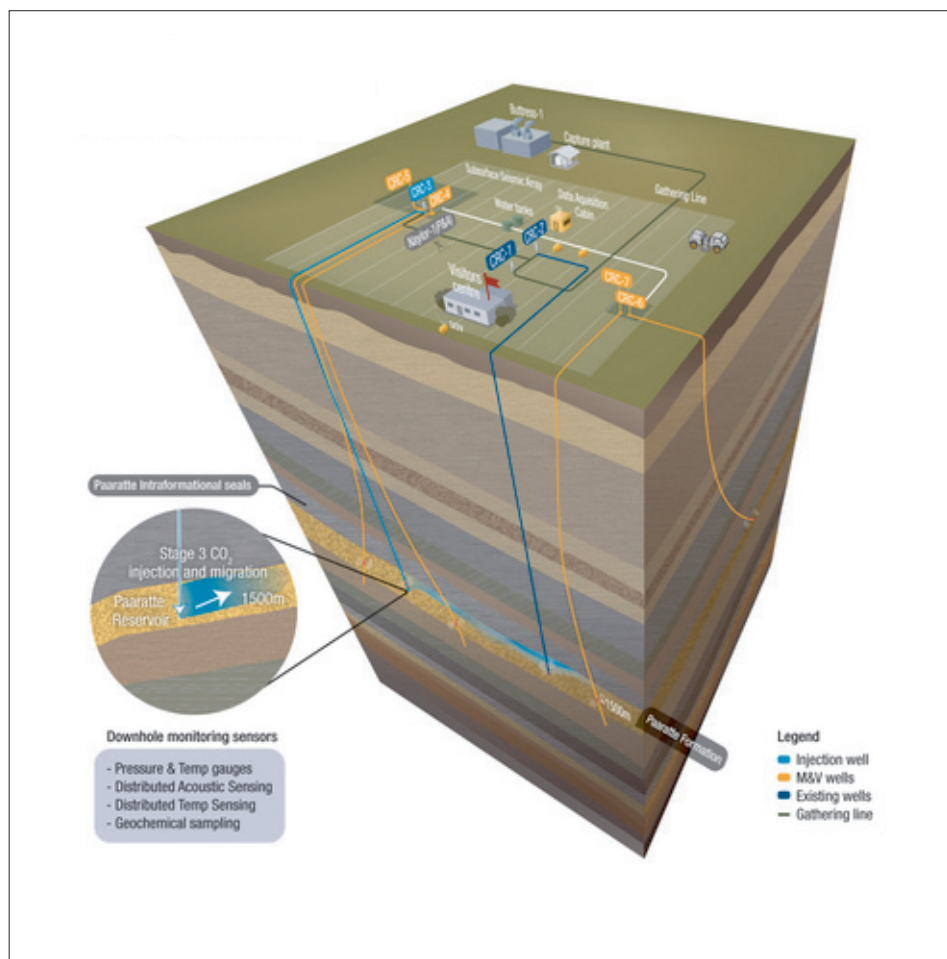
The wells are part of CO2CRC's biggest project to date, known as Otway Stage 3. The project is proving up technologies which provide data on demand, as well as reducing the cost and impact of long-term CO2 storage monitoring for carbon capture and storage (CCS) projects.

The next six months will see teams from CSIRO and Curtin University calibrating the pressure tomography monitoring system and performing baseline seismic acquisitions using fibre optics cables and permanently deployed surface orbital vibrators.

"These new technologies provide data quicker, are much less invasive and cost significantly less than the seismic surveys currently used. Initial estimates show cost savings of up to 75 percent," said David Byers, CEO of CO2CRC.

"Our hope is that the research will lead to more CCS projects around the world, allowing CCS to play a vital role in reducing emissions across all major industry sectors. As the International Energy Agency points out, without CCS as part of the solution, meeting global climate goals will be practically impossible," he said.

With the support of its drilling management team, InGauge Energy, the drilling company, Easternwell Drilling and with multiple specialist service providers, the CO2CRC team drilled almost 7km of directional wells, ran 11km of steel casing, 13km of fibre optic cable and pumped 458 tonnes of cement.



Layout of CO2 injection and monitoring wells for CO2CRC's Otway Stage 3 Project

This represents the largest single project undertaken by CO2CRC in support of testing new and innovative techniques that will support current and future CCS projects both within Australia and globally.

The \$45 million project is jointly funded by the Commonwealth Government's Education Investment Fund (EIF), COAL21 through ANLEC R&D, BHP and the Victorian State Government.

Technical and scientific work programs are being carried out in partnership with Curtin University and CSIRO and are expected to be complete by June 2022.

More information

www.co2crc.com.au



Australian gas fields show that CO₂ storage is secure

New research shows that carbon dioxide emissions can be captured and securely stored beneath deep-seated and impermeable underground rocks.

Researchers studied natural CO₂ gas fields and CO₂ mineral springs in south-east Australia to improve the understanding of how to safely store CO₂ underground.

By measuring tiny traces of inactive natural gases, known as noble gases, found in the CO₂ they were able to show that, in both the gas fields and mineral springs, the CO₂ had come from the same source, the Earth's mantle.

The Earth's mantle is around 40 kilometres below the depth where the samples were collected from. Despite such a long distance of travel, the unique noble gas signature preserves the record of the gas origin. The same techniques can therefore be confidently applied for monitoring injected CO₂, where travel distances are much shorter than in these natural samples.

Dr Ruta Karolyte, who led the research at the University of Edinburgh said: "We were able to show for the first time that noble gases remain very sensitive tracers of the source of CO₂ even after it mixes with large volumes of

water. This means that we can use noble gas techniques to sensitively fingerprint stored CO₂ once it is injected underground."

Dr Stuart Gilfillan, who directed the study said: "Our work clearly shows the unique capability of using noble gases to monitor CO₂ injected for geological storage. This paves the way for safe storage of CO₂ in old gas and oil fields, such as those present in the North Sea."

Such an approach can reduce emissions of CO₂ and help to limit the impact of climate change. Adoption of CCS technologies could greatly help the UK cut its greenhouse gas emissions to almost zero by 2050, necessary to meet recently announced targets.

The study, published in *Geochimica et Cosmochimica Acta*, was supported by the UK Engineering and Physical Sciences Research Council and the Australian research organisation CO₂CRC. The paper is titled "Tracing the migration of mantle CO₂ in gas fields and mineral water springs in south-east Australia using noble gas and stable isotopes".



Ruta Karolyte collecting gas samples for noble gas analysis at the CO₂CRC Orway National Research Facility in Australia. Photo: Stuart Gilfillan

Australia news

Minerals Council of Australia advocates for CCS

www.minerals.org.au

Carbon capture and storage is critical to reducing emissions says the Minerals Council of Australia.

BP's Statistical Review of World Energy shows coal generation is now the highest it has ever been – increasing 6.24 percent over the past two years, representing 38 per cent of all electricity generation.

200,000 MW of new coal-fired generation capacity is now under construction globally. Zero emission nuclear energy is also providing more than 10% of all electricity, and continues to grow – now at its highest since 2008.

The global emissions trend means the ongoing development and cooperation in the region on carbon capture, utilisation and storage (CCUS) is more important than ever.

MCA supports participation in global agreements such as the Paris Agreement, which would hold the increase in the global average temperature to well below 2°C.

CCUS is the only clean technology capable of decarbonising major industry.

The Intergovernmental Panel on Climate Change (IPCC) and International Energy Agency (IEA) have confirmed that CCUS is the only technology able to decarbonise large industrial sectors, particularly the steel, cement, fertiliser and petrochemical industries.

CCUS has been working safely and effectively for 45 years. There are now 18 large-scale facilities in commercial operation around the world which complement investments in renewables.

Zero emission nuclear energy providing more than 10 per cent of all electricity, and that it continues to grow with it being at its highest since 2008

Australian business and industry are actively working on pathways to net zero emissions. A least cost approach to reducing greenhouse emissions is critical to ensuring Australian businesses and families and our energy trading partners continue to have access to affordable, reliable and sustainable supplies.



ASME TURBO EXPO
Power for Land, Sea & Air



TU Graz
Graz University of Technology

Institute for Thermal Turbomachinery and Machine Dynamics


Graz University of Technology
Erzherzog-Johann-University

Design Concept for Large Output **Graz Cycle** Gas Turbines

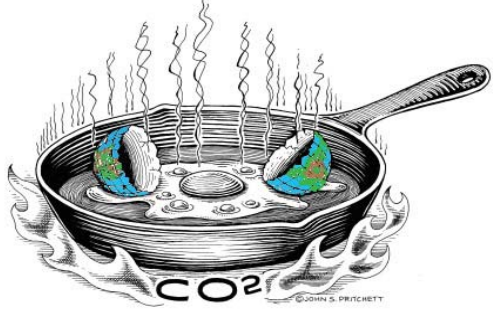
Presentation at the
ASME Turbo Expo 2006
Barcelona, Spain, May 8 - 11, 2006

Herbert Jericha, Wolfgang Sanz and Emil Göttlich
Institute for Thermal Turbomachinery and Machine Dynamics
Graz University of Technology
Austria

Motivation




How do you want your egg(s)? - Sunny side up?
But do not have it burned!




© JOHN S. PRITCHETT

Background




- Toronto Conference 1988, a Call for Action
- Kyoto Protocol** demands the reduction of greenhouse gases, mainly CO₂
- In EU**: strong pressure on utilities and companies to reduce CO₂ emissions
- In 2005: **emission allowances** to about 10 000 companies within the EU covering about 46 % of the overall EU CO₂ emissions
- As emission allowances become scarce: CO₂ generates costs (European Emission Allowances in March 2006: **27 €/ton CO₂**)
- CO₂ and N₂ from ASU can be utilized for **Enhanced Oil Recovery (EOR)**
Return: 20 – 40 \$/ton CO₂

Oxy-Fuel Cycles

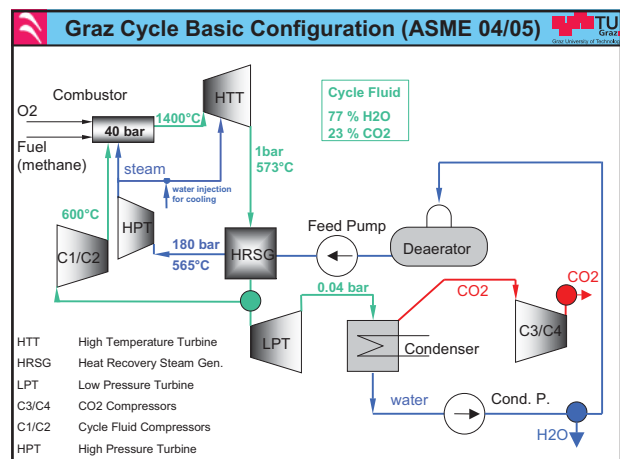


- Oxy-fuel cycles** with internal combustion with pure oxygen are a very promising technology (Global Gas Turbine News 10/2005)
- + CO₂ can be **easily** separated by **condensation** from working fluid consisting of **CO₂** and **H₂O**, no need for very penalizing scrubbing
- + Very low NO_x generation (fuel bound N₂)
- + Flexibility regarding fuel: natural gas, syngas from coal, biomass or refinery residue gasification
- New equipment required
- Additional high costs of oxygen production
- + These new cycles show higher efficiencies than current air-based combined cycles (**Graz Cycle**, Matiant cycle, Water cycle,...)

History of the Graz Cycle



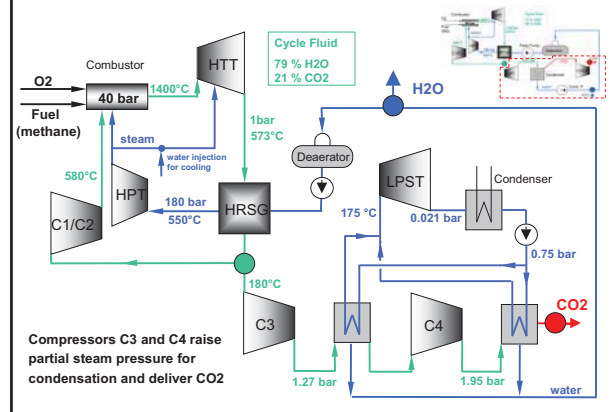
- 1985**: presentation of a power cycle without any emission (CIMAC Oslo)
 - H₂/O₂ internally fired steam cycle, as integration of top Brayton steam cycle and bottom Rankine cycle
 - efficiency 6 % - points higher than state-of-the art CC plants
- 1995**: Graz cycle adopted for the combustion of fossil fuels like methane (CH₄) (CIMAC Interlaken & ASME Cogen Vienna)
 - cycle fluid is a mixture of H₂O and CO₂
 - thermal cycle efficiency: 64 %
- 2000**: thermodynamically optimized cycle for syngas from coal gasification (VDI Essen)
- 2002/2003**: conceptual layout of prototype Graz Cycle power plant: detailed design of components (ASME Amsterdam, VDI Leverkusen, ASME Atlanta)
- 2004/2005**: presentation of **S-Graz Cycle** with 69% thermal efficiency and 57 % net efficiency for syngas firing (ASME Vienna, ASME Reno)



Power Balance ASME 2005

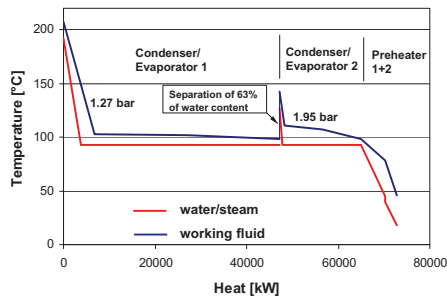
- Electrical cycle efficiency for **methane** firing:
Efficiency: 64.6 % (same for syngas firing)
- Oxygen production (0.15 - 0.3): 0.25 kWh/kg
Oxygen compression (2.38 to 40 bar, inter-cooled): 325 kJ/kg
Efficiency: 54.8 %
- Compression of separated CO₂ for liquefaction (1 to 100 bar, inter-cooled): 270 kJ/kg (3.7 MW)
Efficiency: 52.7 %

Condensation/Re-Vaporization at around 1 bar



Heat Transfer in Condenser/Evaporator

- Constant re-evaporation pressure of 0.75 bar for the bottoming steam cycle
- LPST inlet temperature of 175 °C; expansion line crosses Wilson line at last blade inlet, thus low humidity losses



S-Graz Cycle Power Balance for 400 MW net power

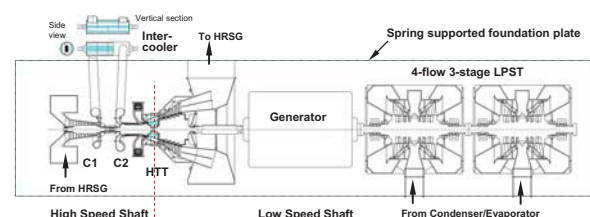
	Basic Layout	New Layout
HTT power [MW]	635	638
Total turbine power [MW]	753	739
Total compression power [MW]	249	235
Net shaft power [MW]	504	505
Total heat input [MW]	759	759
Thermal cycle efficiency [%]	66.5	66.5
Electrical cycle efficiency [%]	64.6	64.6

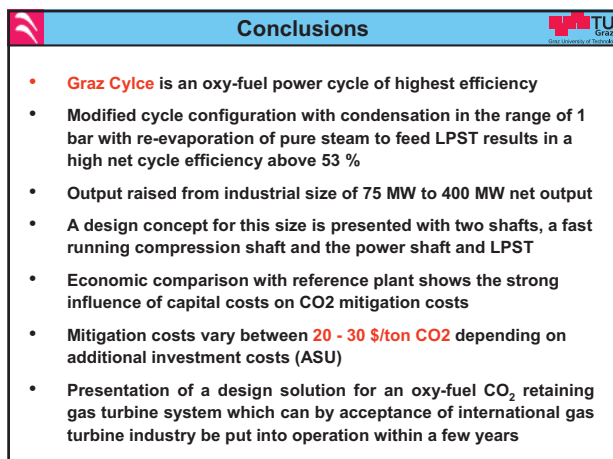
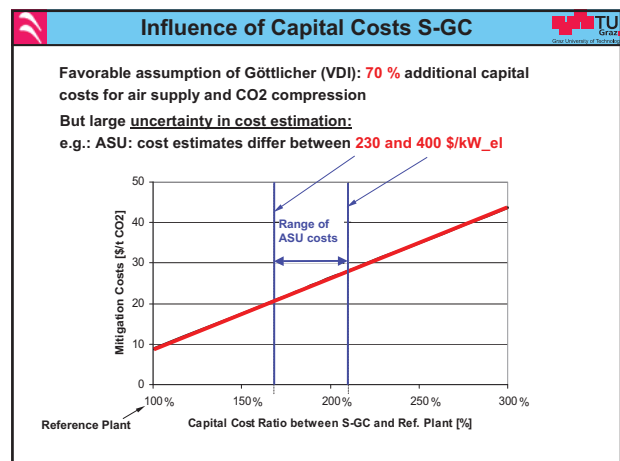
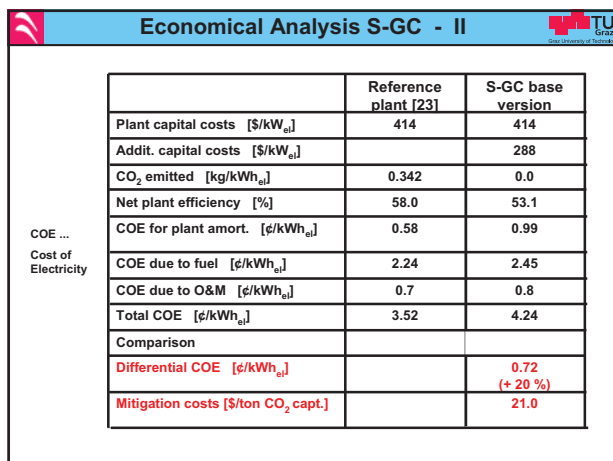
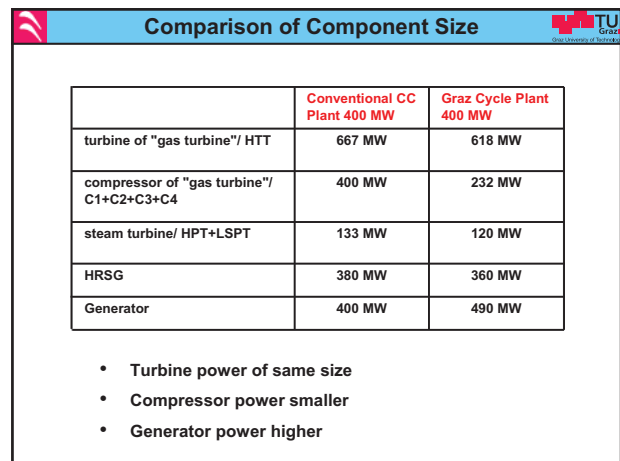
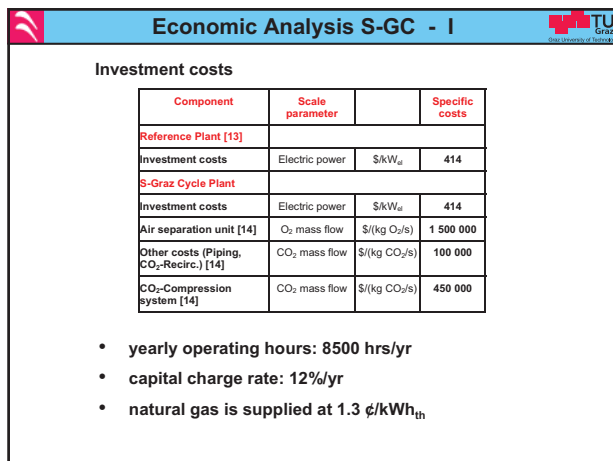
Additional Losses and Expenses

- Oxygen production: 0.25 kWh/kg = 900 kJ/kg
Oxygen compression (2.38 to 42 bar, inter-cooled): 325 kJ/kg
Efficiency: 54.8 %
- Compression of separated CO₂ for liquefaction (1.9 to 100 bar): **13 MW** (1 to 100 bar: 15.6 MW)
Efficiency: 53.1 % (compared to 52.7 %)

490 MW Turbo Shaft Configuration

- Main gas turbine components on two shafts
- Compression shaft of 8500 rpm: cycle compressors C1 and C2, driven by first part of HTT, the compressor turbine HTTC
- Power shaft of 3000/3600 rpm: power turbine HTTP as second part of HTT drives the generator
- Four-flow LPST at the opposite side of the generator
- Shafts on same spring foundation
- Intercooler between C1 and C2 on fixed foundation connected to HRSG





GT2006-90032

DESIGN CONCEPT FOR LARGE OUTPUT GRAZ CYCLE GAS TURBINES

H. Jericha, W. Sanz, E. Göttlich

Institute for Thermal Turbomachinery and Machine Dynamics
Graz University of Technology, Graz, Austria
wolfgang.sanz@tugraz.at

ABSTRACT

Introduction of closed cycle gas turbines with their capability of retaining combustion generated CO₂ can offer a valuable contribution to the Kyoto goal and to future power generation. Therefore research and development work at Graz University of Technology since the nineties has led to the Graz Cycle, a zero emission power cycle of highest efficiency. It burns fossil fuels with pure oxygen which enables the cost-effective separation of the combustion CO₂ by condensation. The efforts for the oxygen supply in an air separation plant are partly compensated by cycle efficiencies far higher than for modern combined cycle plants.

Upon the basis of the previous work the authors present the design concept for a large power plant of 400 MW net power output making use of the latest developments in gas turbine technology. The Graz Cycle configuration is changed insofar, as condensation and separation of combustion generated CO₂ takes place at the 1 bar range in order to avoid the problems of condensation of water out of a mixture of steam and incondensable gases at very low pressure. A final economic analysis shows promising CO₂ mitigation costs in range of 20 – 30 \$/ton CO₂ avoided. The authors believe that they present here a partial solution regarding thermal power production for the most urgent problem of saving our climate.

INTRODUCTION

In the last hundred years the concentration of some greenhouse gases in the atmosphere has markedly increased. There is a wide consensus in the scientific community that this seems to influence the Earth surface temperature and thus the world climate.

Therefore, in 1997 the Kyoto conference has defined the goal of global greenhouse gas emission reduction of about 5 % in the next years compared to the 1990 emission level. CO₂ is

the main greenhouse gas due to the very high overall amount emitted by human activities. And about one third of the overall human CO₂ emissions are produced by the power generation sector. In the EU there is a strong pressure on utilities and industry to reduce the CO₂ emissions from power generation. So there is a strong driving force to develop commercial solutions for the capture of CO₂ from power plants.

The authors believe that oxy-fuel cycles with internal combustion of fossil fuels with pure oxygen are a very promising technology and that their Graz Cycle can be the most economic solution for CO₂ capture from fossil power generation once the development of the new turbomachinery components needed are done. Oxygen is needed in large quantities for this kind of cycle and can be generated by air separation plants which are in use worldwide with great outputs in steel making industry and even in enhanced oil recovery (EOR) [1].

The basic principle of the so-called Graz Cycle has been developed by H. Jericha in 1985 [2] for solar generated oxygen-hydrogen fuel, in 1995 changed to fossil fuels [3, 4]. This was a first proposal for gas turbine oxy-fuel CO₂ capture. Improvements and further developments since then were presented at several conferences [5-9]. Any fossil fuel gas (preferable with low nitrogen content) is proposed to be combusted with oxygen so that neglecting small impurities only the two combustion products CO₂ and H₂O are generated. The cycle medium of CO₂ and H₂O allows an easy and cost-effective CO₂ separation by condensation. Furthermore, the oxygen combustion enables a power cycle with a thermal efficiency among the very best ever proposed, thus largely compensating the additional efforts for oxygen production.

At the ASME IGTI conference 2004 in Vienna a Graz Cycle power plant (High Steam Content Graz Cycle, S-Graz Cycle) was presented with a thermal cycle efficiency of nearly

70 % (excluding work for oxygen supply and CO₂ compression) based on syngas firing and relatively low CO₂ retention costs [10].

The very promising data aroused interest in several institutions in Europe, among them the Norwegian oil and gas company Statoil ASA. In cooperation with Statoil the S-Graz Cycle was re-evaluated and optimised with assumptions on component losses and efficiencies that Statoil and Graz University of Technology had agreed on. At the ASME IGTI conference 2005 [11] the results were presented with a net cycle efficiency of 52.7 % for methane firing, if the efforts of oxygen supply and compression of captured CO₂ for liquefaction are considered. The CO₂ mitigation costs were evaluated to 20.7 \$/ton CO₂ avoided.

These investigations also formed the basis of a techno-economic evaluation study by the two most important and most successful gas turbine companies in Europe. The feasibility of the S-Graz Cycle was accepted and the cost structure discussed in detail. The result was on one side that the cryogenic Air Separation Unit ASU appeared to have too high investment costs. On the other side the condensation of water out of a mixture of steam and incondensable gases, a thermodynamic technical problem not yet solved in European science, had to be more clearly investigated.

Therefore the object of this paper is to present author's work on the following subjects:

- Modification of S-Graz Cycle configuration to condensation in the range of 1 bar providing for separation of combustion generated CO₂ to the delivery compressor. By slight recompression evaporation of pure steam at reasonably high pressure and efficient expansion in a large output steam turbine (LPST) is made possible.
- Increase of net plant output to 400 MW providing for the additional tasks of oxygen production, CO₂ capture and delivery for pipeline use or liquefaction. The power effort is included in the overall efficiency raising the shaft output design value to 490 MW
- Two-shaft design of the turbo set with a fast running shaft comprising the main compressors C1 and C2 and the compressor turbine and with the power output shaft from high temperature turbine and steam turbine
- Incorporation of advanced flow and cooling development throughout the gas turbine components for smaller size and cost and reduction of high temperature material by rotor steam cooling on all accessible surfaces

Deliberations on part load and cold start for the situation of the novel cycle medium are also presented.

In this work the nomination "Graz Cycle" means "S-Graz Cycle", which is the more efficient variant and will be prosecuted in the future.

GRAZ CYCLE BASIC CONFIGURATION

The Graz Cycle is suited for all kinds of fossil fuels. Best results regarding net cycle efficiency and mitigation costs can

be obtained for syngas firing from coal gasification, if the syngas production effort is not considered in the thermodynamic balance (but only in the economic balance by elevated fuel costs). The higher net cycle efficiency is due to the fact that the lower oxygen demand of syngas per heat input reduces the effort of oxygen supply considerably. And finally, the higher carbon content results in more favorable mitigation costs per ton CO₂ avoided. But in this work thermodynamic data presented are for a cycle fired with methane, because it is the most likely fuel to be used in a first demonstration plant.

Figure 1 shows the principle flow scheme of the S-Graz Cycle with the main cycle data as published in [11].

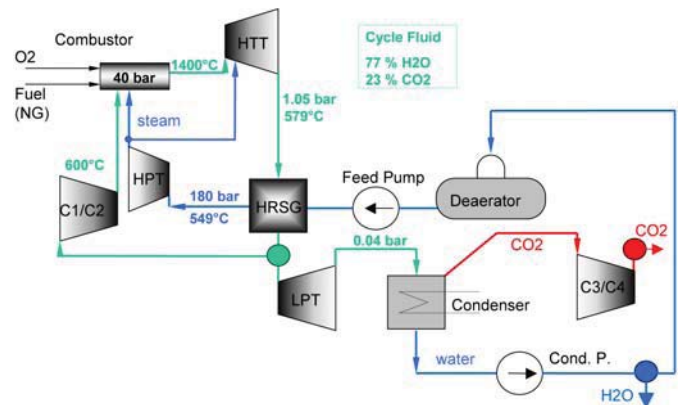


Fig. 1: Principle flow scheme of the basic Graz Cycle power plant

Basically the Graz Cycle consists of a high temperature Brayton cycle (compressors C1 and C2, combustion chamber and High Temperature Turbine HTT) and a low temperature Rankine cycle (Low Pressure Turbine LPT, condenser, Heat Recovery Steam Generator HRSG and High Pressure Turbine HPT). The fuel together with the nearly stoichiometric mass flow of oxygen is fed to the combustion chamber, which is operated at a pressure of 40 bar. Steam as well as a CO₂/H₂O mixture is supplied to cool the burners and the liner.

A mixture of about 74 % steam, 25.3 % CO₂, 0.5 % O₂ and 0.2 % N₂ (mass fractions) leaves the combustion chamber at a mean temperature of 1400°C, a value achieved by G and H class turbines nowadays. The fluid is expanded to a pressure of 1.053 bar and 579°C in the HTT. Cooling is performed with steam coming from the HPT using 330°C (13.7 % of the HTT inlet mass flow), increasing the steam content to 77 % at the HTT exit. It is quite clear that a further expansion down to condenser pressure would not end at a reasonable condensation point for the water component, so that the hot exhaust gas is cooled in the following HRSG to vaporize and superheat steam for the HPT; the pinch point of the HRSG is 25°C at the superheater exit. But after the HRSG only 45 % of the cycle mass flow are further expanded in the LPT. For a cooling water temperature of 8°C the LPT exit and thus condenser pressure would be 0.041 bar.

Gaseous and liquid phase are separated in the condenser. From there on the gaseous mass flow, which contains the combustion CO_2 and half of the combustion water, is compressed to atmosphere by C3 and C4 with intercooling and further extraction of condensed combustion water, and supplied for further use or storage. At atmosphere the CO_2 purity is 96 %; further water extraction is done during further compression for liquefaction.

After segregating the remaining combustion H_2O , the water from the condenser is preheated, vaporized and superheated in the HRSG. The steam is then delivered to the HPT at 180 bar and 549 °C. After the expansion it is used to cool the burners and the HTT stages.

The major part of the cycle medium –the return flow after the HRSG- is compressed using the main cycle compressors C1 and C2 with intercooler and is fed to the combustion chamber with a maximum temperature of 600°C.

The cycle arrangement of the Graz Cycle offers several advantages: On one hand, it allows heat input at very high temperature, whereas on the other hand expansion takes place to vacuum conditions, so that a high thermal efficiency according to Carnot can be achieved. But only less than half of the steam in the cycle releases its heat of vaporization by condensation. The major part is compressed in the gaseous phase and so takes its high heat content back to the combustion chamber.

LARGE POWER GRAZ CYCLE WITH WORKING FLUID CONDENSATION/ EVAPORATION IN 1 BAR RANGE

In the basic S-Graz Cycle configuration the authors have proposed to expand the portion of the working fluid which has to be segregated from the circulating flow to be expanded down to condenser pressure. This flow contains the captured CO_2 and steam from the combustion as well as the cooling steam flow. Recent research [12] shows that difficulties in condensation arise in the formation of water films on the cooling tubes and in concentration of CO_2 forming a heat transfer hindering layer so that only a low heat transfer coefficient in condensation will be achieved. This results in excessively large condenser heat transfer surface and related high costs.

Therefore it was suggested in the Austrian patent of the Graz Cycle [13] to condense this mass flow at atmosphere, separate the combustion CO_2 and re-vaporize the water at a reduced pressure level using the condensation heat. The pure steam is then fed to a Low Pressure Steam Turbine LPST, where it can be expanded to a condenser pressure lower than that for the working fluid mixture.

Thermodynamic investigations presented at the ASME 2005 conference [11] showed that best results can be obtained for a dual pressure evaporation at 0.55 and 0.3 bar. But for these low evaporation pressures, large volume flows arise and the losses of live steam pipes and valves counteract the gains of this process.

Therefore a novel configuration is proposed in this work which allows single-pressure evaporation at a reasonable

pressure level. The process is now split into the high-temperature cycle and a separate low temperature condensation process as shown in the simplified scheme of Fig. 2. The high temperature part consists of HTT, HRSG, C1/C2 compressors and HPT. Again condensation of the working fluid in the 1 bar range is proposed in order to avoid the problems of a working fluid condenser at vacuum conditions as described above. The heat content in the flow segregated after the HRSG for condensation is still quite high so re-evaporation and expansion in a bottoming cycle is mandatory. The detailed flow sheet used for the thermodynamic simulation is included in the appendix (Fig. 10) and gives mass flow, pressure, temperature and enthalpy of all streams.

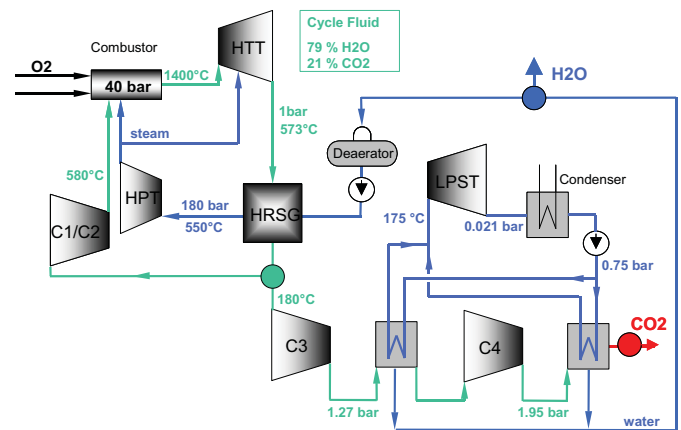


Fig. 2: Principle flow scheme of modified Graz Cycle power plant with condensation/evaporation in 1 bar range

This bottoming cycle operates by pure steam with extensively cleaned feed water and thus allows together with the very low cooling water temperatures of northern Europe to attain condenser pressures down to 0.02 bar.

For proper re-evaporation two sections of working fluid condensations are provided, each following a compressor stage with reasonable increase of flow pressure resulting in a higher partial condensation pressure of the water content. The two compressor stages can be regarded as pre-runners of the CO_2 delivery compressor and will be helpful in cleaning the turbomachinery, piping and HRSG interior from air in preparation of a cold start. The heat exchangers are well developed modern boiler elements providing steam just below 1 bar for the condensing steam turbine.

At the first pressure level of 1.27 bar about 63 % of the water content can be segregated, so that the power demand of the second compression stage is considerably reduced. It compresses up to 1.95 bar, which allows the segregation of further 25 % of the contained water. Further cooling of the working fluid, also for water preheating, leads to the separation of additional 11 %, so that the water content of the CO_2 stream supplied at 1.9 bar for further compression is below 1 %. After segregation of the water stemming from the combustion process, the water flow is degassed in the deaerator with steam

extracted after the HPT and fed to the HRSG for vaporization and superheating.

This two-step pre-compressed condensation counteracts the effect of sinking H_2O partial pressure due to condensed water extraction from working fluid and thus allows a reasonably high constant re-evaporation pressure of 0.75 bar for the bottoming steam cycle. Fig. 3 shows the heat – temperature diagram for this condensation/ evaporation process. After the start of water condensation, the working fluid temperature decreases only slightly, leading to relatively small mean temperature differences of 8 K in the first evaporator and 12 K in the second evaporator. After having condensed and separated most of the water content, the temperature of the working fluid decreases strongly in the water preheaters of the bottoming cycle (see Fig. 10).

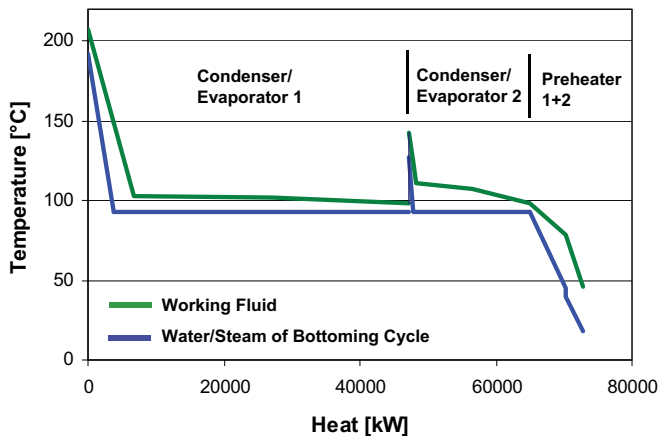


Fig. 3: Heat - temperature diagram of the condensation/ evaporation process

About three quarters of the condensation cycle mass flow is evaporated and superheated in the first condenser. It is mixed with the steam of the second condenser/evaporator unit providing steam of 0.75 bar and 175°C at the LPST inlet. Expanding the steam to a condensation pressure of 0.021 bar for a cooling water temperature of 8°C provides about 72 MW power output. A four-flow design is necessary to handle the high volume flow for a 400 MW Graz Cycle.

Steam is extracted at a pressure of 0.12 bar from the LPST and fed to the deaerator. The expansion line is to the major part in the dry steam region and crosses the Wilson line only before the last stage, so that only very fine droplets in the outer last stage sections are formed. A very high expansion efficiency hardly hindered by formation of humidity is to be expected.

Table 1 gives the power balance of the modified Graz Cycle plant of 400 MW net power output in comparison with the scaled-up basic configuration published in [11]. The heat input is the same for both cycles allowing a better comparison of the turbomachinery sizes. The C3 and C4 compressor have different tasks in both cycles. In the basic cycle they re-compress the separated CO_2 flow to 1 bar, whereas in the modified cycle they increase the working fluid pressure for a

more favorable condensation/evaporation condition as described above. The modified Graz Cycle works with a smaller mass flow of the working fluid, so that both turbine and compressor total power decrease, whereas the net power output remains nearly the same. This leads to a similar thermal efficiency of about 66.5 % or an electrical net efficiency of about 64.65 %.

If considering the efforts for oxygen production and compression as well as the efforts of CO_2 compression to 100 bar for liquefaction, the net efficiency further reduces to 52.72 % for the basic cycle and 53.12 % for the modified cycle. This higher efficiency stems from a reduced CO_2 compression effort due to the higher supply pressure of 1.9 bar in the modified cycle. Thus the specific energy consumption reduces from 350 kJ/kg to 300 kJ/kg CO_2 . The net efficiency of 53.12 % is higher than that of most other CO_2 capture technologies if evaluated under the same conditions, so that this new concept is worth a further feasibility investigation.

Table 1: Graz Cycle Power Balance

	Basic layout	New layout
HTT power [MW]	634.7	617.9
HPT power [MW]	48.0	49.9
LPT/LPST power [MW]	70.5	71.6
Total turbine power P_T [MW]	753.2	739.4
C1 power [MW]	137.2	131.1
C2 power [MW]	90.2	82.6
C3 power [MW]	11.5	8.9
C4 power [MW]	4.8	6.6
Pump power [MW]	5.3	5.5
Total compression power P_C [MW]	249.0	234.7
Net shaft power [MW] without mechanical losses	504.2	504.7
Total heat input Q_{zu} [MW]	758.6	758.6
Thermal cycle efficiency [%]	66.47	66.52
Electrical power output [MW] incl. mechanical, electrical & auxiliary loss	490.3	490.7
Net electrical cycle efficiency [%]	64.63	64.68
O_2 generation & compression P_{O_2} [MW]	74.7	74.7
Efficiency considering O_2 supply [%]	54.78	54.83
CO_2 compression to 100 bar P_{CO_2} [MW]	15.6	13.0
Net power output [MW]	400.0	403.0
Net efficiency η_{net} [%]	52.72	53.12

DESIGN CONCEPT FOR A VERY LARGE GRAZ CYCLE PLANT OF 400 MW NET OUTPUT

In this work the design concept for a Graz Cycle power plant of 400 MW electrical net output is presented. This power is derived from a 490 MW turbo shaft configuration. The difference is caused by the power demand of the ASU and by the driving power for the oxygen compressor in order to deliver

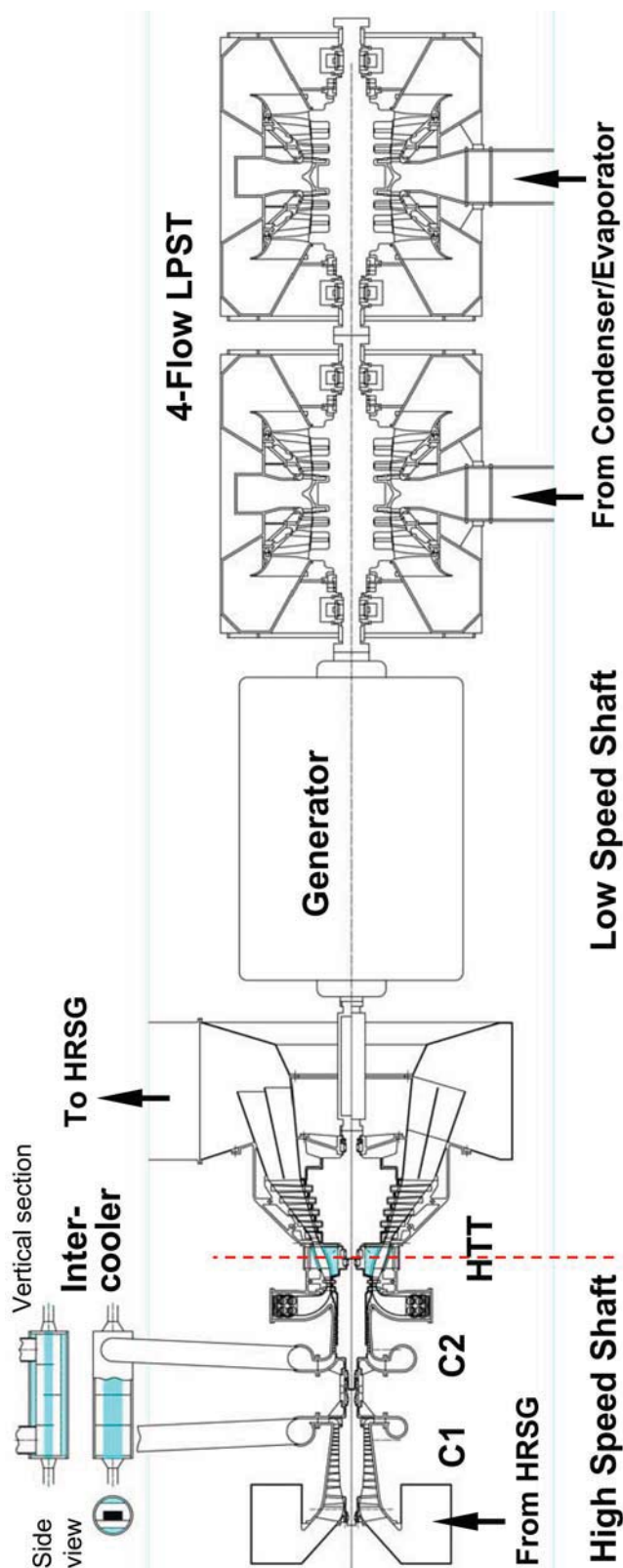


Fig. 4: Arrangement of the main turbomachinery for a 400 MW Graz Cycle plant

oxygen to the combustor at 42 bar and by the CO₂ compressor which has to deliver the captured CO₂ at a pipeline pressure of over 100 bar.

Gas turbines, compressors and combustors require the best flow development achieved up to now in gas turbine technology. In the course of this project our institute has found novel solutions for blade cooling, steam cooled combustor burner design and optimal rotor construction and rotor dynamics. The innovative cooling burner design helps to achieve the mentioned extreme high thermal efficiency (see [6] for details of the burner design), further improved by the positive change on the lower temperature end of the power cycle flow scheme as described above.

In this design proposal intensive use of steam cooling is made, not only for blades, but for all rotors in the high-speed high-temperature region. In that manner a solid and simple rotor design forged from one piece or welded from separate disks can be used with no internal friction between rotor disks as might be possible in a rotor assembled from separate disks. This type of rotor design provides for high blade load carrying capability with acceptable radial stress. The newly developed high chromium ferritic steels will be applied making use of their superior heat conduction and low thermal expansion properties. The relatively high speed selected provides for long blades in the last stages with high flow efficiency and low tip clearance loss.

The one-shaft system as in air-breathing gas turbines is not applicable since in the Graz Cycle system the amount of compressor flow volume is smaller and the number of stages required considerably higher. Therefore a much higher compressor speed as power turbine speed is an effective solution.

The main gas turbine components are arranged on two shafts, the compression shaft and the power shaft (see Fig. 4). The compression shaft consists of the cycle compressors C1 and C2, which are driven by the first part of the high temperature turbine HTT, the compressor turbine HTTC. It runs free on its optimal speed of 8500 rpm. This relatively high speed is selected for reason of obtaining sufficient blade length at outlet of C2 and to reduce the number of stages in both compressors. The second part of the HTT, the power turbine HTTP, delivers the main output to the generator. A further elongation of the shaft is done by coupling the four-flow LPST at the opposite side of the generator. The HPT can be coupled to the far end of the LPST or can drive a separate generator. The two shafts are based on the same spring foundation. The intercooler between C1 and C2 is located on the fixed foundation.

C1/C2 compressor design with intercooler:

The working fluid compressor C1 is driven by the HTTC at 8500 rpm. The high speed poses a special problem for the first stage of C1 which has yet been solved by flow research and is now applied in many aircraft jet engines and also stationary compressor designs [14, 15]. The high tip Mach number on the

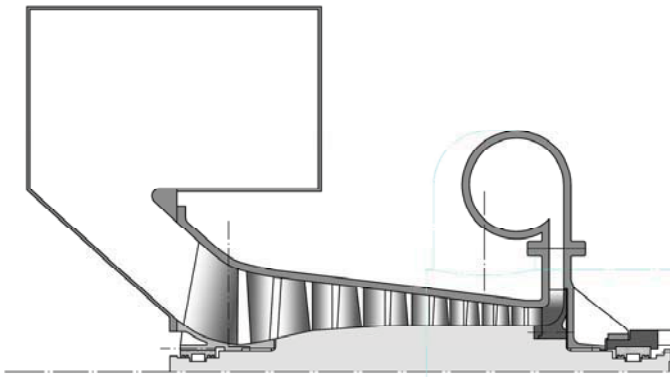


Fig. 5: C1 design with an uncooled drum rotor and an additional radial stage from nickel alloy, with radial diffuser and exit scroll to intercooler

first stage should not exceed the value of 1.4 for reasons of shock formation. With the help of a slight positive inlet swirl an inlet Mach number of 1.3 is designed.

Compression at C1 starts at 106°C and reaches 442°C at the outlet to the intercooler. For reasons of rotor dynamics the shafts of C1 and C2 are separated with intermediate bearings and a solid coupling. This makes the transfer of cooling flow difficult, so that cooling of the drum rotor of C1 will not be applied. This is possible by a combination of rotor materials.

The first part with seven axial stages is a ferritic steel drum, which reaches only 390°C. This material can be highly stressed without creep at temperatures below 400°C. By the application of a final radial wheel which has to be milled separately from nickel alloy and which is mounted to the main

drum by elastic centering completes the rotor construction of C1, as shown in Fig. 5. The radial wheel with a wide vaneless diffuser and scroll improves the flow transfer to the intercooler.

The inlet temperature to C2 is somewhat lowered by the intercooler but still reaches 380°C. During course of compression the working fluid reaches an outlet temperature of 580°C, so that from the second stage onwards cooling has to be applied on the rotor surface of the bladed annular flow channel. Seven axial stages with a stepwise decrease of blade length from 90 to 40 mm are supported on a drum rotor with disk extensions of constant diameter. Fig. 6 shows the C2 rotor with the counter flow of cooling steam on the drum surface. It is guided by means of openings under the bladed disk extensions and is prevented by sealing strips from flowing into the main flow. These strips are carried on both sides of the stationary blades. By proper selection of the feed pressure this flow can be optimized at a small penalty in dilution of the main flow.

Excellent flow properties of this compressor can be expected due to its blade mounting on a stiff rotor with very small radial tip clearances and flow losses together with an aspect ratio of outer to inner flow radius of 440 to 400 mm.

The intercooler requires some development work. The fluids on both sides are unconventional insofar as the working fluid on one side is to be cooled by high pressure steam on the other side. Heat transfer from compression work to steam superheat is thus achieved. The authors can point at previous development work at their institute in a similar problem, i.e. the design of an 850°C steam plant in double loop configuration as published by Perz et al. [16], where many boiler heat transfer problems had been treated.

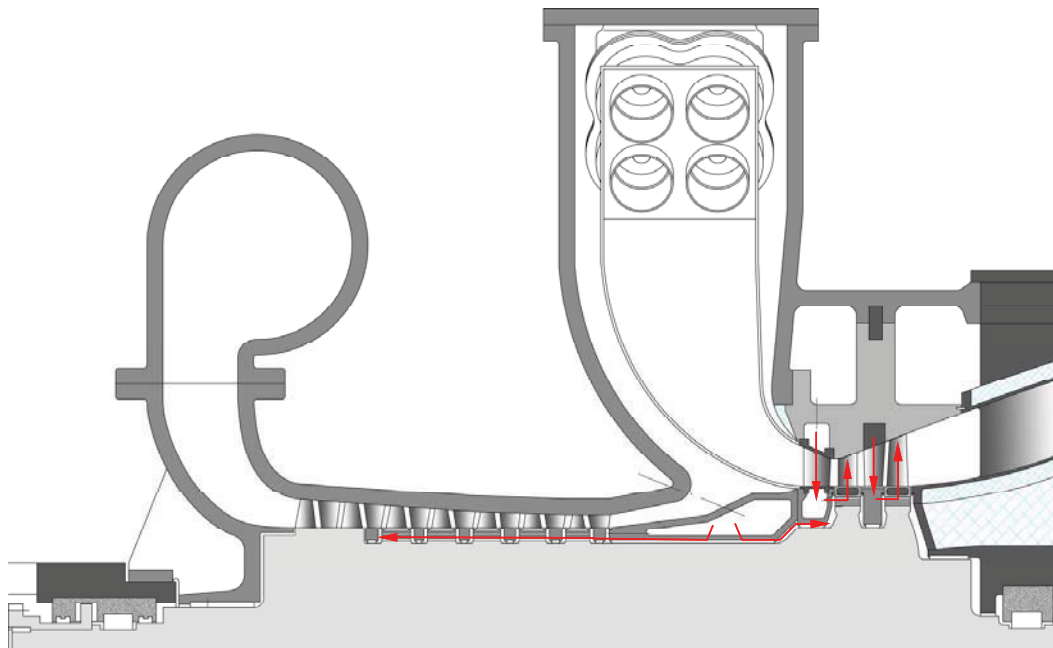


Fig. 6: Design of C2 drum rotor with cooling steam flow arrangement, combustor and HTTC

In the case given the intercooler is thermodynamically part of the HRSG superheater and is thus arranged close to the HRSG. Its cooling flow is steam of 196 bar pressure. It is designed as a solid tube which should be supported on solid ground foundation. The heat transfer surface is realized by 180 tubes of 3.1 m length held in support plates which guide the working gas flow from C1 outlet to C2 inlet. The outer shell of the intercooler is internally insulated and is connected by ample flow areas in flexible scroll and tube arrangements to both compressors (see Fig. 4).

HTT compressor turbine (HTTC)

The same drum rotor either forged in one piece or welded up from separated disks carries not only the C2 but also the compressor turbine HTTC. The flow design of the HTTC will be a two-stage reaction turbine with 50 % reaction at the mean section of both blade rows. The high rotor speed of 8500 rpm as mentioned before provides for long blade lengths, i.e. a first stage blade of 100 mm and a second stage blade of 164 mm with an inner radius of 533 mm (see Fig. 7). This results in excellent flow properties in subsonic condition and together with the high reaction of the blade on all radii (55 % at mean section and at least 25 % at hub) a high blade flow efficiency is expected. Low tip clearances are applied also contributing to this goal and can be achieved by the excellent rotor dynamics of the stiff drum rotors and very careful blade cooling.

The high speed and power of this turbine is made possible by ample steam cooling. Nozzles and blades are cooled in conventional serpentine passage design with holes as well as the rotor inlet edge as shown in the cooling arrangement of Fig. 7. Rotor cooling steam is supplied along the whole drum

surface. It is fed into a labyrinth seal in the inner range of the combustion chamber allowing the steam to flow to both sides. One flow is directed backwards under the dump diffuser into the outer surface of the C2 providing cooling steam as described above. The main amount of cooling steam flows along the rotor drum at the inner radius of the combustor casing towards the first disk of the HTTC.

The first nozzles are hollow with proper cooling passages and are cooled by steam fed from the casing outside in radial inwards direction. The steam is collected in a chamber of the diaphragm just opposite the first blade root. Via nozzles, blowing in direction of rotor speed, the cooling steam is then fed to the lower part of the blade fir-tree root. From there it flows along the serpentine passages under pumping action of the rotor wheel and is delivered to the blade surface via laser drilled holes to form the conventional cooling films at the appropriate locations of the blade. The second guide vanes are supplied with cooling steam which is fed into the outer rim of the diaphragm. There it flows radially inwards also to supply the rotor surface in-between stages and the inlet to the second stage blades which are also built with serpentine passages and the appropriate cooling holes. In principle this design was applied for the well-known gas turbine model GT10, originally designed by F. Zerlauth [17].

In terms of rotor dynamics the drum rotor of C2 and HTTC will be designed for the high stress considering the effect of steam cooling on all surfaces. Stiff bearing shaft extensions and solid double-lobe oil bearings provide for high shaft and high bearing stiffness in order to have all critical speeds sufficiently high above running speed.

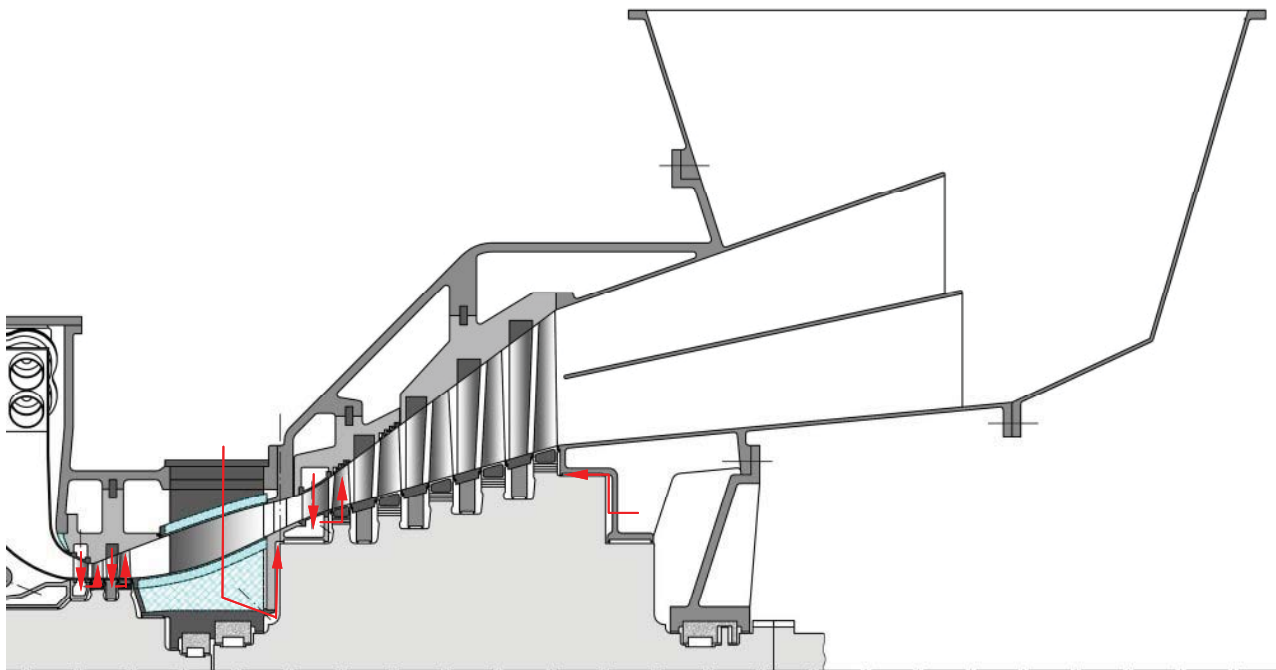


Fig. 7: Design of two-stage HTTC and 50 Hz HTTP

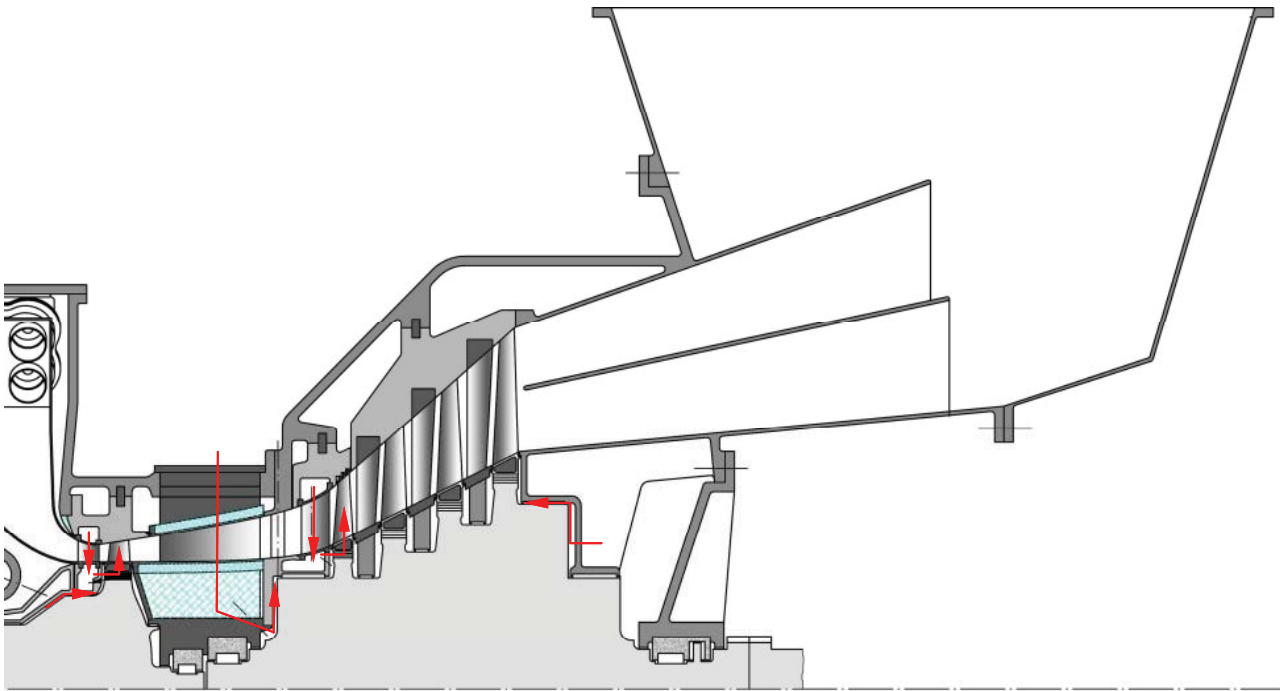


Fig. 8: Design of transonic one-stage HTTC and 60 Hz HTTP

HTTC alternative transonic stage design

The authors' institute has done extensive development work for the design of transonic turbine stages. Not only several computer programs have been developed for investigating three-dimensional transonic flow, but a unique test installation for transonic stages was built where many effects of unsteady viscous transonic flow were investigated (e.g. [18, 19]). The test installation has aided the development of industrial gas turbines and is now in use for several EU projects.

A novel innovative cooling system has also been developed and could be applied here in order to save cooling medium, high temperature material and cost of manufacture at the same time providing most effective blade cooling at the blade leading edge in transonic flow [20, 21]. The design could follow the development path of General Electric in providing thermal barrier coating on the rotating blades since these are free of the multitude of cooling holes and are supplied only by low number of slots creating cooling steam films covering the whole surface.

Therefore, alternatively the HTTC expansion could also be done with one transonic stage as shown in Fig. 8. This can be achieved by a higher radius and stage loading at a somewhat reduced degree of reaction. Such a stage would sit on the same rotor as described before and it would have a mean radius of 750 mm at a blade length of 120 mm. A further advantage of a transonic stage would be the much smaller radius difference from compressor turbine outlet to power turbine inlet, depending also on the speed of the power turbine for which design proposals for 50 and 60 Hz are presented here.

HTT power turbine (HTTP)

A gas turbine system with two shafts at highly different speed as it has to be built here, requires an intermediate bearing to be arranged right between the stages of compressor turbine outlet and power turbine inlet. The flow of gas transmitted is at very high velocity, at temperatures of 1075°C and at a pressure of 14 bar. A conventional design would provide an outlet diffuser, an outlet casing, a transition duct and an inlet casing in between this gas turbine parts. Frictional loss, heat loss, even with internal and external insulation, would be unavoidable. In previous design solutions for industrial size turbines with almost the same cycle conditions the authors have proposed a single overhung disk with a transonic stage for the compressor turbine and one or two overhung disks for the power turbine directly opposite to take over the gas flow in a common casing [10]. This solution requires a high speed power turbine which is only possible to build relying on gears of high speed and high power. The power output of 92 MW in that case made it possible since gas turbines transferring around 100 MW from gas turbine speeds at 5400 rpm to 3000 rpm are in use in industry.

The large power output in the case presented here forbids the use of gears for such high-speed power transfer. Therefore the possible electrical frequencies of 50 Hz in Europe and 60 Hz in USA and western hemisphere were investigated. The power turbine is proposed with a strong change of inner radius on a solid shaft. Five stages are necessary for the 50 Hz design of Fig. 7 and four stages for the 60 Hz of Fig. 8. So the axial outlet speed should be kept at medium value in order to reduce

the exhaust loss, to reduce axial diffuser exit length and to facilitate the flow transfer to the HRSG inlet.

The design proposed provides last blade lengths of 750 mm at 50 Hz and of 600 mm at 60 Hz, both at 1300 mm inner radius. At the inlet the inner radius at 50 Hz is somewhat larger than the HTTC outlet, but at 60 Hz, together with a transonic HTTC, it provides a flow path at almost the same radius as shown in Fig. 8.

The intermediate bearing casing in its hot environment has to be insulated on its outer surface in a mode of insulation withstanding the friction of the hot outer flow. The same holds true for the three supporting ribs, which have to provide ample inner space for transfer of oil, cooling air and steam leakage outlet from labyrinths on both shaft sides as well as for monitoring equipment. At the same time the bearing should be as short as possible and the ribs should provide only a minimum of flow resistance. Certainly this is an object that deserves intensive flow, stress and heat transfer deliberations.

The thrust equalization of both types of power turbines cannot be made in the conventional manner of steam turbines. A balance piston requires a diameter of about the mean blade mean diameter to give proper balance of axial forces. In this case such a design would require an unacceptable flow turn and deviation of the hot gas flow. (In a one-shaft gas turbine the problem does not exist, since compressor thrust and turbine thrust balance each other.) On the other hand, to carry the axial thrust of a large power turbine especially in the conical form is impossible for oil thrust bearings. Size and oil friction power loss would be too high. Therefore a stepped labyrinth on the exhaust side of the rotor drum is proposed as shown in Figs. 7 and 8, which is supplied with internal steam pressure to provide for the necessary thrust equalization. The steam supply feeds also the cooling flow which is led along the rotor drum surface under the root sealing plates for the last and the penultimate stage, whereas cooling flow to the first and second stage is supplied via the hollow nozzle blades to an inner diaphragm cavity from which the inflow to the hollow rotor blades is effected. Power turbine thrust bearing is arranged outboard of casing in vicinity of steam operated balance piston (see Figs. 7 and 8).

Low Pressure Steam Turbine (LPST)

The LPST is fed with steam of 0.75 bar and 175°C. Expanding the steam to a condensation pressure of 0.021 bar leads to a high volume flow. At 50 Hz a four-flow design with three stages, as shown in Fig. 4, is able to handle the high steam flow with excellent efficiency. The last stage is transonic with a blade length of 970 mm. In the shaft arrangement this steam turbine is coupled to the far side of the main generator.

HPT

The HPT is a standard high-speed back-pressure steam turbine of 50 MW power output for which many designs are in the market. A geared type seems to be a superior solution since better flow efficiency and operability due to nozzle boxes and low number of stages with long blades and low leakage loss can

be achieved. It can be coupled to the far end of the LPST or can be used to drive a separate smaller electric generator.

Compressors C3 and C4

The delivery compressors C3 and C4, which increase the pressure of the working fluid prior to condensation in order to obtain better evaporation conditions for the bottoming steam cycle, are also needed to vent the internal volume before start up. They are driven by two separate speed-controlled motors.

Combustion

The combustion chamber and burner design proposed has been thoroughly tested in science of combustion. Research partners have run CH₄/oxygen burners in a steam environment successfully [22, 23]. The authors' proposal [7] of setting a separate oxygen and fuel inlet in the center of a strong steam vortex in a large number of separate burners within the combustion chamber provides for easy control of amount and ratio of oxygen and fuel together with ignition and flame observation. The steam vortex keeps together both reactants. The independent supply of both reactants together with the high flame speed caused by pure oxygen lets expect improvements compared to the otherwise acoustic vibration prone conventional low-NO_x combustion chamber flows.

PART LOAD AND START-UP

In part load the maximum gas turbine temperature can be lowered by reduction of heat input. With the free running compressor shaft adjustment of flow and temperature can be effected precisely in operating IGVs and turbine valves accordingly.

To keep the working fluid and the CO₂ delivery line free of nitrogen in each cold start careful scavenging of all internal volumes in turbomachinery, HRSG and piping has to be done. Since fuel and oxygen input can be governed for each burner quadruple ignition and safe operation of flames is secured. See further details of the start-up process in the appendix.

ECONOMIC EVALUATION

Despite the high efficiency and the positive impact on the environment by a Graz Cycle power plant, a future application of this technology and an erection of a power plant mainly depends on the economical balance. The main indicator characterizing the economical performance of a power plant for CO₂ capture are the mitigation costs. They represent the increased capital and operational costs incurred by new and additional equipment and lower cycle efficiencies in relation to the CO₂ mass flow avoided. The CO₂ captured has an economic value of about 10 \$/ton, if it can be used for enhanced oil recovery (EOR) or of about 30 \$/ton in the future CO₂ emission trading scenario. These prices show the current threshold for the economic operation of zero emission power plants.

In order to estimate the mitigation costs for a Graz Cycle plant, an economic comparison with a state-of-the-art combined

cycle power plant of 58% efficiency is performed. The economic balance is based on following assumptions: 1) the yearly operating hours is assumed at 8500 hrs/yr; 2) the capital charge rate is 12%/yr, which corresponds to an interest rate of 8 % over a depreciation period of 15 years; 3) methane fuel costs are 1.3 ¢/kWh_{th}; 4) the investment costs per kW are the same for the reference plant of about 400 MW net power output and the Graz Cycle plant (see below); 5) additional investment costs are assumed for the air separation unit (ASU), for additional equipment and CO₂ compression to 100 bar (see Table 2 [24]); 6) the costs of CO₂ transport and storage are not considered because they depend largely on the site of a power plant.

Table 2: Estimated investment costs

Component	Scale parameter		Specific costs
Reference Plant			
Investment costs	Electric power	\$/kW _{el}	414
Graz Cycle Plant			
Plant investment costs	Electric power	\$/kW _{el}	414
Air separation unit [24]	O ₂ mass flow	\$(kg O ₂ /s)	1 500 000
Other costs (Piping, CO ₂ -Recirc.) [24]	CO ₂ mass flow	\$(kg CO ₂ /s)	100 000
CO ₂ -Compression system [24]	CO ₂ mass flow	\$(kg CO ₂ /s)	450 000

The assumption of similar investment costs for a conventional and a Graz Cycle power plant is based on a comparison with typical turbomachinery sizes for a 400 MW combined cycle plant as given in Table 3. It shows that the turbine power and the HRSG is of similar size, whereas the compressor power is remarkably smaller. On the other hand the Graz Cycle needs a larger generator due to the additional power consumption for ASU and CO₂ compression. Development efforts needed especially for HTT and combustor are not considered in the investment costs.

Table 3: Comparison of equipment size for a 400 MW plant in terms of power

	Conventional CC plant	Graz Cycle plant
turbine of "gas turbine"/ HTT	667 MW	618 MW
compressor of "gas turbine"/ C1+C2+C3+C4	400 MW	232 MW
steam turbine/ HPT+LSPT	133 MW	120 MW
HRSG	380 MW	360 MW
Generator	400 MW	490 MW

Table 4 shows the result of the economic evaluation. Compared to the reference plant, the capital costs are about 70 % higher only by considering the additional components for O₂ generation and CO₂ compression. So they contribute mostly to the difference in COE. The fuel costs have the major influence on the COE, especially for syngas firing, but they do not differ largely between reference and Graz Cycle plant. The O&M costs are assumed 15 % higher for a Graz Cycle plant due to the operation of additional equipment.

Based on these assumptions, the COE of a methane fired Graz Cycle plant of 53.1 % net efficiency is 0.72 ¢/kWh_{el} higher than for the reference plant. The mitigation costs are 21.0 \$/ton of CO₂ avoided, if CO₂ liquefaction is considered. This value is clearly below the threshold value of 30 \$/ton showing the economic potential of the Graz Cycle.

Table 4: Economic data for a 400 MW Graz Cycle plant

	Reference plant	S-GC base version
Reference Plant		
Plant capital costs [\$/kW _{el}]	414	414
Addit. capital costs [\$/kW _{el}]		288
CO ₂ emitted [kg/kWh _{el}]	0.342	0.0
Net plant efficiency [%]	58.0	53.1
COE for plant amort. [¢/kWh _{el}]	0.58	0.99
COE due to fuel [¢/kWh _{el}]	2.24	2.45
COE due to O&M [¢/kWh _{el}]	0.7	0.8
Total COE [¢/kWh_{el}]	3.52	4.24
Comparison		
Differential COE [¢/kWh_{el}]		0.72
Mitigation costs [\$/ton CO₂ avoided]		21.0

The results of the economic study depend mainly on the assumptions about investment costs, fuel costs and capital charge rate. A cost sensitivity analysis performed in [11] showed that a variation of the capital costs has the main influence on the economics, since they contribute most to the mitigation costs. Unfortunately, there is a large uncertainty of these costs. A survey of the ASU costs vary in the range of 230 to 400 \$/kW_{el} (the same price as for a complete power plant). These costs are for a cryogenic ASU as used e.g. in steel industry for half a century. There is certainly a potential for effectivity increase. Oxygen from membranes which are under intensive development now are not yet available for plants of the output in discussion. The ASU appears to be a decisive cost factor. Only considering its cost variation, the mitigation costs vary between 21.0 and 27.9 \$/ton CO₂ for the methane fired plant (see Fig. 9).

This high sensitivity to the capital costs shows the dilemma in performing an exact economic evaluation, since their estimation for a Graz Cycle power plant is very difficult because of new turbomachinery components. But the authors

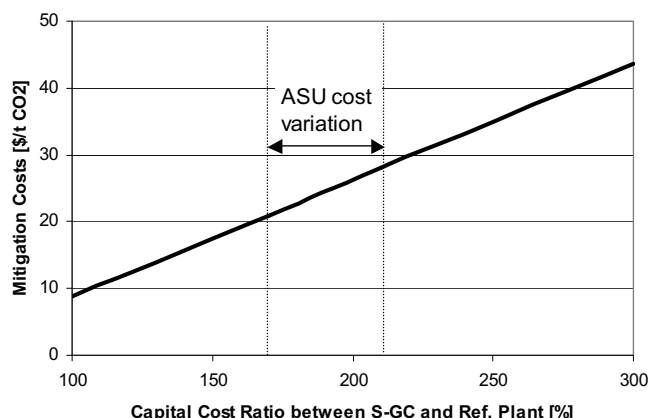


Fig. 9: Influence of capital costs on the mitigation costs (CO₂ provided at 100 bar)

claim that their design of high-speed transonic stages with innovative steam cooling allows a cost-effective manufacture. In these considerations about the height of additional investment costs, a further advantage of the Graz Cycle, the almost NO_x-free combustion was not evaluated. According to [25] exhaust flow NO_x and CO catalytic reduction to achieve single-digit emissions (in strict attainment areas) can increase gas turbine genset plant costs by 40 to 50 percent.

CONCLUSIONS

The Graz Cycle is an oxy-fuel power cycle with the capability of retaining all the combustion generated CO₂ for further use. In order to avoid the difficulties of condensation of water out of a mixture of steam and incondensable gases at very low pressures, a modified cycle configuration was presented with condensation in the range of 1 bar. It allows a separate bottoming steam cycle with reasonably high pressures and efficiencies, so that a high net cycle efficiency above 53 % can be expected.

The output of the Graz Cycle plant is raised from industrial size to 400 MW net output. A design concept for this size is presented with two shafts. A fast running compression shaft is driven by the compressor turbine HTTC, whereas the power shaft comprises the power turbine HPT and the LPST.

In an economical analysis the Graz Cycle power plant is compared with a reference plant. The resulting mitigation costs are in the range of 20 – 30 \$/ton CO₂ avoided depending on the costs of the ASU and thus are below a threshold value of 30 \$/ton CO₂ (assumed for future CO₂ emission trading).

The authors have thus presented a design solution for an oxy-fuel CO₂ retaining gas turbine system which can by acceptance of international gas turbine industry be put into operation within a few years. The authors believe, that this system is equal in thermodynamic performance to any other proposal in the field of CO₂ reduction and is superior in applying gas turbine experience and research accumulated to our day.

REFERENCES

- [1] **Gas Turbine World**, 1998, "Pemex Injection for Cantarell Field EOR", Pequot Publishing Inc.
- [2] **Jericha, H.**, 1985, "Efficient Steam Cycles with Internal Combustion of Hydrogen and Stoichiometric Oxygen for Turbines and Piston Engines", CIMAC Conference Paper, Oslo, Norway
- [3] **Jericha, H., Sanz, W., Woisetschlager, J., Fesharaki, M.**, 1995, "CO₂ - Retention Capability of CH₄/O₂ – Fired Graz Cycle", CIMAC Conference Paper, Interlaken, Switzerland
- [4] **Jericha, H., Fesharaki, M.**, 1995, "The Graz Cycle – 1500°C Max Temperature Potential H₂ – O₂ Fired CO₂ Capture with CH₄ – O₂ Firing", ASME Paper 95-CTP-79, ASME Cogen-Turbo Power Conference, Vienna, Austria
- [5] **Jericha, H., Lukasser, A., Gatterbauer, W.**, 2000, "Der "Graz Cycle" für Industriekraftwerke gefeuert mit Brenngasen aus Kohle- und Schwerölvorgasung" (in German), VDI Berichte 1566, VDI Conference Essen, Germany
- [6] **Jericha, H., Göttlich, E.**, 2002, "Conceptual Design for an Industrial Prototype Graz Cycle Power Plant", ASME Paper 2002-GT-30118, ASME Turbo Expo 2002, Amsterdam, The Netherlands
- [7] **Jericha, H., Göttlich, E., Sanz, W., Heitmeir, F.**, 2003, "Design Optimisation of the Graz Cycle Prototype Plant", ASME Paper 2003-GT-38120, ASME Turbo Expo 2003, Atlanta, USA, Journal of Engineering for Gas Turbines and Power, Vol. 126, Oct. 2004, pp. 733-740
- [8] **Heitmeir, F., Sanz, W., Göttlich, E., Jericha, H.**, 2003, "The Graz Cycle – A Zero Emission Power Plant of Highest Efficiency", XXXV Kraftwerkstechnisches Kolloquium, Dresden, Germany
- [9] **Jericha, H., Sanz, W., Pieringer, P., Göttlich, E., Erroi, P.**, 2004, "Konstruktion der ersten Stufe der HTT-Gasturbine für den Graz Cycle" (in German), VDI Berichte 1857, VDI Tagung "Stationäre Gasturbinen: Fortschritte und Betriebserfahrungen", Leverkusen
- [10] **Sanz, W., Jericha, H., Moser, M., Heitmeir, F.**, 2004, "Thermodynamic and Economic Investigation of an Improved Graz Cycle Power Plant for CO₂ Capture", ASME Paper GT2004-53722, ASME Turbo Expo 2004, Vienna, Austria, Journal of Engineering for Gas Turbines and Power, Vol. 127, Oct. 2005, pp. 765-772
- [11] **Sanz, W., Jericha, H., Luckel, F., Heitmeir, F.**, 2005, "A further step Towards a Graz Cycle Power Plant for CO₂ Capture", ASME Paper GT2005-68456, ASME Turbo Expo 2005, Reno-Tahoe, USA
- [12] **Karl, J., Hein, D.**, 1999, "Effect of Spontaneous Condensation on Condensation Heat Transfer in the Presence of Non Condensable Gases", Proceedings of the

- 5th ASME/JSME Joint Thermal Engineering Conference, San Diego, CA, USA
- [13] **Jericha, H., Sanz, W.**, 2001, "Wärmekraftanlagen mit Verbrennung von Kohlenwasserstoffen mit reinem Sauerstoff zur Stromerzeugung bei Rückhaltung von Kohlendioxyd" (in German), Austrian Patent No. AT 409 162 B
 - [14] **Benvenuti, E.**, 1997, "Design and Test of a New Axial Compressor for the Nuovo Pignone Heavy-Duty Gas Turbine", *Journal of Engineering for Gas Turbines and Power*, Vol. 119, 633 - 639
 - [15] **Hennecke, D. K.**, 1997, "Transsonik-Verdichter-Technologien für stationäre Gasturbinen und Flugtriebwerke" (in German), *Festschrift zum Jubiläum 100 Jahre Turbomaschinen TU-Darmstadt*, published by TU-Darmstadt, Darmstadt, Germany
 - [16] **Perz, E., Gasteiger, G., Steinrück, P., Mader, O., Jericha, H.**, 1988, "Design of a 50 MW Pilot Plant for a High Efficiency Steam Cycle", *ASME Gas Turbine and Aeroengine Congress*, Amsterdam, The Netherlands
 - [17] **Zerlauth, F.**, 1986, "Sulzer Gasturbinen-Konstruktionen (in German)", *Conference on Turbomachinery Developments*, Graz University of Technology
 - [18] **Göttlich, E., Neumayer, F., Pieringer, P., Woisetschläger, J., Sanz, W., Heitmeir, F.**, 2004, "Investigation of Stator-Rotor Interaction in a Transonic Turbine Stage Using Laser-Doppler-Velocimetry and Pneumatic Probes", *ASME Journal of Turbomachinery*, April 2004, 126: 297-305
 - [19] **Göttlich, E., Woisetschläger, J., Pieringer, P., Hampel, B., Heitmeir, F.**, 2005, "Investigation of vortex shedding and wake-wake interaction in a transonic turbine stage using Laser-Velocimetry and Particle-Image-velocimetry", *ASME paper GT2005-68579*, ASME Turbo Expo 2005, Reno-Tahoe, USA
 - [20] **Göttlich E., Lang H., Sanz W., Woisetschläger J.**, 2002, "Experimental Investigation of an Innovative Cooling System (ICS) for High Temperature Transonic Turbine Stages", *ASME paper 2002-GT-30341*, Amsterdam, The Netherlands
 - [21] **Göttlich, E., Innocenti, L., Vacca, A., Sanz, W., Woisetschläger, J., Facchini, B., Jericha, H., Rossi, E.**, 2004, "Measurement and Simulation of a Transonic Innovative Cooling System (ICS) for High-Temperature Transonic Gas Turbine Stages", *ASME Paper GT2004-53712*, ASME Turbo Expo 2004, Vienna
 - [22] **Chorpening, B.T., Casleton, K.H., Richards, G.A.**, 2003, "Stoichiometric Oxy-Fuel Combustion for Power Cycles With CO₂ Sequestration", *Proceedings of the Third Joint Meeting of the U.S. Sections of The Combustion Institute*, Chicago, IL
 - [23] **Inoue, H., Kobayashi, N., Koganezawa, T.**, 2001, "Research and Development of Methane-Oxygen Combustor for Carbon Dioxide Recovery Closed-Cycle Gas Turbine", *CIMAC*, Hamburg, Germany
 - [24] **Göttlicher, G.**, 1999, "Energetik der Kohlendioxidrückhaltung in Kraftwerken" (in German), *Fortschritt-Berichte VDI, Reihe 6, Energietechnik*, Nr. 421. Düsseldorf: VDI Verlag
 - [25] **Gas Turbine World**, 2003, "2003 Handbook for Project Planning, Design and Construction", Pequot Publishing Inc.

Characteristics of Cycle Components for CO₂ Capture

Flavio J. Franco¹, Theo Mina¹, Gordon Woollatt¹, Mike Rost², Olav Bolland³

¹ALSTOM (LE8 6LH,UK), ²Siemens Power Generation (Germany),

³The Norwegian University of Science and Technology (NO-7491, Norway)

Abstract

Within the ENCAP Project – ENhanced CO₂ CAPture - the benchmarking of a number of novel power cycles with CO₂ capture was carried out. Some of these cycles show good efficiencies but the ultimate implementation of any of them in commercial power plants depends upon the feasibility, technical and economic, of their components. In this paper, the methodology used to evaluate the components and some results are described. It had two stages. The first stage was a first evaluation of all components, based on expert opinion, resulting basically in three classes of components, involving: 1) current engineering practices, 2) new engineering practices but not new scientific developments and 3) substantial scientific developments. The second stage, still in progress, is a more elaborate numerical analysis, leading to basic design concepts. One example cycle is discussed in this paper.

1. Introduction

The ENCAP Project – Enhanced CO₂ Capture is a European Union funded research project with more than twenty partners from industry and universities. Its objective is the investigation of technologies for power generation that would meet the target of at least 90% CO₂ capture rate and 50% CO₂ capture cost reduction. ENCAP focuses on pre-combustion and oxy-fuel types of cycles. Benchmarking of a number of novel gas turbine based power cycles with CO₂ capture was carried out in work package WP6.1. These are shown in Fig.1. The first four cycles on the left are natural gas (NG) oxy-fuel cycles, the following ten cycles are natural gas pre-combustion cycles, including different configurations of novel reforming reactors and/or selective membranes, and the last three are coal Integrated Gasification Combined Cycles with Chemical Absorption, with integrated Air Separation Unit and with Oxygen Transport Membrane respectively. For the meaning of other initials, please see Figs. 3 and 4.

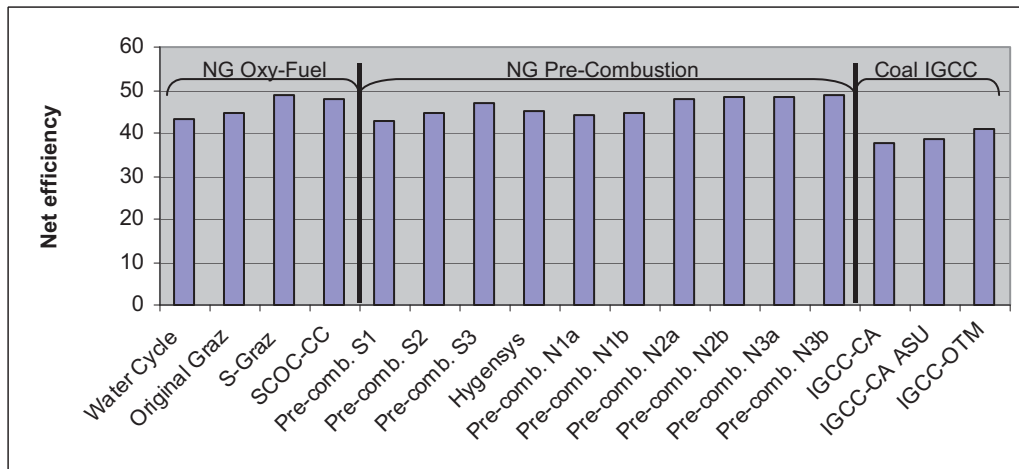


Fig. 1 – Efficiencies of the cycles studied in WP6.1

Work package WP6.2 of ENCAP has the objective of identifying the potential difficulties of practical implementation of these cycles in real world power plants, from the point of view of the equipment manufacturers. The ultimate practical implementation in power plants will depend upon attributes such as capital cost, efficiency, reliability, availability, maintainability and life expectancy. These attributes of the whole electricity generation system will depend on the corresponding attributes of its components: compressors, turbines, combustors, heat exchangers and novel components. The mission is thus to examine the components of those cycles and to evaluate them with respect to those attributes. If it is assumed that each cycle has on average five critical components, the task would involve around one hundred components. As a detailed study of all components would not be practical within a reasonable timescale, a two-stage approach was adopted.

In the first stage, a so-called ‘component book’ was created, containing some basic information for each component:

- Inlet conditions: streams, compositions, mass flows, pressures and temperatures
- Power, polytropic and isentropic efficiencies
- Outlet conditions: streams, compositions, mass flows, pressures and temperatures

Expert opinion was then sought about the critical components, covering materials, gas turbines with or without cooling, compressors, combustors, steam turbines, heat exchangers and special reactors. The components were classified into three levels, technically and economically, as shown in Table 1. In the second stage, more detailed numerical analysis was made of selected components from the most promising cycles studied in WP6.1 - at this point in the project, turbo-machinery components and combustors. It would not be appropriate to report the whole set of data and results produced in the ENCAP project. So, only the summary charts of stage one and one example including the analyses of stages one and two are presented in sections 2 and 3.

Table 1 - Classification of components according to expert opinion

Class	Technical evaluation	Economic evaluation
Green	commercially available or current engineering practice	usual costs of commercially available equipment
Yellow	new engineering practices but not new significant scientific developments	cost of new design or high capital costs due to size, quantity or special materials
Red	considerable scientific developments and new engineering practices	high development costs, high capital cost and/or high operation and maintenance costs

2. The ‘Component Book’

Initially the example of the Semi-Closed Oxy-Fuel Combustion Combined Cycle (SCOC-CC) will be discussed. Its flow diagram is shown in Fig. 2 and its individual evaluation sheet is shown in Fig. 3.

Basically, the main difficulties of this cycle result from the combustion process and from the working fluid in the compressor and in the gas turbine. The compressor and the turbine require a new design because of the working fluid, but it is unlikely that new scientific developments will be necessary. About the combustor, re-circulation of CO₂ is necessary, so that a design exit temperature is achieved and combustor cooling is made with CO₂. Also the starting transient process should be studied in a laboratory

first and then in large scale. Considering the need for re-circulation and the transient regime, where combustion starts with air, moving slowly to oxygen with re-circulation, a new control system should be developed. However, all these developments, though outside the current engineering practices, do not include considerable scientific new developments. Finally, with regard to heat exchangers, low pressures are considered but they are not as low as the pressures of the Water Cycle.

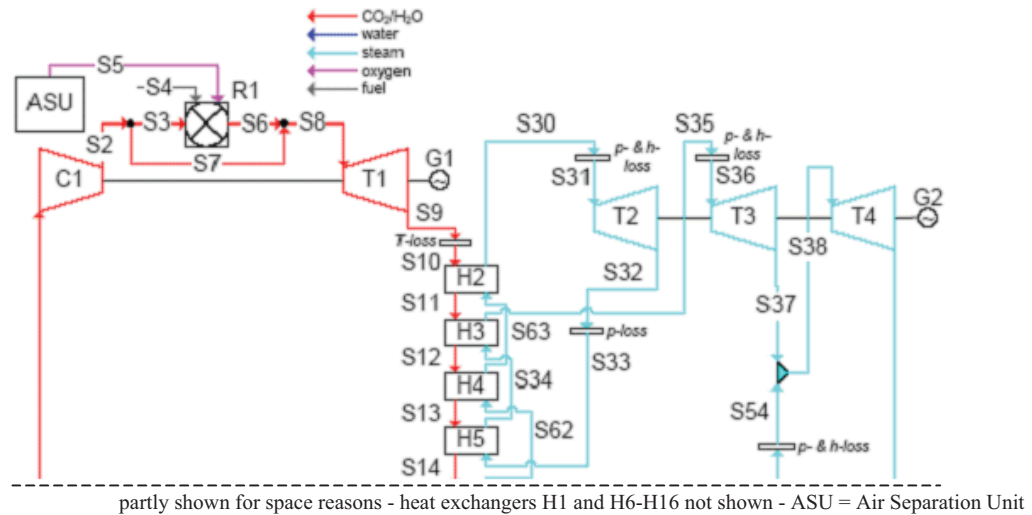


Fig. 2 – The Semi-Closed Oxy-Fuel Combustion Combined Cycle

8 - Semi-closed oxygen combustion combined cycle - SCOC-CC															
Compo nent	Inlet					Outlet					Technical Comments	Economic Comments			
	stream no.	comp.	mass flow (kg/s)	press. [bar]	temp. [°C]	P _{th/mech} [MW]	η _p [%]	η _{is} [%]	stream no.	comp.			mass flow (kg/s)	press. [bar]	temp. [°C]
C1	S1	CO ₂ 88.17% + N ₂ 4.29% + Ar 5.35% + 2.18% steam	536.14	1.01	19.00	193.9	91.5	88.37	S2	CO ₂ 88.17% + N ₂ 4.29% + Ar 5.35%, 2.18% H ₂ O	536.14	40.53	393.74	The compressor is similar to a gas turbine compressor, but the fluid is a mixture of CO ₂ and steam for which the molecular weight is higher than for air, thus a new design is required.	New design required
T1	S8	CO ₂ 78.71% + Steam 12.68%	608.2	39.31	1231.5	468.96	86.37	89.75	S9	CO ₂ 78.71% + Steam 12.68%	608.2	1.06	629.11	The fluid is a mixture of CO ₂ and steam for which the molecular weight is higher than for air, thus a new design is required. To be studied as a gas turbine. Potential steam/CO ₂ mixture effects on materials would need to be investigated (acidic mixture - aggressive environment for materials)	New design required
T2	S31	Steam	82.83	116.25	556.24	29.81		90.00	S32	Steam	82.83	32.05	362.71	Standard steam turbine	
T3	S36	Steam	82.83	28.95	559.14	46.39		92.00	S37	Steam	82.83	3.96	282.39	Standard steam turbine	
T4	S38	Steam	98.90	3.96	287.54	65.37		88.00	S39	Steam	98.90	0.05	32.15	Standard steam turbine	
R1		88.17% CO ₂ , 4.29% N ₂ , 5.35% Ar, 2.18% H ₂ O	411.23	40.53	393.74	696.02			S6	CO ₂ 76%, H ₂ O 15%	483.29	39.31	1425.00	The O ₂ needs to be mixed with part of the CO ₂ to give the design combustor exit temperature. The CO ₂ can be used for combustor cooling.	New design required
	S3														
	S4	Fuel	14.67	70.00	10										
	S5	95% O ₂ , 2% N ₂ , 3% Ar	57.39	40.53	15										
H1	S23	13% H ₂ O, 78% CO ₂	608.2	1.02	86.7	110.1			S24	water	29.5	1.01	19.0	The condenser pressure is 1 bar (in the Water cycle, the pressure is 0.07 bar). Corrosion is a challenge where condensation takes place. Condensation with inert gases present must be taken into account.	
					S25				2% H ₂ O, 98% CO ₂	578.7	1.01	19.0			
	S28	water	2632.6	2.50	15						S29	water	2632.6		
H2-H16														Standard HRSG technology, but with somewhat different fluid composition compared to air-based system	

Fig. 3 – Evaluation sheet of the Semi-Closed Oxy-Fuel Combustion Combined Cycle

General type of component	Oxy-fuel Water Cycle		Oxy-fuel Original Graz Cycle		Oxy-fuel Steam Graz Cycle		Oxy-fuel SCOC-GT		Oxy-fuel SCOC-CC		Pre-Combustion Siemens 1	
	4		5		6		7		8		9	
	Tech	Eco	Tech	Eco	Tech	Eco	Tech	Eco	Tech	Eco	Tech	Eco
Compressors			Very high volume flow rate (860 m ³ /s). Potential corrosion problems. Unknown corrosion effects of CO ₂ and steam in the cycle concentrations.	Two units in parallel required. Complex design.	CO ₂ + Steam. Potential corrosion problems.	Cost of materials development.	Mixture of CO ₂ and Steam. Potential corrosion.	New design due to properties of CO ₂ .	Working fluid is a mixture of CO ₂ and Steam.	New design due to working fluid.	Large fractions of CO ₂ and steam. Potential effects on materials.	New design due to working fluid.
Turbines	Very high pressure ratio = 158. Potential sealing problems. Steam cooling. Turbine inlet temperature is 1254 °C after mixing with coolant. Working fluid is 87% steam + 12% CO ₂ .	Completely new design due to working fluid and pressure ratio.	Steam cooling. CO ₂ + Steam. Potential corrosion problems with inlet temperature 1247 °C.	High power output (470 MW). High development costs.	Slow pressure uncooled turbine for 10% CO ₂ and 89% steam. Exit gas below dew point temperature (32.54 °C). Corrosion potential problems.	Completely new design due to working fluid.	Mixture of CO ₂ and Steam. Potential corrosion.	New design due to working fluid.	Mixture of CO ₂ + Steam. Corrosion to be investigated.	New design due to working fluid.		
Combustors and Other Reactors	High pressure (92 bar). Extensive development required. Desired temperature may be achieved by mixing steam to O ₂ .	High development cost.	Need to cool combustor with water & ex. gas.	Some cooling development cost.	Steam to be added for temperature control.	Cost of development of cooling system.	O ₂ to be mixed with CO ₂ for combustor temperature.	New design for CO ₂ circulation.	O ₂ to be mixed with CO ₂ for combustor temperature.	New design due to circulation.	Syngas splitting with H ₂ permeable membrane.	High development cost and unknown capital cost. Unknown reliability and effectiveness.
Heat Exchangers	Very low pressure. Low heat transfer coefficient.	Large size equipment: high capital cost.			Low pressure condenser for CO ₂ & steam. Corrosion in condensation section.	Very low heat transfer coefficient. Exit pressure very low. Large size and capital cost.	Corrosion may be a problem in condensation section.		Corrosion may be a problem.		High temperature / multiple media.	Development costs and capital cost.

SCOC=Semi-Closed Oxy-fuel Combustion, GT=Gas Turbine, CC=Combined Cycle

Fig. 4.a - Summary of evaluation of components of all cycles studied

General type of component	Pre-Combustion Siemens 2		Pre-Combustion Siemens 3		Pre-Combustion IFP Hygensys		Pre-Combustion NTNU 1a		Pre-Combustion NTNU 1b		Pre-Combustion NTNU 2a	
	10		11		12		13		14		15	
	Tech	Eco	Tech	Eco	Tech	Eco	Tech	Eco	Tech	Eco	Tech	Eco
Compressors	Three-stage compressor with intercooling.	Capital cost.	Three-stage compressor with intercooling.	Capital cost.			74% H ₂ and 26% steam working fluid: possible material embrittlement problems.	Cost in materials developments.	74% H ₂ and 26% steam working fluid: possible material embrittlement problems.	Cost in materials developments.		
Turbines					Air with large fraction of steam. Cooling to be considered.	Development costs. High capital cost?	Working fluid from combustion of H ₂ : 22% water 1229 °C. High cooling fraction: 31%.	Moderately new turbine design due to different working composition and operation conditions.	Working fluid from combustion of H ₂ : 22% water 1229 °C. High cooling fraction: 31%.	Moderately new turbine design due to different working composition and operation conditions.	Working fluid from combustion of H ₂ : 22% water 1229 °C. High cooling fraction: 31%.	Moderately new turbine design due to different working composition and operation conditions.
Combustors and Other Reactors	Syngas splitting with H ₂ permeable membrane	Development costs, reliability, effectiveness.	Syngas splitting with H ₂ permeable membrane	Development costs, reliability, effectiveness.	High flame speed for pre-mixed system, leading to 2480 °C. Fuel dilution with steam and combustor cooling with steam needed.	Development costs.	a) Membrane reactor for autothermal reforming. b) Membrane for water gas shift with palladium-silver. c) Membrane combustor to convert CH ₄ , CO and H ₂ from WGS membrane to CO ₂ and H ₂ O.	No similar reactors available today. Very high development costs and probably high capital costs. Effectiveness and reliability?	a) Membrane reactor for autothermal reforming. b) Membrane for water gas shift with palladium-silver. c) Membrane combustor to convert CH ₄ , CO and H ₂ from WGS membrane to CO ₂ and H ₂ O.	No similar reactors available today. Very high development costs and probably high capital costs. Effectiveness and reliability?	a) Membrane reactor for autothermal reforming. b) Membrane for water gas shift with palladium-silver. c) Membrane combustor to convert CH ₄ , CO and H ₂ from WGS membrane to CO ₂ and H ₂ O. Very high temperatures.	No similar reactors available today. Very high development costs and probably high capital costs. Effectiveness and reliability?
Heat Exchangers	High temperature / multiple media.	Development costs and capital cost.	High temperature / multiple media.	Development costs and capital cost.			Large number of exchangers. Possible material problems due to composition of syngas (hydrogen) or to CO ₂ & steam and high temperature.	Materials development costs and extensive test work.	Large number of exchangers. Possible material problems due to composition of syngas (hydrogen) or to CO ₂ & steam and high temperature.	Materials development costs and extensive test work.	Large number of exchangers. Possible material problems due to composition of syngas (hydrogen) or to CO ₂ & steam and high temperature.	Materials development costs and extensive test work.

NTNU = Norwegian University of Science and Technology, IFP = Institut Francais du Petrole

Fig. 4.b - Summary of evaluation of components of all cycles studied

General type of component	Pre-Combustion NTNU 2b		Pre-Combustion NTNU 3a		Pre-Combustion NTNU 3b		IGCC-CA UPB		IGCC-CAASU UPB		IGCC-OTM UPB	
	16		17		18		21		22		23	
	Tech	Eco	Tech	Eco	Tech	Eco	Tech	Eco	Tech	Eco	Tech	Eco
Compressors										High mass flow with 15% extraction. New design needed.		
Turbines	Working fluid from combustion of H ₂ : 22% water 1229 °C. High cooling fraction: 31%.	Moderately new turbine design due to different working composition and operation conditions.	Working fluid from combustion of H ₂ : 22% water 1229 °C. High cooling fraction: 31%.	Moderately new turbine design due to different working composition and operation conditions.	Working fluid from combustion of H ₂ : 22% water 1229 °C. High cooling fraction: 31%.	Moderately new turbine design due to different working composition and operation conditions.	Three steam extractions in steam turbine.	Complex design.	Three steam extractions in steam turbine.	Complex design.	Three steam extractions in steam turbine.	
Combustors and Other Reactors	a) Membrane reactor for autothermal reforming Oxygen transport membrane. b) Membrane for water gas shift with palladium-silver.	No similar reactors available today. Very high development costs and probably high capital costs. Effectiveness and reliability?	a) Membrane reactor for autothermal reforming Oxygen transport membrane. b) Low temperature with CO ₂ polymeric membrane for water gas shift.	No similar reactors available today. Very high development costs and probably high capital costs. Effectiveness and reliability?	a) Membrane reactor for autothermal reforming Oxygen transport membrane. b) Low temperature with CO ₂ polymeric membrane for water gas shift.	No similar reactors available today. Very high development costs and probably high capital costs. Effectiveness and reliability?	Technology not tested for the fuel composition.		Technology not tested for the fuel composition.		High temperature Oxygen Transport Membrane.	High development costs. Reliability?
Heat Exchangers	Large number of exchangers. Possible material problems due to composition of syngas (hydrogen) or to CO ₂ & steam and high temperature.	Materials development costs and extensive test work.	Large number of exchangers. Possible material problems due to composition of syngas (hydrogen) or to CO ₂ & steam and high temperature.	Materials development costs and extensive test work.	Large number of exchangers. Possible material problems due to composition of syngas (hydrogen) or to CO ₂ & steam and high temperature.	Materials development costs and extensive test work.			Three heat exchangers: high capital cost.		Due to the high temperature of the OTM.	High operating temperature of the OTM requires high cost heat exchanger.

UPB = University of Paderborn, IGCC=Integrated Gasification Combined Cycle, CA=Chemical Absorption, ASU=Air Separation Unit, OTM=Oxygen Transport Membrane

Fig. 4.c – Summary of evaluation of components of all cycles studied

These necessary technical developments are reflected in the costs. The concern about costs is moderate as new designs are necessary for compressor, turbine and combustor, but no scientific investigations seem to be required. As a consequence of these findings, no ‘red’ components are seen in the evaluation sheet of this cycle (Fig. 3).

The summary evaluation sheets shown in Fig. 4, obtained from all detailed individual sheets made for all cycles, are self-explanatory.

3. The Semi-Closed Oxy-Fuel Combustion Combined Cycle (SCOC-CC)

Considering the good position of the SCOC-CC cycle in the overall comparison made within WP6.1 and the absence of great challenges in the first-stage evaluation of components, a more detailed numerical analysis – second stage analysis - was made of some of these components. Highlights are given here about the compressor and the combustor.

Compressor

The gas in the SCOC-CC compressor is largely carbon dioxide. Compared to air, the gas has significantly lower values of both the gas constant and the ratio of specific heats. It can be shown that to achieve dynamic similarity with an air compressor, the ‘CO₂’ compressor should run with approximately a 25% reduction in the blade tip speed and a 15% increase in the mass flow. In this cycle the rotational speed is 3000 rpm, i.e. the same value as that of existing 50 Hz power generation gas turbine compressors, while the mass flow is lower than that of typical heavy-duty compressors. Hence the diameter of the SCOC-CC compressor has to be reduced as

compared to a compressor running with air in order to reduce the blade speed and the associated Mach numbers.

Further the pressure ratio of 40.13 is higher than that of current power generation gas turbines. At this high exit pressure the density of the gas is significantly higher than air. Hence in order to achieve a reasonable hub/tip ratio of the exit stage (to avoid large clearance losses) either the flow coefficient (axial velocity/blade speed) or the mean radius has to be reduced. If it is assumed that flow coefficients should not be reduced below a certain level, then the mean radius at the exit must be lower than in a conventional gas turbine compressor. The lower radius means that for a given limiting level of work coefficient (stage enthalpy rise over blade speed squared) more stages are required for a compressor using CO₂.

As a first step in defining the compressor a parametric study was carried out on the first stage in isolation. An ALSTOM in-house code was run over a range of inlet guide vane exit angles, mean radii, flow coefficients and work coefficients. Having defined the first stage, candidate compressors were investigated. It was found that around 24 stages were required to achieve a pressure ratio of 40 in order to stay within conservative limits of work coefficient. A parametric study was then carried out over a range of mean radii, flow coefficients and work coefficients for the last stage. Distributions of the above were assumed for each stage through the compressor. The code was then run to the required pressure ratio adjusting the level of the stage work coefficients. After several calculations involving considerations of losses associated to blade tip clearances and of surge margin, a configuration was selected with 24 stages and the following last stage mean line parameters: radius = 0.64 m, flow coefficient = 0.45 and work coefficient = 0.25. A schematic view of the blade path of the final conceptual design is shown in Fig. 5 and the relevant parameters are given in table 2.

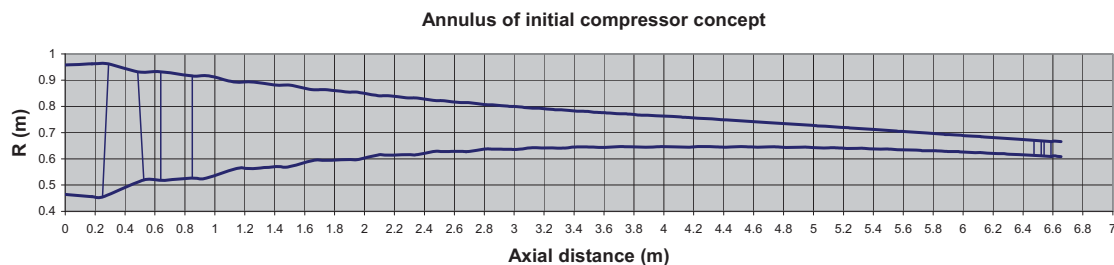


Fig. 5 – Compressor profile

Table 2 - Compressor calculated parameters

Number of stages	24	Rotor 1 hub Mach number	.841
Rotor 1 hub/tip ratio	.473	Stator 1 hub Mach number	.819
Rotor 24 hub/tip ratio	.915	Exit Mach number	.221
Rotor 1 tip Mach number	1.17	Length (m)	6.654

The working fluid of the SCOC-CC compressor necessitates the design of a radically different compressor from those currently in use in 50Hz power generation gas turbines and requires more stages at lower exit radius. The longer and slender rotor may result in rotor dynamics problems. Ways of reducing the overall length should be investigated. If the parameters are not significantly modified, high efficiencies should be attainable in line with the values currently assumed in the cycle calculations.

Combustor

The input and output streams to the combustor (R1) with their compositions are given in Figure 6. The numerical investigations began from general concepts acquired in previous experience [1] and some specific design concepts were then defined for the combustor of the SCOC-CC cycle, briefly explained below. In this cycle, natural gas (S4) is burnt with an oxygen-rich stream (S5) in the combustion chamber (R1). The temperature is controlled by a recycled exhaust stream (S3). The combustor exit stream (S6) is a mixture of CO₂ and steam.

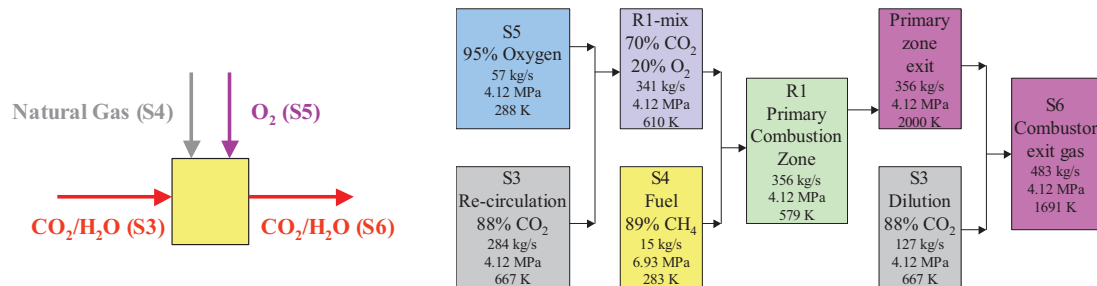


Fig. 6 – Input and output streams to combustor

Fig. 7 – Proposed flow split for the combustor

The O₂ (S5) and part (approximately 69%) of the re-circulating exhaust gas (S3) (after it has been used for primary zone cooling) are mixed and used to give the design combustor primary zone exit temperature of approximately 2000K. The design combustor exit temperature (1691 K) is achieved by diluting the combustor primary zone exhaust gases with the remainder (approximately 31%) of the re-circulating exhaust gas (S3). The proposed flow split for this combustor, given in Figure 7, is based on one-dimensional combustor calculations.

4. Conclusions


The evaluation of all novel cycles summarized in the sheets reproduced in Fig. 4 suggests that the following cycles incorporating gas turbines would require least effort to turn them into real power plants:

- Semi-Closed Oxy-Fuel Combustion – Gas Turbine (simple cycle)
- Semi-Closed Oxy-Fuel Combustion – Combined Cycle
- Integrated Gasification Combined Cycle – Chemical Absorption
- Integrated Gasification Combined Cycle – Chemical Absorption with Air Separation Unit

This does not mean that they are the best solutions for the problem of reducing CO₂ emissions. Within other sub-projects of ENCAP other solutions are being studied for coal and natural gas. In the remainder of the project, some refinement is to be made of the evaluation and classification of components shown here and deeper analysis will be made of further components of the cycles that are in the scope of work package WP6.2.


References

1. Mina, T. and Chen, J. X., 2005, 'Combustion system design for GAS-ZEP cycle', Fuels for the Future, Institute of Physics, Cardiff, April 14.



TURBO EXPO
Gas Turbine Technical Congress & Exposition
Powered by the International Gas Turbine Institute

ASME Turbo Expo 2007
May 14-17, 2007
Palais des Congrès • Montreal, Canada



TU Graz
Graz University of Technology

Institute for
Thermal Turbomachinery
and Machine Dynamics


Graz University of Technology
Erzherzog-Johann-University

Qualitative and Quantitative Comparison of Two Promising **Oxy-Fuel** Power Cycles for CO₂ Capture


Presentation at the
ASME Turbo Expo 2007
Montreal, Canada, May 14 - 17, 2007

Wolfgang Sanz, Herbert Jericha, Bernhard Bauer and Emil Göttlich
Institute for Thermal Turbomachinery and Machine Dynamics
Graz University of Technology
Austria


Background - I



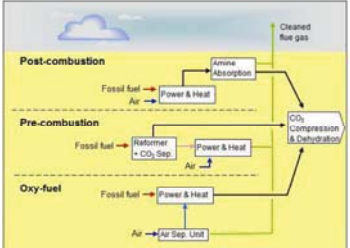
- Worldwide ever rising emissions of greenhouse gases to atmosphere -> global warming and environmental change
- Kyoto Protocol** demands the reduction of greenhouse gases, mainly CO₂
- In EU**: strong pressure on utilities and companies to reduce CO₂ emissions
- Carbon capture and storage (**CCS**) as short and mid term solution



Background - II (CCS Technologies)




- Post-combustion**: CO₂-Capture from exhaust gas (chemical absorption, membranes, ...)
- Pre-combustion**: Decarbonization of fossil fuel to produce pure hydrogen for power cycle (e.g. steam reforming of methane, ...)
- Oxy-fuel power generation**: Internal combustion with pure oxygen and CO₂/H₂O as working fluid enabling CO₂ separation by condensation

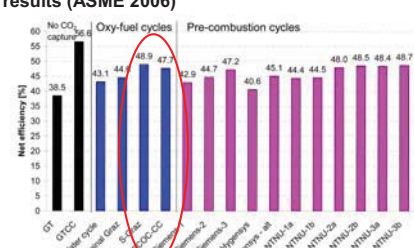


Which technology has the best chances to dominate future power generation ?

Background - III




- EU project **ENCAP** (Enhanced CO₂ Capture): benchmarking of a pre-combustion and oxy-fuel cycles
- Among oxy-fuel cycles:
highest efficiencies for **S-Graz Cycle** and **Semi-Closed Oxy-Fuel Combustion Combined Cycle (SCOC-CC)**
- ENCAP efficiency for S-Graz Cycle is by 3.6 %-points lower than own results (ASME 2006)




Cycle	Net efficiency (%)
GT	38.5
GTCC	43.1
Water cycle	44.0
Oxy-fuel cycles	44.0
S-Graz	48.9
SCOC-CC	47.3
Pre-combustion cycles	42.9
Semirank-2	44.7
Hydrogen	47.2
Hydrogen-air	40.6
HTU-1a	45.1
HTU-1b	44.4
HTU-2a	44.6
HTU-2b	48.0
HTU-3a	48.5
HTU-3b	48.4
HTU-3c	48.7

Background - III



- EU project **ENCAP** (Enhanced CO₂ Capture): benchmarking of a pre-combustion and oxy-fuel cycles
- Among oxy-fuel cycles:
highest efficiencies for **S-Graz Cycle** and **Semi-Closed Oxy-Fuel Combustion Combined Cycle (SCOC-CC)**
- ENCAP efficiency for S-Graz Cycle is by 3.6 %-points lower than own results (ASME 2006)
- Feasibility study of key components:
 - SCOC-CC plant was evaluated technically favorable
 - 3 components of S-Graz Cycle were ranked as critical.

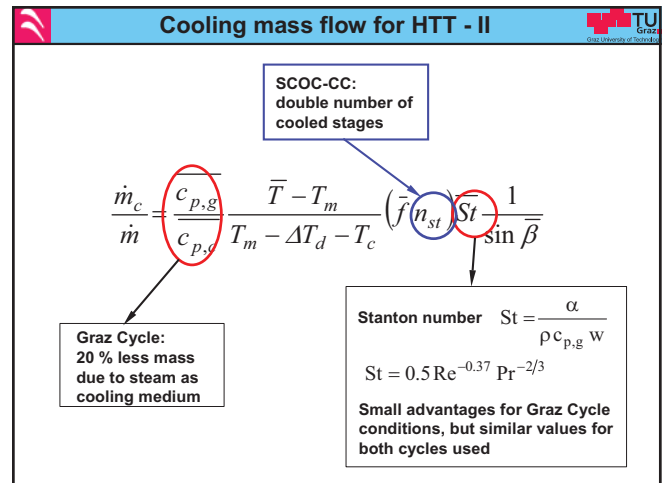
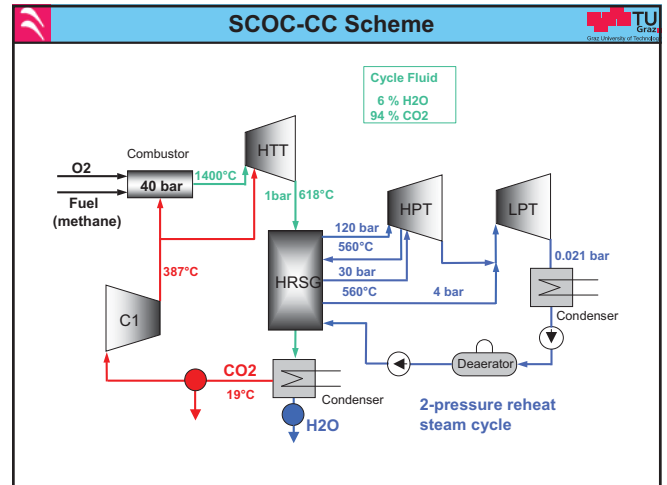
Objective

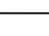


- Differences in efficiency to ENCAP and
- New scheme of the Graz Cycle (ASME 2006) not considered in the study


Thus comparison between both plants is repeated in this work

- Thermodynamic comparison
- Layout and discussion of the main components for a 400 MW power plant.



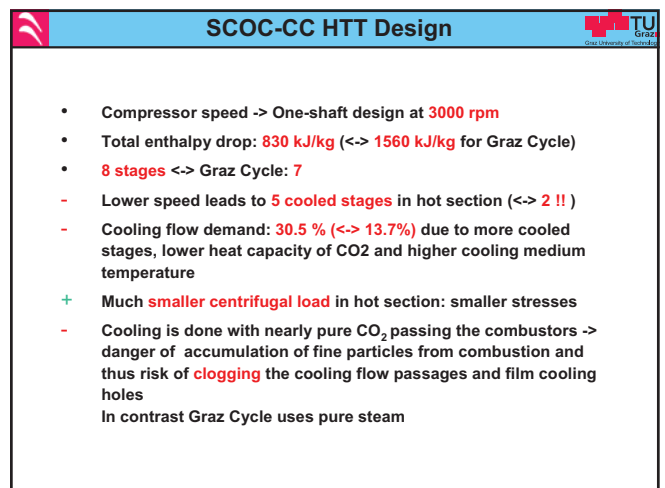
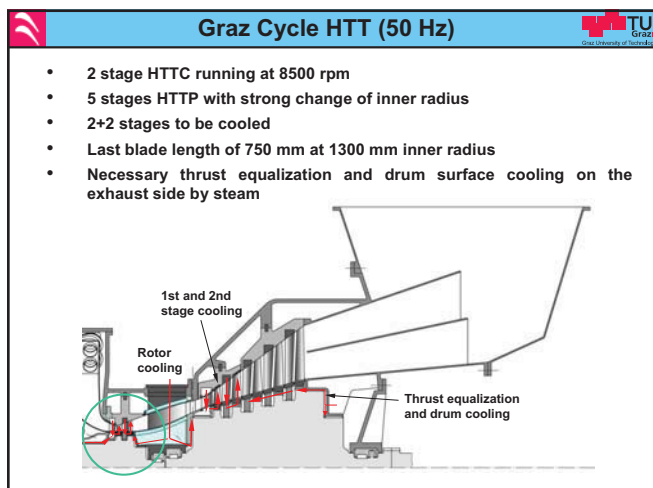
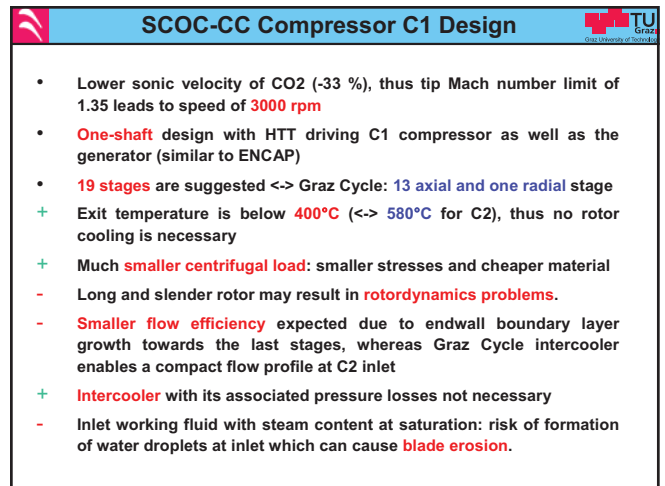
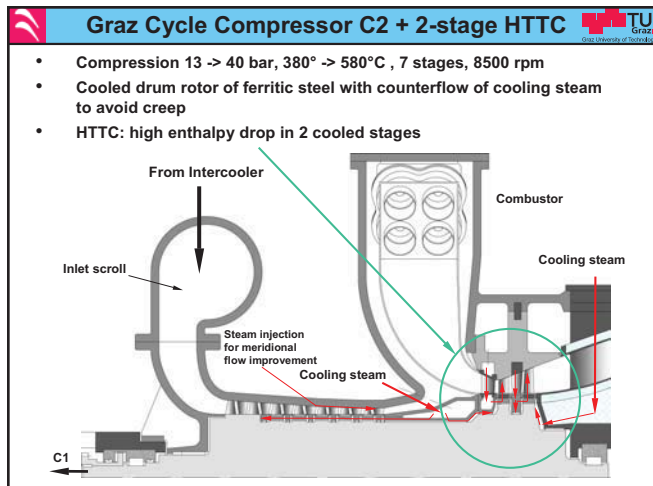
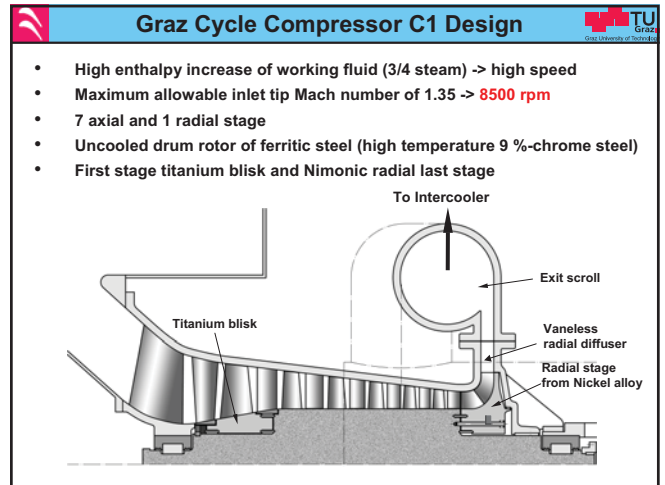
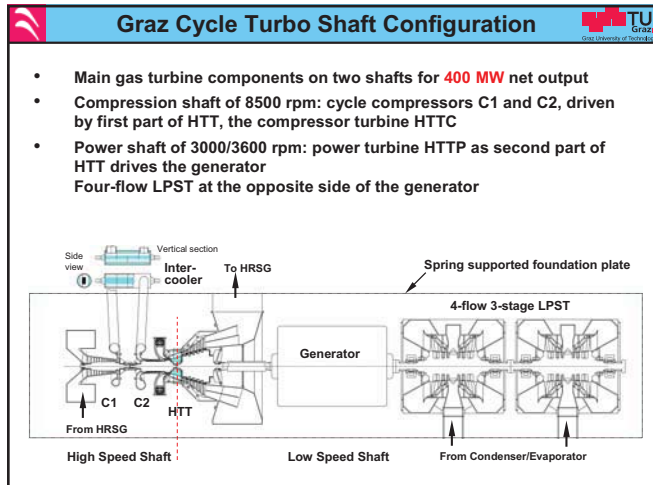


Differences to ENCAP



	Graz Cycle	SCOC-CC
Net efficiency [%]	53.1	49.8
Net efficiency ENCAP [%]	48.9	47.7

- Higher inlet temperature of oxygen and fuel of 150°C
- Oxygen is provided with 99 % purity at an energy requirement of 0.25 kWh/kg compared to 95 % purity at 0.30 kWh/kg
- Probably different assumptions of component efficiencies and losses
- ENCAP: difference of 1.2 %-points
this study: difference of 3.3 %-points (1.8 %-points due to higher cooling flow demand of the SCOC-CC HTT)



Economic Analysis - I			
Investment costs			
Component	Scale parameter		Specific costs
Reference Plant			
Investment costs	Electric power	\$/kW _{el}	414
Oxyfuel Plant			
Investment costs	Electric power	\$/kW _{el}	414
Air separation unit	O ₂ mass flow	\$/kg O ₂ /s	1 500 000
Other costs (Piping, CO ₂ -Recirc.)	CO ₂ mass flow	\$/kg CO ₂ /s	100 000
CO ₂ -Compression system	CO ₂ mass flow	\$/kg CO ₂ /s	450 000

- yearly operating hours: 8500 hrs/yr
- capital charge rate: 12%/yr
- natural gas is supplied at 1.3 ¢/kWh_{th}

Comparison of Component Size			
400 MW net power output			
	Convent. CC plant	Graz Cycle	SCOC-CC
turbine of "gas turbine"/ HTT	667 MW	623 MW	557 MW
compressor of "gas turbine"/C1+C2+C3+C4	400 MW	241 MW	235 MW
steam turbines/ HPT+LSPT	133 MW	120 MW	190 MW
HRSG	380 MW	360 MW	461 MW
Generator	400 MW	487 MW	495 MW

Conventional plant vs. Graz Cycle/SCOC-CC:

- total turbine power of same size
- compressor power smaller
- generator power higher

Economical Analysis - II			
COE ... Cost of Electricity		Reference plant	GC plant
			SCOC-CC plant
	Plant capital costs [\$/kW _{el}]	414	414
	Addit. capital costs [\$/kW _{el}]	-	288
	CO ₂ emitted [kg/kWh _{el}]	0.342	0.0
	Net plant efficiency [%]	58.0	53.1
	COE f. plant amort. [¢/kWh _{el}]	0.58	0.99
	COE due to fuel [¢/kWh _{el}]	2.24	2.45
	COE due to O&M [¢/kWh _{el}]	0.7	0.8
	Total COE [¢/kWh _{el}]	3.52	4.24
	Comparison		
	Differential COE [¢/kWh _{el}]		0.72
	Mitigation costs [\$/ton CO ₂]		21.0

Conclusions	
<ul style="list-style-type: none"> ENCAP study of oxy-fuel power cycles: two very promising variants Graz Cycle and SCOC-CC Graz Cycle: high efficiency, SCOC-CC: relatively low complexity This work: thermodynamic and design study of both cycles SCOC-CC: lower efficiency because of very high HTT cooling demand due to less favorable properties of CO₂. Both cycles need new designs for HTT and compressors SCOC-CC: low sonic velocity of CO₂ leads to one shaft of 3000 rpm -> more stages for compressor and HTT Lower operating temperature of SCOC-CC compressor All turbomachinery of both cycles is regarded as feasible and of similar complexity. Mitigation costs vary between 20 - 30 \$/ton CO₂ depending on additional investment costs (ASU), 5 \$/ton lower for Graz Cycle So Graz Cycle is a very efficient and feasible solution for a future CCS scheme 	

H. J. Yang

D. W. Kang

J. H. Ahn

Graduate School,
Inha University,
Incheon, 402-751 Korea

T. S. Kim

Department of Mechanical Engineering,
Inha University,
Incheon, 402-751 Korea
e-mail: kts@inha.ac.kr

Evaluation of Design Performance of the Semi-Closed Oxy-Fuel Combustion Combined Cycle

This study aims to present various design aspects and realizable performance of the natural gas fired semi-closed oxy-fuel combustion combined cycle (SCOC-CC). The design parameters of the cycle are set up on the basis of the component technologies of today's state-of-the-art gas turbines with a turbine inlet temperature between 1400°C and 1600°C. The most important part of the cycle analysis is the turbine cooling, which considerably affects the cycle performance. A thermodynamic cooling model is introduced in order to predict the reasonable amount of turbine coolant needed to maintain the turbine blade temperature of the SCOC-CC at the levels of those of conventional gas turbines. The optimal pressure ratio ranges of the SCOC-CC for two different turbine inlet temperature levels are researched. The performance penalty due to the CO₂ capture is examined. The influences of the purity of the oxygen provided by the air separation unit on the cycle performance are also investigated. A comparison with the conventional combined cycle, adopting a post-combustion CO₂ capture, is carried out, taking into account the relationship between the performance and the CO₂ capture rate. [DOI: 10.1115/1.4007322]

Introduction

Diverse research on CO₂ capture technology in power plants has been initiated in recent years and several distinct power plant configurations have been suggested. Oxy-fuel combustion is one of the leading technologies competing with pre- and postcombustion capture techniques. The major advantage of the power plant systems that are adopting oxy-fuel combustion is that CO₂ in the flue gas can be separated by using a simple mechanical scheme instead of complex chemical processes because its combustion gas consists mainly of CO₂ and H₂O. On the contrary, oxy-fuel combustion systems require an oxygen generation and supply subsystem. A cryogenic air separation unit (ASU) is usually adopted for the oxygen supply. Natural gas fired oxy-combustion systems are usually designed as a closed cycle with a recirculation fluid as a diluting medium in order to maintain the flame temperature in the combustor at a target value. The recirculation fluid is none other than one of the combustion gas components: H₂O or CO₂. Until now, the representative CO₂ recirculating cycle proposed has been the semiclosed oxy-fuel combustion combined cycle (SCOC-CC) [1]. The liquid phase containing much more H₂O than CO₂ is extracted at the condenser. The CO₂-rich gas phase is recirculated and redundant CO₂ is extracted for capture from the recirculating fluid.

A comparison between several recently proposed oxy-fuel combustion cycles such as the GRAZ cycle [2], the CES cycle [3], and the SCOC-CC is interesting. Recently, comparative evaluations of the performance expectations between these three cycles were reported [4,5]. However, a direct performance comparison is difficult to conduct because cycle configurations are very different between these three cycles and the major components require quite different design technologies due to a difference in the working fluids and conditions. A generally accepted relative merit of the SCOC-CC is as follows. The layout of the power generation

part of the SCOC-CC is the same as the conventional combined cycle (CC). The major exceptions are that the combustor is an oxy-fuel burner with a recirculating flow and the working fluid properties are different. Thus, the component design modifications from existing CC systems are expected to be much fewer in comparison to in other oxy-fuel cycles. This is a very promising advantage of the SCOC-CC. It was reported that the SCOC-CC is favored, considering the diverse technical and economic aspects [1].

The studies on CO₂-rich gas as a working fluid in gas turbines and combined cycles have become relatively active during the past decade. Since specific development plans do not seem to have been initiated yet, most of the related studies have presented the fundamental performance analyses and basic component design features. Research topics include the basic design characteristics of gas turbines and combined cycles using CO₂-rich gas as a working fluid [6,7], comparative analyses focused on performance studies [4,8,9], and considerations on using existing gas turbines for the CO₂-rich working fluid environment [10]. Besides, studies on component modeling and designs such as turbine cooling modeling [11,12] and conceptual designs of the compressor and turbine [13] have been performed.

Even though some performance forecasts and component design characteristics of the SCOC-CC have been reported, as previously described, numerous tasks still remain in order to realize a working system. In particular, the cycle performance analysis, which is the first step in developing a power plant system, should include as many realistic factors as possible and provide a systematic view of the design features. In this study, a parametric performance analysis of the SCOC-CC has been conducted. The component design parameters of two gas turbines, which are commercially available or achievable in the near future, were adopted as references. To take into account the change in working the fluid properties, a reasonable allocation of turbine blade coolant flows was tried. In this paper, the selection of the optimal design conditions, considering turbine cooling, is discussed and the influences of secondary design parameters such as the oxygen purity provided by the air separation unit are examined. Then, the SCOC-CC performance is compared with

Contributed by the International Gas Turbine Institute (IGTI) of ASME for publication in the JOURNAL OF ENGINEERING FOR GAS TURBINES AND POWER. Manuscript received June 18, 2012; final manuscript received June 29, 2012; published online September 28, 2012. Editor: Dilip R. Ballal.

that of the conventional combined cycle adopting a postcombustion CO_2 capture from the perspective of the relationship between the performance and the capture rate.

Cycle Configuration and Modeling

Configuration. The entire layout of the SCOC-CC modeled in this study is shown in Fig. 1. The power block consists of a gas turbine, a heat recovery steam generator (HRSG), and a steam turbine. It is very close to the conventional combined cycle, except that the major part of the working fluid circulates inside a closed loop, consisting of a semi-closed cycle. The combustor is an oxy-fuel combustor wherein highly pure oxygen is supplied. Part of the HRSG exhaust gas, which is the net mass added to the combustor from outside (oxygen rich flow from the ASU and fuel), is extracted from the cycle.

The parameters of two types of high-performance gas turbines were assumed: the 1400°C and 1600°C classes. The component models, including turbine cooling, were modeled by referring to those of practical gas turbines, as will be explained in the next section. A triple pressure HRSG and steam turbine system with reheat was adopted. A cryogenic ASU was used to separate oxygen from the ambient air because it is the most suitable separation scheme, considering technical readiness. The ASU was modeled after the literature and delivered oxygen at a high pressure (27 bar), which was sufficiently high to be injected into the combustor if the pressure of the combustor inlet mainstream flow is lower than this pressure. If the pressure ratio of the gas turbine is higher than the ASU exit oxygen pressure, the oxygen was further compressed using an auxiliary compressor. The purity of the oxygen supplied to the combustor affects both the purity of the captured CO_2 and the power consumption of the CO_2 separation unit. Most of the oxy-fuel combustion studies have assumed over 90% purity of the ASU exit oxygen [4,14]. A purity that is too high (over 95%) is not recommendable because the specific power consumption (power per unit oxygen generation) excessively increases [14]. Therefore, a 95% oxygen purity was assumed in this study as a primary case, and then a 90% case was also considered in order to examine the effect of oxygen purity on the

performance of the entire system. All of the compositions cited in this study are mole fractions.

Natural gas is burned with the oxygen-rich stream at the combustor and the CO_2 -rich combustion gas enters the turbine. The working fluid properties are the key difference, in comparison to the conventional combined cycle in which the turbine inlet flow is nitrogen-rich. At the end of the HRSG, a condenser is installed, where the working fluid is cooled down to a sufficiently low temperature to achieve condensation of the water vapor. Due to a considerably larger difference in the condensing temperatures between the CO_2 and H_2O , the liquid phase at the end of the condenser is H_2O -rich and the gas phase is CO_2 -rich. The condensate is simply removed, and the gas phase is recirculated, thereby forming a semi-closed cycle. The condenser exit (i.e., the compressor inlet) temperature was set at 18°C , which is achievable through cooling by ambient air or water. A relatively small amount of the recirculating flow is extracted for the CO_2 capture. The recirculating flow mainly consists of CO_2 but also contains a small portion of H_2O .

The CO_2 capture mechanism of the SCOC-CC is quite different from those of the other capture schemes, such as the chemical absorption process of the postcombustion capture. Since the gaseous phase after the condenser is sufficiently CO_2 -rich, some of it is simply extracted and is sent to the carbon separation unit (CSU), which pressurizes the gas and simultaneously purifies the CO_2 further by removing the water content. Actually, the CO_2 purity depends on the purity of the ASU exit oxygen. The extraction pressure is set at the ambient pressure. A three-stage compression with intercooling was adopted, as shown in Fig. 1.

Modeling. The gas turbine part (from the compressor inlet to the turbine exit, including the combustor) was simulated using GateCycle [15]. All of the other components such as the steam turbine cycle, including the HRSG and the condenser, the ASU, and the carbon separation unit (CSU) were simulated using ASPEN HYSYS [16], which was more suitable for modeling the calculation of general processes including material separation processes. Mass flows and thermodynamic properties at all of the flow streams between the gas turbine and the remaining parts (separately simulated by GateCycle and ASPEN HYSYS, respectively) were

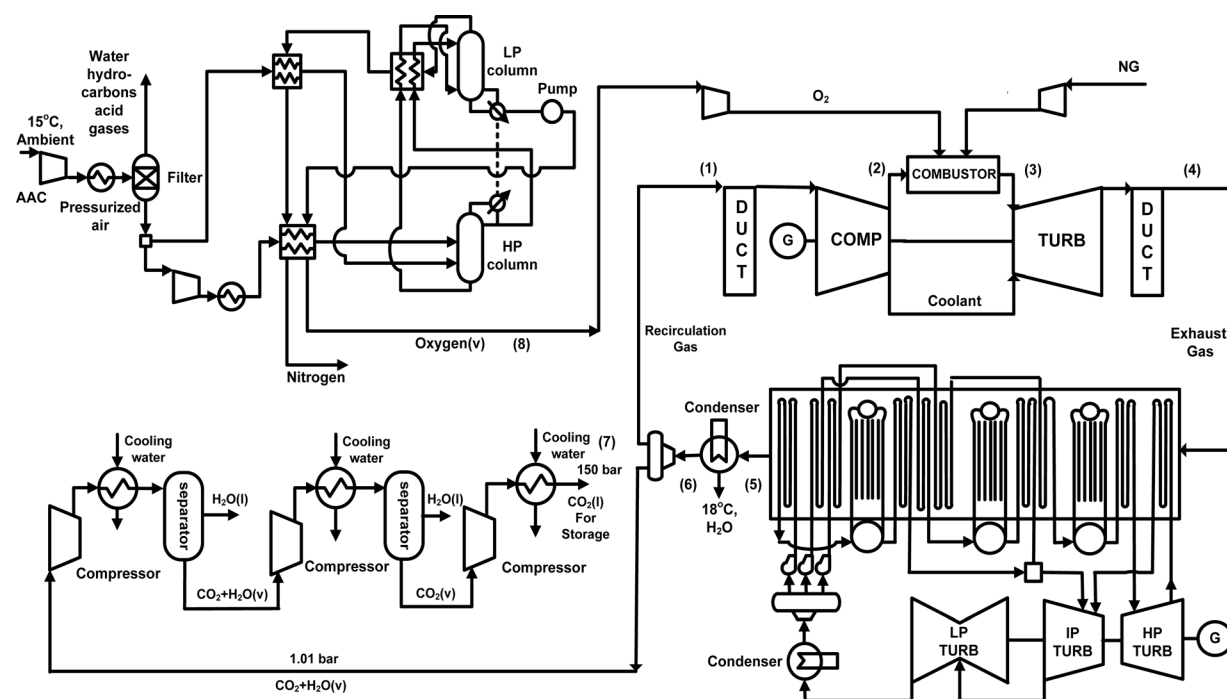


Fig. 1 Schematic diagram of the SCOC-CC system

deliberately matched to ensure the mass and energy balances of the entire plant.

We selected two turbine inlet temperatures that correspond to the current state-of-the-art and advanced technologies (F and J class gas turbines, respectively): 1418 °C and 1600 °C. To obtain a practically feasible performance of the SCOC-CC, we simulated commercial gas turbines in the two temperature classes and used the component performance characteristic parameters, such as compressor and turbine efficiencies and turbine cooling parameters, as reference data for the SCOC-CC analysis. The performance summaries of the conventional combined cycle plants using the two engines are shown in Table 1. The simulated performance is also shown, which corresponds very well with the data from the literature [17,18].

In the SCOC-CC, the compressor pressure ratio was varied to obtain optimal design conditions for each turbine inlet temperature. An ASU having an oxygen delivery pressure of 27 bar was modeled with a reference to the literature [14]. The details of the ASU are shown in Fig. 1. The ASU consumes a considerable amount of electric power to separate the oxygen, penalizing the SCOC-CC's performance. Thus, a precise calculation of the ASU is important. Our calculated specific power consumption (power per unit oxygen generation) agreed very well with the literature data in a practical oxygen purity range: 260.4 kW h/ton-O₂ (simulated) versus 260.2 kW h/ton-O₂ (see Ref. [14]) for 95% O₂ purity, and 242.2 kW h/ton-O₂ (simulated) versus 239.2 kW h/ton-O₂ (see Ref. [14]) for 90% O₂ purity, respectively. The ASU power consumption was calculated by using the following equation

$$\dot{W}_{ASU} = (\dot{W}_{AAC} + \dot{W}_{C,air} + \dot{W}_{P,O_2} + \dot{W}_{C,O_2})/\eta_{mo} \quad (1)$$

When the gas turbine pressure ratio is sufficiently high, the auxiliary oxygen compressor is used to supply the oxygen-rich stream out of the ASU to the combustor. The fuel in the SCOC-CC is also natural gas, as in conventional combined cycles. The natural gas consists of 90% CH₄, 6% C₂H₆, 2.5% C₃H₈ by volume, and other miscellaneous higher hydrocarbons and its lower heating value (LHV) is 49,244 kJ/kg. It was assumed that the pressure of the natural gas supplied to the plant is 30 bar. A fuel compressor was used to pressurize the fuel up to a pressure which is 30% higher than the combustor pressure. In the oxy-combustor, natural gas reacts with the oxygen-rich stream from the ASU and the CO₂-rich recirculating flow supplied by the gas turbine

compressor plays the role of the diluting medium. Given a compressor inlet air flow and pressure ratio, the fuel flow and oxygen flow rates were determined to achieve the specified turbine inlet temperature.

From the simulation of the two reference commercial gas turbines, we obtained the component parameters, as listed in Table 1. The compressor and turbine efficiencies were feasible as design values for advanced gas turbines. We used them as reference values for the SCOC-CC simulation. Turbine cooling considerably affects the gas turbine performance. The estimated total coolant fractions (total cooling air flow divided by compressor inlet air flow) are also shown in Table 1. It did not seem very reasonable to assign the same coolant fractions to any other design conditions. Especially, in the SCOC-CC, the pressure ratio and the properties of the working fluids deviate a great amount from those of the two conventional gas turbines. Therefore, a reasonable assumption is required to assign feasible coolant flows. First, we assumed that similar materials and cooling technologies, as in the two gas turbines, would be adopted in the two turbine inlet temperature (TIT) classes, respectively. The temperatures of all of the cooled blades of the two reference gas turbines were assumed to be 870 °C, considering the current technology status. We assumed that the temperature of the first stage nozzle blade of the SCOC-CC gas turbine would be the same as in the conventional gas turbines. Then, a thermodynamic cooling model [19] was used to calculate the coolant flows. The cooling effectiveness and the relation between the effectiveness and the heat capacity ratio (between the coolant and hot gas) were represented by the following equations. The second equation forms a cooling effectiveness curve

$$\phi = \frac{T_g - T_b}{T_g - T_c}, \quad \frac{\dot{m}_c c_{pc}}{\dot{m}_g c_{pg}} = C \cdot \frac{\phi}{1 - \phi} \quad (2)$$

In the reference calculation of the two engines in Table 1, the cooling parameter C , which represents the cooling technology level, was determined for each cooled blade. Then, in the calculation of the SCOC-CC, the parameter C was retained and the coolant flow rate was determined to achieve the same nozzle blade temperature for a new design condition which greatly deviated from the reference design condition in terms of the properties and temperatures of both the hot gas and the coolant.

The coolant flows of all of the other cooled blades (both the nozzle and rotor blades) were determined using the following proportional equation instead of the detailed calculation adopted in the first stage. The feasibility of this method will be discussed in the section titled "Results and Discussion"

$$\frac{(C_p \cdot \dot{m}_c)_{others}}{(C_p \cdot \dot{m}_c)_{others,ref}} = \frac{(C_p \cdot \dot{m}_c)_{1N}}{(C_p \cdot \dot{m}_c)_{1N,ref}} \quad (3)$$

Since a wide range of pressure ratios were investigated in this work, corrections for the compressor and turbine efficiencies were taken into account. In the compressor, since the polytropic efficiency naturally accounts for a correction of the isentropic efficiency depending on pressure ratio, the reference polytropic efficiencies in Table 1 were used. A recent study on detailed aerodynamic designs [13] confirmed that a pressure ratio which exceeds conventional design values considerably can still be designed with four turbines stages. Hence, the number of turbine stages (four) of the reference engines in Table 1 was maintained. However, the stage efficiency needed to be corrected because, in general, it tends to decrease as the blade loading increases. Since a full aerodynamic design was not used in this study, a simple efficiency correction using a database was used. The database of the Smith chart [20], showing the relation between stage efficiency and loading coefficient, was appropriate for this purpose. We selected a reference design condition (flow coefficient and loading coefficient) on the chart and generated the following efficiency

Table 1 Performance of combined cycle plants using two reference gas turbines

Item	1400 °C class		1600 °C class	
	Ref. [17]	Simulation	Ref. [18]	Simulation
Compressor inlet mass flow(kg/s)		507.2		598.7
Pressure ratio		17.4		23
Total coolant fraction (%)	—	20.2	—	16.7
Number of turbine stages		4		4
Turbine inlet temperature (°C)		1418		1600
Turbine exhaust temperature (°C)	578	582	632	631.5
Comp. polytropic efficiency (%)	—	89.3	—	91.5
Combustor pressure drop (%)	—	4.0	—	4.0
Turbine stage efficiency (%)	—	89.2	—	91
GT power (MW)	196.4	198.6	320	326.8
ST power (MW)	112.6	105.5	140	143.1
CC power output (MW)	309.0	304.1	460.0	469.9
CC efficiency (%)	57.0	56.8	61.0	60.6

Table 2 Parameters of the bottoming cycle and the auxiliary losses

HPT pressure (kPa)	12,400
IPT pressure (kPa)	2350
LPT pressure (kPa)	240
Maximum HP/IP steam temperature (°C)	565
ST polytropic efficiency (HP/IP/LP) (%)	86.4/89.0/90.5
Condensing pressure (kPa)	4.62
Pinch temperature difference (HP/IP/LP) (°C)	35/40/5
Pump isentropic efficiency (%)	80
Pressure losses (%)	0.5~5.0
Motor efficiency (%)	95
Generator efficiency (%)	98.5

correction function, in terms of loading change, as a linear equation

$$\frac{\eta_{st}}{\eta_{st,ref}} = f\left(\frac{\psi}{\psi_{ref}}\right) \quad (4)$$

We applied this correction factor to every stage in our calculation. The aforementioned models for the blade cooling and the stage efficiency correction were additionally embedded in the GateCycle using macro functions. The gas turbine power output was calculated as follows

$$\dot{W}_{GT} = (\dot{W}_T - \dot{W}_C/\eta_{mech}) \cdot \eta_{gen} \quad (5)$$

The design parameters of the steam bottoming cycle and auxiliary losses are shown in Table 2. The high pressure/intermediate pressure (HP/IP) steam temperature shown in the table is an allowable limit. If the gas turbine exhaust temperature is not sufficiently high to achieve this steam temperature, it was set at 10 °C lower than the gas temperature. The HRSG exit gas is CO₂-rich (over 80% for the ASU O₂ purity over 90%). At the condenser exit, the condensate is dumped out and a portion of the gaseous phase is extracted and fed to the CSU, which compresses the CO₂ and simultaneously purifies it by removing the water. Since the removed water at the CSU contains only a very small amount of dissolved CO₂, nearly all of the net CO₂ generation in the cycle can be captured; that is, the CO₂ capture rate, defined by the following equation, is very high (over 99%), which must be an advantage of the SCOC-CC

$$\text{capture rate} = \frac{\text{CO}_{2,\text{captured}}}{\text{CO}_{2,\text{generated}}} \quad (6)$$

The CSU requires power consumption for gas compression and cooling water pumping and it was calculated as follows. The delivery state of the captured CO₂ is 150 bar and 40 °C (liquid) and the two intermediate pressures are 5.47 and 29.7 bar [21]

$$\dot{W}_{CSU} = (\dot{W}_{C,\text{CO}_2} + \dot{W}_{P,\text{H}_2\text{O}})/\eta_{mo} \quad (7)$$

The net SCOC-CC power output and efficiency were defined as follows

$$\dot{W}_{\text{SCOC-CC,net}} = \dot{W}_{GT} + \dot{W}_{ST} - \dot{W}_{ASU} - \dot{W}_{CSU} \quad (8)$$

$$\eta_{\text{SCOC-CC,net}} = \frac{\dot{W}_{\text{SCOC-CC,net}}}{(\dot{m} \cdot \text{LHV})_{\text{NG}}} \quad (9)$$

Results and Discussion

Overview. First, the design performance expectations with the pressure ratio as a primary design parameter for the two turbine inlet temperatures will be presented. Then, the influence of the

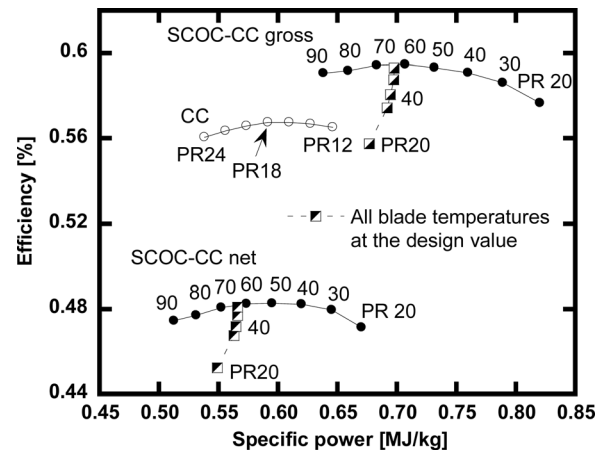


Fig. 2 Efficiency versus the specific power chart for the SCOC-CC using the 1400 °C class gas turbine

ASU oxygen purity will be explained. Finally, the SCOC-CC performance will be compared with the performance of the conventional CC coupled with a postcombustion CO₂ capture.

Performance Characteristics. The predicted SCOC-CC performance for a wide pressure ratio (PR) range with a TIT of 1418 °C was summarized in the specific power versus efficiency chart of Fig. 2. The ASU exit oxygen purity for all of the simulations in this section is 95% (by mole). Also shown is the performance of a conventional combined cycle adopting the same TIT. Pay attention only to the markers with solid lines. The dotted lines will be explained later. First, we confirmed that the pressure ratio of the commercial engine in Table 1 (17.4) is the optimal design point in terms of the CC efficiency. This is a reasonable result considering that the combined cycle is targeted to achieve maximum fuel economy (efficiency), which can also be confirmed from the manufacturer's design criteria. In this respect, the current simulation result seems to be quite feasible. The optimal pressure ratio of the SCOC-CC is considerably higher in comparison to the conventional CC. In addition, the gross performance of the SCOC-CC is much higher than that of the conventional CC. The SCOC-CC yields a much larger power output per compressor inlet air flow (i.e., the specific power is greater), mainly due to the increased turbine mass flow (remember that the oxygen for the combustor is supplied from outside of the cycle). The thermodynamic properties of the CO₂-rich working fluid are different from those of the ambient air and its combustion gas in the conventional CC. In particular, the difference in specific heat is one of the major causes for the performance difference. The CO₂-rich gas has a lower specific heat at relatively low temperatures (e.g., the compressor part) and a higher specific heat at higher temperatures (e.g., the turbine part) in comparison to the working fluids of the conventional CC. As a result, the optimal efficiency of the SCOC-CC appears at a much higher pressure ratio than in the conventional CC. The gross efficiency reaches almost 60% with a pressure ratio around 60. The net SCOC-CC efficiency reduces by more than 10 percentage points. The best net efficiency is about 48.5% and is also achieved by a pressure ratio around 60.

The turbine blade cooling needed to be checked. Figure 3 shows the variations in the compressor discharge temperature (CDT) and the turbine exit temperature (TET). Let's compare the results of the conventional CC and the SCOC-CC at a same pressure ratio. The CDT of the SCOC-CC is more than 100 °C lower than that of the conventional CC. In the turbine, temperature drop of the SCOC-CC is lower than in the conventional CC, resulting in a higher TET at the same pressure ratio. The lower CDT is positive in the viewpoint of the first stage nozzle cooling because the cooling effectiveness becomes lower as the coolant temperature

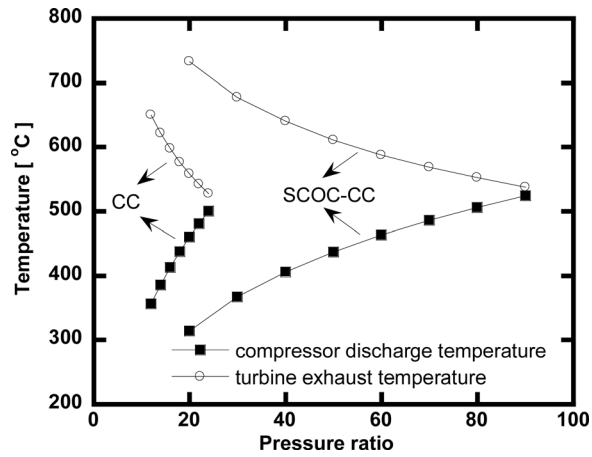


Fig. 3 Variations in the compressor discharge temperature and turbine exhaust temperature with the pressure ratio (1400 °C class)

(CDT) becomes lower (see the first equation of Eq. (2)). Figure 4 shows the cooling effectiveness curve, which is a graphical representation of the second equation of Eq. (2), with several design points of both the SCOC-CC and the conventional CC. The increased specific heat of hot gas is a negative factor. However, since the positive effect prevails, the coolant fraction of the SCOC-CC is less than in the conventional CC at the same pressure ratio. Figure 5 shows the total coolant fractions for the two cases. The dotted line will be explained in the next paragraph. Since the coolant flow after the first stage was assigned by the rather simple scaling of Eq. (3), we checked the temperatures of the 2nd and 3rd stage nozzles. Figure 6 shows the results. The first stage temperature was kept constant, as explained. In the lower pressure ratio range, the temperatures of the 2nd and 3rd stage nozzles exceed the design value because the stage inlet gas temperature (T_g in Eq. (2)) is higher than the reference temperatures of the conventional CC (i.e., the temperature drop at a given pressure ratio is smaller in the SCOC-CC, as previously explained; see Fig. 3). At around the optimal efficiency point (a PR of 60), they become similar to the reference design value of 870 °C. Above this pressure ratio, they become lower. At the optimal pressure ratio, the temperatures of all of the blades would be very close to the reference design value but require more total coolant flows (see the difference between the PR 60 of the SCOC-CC and the PR 18 of the conventional CC in Fig. 5).

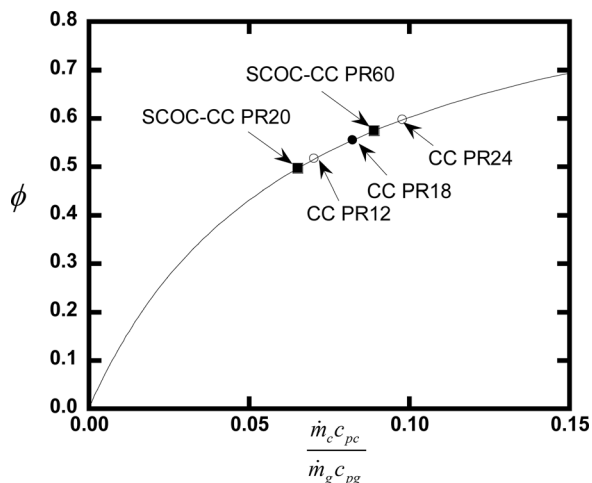


Fig. 4 Cooling effectiveness of the 1st stage nozzle blade (1400 °C class)

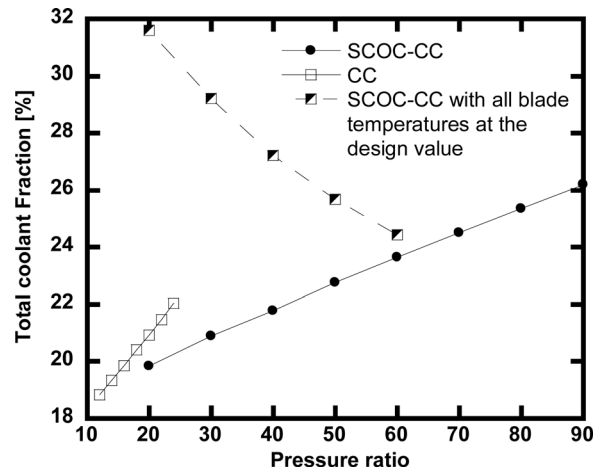


Fig. 5 Variations in the total coolant fraction (total coolant divided by compressor inlet air) with the pressure ratio (1400 °C class)

In any case, we may want to select a relatively low pressure ratio because the optimal pressure ratio is much higher than those of currently available commercial gas turbines. Furthermore, a large reduction in the pressure ratio from the optimal point provides a greater enhancement of the specific power while the efficiency loss is only marginal. For example, with a pressure ratio of 30, the efficiency decreases by 0.5% point from the optimal value, but the specific power increases by 15%. However, with the selection of a much lower pressure ratio than the optimal pressure ratio, we would have much higher blade temperatures, as shown in Fig. 6 (30 °C to 50 °C increases for a PR of 30, compared with a PR of 60). This means that we should have higher-quality blade materials, which increases the development cost. The other option, to select the lower pressure ratio as a design point while maintaining the blade temperatures of the 2nd and 3rd stage without enhancing the material capability and cooling technologies, is to use more coolant to those locations. A calculation wherein the temperatures of all the blades were kept at the reference temperature (870 °C) by increasing coolant flows of the 2nd and 3rd stages was performed and the results are indicated in Fig. 2 by markers with dotted lines. The required total coolant flow is also indicated in Fig. 5 as a dotted line. It is confirmed that an increase of coolant flows causes a remarkable power and efficiency reduction. The result means that a simple increase in coolant flows to achieve blade temperatures as in conventional gas turbines cannot be a good solution. Therefore, material reinforcement should be a better

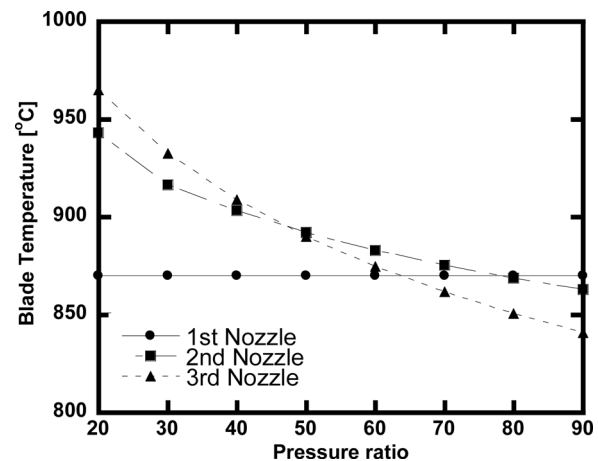


Fig. 6 Variations in the nozzle blade temperatures with the pressure ratio (1400 °C class)

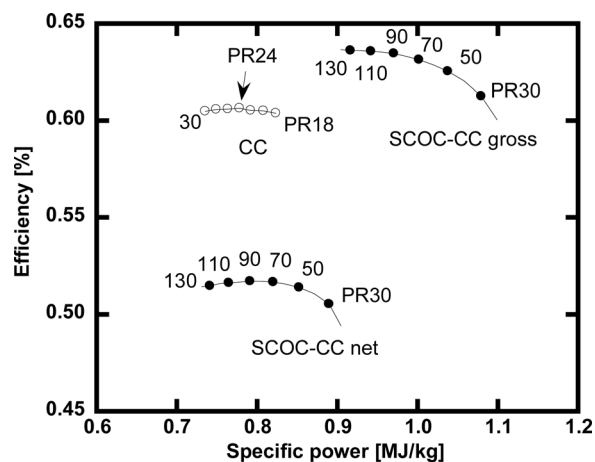


Fig. 7 Efficiency versus the specific power chart for the SCOC-CC using the 1600 °C class gas turbine

option. Or, using a better cooling technology which requires the same coolant flows but decreases blade temperatures can be another option. However, both of these two options cause an increase of the development cost. In summary, pressure ratios around the optimal point in terms of net cycle efficiency are also feasible as a design point in the viewpoint of the thermal design of turbine blades. Consequently, the result of the present study suggested that a pressure ratio of around 60 would be appropriate as a design point of the SCOC-CC using a TIT around 1400 °C, considering both the net cycle efficiency and the design feasibility of the turbine.

Figure 7 presents the specific power-efficiency chart for the case using the 1600 °C class gas turbine. The trend is quite similar to Fig. 2, except that efficiency and specific power are higher than in Fig. 2 and the optimal pressure ratio is higher. The optimal pressure ratio, in terms of the net cycle efficiency, is around 90 where both the gross and net efficiencies are about 4 percentage points higher than the corresponding optimal efficiencies in Fig. 2. It is noticeable that the net efficiency of over 50% is possible. The trends in the variations in the blade temperatures were similar to those in Fig. 6: the temperatures of the 2nd and 3rd stage blades are close to the design values at the optimal pressure ratio (90) and become higher as the pressure ratio decreases. Thus, the same conclusion regarding the design point selection as in the cycle with 1400 °C TIT is possible: the best efficiency point should be the most feasible design

point, while a selection of relatively lower pressure ratios requires material reinforcement of the turbine blades or upgrades of the turbine cooling technology.

Table 3 summarized the performance data for the optimal design points. Results for both the conventional cycle and the SCOC-CC are compared in the two TIT classes, respectively. We now focus our interest on the case with a 95% ASU oxygen purity. The case with 90% purity will be discussed in the next section. In both TIT classes, the auxiliary power consumption penalizes the cycle efficiency by about 18% (about 11 percentage points). In comparison with the reference efficiency of the conventional CC, the net cycle efficiency is about 8 percentage points lower. The ASU power consumption is much larger than the CSU power consumption, which means that the technology advancement in the ASU would enhance the SCOC-CC efficiency. For example, a 20% reduction in the ASU power would yield a 1.7 percentage points improvement in the net cycle efficiency in the 1400 °C class: the net efficiency would be over 50%. The CO₂ capture rate is very high because only a very small amount of CO₂ dissolved in the water is extracted out from the CSU. The purity of the captured CO₂ is close to 90% with a 95% ASU oxygen purity.

Since the pressure ratios of the optimal design conditions of the SCOC-CC are much higher than for the conventional CC, special attention should be given to the compressor design. A recent conceptual aerodynamic design of the same cycle [13] demonstrated that a pressure ratio of 39 could be designed with 18 compressor stages. According to their study, the average stage pressure ratio is around 1.2-1.23, which is very similar to that of the state-of-the-art conventional gas turbines (14-15 stages for a pressure ratio of 17-18). Thus, we can expect that 20-21 stages and 22-23 stages would be appropriate for the pressure ratios of 60 and 90. Even though the pressure ratios are high, the compressor discharge temperature is acceptable. As Table 3 shows, it remains between 463 °C and 525 °C in the SCOC-CC. It is somewhat higher than that of the conventional CC (437 °C to 479 °C). However, it is quite achievable without critical material reinforcement because temperatures much higher than 500 °C are already available in industrial gas turbines which have a pressure ratio of over 30 [22]. Of course, such a high temperature is quite the norm in aeroderivative gas turbines, which have higher pressure ratios than industrial gas turbines.

Effect of Oxygen Purity. The purity of the oxygen supplied by the ASU affects the compositions of the working fluid. Tables 4 and 5 show the compositions and properties of the working fluid at several locations. As the oxygen purity decreases, the nitrogen

Table 3 Performance of the SCOC-CC and comparison with the conventional CC

	CC		SCOC-CC		CC		SCOC-CC	
Turbine inlet temperature (°C)		1418				1600		
Pressure ratio	18	60	60	24	90	90		
ASU O ₂ purity (%)	—	95	90	—	95	90		
Compressor inlet temperature (°C)	15	18	18	15	18	18		
Inlet mass flow (kg/s)		507.2			598.7			
Compressor discharge temperature (°C)	437.3	463.1	478.5	478.9	508.6	525.9		
Fuel supply (kg/s)	10.74	12.25	12.00	15.60	18.61	18.31		
Fuel compression power (MW)	—	−1.9	−1.9	—	−4.4	−4.4		
Turbine exit temperature (°C)	576.4	587.7	572.2	623.5	635.0	617.3		
GT power output (MW)	197.6	244.6	242.4	325.8	420.9	419.4		
ST power output (MW)	102.7	114.2	108.9	140.3	160.4	153.3		
Gross power output (MW)	300.3	358.8	351.3	466.1	581.3	572.7		
Gross cycle efficiency	56.8	59.5	59.4	60.6	63.4	63.5		
ASU power (MW)	—	−52.0	−50.0	—	−82.8	−80.1		
CSU power (MW)	—	−15.8	−17.1	—	−24.7	−27.1		
CO ₂ capture rate (%)	—	99.5	99.5	—	99.5	99.5		
CO ₂ purity (%)	—	89.5	81.5	—	89.5	81.5		
Net cycle power output (MW)	300.3	291.1	284.2	466.1	473.8	465.5		
Net cycle efficiency (%)	56.8	48.2	48.1	60.6	52.2	51.6		

Table 4 Compositions and properties at several locations (1400 °C class, PR 60, 95% oxygen purity)

Item	Mass flow (kg/s)	T (°C)	P (kPa)	Composition (mole fraction)					Density (kg/m ³)	c_p (kJ/kg °C)
				CO ₂	H ₂ O	N ₂	Ar	O ₂		
(1) Compressor inlet	507.2	18.0	101.3	0.885	0.020	0.03	0.065	—	1.799	0.861
(2) Compressor outlet	387.3	463.1	6049	0.885	0.020	0.03	0.065	—	41.98	1.128
(3) Combustor outlet	450.4	1418.0	5807	0.774	0.144	0.026	0.056	—	16.20	1.410
(4) Turbine outlet	570.3	587.7	103.5	0.796	0.119	0.027	0.058	—	0.582	1.192
(5) HRSG outlet	570.3	117.0	101.8	0.796	0.119	0.027	0.058	—	1.266	0.966
(6) Condenser outlet	544.5	18.0	101.3	0.885	0.020	0.030	0.065	—	1.799	0.861
(7) CSU outlet	37.2	40.0	15000	0.895	0.0094	0.030	0.0656	—	647.8	3.195
(8) ASU outlet	50.9	25.0	2700	0.001	—	0.013	0.035	0.95	35.95	0.944

Table 5 Compositions and properties at several locations (1400 °C class, PR 60, 90% oxygen purity)

Item	Mass flow (kg/s)	T (°C)	P (kPa)	Composition (mole fraction)					Density (kg/m ³)	c_p (kJ/kg °C)
				CO ₂	H ₂ O	N ₂	Ar	O ₂		
(1) Compressor inlet	507.2	18.0	101.3	0.806	0.020	0.110	0.065	—	1.753	0.870
(2) Compressor outlet	383.6	478.5	6049	0.806	0.020	0.110	0.065	—	39.80	1.130
(3) Combustor outlet	447.9	1418.0	5807	0.709	0.139	0.097	0.056	—	15.80	1.402
(4) Turbine outlet	571.4	572.2	103.5	0.729	0.114	0.099	0.058	—	0.578	1.183
(5) HRSG outlet	571.4	117.7	101.8	0.729	0.114	0.099	0.058	—	1.231	0.972
(6) Condenser outlet	544.5	18.0	101.3	0.806	0.0201	0.110	0.064	—	1.753	0.870
(7) CSU outlet	38.9	40.0	15000	0.815	0.0093	0.111	0.065	—	518.6	3.092
(8) ASU outlet	52.2	25.0	2700	0.001	—	0.065	0.034	0.90	35.69	0.950

content increases and the CO₂ content decreases inside the cycle. Therefore, the purity of the CO₂ extracted from the cycle for capture also decreases. The final CO₂ purity at the end of the capture process with a 90% oxygen purity is barely over 80%, which is much lower than the almost 90% in the case of a 95% oxygen purity. The change in oxygen purity also affects the cycle performance: see Table 3 for a performance comparison between the 90% and 95% oxygen purity cases. A decrease in oxygen purity slightly reduces the gas turbine power and further reduces the steam turbine power contributed by the lower gas turbine exit temperature. Since the fuel supply also decreases a bit due to the increased compressor discharge temperature, the net efficiency does not effectively change.

All of our simulations were based on the stoichiometric reaction at the combustor, i.e., no excess oxygen supply. However, some excess oxygen may exist in a real plant. Additionally, a sensitivity analysis was performed to determine the influence of the presence of excess oxygen on the cycle performance. It was found out that 1% excess oxygen would decrease the system efficiency by 0.5 and 0.2 percentage points in the 1418 °C and 1600 °C cases, respectively.

Comparison With Postcombustion Capture. Postcombustion CO₂ capture is the conceptually simplest idea wherein the power cycle modification is minimized. However, a complicated absorption capture process is required. We intended to compare the thermodynamic performance of the SCOC-CC with the conventional CC coupled with a postcombustion capture. A special focus was given to the capture rate of the absorption process and its effect on net system performance.

Figure 8 shows the entire power system adopting a postcombustion capture. An amine-based (monoethanol amine (MEA)) absorption capture process was modeled after the literature [23]. After being captured at the absorption process, the CO₂ is purified and compressed up to the same state as in the SCOC-CC using the CSU. The details of the absorption process need not be explained here because they are relatively well known. The absorption process requires a great amount of energy consumption at the

reboiler. The heat for the reboiler is supplied using the steam from the bottoming cycle. In this study, the IP steam was used and returned to the feedwater stream, as shown in the figure. Based on the published technology status, the CO₂ capture rate of the absorption process (CO₂ at the exit (point 6) divided by CO₂ from the HRSG (point 5)) was set at over 85%; the usual capture rate that appears in the literature is 85% to 90% [24,25]. A reference calculation was performed for an 85% capture rate and the thermal energy for the reboiler was estimated to be 3.63 GJ/ton-CO₂. This is very well matched with the reference data (3.4 to 3.65 GJ/ton-CO₂ for the 82% to 85% capture rate) [23], which validated the absorption process modeling of this study.

The overall capture rate, the definition of which is the same as in Eq. (6), does not change much from the capture rate of the absorption process because the CSU process is the same as before and only purifies the CO₂. Therefore, the overall capture rate of this reference case (~85%) is much lower compared with those of the SCOC-CC (over 99%). Since a direct performance comparison between the present case with only an 85% capture rate with the SCOC-CC case with over a 99% capture rate does not seem reasonable, the capture rate was varied and its effect on the net cycle performance was evaluated. Figure 9 shows the impact of the absorption CO₂ capture. An increase in the absorption CO₂ capture rate requires more thermal energy of the reboiler because it requires an increase in the MEA flow rate. The heat demand abruptly increases as the absorption CO₂ capture rate exceeds 90%, resulting in a large penalty in the steam turbine power and cycle efficiency. The performance summaries for the combined cycle plants with the postcombustion capture using 1400 °C and 1600 °C class gas turbines are shown in Table 6 (the reference CC performance is shown in Table 3).

For example, with an absorption capture rate of 85% in the case of the gas turbine of the 1400 °C class, the steam turbine power loss due to the heat transport to the reboiler is about 21 MW (81.0 MW in Table 6 versus 102.7 MW in Table 3). Since the power consumption of the absorption process is relatively very small, most of the auxiliary power consumption is due to the CSU. The net cycle efficiency was predicted to be 50.4%, which is 6.4 percentage points lower than the gross CC efficiency

Table 7 Compositions and properties at several locations in the conventional CC with the postcombustion capture (1400 °C class, PR 18)

Item	Mass flow (kg/s)	T (°C)	P (kPa)	Composition (mole fraction)					Density (kg/m ³)	c_p (kJ/kg °C)
				CO ₂	H ₂ O	N ₂	Ar	O ₂		
(1) Compressor inlet	507.2	15.0	101.3	0.0003	0.010	0.773	0.0092	0.207	1.221	1.009
(2) Compressor outlet	403.8	437.3	1814	0.0003	0.010	0.773	0.0092	0.207	8.816	1.099
(3) Combustor outlet	414.5	1418.0	174	0.047	0.097	0.739	0.0088	0.109	3.501	1.332
(4) Turbine outlet	518.0	576.4	103.5	0.038	0.080	0.746	0.0089	0.128	0.417	1.175
(5) HRSG outlet	518.0	118.8	101.8	0.038	0.080	0.746	0.0089	0.128	0.889	1.071
(6) Condenser outlet	32.6	93.9	200	0.596	0.403	0.0003	0.0003	0.0004	2.216	1.127
(7) CSU outlet	25.6	40.0	15,000	0.990	0.0096	0.0003	0.0003	0.0001	766.2	2.925

evaluation, especially the initial investment cost analysis, is beyond the scope of this work. However, it seems quite feasible to imagine that the relative economic merit of the SCOC-CC over the postcombustion capture would be dominant as the CO₂ capture requirement becomes tighter.

Conclusion

The design performance of the SCOC-CC was evaluated for two turbine inlet temperatures, taking into account practical component parameters including turbine cooling. The performance characteristics were investigated and compared with those of the conventional combined cycle coupled with a postcombustion capture. The results are summarized as follows:

- (1) The optimal pressure ratio (the best efficiency condition) of the SCOC-CC is much higher than for the conventional combined cycle. The optimal pressure ratio, in terms of the net cycle efficiency, is around 60 and 90 for turbine inlet temperatures of 1418 °C and 1600 °C, respectively. With a relatively lower pressure ratio, the turbine blade temperatures would be higher than for conventional gas turbines or better cooling schemes should be adopted. Otherwise, the performance penalty due to cooling would be considerable.
- (2) With optimal design conditions, the net cycle efficiency is lower than the efficiency of the conventional CC by about 8 percentage points for both of the two turbine inlet temperatures. The oxygen purity of the ASU exit stream affects the net power output, but its effect on the net cycle efficiency is only marginal. The CO₂ capture rate is extremely high (over 99%) and is not affected by the oxygen purity. However, the oxygen purity considerably affects the purity of the captured CO₂. The CO₂ purity is almost 90% with a 95% oxygen purity, but is reduced to 81.5% with a 90% oxygen purity.
- (3) The very high CO₂ capture rate of the SCOC-CC cannot be achieved by the postcombustion capture. The postcombustion capture could provide a similar, or slightly higher, net efficiency than the SCOC-CC only when the CO₂ capture rate remains under 90%. Otherwise, the energy consumption of the postcombustion capture is too high for its net efficiency to be comparable to the SCOC-CC.

Acknowledgment

This research was supported by the Basic Research Program through the National Research Foundation of KOREA (NRF) funded by the Ministry of Education, Science and Technology (Grant No. 2011-0002491).

Nomenclature

ASU = air separation unit
 c_p = specific heat (kJ/kg K)
 C = cooling parameter
 CC = combined cycle

CDT = compressor discharge temperature
 CSU = carbon separation unit
 GT = gas turbine
 HP = high pressure
 HRSG = heat recovery steam generator
 IP = intermediate pressure
 LHV = lower heating value (kJ/kg)
 LP = low pressure
 \dot{m} = mass flow rate (kg/s)
 PR = pressure ratio
 SCOC-CC = semi-closed oxy-fuel combustion combined cycle
 ST = steam turbine
 T = temperature (°C)
 TET = turbine exhaust temperature (°C)
 TIT = turbine inlet temperature (°C)
 \dot{W} = power (MW)
 η = efficiency
 ϕ = cooling effectiveness
 ψ = loading coefficient

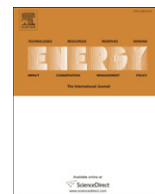
Subscripts

AAC = auxiliary air compressor
 b = blade
 c = coolant
 C = compressor
 g = main stream gas
 gen = generator
 mech = mechanical
 mo = motor
 net = net performance
 NG = natural gas
 P = pump
 ref = reference
 st = stage
 T = turbine
 1 N = 1st stage nozzle

References

- [1] Franco, F. J., Mina, T., Woollatt, G., Rost, M., and Bolland, O., 2006, "Characteristics of Cycle Components for CO₂ Capture," Proceedings of the 8th International Greenhouse Gas Control Technologies, Trondheim, Norway, June 19–22.
- [2] Jericha, H., Sanz, W., Gottlich, E., and Neumayer, F., 2008, "Design Details of a 600 MW Graz Cycle Thermal Power Plant for CO₂ Capture," *ASME Paper No. GT2008-50515*.
- [3] Anderson, R. E., MacAdam, S., Viteri, F., Davies, D. O., Downs, J. P., and Paliszewski, A., 2008, "Adapting Gas Turbines to Zero Emission Oxy-Fuel Power Plants," *ASME Paper No. GT2008-51377*.
- [4] Sanz, W., Jericha, H., Bauer, B., and Gottlich, E., 2008, "Qualitative and Quantitative Comparison of Two Promising Oxy-Fuel Power Cycles for CO₂ Capture," *ASME J. Eng. Gas Turbines Power*, **130**, pp. 1–11.
- [5] Tak, S. H., Park, S. K., Kim, T. S., Sohn, J. L., and Lee, Y. D., 2010, "Performance Analyses of Oxy-Fuel Power Generation Systems Including CO₂ Capture: Comparison of Two Cycles Using Different Recirculation Fluids," *J. Mech. Sci. Technol.*, **24**, pp. 1947–1954.
- [6] Ulizra, I. and Pilidis, P., 1997, "A Semi Closed-Cycle Gas Turbine With Carbon Dioxide-Argon as Working Fluid," *ASME J. Eng. Gas Turbines Power*, **119**, pp. 612–616.

- [7] Jackson, A. J. B., Neto, A. C., Whellens, M. W., and Audus, H., 2000, "Gas Turbine Performance Using Carbon Dioxide as Working Fluid in Closed Cycle Operation," ASME Turbo Expo 2000, Munich, Germany, May 8–11, ASME Paper No. 2000-GT-153.
- [8] Bolland, O., and Mathieu, P., 1998, "Comparison of Two CO₂ Removal Options in Combined Cycle Power Plants," *Energy Convers. Manage.*, **39** (16–18), pp. 1653–1663.
- [9] Kvamsdal, H. M., Jordal, K., and Bolland, O., 2007, "A Quantitative Comparison of Gas Turbine Cycles With CO₂ Capture," *Energy*, **32**, pp. 10–24.
- [10] Yang, H. J., Kang, S. Y., Kang, D. W., and Kim, T. S., 2011, "Performance Expectation of a Semi-Closed Oxy-Fuel Combustion Combined Cycle Using an Existing Gas Turbine," International Gas Turbine Congress, Osaka, Japan, Nov. 14–18, Paper No. IGTC2011-0231.
- [11] Jordal, K., Bolland, O., and Klang, A., 2003, "Aspects of Cooled Gas Turbine Modelling for the Semi-Closed O₂/CO₂ Cycle With CO₂ Capture," ASME Paper No. GT2003-38067.
- [12] Jonsson, M., Bolland, O., Buckner, D., and Rost, M., 2005 "Gas Turbine Cooling Model for Evaluation of Novel Cycles," Proceedings of ECOS 2005, Trondheim, Norway, June 20–22.
- [13] Sammak, M., Jonshagen, K., Thern, M., Genrup, M., Thorbergsson, E., Gronstedt, T., and Dahlquist, A., 2011, "Conceptual Design of a Mid-Sized Semi-Closed Oxy-Fuel Combustion Combined Cycle," ASME Paper No. GT2011-46299.
- [14] Amann, J. M., Kanniche, M., and Bouallou, C., 2009, "Natural Gas Combined Cycle Power Plant Modified Into O₂/CO₂ Cycle for CO₂ Capture," *Energy Convers. Manage.*, **50**, pp. 510–521.
- [15] Enter Software Inc., GATECYCLE, Ver. 6.0, 2006.
- [16] Aspen Technology Inc., ASPENONE HYSYS, Ver. 7.2, 2006.5.
- [17] Gas Turbine World 2011 Performance Specifications, **41**(1), p. 20, 39.
- [18] Biasi, V., 2010, "1600 °C-Class M501J Plant Rated 460 MW and Over 61% Efficiency," *Gas Turbine World*, **40**, pp. 10–14.
- [19] Kim, T. S., and Ro, S. T., 1995, "Comparative Evaluation of the Effect of Turbine Configuration on the Performance of Heavy-Duty Gas Turbines," ASME Paper No. 95-GT-334.
- [20] Moustapha, H., Zelesky, M. F., Baines, N. C., and Japikse, D., 2003, "Turbine Fundamentals and Parameters," *Axial and Radial Turbines*, Concepts NREC, White River Junction, VT, Chap. 1.
- [21] Park, S. K., Ahn, J. H., and Kim, T. S., 2011, "Performance Evaluation of Integrated Gasification Solid Oxide Fuel Cell/Gas Turbine Systems Including Carbon Dioxide Capture," *Appl. Energy*, **88**, pp. 2976–2987.
- [22] Jeong, D. H., Yoon, S. H., Lee, J. J., and Kim, T. S., 2008, "Evaluation of Component Characteristics of a Reheat Cycle Gas Turbine Using Measured Performance Data," *J. Mech. Sci. Technol.*, **22**, pp. 350–360.
- [23] Oei, L. E., 2007, "Aspen HYSYS Simulation of CO₂ Removal by Amine Absorption From a Gas Based Power Plant," SIMS2007 Conference, Goteborg, Sweden, October 30–31.
- [24] Pfaff, I., Oexmann, J., and Kather, A., 2010, "Optimised Integration of Post-Combustion CO₂ Capture Process in Greenfield Power Plants," *Energy*, **35**, pp. 4030–4041.
- [25] Kanniche, M., Gros-Bonnivard, R., Jaud, P., Valle-Marcos, J., Amann, J., and Bouallou, C., 2010, "Pre-Combustion, Post-Combustion and Oxy-Combustion in Thermal Power Plant for CO₂ Capture," *Appl. Therm. Eng.*, **30**, pp. 53–62.



Zero CO₂ emission SOLRGT power system

Chending Luo^{a,b}, Na Zhang^{a,*}

^a Institute of Engineering Thermophysics, Chinese Academy of Sciences, P.O. Box 2706, Beijing 100190, PR China

^b State Nuclear Electric Power Planning Design & Research Institute, No. 5 Dijin Road, Haidian Distric, Beijing 100195, PR China

ARTICLE INFO

Article history:

Received 26 September 2011

Received in revised form

20 April 2012

Accepted 29 April 2012

Available online 2 July 2012

Keywords:

Hybrid system

Oxy-fuel cycle

Solar energy

Natural gas reforming

Zero CO₂ emission

ABSTRACT

A novel hybrid power system with zero CO₂ emission (ZE-SOLRGT) has been proposed and analyzed in this paper. It consists of a high temperature Brayton-like topping cycle and a high pressure-ratio Rankine-like bottoming cycle, integrated with methane-steam reforming, solar heat-assisted steam generation and CO₂ capture and compression. Water is selected to be the working fluid. Solar heat input enhances the steam generation and power output, and reduces fossil fuel consumption. Besides CO₂ capture with oxy-fuel combustion and cascade recuperation of turbine exhaust heat, the system is featured with indirect upgrading of low-mid temperature solar heat and cascade release of fossil fuel chemical exergy, which is described by the energy level concept. With nearly 100% CO₂ capture, the system attains a net energy efficiency of 50.7% (including consideration of the energy needed for oxygen separation). The cost of generated electricity and the payback period of ZE-SOLRGT are found to be \$0.056/kWh and 11.3 years, respectively. The system integration accomplishes the complementary utilization of fossil fuel and solar heat, and attains their high efficiency conversion into electricity.

© 2012 Elsevier Ltd. All rights reserved.

1. Introduction

Solar power can play an important role in meeting energy demand and reducing greenhouse gas emissions. In the past few decades, to improve the thermodynamic and economic performances of the conventional solar-only thermal power systems, some hybrid systems were proposed that use multiple heat sources at different temperature levels in a way that low/mid-temperature solar thermal energy sources are used when they are relatively inexpensive, and higher temperature fossil fuel energy sources are integrated to raise the energy efficiency. The solar thermal energy helps to increase the mass flow of the working fluid and thus the power output, or save fossil fuel, or both.

An earlier such hybrid system was proposed by Lior and co-workers [1–3], named SSPRE (Solar Steam Powered Rankine Engine), which integrated steam Rankine cycle with a solar collector loop (solar flat plates) for the evaporation process, at a temperature of only ~100 °C. The solar heat contributes nearly 80% of the input energy. Fossil fuel is burned to provide the remaining 20% heat demand to superheat the steam and boost its temperature up to 600 °C. The cycle efficiency achieves about 18%, doubling the efficiency of the organic fluid or steam Rankine cycles operating at similar (~100 °C) solar collector temperatures.

Later solar energy was introduced into combined cycles (CC) for the significant advantages it brings about. The integrated solar combined cycle systems (ISCCS) were built in Egypt, Iran, Germany and many other countries. Depending on its temperature level, solar thermal energy can principally be integrated into either the gas turbine topping cycle (for air preheating prior to the combustor) or into the steam turbine bottoming cycle (for steam generation) [4–7]. For a 310 MW ISCCS in California it was estimated that the electricity cost of the ISCCS with a trough solar field could attain 9 ¢cent/kWh without thermal storage, or 7.5 ¢cent/kWh with; but the achievable annual solar share is small, 4% without thermal storage and 9% with [6].

Thermal integration integrates solar heat into some heat absorption process in power plants, such as for evaporation and recuperation processes, and converts solar heat into working fluid sensible heat, noting also that the energy quality of collected solar heat drops because of the necessary heat transfer temperature difference. Thermo-chemical integration, on the other hand, integrates with some endothermic reactions like reforming and decomposition, which convert the absorbed solar heat into chemical energy of the reaction product, thus achieving an upgrading of the solar heat. Hong, Jin and co-workers proposed a methanol combined cycle (Solar CC) that integrates power generation with solar heat-driven methanol decomposition at relatively low temperature (~220 °C) [8,9]. Low-mid temperature solar thermal energy is first upgraded to the chemical energy of the reaction produced syngas, and then efficiently converted to electricity in an

* Corresponding author. Tel.: +86 10 82543030; fax: +86 10 82543019.
E-mail addresses: zhangna@iet.cn, zhangna@mail.etp.ac.cn (N. Zhang).

Nomenclature

A	Energy level
C	Cost [M\$]
COE	Cost of electricity [\$/kWh]
DNI	Direct solar radiation [W/m ²]
E	Exergy [MW]
H	Annual operating hours [h]
I	Annual solar radiation [kWh/(m ² ·y)]
i	Interest rate
m	Mass flow [kg/s]
NG	Natural gas
PBP	Payback period [y]
Q_f	Fuel low-heating-value input [MW]
Q_{sol}	Absorbed solar heat by power block [MW]
Q_{rad}	Solar energy irradiated to the solar field [MW]
R	Annual revenue of the plant [M\$]
R_{SN}	Steam to NG mole ratio in reforming reaction
S	Area of solar field [km ²]
SM	solar multiple
SR_f	Fossil fuel saving ratio
T/t	Temperature [K]/[°C]
TIT	Turbine inlet temperature [K]
TPC	Total plant cost [M\$]

U	Heat-transfer coefficient
VF	Vapor fraction
W	Power output [MW]
w	Specific work output [kJ/kg]
X_{sol}	Solar thermal share in total energy input

Greek symbols

β	Annual average investment coefficient
η_{col}	Solar collector efficiency
ϵ	Exergy efficiency
η	Thermal efficiency
η_{sol}	Net solar-to-electricity efficiency

Subscripts and superscripts

a	Ambient state
col	Solar collector
f	Fuel
in	Input
net	Net value
om	Operation and maintenance
rad	Radiation
ref	Reference system
sol	Solar heat
tr	Heat transfer

advanced combined cycle power system. The system simulation showed that the solar heat share and system exergy efficiency of the Solar CC were 18% and 60.7%, respectively [8]. The methane-steam reforming reaction is highly endothermic and requires a high temperature (above 800 °C with Ni-based catalyst) to obtain a reasonably high methane conversion. Methane conversion does not occur for temperatures <330 °C [10]. Research of solar thermochemical technology with methane conversion is therefore mainly focused on high temperature solar heat application (900–1000 °C) [11–14].

To integrate low/mid-temperature solar heat (below 400 °C) into methane-steam reforming and achieve its chemical conversion, Zhang and Lior proposed the concept of indirect upgrading of low/mid level solar heat [15,16]. Rather than driving the endothermic reforming reaction directly, the solar thermal energy collected at ~220 °C is used for water evaporation and thus first transformed into the latent heat of vapor supplied to a reformer and then via the reforming reactions to the produced syngas chemical exergy. It is a two-step conversion, a combination of thermal integration and thermo-chemical conversion. A hybrid solar assisted chemically recuperated gas turbine (SOLRGT) system was proposed to embody this concept, in which the produced syngas is burned to provide high temperature working fluid to a gas turbine. The solar-driven steam production helps improve both the chemical and thermal recuperation of the system. That study shows that compared to an intercooling chemically recuperated gas turbine cycle (IC-CRGT) without solar assistance, the overall exergy efficiency could be about 5.6%-points higher. Because of the replacement of partial fossil fuel with solar heat input, the SOLRGT attains a reduced specific CO₂ emission of 343 g/kWh compared with a reference system with the same configuration but without solar assistance [16].

In the SOLRGT system, the low concentration of CO₂ (2.9% mol) in the flue gas and the low methane conversion rate (37.8%) in the reformer make neither the post- nor the pre-combustion decarbonization attractive for this application. Because of the introduction of large amount of steam, the mixing

exergy loss between steam and air in the combustor is large. In addition, the turbine working fluid is vapor-rich (~25% mol), and it is exhausted at a relatively high temperature. A large amount of steam latent heat is dumped to the environment, leading to a high flue gas exergy loss. This suggests that the exergy loss may be reduced by recycling part of the flue gas so as to bring its latent heat back to the combustor as done in some oxy-fuel combustion power systems [17–22]. In [23], an exergy analysis was conducted to identify the exergy loss in each main component of the system and the potential for improvement, and the major exergy losses were confirmed to be in the combustion, the turbine and compressors, and in the flue gas exhaust. Guided by the exergy analysis results, an improved system configuration with oxy-fuel combustion and CO₂ capture (named ZE-SOLRGT) was thus proposed in [23] with steam as its main working fluid, but without a detailed analysis. It is a solar assisted oxy-fuel combustion cycle, and the power section is configured on a Graz-like cycle to take advantage of the combination of a high-temperature Brayton topping cycle with a high-pressure ratio Rankine like bottoming cycle.

Integrated with solar heat driven steam generation and methane reforming process, the ZE-SOLRGT (zero CO₂ emission SOLRGT) system is featured with indirect upgrading of low-mid temperature solar heat and indirect combustion of fossil fuel with cascade release of chemical exergy, conjoining each other at the reforming process. Attention has been paid to the integration of turbine exhaust heat recovery in both reforming and steam-generation processes. In this paper, the system is simulated with ASPEN PLUS software [24], thermodynamic performances are analyzed and discussed, and a preliminary economic estimation is also preformed. With nearly 100% CO₂ capture, the system attains a net energy efficiency of 50.7% (with accounting for the energy needed for oxygen separation). The cost of electricity (COE) and the payback period of ZE-SOLRGT are found to be \$0.056/kWh and 11.3 years (including 2 years of construction), respectively. The results demonstrate the advantages of system integration with multiform energy inputs.

2. System configuration description

As depicted in Fig. 1, the layout of the ZE-SOLRGT system can be divided into the following five sections: fuel reforming process, combustion, power generation, steam generation (stream 19–23), and CO₂ compression (stream 26–28). Fig. 2 is the t – s diagram of ZE-SOLRGT, which shows the combination of the Brayton-like topping cycle with the Rankine-like bottoming cycle, and the integration of solar heat driven steam generation.

The power generation section is configured based on the Graz cycle [19–22]. With steam as the main working fluid, the solar heat collection can be easily integrated for steam generation. The main merit of this configuration is the combination of a high-temperature Brayton topping cycle with a high-pressure ratio Rankine-like bottoming cycle, thus the cycle has both a high heat absorption temperature and a low heat release temperature. In addition, the steam bottoming cycle has the advantage of high-pressure ratio and low backpower ratio. All these features contribute to the system efficiency improvement and depletable fossil fuel saving.

As shown in Fig. 1, the system has two gas turbines (high-pressure gas turbine HPT and low-pressure gas turbine LPT) and one high-pressure steam turbine (HPST). The high-temperature combustion gas first flows through HPT. The HPT flue gas is composed of 90.3% H₂O and 8.5% CO₂ (mole fraction), and a small fraction of O₂, N₂ and Ar. After transferring heat to the reforming reaction and steam superheating in turn, it is split into two streams (streams 9 and 13). Stream 9 is recycled back to the combustor after being cooled by water preheating and compressed thus constitutes the “Brayton-like cycle”. Stream 13 is expanded further for power generation in LPT to a vacuum (0.082 bar), and its vapor component condensed. The combustion-generated CO₂ is separated and compressed to 110 bar (stream 27) in a separate seven-stage compressor with intercooling for further disposition. The excess water from combustion is drained, and the rest is recycled as the Rankine-like cycle working fluid (stream 17). It is pumped to the highest pressure of the cycle (~150 bar) and heated by retrieving heat from the Brayton-like cycle exhaust heat. Solar heat is

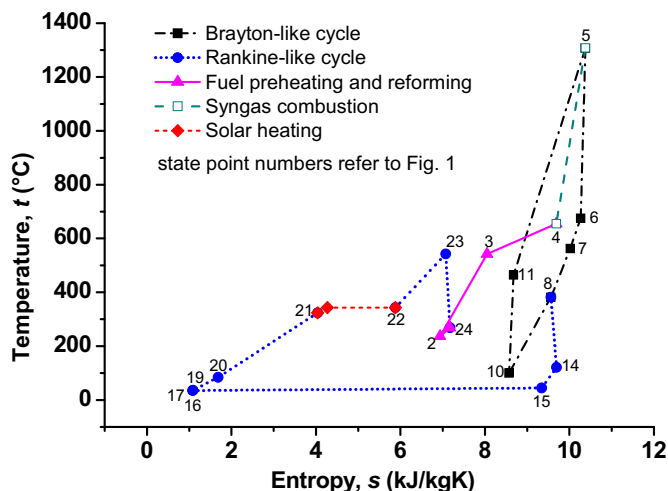


Fig. 2. The t – s diagram of the ZE-SOLRGT system.

introduced upstream of the steam superheater. The collected solar heat is used for water evaporation and produces saturated steam at a temperature of 343 °C.

Despite the overall high system pressure ratio (the HPST inlet pressure is 150 bar), the pressure ratios of the gas turbines HPT and LPT are only ~13.9 and ~12.6, respectively, similar to those in the standard air-based ones. While using steam as the working fluid, the HPST works more like a gas turbine, with the working fluid being always in the gaseous phase and with a pressure ratio of only ~10.

Open-loop steam cooling is adopted for the HPT blade cooling, and the coolant steam (25) is extracted from the HPST turbine outlet. Because of the higher specific heat capacity of steam than that of air, steam cooling is superior to air cooling in its reduction of coolant demand. Different from the steam injection to combustion in the Graz cycle, the remainder of the HPST outlet fluid is fed to the reforming reaction (stream 24), attaining a possibly highest H₂O/CH₄ ratio of 4.9 in the reformer. The reformer operates at

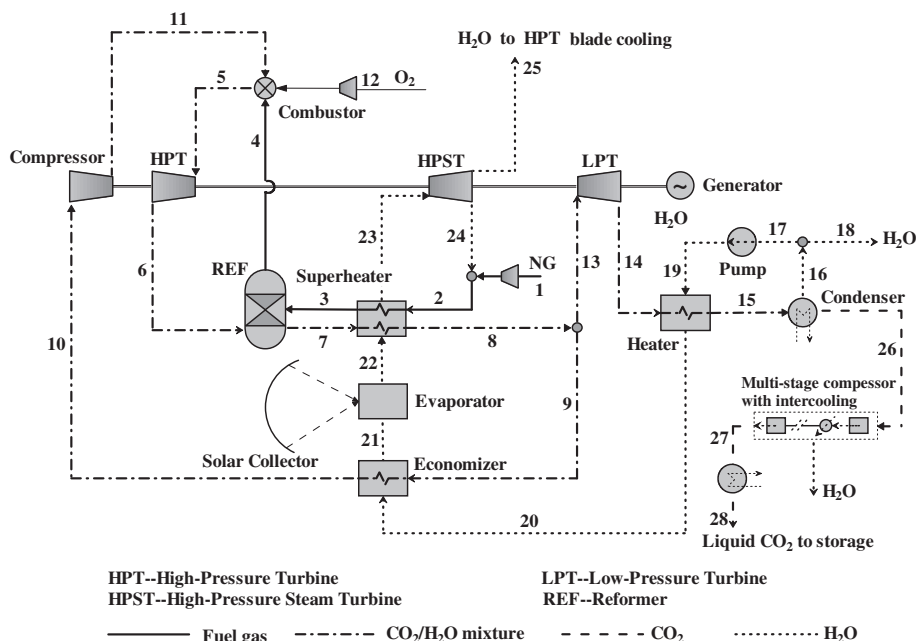


Fig. 1. Process flowsheet of the ZE-SOLRGT system.

a pressure of 19.2 bar, for which the conventional counterflow design with the reformer tubes filled with suitable catalyst could be adopted. Fuel gases flow through a packed bed, the high-pressure gas turbine (HPT) exhaust (stream 6–7) flows through the shell side to provide the heat necessary for reforming. The minimal heat transfer temperature difference inside the reformer is set to be 20 °C.

The reformed syngas serves as the fuel to the combustor. 2% excess O₂ beyond the stoichiometric rate is assumed for the syngas combustion. The oxygen is assumed to be produced in a conventional cryogenic vapor compression air separation plant with the specific energy consumption of 812 kJ/kgO₂ [18].

Restricted by the HPT exhaust temperature, the conversion ratio of CH₄ achieves 52%. Similar to that in a chemically recuperated gas turbine (CRGT) cycle, here reforming aims at improving fuel heating value by the turbine exhaust heat recuperation via the endothermic reaction of methane conversion to H₂ and CO. The reformed syngas together with the unreacted methane feeds as fuel to the combustor. This is different from that in the low-emission systems with pre-combustion decarbonization, in which the priority is on pursuing high methane conversion ratio.

The fuel methane is first converted to syngas via reforming and then to combustion products via combustion, which is therefore called “indirect combustion” where the fuel chemical exergy is released in a cascading manner. As will be explained in detail below, the indirect combustion reduces the combustion exergy loss as compared with the direct combustion of methane, by making more efficient use of the source fuel chemical exergy. Furthermore, it also allows the use of lower temperature energy sources, such as solar heat, to be integrated and upgraded thermo-chemically in a way that contributes to the overall energy input and thus reduces the use of fossil fuel and the associated undesirable emissions.

The concept of “Energy Level”, A , proposed by Ishida and co-workers [25,26] is used to evaluate the quality of released or accepted energy in an energy transformation process. It is defined as the ratio of exergy change ΔE to enthalpy change ΔH , i.e.

$$A = \Delta E / \Delta H = 1 - T_a \cdot \Delta S / \Delta H \quad (1)$$

The energy level of heat is $A = 1 - T_a / T$, where T_a is the environmental temperature and T is the temperature of the heat source. Similarly, the energy level of solar thermal energy may be expressed as $A_{sol} = 1 - T_a / T_{sol}$, where T_{sol} is the temperature of the collected solar heat.

Fig. 3 shows the upgrading of the low/mid temperature solar heat and cascade release of the fossil fuel chemical exergy. On the solar heat side, it first transforms into the steam latent heat in the process of steam generation, experiencing the energy level drop from A_{sol} to A_s ; and then in the steam reforming process, the generated steam takes part in the chemical reaction in which the energy level of steam is elevated to that of the syngas chemical exergy A_{syn} . At the same time, the reforming reaction absorbs heat from turbine exhaust and converts it into the syngas chemical exergy as well. On the fossil fuel side, the fossil fuel is first converted into syngas in the reforming process, experiencing an energy level drop from A_f to A_{syn} . Then in the process of combustion, the syngas chemical exergy converts into thermal exergy, and the energy level drops to that of the combustion produced thermal heat A_T . Thus both solar heat and fossil fuel chemical exergy experience a two-step conversion, and they conjoin each other in the process of reforming which functions like a lever, the upgrading of the steam energy level is at the cost of the degrading of fuel energy level from methane to syngas. The cascade release of fuel chemical exergy on one side reduces the energy level drop in the combustion process from $(A_f - A_T)$ of methane combustion to $(A_{syn} - A_T)$ of syngas combustion, the exergy destruction in the conversion from chemical into thermal energy is therefore lower in

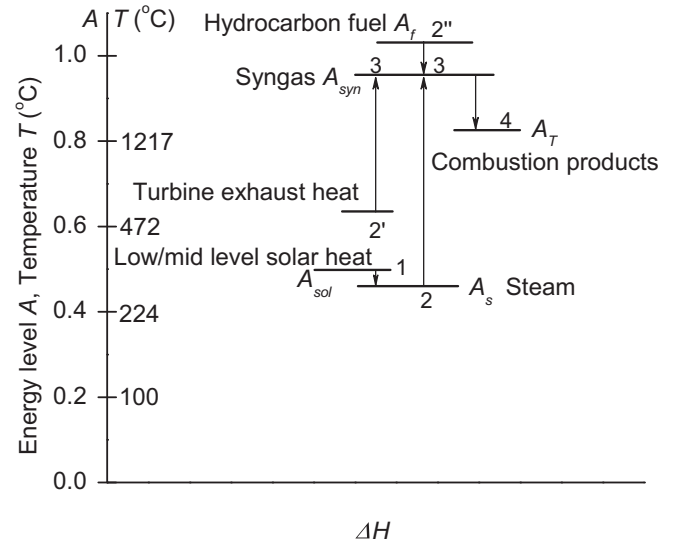


Fig. 3. Upgrading of low-mid temperature solar heat and cascade utilization of fossil fuel chemical exergy.

syngas combustion than that in the unreformed methane fuel combustion; it on the other side boost the upgrading of solar heat into syngas chemical exergy, enabling the low/mid solar heat collected at a relatively low expense to achieve a high-efficiency conversion into electricity in the advanced power system.

Besides the CO₂ capture with oxy-fuel combustion, major features of this ZE-SOLRGT system are summarized below:

1. Nearly 60% of the HPT flue gas is recycled back via a compressor to the combustor, bringing its internal heat back to the combustor. Only the rest of the working fluid is condensed and the condensation is at a temperature below 40 °C, so the associated exergy loss to the environment is relatively small.
2. Heat exchangers are arranged in a cascade manner according to their temperature levels, for reduction of irreversibility in the heat transfer process.
3. Due to input of solar heat, the temperature match in the turbine exhaust heat recuperation process has been improved since it releases heat only to a sensible heat sink with varying temperature, thus reducing the heat transfer exergy loss.
4. Indirect upgrading of low-mid temperature solar heat and its high efficiency conversion into electricity.
5. Indirect combustion with cascade fossil fuel chemical exergy release.

The indirect upgrading of solar heat has been explained in detail in [15,16]; the cascade utilization of fossil fuel chemical exergy is further explored in the following section.

3. Cascade release of fossil fuel chemical exergy

Fig. 4 illustrates two different ways of chemical energy release via methane combustion. The conventional direct combustion process is shown in Fig. 4a, while Fig. 4b depicts the indirect combustion process in the ZE-SOLRGT system, including water evaporation, methane-steam reforming, and combustion of syngas with enriched oxygen.

3.1. Exergy destruction in the direct combustion

For comparison, it is assumed that the direct and indirect combustions of methane proceed at the same temperature T , with

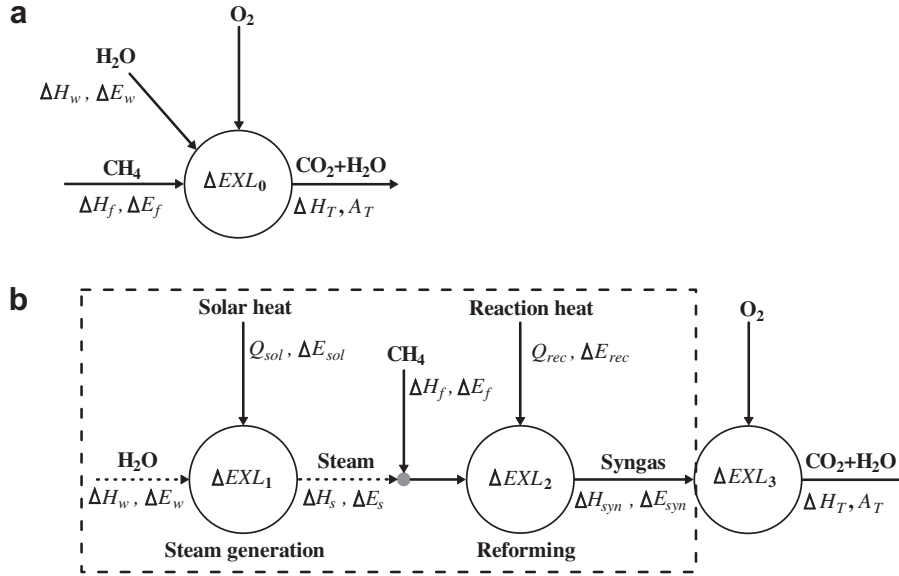


Fig. 4. Chemical energy release of methane: a) direct combustion way, b) indirect combustion way.

the same water input. The direct combustion process thus involves water heating and steam injection. Fig. 4a, however, shows only the inlet and outlet states of the combustion. For the direct combustion process (Fig. 4a), the energy balance and exergy balance are:

$$\Delta H_w + \Delta H_f = \Delta H_T \quad (2a)$$

$$\Delta E_w + \Delta E_f = \Delta E_T + \Delta EXL_0 \quad (2b)$$

where the subscripts w, f, T represent the water, fuel methane and combustion product, respectively. ΔEXL_0 is the exergy loss in the direct combustion process. ΔH_f and ΔE_f denote the released enthalpy and exergy of the methane combustion, ΔH_w and ΔE_w are the physical enthalpy and exergy brought in by water, and ΔH_T and ΔE_T are the thermal enthalpy and exergy contained in the combustion products. The reference state for this calculation is 25°C/1.013 bar.

For the definition of energy level A (1), we have,

$$\Delta E_w = \Delta H_w \cdot A_w \quad (3a)$$

$$\Delta E_f = \Delta H_f \cdot A_f \quad (3b)$$

$$\Delta E_T = \Delta H_T \cdot A_T \quad (3c)$$

Substituting (2a) and (3a–c) into (2b) gives,

$$\Delta EXL_0 = \Delta H_w \cdot (A_w - A_T) + \Delta H_f \cdot (A_f - A_T) \quad (4)$$

ΔEXL_0 represents the exergy destruction in the direct combustion caused by the energy level differences between the chemical energy provided by methane A_f , combustion products heat A_T , and the input water A_w .

3.2. Exergy destruction in the indirect combustion

The total chemical exergy loss in the indirect combustion of methane (Fig. 4b) includes three parts, ΔEXL_1 in steam generation, ΔEXL_2 in methane-steam reforming, and ΔEXL_3 in syngas combustion.

In the steam generation process, the water absorbs solar heat and converts it into the steam internal heat. The subscripts s and sol

represent the steam and solar heat, respectively. The energy balance and exergy balance for the steam generation process are,

$$\Delta H_w + Q_{sol} = \Delta H_s \quad (5a)$$

$$\Delta E_w + \Delta E_{sol} = \Delta E_s + \Delta EXL_1 \quad (5b)$$

Q_{sol} and ΔE_{sol} are the solar thermal energy and exergy absorbed by the system; ΔH_s and ΔE_s are the physical enthalpy and exergy of the produced steam; ΔEXL_1 is the exergy loss. From energy level definition, we get,

$$\Delta E_{sol} = Q_{sol} A_{sol} \quad (6a)$$

$$\Delta E_s = \Delta H_s A_s \quad (6b)$$

Substituting (5a), (6a), (6b) and (3a) into (5b), we obtain:

$$\Delta EXL_1 = Q_{sol} (A_{sol} - A_s) + \Delta H_w (A_w - A_s) \quad (7)$$

ΔEXL_1 represents the exergy destruction caused by the energy level difference between the provided solar heat A_{sol} and the steam generation, caused by the temperature difference between the heat donation and acceptance.

In the methane-steam reforming process, the reforming reaction receives heat Q_{rec} from the turbine exhaust. The energy conservation and the exergy balances are,

$$\Delta H_f + \Delta H_s + Q_{rec} = \Delta H_{syn} \quad (8a)$$

$$\Delta E_f + \Delta E_s + \Delta E_{rec} = \Delta E_{syn} + \Delta EXL_2 \quad (8b)$$

where Q_{rec} and ΔE_{rec} are the turbine exhaust heat and exergy absorbed by the reforming reaction; ΔH_{syn} and ΔE_{syn} denote the released enthalpy and exergy of the syngas combustion; ΔEXL_2 is the exergy loss. From the energy level definition, we obtain,

$$\Delta E_{rec} = Q_{rec} A_{rec} \quad (9a)$$

$$\Delta E_{syn} = \Delta H_{syn} A_{syn} \quad (9b)$$

Substituting Eqs. (8a) and (9a), (9b), (3b), (6b) into (8b),

$$\Delta \text{EXL}_2 = \Delta H_f (A_f - A_{\text{syn}}) + \Delta H_s (A_s - A_{\text{syn}}) - Q_{\text{rec}} (A_{\text{rec}} - A_{\text{syn}}) \quad (10)$$

ΔEXL_2 represents the exergy destruction caused by the energy level difference between heat donation and acceptance in the reforming reaction.

In the syngas combustion, the chemical exergy degrades into the thermal exergy, thus the exergy loss in the syngas combustion ΔEXL_3 can be expressed as,

$$\Delta \text{EXL}_3 = \Delta H_{\text{syn}} (A_{\text{syn}} - A_T) \quad (11)$$

The total exergy destruction in the indirect combustion is $\sum_{i=1}^3 \Delta \text{EXL}_i$.

We can derive the reduction of the chemical exergy loss in the indirect combustion of methane is:

$$\Delta \text{EXL}_0 - \sum_{i=1}^3 \Delta \text{EXL}_i = Q_{\text{sol}} \cdot (A_T - A_{\text{sol}}) + Q_{\text{rec}} \cdot (A_T - A_{\text{rec}}) \quad (12)$$

Since the temperature of combustion products is much higher than that of solar thermal energy and the reforming temperature, the energy level A_T is larger than A_{sol} and A_{rec} . Hence, the value expressed by (12) is always positive, which means that the chemical exergy loss of indirect combustion is lower than that of direct combustion. This reduction in exergy destruction increases the maximal available work of the combustion products.

It is interesting to notice that the reduction of the exergy loss includes two parts, the first part $Q_{\text{sol}} \cdot (A_T - A_{\text{sol}})$ comes from indirect upgrading of solar heat; and the second part $Q_{\text{rec}} \cdot (A_T - A_{\text{rec}})$ comes from the upgrading of reforming absorbed heat. Both convert into the combustion-produced high temperature heat, and achieve the high efficiency conversion into electricity in the power system.

4. The computation model and its validation

4.1. Main assumptions for the simulation

The proposed system was simulated with the ASPEN PLUS software [24]. The component models are based on energy balance, mass balance and species balance, with the default relative convergence error tolerance of 0.01%, which is the specified tolerance for all tear convergence variables. The RK-SOAVE and STEAM-TA physical properties (available in ASPEN PLUS) were selected for dealing with the processes where the working media are gas and water respectively [15,16,27].

In the solar block of ZE-SOLRGT, the solar field is assumed to be installed with the SEGS (Solar Energy Generating Systems) LS-2 parabolic trough solar collectors, and the heat transfer fluid (HTF) is taken as the Therminol VP-1 synthetic oil (Vapor Phase/Liquid Phase heat transfer fluid by Solutia) [28–32]. At the design point (basic cycle), the solar collector efficiency η_{col} is chosen to be the peak efficiency and mainly decided by the DNI (direct solar radiation) and temperature of the solar concentrators [33,34]; the DNI (944.5 W/m^2) refers to the measured value at noon in the summer solstice day, Barstow, California [35].

For longer operating time of the system, solar thermal storage section was introduced, in which a molten salt is chosen to be the heat accumulation medium [28–34]. The solar multiple (SM) is defined as the ratio between the thermal power produced by the solar field ($Q_{\text{th,solar field}}$) at the design point and the insolation of the solar power block at nominal conditions (Q_{rad}) [29–31],

$$\text{SM}_{\text{design point}} = \left(Q_{\text{th,solar field}} / Q_{\text{rad}} \right)_{\text{design point}} \quad (13)$$

This parameter represents the thermal storage capacity of the solar field. In this paper, SM is chosen to be 1.4 to achieve nominal conditions in the power block during a time interval longer than the one obtained if SM was equal to 1.0 [32].

Some properties of feed streams are reported in Table 1, the main assumptions for simulations are summarized in Table 2, and the same system assumptions and conditions were also used in [15,16,23].

4.2. Model validation

The reforming reaction is the key process of energy conversion in the ZE-SOLRGT system; it associates the indirect upgrading of solar heat with the cascade release of fossil fuel chemical exergy. Besides the combustor, it is the only component which involves complicated chemical reactions. We believe that the precision of the reformer simulation is the key to the whole system simulation. In this paper, the reformers are simulated with the Gibbs Reactor module available in the ASPEN PLUS model library, which determines the equilibrium conditions by minimizing the Gibbs free energy [15,16,27]. To validate the simulation, we have simulated the reforming reactions under different temperatures and pressures, and compared the results with that from the literature. Table 3 reports the reforming product compositions and their heating values, and the results show good agreement with the data from literature.

5. System performance analysis and comparison

5.1. Performance criteria

The absorbed solar heat by steam generation at the design point is denoted as Q_{sol} ,

$$Q_{\text{sol}} = Q_{\text{rad}} \cdot \eta_{\text{col}} \cdot \eta_{\text{tr}} = \text{DNI} \cdot S_0 \cdot \eta_{\text{col}} \cdot \eta_{\text{tr}} \quad (14)$$

where Q_{rad} is the entire insolation energy to the solar field at the design state; DNI is the direct solar radiation, S_0 is the area of the solar field without considering heat storage, η_{col} is the solar collector efficiency, η_{tr} is the heat transfer efficiency from the heated fluid in the solar block to the power cycle working fluid.

The contribution of the low/mid-temperature solar heat can be measured by its share in the system total energy input,

$$X_{\text{sol}} = Q_{\text{sol}} / (Q_f + Q_{\text{sol}}) = Q_{\text{sol}} / (m_f \cdot \text{LHV} + Q_{\text{sol}}) \quad (15)$$

where $Q_f = m_f \times \text{LHV}$ is the fuel low-heating-value input.

To give an overall assessment of ZE-SOLRGT, the thermal efficiency is defined as,

$$\eta = W_{\text{net}} / (Q_f + Q_{\text{sol}}) = W_{\text{net}} / (m_f \cdot \text{LHV} + Q_{\text{sol}}) \quad (16)$$

Table 1
Composition and some properties of feed streams.

Items	Natural gas	Oxygen
	Zhang et al., 2008 [27]	Zhang et al., 2008 [27]
CH ₄ (mol%)	100	–
N ₂ (mol%)	–	2
O ₂ (mol%)	–	95
Ar (mol%)	–	3
Temperature (°C)	25	25
Pressure (bar)	4.93	2.38
Lower heating value (kJ/kg)	50,030	–
Power consumption for O ₂ production (kJ/kg)	–	812

Table 2

Main assumptions for the simulation and calculation.

Configurations	Parameters	Value	Source
Gas turbine	HPT inlet temperature/pressure	1308 °C/14.5 bar	Zhang and Lior, 2012 [16]
	HPT isentropic efficiency	89%	Zhang and Lior, 2012 [16]
	LPT inlet temperature/pressure	382 °C/1.03 bar	Zhang and Lior, 2012 [16]
	LPT isentropic efficiency	90%	Zhang and Lior, 2012 [16]
Steam turbine	HPST inlet temperature/pressure	542 °C/150 bar	Zhang and Lior, 2012 [16]
	HPST isentropic efficiency	90%	Zhang and Lior, 2012 [16]
Condenser	Pressure	0.08 bar	Zhang and Lior, 2012 [16]
Reformer	Pressure	19.2 bar	Zhang and Lior, 2012 [16]
	Pressure drop (cold side)	10%	Zhang and Lior, 2012 [16]
	Pressure drop (heat side)	2%	
	Minimal heat transfer temperature difference gas/gas	20 °C	Zhang and Lior, 2012 [16]
Steam generation process	Pressure drop (of inlet pressure)	3%	Zhang and Lior, 2012 [16]
	Minimum heat transfer temperature difference gas/liquid	15 °C	Zhang and Lior, 2012 [16]
	Solar collector temperature	343 °C	Pitz-Paal et al., 2005 [31]
Parabolic trough solar collector (peak point) and evaporator	Solar collector efficiency	68.1%	Odeh et al., 1998 [32]
	DNI	944.5 W/m ²	TRNSYS, 2010 [34]
	Solar multiple	1.4	Pitz-Paal et al., 2005 [31]
	Minimal heat transfer temperature difference in evaporator	20 °C	Zhang and Lior, 2012 [16]
	Heat transfer efficiency	0.95	Pitz-Paal et al., 2005 [31]
	Isentropic efficiency	88%	Zhang and Lior, 2012 [16]
Compressor	Isentropic efficiency	85%	Zhang and Lior, 2012 [16]
O ₂ compressor	Pressure drop (of inlet pressure)	3%	Zhang and Lior, 2012 [16]
Combustor	Excess O ₂ (of inlet O ₂ mass flow)	2%	Zhang and Lior, 2012 [16]
	Stage number	7	Zhang and Lior, 2012 [16]
Multi-stage compressor for CO ₂ compression	Stage isentropic efficiency	80%	Zhang and Lior, 2012 [16]
	Intercooler temperature	35 °C	Zhang and Lior, 2012 [16]
	Efficiency	85%	Zhang and Lior, 2012 [16]
Pump	Temperature	25 °C	
Ambient state	Pressure	1.013 bar	

where W_{net} is the net electricity power output of the hybrid system. The exergy efficiency ε is,

$$\varepsilon = W_{\text{net}} / (E_f + E_{\text{sol}}) = W_{\text{net}} / [m_f \cdot e_f + Q_{\text{sol}} \cdot (1 - T_a / T_{\text{sol}})] \quad (17)$$

where the methane fuel exergy is approximately 1.05 fold of the fuel low heating value, i.e. $E_f = 1.05Q_f$; the exergy of the solar heat at a temperature of T_{sol} is calculated as the maximal work availability between T_{sol} and the ambient temperature T_a [15,16].

To assess the performance of solar heat conversion in the hybrid system, the following net solar-to-electricity efficiency is defined as,

$$\eta_{\text{sol}} = (W_{\text{net}} - W_{\text{ref}}) / Q_{\text{rad}} = (W_{\text{net}} - Q_f \cdot \eta_{\text{ref}}) / Q_{\text{rad}} \quad (18)$$

in which W_{ref} is the power output generated by the reference system with same fossil fuel input ($W_{\text{ref}} = Q_f \times \eta_{\text{ref}}$). The reference system in this study is chosen to be the conventional dual-pressure reheat combined cycle with post-combustion amine-absorption decarbonisation (CC-PC) [18].

In addition, because of the replacement of part of the fossil fuel with solar heat input, the fossil fuel saving ratio SR_f is defined as,

$$SR_f = (Q_{\text{ref}} - Q_f) / Q_{\text{ref}} = 1 - Q_f / (W_{\text{net}} / \eta_{\text{ref}}) = 1 - W_{\text{ref}} / W_{\text{net}} \quad (19)$$

where the numerator ($Q_{\text{ref}} - Q_f$) is the fossil fuel saving in comparison with the reference system, for generating the same amount of electricity ($Q_{\text{ref}} = W_{\text{net}} / \eta_{\text{ref}}$).

5.2. System performance and discussions

Using the computational assumptions and models given in Section 4.1, the ZE-SOLRGT and CC-PC systems were simulated and compared with the same NG input (1 kmol/s). For CC-PC, the CO₂ removal section consists essentially of an absorber and stripper. The

solution for CO₂ absorption is 40 wt% methyl diethanolamine (MDEA) and it is assumed 90% of the CO₂ is captured. The rich solution from the absorber is preheated by lean solution and regenerated in the stripper by extracting heat from the low-pressure (LP) steam upstream of the LP steam turbine. The minimal temperature differences in the preheater and reboiler are chosen to be about 10 °C [18,38]. The captured CO₂ is compressed to 110 bar for transportation and storage.

The stream state parameters for ZE-SOLRGT are reported in Table 4. The overall performances of the ZE-SOLRGT and CC-PC systems are summarized in Table 5 and Table 6. In ZE-SOLRGT and CC-PC systems, the NG energy input (802.6 MW) and HPT inlet temperature (1308 °C) are all the same.

In the ZE-SOLRGT system, solar heat contributes an additional 18% to the total energy input leading to a much higher power

Table 3

Validation of the reformer simulation.

Items	Lozza, 2002 [36]	Simulation results	Kesser, 1994 [37]	Simulation results
Reformer inlet state				
P [bar] ^a	1.15		21.3	
t [°C] ^a	565		207.9	
m [kg/s] ^a	60.6		0.165	
H ₂ O mole fraction ^a	0.747		0.859	
CH ₄ mole fraction ^a	0.230		0.141	
N ₂ mole fraction ^a	0.011		—	
Reformer exit state				
P [bar] ^a	1.15		19.1	
t [°C] ^a	700		575.9	
H ₂ O mole fraction	0.267	0.292	0.68	0.678
CH ₄ mole fraction	0.006	0.005	0.081	0.077
N ₂ mole fraction	0.007	0.008	—	—
CO mole fraction	0.092	0.083	0.004	0.004
CO ₂ mole fraction	0.072	0.073	0.045	0.046
H ₂ mole fraction	0.555	0.540	0.19	0.196
Reformer heat duty [kJ/kg]	—	3023	—	1464

^a Input data to the simulation.

output by 28.8% as compared with that in the CC-PC system (496 MW vs. 385 MW), resulting to a thermal efficiency of 50.7% with nearly 100% CO₂ capture. For the combined cycle system, the thermal efficiency drops from 55% to 48% taking into account the energy penalty for ~90% CO₂ capture rate. The net solar-to-electricity efficiency, which is an indicator of solar heat conversion performance in the hybrid system, is found to be 40.6%, much higher than that in the solar-alone system operating at the same temperature level. For generating the same electricity as the referenced CC-PC system, the fossil fuel saving ratio in ZE-SOLRGT reaches 22.4%.

An exergy analysis was performed in [23]. The exergy efficiency of the ZE-SOLRGT system is found to be 53%, 7.3 %-points higher than that of CC-PC system. The difference between the thermal and exergy efficiencies in the hybrid system is mainly due to the fact that the exergy input of solar thermal energy is much lower than its corresponding heat input at a relatively low temperature level (343 °C). The largest exergy loss takes place in the combustion process, and the turbines and compressor, which are 22% and 7.6% of the system input exergy, respectively. Because only ~40% of the HPT working fluid is condensed at a relatively low temperature (the other 60% of the working fluid is recycled via compression, thus taking their internal heat back to the combustor), the exergy loss to the environment is 4.2% of the system input exergy.

The *t*–*Q* diagrams of the steam generation and superheating processes in the ZE-SOLRGT and CC-PC systems are shown in Fig. 5 and Fig. 6, respectively. In both systems the turbine exhaust heat is recovered in a high to low temperature cascade. In the ZE-SOLRGT system, the arrangement of the higher pressure (higher heat capacity) but lower mass flow rate fluid on the Rankine cycle side in the heat recovery section, with the lower pressure (lower heat capacity) but higher mass flow rate fluid on the Brayton cycle side, is intended for reducing heat transfer irreversibility in the heat exchangers. In addition, the isothermal evaporation process of water is heated by solar thermal energy and thus the turbine

Table 5

Breakdown of power generation and consumption in % of input energy for the ZE-SOLRGT and CC-PC systems.

Items	ZE-SOLRGT system			CC-PC system	
	MW	%		MW	%
Natural gas LHV input	802.62	82.0	100	802.62	100
Solar heat input	176.37	18.0		—	—
HPT turbine	651.46	66.5		618.12	77.0
LPT turbine	110.96	11.3		—	—
HPST turbine	79.86	8.16		121.59	15.2
Compressor	226.77	23.2		331.12	41.3
Pump	2.90	0.30		1.44	0.18
CO ₂ compression	35.21	3.60		17.39	1.79
O ₂ production	56.07	5.73		—	—
O ₂ compression	15.13	1.55		—	—
Generator and mechanical loss	10.12	1.03		7.86	0.98
Net power output	496.07	50.7		384.90	48.0

exhaust heat just provides sensible heat for the variable temperature heat-sink in the reformer, superheater and economizer. This helps achieve a good thermal match between the heating and heated streams and reduced heat transfer exergy loss of 2.7% of the system input exergy.

6. Economic analyses

6.1. Evaluation of the total plant cost TPC

For the designed ZE-SOLRGT system with a capacity of 496 MW and an efficiency of 50.7% (shown in Tables 5 and 6), a preliminary economic analysis was carried out based on following assumptions:

- 1) Price of methane is 0.144 \$/Nm³ for power generation [39].
- 2) The price of electricity is 0.08 \$/kWh [40].
- 3) The plant life *n* is 30 years [29–34].

Table 4

Stream states of the ZE-SOLRGT system.

No.	<i>t</i> (°C)	<i>p</i> (bar)	<i>m</i> (kg/s)	VF	Molar composition							
					N ₂	O ₂	H ₂ O	H ₂	CH ₄	CO ₂	CO	Ar
1	25	4.93	16.0	1	0	0	0	0	1	0	0	0
2	237.2	21.33	104.2	1	0	0	0.83	0	0.17	0	0	0
3	542.4	21.12	104.2	1	0	0	0.83	0	0.17	0	0	0
4	654.6	19.2	104.2	1	0	0	0.572	0.283	0.07	0.06	0.015	0
5	1308	14.55	519.6	1	0.004	0.004	0.888	0	0	0.098	0	0.006
6	674.6	1.05	587.0	1	0.004	0.003	0.903	0	0	0.085	0	0.005
7	562.4	1.04	587.0	1	0.004	0.003	0.903	0	0	0.085	0	0.005
8	381.9	1.03	587.0	1	0.004	0.003	0.903	0	0	0.085	0	0.005
9	381.9	1.03	346.3	1	0.004	0.003	0.903	0	0	0.085	0	0.005
10	100.3	1.02	346.3	1	0.004	0.003	0.903	0	0	0.085	0	0.005
11	464.3	15	346.3	1	0.004	0.003	0.903	0	0	0.085	0	0.005
12	25	2.38	69.1	1	0.02	0.95	0	0	0	0	0	0.03
13	381.9	1.03	240.7	1	0.004	0.003	0.903	0	0	0.085	0	0.005
14	121.4	0.08	240.7	1	0.004	0.003	0.903	0	0	0.085	0	0.005
15	45.1	0.08	240.7	1	0.004	0.003	0.903	0	0	0.085	0	0.005
16	35	0.08	168.6	0	0	0	1	0	0	0	0	0
17	35	0.08	155.6	0	0	0	1	0	0	0	0	0
18	35	0.08	13.0	0	0	0	1	0	0	0	0	0
19	36.1	157.5	155.6	0	0	0	1	0	0	0	0	0
20	84	156	155.6	0	0	0	1	0	0	0	0	0
21	323.8	154.5	155.6	0	0	0	1	0	0	0	0	0
22	342.9	151.5	155.6	1	0	0	1	0	0	0	0	0
23	542.4	150	155.6	1	0	0	1	0	0	0	0	0
24	268.8	21.33	88.1	1	0	0	1	0	0	0	0	0
25	230.7	15	67.4	1	0	0	1	0	0	0	0	0
26	35	0.08	72.1	1	0.018	0.016	0.527	0	0	0.412	0	0.027
27	35	110	49.1	1	0.037	0.035	0.002	0	0	0.87	0	0.056
28	16.6	110	49.1	0	0.037	0.035	0.002	0	0	0.87	0	0.056

Table 6
Thermal performances of the ZE-SOLRGT and CC-PC systems.

Items	ZE-SOLRGT	CC-PC
Mole flow rate of NG input [kmol/s]	1	1
Steam to NG mole ratio in reformer, R_{SN}	4.89	—
Carbon conversion rate of NG	51.6%	—
Solar thermal share, X_{sol} [%]	18.02	—
Net solar-to-electricity efficiency, η_{sol} [%]	40.6%	—
Fossil fuel saving ratio, SR_f [%]	22.4%	—
Specific CO ₂ emission [g/kWh]	0	41.1
Net power output [MW]	496.07	384.90
Thermal efficiency, η [%]	50.7	48.0
Exergy efficiency, ϵ [%]	53.0	45.7

- 4) The interest rate is 8% [41,42].
- 5) The CO₂ credit price is assumed as 33 \$/ton [41,42].
- 6) The construction period is 2 years, and 50% of total investment cost is an interest-bearing loan [41,42].
- 7) The annual operating time H of the hybrid system depends on the capacity of the solar heat subsystem.

The total plant cost (TPC) estimation of ZE-SOLRGT is listed in Table 7. The TPC consists of the equipment costs and the balance of plant (BOP). The BOP contains the remaining components, and structures that comprise a complete power plant or energy system that is not included in the prime mover. For a power generation system, the BOP is usually assumed to be 15% of the known component cost [41–44].

The cost of the solar field is evaluated as the area multiplied by the unit price. Considering the solar multiple (SM), the actual surface area S is larger by SM fold:

$$S = SM \cdot Q_{rad} / DNI = (SM \cdot Q_{sol}) / (DNI \cdot \eta_{col} \cdot \eta_{tr}) \quad (20)$$

where the heat transfer efficiency η_{tr} is 0.95 [34].

The annual running hours H of the hybrid systems are calculated from,

$$H = S \cdot I \cdot \overline{\eta_{col}} \cdot \eta_{tr} / Q_{sol} = SM \cdot I \cdot \overline{\eta_{col}} / (\eta_{col} \cdot DNI) \quad (21)$$

where $\overline{\eta_{col}}$ is the annual average collector efficiency. In the base cycle, $\overline{\eta_{col}}$ of the parabolic trough solar collector is 45.6% [34]. The annual solar radiation I is taken as 2717 kWh/(m²·y) [30,31]. As a result, the H is calculated to be 2914 h/y.

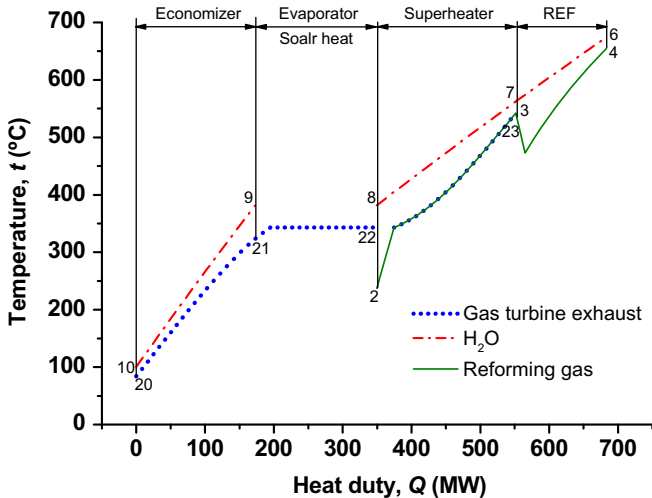


Fig. 5. The t - Q diagrams of the ZE-SOLRGT system.

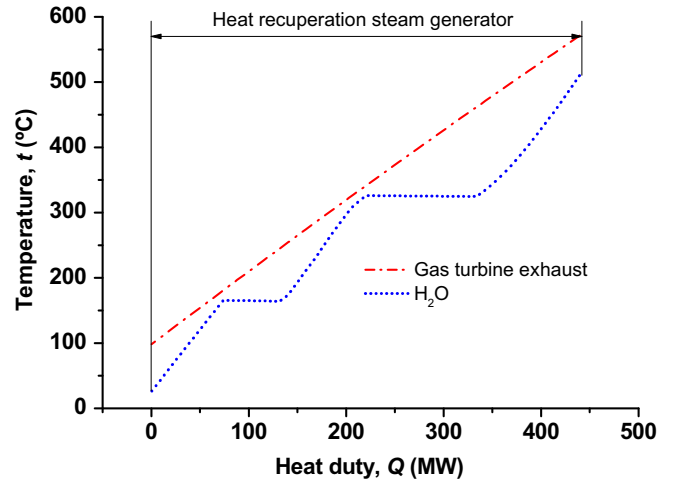


Fig. 6. The t - Q diagram of the referenced CC-PC system.

The estimation of other component costs is explained in the footnotes of Table 7. From Table 7 we can find that the TPC for ZE-SOLRGT is about 954.2 \$/kW, and the solar field and turbines are the two most expensive parts of the whole system.

6.2. Evaluation of the electricity cost COE and payback period PBP

The cost of electricity COE is calculated by,

$$COE = (\beta \cdot TPI + C_{om} + C_f - C_{CO_2}) / (H \cdot W_{net}) \quad (22)$$

where the numerator is the average annual electricity cost. TPI is the total plant investment, with the consideration of interest rate and the 2 years construction period. β is the average annual investment coefficient, a function of the interest rate i and plant life n :

$$\beta = i / [1 - (1 + i)^{-n}] \quad (23)$$

C_{om} is the annual O&M cost of the systems. The term O&M represents the cost of operating and maintenance, assumed to be 4% of the first capital cost of the system [41–44]. It covers both fixed and variable parts. Fixed O&M consists primarily of plant operating labour. Variable O&M represents periodic inspection, replacement, repair of system components (i.e., solar collector, turbine, etc.), and consumables (i.e., water, catalyst, etc.) [46,47].

C_f is the annual fuel cost of the hybrid system; W_{net} is the power output.

C_{CO_2} is the annual CO₂ credit, defined as the capture amount multiplied by the credit price.

The payback period PBP is the time by which the current value of all the revenue becomes equal to that of the total plant investment [41,42]:

$$R \cdot [(1 + i)^{PBP} - 1] / [i(1 + i)^{PBP}] = TPI \quad (24)$$

where R is the annual net revenue of the plant:

$$R = R_e - C_f - C_{om} + C_{CO_2} \quad (25)$$

R_e is the annual revenue of the net power product, defined as the electricity output multiplied by the electricity price.

Table 8 presents the economic analysis results. With a thermal solar share of 18.0%, the COE (cost of the electricity) is 0.056 \$/kWh and the PBP (payback period) is 11.3 years (including two years of construction).

Table 7
Investment cost of the ZE-SOLRGT system.

Items	ZE-SOLRGT	Percentage
Power block (BOP included)		
Air separation unit (10^6 \$) ^a	109.3	23.1%
Gas turbines and steam turbine (10^6 \$) ^b	140.0	29.6%
Heat exchangers (10^6 \$) ^c	31.1	6.6%
Compressors (10^6 \$) ^d	13.9	2.9%
Reformer (10^6 \$) ^e	9.5	2.0%
Solar block (BOP included)		
Solar field (10^6 \$) ^f	134.0	28.3%
Thermal storage system (10^6 \$) ^g	29.3	6.2%
Solar evaporator (10^6 \$) ^h	1.2	0.3%
Land cost (10^6 \$) ⁱ	5.1	1.1%
Total plant cost, TPC (10^6 \$)	473.4	100%
Specific cost (\$/kW)	954.2	—

^a The price is taken from [41,42], 1376×10^3 \$/(kg O₂/s).

^b The combustor and generators are included in this part. The unit cost of the gas turbine is taken from the simple cycle specifications of the PG9351FA model (GE company, 50 Hz) [45], and the Hangzhou Steam Turbine Work was consulted for the steam turbine cost.

^c The heat transfer area of each heat exchanger or condenser is calculated with the formula $A = Q/(U \cdot \Delta T)$. The heat duty Q and temperature approaches ΔT (taken as the mean logarithmic temperature difference) are calculated by ASPEN PLUS. The heat transfer coefficients U , and unit costs are taken from the research in [41,42].

^d The oxygen compressor, exhaust gas compressor and CO₂ compressors are all considered. According to [41,42], the unit price is 164.5×10^3 \$/(kg/s).

^e The Ni-based catalyst is used. It is not necessary to obtain an elevated conversion rate because the unconverted reactants are all used as fuel. Hence the unit cost of the reformer is quite lower than that of the high-temperature reforming reactor in traditional hydrogen-producing process. The cost is calculated with formula $C = C_0[S/(S_0)]^f$, where C_0 (39.8 M\$) is the cost of the reference component (reformer) of size S_0 (1377MW_{th}), and f is the scale factor 0.67 [43,44].

^f The solar field cost includes parabolic trough solar collectors and HTF fluid (Therminol VP-1), 288.4 \$/m² [28–32].

^g The nitrate salt inventory, tanks and oil-to-salt heat exchanger are included; the heat storage efficiency is taken as 0.95 [32]; the storage capacity achieves 3 h when the solar multiple SM is 1.4 [32]; and the unit cost is 12.06 \$/MJ [30].

^h The capacity is the heat duty of the oil-to-water heat exchanger, Q_{sol} . The unit cost is 5.6 \$/kW_{th} [31].

ⁱ The total area of the plant is amplified proportionally from the solar field area by 3.89 folds [32], and the unit cost is 2.8 \$/m² [32].

The electricity cost structure of the ZE-SOLRGT is shown in Fig. 7. It can be seen that the average annual total plant investment (TPI) occupies the largest part of the COE (46.4%), while the annual fuel and O&M (operation and maintenance) costs account for 34.5% and 19.1% respectively. In the subdivision graph of the TPI part, it is shown that the investments of the power block and solar block have played the most important economic roles. A parametric sensitivity analyses is conducted to investigate the influences of different parameters on COE and PBP.

Table 8
Economic analysis results of the ZE-SOLRGT system.

Items	ZE-SOLRGT
Annual operating time, H (h)	2914
Annual electricity output (10^6 kWh/y)	1446
Annual CO ₂ recovery (10^3 tons/y)	515
Annual natural gas consumption (10^6 Nm ³ /y)	235
Annual solar thermal energy input (10^6 kWh/y)	514
Total plant cost, TPC (10^6 \$)	473.4
Construction interest (10^6 \$)	39.4
Total plant investment, TPI (10^6 \$)	512.7
Annual income from produced electricity, R_e (10^6 \$/y)	63.1
Annual CO ₂ credit, C_{CO_2} (10^6 \$/y)	17.0
Annual fuel cost, C_f (10^6 \$/y)	33.8
Annual O&M cost, C_{om} (10^6 \$/y)	18.7
Payback period, PBP (y)	11.3
Cost of electricity, COE (\$/kWh)	0.056

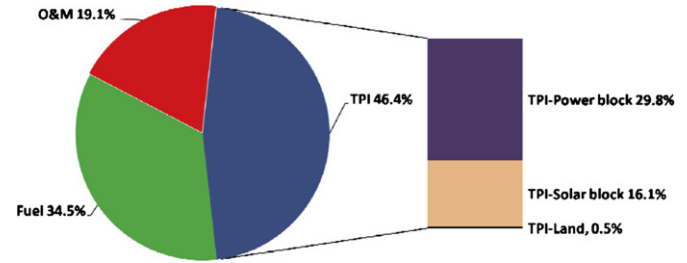


Fig. 7. The electricity cost structure of the ZE-SOLRGT system.

6.3. Parametric sensitivity analyses

Fig. 8 shows the influence of different parameters on COE. The total plant investment (TPI) is the most influential one, followed by NG price and CO₂ tax. For PBP, the electricity price has the most significant influence (Fig. 9), followed by the total plant investment (TPI).

When either CO₂ tax or natural gas price varies by about 20%, the electricity cost varies by about 8.3% and the payback period remains within 10–13 years. However, if TPI increases by 20%, the COE rises from 0.056 \$/kWh to 0.065 \$/kWh (nearly 16% variation), and the PBP rises from 11.3 years to 15.4 years. When the electricity price

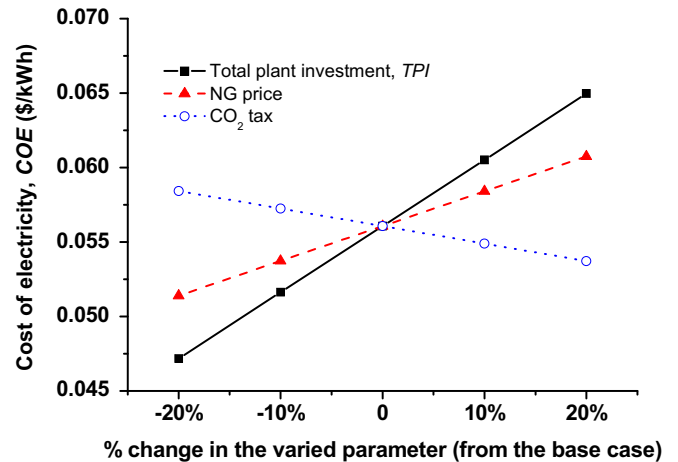


Fig. 8. The parametric sensitivity analyses of electricity cost COE.

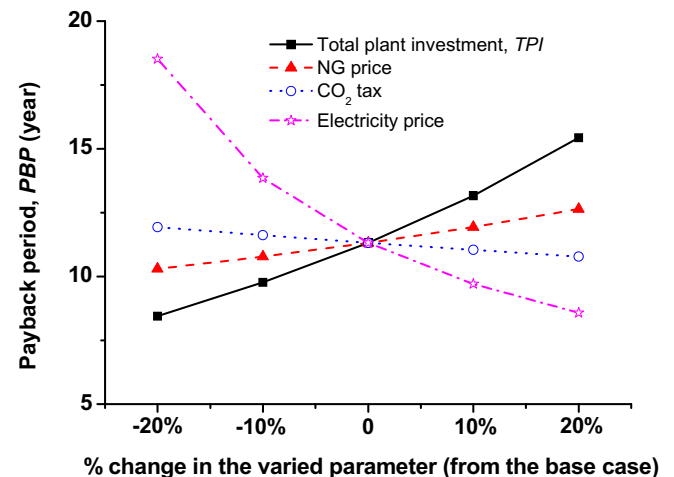


Fig. 9. The parametric sensitivity analyses of payback period PBP.

decreases to be equal to COE (0.056 \$/kWh), the PBP extends to be 32 years, the assumed plant life (30 years) plus the construction period (2 years). It can be seen the economic benefit of ZE-SOLRGT system mostly depends on the electricity pricing; obviously, the higher the electricity price is, the more profitable the solar hybrid system will be. At present, the CO₂ credit has not been implemented yet in China, which demands more practical experience and establishment of standard practices and regulations.

It is obvious that achieving a lower COE and shorter PBP requires improvements in the system efficiency and lowering of the equipment costs. It is important to develop relatively inexpensive parabolic trough solar collectors with higher collector efficiency. If instituted, a proper credit for CO₂ emissions abatement would improve the economic competitiveness of power generation from the hybrid system.

7. Conclusion

A novel hybrid solar-assisted integrated chemically recuperated gas turbine with oxy-fuel combustion was proposed as the new zero CO₂ emission hybrid system (ZE-SOLRGT). The power generation section of the system is configured as a Graz-like cycle, which combines a high temperature Brayton-like topping cycle and a high-pressure ratio Rankine-like bottoming cycle with water as the main working fluid.

The system features CO₂ capture with oxy-fuel combustion and cascade recuperation of turbine exhaust heat, and indirect upgrading of low-mid temperature solar heat and cascade release of chemical exergy in the indirect combustion of fossil fuel, which is explained by the energy level concept in this paper.

By integrating with steam generation, the collected mid-level solar heat of about 350 °C is first transformed into the latent heat of vapor supplied to the reformer and then via the reforming reactions to the produced syngas chemical exergy. This conversion on the solar heat side is conjoined with the conversion of fossil fuel chemical exergy into syngas chemical exergy, the latter is further transformed into high temperature thermal heat via combustion and accomplishes high efficiency conversion into electricity in the advanced CC power generation system. Solar heat input raises the system work output and reduces fossil fuel consumption.

The system was simulated and compared with a conventional dual-pressure reheat combined cycle with post-combustion decarbonisation (CC-PC). The low-mid temperature solar heat helps improve the thermal match in ZE-SOLRGT and raises the specific power output. The analysis shows that with a solar thermal share of 18.0% and nearly 100% CO₂ capture, the power output of ZE-SOLRGT is higher by 28.8% than that in the CC-PC system with the same fossil fuel input, and the exergy efficiency is 7.3 %-points higher. The net solar-to-electricity conversion efficiency attains 40.6%, which is much higher than that in the solar-only system at the same temperature level.

A preliminary economic analysis predicts the COE and PBP of the ZE-SOLRGT to be \$0.056/kWh and 11.3 years (including two years of construction), respectively. The ZE-SOLRGT system integration exhibits a successful complementary utilization of multiple energy resources and their high efficiency conversion into electricity.

Acknowledgments

The authors gratefully acknowledge the support of the National Natural Science Foundation of China (Grant Nos. 50836005, 51076152) and the National Basic Research Program of China ("973" Program) (Grant No. 2010CB227301).

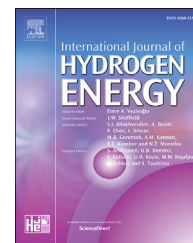
References

- [1] Lior N, Koai K. Solar-powered/fuel-assisted Rankine cycle power and cooling system: simulation method and seasonal performance. *J Solar Energy Eng* 1984;106:142–52.
- [2] Lior N, Koai K. Solar-powered/fuel-assisted Rankine cycle power and cooling system: sensitivity analysis. *J Solar Energy Eng* 1984;106:447–56.
- [3] Koai K, Lior N, Yeh H. Performance analysis of a solar-powered/fuel-assisted Rankine cycle with a novel 30hp turbine. *Solar Energy* 1984;32:753–64.
- [4] Buck R, Brauning T, Denk T, Pfander M, Schwarzbozl F, Tellez F. Solar-hybrid gas turbine-based power tower systems (REFOS). *J Solar Energy Eng* 2002;124:2–9.
- [5] Horn M, Hring H, Rheinla J. Economic analysis of integrated solar combined cycle power plants a sample case the economic feasibility of an ISCCS power plant in Egypt. *Energy* 2004;29:935–45.
- [6] Schwarzbo P, Buck R, Sugarmen C. Solar gas turbine systems design cost and perspectives. *Solar Energy* 2006;80:1231–40.
- [7] Dersch J, Geyer M, Herrmann U, Jones SA, Kelly B, Kistner R, et al. Trough integration into power plants - a study on the performance and economy of integrated solar combined cycle systems. *Energy* 2004;29:947–59.
- [8] Hong H, Jin H, Ji J. Solar thermal power cycle with integration of methanol decomposition and middle-temperature solar thermal energy. *Solar Energy* 2005;78:49–58.
- [9] Jin H, Hong H, Sui J, Liu Q. Fundamental study of novel mid- and low-temperature solar thermochemical energy conversion. *Sci China Ser E Eng Mater Sci* 2009;52:1135–52.
- [10] Abdallah H, Harvey S. Thermodynamic analysis of chemically recuperated gas turbines. *Int J Thermal Sci* 2001;40:372–84.
- [11] Tamme R, Buck R, Epstein M, Fisher U, Sugarmen C. Solar upgrading of fuels for generation of electricity. *ASME Trans J Solar Energy Eng* 2001;123:160–3.
- [12] Kodama T. High-temperature solar chemistry for converting solar heat to chemical fuels. *Prog Energy Combust Sci* 2003;29:567–97.
- [13] Zedtwitz P, Petrasch J, Trommer D, Steinfeld A. Hydrogen production via the solar thermal decarbonization of fossil fuels. *Solar Energy* 2006;80:1333–7.
- [14] Alexopoulos S, Hoffschmidt B. Solar tower power plant in Germany and future perspectives of the development. *Renew Energy* 2010;35:1352–6.
- [15] Zhang N, Lior N. Use of low/mid-temperature solar heat for thermochemical upgrading of energy, with application to a novel chemically-recuperated gas-turbine power generation (SOLRGT) system; 2009. ASME Paper IMECE2009-13037.
- [16] Zhang N, Lior N. Use of low/mid-temperature solar heat for thermochemical upgrading of energy, part I: application to a novel chemically-recuperated gas-turbine power generation (SOLRGT) system. *ASME J Eng Gas Turb Power*, 2012;134:072303-1–072303-14.
- [17] Mathieu P, Nihart R. Zero-emission MATIANT cycle. *ASME J Eng Gas Turb Power* 1999;121:116–20.
- [18] Kvamsdal HM, Jordal K, Bolland O. A quantitative comparison of gas turbine cycles with CO₂ capture. *Energy* 2007;32:10–24.
- [19] Jericha H, Gottlich E, Sanz W, Heitmeir F. Design optimization of the Graz cycle prototype plant. *ASME J Eng Gas Turb Power* 2004;126:733–40.
- [20] Jericha H, Sanz W, Gottlich E. Design concept for large output Graz cycle gas turbines. *ASME J Eng Gas Turb Power* 2008;130:011701.
- [21] Sanz W, Jericha H, Moser M, Heitmeir F. Thermodynamic and economic investigation of an improved Graz cycle power plant for CO₂ capture. *ASME J Eng Gas Turb Power* 2005;127:765–72.
- [22] Sanz W, Jericha H, Bauer B, Gottlich E. Qualitative and quantitative comparison of two promising oxy-fuel power cycles for CO₂ capture. *ASME J Eng Gas Turb Power* 2008;130:031702-1–031702-11.
- [23] Zhang N, Lior N, Luo C. Use of low/mid-temperature solar heat for thermochemical upgrading of energy, part II: a novel zero-emissions design (ZE-SOLRGT) of the solar chemically-recuperated gas-turbine power generation system (SOLRGT) guided by its exergy analysis. *ASME J Eng Gas Turb Power*, 2012;134:072301-1–072301-8.
- [24] Aspen Plus. Aspen technology, Inc., version 11.1, Available at: <http://www.aspentech.com/>, [accessed 30.09.10].
- [25] Ishida M, Kawamura K. Energy and exergy analysis of a chemical process system with distributed parameters based on the energy direction factor diagram. *Ind Eng Chem Process Des Dev* 1982;21:690–5.
- [26] Ishida M. Thermodynamics made comprehensible. New York: Nova Science; 2002.
- [27] Zhang N, Lior N. Two novel oxy-fuel power cycles integrated with natural gas reforming and CO₂ capture. *Energy* 2008;33:340–51.
- [28] Therminol VP-1. Solutia, Inc. Available at: <http://www.therminol.com/>, [accessed 09.30.10].
- [29] Geyer M, Lupfer E, Osuna R, Esteban A, Schiel W, Schweitzer A, et al. EURO TROUGH - parabolic trough collector family developed and qualified for cost efficient solar power generation. In: Proceedings of 11st international symposium on concentrating solar power and chemical technologies; 2002. Zurich, Switzerland. No.2009102502.
- [30] Herrmann U, Kelly B, Price H. Two-tank molten salt storage for parabolic trough solar power plants. *Energy* 2004;29:883–93.

- [31] Montes MJ, Abánades A, Martínez-Val JM, Valdes M. Solar multiple optimization for a solar-only thermal power plant, using oil as heat transfer fluid in the parabolic trough collectors. *Solar Energy* 2009;83:2165–76.
- [32] Pitz-Paal R, Dersch J, Milow B. European concentrated solar thermal road-mapping. The German Aerospace Center (DLR). Available at: http://www.pre.ethz.ch/publications/0_pdf/various/ECOSTAR_Executive_Summary.pdf; 2005 [accessed 30.09.10].
- [33] Odeh SD, Morrison GL, Behnia M. Modelling of parabolic trough direct steam generation solar collectors. *Solar Energy* 1998;62:395–406.
- [34] Price H. Assessment of parabolic trough and power tower solar technology cost and performance forecasts. America. National Renewable Energy Laboratory. Available at: <http://www.nrel.gov/docs/fy04osti/34440.pdf>; 2003 [accessed 30.09.10].
- [35] TRNSYS, A TRANSIENT systems simulation program, version 16, Available at: <http://sel.me.wisc.edu/trnsys/>, [accessed 30.09.10].
- [36] Lozza G, Chiesa P. Natural gas decarbonization to reduce CO₂ emission from combined cycles—part II: steam-methane reforming. *ASME J Eng Gas Turb Power* 2002;124:89–95.
- [37] Kesser KF, Hoffman MA, Baughn JW. Analysis of a basic chemically recuperated gas turbine power plant. *ASME J Eng Gas Turb Power* 1994;116:277–84.
- [38] Zhang N, Lior N. Comparative study of two low CO₂ emission power generation system options with natural gas reforming. *ASME J Eng Gas Turb Power* 2008;130:051701-1–051701-11.
- [39] U.S. Energy Information Administration. Natural gas weekly update. Available at: <http://www.eia.doe.gov/oog/info/ngw/ngupdate.asp> 2010.9.30, [accessed 30.09.10].
- [40] U.S. Energy Information Administration. Average retail price of electricity to ultimate customers by end-use sector, by state. Available at: http://www.eia.doe.gov/electricity/epm/table5_6_a.html, [accessed 30.09.2010].
- [41] Zhang N, Lior N, Liu M, Han W. COOLCEP (cool clean efficient power): a novel CO₂-capturing oxy-fuel power system with LNG (liquefied natural gas) coldness energy utilization. *Energy* 2010;35:1200–10.
- [42] Liu M, Lior N, Zhang N, Han W. Thermoeconomic analysis of a novel zero-CO₂-emission high-efficiency power cycle using LNG coldness. *Energ Conv Manage* 2009;50:2768–81.
- [43] Larson ED, Ren T. Synthetic fuel production by indirect coal liquefaction. *Energ Sust Dev* 2003;VII(4).
- [44] Kreutz T, Williams R, Consonni S, Chiesa P. Co-production of hydrogen, electricity and CO₂ from coal with commercially ready technology part B: economic analysis. *Int J Hydrogen Energy* 2005;30:769–84.
- [45] Gas turbine world 2009 handbook. 654 Hillside Rd., Fairfield, CT 06824: Pequot Publishing Inc.; 2009.
- [46] The energy of California. Operation and maintenance costs. Available at: <http://www.energy.ca.gov/distgen/economics/operation.html>, [accessed 30.09.10].
- [47] Caldés N, Varela M, Santamaría M, Saez R. Economic impact of solar thermal electricity deployment in Spain. *Energ Policy* 2009;37:1628–36.

Available online at www.sciencedirect.com

ScienceDirect

journal homepage: www.elsevier.com/locate/he

Adapting the zero-emission Graz Cycle for hydrogen combustion and investigation of its part load behavior

Wolfgang Sanz ^{a,*}, Martin Braun ^a, Herbert Jericha ^a, Max F. Platzer ^{a,b}

^a Institute for Thermal Turbomachinery and Machine Dynamics, Graz University of Technology, Graz, Austria

^b AeroHydro Research & Technology Associates, Pebble Beach, CA, USA

ARTICLE INFO

Article history:

Received 12 September 2017

Received in revised form

9 January 2018

Accepted 26 January 2018

Available online 15 February 2018

Keywords:

Graz Cycle

Hydrogen combustion

Power generation

Part load behavior

ABSTRACT

A modern energy system based on renewable energy like wind and solar power inevitably needs a storage system to provide energy on demand. Hydrogen is a promising candidate for this task. For the re-conversion of the valuable fuel hydrogen to electricity a power plant of highest efficiency is needed.

In this work the Graz Cycle, a zero-emission power plant based on the oxy-fuel technology, is proposed for this role. The Graz Cycle originally burns fossil fuels with pure oxygen and offers efficiencies up to 65% due to the recompression of about half of the working fluid. The Graz Cycle is now adapted for hydrogen combustion with pure oxygen so that a working fluid of nearly pure steam is available. The changes in the thermodynamic layout are presented and discussed. The results show that the cycle is able to reach a net cycle efficiency based on LHV of 68.43% if the oxygen is supplied “freely” from hydrogen generation by electrolysis.

An additional parameter study shows the potential of the cycle for further improvements. The high efficiency of the Graz Cycle is also achieved by a close interaction of the components which makes part load operation more difficult. So in the second part of the paper strategies for part load operation are presented and investigated. The thermodynamic analysis predicts part load down to 30% of the base load at remarkably high efficiencies.

© 2018 Hydrogen Energy Publications LLC. Published by Elsevier Ltd. All rights reserved.

Introduction

In order to counteract the threatening climate change most countries regard it as virtually self-evident that they must concentrate on the development of the renewable energy resources within their national boundaries. However, there is a growing realization that the national resources are insufficient to achieve this objective. For example, MacKay [1]

showed quite convincingly that the United Kingdom cannot replace fossil-based energy generation without recourse to nuclear power generation or without importation of energy from the outside.

Germany came to a similar conclusion and therefore proposed to take advantage of the elevated solar power densities in North Africa and the Middle East by building concentrated solar power plants there and transmitting the electric energy via high voltage direct current cables. The technical challenges

* Corresponding author.

E-mail addresses: wolfgang.sanz@tugraz.at (W. Sanz), platzer@redshift.com (M.F. Platzer).

<https://doi.org/10.1016/j.ijhydene.2018.01.162>

0360-3199/© 2018 Hydrogen Energy Publications LLC. Published by Elsevier Ltd. All rights reserved.

and the political instabilities in this region have impeded the implementation of this Desertec Initiative [2].

As an alternative in 2009 Platzer and Sarigul-Klijn [3] proposed a concept to exploit the global wind sources more easily. They suggest the use of sailing ships instead of stationary floating platforms so that the ships can be operated in areas of optimum wind conditions. In this concept the available wind power is converted into propulsive ship power which, in turn, is converted into electric power by means of ship-mounted hydropower generators. Hydrogen produced by electrolysis will be used for energy storage. In a number of papers Platzer et al. analyzed this concept in more detail, e.g. Refs. [4,5].

Due to the fluctuating nature of solar and wind power a storage system is also inevitable for land-based electricity generation from renewable energy in order to provide energy at the times of demand [6]. The limited storage potential of pumped hydroelectric storage, compressed air energy storage, flywheels and batteries, make Power-to-Gas (PtG) technology one promising option to overcome these limitations [7]. Surplus or intermittent power is used to produce hydrogen via water electrolysis. At demand, hydrogen can then be reconverted to electricity.

In order to find the optimum storage technology for electricity generated from renewable energy, in 2016 Walker et al. [8] compared Power-to-Gas with other energy storage technologies in applications ranging from residential load shifting to bulk energy storage and utility-scale frequency support. The authors found that Power-to-Gas is favorable for utility-scale energy storage where criteria such as energy portability, energy density and ability for seasonal storage are considered. PtG can provide significantly higher energy density than competing energy storage technologies. The ability of PtG for long-term storage of large amounts of energy led to studies of this concept for future renewable energy based systems in Great Britain [9], Germany [10] and Italy [11]. They showed that PtG is able to reduce the overall costs of the gas and electricity network and to improve system reliability in the case of large-scale use of renewable energy. E.g., in Great Britain electricity curtailment of 50–100 TWh in 2050 is possible without a large-scale storage technology.

Regarding electricity-to-electricity efficiency Walker et al. [8] showed that for bulk energy storage the storage efficiency of PtG is only about 35% at current technologies compared to pumped hydro with 82% and batteries ranging from 60 to 90% depending on the technology. But the batteries are far more expensive and do not have seasonal storage capability. In Ref. [12] a hybrid PtG-battery system was investigated with the result that batteries can support electrolyser operation but at too high costs.

So if hydrogen will be used as an energy storage system on a large scale, there is a need for highly efficient power plants for the re-conversion to electricity. In this sense Jericha et al. [13] proposed a hydrogen/oxygen fuelled steam power plant using fuel cells and gas turbine cycle components. The concept is based on the assumption that oxygen is provided “freely” together with hydrogen from the electrolyzers. In their hybrid cycle about 20% of the net power output are generated by fuel cells, whereas the main output comes from the succeeding power plant. They predicted a net cycle

efficiency of 74% which is far above the efficiency of state-of-the-art combined cycle power plants of 60%. In Ref. [14] Platzer et al. analyzed the energy conversion chain of the energy ship concept combined with the hybrid cycle and predicted that 44% of the hydro-turbine electrical power can be regained. Other researchers also proposed novel fuel cell/gas turbine hybrid cycles with the goal of highest efficiency. So Evely et al. [15] combined the hybrid cycle with an organic Rankine cycle, Wang et al. [16] proposed the combination with a Kalina cycle and Meng et al. [17] used an additional supercritical CO₂ process. The achieved efficiencies varied between 64 and 70%.

But the realization of the hybrid cycle concept lacks – besides the development work needed for the turbomachinery components – the availability of fuel cells of large power output. Therefore, in this work a concept is presented which also additionally uses the oxygen from the electrolysis for the hydrogen combustion thus leading to a power cycle of remarkably high efficiency without the need for fuel cells. In contrast to Ref. [6] where the hydrogen/oxygen combustion takes place in an internal combustion engine, a power cycle based on turbomachinery technology is proposed.

This cycle is more or less the Graz Cycle, an oxy-fuel cycle for CO₂ capture which has been developed at Graz University of Technology since 1995 [18]. Since then many further thermodynamic studies as well as component developments have been published, e.g. Refs. [19–22]. It is based on the internal combustion of fossil fuels with oxygen so that a working fluid consisting mainly of steam and CO₂ is generated thus allowing an easy CO₂ separation by condensation. Net efficiencies of more than 65% were predicted when the efforts for oxygen generation and CO₂ compression were not considered [22].

In this work the Graz Cycle is adapted for hydrogen/oxygen combustion so that a working fluid of nearly pure steam is available. This can be considered as a return to its origin, when Jericha firstly proposed a high-temperature steam cycle with internal combustion of hydrogen and stoichiometric oxygen [23]. A thermodynamic layout of the cycle is presented resulting in a power balance promising highest efficiency. Then a variation of important cycle parameters is performed to study the sensitivity of the plant to parameter changes. A final investigation of the part load behavior will prove the applicability of a Graz Cycle plant in a future energy system based on renewable energy and hydrogen as storage medium.

Thermodynamic layout

All thermodynamic simulations were performed using the commercial software IPSEpro v7 by SIMTECH Simulation Technology [24]. This software allows implementing user-defined fluid properties to simulate the real gas properties of the cycle medium as well as to add new models to the model library as the hydrogen combustion chamber. The physical properties of water and steam are calculated using the IAPWS-IF97 formulations.

Furthermore, a turbine module was developed for the calculation of cooled turbine stages. A simple stage-by-stage approach similar to Ref. [25] is assumed which allows calculating the amount of cooling steam needed per stage. The module assumes that half of the cooling mass flow is mixed to

the main flow at stage inlet, thus contributing to the stage expansion work. The rest is added at the stage exit.

Efficiencies and losses of the components of the power cycle as well as important parameters are listed in Table 1.

Process description of a Graz Cycle plant for hydrogen combustion

Fig. 1 shows the principle flow scheme of the Graz Cycle plant for hydrogen combustion, and Fig. 2 the associated temperature-entropy (T-s) diagram generated by the software IPSEpro. The plant is based on a proposal by Jericha [18] and consists basically of a high-temperature Brayton cycle and a low-temperature Rankine cycle – a combined cycle. The Brayton part consists of the combustion chamber (CC), the high-temperature turbine (HTT) and the compressors (C1/C2). The Rankine steam loop consists of the heat recovery steam generator (HRSG), high-pressure steam turbine (HPT), low pressure steam turbine (LPT), condenser, condensate pump, deaerator and finally the feed pump supplying high pressure water to the HRSG.

In the following, the cycle will be explained in more detail. The flow sheet used for the thermodynamic simulation can be found in the appendix (Fig. 14) and gives mass flow, pressure, temperature and enthalpy of all streams.

Table 1 – Component efficiencies and losses as well as important parameters used in the thermodynamic simulation.

Fuel	Pure hydrogen
Hydrogen LHV	120,0 MJ/kg
Hydrogen HHV	146.8 MJ/kg
Oxygen purity	100%
Oxygen excess	0%
Fuel and oxygen supply temperature	15 °C
Combustor pressure loss	1.7 bar
Combustor heat loss	0.25% of heat input
Turbine inlet temperature	1500 °C
Turbine inlet pressure	40 bar
Turbine isentropic efficiency	HTT: 92%, HPT, LPT: 90%
Maximum turbine metal temperature	750 °C
Compressor isentropic efficiency	88%
Pump isentropic efficiency	70%
HRSG pressure loss: cold side	3.15% per heat exchanger = 29.6 bar in total
HRSG pressure loss: hot side	2.5% per heat exchanger = 12 kPa in total
Condenser pressure loss	3%
HRSG minimum temperature difference	Economizer: 5 K Superheater: 15 K
Condenser pressure	0.025 bar
HRSG heat loss	0.5% of transferred heat
Mechanical efficiency η_{m}	99.6% of net power
Generator efficiency η_{gen}	98.5%
Transformer efficiency η_{tr}	99.65%
Auxiliary losses P_{aux}	0.35% of heat input
Oxygen production	0.25 kWh/kg = 900 kJ/kg
Oxygen compression	2.4–42 bar: 325 kJ/kg

Pure hydrogen together with a stoichiometric mass flow of pure oxygen is fed to the combustion chamber, which is operated at a pressure of 40 bar. The high purity can be obtained by producing hydrogen and oxygen with electrolyzers supplied by electricity from renewable energy as discussed above. In order to obtain reasonable combustion temperatures steam stemming from the steam compressor as well as from the HPT are supplied to form the environment for the combustion process and to cool the burners and the liner. As experiments on oxygen combustion have shown (see below) an oxygen surplus of at least 3% is necessary for nearly complete fuel conversion. In this case a small amount of oxygen would accumulate in the cycle, which is extracted in the deaerator. In the simulation stoichiometric combustion is assumed.

Steam leaves the combustion chamber at a mean temperature of 1500 °C, a value achieved by H class turbines nowadays (point 1 in the T-s diagram of Fig. 2). The fluid is expanded to a pressure of 1.2 bar and 596 °C in the HTT (point 2). Cooling is performed with steam coming from the HPT at 41.7 bar/364 °C for the high pressure section and at 15 bar/240 °C for the low-pressure section (see dashed lines in Fig. 2). Cooling is assumed to an expansion temperature of 750 °C, leading to a cooling mass flow of 21.8% of the HTT inlet mass flow.

It is quite clear that a further expansion down to condenser pressure would not end at a reasonable condensation point, so that the hot exhaust steam is cooled in the following HRSG to vaporize and superheat steam for the HPT; the pinch point of the HRSG is 5 K at the economizer outlet, the approach point is 15 K at the superheater exit. The associated temperature-heat diagram (T-Q) is shown in Fig. 3; the transferred heat is 128 MW for a heat input of 300 MW (see below). But after the HRSG (point 3) only 52% of the steam mass flow at 150 °C are further expanded in the LPT, a typical condensing turbine. For a cooling water temperature of 10 °C the LPT exit and thus condenser pressure is 0.025 bar which corresponds to a condenser temperature of 21.1 °C. The steam quality at the LPT exit is 89% (point 4).

After the condensate pump excess water stemming from the combustion process is separated, before the water is degassed in the deaerator (point 5). It is then further compressed in the feed pump and delivered to the HRSG. After preheating, evaporation and superheating steam of 170 bar and 581 °C is fed to the HPT (point 6). After the expansion it is used to cool the burners and the HTT stages as described above.

Nearly half of the cycle steam - the return flow after the HRSG - is compressed using the main cycle compressors C1 and C2 with intercooler (see Fig. 14) and is fed to the combustion chamber with a temperature of 538 °C (point 7). Intercooling is performed to keep the compressor exit temperature at reasonable levels; its heat partially superheats the high pressure steam which causes the jump in the T-Q diagram of Fig. 3. The split ratio is mainly determined by the heat balance in the HRSG and the request of having superheated steam at the compressor inlet to avoid possible condensation there. The proposed return rate of 48% is found by an efficiency optimization. Considering reasonable boundaries for combustion pressure and temperature, condenser efficiency and pinch points, the optimum efficiency was found by a Design of

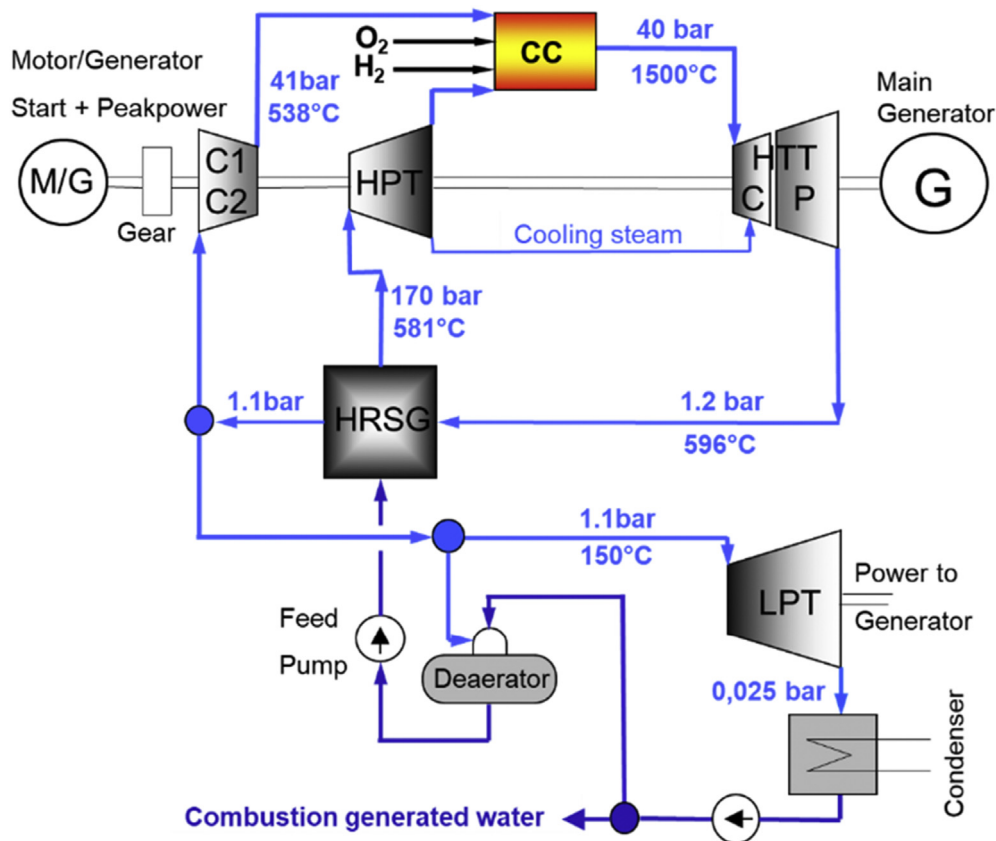


Fig. 1 – Principle flow scheme of the Graz Cycle for hydrogen/oxygen combustion.

Experiments (DoE) approach for the parameters condensation pressure, feed pump pressure, combustion pressure and temperature and pressure of compressor intercooling.

The cycle arrangement of the Graz Cycle offers several advantages: On one hand, it allows heat input at very high temperature, whereas on the other hand expansion takes place to vacuum conditions, so that a high thermal efficiency according to Carnot can be achieved. But the fact that only half of the steam in the cycle releases its heat of vaporization by condensation whereas the other half is compressed in the gaseous phase and so takes its high heat content back to the combustion chamber leads to the remarkably high efficiencies of a Graz cycle plant. But on the other hand the close integration of Brayton and Rankine cycle makes the operation more complex especially when part load is considered.

But the idea of a top Joule and a bottom Rankine cycle with the common working fluid steam was presented much earlier. Horlock [26] assigned them to the category of “doubly cyclic plants”. In the Field Cycle [27] evaporation is done by mixing with HTT exhaust gas. The complete mass flow is then compressed to the cycle peak pressure which leads to very high pressures at peak temperature if high efficiency is aimed at. Another process described by Horlock [26] is the Sonnenfeld Cycle, which can be considered as a supercritical Rankine cycle with three stages of reheat and an internal Joule cycle. Both cycles achieve efficiencies up to 55%. In order to use oxy-fuel technology for CO₂ separation, in 2002 Gabbrilli and Singh [28] presented three cycles based also on the principle of a top Brayton and a bottom Rankine cycle. In contrast to the

Graz Cycle, steam evaporation takes place at compressor inlet pressure or at compression exit pressure at most. An additional high-pressure steam turbine as in the Graz Cycle does not exist. Efficiencies predicted are lower than for a Graz cycle plant. In 2007 Stankovic [29] presented a very intensive investigation of doubly cyclic plants also based on steam. Their common feature is again the addition of a recirculating steam compressor. His high temperature turbine operates at elevated steam turbine inlet conditions (900 °C, 300 bar), but does not apply gas turbine technology as the Graz Cycle. In the best case efficiencies up to modern combined cycle plants can be achieved. So although many efficient cycles have been proposed in the past based on the doubly cyclic concept, the Graz Cycle stands out by applying both state-of-the-art gas turbine and steam cycle technology at the same time leading to highest efficiency.

Power balance

Table 2 gives the power balance of the hydrogen fuelled Graz Cycle plant for a heat input of 300 MW based on lower heating value. This corresponds to a hydrogen supply of 2.5 kg/s.

Whereas in a conventional combined cycle plant the compressor power is roughly half of the total turbine power, in the Graz Cycle plant it is only about a quart. This is a result of the compression of about half of the cycle mass flow in the liquid state. The HTT turbine, the counterpart of the gas turbine expander in a conventional combined cycle plant, is also

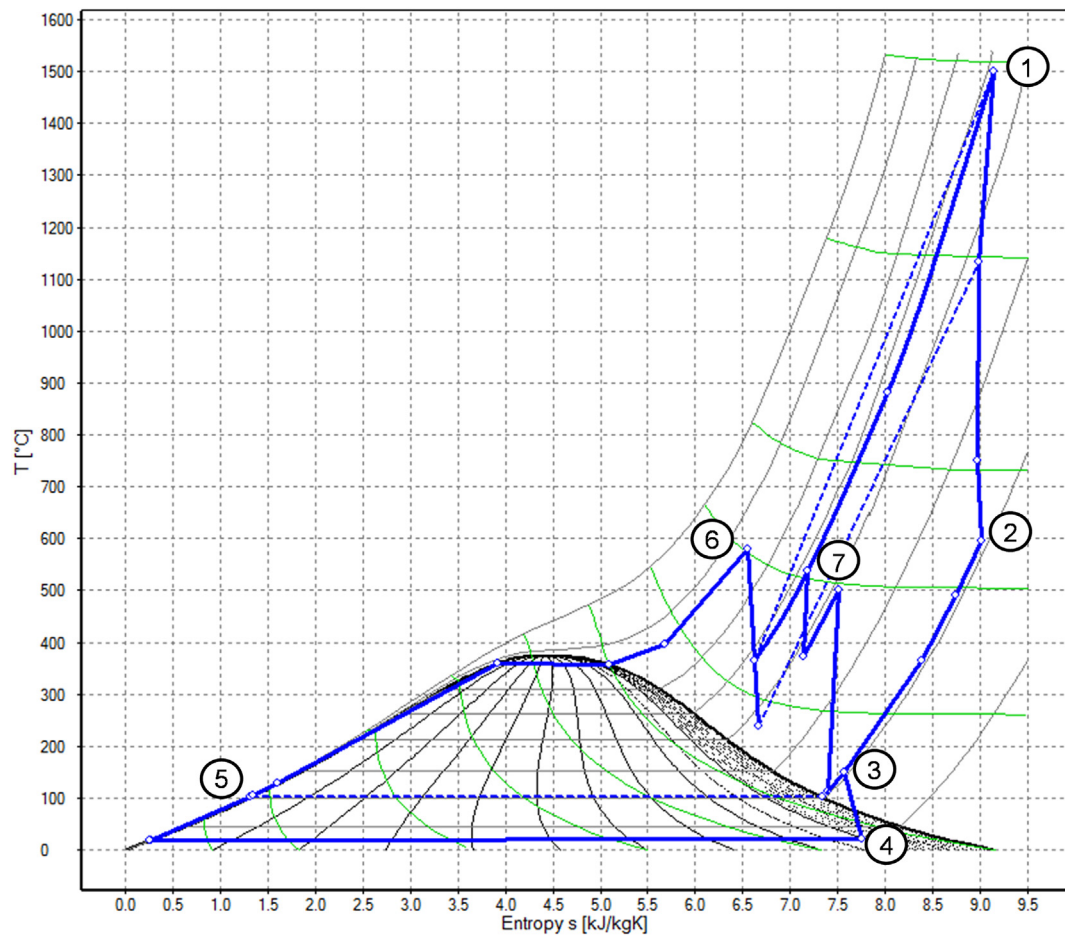


Fig. 2 – Temperature-entropy diagram of the Graz Cycle for hydrogen/oxygen combustion.

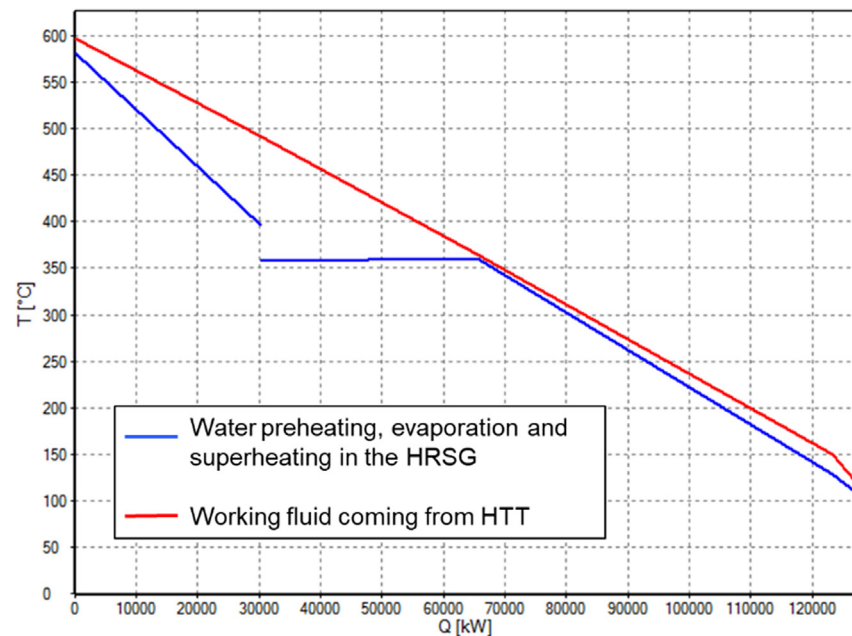


Fig. 3 – Temperature-heat diagram of the HRSG.

the dominant working machine generating more than 80% of the total turbine power. The favorable ratio of turbine to compression power leads to a remarkably high thermal efficiency of 70.35% based on LHV. If mechanical, electrical and

auxiliary losses are considered the net output is 205 MW which corresponds to a net cycle efficiency of 68.43% according to Eq. (1) which is far above the efficiency of state-of-the-art combined cycle plants.

Table 2 – Graz Cycle power balance.

HTT power [MW]	231.85
Total turbine power P_T [MW]	283.80
Total compression power P_C [MW]	72.75
Net shaft power [MW] without mechanical losses	211.05
Total heat input Q_{zu} [MW]	300.0
Thermal cycle efficiency [%]	70.35
Electrical power output [MW] incl. mechanical, electrical & auxiliary losses	205.28
Net efficiency η_{net} [%]	68.43
O ₂ generation & compression [MW]	24.30
Additional power by preheat of hydrogen and oxygen with ASU compressor intercooler to 150 °C [MW]	4.70
Net efficiency considering O ₂ supply $\eta_{O2,net}$ [%]	61.89

$$\eta_{net} = \frac{(P_T - P_C) \cdot \eta_m \cdot \eta_{gen} \cdot \eta_{tr} - P_{aux}}{Q_{zu}} \quad (1)$$

But one should be aware that the difference between higher and lower heating value is with 18% the highest for the fuel hydrogen. Compared to natural gas this leads to an increase in efficiency by 7%, if the efficiency definition is based on the lower heating value. The jump in efficiency compared to a fossil fuel fired Graz Cycle is also caused by this effect.

In this power balance, it was assumed that oxygen of high purity is available “free” from the hydrogen producing electrolysis. If this is not the case, oxygen has to be provided by an air separation unit (ASU). The oxygen demand of the presented plant is 1715 tons/day, which is the capacity of large ASU nowadays. A typical value for the oxygen generation is 0.25 kWh/kg. Since oxygen is usually provided at an elevated pressure, an effort for the intercooled compression from 2.4 to 42 bar of 325 kJ/kg is taken into account. This leads to a total power consumption of 24.3 MW for the oxygen supply. On the other hand, it was found that the heat of compression of ASU air and oxygen can be used to preheat the fuel, so that hydrogen and oxygen can be fed to the combustion chamber at a temperature of 150 °C resulting in a power increase of 4.7 MW. With these assumptions the net efficiency of the Graz Cycle plant is found with 61.89% if oxygen has to be generated on-site. This value is still above current plant efficiencies.

Turbomachinery layout

Since the working fluid is pure steam, new turbomachinery components have to be developed for this plant. The high temperature turbine with steam cooling and steam as working fluid is expected to require the highest development efforts.

The combustion chamber for the nearly stoichiometric combustion of hydrogen with oxygen in a steam environment also demands development work. Experiments for oxy-fuel combustion in a steam vapor environment were performed for natural gas as fuel. Chorpene et al. [30] and Richards et al. [31] operated a combustion chamber for 1 MW thermal output at 10 bar and an exhaust temperature of 1200 °C. Oxygen was mixed with 80% total steam entering the primary combustion zone. 20% total steam entered through dilution ports downstream in order to operate the primary zone at higher

temperatures. Based on their CO measurements they suggest an oxygen surplus of 6%; and they concluded that the concept of oxy-fuel combustion using steam dilution is viable. Griffin et al. [32] also investigated oxy-fuel combustion of natural gas in an inert steam/CO₂ environment. They concluded that an excess amount of oxygen of 3% is necessary to ensure a nearly full fuel conversion. Experience can also be taken from Clean Energy Systems, Inc., who conducted combustion tests in a steam environment using a combustor can of a GE J79 engine [33].

The development work needed for the steam compressors and the HRSG are considered to be small. All other components are regarded as state-of-the-art. As Fig. 14 in the appendix shows, about one third of the cooling steam is expanded in a small steam turbine of 4 stages running at 20000 rpm. Omitting it would lead a decrease of efficiency of 0.65 %-points so that it is a matter of economics if it will be installed.

Since the heat capacity of steam is about twice the value of the working gas of an air-breathing gas turbine, the HTT and the steam compressors have to cope with a larger enthalpy drop for the same pressure ratio. In order to keep the number of stages low it was suggested in previous publications on the Graz Cycle (e.g. Refs. [21,22]) to arrange the compressors and the first two stages of the HTT on a fast-running shaft. The larger speed of sound of steam also allows a higher rotational speed without surpassing a relative tip Mach number of 1.3 at the compressor inlet. A faster speed is also advantageous for the HPT due to its relatively small volume flow. Therefore, it is suggested to group the compressors, the compressor turbine HTT-C and the HPT on a fast running shaft, which is connected via a gear box with a generator/motor indicated in the cycle scheme of Fig. 1. This electrical machine has to cope with the difference in power and can also be used as motor for start-up. The HTT power turbine and the LPT run at 3000 rpm and can be connected to the same generator.

Parameter study

The main parameters of the plant are chosen to obtain high efficiency at realistic values. In order to see the chances for improving the process efficiency and the sensitivity of the cycle if design variables cannot be met a parameter study is conducted. HTT inlet temperature and pressure, condenser pressure and HPT feed pressure are varied to see their influence on the cycle net efficiency. In the following Figs. 4–7 the square marks the design value.

Fig. 4 shows the influence of the cycle peak temperature on the net efficiency, which is quite strong. Reducing the temperature to 1400 °C leads to a decrease in efficiency of nearly 1 %-point. A further reduction goes along with an increasing penalty in efficiency with a value of 64.9% at 1200 °C, about 3.5 %-points lower. If an increase to 1600 °C could be done, the net efficiency would slightly increase by 0.7 %-points.

Increasing the HTT inlet pressure from 40 bar to 60 bar leads to a nearly linear increase in efficiency as shown in Fig. 5, with a value of 69.38% at 60 bar. The increasing efficiency indicates that the optimum cycle pressure has not yet been achieved. On the other hand, efficiency decreases considerably with decreasing pressure; a reduction by 20 bar leads to a loss in efficiency by 2.8 %-points.

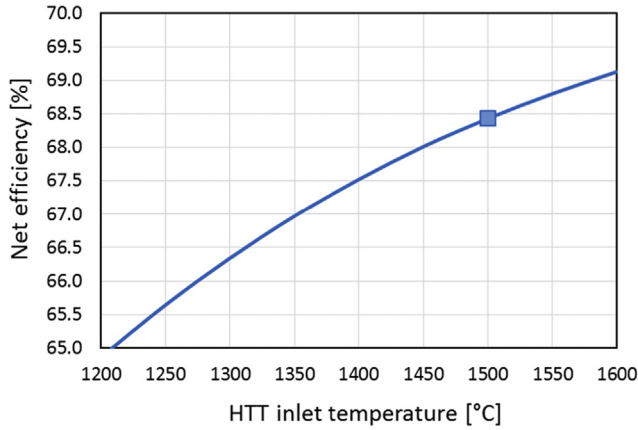


Fig. 4 – Net efficiency as a function of HTT inlet temperature.

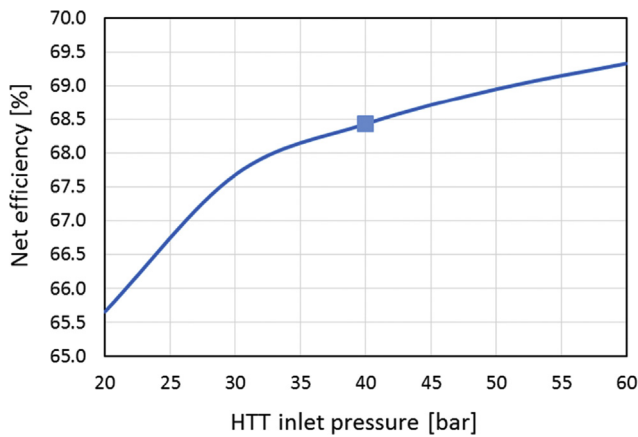


Fig. 5 – Net efficiency as a function of HTT inlet pressure.

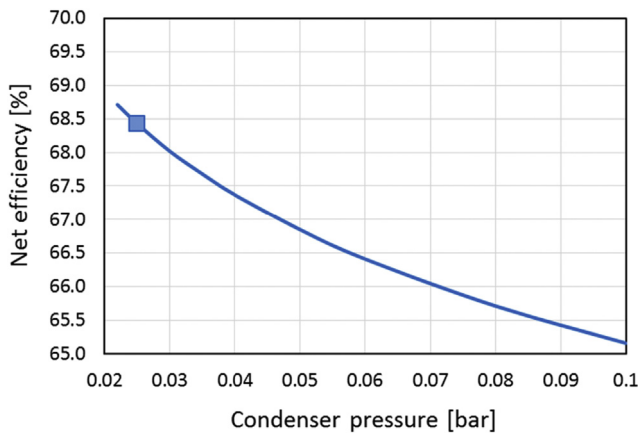


Fig. 6 – Net efficiency as a function of condenser pressure.

The cycle reacts very sensible to a change in condenser pressure as shown by Fig. 6. Increasing the condenser pressure to 0.1 bar and thus the condensation temperature to 46 °C, which is typical for hot regions like India, reduces the cycle efficiency by 3.2 %-points to 65.3%.

The influence of the HPT feed pressure is relatively small. Varying it in a relatively wide range of 120–190 bar leads only to a moderate change in efficiency of 1.4 %-points as shown in Fig. 7.

Part load performance

Since a Graz Cycle plant is characterized by a closer interaction between Brayton and Rankine part than a conventional combined cycle plant, the question arises to what extent a part-load operation is possible. Therefore, in the following the results of a part-load simulation are presented.

There are several ways to control the power output of a combined cycle plant in part load. First, mostly the mass flow in the gas turbine is reduced with the help of variable guide vanes at the compressor inlet. The peak temperature is kept nearly constant to maintain a high efficiency. In this case the gas turbine exhaust temperature also remains nearly constant which has a positive impact on the bottoming steam cycle. If the load is further decreased the peak temperature has to be reduced additionally. For the steam cycle the power is controlled by throttling the feed mass flow or by floating pressure operation which promises higher efficiency.

For the simulation of the part load behavior of the Graz Cycle plant, as a first guess the main cycle parameters, i.e. the mass flow to the HTT as well as HTT inlet pressure and temperature are varied simultaneously whereas a floating pressure control is assumed for the HPT. This control strategy is mostly dictated by the need to maintain reasonable temperature differences in the heat exchangers.

In order to simulate the part load behavior of the turbines and compressors Stodola's law [34] is applied which relates mass flow (\dot{m}), inlet and outlet pressure (p_{in} and p_{out}) and inlet temperature T_{in} between design point (DP) and part load (PL). Eq. (2) gives the formula for a turbine, for a compressor the pressure difference between outlet and inlet is used.

$$\frac{\dot{m}_{PL}}{\dot{m}_{DP}} = \frac{\sqrt{\frac{p_{in,PL}^2 - p_{out,PL}^2}{T_{in,PL}}}}{\sqrt{\frac{p_{in,DP}^2 - p_{out,DP}^2}{T_{in,DP}}}} \quad (2)$$

A simple relation between isentropic efficiency and mass flow as shown in Fig. 8 considers the drop in efficiency for the turbomachinery components in part load. For the heat exchangers the pressure loss is assumed proportional to the square of the mass flow according to Eq. (3). The change in heat transfer is considered by relating the heat transfer coefficient k to the transferred heat (q_{trans}) according to Eq. (4).

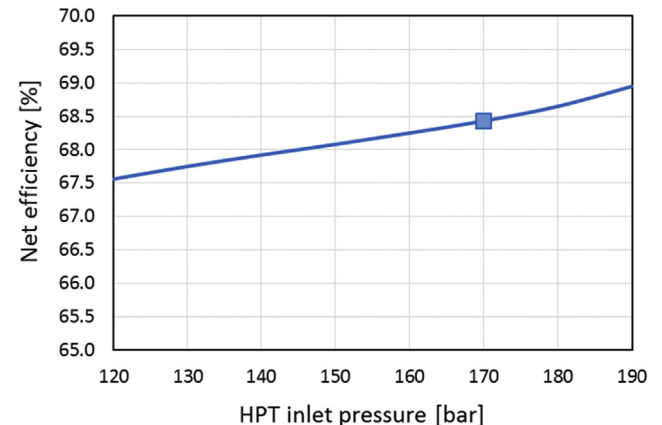


Fig. 7 – Net efficiency as a function of HPT feed pressure.

$$\frac{\Delta p_{PL}}{\Delta p_{DP}} = \left(\frac{\dot{m}_{PL}}{\dot{m}_{DP}} \right)^2 \quad (3)$$

$$\frac{k_{PL}}{k_{DP}} = \left(\frac{q_{trans,PL}}{q_{trans,DP}} \right)^{0.6} \quad (4)$$

For the evaporator and superheater the full load model was used. All other parameters, i.e. combustor pressure and heat

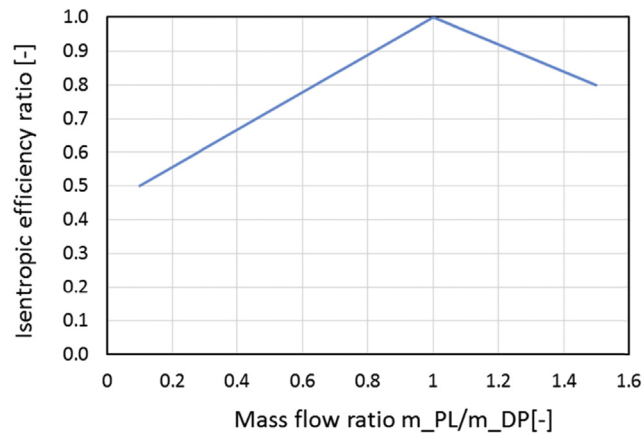


Fig. 8 – Isentropic efficiency ratio vs. mass flow ratio.

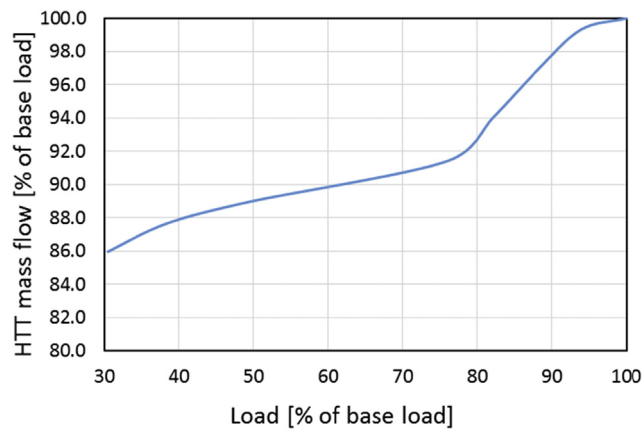


Fig. 9 – HTT inlet mass flow at part load operation.

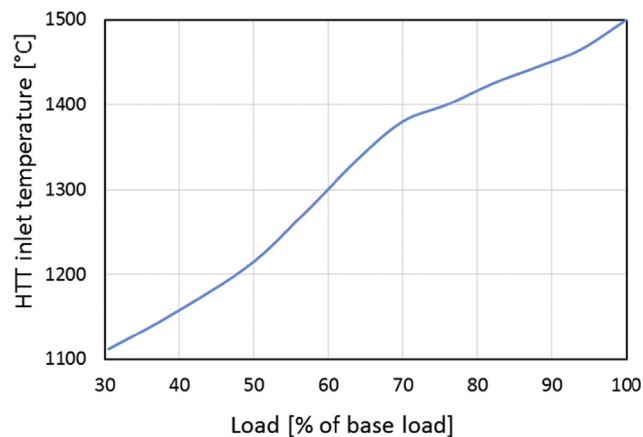


Fig. 10 – HTT inlet temperature at part load operation.

loss, pump efficiencies, mechanical and electrical efficiencies as well as auxiliary losses were kept constant for simplicity reasons.

The simulations demonstrate that for the chosen operation strategy part load down to 30% of the base load can be achieved. Figs. 9–12 show the change of HTT mass flow, inlet temperature and pressure as well as HPT feed pressure over the load. The HTT inlet mass flow is decreased strongly down to about 91.5% at 75% load whereas the peak temperature is reduced more

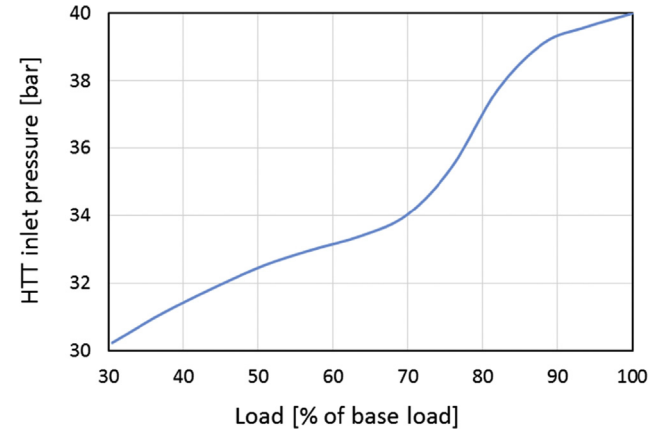


Fig. 11 – HTT inlet pressure at part load operation.

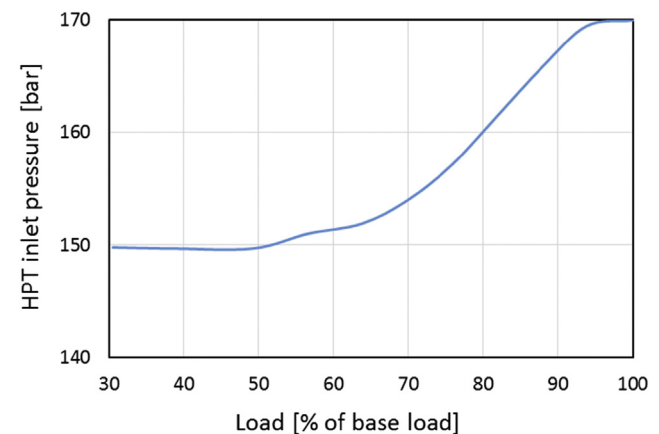


Fig. 12 – HPT inlet pressure at part load operation.

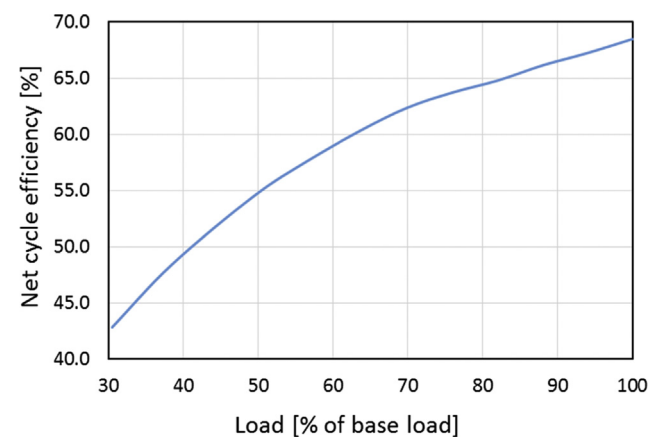


Fig. 13 – Net cycle efficiency at part load operation.

slightly to about 1400 °C. Then the control strategy is changed. The mass flow decline is less pronounced and it reduces slowly to 86% at 30% load, whereas the temperature drops significantly to 1100 °C in the same load interval.

The HTT inlet pressure follows more or less the tendency of the mass flow with a sharp decrease at the beginning down to 34 bar at 70% load. Then the pressure falls slowly to 30 bar at 30% load. The pressure of the HPT steam turbine decreases from 170 bar at base load to 150 bar at 50% load and then remains constant.

The resulting change of the net cycle efficiency is displayed in Fig. 13. There is a nearly linear decrease from 68.5% to 62.4% at 70% part load. Then the efficiency drops more substantially to 42.8% at 30% load. This behavior is mainly caused by peak temperature, which shows a similar trend and influences strongly the cycle efficiency.

The part load efficiency can be considered as remarkably high, which allows an economic operation of the Graz Cycle plant even at part load. This is a valuable feature since the fluctuating nature of renewable energy forces power plants more often to operate at part load. But it has to be kept in mind that this result is based on a relatively rough assumption of the part load behavior of the main components. A more thorough study with different control strategies can lead to a more negative, but also to a more positive part load behavior.

Summary and conclusions

The Graz Cycle, a power plant of highest efficiency, is proposed for the energy conversion of hydrogen to electricity in a future energy system based on renewable energy.

The Graz Cycle in this work is based on the internal combustion of hydrogen with pure oxygen, so that a working fluid of nearly pure steam is obtained. The thermodynamic layout at the design point assumes state-of-the-art gas turbine technology with a peak cycle condition of 1500 °C and 40 bar. At design point the net cycle efficiency is 68.5% which is remarkably higher than the efficiency of modern power plants.

The high efficiency is obtained amongst others by the recompression of about half of the cycle fluid thus reducing the heat extraction out of the process. But this leads to a close interaction of the components so that the feasibility of part-load operation is studied.

For the proposed control system part load down to 30% of the base load could be achieved at remarkably high efficiencies. These high efficiencies at part and full load make the Graz Cycle to a promising candidate for the re-conversion of hydrogen in a future energy system based on hydrogen as storage medium.

Appendix

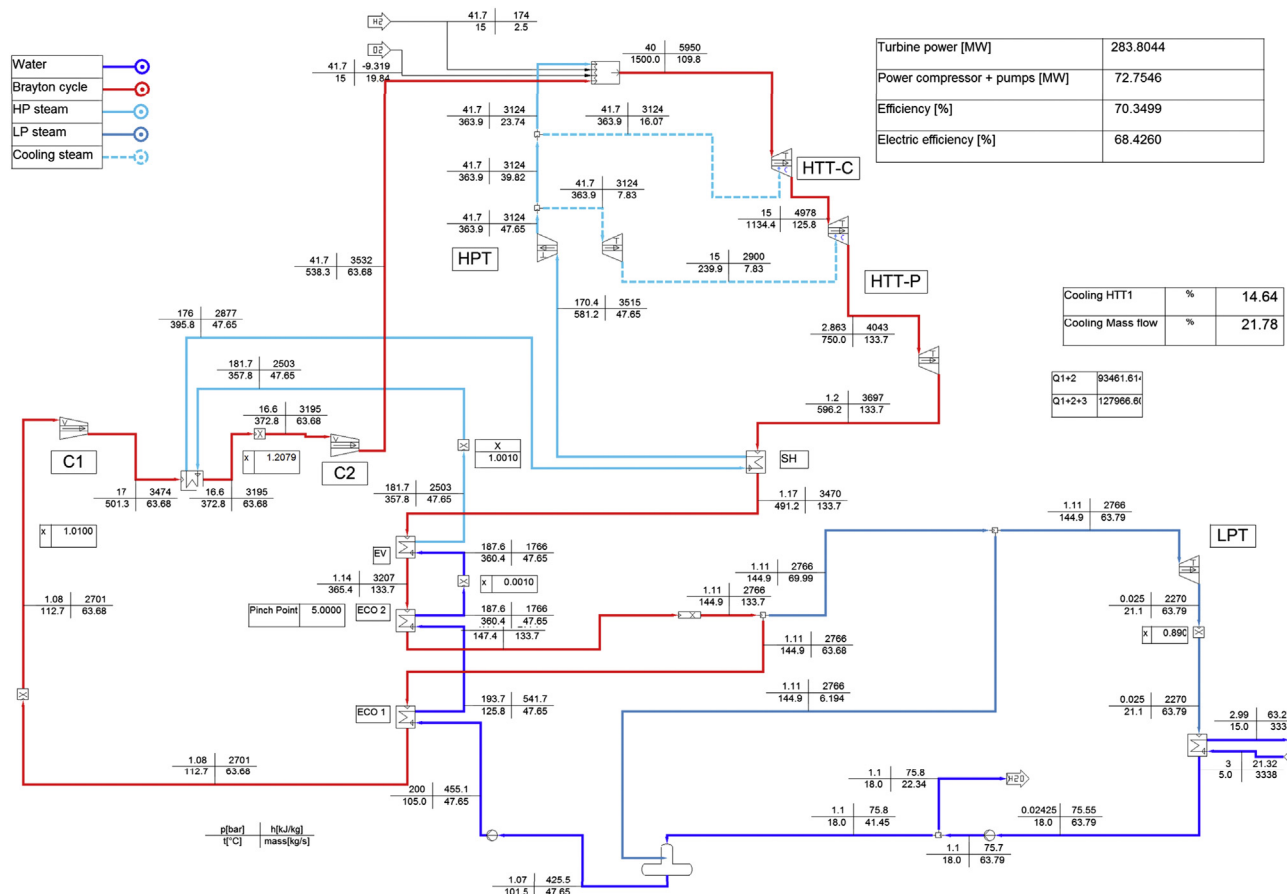


Fig. 14 – Detailed thermodynamic cycle data of the hydrogen/oxygen fuelled Graz Cycle plant.

REFERENCES

- [1] MacKay DJ. Sustainable energy – without the hot air. UIT Cambridge Ltd.; 2009.
- [2] www.desertec.org.
- [3] Platzer M, Sarigul-Klijn N. A novel approach to extract power from free-flowing water and high altitude jet streams. In: Proceedings of ES2009, energy sustainability 2009, San Francisco, USA; 2009.
- [4] Platzer M, Sarigul-Klijn N, Young J, Ashraf MA, Lai JCS. Renewable hydrogen production using sailing ships. ASME J Energy Resour Technol 2014;136. 021203-1 to 5.
- [5] Platzer MF, Sarigul-Klijn N. Energy ships and plug-in hybrid electric vehicles: are they the key for a rapid transition to an emission-free Economy? ASME IMECE-2015–50652. 2015.
- [6] Haller J, Link T. Thermodynamic concept for an efficient zero-emission combustion of hydrogen and oxygen in stationary internal combustion engines with high power density. Int J Hydrogen Energy 2017;42(44).
- [7] Bailera M, Lisbona P, Romeo LM. Power to gas-oxyfuel boiler hybrid systems. Int J Hydrogen Energy 2015;40(32).
- [8] Walker SB, Mukherjee U, Fowler M, Elkamel A. Benchmarking and selection of Power-to-Gas utilizing electrolytic hydrogen as an energy storage alternative. Int J Hydrogen Energy 2016;41(19).
- [9] Qadrdan M, Abeysekera M, Chaudry M, Wu J, Jenkins N. Role of power-to-gas in an integrated gas and electricity system in Great Britain. Int J Hydrogen Energy 2015;42(17).
- [10] Michalski J. Investment decisions in imperfect power markets with hydrogen storage and large share of intermittent electricity. Int J Hydrogen Energy 2017;42(19).
- [11] Guandalini G, Robinius M, Grube T, Campanari S, Stolten D. Long-term power-to-gas potential from wind and solar power: a country analysis for Italy. Int J Hydrogen Energy 2017;42(19).
- [12] Gillessen B, Heinrichs HU, Stenzel P, Linssen J. Hybridization strategies of power-to-gas systems and battery storage using renewable energy. Int J Hydrogen Energy 2017;42(19).
- [13] Jericha H, Hacker V, Sanz W, Zotter G. Thermal steam power plant fired by hydrogen and oxygen in stoichiometric ratio, using fuel cells and gas turbine cycle components. In: ASME GT2010-22282, ASME turbo expo 2010, Glasgow, UK; 2010.
- [14] Platzer MF, Sanz W, Jericha H. Renewable power via energy ship and Graz Cycle. In: 15th international symposium on transport phenomena and dynamics of rotating machinery, ISROMAC-15, Honolulu, HI, USA; 2014.
- [15] Eveloy V, Karunkeyoon W, Rodgers P, Al Alili A. Energy, exergy and economic analysis of an integrated solid oxide fuel cell – gas turbine – organic Rankine power generation system. Int J Hydrogen Energy 2016;41(31).
- [16] Wang J, Yan Z, Ma S, Dai Y. Thermodynamic analysis of an integrated power generation. Int J Hydrogen Energy 2012;37(3).
- [17] Meng Q, Han J, Kong L, Liu H, Zhang T, Yu Z. Thermodynamic analysis of combined power generation system based on SOFC/GT and transcritical carbon dioxide cycle system driven by solid oxide fuel cell. Int J Hydrogen Energy 2017;42(7).
- [18] Jericha H, Sanz W, Woisetschlager J, Fesharaki M. CO₂-Retention capability of CH₄/O₂ – fired Graz Cycle. In: CIMAC conference paper, Interlaken, Switzerland; 1995.
- [19] Jericha H, Göttlich E, Sanz W, Heitmeir F. Design optimisation of the Graz Cycle prototype plant. In: ASME paper 2003-GT-38120, ASME turbo expo 2003, Atlanta, USA, journal of engineering for gas turbines and power, vol. 126, Oct. 2004; 2003. p. 733–40.
- [20] Sanz W, Jericha H, Moser M, Heitmeir F. Thermodynamic and economic investigation of an improved Graz Cycle power plant for CO₂ capture. In: ASME paper GT2004-53722, ASME turbo expo 2004, Vienna, Austria, journal of engineering for gas turbines and power, vol. 127, Oct. 2005; 2004. p. 765–72.
- [21] Jericha H, Sanz W, Göttlich E. Design concept for large output Graz Cycle gas turbines. In: ASME paper GT2006–90032, ASME turbo expo 2006, Barcelona, Spain; 2006.
- [22] Jericha H, Sanz W, Göttlich E, Neumayer F. Design details of a 600 MW Graz Cycle thermal power plant for CO₂ capture. In: ASME paper GT2008–50515, ASME turbo expo 2008, Berlin, Germany; 2008.
- [23] Jericha H. Efficient steam cycles with internal combustion of hydrogen with stoichiometric oxygen for turbines and piston engines. In: CIMAC international congress on combustion engines, Oslo, 1985; 1985.
- [24] SimTech Simulation Technology. IpsePro overview. 2015. <http://www.simtechnology.com/IPSEpro>.
- [25] Jordal K, Bolland O, Klang A. Effects of cooled gas turbine modelling for the semi-closed O₂/CO₂ cycle with CO₂ capture. In: ASME paper 2003-GT-38067, ASME turbo expo 2003, Atlanta, USA; 2003.
- [26] Horlock JH. Combined power plants. Pergamon Press; 1992.
- [27] Field JF. The application of gas turbine technique to steam power. Proc Inst Mech Eng Transport Eng 1950;162:209.
- [28] Gabbriellini R, Singh R. Thermodynamic performance analysis of new gas turbine combined cycles with no emissions of carbon dioxide. In: ASME paper GT2002-30117, ASME turbo expo 2002, Amsterdam, Netherlands; 2002.
- [29] Stankovic B. Combined steam-turbine power producing concept with recirculating steam compressor. In: ASME paper GT2007–28090, ASME turbo expo 2007, Montreal, Canada; 2007.
- [30] Chorpeneing BT, Richards GA, Casleton KH, Woike M, Willis B, Hoffman L. Demonstration of a reheat combustor for power production with CO₂ sequestration. In: ASME paper 2003-GT-38511, ASME turbo expo 2003, Atlanta, USA; 2003.
- [31] Richards GA, Casleton KH, Chorpeneing BT. CO₂ and H₂O diluted oxy-fuel combustion for zero-emission power. Proc Inst Mech Eng Transport Eng 2005;219. Part A: J Power and Energy.
- [32] Griffin T, Sundkvist SV, Asen K, Bruun T. Advanced zero emissions gas turbine power plant. J Eng Gas Turbines Power 2005;127.
- [33] Anderson R, Viteri F, Hollis R, Keating A, Shipper J, Merrill G, et al. Oxy-fuel gas turbine, gas generator and reheat combustor technology development and demonstration. In: ASME paper GT2010-23001, ASME turbo expo 2010, Glasgow, UK; 2010.
- [34] Stodola A. Die Dampfturbinen. Berlin (in German): Springer Verlag; 1903.

Thermodynamic Analysis of Zero-Atmospheric Emissions Power Plant

Joel Martinez-Frias
e-mail: martinezfrias@llnl.gov

Salvador M. Aceves

J. Ray Smith

Lawrence Livermore National Laboratory,
7000 East Avenue, L-644,
Livermore, CA 94551

Harry Brandt

Clean Energy Systems, Inc.,
2530 Mercantile Drive, Suite A,
Rancho Cordova, CA 95742
e-mail: hbrandt@cleanenergysystems.com

This paper presents a theoretical thermodynamic analysis of a zero-atmospheric emissions power plant. In this power plant, methane is combusted with oxygen in a gas generator to produce the working fluid for the turbines. The combustion produces a gas mixture composed of steam and carbon dioxide. These gases drive multiple turbines to produce electricity. The turbine discharge gases pass to a condenser where water is captured. A stream of pure carbon dioxide then results that can be used for enhanced oil recovery or for sequestration. The analysis considers a complete power plant layout, including an air separation unit, compressors and intercoolers for oxygen and methane compression, a gas generator, three steam turbines, a reheater, two preheaters, a condenser, and a pumping system to pump the carbon dioxide to the pressure required for sequestration. This analysis is based on a 400 MW electric power generating plant that uses turbines that are currently under development by a U.S. turbine manufacturer. The high-pressure turbine operates at a temperature of 1089 K (1500°F) with uncooled blades, the intermediate-pressure turbine operates at 1478 K (2200°F) with cooled blades and the low-pressure turbine operates at 998 K (1336°F). The power plant has a net thermal efficiency of 46.5%. This efficiency is based on the lower heating value of methane, and includes the energy necessary for air separation and for carbon dioxide separation and sequestration. [DOI: 10.1115/1.1635399]

Introduction

The main contributor to increasing atmospheric carbon dioxide (CO_2) concentration is the combustion of fossil fuels for electricity generation, transportation and industrial and domestic uses. Fossil fuels (coal, oil, and natural gas) have underpinned the development of the economies in the industrialized countries around the world. The demand for energy is expected to grow in the developed countries and in particular in the developing countries as they strive to obtain a higher standard of living. This increase in energy demand will increase the carbon dioxide concentration in the earth's atmosphere.

Carbon dioxide capture and geologic storage offer a new set of options for reducing greenhouse gas emissions that can complement the current strategies of improving energy efficiency and increasing the use of nonfossil energy resources.

Production of electric power with zero-atmospheric emissions is one of the goals of the Vision 21 Program of the U.S. Department of Energy (DOE), [1]. A decade ago, such a concept would not have been considered to be viable. However, recent research, [2–10], has addressed technical and economic issues associated with the concept, making it a viable option.

The power plant concept uses a Rankine cycle to drive three turbines connected in series. However, unlike conventional steam power plants, the plant does not use a boiler to generate steam. Use of a boiler presents two disadvantages to the efficiency of the Rankine cycle. First, the maximum cycle temperature is limited by the maximum metal temperature that boiler components can withstand; and second, 10 to 15% of the available energy in the fuel is lost by the exhaust gases that are vented to the atmosphere.

In this study, the turbine working fluid is produced in a gas generator by the stoichiometric combustion of natural gas and oxygen. Hence, the maximum operating temperature of the Rank-

ine cycle is no longer controlled by the maximum operating temperature of a boiler. Rather, the maximum operating temperature that the turbines can withstand becomes the efficiency-limiting temperature. The hydrocarbon fuel does not need to be natural gas, but could, for example, be syngas derived from coal, or gas derived from biomass.

The adiabatic flame temperature of the stoichiometric combustion of methane and oxygen at a pressure of 2.07 MPa (300.2 lb/in²) is 3460 K (5768°F), [11]. No turbines are available that can operate at this temperature. Therefore, in the gas generator, water is premixed with the natural gas and oxygen before the mixture enters the combustion chamber. In addition, the gas generator, [8–10], has several sections in which water is added to the combustion products to bring the gas temperature to a level acceptable to available turbines.

The turbine discharge gases pass to a condenser where water is captured as liquid and gaseous carbon dioxide is pumped from the system. The carbon dioxide can be compressed for enhanced recovery of oil or coal-bed methane, or the compressed carbon dioxide can be injected for sequestration into a subterranean formation. The technology described in this paper is the subject of several US patents, [12–21].

The next section describes the specific plant configuration analyzed in this paper. The analysis section discusses the methodology used for analyzing the power plant.

Power Plant Configuration

Figure 1 presents the power plant configuration analyzed in this paper. The power plant has four major sections: methane compression, air separation and oxygen (O_2) compression, power generation, and carbon dioxide separation and sequestration. Each of these sections consists of multiple components as shown in the figure. For the analysis, the plant is assumed to operate on methane that is combusted with oxygen. Methane is compressed to the operating pressure of the gas generator (12.4 MPa, 1800 lb/in², point 22, Fig. 1). Part of the methane is compressed to a pressure of 1.38 MPa (200 lb/in²) for a reheater that is installed between the high-pressure turbine and the intermediate-pressure turbine

Contributed by the Advanced Energy Systems Division of THE AMERICAN SOCIETY OF MECHANICAL ENGINEERS for publication in the ASME JOURNAL OF ENGINEERING FOR GAS TURBINES AND POWER. Manuscript received by the AES Division July 2002; final revision received March 2003. Associate Editor: G. M. Reistad.

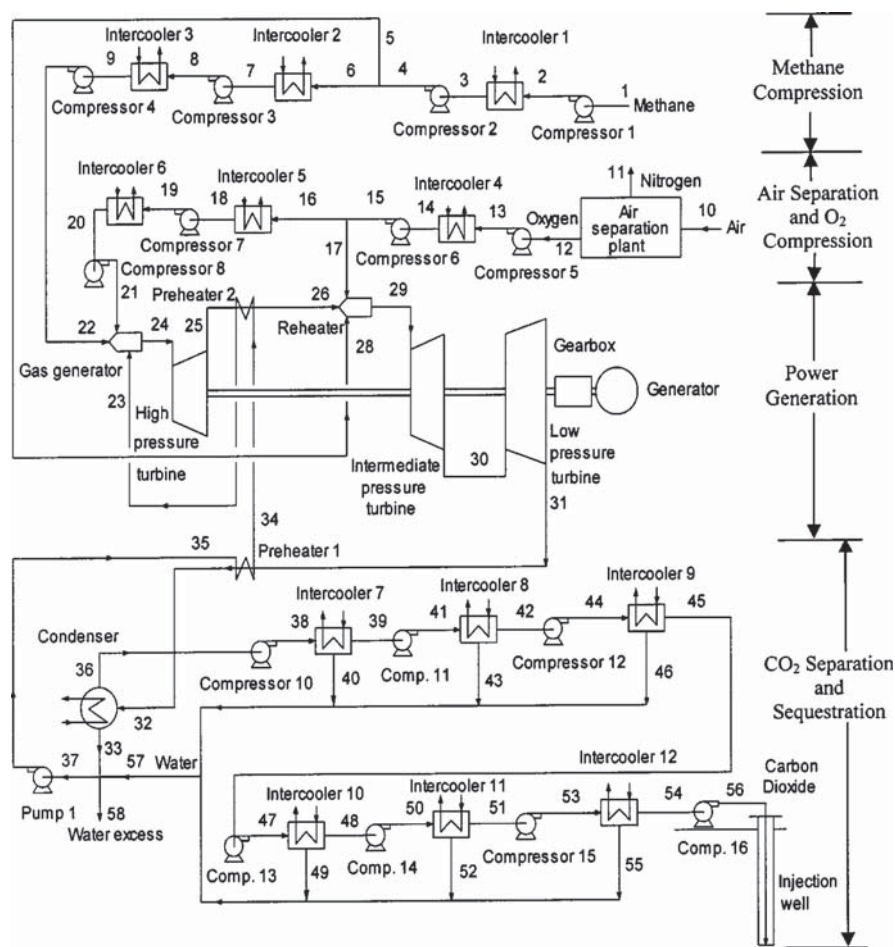


Fig. 1 Schematic of the zero-atmospheric emissions 400 MW power plant

(point 28). The compression system for methane consists of four compressors (Compressors 1 to 4) and three intercoolers (Intercoolers 1 to 3). Oxygen is generated in an air separation plant and is compressed to feed the gas generator and the reheater. The oxygen compression system consists of four compressors (Compressors 5 to 8) and three intercoolers (Intercoolers 4 to 6).

The water for this cycle is generated by the cycle itself. The water leaving the condenser is heated in Preheaters 1 and 2 before the water is injected into the combustion products in the gas generator. These preheaters increase the efficiency of the cycle.

In this study, the preheaters are located in the discharge lines of both the high-pressure turbine and the low-pressure turbine. The preheaters heat the water that is routed from the condenser to the gas generator where the water is evaporated to cool the combustion products in the gas generator. If the water were not preheated, a smaller amount of water would be required to cool the gases in the gas generator. However, taking thermal energy out of the discharge of the drive gas from the low-pressure turbine reduces the energy that is delivered to the condenser. As a result, less heat is transferred in the condenser to the condenser cooling water. This reduced condenser cooling water heat loss increases plant efficiency. The location of the preheaters, the amount of heat removed from the turbine drive gas and the temperature of the cooling water entering the gas generator, all affect cycle efficiency. How this increase in efficiency is obtained is not a priori clear, but is determined from optimization studies of the entire cycle.

Combustion products from the gas generator are delivered to the high-pressure turbine (point 24) where the mixture of steam and carbon dioxide expands, thereby producing power in the tur-

bine and electrical generator system. The mixture consists of a 0.88 mass fraction of steam and 0.12 mass fraction of carbon dioxide. After the steam and carbon dioxide mixture leaves the high-pressure turbine, the mixture is heated by a reheater (point 26). The reheater increases the temperature of the mixture before it enters the intermediate-pressure turbine. After the reheater, the working fluid entering the intermediate-pressure turbine consists of a 0.79 mass fraction of steam and a 0.21 mass fraction of carbon dioxide. After leaving the intermediate-pressure turbine, the mixture enters a low-pressure turbine for its final expansion (point 30). The exhaust from the low-pressure turbine flows through Preheater 1 to preheat the water that was separated from the turbine working fluid in the condenser.

Most of the water that is generated in the cycle is separated from the turbine working fluid mixture in the condenser. Liquid water is extracted from the condenser by Pump 1 and is recycled to the system. The water temperature is increased in Preheaters 1 and 2, before the water goes to the gas generator (point 23) to control the temperature of the combustion products.

A mixture consisting primarily of carbon dioxide, but containing a substantial amount of moisture, is extracted from a port (point 36) at the top of the condenser. The carbon dioxide with the remaining moisture from the condenser is then delivered to several compressors and intercoolers to obtain high-pressure carbon dioxide with almost no moisture. The compression-sequestration system consists of seven compressors (Compressors 10 to 16) and six intercoolers (Intercoolers 7 to 12).

Table 1 Values of the parameters used in the base case simulation of the zero-atmospheric emissions power plant

System Parameters	Value
Preheater effectiveness	0.85
Condenser effectiveness	0.90
Intercooler effectiveness	0.85
Ambient temperature	288 K
Isentropic efficiency of the high-pressure turbine	90%
Isentropic efficiency of the intermediate-pressure turbine	91%
Isentropic efficiency of the low-pressure turbine	93%
Isentropic efficiency of the compressors	85%
Efficiency of the water pump	85%
Efficiency of the electric generator	98%

Analysis

The power plant system consists of a gas generator, three turbines, a reheater, a condenser, an oxygen separation plant, 15 compressors, a pump to recirculate the water from the condenser to the gas generator and a pump for the condenser cooling water, 12 intercoolers, two preheaters, and an electric generator. Energy and mass conservation laws are applied to every system component. The equations used to describe the power plant components are solved simultaneously in a computer code. A computer code using F-Chart software, [22], was developed to analyze plant efficiencies. Individual system components are described next.

Gas Generator and Reheater. Methane and oxygen are combusted in the gas generator to produce the turbine drive fluid. The temperature of the combustion products of methane with oxygen is controlled by adding water to the combustion products in the gas generator. The mass flow rate of water into the gas generator depends on the desired inlet temperature of the working fluid for the high-pressure turbine.

A reheater is used to increase the temperature of high-pressure turbine exhaust to the desired temperature for the intermediate-pressure turbine. The reheater produces this temperature increase by burning methane with oxygen and mixing the combustion products with the high-pressure turbine exhaust.

In the gas generator and the reheater, assuming an adiabatic process, the rate of change with time of the absolute enthalpy (including both sensible enthalpy and enthalpy of formation) of the products is equal to the rate of change of the absolute enthalpy of the reactants. Complete combustion is considered in the gas generator and in the reheater.

Turbines. Turbines are modeled by the equation of isentropic efficiency, [23], which is defined as the ratio of the power generated for the actual expansion of the gases in the turbine (\dot{W}_a) and the power generated in an isentropic expansion of the gases in the turbine (\dot{W}_s). For the three turbines the following equation is used for turbine efficiency:

$$\eta_t = \frac{\dot{W}_a}{\dot{W}_s} = \frac{\dot{H}_{in} - \dot{H}_{out,a}}{\dot{H}_{in} - \dot{H}_{out,s}} \quad (1)$$

The turbine efficiencies for the high-pressure turbine, the intermediate-pressure turbine, and the low-pressure turbine were assumed to be 90%, 91%, and 93%, respectively (see Table 1). The efficiency of the high-pressure turbine takes into account the use of short blades; the efficiency of the intermediate-pressure turbine takes into account the blade cooling losses. These efficiencies compare to values of 93% used by Bannister et al. [24], 85% used by Bolland et al. [25], and 93% by Aoki et al. [26].

Heat Exchangers. To determine the performance of the heat exchangers (intercoolers, preheaters, and condenser) an effective-

ness equation is used. The heat exchanger effectiveness is defined as the ratio of the actual rate of heat transfer in a given heat exchanger to the maximum possible rate of heat exchange. If the heat capacity rate of the warmer fluid ($\dot{m}_h c_{ph}$) is smaller than the heat capacity rate of the colder fluid ($\dot{m}_c c_{pc}$) then the equation for effectiveness, ε is

$$\varepsilon = \frac{\dot{Q}}{\dot{Q}_{\max}} = \frac{\dot{H}_{h,in} - \dot{H}_{h,out}}{\dot{H}_{h,in} - \dot{H}_{c,in}} \quad (2)$$

If the heat capacity rate of the colder fluid ($\dot{m}_c c_{pc}$) is smaller than the heat capacity rate of the warmer fluid ($\dot{m}_h c_{ph}$) then the effectiveness equation is

$$\varepsilon = \frac{\dot{Q}}{\dot{Q}_{\max}} = \frac{\dot{H}_{c,out} - \dot{H}_{c,in}}{\dot{H}_{h,in} - \dot{H}_{c,in}} \quad (3)$$

This analysis assumes an effectiveness of 85% for intercoolers and preheaters (see Table 1), [25]. The temperature of the environment and cooling water is assumed to be 288 K (59°F) to be consistent with the environment temperature used in the analysis of combined cycle plants.

Compressors. Compressors are modeled by the equation of isentropic efficiency [23] defined as the ratio of power needed to compress gases in an isentropic process and the actual power needed in the compression of the gases. For all compressors, the following equation is used for compressor efficiency, η_{comp} ,

$$\eta_{\text{comp}} = \frac{\dot{W}_s}{\dot{W}_a} = \frac{\dot{H}_{out,s} - \dot{H}_{in}}{\dot{H}_{out,a} - \dot{H}_{in}} \quad (4)$$

The compressors were assumed to have an isentropic efficiency 85%. Previous researchers, [24,26], have used compressor efficiencies in the range of 85–89%.

Water Recirculation Pump. The isentropic efficiency of the water pump is assumed to be 85%. Previous researchers, [24,26], have used pump efficiencies in the range of 85–99%.

Oxygen Separation Plant. The power to operate the oxygen separation plant, 0.22 kWh per kg of oxygen, was obtained from data presented the literature, [27], for a cryogenic air separation plant. Advances in oxygen separation are expected to reduce this power, especially when ion transport membrane (ITM) technology matures.

Computational Assumptions. Complete combustion was assumed in the gas generator. This assumption is justified because the gas generator uses platelet injectors that provide extremely uniform mixing of oxygen, fuel, and water. In addition, bench-scale tests recently made at the University of California at Davis show an absence of hydrocarbons in the exhaust and only minor concentrations of carbon monoxide. These results are in agreement with predictions based on the use of the chemical kinetics code Chemkin-II, [28,29].

Pressure drops are considered negligible in all pipelines. Heat transfer losses to the environment from lines connecting plant components are also considered to be negligible. Heat losses to the environment from heat exchangers are neglected. In a conventional power plant, natural gas would be used instead of pure methane. Natural gas typically may contain about 1% nitrogen. Similarly, a commercial oxygen separation plant for this type of application would produce an oxygen stream that contains about 1 to 2% argon. In this analysis, the contributions of the nitrogen and argon in the turbine working fluid are neglected. Addition of nitrogen and argon to the working fluid mixture of steam and carbon dioxide makes the convergence of the iterative computations more complex. Studies show that these non-combustible gases do not

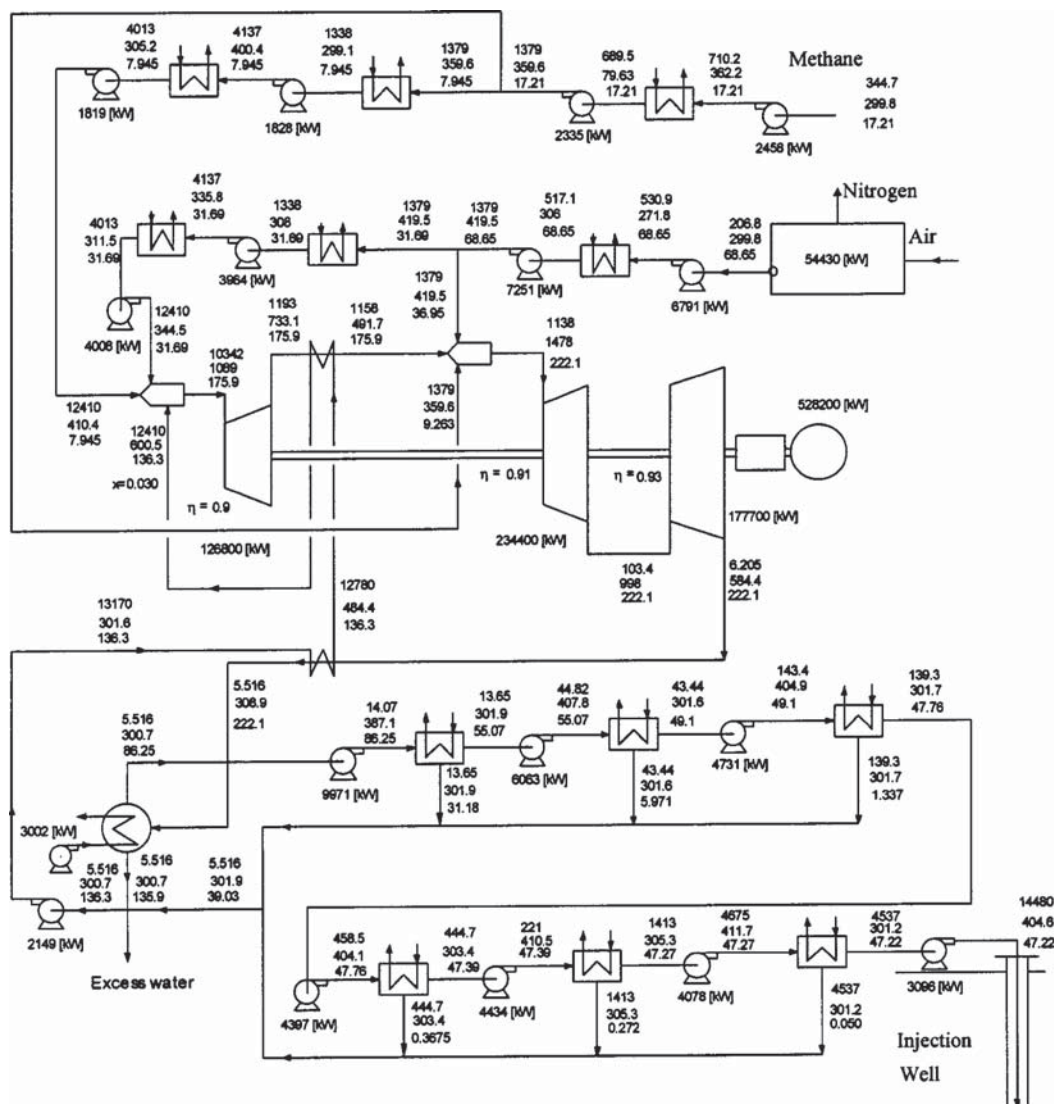


Fig. 2 Zero-atmospheric emissions power plant data for base-case analysis. Notation: pressure—kPa, temperature—K, mass flow—kg/sec. Input Power=860.4 MW, LHV, electric power generated=528.2 MW, parasitic power=128.2 MW. Net electric power=400.0 MW, net LHV thermal efficiency=0.4649.

change significantly the efficiency calculations, but primarily change the output power due to the change in molecular weight of the working fluid.

The system of equations is solved with an iterative equation solver, [22], by using computer-based tables of properties for all the substances involved (water, oxygen, methane, and carbon dioxide). The thermodynamic properties of water were obtained from the 1995 data of the International Association for the Properties of Water and Steam, [30]. Carbon dioxide properties were obtained from a fundamental equation of state by Span and Wagner [31]. Properties for methane were obtained from the 1991 equation of state by Setzmann and Wagner [32]. Properties of oxygen were obtained from Sonntag and Van Wylen [33].

Table 1 shows the values of the system parameters used in the analysis.

Results

Figure 2 shows the results for the base case power plant analysis. Figure 2 shows pressures, temperatures and mass flow rates for this power plant at more than fifty locations. In Figure 2, power is given in kW, pressures in kPa, temperatures in K, and

mass flow rates in kg/s. The base case assumes a high-pressure turbine with an inlet temperature of 1089 K (1500°F) and isentropic efficiency of 90%. The intermediate-pressure turbine operates at 1478 K (2200°F) and isentropic efficiency of 91%, and the low-pressure turbine operates at an inlet temperature of 998 K (1336°F) and isentropic efficiency of 93%. Steam turbines operating at these temperatures are being designed by a major U.S. manufacturer.

This power plant configuration has a net thermal efficiency of 46.5% and a net electrical output of 400 MW. The net thermal efficiency is based on the lower heating value of methane, and includes the energy required to separate oxygen from air and the energy required to compress the carbon dioxide for underground sequestration at a pressure of 14.5 MPa (2100 lb/in²). This sequestration pressure is sufficient to inject the carbon dioxide either into an oil zone for enhanced oil recovery, or into a subterranean aquifer at an approximate depth of 1200 m (3937 ft).

Figure 3 presents the net thermal efficiency of the power plant as a function of two important power plant parameters: turbine inlet temperature and turbine isentropic efficiency. Figure 3 shows the efficiency advantage of being able to operate the power plant

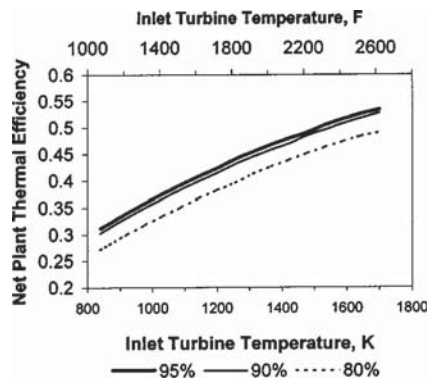


Fig. 3 Net thermal efficiency of the zero-atmospheric emissions power plant as a function of inlet turbine temperature for three values of turbine isentropic efficiency (95%, 90%, and 80%). Data shown in this figure are obtained for the same inlet temperature of both the high-pressure turbine and the intermediate-pressure turbine.

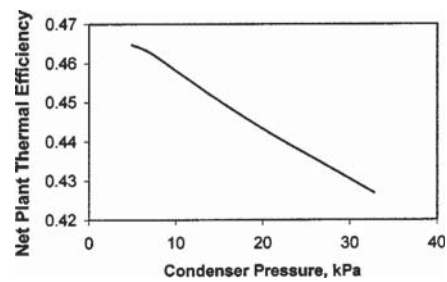


Fig. 4 Net thermal efficiency of the zero-atmospheric emissions power plant as a function of condenser pressure. The data were obtained for the base-case conditions shown in Fig. 2 and Table 1. The high-pressure turbine inlet temperature is 1089 K (1500°F), and the intermediate-pressure turbine inlet temperature is 1478 K (2200°F).

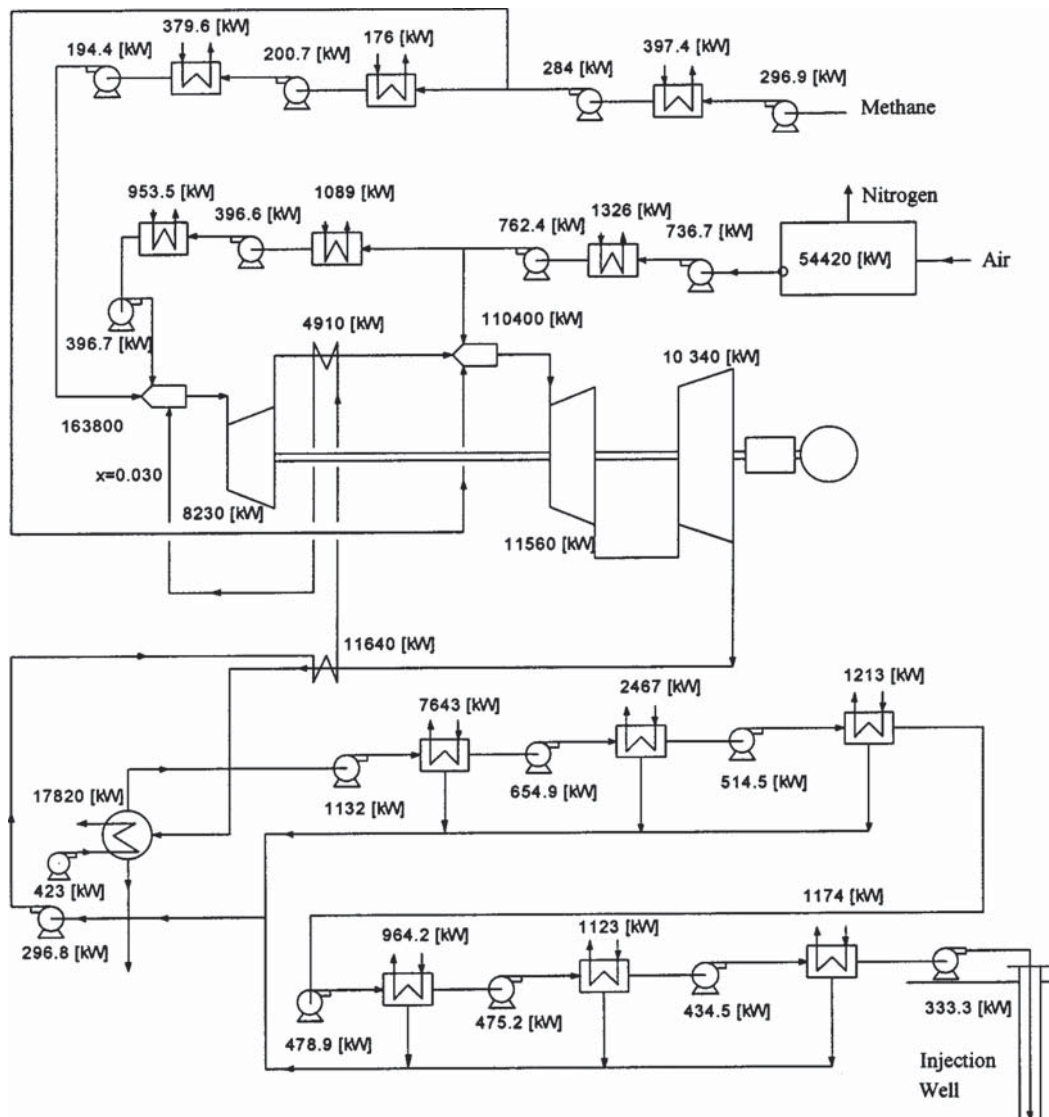


Fig. 5 Irreversibilities in components of the zero-atmospheric emissions power plant. Input power = 860.4 MW LHV, electric power generated = 528.2 MW, parasitic power = 128.2 MW, net electric power = 400.0 MW, net LHV thermal efficiency = 0.4649.

with advanced-technology high-temperature turbines. The thermal efficiency is close to 50% for 90% turbine efficiency and 1644 K (2500°F) turbine inlet temperature. This is an excellent value considering that no regulated, or greenhouse gas emissions are emitted into the atmosphere.

Figure 4 shows the effect of variations in the condenser pressure on net plant thermal efficiency. Although lowering condenser pressure will increase the power required to pump the water and the carbon dioxide from the condenser, the increase in efficiency of the Rankine cycle more than offsets this pumping power increase, thereby giving a net increase in overall plant efficiency.

A second-law analysis, [34], of the power plant was conducted as a part of this study. Irreversibilities were calculated for all components of the power plant, operating at the base-case conditions (Fig. 2). Figure 5 shows the calculated irreversibilities in kW. Figure 5 shows that the main source of irreversibilities is the combustion process. This is typical of existing power plants. The exergy lost in the gas generator and the reheater is 274 MW, which is 32% of the total exergy fed into the power plant. This irreversibility can be reduced by increasing the operating temperature of the gas turbine. However, this is difficult to accomplish due to the limits of operating temperature of current turbine materials. The second most important source of irreversibility is the air separation plant, where 54.4 MW of power is lost. This points to alternative methodologies to cryogenic air separation as important for improving the efficiency of this power plant. A possible alternative methodology is ion transport membrane (ITM). On the other hand, little exergy is consumed in carbon dioxide separation and sequestration. This process only generates 18.6 MW of irreversibility, which corresponds to 2.2% of the exergy input to the system. This is one of the main advantages of this cycle: carbon dioxide sequestration can be accomplished with little additional work.

Finally, it is worth noticing that the capital cost of a typical power plant accounts for more than half of the electricity cost. Although plant efficiency is a major factor in the cost of electricity generation, the reduced capital cost of the power plant described in this paper will result in reduced electricity cost. The reader is referred to previous publications, [8,9,35], for electricity costs per kWh and a comparison of the costs of the current technology with the electricity costs of combined cycle plants with exhaust gas clean up.

Conclusions

This paper presents a thermodynamic analysis of a zero-atmospheric emissions power plant. The simulation considers the compression process of methane and oxygen to feed the gas generator and the reheater, a Rankine cycle with three turbines and the carbon dioxide separation and sequestration processes.

The analysis predicts a 46.5% net thermal efficiency in a zero-atmospheric emissions 400 MW power plant that can be constructed with turbine technology that is under current development. The net thermal efficiency is based on the lower heating value of methane, and includes the energy required to separate oxygen from air and the energy required to compress the carbon dioxide for underground sequestration. A thermal efficiency of more than 50% is expected in a system that uses future high-temperature turbine technology.

The separation and sequestration process of the carbon dioxide demands only a small part of the auxiliary power of the system. Current research and development of the air separation technology is expected to reduce the energy required to separate oxygen from air. This would increase the efficiency of the power plant.

Acknowledgments

This work was performed under the auspices of the U.S. Department of Energy by the University of California, Lawrence Livermore National Laboratory under Contract No. W-7405-Eng-

48. Some of the concepts in this publication are based on the intellectual property of Clean Energy Systems, Inc.

Nomenclature

- c_p = constant pressure specific heat, kJ/(kg K)
- \dot{H} = rate of absolute enthalpy (includes enthalpy of formation), kW
- LHV = lower heating value, kJ/kg
- \dot{m} = mass flow rate, kg/s
- P = pressure, kPa
- \dot{Q} = heat transfer rate, kW
- T = temperature, K
- v = specific volume, m³/kg
- \dot{W} = power, kW
- ε = effectiveness (Intercoolers, preheaters, and condenser)
- η = efficiency

Subscripts

- a = actual
- c = cold side in the heat exchanger
- comp = compressor
- h = hot side in the heat exchanger
- in = inlet condition in the power plant component
- max = maximum
- out = outlet condition in the power plant component
- s = isentropic process
- t = turbine

References

- [1] DOE, 1999, "Vision 21 Program Plan: Clean Energy Plants for the 21st Century," US Department of Energy, Federal Energy Technology Center, Pittsburgh, PA.
- [2] Bilger, R., D., 1999, "Zero Release Combustion Technologies and the Oxygen Economy," *Proceedings of the Fifth International Conference on Technologies and Combustion for a Clean Environment*, Research Group on Energy and Sustainable Development, Portugal.
- [3] Falk-Pederson, O., and Dannström, H., 1997, "Separation of Carbon Dioxide From Offshore Gas Turbine Exhaust," *Energy Convers. Manage.*, **38**, pp. S81–S86.
- [4] Herzog, H., Drake, E., and Adams, E., 1997, "CO₂ Capture, Reuse, and Storage Technologies for Mitigation Global Climate Change," Final Report No. DE-AF22-96PC01257, U.S. Department of Energy, Washington, DC.
- [5] Stevens, S. H., and Gale, J., 2000, "Geologic CO₂ Sequestration May Benefit Upstream Industry," *Oil Gas J.*, **98**, pp. 40–44.
- [6] Wildenborg, T., 2000, "Costs of CO₂ Sequestration by Underground Storage," *Greenhouse Issues*, International Energy Agency Greenhouse Gas R&D Program, (47), pp. 2–4.
- [7] Wong, S., and Gunter, B., 1999, "Testing CO₂-Enhanced Coalbed Methane Recovery," *Greenhouse Issues*, International Energy Agency Greenhouse Gas R&D Program, (45), pp. 1–3.
- [8] Anderson, R., E., Brandt, H., Mueggenburg, H., H., Taylor, J., and Viteri, F., 1998, "A Power Plant Concept Which Minimizes the Cost of Carbon Dioxide Sequestration and Eliminates the Emission of Atmospheric Pollutants," *Proceedings of the Fourth International Conference on Greenhouse Gas Control Technologies*, P. Reimer, B. Eliasson, and A. Wokaun, eds., Interlaken, Switzerland, Pergamon, London.
- [9] Anderson, R. E., Brandt, H., Doyle, S. E., Mueggenburg, H. H., Taylor, J., and Viteri, F., 2000, "A Unique Process for Production of Environmentally Clean Electric Power Using Fossil Fuels," *Proceedings of the 8th International Symposium Transport Phenomena and Dynamics Rotating Machinery (ISROMAC-8)*, Pacific Center of Thermal-Fluids Engineering, Honolulu, HI.
- [10] Smith, J. R., Surles, T., Marais, B., Brandt, H., and Viteri, F., 2000, "Power Production With Zero Atmospheric Emissions for the 21st Century," *Proceedings of the 5th International Conference on Greenhouse Gas Control Technologies*, CSIRD Publishing, Cairns, Queensland, Australia.
- [11] Glassman, I., 1977, *Combustion*, Academic Press, San Diego, CA.
- [12] Viteri, F., 1993, "Turbomachinery for Modified Ericsson Engines and Other Power/Refrigeration Applications," U.S. Patent 5473899.
- [13] Viteri, F., 1997, "Turbocharged Reciprocation Engine for Power and Refrigeration Using the Modified Ericsson Cycle," U.S. Patent 5590528.
- [14] Viteri, F., 1997, "Clean Air Engines for Transportation and Other Power Applications," U.S. Patent 5680764.
- [15] Beichel, R., 1998, "Reduced Pollution Hydrocarbon Combustion Gas Generator," U.S. Patent 5709077.
- [16] Beichel, R., 1998, "Reduced Pollution Power Generation System," U.S. Patent 5715673.
- [17] Beichel, R., 1999, "Reduced Pollution Power Generation System Having Multiple Turbines and Reheater," U.S. Patent 5956937.

- [18] Beichel, R., 1999, "Reduced Pollution Hydrocarbon Combustion Gas Generator," U.S. Patent 5970702.
- [19] Viteri, F., Taylor, J. P., Brandt, H., and Anderson, R. E., 2000, "Hydrocarbon Combustion Power Generation System With CO₂ Sequestration," U.S. Patent 6170264.
- [20] Mueggenburg, H., 2001, "Steam Generator Injector," U.S. Patent 6206684.
- [21] Viteri, F., 2001, "Clean Air Engines for Transportation and Other Power Applications," U.S. Patent 6247316.
- [22] Klein, S. A., and Alvarado, F. L., 2002, "Engineering Equation Solver," F-Chart Software, Madison, WI.
- [23] Wilson, D. G., and Korakianitis, T., 1998, *The Design of High-Efficiency Turbomachinery and Gas Turbines*, Prentice-Hall, Englewood Cliffs, NJ.
- [24] Bannister, R. L., Newby, R. A., Yang, W. C., 1999, "Final Report on the Development of a Hydrogen-Fueled Combustion Turbine Cycle for Power Generation," ASME J. Eng. Gas Turbines Power, **121**, pp. 38–45.
- [25] Bolland, O., Kvamsdal, H. K., and Boden, J. C., 2001, "A Thermodynamic Comparison of the Oxy-Fuel Power Cycles Water-Cycle, Gratz-Cycle and Matiant-Cycle," International Conference of Power Generation and Sustainable Development, Liège, Belgium.
- [26] Aoki, S., Uematsu, K., Suenaga, K., Mori, H. H., and Sugishita, H., 1998, "A Study of Hydrogen Combustion Turbines," *Proceedings of the International Gas Turbines & Aeroengines Congress & Exhibition*, Stockholm, Sweden, ASME, New York.
- [27] Kobayashi, H., and Prasad, R., 1999, "A Review of Oxygen Combustion and Oxygen Production Systems," Praxair Technology, Inc.
- [28] Kee, R. J., Rupley, F. M., and Miller, J. A., 1991, "Chemkin-II: A Fortran Chemical Kinetics Package for the Analysis of Gas Chemical Kinetics," SAND89-8009B, UC-706, Sandia National Laboratories, Albuquerque, NM and Livermore, CA.
- [29] Bowman, C. T., Frenklach, M., Wang, H., Goldberg, M., Smith, G. P., Golden, D. M., Hanson, R. K., Davidson, D. F., Gardiner W. C., Jr., and Lissianski, V., 1997, "GRI-MECH2.11—An Optimized Detailed Chemical Reaction Mechanism for Natural Gas Combustion and NO Formation and Reburning," *Proceedings of the American Institute Chemical Engineers*, Los Angeles, CA, AIChE, New York.
- [30] IAPWS, "Formulation 1995 for the Thermodynamic Properties of Ordinary Water Substance for General and Scientific Use," The International Association for the Properties of Water and Steam (IAPWS).
- [31] Span, R., and Wagner, W., 1996, "A New Equation of State for Carbon Dioxide Covering the Fluid Region From the Triple-Point Temperature to 1100 K at Pressures up to 800 MPa," J. Phys. Chem. Ref. Data, **25**(6), pp. 1509–1596.
- [32] Setzmann, U., and Wagner, W., 1991, "A New Equation of State and Tables of Thermodynamic Properties for Methane Covering the Range From Melting Line to 625 K and Pressures up to 1000 MPa," J. Phys. Chem., **20**(6), pp. 1061–1155.
- [33] Sonntag, R. E., and Van Wylen, G. J., 1986, *Fundamentals of Classical Thermodynamics*, John Wiley and Sons, New York.
- [34] Moran, M. J., 1982, *Availability Analysis: A Guide to Efficient Energy Use*, Prentice-Hall, Englewood Cliffs, NJ.
- [35] Simbeck, D., 1998, "A Portfolio Selection Approach for Power Plant CO₂ Capture, Separation and R&D Options," *Fourth International Conference on Greenhouse Gas Control Technologies*, Interlaken, Switzerland, P. Reimer, B. Eliasson, and A. Wokaun, eds., Interlaken, Switzerland, Pergamon, London.



Rev-1: July 2005

OPTIMIZATION OF THERMODYNAMICALLY EFFICIENT NOMINAL 40 MW ZERO EMISSION PILOT AND DEMONSTRATION POWER PLANT IN NORWAY

Carl-W. Hustad,
CO2-Norway AS, Kongsberg, Norway

Inge Tronstad,
Nebb Engineering AS, Asker, Norway

Roger E. Anderson

Keith L. Pronske
Clean Energy Systems Inc., Sacramento, Ca.

Fermin 'Vic' Viteri

ABSTRACT

In Aug 2004 the *Zero Emission Norwegian Gas (ZENG)* project team completed *Phase-1: Concept and Feasibility Study* for a 40 MW Pilot & Demonstration (P&D) Plant, that is proposed will be located at the Energy Park, Risavika, near Stavanger in South Norway during 2008.

The power plant cycle is based upon implementation of the natural gas (NG) and oxygen fueled Gas Generator (GG) (1500 °F / 1500 psi) successfully demonstrated by *Clean Energy Systems (CES) Inc.* The GG operations was originally tested in Feb 2003 and has currently (July 2005) undergone extensive commissioning at the CES 5MW Kimberlina Test Plant, near Bakersfield, California.

The ZENG P&D Plant is an important next step in an accelerating path towards demonstrating large-scale (+200 MW) commercial implementation of zero-emission power plants before the end of this decade. However, development work also entails having a detailed commercial understanding of the techno-economic potential for such power plant cycles: specifically in an environment where the future penalty for carbon dioxide (CO₂) emissions remains uncertain.

Work done in dialogue with suppliers during ZENG Project Phase-1 has cost-estimated all major plant components to a level commensurate with engineering pre-screening. The study has also identified several features of the proposed power plant that has enabled improvements in thermodynamic efficiency from ~38% up to ~45% without compromising the criteria of implementation using "near-term" available technology. The work has investigated:

- (i) Integration between the cryogenic air separation unit (ASU) and the power plant.
- (ii) Use of gas turbine technology for the intermediate pressure (IP) steam turbine.

- (iii) Optimal use of turbo-expanders and heat-exchangers to mitigate the power consumption incurred for oxygen production.
- (iv) Improved condenser design for more efficient CO₂ separation and removal.
- (v) Sensitivity of process design criteria to "small" variations in modeling of the physical properties for CO₂ / steam working fluid near saturation.
- (vi) Use of a second "conventional" pure steam Rankine bottoming cycle.

In future analysis, not all these improvements may necessarily be "cost-effective" when taking into account total overall objectives such as; thermodynamic efficiency, capital investment, operations and maintenance cost, project life, etc. However, they do represent important considerations towards "total" optimization when designing the P&D Plant.

Project Phase-2: Pre-Engineering & Qualification is currently focusing on further improved thermodynamic efficiency and optimization of plant size with respect to total capital investment (CAPEX). We are also collaborating on turbine development for technology migration from the gas turbine environment that will permit raising turbine inlet temperatures (TIT) and attaining "medium-term" thermodynamic efficiency of ~55% (US-DOE, 2005).

INTRODUCTION

The purpose of the ZENG Project Phase-1 was to gather information and propose a "Base Case" zero-emission plant that is appropriate for the pilot and demonstration (P&D) phase of technology development. A main criterion was to use components compatible with an investment decision being made in 3Q-2006 and plant commissioning in 2008.

Furthermore emphasis has throughout been placed on ensuring that such a P&D Plant would provide the necessary

knowledge and experience to permit construction for “commercial” power plants of 240-400 MW_e (net export) in the 2010-2014 timeframe.

Such a goal for commercialization in the “medium-term” necessitates attaining power plant thermodynamic efficiency ~55% and ensuring that specific CAPEX is significantly reduced compared with what we estimate for the initial proposed nominal 40 MW P&D Plant.

There still remains considerable scope for optimizing and integrating the CES Gas Generator (GG) within a total balance of plant concept: the “Base Case” described extensively in the [Phase-1 Report](#) (Hustad *et al.*, 2004) has already been further developed and improved with respect to thermodynamic efficiency, as described in this paper.

We are also confident that a focussed effort in [Project Phase-2](#) will enable a reduction in CAPEX as we continue to optimize plant integration and work closely alongside the main equipment suppliers.

Furthermore, there continues to be a need for work regarding integration with CO₂-handling, interim storage, transportation and commercial sale of CO₂ for enhanced oil recovery (EOR), as described by Sæther and Hustad (2005).

DESIGN BASE FOR 40 MW P&D PLANT

Proposed Plant location is on reclaimed “brown field” land made available at the Energy Park, Risavika, shown in Fig. 1. Selection of the P&D Plant nominal design capacity equal to 40 MW_e (net export) corresponds to ~100 MW_t thermal power from the GG.



Fig. 1: Aerial view of reclaimed land area at the Energy Park, Risavika, nr. Stavanger, South Norway. Highlighted rectangle shows proposed location for the P&D Plant.

This size of plant was initially chosen as being a reasonable compromise between development risk, economy of scale, CAPEX and technology status. It also provides a useful

“next-step” on the path to commercialization from the 5 MW_e Kimberlina Test Plant that CES started commissioning near Bakersfield, Ca. during 4Q-2004.

The GG thermal power output scales with cross-sectional area: for the proposed P&D Plant the current (20 MW_t) GG diameter increases by a factor of 2.4—whilst length remains the same. This is considered to be within practical limits for scaling from the on-going test and operating experience.

Natural Gas (NG) is made available to the Stavanger region by *Lyse Gass AS* through a recently laid 10-inch diameter sub-sea pipeline from Kårstø with shore landing adjacent to the proposed plant site as indicated in Fig. 1.

Fuel Composition	Concentration (%-mol)
Methane (CH ₄)	88.54
Ethane	7.71
Propane	0.50
i-Butane	0.03
n-Butane	0.04
Nitrogen (N ₂)	0.69
Carbon dioxide (CO ₂)	2.49

Table 1: Summary of Fuel Composition for Natural Gas (NG). For the economic analysis we have assumed NG fuel cost to be 85 øre/Nm³ (3.29 \$/GJ).

The fuel gas in Table 1 has heat value (LHV) assumed to be 39.8 MJ/Nm³ (equivalent to 47.7 MJ/kg) and a line pressure in the range 120-180 bar. With the “Base Case” this will be reduced to 94 bar for the GG and 30 bar for reheat (RH) combustion.

PROCESS DESIGN PHILOSOPHY

The process design was based on “current technology” and required that all major equipment items should be commercially available. We utilize a conventional cryogenic air separation unit (ASU), as shown in Fig. 2, to supply pure oxygen to the GG—this being the most cost-efficient commercial method available to date.

For the power train we employ a conventional steam turbine coupled to an electric power generator; if necessary through a speed reducer.

The high-pressure (HP) turbine inlet steam temperature is restricted to 565 °C, with an increase to 705 °C for the intermediary-pressure (IP) turbine (as is acceptable from potential suppliers). The low-pressure (LP) steam turbine exhaust flows to a vacuum condenser with 0.08 bar pressure.

A condenser pressure of 0.04 bar was investigated but this would have considerably increased the condenser size; bearing also in mind that the presence of CO₂ gas in the condensing steam will significantly increase the heat transfer resistance across the condenser compared to a conventional vacuum steam condenser. Furthermore it is advisable to keep the steam

conditions upstream of the condenser above saturation level, to avoid corrosion (or erosion-corrosion) on turbine internals.

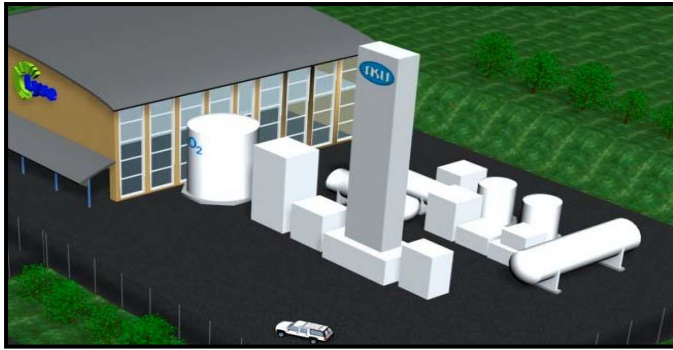


Fig. 2: Schematic view of the Air Separation Unit (ASU) adjacent to the main P&D Plant building.

The mass flow and energy balance data necessary for the selection and dimensioning of the process equipment, fuel feed, utilities consumption, etc., are generated by CHEMCAD (see www.chemstations.net). This includes comprehensive subroutines calculating thermodynamic, physical and transportation properties for the actual mixtures of the fluids involved in the main process, as well as in the utility systems.

We experienced some variation in the results depending on the simulation subroutine models utilized. These originated from differences in the calculated physical properties for the CO_2 /steam mixtures within the lower pressure and temperature regimes. Subsequent discussions have confirmed that there would appear to be limited reliable data available in this region. This means that process data and equipment parameters in the low-pressure (sub-atmospheric) regime should be treated as preliminary for the time being.

Intermediate steam data is based on thermodynamic efficiency specifications obtained from recognized suppliers of steam turbines or “state-of-the-art” efficiency properties for such equipment, as indicated in Table 2. Efficiency factors for gas compressors are based on catalogue values.

Component	Efficiency Factor
HP turbine	0.89
IP turbine	0.90
LP turbine	0.93
Electric Power Generator	0.95

Table 2: Assumed power train efficiency factors.

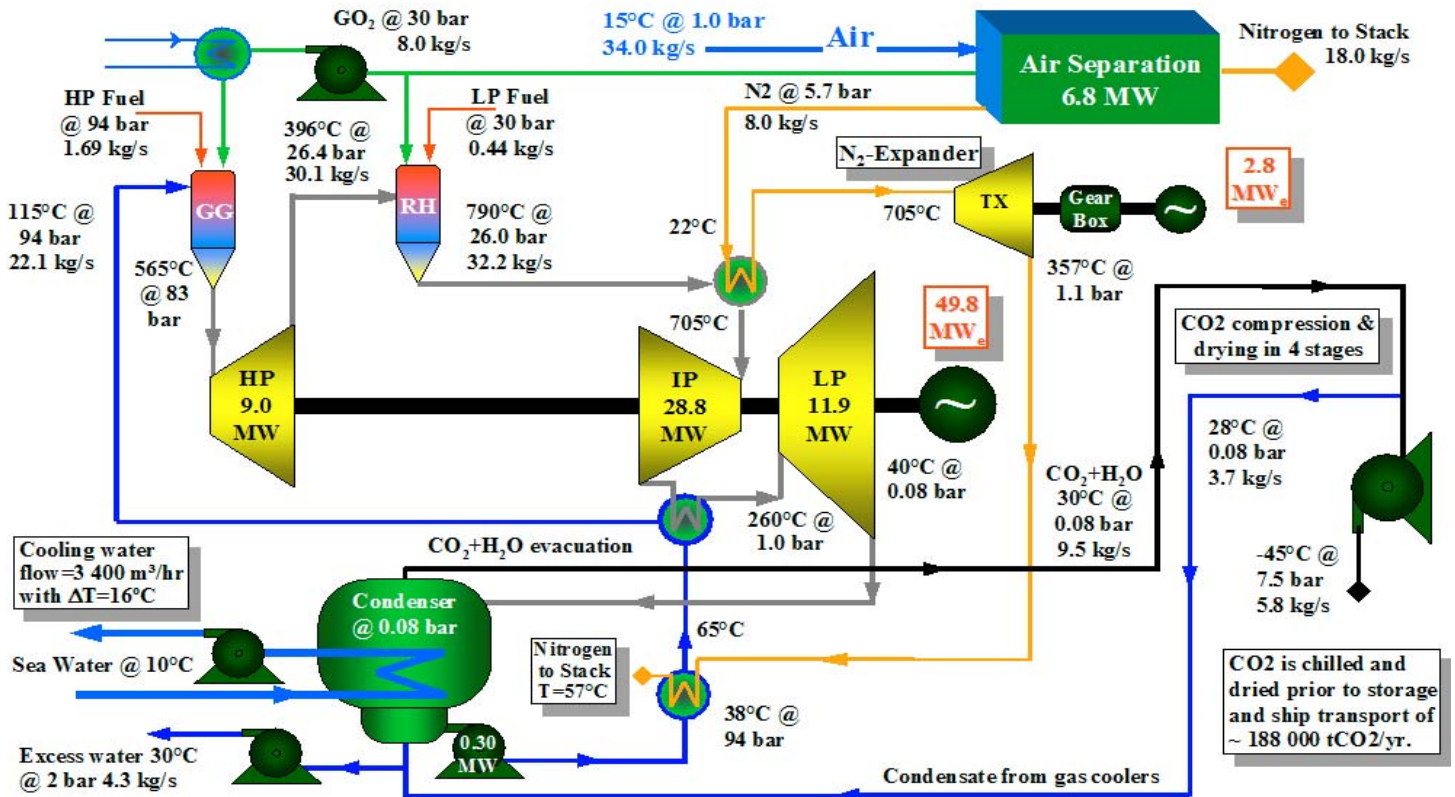


Fig. 3: Process flow schematic for “Base Case” configuration with 42 MW_e net output and cycle efficiency of ~ 38%.

DESCRIPTION OF BASE CASE PROCESS

The NG fuel is supplied at 94 bar to the GG injection nozzles through a filtering and pressure reduction control station (see Fig. 3). The gaseous fuel and pure oxygen are combusted in combination with injection of water in a complex manifold and nozzle system; establishing near ideal conditions for stoichiometric combustion and temperature control within the combustor section of the GG shown in Fig. 4.

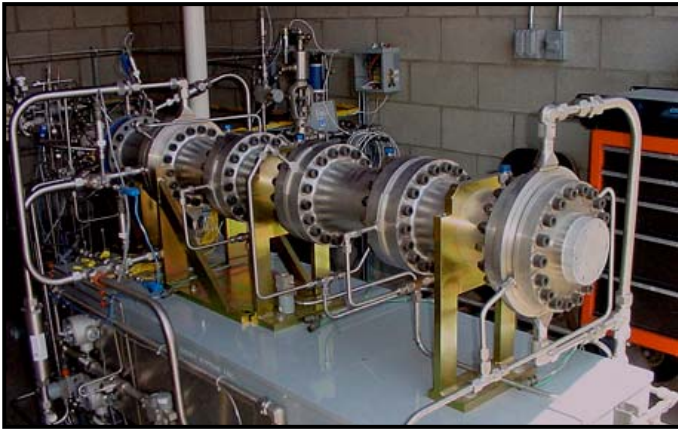


Fig. 4: The 20 MW_i CES Gas Generator (GG). Combustor section is at far end followed by 4 sequential water-cooldown sections. Closest to observer is the downstream endplate that provided back-pressure during testing ‘in lieu’ of HP turbine.

The GG exit pressure is controlled at 83 bar by the rate of fuel and oxygen flow. The process “drive” gas (CO₂ / steam) temperature is maintained at 565 °C by the water-injection rate in the cooldown sections. The GG wall temperature is controlled by the flow of water through internal cooling passages within the housing.

The process gas stream is routed through the HP turbine and expanded to the outlet pressure at 26.4 bar and 396 °C. The HP turbine shaft duty is 9.0 MW.

Next the process gas temperature is raised to 790 °C using a reheat (RH) combustion chamber operating at 26 bar pressure and fed with NG fuel and oxygen at near stoichiometric ratio (Chorpening *et al.*, 2003). The process gas stream at the RH outlet comprises a mixture of 17% CO₂ and 83% H₂O (steam) based on %-weights.

Before the IP turbine the process gas passes through a nitrogen gas heater and is cooled to 705 °C; close to currently maximum acceptable IP turbine inlet temperature (TIT). The IP turbine expands the process gas from 26 to 1 bar and a temperature of 260 °C. The IP turbine shaft duty is 28.8 MW.

The nitrogen gas (partially taken from the ASU) is expanded in a N₂-turbine expander from 5.7 bar (705 °C) to 1.1 bar (357 °C) producing 2.8 MW_e additional power.

Next the process gas is led to the LP turbine where it is expanded to the condenser pressure of 0.08 bar and a temperature of 40 °C. This is maintained sufficiently above

steam saturation temperature, in order to avoid corrosion problems in the steam turbine and exhaust channels. The LP turbine shaft duty is 11.9 MW. The total turbine duty is 49.8 MW, whilst the electric generator efficiency is assumed to be 95%.

The exhaust steam from the LP turbine is condensed in a seawater-cooled condenser. In addition to CO₂ / steam mixture, the flow to the condenser contains a small amount of oxygen and a trace of carbon monoxide. The concentrations of unburned hydrocarbons and NO_x are anticipated to be essentially zero. At an absolute pressure of 0.080 bar, partial pressures of the main components are 0.0065 bar for the CO₂ and 0.0735 bar for the steam (at which pressure the condensation temperature is estimated to be 39.9 °C).

The seawater flow requirement for the condenser is calculated to be ~3,400 m³/h with assumed cooling-water inlet temperature of 10 °C which is standard Norwegian West Coast North Sea.

“Base Case” Cycle Summary Data	
Thermal power input	111.0 MW
Gross power output	52.6 MW
Parasitic power*	10.7 MW
Net power	42.0 MW _e
Overall cycle efficiency	~ 38%
Fuel consumption	7 670 kg/h
Oxygen consumption	28 800 kg/h
Cooling water flow (total)	~ 4 300 m ³ /h
Excess water production	15.5 m ³ /h
HP Turbine inlet pressure	83 bar
HP Turbine inlet temperature	565 °C
HP Turbine exhaust temperature	~ 396 °C
IP Turbine inlet pressure	25.9 bar
IP Turbine inlet temperature	705 °C
LP Turbine inlet temperature	260 °C
LP Turbine inlet pressure	1.0 bar
LP Turbine exhaust temperature	40 °C
Condenser pressure	0.08 bar [†]

Table 3: Summary Data for “Base Case” Configuration.

* The “parasitic” power also includes electric energy consumption for the ASU, oxygen and CO₂-compressors, as well as cooling-water supply pumps.

† The condenser pressure was also increased from 0.08 bar to 0.15 bar due to recommendation from the CO₂-compressor suppliers. A higher pressure could significantly decrease the dimensions and costs for both the compressors and intercoolers. This increase in condenser operating pressure would have reduced the cycle efficiency from 37.8 to 36.3%.

OPTIMIZED PROCESS DESCRIPTION

To date the practical limit for steam temperature from conventional boilers has been around 565 °C; and no strong market incentive has existed for the development of steam turbines with higher temperatures. The CES GG presents new possibilities for cycle improvement with increased steam temperature and process pressure. However, steam turbines will not accommodate significant increase of TIT without introduction of secondary flow and internal blade-cooling, together with utilization of sophisticated materials.

But current gas turbine (GT) technology is already operating at significantly higher TIT, albeit at comparatively lower intermediary pressures: these present an excellent opportunity for inclusion as IP turbines in an “Optimized” process scheme as shown in Fig. 5. In such cycles the IP turbine TIT may potentially be elevated to 1,450 °C thereby resulting in a very substantial increase in cycle efficiency.

However for practical purpose this would require some—but still limited—redesign of a suitable gas turbine. Commercial availability of such GT’s is still considered being “a few years” ahead of the initial demonstration goals for the

current P&D Plant (but see also US-DOE, 2005) and requires commercial drivers for the equipment suppliers.

To provide an indication of the “near-term” potential for improvement of thermodynamic efficiency we have maintained a TIT of ~700 °C whilst including here an optional process scheme based on cycle integration using a RR-WR21 recuperated gas turbine as proposed by Phillips (2004).

Included in the “Optimized” configuration is also a “double” Rankine steam cycle, together with further integration of the air compressor and nitrogen expansion from the ASU. (N₂-expansion is here principally the same as for the “Base Case”, but now with the total nitrogen flow routed through the expander, thereby increasing power production and cycle efficiency.)

The benefit of the double Rankine cycle is that separation of CO₂ occurs at a pressure of 3.0 bar, thus reducing the number of CO₂-compressors and dimensions for the CO₂-handling equipment. Furthermore the LP “pure” steam Rankine cycle can now have a reduced condensation pressure (0.03 bar) compared with the “Base Case” process (0.08 bar)—this too contributes significantly to overall cycle efficiency.

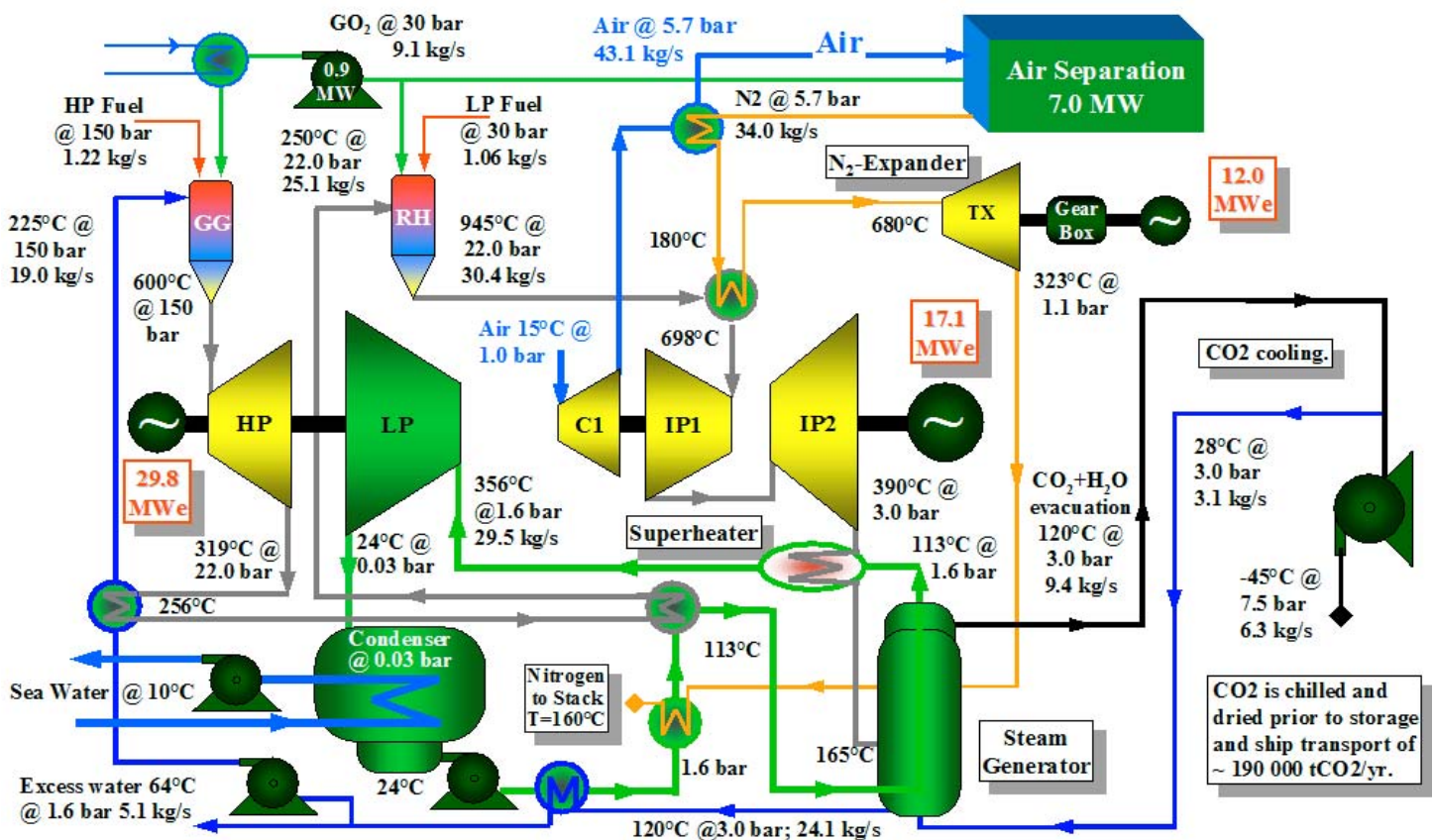


Fig. 5: Process flow schematic for “Optimized” configuration with 50.5 MW_e net output and cycle efficiency of ~ 45%.

The GG, HP turbine, reheater (RH), nitrogen heater and turbine expander, feed-water heaters and oxygen compressors are principally the same as in the “Base Case”. While the LP cycle is now a conventional “Cogen” condensing steam turbine. Furthermore the compressor (C1) delivers compressed air to the cryogenic ASU (see Fig. 5).

The GG is here operated at 150 bar and therefore a separate pressure reduction station for initial fuel handling is not necessary. Total fuel feed to the GG injection nozzle is 1.22 kg/s. The fuel energy supplied is 61 MW and the outlet energy flux is 80 MW. The process gas at the GG exit contains approximately 5.3 %-mol CO₂ while the combustion generates 3.35 kg/s CO₂ and 2.74 kg/s steam.

The process gas at 150 bar and 600 °C is routed to the HP turbine where it is expanded to 22 bar and ~ 320 °C. With turbine efficiency maintained throughout as specified in Table 2 the HP turbine stage shaft duty is now 12.4 MW.

The process gas is passed through a heat exchanger to raise GG feed-water temperature to 225 °C. The process gas stream also heats feed-water to the LP steam generator up to near vaporization temperature of 113 °C.

Next the process gas stream is routed to the RH operating at 22 bar and where the process gas temperature is raised to 945 °C by stoichiometric combustion of fuel gas with oxygen. Fuel consumption is 1.06 kg/s (equivalent to 53 MW fuel energy). The RH combustion produces 2.91 kg/s CO₂ and 2.38 kg/s steam; the gas stream now comprises 6.26 kg/s CO₂ and 24.1 kg/s steam, with the CO₂ concentration being 9.5 %-mol and energy stream flux is 116 MW.

Next the process gas stream flows to the N₂-turbine expander heater where 34 kg/s (all available) nitrogen is heated to 680 °C whilst the process gas temperature is reduced to ~ 700 °C in order to be compatible with TIT for the IP1 gas turbine.

The N₂-turbine expander produces 12 MW_e power and has an exhaust temperature of 323 °C; this is heat-exchanged against feed-water in the LP steam cycle, reducing temperature of the nitrogen exhausting to atmosphere to ~ 160 °C. (Which is still comparatively high and we should be able to make better use of this with further optimization!)

The IP gas turbine is based on a modified design derived from a recuperated GT (e.g. Rolls-Royce WR-21) where the recuperator is removed and principally replaced by the gas reheater. The process fluid expands from 22 to 3.0 bar—through two stages (IP1 and IP2)—with temperature decrease from 705 to ~ 390 °C. Normal exhaust condition for the WR-21 is atmospheric pressure, hence the last turbine stage(s) will need to be modified or removed. The turbine shaft duty is estimated to be ~17.1 MW.

The IP2 exhaust steam is led to the steam superheater for the LP steam cycle, where saturated steam from the steam generator is heated from 113 to 356 °C. The steam generator is a conventional unit, as normally utilized for production of clean steam from “unclean” steam sources.

The superheater for the produced clean steam is also a conventional free-standing unit, comprising of tube banks in a countercurrent arrangement. The exhaust steam is routed to the steam generator, where the steam fraction is condensed by heat-exchange against the (boiling) feed-water to the steam generator—mol-fraction of steam in the process fluid is 0.90.

The superheated steam (at 1.6 bar and 356 °C) is routed to the LP turbine where the steam is expanded to condenser pressure at 0.03 bar and ~ 24 °C. The LP turbine stage duty is estimated to be 17.6 MW_e.

The exhaust steam from the LP turbine is condensed in a seawater-cooled condenser. At an absolute pressure of 0.03 bar the condensation temperature for the steam is 24.1 °C.

In this preliminary study we have not to date included recompression of CO₂ from 3.0 bar to 7.5 bar followed by chilling to -45 °C, thereby making it completely ready for interim storage and subsequent ship transportation. However this will only have a small impact on the total cycle efficiency.

“Optimised” Cycle Summary Data	
Thermal power input	114 MW
Gross power output	58.6 MWe
Parasitic power	8.1 MWe
Net power	50.5 MWe
Overall cycle efficiency	~ 45 %
Fuel consumption	8 210 kg/h
Oxygen consumption	32 760 kg/h
Cooling water flow (total)	~ 4 300 m ³ /h
Excess water production	19.0 m ³ /h
HP Turbine inlet pressure	150 bar
HP Turbine inlet temperature	600 °C
HP Turbine exhaust temperature	~ 320 °C
IP Turbine inlet pressure	22.0 bar
IP Turbine inlet temperature	698 °C
IP Turbine exhaust temperature	~ 390 °C
CO ₂ / Steam Condenser pressure	3.0 bar
LP Steam Rankine Cycle	
LP Turbine inlet pressure	1.6 bar
LP Turbine inlet temperature	356 °C
LP Turbine exhaust temperature	24 °C
Steam Condenser pressure	0.03 bar

Table 4: Summary Data for “Optimized” Configuration.

In recent (unpublished) work we have further increased cycle efficiency by 2-3%-point. And therefore now consider our main focus in [Project Phase-2](#) should be to ensure similar progress in reducing the plant specific CAPEX (\$/kW) and ensuring plant availability of ~ 95%, as is achievable with typical steam cycles.

ECONOMIC ANALYSIS

Within the present study we have identified and cost-estimated all major components for the “Base Case” configuration and made comparison with a conventional NG Combined Cycle (NGCC) Power Plant. Included here are also cost-factors based on accumulated project experience in Norway—with high labor costs and strong local currency these can typically lead to estimates that are 20-25% above US Gulf Coast estimates!

The economic model permits input of all main power plant parameters; CAPEX, operating costs, internal rate of return, project duration, efficiency, net power generation, sale of CO₂, etc. Model output is derived using annualized cash flow and calculates cost of electricity (CoE) by prescribing a zero net present value. All modeling is pre-tax. We have made the following generalized basic assumptions:

- 10% discount rate and project economic life of 25-yrs.
- Fuel cost is 85 øre/Nm³ NG (equivalent to 3.29 \$/GJ).
- For P&D Plant we assume 60% financed debt at 5% interest. This reflects some “goodwill” from the Norwegian government’s interest to help promote development and demonstration of such “new” power generation technology¹.
- For comparison between the conventional NGCC Reference Plant and a “commercial” ZENG-CES plant we revert to assuming 100% equity financing.
- Assume two years for total investment and construction.
- Assume 6 weeks for commissioning during first year.
- Exchange rate is 6.50 NOK/US\$.
- CoE is expressed in mills/kWh (1,000 mills/US\$) and in Norwegian currency as øre/kWh (100 øre/NOK).

Using Reference CoE from the NGCC without CO₂-capture² we can also calculate a CO₂-capture cost (in US\$ per ton of CO₂) for comparison with sale of CO₂ for EOR to a CO₂-aggregator / transporter / oilfield operator.

For the “Base Case” 42 MW_e P&D Plant (inclusive of the ASU) we have total CAPEX of \$97.7 million (equivalent to 635 MNOK). With further focus on cost optimization in Project Phase-2 and with economies of scale, we believe there is considerable opportunities for reducing this CAPEX.

The incremental CoE for the “Base Case” is estimated to be +26.0 mills/kWh compared with the 400 MW Reference CoE. Alternatively, the plant would need to recover a CO₂-

capture cost of \$28.0 /ton (at perimeter fence) in order to be competitive with electricity from the Reference Plant³.

For the “Optimized” Configuration we have estimated total CAPEX to be \$109.9 million (equivalent to 714 MNOK). Net export power is 50.5 MW_e resulting in incremental CoE of +19.0 mills/kWh compared with the Reference CoE. Alternatively the “Optimized” P&D Plant must sell the CO₂ at a price of \$19.3 /ton (at perimeter fence) to cover extra costs.

The CO₂-liquefaction plant (with storage facilities) and transportation to offshore platform are outside Scope of Work for the P&D Plant (but see Sæther and Hustad, 2005). However, as described by Hustad and Austell (2004) one may conservatively account for this incremental cost in CO₂-handling by assuming an additional ~\$12 /ton whereby delivered price will be ~\$31 /tCO₂.

Recent alternative studies have indicated delivered cost for CO₂ on North Sea platform to be in the range from \$35 /tCO₂ as proposed by Elsam / Kinder Morgan, CENS Project (Markussen *et al.*, 2002). Alternatively up to \$48 /tCO₂ as presented by Statoil for proposed CO₂-flooding at Gullfaks.

In the near- to medium-term (2010-2014) we have identified cycle optimization opportunities that could ensure plant efficiency of ~51%. Furthermore, we believe cost-optimization, economies of scale and early commercial introduction can contribute to ensure an additional one-third reduction in specific CAPEX. This would entail that a “100% equity financed” commercial 240 MW ZENG-CES Power Plant could have a CO₂-capture cost (at perimeter fence) of \$17.9 /tCO₂ whilst delivering 0.80 mtCO₂/yr for EOR.

In this context the key economic variable is the market price of crude oil which determines the sales value of CO₂ for EOR. Again we may assume, using larger volumes, that delivered cost of CO₂ at the offshore platform from such a 240 MW ZENG-CES Power Plant could be ~\$28 /tCO₂. Thus, even with the current fiscal regime in the North Sea—which is not yet optimized to create incentives for CO₂-EOR—the pre-requisite crude oil price needed to sustain project economics would be in the range \$25-\$28 /bbl (see Hustad and Austell, 2004).

In the medium- to longer-term (2012-2015) we foresee technology improvements⁴ and economies of scale that should permit a 400 MW ZENG-CES Power Plant to operate with ~55% efficiency and have specific investment cost below 1 400 \$/kW. Economic modeling for such a plant suggest it would have a CO₂-capture price of ~\$10 /tCO₂ whilst producing 1.25 mtCO₂/yr. The long-term goal is to achieve 60% plant efficiency by 2015 (US-DOE, 2005).

¹ In 2004 the Norwegian government specifically set aside a fund of \$310 million to promote P&D Power Plants with CO₂-capture & storage (CCS). They have also indicated that as cost-effective technologies emerge, then they shall be willing to further add to this level of support if necessary.

² The Reference Plant assumes a new build on the West Coast of Norway with specific CAPEX of 745 \$/kW installed. We obtain CoE at 35.2 mills/kWh (22.9 øre/kWh) exclusive of CO₂-emissions. We assume that the Reference Plant will need to purchase CO₂-credits for an additional cost of \$12 /tCO₂ starting in 2008 and rising linearly to \$24 /tCO₂ at end of project economic lifetime. With these assumptions we derive a Reference CoE equal to 40.7 mills/kWh (26.5 øre/kWh). For further details see Hustad *et al.* (2004).

³ Here we assume “Base Case” P&D Plant will capture 100% of its CO₂-emissions at a pressure of 7.5 bar. This will subsequently need to be dried and cooled to -45 °C (near triple point) for liquefied storage and ship transportation.

⁴ Specifically we here foresee commercial introduction of; (i) oxygen membrane technology, and (ii) blade-cooling to permit increased TIT for the HP and—in particular—the IP turbine expansion stages.



Fig. 6: Schematic sketch of the proposed 40 MW (nominal) Pilot & Demonstration Power Plant at the Energy Park in Risavika.

In this timeframe we may also assume that the cost of CO₂ transportation from the power plant perimeter fence out to an oilfield will be aggregated and handled in a more cost-effective manner through a dedicated CO₂-infrastructure. We therefore estimate future delivered price for CO₂ to be ~ \$17 /ton. The sustaining market price of crude oil would then need to be ~ \$22 /bbl.

The long-term market expectation is that crude oil will be above \$35 /bbl; highlighting a substantial commercial upside on the basis of EOR. Furthermore, CO₂-credits are already trading at ~ \$20 /ton on EU and US exchanges. Thus there are already two strong economic incentives to develop zero-emission fossil power generation.

CONCLUSIONS

Results suggest that a ZENG-CES Power Plant, in combination with sale of CO₂ for EOR could provide 3.2 TWh of base load (+8 000 hours per year) zero-emission electricity by 2011. And will, through project economic lifetime in a “carbon-constrained” market be more cost-effective than a conventional power plant having to pay for its CO₂ emissions.

Zero-emission power in combination with recognized CO₂-EOR potential creates a business opportunity providing an important contribution to the use of NG in Norway, life-extension for the mature oil reservoirs on the Norwegian Continental Shelf, and technology export opportunities.

ACKNOWLEDGMENTS

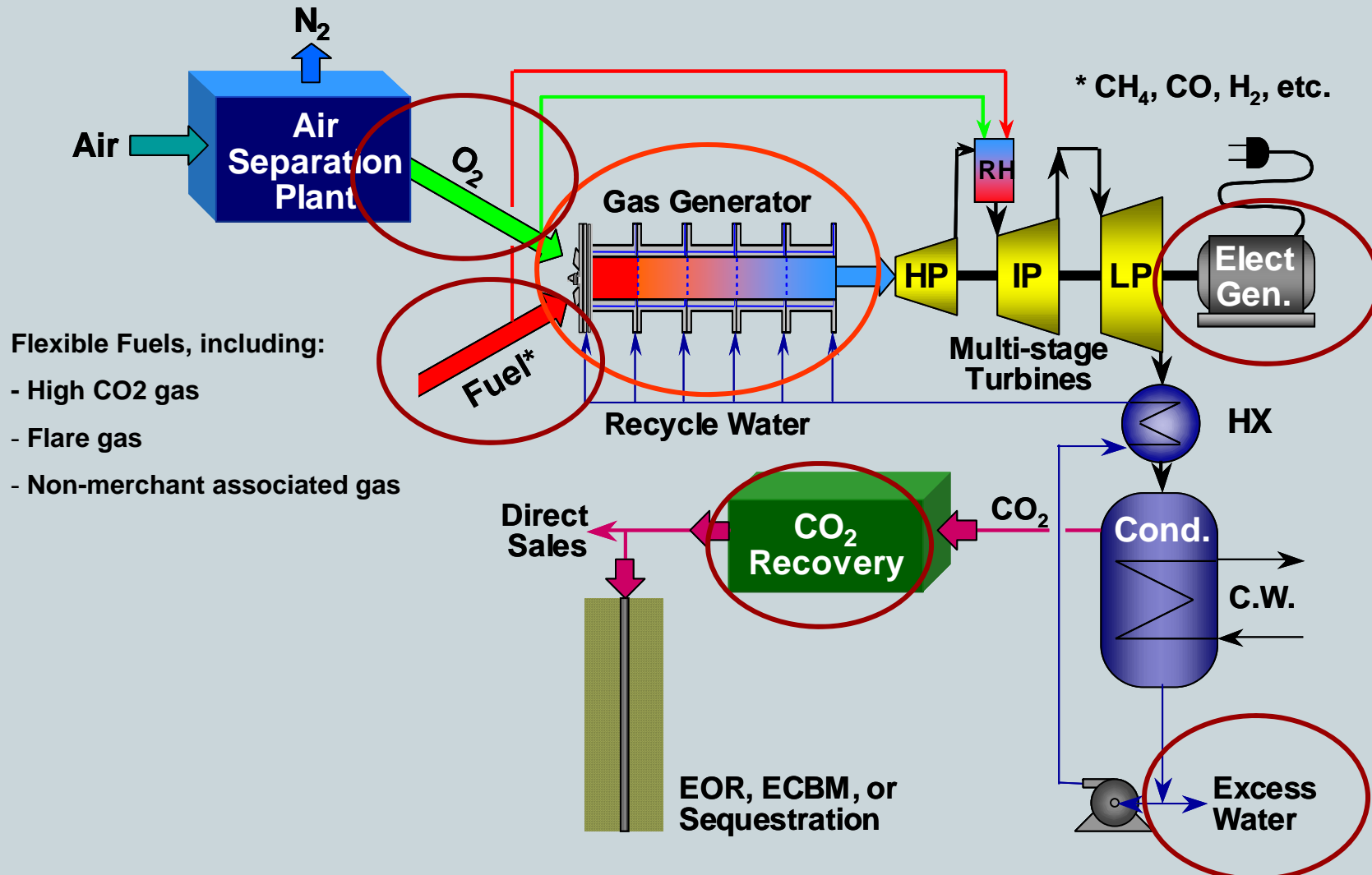
The following have participated and contributed to the ZENG Project Phase-1 Study Report: **Sweco Grøner AS** (a Swedish / Norwegian engineering consultancy); **Nebb Engineering AS** (a Norwegian power and process engineering consultancy); **Det Norske Veritas** (the Norwegian safety, risk and certification company); **Clean Energy Systems Inc.** (California-based technology developer); **CO₂-Norway AS** (a

Norwegian technology & project developer); **Lyse Energi AS** (regional utility company); **Energiparken AS** (Manager, Energy Park, Risavika, near Stavanger).

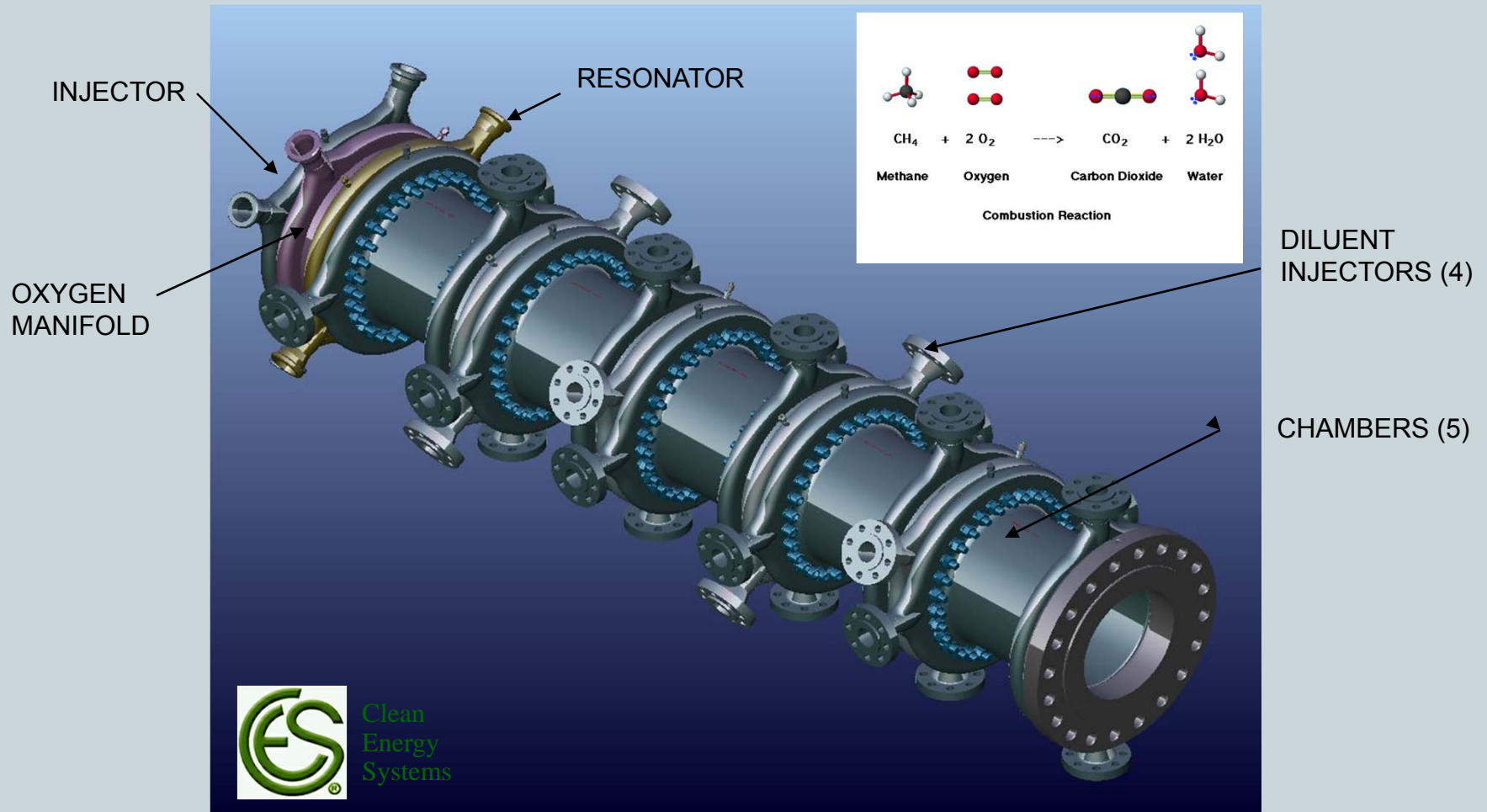
REFERENCES

- US-DOE, (2005). “Enabling Turbine Technologies for High-Hydrogen Fuels (incl. oxygen combustion cycles)”. Funding opportunity DE-PS26-05NT42380, March. (Available at <http://www.co2.no/download.asp?DAFID=8&DAAID=3>).
- Hustad, C-W. *et al.*, (2004). “Zero Emission Norwegian Gas (ZENG) Phase-1: Concept and Feasibility Study”. Final Report, Rev. date 15th October, CO₂-Norway AS. (Available at <http://www.co2.no/download.asp?DAFID=20&DAAID=3>).
- Sæther, T. and Hustad, C-W., (2005). “A CO₂-Hub at Risavika”. Scope of Work (in preparation). Project Invest AS / CO₂-Norway AS, August.
- Chorpening, B. *et al.*, (2003). “Demonstration of a Reheat Combustor for Power Production with CO₂ Sequestration”. GT-2003-38511, *ASME Turbo Expo*, Atlanta, GA, June 16-19.
- Phillips, J. N., 2004. “Integration of Commercial Gas Turbine Technology into a CES Zero Emissions Power Plant”. Report No. 5909-08-3 *Fern Engineering*, CES – DOE Funded Contract, June.
- Markussen, P., Austell, J.M. and Hustad, C-W. (2002). “A CO₂-Infrastructure for EOR in the North Sea (CENS): Macroeconomic Implications for Host Countries”. Presented at *GHGT-6*, Kyoto. Paper No.324, Sept 30 – Oct 4. (Available at <http://www.co2.no/files/files/co2/16.pdf>).
- Hustad, C-W. and Austell, J. M., 2004. “Mechanisms and Incentives to Promote the Use and Storage of CO₂ in the North Sea”. In *European Energy Law Report I*, pp. 355-380. Eds. Roggenkamp, M.M. and Hammer, U., Intersentia. (Available at <http://www.co2.no/files/files/co2/12.pdf>).

Oxy Fuel Plant Concept



Gas Generator



- Combustion Technology for injector design promotes intimate mixing and cooling

Protection notice / Copyright notice

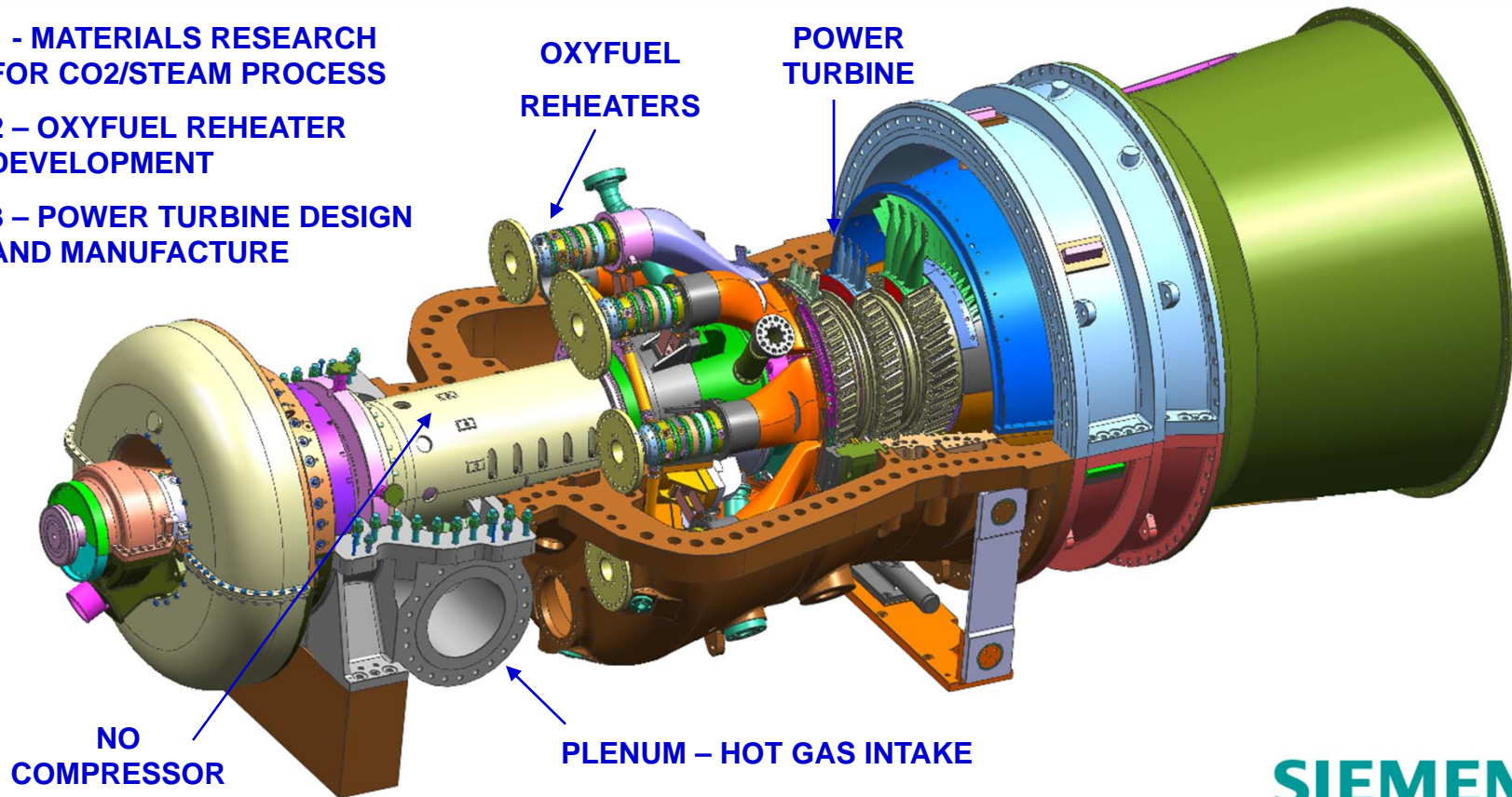
Power Turbine

SIEMENS

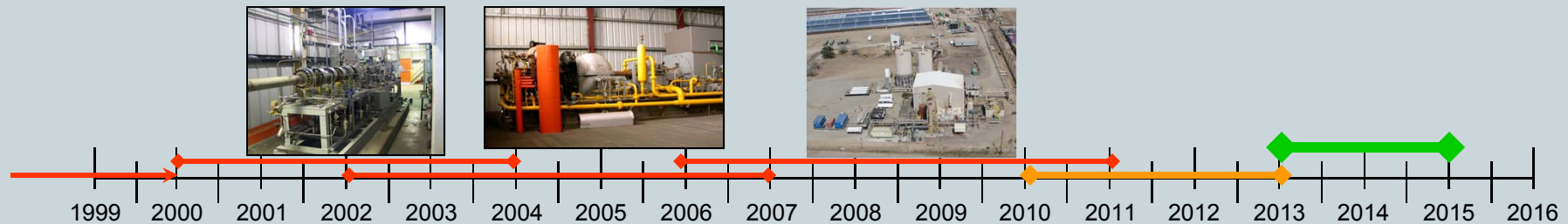
1 - MATERIALS RESEARCH
FOR CO₂/STEAM PROCESS

2 - OXYFUEL REHEATER
DEVELOPMENT

3 - POWER TURBINE DESIGN
AND MANUFACTURE



Development History



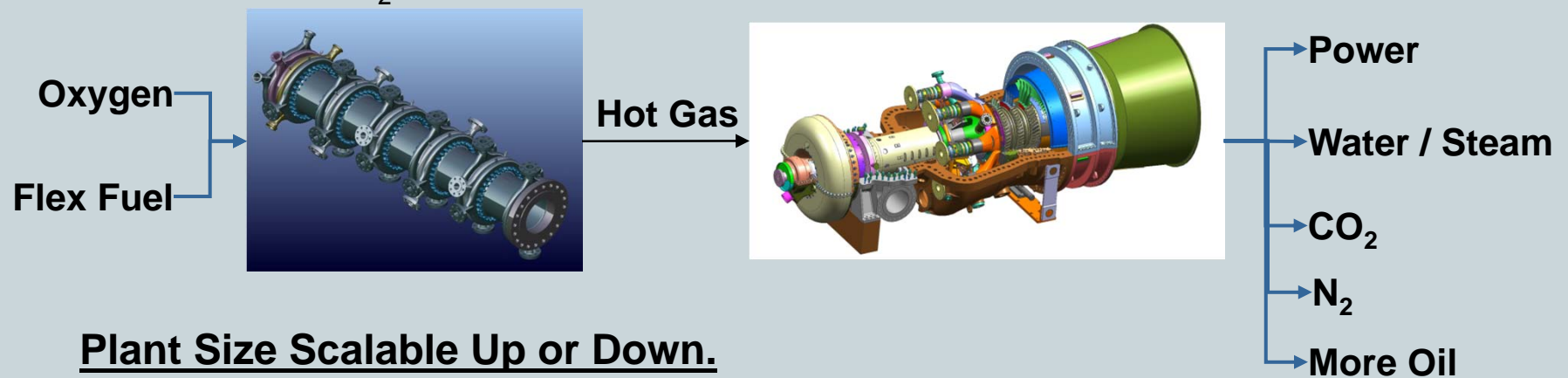
- Past Development:

- 1999: First demonstration of CES oxy fuel technology done under CEC grant
- 2000-2003: 20MWt generator tested under DOE grant
- 2002-2006: 2.7 MWe pilot-scale oxy fuel plant commissioned and connected
 - > Over 400 starts and 2,000 running hours
- 2006-2010: 170 MWt CES combustor tested with 1st generation oxy fuel turbine
- Current: DOE grant awarded to CES in partnership with Siemens
 - USD \$30M awarded Sep 2010
 - Goal: Development of 2nd generation oxy fuel gas turbine technology
 - CES to further enhance combustor technology
 - Siemens to design, manufacture, and package oxy fuel turbine
 - DOE project completion: 2012
- Future: Commercial deployment of oxy fuel solution: 2014-2015

Technology Targets

2nd generation Oxy Fuel Turbine Cycle capable of producing:

- Up to 150 to 200 MWe net power = 200,000 to 270,000 hp compression
- Start and synchronize to grid within 10 minutes
- No NO_x
- 30-40% cycle efficiency
 - Includes CO₂ capture/compression, and O₂ separation/compression
 - Use of low calorific and non-merchant fuels (25%-90% CO₂)
- 2,500 tonnes/day or 48 MMSCFD CO₂ → Enhanced Oil Recovery
- 13,000 BWPD net produced, or 190 kpph steam → net water
- 500 MMSCFD N₂ → ??



Plant Size Scalable Up or Down.

Protection notice / Copyright notice
Energy Oil & Gas

13th International Conference on Greenhouse Gas Control Technologies, GHGT-13, 14-18
November 2016, Lausanne, Switzerland

Demonstration of the Allam Cycle: An update on the development status of a high efficiency supercritical carbon dioxide power process employing full carbon capture

Rodney Allam, Scott Martin*, Brock Forrest, Jeremy Fetvedt, Xijia Lu, David Freed,
G. William Brown Jr.^a, Takashi Sasaki, Masao Itoh^b, James Manning^c

^a8 Rivers Capital, 406 Blackwell Street, Crowe Building 4th Floor, Durham, North Carolina 27701, US

^bToshiba Corporation, 2-4, Suehiro-Cho, Tsurumi-ku, Yokohama 230-0045, Japan

^cHeatric, 46 Holton Road, Poole BH16 6LT, United Kingdom

Abstract

The Allam cycle is a novel CO₂, oxy-fuel power cycle that utilizes hydrocarbon fuels while inherently capturing approximately 100% of atmospheric emissions, including nearly all CO₂ emissions at a cost of electricity that is highly competitive with the best available energy production systems that do not employ CO₂ capture. The proprietary system achieves these results through a semi-closed-loop, high-pressure, low-pressure-ratio recuperated Brayton cycle that uses supercritical CO₂ as the working fluid, dramatically reducing energy losses compared to steam- and air-based cycles. In conventional cycles, the separation and removal of low concentration combustion derived impurities such as CO₂ results in a large additional capital cost and increased parasitic power. As a result, removal in conventional cycles can increase the cost of electricity by 50% to 70% [1]. The compelling economics of the Allam Cycle are driven by high target efficiencies, 59% net for natural gas and 51% net for coal (LHV basis) while inherently capturing nearly 100% CO₂ at pipeline pressure with low projected capital and O&M costs. Additionally, for a small reduction in performance the cycle can run substantially water free. The system employs only a single turbine, utilizes a small plant footprint, and requires smaller and fewer components than conventional hydrocarbon fueled systems. The Allam Cycle was first presented at GHGT-11 [2]. Since then, significant progress has been made, including detailed system design, component testing and the construction of a 50 MWth demonstration plant commencing in Q1 2016 and now entering commissioning as of Q4 2016. This paper will review the development status of the Allam Cycle; for the demonstration plant, the construction and commissioning status, schedule, key components, layout, and detailed design; turbine design, manufacturing status; development of a novel dynamic control system and control simulator for the demonstration plant; and other key aspects of the cycle. It will provide an

* Corresponding author. Tel.: +1-919-667-1800; fax: +1-919-287-4798.

E-mail address: scott.martin@8rivers.com

update on the progress of the gasified solid fuel Allam Cycle and then address the overall Allam Cycle commercialization program, benefits and applications, and the expected design of the natural gas 300 MWe commercial NET Power plant projected for 2020.

© 2017 The Authors. Published by Elsevier Ltd. This is an open access article under the CC BY-NC-ND license (<http://creativecommons.org/licenses/by-nc-nd/4.0/>).

Peer-review under responsibility of the organizing committee of GHGT-13.

Keywords: natural gas, coal, Allam Cycle, carbon, capture, supercritical, update, demonstration, 8 Rivers, Heatric, Toshiba, NET Power, CO₂, sCO₂

1. Introduction

It is imperative that the global community implements a path to achieve significant reductions in current greenhouse gas emissions, principally CO₂. This resolve is set out in the COP-21 protocol [3]. At present, efforts focus on using nuclear and renewable energy sources to meet low-carbon power needs. While these are important clean energy sources, the IPCC 5th Assessment shows that a broader portfolio of low-carbon energy sources is necessary to offer the greatest chance of meeting global climate change targets. In particular, the IPCC 5th Assessment finds that climate models that do not include carbon capture and sequestration in addition to renewable and nuclear energy result in the fewest scenarios in which global temperature rise is maintained below agreed limits. Additionally, the assessment shows that scenarios without carbon capture and sequestration achieve results only with substantially higher costs [4].

The Allam Cycle offers a path to a sustainable energy future by cleanly and economically employing hydrocarbon energy reserves in a process that inherently captures combustion derived CO₂ for sequestration or reuse. The Allam Cycle was originally presented in Kyoto at GHGT-11. It has now reached a mature state of development and will soon be demonstrated using a pilot plant now entering the commissioning stage.

Traditional power cycles, such as natural gas combined cycle (NGCC), supercritical coal cycles, and integrated gasification combined cycles (IGCC), require the addition of expensive, efficiency-reducing equipment in order to reduce and capture emissions of CO₂ and other pollutants. Analyses of these cycles have shown that the additional CO₂ removal systems can increase the cost of electricity by 50% to 70% when capturing typically 90% of the CO₂ generated from hydrocarbon fuel combustion [1]. The Allam Cycle takes a novel approach to reducing emissions by employing oxy-combustion and a high-pressure supercritical CO₂ working fluid in a highly recuperated cycle [5]. The CO₂ that must be vented from the process leaves at pipeline pressure and high quality as a result of the operating conditions of the cycle, thereby mitigating the common necessity of an additional capture, clean-up, and compression system. The cycle is able to utilize a variety of hydrocarbon fuels, including natural gas, unprocessed raw and sour natural gas streams containing H₂S and CO₂, and gasified solid fuels such as coal, oil refining residuals, and biomass. The result is a power cycle with major advantages over conventional systems that do not capture CO₂, attaining 59% LHV efficiency (comparable to best-in-class NGCC power plants not capturing CO₂); significantly higher efficiencies than state-of-the-art coal plants, currently reaching 51% LHV; low capital costs due to the simplicity and high-pressure of the cycle; low ambient cooling requirements, depending on cooling configurations used; and virtually no air emissions, including full CO₂ capture. Additionally, for a small reduction in performance the Allam Cycle can run substantially water free [6, 7, 8].

The Allam Cycle has been under development for 7 years by 8 Rivers Capital. Specific development of the natural gas Allam Cycle has been undertaken by NET Power, a company owned by 8 Rivers, Exelon Generation, and CB&I. NET Power is currently building a 50 MWth natural gas demonstration power plant in La Porte, Texas, soon entering commissioning. The plant will be a fully operational, grid-connected power plant containing all key system components. Further, it will demonstrate the full operability of the cycle, including start-up, shut-down, load following, emergency operations, and partial-load operation in addition to component duration testing.

NET Power is working closely with Toshiba Corporation which is developing and supplying a novel supercritical CO₂ combustion turbine for the cycle [9, 10]. The turbine for the demonstration plant is completed and is in the process of being shipped to site with its electric generator and auxiliary equipment. The advanced high pressure recuperative heat exchanger has been designed and fabricated by Heatric and is already on site.

The first full-scale, 300 MWe Allam Cycle commercial plant based on natural gas fuel is currently in the design phase. A pre-FEED study of the commercial-scale plant has been completed. Numerous commercial partners are already engaged and vetting potential sites. The first commercial plant is expected to become operational in 2020.

In addition to the demonstration of the natural gas Allam Cycle, 8 Rivers Capital continues to advance the gasified coal-based Allam Cycle, having completed several feasibility design studies. Current activity covers the design of the combustor, validation of 8 Rivers' proprietary, novel coal-derived impurity removal system, corrosion testing, and gasifier selection. This work is being completed with a consortium of stakeholders from the State of North Dakota that includes the Energy & Environment Research Center, ALLETE, and Basin Electric.

2. Core Allam Cycle Description

2.1. Allam Cycle for Natural Gas Fuel

The Allam Cycle is a power cycle that utilizes a recirculating, trans-critical CO_2 working fluid in a high-pressure, low-pressure-ratio, highly recuperated Brayton cycle [8]. The cycle operates with a single turbine that has an inlet pressure of approximately 300 bar and a pressure ratio of 10. The basic schematic employing natural gas fuel is depicted in Figure 1 with a stream flow summary in Table 1. These values are a simplified representation of a commercial scale plant without depicting additional detail for optimized heat exchanger, compressor, and turbine performance. A pressurized gaseous fuel (14) is combusted in the presence of a hot oxidant flow containing a mixture of CO_2 and nominally pure oxygen (13, provided by a co-located Air Separation Unit (ASU)) and a hot CO_2 diluent recycle stream (9) at approximately 300 bar under lean combustion conditions. The exhaust flow exiting the combustor is expanded through a turbine to approximately 30 bar, reducing in temperature to above 700°C (1). Following the turbine, the exhaust flow enters a recuperating heat exchanger which transfers heat from the hot exhaust flow to the

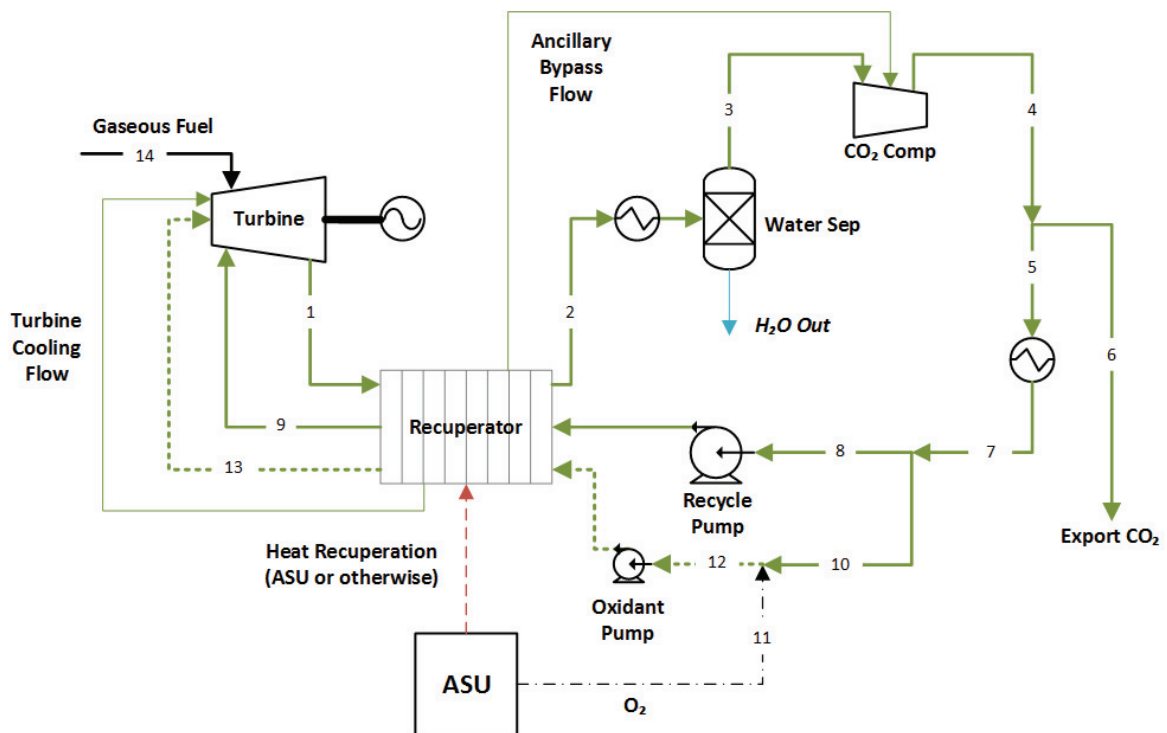


Figure 1: Process schematic of a simplified commercial scale natural gas Allam Cycle

aforementioned high pressure CO₂ recycle stream which acts as diluent quench for the combustion products and lowers the turbine inlet temperature to an acceptable level of 1150°C, as well as the oxidant flow providing oxygen to the combustor flame zone. Exiting the primary heat exchanger (2), the turbine exhaust flow is cooled to near ambient temperature and combustion derived water is separated (3). The predominantly CO₂ fluid stream is then recompressed (4), cooled (7), and pumped to approximately 300 bar pressure where it then reenters the cold end of the recuperative heat exchanger. At a point before entering the heat exchanger, a portion of the recycle CO₂ (10) is mixed with oxygen (11) to form an oxidant mix stream (12) which is fed separately to the heat exchanger and turbine. Within the main process heat exchanger, the recycle flows undergo reheating against the hot turbine exhaust before returning to the combustor at temperatures exceeding 700°C. In order to maintain mass balance within the semi-closed cycle, a portion of the high purity CO₂ process gas is exported at a point within recompression to a high pressure CO₂ pipeline for sequestration or utilization. This net export is approximately 5% of the total recycle flow, meaning the majority of the process inventory is recirculated.

Table 1: Stream flow summary of a simplified commercial scale natural gas Allam Cycle

Stream	Temperature (°C)	Pressure (bar)	Mass Flow (kg/s)
1	727	30	923
2	43	29	564
3	17	29	563
4	23	100	909
5	23	100	881
6	23	100	28
7	16	100	881
8	16	100	689
9	717	312	586
10	16	100	191
11	16	100	41
12	2	99	233
13	717	310	233
14	266	330	10

The operating points for a simplified Allam Cycle CO₂ power cycle are shown on a pressure-enthalpy diagram for pure CO₂ in Figure 2. This diagram shows a turbine inlet condition of 300 bar and 1150°C and an outlet pressure of 30 bar. Note that the presence of H₂O, inert N₂, Ar, and O₂ plus fuel and combustion-derived impurities will modify the physical properties of pure CO₂ slightly. The turbine inlet is defined by point A and the turbine outlet at point B, which also refers to the inlet of the hot end of the recuperating heat exchanger. The fuel heat input to the combustor is equivalent to A-K. The heat transferred from the turbine exhaust to the high pressure recycle stream is B-C and the heat received by the recycle stream from this heat transfer is K-J. Following ambient cooling from points C to D and water separation, the cooled turbine exhaust enters a two stage CO₂ compressor with an intercooler inlet at point E. In the second stage it is compressed from point F to G, at a pressure above the critical pressure of the predominantly CO₂ stream. The compressor after-cooler then cools the supercritical CO₂ stream to near ambient temperature at point H. This results in an increase in density from 0.15 kg/m³ to 0.85 kg/m³. A multi-stage centrifugal pump then raises the CO₂ working fluid pressure from point H to 300 bar at point I. The net product CO₂ is removed at or before this point and the remaining process flow enters the recuperating heat exchanger. A portion of heat from a collocated ASU or other source of waste heat provides energy from J-I (to be addressed below) and then the hot exhaust provides recuperated energy in K-J to provide the total reheating energy of K-I. The heated recycle CO₂ flow leaves the economizer heat exchanger and enters the combustor at point K, where it mixes with the combustion products from a methane stream burned with oxygen.

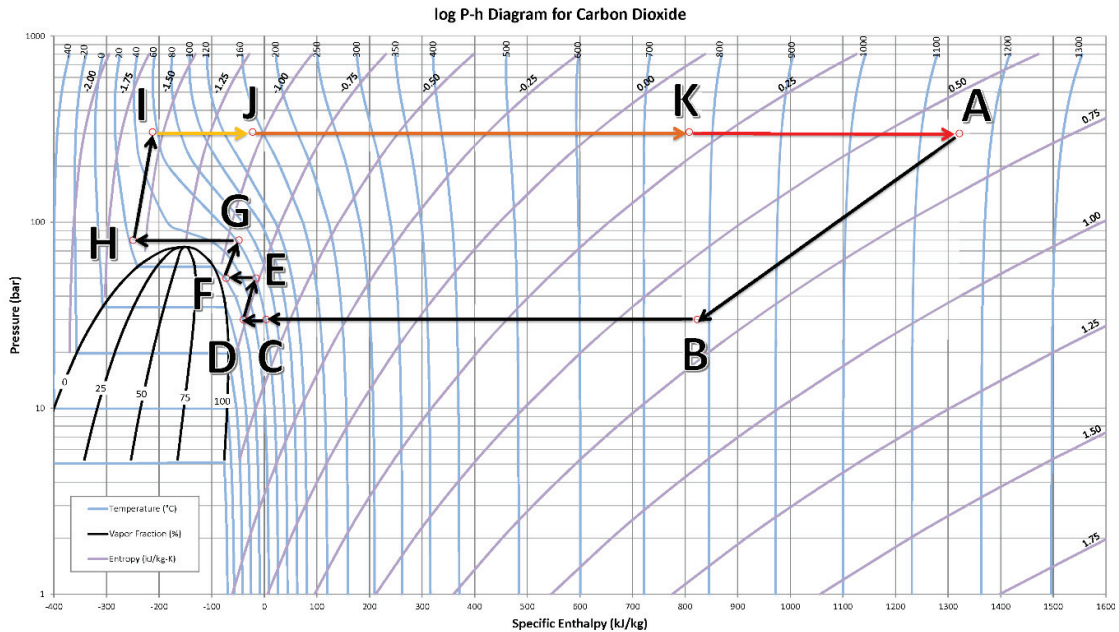


Figure 2: Simplified Allam Cycle Pressure-Enthalpy diagram for pure CO₂

To achieve high overall power generation efficiency, a close temperature approach is required at the hot end of the heat exchanger. It can be seen that there is a very significant imbalance between the heat liberated by the low pressure turbine exhaust (B-C) and the heat required to raise the temperature of the high pressure recycle stream (K-I). This imbalance is due to the very large difference in the specific heat of CO₂ in the 300 bar recycle stream compared to the 30 bar turbine exhaust stream at the low temperature end of the recuperating heat exchanger. The imbalance can be corrected by adding a significant quantity of externally generated heat in the range of 100°C to 400°C into the 300 bar recycle CO₂ stream corresponding to the heat required from points I to J. A convenient source of heat can come from the adiabatic operation of the ASU air compressors and the CO₂ recycle compressor. Although this increases the compressor power, the overall effect is net positive. The total adiabatic power input to the recycle CO₂ stream produces an equivalent drop in required fuel energy input due to the reduction of temperature difference at the hot end of the recuperating heat exchanger.

An important factor in achieving high net cycle efficiency is to use a high turbine inlet temperature. This temperature, however, is limited by the maximum allowable temperature of the 30 bar turbine exhaust that exits the turbine and enters the hot end of the recuperating heat exchanger. This maximum allowable temperature depends on the operating pressure selected and the allowable stress level for high nickel alloy such as INCONEL alloy 617 [11]. The operating temperature at the hot end of the heat exchanger is in the range of 700°C to 750°C. This leads to a typical turbine inlet temperature constraint in the range of 1100°C to 1200°C.

2.2. Allam Cycle for Solid Fuels

A solid fuel such as coal or biomass must be converted to a fuel gas before it can be utilized in the core Allam cycle power system described above. This system has been detailed extensively in previous work and only a cursory introduction is made here [7]. A basic process schematic of the coal based Allam Cycle can be found in Figure 3, which incorporates the process with a water quenched coal gasifier. Exiting the quenched gasifier between 250°C to 300°C, the product fuel gas will contain all coal- and POX-derived impurities as well as high quantities of steam. The water quench, plus an additional water scrub followed by final fine particle filtration will remove all slag and inorganic material from the steam/fuel gas mixture. The filtered gas stream is then cooled to near ambient temperature in a heat

exchanger. This cooling condenses the steam content for removal, cools the fuel gas, and transfers the released low grade heat to the recycle quench water and the low temperature region of the high pressure CO₂ recycle stream in the power cycle.

Following pre-combustion cleanup, the fuel gas is combusted under lean conditions and any impurities, such as H₂S, COS, CS₂, NH₃, and HCN, are converted to their oxidized forms: SO₂, NO, H₂O, and N₂. The predominant impurities in the low pressure turbine exhaust stream are SO₂ and NO/NO₂. As above, the exhaust gases are expanded through a turbine and heat is recuperated in the primary process heat exchanger to the incoming cold recycle stream.

At the cold end of the plant the exhaust gas undergoes direct contact cooling to condense combustion derived water and further oxidize and remove any remaining impurities as aqueous acids such as H₂SO₄ and HNO₃ using the remaining oxygen in the process stream. Table 2 shows the reaction sequence [12]. The 30 bar pressure of the turbine exhaust stream ensures that the reaction kinetics of the NO oxidation Step 1 are fast enough for the reaction sequence to proceed with a residence time of only several seconds. This process step has been demonstrated in several locations, including Vattenfall's Schwarze Pumpe pilot plant in Germany [13, 14, 15, 16, 17]. The concentration of H₂SO₄ will depend on the ambient cooling temperature and the sulfur content in the coal used, varying in the range of 10% to 40% by weight. The H₂SO₄ can be converted directly to CaSO₄ by reaction with a limestone slurry in a simple stirred tank reactor. Ca(NO₃)₂ is highly soluble in water and can be separately recovered if desired. The nitric acid present will also largely remove any mercury contaminant.

Following post-combustion impurity removal, the process occurs as described above in Section 2.1, returning the recycle CO₂ back to the combustor via the main process heat exchanger while venting a portion of the now clean CO₂ to a pipeline to maintain inventory mass balance. Additionally, a small portion of the recycle flow may be allocated back to the coal preparation and feeding step.

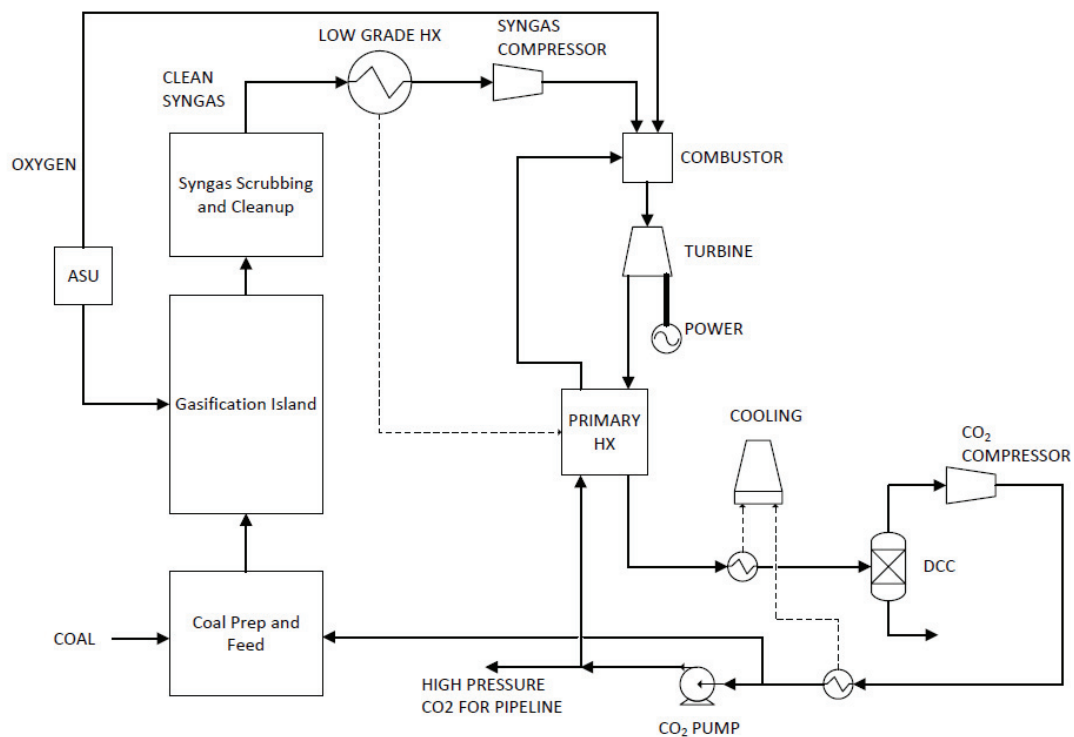


Figure 3: Process schematic of the solid fuel Allam Cycle [7]

Table 2: Impurities removal reaction sequence

Reaction	Sequence and Relative Speed
$\text{NO} + \frac{1}{2} \text{O}_2 \rightarrow \text{NO}_2$	(1) Slow
$2 \text{NO}_2 \rightarrow \text{N}_2\text{O}_4$	(2) Fast
$2 \text{NO}_2 + \text{H}_2\text{O} \rightarrow \text{HNO}_2 + \text{HNO}_3$	(3) Slow
$3 \text{HNO}_2 \rightarrow \text{HNO}_3 + 2 \text{NO} + \text{H}_2\text{O}$	(4) Fast
$\text{NO}_2 + \text{SO}_2 \rightarrow \text{NO} + \text{SO}_3$	(5) Fast
$\text{SO}_3 + \text{H}_2\text{O} \rightarrow \text{H}_2\text{SO}_4$	(6) Fast

2.3. Process Modeling

The demonstration plant has been thermodynamically modeled using Aspen Plus. Due to the high operating temperatures and pressures, equations of state for CO_2 and its impurities (such as O_2 , Ar, CH_4 and higher chain hydrocarbons, acid gases such as NO_x and SO_x , and N_2) must be selected carefully. These additional trace compounds can have drastic impacts on the compressibility of the working fluid and must be considered. 8 Rivers Capital undertook an extensive literature analysis prior to modeling work to ensure that the equations of state were selected properly. The results demonstrated that RK-Soave and Peng-Robinson equation of state provided the best empirical match to the operational region of Allam Cycle operation. Static models have been completed using Aspen Plus and dynamic simulations have been completed using Aspen Dynamics and Aspen Custom Modeler.

3. Technical Development of the Allam Cycle

3.1. Overview

In 2012 at GHGT-11 in Kyoto, Japan, the Allam Cycle was presented as a breakthrough carbon capture technology just entering the demonstration pathway. Since GHGT-11, the Allam Cycle has progressed rapidly, garnering significant commercial support, securing substantial investment in its development, undergoing major design advancements, and entering the demonstration phase. A 50 MWth demonstration-scale natural gas version of the plant is currently in construction by NET Power to prove out operation of the cycle and validate performance, control methodology, operational targets, and component durability. In tandem, a commercial effort is underway, with planned operation of the first commercial scale 300 MWe Allam Cycle plant targeted for 2020. Meanwhile, the solid fuel analog of the Allam Cycle is under research and development with a consortium from the State of North Dakota. Preliminary design work is also completed on several other practical integrations of the Allam Cycle.

A summary of the activities:

- In order to demonstrate the characteristics of the cycle and verify the design and operation of the integrated system and individual components, a demonstration plant in La Porte, Texas with a 50 MWth natural gas fuel input is now at an advanced stage of construction. Commissioning will commence by the end of 2016. The plant is expected to reach continuous operation and begin transferring power to the grid by the autumn of 2017. The plant process design has been developed by 8 Rivers. The engineering, procurement, and construction of the plant has been carried out by CBI. The plant will be operated by Exelon. The oxygen will be supplied by pipeline from an Air Liquide facility. The turbine and electric generator are supplied by Toshiba and the high pressure recuperative heat exchanger by Heatric. Comparing the plant operating characteristics to design assumptions and validating the performance of individual components are among

important goals of the testing period. Further, the results of the Demonstration Plant will provide future commercial partners the chance to assess performance over various operating modes.

- Toshiba corporation has developed a preliminary turbine design for a 500 MWth system. The objective in the design of the turbine for the demonstration unit has been to scale the size of the unit to provide the necessary confidence in performance guarantees for the full-size commercial turbine. The demonstration turbine utilizes partial arc inlet admission to enable the 50 MWth input to be accommodated on a turbine sized for a possible thermal input of approximately 200 MWth. The turbine was constructed combining high pressure steam turbine technology (utilizing an inner and outer pressure casing) and demonstrated gas turbine technology (for coatings and internal cooling of the turbine blades and inner casing). Beginning with successful operation of a 5 MWth test unit, Toshiba has developed the high pressure combustor, which attained the required maximum test pressure of 300 bar in 2013. The scaled demonstration combustor will be tested using the facilities of the demonstration plant before being commissioned as an integrated part of the complete combustion turbine assembly. In practice, the 200 MWth turbine will use a disproportionately large CO₂ cooling flow which will lower the overall system efficiency versus a commercial plant. Toshiba has also developed a proprietary turbine control system in cooperation with the NET Power process design methodology.
- Heatric has completed the design and manufacturing of the primary high pressure recuperative heat exchanger. Their fabrication technique involved construction of a multi-channel diffusion bonded unit. The units were combined to form monolithic blocks which comprise the heat exchanger battery. This heat exchanger unit was produced in 4 separate assemblies. The high temperature section operates to cool the turbine exhaust flow from approximately 700°C down to 550°C. It is fabricated from 617 alloy which is able to withstand the required operating temperature under 300 bar pressure. The remaining 3 sections cool the turbine exhaust to an exit temperature of approximately 60°C. These are fabricated from 316L stainless steel.
- 8 Rivers has developed a dynamic simulation model for the 50 MWth demonstration plant. This model is based on the actual design sizing and capacity, process conditions, configuration, and control methodology of the demonstration facility. The model will be further calibrated with empirical data from the demonstration plant. In addition to ongoing process development, the simulator is providing advanced validation of the DCS provided by Emerson. Operator training utilizing the simulator via the control system and software is in progress. In addition to its primary use in demonstration plant control, it will serve to further demonstrate the expected functionality of a commercial scale plant.
- The NET Power team is in the process of designing the 300 MWe commercial plant (at ISO ambient conditions). The lessons learned from the design and construction of the demonstration plant have already proven valuable in achieving the objectives of high efficiency, low capital cost and reliability. Operational feedback from the demonstration plant will be available before the detailed design is completed to further inform design.
- 8 Rivers has completed design studies on application of the core Allam Cycle to various practical operating situations. Studies have continued to improve the design of the gasified solid fuel Allam Cycle which has included experimental work on an SO_x/NO_x purification system with the cooperation of a consortium from the state of North Dakota. Further studies have suggested the use of liquefied natural gas will allow the turbine exhaust (following drying and cooling to near atmospheric temperature) to be liquefied and then pumped to the 300 bar operating pressure for the CO₂ recycle stream. This eliminates the energetically costly step of compression to the supercritical CO₂ state and likewise saves the heat required for LNG heating to ambient temperature. Existing coal-fired steam cycle power stations can be upgraded by heating the

superheated steam exiting the boiler to 700°C to 750°C in the primary Allam Cycle recuperative heat exchanger allowing for extra production at higher efficiency with no additional CO₂ emissions.

4. Demonstration Plant: Components, Layout, and Modeling

The Allam cycle design operates largely with the use of equipment already proven in the energy, petrochemical or oil/gas industries. However, several vital pieces of equipment required development. The two most critical are the novel combustion turbine provided by Toshiba, and the printed circuit heat exchanger provided by Heatric. These are described in greater detail below. Following these descriptions are an overview of the demonstration plant layout, an introduction to the dynamic simulation work and DCS implementation, and an overview of the demonstration testing plan.

4.2. Toshiba: Turbine and Combustor

Toshiba has developed a novel turbine and combustor to match the unique conditions of the Allam Cycle through the integration of technology found in both gas turbines and steam turbines. This hybrid design allows the combustor and turbine to operate at the combination of relatively high inlet temperature and high pressure required by the process. To expedite the commercialization of this technology, Toshiba began with basic engineering design of the anticipated future commercial turbine. This commercial design was then translated to the demonstration plant turbine while ensuring that design similarity was maintained as much as possible. Due to this design process the combustor and turbine, after validation within the demonstration plant, will therefore follow an expedited path to commercialization once the demonstration plant operation is confirmed [9, 10].

In order to cope with the high inlet temperature, cooling designs and thermal barrier coatings adopted from gas turbine technology were used for the rotor, moving blades, and stationary blades, among other parts. Proven gas turbine materials can be used for most of the hot gas path area since the temperature is not extremely high when compared to existing gas turbines (compare temperatures here). However, large Ni base forging is used in the central portion of rotor to ensure several key design criteria are met: first, that the rotor design remain simple and free of complex geometry, second, to minimize the required amount of cooling flow, and third, to cope with large torque transmission between stages.

A double shell structure consisting of one outer casing and several inner casings is used to safely operate under the required high inlet pressure. This arrangement is typical in high pressure steam turbine technology but differs from gas turbine technology which normally operates at considerably lower pressures. Proven materials in steam turbine technology can thus be applied to the casing when coupled with a small amount of cooling flow. However, Ni base casting is also employed in selected areas where cooling is not applied.

In addition to the turbine development work, the combustor required significant development since GHGT-11. The combustor is highly novel from the viewpoint of both the working fluid present in the combustion region as well as the elevated pressure. The combustion flame involves further challenges as it must maintain stability across a much greater pressure range than typical gas turbine combustors, starting at low ignition pressures and ramping to operating pressure of 300 bar. Initial development of the combustor aerodynamics via thermal and reacting flow modeling with Computational Fluid Dynamic (CFD) analysis guided the development process to a small-scale (5 MWth) rig test. These tests proved fruitful, reaching and validating operation at the required nominal full load combustion pressure of 300 bar successfully in 2013. Figure 4 depicts the test stand for the combustor from these tests [18]. In these tests the oxy-fuel flame exhibited stable diffusion behavior.

Inherent to the design of the oxy-fuel cycle is the absence of nitrogen in the combustor, thereby preventing the formation of NO_x. From the standpoint of natural gas combustor design this is one highly beneficial aspect of oxy-fuel combustion. One of the most difficult engineering challenges of existing combustors for gas turbines is to design for reduced NO_x emissions. The existing development pathway for dry, low NO_x combustors typically employs pre-mixed fuel and oxidant as a countermeasure against NO_x emissions. However, pre-mixed combustors present concerns with flame stability leading to difficulty in sustained plant operation with varying loading. The Toshiba combustor is low NO_x by virtue of oxy-combustion and thus does not necessitate pre-mixed combustion. This implies that very stable operation can be anticipated for the new Allam Cycle combustor under many operational conditions.

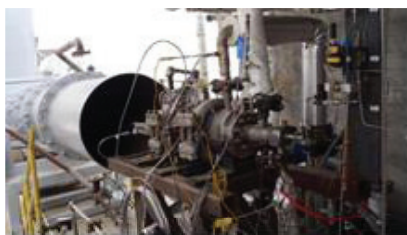


Figure 4: Test stand for a 5 MWth combustor operating at 300bar (Courtesy: Toshiba)



Figure 5: Rotor of Demonstration Turbine (Courtesy: Toshiba)



Figure 6: Outer Casing of Demonstration Turbine (Courtesy: Toshiba)

The design work and research and development described above has now informed the ongoing factory production of the turbine and combustor for the demonstration plant. Figure 5 and Figure 6 show important parts of turbine, its rotor and outer casing respectively. The turbine will be assembled and shipped from Toshiba in October 2016, and the combustor will be shipped early 2017.

4.3. Heatric: Main Process PCHE

Heatric are the heat transfer technology specialists and are designing and manufacturing a set of high pressure, high integrity and high performance heat exchangers for NET Power's demonstration plant. Maximizing energy recovery is a key driver in the thermally driven power market. In particular, the Allam Cycle has exacting performance requirements that are nearly impossible to achieve using conventional heat transfer equipment. Heatric's diffusion bonded heat exchangers are able to achieve the very close temperature approaches required.

Each Exchanger is constructed from individual 1.6mm thick plates into which the process channels are chemically etched in a complex arrangement of patterns optimized for the application, allowing for counter-current, parallel or multi-pass cross-flow geometries. The channel pattern is applied using methods similar to the manufacture of Printed Circuit Boards in the electronics industry. While in this particular case there is one process stream per plate, the flexibility of the manufacturing method allows for two or more separate flow streams with the necessary inlet and outlet channels to co-exist on individual plates as well. The plates are then stacked to form a block and are diffusion bonded together. The solid state joining process – which does not include any joining consumables – promotes grain growth across the faying surfaces of the stacked plates such that the product is a homogeneous block with the engineered process channels encased within. To achieve the required duty, multiple blocks are joined together. The inlet and outlet connections of the core faces are covered with headers which are welded to the diffusion bonded cores, which distributes the process evenly throughout the core.

The Heat transfer package is comprised of a four stage high pressure, high temperature heat exchanger network for the main process stream and a separate main recycle compressor aftercooler. The vessels are designed for temperatures between 100°C and 705°C as well as pressures up to ~300 bar. Figure 7 is a photograph of the low temperature section

of this network. Figure 8 is a photograph of the main compressor aftercooler. A CFD layout of the demonstration plant main heat exchanger network is found in Figure 9. This configuration is not indicative of the full commercial scale main process network as ongoing development has led to significant improvement of its design and configuration.

The design of the main process heat exchanger uses the common 30 bar hot exhaust stream exiting the Toshiba combustion turbine to provide for the duties of the high pressure CO₂ main process recycle stream and the oxidant mixture stream returning to the combustor. The staged heat exchanger network enables the bulk of the required surface area to be manufactured from Stainless Steel 316, minimizing the expense of exotic alloys, which are reserved only for the hottest section, with the high temperature heat exchanger constructed from Alloy 617.



Figure 7: Low Temperature Section (Courtesy: Heatric)



Figure 8: Aftercooler being lowered into position (Courtesy: Heatric)

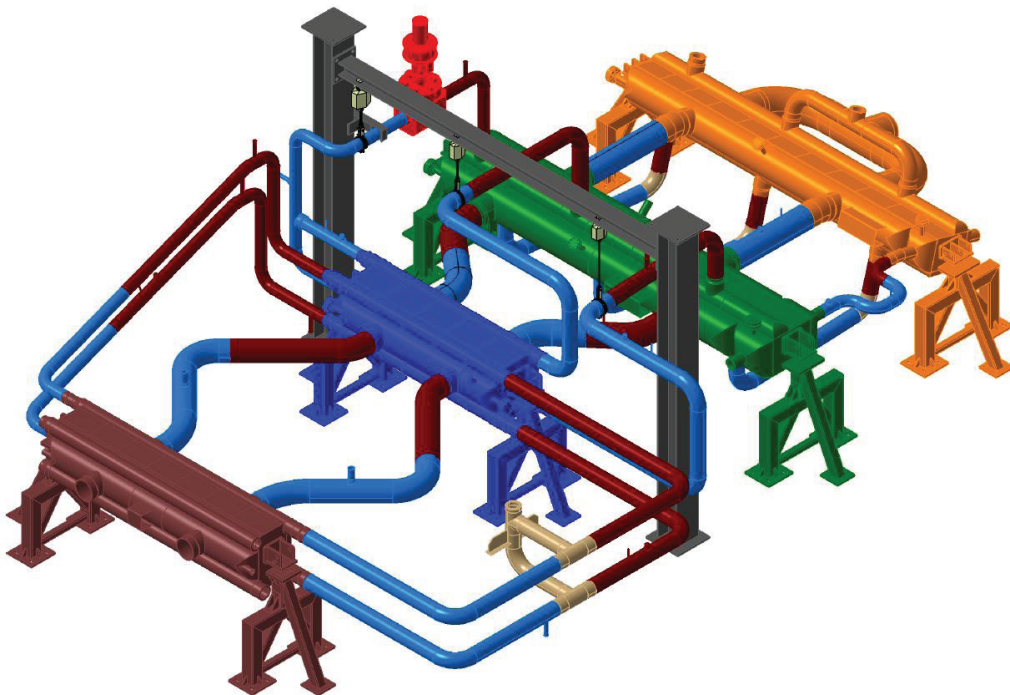


Figure 9: Demonstration plant main process heat exchanger network (Courtesy: Heatric)

Three of the four stages and the associated pipework have been delivered to site in La Porte, Texas with the remaining stage well into the construction phase at Heatric's main manufacturing base in Poole, England.

4.4. Plant Construction and Layout

Commencing Q1 2016, NET Power began construction on the Allam Cycle demonstration plant using natural gas fuel at La Porte, Texas. The detailed engineering, procurement and construction of the plant has been undertaken by CB&I. The operation of the plant will be handled by Exelon. 8 Rivers has been responsible for providing the process design and technology package to NET Power together with the control system and the dynamic simulation models for plant operation.

The demonstration process will match the operating conditions of the core Allam Cycle and the expected commercial temperatures and pressures. As described above, Toshiba has provided the combustion turbine. Exiting the turbine, the exhaust gas enters the main recuperator heat exchanger provided by Heatric. The turbine exhaust exiting the cold end of the recuperator is then cooled to near ambient temperature and combustion-derived H_2O condensed in the direct contact condensing column. The predominantly CO_2 recycle flow then reaches the compression step. The primary process compressors are multi-stage, intercooled centrifugal compressors. These compressors have been extensively operated in commercial applications at comparable temperature and pressure profiles. Following compressor after-cooling to achieve the correct pump suction density, the process fluid reaches the primary process pumps which provide the driving force for mass flow to the heat exchanger and combustor, increasing pressure back to approximately 310 bar.

In lieu of a devoted on-site ASU, the demonstration plant will receive a pure oxygen supply at approximately 30 bar pressure by pipeline from an adjacent Air Liquide air separation plant. This is mixed with the cooled and condensed CO_2 recycle stream exiting the direct contact condenser to create an oxidant stream separate from the main recycle stream to provide an oxidant chemistry containing about 25% by mole of O_2 . The oxidant stream is compressed in a separate compressor followed by a cooler and a separate multi-stage centrifugal pump to raise the pressure to 310 bar. This high pressure oxidant stream is heated against the turbine exhaust within the recuperator heat exchanger alongside the primary recycle flow.

The turbine pedestal requires special consideration. The high pressure CO_2 turbine provided by Toshiba drives an electric motor through a gearbox. Natural gas fuel is supplied by pipeline and compressed to the appropriate upstream control pressure which is fed through valves to the combustor. Additionally, recirculating hot oxidant and recycle flows are fed from the hot end of the Heatric heat exchanger to the combustor using high pressure and high temperature nickel alloy piping. At the opposite end of the turbine sits the main CO_2 recycle compressor which is coupled to the turbine rotor shaft. This allows the compressor to act as a brake to limit turbine over-speed in the event of load disconnection. The seal of the turbine shaft leaks a portion of the recycling CO_2 which can be recovered. At full load conditions this leak is negligible compared to the mass inventory addition provided by the fuel and oxidant. However, during plant startup it is desired that this inventory be conserved. A piston style compressor elevates the pressure of captured process gas emanating from the gland seal to approximately 30 bar and returns this flow to the cycle.

Construction on the Demonstration Facility began in March 2016 and is planned to be completed in Q2 of 2017. Exelon Generation supported the site selection, permitting and initial development work. CB&I has managed the construction of the facility, with on-site support from Exelon and 8 Rivers. All foundations have been laid, all major equipment is on site or in transit to the site, and pipe work is underway. Status of the construction as of September 20, 2016 can be seen in the photograph in Figure 10. Commissioning is presently underway. The plant is scheduled to enter into operation in 2016. Exelon will operate the plant and sell the power into Texas' power market.

4.5. Simulator Development and DCS Implementation

Being a first-of-a-kind project, 8 Rivers is in the process of developing a dynamic simulator for NET Power for the demonstration power plant to support control system design, process and control optimization, kinetic modeling, operating training, commissioning diagnostics and ongoing research and development. The simulator will be a predictive tool that will be continually improved as empirical data becomes available through demonstration plant testing. The simulator has been built using Aspen Plus Dynamics and Aspen Custom Modeler for the main process



Figure 10: NET Power 50 MWth Demonstration facility in La Porte, Texas (taken September 20, 2016)

and Emerson's Ovation Platform for the balance of plant equipment and the graphics of the actual plant operation as the interface to operators. The NET Power simulator acts as a near digital twin of the demonstration plant, capturing the expected performance of minor and major equipment and the overall plant configuration, inclusive of pipe volumes, dynamic heat exchange, turbine, compressor and pump maps and the NET Power Control System. The simulator will capture the operation of the plant from below ignition to full load performance.

For the Allam Cycle, dynamic simulation is particularly necessary and informative. As a highly recuperated process, the Allam Cycle presents added complexity in the high recirculation flowrates seen within the main loop and the high amount of main process heat transfer. As detailed previously, one of the benefits of using CO_2 is the difference in specific heat between the cold-end, high pressure recycle streams and the hot-end, lower pressure exhaust stream. Therefore, large quantities of high temperature heat can be transferred to the incoming high pressure cold streams without large increases in temperature, adding a barrier to process upsets. However, under varying pressure and changes in temperature of the cold recycle streams, the specific heat of the fluid can vary, resulting in potential non-linear profile changes within the heat exchangers. The ensuing response can involve behavior across the entire process, as pressures, temperatures, and flowrates resettle at their new equilibrium values. Similarly, as loading and inventory change throughout startup, load change, and shutdown, the impact of changes in demanded mass flowrates and physical properties such as specific heat adds enormous complexity to the heat exchanger balance. This means that the majority of the process complexity is carried in the performance of the main process heat exchanger, which then carries to other parts of the process.

The importance of modeling adequate heat exchange has required close cooperation with Heatric to develop a rigorous model of the heat exchanger network. The dynamic heat exchanger network has laid the foundation for the operation of the other major subcomponents in the model. As a result of this complex interplay, the dynamic simulator provides great predictive power in estimating the impact of process disturbances as well as changes in demand on the performance and operation of the cycle. From an engineering perspective, the simulator has reduced iteration on a "static" thermodynamic simulation software such as Aspen Plus and has likewise provided insight into expected control methodologies, instrument placement, and necessary interlocks and alarm limits. From an operational

perspective, the simulator will soon provide operators with a key commissioning and operational diagnostic tool for the demonstration plant. As mentioned above, instrumentation data in the demonstration plant will be used to continually validate, update, and calibrate the property and process models. This work will help to build better understanding of the process responsiveness, and ensure the commercial plant can be optimized across operational regimes and for any given location and performance.

4.6. Anticipated Performance, Purpose, and Test Plan

After individual systems have been tested for safety and checked out, overall plant commissioning will focus on reaching full load operation. This will include load rejection tests and run-back tests at various partial load conditions. The testing philosophy for the first several hundred hours is to gather operational data that defines initial performance criteria and to validate the control system with a focus on adjusting warnings, alarms, and trip set points to ensure the plant can be started and tested in a safe and controllable manner. Other tests can be run once the plant has attained sustained full power. These include quantifying the time to start under automated control and varying several key set-points in the plant's operation to validate and map the performance of the combustor turbine, recuperative heat exchanger, compressors, pumps and water separator. Once the initial performance testing has been completed, mechanical integrity testing will be performed to understand expected turbine cooling effectiveness and perform emergency and abnormal routines.

Of particular importance will be the ongoing validation of thermodynamic models and equation of state, and the refinement of the control methodology based on improved predictive capabilities from empirical data.

5. Ongoing Development of the Allam Cycle

5.1. Solid Fuel Allam Cycle

In parallel to the development of Allam Cycle natural gas system with NET Power, 8 Rivers is developing a process for utilizing solid fuels in the Allam Cycle, including coal and biomass which is reaching an advanced stage of research, development, and component demonstration. It has been reviewed extensively in an earlier paper [7].

The solid fuel Allam Cycle has the advantage of utilizing the basic power cycle described above, together with its associated cost and performance benefits, but with a derived "syngas" ($\text{CO} + \text{H}_2$) fuel which is generated by a conventional gasification process. Possible feedstock for this process include coal, refinery residuals such as tar and petroleum coke, prepared biomass, and solid wastes. In the case of coal, the fuel is first prepared via coal grinding and feed (using either slurry or dry-fed processes) followed by gasification in a commercially available gasifier using pure oxygen, syngas cooling and ash removal, and final cooling to near atmospheric temperature. Several advantageous aspects of the coal-based Allam Cycle that demand special consideration when designing optimum system integration are [7]:

- *Gasifier and Coal Input:* The Allam cycle can utilize existing gasifier technology and registers high efficiencies regardless of coal rank and type. The optimum Allam Cycle gasifier type is a simple water quench gasifier which provides greater process simplification with a corresponding reduction in capital cost and higher reliability. These also offer excellent ash removal without the issues of deposition and plugging due to condensation of contaminants. The gasifier produces a product gas stream comprising a mixture of 30% to 50% syngas plus steam, with exact composition dependent on the gasification pressure. The syngas cooling from typically 260°C to 290°C down to near ambient temperature releases all this large low temperature quantity of heat, derived principally from the condensing steam, by transferring it into the Allam cycle. The effect of this is to recover most of the sensible heat present in the syngas produced from the gasified coal which is leaving the partial oxidation section of the gasifier at over 1400°C as extra heat input to the Allam Cycle where it has the same fuel value as the syngas. This means that the water quench gasifier has an effective efficiency of about 90%.

- *No need for a Water Gas Shift Reactor:* The integration of coal gasification and Allam Cycle power eliminates the need to convert CO to H₂ saving the cost of the catalytic shift converters with their large evolution of low temperature heat. The Allam Cycle ensures that near 100% of the carbon derived from the coal is produced as CO₂ at pipeline pressure of typically 150bar.
- *Ease of Pollutant Removal:* Section 2.2 describes in detail the procedure for removal of coal and gasifier derived contaminants from the coal based power system as H₂SO₄, HNO₃, Hg(NO₃)₂ and CO₂. The complex and expensive gas treating systems required on conventional coal gasification plants to remove H₂S, COS CS₂ and the large quantity of CO₂ produced by shift conversion of CO to H₂ for CO₂ free gas turbine power are simply not required.
- *Reduced Water Consumption:* The solid fuel Allam Cycle has considerable water savings versus IGCC and SCPC baselines, with the ability to run substantially water free with only minor impacts to overall efficiency.

The coal-based Allam Cycle has been the subject of several feasibility, design, and academic analyses that provide a sound understanding of anticipated cost and performance of the cycle when integrated with various commercial gasification and clean-up systems [19, 20, 21, 22, 23, 7]. This work has shown that the system can perform with a baseload efficiency of up to 52% LHV utilizing commercially available gasification systems and with full carbon capture. This is a significant improvement over new advanced ultra-supercritical pulverized coal (USCPC) at 45% LHV and IGCC at 42% to 48% LHV, each of which operates without carbon capture. Studies have shown that these efficiencies decline by about 8% points when systems capable of achieving about 90% CO₂ capture are added. Furthermore, the coal-based Allam Cycle has been found to achieve significant capital cost savings. The cost and performance benefits of the Allam Cycle over existing USCPC and IGCC systems are even more substantial when costly carbon capture systems are considered for those legacy systems.

Four additional development hurdles have been identified for the commercialization of the solid fuel Allam Cycle:

- 1) Selection of the appropriate gasifier technology (optimizing for cost and performance)
- 2) Handling of corrosion from additional impurities found in coal-derived syngas
- 3) Methods of contaminant removal from the system [7]
- 4) Development of the Allam Cycle combustor for low calorific value and hydrogen-containing fuels [23]

8 Rivers has partnered with the EERC and several industry and government organizations in the state of North Dakota to undertake a \$5 million program to address each of these incremental developments. The initial results for each are very promising.

6. Commercial Development of the Allam Cycle

6.1. Market and Applications Overview

At present, the world must pay more for electricity to capture CO₂ produced by the combustion of hydrocarbon fuels. The Allam Cycle breaks this paradigm, allowing CO₂ capturing plants to produce electricity at prices comparable to traditional power sources that emit CO₂ to the atmosphere. At no additional cost to electricity, vented CO₂ from the Allam Cycle is captured at purity and pressure to be immediately exported. This technology presents a clear and significant market potential in the electricity sector. However, as a platform technology with many applications and the ability to co-produce a number of byproducts, the Allam Cycle technology is capable of dramatically impacting a wide variety of energy markets and sectors.

The Allam Cycle drives important synergies between electric power generation and transportation. In the long term, as improved batteries and fuel cells increase the role of electric and hydrogen powered vehicles, the Allam Cycle may be critical to both technologies: it can be a source of low-cost, low-carbon electricity for a growing electric vehicle load, and technology developments are underway to use the Allam Cycle for low-cost hydrogen production.

In the more immediate term, the Allam Cycle can play a critical role in producing more conventional transportation fuels while sequestering emissions from the power sector. Allam Cycle plants can export to the large network of CO₂ pipelines already in existence in the US, which are primarily used by the enhanced oil recovery industry. These networks exist in the United States due to the presence of several geologic domes that contain low-cost CO₂. The broader adoption of the Allam Cycle would justify and motivate the development of these pipeline networks in other regions where enhanced oil recovery is possible, but CO₂ previously has not been available.

When CO₂ captured from power production is utilized for enhanced oil recovery, the net effect of the process improves the emissions profile of the aggregate transportation and power sectors significantly. CO₂ captured from power sources offsets transportation fuels with carbon that would otherwise be released to the atmosphere. By combining the power generation fuel “system” with the transportation fuel “system,” we cease emitting CO₂ from both systems and, instead, limit it to the CO₂ emissions from the transportation system. In addition, the demand for CO₂ for enhanced oil recovery drives the development of a CO₂ transportation infrastructure that can later be used for other purposes, such as for direct geologic sequestration of CO₂.

The coal version of the Allam Cycle also presents important opportunities. The two primary forces driving decreased coal usage are its environmental impact and the prevalence of low cost natural gas (especially in the United States). When applied to coal, the Allam Cycle helps address both of these issues. First, it allows for coal to be used in a way that allows for full capture/abatement of not just CO₂, but also SO_x, NO_x, and mercury. In addition, the Allam Cycle increases coal’s competitiveness versus natural gas because it is about 10 percentage points more efficient than traditional coal cycles. Moreover, CO₂ from the Allam Cycle can be used to extract methane from coal through the process of enhanced coal bed methane recovery. Thus, whether through using coal directly for power generation or through ECBMR, the Allam Cycle can drive economic relief for regions that have been hard hit by the diminished demand for coal and enable regions of the world that are likely to continuing to burn coal for power generation, such as China and India, to do so economically and without generating air emissions.

The Allam Cycle can also impact natural gas utilization and markets. A version of the Allam Cycle has been designed where it is coupled with an LNG regasification plant, allowing for efficiencies approaching 67%. This is achieved by utilizing the cold LNG to cool the Allam Cycle CO₂ recycle stream to a point where it can be directly pumped, eliminating the energy-intensive compression step. In high gas price environments, such as nations that rely on imported LNG, these high efficiencies can enable gas-based power generation to become more economical and would cause combined cycle technologies to become economically obsolete. Separately, for natural gas producing regions, the Allam Cycle can further reduce the cost of natural gas. The cycle accomplished this through being able to directly combust unprocessed gases (including flare gas, acid gas and sour gas), thereby avoiding the expensive steps needed to process the gas for pipeline transportation and power generation.

Other commercial opportunities derive from the gases inherent in the Allam Cycle oxy-combustion process. Valuable gasses that can be co-produced by the Allam Cycle’s oxygen-producing air separation units include argon and nitrogen. In particular, nitrogen’s role in the manufacture of ammonia, urea and fertilizer, and the agriculture that could follow, would benefit large parts of the world.

6.2. Core Market Size

Four different markets have been analyzed to determine a total addressable market for the Allam Cycle. The results of that analysis are shown in Figure 11. These include the following, estimated by the IEA and independent sources:

1. The global market for new and replacement fossil fuel plants through 2025 [24]
2. The global market for new and replacement fossil fuel plants through 2040 [24]
3. The needs for CO₂ for enhanced oil recovery [25].
4. The needs for CO₂ for enhanced coal bed methane recovery [26].

As can be seen, the total addressable markets are substantial. Several important notes about this data should be considered:

NUMBER OF ALLAM CYCLE TURBINES NEEDED TO SATISFY DIFFERENT MARKETS

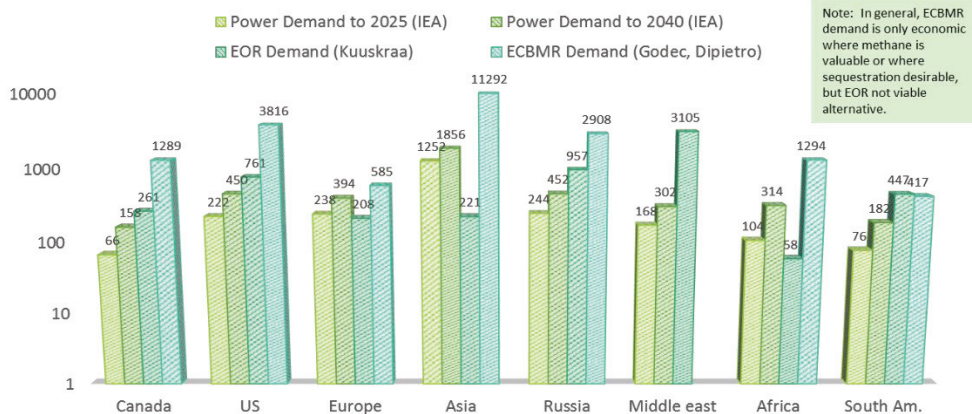


Figure 11: Total addressable market for the Allam Cycle

- Transportation (pipeline) costs are disregarded (note, however, that 14 Allam Cycle natural gas turbines or 7 coal turbines will justify the construction of 800 miles of CO₂ pipelines if the CO₂ is used for enhanced oil recovery).
- If given a choice of using CO₂ to produce a long chain hydrocarbon (in enhanced oil recovery) or a methane molecule (in enhanced coal bed methane recovery), the long-chain hydrocarbon is preferable if transportation costs are equal.
- Enhanced coal bed methane justifies smaller pipeline networks, but coal beds provide excellent sinks for cash-positive CO₂ sequestration
- Tax laws can provide substantial enhancements to CO₂ sequestration and enhanced fuel recovery
- Low-carbon fuel standards, such as in California, have been underestimated as potential revenue sources for using technologies like the Allam Cycle to reduce the carbon intensity in the fossil fuel business and could lead to further market opportunities.
- There are many more uses for CO₂ than EOR and ECBMR, and many of these are currently being developed in connection with an X-Prize competition.

6.3. Commercialization Steps

Given the various applications and benefits of the Allam Cycle that have been discussed, it is clear that a variety of developmental opportunities exist. At present, the commercial development program for the Allam Cycle is centered around developing a 300 MWe natural gas plant design, viewed as the core of the Allam Cycle process, with a focus on driving competitiveness through a high level of modularity and manufacturing efficiency. From there, the first commercial natural gas plant can be built. Meanwhile, the components that are unique to the coal Allam Cycle will be developed and demonstrated so that it can rapidly follow the commercial deployment of the gas cycle. Development of a low-BTU-fuel combustor, capable of burning natural gas, unprocessed gases, and syngas, is essential to that process. Following these critical steps, Allam Cycle development can be extended into new fields or more advanced versions of the cycle, including: further exploitation of economics of scale (e.g. the cost benefits seen as conventional turbine manufacturers have moved from F frame to H frame units); development of smaller, more modular units; and extension into LNG applications and the fields of N₂ and H₂ production.

The demonstration plant is a key gating factor for the development of the first commercial plant. Given the anticipated timeline for start-up and initial testing of the demonstration plant, sufficient data is expected to be available by late 2017 to allow Toshiba to commence design and manufacture of the 300 MWe turbine, and to allow financial

close to be reached by the end of 2017 or the beginning of 2018. Based on current design and construction timeline estimates, this would lead to a commercial operation date in early-to-mid 2020. Several electrical power producers and oil and gas companies are currently in the due diligence phase for partnering in the construction and operation of this plant.

6.4. The First 300 MWe Plant

A pre-FEED for the first 300 MWe commercial plant was first completed in 2013 and was used as the basis for the design of the demonstration plant. At present, that pre-FEED is undergoing an update, building off of lessons learned from the demonstration plant. Learnings from the demonstration plant will continue to be incorporated into the commercial plant design throughout the completion of construction, start-up and testing of the demonstration facility. The commercial unit is being designed around principles of cost and performance optimization, with a particular focus on incorporating advanced modular design concepts where possible. Customer feedback is being solicited throughout the design process to ensure feedback on sizing, flexibility, operational profile, maintenance, and other key design features are incorporated.

The current performance targets, at ISO conditions, for the first commercial plant are presented in Table 3 below:

Table 3: Expected Performance of a 300 MWe NET Power Commercial Power Plant

Cycle Attribute	Expected Value
Net power output	303 MW
Natural gas thermal input	511 MW
Oxygen consumption	3555 MT/day (contained)
Turbine outlet flow	923 kg/s
Turbine inlet condition	300 bar at 1158°C
Turbine outlet condition	30 bar at 727°C (approximately)
Oxygen plant power	56 MW
CO ₂ compression power	77 MW

7. Conclusions

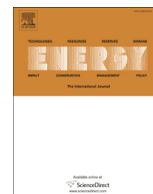
The Allam cycle power system offers a pathway to the continuing use of hydrocarbon fuels for the generation of power at low cost with near complete capture of greenhouse gases, making it a critical technology in addressing global climate change. The 50 MWth Demonstration Plant construction is well underway, and is planned to be operational in 2017. The first full-scale commercial plant should enter operation in 2020. The gasified solid fuel and coal based system offers CO₂ free power at high efficiencies and costs lower than comparable systems which do not employ carbon capture. This system is currently being advanced. The disrupting economics of Allam Cycle carbon capture Cycle and its ability to integrate with a variety of processes presents several viable and unique commercialization opportunities under continual development.

Acknowledgements

We would like to thank NET Power and the development partners, 8 Rivers Capital, Exelon, and CB&I for their ongoing contributions to the Allam Cycle and the significant support of the work provided by Toshiba and Heatric. For their ongoing work on coal, we would like to thank the State of North Dakota and the development consortium working on aspects of the gasified lignite Allam Cycle, including EERC, ALLETE/Minnesota Power, BEPC/Dakota Gasification, EPRI, the Lignite Energy Council, and the US Department of Energy. In addition, we would like to thank the former UK Department of Energy and Climate Change (now part of the UK Department for Business, Energy and Industrial Strategy) for their early support of the technology.

References

- [1] Intergovernmental Panel on Climate Change, "IPCC Special Report on Carbon Dioxide Capture and Storage," Cambridge University Press, Cambridge, 2005.
- [2] R. J. Allam, M. R. Palmer and et al, "High Efficiency and low cost of electricity generation from fossil fuels while eliminating atmospheric emissions including carbon dioxide," *Energy Procedia (GHGT-11)*, 2012.
- [3] United Nations Framework Convention on Climate Change, "Report of the Conference of the Parties on its twenty-first session, held in Paris from 30 November to 13 December 2015," United Nations, Paris, 2016.
- [4] Intergovernmental Panel on Climate Change, "Climate Change 2014," Geneva, 2014.
- [5] R. J. Allam, M. Palmer and G. W. Brown, "System and Method for High Efficiency Power Generation Using a Carbon Dioxide Circulating Working Fluid". USA Patent 8,596,075 B2, 03 December 2013.
- [6] Parsons Brinckerhoff (PB), "Electricity Generation Model: Update of Non-Renewable Technologies," 2013.
- [7] X. Lu, B. Forrest, S. Martin, J. Fetvedt and et al, "Integration and Optimization of Coal Gasification Systems with a Near-Zero Emissions Supercritical Carbon Dioxide Power Cycle," in *Proceedings of ASME Turbo Expo 2016: Turbine Technical Conference and Exposition*, Seoul, South Korea, June 13-17, 2016.
- [8] R. J. Allam, J. E. Fetvedt, B. A. Forrest and D. A. Freed, "The Oxy-Fuel, Supercritical CO₂ Allam Cycle: New Cycle Developments to Produce Even Lower-Cost Electricity from Fossil Fuels Without Atmospheric Emissions," in *Proceedings of ASME Turb Expo 2014: Turbine Technical Conference and Exposition*, Dusseldorf, Germany, June 16-20, 2014.
- [9] H. Nomoto and et al, "Cycle and Turbine Development for the Supercritical Carbon Dioxide Allam Cycle," *Proceedings of the International Conference on Power Engineering*, 2015.
- [10] J. Isles, "Gearing up for a new supercritical CO₂ power cycle system," *Gas Turbine World*, pp. 14-18, December 2014.
- [11] Special Metals, "INCONEL alloy 617," 05 March 2005. [Online]. Available: <http://www.specialmetals.com/assets/documents/alloys/inconel/inconel-alloy-617.pdf>. [Accessed 10 October 2016].
- [12] R. J. Allam, V. White and E. J. Miller, "Purification of Carbon Dioxide". USA Patent 8,580,206 B2, 12 November 2013.
- [13] V. White, R. J. Allam and E. Miller, "Purification of Oxyfuel-Derived CO₂ for Sequestration or EOR," in *8th International Conference on Greenhouse Gas Control Technologies GHGT-8*, Trondheim, Norway, 2006.
- [14] V. White, L. Torrente-Murciano, D. Sturgeon and D. Chadwick, "Purification of Oxyfuel-Derived CO₂," *Energy Procedia (GHGT-9)*, vol. 1, pp. 399-406, 2009.
- [15] V. White, L. Torrente-Murciano, D. Sturgeon and D. Chadwick, "Purification of oxyfuel-derived CO₂," *International Journal of Greenhouse Gas Control*, vol. 4, pp. 137-142, 2010.
- [16] V. White, A. Wright, S. Tappe and J. Yan, "The Air Products - Vattenfall Oxyfuel CO₂ Compression and Purification Pilot Plant at Schwarze Pumpe," *Energy Procedia (GHGT-11)*, vol. 37, pp. 1490-1499, 2013.
- [17] Murciano, et al., "Sour Compression Process for the Removal of SOX and NOX from oxyfuel-derived CO₂," *Energy Procedia*, 2011.
- [18] Y. Iwai, M. Itoh, Y. Morisawa, S. Suzuki, D. Cusano and M. Harris, "Development Approach to the Combustor of Gas Turbine for Oxy-fuel, Supercritical CO₂ Cycle," in *Proceedings of ASME Turbo Expo 2015: Turbine Technical Conference and Exposition*, Montreal, Canada, June 15-19, 2015.
- [19] R. J. Allam and et al, "New Power Cycle Provides High Efficiency and Lower Cost Electricity Generation from Coal while Eliminating Atmospheric Emissions," *COAL-GEN*, 2013.
- [20] R. J. Allam and et al, "Allam Cycle Path to Coal," *Prepared for the UK Department of Energy and Climate Change*, 2013.
- [21] J. Fetvedt, B. Forrest, X. Lu and M. McGroddy, "Applying the Supercritical CO₂ Allam Cycle to Lignite: Improved Efficiency, Lower Cost, and Near-Zero Air Emissions from Coal," in *COAL GEN 2014*, Nashville, 2014.
- [22] B. Forrest and et al, "Oxy-lignite Syngas Fuelled Semi-closed Brayton Cycle Process Evaluation," *Prepared for Lignite Research Council, BNI Coal, Minnesota Power, and Dakota Gasification Company*, (In Press).
- [23] J. Fetvedt, "Coal Syngas Combustor Development for High-Pressure, Oxy-Fuel SCO₂ Cycle Applications," US Dept of Energy - NETL, Award Number FE0023985, October 2014.
- [24] V. Kuuskraa, M. Godec and P. Dipietro, "CO₂ Utilization from "Next Generation" CO₂ Enhanced Oil Recovery Technology," in *GHGT-11*, 2013.
- [25] M. Godec, H. Jonsson and B. Basava-Reddi, "Potential Global Implications of Gas Production from Shales and Coal for Geological CO₂ Storage," in *GHGT-11*, 2013.



A modified Allam cycle without compressors realizing efficient power generation with peak load shifting and CO₂ capture

Zilong Zhu, Yaping Chen^{*}, Jiafeng Wu, Shaobo Zhang, Shuxing Zheng

Key Laboratory of Energy Thermal Conversion and Control of Ministry of Education, School of Energy and Environment, Southeast University, Nanjing, 210096, China

ARTICLE INFO

Article history:

Received 4 October 2018

Received in revised form

28 January 2019

Accepted 31 January 2019

Available online 1 March 2019

Keywords:

Power generation

Oxy-fuel combustion

CO₂ and H₂O mixture

CO₂ capture

Allam cycle

Allam-Z cycle

ABSTRACT

A modified Allam cycle (Allam-Z cycle) with a simpler system was proposed and investigated using NG (natural gas)/O₂ combustion products mixing with the circulation CO₂ as the working medium for power generation with high efficiency, zero CO₂ emission and peak load shifting. The modifications are that all the working media are pumped to high pressure by pumps instead of compressors, the cold energy of both liquid oxygen and LNG is used for degrading the cooling water for CO₂ liquefaction and a set of regenerative heat exchangers are arranged for turbine exhaust heat recovery. The influences of turbine parameters on the performances of the cycle were investigated. The comparison was performed under the conditions of condensation temperature of 30 °C, turbine inlet pressure of 30 MPa, inlet temperature of either 700 °C or 900 °C and the turbine outlet pressures of Allam-Z cycle and Allam cycle are 7.21 MPa and 4 MPa respectively. The results show that the output power efficiency and the equivalent net efficiency of the Allam-Z cycle with full CO₂ capture are 43.64% and 40.83% respectively or 50.87% and 48.05% respectively, which are 2.15% or 2.96% higher than those of the Allam cycle under the same condition.

© 2019 Elsevier Ltd. All rights reserved.

1. Introduction

The application of CCS (carbon capture and storage) technology in power generation for reduction CO₂ emission into the atmosphere is considered as the main technology to solve the problem of climate change [1,2]. The biggest problem for CO₂ capture in traditional coal power plants is the huge economic cost on complex technical processes with massive power consumption and it also needs a lot of chemicals [3,4]. In a traditional coal power plant with CO₂ capture, the carbon dioxide composition of flue gas is decreased by about 65% while the thermal efficiency will drop around 18%. Obviously, oxy-fuel combustion has more advantages than traditional combustion since the CO₂ content is concentrated with oxy-fuel combustion and can be easily separated from the mixture by conventional cooling technologies [5], therefore it provides a simple and valuable measure for CO₂ capture. Many scholars and experts performed economic and technical analysis on the operation of oxy-fuel combustion power plants [6–11] in recent years, and got a conclusion that oxy-fuel combustion power plants

are feasible with environment-friendly features.

Beside the emissions of greenhouse gases, the limited resources and increasing global energy demand compel to reform energy structure through improving energy efficiency and developing renewable energies. Some new thermal cycles used in solar energy, biomass energy and waste heat have been proposed or studied [12–16]. The supercritical or transcritical carbon dioxide power cycles with simple loop and high thermal efficiency have captured increasing attention in recent years [17]. Carbon dioxide is a natural working fluid, nontoxic and nonflammable, and has good thermophysical properties with fairly high heat transfer coefficient. Supercritical or transcritical carbon dioxide power cycles have been applied in waste heat [18], solar energy [19] and nuclear energy [20] in different occasions. Zhang and Lior [21] proposed a CO₂ and H₂O mixture Rankine cycle and CO₂ Brayton cycle combined power cycle using LNG and O₂ as fuel and oxidant, respectively. Although the thermal efficiency of this power cycle is higher than 50%, the cycle system with both gas turbine and steam turbine loops is rather complicated. Purjam et al. [22] studied a supercritical carbon dioxide cycle and investigated the impacts of some important parameters on cycle efficiency in different temperature heat resources. Chen et al. [23] and Wu et al. [24] proposed and studied a novel LNG/O₂ combustion gas and steam mixture cycle (GSMC)

^{*} Corresponding author.

E-mail address: ypgchen@sina.com (Y. Chen).

Nomenclature*Latin letters*

G	mass flow, mass flow in turbine ($\text{kg} \cdot \text{s}^{-1}$)
h	specific enthalpy ($\text{kJ} \cdot \text{kg}^{-1}$)
p	pressure (MPa)
Q	heat ($\text{kJ} \cdot \text{kg}^{-1}$)
R_{ASU}	percentage of ASU consumed power
R_{aux}	percentage of auxiliary power
T, t	temperature ($\text{K}, ^\circ\text{C}$)
W	power output or consumption (kW)

Greek letters

γ	ratio of prices of off-peak and peak electricity
Δ	difference
Δt_p	pinch temperature difference (K)
$\eta_{\text{el out}}$	output power efficiency
$\eta_{\text{eq net}}$	equivalent net efficiency

Subscript

digit	status point in Fig. 1
a	O_2
ASU	air separation unit
b	NG
c	CO_2
w	H_2O
cp	combustion product
el	electricity
g	electric generator
in	inlet
m	mass
out	output, outlet
p	pressure
P	pump
s	isentropic
sat	saturate
t	temperature
T	turbine

which is supercritical Rankine cycle using $\text{H}_2\text{O}/\text{CO}_2$ mixture working fluid. In the GSMC system, the CO_2 is liquefied and captured by cryogenic liquids of both LNG and oxygen. In order to solve the problem of excessive circulation operation pressure of supercritical carbon dioxide cycle, Jeong and Yong [25] investigated a supercritical CO_2 –Xe and CO_2 –Kr mixture Brayton cycle at variable critical points. The results show that the mixture cycle can achieve higher thermal efficiency than S- CO_2 cycle with lower operation pressure. Amann et al. [26] modified natural gas fueled combined cycle into O_2/CO_2 power cycle to realize CO_2 capture. Zhang et al. [27] presented a novel combined gas and steam power cycle using cryogenic LNG and liquid oxygen to cool the inlet air and the results show a slightly higher thermal efficiency in comparison with the original cycle.

With the rapid development of China's economy, the increasing gap of peak-valley of power grids is becoming hot issue. At present, peak load regulation of coal fired power units is still the main means of peak shaving for power grids in China [28]. The peak load regulation by coal fired power units has huge influence on its service life and also reduces its thermal efficiency. Since the application of hydraulic pumped storage stations are limited by geographic conditions, while the other large-scale energy storage approaches such as air compression and air liquefaction are still under development or lack of economic justification, there are urgent demands of large-scale energy storage or shifting for the modern and future smart grid operation [29,30]. In this paper the energy storage or shifting is merged with the oxy-fuel combustion technology for power generation with CO_2 capture.

Allam et al. [31,32] proposed a novel *trans*-critical carbon dioxide power cycle (Allam cycle) that utilizes combustion products and recirculation CO_2 mixture as working fluid. Allam cycle adopts oxy-fuel combustion technology with little nitrogen in combustion to realize nearly zero NO_x emission, to overcome the deficiency of high NO_x emission of the conventional LNG fueled power plants. Allam cycle can dramatically achieving higher thermal efficiency compared to steam Rankine cycle and Brayton cycle.

It is apparent that the thermal efficiency of a power cycle depends mainly on the cycle operation parameters of working medium especially the turbine inlet pressure and temperature. Adopting high parameters of supercritical or ultra-supercritical is becoming the trend in the modern and future development of power plants [33]. With the rapid development of material

technology and cooling methods, the biggest obstacle of supercritical and ultra-supercritical power plant is going to be eliminated [34,35]. To improve the thermal efficiency, the turbine inlet parameters in the Allam cycle [31,32] are about 30 MPa and 1150°C respectively. The Allam cycle uses gaseous fuel with oxygen combustion products with the addition of circulation CO_2 as working fluid, and the liquid or solid fuel such as coal or biomass should be converted to gaseous fuel before combustion. Liquefied natural gas (LNG), as a clean energy, with considerable cold energy and high calorific value, is widely used as fuel in peak shaving power generation plant and should be utilized first adopting CCS with the oxy-fuel combustion technology from the economic consideration.

The turbine backpressure in the Allam cycle is set considerably lower than the critical value of CO_2 in consideration of the proper turbine exhaust temperature for the recuperating heat exchangers. Thus a set of compressors with intercooling are used to raise the pressure of working medium for condensing by the cooling water which makes the Allam cycle system rather complicated. In this paper, with the lower turbine inlet temperature ($\leq 900^\circ\text{C}$) cases without cooling approach or with only static vane cooling in turbine first stage, a simplified but still efficient power cycle based on the Allam cycle (thereafter referenced as the Allam-Z cycle) is proposed and studied for power generation with peak load shifting and CO_2 capture.

2. Description of the Allam-Z cycle

2.1. Main circulation loop

As shown in Fig. 1, the distinguishes of the Allam-Z cycle with the Allam cycle are that the turbine backpressure is around the supercritical value rather than the lower one, thus the compressors can be eliminated and all the working media can be raised to high pressure by pumps instead of compressors; the cold energy of both LNG and liquid oxygen is used for declining the cooling water temperature in a heat exchanger (HX5) and a set of other regenerative heat exchangers are properly arranged to make full use of the turbine exhaust heat. Since the turbine back pressure of the Allam-Z cycle is higher than that of the original Allam cycle and the partial pressure of the H_2O in the mixture is higher than the H_2O saturation pressure of corresponding temperature at outlet of the heat exchanger HX3, H_2O can be easily separated in the separator as

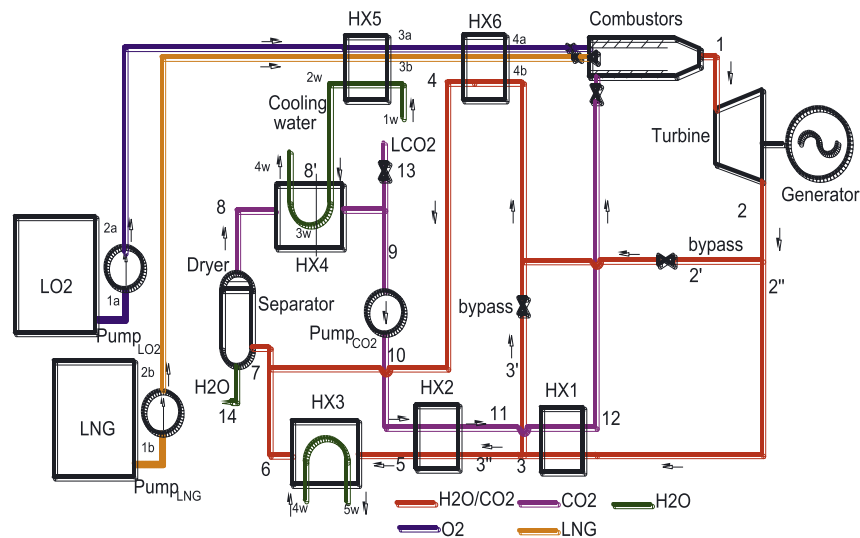


Fig. 1. Schematic diagram of Allam-Z cycle.

liquid state and the remaining moisture in gaseous phase can be eliminated with the aid of a dryer. The gaseous CO_2 is then cooled and condensed in HX4 by the cooling water from the HX5. The amount of CO_2 corresponding to combustion product is detached as the captured CO_2 at purity and liquid status.

The main components of the Allam-Z cycle include combustors, turbine, pumps, separator, and a set of heat exchangers. This power cycle uses CO_2 with very small amount of H_2O from combustion products as the working fluid operating with a turbine that has inlet pressure in the range of 20–30 MPa and outlet pressure around 7.21 MPa, respectively. This cycle uses pumps to raise pressure of both liquid fuel and oxidant to high value for combustion, and the high temperature combustion products mix with the circulation CO_2 in the combustors to produce CO_2 dominated CO_2 and H_2O mixture vapor as the working medium, which expands in a supercritical turbine unit for power generation. The turbine exhaust medium enters a set of recuperating heat exchangers for heating the aforementioned high pressure circulation CO_2 , oxygen and NG streams ready for combustion.

The combustion takes place in the flame tubes of a set of combustors in parallel, some of the circulation CO_2 can be mixed with the O_2 before entering the combustors, while the rest of circulation CO_2 flows in the annular channel of each combustor between cylinder and flame tube. The CO_2 is directly mixed with the combustion products through the holes of the flame tube and at the outlet end of the annular channel of each combustor, forming predominant CO_2 and minor H_2O mixture working fluid which expands and produces power work in the turbine. LNG as the fuel is purchased from overseas market, while the liquid oxygen (LO_2) is produced by consuming the off-peak electricity in the air separation unit (ASU). Pure O_2 with complete combustion assumption is postulated in the simulation of the system. If only the NG/oxygen combustion products absorb calorific value released by NG and O_2 combustion, the combustion products temperature might raise to more than 7000 K, so the circulation medium must be added for degrading temperature. The possible circulation medium is either H_2O or CO_2 . Since CO_2 has excellent thermodynamic properties above its critical point (31.1 °C and 7.38 MPa) and also the cycle system is much simpler than the one using H_2O , the CO_2 is preferably selected as the circulation medium.

The fuel LNG is transported to the coastal cities by ships and stored in tanks at cryogenic temperature and low pressure. The

pressure and temperature in LNG and LO_2 tanks are set as $p_{1a} = p_{1b} = 0.1$ MPa and $t_{1b} = -162$ °C, $t_{1a} = -185$ °C, which are a bit lower than the bubble temperatures of NG and O_2 , respectively. Before entering the combustors, the NG and oxygen are pumped and heat up to high pressure and high temperature. Because of the pump power consumption, the temperature of the liquids will increase considerably and also both NG and oxygen can only transmit the sensible heat under turbine inlet pressure which is much higher than their critical pressures. The “cold energy” of both LNG and LO_2 is used for decreasing temperature of the cooling water in HX5 thus a lower temperature cold sink is resulted in this Allam-Z cycle.

In the combustors the high temperature combustion zone is confined in the flame tube which is well protected by the circulation CO_2 at other side and also by injected gaseous film through holes. The circulation CO_2 mixes with the combustion products of H_2O and CO_2 , forming CO_2 predominant mixture of CO_2 and H_2O at point 1. The turbine inlet temperature of the Allam-Z cycle could be 1150 °C, the same as that of the Allam cycle, or even higher if references to the working temperature of gas turbine (up to 1600 °C), however, 600–900 °C with the turbine inlet pressure of 30 MPa might be reasonably selected in comparison with that of the conventional steam Rankine cycle power plant without or with only simple cooling technique. Considering the material used in heat exchangers, the maximum temperature at the turbine outlet is set as not to exceed 705 °C [31,32], and thus the turbine inlet temperature is set as not to exceed 900 °C. Since the turbine outlet temperature is higher with higher turbine back pressure, for economic consideration only HX1 is used to reduce the turbine exhaust gas temperature from about 705 °C to 560 °C for heating the circulation CO_2 and then split to two streams to both HX2 and HX6. If the temperature at the turbine outlet is below 560 °C, then the exhaust gas of the turbine splits directly into two streams which enter HX1 and HX6 respectively. Then the exhaust flows are cooled to temperatures of 35 °C at the both outlets of HX3 and HX6, higher than the saturation temperature of carbon dioxide (about 30 °C), and the two streams merge again (point 7) before the separator. So the water is easily separated from mixture in the vapor-liquid separator, with a dryer set at the outlet of the gaseous port. The vapor CO_2 is liquefied further by cooling water in HX4. Then the captured CO_2 splits from the main flow, while the circulation CO_2 stream is raised to high pressure by a CO_2 pump before entering the regenerator HX2 and HX1 in series.

2.2. Main advantage features

The pressure–enthalpy diagrams of both original Allam cycle and Allam-Z cycle are showed in Fig. 2. It can be seen from the diagrams that the most notable difference between them is the simplicity.

The main advantage features of the Allam-Z cycle are as follows: Firstly, since its combustion products become part of the working medium, which expand in the turbine, this system can eliminate exhaust flue gas loss and make almost full use of the calorific value of the fuel with reduced exergy loss. Secondly, the carbon capture process in this cycle is of high conversion efficiency that needs no additional cost of both electricity and chemical additives, and the captured CO₂ can be used in oil industry for squeezing the remaining oil out from underground which makes a perfect sequestration of CO₂ and in other industrial usages; while in the conventional carbon capture approaches with absorption or adsorption, a lot of energy might be consumed for separation and fluid transmission with pumps and fans, and also considerable chemical materials will be consumed [36–38]. Thirdly, the Allam-Z cycle system is very simple and has less thermal equipment. The turbine is compact and needs fewer stages with raised back pressure. The recuperation is performed in limited number of heat exchangers for heating the circulation CO₂ and fuel/oxidant, while in a steam Rankine cycle or a gas and steam mixture cycle (GSMC) [23,24] 8 sets of feedwater heaters are usually adopted. The gas and steam turbine combined cycle system needs gas turbine and steam turbine two cycle systems with much higher equipment cost, and the heat transfer area of the waste heat boiler which connects two sets of systems is also very large due to poor heat transfer coefficient at flue gas side. The related equipment cost and space with the replacement of combustors to the conventional boiler can be greatly reduced too. Fourthly, the economic and ecological benefits are remarkable with features of high efficiency, peak load shifting and minute quantity NO_x emission and zero CO₂ emission. The liquid oxygen production technology and storage facilities are relatively safe (low pressure) and of high energy storage density. The large scaled liquid oxygen production by air separation unit (ASU) with the massive consumption of off-peak electricity is beneficial to the balance and safety of power grid. Because of the very compact configuration compared to the air compression energy storage unit and free of geographic limitation as pumped storage power station, both the investment and space for energy storage facility can be greatly reduced. It is a unique stack-free environment friendly power plant.

3. Methods

3.1. Parameter conditions and constraints

The thermodynamic properties of pure or mixture CO₂ and H₂O at vapor, liquid and two phase states data were calculated by the software of REFPROP 8 based on the NIST [39]. The inlet and outlet parameters of each component of the Allam-Z cycle are labeled subscripts consistent to the state points in the Fig. 1. Then the thermodynamic models of the cycle system and the component equipment are established with governing equations of conservation laws of mass and energy. By thermodynamic analysis of quantitative evaluation for cycle efficiency, the trends of the influence parameters on the features of the new cycle can be revealed. MATLAB code was written to call the software functions and to organize the whole calculation. Table 1 shows the known parameter conditions and the constraints for the calculation. The assumptions are listed as following:

- 1) The composition of NG is simplified as CH₄, CO₂ and C₂H₆ which are the three most abundant components in NG [24] as show in Table 2. The combustion is complete for oxidant O₂ to CH₄ and

Table 1
Known parameter conditions and constraints.

Item	Symbol	Unit	Value
Turbine inlet pressure	p_1	MPa	20–30
Turbine inlet temperature	t_1	°C	600
			–900
Condensation temperature	t_8	°C	30
Temperature of storage LNG	t_{1b}	°C	–162
Pressure of storage LNG	p_{1b}	MPa	0.1
Flow rate of LNG	G_{1b}	kg·s ^{–1}	1
Temperature of storage LO ₂	t_{1a}	°C	–185
Pressure of storage LO ₂	p_{1a}	MPa	0.1
Flow rate of LO ₂	G_{1a}	kg·s ^{–1}	3.72
Flow rate of CO ₂	G_{1CO_2}	kg·s ^{–1}	2.64
Flow rate of ejected H ₂ O	G_{1H_2O}	kg·s ^{–1}	2.08
Pinch temperature difference of heat exchangers	Δt_p	K	10
Isentropic efficiency of turbine	η_T		0.85
Isentropic efficiency of pumps	η_P		0.80
Isentropic efficiency of compressors	η_C		0.85
Efficiency of electric generator	η_g		0.985
Ratio of prices of off-peak and peak electricity	γ		1/4
Unit power consumption for oxygen production of ASU		kWh kg ^{–1} (O ₂)	0.42
LNG calorific value	E	MJ·kg ^{–1}	50

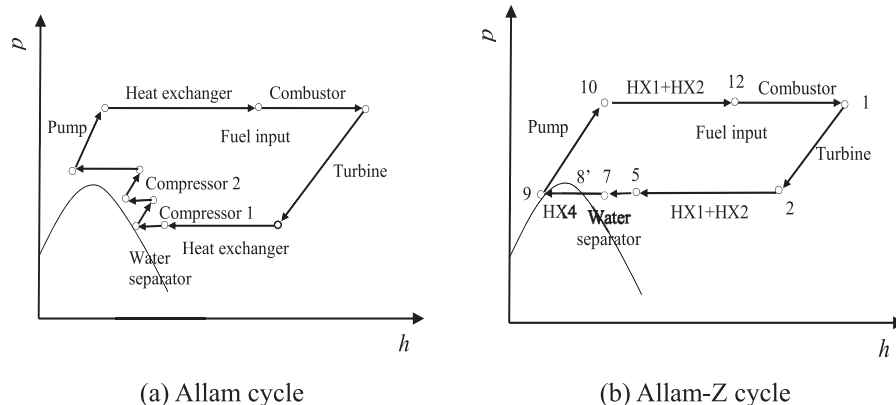
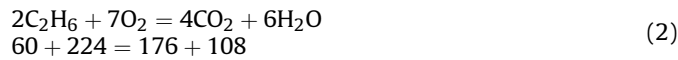


Fig. 2. Pressure–enthalpy diagrams of the Allam cycle and the Allam-Z cycle.

Table 2
Simplified composition of NG.

component	Molecular weight	Mass fraction
CH ₄	16	88.8%
C ₂ H ₆	30	4.51%
CO ₂	44	6.69%
Total		100%

C₂H₆ according to the theoretical proportional value 4:1 and 56:15 separately as show in Eqs.(1) and (2).



- 2) Gaseous carbon dioxide and liquid water are separated completely from the vapor-liquid separator.
- 3) The minimum pinch temperature difference Δt_p is set as 5 K in CO₂ condensation heat exchanger HX4, while the other heat exchangers are set as 10 K, due to worse heat transfer coefficient of gas-like supercritical CO₂.

Table 3
Mathematical model of Allam-Z cycle.

Item	Calculation formula	No.
Parameters		
Super-heated vapor or sub-cooled liquid	$h(\text{or } \rho, s) = f(t, p, \xi)$	(3)
Saturate vapor or liquid	$p_{\text{sat}}(\text{or } h_{\text{sat}}, \rho_{\text{sat}}, s_{\text{sat}}); h_{2s} = f(t, \xi)$	(4)
	or $t_{\text{sat}}(\text{or } h_{\text{sat}}, \rho_{\text{sat}}, s_{\text{sat}}); h_{2s} = f(p, \xi)$	(5)
Combustor	$G_1 = G_{1a} + G_{1b} + G_{10} = G_{1c} + G_{1w}$	(6)
	$G_{1c} = 2.75G_{1b} + G_{10}; G_{1w} = 2.25G_{1b}$	(7)
	$\xi_{\text{cp}} = 2.75/5; h_{\text{cptab}} = f(t_{4b}, p_1, \xi_{\text{cp}})$	(8)
	$G_1 h_1 = G_{10}(h_{\text{cptab}} + E) + G_{1a} h_{\text{cptab}} + G_{10} h_{10}$	(9)
	$R_C = G_{10}/(G_{1a} + G_{1b})$	(10)
CO ₂ circulation ration		
Turbine		
isentropic outlet	$h_{2s} = f(p_2, s_1, \xi_2)$	(11)
actual outlet	$h_2 = h_1 - (h_1 - h_{2s})\eta_T$	(12)
turbine work	$W_T = G_1(h_1 - h_2)$	(13)
HX1	$G_{2'}(h_2 - h_3) = G_{12}(h_{12} - h_{11})$	(14)
	$t_3 - t_{11} \geq \Delta t_p; t_2 - t_{12} \geq \Delta t_p$	(15)
HX2	$G_{3'}(h_3 - h_5) = G_{10}(h_{11} - h_{10})$	(16)
	$t_5 - t_{10} = \Delta t_p; t_3 - t_{11} \geq \Delta t_p$	(17)
HX3	$G_w(h_{5w} - h_{4w}) = G_5(h_5 - h_6)$	(18)
	$t_6 - t_{4w} \geq \Delta t_p; t_5 - t_{5w} \geq \Delta t_p$	(19)
HX4	$G_w(h_{4w} - h_{2w}) = G_8(h_8 - h_9)$	(20)
	$t_9 - t_{2w} \geq \Delta t_p; t_{8\text{sat}} - t_{3w} = \Delta t_p; t_8 - t_{4w} \geq \Delta t_p$	(21)
HX5	$G_{1w}(h_{1w} - h_{2w}) = G_{1a}(h_{3a} - h_{2a}) + G_{1b}(h_{3b} - h_{2b})$	(22)
	$t_{1w} - t_{3a}(t_{3b}) = \Delta t_p; t_{2w} - t_{2a}(t_{2b}) \geq \Delta t_p$	(23)
HX6	$G_4(h_2 - h_4) = G_{1a}(h_{4a} - h_{3a}) + G_{1b}(h_{4b} - h_{3b})$	(24)
	$t_2 - t_{4a}(t_{4b}) \geq \Delta t_p; t_4 - t_{3a}(t_{3b}) \geq \Delta t_p$	(25)
Pumps	$s_{\text{in}} \text{ or } h_{\text{in}} = f(t_{\text{in}}, p_{\text{in}})$	(26)
	$h_{\text{outs}} = f(s_{\text{in}}, p_{\text{out}})$	(27)
	$h_{\text{out}} = h_{\text{outs}} + (h_{\text{outs}} - h_{\text{in}})(1 - \eta_p)$	(28)
Cycle		
Pump work consumed	$W_p = G(h_{\text{outs}} - h_{\text{in}})/\eta_p = G(h_{\text{out}} - h_{\text{in}})$	(29)
Output power efficiency	$\eta_{\text{el out}} = (W_T \eta_g - \sum W_p)/Q_{\text{cp}}$	(30)
Equivalent net efficiency	$\eta_{\text{eq net}} = (W_T \eta_g - \sum W_p - W_{\text{ASU}} \gamma)/Q_{\text{cp}}$ $= \eta_{\text{el out}}(1 - R_{\text{ASU}} \gamma)$	(31)
Pct. of ASU consumed power	$R_{\text{ASU}} = W_{\text{ASU}} \gamma / (W_T \eta_g - \sum W_p)$ $= W_{\text{ASU}} / W_{\text{el out}}$	(32)
Pct. of auxiliary power	$R_{\text{aus}} = \sum W_p / W_{\text{el out}}$	(33)
Heat released by cooling water	$Q_{\text{cw}} = G_w(h_{5w} - h_{1w})$	(34)
Heat input by fuel combustion Q_{cp}	$Q_{\text{cp}} = E$	(35)

Note: $f()$ stands for the state function; G stands for the flow rate, kg/s; the subscripts a, b, c and w stand for NG, O₂, CO₂ and H₂O respectively; the subscripts sat stand respectively for the saturation point parameter; the subscript digit number stands for the state point shown in Fig. 1; and the subscript s stands for the isentropic process of turbine and pump. The turbine back pressure is fixed at 7.21 MPa and its corresponding CO₂ saturation temperature is 30 °C (point 9).

- 4) The heat dissipation losses are neglected, while the pump outlet pressure of all fluids is set 1 MPa more than the turbine inlet pressure considering the additional pump power consumption due to flow resistance.

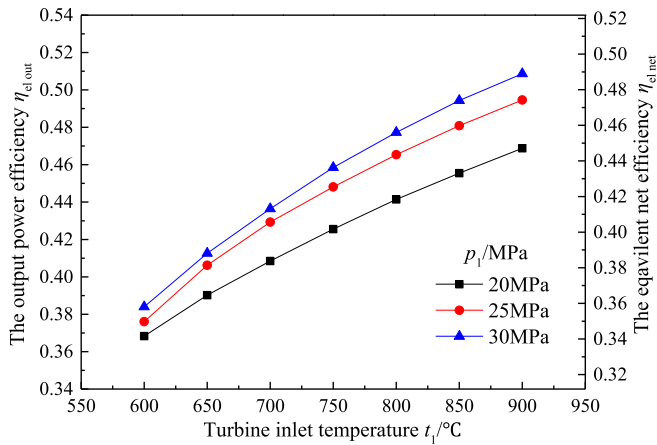
3.2. Mathematical model

Table 3 shows the calculation model of this cycle with the conservation laws. Eqs. (30) and (31) are respectively performance evaluations of cycle system of the output power efficiency and the equivalent net efficiency of this system, the former only consider the subtraction of auxiliary pump power, while the latter further subtracted 1/4 off-peak electricity by ASU in consideration of the ratio of the off-peak/peak electricity prices. Usually, the ratio of the price of off-peak electricity over that of peak electricity γ varies in the range of 1/3 to 1/5 in different circumstances, while in this paper γ is taken a mean value of 1/4 [23,24].

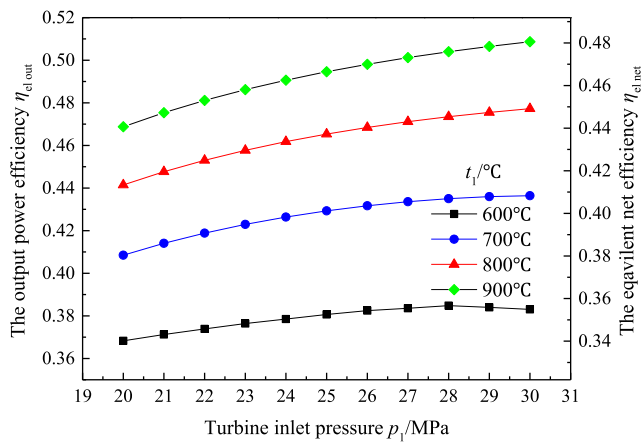
4. Results and discussion

4.1. Impacts of turbine inlet parameters

Fig. 3 shows variations of the output power efficiency and the



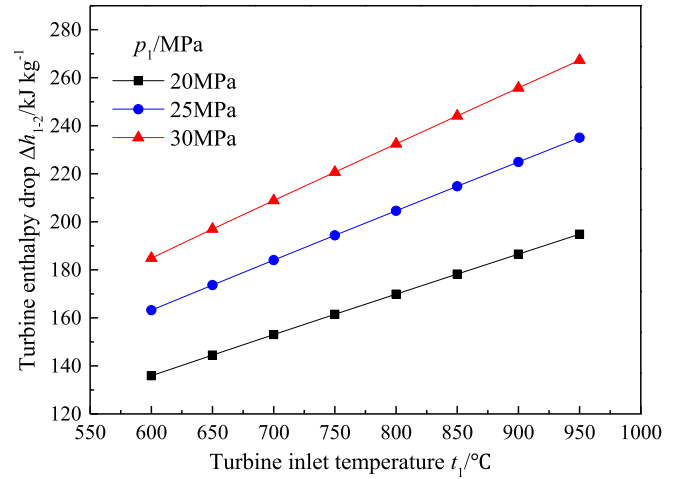
(a) Variations of efficiencies with turbine inlet temperature



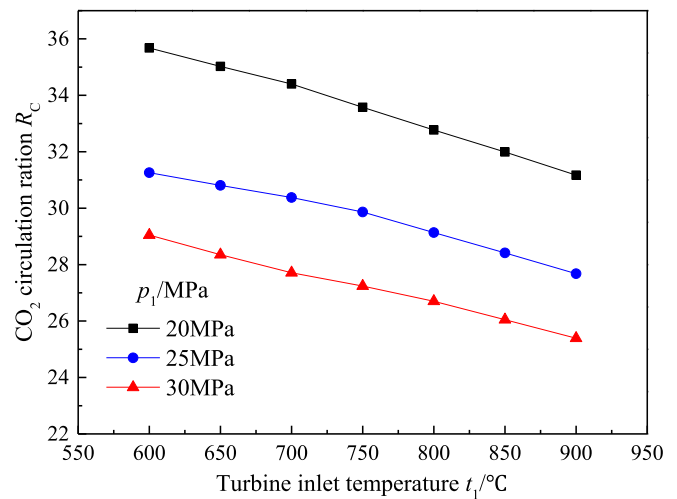
(b) variations of efficiencies with turbine inlet pressure

Fig. 3. Equivalent net efficiency of Allam-Z cycle versus turbine inlet temperature and pressure ($t_9 = 30^\circ\text{C}$, $p_2 = 7.21\text{ MPa}$).

equivalent net efficiency of the Allam-Z cycle with turbine inlet temperature and pressure. Since the differential efficiency ($\eta_{el,out} - \eta_{eq,net}$) is a constant, the trend curves of the equivalent net efficiency and the output power efficiency are plotted with the same curves but different ordinate scales. Fig. 3(a) shows the variation curves of both efficiencies versus the turbine inlet temperature at constant turbine inlet pressure 20 MPa, 25 MPa and 30 MPa. It can be seen that with the inlet temperature of the turbine is limited to 900°C , the limit temperature of 705°C in the heat exchanger HX1 can be satisfied [31,32]. It is clear that both output power efficiency and the equivalent net efficiency increase with the rise of turbine inlet temperature or pressure. In order to further reveal the impact of turbine inlet pressure on the output power efficiency and equivalent net efficiency, the variation curves of previously mentioned efficiencies are illustrated in Fig. 3(b). There are four similar upward trend curves that increase with the rise of the turbine inlet pressure at constant turbine inlet temperature 600°C , 700°C , 800°C and 900°C . However, the curve of both output power efficiency and equivalent net efficiency at turbine inlet temperature of 600°C has a maximum value at turbine inlet pressure of 28 MPa, while the other two curves show increasing trends only, and it seems that the peak moves to higher pressure with the increase of turbine inlet temperature. Thus it can be postulated that the optimal turbine inlet pressure should be over 30 MPa with



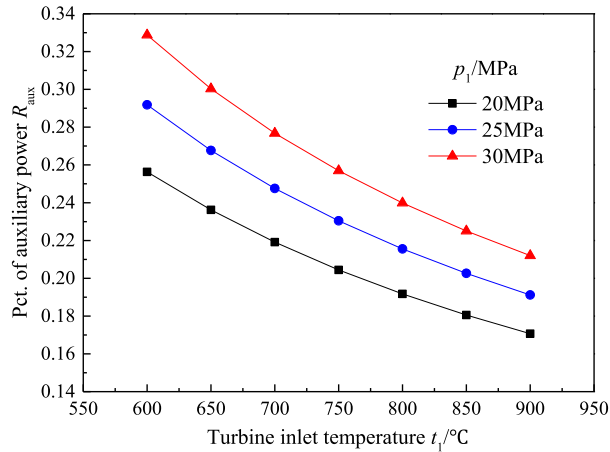
(a) Enthalpy drop of turbine

(b) CO₂ circulation ratio**Fig. 4.** Enthalpy drop of turbine and CO₂ circulation ratio versus turbine inlet temperature and pressure.

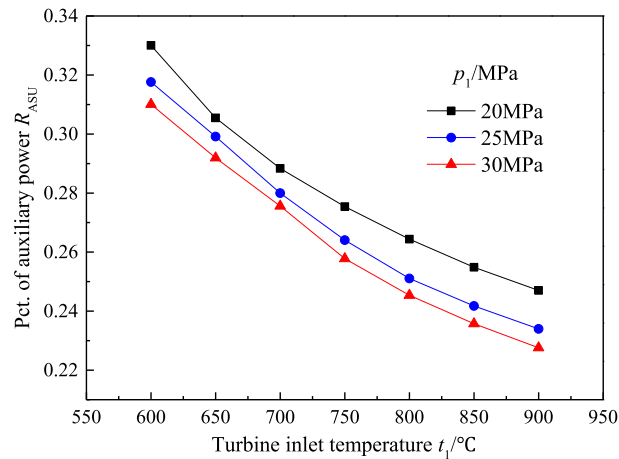
higher turbine inlet temperature. It means that the turbine inlet pressure should be selected correspondingly to the turbine inlet temperature for higher efficiency. Nevertheless, since the slope near the summit of the curves are quite flat, while the cost for higher pressure is high, the maximum pressure of 30 MPa is recommended in this paper. Fig. 3 also indicates that the output power efficiency or the equivalent net efficiency is more easily influenced by temperature than by pressure at turbine inlet.

Under the conditions of turbine inlet parameters of 30 MPa/ 900°C and condensation temperature of 30°C , the output power efficiency and the equivalent net efficiency are 50.87% and 48.05% respectively. The value of the equivalent net efficiency is higher than the conventional power plant without CCS.

Turbine inlet working fluid flow and enthalpy drop are two main indexes of turbine power. Variations of enthalpy drop of turbine with turbine inlet temperature and pressure is shown in Fig. 4(a). According to the graph, the enthalpy drop of turbine always increases with the increase of turbine inlet temperature or pressure. Fig. 4(b) demonstrates the variations of CO₂ circulation ratio with



(a) Percentage of auxiliary power consumption by pumps



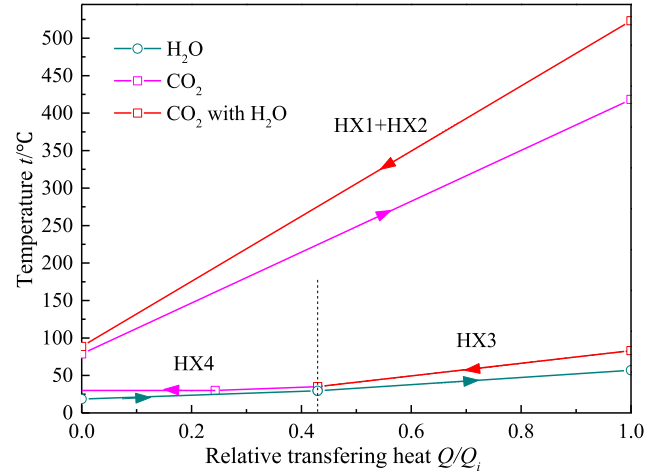
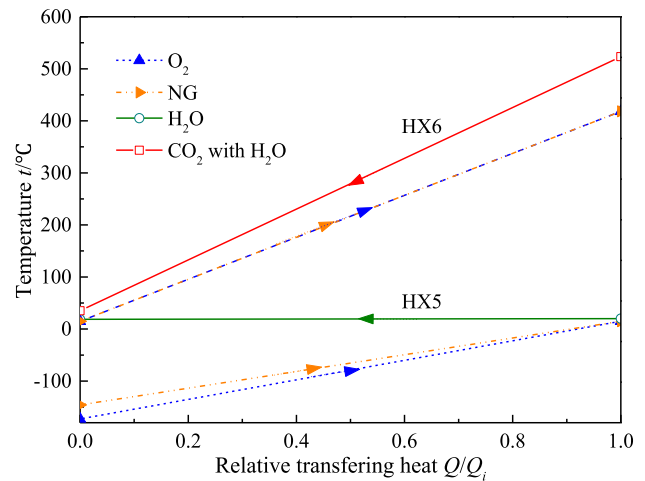
(b) percentage of ASU consumed power

Fig. 5. Percentage of auxiliary power consumption and percentage of ASU consumed power over output power versus turbine inlet parameters.

turbine inlet temperature and pressure. CO₂ circulation ratio R_c is defined as the ratio of CO₂ circulation flow rate over LNG plus O₂ flow rate. It shows that the CO₂ circulation ratio decreases with the increase of turbine inlet temperature or pressure which is just contrary to the trend of enthalpy drop mentioned before.

For a fixed turbine power, cycle thermal efficiency always increases with the decrease of total auxiliary power consumption by the pumps. The percentage of auxiliary power consumption by pumps over output power under different turbine inlet parameters is illustrated in Fig. 5(a). It is clear that the percentage of auxiliary power consumption decreases with the increase of the turbine inlet temperature or the decrease of the turbine inlet pressure and the downward trend is gradually slow. The reason is apparent that higher temperature increases the enthalpy drop thus decrease the CO₂ circulation flow rate and the power consumption while the higher pressure requires higher pump power consumption.

The liquid oxygen is produced by consuming the off-peak electricity in the air separation unit (ASU) with unit power consumption at 0.42 kWh/kg (O₂) which is also a kind of peak load shifting or energy storage approach. Fig. 5(b) reveals variations of the percentage of ASU consumed power over output power with

(a) CO₂ condensation and recuperating(b) NG and O₂ preheating and recuperating**Fig. 6.** Heat transfer curves of heat exchangers.

turbine inlet temperature and pressure at equal operation time of ASU. As is illustrated in Fig. 5(b), the percentage of ASU consumed power decreases with the increase of either the turbine inlet temperature or the turbine inlet pressure. The value of the percentage of ASU consumed power is around 23%–33% of the output power which indicates that this scheme power plant has capacity of peak load shifting. Beside the oxygen production, the ASU can also produce even more nitrogen which also has great economical value.

4.2. Specific example of the Allam-Z cycle

Under the conditions of condensation temperature of 30 °C, turbine inlet pressure of 30 MPa and temperature of 700 °C, the output power efficiency is 43.64% and the percentage of ASU consumed power over output power is 25.78%. A 200 MW peak shaving power plant which generates peak electricity on full load and consumes off-peak electricity with ASU for 8 h per day is analyzed for an example of this power cycle. 264 ton of LNG fuel and 982 ton of LO₂ are consumed for combustion which indicates that large volumes of the storage tanks are needed in this power

plant. Meanwhile, the superfluous liquid CO_2 and H_2O are reclaimed 697 tons and 549 tons respectively. At off-peak period, the electric power of 412 MW h is consumed by ASU for oxygen production at the rate of 0.42 kW h/kg (O_2). The equivalent net efficiency is 40.83% considering 1/4 ASU consumed off-peak power. Under the same turbine inlet parameter conditions, the equivalent net efficiency of the Allam cycle is 38.15% with much complicated system.

Fig. 6(a) reveals the heat transfer curves of fuel and oxidant preheating process under abovementioned turbine inlet conditions in HX5 and HX6 successively and Fig. 6(b) shows the heat transfer curves of the pure substance or mixture of CO_2 and/or H_2O in recuperating and condensing heat transfer processes in HX1+HX2, HX3 and HX4. Turbine outlet temperature is 523 °C, so the exhaust gas is directly divided into two streams entering HX1+HX2 and HX6 respectively. The latent heat of CO_2 accounts only 24% of heat carried away by cooling water in HX3 and HX4. To make the thermodynamic process of this power cycle more clear, parameters of status points of this case is also listed in Table 4.

4.3. Comparison of the Allam-Z cycle with the Allam cycle

The aim for comparison of the Allam-Z cycle with the Allam cycle is to see the quantitative deviation of performances due to a decreased turbine enthalpy drop without compression power consumption with a higher turbine back pressure. The schematic diagram of the Allam cycle for comparison is showed in Fig. 7(a). The Allam cycle has similar loop as the Allam-Z cycle, but has an additional compressor. The Pressure-enthalpy diagrams of the Allam cycle is also given in Fig. 7(b). Theoretically, the isotropic expansion enthalpy drop in high temperature range is larger than the isotropic compression enthalpy rise in low temperature range between two pressures, however, the entropy increases in real process of either expansion or compression, thus the power gain in

the turbine might not compensate the loss in the compressor especially when the turbine inlet temperature is not very high.

Table 5 shows the performance comparison of the Allam-Z and Allam cycle under two sets of conditions that the turbine inlet parameters are 30 MPa/700 °C and 30 MPa/900 °C respectively and the condensation temperature is kept 30 °C, the minimum pinch temperature difference of each heat exchange takes the same value. The turbine outlet pressures of Allam-Z cycle and Allam cycle are respectively 7.21 MPa and 4 MPa. Under turbine inlet parameters of 30 MPa/700 °C, the Allam-Z cycle has output power efficiency and equivalent net efficiency of 43.64% and 40.83% respectively, which are all 2.15% higher than those of the Allam cycle. Under turbine inlet parameters of 30 MPa/900 °C, the Allam-Z cycle has output power efficiency and equivalent net efficiency of 50.87% and 48.05% respectively which are all 2.97% higher than those of the Allam cycle under the same condition.

The calculation verified that the modification to raise the turbine back pressure and eliminate the compressors is justified when the turbine inlet temperature is not higher than 900 °C.

5. Conclusions

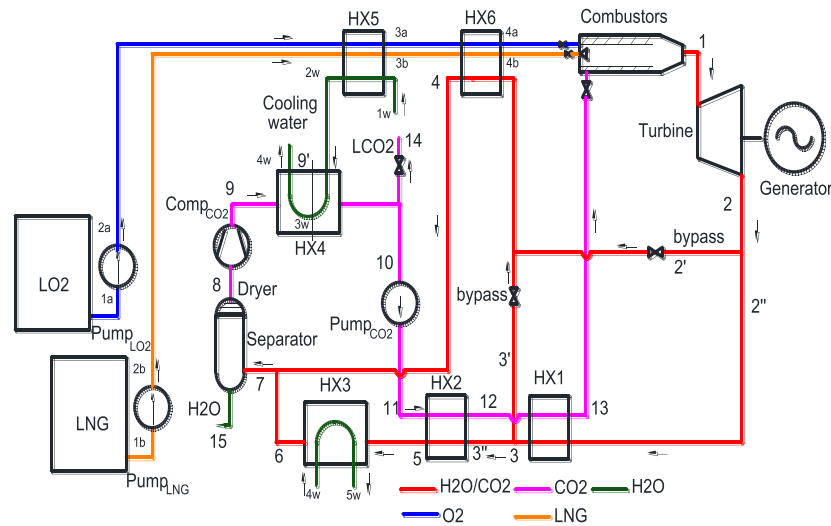
Under the turbine inlet temperature not higher than 900 °C, the Allam-Z cycle with higher turbine back pressure to eliminate compressors was investigated using combustion product and circulation CO_2 as working medium aiming at high efficiency power generation, nearly zero NO_x emission, peak load shifting and CO_2 capture. The conclusions are as follows:

- 1) The output power efficiency increases with the increase of turbine inlet temperature at constant turbine inlet pressure. The cycle efficiency varying with turbine inlet pressure at constant turbine inlet temperature has a maximum value, and the peak moves to higher pressure with the increase of turbine inlet

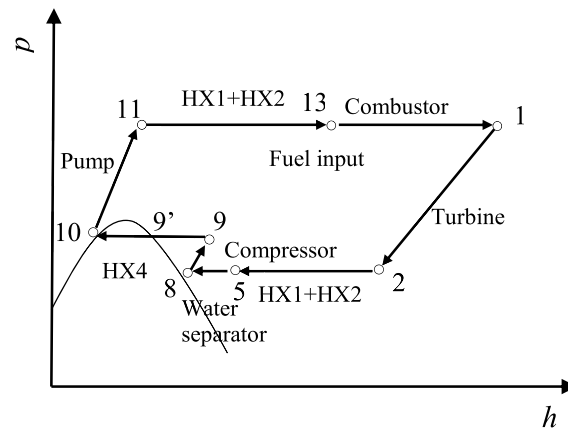
Table 4

Parameters of status points of the example of Allam-Z cycle.

Status point	Temperature °C	Pressure MPa	Enthalpy kJ·kg ⁻¹	Flow rate kg·s ⁻¹	CO_2 fraction kg·kg ⁻¹
1	700	31	1265.7	133.31	0.9844
2	523.4	7.21	1056.8	133.31	0.9844
4	35	7.21	406.0	4.77	0.9844
5	88.6	7.21	543.6	128.54	0.9844
6	35	7.21	406.0	128.54	0.9844
7	35	7.21	406.0	133.31	0.9844
8	35	7.21	410.0	131.23	1
8'	30	7.21	354	131.34	1
9	30	7.21	304.6	128.59	1
10	78.6	31	346.5	128.59	1
12	416.8	31	860.4	128.59	1
13	30.0	7.21	304.6	2.64	1
14	35	7.21	153.1	2.08	—
1a	−185	0.1	−136.8	3.72	—
1b	−162	0.1	−3.1	1	—
2a	−175.4	31	−103.8	3.72	—
2b	−149.1	31	80.9	1	—
3a	15	31	200.2	3.72	—
3b	15	31	618.1	1	—
4a	416.8	31	651.2	3.72	—
4b	416.8	31	1917.7	1	—
1w	20	0.1	84.0	459.89	—
2w	19.1	0.1	80.4	459.89	—
3w	25	0.1	104.9	459.89	—
4w	28.1	0.1	117.7	459.89	—
5w	37.3	0.1	156.2	459.89	—



(a) Schematic diagram of the Allam cycle



(b) pressure-enthalpy diagram of the Allam cycle

Fig. 7. Schematic and pressure-enthalpy diagram of the Allam cycle.

Table 5
Comparison of performances of Allam-Z and Allam cycle.

item	unit	Allam-Z	Allam
Turbine inlet pressure p_1	MPa	30	30
Turbine outlet pressure p_2	MPa	7.214	4
Cooling water temperature t_{1w}	°C	20	20
LNG flow rate G_{1b}	kg·s ⁻¹	1	1
LO ₂ flow rate G_{1a}	kg·s ⁻¹	3.72	3.72
Turbine inlet temperature t_1	°C	700	900
Turbine enthalpy drop Δh_{1-2}	kJ·kg ⁻¹	208.9	255.8
CO ₂ circulation ration R_c	%	27.24	24.67
Power output by turbine W_T	MW	27.85	31.00
Power consumption of pumps W_P	MW	5.61	5.10
Power consumption of compressor W_C	MW	—	—
Power output	MW	21.82	25.43
Transferring heat of HX1+HX2	MW	66.08	85.45
Transferring heat of HX3	MW	17.69	17.18
Transferring heat of HX4	MW	13.83	12.56
Transferring heat of HX5	MW	1.67	1.67
Transferring heat of HX6	MW	2.98	3.98
Heat released by cooling water Q_{cw}	MW	29.86	28.07
Heat input by combustion product Q_{cp}	MW	50	50
Output power efficiency $\eta_{el out}$	%	43.64	50.87
Equivalent net efficiency $\eta_{eq net}$	%	40.83	48.05

temperature. Moreover, the impact of turbine inlet pressure on the efficiency is smaller than that of the turbine inlet temperature.

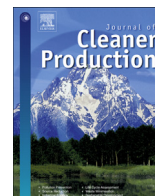
- The enthalpy drop of turbine always increases with the increase of the turbine inlet temperature and/or pressure. The circulation CO₂ ratio decreases with the increase of turbine inlet temperature or pressure.
- The percentage of auxiliary power consumption decreases with the increase of the turbine inlet temperature or the decrease of the turbine inlet pressure. The percentage of ASU consumed power decreases with the increase of either temperature or pressure at turbine inlet and ranges from 23% to 33% of the output power at equal operation time of ASU with consumption rate of 0.42 kW h/kg (O₂) in the investigated turbine inlet parameter range of temperature 600–900 °C and pressure 20–30 MPa.
- Under turbine inlet parameters of 30 MPa/700 °C or 30 MPa/900 °C and condensation temperature of 30 °C, the equivalent net efficiency of the Allam-Z cycle is 40.80% or 48.05% which is higher than that of the Allam cycle (38.68% or 45.09%).

Acknowledgement

This work is supported by the National Nature Science Foundation Program of China (No. 51776035).

References

- [1] Global CCS Institute (GCCSI). The status of CCS projects interim report 2010. GCCSI; 2010.
- [2] International Energy Agency (IEA). United Nations Industrial Development Organization (UNIDO). Technology roadmap carbon capture and storage roadmap. IEA Publication; 2011.
- [3] Davison J. Performance and costs of power plants with capture and storage of CO₂. *Energy* 2007;32(7):1163–76.
- [4] Supekar SD, Skerlos SJ. Reassessing the efficiency penalty from carbon capture in coal-fired power plants. *Environ Sci Technol* 2015;49(20):12576–84.
- [5] Oboirien BO, North BC, Kleyn T. Techno-economic assessments of oxy-fuel technology for South African coal-fired power stations. *Energy* 2014;66(4):550–5.
- [6] Scaccabarozzi R, Gatti M, Martelli E. Thermodynamic analysis and numerical optimization of the NET Power oxy-combustion cycle. *Appl Energy* 2016;178:505–26.
- [7] Cormos CC. Oxy-combustion of coal, lignite and biomass: a techno-economic analysis for a large scale Carbon Capture and Storage (CCS) project in Romania. *Fuel* 2016;169:50–7.
- [8] Gladysz P, Ziębik A. Life cycle assessment of an integrated oxy-fuel combustion power plant with CO₂ capture, transport and storage – Poland case study. *Energy* 2015;92:328–40.
- [9] Kanniche M, Gros-Bonnivard R, Jaud P, Valle-Marcos J, Amann J, Bouallou C. Pre-combustion, post-combustion and oxy-combustion in thermal power plant for CO₂ capture. *Appl Therm Eng* 2010;30(1):53–62.
- [10] Pak PS, Lee YD, Ahn KY. Characteristics and economic evaluation of a power plant applying oxy-fuel combustion to increase power output and decrease CO₂ emission. *Energy* 2010;35(8):3230–8.
- [11] Hong J, Field R, Gazzino M, Ghoniem A. Operating pressure dependence of the pressurized oxy-fuel combustion power cycle. *Energy* 2010;35(12):5391–9.
- [12] Peng S, Hong H, Jin H, Wang Z. An integrated solar thermal power system using intercooled gas turbine and Kalina cycle. *Energy* 2012;44(1):732–40.
- [13] Zhao ZY, Yan H. Assessment of the biomass power generation industry in China. *Renew Energy* 2012;37(1):53–60.
- [14] Chen Y, Guo Z, Wu J, Zhang Z, Hua J. Energy and exergy analysis of integrated system of ammonia–water Kalina–Rankine cycle. *Energy* 2015;90:2028–37.
- [15] Zhu Z, Zhang Z, Chen Y, Wu J. Parameter optimization of dual-pressure vaporization Kalina cycle with second evaporator parallel to economizer. *Energy* 2016;112:420–9.
- [16] Luu MT, Milani D, McNaughton R, Abbas A. Dynamic modelling and start-up operation of a solar-assisted recompression supercritical CO₂ Brayton power cycle. *Appl Energy* 2017;199(2017):247–63.
- [17] Crespi F, Gavagnin G, Sánchez D, Martínez GS. Supercritical carbon dioxide cycles for power generation: a review. *Appl Energy* 2017;195:152–83.
- [18] Cayer E, Galanis N, Nesreddine H. Parametric study and optimization of a transcritical power cycle using a low temperature source. *Appl Energy* 2010;87(4):1349–57.
- [19] Osorio JD, Hovsapien R, Ordonez JC. Effect of multi-tank thermal energy storage, recuperator effectiveness, and solar receiver conductance on the performance of a concentrated solar supercritical CO₂-based power plant operating under different seasonal conditions. *Energy* 2016;115:353–68.
- [20] Abram T, Ion S. Generation-IV nuclear power: a review of the state of the science. *Energy Policy* 2008;36(12):4323–30.
- [21] Zhang N, Lior N. Two novel oxy-fuel power cycles integrated with natural gas reforming and CO₂ capture. *Energy* 2008;33(2):340–51.
- [22] Purjam M, Goudarzi K, Keshtgar M. A new supercritical carbon dioxide Brayton cycle with high efficiency. *Heat Transf Asian Res* 2017;46(5):465–82.
- [23] Chen Y, Zhu Z, Wu J, Yang S, Zhang B. A novel LNG/O₂ combustion gas and steam mixture cycle with energy storage and CO₂ capture. *Energy* 2017;120:128–37.
- [24] Wu J, Chen Y, Zhu Z, Mei X, Zhang S, Zhang B. Performance simulation on NG/O₂ combustion gas and steam mixture cycle with energy storage and CO₂ capture. *Appl Energy* 2017;196:68–81.
- [25] Jeong WS, Yong HJ. Performance of supercritical Brayton cycle using CO₂-based binary mixture at varying critical points for SFR applications. *Nucl Eng Des* 2013;262:12–20.
- [26] Amann JM, Kanniche M, Bouallou C. Natural gas combined cycle power plant modified into an O₂/CO₂ cycle for CO₂ capture. *Energy Convers Manag* 2009;50(3):510–21.
- [27] Zhang G, Zheng J, Yang Y, Liu W. A novel LNG cryogenic energy utilization method for inlet air cooling to improve the performance of combined cycle. *Appl Energy* 2016;179:638–49.
- [28] Cheng C, Su C, Wang P, Shen J, Lu J, Wu X. An MILP-based model for short-term peak shaving operation of pumped-storage hydropower plants serving multiple power grids. *Energy* 2018;163:722–33.
- [29] Chen H, Cong TN, Yang W, Tan C, Li Y, Ding Y. Progress in electrical energy storage system: a critical review. *Prog Nat Sci* 2009;19(3):291–312.
- [30] Fu C, Gundersen T. Using exergy analysis to reduce power consumption in air separation units for oxy-combustion processes. *Energy* 2012;44(1):60–8.
- [31] Allam RJ, Palmer Jr MR, B GW, Fetvedt J, Freed D, Nomoto H, et al. High efficiency and low cost of electricity generation from fossil fuels while eliminating atmospheric emissions, including carbon dioxide. *Energy Proc* 2013;37:1135–49.
- [32] Allam R, Martin S, Forrest B, Fetvedt J, Lu X, Freed D, et al. Demonstration of the Allam cycle: an update on the development status of a high efficiency supercritical carbon dioxide power process employing full carbon capture. *Energy Proc* 2017;114:5948–66.
- [33] Kumar PR, Raju VR, Kumar NR. Simulation and parametric optimization of thermal power plant cycles. *Perspectives in Sci* 2016;8(C):304–6.
- [34] Purgert R, Shingledecker J, Saha D, Thangirala M, Booras G, Powers J, et al. Materials for advanced ultrasupercritical steam turbines. 2015.
- [35] Wang L, Yang G, Lei T, Yin S, Wang L. Hot deformation behavior of GH738 for A-USC turbine blades. *Iron Steel Res* 2015;22(11):1043–8.
- [36] Urech J, Tock L, Harkin T, Hoadley A, Maréchal F. An assessment of different solvent-based capture technologies within an IGCC–CCS power plant. *Energy* 2014;64(1):268–76.
- [37] Lindqvist K, Jordal K, Haugen G, Hoff KA, Anantharaman R. Integration aspects of reactive absorption for post-combustion CO₂ capture from NGCC (natural gas combined cycle) power plants. *Energy* 2014;78(2):758–67.
- [38] Park SH, Lee SJ, Jin WL, Chun SN, Lee JB. The quantitative evaluation of two-stage pre-combustion CO₂ capture processes using the physical solvents with various design parameters. *Energy* 2015;81:47–55.
- [39] NIST reference fluid thermodynamic and transport properties-REFPROP (Version 8.0). NIST Standard Reference Database 2007;23.



Thermodynamic optimization and equipment development for a high efficient fossil fuel power plant with zero emissions

Andrey Rogalev ^a, Evgeniy Grigoriev ^{a, b}, Vladimir Kindra ^{a, *}, Nikolay Rogalev ^a

^a National Research University "Moscow Power Engineering Institute", Krasnokazarmennaya str. 14, Moscow, 111250, Russian Federation

^b Ivanovo State Power Engineering University, Rabfakovskaya str. 34, Ivanovo, 153003, Russian Federation

ARTICLE INFO

Article history:

Received 29 January 2019

Received in revised form

25 May 2019

Accepted 7 July 2019

Available online 8 July 2019

Handling editor is Zheming Tong

Keywords:

Global warming

Carbon dioxide emissions

Oxy-fuel combustion cycle

Thermodynamic optimization

Supercritical CO₂ gas turbine

ABSTRACT

The transition to oxy-fuel combustion cycles is a perspective way to decrease harmful emissions into the atmosphere in the energy sector. The oxy-fuel, supercritical carbon dioxide Allam cycle (NET Power oxy-combustion cycle) is a promising technology with high efficiency. Emissions of carbon dioxide into the atmosphere could be decreased by 98.9% using this cycle for electricity production, which is 8–17% higher compare to gas turbine combined cycle with post-combustion carbon capture. However, there are several challenges on the way of its implementation, one of which is the development of a supercritical carbon dioxide gas turbine. The aim of the present study was to develop a construction of a high-power supercritical CO₂ gas turbine with optimal thermodynamic parameters of the Allam cycle and to evaluate technical, environmental and economic characteristics of zero emission technology for the electricity production. To reach the goal, the calculation algorithm allowing to model the oxy-fuel combustion cycles was developed. The results of thermodynamic optimization showed that the highest value of cycle net efficiency equal to 56.5% is achieved for the turbine inlet temperature and pressure of 1083 °C and 30 MPa, the turbine outlet pressure of 3 MPa and the coolant temperature of 200 °C. The formed equipment requirements were used to create the design of a 335 MW supercritical carbon dioxide gas turbine, the main features of which were described in detail. The results of environmental characteristics analysis showed, that the specific amount of CO₂ emitted from the cycle to the atmosphere is 0.0038 kg/kWh. The results of economic feasibility evaluation for the Allam cycle showed that the total specific investment costs including the price for carbon storage are equal to \$1307.5/kW, which is quite competitive value.

© 2019 Elsevier Ltd. All rights reserved.

1. Introduction

1.1. Anthropogenic carbon dioxide emissions sources

The world's energy consumption is rising over the past 50 years due to population growth and increasing industrialization of countries in the third tier. The emerging trend has predetermined a number of serious environmental consequences, among which is the global warming. With a high probability, a rising concentration of CO₂ in the atmosphere is the main reason for the observed process.

Continuous measurements of the CO₂ concentration in the atmosphere have been carried out since the middle of the last century. The results are presented in the form of the Killing graph and indicate a continuous increase in the average annual concentration of CO₂ in the period from 1958 to 2017: from 318 to 403 ppm.

Such a significant change in a relatively short time period could not be due to natural causes only (Wang et al., 2018; Nejat et al., 2015). The concern of the world community about global climate change has contributed to the creation of a number of international agreements that oblige developed countries and countries in transition to stabilize or reduce greenhouse gas emissions. In particular, in 1997 the Kyoto Protocol was adopted, and in 2015 the Paris Agreement was signed (Ari and Sari, 2017).

The world largest producers of CO₂ emissions are China, the United States, India and Russia. Despite the fact that the energy consumption is similar to the one in the United States, the total contribution of the European Union countries is less significant

* Corresponding author. Department of Thermal Power Plants, National Research University "Moscow Power Engineering Institute", Krasnokazarmennaya str. 14, Moscow, 111250, Russian Federation.

E-mail addresses: r-andrey2007@yandex.ru (A. Rogalev), grigorieff007@mail.ru (E. Grigoriev), kindra.vladimir@yandex.ru (V. Kindra).

(about 14%) due to the intensive development of renewable energy sources (Lisin et al., 2014).

Forecasting changes in CO₂ concentration during the next few decades can be made by analyzing the dynamics of this indicator in the past for the regions with the largest emissions and determining the most significant impact factors. Since 1970, in the United States, Russia, and the European Union, total CO₂ emissions have remained roughly at the same level, and in China and India, this value has increased significantly (Smith and Wigley, 2000; Liu and Bae, 2018). The largest increases were observed in the early 21st century due to the rapid industrialization of these countries.

Analysis of numerous forecast data, in particular (OECD, 2012), allows concluding that with no implementation of environmentally friendly production technologies, such a tendency appears likely to continue and lead to significant economic losses in various regions of the planet. About three-quarter of the anthropogenic CO₂ emissions is the result of oil, natural gas, and coal production and combustion. About 25% of global emissions are produced by power plants. In the United States, the contribution of the energy industry to the overall structure of anthropogenic CO₂ emissions is 35%, in China – 6%, in Europe – 31%, in Russia – 33%.

The reason for such a significant energy industry contribution in the overall structure of CO₂ emissions is the prevalence of generating power plants operating by the typical Rankine and Brayton-Rankine cycles, with the heat supply due to the combustion of a hydrocarbon in the air. The research and development of zero emission technologies for electricity production is necessary for sustainable development.

1.2. Different ways to reduce CO₂ emissions pollution from the energy sector

There are several ways to reduce the amount of CO₂ emissions by the energy industry. First of all, it is possible to make a qualitative step forward by increasing the energy efficiency of existing fossil fuel power plants (Konova et al., 2012). This approach could slow down somewhat the growing CO₂ concentration in the atmosphere, but not stabilize it since combustion products consisting mainly of greenhouse gases will still be discharged into the air (Mallapragada et al., 2018). But CO₂ extraction from nitrogen-rich low-temperature waste gases is associated with high capital costs for special equipment, lower cycle efficiency and, ultimately, leads to an increase in the electricity cost by 1.5–2 times.

The second promising growth area is renewable energy sources. The growth of solar cell energy efficiency and wind turbine capacity led to a significant reduction in the payback period for this type of units. Currently, the proportion of the world's renewable energy sources in the total power structure is less than 5% (excluding hydropower industry). That is due to the complexity of power loading control and the high cost of energy storage.

An efficient way to reduce CO₂ emissions into the atmosphere, which implies maintaining economic growth, is the creation of closed thermodynamic cycles with oxy-fuel combustion (Barba et al., 2016; Rogalev et al., 2018). The energy efficiency of power generation and the absence of pollutant emissions in the air are the main advantages of these technologies.

The following closed thermodynamic cycles have become widely known: semi-closed oxy-fuel combustion combined cycle (SCOC-CC), MATIANT cycles, NET Power oxy-combustion cycle, Graz cycles as well as supercritical CO₂ Brayton cycles (International Energy Agency, 2015; Zhao et al., 2017; Padilla et al., 2016; Gkoutas et al., 2017; Shi, et al., 2018). The first modifications of these cycles appeared at the end of the last century. Today the USA, Japan, and European countries invest heavily in this area.

1.3. High-efficient, near-zero emissions technology for electricity production

The Allam cycle is currently one of the most promising among the oxy-fuel power plants of the new generation (Allam et al., 2013). The technology patented in 2010 by the inventor Rodney John Allam, allows achieving a record net efficiency of 58.9% for natural gas and of 51.44% for gasified coal, taking into account the costs of CO₂ disposal. The technology developers also highlight CAPEX of installed capacity. For the Allam cycle on natural gas, it may be \$800–1000/kW, on gasified coal – \$1500–1800/kW (Allam et al., 2017).

A big advantage of the Allam cycle technology is low atmospheric emissions. The traditional post-combustion carbon capture technology allows preventing 80–89% of carbon dioxide emissions and the Allam cycle – 98.9%. It means that the mass of the produced CO₂ emissions for the Allam cycle is three to six times lower than for combined cycle with post-combustion carbon capture.

The operating points for the Allam cycle are shown on a pressure-enthalpy diagram for pure carbon dioxide in Fig. 1. CO₂ is compressed in a multistage compressor with intercooler up to 80 bar and then pumped to the maximum pressure in the cycle, ranging from 200 to 400 bar. After being pumped, CO₂ is sent to the regenerator where it is heated up to 700–750 °C due to the turbine exhaust heat and the internal low-grade heat from the air separation unit (ASU). After the regenerator, most of the CO₂ stream is directed to the combustion chamber in order to limit the maximum temperature, and a smaller part is used for gas turbine cooling. The rest of CO₂ is mixed with a compressed oxygen stream and is also directed to the combustion chamber. The working fluid temperature increases in the combustion chamber up to 1100–1200 °C due to the oxy-fuel combustion. The CO₂ recycle flow is used to limit the turbine inlet temperature. The turbine outlet pressure is in the range from 20 to 40 bar, which is less than the CO₂ critical pressure. After the turbine, the working fluid is sent to the regenerator.

The high performance of the Allam cycle, as well as the unconventional chemical composition of the working fluid, make it necessary to develop a framework for power equipment, among which a supercritical CO₂ gas turbine deserves a special mention. When designing the CO₂ turbine, it is rational to use the existing practices in developing of steam and gas turbine technologies (González-Salazar, 2015; Best et al., 2018). The temperatures in the Allam cycle are lower than in modern gas turbine units and combined cycles, but much higher than in steam turbine units. At the same time, the maximum pressure in the Allam cycle does not exceed the maximum pressure in the newest steam turbine units but exceeds the maximum pressure in gas turbine units.

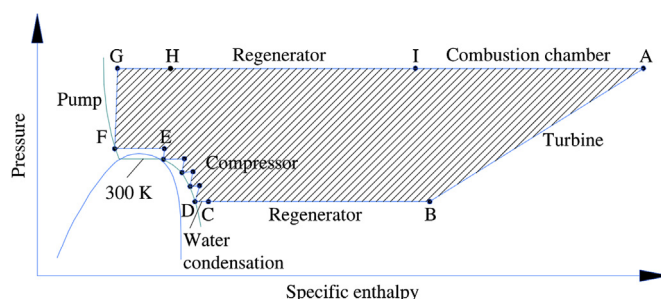


Fig. 1. Pressure-enthalpy diagram for the Allam cycle.

1.4. Current progress on the high-power supercritical carbon dioxide gas turbines

In the Soviet Union, the transition to supercritical steam pressure (240 bar) was carried out back in the late 50s and early 60s of the last century when the prototype model of the turbine K-300-240 was created. However, the metallurgy development level did not allow the steam temperature to rise above 565 °C back then. In 1968, the commercialization of the SKR-100 turbine with initial parameters of 300 bar and 650 °C was executed for the first time. A great deal of emphasis had recently been laid on to the development of power units with supercritical and ultra-supercritical initial parameters (Rogalev et al., 2016; Petrescu et al., 2017; Zaryankin et al., 2016). The key challenge to their large-scale effective implementation is the high capital cost, associated with the increase of heat-resisting alloys used for the production of high-temperature elements. The specific cost of installed capacity can be decreased by increasing the power of energy unit, as well as reducing the metal content of equipment. The lack of proper strength of the last stage blades of the low-pressure turbine prevents the power improvement of the steam-turbine unit achieved by increasing the flow path. However, the problem can be solved using a low-pressure turbine of increased capacity (Zaryankin et al., 2015) and related technical solutions (Inozemtsev et al., 2008; Zaryankin et al., 2017a, 2017b). Nonetheless, the working fluid temperature in such units does not exceed 700 °C. The significantly higher maximum temperature in the Allam cycle makes it impossible to directly adapt all technical solutions used for steam turbines to a supercritical CO₂ gas turbine. Nevertheless, the engineering algorithm for existing steam turbines can be used as a first iteration to obtain the most suitable design.

Because of the new concept, there is little information about developing methods of high-power supercritical CO₂ gas turbines up to this date. The cycle developers propose some recommendations on the rotor design in (Allam et al., 2013), including the choice of materials for its manufacture and the possible way of blade cooling. The turbine design of a demonstration unit with a capacity of 50 MW is described by (Allam et al., 2017).

The results of characteristics comparison for the impulse and reaction turbines designed for supercritical CO₂ cycle of 100 MW are presented in (Moroz et al., 2014). Based on calculation results presented in the work, the authors conclude that the efficiency of

the reaction turbines is higher by 1.5%. On the other hand, the flow path of the reaction turbine is more expensive due to the relatively big number of stages. Moreover, the turbine stages are overloaded compare to gas and steam turbines, which leads to an increase in the axial chords of the blades due to the significant density of the supercritical carbon dioxide.

Another example of a high-power supercritical CO₂ gas turbine construction having six stages is presented in (Schmitt et al., 2014). In the work, the cooled vane development process for the first stage with an inlet temperature of 1350 K is described in detail. At the same time, the design features of the other elements of the turbine flow path are not considered.

1.5. Aims and objectives

The aim of this study is to develop a construction of a high-power supercritical CO₂ gas turbine for optimal parameters of the Allam cycle and to evaluate technical, environmental and economic characteristics of zero emission technology for the electricity production. The next objectives were fulfilled to achieve the stated aim:

- The precise simulation model of the oxy-fuel combustion cycle was created using AspenONE software and the recommendations for the cycle modeling process were formed including estimation of penalties for the oxygen production, the approaches to identify real properties of the working fluid and the calculation algorithm.
- The optimal values of the turbine inlet, outlet parameters and the coolant temperature allowing to achieve maximum cycle efficiency were identified.
- The design of the high-power supercritical CO₂ for the Allam cycle with optimal thermodynamic parameters was developed.
- The specific amount of CO₂ emitted from the cycle to the atmosphere was identified and the overall volume of the carbon storage was estimated for the Allam cycle.
- Economic feasibility evaluation for the Allam cycle.

2. Methodology

Mathematical modeling is considered as a tool for the thermodynamic optimization of the Allam cycle parameters. Fig. 2 shows

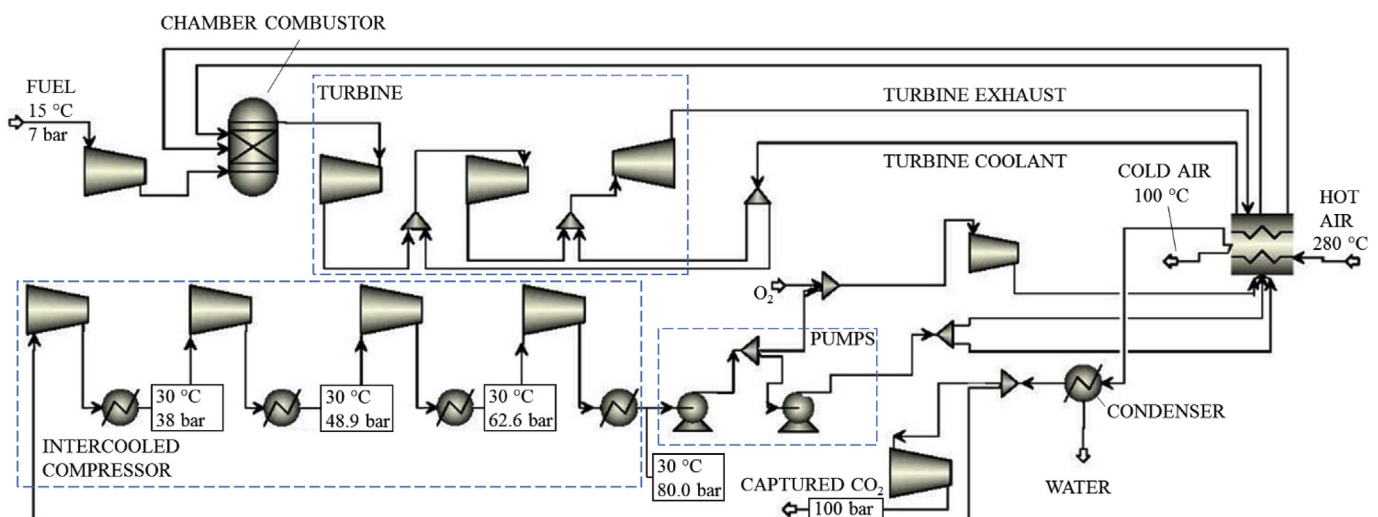


Fig. 2. Simulation flowchart.

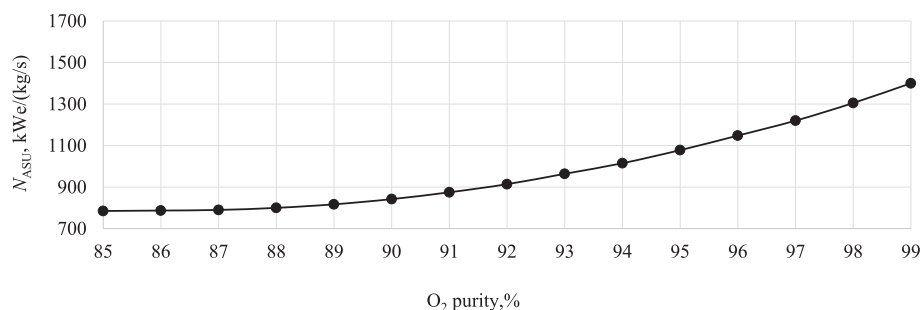


Fig. 3. An influence of oxygen purity on the power consumption of the air separation unit.

the simulation model of the Allam cycle operated on natural gas, which has been created using the AspenONE software. The thermal scheme consists of several elements: intercooled compressor, pumps, combustion chamber, cooled turbine, regenerator, condenser, and auxiliary equipment.

The cycle thermodynamic simulation included the specially developed model of air separation unit. The technical and financial reasons determine the ASU type as the cryogenic high pressure two-stage. The developed model includes estimation of the energy consumption for oxygen production and evaluation of the amount of low potential heat transferred to the regenerator.

The analysis of ASU with different oxygen purity production is disclosed in the relation between oxygen purity and power consumption shown in Fig. 3. The oxygen purity above 90–91% requires a remarkable power consumption increase. In this work the purity degree is assumed as 91.25% with the argon main impurity, then the ASU power consumption is 900 kW/(kg/s). The air to oxygen ratio used for evaluation of the low potential heat the air takes away from ASU is 5.46. In addition, the simulation model assumes the air temperature increase caused by its compression up to 280°C.

Carbon dioxide is the main component of the working fluid of the Allam cycle and the correct definition of CO₂ thermodynamic properties is very important to ensure the accuracy of simulation results. Several approaches for estimation of CO₂ thermodynamic properties were considered: two equations of state (the Peng-Robinson EOS and the Redlich-Kwong EOS) and the NIST REFPROP database. Reference values were taken from (Vargaftik, 1972).

According to the plots presented in Fig. 4 the minimum average deviation of the CO₂ specific volume definition equal to 0.03% is achieved for NIST REFPROP database based on the Span and Wagner equation of state (Span and Wagner, 1996). An increase of CO₂ pressure usually leads to an increase in deviation. However, the

temperature increase affects ambiguously. To simulate the Allam cycle we used the NIST REFPROP database because of the highest accuracy.

Open-loop internal (convection) cooling of the high-temperature supercritical carbon dioxide gas turbine was considered due to relatively low turbine inlet temperature. The coolant flow fraction was determined according to the method outlined in (Wilcock et al., 2005). The turbine cooling losses were estimated according to (Thorbergsson and Grönstedt, 2016). Pinch analysis technique was used for the modeling of the multithreaded high-temperature regenerator (Kemp, 2011; Scaccabarozzi et al., 2016). The algorithm for estimation of energy characteristics of the Allam cycle is presented in Fig. 5 and the input data are presented in Table 1.

3. Results and discussion

3.1. Thermodynamic optimization of turbine parameters for the Allam cycle

To achieve the maximum net efficiency of the NET Power oxy-combustion cycle, the turbine inlet and outlet parameters were optimized. The results of thermodynamic investigations of the turbine inlet parameters influence on the Allam cycle net efficiency are presented in Fig. 6a. The maximum value of the Allam cycle net efficiency η_{net} of 56.5% (including ASU penalty and carbon capture and storage at 100 bar) is achieved for the turbine inlet temperature T_0 of 1083 °C and pressure P_0 of 300 bar. The turbine outlet pressure P_{out} value was fixed at 30 bar during the optimization of turbine inlet parameters.

Usually, a rise of the turbine inlet temperature is accompanied by an increase of cycle thermodynamic efficiency due to the growth of the heat source average temperature. However, the Allam cycle contains a multithreaded regenerator, parameters of which

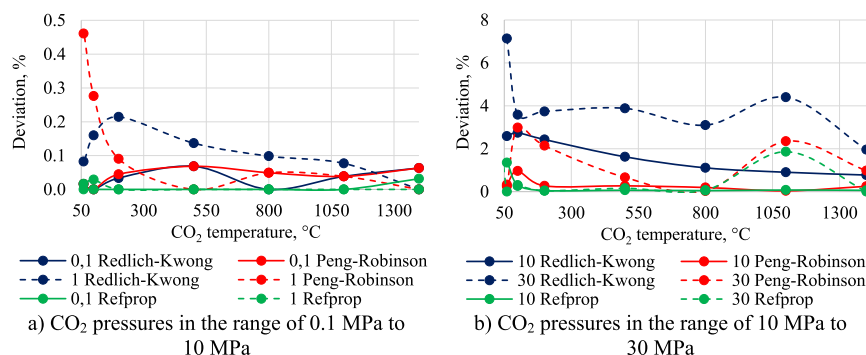


Fig. 4. An influence of the CO₂ temperature and pressure on the definition error of the CO₂ specific volume.

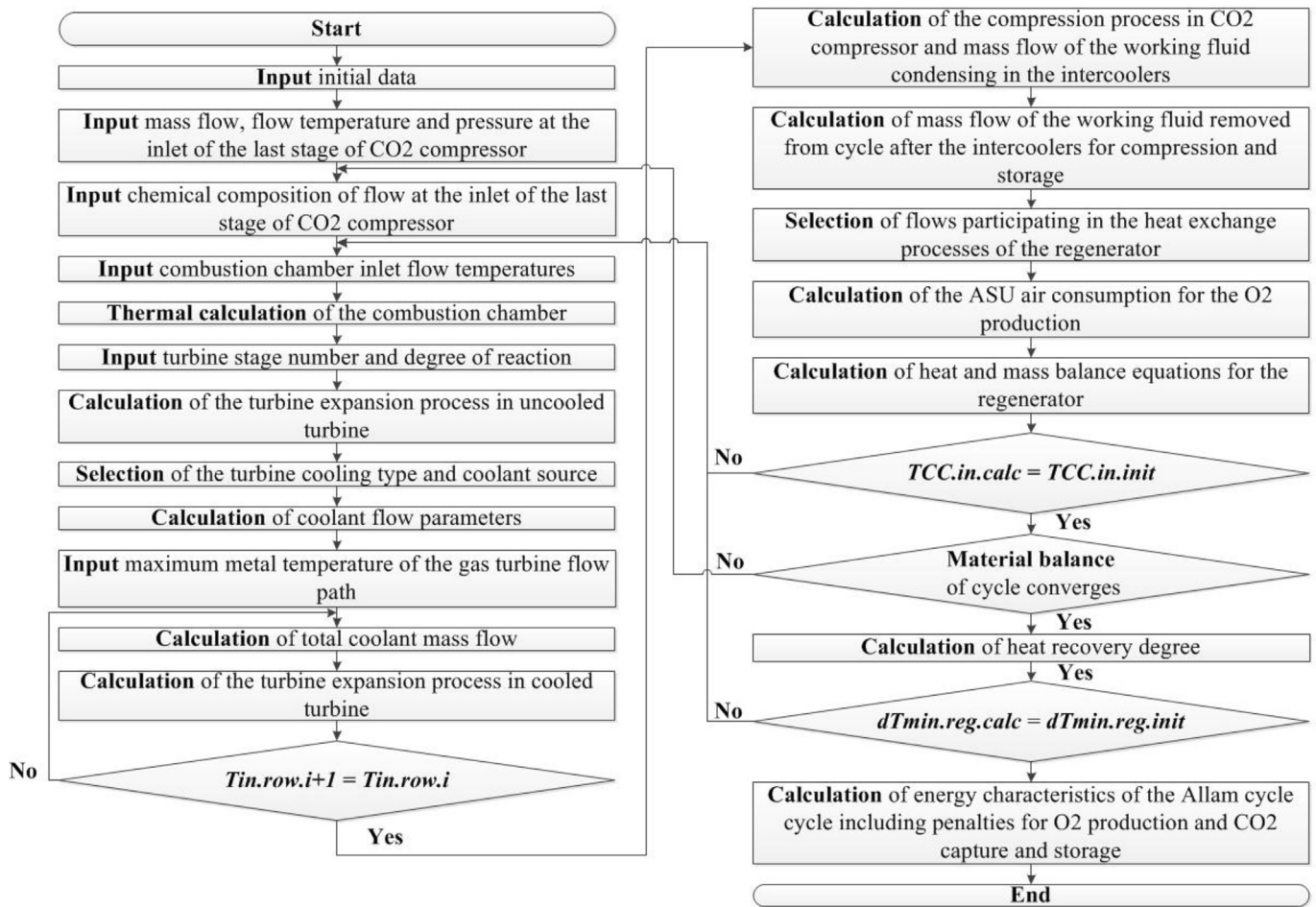


Fig. 5. Calculation algorithm.

significantly affect the cycle efficiency. An excessive increase of the turbine inlet temperature leads to an increase of the turbine exhaust temperature (the main hot flow entering the regenerator) and the position of the pinch point in the regenerator changes, which results in an increase of the cold source losses. Moreover, an increase in the turbine inlet temperature leads to an increase in the turbine cooling losses. Therefore, the optimal turbine inlet temperature at a fixed turbine inlet pressure for the Allam cycle could be observed.

The results of studies of the turbine outlet pressure influence on cycle efficiency are shown in Fig. 6b. The maximum net efficiency is achieved for the turbine outlet pressure of 30 bar. The turbine inlet temperature of 1083 °C and the turbine outlet pressure of 300 bar were fixed during the optimization of the turbine outlet pressure. A decrease in the turbine outlet pressure from 3 MPa to 0.1 MPa leads to a decrease in the cycle net efficiency by 6.3%.

The reason for the existence of the optimal turbine inlet and outlet pressures are the redistribution of turbomachines' heat drops and heat losses in the regenerator.

Optimal turbine inlet parameters for the maximum net efficiency of the Allam cycle operated on natural gas are presented in Table 2.

An important feature of the Allam cycle is the presence of the optimum coolant temperature. According to the simulation results, the maximum cycle net efficiency is achieved for a coolant temperature of 200 °C. Despite the fact that a decrease of a coolant temperature below 200 °C is accompanied by a decrease in the

required coolant mass flow (Fig. 7a) and turbine cooling losses, the amount of heat utilized in the regenerator decreases (Fig. 7b) and the cold source losses increases.

An influence of turbomachines flow path efficiency on the Allam cycle efficiency illustrated in Fig. 8 shows that an increase of turbine polytropic efficiency by 1% is accompanied by an increase of the cycle net efficiency by 0.28–0.43% and an increase of compressor polytropic efficiency by 1% is accompanied by an increase of the cycle net efficiency by 0.09–0.12%.

Such a small influence of the compressor flow path perfection on the Allam cycle net efficiency is because the final increase of the working fluid pressure is carried out in the pumps, which polytropic efficiency was remained unchanged in the research.

The following parameters based on the thermodynamic optimization of the Allam cycle were chosen for the design of supercritical carbon dioxide gas turbine: $T_0 = 1083$ °C, $P_0 = 300$ bar, $P_{out} = 30$ bar, turbine polytropic efficiency = 90%.

3.2. Design features of supercritical turbines for high-power energy units

The aims of a preliminary turbine design are:

- Design method selection of the flow path.
- Definition of the turbine stages' main parameters (specific work, diameter, the degree of reaction, etc.).
- Definition of the number of stages.

Table 1
Input data for the Allam cycle simulation.

Parameter	Unit	Value
Ambient temperature, pressure and humidity	°C/bar/%	15/1.013/60
Fuel low calorific value (89% CH ₄ , 7% C ₂ H ₆ , 1% C ₃ H ₈ , 0.1% C ₄ H ₁₀ , 0.01% C ₅ H ₁₂ , 2% CO ₂ , 0.89% N ₂)	kJ/kg	46502
Fuel temperature and pressure	°C/bar	15/7
Multi-stage intercooled compressor exit pressure	bar	80
CO ₂ pressure before storage	bar	100
Fluid temperature at coolers exit or cycle minimal temperature	°C	30
Regenerator hot and cold flows minimal temperature difference (in the pinch point)	°C	5
Underheating in condensers	°C	5
Turbine, compressors and pumps specific polytropic efficiency	%	90
Compressors and pumps mechanical efficiency	%	97.5
Turbine and power generator mechanical efficiency	%	99
Power generator electric efficiency	%	98.5
Specific power spent on O ₂ production	kW/(kg/s)	900
Oxygen purity	%	91.25

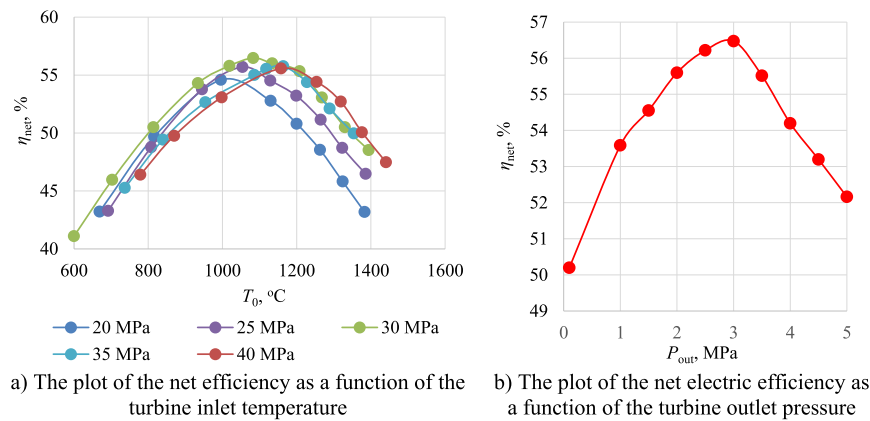


Fig. 6. The thermodynamic optimization results of turbine inlet and outlet parameters.

Table 2
Optimal turbine inlet parameters.

Parameter	Unit	Value
Turbine inlet temperature	°C	996 1054 1083 1164 1158
Turbine inlet pressure	MPa	20 25 30 35 40
Cycle net efficiency	%	54,6 55,7 56,5 55,8 55,8
Coolant flow fraction	%	3,9 6,6 7,7 11,4 10,5

It is expedient to choose the turbine design presented in (Allam et al., 2017) for a power plant with a capacity of 50 MW as a prototype. Despite the fact that the turbine is not a serial one and is designed for gaining experience of implementation of the Allam cycle, some technical solutions are quite suitable for high-power units. For example, a single shell design decreases aerodynamic

losses due to the reduction of axial dimensions of the turbine. This technical solution is taken from gas turbines. However, there is a difference in the number of stages: it does not exceed four to five for the existing gas turbines but in the Allam cycle the number of stages increases due to the large isentropic work.

A preliminary assessment of the isentropic work of a supercritical CO₂ gas turbine shows that it equals 610.1 kJ/kg with predefined initial and final steam parameters, which is comparable to existing gas turbines. With a working fluid mass flow of 600 kg/s and a predefined turbine efficiency of 90%, the turbine power will be about 335 MW. The operating parameters for the developed turbine are presented in Table 3.

Following the recommendations in (Bogard and Thole, 2006), the convective cooling of the blades and rotor of the designed turbine was chosen, which is acceptable at today's material

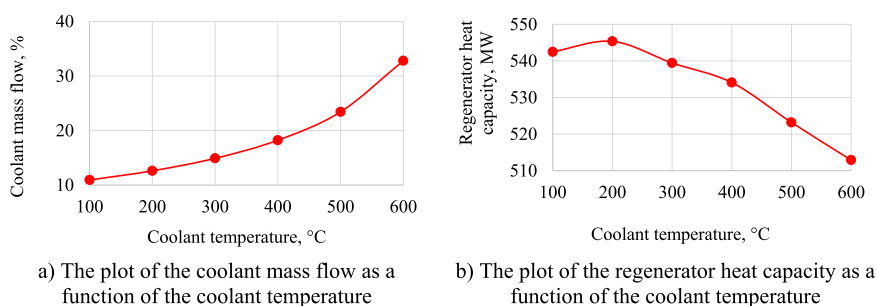


Fig. 7. An influence of the coolant temperature on cycle parameters.

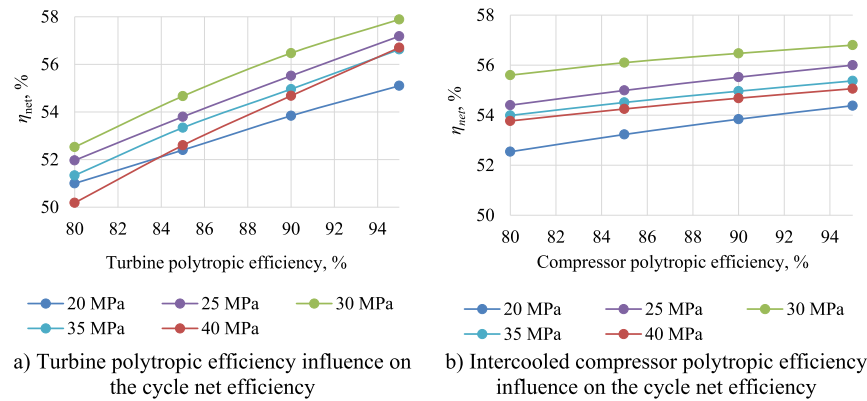


Fig. 8. An influence of polytropic efficiency of turbomachines on cycle net efficiency.

development level for gas turbines and at initial temperatures of up to 1200 °C. The closed cooling system allows ignoring the coolant consumption when designing the flow path. A similar technical solution is proposed in (Allam et al., 2017).

The main feature of the designed turbine is the low specific volume of working fluid at the turbine inlet: about 0.01 m³/kg. Even with a large CO₂ mass flow of 600 kg/s, there is a relatively low volume flow through the first stages. This requires the use of low-profile blades. However, the use of blades with a height of less than 15–17 mm for the first stage would increase the blade tip losses in turbine cascades and reduce stage efficiency.

This problem can be solved by reducing the root diameter d_{root} . At the same time, the velocity ratio U/c_s will be much less than optimal with a constant stage specific work. In this case, in order to maintain the stage efficiency, it is possible to reduce its specific work, which in turn will lead to an increase in the number of turbine stages.

At the beginning of turbine design, it is important to choose the variant of its flow path, as it affects the further design method. It is advisable to develop the supercritical CO₂ gas turbine using mainly the method for steam turbines by selecting a flow path with a constant root diameter due to the low cost of the rotor discs and the possibility of using the “sample stage” method at their design period, when the highest stage is made, and all the others are obtained by their peripheral trimming, as a result of which it is possible to keep the same blade root for all stages.

Thus, it is advisable to develop the supercritical CO₂ gas turbine design using mainly the method for steam turbines by selecting the first variant of a flow path with a constant root diameter.

3.3. The development of supercritical CO₂ turbine

The preliminary flow path design method with a constant root diameter consists of the steps of determining the first, last and intermediate stages' geometric parameters.

Table 3
Operating parameters of the supercritical CO₂ gas turbine.

Parameter	Unit	Value
Turbine power	MW	335
Working fluid mass flow	kg/s	600
Turbine inlet pressure/temperature	MPa/°C	30/1083
Turbine outlet pressure/temperature	MPa/°C	3/689
Turbine isentropic work	kJ/kg	610.1
Turbine rotational speed	rpm	3000
Turbine length	m	6
Turbine height	m	2.8
Turbine casing length	m	3.55
Turbine mass	ton	96

The parameter that determines the stage efficiency and its mean diameter is the velocity ratio U/c_s . For reaction stages, the optimum velocity ratio is defined as follows:

$$(U/c_s)_{opt} \approx \varphi \cdot \cos \alpha_1 / (2 \cdot (1 - \rho) 0.5) \quad (1)$$

where φ represents the velocity coefficient of the nozzle cascade; α_1 represents the outlet angle of working fluid flow from the nozzle cascade channels in the absolute coordinate system; ρ represents the degree of stage reaction.

It should be noted that increasing the degree of stage reaction has a positive effect on the operation of the turbine stage. Usually, in modern steam turbines, the degree of reaction for mean diameter is 5–10% (in active stages) up to 40–50% (in reaction stages). In gas turbines, the reaction stages of 20–25% are usually used.

The choice of the degree of stage reaction ρ and the velocity ratio U/c_s is a difficult technical and economic task. On the one hand, an increase in the degree of reaction leads to an improvement of aerodynamic efficiency due to an increase in the narrowing flow in blade cascade, which is especially important for long blades of the last stages. On the other hand, according to (1), an increase in the degree of stage reaction is accompanied by a decrease in the optimal specific work and by an increase in the number of turbine stages, or by an increase in tip speed due to the stage diameter growth and a height reduction of the first blades. Moreover, an increase in the degree of stage reaction leads to an increase in the peripheral steam leakage.

At the same time, an increase in the degree of stage reaction leads to an increase of axial force on the turbine bearing. In steam turbines, an axial force is traditionally reduced by the implementation of the balancing holes in rotor disks. However, it causes steam leakage, which reduces the stage efficiency. In gas turbines, an axial force is partially compensated by a back-directed axial force on the compressor rotor.

To unload the turbine bearings, it is advisable to use balance pistons in the design of a turbine rotor to compensate a turbine axial force in the Allam cycle while preserving the high efficiency of a single-flow turbine.

Thus, with the specified design features of a single-flow supercritical CO₂ gas turbine in conditions of small volume flow in the first stages and limited axial dimensions, the reaction $\rho = 25\%$ and the velocity ratio $U/c_s = 0.4$ turned out to be optimal.

Despite the fact that the optimal velocity ratio estimated by (1) is $(U/c_s)_{opt} = 0.55$ with the degree of reaction $\rho = 25\%$, the reduction of the assumed velocity ratio down to 0.4 significantly decreases the stage number, thereby fulfilling the restrictions of the limited axial dimensions of the turbine. It should be noted that this solution

is used in the design of gas turbines, where the stage number is usually limited to four to five. At the first iteration, these parameters are the same for all stages.

When determining the dimensions of the first stage, variant calculations are made for different specific work per stage. During this process, the main characteristics of stages (blade length, mean and root diameters, specific work) are determined, as well as the number of the turbine stages $n = z$ is preliminarily estimated.

For the designed supercritical CO₂ gas turbine, seven stages ($n = 7$) were chosen according to the turbine prototype of lower power, but with the same specific work (Allam et al., 2017). A greater number of stages is not advisable because of limited axial dimensions of the turbine.

The last stage dimensions and its specific work are estimated based on the variant calculation with different values of its mean diameter:

$$d^z_{\text{mean}} = \alpha \cdot d^1_{\text{mean}} \quad (2)$$

where d^1_{mean} represents the mean diameter of the first stage, m ; d^z_{mean} represents the mean diameter of the last stage, m ; α represents nondimensional coefficient, ranged from 1 to 1.3.

The characteristics of the intermediate stages are determined by the interpolation method (Fig. 9).

Taking into account the heat recovery coefficient, when determining the characteristics of the intermediate stages at the first iteration, causes an unbalance of the sum of all specific work in the stages relative to the turbine isentropic work H_0 . In this case, it is necessary to change the number of turbine stages ($n = m$) and redefine the characteristics of the intermediate stages, or correct the specific work H_{0i} with the same number of stages z , followed by reassessing the characteristics of the stages at the next iteration. In this work, unbalance was eliminated by recalculating the characteristics of the stages without changing their number $n = z$.

The design of supercritical CO₂ gas turbine of 335 MW power for the Allam cycle is presented in Fig. 10. The turbine length is 6 m, height – no more than 3 m. Single flow, double casing construction was proposed to reduce the pressure drop on the casing wall. The first four turbine stages operating at maximum pressures and temperatures are located directly in the inner casing. The diaphragms of the fifth, sixth and seventh stages are installed in the cage, which connected with the outer casing. Such a solution allows the hydraulic connection of space between inner and outer casing with the compartment behind the fourth stage of the turbine.

When the fourth stage outlet pressure is 13 MPa, the maximum pressure drop on the wall of the inner casing is 17 MPa. Strength calculations of the inner casing using a simple cylindrical model show that the maximum wall thickness in the area of the first stage is not more than 200 mm. The reduced thickness of the inner casing made of Cr–Ni alloys decreases its mass, cost and improves the maneuverability of the turbine.

The rotor has a one-piece design of the shaft and turbine disks. The workpiece size is determined by the turbine root diameter (895 mm) and the required tolerance for metalworking.

In the front part of the turbine on the rotor is a crest of the thrust bearing and a slot for the support bearing. The front seals compensating for the axial force and the partial unloading of the thrust bearing are located on the balance piston. The rear part of the rotor also contains a slot for the support bearing and grooves for the labyrinth seals. To organize the cooling of the rotor the shaft is provided with a cavity into which the coolant enters.

The main characteristics obtained as a result of the flow path design of the 335 MW supercritical CO₂ gas turbine are presented in Table 4.

The resulting mean diameters of the stages provide quite an

acceptable cross-sectional dimensions of the designed turbine. The most interesting fact is the results estimating the lengths of the turbine first blades. In the context of low volume fluid flow rate with a large specific work, it was possible to obtain acceptable lengths of the first stage blades (vane – 34 mm, blade – 37 mm) without using the partial stage scheme, which is most often used in steam turbines. This can lead to a high internal efficiency of the turbine flow path.

Further research will focus on the design of the remaining key elements of the Allam cycle: an oxy-fuel combustion chamber operating at ultra-high pressures and a multi-throated regenerator operating at significant pressure and temperature differences.

3.4. Economic feasibility of the oxy-fuel, supercritical CO₂ Allam cycle

Despite the high thermodynamic efficiency of the Allam cycle and the almost complete absence of emissions, the large-scale implementation of such facilities requires economic feasibility, which in turn, depends on cycle specific investment cost including the price for the carbon capture and storage system (CCS). The results of the evaluation of the main performance characteristics for the different cycle operated on the natural gas are presented in Table 5.

Despite the fact that the Allam cycle has 500 °C lower turbine inlet temperature, its net efficiency is comparable with the state-of-the-art combined cycle power plants (CCPP) without CCS due to the presence of multithroated high-temperature regenerator utilizing heat from the both gas turbine exhaust and hot air from the ASU, and intercooling during the compression of the working fluid. Efficiency penalties related to the CCS for the Allam cycle are 20–30 times lower than for the CCPP due to both thermodynamic principles of CO₂ separation and a higher level of the minimum cycle pressure.

The lowest value of the specific amount of CO₂ removed from the cycle could be observed for the CCPP without CCS in consequence of highest net efficiency among all the cycles. However, the specific amount of CO₂ emitted from the CCPP to the atmosphere is 80–90 times higher than for the Allam cycle due to the absence of CCS.

To estimate total specific investment costs for a fossil fuel power plant with near-zero emissions, the specific investment costs for carbon storage system was evaluated with the assumption that the power plant of 100 MW net power is designed for 30 years of operation (6000 h per year) and CO₂ will be stored in artificial storage at 100 bar. The results of calculation presented in Table 5 show that the specific investment costs for a carbon storage system for the Allam cycle will be equal to \$307.5/kW, which is 5.5% lower than for CCPP due to a lower volume of the carbon storage. The total specific investment costs including the price of CCS for the Allam cycle is \$1307.5/kW, which is cheaper by 85% compare to CCPP with CCS, and 25% more expensive than CCPP without CCS.

4. Conclusions

Overall, it appears that the Allam cycle is one of the most promising technologies for the electricity generation with low emissions releases in the air due to high efficiency and competitive specific cost of installed capacity meeting the requirements of sustainable development. The mass of the produced CO₂ emissions for the Allam cycle is twelve times lower than for combined cycle with post-combustion carbon capture.

A unique calculation algorithm allowing estimate the main thermodynamic parameters and performance characteristics of the Allam cycle considering the efficiency penalty for turbine cooling

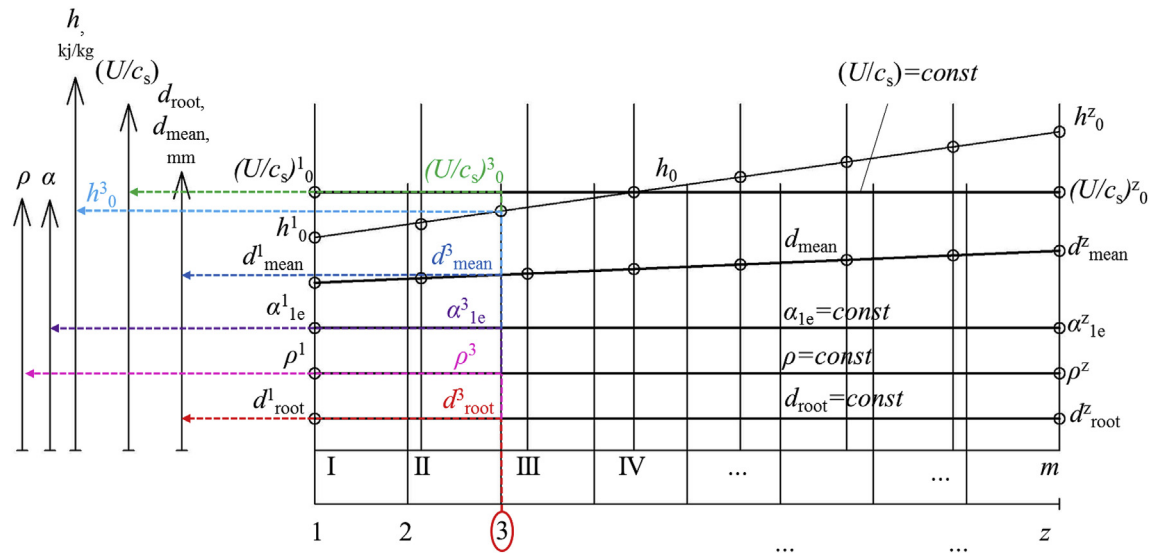


Fig. 9. Defining characteristics of intermediate stages.

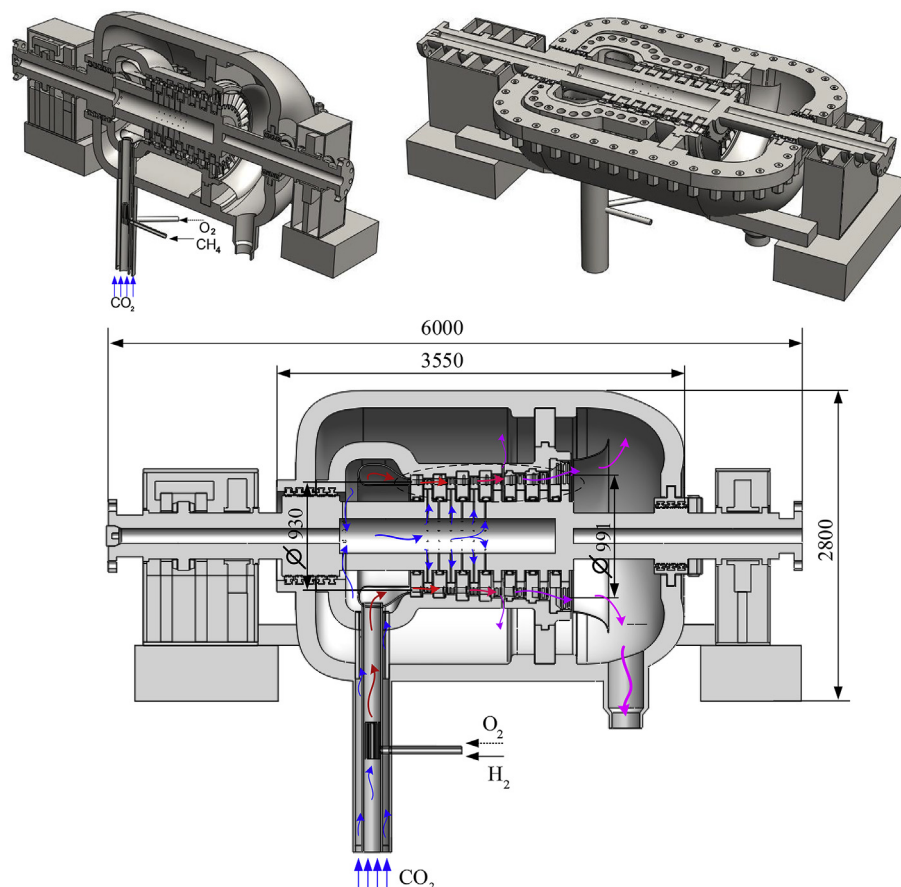


Fig. 10. Design of 335 MW supercritical CO₂ gas turbine.

and fixation of the temperature difference at the pinch point of the regenerator was developed. To estimate the working fluid thermodynamic properties for the oxy-fuel combustion cycles it is

recommended to use the NIST REFPROP database. The average deviation of the CO₂ specific volume definition using the database from experimental data is equal to 0.03%. The technical and

Table 4The results of the flow path design of a 335 MW supercritical CO₂ gas turbine.

Stage	$d_{\text{mean},i}^i$, m	H_{i0}^i , kJ/kg	$(U/c_s)_i$	$\alpha_{1e,i}^i$, °	$\rho_{\text{mean},i}^i$, m	l_1^i , mm	P_{per}^i , mm	P_{root}^i , mm	l_2^i , mm
1	0.9294	78.20	0.4	12	0.25	34.0	2	1	37.0
2	0.9397	85.45	0.4	12	0.25	44.3	2	1	47.3
3	0.9499	87.33	0.4	12	0.25	54.6	2	1	57.6
4	0.9602	89.23	0.4	12	0.25	64.8	3	2	69.8
5	0.9705	91.15	0.4	12	0.25	75.1	3	2	80.1
6	0.9807	93.08	0.4	12	0.25	85.4	3	2	90.4
7	0.991	94.81	0.4	12	0.25	170.9	4	3	177.9

Note: ρ_{mean}^i – degree of stage reaction at the mean diameter; l_1^i – output height of the nozzle cascade; P_{per}^i – peripheral lap; P_{root}^i – root lap; l_2^i – output height of working cascade; i – stage number.

Table 5

Efficiency, environmental and economic characteristics comparison for cycles operated on the natural gas.

Cycle	Allam cycle	CCPP with CCS	CCPP without CCS
Turbine inlet temperature, °C	1083	1600	1600
Turbine inlet pressure, bar	300	25–35	25–35
Turbine outlet pressure, bar	30	1	1
Net efficiency (including penalties for the oxygen production and carbon capture and storage), %	56.5	46–48	58–60
Net efficiency decrease due to the carbon capture and storage at 100 bar, %	0.4	9–12	0
Net efficiency decrease due to the oxygen production and compression, %	7.2	0	0
CO ₂ capture rate, %	98.9	89	0
Specific amount of CO ₂ removed from the cycle, kg/kWh	0.3431	0.4127	0.3287
Specific amount of CO ₂ captured from the cycle, kg/kWh	0.3393	0.3673	0
Specific amount of CO ₂ emitted from the cycle to the atmosphere, kg/kWh	0.0038	0.045	0.3287
Specific investment costs (without carbon storage system), \$/kW	1000	2100	900–1100
The volume of carbon storage at 100 bar for the 100 MW power plant operating 6000 h per year for 30 years, m ³	$13.5 \cdot 10^6$	$14.6 \cdot 10^6$	0
Specific investment costs for carbon storage system, \$/kW	307.5	324.3	0
Total specific investment costs (with carbon storage system), \$/kW	1307.5	2424.3	900–1100

financial reasons determine the ASU type for the Allam cycle as the cryogenic high pressure two-stage. To minimize the power consumption of the air separation unit and compressor for CO₂ storage, an oxygen purity should be not higher than 90–91%.

According to the results of thermodynamic optimization, the optimal turbine inlet parameters for the NET Power oxy-combustion cycle are 1083 °C and 300 bar, optimal turbine outlet pressure is 30 bar and optimal coolant temperature – 200 °C. An increase of turbine polytropic efficiency by 1% is accompanied by an increase of the Allam cycle net efficiency by 0.28–0.43% and an increase of compressor polytropic efficiency – by 0.09–0.12%.

Single flow, double casing construction was proposed for the developed supercritical CO₂ gas turbine of 335 MW power. Flow path with a constant root diameter is recommended. Under the conditions of limited axial dimensions when the combustion chamber and the gas turbine are interconnected, the number of stages of the supercritical CO₂ gas turbine was chosen equal to seven. It is then expedient to choose the degree of stage reaction ρ and the velocity ratio U/c_s by the type of gas turbines: $\rho = 20$ –25% and $U/c_s = 0.35$ –0.45.

The results of efficiency, environmental and economic characteristics comparison for cycles operated on the natural gas showed high perspectives of the Allam cycle compare to CCPP with CCS. Particularly, a specific amount of CO₂ emitted from the cycle to the atmosphere for the Allam cycle is equal to 0.0038 kg/kWh and the specific amount of CO₂ captured from the cycle is equal to 0.3393 kg/kWh.

The total specific investment costs including the price of CCS are equal to \$1307.5/kW for the Allam cycle and \$2424.3/kW for the CCPP with CCS. Such a big difference is caused by the fact that the cost of CO₂ capture technology for CCPP is about 50% of the total cost. In turn, the principle of CO₂ separation in the Allam cycle is thermodynamic and does not require significant costs. Moreover,

the specific investment costs for a carbon storage system for the Allam cycle is 5.5% cheaper than for the CCPP with CCS due to lower volume of carbon storage.

Acknowledgements

This work was supported by the Russian Science Foundation under Agreement No. 17-79-20371 dated July 28, 2017.

References

- Allam, R., Martin, S., Forrest, B., Fetvedt, J., Lu, X., Freed, D., Brown, G.W.J., Sasaki, T., Itoh, M., Manning, J., 2017. Demonstration of the Allam Cycle: an update on the development status of a high efficiency supercritical carbon dioxide power process employing full carbon capture. *Energy Procedia* 114, 5948–5966. <https://doi.org/10.1016/j.egypro.2017.03.1731>.
- Allam, R.J., Palmer, M.R., Brown, G.W.J., Fetvedt, J., Freed, D., Nomoto, H., Itoh, M., Okita, N., Jones, C.J., 2013. High efficiency and low cost of electricity generation from fossil fuels while eliminating atmospheric emissions, including carbon dioxide. *Energy Procedia* 37, 1135–1149. <https://doi.org/10.1016/j.egypro.2013.05.211>.
- Ari, I., Sari, R., 2017. Differentiation of developed and developing countries for the Paris agreement. *Energy Strateg. Rev.* 18, 175–182. <https://doi.org/10.1016/j.esr.2017.09.016>.
- Barba, F.C., Sanchez, G.M.-D., Segui, B.S., Darabkhani, H.G., Anthony, E.J., 2016. A technical evaluation, performance analysis and risk assessment of multiple novel oxy-turbine power cycles with complete CO₂ capture. *J. Clean. Prod.* 133, 971–985. <https://doi.org/10.1016/j.jclepro.2016.05.189>.
- Best, T., Finney, K.N., Ingham, D.B., Pourkashanian, M., 2018. CO₂-enhanced and humidified operation of a micro-gas turbine for carbon capture. *J. Clean. Prod.* 176, 370–381. <https://doi.org/10.1016/j.jclepro.2017.12.062>.
- Bogard, D.G., Thole, K.A., 2006. Gas turbine film cooling. *J. Propuls. Power* 22 (2), 249–270. <https://doi.org/10.2514/1.18034>.
- Gkoutas, A.A., Stamatelos, A.M., Kalfas, A.I., 2017. Recuperators investigation for high temperature supercritical carbon dioxide power generation cycles. *Appl. Therm. Eng.* 125, 1094–1102. <https://doi.org/10.1016/j.applthermaleng.2017.07.092>.
- González-Salazar, M.A., 2015. Recent developments in carbon dioxide capture technologies for gas turbine power generation. *Int. J. Greenh. Gas. Con.* 34, 106–116. <https://doi.org/10.1016/j.ijggc.2014.12.007>.

- Inozemtsev, A.A., Nihamkin, M.A., Sandratskii, V.L., 2008. The Design Fundamentals of Aircraft Engines and Power Plants. Mech. Eng., Moscow, p. 365.
- International Energy Agency, 2015. Oxy-Combustion Turbine Power Plants, 2015/05. IEA Environmental Projects Ltd., Cheltenham.
- Kemp, I.C., 2011. Pinch Analysis and Process Integration: a User Guide on Process Integration for the Efficient Use of Energy. Elsevier.
- Konova, O., Komarov, I., Lisin, E., 2012. The relevance of power generating capacities based on the combined cycle power plants of high power. Czech J. Soc. Sci. Bus. Econ. 1 (1), 101–109. <https://doi.org/10.24984/cjsbe.2012.1.1.11>.
- Lisin, E., Lebedev, I., Sukhareva, E., Komarov, I., 2014. Analysis of scenario of structural and technological modernization of the power industry in the context of competitive electricity markets. Int. Econ. Lett. 3 (3), 105–114. <https://doi.org/10.24984/iel.2014.3.3.3>.
- Liu, X., Bae, J., 2018. Urbanization and industrialization impact of CO2 emissions in China. J. Clean. Prod. 172, 178–186. <https://doi.org/10.1016/j.jclepro.2017.10.156>.
- Mallapragada, D.S., Reyes-Bastida, E., Roberto, F., McElroy, E.M., Veskov, D., Laurenzi, I.J., 2018. Life cycle greenhouse gas emissions and freshwater consumption of liquefied Marcellus shale gas used for international power generation. J. Clean. Prod. 205, 672–680. <https://doi.org/10.1016/j.jclepro.2018.09.111>.
- Moroz, L., Frolov, B., Burlaka, M., Guriev, O., 2014. Turbomachinery flowpath design and performance analysis for supercritical CO2. In: Proceeding of ASME Turbo Expo 2014: Turbine Technical Conference and Exposition, GT2vols. 014–25385. V02BT45A004. <http://doi:10.1115/GT2014-25385>.
- Nejat, P., Jomehzadeh, F., Taheri, M.M., Gohari, M., Majid, M.Z.A., 2015. A global review of energy consumption, CO2 emissions and policy in the residential sector (with an overview of the top ten CO2 emitting countries). Renew. Sustain. Energy Rev. 43, 843–862. <https://doi.org/10.1016/j.rser.2014.11.066>.
- OECD, 2012. OECD Environmental Outlook to 2050: the Consequences of Inaction. OECD Publishing, Paris. <https://doi.org/10.1787/9789264122246-en>.
- Padilla, R.V., Too, Y.C.S., Benito, R., McNaughton, R., Stein, W., 2016. Thermodynamic feasibility of alternative supercritical CO2 Brayton cycles integrated with an ejector. Appl. Energy 169, 49–62. <https://doi.org/10.1016/j.apenergy.2016.02.029>.
- Petrescu, L., Bonalumi, D., Valenti, G., Cormos, A.M., Cormos, C.C., 2017. Life Cycle Assessment for supercritical pulverized coal power plants with post-combustion carbon capture and storage. J. Clean. Prod. 157, 10–21. <https://doi.org/10.1016/j.jclepro.2017.03.225>.
- Rogalev, A., Komarov, I., Kindra, V., Zlyvko, O., 2018. Entrepreneurial assessment of sustainable development technologies for power energy sector. Entrep. Sustain. Issues 6 (1), 429–445. [http://doi.org/10.9770/jesi.2018.6.1\(26\)](http://doi.org/10.9770/jesi.2018.6.1(26)).
- Rogalev, N., Prokhorov, V., Rogalev, A., Komarov, I., Kindra, V., 2016. Steam boilers' constructive solutions for the ultra-supercritical power plants. Int. J. Appl. Eng. Res. 11 (18), 9297–9306.
- Scaccabarozzi, R., Gatti, M., Martelli, E., 2016. Thermodynamic analysis and numerical optimization of the NET Power oxy-combustion cycle. Appl. Energy 178, 505–526. <https://doi.org/10.1016/j.apenergy.2016.06.060>.
- Schmitt, J., Willis, R., Amos, D., Kapat, J., Custer, C., 2014. Study of a supercritical CO2 turbine with TIT of 1350 K for Brayton cycle with 100 MW class output: aerodynamic analysis of stage 1 vane. In: Proceeding of ASME Turbo Expo 2014: Turbine Technical Conference and Exposition, GT2vols. 014–27214. V03BT36A019. <http://doi:10.1115/GT2014-25385>.
- Shi, B., Xu, W., Wu, E., Wu, W., Kuo, P.C., 2018. Novel design of integrated gasification combined cycle (IGCC) power plants with CO2 capture. J. Clean. Prod. 195 (11), 176–186. <https://doi.org/10.1016/j.jclepro.2018.05.152>.
- Smith, S.J., Wigley, T.M.L., 2000. Global warming potentials: 2. accuracy. Clim. Change 44 (4), 459–469. <https://doi.org/10.1023/A:1005537014987>.
- Span, R., Wagner, W., 1996. A new equation of state for carbon dioxide covering the fluid region from the triple-point temperature to 1100 K at pressures up to 800 MPa. J. Phys. Chem. Ref. Data 25 (6), 1509–1596. <https://doi.org/10.1063/1.555991>.
- Thorbergsson, E., Grönstedt, T., 2016. A thermodynamic analysis of two competing mid-sized oxyfuel combustion combined cycles. J. Energy 2016, 2438431. <http://doi.org/10.1155/2016/2438431>.
- Vargaftik, N.B., 1972. Handbook of Thermophysical Properties of Gases and Liquids. Nauka, Moscow, p. 721.
- Wang, G., Wu, C., Wang, J., Chen, J., Li, Z., 2018. Scenario analysis of emissions structure under climate change in China. J. Clean. Prod. 203, 708–717. <https://doi.org/10.1016/j.jclepro.2018.08.045>.
- Wilcock, R.C., Young, J.B., Horlock, J.H., 2005. The effect of turbine blade cooling on the cycle efficiency of gas turbine power cycles. J. Eng. Gas Turbines Power 127 (1), 109–120. <https://doi.org/10.1115/1.1805549>.
- Zaryankin, A., Rogalev, A., Kindra, V., Khudyakova, V., Bychkov, N., 2017b. Reduction methods of secondary flow losses in stator blades numerical and experimental study. In: Proceedings of 12th European Conference on Turbomachinery Fluid Dynamics and Thermodynamics, ETC2vols. 017–158, pp. 3–7. https://doi.org/10.29008/ETC12_7c_ISSN:2410-4833.
- Zaryankin, A., Rogalev, A., Komarov, I., Kindra, V., Osipov, S., 2017a. The boundary layer separation from streamlined surfaces and new ways of its prevention in diffusers. In: Proceedings of 12th European Conference on Turbomachinery Fluid Dynamics and Thermodynamics, pp. ETC2017–E2168. <https://DOI:10.29008/ETC2017-168>.
- Zaryankin, A., Rogalev, A., Komarov, I., Kindra, V., Osipov, S., 2015. Multi-tier steam turbines. Prospects and particularities. Part 1: overview of two-tier lowpressure turbines. Contemp. Eng. Sci. 8 (22), 1021–1037. <https://doi.org/10.12988/ces2015.58234>.
- Zaryankin, A.E., Garanin, I.V., Grigoriev, E.Y., Kindra, V.O., Khudyakova, V.P., 2016. CFD assessment of aerodynamic efficiency improvement methods for steam turbine exhaust hood. Int. J. Appl. Eng. Res. 11 (21), 10648–10654.
- Zhao, Y., Chi, J., Zhang, S., Xiao, Y., 2017. Thermodynamic study of an improved MATIANT cycle with stream split and recompression. Appl. Therm. Eng. 125, 452–469. <https://doi.org/10.1016/j.applthermaleng.2017.05.023>.

Advanced Zero Emissions Gas Turbine Power Plant

Timothy Griffin

ALSTOM Power Technology Center,
CH-5405 Dättwil/Baden, Switzerland

Sven Gunnar Sundkvist

Demag Delaval Industrial Turbomachinery AB,
SE-612 83 Finspong, Sweden

Knut Åsen

Tor Bruun

Norsk Hydro Oil & Energy Research Center,
N-3960 Porsgrunn, Norway

The AZEP "advanced zero emissions power plant" project addresses the development of a novel "zero emissions," gas turbine-based, power generation process to reduce local and global CO₂ emissions in the most cost-effective way. Process calculations indicate that the AZEP concept will result only in a loss of about 4% points in efficiency including the pressurization of CO₂ to 100 bar, as compared to approximately 10% loss using conventional tail-end CO₂ capture methods. Additionally, the concept allows the use of air-based gas turbine equipment and, thus, eliminates the need for expensive development of new turbomachinery. The key to achieving these targets is the development of an integrated MCM-reactor in which (a) O₂ is separated from air by use of a mixed-conductive membrane (MCM), (b) combustion of natural gas occurs in an N₂-free environment, and (c) the heat of combustion is transferred to the oxygen-depleted air by a high temperature heat exchanger. This MCM-reactor replaces the combustion chamber in a standard gas turbine power plant. The cost of removing CO₂ from the combustion exhaust gas is significantly reduced, since this contains only CO₂ and water vapor. The initial project phase is focused on the research and development of the major components of the MCM-reactor (air separation membrane, combustor, and high temperature heat exchanger), the combination of these components into an integrated reactor, and subsequent scale-up for future integration in a gas turbine. Within the AZEP process combustion is carried out in a nearly stoichiometric natural gas/O₂ mixture heavily diluted in CO₂ and water vapor. The influence of this high exhaust gas dilution on the stability of natural gas combustion has been investigated, using lean-premix combustion technologies. Experiments have been performed both at atmospheric and high pressures (up to 15 bar), simulating the conditions found in the AZEP process. Preliminary tests have been performed on MCM modules under simulated gas turbine conditions. Additionally, preliminary reactor designs, incorporating MCM, heat exchanger, and combustor, have been made, based on the results of initial component testing. Techno-economic process calculations have been performed indicating the advantages of the AZEP process as compared to other proposed CO₂-free gas turbine processes. [DOI: 10.1115/1.1806837]

The AZEP Concept

The AZEP concept (see Ref. [1]) is shown in Fig. 1. The combustor in an ordinary gas turbine is here replaced by the MCM-reactor, which includes a combustor, an air preheater, a membrane section (mixed conducting membrane, MCM), and a high temperature heat exchanger section (see [2]). As shown in the figure, air is compressed in a conventional gas turbine compressor. Typically air can be extracted from the compressor at 20 bar and 450 °C. A major part, about 90%, of the extracted compressed air is preheated to about 900–1100 °C in the lower section of the MCM-reactor. The reason for this high preheating temperature is to reduce the membrane area.

The transport of oxygen through the membrane is increasing with increasing temperature. However, in order to avoid significant degradation of the membrane there is also an upper temperature limit, which is material dependent. In the membrane section 40%–50% of the oxygen in the air stream is transported through the dense MCM.

The membrane is made from materials with both ionic and electronic conductivity (see Fig. 2). An oxygen partial pressure difference causes oxygen ions to be transported through the membrane by means of a diffusive process. Simultaneously the electrons flow from the permeate side back to the retentate side of the membrane.

Oxygen is picked up by means of a circulating sweep gas containing mainly CO₂ and H₂O (see [3]). The concentration of oxygen in the combustor inlet is about 10%. The natural gas is typically provided at pressures of 25 to 35 bar and the temperature in the combustor may be over 1200 °C. About 90% of the hot combusted gas then enters the high temperature heat exchanger section in the MCM-reactor in countercurrent flow to the air stream. The air stream then can be heated to above 1200 °C. About 10% of the combusted gas is bled off and heat is recovered by heating a minor part (10%) of the compressed air.

Hot compressed air then enters the turbine to generate electrical power. Waste heat in both the oxygen-depleted air stream and the CO₂ containing bleed gas stream is recovered by generating steam at different pressure levels. The steam is utilized in steam turbines for power generation. The CO₂ containing bleed gas is further cooled to condense water. CO₂ is recovered at about 20 bar and is then compressed to final pressure. Main features of the AZEP process are

- efficiency reduction of about 4% points after CO₂ removal,
- 100% capture of CO₂,
- no NO_x emissions, and
- predicted 30%–50% CO₂ removal cost reduction compared with conventional tail-end CO₂ capture methods (see [4]).

The AZEP Project

A joint feasibility study on the AZEP concept was first performed by Norsk Hydro, Norway, the original inventor of the concept, and the gas turbine manufacturer ABB ALSTOM Power Sweden AB (today Demag Delaval Industrial Turbomachinery AB). As this study showed a high potential of the technology, not

Contributed by the International Gas Turbine Institute (IGTI) of THE AMERICAN SOCIETY OF MECHANICAL ENGINEERS for publication in the ASME JOURNAL OF ENGINEERING FOR GAS TURBINES AND POWER. Paper presented at the International Gas Turbine and Aeroengine Congress and Exhibition, Atlanta, GA, June 16–19, 2003, Paper No. 2003-GT-38426. Manuscript received by IGTI, October 2002, final revision, March 2003. Associate Editor: H. R. Simmons.

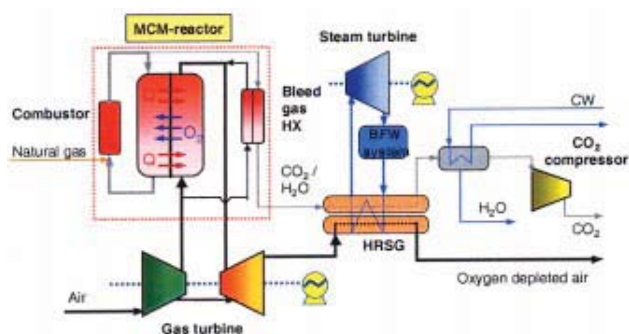


Fig. 1 AZEP process flow sheet

only on performance like gas turbine efficiency and CO₂ capture, but also indicated a much lower CO₂ avoidance cost compared to alternative technologies (see [5]), it was decided to develop this technology in a consortium by inviting other partners with complementing skills.

The project is characterized by a vertically integrated industrial involvement supplemented by well-established academic partners essential for this novel and important development. Ten partners from six European countries (see website www.azep.org) represent a combination of expertise covering all necessary skills (development of materials, ceramic manufacturing methods, high temperature heat exchanger, combustion technology for AZEP gas mixtures, gas turbine and power plant technology, and techno-economic and environmental analysis).

A modular approach has been adopted for the work such that know-how is developed within individual work packages, which deliver components, designs, and process data to the project (see Fig. 3). The on-going first three-year phase (started December 2001) primarily focuses on research and development of the MCM-reactor upon its constituent units, the combination of these components into an integrated reactor, and its subsequent scale-up for future integration in a gas turbine. After the components have been identified and manufactured, they will be integrated into a complete MCM-reactor design, and subsequently tested at simulated gas turbine conditions to verify overall functionality.

In order to develop the optimum AZEP with an integrated MCM-reactor, process simulation and economic evaluation is being continuously performed. The resulting data will be used to define benchmarks (e.g., cost of electricity, net present value). Market potential for AZEP plants will be identified considering the growing CO₂ market for oil and gas recovery as well as emerging financial measures to curb CO₂ emissions, including CO₂ trading.

Project cost for phase 1 is M€ 9.3 with funding by EC (M€ 3.4) and the Swiss government (M€ 1.5).

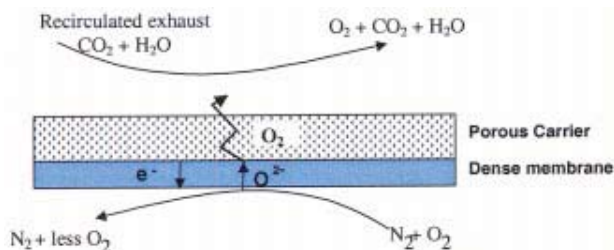


Fig. 2 Schematic drawing of MCM membrane, with oxygen swept from the permeate side of the membrane by recirculated exhaust gas

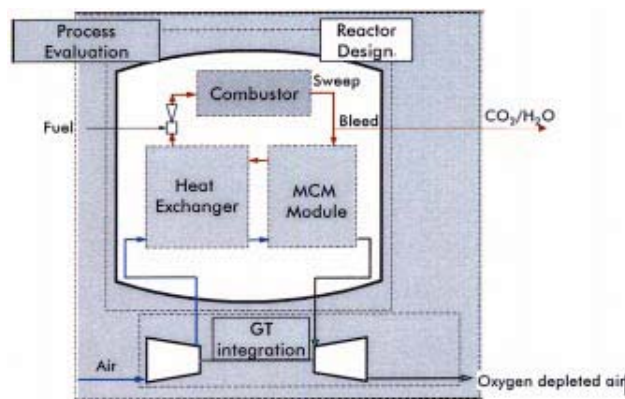


Fig. 3 AZEP project work packages

Technical Challenges

The technical challenges within the project are associated with the following areas:

- combustion of natural gas in highly diluted exhaust gas streams at low temperature (<1300 °C) and with little excess oxygen present,
- the air separation membrane and its stable operation within the gas turbine system (target >30,000 h),
- a heat exchanger stable at high temperatures (>1200 °C) and in the presence of steam and carbon dioxide,
- high temperature (>1100 °C) sealing between ceramic elements,
- achieving highest surface to volume ratios within ceramic components for the required oxygen and heat transport rates,
- integration of the MCM-reactor in the gas turbine system, and
- start-up philosophy and gas turbine trips.

The project is focusing its main efforts on addressing these challenges, and the present paper will discuss progress in some of these areas.

The MCM Reactor

The MCM-reactor is comprised of three main integrated process units: oxygen transporting membrane (MCM), low and high temperature heat exchangers, and a combustion section (see Figs. 3 and 4). Compressed low temperature air (at 20 bar, 450°C) from the gas turbine compressor enters the reactor through a transition duct leading to the inlet openings of the low temperature heat exchanger. This heat exchanger increases the temperature level above 800 °C, so that air may enter into the MCM section and “give off” oxygen to the recirculated exhaust gas stream. From the MCM section the air enters the high temperature heat exchanger where its temperature is raised to a value close to the hot

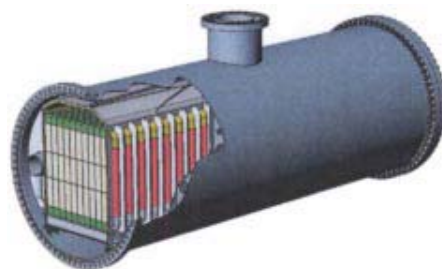


Fig. 4 MCM reactor showing the ceramic monolithic structure

exhaust gas temperature from the combustor ($>1200^{\circ}\text{C}$). From the high temperature section the now hot and oxygen-depleted air is led out of the reactor to the power-generating turbine.

Both the MCM and the heat exchangers are based on ceramic monolith structures (honeycombs) with high surface-to-volume ratio and low pressure drop. Exhaust gas from the combustion chamber flows counter-currently to the airflow, heating up air and picking up and transporting oxygen to the combustion section. The oxygen is transported through the ceramic walls of the MCM monolith structure. Materials are identified for the MCM and heat exchanger and have been demonstrated at laboratory scale and AZEP conditions.

Modeling has been performed to determine the optimal configuration of these process units, and to determine their boundary conditions. The pressures and mass flows of air and oxygen to the combustion cycle are set by the overall turbine process. By utilizing ceramic monolith structures for both heat transport and oxygen transport these operations can be performed in an integrated monolith stack.

A monolith structure with given channel width and wall thickness has a fixed specific surface to volume ratio (m^2/m^3) available for heat and mass (oxygen) transfer. The required total volume of the monolith structures can then be calculated. In principle the ratio between length and width can be chosen freely. However, in order to maintain laminar flow and avoid excessive pressure losses, the free flow area must be above a certain value.

In current design the total height of the monolithic stack is ca. 2 m, and the design is based on standard sized monoliths (with side length of ca. 15×15 cm). Internal channels sizes are in the range of 1–2 mm, giving surface to volume ratios in the range $500\text{--}1000 \text{ m}^2/\text{m}^3$. This unit or standard sized system has a thermal load between 50 and 100 kW (corresponding to an energy density of $1\text{--}2 \text{ MW}/\text{m}^3$). Based on such a modular system any size of capacity can be performed by simply increasing the number of standard ceramic monolith stacks. Thus the heat and oxygen transfer capacity is adjusted to fit the gas turbine system capacity by simply adjusting the number of standard sized monolithic stacks. This acts to increase the length of reactor (see [6]).

For comparison also plate and pipe solutions that have a similarity with SOFC design solutions have been evaluated together with honeycomb structures. Our membrane/heat exchanger structures differ from SOFC solutions in that electric circuit connectors are not necessary. The reason is that the membrane material transfers both oxygen ions and electrons internally and therefore is electrically neutral. This makes it possible to use ceramic monolithic structures. As honeycomb structures have both low pressure drop and high surface-to-volume ratios, the chosen design is based on monolithic structures both for the MCM membrane and the heat exchangers.

Combustion Methodology

The working fluid in the AZEP process consists of extremely diluted fuel/oxidant mixtures (e.g., 5% CH_4 , 10% O_2 , 28% CO_2 , 57% H_2O , by volume). Since the exhaust gas is formed by stoichiometric methane combustion the molar ratio of H_2O and CO_2 is always 2:1. The reactivity of such mixtures in existing lean, premix burners and catalytic combustors is lower than those of standard CH_4/air mixtures at similar temperatures in the following ways:

- Ignition delay times are nearly an order of magnitude higher (based on CHEMKIN calculations).
- Residence times for complete burn out of CO and UHCs are higher.
- Flame speeds are lower.

On the positive side, there is very limited nitrogen within the gas (associated with the natural gas), and thus NO_x formation is not an issue.

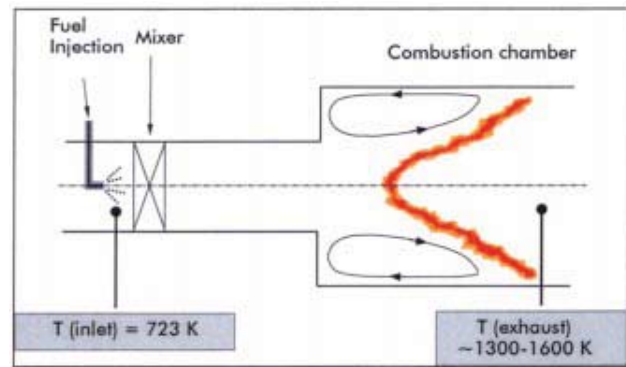


Fig. 5 Backward-facing step combustion stabilization

The situation is exacerbated by the fact that the overall temperature of the combustion products must be relatively low (e.g., 1200°C). The low temperatures are dictated by the fact that the membrane materials are limited in their thermal stability. This signifies that current combustion methods may have to be considerably modified/developed.

Currently available burning methods are swirl-stabilized, diffusion burners, lean premixed burners, and catalytic burners. However, these on their own are not optimized for the AZEP processes. Traditional, vortex stabilized combustion methods, utilizing turbulent recirculation zones for flame stability may not be relevant to this process due to the low pressure drops and low velocities present.

In the present paper initial results on the combustion of AZEP mixtures at high-pressure conditions in a lab-scale combustion chamber will be discussed. (Previous results on AZEP combustion at atmospheric pressure may be found in [7]). In this experiment the combustion was stabilized by vortex regions formed after a sudden expansion of the inlet gases as shown in Fig. 5. The backward-facing step expansion, in a cylindrical configuration, was from 25 to 75 mm diameter.

Experiments were performed at a given inlet temperature and velocity. The gas was ignited and the fuel concentration was gradually reduced until the flame became unstable and the CO emissions rapidly increased. When the flame started to pulsate and unburned hydrocarbons started to be emitted the “lean blow out” (LBO) limit was recorded. The results of the testing are given in Fig. 6 in terms of the lean blow out limit as a function of the combustion pressure. Experiments were performed for both air and an AZEP mixture ($\text{O}_2 + \text{exhaust gas}$).

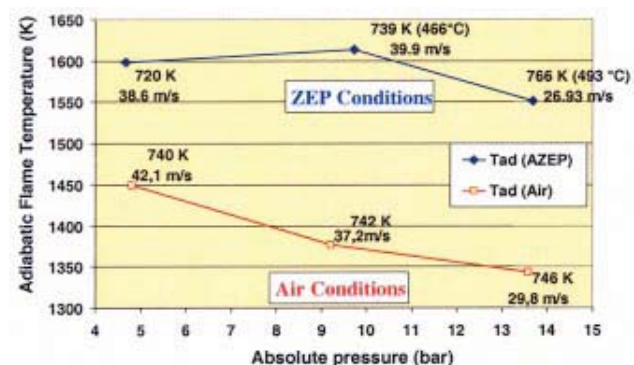


Fig. 6 Lean blowout limit of combustion for methane in both an air and AZEP ($\text{O}_2 + \text{exhaust gas}$ environment. (The inlet temperature and velocity of each data point are indicated.)

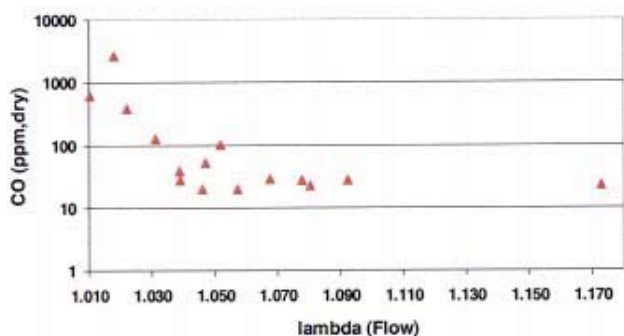


Fig. 7 CO emissions as a function of the excess oxidant ratio of combustion. The data were taken at flame temperatures between 1700 and 1800 K.

As expected, the high levels of CO_2 and H_2O inhibit combustion, leading to an increase in the LBO of more than 150 K, as compared to the results obtained with air. Although the LBO decreases with increasing pressure, it is still at 1550 K (1277 °C) at a pressure of 14 bar, above the goal temperature of 1200 °C.

A further challenge associated with AZEP combustion is related to the complete burnout of the combustion intermediate CO. Figure 7 shows the CO emissions as a function of the lambda value (excess oxidant ratio of combustion). As seen, even at high flame temperatures, where flame stability is not an issue, an excess amount of oxygen is necessary to ensure that the CO will be fully converted to carbon dioxide. This is undesired since it would add to the cost and size of the required membranes.

Another option for flame stabilization is catalytic combustion, proposed to have advantages to homogeneous gas phase combustion for standard gas turbine systems with air as the oxidant. With catalytic combustion it is possible to obtain complete and stable combustion at much lower temperatures, allowing extremely lean fuel combustion outside the flammability limits of homogeneous reactions. More detailed description of the basics of catalytic combustion can be found in [8–12]. In the next phase of the project various catalytic combustion concepts will be evaluated regarding their application in the current AZEP process.

Integration in the Gas Turbine System

The AZEP gas turbine set and its auxiliary systems consist mainly of standard equipment with one exception: as mentioned the conventional combustion chamber in a standard gas turbine will be replaced by the MCM-reactor. Necessary turbine modifications are therefore essentially concentrated to the integration of the MCM-reactor to the gas turbine system, which substantially reduces technical and commercial risks.

Gas Turbine Selection. Several criteria have been put up for the selection of the gas turbine in AZEP:

- It must be a high performance, modern gas turbine with high turbine inlet temperature and potential for higher pressure ratio that can also form the basis for larger machine developments in the future.
- Its design should have a potential for retrofitting existing gas turbine systems with AZEP gas turbine systems in the future.
- Space must be available for a transition duct to the MCM-reactor.
- The start-up procedure for an AZEP gas turbine system must not be too complicated.

After evaluation of three alternative gas turbines the 43 MW (simple cycle) one-shaft gas turbine GTX100 has been selected as

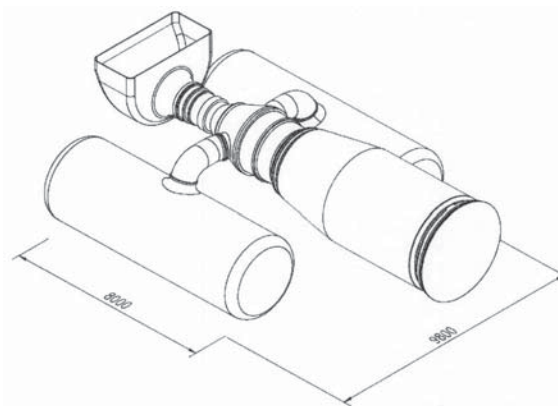


Fig. 8 Gas turbine GTX100 in the middle modified for AZEP with one MCM reactor on each side

the best alternative for a future AZEP gas turbine system. It meets the above-mentioned criteria and it also has the following properties:

- The GTX100 is less complicated and safer to redesign than the other evaluated alternatives.
- A single shaft turbine facilitates the start-up of the AZEP gas turbine system.
- The gas turbine combustor has a double wall for convection cooling, which is the method that will be used in the AZEP-turbine, and this makes it easier to integrate the MCM-reactor to the gas turbine.

Transition Ducts Between Gas Turbine and MCM-Reactor.

Due to the size of the MCM membrane and the heat transfer areas preliminary design has been made for two transition ducts between the gas turbine and two parallel MCM-reactors (see Fig. 8). The chosen principle for the transition duct is to use coaxial ducts with hot gas (depleted air) from the reactor in the inner duct cooled by the air from the compressor in the annulus between the ducts.

A non-insulated inner duct for the hot air (ca 1250 °C) air is proposed, which will allow a fairly simple design of the transition duct. In combination with thermal coating on the inside of the hot duct the maximum temperature of the wall material will be around 800 °C. With chosen design and a short length of the transition duct the temperature loss on the hot side can be kept around 16 °C and the heat expansion can be kept low.

Start-Up Philosophy. At start-up the ceramic core structure is heated up from ambient condition with an external heat source in such a way that temperature gradients are within acceptable limits. The gas turbine is speeded up from stand still with a starting motor. This must be done so that the outlet temperature of the gas turbine compressor matches the cool side of the sweep gas. The pressure difference between compressor outlet and sweep gas side must be controlled but is not critical since the membrane walls can withstand considerable pressure differences. When the temperature in the membrane core is sufficient to start the oxygen transport, fuel is fed to the combustion zone. Heat from the combustion is then transferred to the oxygen depleted air and the turbine inlet temperature increases. The starting motor power can then be reduced. Temperature and oxygen transport to the reactor core is thereafter increased until normal running conditions are achieved.

To facilitate start-up a by-pass duct will connect the cold air side with the turbine inlet. With a valve on the by-pass duct and a valve on the cold air transition duct to the reactor it is possible to gradually control the gas turbine almost as fast as burners at the ordinary gas turbine are controlled (see [13]). With this strategy

the outlet of the MCM-reactor will be kept at constant high temperature after the initial heating of the core irrespective of the load. The inlet temperature of the core will follow the outlet temperature of the compressor.

Transient calculations have been made to simulate the reactor temperature propagation at start-up. These calculations indicate a start-up time comparable with an ordinary GTCC start-up time. The challenge is here to avoid overheating and inhomogeneous temperature distributions in the ceramic structures in the MCM-reactor.

Gas Turbine Trips. The proposed valve arrangement will also make it possible to bypass the reactor at gas turbine trips. However, the pressure cannot be allowed to change too rapidly for reasons related to the mechanical integrity of the MCM-reactor. During shorter stops the temperature profile of the core can be maintained with the help of a small airflow through the core and a corresponding small amount of external firing. Controlling the mixing of heated and unheated air will then control the temperature at the turbine inlet.

Summary

The paper describes AZEP, a membrane based concept, to sequester CO_2 from gas turbine-based power generation processes. Results of the on-going EU funded development project are presented. The MCM-reactor, which replaces the combustion chamber in an ordinary gas turbine, is described together with its integrated components: the oxygen selective MCM membrane and the heat exchangers (all built on a monolithic ceramic structure) and the combustor. Alternative combustion methods for the extremely diluted fuel/oxidant mixtures in AZEP (e.g., 5% CH_4 , 10% O_2 , 28% CO_2 , 57% H_2O) are investigated and results of lean blow out (LBO) limit and CO emissions are shown. Integration of the MCM-reactor (via transition ducts) to the selected gas turbine GTX100 for AZEP is described and start-up philosophy is given for the AZEP gas turbine system.

Acknowledgments

The AZEP project is partly funded by the European Commission in FP5, Contract No. ENK5-CT-2001-00514, and the Swiss Government.

References

- [1] Linder, U., Eriksen, E. H., and Åsen, K. I., 2000, "A Method for Operating a Combustion Plant and a Combustion Plant," SE Patent Application 0002037.
- [2] Bruun, T., Werswick, B., Grönstad, L., Kristiansen, K., and Linder, U., 2000, "A Device and a Method for Operating Said Device," NO Patent Application 20006690.
- [3] Åsen, K. I., and Julsrud, S., 1997, "Method for Performing Catalytic or Non-Catalytic Processes, Wherein Oxygen is One of the Reactants," NO Patent Application 19972630.
- [4] Bill, A., Span, R., Griffin, T., Kelsall, G., and Sundkvist, S. G., 2001, "Technology Options for Zero Emissions' Gas Turbine Power Generation," *International Conference Power Generation and Sustainable Development*, Liège, Belgium, 8–9 October.
- [5] Hellberg, A. et al., 1999, "Zero Emission Power Plant—Process Selection," Internal Report ABB ALSTOM Power, RT T10 57/99, July.
- [6] Bruun, T., Werswick, B., Grönstad, L., and Kristiansen, K., 2001, "Method and Apparatus for Feeding and Output of Two Gases to a Monolithic Structure," NO Patent Application 20015134.
- [7] Reinke, M., Carroni, R., Winkler, D., and Griffin, T., 2002, "Experimental Investigation of Natural Gas Combustion in Oxygen/Exhaust Gas Mixtures for Zero Emissions Power Generation," *Proceedings of 6th International Conference on Technologies and Combustion for a Clean Environment*, Porto, July 2001. (to appear in *International Journal on Environmental Combustion Technologies*, 2002).
- [8] Kesselring, J. P., 1986, "Catalytic Combustion," in *Advanced Combustion Methods*, edited by F. J. Weinberg, Academic, London, pp. 237–275.
- [9] Trimm, D. L., 1985, "Catalytic Combustion (Review)," *Appl. Catal.*, **7**, pp. 249–282.
- [10] Pfefferle, L. D., and Pfefferle, W. C., 1987, "Catalysis in Combustion," *Catal. Rev. - Sci. Eng.*, **29**(2&3), pp. 219–267.
- [11] Griffin, T., and Scherer, V., 1995, "Katalytisch unterstützte Verbrennung in Gasturbinen: Potentiale und Grenzen," *VGB Kraftwerkstechnik*, **75**, Heft 5, pp. 421–426.
- [12] Appel, C., Mantzaras, I., Scharen, R., Bombach, R., and Inauen, A., 2001, "Catalytic Combustion of H_2 /Air Mixtures Over Platinum," *accepted Sixth International Conference on Technologies and Combustion for a Clean Environment*, 9–12 July, Porto, Portugal.
- [13] Hamrin, S., 2003, "Styrning av Gasturbin Med MCM-Reaktor," SE Patent Application 0300131-0.

Proposal and Analysis of a Novel Zero CO₂ Emission Cycle With Liquid Natural Gas Cryogenic Exergy Utilization

Na Zhang

Institute of Engineering Thermophysics,
Chinese Academy of Sciences,
Beijing 100080, P. R. China
e-mail: zhangna@mail.etp.ac.cn

Noam Lior

Department of Mechanical Engineering and
Applied Mechanics,
University of Pennsylvania,
Philadelphia, PA 19104-6315

A novel liquefied natural gas (LNG) fueled power plant is proposed, which has virtually zero CO₂ and other emissions and a high efficiency. Natural gas is fired in highly enriched oxygen and recycled CO₂ flue gas. The plant operates in a quasi-combined cycle mode with a supercritical CO₂ Rankine type cycle and a CO₂ Brayton cycle, interconnected by the heat transfer process in the recuperation system. By coupling with the LNG evaporation system as the cycle cold sink, the cycle condensation process can be achieved at a temperature much lower than ambient, and high-pressure liquid CO₂ ready for disposal can be withdrawn from the cycle without consuming additional power. Good use of the coldness exergy and internal exergy recovery produced a net energy and exergy efficiencies of a base-case cycle over 65% and 50%, respectively, which can be increased up to 68% and 54% when reheat is used. Cycle variants incorporating reheat, intercooling, and reheat+intercooling, as well as no use of LNG coldness, are also defined and analyzed for comparison. The approximate heat transfer area needed for the different cycle variants is also computed. Besides electricity and condensed CO₂, the byproducts of the plant are H₂O, liquid N₂ and Ar. [DOI: 10.1115/1.2031228]

Introduction

Liquefied natural gas (LNG) is regarded as a relatively clean energy resource. During the process of its preparation, approximately 500 kWh energy per ton LNG is consumed for compression and refrigeration and a considerable portion of this invested exergy is preserved in the LNG [1], which has a final temperature of about 110 K, much lower than that of the ambient or of seawater. The liquefaction reduces its volume 600 fold, and thus makes long distance transportation convenient.

LNG is loaded into insulated tankers and transported to receiving terminals, where it is off loaded and first pumped to certain pressure, and then revaporized and heated, by contact with seawater or with ambient air, to approximately ambient temperature for pipeline transmission to the consumers. It is thus possible to withdraw cryogenic exergy from the LNG evaporation process which otherwise will be wasted by seawater heating. This can be achieved with a properly designed thermal power cycle using the LNG evaporator as the cold sink [1–13].

Use of the cryogenic exergy of LNG for power generation includes methods which use the LNG as the working fluid in natural gas direct expansion cycles, or its coldness as the heat sink in closed-loop Rankine cycles [1–5], Brayton cycles [6–9], and combinations thereof [10,11]. Other methods use the LNG coldness to improve the performance of conventional thermal power cycles. For example, LNG vaporization can be integrated with gas turbine inlet air cooling [5,12] or steam turbine condenser system (by cooling the recycled water [11]), etc. Some pilot plants have been established in Japan from the 1970s, combining closed-loop Rankine cycles (with pure or mixture organic working fluids) and direct expansion cycles [1].

Increasing concern about greenhouse effects on climatic change prompted a significant growth in research and practice of CO₂

emission mitigation in recent years. The technologies available for CO₂ capture in power plants are mainly physical and chemical absorption, cryogenic fractionation, and membrane separation. The amount of energy needed for CO₂ capture could lead to the reduction of power generation efficiency by up to 10 percentage points [14,15].

Besides the efforts for reduction of CO₂ emissions from existing power plants, concepts of power plants with zero CO₂ emission were proposed and studied. Particular attention has been paid to the research of trans-critical CO₂ cycle with fuel burning in highly enriched oxygen (99.5%+) and recycled CO₂ from the flue gas [16–25]. The common features of these cycles are the use of CO₂ as the working fluid and O₂ as the fuel oxidizer, produced by an air separation unit. With CO₂ condensation at a pressure of 60–70 bar (temperature 20–30 °C), efficiencies of 0.35–0.49 were reported for plants based on such cycles, despite the additional power use for O₂ production and CO₂ condensation. Staicovici [26] proposed an improvement to these cycles by coupling with a thermal absorption technology to lower the CO₂ condensation below ambient temperature (30 bar, 5.5 °C), and estimated a net power efficiency of 54%.

In a proposal by Velautham et al. [13], an LNG evaporation system is included in a gas-steam combined power plant just for captured CO₂ liquefaction and for air separation to provide oxygen for gas combustion. Deng et al. [9] proposed a gas turbine cycle with nitrogen as its main working fluid. The stoichiometric amount of air needed for the combustion is introduced at the compressor inlet, and mixed with the nitrogen. The turbine exhaust contains mainly nitrogen, combustion generated CO₂, and H₂O. With the cycle exothermic process being integrated with the LNG evaporation process, CO₂ and H₂O are separated from the mainstream by change of their phase, from gas to solid and liquid states, respectively, and the extra nitrogen is discharged. The main merit of this cycle is the absence of the air separation unit, but the combustion product may contain NO_x as well, and the collection and removal of solidified CO₂ may be difficult.

In this paper, a novel zero emission CO₂ capture system is

Contributed by the International Gas Turbine Institute of ASME for publication in the JOURNAL OF ENGINEERING FOR GAS TURBINES AND POWER. Manuscript received November 13, 2003; final revision received May 20, 2004. Associate Editor: R. F. Boehm.

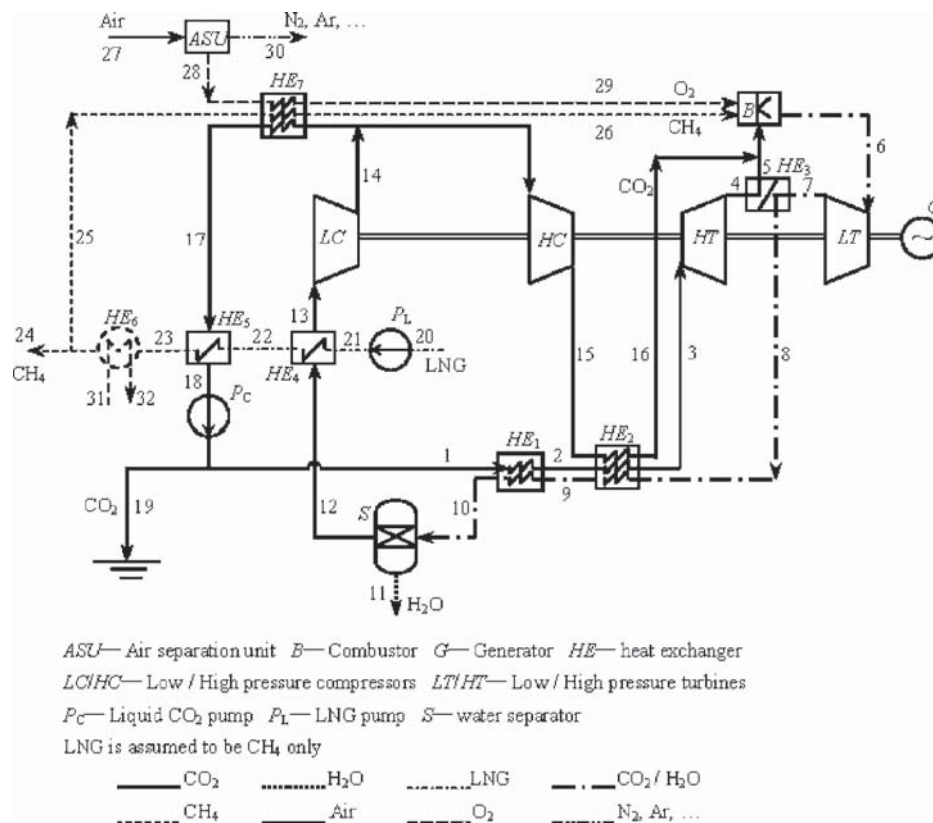


Fig. 1 CO₂ cycle flow sheet

proposed and thermodynamically modeled. The plant is operated by a CO₂ quasi-combined two-stage turbine cycle with methane burning in an oxygen and recycled-CO₂ mixture. Compared to the previous works, two new features are developed in this study: The first is the integration with LNG evaporation process. As a result, the CO₂ condensation and cycle heat sink are at temperatures much lower than ambient. The second one is the thermal cross-integration of the CO₂ Rankine-type cycle and Brayton cycle inside the recuperation system, so the heat transfer related irreversibility could be reduced to improve the global plant efficiency. Our cycle has both high power generation efficiency and extremely low environmental impact. Further, variations of the cycle which incorporate intercooling, reheat, and both, as well as comparison to a similar cycle which does not use LNG coldness, are also described and analyzed.

The Cycle Configuration

The base-case cycle layout and the corresponding t - s diagram are shown in Figs. 1 and 2, respectively. Variations on this cycle are described and analyzed further below. It follows the well-established general principle of a topping Brayton cycle (working fluid here is CO₂/H₂O; TIT=1300 °C), with heat recovery in a bottoming supercritical CO₂ Rankine cycle (TIT=624 °C; a similar idea was first proposed by Angelino [2] in an organic Rankine cycle with CF₄ as its working fluid), but here with some sharing of the working fluids, to take best advantage of the properties of available hardware for these cycles and of good exergy management in the cycles and heat exchangers. The fuel is a small fraction of the evaporated LNG, and the combustion oxidizer is pure oxygen produced in a conventional cryogenic vapor compression air separation plant. The system produces power, evaporates the LNG for further use while preventing more than 50% of the LNG exergy from going to waste during its evaporation, and produces

liquefied CO₂ and water as the combustion products and liquid nitrogen and argon as the air separation products.

The topping Brayton cycle can be identified as 12→13→14→15→16→6→7→8→9→10→12. The bottoming Rankine cycle is 18→1→2→3→4→5→...→14→17→18. The LNG evaporation process is 20→21→22→23→24 and 25. The air separation process is 27→28 and 30. The process material products are liquid CO₂ (19), water (11), nitrogen and argon (30), and gaseous methane (24).

The Brayton cycle uses its exhaust gas heat to preheat its working fluid (CO₂) before entrance to the combustor (B), by (HE)₂,

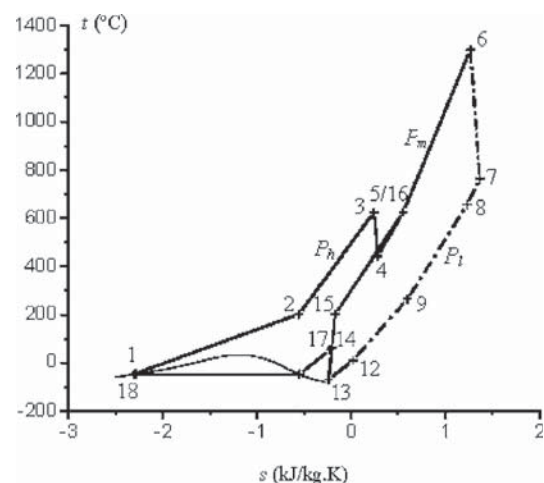


Fig. 2 t - s diagram for CO₂ cycle

Table 1 Main assumptions for the calculation

Cycle parameter	High pressure P_h^a [bar]	150
	Intermediate pressure P_m [bar]	30
	Low pressure P_l [bar]	1
	CO ₂ condensation pressure [bar]	6.5
	CO ₂ condensation temperature [°C]	−48.8
	Lowest temperature t_{13} [°C]	−70
	Mass flow rate ratio of Brayton cycle R_g [%]	30
Turbine	Methane LHV H_u [kJ/kg]	50,010
	LT Inlet temperature t_6 [°C]	1,300
	Isentropic efficiency [%]	88
Compressor	Pressure ratio	30.6
	Isentropic efficiency [%]	88
Combustor	Efficiency [%]	100
	Pressure loss [%]	3
Recuperation system	Water separator working temperature [°C]	10
	Heat exchangers Pressure loss [%]	2
ASU	Specific work for O ₂ production at 30.6 bar and 15°C [kJ/kg O ₂]	900
	LNG pump efficiency [%]	77
LNG vaporization system	Pressure loss [%]	3
	Evaporation pressure [bar]	30.6
	Delivery temperature [°C]	15

^aThe highest pressure of the cycle is $P_1=156$ bar, 6 bar is for pressure losses in the heat exchangers.

and then to evaporate the working fluid (CO₂) for the Rankine cycle by HE₁, the three-pass HE₂, and HE₃. The exhaust gas is then cooled further, by heating the LNG in HE₄, before compression by compressors LC and HC (this cooling reduces the compression work). The first compressor, LC, is used then to compress the working fluid to a pressure that would allow its condensation (in HE₅, the triple point of CO₂ is 5.18 bar and −56.6 °C), and some of the working fluid is withdrawn and first used to preheat combustion methane and oxygen in HE₇, and then condensed in HE₅. The remainder of the working fluid is compressed further in HC to the top pressure of the Brayton cycle, and then passed through the preheater HE₂ and combustor (B) before passing into the Brayton cycle turbine (LT). Assuming stoichiometric combustion, the exhaust gas of the Brayton cycle contains the combustion products CO₂ and H₂O through the path 6→7→8→9→10 only, with the H₂O separated from the CO₂ by condensation and withdrawal in S. A minute amount of CO₂ may be released along with water; but it is assumed here that the water and carbon dioxide are fully separated to simplify the calculation.

In the Rankine cycle, the Brayton cycle recuperators HE₁ and HE₂ serve as the 2-stage boiler of the working fluid (CO₂), HE₇ is a pre-condenser cooler and HE₅ is the condenser using the LNG as coolant, and P_C is the pump to raise the liquid CO₂ pressure to the top value of the Rankine cycle, and for the withdrawal of the excess liquid CO₂ for sequestration (at 19). The Rankine cycle turbine (HT) exhaust is preheated by the Brayton cycle exhaust recuperator HE₃ before being brought as additional working fluid into the combustor (B).

The air separator unit (ASU) is assumed here to produce oxygen for the combustor (B) at the combustor pressure. Liquid O₂ is pumped within the ASU to the combustor pressure by a cryogenic pump, and its cryogenic exergy is regenerated within the ASU (as in [26]). The O₂ (28) and fuel (25) are preheated in HE₇ before entering the combustor B. Further analysis is under way to explore the integration of the air separation process into the cycle, thus taking advantage of the coldness of its products.

LNG off loaded from its storage (20) is first pumped by pump P_L to its evaporation pressure (21), and then heated in the evaporation system (HE₄ (22) and HE₅ (23)) to near-ambient temperature. If the natural gas temperature at point 23 remains below that desired for distribution, the remaining coldness can be used for air conditioning or some other purposes in HE₆. A small portion (typically ~4%) of the natural gas (25) is preheated in HE₇ first and then sent to the combustor as fuel, and the remainder is sent

out to customers via pipeline. It is assumed in this paper that LNG is pure methane. It is noteworthy that both the thermal energy required for evaporation and the power that can be produced with the cryogenic cycle depend strongly on the LNG evaporation pressure. Different delivery pressures are typically made available at the receiving terminals: Supercritical (typically 70 bar) for long distance pipeline network supply, and subcritical (typically 30 bar) for local distribution and power stations based on heavy-duty combined cycles [10]. In this paper, only the subcritical natural gas evaporation process (30 bar) is considered, and the influence of different evaporation parameters will be investigated in forthcoming studies.

The placement of the heat exchangers in the cycle, and the choice of temperatures were made to reduce heat transfer irreversibilities. Furthermore, a combination of the higher-pressure (higher heat capacity) but lower mass flow rate fluid on the Rankine cycle side of the recuperators, with the lower-pressure (lower heat capacity) but higher mass flow rate fluid on the Brayton cycle side is also intended for reduction of irreversibilities.

The Cycle Performance

The simulations were carried out using the commercial Aspen Plus [27] code. To simplify computation, it was assumed that the system operates at steady state, the natural gas is pure methane, the combustion is stoichiometric with CO₂ and H₂O the only combustion products, no turbine blade cooling, and the stoichiometric amount of the water evacuated from the cycle does not contain dissolved CO₂. Besides, the outlet temperatures of the cold streams from HE₂ and HE₃ are set to be the same, i.e., $t_3 = t_{16} = t_5$, since the calculation results suggest a worse efficiency for $t_3 < t_{16} = t_5$. The most relevant assumptions for the calculations in this paper are summarized in Table 1.

The cycle minimal temperature is chosen as −70 °C to avoid gas condensation, since the saturated temperature of CO₂ under ambient pressure (1 bar) is −78.4 °C.

The energy efficiency is calculated as the ratio between overall power output and heat input in the topping cycle [11]:

$$\eta_1 = W_{\text{net}} / (m_f \cdot H_u) \quad (1)$$

where W_{net} is the overall power output from the turbines, reduced by the power input to the compressors (LC and HC) and pumps (P_C, P_L), m_f is the fuel mass flow rate input. This cycle employs both fuel and LNG coldness (via its evaporation) as its input resources, but we have used only the fuel energy in the definition of

Table 2 The stream parameters of CO₂ cycle

No.	<i>t</i> [°C]	<i>P</i> [bar]	<i>G</i> [kg/s]	<i>h</i> [kJ/kg]	<i>s</i> [kJ/kg K]	<i>a</i> [kJ/kg]	Mole Composition			
							CO ₂	H ₂ O	CH ₄	O ₂
1	-44.8	156	70	-9388.7	-2.289	255.9	1			
2	201.6	153	70	-8832.3	-0.555	295.1	1			
3	623.5	150	70	-8307.9	0.242	582.0	1			
4	442.7	30.6	70	-8522.2	0.284	355.3	1			
5	623.5	30	70	-8309.0	0.553	488.2	1			
6	1300	29.1	110.96	-7578.1	1.266	1194.8	0.9	0.1		
7	761.9	1.07	110.96	-8307.4	1.366	435.8	0.9	0.1		
8	656.2	1.05	110.96	-8441.8	1.233	341.0	0.9	0.1		
9	264.4	1.03	110.96	-8902.4	0.598	69.9	0.9	0.1		
10	10	1.01	110.96	-9253.1	-0.349	1.368	0.9	0.1		
11	10	1.01	4.93	-15,936.0	-9.298	1.677		1		
12	10	1.01	106.03	-8955.0	0.021	0.886	1			
13	-70	1	106.03	-9018.3	-0.239	15.18	1			
14	61.1	6.63	106.03	-8915.4	-0.202	106.8	1			
15	201.6	30.6	30	-8788.7	-0.169	223.8	1			
16	623.5	30	30	-8309.0	0.553	488.2	1			
17	53.8	6.565	76.03	-8922.0	-0.220	105.6	1			
18	-48.8	6.5	76.03	-9406.9	-2.309	243.5	1			
19	-44.8	156	6.03	-9388.7	-2.289	255.9	1			
20	-162	1	54.69	-5557.9	-11.721	1086.2				1
21	-160.5	31.5	54.69	-5548.5	-11.702	1089.9				1
22	-126.7	31.2	54.69	-5425.8	-10.75	928.8				1
23	-5	30.9	54.69	-4751.8	-7.143	527.4				1
24	15	30.6	52.49	-4702.4	-6.961	522.4				1
25	15	30.6	2.2	-4702.4	-6.961	522.4				1
26	51.1	30	2.2	-4613.3	-6.659	521.7				1
27	25	1	~37.76	/	/	/		air		
28	15	30.6	8.76	-17.5	-0.942	264.3				1
29	51.1	30	8.76	17.8	-0.821	263.7				1
30	/	/	~29.0	/	/	/		N ₂ , Ar,...		
31	25	1.01	130	-15,865.6	-9.056	0		1		
32	20	1	130	-15,886.4	-9.126	0.098		1		

Note: Combustor inlet CO₂ mass flow rate of 100 kg/s assumed as references.

η_1 , the energy efficiency, because the LNG coldness is free, and it is actually of benefit to the user. Both input resources are, however, used in defining η_2 , the exergy efficiency, which is the more appropriate criterion for performance evaluation than the fuel energy alone. It is defined here as the ratio between the net obtained and total consumed exergy

$$\eta_2 = W_{\text{net}} / (m_f \cdot H_u + m_L \cdot a_L) \quad (2)$$

assuming that the fuel exergy is approximately equal to its lower heating value H_u , m_L is the treated LNG mass flow rate, and a_L the exergy difference between the initial and the final states of the LNG evaporation process:

$$a_L = (h_{20} - h_{23}) - T_0(s_{20} - s_{23}) \quad (3)$$

and in the subcritical evaporation case (30.6 bar), it is about 560 kJ/kg_{LNG}, depending on the final temperature T_{23} .

For a given mass flow rate of the cycle working medium, the mass flow rates of needed fuel, of water and carbon dioxide recovered, and of LNG regasified can all be determined.

With 100 kg/s mass flow rate of CO₂ at the combustor inlet taken as reference, Table 2 summarizes the parameters, including temperature, pressure, flow rate and composition, and thermodynamic properties including exergy, of each stream for the subcritical pressure (30.6 bar) and temperature of 15 °C natural gas delivery. The mass flow rate of LNG regasified is found to be 54.69 kg/s, of which about 4% (2.2 kg/s) are sent to the combustor as fuel for the cycle; and the amount of water and CO₂ recovered are found to be 4.93 kg/s and 6.03 kg/s, respectively.

The computed performance of the cycle is summarized in Table 3 (first column). The total power produced is found to be 79.3

MW. Reduced by the power consumed for O₂ separation, which is roughly 7.9 MW (~10%), the net power output is 71.4 MW, resulting in an energy efficiency (η_1) of 65% and exergy efficiency (η_2) of 51%. The difference between the efficiencies is due to their definition (Eqs. (1) and (2)), where η_1 does not take into account the LNG coldness exergy, while η_2 does. Consequently, such a plant would produce about 124 MWe if installed with the first Chinese LNG receiving terminal that has an import capacity of 3,000,000 t per year (95 kg/s).

Figures 3 and 4 are the t - Q diagrams for the recuperation system and the LNG evaporation system, respectively, where Q is the heat duty of a heat exchanger. Heat load distribution is not even among the different heat exchangers. The minimal temperature differences are present in HE₁ and HE₅. The pinch point in HE₁ appears at the point where the H₂O vapor contained in the hot LT exhaust stream begins to condense. The minimal temperature difference, ΔT_{p1} , is 10 K in this case and one way to raise it is to increase the flue gas temperature out of HE₁(t_{10}), which will lead to more flue gas exhaust heat for LNG evaporation. The pinch point in HE₅ appears at the point where CO₂ begins to condense, and ΔT_{p5} is 5 K in this calculation. Reducing the pinch point temperatures will increase the thermal performance, but larger heat transfer surface area and more equipment investment will be required.

The NG temperature at the HE₅ outlet is -5 °C, still cold enough to be used for local applications such as refrigeration and air conditioning. The total heat duty of HE₆ is 2.7 MW, and if practical cooling can be accomplished up to t_{24} =5 °C (rather than

Table 3 Performance summary of different cycle configurations

	Base-case	No-LNG	Reheat	Intercooling	Reheat+ intercooling
LT turbine work [MW]	80.9	80.5	44.6	81.3	44.9
MT turbine work [MW]	0	0	43.0	0	43.2
HT turbine work [MW]	15.0	15.1	16.3	14.6	16.3
LC compressor work [MW]	10.9	14.0	11.0	10.9	11.0
MC compressor work [MW]	0	13.7	0	0	0
HC compressor work [MW]	3.8	4.6	3.9	2.6	2.6
LNG pump work [MW]	0.5	0	0.5	0.5	0.5
CO ₂ pump work [MW]	1.4	1.3	1.4	1.4	1.4
Fuel/O ₂ expander [MW]	0	0	0.6	0	0.6
O ₂ separation work [MW]	7.9	7.7	8.4	8.1	8.7
Net power output [MW]	71.4	54.1	79.4	72.4	80.8
LNG mass flow rate [kg/s]	54.7	0	54.9	54.7	55.0
Fuel ratio [%]	4.02	/	4.28	4.14	4.42
Fuel energy input $m_f \cdot H_u$ [MW]	109.9	107.2	117.6	113.3	121.5
LNG exergy input $m_L \cdot a_L$ [MW]	30.5	0	30.7	30.9	31.0
Energy efficiency [%]	65.0	50.5	67.5	63.9	66.5
Exergy efficiency [%]	50.9	50.5	53.6	50.2	53.0

all the way to 15 °C), a modest contribution of about 1.3 MW of cooling can be obtained and added to the overall useful output of the system.

Table 4 shows the heat duties of the heat exchangers, and the estimated required heat exchanger surface areas. There are seven

heat exchangers in the system: Recuperators (HE₁, HE₂, and HE₃), LNG evaporators (HE₄, HE₅, and HE₆), and a fuel/O₂ pre-heater, HE₇. The recuperators are conventional heat exchangers with gas streams flow through both sides (ignoring the small amount water condensation in HE₁). HE₄ is a CO₂ gas-to-CH₄ liquid heat exchanger. As shown in Fig. 4, HE₅ consists of two parts, in the first part heat is exchanged between CO₂ gas and natural gas, in the second part CO₂ is condensed due to cooling by liquid, boiling, and gaseous CH₄ with an overall heat transfer coefficient estimated as 600 W/m² K [28]¹. In the calculation in Table 4, the hot stream in HE₆ is assumed to be water with the inlet and outlet temperatures of 25 and 20 °C, respectively. The total heat transfer area for the cycle is estimated to be 27,856 m², nearly 80% of which are the recuperators, and 20% the LNG evaporators, the latter accommodating about 30% of the total heat duty.

The exergy inputs, outputs, and losses are shown in Fig. 5 and Table 5. Some important conclusions are: (1) The amount of coldness exergy of the LNG adds about 28% to the fuel exergy used in the cycle, and is 22% of the overall cycle exergy input ($m_f \cdot H_u + m_L \cdot a_L$), (2) the base-case cycle uses 54% of the coldness exergy of the LNG for power generation, (3) the largest exergy loss, 21%, is in the combustor, consistent with general values found in the literature [29]; this loss can be straightforwardly decreased only by increasing the inlet temperature of the LT turbine beyond the assumed 1300 °C, which would be possible if more advanced turbines are used, (4) obviously, the addition of any component for improving cycle efficiency introduces exergy losses associated with the component, here the most significant ones are in the heat exchangers HE₅ (8.2%), HE₄ (5.2%), and HE₁ (3.4%); these losses can be decreased by decreasing the temperature differences between the heat exchanging streams (Figs. 3 and 4), but this would obviously require larger or/and more complex heat exchangers. The LMTDs of different heat exchangers are shown in Table 4. HE₃ and HE₄ have the biggest LMTDs among the heat exchangers, while exergy loss in HE₃ is relatively smaller because of the high heat transfer temperature. To reduce the system exergy loss further calls for synthetic optimization of both cycle configu-

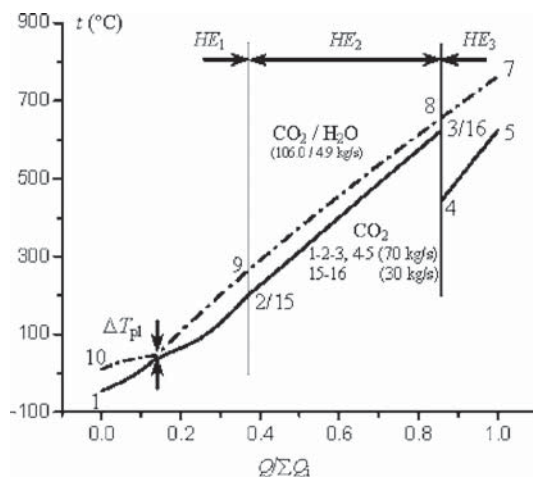


Fig. 3 t - Q diagram in CO₂ recuperation system

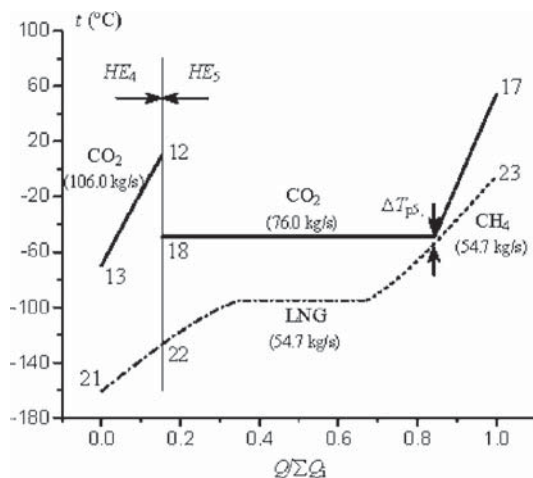


Fig. 4 t - Q diagram in LNG evaporation system

¹Precise determination of heat exchanger areas requires their detailed design specification. The estimates here are very rough, based on the assumption that the heat exchangers are of the shell-and-tube type, and using average typical overall heat transfer coefficient values for these heat exchanger processes and fluids as found in the process heat transfer literature [28]. Use of better heat exchangers, such as plate type, may reduce the required heat transfer area by as much as an order of magnitude.

Table 4 Heat exchanger surface area estimation

	Heat exchanger	Q [MW]	UA [kW/K]	LMTD [K]	U [28] [W/m ² K]	A [m ²]	A [%]	ΣA [m ²]
Recuperators	HE ₁	38.95	1005.76	38.7	99	10,159.2	36.5	21,968
	HE ₂	51.10	1011.75	50.5	93	10,879.0	39.0	
	HE ₃	14.93	86.47	172.7	93	929.8	3.3	
LNG evaporators	HE ₄	6.71	59.63	112.5	99	602.3	2.2	5,632
	HE ₅	36.86	1124.2	32.8	93/600	4645.6	16.7	
	HE ₆	2.699	164.97	16.4	429	384.6	1.4	
Fuel/O ₂ preheater	HE ₇	0.50	23.73	21.1	93	255.1	0.9	255

ration and stream parameters. (5) Figure 5 shows clearly that the proposed configuration of the cycle allows a large fraction of the exergy to be usefully reused internally.

Key Parameters and Discussion

The key parameters that have influence on the cycle performance include the Brayton cycle mass flow rate ratio R_g , the low-pressure turbine inlet temperature t_6 , the cycle high and intermediary pressure level P_h and P_m .

The Brayton cycle mass flow rate ratio R_g is defined as the ratio of the mass flow rate of stream 16 (Fig. 1) over that of the total CO₂ recycled in the system.

$$R_g = m_{16}/(m_5 + m_{16}) \quad (4)$$

If R_g equals 1, the plant becomes a pure Brayton cycle, and less flue gas exhaust heat will be recovered in the recuperation system due to the sizeable increase of the flue gas temperature at the inlet of the LNG evaporation system. This temperature equals to the sum of t_{15} and a temperature difference needed for heat transfer in HE₂. At the other extreme, if $R_g=0$, it is still a kind of quasi-combined cycle of a Brayton and a supercritical Rankine-type one, similar to the "MATIANT" cycle [25], and the higher heat capacity of the compressed liquid CO₂ will lead to a larger temperature difference between LT outlet flue gas and CO₂ entering the combustor, t_7-t_5 . Variation of R_g will thus not only change the flue gas heat distribution between the recuperation system and the LNG evaporation system, but also the heat balance inside the recuperation system itself. Calculation shows that both energy ef-

iciency and exergy efficiency increase by about 3 to 4 percentage points for every 100 °C increase of t_6 (LT inlet temperature) or 20% increase of R_g . Increasing R_g means that more flue gas waste heat is recovered in the recuperation system, and the pinch point temperature difference in HE₁(ΔT_{p1}) will drop accordingly, R_g reaches its upper limit when ΔT_{p1} drops to the accepted lowest value. The specific power output w increases with the increase of t_6 and with the decrease of R_g .

A relatively high level for P_h and P_m was employed in some past studies of power cycles with CO₂ separation, for example, they are 240 bar and 60 bar, respectively, in the "COOPERATE" [20,22] and "COOLENERG" cycles [26], and 300 bar and 40 bar in the "MATIANT" cycle [25]. To relieve the technical problems incurred by these high pressure levels, the pressure P_h and P_m is chosen in our cycle to be 150 and 30 bar for the design point.

Computations show that both P_h and P_m have positive impact on the efficiencies and specific power output within certain calculation range ($P_m=15-55$ bar and $P_h=100-200$ bar). When P_h increases from 150 bar to 200 bar for $P_m=25$ bar, the efficiencies increase by about 0.6 percentage point; and they increase by 1.7 percentage points when P_m increases from 15 to 25 bar for $P_h=150$ bar. Obviously P_m has a more notable influence on the cycle thermal performance than P_h , clearly because the power output of the LT turbine is several fold bigger than that of the HT turbine. Increasing P_h and P_m results in the lowering of the HT and LT turbine flue gas temperature, respectively, leading to the drop of

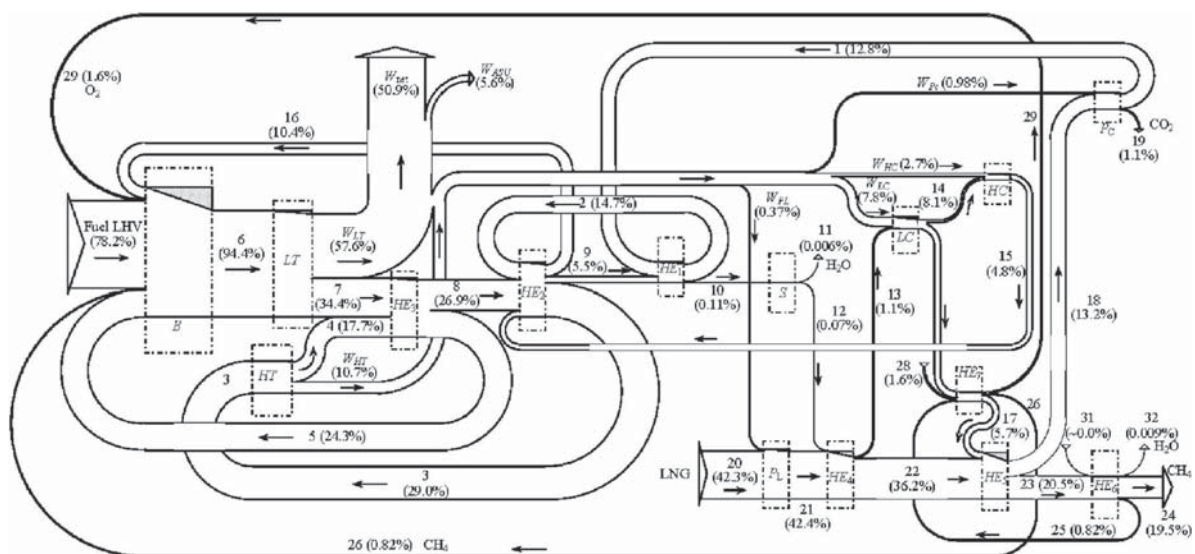


Fig. 5 The exergy flow diagram for the base-case cycle

Table 5 Exergy inputs, outputs, and losses decomposition in the cycle

Exergy input ^a (%)		
Chemical exergy	Fuel LHV	78.238
Physical exergy (stream in)	20; LNG	42.300
	28; O ₂	1.649
	31; H ₂ O	0.0
Sum		122.187
Exergy output ^a (%)		
Power output	W_{net}	50.860
	W_{ASU}	5.617
Physical exergy (stream out)	11; H ₂ O	0.0059
	19; CO ₂	1.099
	24; CH ₄	19.525
	32; H ₂ O	0.0091
Component exergy losses	B	21.058
	HE ₅	8.167
	HE ₄	5.194
	HE ₁	3.461
	LT	2.352
	HE ₂	1.471
	HE ₃	0.866
	LC	0.853
	HT	0.619
	P_C	0.312
	P_L	0.222
	HC	0.206
	HE ₆	0.186
	HE ₇	0.07
	S	0.035
Sum		122.188

^aValues are based on $(m_f \cdot Hu + m_{LNG} \cdot a_L) = 78.238\% + (42.3 - 20.538)\% = 100\%$ (Eqs. (2) and (3)).

the pinch point temperature difference ΔT_{p1} , but it is not necessary to have very high values of P_h , since the HT turbine contributes less to the cycle power output.

Compared with the above-mentioned cycles, our cycle has two new features: first, while $R_g=0$ (no HC compressor) in those cycles, $R_g>0$ in our cycle, which allows a much better turbine exhaust heat recovery in the recuperation system; second, integration here with the LNG evaporation process accomplishes CO₂ condensation at a much lower pressure. As a result, the computed energy efficiency is as high as 65% with the enabling technologies (TIT=1300 °C, $P_h=150$ bar and $P_m=30$ bar), which is about 10 to 15 percentage points of increment compared with the other above-mentioned cycles.

The typical cryogenic equipment for air separation consumes about 0.2–0.28 kWh of electric power per kilogram of O₂ separated [13], depending on the product purity, production capacity and so on. It is found through the calculation that the power consumed for O₂ production is nearly 10% of the total power output, and every 10% reduction in the power needed for air separation will increase both efficiencies and power output by about 1.1%. Clearly, one way to improve system performance is to optimally integrate the air separation with the rest of the system.

Comparison of Different Cycle Configurations

With the base-case cycle described in Figs. 1 and 2 as reference, different system configurations were modeled and analyzed to further explore the effect of LNG exergy application and to examine the potential for performance improvement. These configurations include one where no LNG is used, one in which intercooling is used, one with reheat, and one with reheat and plus inter cooling. The corresponding t - s diagrams are shown in Figs. 6–9, respectively.

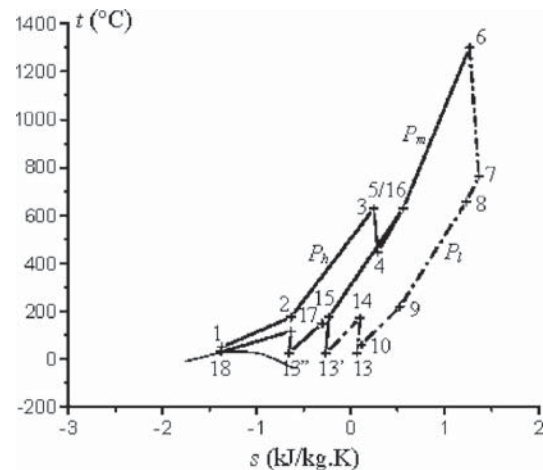


Fig. 6 t - s diagram for CO₂ cycle without LNG

Figures 10 and 11 show the cycle layout for the cycle without use of LNG coldness (no-LNG case), and the intercooling+reheat cycle, respectively. The reheat cycle is the combination of the left part of the schematic shown in Fig. 1 and the right part of that in Fig. 11. Similarly, the intercooling cycle is the combination of the right part of Fig. 1 and the left part of Fig. 11.

If LNG is not used for its coldness, as in reference [30], then a multi-stage compression process with intercooling $13 \rightarrow 14 \rightarrow 13 \rightarrow 15 \rightarrow 17 \rightarrow 13'' \rightarrow 14' \rightarrow 18$ (in Fig. 10) is adopted to bring the CO₂ up to a liquid state of 80 bar and 30 °C, instead of the CO₂ condensation process. This brings two advantages: Elimination of noncondensable gases and the associated problems, and elimination of the need for a condenser. The cycle in Fig. 6 can hence be regarded as a combination of the “MATIANT” cycle and a CO₂ Brayton cycle with intercooling. Unlike all the other ones, this cycle works above the ambient temperature. It uses cold water as the intercooler coolant with the temperature varying from 15 to 20 °C. The specific power output is about 76% of that of the base-case cycle, and it has the same energy efficiency and exergy efficiency, which can reach 50%.

When reheat is employed, the low-pressure turbine outlet temperature t_7 can be raised significantly (to over 1000 °C, Figs. 7 and 9), and the turbine exhaust heat is large, able to raise temperature of the cold streams in HE₂ to a higher magnitude. However, for practical turbine materials, the high pressure turbine HT inlet temperature is restricted to 700 °C in the calculations, and

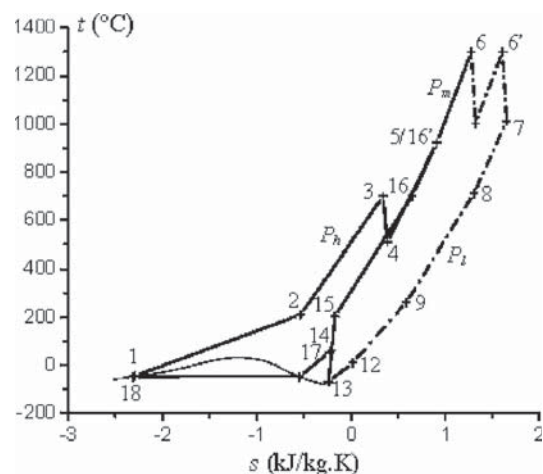


Fig. 7 t - s diagram for CO₂ cycle with reheat

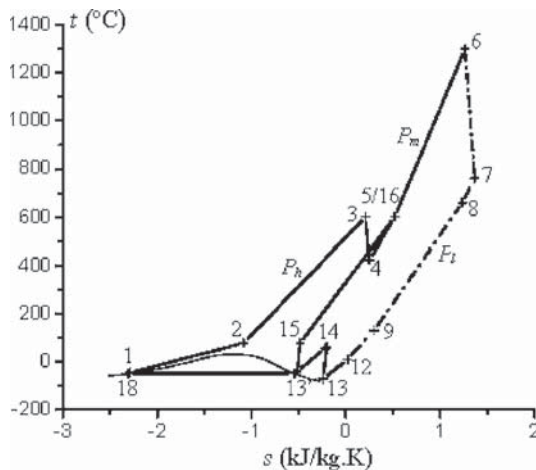


Fig. 8 t - s diagram for CO₂ cycle with intercooling

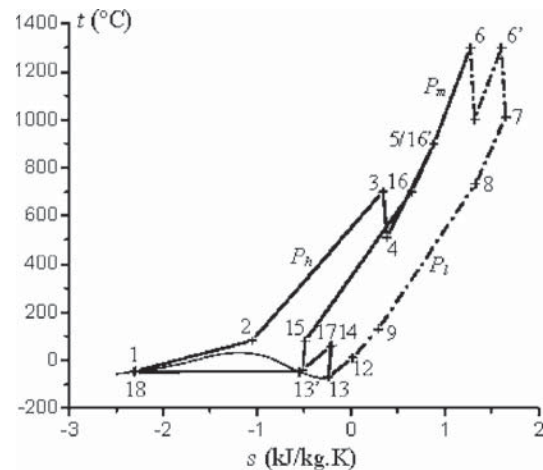


Fig. 9 t - s diagram for CO₂ cycle with intercooling and reheat

the excess amount of LT exhaust heat is used to raise the combustor inlet temperature to a higher level (point 5/16' in Figs. 7 and 9). The layouts of the cycles in Figs. 10 and 11 are somewhat different from that in Fig. 1 in terms of the number and the order of the heat exchangers).

The performances are summarized and compared in Table 3 and Figs. 12–14 as functions of the intermediary pressure P_m . A fuel compressor (or expander) is needed when the combustion pressure in B is higher (or lower) than the natural gas delivery pressure. The efficiencies and power output are found to increase monotonically with P_m within the whole calculation range of P_m (from 20 to 40 bar), with a diminishing rate.

Employing reheat is seen to improve performance: both the energy efficiency and exergy efficiency increase by 2 to 3 percentage points, and the specific power output increases by about 11%.

Employing intercooling increases the specific power output slightly, by 1.3% on average, but the energy and exergy efficiency coincidentally drop by more and less than 1 percentage point, respectively. From Figs. 8 and 9, in the intercooling cycle, the working fluid temperature after compression is lower, but the hot stream temperature at the recuperator outlet t_{10} is fixed. This results in a lower combustor inlet temperature and thus more fuel is needed to raise the temperature to the desired turbine inlet temperature, which explains the efficiency drop. In the intercooling

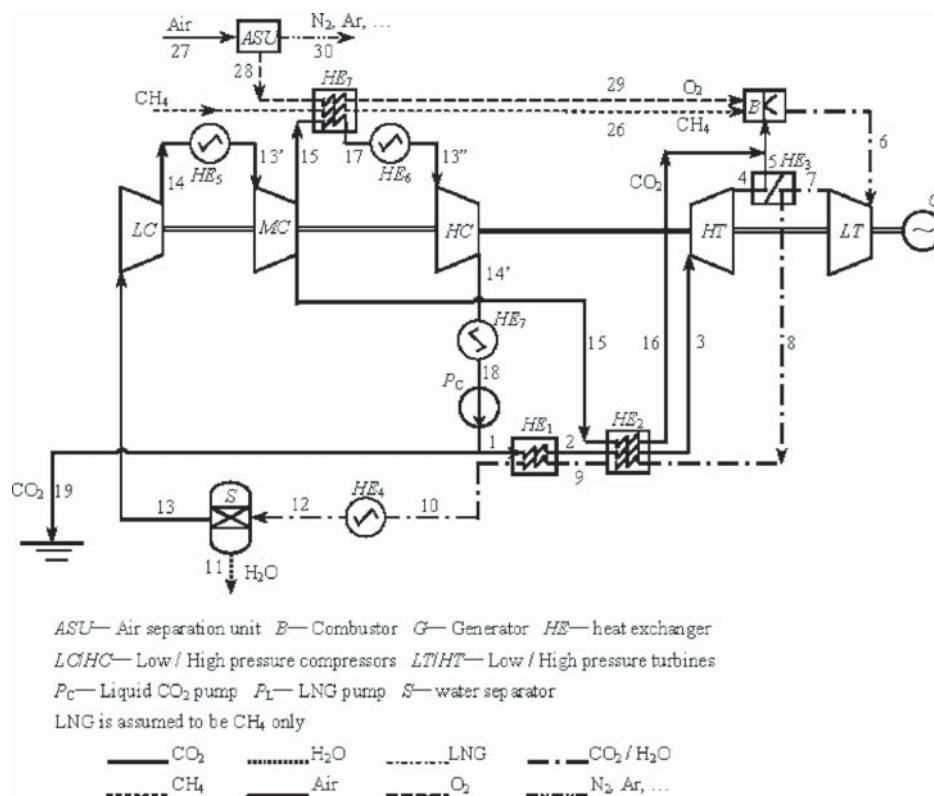


Fig. 10 CO₂ cycle flow sheet without LNG cold exergy utilization

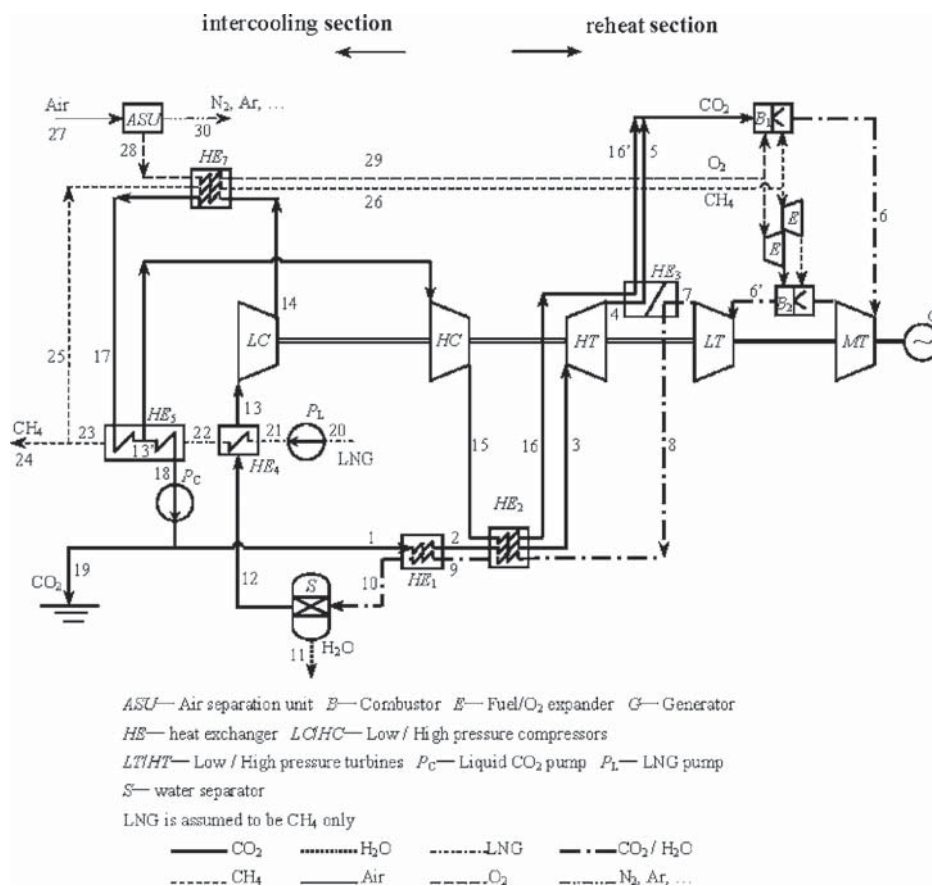


Fig. 11 CO₂ cycle flow sheet with reheat and intercooling

cycle, all of the working fluid needs to be cooled down by LNG after the first stage of compression (14→17→13' in Fig. 11). Therefore, the amount of heat available in the LNG evaporation system will bring the evaporated natural gas to the near-ambient temperature, leaving no extra coldness for air conditioning.

The comparison between the reheat+intercooling cycle with the reheat cycle is similar to the comparison between the intercooling cycle with the base-case cycle. As known in general, incorporation of reheat or intercooling alone can increase the cycle power output, but not necessarily improve the efficiency, because of the

higher turbine flue gas temperature in the cycle with reheat, or the lower compressor outlet temperature in the cycle with intercooling. It is also known that incorporation of recuperation (internal heat regeneration) may have other consequences. Unlike the situation in this paper, if the recuperator hot stream outlet temperature drops in the cycle with intercooling, it is possible to increase the overall efficiency as well.

Compared with the base-case cycle, the energy efficiency of the no-LNG case is lower by nearly 15 percentage points, but their exergy efficiencies are about the same. Its exergy efficiency is

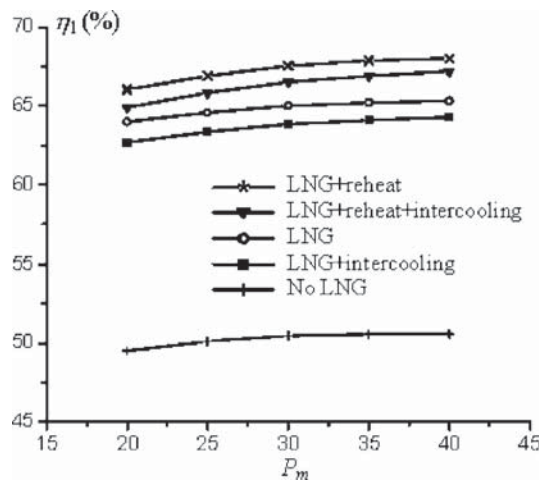


Fig. 12 The influence of P_m on thermal efficiency

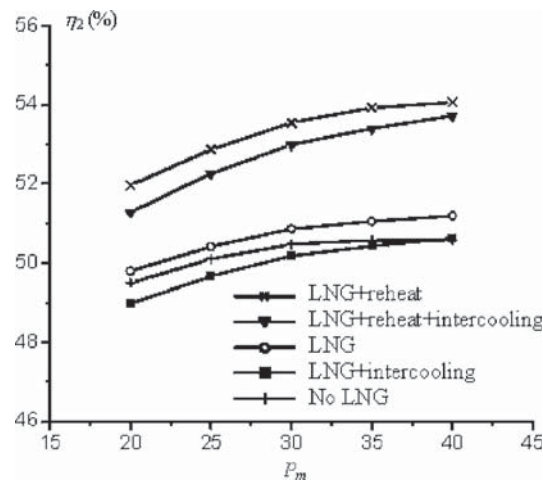


Fig. 13 The influence of P_m on exergy efficiency

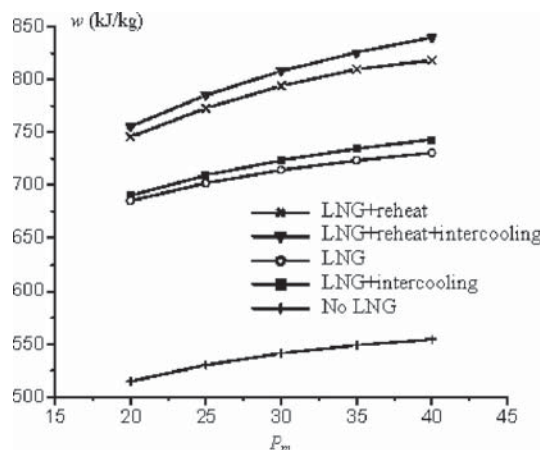


Fig. 14 The influence of P_m on specific power output

between that of the base-case cycle and the one with intercooling (Fig. 13). From Table 3, the LNG coldness contributes nearly 22% to the total base-case cycle exergy input, and it converts to power at almost the same efficiency as the fuel exergy does.

Among the cycle configurations studied in this paper, the reheat cycle has the highest efficiencies, while the reheat+intercooling cycle has the highest specific power output. It should, however, be noted that the recuperator material needs then to bear a temperature as high as 1000 °C.

The heat exchanger surface areas for different cycle configurations are also estimated and compared in Table 6. Differences mainly exist in the recuperation system. Compared with the base-case cycle, it was found that reheat cycle requires 54% additional heat transfer area, and the no-LNG cycle and intercooling cycle require 18% and 9% less, respectively.

Conclusions

A novel power cycle producing zero CO₂ emission by integration of LNG cryogenic exergy utilization is proposed and thermodynamically modeled. The main merits of the system include:

- (1) Good thermodynamic performance, with the energy and exergy efficiencies reaching 65% and 51%, respectively, using conventional technologies, despite the power consumed for air separation; this is in part because the amount of coldness exergy of the LNG adds about 28% to the fuel exergy used in the cycle, and
- (2) Negligible release of pollutants to the environment;
- (3) Removal of high-pressure liquid CO₂ ready for sale or disposal;
- (4) Valuable byproducts: condensed water, liquid N₂, and Ar; and
- (5) Full exploitation of the LNG evaporation process.

The exergy analysis identified the largest exergy loss, 21% (of the total exergy input), to be in the combustor, which can be straightforwardly decreased only by increasing the inlet temperature of the LT turbine beyond the assumed 1300 °C. The most significant other exergy losses are in the heat exchangers HE₅

(8.2%), HE₄ (5.2%), and HE₁ (3.4%), and these losses can be decreased by decreasing the temperature differences between the heat exchanging streams, but this would obviously require larger or/and more complex heat exchangers. The proposed configuration of the cycle allows a large fraction of the exergy to be usefully reused internally.

The influences of some key parameters on the cycle performance, including the Brayton cycle mass flow rate ratio, the low-pressure turbine inlet temperature and pressure levels, are discussed. Energy efficiency and exergy efficiency increase by about 3 to 4 percentage points for every 100 °C increase of t_6 (LT inlet temperature) or 20% increase of R_g . The specific power output w increases with the increase of t_6 and with the decrease of R_g . Both P_h and P_m have a positive impact on the efficiencies and specific power output within the calculation range; and P_m has a more notable influence on the cycle thermal performance than P_h . It is also found that every 10% reduction in the power needed for air separation will increase both efficiencies and power output by about 1.1%.

The total needed heat exchanger area is about 390 m²/MWe for the base-case cycle, ~75% of which are the recuperators HE₁ and HE₂. Employing larger heat transfer temperature differences can effectively reduce the heat transfer surface area, but will lead to a reduction of thermal efficiency. A formal thermoeconomic optimization is obviously called for. The pinch point temperature difference in the recuperation system is one of the main constraints to performance improvement, its influence and parameter optimization call for further study.

Among the different cycle schemes investigated, it was found that highest efficiencies' improvement over the base-case can be obtained by employing reheat but only by 2 to 3 percentage points, and this would also increase the specific power output by more than 10%. The major practical restrictions to employing reheat is the high recuperator inlet temperature for reheat cycle, and a 54% increase in the overall heat transfer surface. Compared with the base-case, incorporation of intercooling lowers efficiencies and slightly increases power output. If no LNG coldness is used, the cycle operates in the same temperature range as conventional power plants do, the required heat exchange area is reduced by 18% (only), the specific power output is reduced by one quarter, and the efficiency can reach 50%, about 15 percentage points lower than that of the base-case cycle.

Based on this analysis, the proposed base-case plant (which was not optimized yet) would produce 124 MWe if installed with the first LNG terminal in China that has an import capacity of 3,000,000 t/yr, and the capacity can be increased up to 137 MWe and 140 MWe for reheat cycle and reheat/intercooling cycle, respectively.

Acknowledgment

The authors gratefully acknowledge the support of the K. C. Wong Education Foundation, Hong Kong; the Chinese Natural Science Foundation Project (No. 50006013); and the Major International (Regional) Joint Research Program: Fundamental Study of CO₂ Control Technologies and Policies in China.

Nomenclature

A = heat exchanger surface area (m²)

Table 6 Heat exchanger surface area comparison of different cycle configurations

	No LNG	Reheat	Intercooling	Reheat/intercooling	Base-case
Recuperators [m ²]	18,664	36,940	18,742.5	28,551.2	21,968
Others [m ²]	4,225.6	5,967.3	6,702.1	6,804.8	5,887.6
Total area ΣA [m ²]	22,889.6	42,907.3	25,444.6	35,356.0	27,855.6
$\Sigma A / \Sigma A_{ref}$ [%]	82.2	154.0	91.3	126.9	1

a = specific exergy (kJ/kg)
 m = mass flow rate (kg/s)
 H_u = fuel LHV value (kJ/kg)
 h = specific enthalpy (kJ/kg)
 P = pressure (bar)
 R_g = mass flow rate ratio of Brayton cycle (%), Eq. (4)
 s = specific entropy (kJ/kg·K)
 T = temperature (K)
 t = temperature (°C)
 Q = heat duty (MW)
 U = overall heat transfer coefficient (W/m² K)
 W = power output (MW)
 w = specific power output (kJ/kg)
 ΔT_p = pinch point temperature difference (K)
 η_1 = energy efficiency
 η_2 = exergy efficiency

Subscripts

f = fuel
 h = high pressure
 m = intermediary pressure
 net = net output
 L = liquefied natural gas
 l = low pressure
 $1...30$ = states on the cycle flow sheet

References

- [1] Karashima, N., and Akutsu, T., 1982, "Development of LNG Cryogenic Power Generation Plant," *Proc. of 17th IECEC*, pp. 399–404.
- [2] Angelino, G., 1978, "The Use of Liquid Natural Gas as Heat Sink for Power Cycles," *J. Eng. Power*, **100**, pp. 169–177.
- [3] Kim, C. W., Chang, S. D., and Ro, S. T., 1995, "Analysis of the Power Cycle Utilizing the Cold Energy of LNG," *Int. J. Energy Res.*, **19**, pp. 741–749.
- [4] Najjar, Y. S. H., and Zaamout, M. S., 1993, "Cryogenic Power Conversion With Regasification of LNG in a Gas Turbine Plant," *Energy Convers. Manage.*, **34**, pp. 273–280.
- [5] Wong, W., 1994, "LNG Power Recovery," *Proc. Inst. Mech. Eng.*, Part A, **208**, pp. 1–12.
- [6] Zhang, N., and Cai, R., 2002, "Principal Power Generation Schemes With LNG Cryogenic Exergy," *Proc. ECOS 2002 15th International Conference on Efficiency, Costs, Optimization, Simulation, and Environmental Impact of Energy Systems*, G. Tsatsaronis et al., eds., Berlin Technical University, Berlin, pp. 334–341.
- [7] Krey, G., 1980, "Utilization of the Cold by LNG Vaporization With Closed-Cycle Gas Turbine," *J. Eng. Power*, **102**, pp. 225–230.
- [8] Agazzani, A., and Massardo, A. F., 1999, "An Assessment of the Performance of Closed Cycles With and Without Heat Rejection at Cryogenic Temperatures," *ASME J. Eng. Gas Turbines Power*, **121**, pp. 458–465.
- [9] Deng, S., Jin, H., Cai, R., and Lin, R., 2004, "Novel Cogeneration Power System With Liquefied Natural Gas (LNG) Cryogenic Exergy Utilization," *Energy*, **29**, pp. 497–512.
- [10] Chiesa, P., 1997, "LNG Receiving Terminal Associated With Gas Cycle Power Plants," *ASME Paper No. 97-GT-441*.
- [11] Desideri, U., and Belli, C., 2000, "Assessment of LNG Regasification Systems With Cogeneration," *ASME Paper No. 2000-GT-0165*.
- [12] Kim, T. S., and Ro, S. T., 2000, "Power Augmentation of Combined Cycle Power Plants Using Cold Energy of Liquefied Natural Gas," *Energy*, **25**, pp. 841–856.
- [13] Velautham, S., Ito, T., and Takata, Y., 2001, "Zero-Emission Combined Power Cycle Using LNG Cold," *JSME Int. J., Ser. B*, **44**, pp. 668–674.
- [14] Riemer, P., 1996, "Greenhouse Gas Mitigation Technologies, an Overview of the CO₂ Capture, Storage and Future Activities of the IEA Greenhouse Gas R&D Program," *Energy Convers. Manage.*, **37**, pp. 665–670.
- [15] Haugen, H. A., and Eide, L. I., 1996, "CO₂ Capture and Disposal: the Realism of Large Scale Scenarios," *Energy Convers. Manage.*, **37**, pp. 1061–1066.
- [16] Yantovski, E. I., Zvagolsky, K. N., and Gavrilenko, V. A., 1992, "Computer Exergonomics of Power Plants Without Exhaust Gases," *Energy Convers. Manage.*, **33**, pp. 405–412.
- [17] Shao, Y., and Golomb, D., 1996, "Power Plants With CO₂ Capture Using Integrated Air Separation and Flue Gas Recycling," *Energy Convers. Manage.*, **37**, pp. 903–908.
- [18] Shao, Y., Golomb, D., and Brown, G., 1995, "Natural Gas Fired Combined Cycle Power Plant With CO₂ Capture," *Energy Convers. Manage.*, **36**, pp. 1115–1128.
- [19] Wall, G., Yantovski, E., Lindquist, L., and Tryggstad, J., 1995, "A Zero Emission Combustion Power Plant for Enhanced Oil Recovery," *Energy*, **20**, pp. 823–828.
- [20] Yantovski, E. I., 1996, "Stack Downward Zero Emission Fuel-Fired Power Plants Concept," *Energy Convers. Manage.*, **37**, pp. 867–877.
- [21] Yantovski, E. I., and Gorski, J., 2000, "Further Elaboration of Quasi-combined Zero-Emission Power Cycle," *Proc. ECOS 2000 13th International Conference on Efficiency, Cost, Optimisation, Simulation and Environmental Aspects of Energy and Process Systems*, G. G. Hirs, ed., University of Twente, Enschede, Netherlands, pp. 1083–1092.
- [22] Yantovski, E. I., Zvagolsky, K. N., and Gavrilenko, V. A., 1995, "The COOPERATE-Demo Power Cycle," *Energy Convers. Manage.*, **36**, pp. 861–864.
- [23] Mathieu, P., Dubuisson, R., Houyou, S., and Nihart, R., 2000, "A Quasi Zero Emission O₂/CO₂ Combined Cycle," *Proc. ECOS 2000 13th International Conference on Efficiency, Cost, Optimisation, Simulation and Environmental Aspects of Energy and Process Systems*, G. G. Hirs, ed., University of Twente, Enschede, Netherlands, pp. 1071–1081.
- [24] Fioravanti, A., Lombardi, L., and Manfrida, G., 2000, "An Innovative Energy Cycle With Zero CO₂ Emissions," *Proc. ECOS 2000 13th International Conference on Efficiency, Cost, Optimisation, Simulation and Environmental Aspects of Energy and Process Systems*, G. G. Hirs, ed., University of Twente, Enschede, Netherlands, pp. 1059–1070.
- [25] Mathieu, P., and Nihart, R., 1999, "Zero-Emission MATIANT Cycle," *ASME J. Eng. Gas Turbines Power*, **121**, pp. 116–120.
- [26] Staicovici, M. D., 2002, "Further Research Zero CO₂ Emission Power Production: the 'COOLENERG' Process," *Energy*, **27**, pp. 831–844.
- [27] Aspen Plus®, Aspen Technology, Inc., version 11.1, <http://www.aspentech.com/>
- [28] Hewitt, G. F., Shires, G. L., and Bott, T. R., 1993, *Process Heat Transfer*, CRC Press and Begell House, Boca Raton, FL.
- [29] Dunbar, W. R., and Lior, N., 1994, "Sources of Combustion Irreversibility," *Combust. Sci. Technol.*, **103**, pp. 41–61.
- [30] Mathieu, P., and Nihart, R., 1999, "Sensitivity Analysis of the MATIANT Cycle," *Energy Convers. Manage.*, **40**, pp. 1687–1700.



A technical evaluation, performance analysis and risk assessment of multiple novel oxy-turbine power cycles with complete CO₂ capture

Fernando Climent Barba, Guillermo Martínez-Denegri Sánchez, Blanca Soler Seguí, Hamidreza Gohari Darabkhani*, Edward John Anthony

Centre for Combustion and CCS, Energy Department, School of Water, Energy and Environment (SWEE), Cranfield University, Cranfield, Bedfordshire MK43 0AL, UK

ARTICLE INFO

Article history:

Received 12 October 2015

Received in revised form

27 May 2016

Accepted 30 May 2016

Available online 3 June 2016

Keywords:

Carbon capture and storage

Oxy-turbine power cycle

Air separation unit

Combined cycle gas turbine

Techno-economic analysis

PESTLE risk analysis

ABSTRACT

In recent years there has been growing concern about greenhouse gas emissions (particularly CO₂ emissions) and global warming. Oxyfuel combustion is one of the key technologies for tackling CO₂ emissions in the power industry and reducing their contribution to global warming. The technology involves burning fuel with high-purity oxygen to generate mainly CO₂ and steam, enabling easy CO₂ separation from the flue gases by steam condensation. In fact, 100% CO₂ capture and near-zero NO_x emissions can be achieved with this technology.

This study examines nineteen different oxy-turbine cycles, identifying the main parameters regarding their operation and development. It also analyses the use of advanced natural gas (NG) combustion cycles from the point of view of the carbon capture and storage (CCS) and considering political, legislative and social aspects of deploying this technology. Six oxy-turbine cycles which are at the most advanced stages of development (NetPower, Clean Energy Systems CES), Modified Graz, E-MATIANT, Advanced Zero Emission Power AZEP 100% and Semi-Closed Oxy-fuel Combustion Combined Cycle (SCOC-CC)), were chosen to conduct a Political, Environmental, Social, Technological, Legislative and Economic (PESTLE) risk analysis. This compares each technology with a conventional combined cycle gas turbine (CCGT) power plant without carbon capture as the base-case scenario. Overall, the net efficiency of the different oxy-turbine cycles ranges between 43.6% and 65%, comparable to a CCGT power plant, while providing the extra benefits of CO₂ capture and lower emissions.

A multi-criteria analysis carried out using DECERNS (Decision Evaluation in Complex Risk Network Systems) software determined that, depending on the specific criterion considered, one can draw different conclusions. However, in terms of technology, environment and social opinion, the most promising cycles are the NetPower and CES cycles, whereas from an economic point of view, E-MATIANT is more competitive in the energy market. Giving each factor equal importance, the NetPower cycle must be considered to be the best oxy-turbine cycle based on our analysis.

Most of the oxy-turbine cycles are still under development and only a few cycles (e.g., CES and NetPower) are progressing to the demonstration phase. In consequence, political measures such as CO₂ tax and emission allowances need to be implemented for oxy-turbine technologies to become the preferred option for fossil fuel power plants burning natural gas.

© 2016 Elsevier Ltd. All rights reserved.

Abbreviations: AHPS, advanced oxy-fuel hybrid power system; ASU, air separation unit; AZEP, advanced zero emission power; CCGT, combined cycle gas turbine; CCS, carbon capture and storage; CES, clean energy systems; COE, cost of electricity; CAPEX, capital expenditure; CPU, compression and purification unit; DECERNS, Decision Evaluation in Complex Risk Network Systems; HICES, Hybrid and Improved CES cycle; HRSG, heat recovery steam generator; HTT, high-temperature turbine; IGCC, integrated gasification combined cycle; ITM, ion transfer membrane; LCA, Life Cycle Assessment; MCDA, multi-criteria decision analysis; NG, natural gas; PESTLE, Political, Environmental, Social, Technological, Legislative and Economic risk analysis; ROC, Renewable Obligation Certificate; SCOC-CC, Semi-Closed Oxy-fuel Combustion Combined Cycle; STHS, Solar Thermal Hybrid H₂O turbine power generation System; TRA, Technology Readiness Assessment.

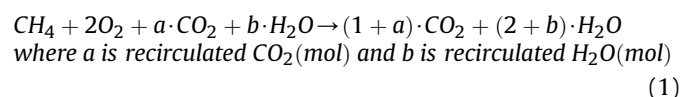
* Corresponding author.

E-mail addresses: h.g.darabkhani@cranfield.ac.uk, h.g.darabkhani@gmail.com (H. Gohari Darabkhani).

1. Introduction

Greenhouse gas emissions from the use of fossil fuels in power generation are a major environmental problem due to their contribution to global warming. In 2013, CO₂ emissions represented 82% of greenhouse gas emissions in the UK and 39% of these CO₂ emissions were produced by the energy supply sector (Department of Energy & Climate Change, 2013). The use of fossil fuels is expected to continue because of their availability and economic importance. As such, technologies such as carbon capture and storage (CCS) are fundamental in reducing the severity of the greenhouse effect (Lee and Hashim, 2014).

Oxyfuel is a promising technology for power generation with carbon capture. It consists of burning fuel with high-purity oxygen at near-stoichiometric conditions and uses flue gas recirculation ($a + b$) to control the combustor temperature. The process follows the global reaction shown in Equation (1).



The flue gases contain mainly CO₂ and steam (and low proportions of NO_x, SO_x, CO) which can be separated by condensation of the steam (Richards and Williams, 2012). Subsequently, the steam-depleted stream is normally treated to obtain high-purity CO₂ for further applications.

The advantages of this technology are near elimination of NO_x by avoiding the ingress of nitrogen into the burner, and the simplicity of the CO₂ sequestration process compared to other techniques since the flue gases contain few impurities. On the other hand, the technology's drawbacks are the energy penalty caused by the requirement of high-purity O₂ and potentially higher materials degradation caused by the presence of excess oxygen at high temperatures and the corrosive potential of any possible fuel sulphur content.

In order to show oxyfuel combustion with carbon capture and storage is feasible, seventeen large-scale projects were initiated worldwide (SCCS, 2015). In most of these projects coal/biomass were the primary fuels. An important example is provided by the Callide Oxyfuel (coal) Project in Australia (Global CCS Institute, 2013) which consists of the retrofit of a unit of 30 MW into an oxyfuel boiler for electricity generation with CO₂ purification, capture and storage. When the project finished in March 2015, the oxy-combustion unit had operated for 10,000 h and the Compression and Purification Unit (CPU) for 5500 h (Komaki et al., 2014). Four of the seventeen projects were recently cancelled or are currently moth-balled due to lack of funding or profitability. The Compostilla Phase II project located in Spain is one of these, which when it was operating showed an impressive net efficiency of 33% capturing 91% of the produced CO₂ (EndesaCiuden and Foster Wheeler, 2013).

There is a growing worldwide attempt to convert coal-fired power plants to gas-fired plants due to their lower emissions. Consequently, by increasing the number of natural gas power plants, CO₂ capture from gas-fired power plants (Gas-CCS) is presently receiving more attention (e.g., Gas-FACTS a CCS Research Council funded project in the UK). One of the alternatives in Gas-CCS is the oxy-combustion gas turbine cycles and, therefore, further investigations on these cycles look more promising than before.

This technical evaluation addresses a specific type of oxyfuel cycles known as oxy-turbine which are characterised by combusting natural gas or syngas with high-purity oxygen previously separated using a cryogenic air separation unit (ASU), ion transfer

membrane (ITM) or other technology. Political, Environmental, Social, Technological, Legislative and Economic (PESTLE) risk analysis and a multi-criteria decision analysis carried out using DECERNS (Decision Evaluation in Complex Risk Network Systems) software have been employed to evaluate and compare different cycles.

This paper assesses nineteen different oxy-turbine power cycles which are shown with their specifications in Table 1.

According to Table 1, the key factors which determine the availability and performance of the oxy-turbine panorama are the current status and the net efficiency. Considering the current status, most of the cycles can be considered as being under development (e.g., at the stage of being investigated via thermodynamic analysis). In fact only AZEP, CES and NetPower can be considered to be at an advanced status given that CES and NetPower cycles have been built at the pilot scale to demonstrate their feasibility (Anderson et al., 2008; Lu, 2014) followed by the AZEP whose components have been tested at laboratory scale (Sundkvist et al., 2007). Overall, the net efficiency of the different cycles ranges between 43.6 and 65%, comparable to a combined cycle gas turbine (CCGT) power plant (Chase and Kehoe, 2010).

The core of CES's design is adapted from rocket engine technology and burns gaseous or liquid fuels with pure gaseous oxygen. The high-pressure oxy-combustor produces a steam/CO₂ working fluid for expansion in a turbine. NetPower, however, uses supercritical CO₂ as the working fluid in a radically new cycle. Carbon capture in oxy power cycles is an inherent feature of the process, not an add-on with very large parasitic loads, as with "conventional" CCS approaches. For most of these cycles compatible fuels include natural gas, syngas from coal, refinery residues, biogases, landfill gas, and oil/water emulsions. A demonstration project for the CES cycle including the design, analysis, and testing of a modified Siemens SGT-900 gas turbine was done by Clean Energy Systems (CES), with support from Siemens Energy and Florida Turbine Technologies (FTT), through a U.S. Department of Energy (DOE) funding programme (Hollis et al., 2012). Component test results proved the feasibility of the gas turbine conversion to an oxy-fuel turbine; however, further testing was recommended to verify performance at higher power levels, and longer durations (Anderson et al., 2010). For demonstration of the NETPower cycle, the company is partnering with CB&I, Toshiba Corporation, and Exelon Corporation to demonstrate this new system in a 50 MWt natural gas power plant (Allam, 2016).

1.1. Classification by recirculation

Regarding the recirculation of flue gases, researchers have carried out several studies in order to determine if recirculating CO₂, steam, or a mixture of both offers more thermodynamic advantages. Thus, these cycles were classified using these criteria, as shown in Table 2.

CO₂ is the most popular recirculation fluid for the oxy-turbine cycles reviewed. In the condenser, CO₂ and steam are separated by steam condensation and the remaining carbon dioxide is divided into two streams. Usually, at least 90% of the CO₂ produced is recirculated to the combustor, whereas the remaining part is purified and compressed for further applications (Yang and Wang, 2015; Luu et al., 2016). For example, in Semi-Closed Oxy-fuel Combustion Combined Cycle (SCOC-CC), recirculated CO₂ is represented as a red line in the diagram shown in Fig. 1.

Another option, only seen in two of the considered oxy-turbine cycles, is to use some of the steam separated in the condenser instead of CO₂. The CES cycle illustrates the recirculation process with water, which is represented in Fig. 2 as a dark blue line (in the web version).

Table 1

Specification review of the nineteen studied oxy-turbine power cycles.

Cycle name	Developers/ year	Current status	Processes	Air separation system	Fuel/LHV [MJ/kg]	Net power [MW]	Gross efficiency [%]	O ₂ separation work [kWh/kg]/ efficiency considering it [%]	Net efficiency [%]	Highest pressure [bar]	TIT [°C]	TIP [bar]	Recirculation gas [w/w %]	Carbon captured [%]	CO ₂ purity [molar %]
1. CES (Anderson et al., 2008)	Gou et al., 2006	Pilot scale	Combined cycle	ASU	CH ₄ /50.02	400	60.94	0.24/50	43.6	80–100	760–927	11.6	H ₂ O	99	100 (ideal)
2. NetPower (Allam et al., 2013)	R.J. Allam et al., 2013	Pilot scale	Regenerative Brayton	ASU	CH ₄ /50.02	250	—	—/70.5	55.1	300	1150	30	CO ₂	100 (ideal)	100 (ideal)
3. GRAZ (Sanz et al., 2005)	H. Jericha, 1985	Thermodynamic analysis (IPSEpro)	Quasi CC (Brayton and Rankine)	ASU	Syngas (0.1 CO ₂ , 0.4CO, 0.5H ₂ molar fraction)	74.75	63.30	0.25/55	52.5	180	1400	40	CO ₂ + H ₂ O — 79.26	100 (ideal)	93
4. S-GRAZ (Sanz et al., 2005)	W. Sanz et al., 2005	Thermodynamic analysis (IPSEpro)	Quasi CC (Brayton and Rankine)	ASU	Syngas (0.1 CO ₂ , 0.4CO, 0.5H ₂ molar fraction)	82.75	68.60	0.25/60.3	57.7	180	1400	40	CO ₂ + H ₂ O — 81.1	100 (ideal)	94
5. Modified GRAZ (Sanz et al., 2007)	H. Jericha et al., 2007	Thermodynamic analysis (IPSEpro)	Rankine + Quasi CC (Brayton and Rankine)	ASU	CH ₄ /50.02	400	66.55	0.25/54.84	53.09	180	1400	40	CO ₂ + H ₂ O	100 (ideal)	99
6. MATIANT (Mathieu and Nihart, 1999a; Mathieu and Nihart, 1999b)	P. Mathieu and E. Iantovski, 1998	Thermodynamic analysis (ASPEN+ & EES)	Quasi CC (Brayton with reheat and Brayton)	ASU	NG/42	642.5 kJ/kg CO ₂ recirculated	49.20	0.28/44.2	44.2(CO ₂ compression in cycle)	300	1300	40	CO ₂ — 92	99.98	99
7. E-MATIANT (Mathieu, 2004)	S. Houyou, P. Mathieu and R. Nihart, 1999	Thermodynamic analysis (ASPEN+ & EES)	Regenerative Brayton with reheat	ASU	NG/42	560 kJ/kg CO ₂ recirculated	60	0.25/47	47 (CO ₂ compression in cycle)	110	1300	60	CO ₂	99	99
8. CC-MATIANT (Bolland et al., 2001)	S. Houyou, P. Mathieu and R. Nihart, 1999	Thermodynamic analysis (ASPEN+ & EES)	Combined cycle with reheat	ASU	NG/42	605 kJ/kg CO ₂ recirculated	—	—	49.75(CO ₂ compression in cycle)	210	1300	—	CO ₂	99	99
9. AZEP 100% (Sundkvist et al., 2004; Möller et al., 2006)	S. Sundkvist et al., 2001	Lab Scale	Combined cycle (Brayton with air)	ITM	NG/48.43	45.7	48.40	—	47.9	20	1200	18	CO ₂ + H ₂ O — ≈90	100	—
10. AZEP 85% (Sundkvist et al., 2004; Möller et al., 2006)	S. Sundkvist et al., 2001	Thermodynamic analysis (IPSEpro)	Combined cycle (Brayton with air) with reheat	ITM	NG/48.43	53.3	50.30	—	49.8	20	1327	—	CO ₂ + H ₂ O — ≈90	85	—
11. SCOC-CC (Sanz et al., 2005)	W. Sanz et al., 2007	Thermodynamic analysis (IPSEpro)	Combined cycle	ASU	CH ₄ /50.02	400	61.45	0.25/51.68	49.75	120	1400	40	CO ₂ — 90.6	100 (ideal)	98.8
12. ZEITMOP (Yantovski et al., 2004)	E. Yantovsky et al., 2002	Thermodynamic analysis (ASPEN+)	Brayton with air + quasi CC (two Brayton cycles)	ITM	CH ₄ /50.02	25.46	50.9	—	50.9 (CO ₂ compression in cycle)	210	1400	14	CO ₂ — 93	100 (ideal)	—
13. OXYF-REF (Zhang and Lior, 2008a, 2008b)	N. Zhang and N. Lior, 2008	Thermodynamic analysis (ASPEN+)	Quasi CC (Brayton and Rankine)	ASU	NG/46.3	404.84	64.33	—/55.42	50.82	150	1300	15	CO ₂ + H ₂ O — 74.1	100 (ideal)	84

(continued on next page)

Table 1 (continued)

Cycle name	Developers/ year	Current status	Processes	Air separation system	Fuel/LHV [MJ/kg]	Net power [MW]	Gross efficiency [%]	O ₂ separation work [kWh/kg]/ efficiency [%]	Net efficiency [%]	Highest pressure [bar]	TIT [°C]	TIP [bar]	Recirculation gas [w/w %]	Carbon captured [%]	CO ₂ purity [molar %]
14. COOLCEP-S (Liu et al., 2008)	S Deng et al., 2002	Thermodynamic analysis (ASPEN+)	Regenerative Rankine-like	ASU	LNG/49.2	20	59.1	0.22/52.29	52.29 (no CO ₂ compression considered)	73.5	900	28	CO ₂ – 97	100	100 (ideal)
15. Water-steam Rankine cycle with a steam- CO ₂ recuperative –reheat cycle (Gou et al., 2006)	C. Gou, R. Cai, and H. Hong, 2006	Thermodynamic analysis (ASPEN+)	Quasi CC (Brayton with reheat and Rankine)	ASU	CH ₄ /50.02	67.63	–	0.25/–	47.12	300	1300	38.8	H ₂ O	>99	>99
16. Water-steam Rankine cycle with steam- CO ₂ recuperative –reheat cycle and a topping Brayton cycle (Gou et al., 2006)	C. Gou, R. Cai, and H. Hong, 2006	Thermodynamic analysis (ASPEN+)	Quasi CC (Brayton with reheat and Rankine)	ASU	CH ₄ /50	72.56	–	0.25/–	50.64	300	1300	38.8	H ₂ O (COMB1) and CO ₂ + H ₂ O (COMB2)	>99	>99
17. Novel O ₂ /CO ₂ (Cao and Zheng, 2006)	W. Cao and D. Zheng, 2006	Thermodynamic analysis (ASPEN+)	Regenerative Brayton	ASU	CH ₄ /50.02	24.8	59.5	0.28/51.1	48.9	10	1300	8.85	CO ₂ – 95.6	100 (ideal)	99.5
18. LNG quasi- combined supercritical CO ₂ Rankine cycle (Zhang and Lior, 2006)	N. Zhang and N. Lior, 2003	Thermodynamic analysis	Quasi CC (Brayton and Rankine-like)	ASU	CH ₄ /50.02 (Assumed that LNG is CH ₄)	71.4	72.3	0.25/65.1	65	156	1300	29.1	CO ₂ – 94.3	100 (ideal)	100 (ideal)
19. ZE-SOURGT (Luo and Zhang, 2011)	Zhang and Lior, 2012	Thermodynamic analysis (ASPEN+)	Quasi CC (Brayton and Rankine)	ASU	CH ₄ /50.03	496.07	61.54	0.25/54.27	50.7	157.5	1308	14.55	CO ₂ + H ₂ O – 59	100 (ideal)	87

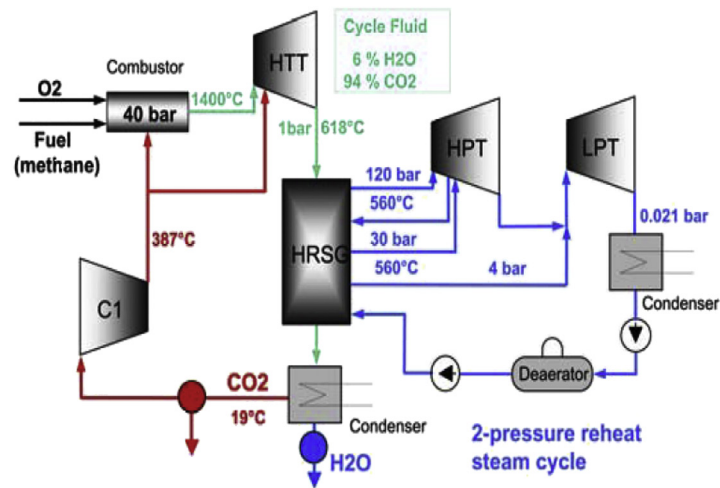
Table 2
Classification of oxy-turbine cycles by recirculation fluid.

Recirculated working fluid		
CO ₂	H ₂ O	CO ₂ + H ₂ O
NetPower	CES	Graz cycles ^a
MATANT ^a	Water cycles ^a	AZEP ^a
SCOC-CC		OXYF-REF
ZEITMOP		ZE-SOLRGT
COOLCEP-S		
Novel O ₂ /CO ₂		
LNG quasi-combined		

^a Refers to all their variants.

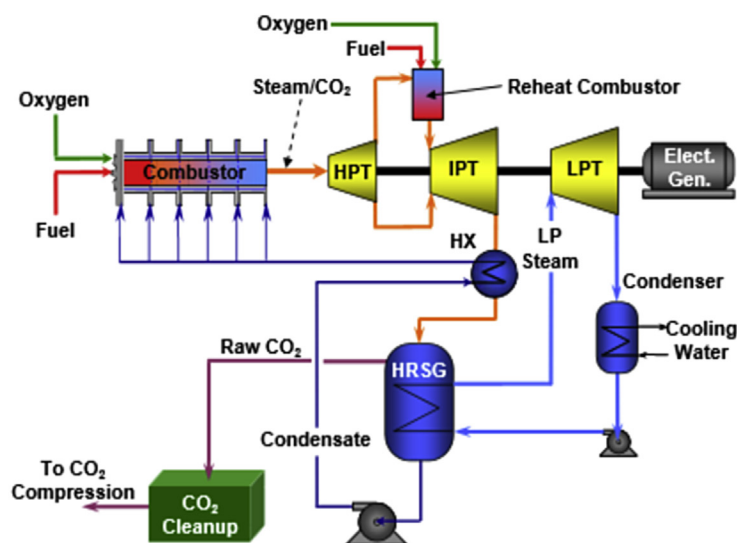
The last group includes those cycles which recirculate a mixture of CO₂ and H₂O. The S-Graz cycle uses this process as it is represented in Fig. 3.

Depending on the recirculation of working fluid in gas turbines (CO₂, H₂O and CO₂ + H₂O), oxy-fuel technologies benefit or suffer depending on their cycles. First of all, recycling CO₂ minimises the CCS costs by the use of almost 96% of the total CO₂; however, the turbomachinery must be completely redesigned (gas turbine, combustor, compressor and heat exchanger) since higher temperatures and pressures are achieved (Tak et al., 2010). In addition, the materials suffer from some limitations such as corrosion and incomplete combustion due to high levels of CO, H₂ and OH⁻ (Bolland and Mathieu, 1998). In the second case, H₂O (steam) lowers capital costs whilst increasing the net efficiencies, since



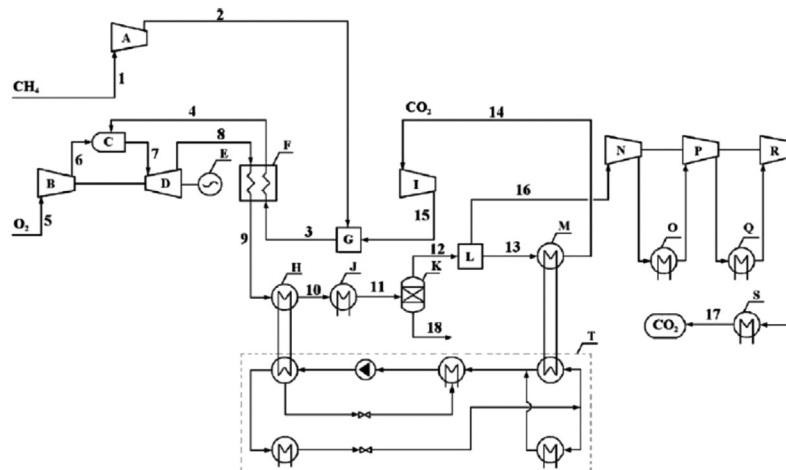
Legend: C1 – Compressor, HTT – High-temperature turbine, HRSG – Heat recovery steam generator, HPT – High-pressure turbine, LPT – Low-pressure turbine

Fig. 1. SCOC-CC schematic (Sanz et al., 2005).



Legend: HX – Heat Exchanger, HTT – High-temperature turbine, HRSG – Heat recovery steam generator, HPT – High-pressure turbine, IPT – Intermediate-pressure turbine, LPT – Low-pressure turbine

Fig. 2. CES cycle schematic (Anderson et al., 2008).



Legend: A CH₄ compressor, B O₂ compressor, C combustor, D turbine, E generator, F CO₂-NG reformer, G mixer, H heat exchanger, I CO₂ compressor, J cooler, O&Q intercooler, K separator, L splitter, M CO₂ inlet cooler, N,P,R compressor, S condenser, T ammonia absorption refrigeration

Fig. 4. Novel O₂/CO₂ cycle schematic (Cao and Zheng, 2006).

fluid and optimising the HRSG, minimising fuel and oxygen consumption. However, in general, they produce low cycle efficiency compared to the standard oxy-turbine cycles. In addition, they are highly affected by the intermittency of solar radiation due to seasonality and geographical limitations.

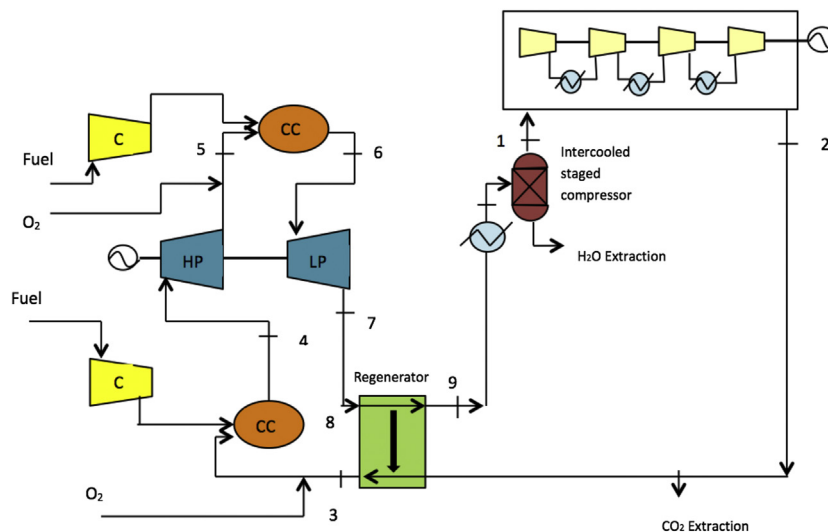
1.3.2. Biomass

Currently, biomass is used as fuel in oxyfuel technologies by using it with different types of coal (anthracite, bituminous, peat and lignite) in a boiler to generate steam. However, the use of solid fuels in oxy-turbine cycles would damage the turbine when flue gases are expanded. The possibility of implementing solid fuels (coal) in an oxy-turbine cycle was studied by Oki et al. (Kidoguchi et al., 2011). They concluded that it would be feasible only by integrating a gasifier into a combined cycle (IGCC). On the other hand, several thermogravimetric analyses have been conducted to

study the feasibility of employing biomass in oxy-turbine cycles. These studies suggest the possibility of using several biological feedstocks such as forest residues (e.g., from poplar and switch-grass), agricultural residues (e.g., corn stover, sugarcane bagasse, pine sawdust, torrefied pine sawdust and olive pits) and waste (e.g., MSW, sewage sludge and slurry) (López et al., 2014, 2015).

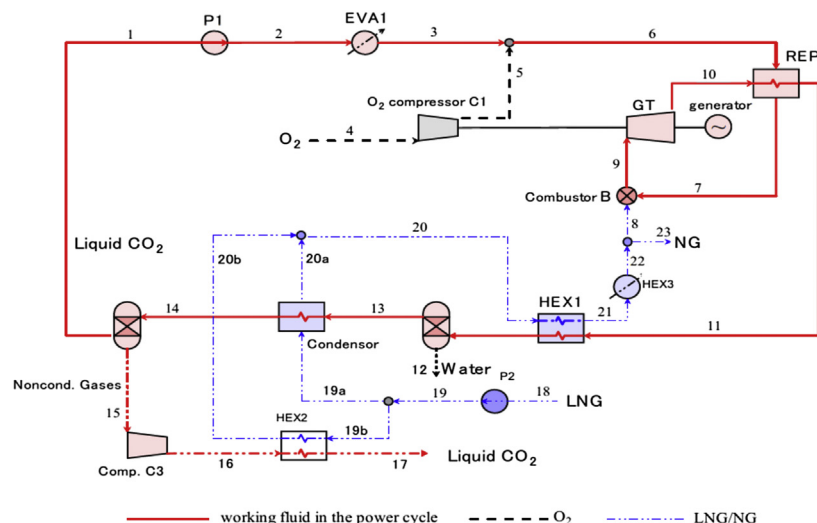
1.3.3. Biofuels (liquid and gaseous states)

There are studies on the use of biofuels such as diesel, ethanol and glycerol (previously treated) in oxy-turbine power plants (Beatrice et al., 2013, 2014; Asdrubali et al., 2015). Indeed, CES offers assurances that its technology is ready to be fuelled from landfill gas, bio-digester gas and glycerine (glycerol) followed by oxyfuel combustion. Additionally, oxyfuel technologies can help third and fourth generation biofuels since both microalgae and bio-engineered microbes are fed with sequestered CO₂ to grow and



Legend: C – Compressor, CC – Combustion chamber, HP – High-pressure turbine, LP – Low-pressure turbine

Fig. 5. E-MATANT cycle schematic (Llorente, 2013).



Legend: P1 & P2 – Pump; HEX1 HEX2, HEX3 – Heat Exchanger; EVA1 – Evaporator; REP – Regenerator; GT – Gas turbine; NG – Natural gas; LNG – Liquefied natural gas

Fig. 6. COOLCEP-S Cycle schematic (Liu et al., 2008).

produce biofuels such as ethanol, diesel, jet fuel and gasoline (Chen et al., 2013).

2. Research methodology

The evaluation of each oxy-turbine cycle is based on a PESTLE risk analysis which stands for assessments of the cycles from Political, Environmental, Social, Technological, Legislative and Economic (PESTLE) points of view (ToughNickel, 2016). The complexity of evaluating the political, legislative and social factors for each cycle has led to a general analysis of these three aspects applied to the CCS field without going into detail for each specific cycle.

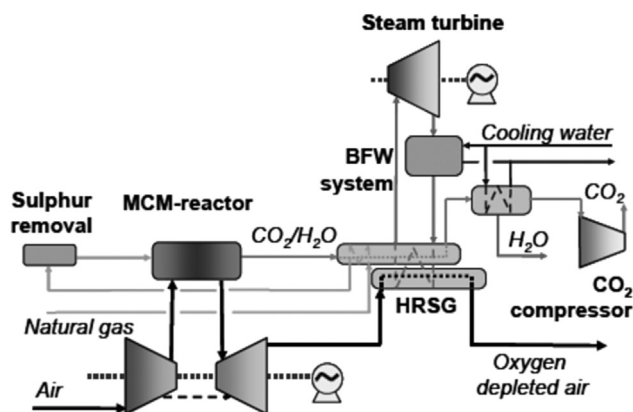
A Multi-Criteria Decision Analysis (MCDA) has been carried out to evaluate the technological, economic, environmental and social factors using DECERNS software (Sullivan et al., 2009). This type of analysis evaluates different alternatives attending to different factors, which have a certain weight assigned in order to decide which alternative is the most appropriate. Due to better availability of the technical information in the literature, AZEP, CES, E-MATIANT,

Modified Graz, NetPower and SCOC-CC have been chosen for this analysis. The results of this study enable the identification of the best cycle for the considered factors. Our contribution is to conduct a MCDA according to the data found in the literature, thus, a robust comparison between the most developed oxy-fuel cycles and a base case (CCGT) can be done.

2.1. Political and legislative

In general, CCS is a developing technology that has not yet been proven at large scale. It has been estimated that commercial power plants with CCS technology will not be deployed until the second tranche of units is built (Chalmers and Gibbins, 2010). The first tranche will, therefore, be useful to identify the technical problems that can arise in real power plants with these technologies. Consequently, several political measures should be applied with the intention of enhancing the economic viability of this type of power plant.

The main driver that will make CCS technology profitable for



Legend: BFW – Boiled feed water, MCM – Oxygen mixed conducting membrane, HRSG – Heat recovery steam generator

Fig. 7. AZEP cycle schematic (Möller et al., 2006).

to a specific stage of development according to the literature review and reports of the oxy-fuel technologies, as shown in Table 4.

2.3. Economic

The two factors used for the economic evaluation are the cost of electricity (COE) which describes how much it costs to generate 1 kWh of electricity taking into account all the expenses to produce this amount of energy (e.g., fuel cost, operation, etc.) and the capital costs (CAPEX). Although the COE seems to be more significant in terms of power plant benefits, a low CAPEX will attract stakeholders to invest in it. For this reason, the same weight (50%) has been assigned to both factors.

The economic data provided for each cycle have different assumptions depending on factors such as the power plant size, the fuel price, the discount rate, etc. Thus, in order to show the results and make them comparable, the costs for each cycle have been divided by the costs for its reference plant (CCGT), obtaining a ratio that represents their overcost. For instance, taking into account a COE of 39.5 €/MWh for the CCGT and 53.32 €/MWh for the AZEP 100% the COE overcost ratio is 1.35. The overcost ratio of each cycle is shown in Table 5.

However, it is important to take into account that these costs include the implementation and financing of these cycles as a project but R&D investment is not included, which would increase the cost considerably. This investment will depend on the complexity and novelty of the cycle and components on them but these costs cannot be estimated by the authors of this study.

2.4. Environmental

The environmental aspect of the different cycles has been evaluated based on the Life Cycle Assessment (LCA). This technique assesses the environmental impacts associated with all stages of a product's life from cradle to grave. Hence, it evaluates the equivalent CO₂ emissions per kWh that each cycle releases during the 25 years of its life cycle including the construction of the plant, the emissions emitted during its use considering possible losses in compressors and during transport, the maintenance and repair operations and the demolition of the plant. Table 6 shows these emissions.

2.5. Social

With the aim of determining the social opinion related to CCS as well as the public investment in this field, the authors of this report conducted a survey which was answered by 136 people between 17 and 61 years of age, where most of the respondents (92%) were between 20 and 30 years old. Moreover, 83% of the samples are science graduates; of these 42% of the degrees are related to

sustainability or environmental science. Here the sampling method is based on the convenience sampling procedure where subjects are selected because of their convenient accessibility and proximity to the researcher (Peterson and Merunka, 2014).

Although most of the respondents were science graduates, first of all a brief introduction describing the CCS process was presented in order to provide a closer picture of the topic to the respondents. The samples were not restricted only to people with a degree related with this topic and, thus, have a wider social opinion. Then, the respondents were asked some personal questions related to their age, their educational background and where they lived (to determine whether their proximity to a power plant affected their survey responses). The survey continued with questions regarding their previous knowledge about CCS techniques and it finished with specific enquiries about their opinion on economic investment by the government for this type of technology.

The results showed that 86% of the respondents would support government investment in CCS technologies, although if they had to choose between CCS and renewable technologies, 82% would choose the latter. From this 82%, 56% claimed not to have heard about CCS before.

Of the 14% who did not support investment in CCS technologies, almost half did not know anything about CCS. The rest noted that they had heard about this concept before but 80% of them were not capable of naming any specific technique.

Although 36% of the respondents had some education related to sustainability or environmental science, 37.5% of this 36% had never been told about CCS. 86% of the respondents from this 36% would prefer that the government invested in renewables instead of CCS technologies.

The answers obtained from the survey were compared to the social opinion from the literature. Thus, Van Alphen et al. (2007) carried out an analysis in which they state that the social opinion should be divided into two sectors: stakeholders and general public. Stakeholders are agents who have a professional interest in CCS such as the industry, the government and the non-governmental organisations (NGOs), whereas all the other opinions are included in the general public. The authors stated that it is necessary to analyse their opinion because their perception of CCS is quite different; while the stakeholders have knowledge about CCS, the public in general does not have an *a priori* point of view and in many cases its responses to questionnaires are affected by the sparse information provided by the interviewers. The stakeholders' support on CCS technologies is based on five factors: safety, temporality/partiality (it should not be a permanent technique), financial stimulation, cooperation/commitment between the different parties such as government, experts and stakeholders, and open communication with the local communities (Wennersten et al., 2015).

All these factors are governed by two facts: renewable

Table 5
CAPEX and COE overcost ratio of each selected cycle.

	AZEP 100% (Möller et al., 2006)	CCGT	CES (Anderson et al., 1998)	E-MATIAN (Houyou et al., 2000)	Modified Graz (Sanz et al., 2005)	NetPower	SCOC-CC (Sanz et al., 2005)
CAPEX overcost	1.23	1	1.36	1.1	1.69	1.27	1.64
COE overcost	1.35	1	1.1	1.1	1.2	1.04	1.26

Table 6
CO₂ emissions for each selected cycle.

	AZEP 100% (Sundkvist et al., 2004)	CCGT (Spath and Mann, 2000)	CES	E-MATIAN (Lombardi, 2003)	Modified Graz	NetPower (Allam, 2016)	SCOC-CC
gCO ₂ eq/kWh	19	366	21	29.84	26.1	8	25.33

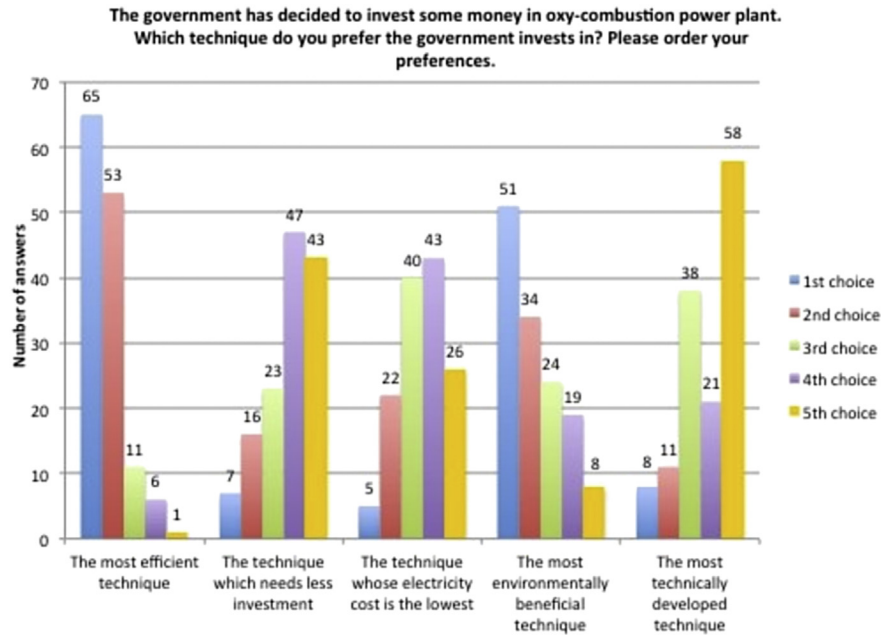


Fig. 9. Responses to the last question of the survey.

technologies should have priority if they can be well established, and both safety and effects should be studied thoroughly before implementing these technologies.

The survey carried out matches with the Van Alphen et al. study in two facts: the general public presents a lack of knowledge on CCS technologies; and society prefers renewable technologies rather than CCS.

In the last question of the survey, the respondents were asked to order different alternatives related to aspects that the government should take into account when investing public funding in a CCS oxy-power plant. The results can be found in Fig. 9.

The social factor has been studied according to the last question of the survey. Thus, each alternative appeals to a specific cycle characteristic that can be used as a criterion to evaluate the social factor.

Hence, the importance that people gave to the different characteristics has been scored from 1 to 5, 5 being the value attributed to the first-preferred one. This value was obtained using the equation shown below (Eq. (2)), normalising it afterwards. Each one of these characteristics has been related to one of the cycle parameters obtained from the literature in order to analyse the different alternatives following an MCDA. The related parameter to each characteristic, score obtained for each factor and its respective normalised value can be observed in Table 7.

Table 7
Weighted and normalised values of each characteristic for the social factor.

Characteristic	Related parameter	Weighted value	Normalised value
The most efficient	Net efficiency	4.29	0.329
The one which needs less investment	CAPEX overcost	2.24	0.124
The one whose electricity cost is the lowest	COE overcost	2.54	0.154
The most environmentally beneficial	CO ₂ eq	3.74	0.274
The most technically developed	Readiness	2.19	0.119

$$\text{Weighted Value}_i = \frac{5 \times N_{i,1} + 4 \times N_{i,2} + 3 \times N_{i,3} + 2 \times N_{i,4} + 1 \times N_{i,5}}{N_{\text{total}}} \quad (2)$$

i = characteristic

j = 1st, 2nd, 3rd, 4th or 5th choice

N_{ij} = Number of answers for characteristic i as choice j

N_{total} = Total number of respondents (always 136)

3. Results and discussion

When the data were entered in the DECERNS software, one cycle was ranked highest for each factor following a Multi-Criteria Decision Analysis.

3.1. Technological

The best performing cycle in terms of technology is, without considering the CCGT, the NetPower cycle. However, the Modified Graz cycle has a similar score to that of the NetPower. The results of the analysis can be seen in Fig. 10.

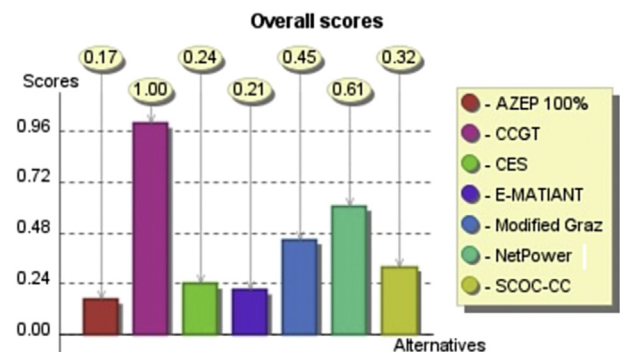
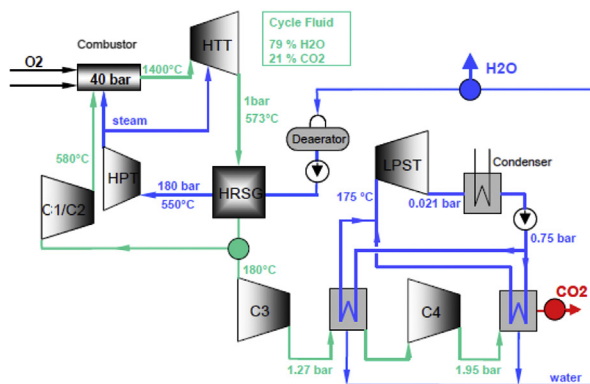


Fig. 10. MCDA results for the technological factor.



Legend: C1/C2, C3 & C4 – Compressor, HTT – High-temperature turbine, HRSG – Heat recovery steam generator, HPT – High-pressure turbine, LPST – Low-pressure steam turbine

Fig. 11. Modified Graz cycle schematic (Sanz et al., 2007).

The Modified Graz and NetPower cycles are represented in Figs. 11 and 12, respectively.

3.2. Economic

The most economically beneficial is, without considering the CCGT, the E-MATIANT cycle (Fig. 5) followed closely by the NetPower (Fig. 12). The results of this analysis can be seen in Fig. 13.

3.3. Environmental

Fig. 14 shows the overall scores for the different cycles regarding their environmental benefits, meaning that the best cycle in terms of emissions is the NetPower, although the results are skewed because of the high amount of emissions released by the CCGT.

3.4. Social

Following the methodology explained in Section 2.5, the social

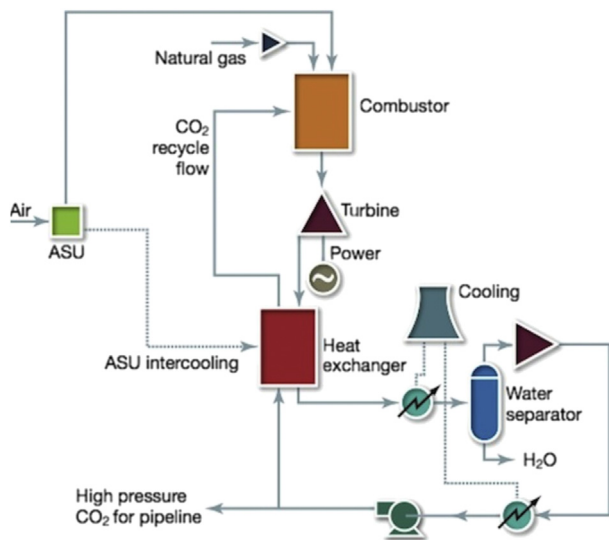
evaluation results are shown in Fig. 15.

The NetPower cycle is the best solution in social terms with a higher score even than for the CCGT.

3.5. Overall results

A way of summarising the results provided by the MCDA is by plotting them in a radial graph (Fig. 16) where the four axes represent each of the aspects considered above.

When all factors are given equal weight, the NetPower is the cycle which stands out from the others, including the CCGT. The assigned weight was equal for each factor because, depending on the sector that analyses the scenario, the importance given to each factor would vary. Although the CCGT has the maximum score in economic and technological factors, its score of 0 in the



Legend: ASU – Air separation unit

Fig. 12. NetPower cycle schematic (Allam, 2016).

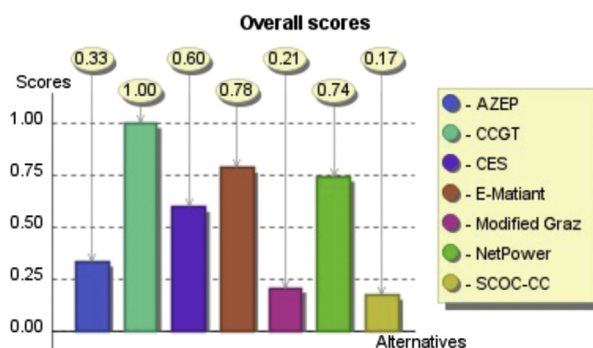


Fig. 13. MCDA results for the economic factor.

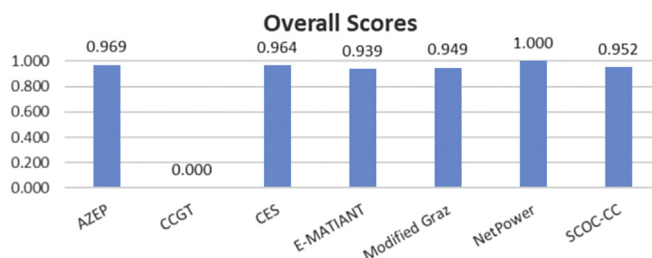


Fig. 14. Results for the environmental factor.

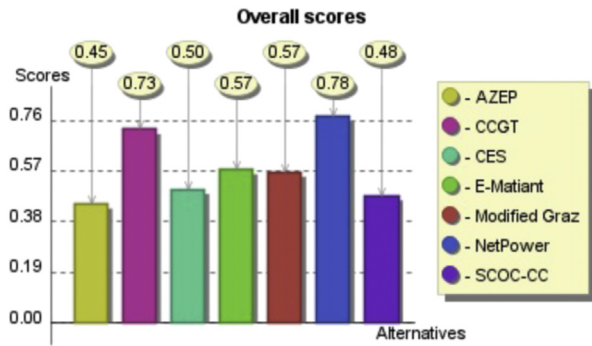


Fig. 15. MCDA results for social factor.

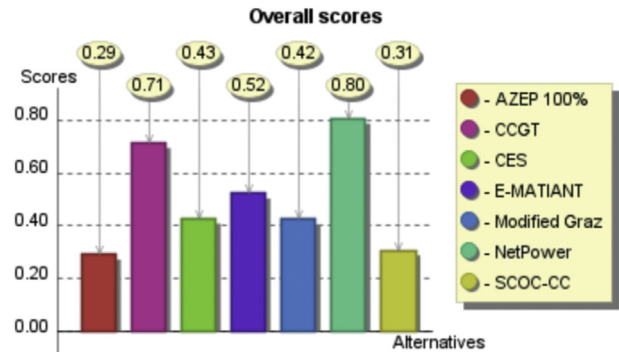


Fig. 17. MCDA of the final results.

environmental factor lowers its overall mark. Fig. 17 shows the final multi-criterial results of all the cycles showing that NetPower has the best overall performance.

The NetPower cycle has a simple design offering high efficiency which provides power generation and CO₂ capture with low investment and low COE. Also, if a Life Cycle Assessment is considered (Allam, 2016) it is the lowest in terms of CO₂e emissions. The main drawback is that the thermodynamic data (e.g., LHV net efficiency) vary markedly depending on the source (company or independent researchers). However, recent publications as well as peer-review have demonstrated a more accurate value compared to past studies (IEAGHG, 2015).

In order to increase the scores for the other cycles, raising them to the NetPower level, their technological and economic aspects must be improved. The adoption of political measures such as CO₂ Tax and Emission Allowances could enhance the undeveloped technologies offering public funding to those technologies that still need to be supported by the government in order to be more attractive economically. However, the result of these measures would be different for each cycle. Hence, more investment by governments would increase the readiness level of cycles but other intrinsic parameters such as the efficiency or the cost in terms of materials and equipment would not vary since they depend on the complexity of the cycles themselves (Wennersten et al., 2015).

4. Conclusions

Nineteen oxy-turbine power cycles were summarised in terms of their main characteristics and parameters, and six of these cycles were analysed. This technical review concludes most of the cycles (except CES and NetPower) are in the early development stage and mainly studied only from a thermodynamic perspective. Overall, all of the oxy-turbine cycles involve complex schemes which require technically advanced equipment but they offer high efficiencies for power generation, while at the same time, offering nearly perfect CO₂ capture without generating hazardous emissions such as NO_x and the best overall cycle efficiencies. Oxy-turbine power cycles also provide net efficiencies up to 65%, comparable to a combined cycle gas turbine (CCGT) power plant (58–60%).

Renewable sources such as solar, biomass and biofuels have also been proposed in some oxy-turbine cycles. Generally, the application of renewable technologies in these cycles does not provide significant advantages in terms of design and efficiency. However, the benefits of renewable implementation are the reduction in fossil fuel consumption and, in the case of solar, decrease in the required oxygen supply providing this can be done without major loss of efficiency or other problems.

The PESTLE analysis has shown that from a political and legislative point of view, the oxy-turbine cycles need to be supported by

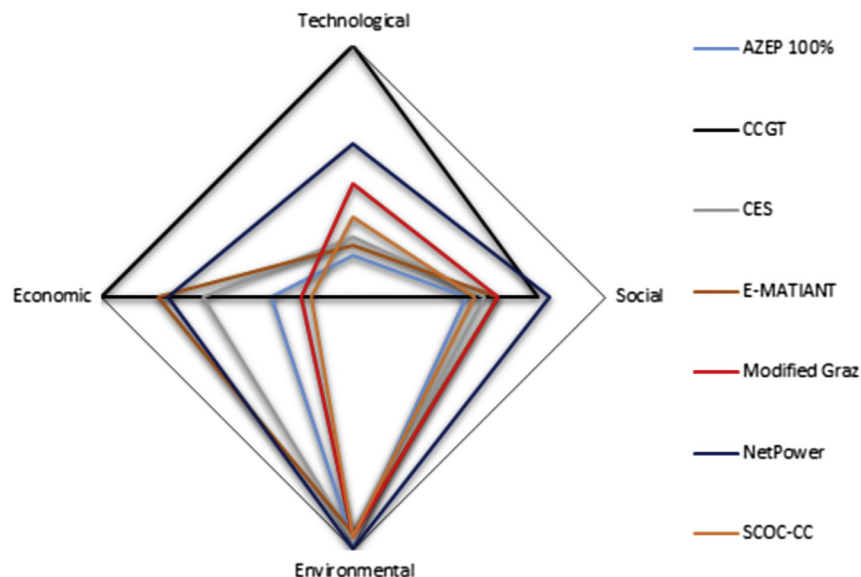


Fig. 16. Radial graph of the MCDA results.

government measures that attract stakeholders to invest in these clean technologies. Concerning social opinion, a survey has been carried out in which 136 respondents were asked specific questions regarding CCS. Their answers show that, in general, society is unaware of the existence and requirement for these techniques, which is in agreement with previous studies on the subject. This lack of public knowledge about CCS science causes the public to favour renewable options instead of CCS technologies even when the latter are more cost effective.

From the MCDA, the NetPower cycle was identified as the best option among the oxy-turbine cycles proposed for the PESTLE analysis. Further research needs to be carried out in order to demonstrate the reliability of these cycles in real industrial situations. For instance, high temperatures and flue gas composition cause an aggressive environment which implies that materials selection needs to be carefully addressed and demonstrated in trials carried out over extensive periods.

Acknowledgements

The editorial assistance of Dr David Granatstein is very much appreciated. Finally, the authors would also like to note that the first three authors have made equal contributions to this work as part of a graduate project.

References

- Allam, R.J., 2016. NET Power's CO₂ Cycle: the Breakthrough that CCS Needs. Available at: <http://www.modernpowersystems.com/features/feature-net-powers-co2-cycle-the-breakthrough-that-ccs-needs> (accessed: 12.08.15.).
- Allam, R.J., Palmer, M.R., Brown, G.W., Fetvedt, J., Freed, D., Nomoto, H., Itoh, M., Okita, N., Jones, C., 2013. High efficiency and low cost of electricity generation from fossil fuels while eliminating atmospheric emissions, including carbon dioxide. *Energy Procedia* 37, 1135–1149. <http://dx.doi.org/10.1016/j.egypro.2013.05.211>.
- Anderson, R.E., Brandt, H., Mueggenburg, H., Taylor, J., Viteri, F., 1998. A power plant concept which minimizes the cost of carbon dioxide sequestration and eliminates the emission of atmospheric pollutants. In: Fourth International Conference of Greenhouse Gas Technologies. Interlaken, Switzerland. Available at: <http://www.co2.no/download.asp?DAFID=30&DAID=4>.
- Anderson, R.E., MacAdam, S., Viteri, F., Davies, D.O., Downs, J.P., Paliszewski, A., 2008. Adapting gas turbines to zero emission oxy-fuel power plants. *Proc. ASME Turbo Expo* 2, 781–791. <http://dx.doi.org/10.1115/GT2008-51377>.
- Anderson, R., Viteri, F., Hollis, R., Keating, A., Shipper, J., Merrill, G., Schillig, C., Shinde, S., Downs, J., Davies, D., Harris, M., 2010. Oxy-fuel gas turbine, gas generator and reheat combustor technology development and demonstration. *Proc. ASME Turbo Expo* 3, 733–743. <http://dx.doi.org/10.1115/GT2010-23001>.
- Asdrubali, F., Cotana, F., Rossi, F., Presciutti, A., Rotili, A., Guattari, C., 2015. Life cycle assessment of new oxy-fuels from biodiesel-derived glycerol. *Energies* 8, 1628–1643. <http://dx.doi.org/10.3390/en8031628>.
- Beatrice, C., Di Blasio, G., Lazzaro, M., Cannilla, C., Bonura, G., Frusteri, F., Asdrubali, F., Baldinelli, G., Presciutti, A., Fantozzi, B., Bidini, G., Bartocci, P., 2013. Technologies for energetic exploitation of biodiesel chain derived glycerol: oxy-fuels production by catalytic conversion. *Appl. Energy* 102, 63–71. <http://dx.doi.org/10.1016/j.apenergy.2012.08.006>.
- Beatrice, C., Di Blasio, G., Guido, C., Cannilla, C., Bonura, G., Frusteri, F., 2014. Mixture of glycerol ethers as diesel bio-derivable oxy-fuel: impact on combustion and emissions of an automotive engine combustion system. *Appl. Energy* 132, 236–247. <http://dx.doi.org/10.1016/j.apenergy.2014.07.006>.
- Bolland, O., Mathieu, P., 1998. Comparison of two CO₂ removal options in combined cycle power plants. *Energy Convers. Manag.* 39 (16–18), 1653–1663. [http://dx.doi.org/10.1016/S0196-8904\(98\)00078-8](http://dx.doi.org/10.1016/S0196-8904(98)00078-8).
- Bolland, O., Kvamsdal, H.M., Boden, J.C., 2001. A thermodynamic comparison of the oxy-fuel power cycles water-cycle, Graz-cycle and Matiant cycle. In: Proceedings of the International Conference POWER Generation and Sustainable Development. Association of Engineers from the Montefiore Electrical Institute (AIM), Liege, Belgium. Available at: http://www.graz-cycle.tugraz.at/pdfs/Bolland_Kvamsdal_Boden_Liege.pdf.
- Cao, W., Zheng, D., 2006. Exergy regeneration in an O₂/CO₂ gas turbine cycle with chemical recuperation by CO₂ reforming of methane. *Energy Convers. Manag.* 47 (18), 3019–3030. <http://dx.doi.org/10.1016/j.enconman.2006.03.010>.
- Chalmers, H., Gibbins, J., 2010. Carbon capture and storage: the ten year challenge. *Proc. Inst. Mech. Eng. Part C J. Mech. Eng. Sci.* 224 (3), 505–518. <http://dx.doi.org/10.1243/09544062JMES1516>.
- Chalmers, H., Gibbins, J., Lucquiaud, M., 2009. Retrofitting CO₂ capture to existing power plants as a fast track mitigation strategy. In: ASME 2009 3rd International Conference on Energy Sustainability Collocated with the Heat Transfer and InterPACK09 Conferences. American Society of Mechanical Engineers, pp. 669–678. <http://dx.doi.org/10.1115/ES2009-90401>.
- Chase, D.L., Kehoe, P.T., 2010. GE Combined-Cycle Product Line and Performance. GE Power Systems, Schenectady. Available at: www.ge-3574g-ge-cc-product-line-performance.pdf.
- Chen, C., Lu, Z., Ma, X., Long, J., Peng, Y., Hu, L., Lu, Q., 2013. Oxy-fuel combustion characteristics and kinetics of microalgae *Chlorella vulgaris* by thermogravimetric analysis. *Bioresour. Technol.* 144, 563–571. <http://dx.doi.org/10.1016/j.biortech.2013.07.011>.
- Department of Energy & Climate Change, 2013. Greenhouse Gas Emissions, Final Figures. National Statistics, London, UK. <http://www.gov.uk/government/collections/uk-greenhouse-gas-emissions-statistics>.
- EndesaCiuden, Wheeler, Foster, 2013. OXYCFB300 Compostilla. Carbon Capture and Storage Demonstration Project, Knowledge Sharing FEED Report. Available at: <http://ccsnetwork.eu/publications/oxyfcb300-compostilla-carbon-capture-and-storage-demonstration-project-knowledge-sharing-feed-report> (accessed: 20.05.15.).
- Franco, F., Mina, T., Woolatt, G., Rost, M., Bolland, O., 2006. June. Characteristics of cycle components for CO₂ capture. In: Proceedings of 8th International Conference on Greenhouse Gas Control Technologies, Trondheim, Norway. Available at: http://www.graz-cycle.tugraz.at/pdfs/franco_et_al_ghg_2006.pdf.
- Global CCS Institute, 2013. The Callide OxyFuel Project. Available at: www.globalccsinstitute.com/insights/authors/dennisvanpuyvelde/2013/02/13/callide-oxyfuel-project (accessed: 20.05.15.).
- Gou, C., Cai, R., Hong, H., 2006. An advanced oxy-fuel power cycle with high efficiency. *Proc. Inst. Mech. Eng. Part A J. Power Energy* 220 (4), 315–325. <http://dx.doi.org/10.1243/09576509JPE215>.
- Gou, C., Cai, R., Hong, H., 2007. A novel hybrid oxy-fuel power cycle utilizing solar thermal energy. *Energy* 32 (9), 1707–1714. <http://dx.doi.org/10.1016/j.energy.2006.12.001>.
- Hollis, R., Skutley, P., Ortiz, C., Varkey, V., LePage, D., Brown, B., Davies, D., Harris, M., 2012. Oxy-fuel turbomachinery development for energy intensive industrial applications. *Proc. ASME Turbo Expo* 3, 431–439. <http://dx.doi.org/10.1016/j.egypro.2014.11.056>.
- Houyou, S., Mathieu, P., Nihart, R., 2000. Techno-economic comparison of different options of very low CO₂ emission technologies. In: Proceedings of the Fifth International Conference on Greenhouse Gas Control Technologies, p. 1003. Available at: <https://books.google.es/books?isbn=0643066721>.
- IEAGHG, 2015. Oxy-Combustion Turbine Power Plants, Report 2015/05. Available at: <http://ieaghg.org/terms-of-use/49-publications/technical-reports/599-2015-05-oxy-combustion-turbine-power-plants>.
- Kidoguchi, K., Hara, S., Oki, Y., Kajitani, S., Umemoto, S., Inumaru, J., 2011. Development of oxy-fuel IGCC system with CO₂ recirculation for CO₂ capture – experimental examination on effect of gasification reaction promotion by CO₂ enriched using bench scale gasifier facility. *Am. Soc. Mech. Eng. Power Div. Publ. POWER* 2 (1), 485–492. <http://dx.doi.org/10.1115/POWER2011-55458>.
- Komaki, A., Gotou, T., Uchida, T., Yamada, T., Kiga, T., Spero, C., 2014. Operation experiences of oxyfuel power plant in Callide oxyfuel project. *Energy Procedia* 63, 490–496. <http://dx.doi.org/10.1016/j.egypro.2014.11.053>.
- Lee, M.Y., Hashim, H., 2014. Modelling and optimization of CO₂ abatement strategies. *J. Clean. Prod.* 71, 40–47. <http://dx.doi.org/10.1016/j.jclepro.2014.01.005>.
- Liu, M., Lior, N., Zhang, N., Han, W., 2008. Thermoeconomic optimization of COOLCEP-S: a novel zero-CO₂-emission power cycle using LNG (liquefied natural gas) coldness. In: Paper IMECE 2008-66467, Proceedings of IMECE 2008, 2008 ASME International Mechanical Engineering Congress and Exposition, October 31. <http://dx.doi.org/10.1115/IMECE2008-66467>.
- Llorente, R., 2013. CO₂ Capture in Power Plants-Using the Oxy-Combustion Principle (Master's thesis). Norwegian University of Science and Technology (NTNU), Trondheim, Norway. Retrieved from: <http://www.diva-portal.org/smash/get/diva2:652833/FULLTEXT01.pdf>.
- Lombardi, L., 2003. Life cycle assessment comparison of technical solutions for CO₂ emissions reduction in power generation. *Energy Convers. Manag.* 44 (1), 93–108. [http://dx.doi.org/10.1016/S0196-8904\(02\)00049-3](http://dx.doi.org/10.1016/S0196-8904(02)00049-3).
- López, R., Fernández, C., Fierro, J., Cara, J., Martínez, O., Sánchez, M.E., 2014. Oxy-combustion of corn, sunflower, rape and microalgae bioresidues and their blends from the perspective of thermogravimetric analysis. *Energy*. <http://dx.doi.org/10.1016/j.energy.2014.07.058>.
- López, R., Fernández, C., Martínez, O., Sánchez, M.E., 2015. Modelling and kinetics studies of a corn-rape blend combustion in an oxy-fuel atmosphere. *Bioresour. Technol.* 183, 153–162. <http://dx.doi.org/10.1016/j.biortech.2015.02.040>.
- Lu, X., 2014. Flexible Integration of the sCO₂ Allam Cycle with Coal Gasification for Low-Cost, Emission-Free Electricity Generation. 8 Rivers Capital [Online]. Available at: http://gasification.org/uploads/eventLibrary/2014_112_8_Rivers_Xijia_Lu.pdf (accessed: 25.02.15.).
- Luo, C., Zhang, N., 2011. Zero CO₂ emission SOLRGT system. In: Proceedings of the 24th International Conference on Efficiency, Cost, Optimization, Simulation and Environmental Impact of Energy Systems, ECOS 2011, pp. 3368–3400. <http://dx.doi.org/10.1016/j.energy.2012.04.058>.
- Luu, M.J., Milani, D., Abbas, A., 2016. Analysis of CO₂ utilization for methanol synthesis integrated with enhanced gas recovery. *J. Clean. Prod.* 112, 3540–3554. <http://dx.doi.org/10.1016/j.jclepro.2015.10.119>.
- Mathieu, P., 2004. Towards the hydrogen era using near-zero CO₂ emissions energy systems. *Energy* 29 (12–15 spec. iss.), 1993–2002. <http://dx.doi.org/10.1016/>

- j.energy.2004.03.007.
- Mathieu, P., Nihart, R., 1999. Zero emission MATIANT cycle. *Am. Soc. Mech. Eng. J. Eng. Gas Turbines Power* 121 (1), 116–120. <http://dx.doi.org/10.1115/1.2816297>.
- Mathieu, P., Nihart, R., 1999. Sensitivity analysis of the MATIANT cycle. *Energy Convers. Manag.* 40 (15), 1687–1700. [http://dx.doi.org/10.1016/S0196-8904\(99\)00062-X](http://dx.doi.org/10.1016/S0196-8904(99)00062-X).
- Möller, B.F., Torisson, T., Assadi, M., Sundkvist, S.G., Sjödin, M., Klang, Å., Åsen, K.I., Wilhelmsen, K., 2006. AZEP gas turbine combined cycle power plants – thermo-economic analysis. *Int. J. Thermodyn.* 9 (1), 21–28. Available at: <http://dergipark.ulakbim.gov.tr/eoguijt/article/view/1034000164/0>.
- Peterson, R.A., Merunka, D.R., 2014. Convenience samples of college students and research reproducibility. *J. Bus. Res.* 67 (5), 1035–1041. <http://dx.doi.org/10.1016/j.jbusres.2013.08.010>.
- Richards, G., Williams, M., 2012. Novel cycles: oxy-combustion turbine cycles. In: Rao, A.D. (Ed.), *Combined Cycle Systems for Near-Zero Emission Power Generation* Elsevier Science, pp. 186–219. Available at: <https://books.google.co.uk/books?isbn=0857096184> (Chap. 6).
- Røkke, P.E., Hustad, J.E., 2005. Exhaust gas recirculation in gas turbines for reduction of CO₂ emissions; combustion testing with focus on stability and emissions. In: ECOS 2005-Proceedings of the 18th International Conference on Efficiency, Cost, Optimization, Simulation, and Environmental Impact of Energy Systems, pp. 1427–1434. Available at: <http://dergipark.ulakbim.gov.tr/eoguijt/article/view/1034000158>.
- Sanz, W., Jericha, H., Moser, M., Heitmeir, F., 2005. Thermodynamic and economic investigation of an improved Graz cycle power plant for CO₂ capture. *J. Eng. Gas Turbines Power* 127 (4), 765–772. <http://dx.doi.org/10.1115/GT2004-53722>.
- Sanz, W., Jericha, H., Bauer, B., Göttlich, E., 2007. Qualitative and quantitative comparison of two promising OXY-fuel power cycles for CO₂ capture. *Proc. ASME Turbo Expo* 3, 161–173. <http://dx.doi.org/10.1115/1.2800350>.
- SCCS, 2015. Global CCS Map. Available at: [sccs.org.uk/expertise/global-ccs-map](https://www.sccs.org.uk/expertise/global-ccs-map) (accessed: 15.05.15.).
- Soothill, C.D., Bialkowski, M.T., Guidati, G.L., Zagorskiy, A., 2013. Carbon dioxide (CO₂) capture and storage for gas turbine systems. In: Jansohn, P. (Ed.), *Modern Gas Turbine Systems – High Efficiency, Low Emission, Fuel Flexible Power Generation* Woodhead Publishing, pp. 685–713 (Chap. 15). Available at: <https://books.google.es/books?id=cVREAgAAQBAJ&printsec=frontcover&hl=es#v=onepage&q&f=false>.
- Spath, P., Mann, M., 2000. Life Cycle Assessment of a Natural Gas Combined-Cycle Power Generation System. NREL/TP-570-27715. [Online]. Available at: <http://www.nrel.gov/docs/fy00osti/27715.pdf> (accessed: 05.05.15.).
- Sullivan, T., Yatsalo, B.I., Grebenkov, A., Linkov, I., 2009. Decision evaluation for complex risk network systems (DECERNS) software tool (Chapter 12). In: *Decision Support Systems for Risk-Based Management of Contaminated Sites*. Springer Book, pp. 257–274. Available at: http://link.springer.com/chapter/10.1007/978-0-387-09722-0_12#page-1.
- Sundkvist, S.G., Klang, Å., Sjödin, M., Wilhelmsen, K., Åsen, K., Tintinelli, A., McCahey, S., Ye, H., 2004. AZEP gas turbine combined cycle power plants – thermal optimisation and LCA analysis. In: *Proceedings of Seventh International Conference on Greenhouse Gas Control Technologies, GHGT-7*, Vancouver, Canada. <http://dx.doi.org/10.1016/B978-0-08044704-9/50027-6>.
- Sundkvist, S.G., Julsrud, S., Vigeland, B., Naas, T., Budd, M., Leistner, H., Winkler, D., 2007. Development and testing of AZEP reactor components. *Int. J. Greenh. Gas Control* 1 (2), 180–187. [http://dx.doi.org/10.1016/S1750-5836\(07\)00025-4](http://dx.doi.org/10.1016/S1750-5836(07)00025-4).
- Tak, S.H., Park, S.K., Kim, T.S., Sohn, J.L., Lee, Y.D., 2010. Performance analyses of oxy-fuel power generation systems including CO₂ capture: comparison of two cycles using different recirculation fluid. *J. Mech. Sci. Technol.* 24 (9), 1947–1954. Available at: <http://link.springer.com/article/10.1007%2Fs12206-010-0623-x>.
- ToughNickel, 2016. What Are the Driving Forces of PESTLE Analysis? Available at: <http://dommccg.hubpages.com/hub/What-is-PESTLE-analysis> (accessed on 26.05.16.).
- U. S. Department of Defence, 2011. Technology Readiness Assessment (TRA) Guidance. Revision Posted 13 May 2011. [Online]. Available at: <http://www.acq.osd.mil/chieftechologist/publications/docs/TRA2011.pdf> (accessed: 20.05.15.).
- Van Alphen, K., Tot Voorst, Q.V.V., Hekkert, M.P., Smits, R.E., 2007. Societal acceptance of carbon capture and storage technologies. *Energy Policy* 35 (8), 4368–4380. <http://dx.doi.org/10.1016/j.jbusres.2013.08.010>.
- Wennersten, R., Sun, Q., Li, H., 2015. The future potential for carbon capture and storage in climate change mitigation – an overview from perspectives of technology, economy and risk. *J. Clean. Prod.* 103, 724–736. <http://dx.doi.org/10.1016/j.jclepro.2014.09.023>.
- Yang, N., Wang, R., 2015. Sustainable technologies for the reclamation of greenhouse gas CO₂. *J. Clean. Prod.* 103, 784–792. <http://dx.doi.org/10.1016/j.jclepro.2014.10.025>.
- Yang, H.J., Kang, D.W., Ahn, J.H., Kim, T.S., 2012. Evaluation of design performance of the semi-closed oxy-fuel combustion combined cycle. *ASME J. Eng. Gas Turbines Power* 134 (11), 111702–111702-10. <http://dx.doi.org/10.1115/1.4007322>.
- Yantovski, E., Gorski, J., Smyth, B., Ten Elshof, J., 2004. Zero-emission fuel-fired power plants with ion transport membrane. *Energy* 29 (12–15 spec. iss.), 2077–2088. Available at: <http://doc.utwente.nl/75712/>.
- Zhang, N., Lior, N., 2006. Proposal and analysis of a novel zero CO₂ emission cycle with liquid natural gas cryogenic exergy utilization. *J. Eng. Gas Turbines Power* 128 (1), 81–91. <http://dx.doi.org/10.1115/1.2031228>.
- Zhang, N., Lior, N., 2008. Comparative study of two low CO₂ emission power generation system options with natural gas reforming. *J. Eng. Gas Turbines Power* 130 (5). <http://dx.doi.org/10.1115/1.2904895> art. No. 051701.
- Zhang, N., Lior, N., 2008. Two novel oxy-fuel power cycles integrated with natural gas reforming and CO₂ capture. *Energy* 33 (2), 340–351. <http://dx.doi.org/10.1016/j.energy.2007.09.006>.

GT2004-53359

CHEMICAL LOOPING COMBUSTION- ANALYSIS OF NATURAL GAS FIRED POWER CYCLES WITH INHERENT CO₂ CAPTURE

Rehan Naqvi, Olav Bolland, Øyvind Brandvoll, Kaare Helle
Norwegian University of Science and Technology (NTNU)
Norway

ABSTRACT

In this paper an alternative to so-called ‘oxy-fuel’ combustion has been evaluated. Chemical Looping Combustion (CLC) is an innovative concept of CO₂ capture from combustion of fossil fuels in power plants. CLC is closely related to oxy-fuel combustion as the chemically bound oxygen reacts in a stoichiometric ratio with the fuel. In CLC, the overall combustion takes place in two steps. In a reduction reactor fuel is oxidised by the oxygen carrier i.e. the metal oxide MeO which is reduced to metal oxide with a lower oxidation number, Me. Me flows to an oxidation reactor where it is oxidised by oxygen in the air. In this way pure oxygen is supplied to fuel without using an energy intensive traditional air separation unit.

This paper presents thermodynamic cycle analysis of a CLC-power plant. A steady-state model has been developed for the solid-gas reactions occurring in the reactor system. The model is applied to analyse the system under two configurations; a combined cycle and a conventional steam cycle. A turbine-cooling model has also been implemented to evaluate the turbine cooling penalty in the combined cycle configuration. Effects of exhaust recirculation for coking prevention and incomplete fuel conversion have also been investigated. Performance of the oxygen carrier has been idealised except for the degrees of reduction and oxidation. Energy needs for CO₂ capture have properly been taken into account.

The results show that an optimum efficiency of 49.7% can be achieved under given conditions with a CLC-combined cycle at zero emissions level. With turbine cooling, efficiency falls by 1.2% points under the same conditions. The CLC-steam cycle is capable of achieving 40.1% efficiency with zero emissions. The results show that CLC has high potential for power generation with inherent CO₂ capture. This work will be useful in designing CLC systems after the reactor system has been analysed experimentally for long-term operations.

NOMENCLATURE

a, b, c, d	coefficients in Eq. (9)	-
C_p	specific heat capacity	kJ/molK
CF	coolant fraction	-
\dot{H}	heat of reaction	kW
HP	high-pressure steam	-
HX	heat exchanger	-
IP	intermediate pressure steam	-
$HRSG$	heat recovery steam generator	-
LHV	lower heating value	kJ/kg
\dot{m}	mass flowrate	kg/s
\dot{n}	molar flowrate	mol/s
OX	oxidation reactor	-
PR	compressor pressure ratio	-
\dot{Q}	heat flow	kW
R	universal gas constant	kJ/molK
RED	reduction reactor	-
T	temperature	K or °C
TIT	turbine inlet temperature	-
\dot{W}	power	KW
w	specific work	kJ/kg
X	degree of reaction	-

Greek

$\alpha, \beta, \gamma, \delta, \varepsilon$	coefficients in Eq. (8)	-
ϕ	degree of fuel conversion	-
η	efficiency	-

Subscripts and superscripts

$comp.$	compression
CO_2-T	CO ₂ -turbine
$el.$	electrical
GT	gas turbine
$m+g+aux$	mechanical+generator+auxiliaries ($\eta_{m+g+aux}$)
ox	oxidation
red	reduction
st	steam
ST	steam turbine

INTRODUCTION

Carbon dioxide is the most prevalent of all man-made greenhouse gases causing global warming effects. Exhaust gases from power plants combusting oil or coal are a major source of CO₂ release. By use of natural gas in power plants, CO₂ emissions per kWh electricity produced can be reduced to below half of that compared to coal combustion¹. However, CO₂ can be completely eradicated by developing more efficient combustion technologies; for instance, Chemical Looping Combustion (CLC) proposed by Richter and Knoche² in 1983. CLC is a novel concept of power production with inherent CO₂ capture. In CLC, unlike conventional combustion processes, combustion is more ordered by avoiding direct contact between air and fuel. Combustion is split up into intermediate oxidation and reduction reactions each approaching near-to-thermodynamic equilibrium². This goal is achieved by introducing a certain metal oxide as an oxygen carrier that circulates between the two reactors, as depicted in Fig. 1.

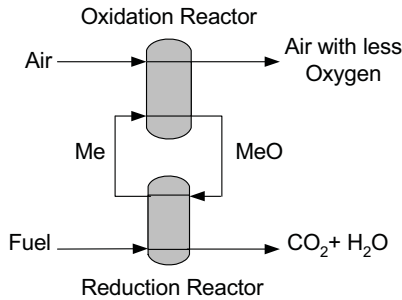
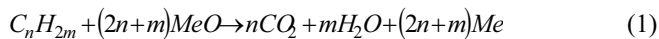
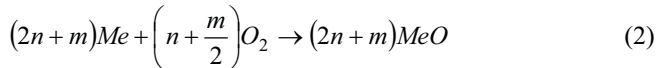


Figure 1: The Chemical Looping Combustion principle

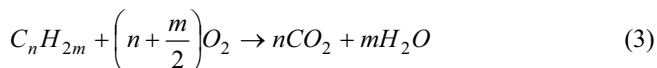
In a reduction reactor, fuel reacts with oxygen in the metal oxide in a stoichiometric ratio thereby reducing the metal oxide. Equation (1) gives the reduction reaction.



In eq. (1) MeO is metal oxide and Me is reduced metal. C_nH_{2m} is fuel and n and m are the stoichiometric factors for fuel molecules. The reduced metal oxide circulates to the oxidation reactor where oxygen in the air oxidises it to metal oxide. The oxidation reaction is given by eq. (2).



Equation (3) gives the net reaction.



The oxidation reaction for a metal is exothermic and the heat released is summation of heats of reaction of both oxidation

and reduction. Metal oxide continuously flows between the reactors and transfers oxygen and heat to the reduction reactor. The heat is utilised for the endothermic reduction reaction. By virtue of the intermediate reactions and heat recovery in the reduction reactor irreversibility of the process is lower and therefore the exergy loss is lesser when compared to conventional combustion³. The exhaust stream out of the reduction reactor is available at high temperatures and can also be utilised for power production. Also, the exhaust contains only CO₂ and H₂O vapour. CO₂ is not diluted with N₂ and can easily be separated by simply condensing the stream, thus giving a very low energy penalty. On the contrary, separation of CO₂ from the exhaust of conventional combustion processes is energy intensive resulting in a decrease in efficiency. CLC is also capable of thoroughly eradicating NO_x formation⁴. By virtue of separate air and fuel reactors there is no fuel NO_x produced. Thermal NO_x increases exponentially with combustion temperatures in conventional processes where local flame temperatures might be as high as 2000 K. In CLC, oxidation takes place at much lower temperatures and high heat capacity of solid particles results in lower local temperature. Thus NO_x is thoroughly eradicated. The choice of an oxygen carrier, which plays the central role in the process, is based on its reaction rates, chemical and mechanical stability and temperature standing abilities. Various metal oxides in combination with different stabilisers have been investigated so far and NiO/NiAl₂O₄ is believed to be the most promising⁵.

CYCLE DESCRIPTION

The schematic sketch of CLC-combined cycle with CO₂ capture is shown in Fig. 2. Air and fuel are introduced into the reactors at the same pressure. The oxidation reactor outlet stream drives the air turbine (or gas turbine) and the exhaust drives CO₂-turbine. Both turbines are assumed to be on the same shaft. For exergy loss minimisation, recuperation is done to heat the fuel prior to its entry into the reduction reactor. This approach also brings the temperature of the exhaust stream down which facilitates its subsequent cooling needed for CO₂ separation. The air turbine exhaust is passed through HRSG to generate steam for a dual pressure steam cycle.

As the losses associated with turbomachinery decrease with increase in plant size, simulations were carried out for fairly high power outputs (320-400 MW). The fuel flow-rate was kept constant at 15 kg/s. The cycle was analysed by varying airflow rate and maintaining turbine inlet temperature (TIT) at different compressor pressure ratios (PR). The term TIT is valid only for the air turbine and is defined as the temperature of stream coming out of the oxidation reactor. The computational assumptions used in the present work are very close to reality and are given in the appendix.

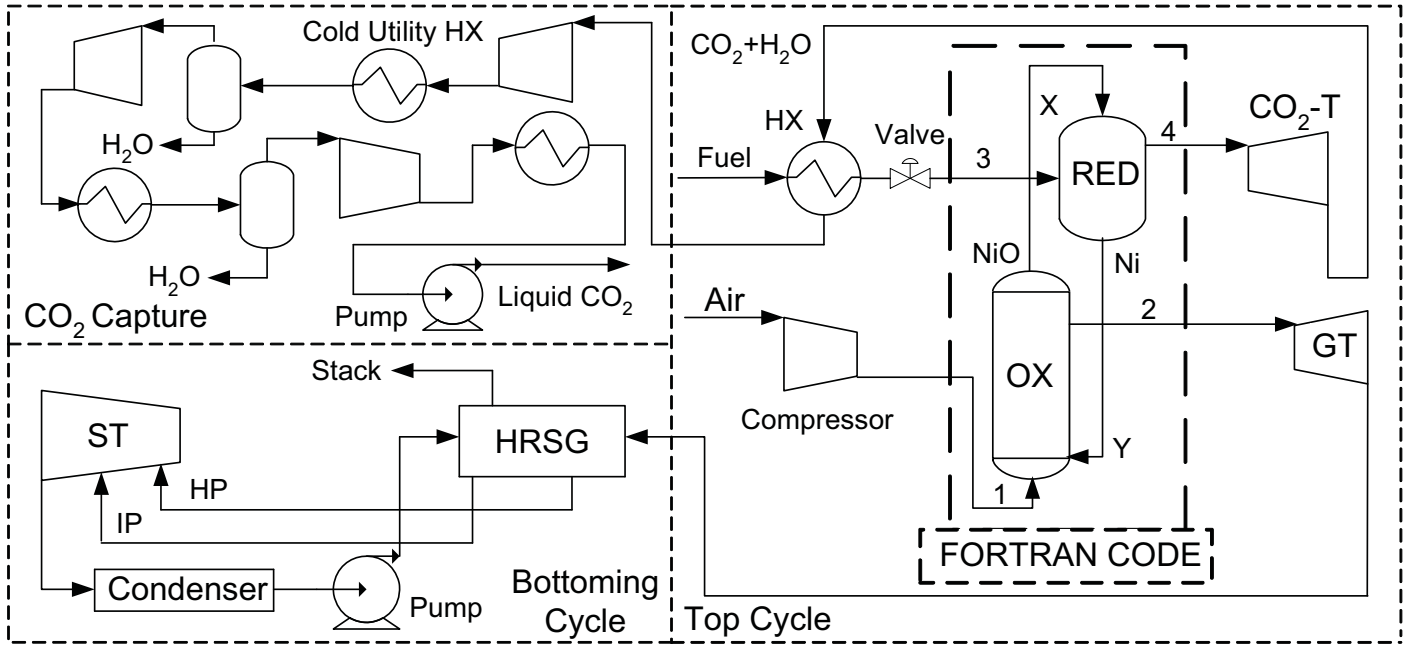


Figure 2: CLC-Combined Cycle with CO₂ Capture (Schematic Sketch)

Model Description

The present work is based on a steady-state model for cycle analysis with two configurations i.e. combined cycle and conventional steam cycle. NiO/NiAl₂O₄ on a 3:2 mass basis is the chosen oxygen carrier. The model is based on heat and mass balance for the solid-gas reactions occurring in the two reactors. Equation (4) gives heat balance over the reduction reactor for both configurations.

$$\dot{Q}_3 + \dot{Q}_X = \dot{Q}_4 + \dot{Q}_Y + \dot{H}_{red} \quad (4)$$

Equations (5) and (6) give heat balance over the oxidation reactor for combined cycle and steam cycle configuration respectively.

$$\dot{Q}_1 + \dot{Q}_Y = \dot{Q}_2 + \dot{Q}_X + \dot{H}_{ox} \quad (5)$$

$$\dot{Q}_1 + \dot{Q}_Y = \dot{Q}_2 + \dot{Q}_X + \dot{Q}_{st} + \dot{H}_{ox} \quad (6)$$

The subscripts used in eq. (4), (5) and (6) correspond to the cycle schematic sketches shown in Figs. 2 and 9.

The heat flow was calculated by using eq. (7).

$$\dot{Q}_i = \dot{n}_i \cdot (Cp_i(T_i) \cdot T_i - Cp_i(T_0) \cdot T_0) \quad (7)$$

Heat of reaction was calculated with the help of standard enthalpy of formation of reacting components at the corresponding reference temperature.

The heat capacities of the constituting components of the gaseous streams entering and leaving the reactor system were calculated by eq. (8)⁶.

$$Cp_i = (\alpha_i + \beta_i T + \gamma_i T^2 + \delta_i T^3 + \epsilon_i T^4) \cdot R \quad (8)$$

The Cp values calculated from eq. (8) were also validated against those calculated with the help of eq. (9)⁷.

$$Cp_i = (a_i + b_i \cdot 10^{-3} \cdot T + c_i \cdot 10^6 \cdot T^{-2} + d_i \cdot 10^{-6} \cdot T^2) \quad (9)$$

The specific heat capacity of the metal oxide was also calculated by eq. (9).

The specific heat capacity of the binding material (or stabiliser) NiAl₂O₄ was calculated by making use of an interpolated table⁸ of specific heat capacity values at different temperatures.

Temperature of various streams going in and coming out of the reactors was calculated by eq. (10)

$$T_i = \frac{\dot{Q}_i + (\dot{n}_i \cdot Cp_i(T_0) \cdot T_0)}{\dot{n}_i \cdot Cp_i(T_i)} \quad (10)$$

The subscripts i and 0 used in eqs. (7), (8), (9) and (10) correspond to the stream and the reference (ambient) condition, respectively.

The function of NiAl_2O_4 is to give mechanical stability to oxygen carrier. This material is inert yet it increases the reaction rate and contributes to heat transportation between the reactors. Therefore it appears in the mass balance equations. Mass balance over the reduction and oxidation reactor is given by eq. (11) and (12), respectively.

$$\dot{m}_{total,red} = X_{red} \dot{m}_{ox} + (1 - X_{red}) \dot{m}_{red} + \dot{m}_{\text{NiAl}_2\text{O}_4} \quad (11)$$

$$\dot{m}_{total,ox} = X_{ox} \dot{m}_{ox} + (1 - X_{ox}) \dot{m}_{red} + \dot{m}_{\text{NiAl}_2\text{O}_4} \quad (12)$$

X is degree of reaction and is defined by eq. (13).

$$X = \frac{m - m_{red}}{m_{ox} - m_{red}} \quad (13)$$

In eq. (13) m_{red} is mass of metal oxide when it is fully reduced and m_{ox} is its mass when it is fully oxidised. The term m stands for mass of metal oxide at a certain time. Hence X_{red} is 0.0 for full reduction and X_{ox} is 1.0 for full oxidation. Recent experiments by Brandvoll⁹ show that the values of $X_{ox}=1.0$ and $X_{red}=0.3$ are quite realistic and the present work is based on these values.

All the streams were defined on molar basis (index ' n '). Figure 3 shows the overall mass balance for the reactor system.

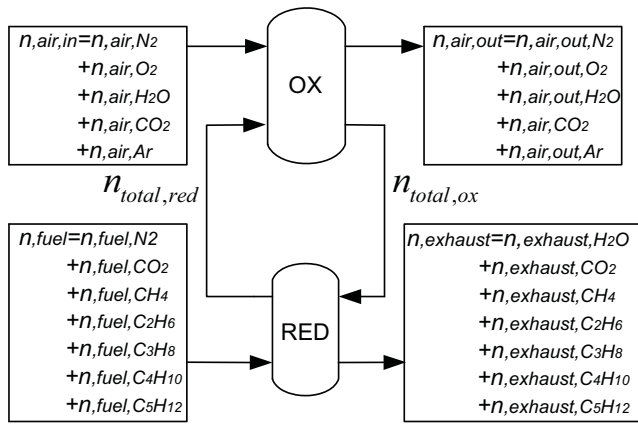


Figure 3: Mass Balance

In case of incomplete fuel conversion there can be some fuel components in the exhaust stream as shown in Fig. 3. In order to analyse the cycle at such condition a factor 'degree of fuel conversion' was defined which is given by eq. (14).

$$\phi = \frac{n_{rx,fuel}}{n_{fuel}} \quad (14)$$

In eq. (14), $n_{rx,fuel}$ is the number of moles of fuel actually reacting with the oxygen carrier and n_{fuel} is the number of moles of fuel supplied.

The model was implemented in a FORTRAN 90 code and embedded into the flow-sheeting simulation tool PRO/II, version 5.6 (SIMSCI Inc.) as 'user added subroutine'. The stream data from PRO/II was provided to the simulation tool GTPRO (Thermoflow Inc.) in order to simulate the heat recovery steam generator (HRSG) and the steam turbine.

Turbine Cooling

The efficiency and specific work output of a gas turbine increase by raising turbine inlet temperature (TIT). Surfaces of the components exposed to hot gas need to be maintained below a certain safe working temperature at which they show mechanical stability and corrosion resistance. The higher the TIT, the higher is the temperature difference between hot gas and blade surface. In cooled turbines, mixing of coolant with hot gas results in thermodynamic penalties due to stagnation temperature and pressure losses, and aerodynamic losses. In the present work, only the mixing loss is accounted for. For a given level of cooling technology, raising TIT beyond a certain limit results in such cooling penalties that cycle efficiency drops. These penalties can be reduced by minimising the coolant flow. It is achieved by improving internal heat transfer between the coolant and the blade; and reducing the blade external heat transfer coefficient. The latter effect can be achieved by employing film cooling in which the spent coolant is caused to form a film on the blade surface which shields it against the hot gas.

The objective of implementing a cooling model in CLC-combined cycle is to determine the coolant flow at elevated turbine inlet temperatures and the efficiency drop associated with the cooling penalty. The nature of the CO_2 -turbine working fluid does not allow application of conventional air cooling techniques. Also the CO_2 -turbine contributes little to the net output power (about 10%); therefore its cooling was not considered. Figure 4 depicts the turbine cooling approach adopted in the present work.

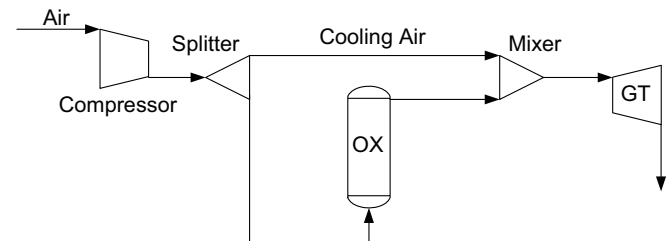


Figure 4: Turbine cooling principle

The air at the compressor discharge is split into two streams; one going to the oxidation reactor and the other mixing with the hot air stream coming out of the oxidation reactor. In order to consider the employment of a state-of-the-art gas turbine, the technology level was derived from data available for the gas turbine GE93519FA in GTPRO. The total flow of coolant and air at the turbine inlet is less than that of air at the compressor inlet due to oxygen consumption in the oxidation reactor. Therefore, the coolant fraction (CF) was determined as a percent of turbine exhaust. Figure 5 presents the CF as a function of TIT at different compressor pressure ratios. The coolant flowrate was then calculated by eq. (15).

$$\dot{m}_{coolant} = CF \cdot \dot{m}_{exhaust} \quad (15)$$

The present work is based on the cooling model with 10 mbar back pressure turbine operating on air/methane combustion products. The model is based on the work done by Bolland and Stadaas¹⁰ which is again based on the work done by Elmasri¹¹.

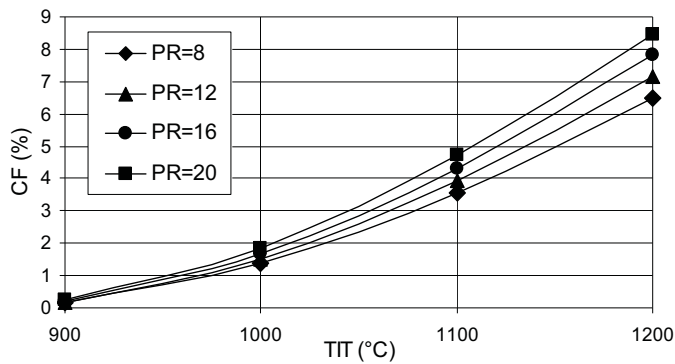


Figure 5: Coolant Fraction (CF) as % of exhaust flowrate

In CLC, the composition of working fluid is different from that of a conventional gas turbine. Also, in practice the coolant and gas mixing occurs in the turbine stage and not before the turbine inlet. Therefore, the results obtained do not have a very high degree of accuracy. However, they are sufficiently reasonable for assessing the turbine cooling demand and its impact on cycle efficiency at the current stage of CLC development.

CO₂ Separation and Compression

A CO₂ separation and compression model (included in Fig. 2) was developed and incorporated into the main model in order to determine power requirements and eventual energy penalty associated with CO₂ capture. CO₂ separation and compression takes place in three stages. In the first two stages the exhaust stream at atmospheric pressure is compressed and cooled followed by H₂O separation in flash drums. After the second stage the stream consists of pure CO₂ which is compressed to

80 bar pressure and further cooled down to 30°C. Finally a pump delivers liquid CO₂ at 100 bar and 36°C.

RESULTS AND DISCUSSION

Results are presented over a range of compressor pressure ratios (PR) and turbine inlet temperatures (TIT). The definitions of cycle efficiency and specific work used in the present work are given by eq. (16) and (17), respectively.

$$\eta_{net} = \frac{(\dot{W}_{GT} + \dot{W}_{CO_2-T} + \dot{W}_{ST} - \dot{W}_{comp}) \cdot \eta_{m+g+aux} - \dot{W}_{CO_2-comp}}{\dot{m}_{fuel} \cdot LHV} \quad (16)$$

$$w = \frac{(\dot{W}_{GT} + \dot{W}_{CO_2-T} + \dot{W}_{ST} - \dot{W}_{comp}) \cdot \eta_{m+g+aux} - \dot{W}_{CO_2-comp}}{\dot{m}_{air}} \quad (17)$$

Figure 6 presents the net cycle efficiency as a function of specific work for different pressure ratios and TIT values.

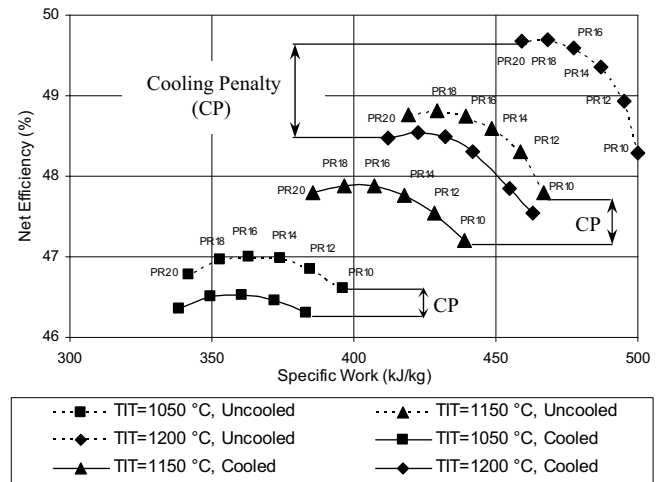


Figure 6: Efficiency vs. Specific Work

The airflow through the system decreases with an increase in desired TIT value in order to maintain the reactor temperature. Therefore, the points of specific work move towards the right with increased TIT values. The maximum specific work is at TIT=1200°C and PR=10. At a certain TIT, increase in PR results in lower specific work. This is due to an increased air flow in order to maintain the reactor temperature when the compressor exit temperature increases with increased PR. However, the net efficiency increases with PR increase at a fixed TIT and the most optimum compressor pressure ratio is found to be 18 for TIT values higher than 1050°C. At high pressure ratios and low TIT values, turbine exit temperature (TET) is insufficiently low (below 420°C). Under such conditions supplementary firing becomes inevitable for production of superheated steam at high-pressure. The effect of supplementary firing is release of CO₂ into the atmosphere.

The present work is intended to analyse a power cycle with zero emissions, therefore the points of supplementary firing have been omitted from Fig. 6. However, the TIT values for different pressure ratios at which supplementary firing is needed are presented in table 1.

Table 1: Supplementary Firing start points

PR	10	12	14	16	18	20
TIT (°C)	----	912	952	980	1010	1040

The results of the thermodynamic analysis show that the efficiency improvement in the region of TIT (900-1000°C) is small at all pressure ratios. Therefore, Fig. 6 takes into account the TIT values ranging from 1050 to 1200°C. The results conclude that the most optimum operating condition for a CLC-combined cycle under the devised configuration is pressure ratio of 18 at TIT of 1200°C. Under this condition, a net electrical efficiency of 49.7% is achieved at zero emissions level. This efficiency is somewhat lower than that of a modern conventional combined cycle power plant which approaches 60% efficiency but does not take into account the energy penalty associated with CO₂ separation and compression.

Although efficiency is a function of TIT and the modern gas turbines can stand elevated temperatures (above 1200°C) thanks to advanced cooling technologies; yet the material constraints associated with the CLC reactor system still hinder the adoption of this approach. In general, turbine blades need to be cooled at TIT values higher than 850°C. Figure 6 presents the efficiency drop due to cooling for different TIT's and PR's. At the optimum condition of TIT=1200 °C and PR=18, the cooling penalty results in an efficiency drop of 1.20% points and the net efficiency is 48.5%. This efficiency is slightly higher than that achieved at the condition of PR=10, TIT=1200°C with no turbine cooling. Therefore, an optimisation of TIT and PR is necessary to obtain a reasonable efficiency, but this is not presented here.

Table 2 presents the combined cycle summary for uncooled and cooled air turbine at the optimum pressure ratio of 18 and different TIT values. It can be seen that the net efficiency for the combined cycle with cooled air turbine is lower as compared to that with uncooled turbine. However, the cooled air turbine gross output power is somewhat higher than that of the uncooled turbine. When employing air turbine cooling, the airflow rate at the compressor inlet increases in the amount required for turbine cooling thereby increasing the power required to drive the compressor. As mentioned earlier, the term TIT refers to the oxidation reactor exit and in case of cooled air turbine the real turbine inlet temperature is lower than TIT due to mixing of the hot air and the coolant air streams. This is more explicable in connection with Fig. 4 depicting the simple approach adopted for turbine cooling.

Table 2: Cycle Summary at the optimum pressure ratio of 18

	Uncooled Air Turbine			Cooled Air Turbine		
TIT (°C)	1050	1150	1200	1050	1150	1200
Airflow at comp. exit (kg/s)	950	812	758	978	862	820
Coolant Flow (kg/s)	0	0	0	28	50	62
Power (MW)						
Fuel Input	713.9	713.9	713.9	713.9	713.9	713.9
Air Turbine	624.3	570.1	548.9	634.2	588.1	571.4
CO ₂ -Turbine	52.60	57.2	59.5	52.6	57.2	59.5
Compressor	-393	-335.7	-313.3	-404.6	-356.6	-339
Steam Turbine	98.35	105.8	109.4	95.5	101.7	104.1
CO ₂ -Compression	-37.3	-38.9	-39.8	-37.3	-38.9	-39.8
Auxiliaries	-3.8	-3.8	-3.8	-3.8	-3.8	-3.8
Mech. Losses	-1.1	-1.1	-1.1	-1.1	-1.1	-1.1
Gen. Losses	-4.8	-4.8	-4.8	-4.8	-4.8	-4.8
Net Power	335.4	348.7	354.8	330.7	341.8	346.5
Specific Work (kJ/kg)	352.8	429.3	468.4	349.7	396.5	422.4
Net Efficiency (%)	46.97	48.84	49.7	46.32	47.9	48.5

Despite a lower turbine inlet temperature, the increased airflow rate results in a higher gross output than that of the uncooled air turbine. But for the same pressure ratio, lower turbine inlet temperature results in lower turbine exit temperature in comparison with the uncooled turbine. The effect of lower turbine exit temperature is less heat available for steam generation in HRSG and hence a lower output power from the steam turbine. This effect together with the increased compressor work results in a lower net efficiency compared to that of the cycle with uncooled air turbine. Turbine cooling has no effect on the reduction reactor and thus the CO₂-turbine power output and the exhaust temperature remain the same in both cases under the same conditions. Therefore the power requirements for CO₂ compression also remain the same.

The selection of an optimum pressure ratio is in fact a trade-off between the output power from the gas turbine and the steam turbine. At low pressure ratios and high TIT's, the work extraction from gas turbine is less so that the turbine exit temperature (TET) is sufficiently high to raise superheated steam in HRSG. At high pressure ratios gas turbine output power and efficiency increase due to higher difference in TIT and TET which results in lower output from the steam cycle at a certain temperature. A steam cycle which is more efficient than the one employed in the present work together with the gas turbine cycle can achieve an optimum efficiency at comparatively lower pressure ratios than 18. This can be beneficial in terms of the proposed pressurised fluidised circulating bed reactors for CLC system. Such reactors can be very costly if manufactured to stand high pressures. Therefore, efforts should be made to achieve an optimum efficiency at a reasonably low reactor pressure (or pressure ratio). This is done through optimisation or employment of different power plant configurations; for instance utilising the exhaust stream to produce additional steam in HRSG instead of expanding it through a CO₂ turbine, and choosing maximum possible

pressure levels in HRSG. Being within the scope of the present work and analysing the devised combined cycle configuration (Fig. 2), the optimisation part is not presented here.

Exhaust Recirculation

One operational problem in CLC is carbon deposition (or coking) on the oxygen carrier particles in the reduction reactor. This affects mass transfer in reduction reactor thereby reducing the rate of reduction. Also carbon is transported to the oxidation reactor with the metal oxide particles which has to be avoided in order to achieve zero emissions. This problem can be dealt with by steam injection in the reduction reactor. An optimum steam to fuel ratio is 2:1⁵. Steam can be supplied by using the steam available in the exhaust stream. Figure 7 shows the principle of exhaust recirculation used in the present work.

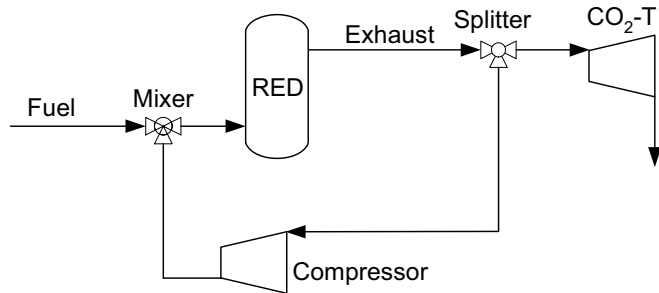


Figure 7: Recirculation of exhaust stream

The exhaust stream was split into two parts one being recycled back to the fuel stream. This is beneficial in the terms that the exhaust stream also contains CO₂ which has the same effect as that of steam for avoiding coking¹².

The results show that recirculation has a very little effect on the efficiency which is in connection with employment of the light duty compressor in order to make up for the pressure loss through the reactor. The efficiency drop due to recirculation of exhaust is 0.04% points, which should be considered negligible.

Incomplete Fuel Conversion

The results shown so far are based on the assumption of complete fuel conversion. In reality solid-gas reactions do not result in full conversion due to the limitations associated with mass transfer. Therefore, the cycle was also analysed under the conditions of incomplete fuel conversion. Table 3 presents net cycle efficiency at the optimum condition of pressure ratio=18 and TIT=1200°C for different degrees of fuel conversion ' Φ '. Table 3 shows that there is 0.5% efficiency drop for each 1% decrease in degree of fuel conversion.

Table 3: Efficiency at different degrees of fuel conversion

Φ	1	0.99	0.98	0.97	0.96	0.95
η (%)	49.7	49.2	48.7	48.2	47.7	47.2

This should be considered as a significant efficiency drop and therefore the reactor system design should be sophisticated enough to avoid such inefficiencies. Since the focus of this paper is not reactor system design, this issue is not discussed here.

THE OXYGEN CARRIER FLOW IN REACTORS

The performance of oxygen carrier is largely dependent on the type of reactor system chosen. The concept of circulating fluidised bed has been proposed¹³ and is believed to be the most suitable setup. The design of reactor system depends on total flowrate through each reactor. For a certain flowrate of air and fuel, the reactor system can be designed if the flowrate of particles through each reactor is known. This flowrate is a function of the difference between X_{ox} and X_{red} . The total flowrate of particles through the reactor system depends on the stoichiometric amount of oxygen needed by the fuel. Therefore, the total flowrate remains constant for a certain amount of fuel supplied. The rate of reaction in each reactor affects the flowrate of particles through the two reactors. The lower the reduction rate, the higher is the flowrate of particles to the oxidation reactor and vice-versa. This is due to the presence of the additional unconverted oxygen carrier in the stream leaving one reactor and going into the other. Figure 8 presents the oxygen carrier flowrate per MJ heat supplied at the reactors exit as a function of ($X_{ox} - X_{red}$).

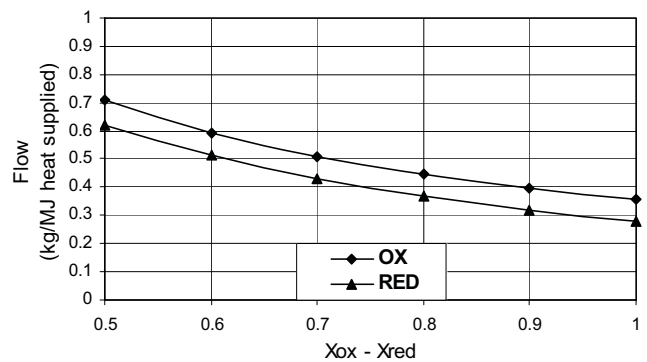


Figure 8: The Oxygen Carrier flow (Combined Cycle) (Constant $X_{ox}=1.0$, varying X_{red})

The results show that the minimum flow of the oxygen carrier is at the state of complete oxidation and reduction. Table 4 presents the key parameters for the reactor system. In Table 4, the particles flowrate per MJ of electricity has been calculated at the optimum condition of TIT=1200°C and PR=18.

Table 4: Reactors exit key parameters for the combined cycle

Xox=1.0	Xred	0.3
	Xox-Xred	0.7
OX (Pure NiO)	kg/s	362.4
	kg/MJ LHV	0.51
	kg/MJ el.(Uncooled)	1.02
	kg/MJ el.(Cooled)	1.05
RED (Unconverted NiO + Ni)	kg/s	308
	kg/MJ LHV	0.43
	kg/MJ el.(Uncooled)	0.87
	kg/MJ el.(Cooled)	0.89

At complete oxidation (Xox=1.0), the particles at the oxidation reactor outlet consist of pure NiO. Due to incomplete reduction (Xred=0.3), the particles entering the oxidation reactor (or leaving the reduction reactor) contain some unreduced NiO. Hence, the particles flowrate through the oxidation reactor is higher as compared to that at complete reduction and oxidation. For the devised combined cycle power plant, the design point flowrate of NiO particles is 362.4 kg/s and hence the total flowrate of particles (NiO/NiAl₂O₄) in the system is 604 kg/s.

CLC-STEAM CYCLE

A CLC power plant operating at atmospheric conditions with steam generation in the oxidation reactor can be a short-term alternative to a gas turbine with pressurised reactors. Such an arrangement is shown in Fig. 9.

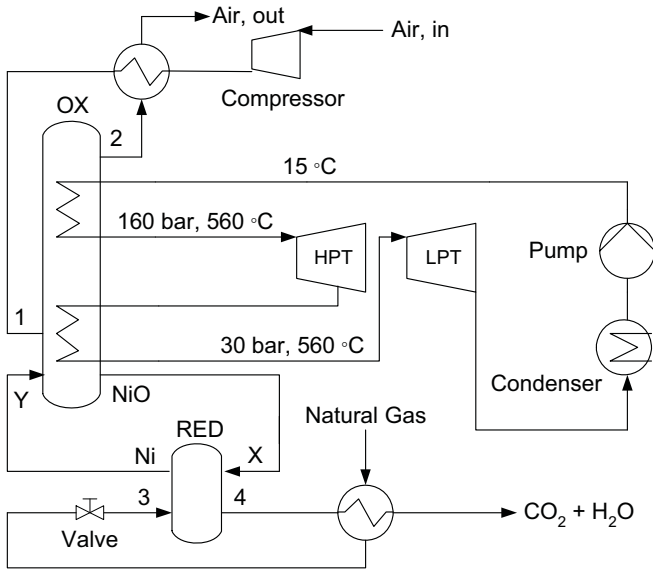


Figure 9: CLC-Steam Cycle schematic sketch

At present, there exist material constraints for the reactors. Also the oxygen carrier has its limitations at elevated temperatures. For such reasons, the oxidation temperature needs to be controlled. This can be done by walls cooling of

the oxidation reactor i.e. steam generation benefited from good heat transfer conditions in a circulating fluidised bed reactor. In the devised configuration (Fig. 9), the oxidation reactor is assumed to have isothermal mixing at a constant temperature of 850°C. In order to minimise exergy loss, the process is configured to have a high degree of heat integration. A light duty compressor is employed for atmospheric air in order to compensate for the pressure drop through the heat exchanger. The steam data is obtained from PRO/II model and supplied to GTPRO to analyse a dual pressure reheat steam cycle. The definition of efficiency used in the present work for the steam cycle is given by eq. (18).

$$\eta_{net} = \frac{(\dot{W}_{ST} - \dot{W}_{comp} - \dot{W}_{pump}) \cdot \eta_{m+g+aux} - \dot{W}_{CO_2-comp}}{\dot{m}_{fuel} \cdot LHV} \quad (18)$$

The results show that for a power plant of the size bigger than 300 MW, an efficiency of 42.8% can be achieved without CO₂ capture. Including energy demands for CO₂ compression, the net electrical efficiency is 40.1%. This efficiency is comparable to that of a modern steam power plant approaching 41% efficiency which does not include energy penalty for CO₂ capture.

CONCLUSIONS

CLC system has been evaluated for two configurations; combined cycle and conventional steam cycle. The results show that at the condition of TIT=1200°C and PR=18, 49.7% efficiency can be achieved with combined cycle configuration at zero emissions level. Under the same conditions, turbine cooling results in 1.20% points efficiency drop. Exhaust recirculation for coking prevention in the reduction reactor has a negligible effect on efficiency. Incomplete fuel conversion due to mass transfer limitations in the reduction reactor has a considerable effect on the efficiency and efficiency drop is 0.5% points for every 1% reduction in fuel conversion. The optimum pressure ratio can be brought down to a value lower than 18 by selecting a power plant configuration which emphasises on the steam cycle thus producing more work from the steam turbine as well as maintaining a reasonable power output from the gas turbine cycle. In case of the conventional steam cycle configuration, an efficiency of 40.1% can be achieved at oxidation temperature of 850°C. The results also show that flow through each of the two reactors can be minimised by achieving high rates of reduction and oxidation. The results of this study support the argument that CLC has high potential of power generation with CO₂ capture.

ACKNOWLEDGEMENTS

This work has been sponsored by the Norwegian Research Council Klimatek Project.

REFERENCES

1. Bolland, O., **2000**, *Removal of CO₂ from Natural Gas Combined Cycle Power Plants*, lecture at the seminar *Flowsheet synthesis and optimisation of CHP power plants*, Nordic Council of Ministers, Helsinki, Finland
2. Richter, H. J., Knoche, K., **1983**, *Reversibility of combustion processes*, Efficiency and Costing. Second Law Analysis of Processes, ACS symposium Series 235, Washington D.C., pp. 71-85
3. Anheden, M. *et al.*, **1995**, *Chemical-looping combustion – efficient conversion of chemical energy in fuels into work*, ASME, IECE paper no. CT-45, pp. 75-81
4. Ishida, M., Jin, H., **2001**, *Fundamental study on a Novel Gas Turbine Cycle*, Journal of Energy Resources Technology, vol. 123, pp. 10-14
5. Jin, H., Okamoto T., Ishida, M., **1999**, *Development of a Novel Chemical-Looping Combustion: Synthesis of a Solid Looping Material of NiO/NiAl₂O₄*, Ind. Eng. Chem. Res., vol. 3, pp. 126-132
6. Moran, M. J., Shapiro, H. N., **1993** *Fundamentals of Engineering Thermodynamics*, 2nd Edition, SI version, pp. 680, John Wiley & Sons, Inc.
7. Knache, O., Kubaschewski, O., Hesselmann, K., **1991**, *Thermochemical Properties of Inorganic Substances*, 2nd Edition, Springer-Verlag Inc.
8. Barin, I., **1995**, *Thermochemical data of pure substances*, 3rd Edition, VCH Verlagsgesellschaft
9. Brandvoll, Ø., **2004**, *Chemical Looping Combustion-Oxy-fuel process with inherent CO₂ capture*, PhD Thesis, Dept. of Energy and Process Engineering, Norwegian University of Science and Technology, submitted for review
10. Bolland, O., Stadaas, J. F., **1993**, *Comparative evaluation of Combined Cycles and Gas Turbine Systems with Water Injection, Steam Injection and Recuperation*, Presented at the International Gas Turbine and Aeroengine Congress and Exposition Cincinnati, ASME Paper No. 93-GT-57, 1993, published in the *ASME Journal of Engineering for Gas Turbines and Power*, Vol. 28, Jan. **1995**
11. Elmasri, M.A., 1986b, *On Thermodynamics of Gas-Turbine Cycles: Part 2-A Model for Expansion in Cooled Turbines*, Journal of Engineering for Gas Turbines and Power, vol. 108, pp. 151-159
12. Dahl, Ivar M., *Hydrocarbon Process Chemistry*, SINTEF, Norway
13. Lyngfelt, A., Leckner, B., Mattisson, T., I., **2000**, *A fluidized-bed combustion process with inherent CO₂ separation-application of chemical-looping combustion*, Chem. Eng. Sci. vol. 56, pp. 3101-3313

APPENDIX

Computational assumptions used in the present work are given below.

Ambient Air:

15°C, 1.013 bar,

60% Relative Humidity

Air Composition (Mole Percent):

N₂ (77.3), O₂ (20.74), CO₂ (0.03), H₂O (1.01), Ar (0.92)

Fuel:

Natural Gas: 15°C, 50 bar,

LHV=47594 kJ/kg

Natural Gas Composition (Mole Percent):

N₂ (0.9), CO₂ (0.7), CH₄ (82), C₂H₆ (9.4), C₃H₈ (4.7), C₄H₁₀ (1.6), C₅H₁₂ (0.7)

CLC- Reactors System:

Adiabatic Reactors, Pressure drop 5%

NiO/NiAl₂O₄=3:2 (mass basis),

H₂O/Fuel=2:1 (Coking prevention)

Gas Turbine Cycle:

Compressor: Adiabatic efficiency 90%

Turbines adiabatic efficiency: 90 %

Air turbine back pressure: 20 mbar

Heat exchangers: 3% pressure drop, 30°C pinch

Efficiency (Mechanical + generator + auxiliaries): 96.6%

HRSG:

2-Pressure levels: 60 bar, 5 bar

Hot side temperature difference: 20°C

IP temperature: 260°C

Pinch (HP, IP): 10 °C

Min. Stack temperature: 80 °C

Steam Cycle:

CLC-Steam cycle: 2-Pressure levels, 160 bar, 30 bar

HP Temperature: 560°C

Steam turbines adiabatic efficiency (HP, IP) (%): 92, 92

Condenser pressure: 0.04 bar

Cooling water (sea water) temperature: 15°C

Maximum allowable cooling water temperature rise: 10°C

CO₂ compression:

Polytropic efficiency (stage 1, 2, 3) (%): 85, 80, 75

Heat exchanger pressure drop (stage 1, 2, 3): 0.15, 1.5, 2.4 bar

Cold utility (water) inlet/outlet temperature: 15°C/24°C

Adiabatic efficiency Pump (%): 75

Compressor intercooler exit temperature: 30 °C

Vattenfall's 30 MW_{th} Oxyfuel Pilot Plant Project

Lars Strömberg¹, Göran Lindgren², Marie Anheden², Nicklas Simonsson²,
Moritz Köpcke²

¹Vattenfall AB

²Vattenfall Utveckling AB,
Jämtlandsgatan 99, SE-16287 Stockholm, Sweden

Abstract

Vattenfall is to build a pilot plant for a carbon dioxide-free coal-fired power station. The plant will be built next to the Schwarze Pumpe lignite-fired power station to the south of Berlin. The technology that will be used, carbon dioxide capture with Oxyfuel technology, entails firing the lignite using pure oxygen and recycled carbon dioxide. The pilot plant, which will have a thermal output of 30 MW, is part of a research and development project aimed at developing and commercializing the new technology allowing designated tests to be performed in the plant. It will take three years to build the plant, which according to plan will be commissioned in 2008. The paper presents an overview of the pilot plant design aspects and some of the test activities that will be performed in the pilot plant.

Oxyfuel combustion has recently been shown to be one of the most promising options of the technologies for CO₂ capture from coal-fired power plants. The possibility to use advanced steam technology and simplified flue gas processing has moved it into an economically competitive position. The paper will, in addition to describing the planned pilot plant, also show Vattenfall's view on the competitiveness of the Oxyfuel technology to other solutions for CO₂ reductions.

Keywords: Vattenfall, Oxyfuel, Pilot, CO₂, Capture, Storage, Schwarze Pumpe

Introduction

Vattenfall began in 2001 with its major research and development programme in Carbon Capture and Storage under the name "CO₂-free Power Plant". The worldwide dependency on fossil fuels in the future and the serious issue of Global Warming demand for committed engagement for technological concepts and political-economical frameworks to ensure safe and reliable electrical power supply. Vattenfall's research program reaches from capture technology engineering over transport scenario development and storage site investigations to all enclosing environmental impact assessments.

From mainly three technological options for coal-fired power plant concepts with CO₂ capture – the pre-combustion decarbonisation after fuel gasification, the post-combustion decarbonisation with chemical solvents and the denitrification and combustion in pure-O₂/recycled-CO₂ atmosphere – Vattenfall chose to intensify its research on the latter, the Oxyfuel technology, and announced in May 2005 the erection of a self-financed Oxyfuel pilot plant at its lignite-fired German power plant in Schwarze Pumpe, south-east of Berlin. The pilot plant is intended for development and verification of the Oxyfuel process for pulverized fuel (PF) combustion, the combustion technology that today provides the backbone of electricity production. Scheduled to be ready for operation in 2008, the 30 MW_{th} pilot plant is intended to validate and support the technical concept on the gas-side of the process and serve as main step towards the construction of a 200 MW_{el} demonstration power plant generating "CO₂-free" electricity from 2015 under commercial conditions.

In the joint European Research Cooperation ENCAP (Enhanced Capture of CO₂) over 30 research institutes and industrial companies investigate various technological concepts for CO₂ capture under Vattenfall's coordination. The Schwarze Pumpe pilot plant was selected as one of the candidates to be considered for future experimental testing of the Oxyfuel technology within the project.

Even though Vattenfall has chosen to focus its efforts on Oxyfuel combustion, Vattenfall is still also involved in development of the other main options for CO₂ capture. This is done through different initiatives such as the participation in the EU project CASTOR with pilot testing of post combustion at the Esbjerg power station in Denmark and in the DYNAMIS project with preparation of a demonstration plant with pre-combustion capture and hydrogen production.

Oxyfuel Technology

The Oxyfuel technology refers to a combustion environment of pure oxygen (>95% volume) with recirculation of exhaust carbon dioxide to control the combustion temperature.

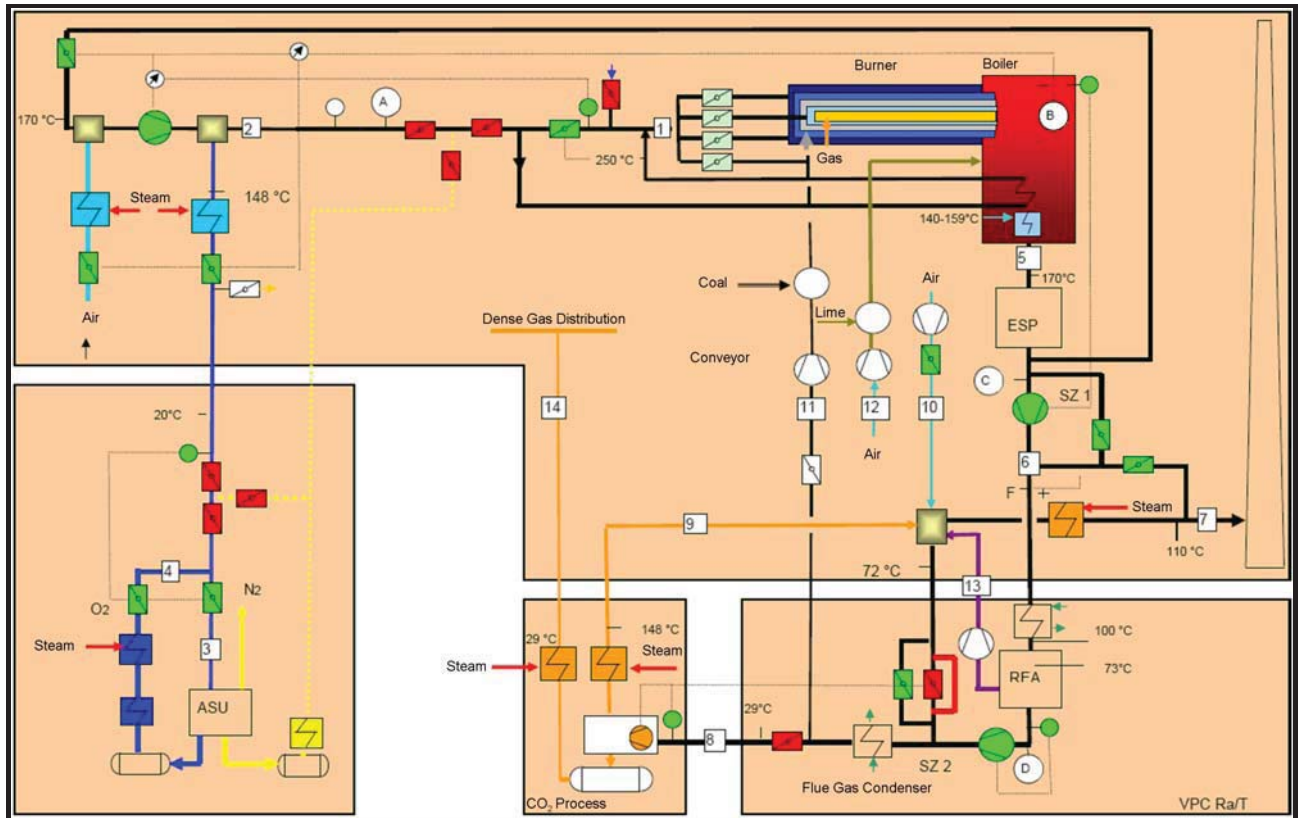


Figure 1 Pilot Plant flow sheet layout

As shown in Figure 1 and further described in literature [1], the oxygen is to be produced by large-scale air separation units and replaces conventional air as oxygen carrier. From the exhaust gas stream, dominated by the contents of carbon dioxide and water vapour, the main fraction of about 70% is redirected into the boiler feed gas. After stages of particle and sulphur removal, the flue gas is cooled and compressed. Purified from water and non-condensable gases, the former flue gas is converted to the supercritical-liquid CO₂ product stream, ready for transport and underground storage.

Pilot Design Aspects

The Vattenfall Oxyfuel pilot plant is designed of 30 MW_{th} size and 40000 hours operating lifetime over 10 years, starting in 2008. In general, the basic purpose of this pilot plant is to validate the concept for being able to later scale up the technology to a 600 MW_{th} demonstration power plant. This requires a fairly complete process with a minimum burner capacity of 30 MW_{th} at one single burner. This 30 MW burner allows scaling up to 70-90 MW_{th} for each burner in a large wall-fired boiler that has to be delivered at normal commercial requirements and warranties.

Full load operation in both Oxyfuel and air mode is a crucial test facility specific requirement. This is to be able to get reference measurements on air combustion. Special arrangements are needed to cope with

the atmospheric emission regulations. A commercial scale facility will use air only for start-up/shutdown.

The main focus is to explore and optimise the combustion of recirculated oxygen enriched flue gas. In the same facility it is also feasible to include all the main components of the Oxyfuel process from the air separation unit (ASU), furnace and boiler system including flue gas recycle, flue gas clean up system including electrostatic precipitator (ESP), wet flue gas desulphurisation (FGD), and flue gas condensation (FGC). It is also the intention to have a CO₂ compression and liquefaction system in place in order to produce CO₂ for truck transport.

While the demo plant would require good heat integration measures in order to operate under commercially viable conditions, this aim is not applicable for the pilot plant. The main objective of the pilot plant is on being able to operate the plant in a flexible manner and perform the tests that are necessary for the development of the Oxyfuel process. The demo plant shall be possible to purchase in good competition for both lignite and bituminous coals. Therefore it is the intention to use the pilot plant for development of the Oxyfuel process both for lignite and bituminous coal. That induces a general flexibility condition but in particular the fuel feeding system and the main recirculation loop with burner, furnace, boiler and primary de-dusting need to be capable of that variation.

Further process requirements were identified as follows:

- Flue gas sulphur removal is needed in order to test this technology under Oxyfuel conditions and also handle the sulphur emissions when the flue gas is vented to the atmosphere.
- NO_x control is performed by in-furnace primary measures. Additional DeNO_x would be considered if needed at the inert off-gas stream from the liquid CO₂ purification.
- Particular measures are to be taken to avoid CO₂ cycle dilution by air or other inert gases
- Operation is intended on both air and oxygen at full load (air only for shorter periods in order to achieve correlations between CO₂ and conventional N₂ based atmospheres).

Other general design requirements, mainly for combustion, boiler and atmospheric flue gas cleaning systems, are:

- A modular approach is aimed at, with flexibility as regards possibilities to modify the system and non-integrated, compact and highly material efficient solutions.
- Plenty of space is required in the buildings and between different components and ducts, in particular the boiler building.
- Additional space must be left in switchgears and I&C systems.

The base fuel to be tested is pre-dried lignite powder as prepared and made available in a briquette factory nearby the Schwarze Pumpe power plant. For bituminous coal test operation, the quality corresponding to today's trade coal will be taken. This will also be pre-dried and milled before delivery to the pilot facility fuel silo.

For the moment, the possible use of the CO₂ is not clear, leaving the specification of the CO₂ an open issue. In any case, the project specific requirements for this "stand-alone" capture test facility makes it difficult to produce a CO₂ quality representative for the targeted optimised complete CCS chain. To avoid a waste classification of the CO₂ product a high product CO₂ quality has to be applied. This means compression, dehydration purification and liquefaction to a CO₂ product of around 98% purity at 20 bar and -35°C. Two storage tanks included are able of storing the CO₂ produced at full capacity during three to four days, corresponding to any storage injection, transport logistics problems or a long weekend without unloading.

Furthermore, a pipeline transport scenario at 110 bar pressure or above and at ambient temperatures is being investigated. Both the latter options are today excluded from the pilot plant design but could be added on later if a pipeline and storage project is connected to this capture pilot plant.

Integration with Schwarze Pumpe power plant

Figure 2 shows the designed location and main equipment arrangement of the pilot plant in close proximity to the existing 2 x 800 MW_{th} lignite-fired power plant in Schwarze Pumpe.

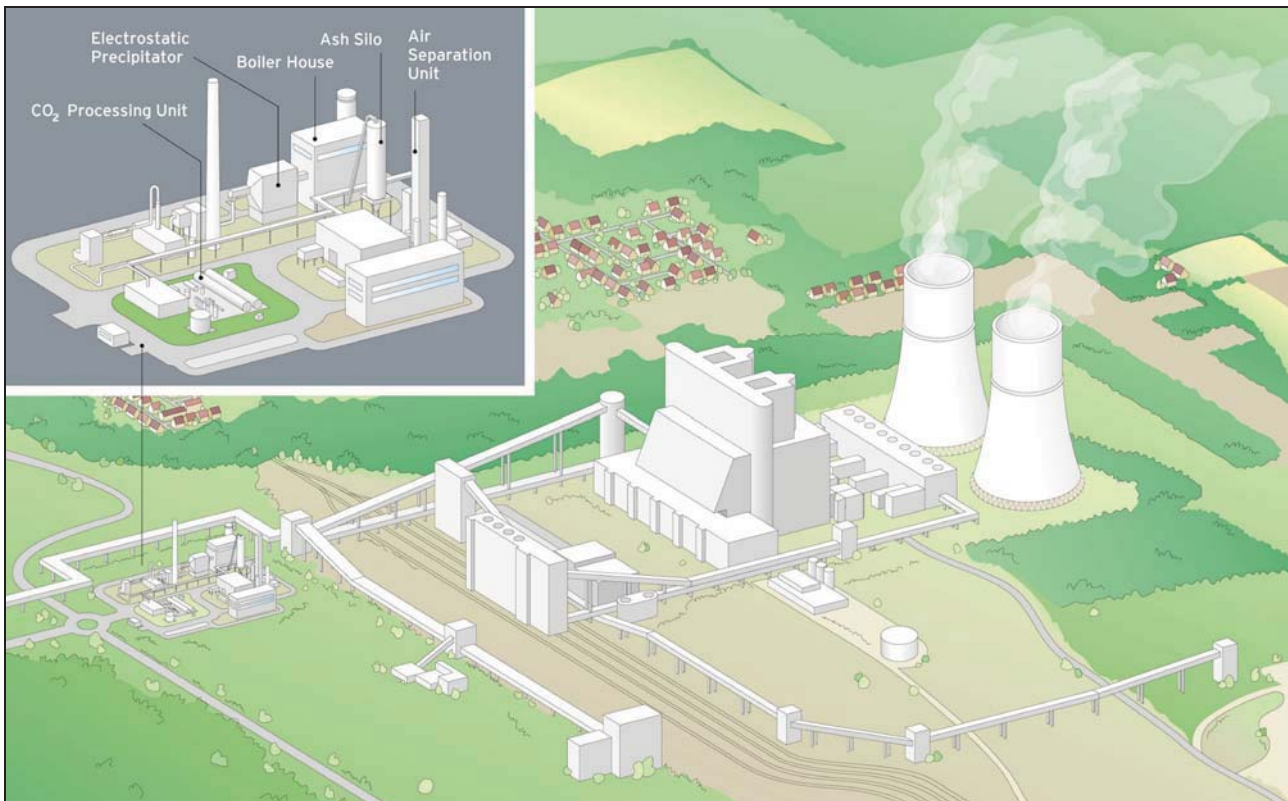


Figure 2 Pilot Plant Location

Several utility systems of the Schwarze Pumpe power plant and adjacent Schwarze Pumpe industrial park could be used for the pilot that shall be summarized as follows.

The delivery of fine lignite powder takes place by Vattenfall Europe Mining AG, located on the area of Schwarze Pumpe industrial park. The loading facilities are about 1.6 km distant from the pilot plant site. The fuel delivery to the Oxyfuel pilot plant takes place with special 25 t silo vehicles from loading facilities to the fuel storage silo. At a fuel consumption of maximal 6 t/h at 30 MW_{th} approximately 144 t/day pulverized lignite are needed, corresponding to average six transports of fuel per day at full pilot capacity. The fuel supply service includes also the reception and disposal of dry ash.

The main purpose with the pilot plant is gathering experience in the Oxyfuel combustion process. A “side effect” of this is the 30 MW of produced heat, which might be used for reduction of operating costs. The planned way to utilise the steam from the pilot plant would be the integration into the power plant auxiliary steam line, which constitutes a very large system being able to buffer the variations of the pilot plant within well-defined limits. That steam would not be injected into the main turbine of the power plant, but connected to the 18 bar auxiliary steam network used for internal consumption and steam export for external consumers, and so indirectly raise the power production of the turbine with about 6-8 MW_{el} at stable full load of the pilot plant.

To avoid the investment of a complete feed water production system, the pilot plant will get about the same amount of condensate back as delivered as steam. It will then only need a minimum of treatment of the condensate. The power plant would have to compensate for losses through its own feed water production and supply condensate water.

For the FGD plant, limestone powder will be delivered to the pilot plant - thus no limestone mill is

required - and mixed on site at the FGD to the required water content. The gypsum suspension though will be fed to the Power Plant Schwarze Pumpe, to avoid the investment of a complete gypsum treatment plant. The gypsum suspension is diluted with the cooling tower bleed-off and flooding and can so reach a lower solid content, which lowers the energy consumption for transport significantly. The gypsum suspension is fed to the limestone slurry preparation plant of the Power Plant Schwarze Pumpe.

Wastewater is generated altogether at about 12 tonnes per hour. Process wastewater is internally put back into the process, thus the Oxyfuel pilot plant runs wastewater-free from a process point of view.

The Power supply to the air and CO₂ compressors will also be supplied from the power plant Schwarze Pumpe via a high voltage (10 kV) connection. This implies daily reports in advance on time, duration and load of operation to the power plant.

Test Objectives

There exist a number of uncertainties even when applying “proven” technology in this Oxyfuel application. The pilot plant concept is defined in order to validate and finding ways of optimisation of the technology up to the point where the design and operating experience is good enough for scale up to commercial size. To enhance further confidence, the plant will be designed for 100% load at both air and oxygen firing, allowing to use the experience from today’s components in full-scale operation with air and to compare it with Oxyfuel conditions at the pilot scale.

These uncertainties are represented by a number of measurement objectives, presented for the combustion section and the gas treatment sections, all for oxygen and air-firing operation:

Combustion and recirculation

- Combustion characteristics (NO_x, SO_x, CO, O₂ level, CO₂, SO₂, SO₃, Hg and HC along flame and boiler path)
- Behaviour of recirculated products in flame (NO_x, SO₂, SO₃, fly ash etc.)
- Mapping of flame characteristics (shape and stability), temperature and velocity profiles
- Slagging / fouling
- Ash quality (incl. recovery of samples for ash /deposit characteristics in the furnace and convective pass)
- Radiation heat transfer in radiative section
- Convective heat transfer in boiler convective section
- Main loop air in-leakage / extracted gas quality
- Material testing and analysis

ASU, FG Treatment and CO₂ purification and compression

- Acid dew point
- SO₂ and SO₃ concentration at FGD exit
- Effect of cooling water temperature on performance of flue gas condenser
- Intercooling temperature in CO₂ compressor train
- Effect of liquefaction operating temperature and pressure
- Effect of different levels of O₂, acidic components and water vapour on CO₂ compressor train
- Condensate quality in FGC and CO₂ compression train

To achieve the recognition of specific characteristics, the following set of stable and “feasible” operating conditions are intended to be investigated at combustion conditions potentially representative for a large-scale plant:

- Coal types: lignite, bituminous, various kinds
- Excess oxygen: 1%(v) – 5%(v) excess O₂ in flue gas

- Flue gas recycle rate: O₂ concentration of 21-39%(v)
- Lignite moisture content: 10.5 up to 20%(w)
- Temperature of recycled flue gas: 150°C – 250°C
- Staged combustion
- Oxygen content in different burner and furnace oxidant (OFA) ports: The different registers in the burner are able to handle an O₂-concentration range from 0 – 40% O₂, also possible to supply 100% O₂ in one of the burner registers.
- Primary / Secondary recirculation alterations
- Air blown reference readings at 100% load (burner and material issues)
- Compression of CO₂ with different levels of inert content

To be studied is also general operating experience such as load changes and dynamic interaction between the different units, in particular the recirculation operation and the connected, for utility boiler plants novel systems, ASU and CO₂ compression and purification. These results then serve as basis for defining further equipment testing and in the end the input for designing the commercial scale plant.

Technology Justification

Oxyfuel combustion for coal has recently established itself as one of the most promising options for CO₂ capture from large-scale coal fired plants. Vattenfall has followed the competitiveness of this technology through benchmarking activities using both results from own and external investigations on performance and costs of the main options for CO₂ capture. An example of benchmarking results is presented below, applicable for typical conditions for large-scale power generation under European conditions as defined within the ENCAP and CASTOR projects. The benchmarking compares the resulting performance of post-combustion CO₂ capture using Fluor's Econamine process, IGCC with pre-combustion capture of CO₂ and Oxyfuel combustion against relevant reference plants without CO₂ capture. The main prerequisites for the evaluation are summarized in Table 1.

Table 1 Basic data used for economic evaluation.

Operating time	7500 hrs/year (Base load power plant)	
Economic lifetime	25 years	
Real interest rate	8% (taking into account the required rate of equity and interest rate on loans, inflation rate equal for all costs. Corporate tax and emission taxes disregarded.	
Fixed O&M	The IEA GHG data is adjusted to level considered as representative for European large-scale power plants. IEA GHG capture cases are adjusted so that the fixed O&M (% of investment) is kept constant between reference and capture cases	
Fuel cost (LHV)	Bituminous coal	1.6 €/GJ _{fuel}
	Lignite	1.1 €/GJ _{fuel}

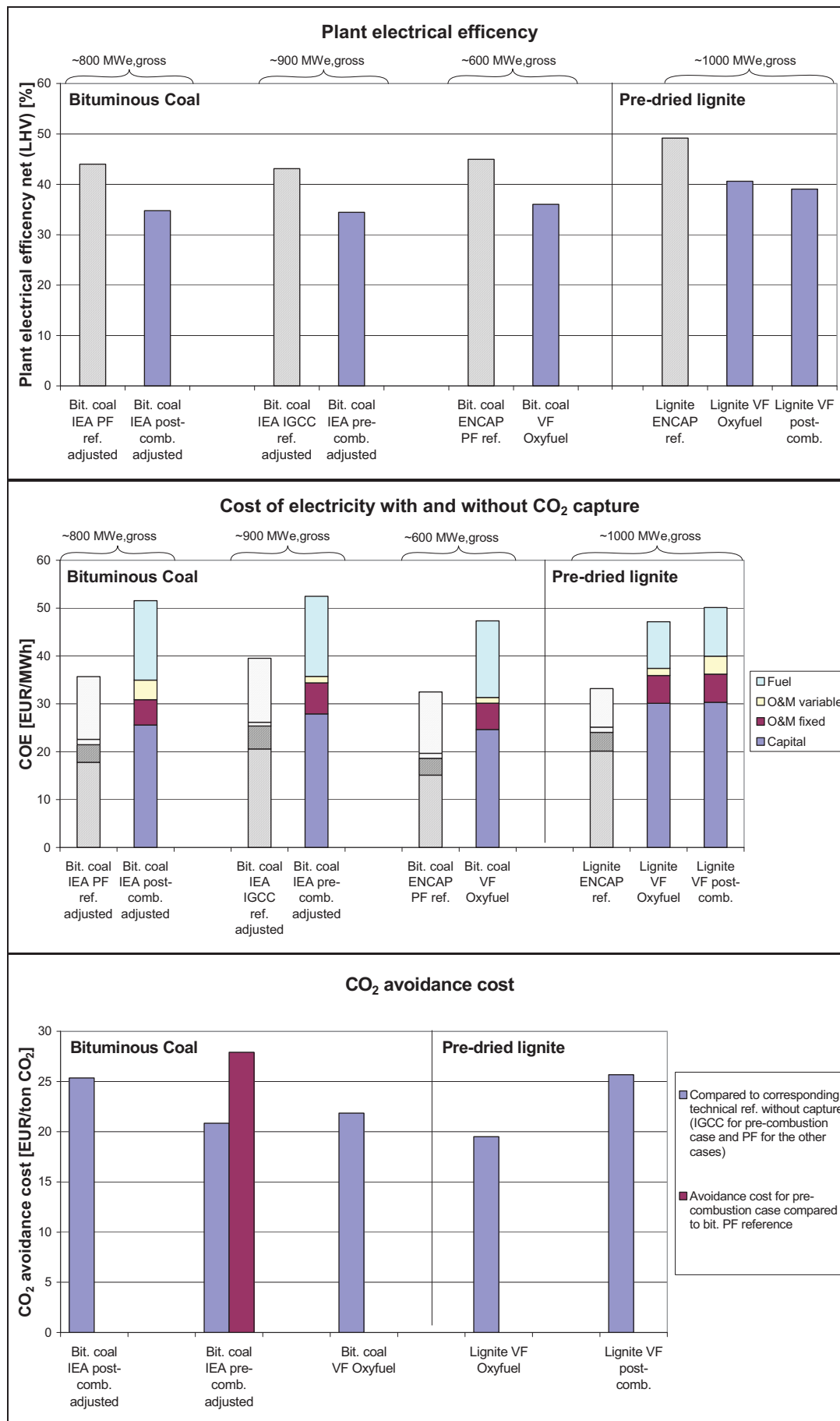


Figure 3 Electric efficiency, cost of electricity and CO₂ avoidance costs for the main options for CO₂ capture. “IEA” – data published by IEA GHG in [2] and [3], “VF” – Vattenfall internal, “g” – gross

The data presented shows that the three options for CO₂ capture come out quite similar with respect to efficiency and cost of electricity, however with a small advantage for Oxyfuel combustion under the conditions used in the evaluation. Considering the uncertainties that still remain in the concept definition and the assessment of the investment costs this is still within the margin of error. Regarding the CO₂ avoidance costs, these costs fall within the range of 20-25 €/ton CO₂ avoided for all options. Again, the Oxyfuel concept comes out quite well in comparison to the other technologies. An opportunity for the Oxyfuel technology is to be able to further optimize the CO₂ capture rate here calculated being 90%.

Concluding Remarks

The Oxyfuel technology applied to combustion of solid fuels, such as bituminous coal and lignite, has lately shown its potential competitiveness compared to other options for CO₂ capture. Activities to further develop the Oxyfuel concept are presently ongoing in different projects worldwide. Vattenfall has taken the initiative to build a 30 MW_{th} Oxyfuel pilot plant to be able to further develop and evaluate the Oxyfuel technology. The plant is scheduled to be in operation by year 2008 and will give important information for scale-up of the technology in a next step to a commercial plant in the size range of 600 MW_{th}.

References

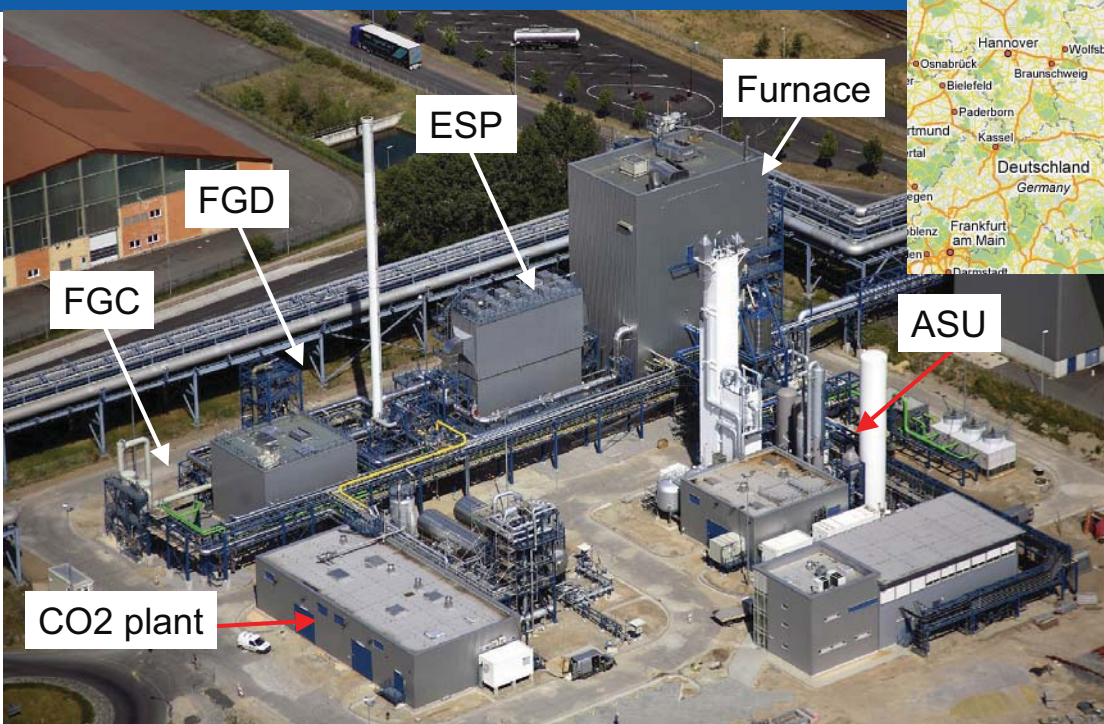
- [1] Andersson K, Birkestad H, Maksinen P, Johnsson F, Strömberg L, Lyngfelt A. An 865 MW lignite-fired CO₂-free power plant – a technical feasibility study. Proceedings of GHGT6, Kyoto, Japan, 2002.
- [2] Flour. Improvements in Power Generation with Post-Combustion Capture of CO₂. IEA GHG report number PH4/33, November 2004.
- [3] Foster Wheeler Energy Ltd. Potential for improvement in Gasification Combined Cycle Power Generation With CO₂ Capture. IEA GHG report number PH4/19, UK and Italy, May 2003.

Vattenfall's 30 MW Oxyfuel pilot plant

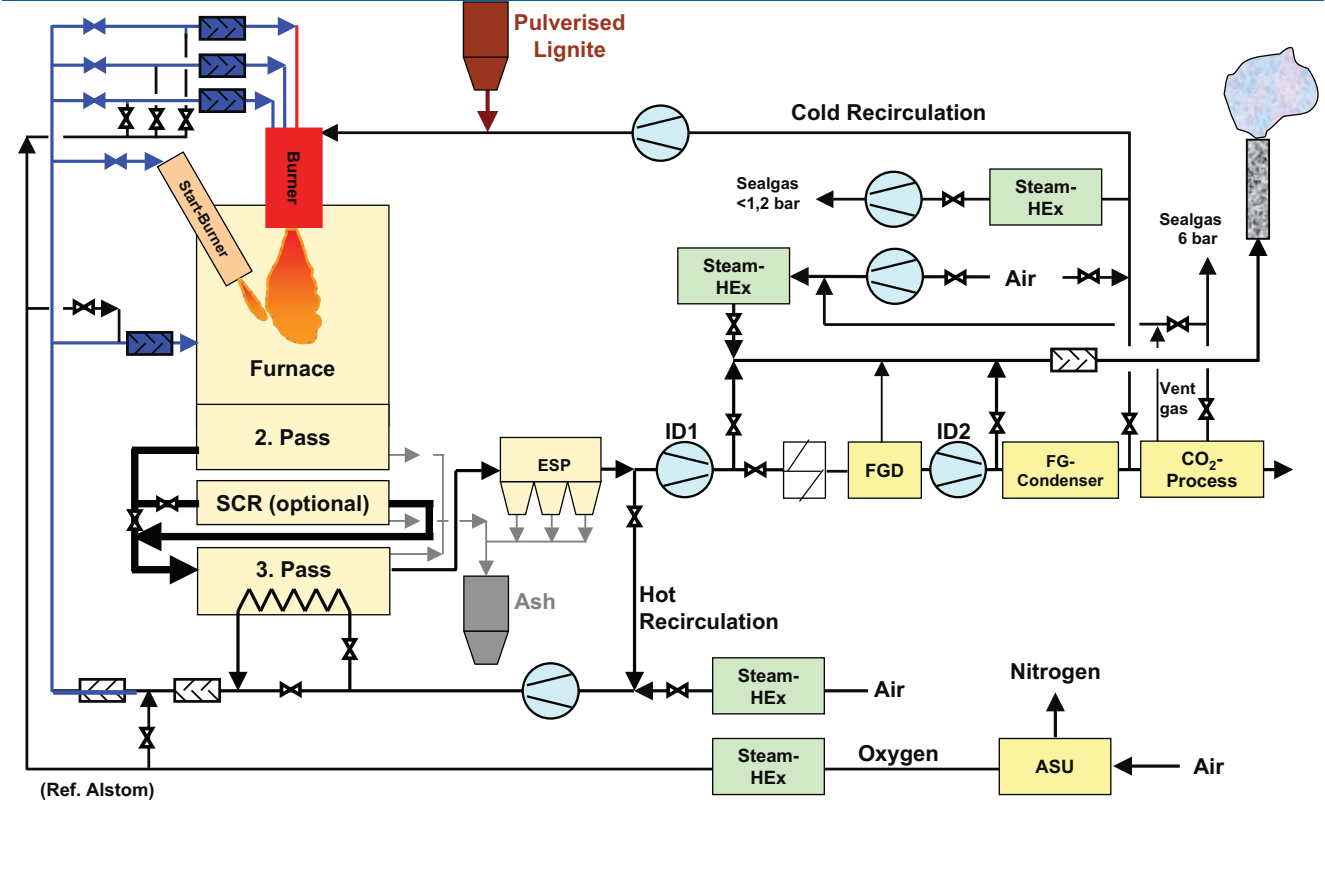


- Vattenfall has constructed a 30 MW_{th} Oxyfuel PF pilot plant
- New-built plant located next to the Schwarze Pumpe power station in Germany
- Investment decision taken by Vattenfall in May 2005.
- Ground breaking ceremony was held at the end of May 2006
- First ignition in May 2008, oxyfuel in July
- Official inauguration in September 2008

The Oxyfuel pilot plant



Plant overview



Basic data of the plant

Boiler: Indirect pulverised fuel fired	Thermal power Steam production Steam parameters	30 MW _{th} 40 t/h 25 bar / 350 °C
Fuel: pulverized lignite (Lausitz)	LHV Moisture Coal demand	21 MJ/kg 10,5 % 5,2 t/h
Media:	Oxygen (purity > 95%) CO ₂ (liquid)	8,5 t/h 9 t/h
Other:	Required area Investment	14.500 m ² ~ € 70 million

First experience from implementation of oxyfuel operation

- Extensive safety measures for handling of CO₂-rich flue gases and O₂
 - Personal gas alarms
 - CO₂ detectors are mounted at different locations
 - Gas ventilation of boiler house
- Implementation of different flue gas paths and requires bypass systems and as well as a new control system.
 - complex control and instrumentation system to handle flexibility
 - Implementation of the control systems for the ASU and the CO₂ plant into the control system of the steam generator presented a challenge
- Fuel transport
 - with air for air operation or dried flue gas for oxyfuel
- Pressure balancing with 5 fans in series, ASU – 2 x ID fan – 2 fans in CO₂ plant
- Corrosion in flue gas ducts due to increased H₂O, CO₂ and SO₂ content and frequent start-ups and shut downs



Initial Operating experiences from ASU

- Standard Linde GOX 6000 plant
- Start-up from ambient temperature requires manual operation and takes about 60-72 hours
- Automatic load change (ALC) and automatic start-up (AST) (for certain conditions) simplifies manual work
 - AST works only for shorter stand-still of less 3 days
- Longer stand-still >5 days require emptying the liquid level from the rectification column (risk for accumulation of C_xH_y)
- ASU has been designed for continuous operation, i.e. during furnace stand-stills, the ASU remains in operation
- Load change of ASU approx. 1 %/min in load window 75 – 100 %
- No difficulties in coupling ASU-furnace coupling !
- Pressure control to burner via GOX-buffer in two pressure stages 2,5 & 1,0 bar



Initial Operating experiences from FGD

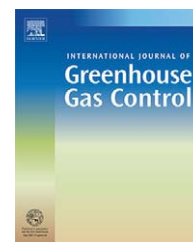
- SO₂-removal efficiency under oxyfuel as expected, >99,5%
- Amount of limestone needed same for air and oxyfuel
- No negative impact due to CO₂-rich atmosphere for FGD operation
- Gypsum quality corresponds to requirements
- No deposits on trays in absorber tower



Initial experience CO₂ compression and purification plant

- Transient load changes ca. 2,5 %/min in load range 60 – 100 %
- Start-up with pre-compressor, venting to ambient until 50% load is reached, main compressor is then started
- External NH₃-cooling loop works well and reduces system response time to liquify CO₂
- Approx. 400 tons CO₂ have been separated in week 6
- QM for CO₂ quality monitoring



available at www.sciencedirect.comjournal homepage: www.elsevier.com/locate/ijggc

CO₂ capture from power plants

Part I. A parametric study of the technical performance based on monoethanolamine

Mohammad R.M. Abu-Zahra^a, Léon H.J. Schneiders^a, John P.M. Niederer^b,
Paul H.M. Feron^{a,*}, Geert F. Versteeg^b

^aDepartment of Separation Technology, TNO Science and Industry, P.O. Box 342, 7300 AH, Apeldoorn, The Netherlands

^bDepartment of Development and Design of Industrial Processes, Twente University, P.O. Box 217, 7500 AE, Enschede, The Netherlands

ARTICLE INFO

Article history:

Received 31 July 2006

Received in revised form

10 November 2006

Accepted 17 November 2006

Published on line 18 December 2006

Keywords:

CO₂ capture

Absorption

Process optimization

MEA

ASPEN Plus

ABSTRACT

Capture and storage of CO₂ from fossil fuel fired power plants is drawing increasing interest as a potential method for the control of greenhouse gas emissions. An optimization and technical parameter study for a CO₂ capture process from flue gas of a 600 MWe bituminous coal fired power plant, based on absorption/desorption process with MEA solutions, using ASPEN Plus with the RADFRAC subroutine, was performed. This optimization aimed to reduce the energy requirement for solvent regeneration, by investigating the effects of CO₂ removal percentage, MEA concentration, lean solvent loading, stripper operating pressure and lean solvent temperature.

Major energy savings can be realized by optimizing the lean solvent loading, the amine solvent concentration as well as the stripper operating pressure. A minimum thermal energy requirement was found at a lean MEA loading of 0.3, using a 40 wt.% MEA solution and a stripper operating pressure of 210 kPa, resulting in a thermal energy requirement of 3.0 GJ/ton CO₂, which is 23% lower than the base case of 3.9 GJ/ton CO₂. Although the solvent process conditions might not be realisable for MEA due to constraints imposed by corrosion and solvent degradation, the results show that a parametric study will point towards possibilities for process optimisation.

© 2006 Elsevier Ltd. All rights reserved.

1. Introduction

Human activity has caused the atmospheric concentration of greenhouse gases such as carbon dioxide, methane, nitrous oxide and chlorofluorocarbons to gradually increase over the last century. The Intergovernmental Panel on Climate Changes (IPCC) has evaluated the size and impact of this increase, and found that since the industrial revolution their concentrations in the atmosphere have increased and carbon dioxide as such is considered to be responsible for about 50% of this increase (IPCC, 2005).

The main CO₂ source is the combustion of fossil fuels such as coal, oil and gas in power plants, for transportation and in homes, offices and industry. Fossil fuels provide more than 80% of the world's total energy demands. It is difficult to reduce the dependency on fossil fuels and switch to other energy sources. Moreover, the conversion efficiency of other energy sources for power generation is mostly not as high as that of fossil fuels. A drastic reduction of CO₂ emissions resulting from fossil fuels can only be obtained by increasing the efficiency of power plants and production processes, and decreasing the energy demand, combined with CO₂ capture and long term storage (CCS).

* Corresponding author. Tel.: +31 55 549 3151; fax: +31 55 549 3410.

E-mail address: Paul.Feron@tno.nl (Paul H.M. Feron).

1750-5836/\$ – see front matter © 2006 Elsevier Ltd. All rights reserved.

doi:10.1016/S1750-5836(06)00007-7

A_p	area of packing (m^2)
C	MEA concentration (mol/m^3)
ΔC	actual driving force (mol/m^3)
$C_{CO_2,i}$	carbon dioxide concentration on the interface (mol/m^3)
C_{MEA}	MEA concentration (mol/m^3)
$D_{CO_2,am}$	CO_2 diffusivity in the MEA solution (m^2/s)
$D_{MEA,am}$	MEA diffusivity in the MEA solution (m^2/s)
E	enhancement factor
E_∞	enhancement factor of an infinitely fast reaction
Ha	Hatta modulus
J	mass transfer flux ($mol/m^2 s$)
k_2	forward second order reaction rate constant ($m^3/mol s$)
K_G	mass transfer coefficient in the gas phase (m/s)
K_L	mass transfer coefficient in the liquid phase (m/s)
K_{ov}	overall mass transfer coefficient (m/s)
K_{-1}	regeneration reaction rate constant ($m^3/mol s$)
m	solubility of carbon dioxide at equilibrium
MEA	monoethanolamine
T	temperature (K)

Greek symbols

α	CO_2 loading ($mol CO_2/mol MEA$)
γ	stoichiometric ratio in the reaction
ϕ_{CO_2}	CO_2 flow (mol/s)

CCS is a promising method considering the ever increasing worldwide energy demand and the possibility of retrofitting existing plants with capture, transport and storage of CO_2 . The captured CO_2 can be used for enhanced oil recovery, in the chemical and food industries, or can be stored underground instead of being emitted to the atmosphere.

Technologies to separate CO_2 from flue gases are based on absorption, adsorption, membranes or other physical and biological separation methods. Rao and Rubin (2002) showed that for many reasons amine based CO_2 absorption systems are the most suitable for combustion based power plants: for example, they can be used for dilute systems and low CO_2 concentrations, the technology is commercially available, it is easy to use and can be retrofitted to existing power plants. Absorption processes are based on thermally regenerable solvents, which have a strong affinity for CO_2 . They are regenerated at elevated temperature. The process thus requires thermal energy for the regeneration of the solvent.

Aqueous monoethanolamine (MEA) is an available absorption technology for removing CO_2 from flue gas streams. It has been used in the Fluor Daniel technology's Econamine FGTM and Econamine FG PlusTM (Mariz, 1998; Chapel et al., 1999) and the ABB Lummus Global technology (Barchas, 1992). Many researchers are aiming to develop new solvent technologies to improve the efficiency of the CO_2 removal. Process simulation and evaluation are essential items to maximize the absorption process performance.

Several researchers have modelled and studied the MEA absorption process (Rao and Rubin, 2002; Mariz, 1998; Chapel et al., 1999; Barchas, 1992; Alie et al., 2005; Singh et al., 2003; Sander and Mariz, 1992; Suda et al., 1992; Chang and Shih, 2005), most of their conclusions focused on reducing the thermal energy requirement to reduce the overall process expenses. The Econamine FGTM requirement was given by Chapel et al. (1999): a regeneration energy of 4.2 GJ/ton CO_2 was used, which was calculated to be responsible for around 36% of the overall operating cost. This high energy requirement makes the capture process energy-intensive and costly. Therefore, it is important to study the conventional MEA process trying to reduce this energy requirement.

Alie et al. (2005) proposed a flow sheet decomposition method, which is a good start to estimate the process tear streams initial guess. However, it is important to use a complete and closed flow sheet to keep the water balance in the system. Alie et al. (2005) found that the lowest energy requirement of 176 kJ/mol CO_2 (4 GJ/ton CO_2) can be achieved at lean solvent loading between 0.25 and 0.30 mol $CO_2/mol MEA$. Singh et al. (2003) found that the thermal energy requirement for MEA process is a major part of the process overall operating cost, and by modelling the MEA process for a 400 MWe coal fired power plant he found a specific thermal energy requirement equal to 3.8 GJ/ton CO_2 .

In this work a parametric study is presented aimed at developing an optimized absorption/desorption process which has a lower thermal energy requirement compared to the available literature data of around 4 GJ/ton CO_2 . The base case flow sheet for this parametric study is the conventional flow sheet which is available in commercial application (Mariz, 1998). However the Fluor improved process Econamine FG PlusTM (Chapel et al., 1999) was not considered as a base case because it has no commercial applications yet. This parametric study uses the ASPEN Plus software package (Aspen Plus, 2005) to the process modelling based on aqueous MEA solution. In this work a variation in several parameters has been included, because the combined effect of several parameters is expected to give a larger effect on the overall process performance compared to a variation of single parameter.

After the process simulation a design model for both the absorber and the stripper was built to investigate the effect of chemical reaction and mass transfer on the absorption process. The following parameters were varied: the CO_2 lean solvent loading, the CO_2 removal percentage, the MEA weight percentage, the stripper operating pressure and the lean solvent temperature. In particular the effect on the thermal energy requirement for the solvent regeneration, the amount of cooling water and the solvent flow rate was amended. These are key performance parameters for the absorption/desorption process and the focal part in the optimization.

2. Process description

The process design was based on a standard regenerative absorption-desorption concept as shown in the simplified flow diagram in Fig. 1 (Rao and Rubin, 2002).

The flue gases from the power plant enter a direct contact cooler (C1) at a temperature depending on the type of the

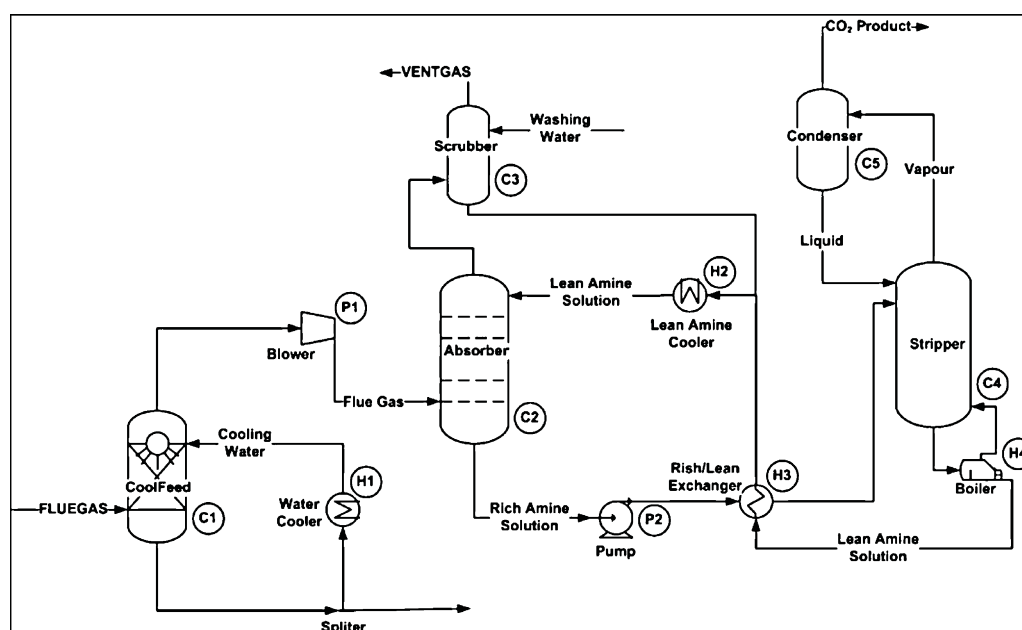


Fig. 1 – CO₂ removal amine process flow sheet.

power plant, after which they are cooled with circulating water to around 40 °C. Subsequently, the gas is transported with a gas blower (P1) to overcome the pressure drop caused by the MEA absorber.

The gases flow through the packed bed absorber (C2) counter currently with the absorbent (an aqueous MEA solution), in which the absorbent reacts chemically with the carbon dioxide (packed bed columns are preferred over plate columns because of their higher contact area). The CO₂ lean gas enters a water wash scrubber (C3) in which water and MEA vapour and droplets are recovered and recycled back into the absorber to decrease the solvent loss. The treated gas is vented to the atmosphere.

The rich solvent containing chemically bound CO₂ is pumped to the top of a stripper via a lean/rich cross heat exchanger (H3) in which the rich solvent is heated to a temperature close to the stripper operating temperature (110–120 °C) and the CO₂ lean solution is cooled. The chemical solvent is regenerated in the stripper (C4) at elevated temperatures (100–140 °C) and a pressure not much higher than atmospheric. Heat is supplied to the reboiler (H4) using low-pressure steam to maintain regeneration conditions. This leads to a thermal energy penalty because the solvent has to be heated to provide the required desorption heat for the removal of the chemically bound CO₂ and for the production of steam, which acts as stripping gas. Steam is recovered in the condenser (C5) and fed back to the stripper, after which the produced CO₂ gas leaves the condenser. Finally, the lean solvent is pumped back to the absorber via the lean/rich heat exchanger (H3) and a cooler (H2) to bring its temperature down to the absorber level.

The absorber was simulated at 110 kPa with a pressure drop of 4.8 kPa, using three equilibrium stages of the RADFRAC subroutine. A preliminary study into the determination of the minimum number of stages required to achieve equilibrium

revealed that three stages were quite adequate in achieving equilibrium. Increasing the number did not result in a more detailed and better description of the absorption process. To simulate the stripper, with an operating pressure of 150 kPa and a pressure drop of 30 kPa, eight equilibrium stages were required.

2.1. Baseline case definition and simulation

The flue gas flow rate and composition for 600 MWe coal-fired power plant, which has been used in the study are presented in Table 1.

Simulations were performed using the ASPEN plus version 13.1 (Aspen Plus, 2005). The thermodynamic and transport properties were modelled using a so-called “MEA Property Insert”, which describes the MEA–H₂O–CO₂ system thermodynamically with the electrolyte-NRTL model. The following base case was defined:

- a 90% CO₂ removal;
- a 30 MEA wt.% absorption liquid;

Table 1 – Flue gas flow rate and composition

Mass flow (kg/s)	616.0
Pressure (kPa)	101.6
Temperature (°C)	48
Composition	Wet gas (vol.%)
N ₂ + Ar	71.62
CO ₂	13.30
H ₂ O	11.25
O ₂	3.81
SO ₂	0.005
NO _x	0.0097

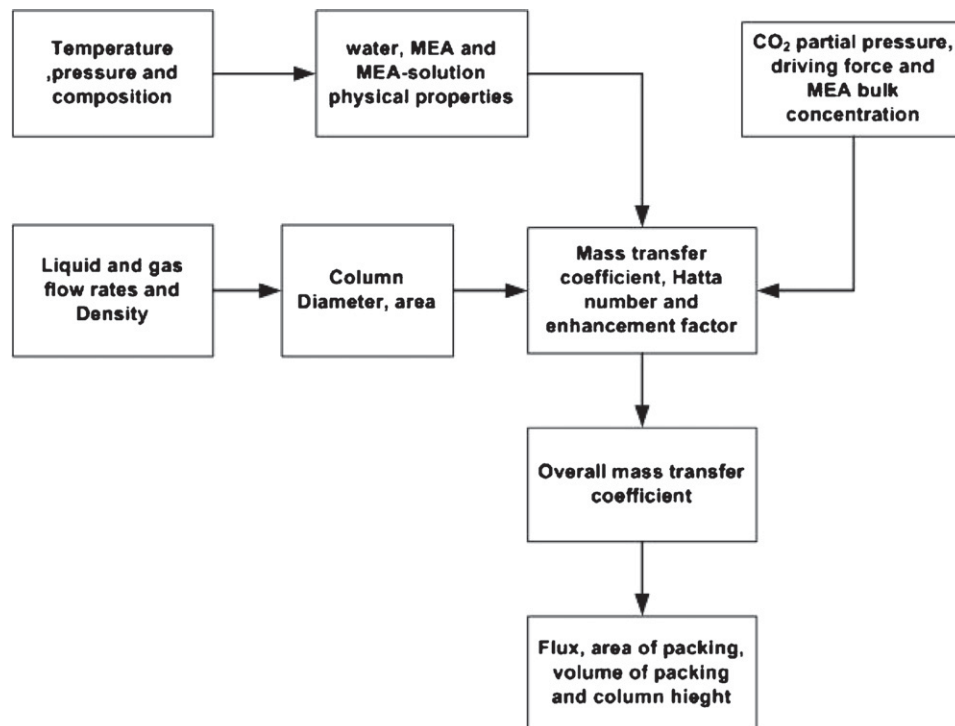
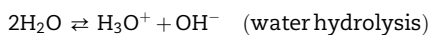
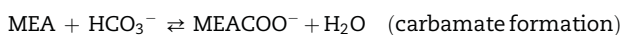
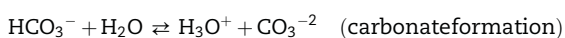
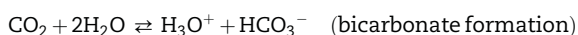
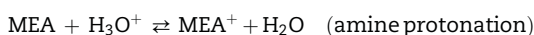


Fig. 2 – Absorber model block diagram.

- using a lean solvent loading of 0.24 mol CO₂/mol MEA (i.e. a 50% degree of regeneration).

2.2. Design model

The reactive absorption of the CO₂-MEA-H₂O system is complex because of multiple equilibrium and kinetic reversible reactions. The equilibrium reactions included in this model are:



The absorber will treat large volumes of flue gases and is therefore the largest equipment in a capture plant. As such it is expected to have a major capital cost, associated with it. Given its importance in investment terms, a design model for the absorber column based on first principles using the equilibrium stage model data, was built. From the overall mass transfer coefficient and the driving force, the mass transfer flux was calculated, which then has been used to estimate the required area of packing. The structure of the absorber model that has been used can be seen in the absorber model block diagram in Fig. 2 and the methods used can be found in more detail in Appendix A. An identical procedure was also followed for the regenerator columns.

2.3. Parameter study

In this study, some of the main parameters affecting the capture process will be varied as an initial step towards an optimization of the process. Starting from the baseline case the following process parameters will be varied:

- The CO₂ lean solvent loading (mol CO₂/mol MEA), by varying the degree of regeneration (20, 30, 40, 50 and 60% degree of regeneration).
- The amount of CO₂ removed (80, 90, 95 and 99% removal).
- The MEA weight percentage in the absorption solvent (20, 30 and 40 wt.%).
- The stripper operating pressure.
- The lean solvent temperature, at the absorber inlet.

The following performance indicators in the absorption/desorption process were used to investigate the effect of the parameters:

- The thermal energy required in the stripper (GJ energy/ton CO₂ removed).
- The amount of cooling water needed in the process (m³ cooling water/ton CO₂ removed).
- The solvent circulation rate needed for the absorption (m³ solvent/ton CO₂ removed).

These indicators were chosen because they present information on both the operating and the capital costs. The thermal energy is expected to be a major contributor to the production cost and a change in the energy required will give a clear effect on the operating costs. Both the

amount of cooling water and solvent required affect the size of the equipment, which in turn influences the capital costs.

3. Results and discussion

3.1. Baseline case

The capture base case was simulated using a complete closed flow sheet to keep the overall water balance to zero. This makes the flow sheet more difficult to converge due to the recycle structure in the flow sheet. However, this is important as only then the results will be realistic. The choice and the initial estimation of the tear streams are important factors in the flow sheet convergence. The results of the baseline case simulations are shown in Table 2. The energy requirement was 3.9 GJ/ton CO₂, which agrees well with the numbers reported in industry today. For example, the Fluor Econamine FGTM process requires 4.2 GJ/ton CO₂ (Chapel et al., 1999), and the Fluor Econamine FG PlusTM technology required a somewhat lower energy requirement of 3.24 GJ/ton CO₂ (IEA, 2004). However, the latter technology consists of different and more complex process configurations (split flow configurations and absorber intercooling) and improved solvent characteristics. The cooling water and solvent requirement for both the base case processes were in line with the data of Fluor Econamine FGTM.

Table 2 – Results of the baseline case

Amine lean solvent loading (mol CO ₂ /mol MEA)	0.242
Amine rich solvent loading (mol CO ₂ /mol MEA)	0.484
Thermal heat required (GJ/ton CO ₂)	3.89
Solvent flow rate required (m ³ /ton CO ₂)	20.0
Cooling water required	
Feed cooling water (m ³ /ton CO ₂)	9
Condenser (m ³ /ton CO ₂)	41.5
Lean cooler (m ³ /ton CO ₂)	42
Scrubber (m ³ /ton CO ₂)	0.2
CO ₂ product compressor intercooling (m ³ /ton CO ₂)	13.16
Total cooling water required (m ³ /ton CO ₂)	106

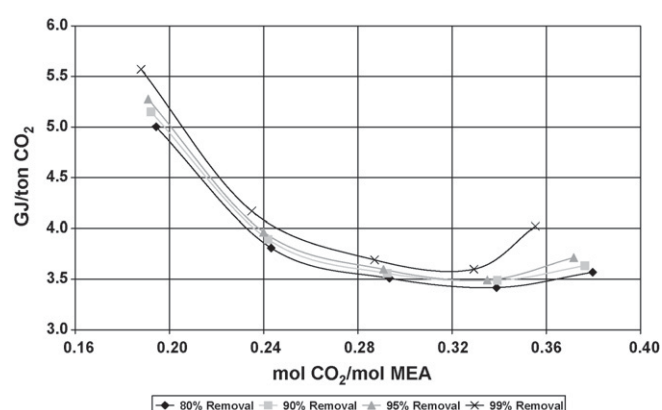


Fig. 3 – Thermal energy requirement at various CO₂/amine lean solvent loadings for different CO₂ removal (%).

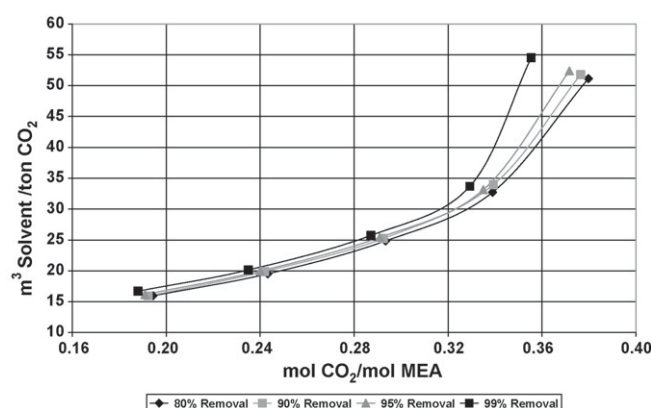


Fig. 4 – Solvent flow rate requirement at various CO₂/amine lean solvent loadings for different CO₂ removal (%).

3.2. Effect of different lean solvent loading including the effect of the CO₂ removal (%)

The lean solvent loading of the MEA solution representing the degree of regeneration, was varied to find the optimum solvent loading for a minimal thermal energy requirement. This can be achieved by changing the reboiler energy input. For a given degree of regeneration, to achieve the same CO₂ removal capacity, the absorption solvent circulation rate was varied.

At low values of lean solvent loading, the amount of stripping steam required to achieve this low solvent loading is dominant in the thermal energy requirement. At high values of lean solvent loading the heating up of the solvent at these high solvent circulation flow rates is dominant in the thermal energy requirement. Therefore a minimum is expected in the thermal energy requirement. From Fig. 3 it is indeed clear that the thermal energy requirement decreases with increasing lean solvent loading until a minimum is attained. The point at which the energy requirement is lowest will be defined to be the optimum lean solvent loading. For 90% removal and a 30 wt.% MEA solution the optimum lean solvent loading was around 0.32–0.33 mol CO₂/mol MEA, with a thermal energy requirement of 3.45 GJ/ton CO₂. This is a reduction of 11.5% compared to the base case. It must be noted, however, that the solvent circulation rate was increased to 33 m³/ton CO₂. Above lean solvent loading of a 0.32 mol CO₂/mol MEA the solvent circulation rate increases more than linearly with the lean solvent loading (see Fig. 4).

For the cooling water required (see Fig. 5) the occurrence of a local minimum was not strictly encountered: the amount of thermal cooling water decreased with increasing lean solvent loadings, in line with the reduced energy requirement. The amount of cooling water needed remained basically constant for a lean solvent loading between 0.26 and 0.33 mol CO₂/mol MEA. This can be explained by the fact that at high lean solvent loadings the lean solvent was not cooled to 35 °C as in the base case. To meet the requirement of a closed water balance, the temperature of the lean solvent entering the absorber was allowed to increase. As a consequence the absorber operates at a higher temperature allowing evaporation of water from the top of the absorber to maintain a closed

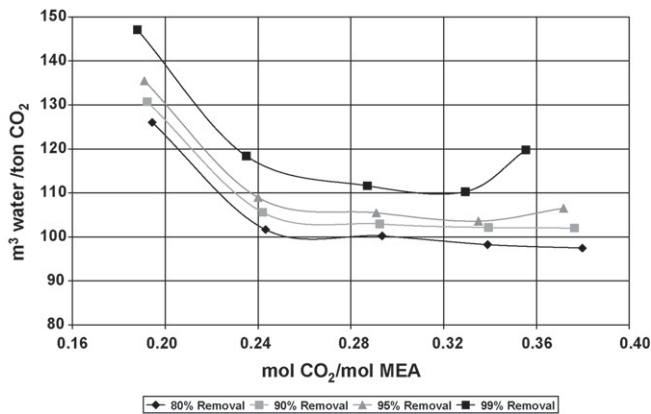


Fig. 5 – Cooling water consumption at various CO₂/amine lean solvent loadings for different CO₂ removal (%).

water balance in the complete process (lean solvent temperatures were varied from 35 °C up to 50 °C). If the lean solvent temperature was kept constant at high solvent flow rates, this would have led to excessive condensation in the absorber. This water would have to be removed in the stripper.

Increasing the percentage of CO₂ removed from 80 to 99% resulted in a small increase in the thermal energy, solvent and cooling water as clearly shown in Figs. 3–5. The differences between the different removal percentages were most pronounced at high lean solvent loadings. To obtain the same removal percentage at high lean solvent loadings, which means lowering the driving force in the top of the absorber, more solvent would be needed, which rapidly increases the energy requirement at high lean solvent loadings.

3.3. Effect of MEA (wt.%)

The thermal energy requirement was found to decrease substantially with increasing MEA concentration (see Fig. 6). It seems attractive to use higher MEA concentrations. However, increasing the MEA concentration is expected to have pronounced corrosive effects. It is therefore required to use better corrosion inhibitors in order to realise the energy saving potential of higher MEA concentrations. Moreover, at high MEA concentration it is expected to have a higher MEA

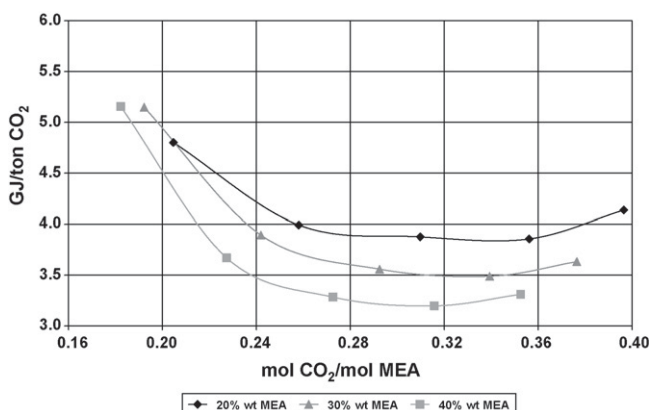


Fig. 6 – Thermal energy requirement at various CO₂/amine lean solvent loadings for different MEA (wt.%).

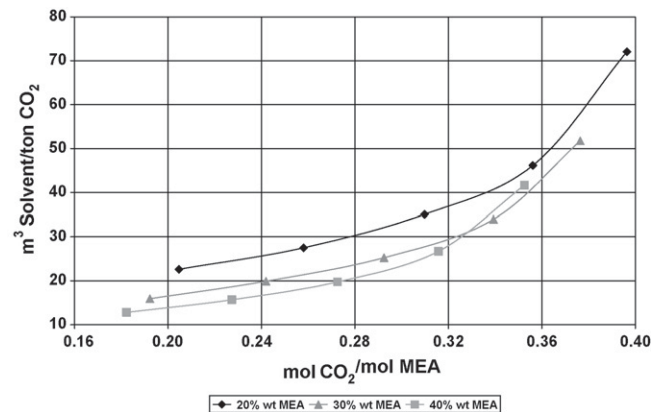


Fig. 7 – Solvent flow rate requirement at various CO₂/amine lean solvent loadings for different MEA (wt.%).

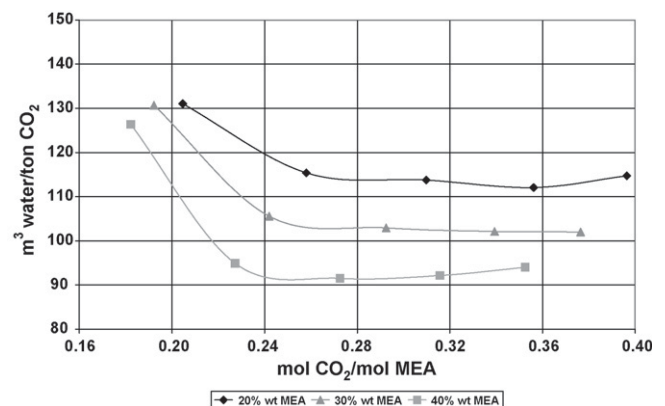


Fig. 8 – Cooling water consumption at various CO₂/amine lean solvent loadings for different MEA (wt.%).

content in the vent gas, but a good washing section can overcome this problem and keep the MEA content in the vent gas as low as possible. The wash section used in the process flow sheets always resulted in an MEA-content much lower than 1 ppm. Upon an increase of the MEA concentration from 30 to 40 wt.%, the thermal energy requirement decreased with 5–8%. Furthermore, the cooling water and solvent consumption decreased with increasing MEA concentration (see Figs. 7 and 8).

The optimum lean solvent loading was for example around 0.32 and 0.29 mol CO₂/mol MEA for 30 and 40 wt.% MEA solutions, respectively. This lower solvent loading with increasing MEA concentration is due to the lower rich solvent loading obtained when using high MEA concentrations.

3.4. Effect of the stripper operating conditions

The effect of different conditions (temperature and pressure) of the stripper has also been investigated. It is expected that at high temperature (and therefore high pressure) the CO₂ mass transfer rate, throughout the stripper column is positively affected via the increased driving force. Starting from the base case (90% CO₂ removal, 30 wt.% MEA solution and 0.24 mol CO₂/mol MEA lean solvent loading) the effect of the

Table 3 – Results of the main process parameters at different stripper pressure

Stripper pressure (kPa)	Stripper temperature (K)	Thermal energy (GJ/ton CO ₂)	Solvent (m ³ /ton CO ₂)	Cooling water (m ³ /ton CO ₂)
90	381	4.87	19.5	128
120	387	4.24	19.7	114
150	393	3.89	19.8	105
180	397	3.68	19.9	101
210	401	3.56	20	98

stripper operating pressure (90–210 kPa) was investigated, assuming a total pressure drop of 30 kPa over the stripper packing and wash section.

Table 3 shows the effect of the stripper pressure and temperature on the process requirement. Clearly, with increased operating pressure of the stripper the energy requirement decreased significantly; i.e., from 150 kPa (base case) to 210 kPa led to an 8.5% reduction in the energy requirement. However, it might be realistic to expect that higher amine degradation rates and corrosion problems will occur at these elevated pressures and temperature. Nevertheless, it demonstrates the possibility of lowering the thermal energy requirement for solvent regeneration by increasing the stripper temperature. The operating pressure of the stripper is more than doubled between 381 and 401 K. The impact of the higher pressure on the design and construction of the stripper has to be taken into account. The amount of solvent required is almost constant with a very small increase (maximum 0.5 m³/ton CO₂) at the maximum stripper pressure used in this study. Because the flue gas specifications and the removal % of CO₂ are the same in all cases, the amount of solvent required does not depend much on the stripper conditions. The cooling water requirement is decreased, from ca. 128 m³/ton CO₂ at 90 kPa to ca. 98 m³/ton CO₂ at 210 kPa (see Table 3). Increasing the stripper temperature will increase the driving force; this will result in a smaller column and hence a lower capital investment.

3.5. Effect of the lean solvent temperature

In Section 3.2, it was mentioned that, at high lean solvent loadings the absorption temperature needs to be increased to ensure a closed water balance in the process. The lean solvent temperature was varied between 25 and 50 °C for the base case (90% removal, 30 wt.% MEA and 50% regeneration) to investigate the effect of the lean solvent temperature on the process parameters.

Increasing the lean solvent temperature had a negative effect on the thermal energy requirement because the rich solvent loading is lower at higher lean solvent temperature. This will result in a higher regeneration energy (see Fig. 9). Decreasing the temperature to 25 °C led to a 4% reduction in the thermal energy requirement compared to the base case. The solvent circulation rate is nearly constant over the temperature range, because the lean solvent loading is almost constant in all cases and the CO₂ recovery was kept the same. However, the effect on the cooling water was the opposite because less cooling energy is required in the lean cooler, resulting in a lower total cooling water consumption with an increased solvent temperature (see Fig. 10). At a higher lean

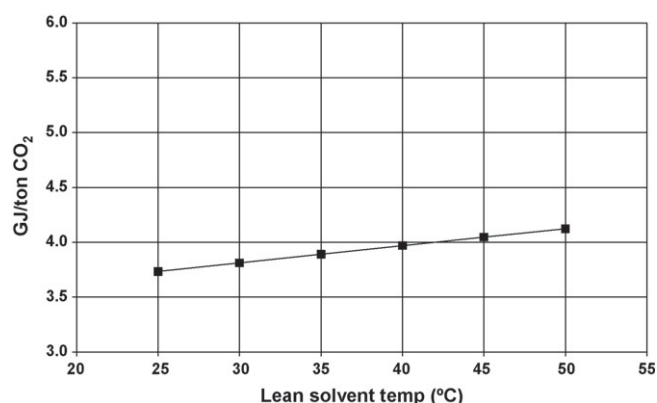


Fig. 9 – Thermal energy requirement for different lean solvent temperatures.

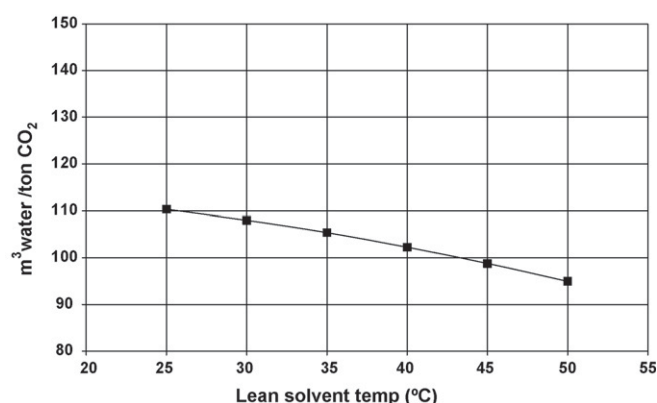


Fig. 10 – Cooling water consumption with different lean solvent temperatures.

solvent temperature, the absorber as a whole will be operated at a higher temperature. This higher operating temperature will increase the evaporation rate of MEA from the top of the absorber. To avoid this high evaporation rate of MEA, the washing section is required to operate at a higher washing water rate.

4. Process optimisation with respect to thermal energy requirement

4.1. Definition of the optimum process

The thermal energy requirement in the capture process is the most important factor, because it is responsible of the major

Table 4 – Optimum process specifications

	30 wt.% MEA	40 wt.% MEA
CO ₂ removal (%)	90	90
MEA (wt.%)	30	40
Lean solvent loading (mol CO ₂ /mol MEA)	0.32	0.30
Stripper operating pressure (kPa)	210	210
Absorption solution temperature (°C)	ca. 25	ca. 25

reduction of the power plant overall thermal efficiency. The optimum process will be defined as the process which has the lowest thermal energy requirement for the five parameters investigated, i.e. CO₂ removal %, MEA solvent concentration, lean solvent loading, stripper operating pressure and lean solvent temperature.

For the optimization 90% CO₂ removal was chosen, because the analysis showed that this parameter was not a critical factor.

Increasing the MEA wt.% decreased the energy requirement, with a minimum observed for a 40 wt.% solutions. Two optimum processes were defined: the first one with a MEA concentration of 40 wt.% MEA and the second one, chosen close to currently used solvent composition, with a concentration of 30 wt.% MEA. The latter concentration is probably more realistic due to the practical constraints imposed by solvent corrosion and degradation. The optimum lean solvent loading equalled 0.30 and 0.32 mol CO₂/mol MEA for 40 and 30 wt.% MEA solutions, respectively.

Higher stripper operating pressures always resulted in a lower thermal energy requirement and an optimum stripper operating pressure of 210 kPa, which was the maximum considered in this study. Decreasing the absorption lean solvent temperature resulted in lower thermal energy requirement. Therefore, a lean solvent temperature of 25 °C will be used in the process optimization. However, as discussed earlier, for high lean solvent loadings the lean solvent temperatures had to be increased in order to maintain the water balance over the complete process, therefore it may be difficult to realize convergence for all of the process simulations at 25 °C. Therefore, the optimum lean solvent temperature will be defined as the lowest temperature which can be achieved; for some cases this could be higher than 25 °C. The specifications of the two optimum processes are summarised in Table 4.

4.2. The optimum processes

The defined processes in Table 4 were simulated with ASPEN Plus; the results are presented in Table 5 including the base case results for a clear comparison.

Clearly, the optimum processes that were defined had a lower thermal energy requirement than the base case process, with a reduction of 16 and 23% for 30 and 40 wt.% MEA solutions, respectively. This decrease in the thermal energy requirement would cause the operating costs to decrease significantly, thereby strongly improving the process. However, it should be noted that, as a result of the changes in the process operating conditions, capital costs could increase as well as the operating costs due to the need of, e.g. corrosion additives and more stringent stripper design requirements at high operating pressure.

For the optimum process the cooling water required in the capture process decreased by 3–10% compared to the base case. Furthermore, the solvent required in the optimum processes increased with 10–40% compared to the base case, and that is because of the higher lean solvent loading used in the optimization.

5. Conclusions

The modelling work and parametric study have shown that that Aspen Plus with RADFRAC subroutine is a useful tool for the study of CO₂ absorption processes.

The lean solvent loading was found to have a major effect on the process performance parameters such as the thermal energy requirement. Therefore it is a main subject in the optimisation of solvent processes.

Significant energy savings can be realized by increasing the MEA concentration in the absorption solution. It is however still to be investigated if high MEA concentrations can be used due to possible corrosion and solvent degradation issues.

Increasing the operating pressure in the stripper would lead to a higher efficiency of the regeneration and would reduce requirement of the thermal energy. Moreover, a high operating pressure would reduce the costs and the energy needed for CO₂ compression.

Table 5 – Optimum process results

	Base case	30 wt.% MEA	40 wt.% MEA
Amine lean solvent loading (mol CO ₂ /mol MEA)	0.242	0.32	0.30
Amine rich solvent loading (mol CO ₂ /mol MEA)	0.484	0.493	0.466
Reboiler heat required (GJ/ton CO ₂)	3.89	3.29	3.01
Solvent flow rate required (m ³ /ton CO ₂)	20.0	27.8	22
Lean solvent temperature (°C)	35	30	25
Cooling water required			
Feed cooling water (m ³ /ton CO ₂)	9	9	9
Condenser (m ³ /ton CO ₂)	41.5	24	19.7
Lean cooler (m ³ /ton CO ₂)	42	57	54
Scrubber (m ³ /ton CO ₂)	0.2	0.03	0.03
CO ₂ product compressor intercooling (m ³ /ton CO ₂)	13	13	13
Total cooling water required (m ³ /ton CO ₂)	106	103	96

Decreasing the lean solvent temperature would save energy in the process, but the amount of cooling water required would counter balance this effect.

From the optimization of the absorption/desorption cycle for the CO₂ capture process, it can be concluded that a reduction of around 20% in the thermal energy requirement seems realistic. For the optimum process using a 30 wt.% MEA solution the energy requirement was found to be 3.3 GJ/ton CO₂, which looks promising in reducing the costs and increase of the efficiency of the capture process. Moreover, when the absorption solution consisting of a 40 wt.% MEA could be used, the energy requirement is 3.0 GJ/ton CO₂, which is a substantial reduction compared to 3.9 GJ/ton CO₂ found for the base case.

Acknowledgements

The authors would like to thank the European Project on the 'Capture and Geological Storage of CO₂' (CASTOR) and the 'CO₂ Capture, Transport and Storage' project in The Netherlands (CATO) for their financial and technical support.

Appendix A. Column design model

The absorber design was based on the data provided from the equilibrium stage Aspen Plus simulation using RADFRAC. This provided the detailed gas and liquid composition (including solvent loading) and temperature data for each equilibrium stage. For each equilibrium stage the logarithmic mean driving force (ΔP) and CO₂ absorption flux can then be determined, which is used in the absorber column sizing.

The two most important parameters for the column sizing are the column diameter and the column volume. The column diameter is function of the liquid and gas flow rates and densities. The two main parameters in determining the column diameter are the flooding limitation and the pressure drop of packed height. The columns diameter has been calculated according to Kister (1992). In order to calculate the height of each stage and then the total column height first the mass transfer flux and the amount of CO₂ absorbed was calculated. The mass transfer flux can be obtained using

$$J = K_{ov} \Delta C$$

Then the area of packing could be determined from

$$A_p = \frac{\phi_{CO_2}}{J}$$

From the required area of packing and in combination with the specific area of packing, the volume of packing was calculated in each stage. The packing volume for each stage was added up resulting in an overall packing volume. The height could be calculated using the estimated column diameter, and then a safety factor (1.25) was applied to the calculated column height to give the overall column height.

For each equilibrium stage the overall mass transfer coefficient needs to be estimated. The overall mass transfer coefficient can be written as

$$K_{ov} = \frac{1}{(1/K_G) + (1/mEK_L)}$$

The enhancement factor E , is the ratio between the chemical and the physical absorption flux at the same driving force. It is given as a function of two parameters, the Hatta number (Ha) and the enhancement factor of an infinitely fast reaction (E_∞). The enhancement factor may be considered a correction to the liquid side mass transfer coefficient due to the chemical reaction occurring in the concentration boundary layer.

The Hatta number, indicative of the rate of diffusion transport vs. chemical reaction, is given by

$$Ha = \sqrt{\frac{D_{CO_2,am} k_2 C_{MEA}}{K_L}}$$

The enhancement factor for an infinitely fast reaction dependent on the choice of the mass transfer model. In case of the film model it may be written as

$$E_\infty = \left[1 + \frac{D_{MEA,am} C_{MEA}}{\gamma D_{CO_2,am} C_{CO_2,i}} \right]$$

The concentrations used in this equation are in the mol/m³ units. C_{MEA} is the free MEA in the bulk, which can be calculated from the MEA concentration and the loading as following: $C_{MEA} = C(1 - 2\alpha)$, as 1 mol of CO₂ used 2 mol of MEA in the reaction.

To calculate the value of enhancement factor an iterative solution for the equation below which is described in Westerterp et al. (1984) was used

$$E = \frac{Ha \sqrt{(E_\infty - E)/(E_\infty - 1)}}{\tanh[Ha \sqrt{(E_\infty - E)/(E_\infty - 1)}]}$$

The value of E was determined for each equilibrium stage at the point where the logarithmic mean driving force equal to the local driving force, as suggested in Kohl and Nielsen (1997). The analysis assumes that the reaction between CO₂ and MEA is simple second order, as shown in Versteeg et al. (1996). The reaction rate is given by

$$k_2 = 4.4 \times 10^8 \exp \left[-\frac{5400}{T} \right]$$

Strictly speaking this relation is valid up to 40 °C, but we assume that this relation is also applicable in the range of absorber temperatures (<55 °C). The reversible reaction constant in the stripper column was estimated using the correlation below developed by Jamal et al. (2004), which is valid to temperatures up to the stripper conditions:

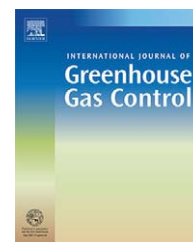
$$K_{-1} = 3.95 \times 10^{10} \exp \left[-\frac{6863.8}{T} \right]$$

Mellapak structure packing Y125 was used for both absorption and stripping columns. The physical mass transfer

coefficient was estimated using the Bravo, Fair's correlation (Kister, 1992).

REFERENCES

- Alie, C., Backham, L., Croiset, E., Douglas, P., 2005. Simulation of CO₂ capture using MEA scrubbing: a flowsheet decomposition method. *Energy Convers. Manage.* 46, 475–487.
- Aspen Plus, 2005. Aspen Plus Version 13.1. Aspen technology Inc., Cambridge, MA, USA.
- Barchas, R., 1992. The Kerr–McGee/ABB Lummus Crest technology for recovery of CO₂ from stack gases. *Energy Convers. Manage.* 33, 333–340.
- Chang, H., Shih, C., 2005. Simulation and optimization for power plant flue gas CO₂ absorption-stripping systems. *Sep. Sci. Technol.* 40, 877–909.
- Chapel, D., Ernst, J., Mariz, C., 1999. Recovery of CO₂ from flue gases: commercial trends. *Can. Soc. Chem. Eng.*
- IEA Greenhouse Gas R&D Programme, 2004. Improvement in power generation with post-combustion capture of CO₂. Report No. PH4/33.
- Intergovernmental Panel on Climate Change (IPCC), 2005. Carbon Dioxide Capture and Storage. Cambridge University Press.
- Jamal, A., Meisen, A., Lim, C., 2004. Kinetics of Carbon Dioxide Absorption and Desorption in Aqueous Alkanolamine Solutions using a Novel Hemispherical Contactor I and II. Department of Chemical and Biological Engineering, the University of British Columbia, Canada.
- Kister, H., 1992. Distillation Design. McGraw Hill Company, Inc..
- Kohl, A., Nielsen, R., 1997. Gas Purification, 5th ed. Gulf Publishing Company.
- Mariz, C.L., 1998. Carbon dioxide recovery: large scale design trends. *J. Can. Pet. Technol.* 37, 42–47.
- Rao, A.B., Rubin, E.S., 2002. A technical, economic and environmental assessment of amine-based CO₂ capture technology for power plant greenhouse gas control. *Environ. Sci. Technol.* 36, 4467–4475.
- Sander, M., Mariz, C., 1992. The Fluor Daniel Econamine FG process: past experience and present day focus. *Energy Convers. Manage.* 33 (5–8), 341–348.
- Singh, D., Croiset, E., Douglas, P., Douglas, M., 2003. Techno-economic study of CO₂ capture from an existing coal-fired power plant: MEA scrubbing vs. O₂/CO₂ recycle combustion. *Energy Convers. Manage.* 44, 3073–3091.
- Suda, T., Fujii, M., Yoshida, K., Lijima, M., Seto, T., Mitsuoka, S., 1992. Development of flue gas carbon dioxide recovery technology. *Energy Convers. Manage.* 33 (5–8), 317–324.
- Versteeg, G., Van Dijck, L., van Swaaij, W., 1996. On the kinetics between CO₂ and alkanolamine both in aqueous and non-aqueous solutions, an overview. *Chem. Eng. Commun.* 144, 113–158.
- Westerterp, K., van Swaaij, W., Beenackers, A., 1984. Chemical Reactor Design and Operation, 2nd ed. Wiley Engineering Company.

available at www.sciencedirect.comjournal homepage: www.elsevier.com/locate/ijggc

CO₂ capture from power plants

Part II. A parametric study of the economical performance based on mono-ethanolamine

Mohammad R.M. Abu-Zahra^a, John P.M. Niederer^b, Paul H.M. Feron^{a,*},
Geert F. Versteeg^b

^aDepartment of Separation Technology, TNO Science and Industry, P.O. Box 342, 7300 AH Apeldoorn, The Netherlands

^bDepartment of Development and Design of Industrial Processes, Twente University, P.O. Box 217, 7500 AE Enschede, The Netherlands

ARTICLE INFO

Article history:

Received 31 July 2006

Received in revised form

14 November 2006

Accepted 8 February 2007

Published on line 21 March 2007

Keywords:

CO₂ capture

Absorption process

MEA

ASPEN plus

Economics

ABSTRACT

While the demand for reduction in CO₂ emission is increasing, the cost of the CO₂ capture processes remains a limiting factor for large-scale application. Reducing the cost of the capture system by improving the process and the solvent used must have a priority in order to apply this technology in the future. In this paper, a definition of the economic baseline for post-combustion CO₂ capture from 600 MW_e bituminous coal-fired power plant is described. The baseline capture process is based on 30% (by weight) aqueous solution of monoethanolamine (MEA). A process model has been developed previously using the Aspen Plus simulation programme where the baseline CO₂-removal has been chosen to be 90%. The results from the process modelling have provided the required input data to the economic modelling. Depending on the baseline technical and economical results, an economical parameter study for a CO₂ capture process based on absorption/desorption with MEA solutions was performed.

Major capture cost reductions can be realized by optimizing the lean solvent loading, the amine solvent concentration, as well as the stripper operating pressure. A minimum CO₂ avoided cost of € 33 tonne⁻¹ CO₂ was found for a lean solvent loading of 0.3 mol CO₂/mol MEA, using a 40 wt.% MEA solution and a stripper operating pressure of 210 kPa. At these conditions 3.0 GJ/tonne CO₂ of thermal energy was used for the solvent regeneration. This translates to a € 22 MWh⁻¹ increase in the cost of electricity, compared to € 31.4 MWh⁻¹ for the power plant without capture.

© 2007 Elsevier Ltd. All rights reserved.

1. Introduction

The amine based absorption systems are the most suitable for CO₂ post-combustion from power plants (Rao and Rubin, 2002a). The technology is commercially available and it has been used in the Fluor technology's Econamine FGTM and Econamine FG PlusTM (Mariz, 1998; Chapel et al., 1999), and the ABB Lummus Global technology (Barchas, 1992).

The estimated cost of CO₂ capture increases the cost of electricity production by 35–70% for natural gas combined cycle (NGCC), and 40–85% for a supercritical pulverized power plant (PC). Overall, the electricity production cost for fossil fuel plants with capture (excluding CO₂ transport and storage costs) ranges from US\$ 0.04 to 0.09 kWh⁻¹, as compared to US\$ 0.03–0.06 kWh⁻¹ for similar plants without capture (IPCC, 2006).

* Corresponding author. Tel.: +31 55 5493151; fax: +31 55 5493410.

E-mail address: Paul.Feron@tno.nl (Paul H.M. Feron).

1750-5836/\$ – see front matter © 2007 Elsevier Ltd. All rights reserved.

doi:10.1016/S1750-5836(07)00032-1

New or improved methods of CO₂ capture, combined with advanced power systems and industrial process designs, could reduce CO₂ capture cost and energy requirements. At present, many research activities are underway trying to improve the capture process or applying improved solvents to reduce the energy requirement and as a result, the CO₂ capture cost.

Several studies have been done in the area of techno-economic modelling. The majority of these activities were focused on defining a baseline case for different power plants, i.e. coal-fired or natural gas combined cycle (Mariz, 1998; Chapel et al., 1999; IEA, 2004) for a single design point, e.g. percent CO₂-removal. Depending on the definitions of the capture baseline cases, other work was focused on the comparison of these baseline cases with new processes like O₂/CO₂ recycle combustion (Singh et al., 2003). None of these studies considered the impact of variation in process design parameters, such as the percentage of CO₂ removal or desorption conditions, on the process economics.

The objective of this work was to develop tools for process design and economic analysis to arrive at an optimised MEA based capture process depending on several technical and economical parameters. The parametric study was based on the conventional technology commercially available on a small scale (Mariz, 1998), without any novel process changes and improvement like split-flow and intercooling (Chapel et al., 1999), because they have not been used yet in commercial applications. This optimization included investigating the effect of CO₂ removal percentage, MEA concentration, lean solvent loading and stripper operating pressure. In addition to the process design parameters, the impact of economic parameters such as fuel prices and interest rate was investigated.

2. Definition of economic baseline

2.1. Methodology and baseline description

The general methodology for the economic evaluation was based on a step-wise approach consisting of the following:

1. Capture process simulation: the CO₂ absorption/desorption process design was based on MEA as the main component in the solvent system. ASPEN Plus was shown to be very useful as the process simulation tool (Abu-Zahra et al., 2006).
2. Modelling and design of the main equipment: the absorber and regenerator column were modelled and designed in detail, using the results from the Aspen Plus simulation. The rest of the equipment was sized to provide information on equipment cost and use of utilities and consumables as required for the economic calculations.
3. Process economics, determination of capital and operating expenses and overall process evaluation with reference to technical and economical performance parameters.

To enable a complete investigation of the capture process, information on both equipment and operating cost was obtained from a number of sources; including vendor input

Table 1 – Economic evaluation assumptions

Project life (years)	25
Equipment salvage value	0
Construction period (years)	3
Plant operating (h/year)	7500
Maintenance cost (% of fixed capital investment)	4
Interest rate (%)	8
MEA price (€/tonne)	1000
Cooling water make up (m ³ /GJ thermal)	1.0
Cooling water price (€/m ³)	0.2
MEA degradation rate (kg/tonne CO ₂) (Rao and Rubin, 2002a,b)	1.5
CO ₂ product temperature (°C)	25
CO ₂ product pressure (bar)	110

and public sources (Rao and Rubin, 2002a,b; Mariz, 1998; Perry et al., 1997; Peters et al., 2003; Matches Engineering Company, 2005). The cash flow analysis method over the project life was used to evaluate the total annual cost. The cost of electricity (CoE) was estimated for the reference power plant before and after adding the capture process. This cost of electricity was considered the one, which resulted in a zero net present value at the end of the project life. Cost of electricity in combination with the CO₂ emission values, can then translated into cost of CO₂ emission avoided. This cost is important for comparative evaluations of CO₂ capture and storage with other measures for reductions of CO₂-emissions. It can be calculated as follows:

cost of CO₂ avoided (€/tonne)

$$= \frac{\text{cost of electricity}_{\text{capture}} - \text{cost of electricity}_{\text{reference}}}{\text{CO}_2 \text{ emission}_{\text{reference}} - \text{CO}_2 \text{ emission}_{\text{capture}}}$$

A 600 MW_e gross coal-fired power plant was chosen as the reference power plant with a constant fuel input before and after adding the capture system. Capital and operating cost for this European reference power plant were readily available. The baseline capture process was designed to remove 90% of the CO₂ present in the flue gas. The solvent used was 30 wt.% MEA and in the baseline process the lean solvent loading was equal to 0.242 mol CO₂/mol MEA lean solvent loading representing a degree of regeneration equal to 50%. The assumptions used in carrying out the economic evaluation are shown in Table 1.

2.2. Base case specifications and results

Capital and operating cost for the capture process were determined using the methodology described in Section 2.1.

2.2.1. Capital cost

The capital cost consists of three main components:

1. Power plant specific cost:

These were defined and agreed upon in joint effort by European power plant companies and plant suppliers supporting the study.

2. Capture plant cost:

The cost of the equipment for the capture process was estimated using several references (Perry et al., 1997; Peters et al., 2003; Matches Engineering Company, 2005).

Table 2 – Overview of equipment cost

Type of equipment	Cost (M€)
Reboiler	0.81
Lean/rich HEX	0.42
Lean cooler	0.21
Reflux condenser	0.14
DC water cooler	0.12
Storage tank	0.73
Gas blower	3.10
Gas scrubber	0.26
Abs. fluid pump	0.59
Condenser fluid pump	0.01
Strip. fluid pump	0.60
Cold water pump	2.04
Absorber	10.94
DCC (feed direct cooler)	0.54
Stripper	3.43
Total	19.96

3. CO₂ compression cost:

Compressor cost has been taken from [Hendriks et al. \(2003\)](#).

Table 2 gives an overview of the equipment cost for solvent process for the base case power plant with 90% CO₂ capture. This does not include the CO₂-compressor.

The most expensive equipment is the absorber, which is responsible for about 55% out of € 20 million for the total equipment purchased cost. In total, the equipment related to the gas path contributes 75% of the equipment cost. Outside the gas path, the second major equipment cost is for the stripper, which also contributes of about 17% of total equipment purchased cost. It is clear that an improved and cheaper packing material or a simpler absorber could reduce the cost of the overall equipment significantly. No auxiliary units or equipment were included in this work, because the fuel input kept constant and no extra boiler is needed. The rest of the direct and indirect cost was estimated as a factor of the overall equipment cost using [Peters et al. \(2003\)](#) and by using factors from the IECM model documentation ([Rao and Rubin, 2002b](#)). Table 3 shows the composition of the total capital investment (CAPEX).

The total capital investment (CAPEX) for the amine plant including CO₂ compression is € 147 million, which compares well to the \$ 179 million (€ 149 million) figure identified in [Singh et al. \(2003\)](#) after removing the cost of the auxiliary units which are not needed in this work.

The total specific capital investment for the power plant after adding the capture process is almost double, which is clear from Table 4. The increase in the power plant capital investment contribution of the overall capital investment is also due to the reduction in the thermal

Table 3 – MEA scrubbing process total capital investment (CAPEX)

	Percentage of purchased cost	Used	Cost (M€)
Direct cost			
ISBL			44.67
Purchased equipment (Perry et al., 1997 ; Peters et al., 2003 ; Matches Engineering Company, 2005)	100	100	19.96
Purchased equipment installation (Peters et al., 2003)	25–55	–	10.54
Instrumentation and control (Peters et al., 2003)	8–50	20	3.99
Piping (Peters et al., 2003)	20–80	40	7.98
Electrical (Peters et al., 2003)	15–30	11	2.20
OSBL			8.98
Building and building services (Peters et al., 2003)	10–80	10	2.00
Yard improvements (Peters et al., 2003)	10–20	10	2.00
Services facilities (Peters et al., 2003)	30–80	20	3.99
Land (Peters et al., 2003)	4–8	5	1.00
Total direct cost			53.66
Indirect cost			
Engineering (Rao and Rubin, 2002b)	10	10	5.37
Construction expenses (Rao and Rubin, 2002b)	10	10	5.37
Contractor's fee (Rao and Rubin, 2002b)	0.5	0.5	0.27
Contingency (Rao and Rubin, 2002b)	17	17	9.12
Total indirect cost			20.12
CO ₂ compressor investment cost (Hendriks et al., 2003)			31.73
Fixed capital investment			105.51
	Percentage of FCI	Used	Cost (M€)
Fixed capital investment	100	100	105.51
Working investment (Peters et al., 2003)	12–28	25	26.38
Start-up cost + MEA cost (Peters et al., 2003)	8–10	10	14.66
Total capital investment (CAPEX)			146.55

Table 4 – Total capital investment and cost of electricity with and without capture process

Item	Without capture	With capture
Total specific investment (€/kW)	980	1855
Power plant	980	1489
CO ₂ capture process	–	254
CO ₂ compression system	–	112
Cost of electricity (€/MWh)	31.4	57.9
Fuel	12.8	18.7
Operating costs	4.6	13.9
Capital costs	14.0	25.3

efficiency of the power plant after addition of the capture process.

2.2.2. Operating cost

The total operating cost (OPEX) includes two main categories:

1. The production cost, which consists of the O&M, cooling water, chemicals, labours, local taxes, and plant overhead.
2. The general expenses, which includes the R&D, administration, and marketing cost.

In Table 5, the total annual cost of amine plant is shown.

The total operating cost found to be € 22 million per year. Thirty-five percent of the direct production cost is MEA make up and almost 32% are maintenance cost. This total operating cost is in a good agreement with Singh et al. (2003) who arrived at a value of \$ 28 million excluding the cost of the natural gas needed for the auxiliary boiler, which is not required in our work. However, adding the capture has a major impact on the overall power plant efficiency. The overall efficiency will decrease from 45% for the reference power plant to 31% due to

Table 6 – Summary of technical and economical results for the base case

Item	Base case	
	No capture	With capture
Capture process performance		
Capacity (tonne/h)	–	408
Energy requirement (GJ/tonne)	–	3.9
Electricity (kWh/tonne)	–	193
Power plant performance		
Fuel input (MW, LHV)	1279	1279
Fuel price (€/GJ)	1.6	1.6
Net power output (MW)	575	399
Thermal efficiency, % (LHV)	45	31
CO ₂ emission (kg/MWh)	772	112
Cost		
Capture investment (€/tonne/h))	–	3.6E+05
Total investment (€/kW)	980	1841
Operating cost (m€/year)	75	96
Cost of Electricity (€/MWh)	31.4	57.4
Cost of CO ₂ avoided (€/tonne)	–	39.3

the addition of the capture process. This 14% reduction is mainly because of the heat needed for solvent regeneration, which is responsible of 55% of total electricity output reduction. The rest is 24% for CO₂ product compression and 21% for process pumps and the flue gas blower. The large regeneration heat demand as well as the large process energy consumption leads to the conclusion that an improved solvent and process innovation are needed to reduce the absorption process energy requirement.

Table 6 shows the overall results of the power plant base case before and after adding the capture process. An increase in the cost of electricity of around € 26 MWh^{−1} can be seen as a result of introducing the amine capture process in the power

Table 5 – MEA scrubbing process total operating cost (OPEX)

	Range	Used	Cost (M€/year)
Production cost			20.33
Fixed charge			3.17
Local taxes (Peters et al., 2003)	1.0–4.0% FCI	2	2.11
Insurance (Peters et al., 2003)	0.5–1% FCI	1	1.06
Direct production cost			14.06
Raw material			0.00
Cooling water			2.65
MEA makeup (Rao and Rubin, 2002a,b)	1.5 kg/tonne CO ₂		4.78
Activated carbon (Chapel et al., 1999)			0.74
Maintenance (Singh et al., 2003)	1.0–10% FCI	4	4.22
Operating labor (OL) (Rao and Rubin, 2002a,b)	Two job per shift	€ 45 h ^{−1}	0.68
Supervision and support labor (Rao and Rubin, 2002a,b)	30% of total labor cost	30	0.29
Operating supplies (Peters et al., 2003)	15% of maintenance	15	0.63
Laboratory charges (Peters et al., 2003)	10–20% OL	10	0.07
Plant overhead cost	50–70% of (M + OL + S)	60	3.11
General expenses			1.29
Administrative cost (Peters et al., 2003)	15–20% of OL	15	0.10
Distribution and marketing (Peters et al., 2003)	2–20% of OPEX	0.5	0.11
R&D cost (Peters et al., 2003)	2–15% of OPEX	5	1.08
Total manufacturing cost (OPEX)			21.62

plant. One of the objectives of this work is to reach an optimum process, which has a lower effect on the overall plant efficiency, by reducing the capture capital and operating cost.

The cost of electricity increases upon addition of the capture process, and 60% of that increase is due to the operating cost in relation to the fuel cost. This was increased due to efficiency reduction (see Table 4).

Comparing these overall results for the base case with the results obtained by the IPCC (IPCC, 2006), we observe that the values in this study are considered in the lower range of the values specified by IPCC. These lower values can be explained by the difference in the euro to dollar currency exchange rates between 2002 (IPCC-report) and 2004 (this study), but also the capacity factor in this study is higher than the one used in the IPCC study. However, comparing the overall results with a European study, which was carried out by VGB power tech (VGB, 2004) we can see that the values from this study are well in line. The power plant specific cost found in the VGB report are € 1020 kW⁻¹ before adding the capture process and increased to € 1860 kW⁻¹ after adding the capture process. Moreover, the cost of electricity was increased from € 37 MWh⁻¹ before capture to € 64 MWh⁻¹ after adding the capture process with an increase of € 27 MWh⁻¹ which is in good agreement with this work. The overall avoided cost was found by VGB to be € 47 tonne⁻¹ CO₂, which is around 20% higher than the avoided cost in this study and this discrepancy can be related to the 20% higher power plant capacity in this study.

3. Effect of process design on cost of electricity and avoided costs

3.1. Variation in process design parameters

It has become clear from our previous study (Abu-Zahra et al., 2006) that the process design can be subjected to optimisation. For instance, by varying the degree of solvent regeneration it is possible to obtain a minimum in the thermal energy required for solvent regeneration. In this section, the effect of variation of the process design parameters on the cost of electricity and costs per tonne CO₂ avoided will be assessed using the economic tools described in Section 2 and the results of the process design from our previous publication (Abu-Zahra et al., 2006).

3.2. Effect of different lean solvent loading including the effect of CO₂-removal percentage

The cost of electricity (CoE) was determined as a function of lean solvent loading, which represents the degree of solvent regeneration the results are shown in Fig. 1 as a function of different value of CO₂-removal.

The results in Fig. 1 show that the CoE has a shallow minimum for the lean solvent loading values between 0.25 and 0.33 mol CO₂/mol MEA. This is the range in which, the thermal energy requirement is at its minimum, indicating a link between the thermal energy requirement, and increased electricity cost. The CoE is obviously influenced by the level of CO₂ removal, with the lowest cost for the lowest value of

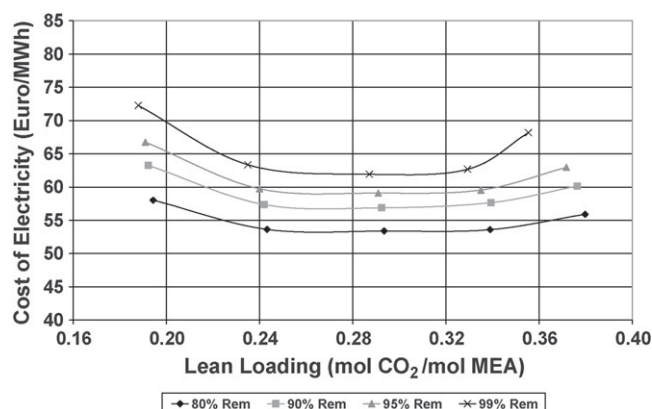


Fig. 1 – Cost of electricity as a function of lean solvent loading for different CO₂ removal.

CO₂ removal. In Fig. 2, the costs per tonne CO₂ avoided are shown for different values of the CO₂ removal as a function of the lean solvent loading.

The results show a near constant cost per tonne CO₂ avoided for lean solvent loading values between 0.25 and 0.33 mol CO₂/mol MEA of around € 40 tonne⁻¹ CO₂. This value does not vary for a CO₂ removal between 80% and 95%. This means that the marginal cost for CO₂ capture is constant in this range but increase at higher CO₂ removal values.

The CoE and cost of CO₂ avoided were studied at low CO₂ removal as well (see Fig. 3). The results show that the CoE increased with increasing CO₂ removal. From these results, it can be concluded that partial removal of CO₂ from the flue gas, i.e. CO₂ removal below 80%, leads to increased costs per tonne CO₂ avoided. It is therefore not economically attractive to aim for partial CO₂-removal.

3.3. Effect of MEA wt. %

In Fig. 4, the cost of electricity is shown as a function of the lean solvent loading for different MEA concentrations. A removal of CO₂ equal to 90% was used in the analysis.

The results in Fig. 4 illustrate that there are clear benefits in increasing the MEA concentration in the solvent. Upon an increase of the MEA concentration from 30 to 40 wt.%, the CoE

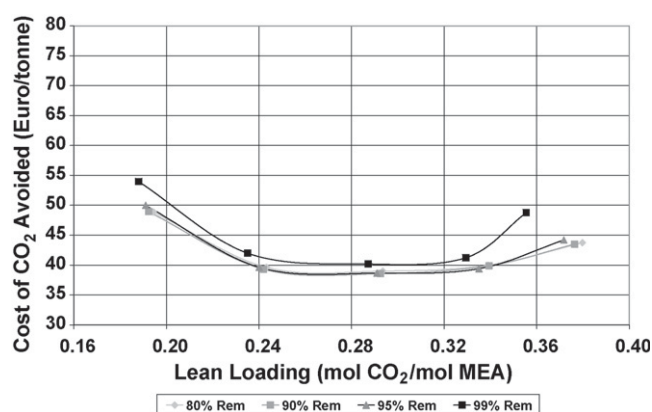


Fig. 2 – Cost per tonne CO₂ avoided as a function of lean solvent loading for different CO₂ removal.

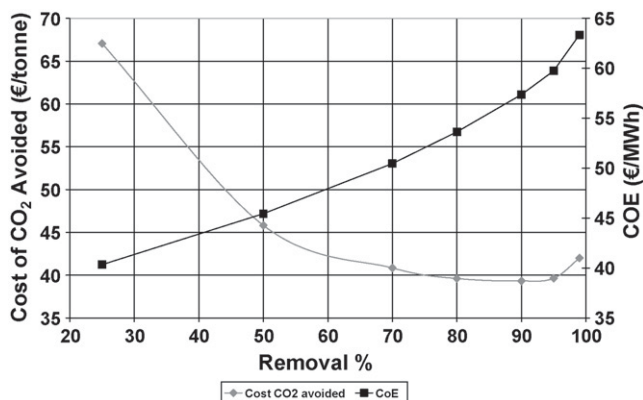


Fig. 3 – Cost per tonne CO₂ avoided and cost of electricity as a function of CO₂ removal.

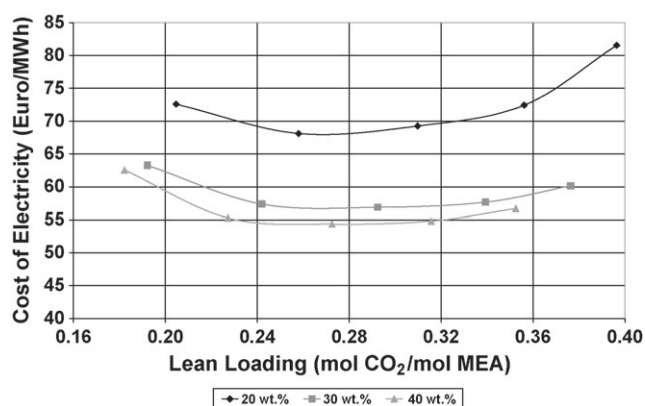


Fig. 4 – Cost of electricity as a function of lean solvent loading for different MEA concentrations.

decreases up to 6%. The minimum CoE occurs for lean solvent loading in the range of 0.26–0.30 mol CO₂/mol MEA, and at 40 wt.% MEA. The costs per tonne CO₂ avoided for different MEA concentrations as a function of the lean solvent loading are shown in Fig. 5.

In Fig. 5, it is shown that higher MEA concentrations will result in lower avoided cost. The cost can be reduced to € 35 tonne⁻¹ using a 40% MEA concentration. The lower cost is

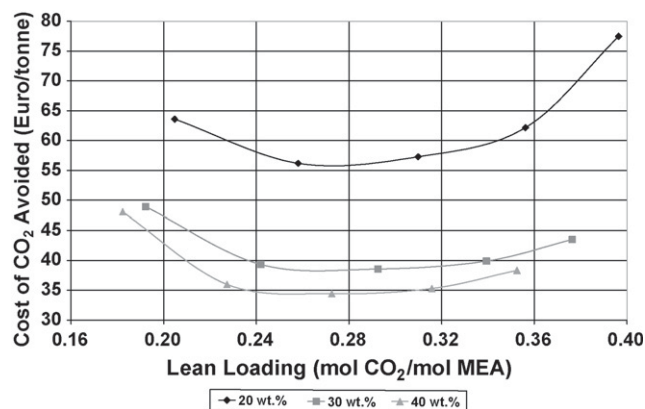


Fig. 5 – Cost per tonne CO₂ avoided as a function of lean solvent loading for different MEA concentrations.

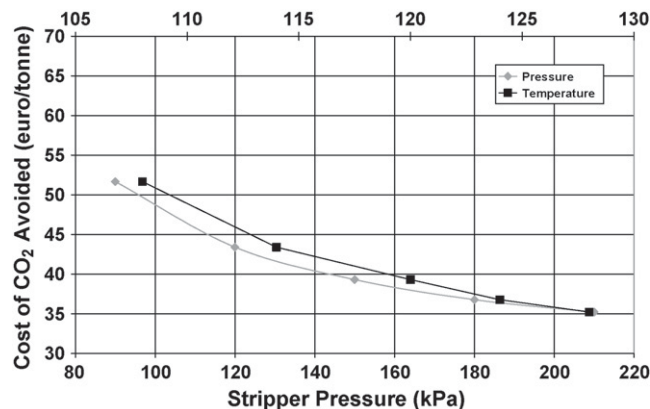


Fig. 6 – Cost per tonne CO₂ avoided as a function of stripper pressure and temperature.

the result of a reduction in the energy requirement for regeneration and lower investment cost for the capture plant as the liquid flow rates are reduced. Furthermore, using a 20% MEA concentration leads to substantially higher cost of CO₂ avoided of at least € 56 tonne⁻¹ CO₂.

3.4. Effect of the stripper operating pressure and temperature

The effect of a higher operating pressure and temperature of the stripper was also investigated. It is expected that the CO₂ mass transfer rate throughout the stripper column is positively affected via the driving force. Starting from the base case, the effect of the stripper operating pressure (90–210 kPa) was investigated, assuming a total pressure drop of 30 kPa over the stripper packing and wash section.

Increasing the stripper operating pressure has a noticeable effect on the capture process by reducing the thermal energy requirement, as was shown in the process study (Abu-Zahra et al., 2006). The effect of different stripper operating conditions on the costs per tonne CO₂ avoided is shown in Fig. 6.

Increasing the pressure from the base case 150 to 210 kPa, will reduce the cost of CO₂ avoided with around 10% (see Fig. 6). This is a significant improvement upon the baseline capture process. There does not appear to be a benefit in lowering the stripper pressure and temperature.

4. Sensitivity analysis

Variations in the values of the economic input parameters will also have a significant impact on the cost of electricity and costs per tonne CO₂ avoided. The effect of the fuel price and interest rate on the CoE and the costs per tonne avoided were determined and shown in Table 7.

For coal prices in the range € 1.2–3.2 GJ⁻¹ the CoE for power plants with CO₂ capture is in the range € 53–76 MWh⁻¹ up from the range € 28 to 44 MWh⁻¹ for the power plant without capture. The increase in CoE is thus € 25–32 MWh⁻¹, which on average represents a 70–90% increase in the cost of electricity.

Table 7 – Effect of interest rate and fuel price variation on the cost of electricity and the costs per tonne avoided CO₂

Fuel price (€/GJ)	Interest rate	COE no capture (€/MWh)	COE with capture (€/MWh)	Cost of CO ₂ avoided (€/tonne CO ₂)
1.2	0.08	28	53	37
1.6	0.08	31	57	39
3.2	0.08	44	76	48
1.6	0.04	27	48	33
1.6	0.08	31	57	39
1.6	0.12	37	68	47

Obviously, the fact that the capture of CO₂ requires additional energy leads to a strong dependence of the CoE on the cost of fuel.

The costs per tonne avoided show a steady increase with increase in fuel price, rising from €37 tonne⁻¹ avoided CO₂, to €48 tonne⁻¹ avoided CO₂ at an interest rate of 0.08. Typically, a doubling of the fuel cost will lead to a 23% increase in the cost per tonne CO₂ avoided.

For interest rates in the range 0.04–0.08 the CoE for power plants with CO₂ capture is in the range €48–68 MWh⁻¹ up from the range €27–37 MWh⁻¹ for the power plant without capture. Costs per tonne CO₂ avoided are in the range €33–47 tonne⁻¹ CO₂ for the interest rate range 0.04–0.08.

5. Process optimization at minimum thermal energy requirement

By the variation of the four operating parameters, i.e. CO₂ removal %, MEA solvent concentration, lean solvent loading, and stripper operating pressure an optimum process was aimed for. It was shown from the comparison between this work and our previous work (Abu-Zahra et al., 2006) that the link between minimum thermal energy requirement and minimal cost of electricity or cost per tonne avoided was close. Therefore, the optimum process was defined as the process, which has the lowest thermal energy requirement for all parameters involved. The minimum was determined using ASPEN Plus as the process-modelling tool.

Table 8 – Optimum process specifications and results

Item	30 wt.% MEA	40 wt.% MEA
Capture process performance		
Capacity (tonne/h)	405	406
Energy requirement (GJ/tonne)	3.3	3.01
Electricity (kWh/tonne)	192	182
Power plant performance		
Fuel input (MW, LHV)	1279	1279
Fuel price (€/GJ)	1.6	1.6
Net power output (MW)	426	426
Thermal efficiency, % (LHV)	33	33
CO ₂ emission (kg/MWh)	108	103
Cost		
Capture investment (€/tonne/h)	4.00E+05	3.50E+05
Total Investment (€/kW)	1865	1712
Operating cost (m€/year)	97	96
Cost of electricity (€/MWh)	56	53
Cost of CO ₂ avoided (€/tonne)	37	33

An optimum process would have the following characteristics: 90% CO₂ removal, 40 wt.% MEA, and 240 kPa stripper bottom pressure equivalent to a temperature of 128 °C. Regarding the optimum lean solvent loading, the results show a shallow minimum at a range of lean solvent loading (0.25–0.33), the optimum value was chosen to be in this range, which give also the lowest energy requirement depending on the results in part one of this study (Abu-Zahra et al., 2006). For the case of 40 wt.% MEA, lean solvent loading of 0.30 mol CO₂/mol MEA was chosen. For currently used solvent compositions (30 wt.% MEA) the optimum lean solvent loading would equal to 0.32 mol CO₂/mol MEA.

The process optimization resulted in a major reduction in the process capital and operating expenses and the cost of CO₂ avoided as shown in Table 8. The optimum process with 40 wt.% MEA has a 23% reduction in the energy requirement compared to the baseline given in Table 6. Moreover, the cost of CO₂ avoided decreases with 16% comparing to the base case.

6. Conclusions

The impact of the degree of regeneration, CO₂-removal, solvent concentration and stripper operating pressure on the economic performance of CO₂ capture from a coal-fired power station has been elaborated. The following conclusions can be drawn from this:

- The costs of CO₂ avoided and cost of electricity were found to show a shallow minimum for lean solvent loading between 0.25 and 0.33 mol CO₂/mol MEA.
- The costs per tonne avoided are quite similar for CO₂ removal in the range between 80% and 95%.
- Increasing the MEA concentration leads to a significant reduction in the costs per tonne CO₂ avoided. Hence, it is advantageous to go the highest concentration, if allowable from the corrosion point of view.
- A high stripper operating pressure will reduce the overall capture process costs and expenses in addition to the cost and the energy required for CO₂ compression.
- The impact of the fuel price on the costs per tonne CO₂ avoided is such that a doubling of the fuel cost will lead to a 23% increase in the cost per tonne CO₂ avoided.
- The overall process economic analysis shows that process optimization will reduce the overall cost of a CO₂ capture process. The avoided cost is equal to €33 tonne⁻¹ CO₂ compared to the base case of €39 tonne⁻¹ CO₂. Furthermore, the cost of electricity would be €53 MWh⁻¹, whereas for the base case the electricity cost would be €57 MWh⁻¹.

Acknowledgements

This work was carried out within the CASTOR Integrated Project, supported by the European Commission (Contract No. SES6-2004-502586) and the CATO project supported by the Dutch Ministry of Economic Affairs (EZ). The authors would like to express their gratitude for their support.

REFERENCES

- Abu-Zahra, M., Schneiders, L., Niederer, J., Feron, P., Versteeg, G., 2006. CO₂ capture from power plants. Part I. A parametric study of the technical performance based on mono-ethanolamine. *Int. J. Green Gas Cont.*, doi:10.1016/S1750-5836(06)00007-7, in press.
- Barchas, R., 1992. The Kerr-McGee/ABB Lummus Crest technology for recovery of CO₂ from stack gases. *Energy Convers. Manage.* 33, 333–340.
- Chapel, D., Ernst, J., Mariz, C., 1999. Recovery of CO₂ from flue gases: commercial trends. *Can. Soc. Chem. Eng.*
- Hendriks, C., Wildenborg, T., Feron, P., Graus, W., Brandsma, R., 2003. EC-case carbon dioxide sequestration. ECOFYS and TNO Report.
- IEA Greenhouse Gas R&D Programme, 2004. Improvement in power generation with post-combustion capture of CO₂. Report No. PH4/33.
- Intergovernmental Panel on Climate Change (IPCC), 2006. Carbon Dioxide Capture and Storage. Cambridge University Press.
- Mariz, C.L., 1998. Carbon dioxide recovery: large-scale design trends. *J. Can. Pet. Technol.* 37, 42–47.
- Matches Engineering Company, 2005 <http://www.matches.com>.
- Perry, R., Green, D., Maloney, J., 1997. *Perry's Chemical Engineers' Handbook*, 7th ed. McGraw-Hill, New York.
- Peters, M., Timmerhaus, K., Ronald, W., 2003. *Plant Design and Economics for Chemical Engineers*, 5th ed. McGraw-Hill.
- Rao, A.B., Rubin, E.S., 2002a. A technical, economic, and environmental assessment of amine-based CO₂ capture technology for power plant greenhouse gas control. *Environ. Sci. Technol.* 36, 4467–4475.
- Rao, A.B., Rubin, E.S., 2002. A technical, economic and environmental assessment of amine-based CO₂ capture technology for power plant greenhouse gas technology. Report 2002. Carnegie Mellon University.
- Singh, D., Croiset, E., Douglas, P., Douglas, M., 2003. Techno-economic study of CO₂ capture from an existing coal-fired power plant: MEA scrubbing vs. O₂/CO₂ recycle combustion. *Energy Convers. Manage.* 44, 3073–3091.
- VGB PowerTech Service GmbH, 2004. CO₂ Capture and Storage, a VGB Report on the State of Art. VGB PowerTech Service GmbH, Essen.

PERFORMANCE AND COST ANALYSIS OF A NOVEL GAS TURBINE CYCLE WITH CO₂ CAPTURE

Matthias Finkenrath¹, Tord Peter Ursin³,
Stéphanie Hoffmann¹, Michael Bartlett¹,
Andrei Evulet², Michael J Bowman²,
Arne Lynghjem³, Jon Jakobsen³.

¹ General Electric, Global Research Center, D-85748 Garching b. München, Germany.

² General Electric, Global Research Center, Niskayuna, NY 12309, New York, USA.

³ Statoil ASA, Technology & Projects, N-4035 Stavanger, Norway.

ABSTRACT

In this paper, a new gas turbine cycle with integrated post-combustion CO₂ capture is presented. The concept advantageously uses an intercooled gas turbine in combination with exhaust gas recirculation to enable CO₂ separation at elevated concentration and pressure. Therefore, less energy is required for the CO₂ separation process. In addition, due to the reduced volume flow entering the CO₂ separation unit, the costs of the CO₂ separation equipment are significantly reduced. The performance and cost of CO₂ avoided of the power cycle have been analyzed. The results show that the concept is able to reach high CO₂ capture rates of 80 % and above. When accounting for CO₂ capture and compression, nearly 50 % (LHV) combined cycle net efficiency is obtained based on an existing medium scale intercooled gas turbine. Furthermore, the cycle has an even higher efficiency potential if applied to larger intercooled gas turbine combined cycles in the future. Using CO₂ separation membrane technology which is currently under development, the cost of CO₂ avoided is estimated at 31 \$/t_{CO2} based on a medium scale intercooled gas turbine. A future scaled-up configuration based on a large-frame intercooled gas turbine has the potential to meet 30 \$/t_{CO2} cost of CO₂ avoided.

INTRODUCTION AND OBJECTIVES

Global warming has been identified as one of the most substantial environmental challenges of the 21st century. As a consequence, the energy industry is facing increasing regula-

tions and governmental pressure regarding carbon dioxide (CO₂) emissions. This is the motivation for significant research efforts in CO₂ capture and sequestration from fossil fueled power plants [1].

Since 2004, Statoil and GE Global Research are jointly developing and evaluating technical options for future power plants that allow for CO₂ capture. The design objectives for these advanced power plants are above 50 % cycle net efficiency, below 30 \$/t_{CO2} cost of CO₂ avoided, and capture of at least 80 % of the generated CO₂. This paper presents a novel gas turbine cycle with integrated CO₂ capture that has the potential to meet these design criteria.

BACKGROUND AND STUDY BASIS

Advanced power plant concepts with integrated post-combustion CO₂ capture are a main focus of the joint Statoil and GE Global Research development project. Due to their positive impact on energy requirements and equipment costs, power cycles with CO₂ separation at elevated pressures and CO₂ concentrations were found to be particularly attractive. The increased partial pressure of CO₂ improves the driving forces for CO₂ separation. This is a substantial advantage compared to a base case using an atmospheric CO₂ amine absorption process applied to for example a 400 MW natural gas combined cycle (NGCC) located on the west coast of Norway. Furthermore, new types of CO₂ separation membranes with even lower energy requirements can be utilized. In addition, the increased

overall pressure reduces the flue gas volume flows to be treated, thus reducing the footprint and size, and thereby cost of the CO₂ separation equipment. An example for this group of cycles utilizing CO₂ separation at elevated pressures and CO₂ concentrations is the Combicap concept, which was developed by Statoil [2]. Results of a joint performance and cost analysis for the Combicap concept have been published earlier. While both performance and cost numbers for this concept looked promising, still substantial component development and the need for simplifications were identified [3].

In the mean time, novel post-combustion capture cycles with lowered cycle complexity have been jointly developed. These concepts advantageously utilize features of an intercooled gas turbine to enable CO₂ separation at pressure. Applied to an intercooled medium scale gas turbine, such as GE's LMS100, existing intercooler scrolls can be used for extraction and reinjection of the gas turbine working fluid at pressure (Figure 1). Hence, only moderate modifications to today's power plant equipment are required, which avoids turbine performance losses and significantly reduces modification costs and thereby costs of CO₂ capture.

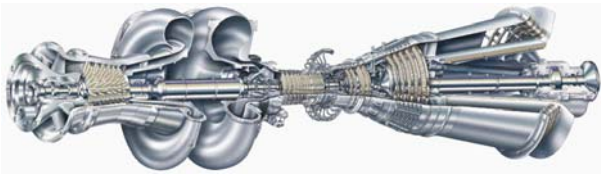


Figure 1: Example of an intercooled gas turbine (LMS100) with intercooler scrolls allowing working fluid extraction between the low and high pressure compressor [4].

The study was based on a medium scale intercooled aeroderivative gas turbine and a 400 MW scale heavy-duty gas turbine. The unmodified medium-scale combined cycle delivers 120 MW net power at around 53.8 % (LHV) net efficiency. To estimate the potential of the new cycle when applied to a large-scale heavy-duty gas turbine, a scale-up to a future intercooled, GE Frame 9FB-size gas turbine was added to the analysis. Today, a (non-intercooled) GE Frame 9FB combined cycle delivers approximately 410 MW net power at around 58 % (LHV) cycle net efficiency.

Both solvent-based as well as membrane-based CO₂ capture have been investigated for the presented cycle. An amine-based plant provides a near term solution for CO₂ separation from pressurized exhaust. A medium to long-term cycle improvement is presented by use of Fixed-Site-Carrier (FSC) CO₂ separation membranes, which currently are under development.

NOVEL CYCLE CONFIGURATION

One of the most promising cycles that were jointly developed by Statoil and GE Global Research is shown in

Figure 2, and will be discussed in more detail in this paper. This post-combustion CO₂ capture cycle shown is based on an intercooled gas turbine in a combined cycle configuration. The gas turbine off-gas is passing the heat recovery steam generator (HRSG) of a bottoming steam cycle, and is recirculated back to the main low pressure compressor (LPC) inlet of the gas turbine.

Prior to entering the compressor, a flue gas cooler is used to lower the temperature of the recirculated exhaust, and separate condensing water. Between the low and high pressure compressor (HPC), the working fluid is extracted utilizing existing scrolls between the two compressor sections of an intercooled gas turbine.

The design of these scrolls used to facilitate intercooling is shown in Figure 1 for the LMS100 aeroderivative gas turbine.

Around 50 % of the recirculated exhaust leaving the low pressure compressor is passed on to the high pressure compressor, and from there back to the combustor of the gas turbine. Thereby, the CO₂ concentration in the gas turbine working fluid is increased to around 8-10 vol-%. The degree of exhaust gas recirculation is limited by minimum oxygen requirements of the gas turbine combustor. The other part of the CO₂-enriched working fluid leaving the low pressure compressor is extracted and sent at pressure to a CO₂ separation unit. If the CO₂ separation unit operates at low temperatures, a heat exchanger and optionally an additional trim cooler (not shown) can be used. In this case, the heat exchanger recovers heat from the CO₂-rich stream coming from the low pressure compressor by heating the cleaned CO₂-lean working fluid leaving the CO₂ separator. The CO₂-lean working fluid leaves the cycle through an expander unit.

In the proposed cycle configuration, an additional air compressor supplies fresh air to the cycle to aid in both mass and oxygen concentration balancing. The air and the recirculated exhaust gas are mixed, intercooled and sent to the high pressure compressor. The expander and the air compressor can be coupled together with an electrical or mechanical drive.

At nominal operation with CO₂ separation, the complete flue gas leaving the gas turbine is recirculated back to the gas turbine low pressure compressor inlet as shown in the drawing. For start-up and shut-down, however, the operation mode can be changed. In this case, similar to a standard gas turbine operation, air can be optionally added to the gas turbine low pressure compressor inlet, and flue gas blown off after the heat recovery steam generator. This operation mode would require an additional fresh air inlet upstream of the low pressure compressor, and a secondary exhaust gas system downstream of the HRSG (both not shown in Figure 2). In this configuration, the gas turbine could even be operated without CO₂ capture if required, for example during maintenance of the CO₂ separation unit.

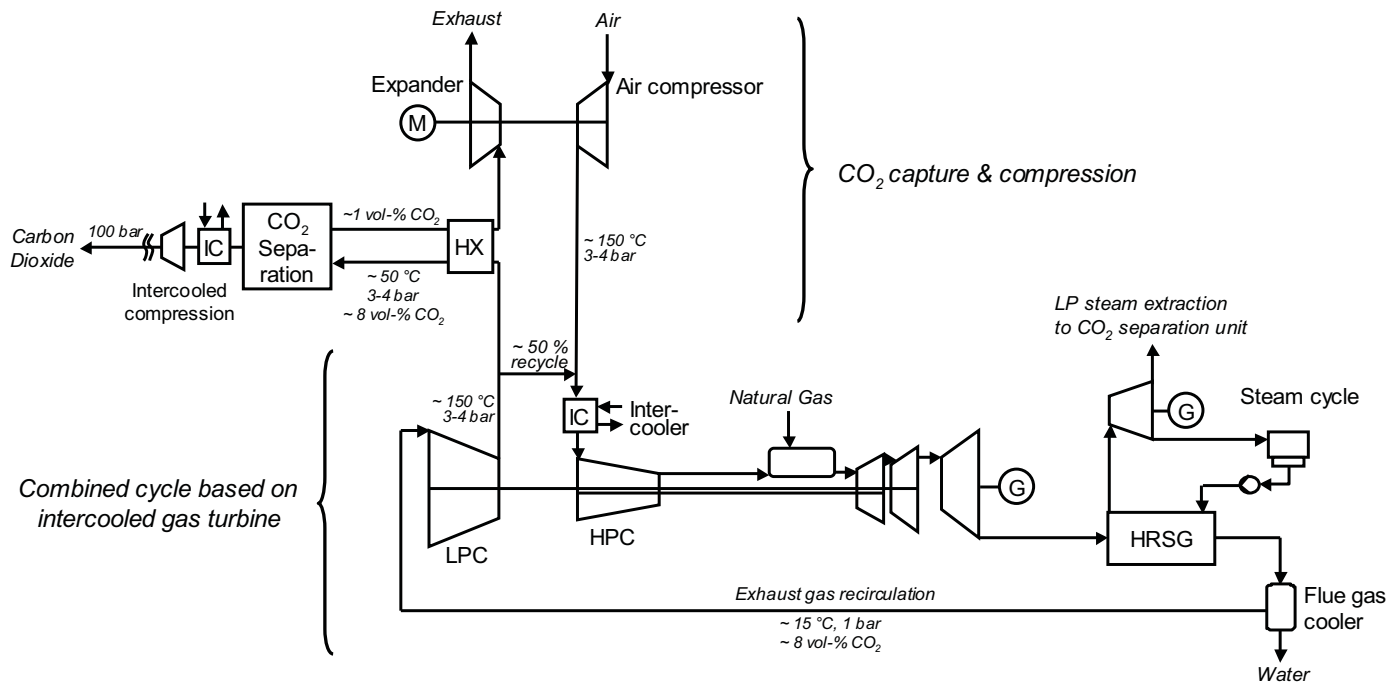


Figure 2: Novel cycle with integrated CO₂ separation at gas turbine intercooler.

MAIN CYCLE FEATURES

Only moderate modifications are needed to implement the proposed cycle to an existing intercooled gas turbine combined cycle. In comparison to previously discussed concepts with CO₂ separation at elevated pressures and CO₂ concentrations, existing intercooler scrolls can be utilized for the gas extraction from and reinjection into the gas turbine. By changing either the fraction of recirculated gas, or the amount of fresh air added through the additional air compressor, the flows to the high pressure compressor of the gas turbine can be adjusted. Thereby, similar flow conditions as in a standard gas turbine operation can be achieved, and the standard intercooler can still be used for cooling the working fluid in front of the high pressure compressor.

Due to the exhaust gas recirculation within the cycle, only about 50 % of the gas turbine working fluid is extracted from the intercooled gas turbine and sent to the CO₂ capture unit, as shown in Figure 2. Thereby, the overall volume flow to be cleaned is halved, which reduces the size and cost of the CO₂ separation unit. This advantage is already known from cycle concepts with atmospheric tail-end CO₂ capture in combination with exhaust gas recirculation. The proposed new concept, however, even leads to an additional CO₂ separation equipment size and cost reduction, as the separation takes place at pressure. In the case of a 3.5 bar intercooler pressure, this leads to a further volume flow reduction by approximately 70 %. As a consequence, the size of the CO₂ separation equipment

needed, and thereby the CO₂ separation equipment costs are substantially reduced.

Besides size and cost reductions, the proposed cycle generates substantially higher CO₂ partial pressures compared to cycles which use atmospheric capture systems. For the example of 3.5 bar intercooler pressure, the combination of exhaust gas recirculation and extraction at pressure leads to increased CO₂ partial pressures of around 0.3 bar at the CO₂ separation unit. For comparison, gas turbines with exhaust gas recirculation and atmospheric CO₂ capture typically cannot exceed a CO₂ partial pressure of 0.1 bar. The higher partial pressure of the proposed cycle increases the driving forces for CO₂ separation, which gives faster reaction kinetics and reduces the specific energy consumption of conventional CO₂ separation systems based on chemical absorption. As discussed before, the decreased volume flow results in a contactor with smaller cross-section and lower height. In addition, new types of CO₂ separation methods could be utilized, which further reduces energy requirements for the CO₂ separation.

As all flue gas passes the CO₂ separation unit, high overall CO₂ capture rates can be achieved. Therefore, considering typical CO₂ separation efficiencies, up to 80 to 90 % of the generated CO₂ can be captured. If chemical absorption is used for CO₂ separation, the proposed configuration avoids carry-over of chemical traces from the CO₂ separation process into the hot gas path of the turbine, as all cleaned flue gas is bled off through an additional expander unit.

COMBUSTION SYSTEM FOR EXHAUST GAS RECIRCULATION

The topic of combustion with exhaust gas recirculation (EGR) is well known from concepts of the time of the dawn of DLN technologies around 1982, when EGR was considered the alternative path to low NO_x . New investigations have been made with more refined assumptions to determine the realistic potential of EGR for CO_2 capture applications. These assumptions include possible levels of EGR, exhaust oxygen levels, emissions and operability. The technical risks may be in fact smaller than predicted, thus the predicted benefits are underestimated.

Based on recent experiments, we estimate that the elements of a successful combustor for EGR will include:

- A simple combustor optimized around EGR operation,
- A good operability and turndown performance,
- Low levels of emissions,
- Combustion efficiencies similar to baseline operation.



Figure 3: Example of DLN combustor system (9FB gas turbine).

CO₂ SEPARATION PLANT

Both solvent-based as well as membrane-based CO_2 capture units have been investigated for the presented cycle. The systems have been designed to separate 80 % of the CO_2 in the exhaust.

a) Solvent based capture unit

The solvent-based plant provides a near term solution for CO_2 separation from pressurized exhaust. These estimates are based on the following assumptions:

- Energy consumption is calculated using an in-house HYSYS[®] simulation model,
- The solvent is 30 wt-% MEA,
- More advanced solvents and/or process optimization by specialized vendors are expected to improve upon the in-house performance estimate. To account for this the calculated thermal energy requirement is reduced by 20 %,
- The electrical energy requirement is used as calculated,
- Capital cost is calculated for a single train configuration.

For pressurized flue gas at around 3.5 bar and 8 vol-% CO_2 , this approach leads to the following results:

- Specific thermal energy consumption: $2.7 \text{ MJ}_{\text{Thermal}}/\text{kg}_{\text{CO}_2}$,
- Specific electrical energy consumption: $0.025 \text{ MJ}_{\text{el}}/\text{kg}_{\text{CO}_2}$,
- CO_2 is supplied to the compression chain at 1.5 bar.

Using this approach for an atmospheric capture unit gives a specific thermal energy consumption of $3.1 \text{ MJ}_{\text{Thermal}}/\text{kg}_{\text{CO}_2}$.

b) CO₂ Selective Membranes

A medium to long-term cycle improvement is presented by use of Fixed-Site-Carrier (FSC) CO_2 separation membranes, see Figure 4. These membranes are currently under development at the Norwegian University of Science and Technology (NTNU) [5].

The FSC membrane material has a demonstrated high selectivity between CO_2 and N_2 , and a one-stage separation process is possible. The flux of CO_2 through the membrane is dependent on the difference in partial pressures between the two sides. Sweep steam is used on the membrane permeate side in order to ensure a positive partial pressure differential. Some nitrogen and oxygen will also permeate to the low pressure side of the membrane. The permeate composition has been calculated and the nitrogen slip (as the largest contribution) is included in the simulations, but equipment to remove these components from the produced CO_2 is not included. Depending on the ultimate use of the captured CO_2 , additional polishing steps may need to be included.

For the performance evaluation, the following operating conditions have been selected for CO_2 separation membranes:

- CO_2 separation efficiency is 80 %,
- The permeate side of the membrane is operated at a pressure of 0.2 bar absolute and the CO_2 is supplied to the compression chain at this pressure,
- 4 kg/s steam at 0.2 bar is extracted from the steam cycle and used as sweep gas in the membrane unit (for the medium-sized cycle with 116 MW net power).

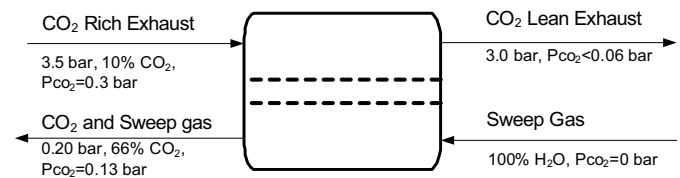


Figure 4. Example of CO_2 separation membrane operating conditions.

Based on the results for the two plants it is concluded that a successful CO_2 capture solution will be based on membrane technology or a solvent that has a significantly improved performance compared to 30 wt-% MEA.

PERFORMANCE MODELING ASSUMPTIONS AND SIMULATION RESULTS

The performance potential of the proposed cycle was evaluated using GateCycle™ as a simulation platform [6]. The analysis was carried out based on a medium scale intercooled aeroderivative gas turbine. For this gas turbine platform, off-design turbomachinery performance was considered to account for the modified operating conditions of the gas turbine due to the exhaust gas recirculation.

Main assumptions used for the performance analysis are given below:

- CO₂ is compressed to 100 bar, specific energy used for CO₂ compression: 0.35 MJ_{el}/kg_{CO₂},
- Natural gas is supplied to the cycle at 50 bar,
- The recirculated exhaust gas is cooled to 15 °C (using 8 °C seawater).

An improved steam cycle is added to the cycle with CO₂ capture compared to the baseline cycle without capture in order to reduce the requirements for cooling the recirculated exhaust gas. The analysis was carried out based on a medium scale aeroderivative gas turbine. At 80 % CO₂ capture, the proposed cycle configuration has the potential to reach a net efficiency of 47.5 % (110 MW) if operating with chemical absorption, or 49.5 % (116 MW) if using membrane technology for CO₂ separation. This is equivalent to comparably low efficiency penalties of 6.3 %-pts or 4.3 %-points due to the CO₂ capture and compression to 100 bar. It has to be noted that even a higher cycle efficiency of around 50 % could be reached, if the CO₂ separation rate is lowered and additional measures for internal heat recovery would be applied. To keep the cycle as simple as possible, however, the cycle configuration shown in Figure 2 is maintained for this analysis.

To evaluate the future potential of applying the new cycle to an even larger gas turbine, a scaled-up version of the process was analyzed. Therefore it was assumed that a 400 MW 9FB-size gas turbine combined cycle with intercooling (or other options for substantial gas extraction and reinjection throughout compression) would be available. Though currently such a large-frame gas turbine with intercooling is not available, this performance estimate gives an indication of the additional cycle potential if being applied to an even larger gas turbine cycle. For the scaled-up system the turbomachinery performance evaluation was based on data from today's non-intercooled 9FB-size gas turbines.

The development of a large-frame intercooled gas turbine would require significant work. If this path would be followed, it would take a substantial amount of time and therefore should be considered a long-term option. Against this background, only membrane technology was considered as CO₂ separation technology for the intercooled large-frame combined cycle option. As this future large-frame intercooled gas turbine does not exist so far, the intercooling pressure was varied to identify the optimum configuration for this specific application with

CO₂ separation. The choice of the intercooler pressure impacts both the performance of the combined cycle, as well as the performance of the CO₂ separation unit, in particular the size (and thereby cost) of the required CO₂ separation membrane. The analysis with varying pressures indicates that intercooler pressures between 2.5 to 3.5 bar would be best for the proposed combined cycle with integrated CO₂ separation. However, any pressures between 2 and 20 bars are possible. On the lower pressure side, however, the application of CO₂ separation membranes becomes more and more challenging, and increasing membrane areas and amounts of sweep steam are necessary to reach the targeted CO₂ capture rates. For a simulation case with 2.5 bar intercooler pressure, the estimated performance results for a future large-frame gas turbine are presented in this paper. Depending on the degree of intercooling, potential net efficiencies are evaluated to lie between 51.1 % (435 MW) and 53.0 % (393 MW) including CO₂ compression to 100 bar.

Table 1 summarizes the performance results for the three main configurations of the new cycle:

- Medium scale plant with chemical absorption CO₂ capture,
- Medium scale plant with CO₂ separation membrane,
- Modified large-scale gas turbine with CO₂ separation membrane.

Table 1: Cycle performance results including CO₂ compression.

	Net Efficiency (LHV)	CO ₂ Capture Rate	Net Power Output
Medium scale NGCC with chemical absorption	47.5 %	80 %	110 MW
Medium scale NGCC with membranes	49.5 %	80 %	116 MW
Future 400 MW NGCC with membranes*	51.1 % (53.0 %)	80 %	435 MW (393 MW)

*depending on the degree of intercooling
(results in parenthesis: without intercooling)

COST ESTIMATION METHODOLOGY AND COST ANALYSIS RESULTS

A cost analysis was carried out to evaluate the economic potential of the proposed cycle. The key element of this analysis is to estimate costs of additionally installed equipment which is needed for CO₂ capture and compression but is not part of a traditional natural gas fired combined cycle. All cost numbers are calculated assuming the cycles and components to be mature technologies.

The economic evaluation is based on the concept of *cost of CO₂ avoided*, which is defined as:

$$\text{Cost of CO}_2 \text{ avoided} [\$/\text{t}_{\text{CO}_2}] = \frac{\text{COE}_{\text{capture}} - \text{COE}_{\text{ref}} [\$/\text{kWh}]}{\text{spec. CO}_2 \text{ emiss.}_{\text{ref}} - \text{spec. CO}_2 \text{ emiss.}_{\text{capture}} [\text{t}_{\text{CO}_2}/\text{kWh}]}$$

In this equation, the term COE stands for cost of electricity and typically is subdivided in capital, fuel, and operation and maintenance costs. The calculation of cost of CO₂ avoided requires the definition of a reference combined cycle plant without CO₂ capture (index: ref) in comparison to the cycle with capture (index: capture). The reference plant is assumed to be a plant of the same type as the plant with CO₂ capture. Depending on the gas turbine platform chosen for the system evaluation, a 120 MW scale LMS100 combined cycle without CO₂ capture, or a 400 MW scale 9FB combined cycle without CO₂ capture are chosen as reference cases. For the 120 MW medium scale cycle configurations, costs of CO₂ avoided were calculated using both an LMS100 and a 9FB combined cycle as reference cases, though there is a substantial difference in power outputs between the 9FB and the medium scale combined cycle. Nonetheless, cost results based on a 400 MW class reference case such as the 9FB were added, as this is typically the focus of today's natural gas based CO₂ cost studies. In the cost calculation potential additional cost for CO₂ transport and sequestration were not included. CO₂ compression to 100 bar and CO₂ dehydration however have been considered. Equipment cost estimates were based both on internal GE and Statoil sources, as well as on preliminary quotes from suppliers. When evaluating the cost results, it has to be kept in mind that they are calculated for an installation in Norway. The results can change when considering other locations.

The calculated cost for all three cases (medium scale with chemical absorption, medium scale with membranes, scaled-up cycle with membranes) are listed together with the performance results in Table 2 below. For a configuration based on a medium scale combined cycle, cost of CO₂ avoided including

compression have been evaluated to be 38 \$/t_{CO2} if using chemical absorption for CO₂ separation. A medium scale combined cycle using CO₂ separation membranes instead of chemical absorption could further reduce these cost to 31 \$/t_{CO2}. In the long run, if a 400 MW-scale combined cycle based on an intercooled gas turbine would be available, an additional cost reduction potential down to 30 \$/t_{CO2} is predicted, which is mainly due to economies of scale.

DISCUSSION OF RESULTS

The proposed novel power plant cycle with integrated CO₂ capture is able to treat all exhaust gas at pressure. Thereby, high CO₂ capture rates can be reached and are only limited by the CO₂ separation efficiency of the CO₂ separation unit. As a result, the cycle is able to capture 80-90 % of the generated CO₂, and meet the CO₂ capture design criteria of at least 80 % capture.

Based on a medium scale combined cycle, net efficiencies including CO₂ compression range between 47.5 % for chemical absorption CO₂ separation, and 49.5 % for membrane-based capture. Though these numbers are below the design target of 50 % efficiency, they are remarkable given the fact that they are not based on a large-scale combined cycle, which typically has a much higher baseline net efficiency (typically 58-60 %). Instead, the analysis shows comparably low efficiency penalties due to the CO₂ capture and compression. Even for the medium scale cycle, above 50 % efficiency could be reached by reducing the CO₂ separation rate, or by additional heat integration. Applied to a future intercooled large-frame machine, the cycle is able to substantially exceed the 50 % efficiency target, reaching net efficiencies between 51.1 % (432 MW) and 53.0 % (393 MW) depending on the degree of intercooling.

From an economic viewpoint, the power cycle has the potential to meet the cost target of 30 \$/t_{CO2} in the long run, if based on a large-scale combined cycle technology in conjunction with CO₂ separation membranes. If it is applied to the already existing medium scale technology, 31 \$/t_{CO2} cost of CO₂

Table 2 Cycle cost and performance analysis results, including CO₂ compression.

	Net Efficiency (LHV)	Net Power Output	CO ₂ Capture Rate	Reference Plant used for Cost Analysis	Cost of CO ₂ avoided
Target	≥ 50 %		≥ 80 %		≤ 30 \$/t _{CO2}
Medium scale NGCC with chemical absorption	47.5 %	110 MW	80 %	LMS100 CC 9FB CC	38 \$/t _{CO2} 54 \$/t _{CO2}
Medium scale NGCC with membranes	49.5 %	116 MW	80 %	LMS100 CC 9FB CC	31 \$/t _{CO2} 46 \$/t _{CO2}
Future 400 MW NGCC with membranes	51.1 %	435 MW	80 %	9FB CC	30 \$/t _{CO2}

avoided are estimated based on membrane technology. Combined with chemical absorption, cost of CO₂ avoided of 38 \$/t_{CO2} have been evaluated. Given the fact that these cost estimates are based on a combined cycle of the 100-120 MW scale, they are very attractive, and could be an interesting option for CO₂ capture opportunities at a medium size.

The novel cycle offers the advantage of combining a comparably high performance and promising economics. Modifications compared to existing technology are needed but evaluated as moderate.

In this context, the following main R&D and optimization areas can be identified:

- Combustion
 - impact of exhaust gas recirculation
 - low O₂ combustion
- CO₂ capture & compression island optimization,
- Selection of solvents optimized for pressurized exhaust,
- Development of CO₂ selective membranes,
- System controls & compressor-expander integration.

To utilize the potential of the large-scale combined cycle in the future, an appropriate intercooled gas turbine would have to be developed.

SUMMARY

A new gas turbine cycle with integrated post-combustion CO₂ capture was developed in a joint Statoil and GE Global Research project. The cycle takes advantage of separating CO₂ at increased CO₂ concentration and elevated pressure. These conditions are facilitated by exhaust gas recirculation and use of a gas turbine intercooler to easily extract and re-inject the working fluid at pressure from the process. Due to the increased CO₂ partial pressure, efficiency penalties and cost of the CO₂ separation unit are reduced. In addition, as only a fraction of the gas turbine working fluid has to be treated, and treatment is carried out under pressure, the size and thereby cost of the CO₂ separation equipment is substantially reduced. The cycle has the potential to capture 80 % or more of the generated CO₂. Using CO₂ separation membrane technology, the cycle approaches the design target of 50 % (LHV) combined cycle net efficiency if based on GE's intercooled LMS100 aeroderivative gas turbine. In the long run, if even larger intercooled gas turbine combined cycles of a 9FB-size would be available, up to 53 % efficiency including CO₂ compression could be reached. The economical analysis shows that using CO₂ membranes the proposed cycle has a potential to

reach 31 \$/t_{CO2} cost of CO₂ avoided if based on the existing medium scale gas turbine platform. In a future scaled-up configuration, the cycle even has the potential of meeting the cost target of 30 \$/t_{CO2}.

Statoil and GE Global Research will continue to jointly investigate additional performance improvements and cost reductions.

ACKNOWLEDGMENTS

This report is based on a joint study of Statoil and GE Global Research. The authors express their appreciation to Statoil ASA and GE for the permission to publish this work.

The authors appreciate the large support by many GE individuals. We would like to thank in particular Narendra Joshi from GE Aviation, Enrico Gori from GE Oil & Gas, Jatila Ranasinghe from GE Energy and Ahmed Elkady, John Bowen and Anthony Brand from GE Global Research for their inputs to this work.

We are also grateful to the many Statoil individuals who offered support and advices on CO₂ separation technologies, in particular Arne Grislingås and Odd Furuseth.

Further, the authors also express their appreciation to May-Britt Hägg and David Grainger from the Norwegian University of Science and Technology (NTNU), for their constructive comments on membrane technology.

REFERENCES

1. Steeneveldt, R., Berger, B., Torp, T.A.: CO₂ capture and storage: Closing the Knowing - Doing Gap, Trans IChemE, Part A, September 2006, Chemical Engineering Research and Design, 84 (A9), pp. 739–763.
2. Lynghjem, A., Jakobsen, J., Kobro, H., Lund, A., Gjerset, M.: The Combicap cycle - efficient combined cycle power plants with CO₂ capture, The Second Trondheim Conference on CO₂ Capture, Transport and Storage, October 25-26, 2004, Trondheim, Norway.
3. Finkenrath, M., Eckstein, J., Hoffmann, S., Bartlett, M., Evulet, A., Bowman, M.J., Lynghjem, A., Jakobsen, J., Ursin, T.P.: Advanced gas turbine cycles with CO₂ removal, 8th International Conference on Greenhouse Gas Control Technologies (GHGT-8), June 19-22, 2006, Trondheim, Norway.
4. Reale, M.: New High Efficiency Simple Cycle Gas Turbine, GE Energy, GER-4222A (06/04), 2004.
5. Hägg, M.-B., Lindbråthen, A.: CO₂ Capture from Natural Gas Fired Power Plants by Using Membrane Technology, Ind. Eng. Chem. Res., 2005, 44 (20), pp. 7668-7675.
6. GateCycleTM Software, website: www.gepower.com/prod_serv/products/plant_perf_software/en/gatecycle/index.htm

GHGT-9

Energy and exergy analyses for the carbon capture with the Chilled Ammonia Process (CAP)

Gianluca Valenti*, Davide Bonalumi, Ennio Macchi

*Politecnico di Milano – Dipartimento di Energia, P.zza L. da Vinci, 32, 20133 Milano, Italy
www.gecos.polimi.it*

Abstract

Post-combustion carbon capture in existing power plants is a strategic technology that can reduce emissions from power generation. The proven approach is scrubbing with amines. However, its drawbacks are energy requirement, 3 to 5 MJ per kg of captured CO₂, as well as solution corrosion and solvent degradation. An alternative approach is scrubbing with chilled aqueous ammonia. This technology aims at mitigating energy usage and solving corrosion and degradation issues. Here an approximate model of the CO₂-H₂O-NH₃ system is coupled with a proposed process to evaluate mass, energy and entropy flows. For 1 kg of captured CO₂, the simulation yields a steam extraction of 0.59 kg, equivalent to a heat duty exceeding slightly 1.5 MJ and a generation loss approaching closely 0.1 kWh, an auxiliary consumption of 0.1 kWh and a delta of almost 0.18 kWh with respect to the ideal case. Assuming a cost of electricity of 7c€/kWh, the sole operation of the capture system totals 14 €/ton CO₂.

© 2009 Elsevier Ltd. All rights reserved.

Chilled Ammonia Process (CAP); Carbon Capture and Storage (CCS); coal-fired power plant; natural gas-fired power plant

1. Introduction

Despite the concerns about rising concentrations of greenhouse gases in the atmosphere, fossil fuels are likely to remain the main source of primary energy for long. Nevertheless, an important contribution towards the reduction of their emissions from fossil fuel-fired power plants may be from Carbon Capture and Storage (CCS) meaning that the CO₂ formed by combustion is captured and stored over an indefinite period. In principle, the CO₂ can be captured according to one of three basic ways: (1) pre-combustion, (2) post-combustion and (3) oxy-fuel combustion. All these ways will play probably a similar role in the short- and the mid-term future, for each of them has peculiar characteristics that makes it appropriate in specific circumstances. Post-combustion capture is strategic for the retrofit of the many existing power plants that will be in service for decades. Traditionally, the sweetening of gases was accomplished with aqueous monoethanol amine (MEA). As it is demanding from the standpoints of energy consumption, corrosion requirement and solvent degradation and as carbon dioxide separation is becoming popular

* Corresponding author. Tel.: +39-02-2399.9845; fax: +39-02-2399.3863.

E-mail address: gianluca.valenti@polimi.it.

in diverse industrial sectors, secondary and tertiary amines have been investigated. Currently, advanced amines, which comprise upload promoters and corrosion inhibitors, are under research. A different approach is to chemically absorb the carbon dioxide into aqueous ammonia at chilled conditions, as patented by EIG Inc. [1]. Among others, Alstom is engaged in an intensive development of the Chilled Ammonia Process (CAP) based on that patent. This paper analyzes a CAP-type process. It begins with a bibliographic review that covers the background of $\text{CO}_2\text{-H}_2\text{O-NH}_3$. Then, it outlines the thermochemical model used to compute mass, energy and entropy flows for a the scheme developed during the investigation. Finally, it reports first- and second-law results from the computer simulation. As to the knowledge of the writers, very little has been written regarding energy balances for complete systems and nothing at all regarding entropy balances. Entropic analysis has the capability of identifying those processes that are responsible for the greater irreversibilities and hence that require an alternative design, if possible.

2. Bibliographic review

$\text{CO}_2\text{-H}_2\text{O-NH}_3$ systems has been investigated by a number of scientists in the last decades. At first the main scope was modeling the chemistry to prepare numerical tools for sour-water treatment. Only in the last decade the interest has shifted onto capturing carbon dioxide. The process is being studied at either room temperature or chilled conditions. The following gives a review of the chemistry of the solution, separating the publications that regard mainly the description of experiments from those that consider primarily the development of models. Thereafter is the review of general manuscripts on ammonia scrubbing and lastly of Alstom's publications on its CAP.

2.1. Chemistry of the $\text{CO}_2\text{-H}_2\text{O-NH}_3$ system

According to the majority of the publications located in the open literature, the species present in the ternary system at working conditions of CAP are: CO_2 , H_2O and NH_3 , in both the vapor and the liquid phases, as well as the aqueous ions H_3O^+ , OH^- , NH_4^+ , HCO_3^- , CO_3^{2-} , NH_2COO^- and, if precipitation occurs in the solution, the pure salt NH_4HCO_3 . In contrast, not all authors agree on the possible formation and combination of the salts made of $(\text{NH}_4)_2\text{CO}_3$ and $\text{NH}_2\text{COONH}_4$. The widely proposed reactions pertinent to the capture and regeneration stages are:



Eqs. 1 and 2 describe the capture of carbon dioxide that is sought inside the absorber whereas eqs. 3 and 4 represent the precipitation of the ammonium bicarbonate salt that occurs at low temperature. On the contrary, the formation of the ion carbamate, eq. 5, may lead to an undesirable capture carbon dioxide, eq. 6, which has a greater enthalpy of reaction for the regeneration. Alternatively, carbamate may combine with ammonium ion, eq. 7.

In 1982 Pawllkowski et al. [2] reported the experimental vapor-liquid equilibrium data of ammonia and carbon dioxide aqueous system, optionally added with salts, at temperatures of 100°C and 150°C. These data were then utilized to calibrate semi-empirical thermodynamic routines (detailed by Edwards et al. and reviewed below).

Almost half a decade later, with the same sake of supporting the design of the equipment for water treatment, Goppert and Maurer [3] conducted an extensive empirical campaign on the equilibria of ammonia and carbon

dioxide aqueous solution in the 333 K to 393 K interval and up to 7 MPa. They re-calibrated those semi-empirical correlations. In 1995 Kurz et al. [4] continued the work both including the solid phase in the equilibrium and expanding the investigation between 313 K and 473 K. They updated the previously-calibrated parameters. Shortly later, Rumpf et al. [5] measured the enthalpy changes upon partial evaporation of aqueous solutions containing ammonia and carbon dioxide and compared them with the predictions from the most-recently regressed models revealing that deviations laid mostly within experimental uncertainty.

Ten years ago, Bai and Yeh [6] provided preliminary experimental data on what was, at that time, going to be referred to as the novel study of ammonia scrubbing. They pointed out the remarkable potential of achieving high removal efficiencies, over 95%, and absorption capacities, as high as 0.9 kg of CO₂ per kg of NH₃. Shortly after, Yeh and Bai [7] completed another experimental campaign with the scope of comparing amine and ammonia scrubbing and they confirmed the potential of the second over the first solvent. Experiments were conducted at room temperature in their first work and between 10°C to 40°C in the later one.

Hsu et al. [8] reported the absorption reaction kinetics of amines and ammonia solutions with carbon dioxide in flue gases. The temperature of investigation was though 50°C, which is relatively high for the CAP. Similarly, Diao et al. [9] also investigated the removal efficiency of the sole ammonia solution in the 25–55°C interval and regressed the parameters of the rate constant, in the Arrhenius form, for the capture reaction.

Interestingly, Mani et al. [10] applied ¹³C NMR spectroscopy at CO₂-NH₃ aqueous solution at room conditions and proved it is a reliable method to investigate the speciation of the ammonium salt of bicarbonate, carbonate and carbamate. They did not detect other species in the solution and determined that NH₂CO₂⁻ is the main species in presence of excess NH₃; in contrast, HCO₃⁻ prevails when most of NH₃ has reacted with CO₂ at lower pH; finally, the CO₃²⁻ anion is always present in solution but at a concentration always lower than carbamate.

In the '70 and '80, the most common approach to the numerical modeling of CO₂-H₂O-NH₃ systems was that developed jointly by two groups lead by the famous scientists Prausnitz and Maurer. As described by Edwards et al. [11], such approach implied combining the molecular-thermodynamic principles with Pitzer's semi-empirical correlation. Bieling et al. [12] introduced in that framework a technique to determine the most important parameters out of the many adjustable ones and applied such technique to ammonia and carbon dioxide aqueous solutions.

A recent approach is the use of the UNIQUAC model for the activity coefficients of the species in the liquid phase. An extended version of the model was started by Sander et al. [13] and later applied by Thomsen and Rasmussen to the CO₂ and/or NH₃ solutions [14,15]. Based on that work, a first assess of a chilled ammonia plant has been lately published (and reported in the next section). In addition to the extended version, Pazuki et al. [16] proposed a UNIQUAC-Non Random Factor (NRF) model for the description of CO₂-H₂O-NH₃ systems.

2.2. Scrubbing of CO₂ with aqueous NH₃

In 2005, Yeh et al [17] published the results of three-cycle absorption-regeneration tests conducted on MEA and ammonia in a batch reactor maintained at about 25°C. They also reported an approximate estimate of energy usage in a cyclical process. According to them, the energy necessary to heat the solution exiting the recuperator and to regenerate is 1017 cal per g of CO₂, which is high with respect to the figures provided by later authors.

Recently, Darde et al. [18] presented a numerical investigation of the phase equilibria for isothermal absorber and regenerator in the range of the working conditions from the original patent by EIG Inc. [1]. In the study, they employed the accurate thermochemical model by Thomsen and Rasmussen [15]. The results include the equilibrium composition of vapor, liquid and solid phases as a function of the CO₂ loading, i.e. the ratio of the number of moles of carbon dioxide and ammonia, the energy requirements for cooling the absorber and, lastly, the energy requirement for heating the regenerator as a function of CO₂ loading and NH₃ initial mass fraction. In short, the CO₂ loading shall be in the 0.33 and 0.67 for the lean solution, 0.67 and 1 for the rich solution. Ammonia initial concentration shall be about 28wt%.

2.3. Alstom's Chilled Ammonia Process

Alstom commenced the development of the CAP in 2006 establishing a 5-year program aiming at commercialization by the end of 2011. The program consisted of 4 phases: (1) small and (2) large scale testing at SRI Int. in the San Francisco Bay Area, CA, (3) field pilot testing of capture on coal-fired exhausts at We Energies' plant in Pleasant Prairie, WI, and at E.ON's plant in Karlshamn, Sweden, and (4) commercial demonstration of capture as well as of storage at the American Electric Power (AEP)'s Mountaineer coal plant. Bench testing is now completed and described in the Electric Power Research Institute (EPRI) technical report [19]. The first pilot testing began in July 2008 and will continue throughout the 2009 whereas the second pilot is under construction, as reported by Black et al. [20,21]. The commercial demonstration is in the engineering design, as detailed by Sherrick et al. [22]. In addition, full-size installations are being programmed for North America and North Europe. As explained in all publications, carbon dioxide is absorbed in an ammoniated solution at temperature below ambient level, 0–20°C, and at almost ambient pressure, generating a slurry containing ammonium bicarbonate. Captured CO₂ is desorbed by turning ammonium bicarbonate into ammonium carbonate at elevated temperatures, moderately above 100°C, and elevated pressures, 20–40 bar. The completed experiments allowed for a first comparison with conventional MEA based on the 460 MW super critical pulverized-coal plant investigated in the Department of Energy (DOE)/EPRI Parson's study [23]: (1) energy consumption for chilling the flue gases, removing absorption enthalpy of reaction and washing the streams can be relatively inexpensive, (2) operating the boiler with minimum excess air and cooling the exhausts reduces the flow volume by a third and increases the CO₂ concentration by a fourth, (3) capture efficiency can exceed 90%, (4) high pressure in the regeneration stage reduces substantially CO₂ compression work, (5) heat duty, and thus steam extraction, in the reboiler is small due to the low regeneration enthalpy of reaction, to the low water concentration in the vapor phase and to the low sensible enthalpy of the rich solution thanks to a high CO₂ loading, (6) direct contact cooling reduces further the SO₂, SO₃, NO₂ and particulate presence, (7) ammonia slip can be minimized to few ppm level by cold-water wash. In contrast to bench results, pilot testing preliminary results are not yet available to the public. However, they are expected to confirm also other key features like: reactants are stable, ammonia can be reintegrated into the process by various forms (anhydrous ammonia, aqueous ammonia, ammonium carbamate) and the system is reliable and cost-effective.

3. Thermochemical model

The thermochemical model adopted in this work is an approximate yet robust one because the scope of the work is to estimate mass, energy and entropy flows with a fair accuracy. In the next stage of the ongoing research the modeling will be brought to greater detail and precision. For that matter, the vapor phase is modeled as a mixture of ideal gases. Information on enthalpy and entropy of formations at standard state of all species are taken from the CRC Handbook [24]. Ideal gas heat capacities are defined as the common NASA Polynomials. The liquid phase is described in either two ways, depending on whether it is chemically reacting or not. In all areas of the process in which liquid water is employed to cool a gaseous stream, liquid phase is treated as pure water. Vapor and liquid equilibrium is computed by means of Raoult's Law assuming that water is the only condensable component. If the liquid phase is chemically reacting, it is assumed that it behaves as an incompressible ideal solution and that all captured carbon dioxide and all ammonia exist only in ionic forms. Moreover, in the lean solutions the only ions present are CO₃²⁻ and NH₄⁺ that react in the absorber with CO₂ and H₂O to form exclusively the ion HCO₃⁻, according to reactions 1 and 2. The lean solution is assumed to be preloaded hypothetically with (NH₄)₂CO₃. Depending upon the temperature, solid ammonium bicarbonate in the rich solution may precipitate, according to reactions 3 and 4. At regeneration conditions the reversal path is followed. Ammonia equivalent concentration in the initial solution, carbon capture efficiency and carbon solution loading are not calculated yet imposed in agreement with experimental results, mainly from Yeh et al. [17]. Being the adopted ammonia concentration relatively low (as stated in the next section), the formation of ion carbamate is neglected, in agreement with Mani et al. [10]. In addition, the model is not structured to compute the ammonia evaporation from the reacting liquid into the vapor phase and the dissolution of components other than carbon dioxide into the liquid. With regards to ions, enthalpy and entropy of formation at standard state are from the CRC [24] and heat capacity as a function of temperature from Thomsen and Rasmussen [15]. With regards to the ammonium bicarbonate salt, standard state data as well as temperature-dependent solubility and specific volume are from the CRC [24] while temperature-independent heat

capacity from Kopp's Rule. Finally, Refprop is used to compute properties of the extracted steam and of the carbon dioxide in the sole compression subsystem (described later), neglecting in the later case that a small quantity of water is included in the flow and making sure the properties are continuous at the boundary with those calculated from the above-described model.

4. Process description

The process analyzed in the present work comprises five subsystems, as illustrated with dashed rectangles in Fig. 1: (1) gas cooling, (2) carbon dioxide absorption and regeneration, (3) treated flue gas wash, (4) regenerated carbon dioxide wash and (5) carbon dioxide compression. It is assumed that upstream of the capture system is a wet desulphurization system. Flue gas cooling is achieved by way of three direct contact coolers, indicated with cooling columns CC1 thru CC3, out of which the first one utilizes water from dry coolers, DC1, while the other two from chillers, CH1 and CH2, operating at different evaporation temperatures. Flue gas chilling yields appreciable condensation of water and thus requires purges, PR1 to PR3, from the columns. After the refrigeration subsystem, the water content and the specific volume of the flow are appreciably reduced hence, at this point, is optimally placed the fan necessary to offset all pressure losses, named FN. Subsequently, the flow enters the absorption column, AB, where it encounters, sprayed from the top, a rich solution recycle, AB4, the lean solution, AC3, and a water make-up, WW4. The recycled stream and the lean stream are refrigerated by a chiller, CH3, in order to counteract the exothermic reaction occurring in the absorber and maintain it at a low temperature at which a moderate quantity of solid ammonium bicarbonate precipitates. Part of this slurry pumped from the bottom of the column, by PS1, is recycled whereas the remainder is boosted to regeneration pressure, by PS2, prior to entering a recuperator, RC, where, as it is heated, the precipitated salt dissolves. At the exit of the heat exchanger, the stream is preheated, in PH, by low pressure steam, ST3, extracted from the turbine and then directed into the regeneration column, RG. Sensible enthalpy and reaction enthalpy inside the column is provided by higher pressure steam, ST1, through an external reboiler, RB. The treated flue gas leaving the absorption column are washed, in WC1, by refrigerated so to minimize ammonia slip to the atmosphere. Similarly, regenerated carbon dioxide is washed, in WC2, so to simultaneously recover the ammonia from the vapor phase, reduce the water content and chill the flow going to the compression subsystem. The treated gas wash has a small water purge, PR4, while carbon dioxide wash a small water make-up. The carbon flow is compressed to slightly supercritical pressure by CC, cooled by dry coolers DC2, and ultimately pumped to transportation conditions by PC. The assumed parameters for the boundary conditions and the working conditions of all operational units are included in Tab. 1.

5. Simulation results

The thermochemical model was implemented in VBA and called by a spreadsheet document containing the first- and second-law analyses of the considered process. As indicated in Tab. 2 in terms specific to 1 kg of captured CO₂, the total heat duty, summing both pre-heater and reboiler, is about 1.5 MJ which is met by a steam extraction of 0.59 kg that results in a loss of electrical production from the turbine of about 0.1 kWh. Tab. 3 summarizes the results for the five subsystems: the first column shows the electrical consumption of the auxiliaries added to the original power plant as well as the electricity penalty related to the two steam extractions, while the second column shows the losses of reversible work related to the irreversible processes occurring in the subsystems along with the discharges of water purges and cold treated gas into the ambient. Referring to the energy analysis, in terms of unit mass of captured CO₂, auxiliaries consume globally almost 0.1 kWh (i.e a value very close to the electricity penalty quoted above for the steam extracted from the turbine), the most of which is for the chiller serving the absorber. As a whole, the absorption-regeneration subsystem takes over almost 58% of all electrical usage. The chillers of the gas refrigeration subsystem are the second most consuming ancillaries, as this subsystem is responsible for more than 20% of the usage. Carbon dioxide compression subsystem has a small share of about 13%, much smaller than in capture systems separating CO₂ at atmospheric pressure. The remainder is equally distributed over the two washing sections. In total, the electrical penalty of carbon capture is 0.2 kWh/kg CO₂. From a second-law perspective, gas cooling and absorption/regeneration subsystems have a similar irreversibility, respectively 39% and 45% of a total work increase of 0.18 kWh per kg of captured CO₂. Interestingly, compression entropy production, 4.4%, is between that of the treated gas wash, 2.9%, and that of the carbon dioxide wash, 6.2%, indicating that is advisable to improve

the second wash by employing a dry cooler in addition to the chiller and allow washing water to return hotter from the column. Entropy production from the discharge of purges and cold gas is very low, about 1% each, as expected, since their discharge temperature is close to the ambient one.

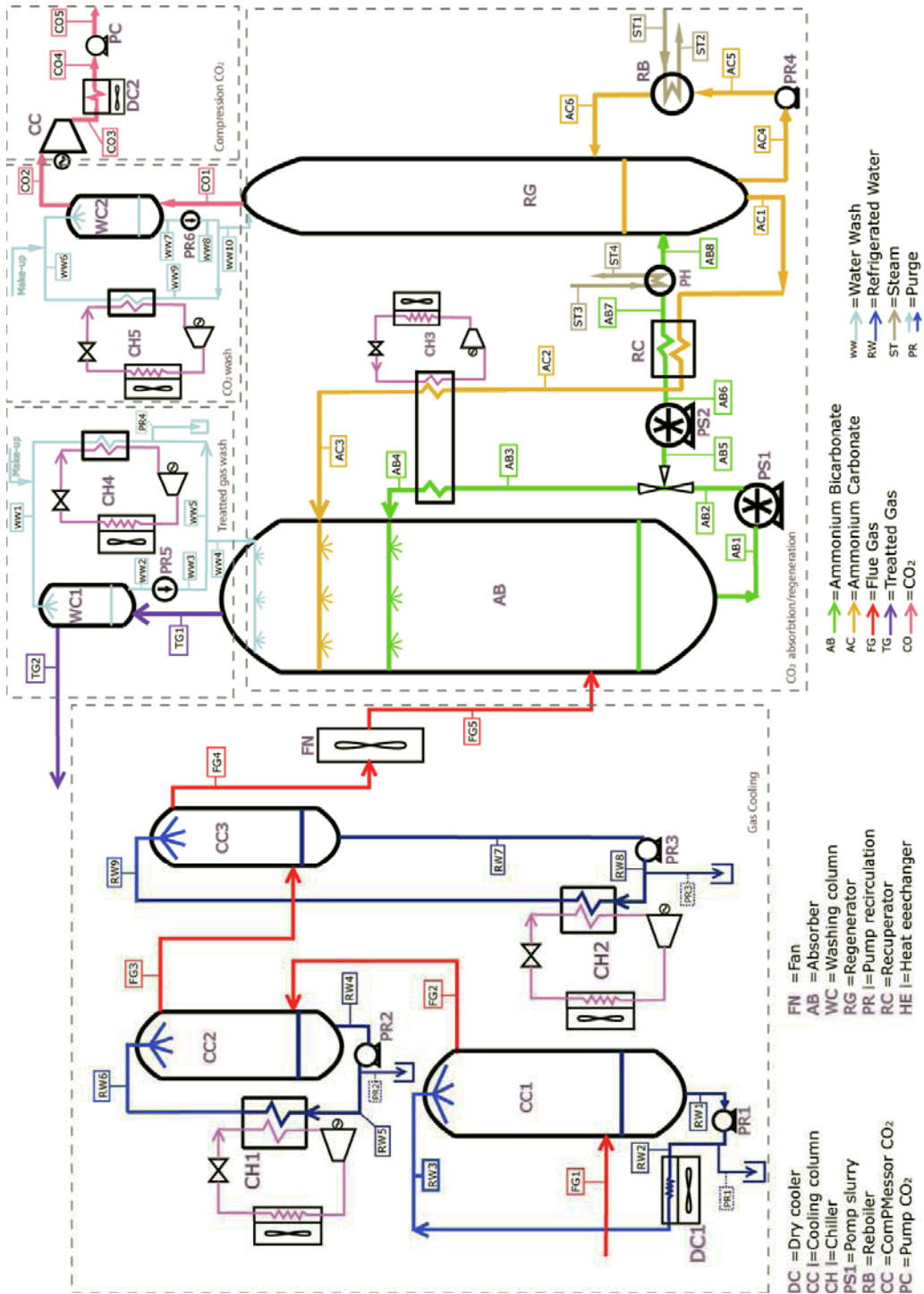


Fig. 1. Schematic of the process analyzed in this work and simulated from first- and second-law points of view.

Tab. 1 – List of the main parameters assumed for the simulation of the process illustrated in Fig. 1.

Ambient		Dry coolers	
Pressure, bar	1.01	Reference thermal power, kW	727
Temperature, °C	15	Reference ΔT inlets, °C	15
Flue gases		Reference electrical power, kW	5.94
Pressure, bar	1.025	ΔT minimum cold side, °C	5
Temperature, °C	60	Chillers	
Ar mol%	0.43	ΔT condensation, °C	10
CO ₂ mol%	11.27	ΔT evaporation, °C	3
H ₂ O mol%	saturated	COP / COP of Carnot cycle	0.65
N ₂ mol%	64.55	Recirculation pumps	
O ₂ mol%	4.24	Hydraulic efficiency, %	80
Reboiler steam		Electro-mechanical efficiency, %	90
Pressure, bar	3.5	Head pressure (PR1, PR2, PR3, PR5), bar	2.50
Temperature, °C	330	Head pressure (PR4, PR6), bar	42.50
Pre-heater steam		Slurry pumps	
Pressure, bar	1	Hydraulic efficiency, %	75
Temperature, °C	200	Electro-mechanical efficiency, %	95
Steam turbine		Head pressure (PS1), bar	5
Adiabatic efficiency, %	90	Head pressure (PS2), bar	40
Electro-mechanical efficiency, %	98	Carbon dioxide pump/compressor	
Exhaust pressure, bar	0.05	Hydraulic/adiabatic efficiency, %	85
Exhaust vapor quality, %	95	Electro-mechanical efficiency, %	92
Absorption reactor		Head pressure (CC/PC), bar	80/150
NH ₃ concentration initial solution, wt%	11.5	Cooling and washing columns	
Capture efficiency, %	90	ΔP , bar	0.015
CO ₂ loading, kg CO ₂ / kg solution	0.10	Hot stream outlet temp (CC1), °C	23
Extracted / regenerated flows, kg / kg	6	Hot stream outlet temp (CC2, WC2), °C	15
Recycle and lean sol inlet temp, °C	10	Hot stream outlet temp (CC3, WC1), °C	6
Regeneration reactor		ΔT cold side, °C	3
Pressure, bar	40	ΔT hot side (CC1), °C	5
Temperature, °C	120	ΔT hot side (CC2), °C	4
Heat exchangers		ΔT hot side (CC3, WC1), °C	3
ΔT min, °C	5	ΔT hot side (WC2), °C	95

Tab. 2 – Steam extraction and loss of electrical production from the steam turbine. All values are given specific to the kilogram of captured CO₂.

	Heat duty MJ / kg CO ₂	Steam extraction kg steam/kg CO ₂	Electrical loss kWh/kg CO ₂
Pre-heater	0.5813	0.2283	0.0271
Reboiler	0.9535	0.3661	0.0688
Total	1.5348	0.5944	0.0959

Tab. 3 – Electrical penalty due to auxiliaries, loss of production from turbine and work increase with respect to ideality due to irreversibilities.

	Electrical penalty		Delta work w/t ideality	
	kWh/kg CO ₂	%	kWh/kg CO ₂	%
Gas cooling	0.0207	20.75	0.0685	38.97
CO ₂ absorption/regeneration	0.0579	57.98	0.0796	45.33
Treated gas wash	0.0039	3.95	0.0051	2.89
CO ₂ wash	0.0039	3.86	0.0109	6.18
CO ₂ compression	0.0134	13.47	0.0077	4.41
Purge discharge	0.0000	0.00	0.0021	1.22
Treated gas discharge	0.0000	0.00	0.0017	0.99
Total auxiliary electrical usage	0.0998	100.00	0.1757	100.00
Total loss from steam turbine	0.0959			
Total electrical penalty	0.1957			

6. Conclusions

The CAP appears to be a promising technology. Compared to MEA, the present simulation confirms it has a reduced reboiler heat duty and a moderate electrical need for auxiliaries, in particular chillers: for 1 kg of captured

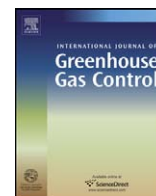
CO₂, a steam extraction of 0.59 kg, equivalent to a heat duty exceeding 1.5 MJ and a generation loss approaching 0.1 kWh, an auxiliary consumption of 0.1 kWh and an increase of work with respect to ideality of 0.18 kWh. The total electrical penalty is 0.2 kWh so, at a cost of electricity of 7 c€/kWh, the sole operation adds about 14 € per captured ton of CO₂. Referring to a modern PC-USC with net electrical output of 600 MW and efficiency of 45.0%, with respect to a coal containing 62wt% of C and having a LHV of 25 MJ/kg, the decrease in output is 76.9 MW, which reduces the efficiency to 39.2%, penalizing the performance less than most of the competing techniques.

Acknowledgements

The authors acknowledge gratefully the support from Enel S.p.A.

References

1. EIG Inc, Ultra cleaning of combustion gas including the removal of CO₂, WO Patent No. WO/2006/022885 (2006).
2. E.M. Pawllkowski, J. Newman and J.M. Prausnitz, Phase equilibria for aqueous solutions of ammonia and carbon dioxide. *Ing. Eng. Chem. Process Des. Dev.* No. 21 (1982) 764-770.
3. U. Göppert and G. Maurer, Vapor-liquid equilibria in aqueous solutions of ammonia and carbon dioxide at temperatures between 333 and 393 K and pressures up to 7 MPa. *Fluid Phase Equilibria* No. 41 (1988) 153-185.
4. F. Kurz, B. Rumpf and G. Maurer, Vapor-liquid-solid equilibria in the system NH₃-CO₂-H₂O from around 310 to 470 K: New experimental data and modeling. *Fluid Phase Equilibria* No.104 (1995) 261-275.
5. B. Rumpf, F. Weyrich and G. Maurer, Enthalpy changes upon partial evaporation of aqueous solutions containing ammonia and carbon dioxide. *Ind. Eng. Chem. Res.* No. 37 (1998) 2983-2995.
6. H. Bai and A.C. Yeh, Removal of CO₂ greenhous gas by ammonia scrubbing. *Ind. Eng. Chem. Res.* No. 36 (1997) 2490-2493.
7. A.C. Yeh and H. Bai, Comparison of ammonia and monoethanolamine solvents to reduce CO₂ greenhouse gas emissions. *The Science of the Total Environment* No. 228 (1999) 121-133.
8. C.H. Hsu, H. Chu and C.M. Cho, Absorption and reaction kinetics of amines and ammonia solutions with carbon dioxide in flue gases. *J. Air & Waste Management Ass.* No 53 (2003) 246-252.
9. Y.-F. Diao, X.-Y. Zheng, B.-S. He, C.-H. Chen and X.-C. Xu, Experimental study on capturing CO₂ greenhouse gas by ammonia scrubbing. *Energy Conv. and Managment* No. 45 (2004) 2283-2296.
10. F. Mani, M. Peruzzini and P. Stoppioni, CO₂ absorption by aqueous NH₃ solutions: speciation of ammonium carbamate, bicarbonate and carbonate by ¹³C NMR study. *Green Chem.* No. 8 (2006) 995-1000.
11. T.J. Edwards, G. Maurer, J. Newman and J.M. Prausnitz, Vapor-liquid equilibria in multicomponent aqueous solutions of volatile weak electrolytes. *Aiche J.* No. 24 (1978) 966-976.
12. V. Bieling, B. Rumpf, F. Strepp and G. Maurer, An evolutionary optimization method for modeling the solubility of ammonia and carbon dioxide in aqueous solutions. *Fluid Phase Equilibria* No. 53 (1989) 251-259.
13. B. Sander, A. Fredenslund and P. Rasmussen, Calculation of vapour-liquid equilibria in mixed solvent/salt systems using an extended UNIQUAC equation. *Chem. Eng. Science* No. 41 (1986) 1171-1183.
14. K. Thomsen, P. Rasmussen and R. Gani, Correlation and prediction of thermal properties and phase behavior for a class of aqueous electrolyte systems. *Chem. Eng. Science* No. 14 (1996) 3675-3683.
15. K. Thomsen and P. Rasmussen, Modeling of vapor-liquid-solid equilibrium in gas-aqueous electrolyte systems. *Chem. Eng. Science* No. 54 (1999) 1787-1802.
16. G.R. Pazuki, H. Pahlevanzadeh and A.M. Ahooei, Prediction of phase behavior of CO₂-NH₃-H₂O system by using the UNIQUAC-Non Random Factor (NRF) model. *Fluid Phase Equilibria* No 242 (2006) 57-64.
17. J.T. Yeh, K.P. Resnik, K. Rygle and H.W. Pennline, Semi-batch absorpion and regeneration studies for CO₂ capture by aqueous ammonia. *Fuel Processing Tech.* No. 86 (2005) 1533-1546.
18. V. Darde, K. Thomsen, W. van Well and E. Stenby, Chilled ammonia process for CO₂ capture. In proceedings of 15th International Conference on the Properties of Water and Steam (ICPWS), Berlin, Germany (2008).
19. Chilled-ammonia Post Combustion CO₂ Capture System—Laboratory and Economic Evaluation Results. EPRI: 2006 1012797.
20. S. Black, O.-M. Bade, E. Gal, E. Morris, G. Krishnan and I.S. Jayaweera, Chilled ammonia process for CO₂ capture. In proceedings of Power-Gen Europe, Madrid, Spain (2007).
21. S. Black, P. Paelinck, F. Kozak, A. Petig, E. Morris, Chilled ammonia process for CO₂ capture. In proceedings of Pennwell Oil Sands Conference, Calgary, Alberta, Canada (2008).
22. B. Sherrick, M. Hammond, G. Spitznogle, D. Muraskin, S. Black, M. Cage, CCS with Alstom's Chilled Ammonia Process at AEP's Mountaineer plant. In proceedings of MEGA Conference, Baltimore, Maryland, U.S.A. (2008).
23. Evaluation of Innovative Fossil Fuel Power Plants with CO₂ Removal, EPRI, Palo Alto, CA, U. S. Department of Energy — Office of Fossil Energy, Germantown, MD and U. S. Department of Energy/NETL, Pittsburgh, PA: 2000. 1000316.
24. D.R. Lide (ed.), CRC handbook of chemistry and physics, 84th Ed.on, CRC Press, 2004.



Quantitative evaluation of the chilled-ammonia process for CO₂ capture using thermodynamic analysis and process simulation[☆]

Paul M. Mathias^{a,*}, Satish Reddy^a, John P. O'Connell^b

^a Fluor Corporation, 47 Discovery, Irvine, CA 92618, USA

^b Department of Chemical Engineering, University of Virginia, Charlottesville, VA 22904, USA

ARTICLE INFO

Article history:

Received 17 April 2009

Received in revised form 14 July 2009

Accepted 23 September 2009

Available online 24 October 2009

Keywords:

Post-combustion CO₂ capture

Thermodynamic analysis

Process simulation

Absorption

Speciation

Heat of reaction

ABSTRACT

There is strong world-wide interest in developing new and improved processes for post-combustion capture of CO₂, often using chemical absorption. Developers of new processes make positive claims for their proposals in terms of low energy consumption, but these are usually difficult to validate. This paper demonstrates that rigorous application of thermodynamic analysis and process simulation provides a powerful way to quantitatively estimate the energy requirements of CO₂-capture processes by applying the methodology to the analysis and evaluation of the chilled-ammonia process.

© 2009 Elsevier Ltd. All rights reserved.

1. Introduction

There is strong world-wide interest in developing new and improved processes for post-combustion capture of CO₂, and current state-of-the-art processes usually use chemical absorption (Aaron and Tsouris, 2005; Bailey and Feron, 2005; Ciferno et al., 2009). Developers of new processes make positive claims for their proposals in terms of low energy consumption, but these are usually difficult to validate. This paper demonstrates that rigorous application of thermodynamic analysis and process simulation provides a powerful way to quantitatively discriminate among various CO₂-capture processes, by applying the methodology to the analysis of an aqueous-ammonia process, specifically the chilled-ammonia process (Gal, 2006).

Chemical absorption is complicated and difficult to analyze because many complexes and ionic species may form and the accuracy of the calculated phase equilibrium and heats of absorption and stripping depend on proper representation of the speciation and the solution non-ideality. But applied thermodynamicists and chemical engineers have many decades of experience in this area (Mather, 2008; O'Connell et al., 2009),

and a variety of data (vapor–liquid and liquid–solid equilibrium, spectroscopic investigation of species distribution, calorimetric measurement of heats of solution, etc.) are usually available to develop, fine-tune and validate the thermodynamic models.

Process simulation of electrolyte systems is also an established tool in chemical engineering, and serves as an effective basis to rapidly and accurately analyze various process schemes (Chen and Mathias, 2002; Mathias, 2005). Process simulation also provides the means to interpret laboratory experiments and quantify the process performance.

This work demonstrates the power of thermodynamic analysis and process simulation by applying these tools to the analysis and quantitative evaluation of the chilled-ammonia process (Gal, 2006).

2. Chemical absorption for CO₂ capture—thermodynamic analysis and process simulation

A wide variety of processes for post-combustion capture of CO₂ are currently being researched, and these include absorption using solvents or solid sorbents, pressure- and temperature-swing adsorption, cryogenic distillation, and membranes (Aaron and Tsouris, 2005; Bailey and Feron, 2005; Ciferno et al., 2009). The focus of the present analysis is on absorption using chemical solvents since this is the current state-of-the-art (Aaron and Tsouris, 2005; Bailey and Feron, 2005; Ciferno et al., 2009). In post-combustion CO₂-capture processes by chemical absorption, the “lean” solvent preferentially absorbs CO₂ from the flue gas at low pressure (about 1 atm). The “rich” solvent is regenerated in a

[☆] Paper previously presented at 9th International Conference on Greenhouse Gas Control Technologies, 16–20 November 2008, Washington, DC (GHGT-9), and invited by Organizing Committee of GHGT-9 and editors of special issue of International Journal of Greenhouse Gas Control (IJGGC) as a submission to IJGGC.

* Corresponding author. Tel.: +1 949 349 3595; fax: +1 949 349 7498.

E-mail address: Paul.Mathias@Fluor.com (P.M. Mathias).

stripper at elevated temperatures to produce the CO₂ product and the lean solvent that is recycled back to the absorber. Chemical-absorption processes for post-combustion CO₂ capture are in successful operation today (Chapel et al., 1999), and hence the competitiveness of a particular process depends on the associated process costs, most significantly the utility costs: heating (low-pressure steam), cooling (cooling water) and, in some cases, chilling (refrigeration).

Thermodynamic analysis offers a powerful technique to perform reliable and accurate analysis of the utility costs of chemical-absorption processes (O'Connell et al., 2009). An accurate thermodynamic model is needed for the complex, electrolytic system, but this can be accomplished today due to the availability of molecular-thermodynamic models and the underlying phase-equilibrium data, analytical data on speciation and calorimetric measurements of the heats of solution (Mather, 2008; O'Connell et al., 2009). Once the thermodynamic model has been developed and validated, commercial software (e.g., Aspen Plus® from Aspen Technology, Inc. and the OLI Engine® from OLI Systems, Inc.) can routinely simulate the entire integrated process, including absorbers, strippers and heat exchangers, as well as heat integration. Darde et al. (2008, 2009) have presented thermodynamic analysis of the chilled-ammonia process.

3. Chilled-ammonia process

Aqueous-ammonia processes (DOE/NETL report, 2007) have been proposed as energy-efficient alternatives to traditional alkanolamine absorption-stripping processes (e.g., Chapel et al., 1999; Mimura et al., 2000) for post-combustion capture of CO₂. This work focuses on the chilled-ammonia process that has been patented by Gal (2006). The process description presented here is concise, and the reader is referred to Gal's patent (2006) for further details. Fig. 1 presents the flow diagram of the process modeled in this work. Flue gas that has been desulfurized (not shown) has its pressure raised slightly using a blower, is cooled to 100 F using cooling water, is chilled to 41 F via refrigeration, and then enters the absorber (represented as a spray tower with chilled-liquid recirculation) where most of the CO₂ in the flue gas (typically 90%) is chemically absorbed in the lean solvent from the stripper. The lean solvent is chilled to 47 F and its CO₂ loading is at the point of imminent precipitation of salts: ammonium bicarbonate (NH₄HCO₃

or ABC) and possibly ammonium carbonate ((NH₄)₂CO₃·H₂O). The absorber removes CO₂ from the flue gas mainly by the precipitation of ABC and has a recirculation loop with refrigerated chilling that maintains it at a target temperature in the range 30–50 F. The refrigeration load comes from three demands: flue-gas-chiller, recycle solvent chiller and absorber chiller. The solvent flow rate is set to absorb 90% of the CO₂ in the flue gas.

The rich solvent is pumped to a higher pressure, heated in a cross exchanger (minimum approach temperature set to 10 F, which is quite aggressive for a heat exchanger with solids in one of the process streams) with the hot lean solvent and enters a stripper that operates at 450 psia and produces the CO₂ product as distillate and the lean solvent as the bottoms. The stripper reboiler duty is set to achieve the required CO₂ loading in the lean solvent.

The absorption system includes a make-up stream of the NH₃ solvent, as shown in Fig. 1.

The specified or control variables in the process flow diagram shown in Fig. 1 are the flow and composition of the flue gas, the absorber temperature (30–50 F) and the NH₃ concentration of the solvent on a CO₂-free basis. The key calculated results are the solvent circulation rate, the heat load (stripper reboiler duty), the refrigeration load (sum of three chiller duties) and the ammonia slip in the absorber.

The NH₃ slip in the absorber overhead is too high (240–2200 ppmv, as further discussed in Section 5) for direct discharge into the environment, and thus requires additional treatment (NH₃ abatement). Fig. 2 presents the NH₃-abatement scheme analyzed in this work. The minimum approach temperature in the NH₃-abatement cross exchanger has been set to 10 F, and the recycle solvent flow rate and the stripper reboiler duty have been calculated to achieve 10 ppmv NH₃ in the vent gas and water flow rate from the stripper overhead to balance water losses from the flow diagram of Fig. 1. In other words, the purpose of the NH₃-abatement system is to control NH₃ discharge into the environment and to maintain a water balance in the plant.

4. Thermodynamic model

The thermodynamic model used here was presented previously at the 7th Annual Conference on Carbon Capture and Sequestration (Mathias et al., 2008). Thermodynamic models for electrolyte systems require a chemistry model, which is a theoretically correct

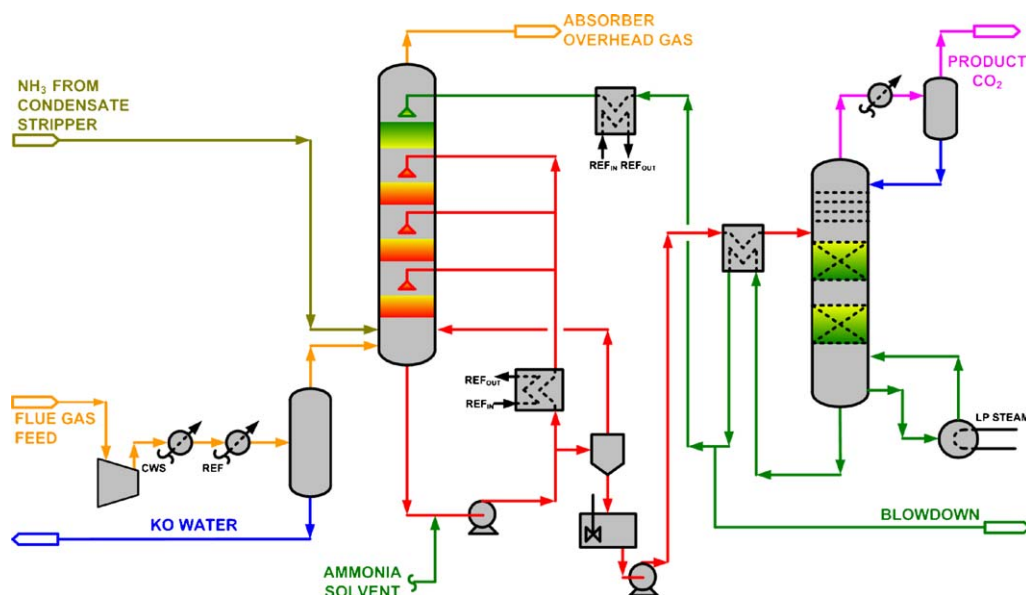


Fig. 1. Flow diagram of the chilled-ammonia process.

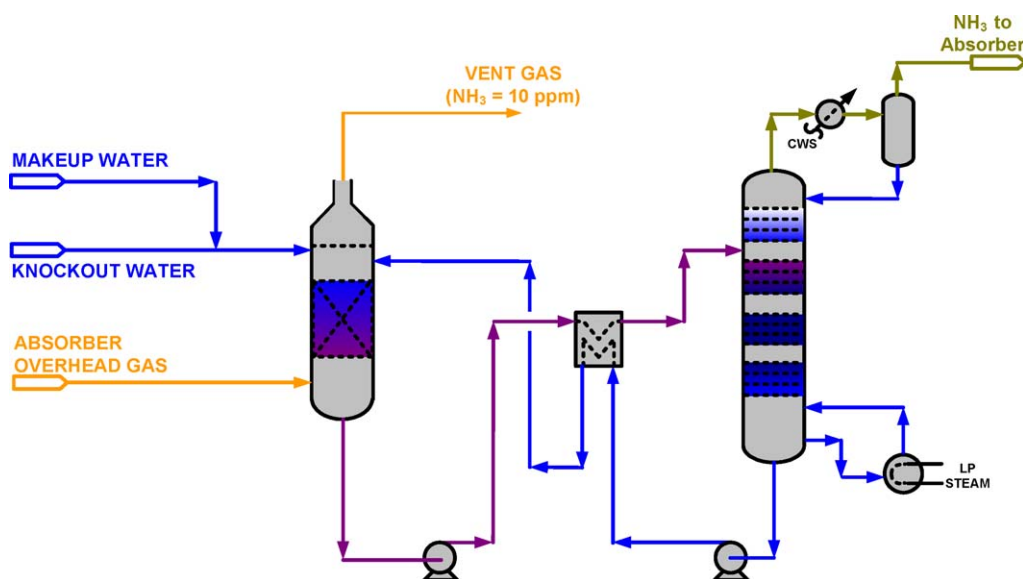


Fig. 2. Absorber-stripper system for NH_3 abatement of stream from the CO_2 absorber overhead.

and practical representation of the ionization reactions that occur in the system, and a non-ideality model (Mather, 2008).

The chemistry model for the NH_3 – CO_2 – H_2O system, which is presented in Table 1, identifies the acid–base effects through which NH_3 as a weak base causes the chemical absorption of the weak acid CO_2 . Absorbed CO_2 exists as molecular CO_2 (very low concentration), and bicarbonate, carbonate and carbamate anions, while NH_3 in solution exists as molecular NH_3 , ammonium cation and carbamate anion. The chemistry model should not only represent the total CO_2 and NH_3 in solution, but also quantitatively describe the concentrations of the various species since effects like heats of solution depend on correct and accurate speciation (Mather, 2008; O’Connell et al., 2009). The chemistry model in Table 1 also includes the formation of $\text{NH}_4\text{HCO}_3(\text{s})$ or ABC since this solid precipitates in the absorber and may remain in the heated rich stream from the cross exchanger. Our analysis indicates that the only other solid that may form in the process is $(\text{NH}_4)_2\text{CO}_3 \cdot \text{H}_2\text{O}$, which possibly precipitates in the chilled lean-solvent feed to the absorber. We have fixed the CO_2 loading of this stream to ensure that both ABC and $(\text{NH}_4)_2\text{CO}_3 \cdot \text{H}_2\text{O}$ do not precipitate in the chilled lean-solvent feed to the absorber.

The non-ideality model used here is the ElectrolyteNRTL (Chen et al., 1982) model available in Aspen Plus[®], and the model parameters were adjusted to provide a good fit of the available vapor–liquid equilibrium (Göppert and Maurer, 1988; Kurz et al., 1995), solid–liquid equilibrium (Jänecke, 1929a,b), calorimetric (Rumpf et al., 1998) and speciation (Wen and Brooker, 1995) data.

Figs. 3 and 4 demonstrate that the model provides good agreement with the vapor–liquid equilibrium data of Kurz et al. (1995), and Figs. 5 and 6 indicate that the speciation predictions of the model agree with the Raman spectra measurements of Wen and Brooker (1995). Mathias et al. (2008) have further shown that the model provides an accurate representation of solid–liquid

equilibrium (Jänecke, 1929a,b) and calorimetric (Rumpf et al., 1998) data.

Fig. 7 presents two independent calculations for the differential heat of solution of CO_2 in aqueous NH_3 : calculation from the present thermodynamic model and “thermodynamic analysis.” The thermodynamic analysis (labeled “From VLE data” in Fig. 7) directly uses the experimental partial pressures of CO_2 (Kurz et al., 1995) to estimate its differential heat of solution through the following thermodynamic relationship and numerical estimation

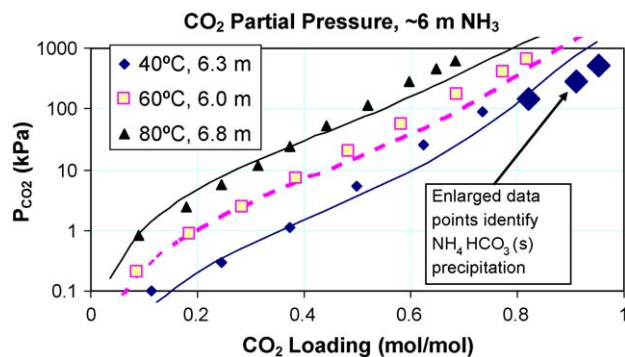


Fig. 3. Comparison between model calculations and data (Kurz et al., 1995) for the partial pressure of CO_2 in ≈ 6 m NH_3 solutions.

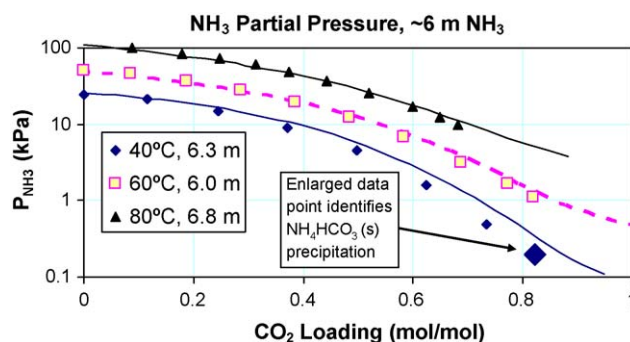
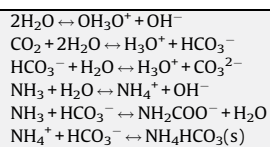


Fig. 4. Comparison between model calculations and data (Kurz et al., 1995) for the partial pressure of NH_3 in ≈ 6 m NH_3 solutions.

Table 1
Chemistry model for the NH_3 – CO_2 – H_2O system.



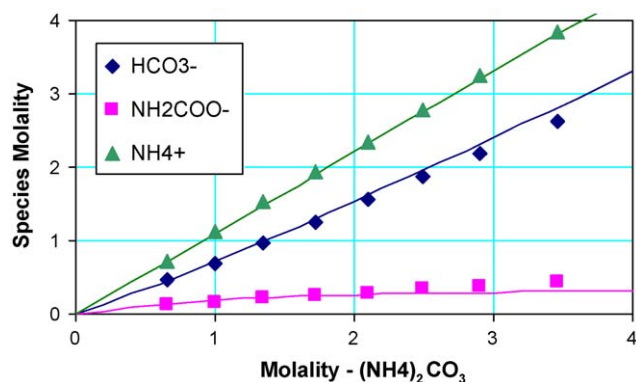


Fig. 5. Speciation in the (NH4)2CO3 system. Comparison between model calculations and data of Wen and Brooker (1995).

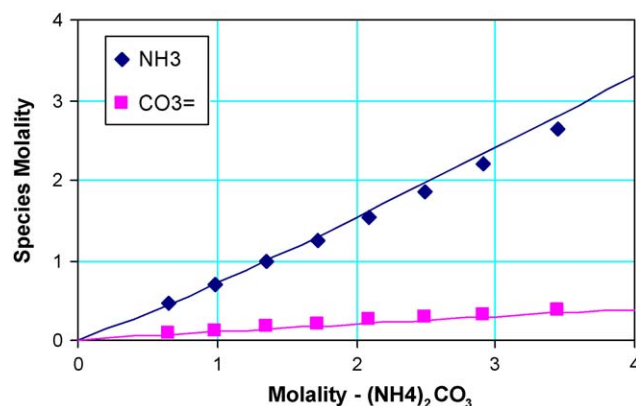


Fig. 6. Speciation in the (NH4)2CO3 system. Comparison between model calculations and data of Wen and Brooker (1995).

of the partial derivative:

$$H_{\text{CO}_2}^{\text{Solution}} = -R \left\{ \frac{\partial \ln(P_{\text{CO}_2})}{\partial (1/T)} \right\}_{\text{Loading}} \quad (1)$$

The agreement between the thermodynamic model and the independent thermodynamic analysis in Fig. 7 is considered good since our estimate of the uncertainty of the thermodynamic analysis (Eq. (1)) is about ± 25 –50 Btu/lb CO₂ due to numerical imprecision in estimating the partial derivative in Eq. (1). This good agreement, as well as the agreement of the model with the calorimetric data of Rumpf et al. (1998), which was previously presented by Mathias et al. (2008), clearly support the validity and accuracy of the model prediction.

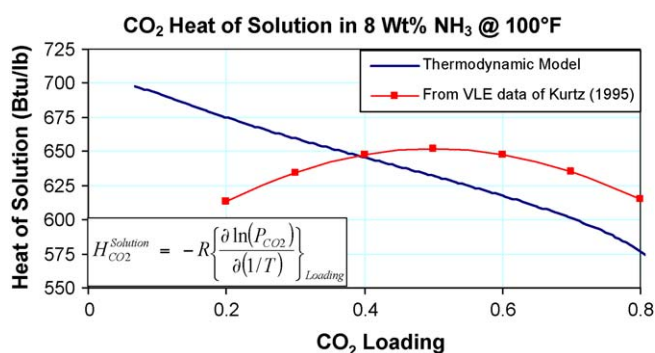
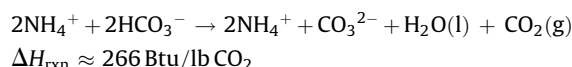


Fig. 7. Heat of solution of CO₂ in 8 wt% NH₃ at 100 F. Comparison between model predictions and thermodynamic analysis of the data of Kurtz et al. (1995).

The CO₂ heat of solution in aqueous MEA (monoethanolamine) at low loadings of CO₂ is about 800 Btu/lb CO₂, as experimentally measured by Carson et al. (2000). Fig. 7 indicates that the heat of solution of CO₂ in aqueous NH₃, also at low CO₂ loadings, is in the range of 600–700 Btu/lb CO₂. Hence, the heat of solution of CO₂ in aqueous ammonia is less than that in aqueous MEA, but is much higher than the ≈ 260 Btu/lb CO₂ reported by many researchers in the field (Resnik et al., 2004; Gal and Olson, 2006; DOE/NETL report, 2007). As discussed by Mathias et al. (2008), the inaccurate estimation of the heat of solution (≈ 260 Btu/lb CO₂) results from imposing fixed speciation rather than allowing the species distribution to follow chemical equilibrium consistent with the chemistry model (Table 1) and measured by Raman spectra analytical data (Wen and Brooker, 1995).

Consider the following reaction as representing the regeneration of CO₂ in the stripper:



This reaction represents the chemical conversion of ammonium bicarbonate in aqueous solution (as ionic species) to ammonium carbonate (as ionic species), liquid water and gaseous CO₂. If this is the only reaction occurring in the stripper, the heat of regeneration would indeed be about 260 Btu/lb CO₂. But, in reality, the regeneration of CO₂ is the overall result of a set of several reactions that are occurring simultaneously (Table 1), and the correct heat of reaction is actually in the range of 600–700 Btu/lb CO₂.

5. Quantitative process analysis and evaluation

The thermodynamic model for the NH₃–CO₂–H₂O system has been used in the Aspen Plus process simulator to study the particular case of post-combustion CO₂ capture by the chilled-ammonia process (Gal, 2006), with flowsheets represented by Figs. 1 and 2. The inlet flue gas stream has a flow rate of 150,000 lb mol/h with mole percents of H₂O, CO₂, N₂ and O₂ as 11.0, 13.7, 71.8 and 3.5, respectively. The feed CO₂ composition of about 14 mol% is typical of flue gases from coal-fired power plants (Ciferno et al., 2009). It should be noted that the process simulation model used here assumes physical and chemical equilibrium, and does not consider reaction kinetics, vapor-to-liquid mass transfer rate in the absorber, solid-precipitation rate in the absorber and solid-dissolution rate in the cross exchanger. Hence, the present simulation model provides an optimistic estimate of process performance; the quantitative extent of the optimism of the equilibrium model is difficult to estimate without developing a rate-based model (Zhang et al., 2009).

The first part of the study kept the absorber temperature fixed at 50 F and varied the NH₃ composition in the solvent. Fig. 8 indicates that increasing the NH₃ concentration in the solvent decreases the solvent circulation rate, and this is because the solids content of the rich solvent increases and the difference between the rich and lean CO₂ loadings also increases, as shown in Fig. 9. The NH₃ slip from the absorber is only weakly dependent on the NH₃ concentration and depends mainly on absorber temperature; at 50 F, the NH₃ slip is approximately constant at 2230 ppmv. Hence, the study further focused on the 26 wt% NH₃ (CO₂-free basis) solvent where the solids content of the rich solvent is 60.2%. For 26 wt% NH₃ and an absorber temperature of 50 F, the stripper duty is 985 Btu/lb CO₂, while the NH₃ abatement regenerator duty is 1022 Btu/lb CO₂, which gives a total LP steam requirement of 2007 Btu/lb CO₂. This LP steam requirement is very high compared to typical LP steam requirements for alkanolamine-based processes, which are usually in the 1200–1500 Btu/lb CO₂ range (DOE/

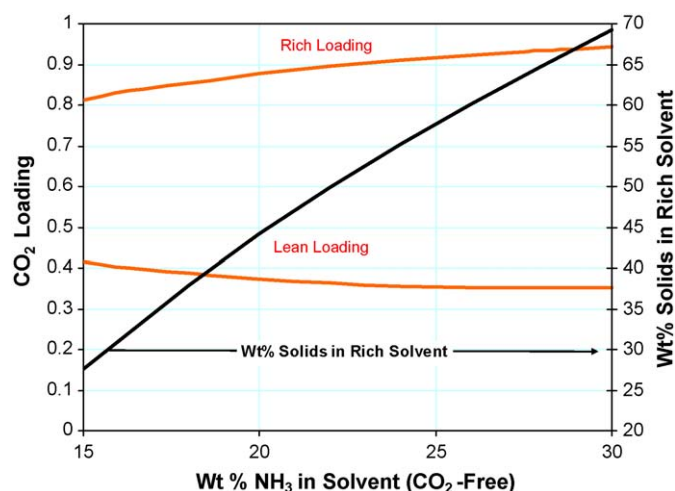


Fig. 8. Effect of NH₃ concentration in the solvent on the solvent flow rate. The absorber temperature is 50 F.

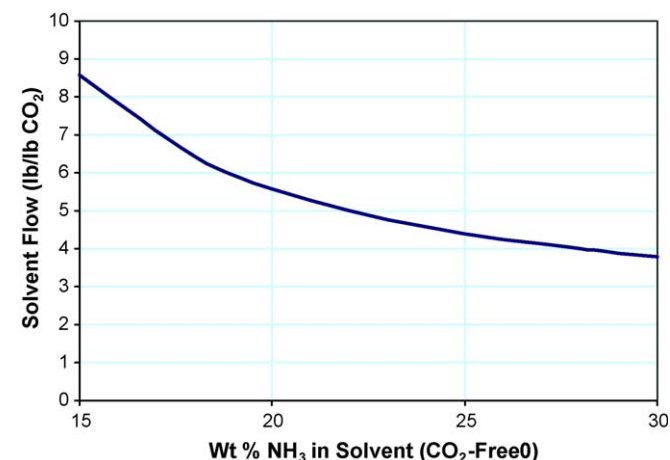


Fig. 9. Effect of NH₃ concentration in the solvent on weight fraction solids in the rich solvent, and lean and rich CO₂ loadings. The absorber temperature is 50 F.

NETL report, 2007). Note also that licensors of the alkanolamine-based processes have made improvements to lower the energy consumption, as, for example, described by Reddy and Gilmartin (2008).

The NH₃-abatement regenerator steam requirement is high because the NH₃ slip is high at the absorber temperature of 50 F. Fig. 10 presents the reduction in NH₃ slip achieved as the absorber temperature is reduced. If the absorber can be run at 30 F, the NH₃

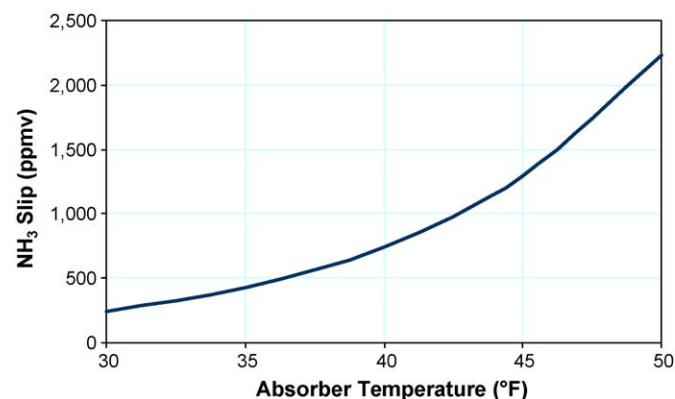


Fig. 10. NH₃ slip in absorber as a function of absorber temperature.

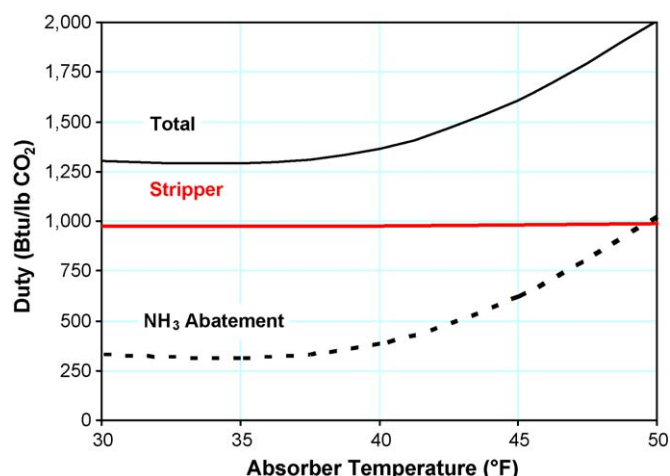


Fig. 11. Utility loads for NH₃ concentration of 26 wt% (CO₂-free) as a function of temperature.

slip will be reduced to 242 ppmv, but NH₃ abatement is still needed to reduce the NH₃ concentration in the flue gas discharged to the stack down to the target level of 10 ppmv. Figs. 11 and 12 show how the absorber stripper duty and NH₃ abatement regenerator duty vary as the absorber temperature is decreased. The total LP steam requirement is approximately constant below about 35 F, and in fact has a weak minimum of about 1291 Btu/lb CO₂ at 35 F. Hence, the steam requirements will be equivalent to alkanolamine-based CO₂-capture processes if the absorber can be run at 35 F. However, Fig. 12 also shows that operation of the absorber below about 50 F will cause solid precipitation in the rich-solvent feed stream to the stripper (following heating in the cross exchanger), which will require pre-heat to mitigate fouling problems in the stripper.

The chilled-ammonia process also incurs a refrigeration load of about 1200 Btu/lb CO₂ (Fig. 12), which will require the use of compressor power for the refrigeration unit. Some of this chilling load is offset by the high pressure of the product CO₂, which reduces the CO₂ compressor power. Our analysis indicates that the chilling-load penalty exceeds the benefits in the reduced compressor power. An optimistic estimate of the coefficient of

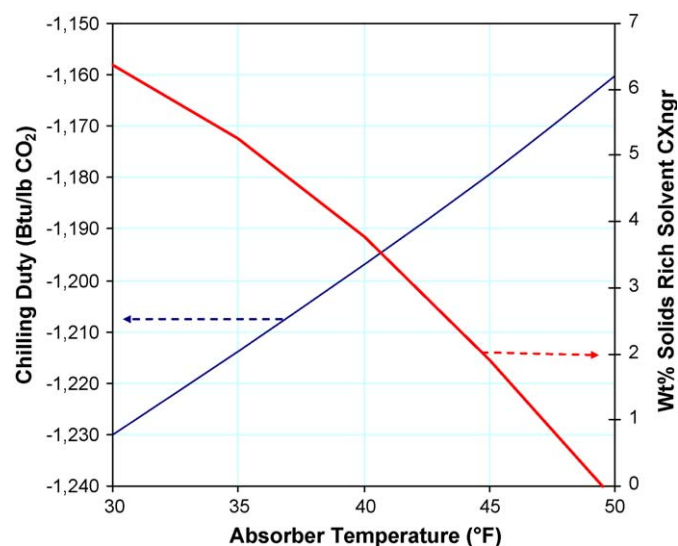


Fig. 12. Chilling duty and weight % solids in the stream leaving the cross exchanger. note that solids will be present in the rich solvent leaving the cross exchanger if the absorber temperature is below 49 F.

performance of the refrigeration system is five, which gives a refrigeration compressor load (i.e., mechanical work or electrical energy) of 240 Btu/lb CO₂. An alkanolamine process condenser typically operates at about 24 psia, and our estimate of the compressor load to raise the pressure of CO₂ from 24 to 450 psia with an isentropic efficiency of 81% is 120 Btu/lb CO₂. Note that both these energy requirements are mechanical work rather than heat, and hence the efficiency of converting heat into work must be taken into account for equivalence with the LP steam requirement.

In summary, the total LP steam requirements of the chilled-ammonia process may be made comparable to alkanolamine processes by running the absorber at a reduced temperature, but temperatures below 50 F require special treatment to avoid fouling problems in the stripper. The chilled-ammonia process requires refrigeration power, which is a net positive energy cost even if the benefits of the higher-pressure CO₂ product from the stripper are taken into account.

6. Conclusions

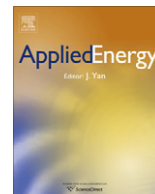
This work has demonstrated that the combination of an accurate and reliable thermodynamic model and process simulation enables a powerful tool to analyze and quantitatively evaluate proposed processes for post-combustion CO₂ capture, which is applicable even to complex processes like chilled ammonia that feature electrolytes and solids formation. The modeling tool reveals how the process performance changes with operating conditions and identifies the optimum conditions to operate the process, which is an NH₃ solvent concentration of about 26 wt% and an absorber temperature at about 35 F; however, note that lowering the absorber temperature below about 50 F requires special pre-heating to avoid fouling problems in the stripper. Finally, the modeling tool provides quantitative estimates of the utility needs of the process. The chilled-ammonia process is judged to be equivalent to alkanolamine-based absorption processes for LP steam consumption, but may be rendered noncompetitive because of the large refrigeration loads that are not needed in alkanolamine-based processes.

It should be noted that the analysis presented here does not address rate limitations that may limit successful achievement of the optimum operating conditions of the chilled-ammonia process. Hence, the results presented here are an optimistic estimate of the process performance.

The thermodynamic analysis provides a reliable way to anticipate operational issues. One indication of an operational problem is that optimization of the absorber temperature may result in a feed temperature of the rich solvent to the stripper that is sufficiently low to cause fouling problems in the stripper.

References

- Aaron, D., Tsouris, C., 2005. Separation of CO₂ from flue gas: a review. *Sep. Sci. Technol.* 40, 321–348.
- Bailey, D.W., Feron, P.H.M., 2005. Post-combustion decarbonization processes. *Oil Gas Sci. Technol.* 60, 461–474.
- Carson, J.K., Marsh, K.N., Mather, A.E., 2000. Enthalpy of solution of carbon dioxide in (water + monoethanolamine, or diethanolamine, or *N*-methyldiethanolamine) and (water + monoethanolamine + *N*-methyldiethanolamine) at $T = 298.15$ K. *J. Chem. Thermodyn.* 32, 1285–1296.
- Chapel, D.G., Maris, C.L., Ernest, J., 1999. Recovery of CO₂ from flue gases: commercial trends. In: Presented at Canadian Society of Chemical Engineers Annual Meeting, Saskatchewan, Canada, October 4–6.
- Chen, C.-C., Britt, H.I., Boston, J.F., Evans, L.B., 1982. Local composition model for excess Gibbs energy of electrolyte systems. Part I: single solvent, single completely dissociated electrolyte systems. *AIChE J.* 28, 588–596.
- Chen, C.-C., Mathias, P.M., 2002. Applied thermodynamics for process modeling. *AIChE J.* 48, 194–200.
- Ciferno, J.P., Fout, T.E., Jones, A.P., Murphy, J.T., 2009. Capturing carbon from existing coal-fired power plants. *Chem. Eng. Progress* 105, 33–41.
- Darde, V., Thomsen, K., van Well, W., Stenby, E., 2008. Chilled ammonia process for CO₂ capture. In: Presented at ICPWS XV, Berlin, September 8–11.
- Darde, V., Thomsen, K., van Well, W., Stenby, E., 2009. Chilled ammonia process for CO₂ capture. *Energy Procedia* 1, 1035–1042.
- DOE/NETL report, 2007. Chilled ammonia-based wet scrubbing for post-combustion CO₂ capture. DOE/NETL-401/02107, February.
- Gal, E., 2006. Ultra cleaning combustion gas including the removal of CO₂. World Intellectual Property, Patent WO 2006022885.
- Gal, E., Olson, S., 2006. Chilled ammonium process (CAP) for post combustion CO₂ capture. In: Presented at the 2nd Annual Carbon Capture and Transportation Working Group Workshop, Palo Alto, March 23.
- Göppert, U., Maurer, G., 1988. Vapor–liquid equilibria in aqueous solutions of ammonia and carbon dioxide at temperatures between 333 and 393 K and pressures up to 7 MPa. *Fluid Phase Equil.* 41, 153–185.
- Jänecke, Z., 1929a. Über das system H₂O, CO₂ und NH₃. *Z. Für Elektrochemie* 39, 332–334.
- Jänecke, Z., 1929b. Über das system H₂O, CO₂ und NH₃. *Z. Für Elektrochemie* 39, 716–728.
- Kurz, F., Rumpf, B., Maurer, G., 1995. Vapor–liquid–solid equilibria in the system NH₃–CO₂–H₂O from around 310–470 K: new experimental data and modeling. *Fluid Phase Equil.* 104, 261–275.
- Mather, A.E., 2008. Vapor–liquid equilibria in chemically reactive systems. In: Presented at the 20th International Conference on Chemical Thermodynamics, Warsaw, Poland, August 3–8.
- Mathias, P.M., 2005. Applied thermodynamics in chemical technology: current practice and future challenges. *Fluid Phase Equil.* 228–229C, 49–57.
- Mathias, P.M., Reddy, S., O'Connell, J.P., 2008. Quantitative evaluation of the chilled-ammonia process. The value of experimental vapor–liquid–solid data and fundamental thermodynamic analysis. In: Presented at the 7th Annual Carbon Capture & Sequestration Conference, Pittsburgh, PA, May 5–8.
- Mimura, T., Matsumoto, K., Iijima, M., Mitsuoka, S., 2000. Development and application of flue gas carbon dioxide recovery technology. In: Williams, D., et al. (Eds.), *Proceedings of the 5th International Conference on Greenhouse Gas Control Technologies*, CSIRO Publishing, Australia, pp. 138–144.
- O'Connell, J.P., Gani, R., Mathias, P.M., Maurer, G., Olson, J.D., Crafts, P., 2009. Properties in chemical process and product engineering: needs, challenges and perspectives. *Ind. Eng. Chem. Res.* 48, 4619–4637.
- Reddy, S., Gilmartin, J., 2008. Fluor's econamine FG PlusSM technology for post-combustion CO₂ capture. In: Presented at the GPA Gas Treatment Conference, Amsterdam, February 20–22.
- Resnik, K.P., Yeh, J.T., Pennline, H.W., 2004. Aqua ammonia process for simultaneous removal of CO₂, SO₂ and NO_x. *Int. J. Environ. Technol. Manage.* 4, 89–104.
- Rumpf, B., Weyrich, F., Maurer, G., 1998. Enthalpy changes upon partial evaporation of aqueous solutions containing ammonia and carbon dioxide. *Ind. Eng. Chem. Res.* 37, 2983–2995.
- Wen, N., Brooker, M.H., 1995. Ammonium carbonate, ammonium bicarbonate, and ammonium carbamate equilibria: a Raman study. *J. Phys. Chem.* 99, 359–368.
- Zhang, Y., Chen, H., Chen, C.-C., Plaza, J.M., Dugas, R., Rochelle, G.T., 2009. Rate-based process modeling study of CO₂ capture with aqueous monoethanolamine solution. *Ind. Eng. Chem. Res.* 48, 9233–9246.



Techno-economic evaluation of the evaporative gas turbine cycle with different CO₂ capture options

Yukun Hu^a, Hailong Li^{b,*}, Jinyue Yan^{a,b}

^a Royal Institute of Technology (KTH), Department of Chemical Engineering and Technology/Energy Processes, SE-100 44 Stockholm, Sweden

^b Mälardalen University, School of Sustainable Development of Society and Technology, SE-721 23 Västerås, Sweden

ARTICLE INFO

Article history:

Received 30 November 2010

Received in revised form 12 July 2011

Accepted 19 July 2011

Available online 23 August 2011

Keywords:

CO₂ capture

Evaporative gas turbines

Chemical absorption

Oxyfuel combustion

Cycle simulation

Economic evaluation

ABSTRACT

The techno-economic evaluation of the evaporative gas turbine (EvGT) cycle with two different CO₂ capture options has been carried out. Three studied systems include a reference system: the EvGT system without CO₂ capture (System I), the EvGT system with chemical absorption capture (System II), and the EvGT system with oxyfuel combustion capture (System III). The cycle simulation results show that the system with chemical absorption has a higher electrical efficiency (41.6% of NG LHV) and a lower efficiency penalty caused by CO₂ capture (10.5% of NG LHV) compared with the system with oxyfuel combustion capture. Based on a gas turbine of 13.78 MW, the estimated costs of electricity are 46.1 \$/MW h for System I, while 70.1 \$/MW h and 74.1 \$/MW h for Systems II and III, respectively. It shows that the cost of electricity increment of chemical absorption is 8.7% points lower than that of the option of oxyfuel combustion. In addition, the cost of CO₂ avoidance of System II which is 71.8 \$/tonne CO₂ is also lower than that of System III, which is 73.2 \$/tonne CO₂. The impacts of plant size have been analyzed as well. Results show that cost of CO₂ avoidance of System III may be less than that of System II when a plant size is larger than 60 MW.

© 2011 Elsevier Ltd. All rights reserved.

1. Introduction

Global warming is considered to be one of the most serious challenges that the world facing today and CO₂ is one of the most important greenhouse gases (GHGs). CO₂ capture and storage (CCS) has the potential to reduce overall mitigation costs and increase flexibility in achieving GHGs emission reductions [1]. In the meantime, natural gas (NG) becomes the second largest energy source accounting for 41% of the total generated electricity respectively [2], surpassing hydropower (20%). According to the Energy Information Administration (EIA) of US, natural gas fired electricity generation is expected to rise further in the next 20 years [3]. Therefore, it is of significance to develop more efficient natural gas based power plants with CO₂ capture facility. However, most of efforts have been focused on the combined cycle (CC) integrated with different CO₂ capture options [4–6].

Evaporative gas turbine (EvGT), which is also called humid air turbine (HAT), is one of the advanced gas turbine cycles [7]. The basic idea of the EvGT cycle is injecting water by evaporation to increase the mass flow rate through the turbine and consequently augment the specific power output. The driving forces for gas turbine humidification have been the potentials of high electrical

efficiency and specific power output, reduced specific investment costs, decreased formation of nitrogen oxides (NO_x) in the combustor, reduced power output degradation caused by high ambient temperatures or low ambient pressure (i.e., at high elevations) and improved part-load performance compared with combined cycle (CC) [8]. Comparing with the CC, the electrical efficiency for an EvGT cycle is fairly close to the efficiency of the CC with the equivalent power output, while the investment costs should be lower since the cost for a steam bottoming cycle is avoided [9–11]. In addition, compared with another kind of humidified gas turbine cycle, steam injection gas turbine cycle (STIG), the EvGT has lower irreversibility. This is due to that water is injected into the cycle by a humidification tower, which has a small temperature difference between the hot and cold fluids. Many studies on EvGT or HAT cycles have been conducted concerning cycle innovations [12–16], water recovery [17–19], humidification process [20–25], and properties of humid air, etc. [26–30]. In this paper, the techno-economic performance is studied when EvGT is integrated with CO₂ capture.

There are two potential CO₂ capture options for power plant retrofit. One is commercialized amine-based chemical absorption. Such a process takes advantage of CO₂ chemical absorption, an acid base neutralization reaction, which enhances absorption rates and hence can be used for exhaust gases with relatively low CO₂ partial pressure (down to 3 kPa) [31]. However, when the CO₂ concentration is low, CO₂ capture becomes less efficient and costs rise. For

* Corresponding author.

E-mail addresses: yukunhu@kth.se (Y. Hu), lihailong@gmail.com (H. Li), yanjy@kth.se (J. Yan).

Nomenclature

<i>C</i>	constant, (dimensionless)
<i>D</i>	column diameter, m
<i>T</i>	temperature, °C
<i>Y</i>	operating life, year

Abbreviations

AIC	amortized investment costs
ASU	air separation unit
BMC	bare module costs
CC	combined cycle
CCS	CO ₂ capture and storage
CEPCI	chemical engineering plant cost index
CF	capacity factor
COA	cost of CO ₂ avoidance
COE	cost of electricity
EIA	Energy Information Administration
EvGT	evaporative gas turbine
FC	fuel cost
FCF	fixed charge factor

FOB	free on board
FOM	fixed operating and maintenance costs
GHGs	greenhouse gases
HAT	humid air turbine
HPC	high pressure column
IR	interest rate
LHV	lower heating value
LPC	low pressure column
LTD	logarithmic temperature difference
MEA	mono ethanol amine
N/A	no applicable
NG	natural gas
PG	power generation
SIC	specific investment costs
STIG	steam injection gas turbines
TEG	triethylene glycol
TIC	total investment costs
TIT	turbine inlet temperature
VOM	variable operating and maintenance costs
WAR	Water/Air ratio

example, it is more challenging to capture CO₂ from natural gas based power generation, which CO₂ in exhaust gas is less than 4 mol%. The main disadvantages of chemical absorption are associated with two aspects: the high-energy consumption to regenerate the solvent and extract CO₂ and the technical issues on corrosion and solvent degradation. The other one is oxyfuel combustion capture. Oxyfuel combustion takes place in a nitrogen-avoided environment. As a result, the exhaust gases mainly consist of CO₂ and water vapor. Therefore, CO₂ can be easily separated by condensation, which can achieve a CO₂ concentration of 95 vol.% or higher [32].

Our previous work focused on characterizing and understanding the features of the integration of the EvGT with CO₂ capture [33]. Many effects were also put on key parameter optimizations [34,35]. The objectives of this work are to evaluate the techno-economic performances of the EvGT combined with CO₂ capture.

2. Methodology

Based on a gas turbine, LM1600PD, which has a capacity of 13.78 MW, manufactured by GE Energy Aero-derivative [36], three EvGT systems, including a reference system without CO₂ capture and two systems combined with chemical absorption and oxyfuel combustion respectively, were set up. The cycle performance was studied by simulating those systems with the simulation tool, Aspen Plus, which calculates the mass and energy balance. The simulation results can further be used to calculate the electricity generation and to identify the capacity of equipment. It shall be noted that the economic analysis in this study is only based on CO₂ capture and CO₂ compression, and the costs associated with transport and storage are excluded according to IPCC special report [1].

CAPCOST [37] is used to estimate the bare module costs (BMC). Based on the results, the key economic parameters, like total investment costs (TIC), operating & maintenance costs (O&M), and cost of electricity (COE) are estimated. The cost of CO₂ avoidance (COA) is evaluated by referring to the reference system. By doing breakdown analysis, the potential to reduce COA is further investigated.

Moreover, the six-tenths-rule [37] is used to scale up/down to a new capacity when investigating the impacts of plant size. If the

cost for a piece of equipment is known for an earlier year, chemical engineering plant cost index (CEPCI) is used to account for the inflation. For such a kind of 'preliminary and study estimation', results provide an accuracy in the range of +40% to −25% [37].

3. The description of processes

3.1. EvGT system without CO₂ capture (reference system, System I)

A sketch of the EvGT system [33] is shown in Fig. 1. Water is heated close to saturated conditions by the compressed air in the aftercooler and exhaust gas in the feedwater heater and the economizer. The heated water enters at the top of a humidification tower and is brought into counter-current contact with the compressed air that enters at the bottom of the tower, which is a column with a packing that is either structured or dumped. Some water is evaporated and the air is humidified. The water evaporates at the water boiling point corresponding to the partial pressure of water in the mixture, i.e., water evaporates below the boiling point corresponds to the total pressure in the tower. Therefore, low temperature heat, which cannot be used to evaporate water in a boiler, can be recovered in an EvGT cycle. Since the water vapor content in the air increases as the air passes upward through the tower, the evaporation temperature also increases. This ensures a close matching of the air and water temperature profiles and small exergy losses compared to evaporation in a conventional steam boiler. The EvGT system has a high efficiency, because the waste heat from the gas turbine exhaust gas can be recovered efficiently through the humidification of compressed air in the humidification tower, the economizer and/or the recuperator.

3.2. EvGT with chemical absorption system (System II)

A sketch of the EvGT system with chemical absorption capture [34] is shown in Fig. 2. Different from the System I, instead of being condensed in the feedwater heater, a part of exhaust gases enters the reboiler of the mono ethanol amine (MEA) stripper to support the heat required for MEA regeneration; after it goes through the recuperator. Two streams of exhaust gases mix again in the exhaust gas condenser 1. Then it is sent into the absorption column

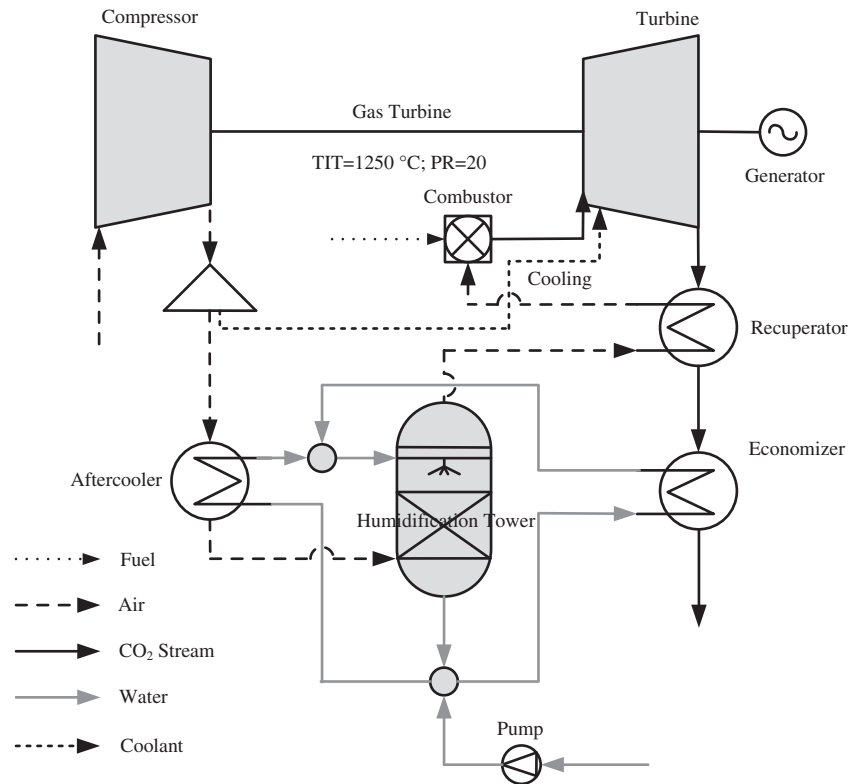


Fig. 1. A sketch of the EvGT system without CO₂ capture.

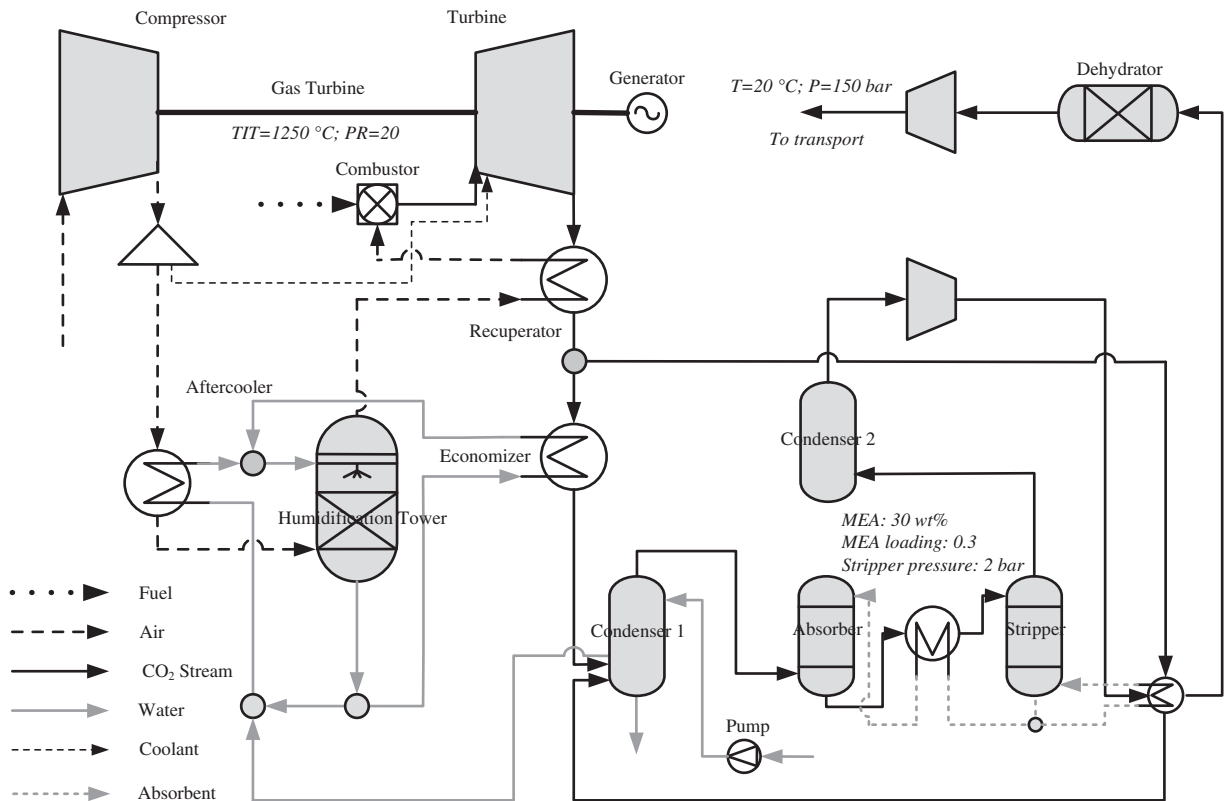


Fig. 2. A sketch of the EvGT system with chemical absorption capture.

where CO₂ is captured. The rich solvent containing chemically bounded CO₂ is stripped at an elevated temperature in the stripper.

Finally, after compression and dehydration, the recovered CO₂ is transported to the storage reservoir. The main penalty caused by

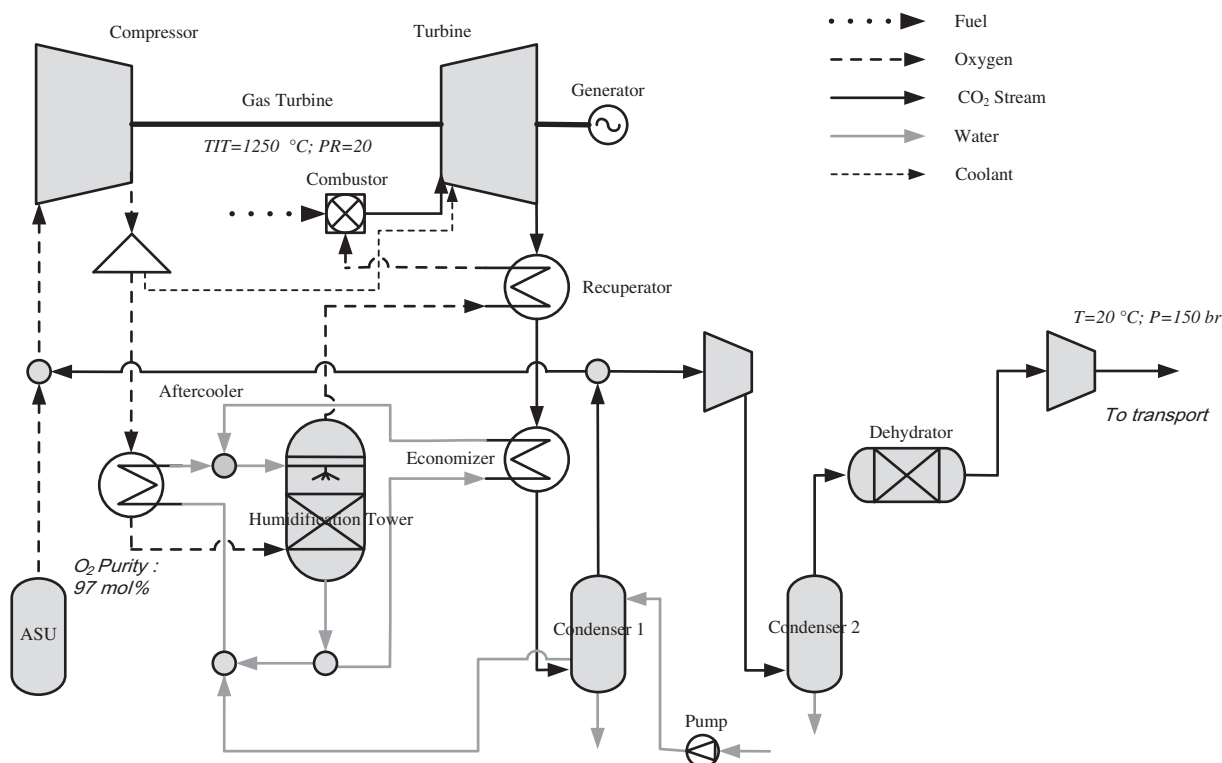


Fig. 3. A sketch of the EvGT system with oxyfuel combustion capture.

CO₂ capture in this system results from the energy requirement of stripper reboiler.

3.3. EvGT with oxyfuel combustion system (System III)

A sketch of the EvGT system combined with oxyfuel combustion capture [35] is shown in Fig. 3. Since exhaust gases consist of mainly H₂O and CO₂, a simplified exhaust gas processing procedure can be used instead of chemical absorption, which is important to achieve a low cost CO₂ capture. However, in the oxyfuel combustion, the removal of nitrogen may cause extremely high flame temperature and decrease the mass flow rate through the gas turbine. In order to control the flame temperature and compensate the reduced volumetric flow, a large fraction of exhaust gases is compressed and recycled back to the system after condensation. The main penalty caused by CO₂ capture in this system results from the power consumption of generating pure oxygen by cryogenic air separation unit (ASU).

4. System simulation results

In order to achieve high efficiencies some operating parameters have been optimized for each system. It has been found that EvGT systems with constant combustion air temperature have an optimum Water/Air ratio (WAR) [38]. The optimized WAR is 14% [34], 11.5% [34] and 13.3% [35] for Systems I–III, respectively. For System II, there exists an optimized exhaust gas condensing temperature regarding the overall electrical efficiency. On one hand, the water contained in the exhaust gas would dilute MEA solvent and result in a higher reboiler duty in the chemical absorption process. In order to remove more water, a lower condensing temperature should be applied in the condenser before absorption column. But on the other hand, a lower condensing temperature will cause a lower temperature of the stream going into the

stripper as well. As the stripping temperature is determined in the stripper, more energy will be required by the reboiler to heat up the stream with a lower temperature. Under the conditions shown in Fig. 2, the optimized condensing temperature is 50 °C [34]. For System III, the variation of oxygen purity will affect the energy consumption of ASU process. Although generating lower purity oxygen could reduce energy consumption, it might introduce more impurities into the system, resulting in an increased energy consumption of CO₂ liquefaction process. According to [35], the oxygen purity applied in this paper is 97%.

Table 1 summarizes the key input parameters and some important cycle simulation results. The electrical efficiency of the EvGT without CO₂ capture (System I) is comparable to that of a combined cycle; but when CO₂ capture is included, the efficiency penalty caused by CO₂ capture of EvGT with chemical absorption and oxyfuel combustion are larger than those of the combined cycle integrated with the same CO₂ capture options. For the option of chemical absorption, the penalties are 10.5% and 8.8% [6] of NG LHV for the EvGT and CC respectively, while 11.8% and 9.7% [6] of NG LHV for the option of oxyfuel combustion. For System II, according to Li et al. [39], air humidification can increase CO₂ concentration in exhaust gas, which will favor the chemical absorption process and reduce the specific duty of reboiler. However, a more negative impact on efficiency is that using exhaust gas to support the heat demand of stripper causes a very large temperature difference in the reboiler and a significantly decreased amount of evaporated water, which reduce the efficiency of the EvGT sharply. As a result, System II has a higher efficiency penalty caused by CO₂ capture than CC. For System III, the larger efficiency penalty compared to CC comes from that high temperature exhaust gas cannot be efficiently used in the humidification tower due to the large temperature difference of heat transfer. In addition, compared with System II, System III has a lower electrical efficiency, but a higher CO₂ capture ratio and therefore, a less CO₂ emission rate.

Table 1
Summary of system simulation results.

	System I	System II	System III
<i>Key input parameters</i>			
Turbine inlet temperature (TIT), °C	1250	1250	1250
<i>Pressure ratio</i>			
Exhaust gas condenser temperature, °C	40	50 [34]	30
WAR ^a , %	14 [34]	11.5 [34]	13.3 [35]
O ₂ purity of ASU, mol%	N/A	N/A	97 [35]
CO ₂ capture ratio, %	N/A	90	99.9
<i>Results</i>			
Power consumption of ASU, kJ/kg O ₂	N/A	N/A	897 [35]
Stripper reboiler duty, MJ/kg CO ₂	N/A	4.0	N/A
CO ₂ % in exhaust gas, mol%	3.2	4.3	89
CO ₂ % to be transported, mol%	N/A	99.9	93.0
CO ₂ emission rate, tonne/MWh	0.38	0.048	Trace
<i>Power output and consumption (in% of fuel LHV)</i>			
Net power output	52.1	41.6	40.3
Power consumption of ASU	N/A	N/A	7.6
Reboiler duty of stripper	N/A	19.9	N/A
CO ₂ compression work	N/A	2.57	2.48

^a Replaced by O₂/CO₂ mixture in System III.

5. Economic evaluation

5.1. Calculation equations

The amortized investment costs (AIC), fixed charge factor (FCF), cost of electricity (COE), and cost of CO₂ avoidance (COA) for a power plant can be calculated by the following equations:

$$AIC = \frac{TIC \times IR \times (1 + IR)^Y}{(1 + IR)^Y - 1}, (\$/\text{year}) \quad (1)$$

$$FCF = IR / [1 - (1 + IR)^{-Y}] \quad (2)$$

$$COE = \frac{TIC \times FCF + FOM}{CF \times PG} + \frac{VOM}{PG} + \frac{FC}{PG}, (\$/\text{MWh}) \quad (3)$$

$$COA = \frac{(COE)_{\text{capture}} - (COE)_{\text{ref}}}{CO_{2,\text{ref}}/\text{kWh} - CO_{2,\text{capture}}/\text{kWh}}, (\$/\text{tonne CO}_2) \quad (4)$$

where TIC is the total investment costs (\$), IR the interest rate (%), Y the operating life (year), FCF the fixed charge factor (fraction/year), FOM the fixed operating costs (\$/year), VOM the variable operating costs (\$/year), FC the fuel cost (\$/year), CF the capacity factor (%), PG is the power generation (MWh/year). Strictly speaking, a cost of CO₂ avoidance should cover a complete CCS system including transport and storage costs, but Eq. (4) is applied only to the capture portion of a full CCS system in this paper.

5.2. Assumptions

Investment costs consist of three main components: power plant cost, capture plant cost, and CO₂ compression cost. They can further be divided into two parts: direct costs and indirect costs. Direct costs, also called bare module costs (BMC), include equipment free on board (FOB) costs, materials required for installation and labor to install equipment and material, etc. Indirect costs include some fees as listed in Table 2. The operation and maintenance costs consist of fixed and variable values. Variable operating and maintenance costs (VOM) are chemical costs and process water, while fixed operating and maintenance costs (FOM) are a function of total investment costs (TIC). The assumptions made in the cost calculation are also listed in Table 2.

5.3. Results and discussions

5.3.1. Base cases

In general, all of the systems can be divided into three subsystems: power plant, capture plant, and CO₂ compression plant. For System II and System III, MEA scrubbing process and air separation process are considered as capture plants. As to dehydration process, it is included in CO₂ compression plant. The capacities of different modules are from system simulation results. Table 3 lists the investment costs of three systems and Table 4 summarizes the direct costs of each subsystem.

Compared with System I, the increments in total investment costs caused by CO₂ capture are significant, which are about 42% for System II and 54% for System III.

For power plant subsystem, heat recovery facilities are the main difference amongst those three systems. In Systems I and III, most of the heat contained in exhaust gases is recovered through a recuperator to heat the humidified air or CO₂/O₂ from the humidification tower; while in System II, a considerable amount of heat of exhaust gases is used to support the thermal energy demand of the stripper reboiler. Therefore, Systems I and III have higher heat transfer duties than System II in the recuperator. As a result, they require larger heat transfer areas. In addition, compared with System I, System III has a higher turbine outlet temperature and a much higher outlet temperature of the recuperator. It implies System III has a much higher temperature difference of heat transfer. Consequently, System III has a smaller heat transfer area than System I. Some results are shown in Table 5.

For capture plant subsystem, ASU costs are higher than that of the chemical absorption plant. As shown in Table 6, for an air separation plant, air compressors are the major modules, and account for 45% of total direct costs of ASU. While for a chemical absorption plant, the columns are the major modules which account for 44% of total direct costs.

For CO₂ compression plant subsystem, the slight difference comes from the cost of CO₂ compressors. It is mainly caused by the different mass flow of captured CO₂.

After the direct and indirect costs were obtained, the annual costs could be calculated by amortizing the total investment costs to represent an annual payment. The annual costs were divided into four criteria for each system as shown in Table 7. It is clear that System III has a little higher total annual costs than System II, which are much higher than System I due to the efficiency penalty and additional equipment for CO₂ capture. Meanwhile, compared with System II, although System III has a higher amortized investment costs, it has lower VOM costs because the costs for absorbents (MEA) are not required.

Costs of electricity of three systems are shown in Fig. 4. Compared with System I, the increments of COE caused by CO₂ capture are about 24.0 \$/MWh for System II and 28.0 \$/MWh for System III. Fuel cost represents the largest fraction of COE in all systems, especially in the system without CO₂ capture (System I). Total investment costs are the second largest component of COE. The sum of fuel cost and investment costs represents about 90% of the total in all systems. For the systems with CO₂ capture (System II and System III), the main cost differences are TIC and VOM. Comparatively, COE of System II is 5.4% lower than that of System III because of the higher electrical efficiency of System II.

Fig. 5 shows the breakdown of the cost of CO₂ avoidance. Similar to the results about COE, System II has a lower COA than System III. The major components of COA for both systems come from the total investment costs and fuel cost. They are corresponding to the large investment cost of capture plants and the large electrical efficiency penalty caused by CO₂ capture.

Table 2
Assumptions made in the cost calculation.

Parameter	Unit	Value
<i>Direct costs</i>		
Bare module costs		Calculated by CAPCOST [37]
<i>Indirect costs</i>		
Specific services (local)	% BMC	1 [11]
Confidence limit	% BMC	2 [11]
Fees in addition to contractors' fee	% BMC	2 [11]
Contractors' fee	% BMC	3 [11]
Land purchase, surveys, site preparations	% BMC	5 [11]
Contingency	% BMC	10 [11]
<i>Assumption for COE</i>		
Annual interest rate	%	8
Economic life	years	20
Natural gas price	\$/MBtu	4.19 [40]
Fix operating and maintenance costs	% TIC	2 [11]
Annual full load hours	h/year	7500
<i>Other assumptions</i>		
MEA price	\$/kg	1.5 [41]
MEA degradation rate	kg/tonne CO ₂	1.6 [42]
TEG price	\$/kg	1 [43]
Make-up water	\$/tonne	0.09 [37]
Cooling water	\$/m ³	0.02 [37]

Table 4
Summary of total direct costs (k\$).

Subsystem	System I	System II	System III
Power plant	11,000	10,078	10,571
Capture plant	N/A	2758	3561
CO ₂ compression plant	N/A	2825	2813
Total direct costs	11,000	15,661	16,945

Table 5
Recuperator specifications.

	System I	System II	System III
$T_{\text{hot,in}}$, °C	588	587	731
$T_{\text{hot,out}}$, °C	202	343	334
$T_{\text{cold,in}}$, °C	138	132	149
$T_{\text{cold,out}}$, °C	558	410	600
Logarithmic temperature difference (LTD ^a), °C	45	194	156
Heat duty, MW	13.27	7.23	14.68
Heat transfer coefficient, kW/m ² C	0.4	0.4	0.4
Heat transfer areas, m ²	739	93	235

$$^a \text{LTD} = \frac{(T_{\text{hot,in}} - T_{\text{cold,out}}) - (T_{\text{hot,out}} - T_{\text{cold,in}})}{\ln \left(\frac{T_{\text{hot,in}} - T_{\text{cold,out}}}{T_{\text{hot,out}} - T_{\text{cold,in}}} \right)}$$

Table 3
Investment costs of three systems (k\$).

Module	System I		System II		System III	
	Capacity	Direct Cost	Capacity	Direct Cost	Capacity	Direct Cost
<i>Power plant</i>						
Gas turbine	13.78 MW	7000	13.78 MW	7000	13.78 MW	7000
Intercooler	3750 kW	383	3263 kW	362	4566 kW	424
Aftercooler	3693 kW	328	3217 kW	318	1825 kW	278
Recuperator	13,267 kW	1571	7228 kW	461	14,642 kW	741
Economizer	3424 kW	212	1592 kW	204	7699 kW	223
Water pump	9 kW	29	6.5 kW	25	8.2 kW	28
Humidification tower		1477		1477		1477
Flue gas condenser			5903 kW	231	11,503 kW	400
<i>Capture plant (MEA scrubbing process)</i>						
Flue gas blower			269 kW	78		
CO ₂ absorber			$D = 3 \text{ m}; H = 15 \text{ m}$	924		
Sorbent stripper			$D = 1.38 \text{ m}; H = 10 \text{ m}$	277		
Pump			6 kW	25		
Lean/rich stream heat exchanger			5017 kW	242		
Stripper reboiler			5282 kW	482		
Stripper condenser			2583 kW	178		
Facilities ^a				552		
<i>Capture plant (Air separation process)</i>						
Air compressors					1972 kW	1602
Air condenser					550 kW	157
Low pressure column					$D = 1.5 \text{ m}; H = 20 \text{ m}$	605
High pressure column					$D = 1.5 \text{ m}; H = 12 \text{ m}$	402
Multistream heat exchangers					1063 kW	83
Facilities ^b						712
<i>CO₂ compression plant</i>						
Dehydration column			$D = 0.7 \text{ m}; H = 3 \text{ m}$	77	$D = 0.7 \text{ m}; H = 3 \text{ m}$	77
Regeneration column			$D = 0.7 \text{ m}; H = 3 \text{ m}$	55	$D = 0.7 \text{ m}; H = 3 \text{ m}$	55
Regeneration column reboiler			26 kW	171	26 kW	174
Dehydration condenser			645 kW	161	642 kW	164
CO ₂ compressors			663 kW	2170	664 kW	2142
CO ₂ condenser			335 kW	136	254 kW	136
CO ₂ pump			14 kW	55	21 kW	65
Total direct costs		11,000		15,661		16,945
Total indirect costs		2530		3602		3897
Total investment costs		13,530		19,263		20,842

^a Facilities includes circulation pump, sorbent processing, sorbent reclaiming etc. It accounts for 20% of total direct costs of chemical absorption process.

^b Facilities includes filter, intercooler of air compressors, condenser/reboiler heat exchanger etc. It accounts for 20% of total direct costs of air separation process.

Table 6

Summary of key modules in capture plants.

Device type	System II		System III	
	Devices	Direct costs, k\$	Devices	Direct costs, k\$
Pressure changers	Flue gas blower	78	Air compressors	1602
Columns	Absorber, Stripper	1201	HPC, LPC	1007

Table 7

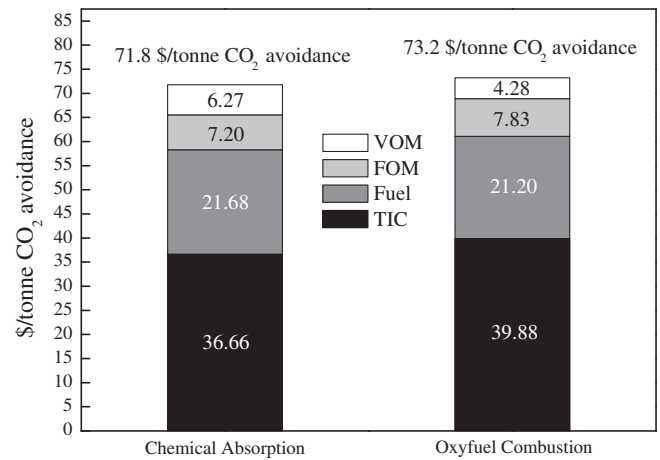
Comparison of annual costs of three systems (k\$/year).

	System I	System II	System III
AIC	1378	1962	2123
Fuel	2853	2853	2853
FOM	271	385	417
VOM	8	178	137
Total annual costs	4510	5378	5530

5.3.2. Effects of plant size

The direct costs are estimated regarding different sizes of the EvGT power plant based on the cost of base case. The results are plotted in Fig. 6. Meanwhile, the prices of the simple cycle and the combined cycle without CO₂ capture [44] and some data about the EvGT without CO₂ capture are also displayed in Fig. 6. All of the numbers published in different years have been revised by considering CEPCI. For the EvGT system without CO₂ capture (System I), the direct costs locate between simple cycle and combined cycle. These results are similar with our previous work [11]. For the EvGT systems with CO₂ capture, the direct costs of System III are a little more expensive than those of System II. In addition, the direct costs of the EvGT system with both capture options are lower than the combined cycle prices without CO₂ capture as plant size is larger than 300 MW. The major reason is due to the absence of the bottoming cycle. For example, for an EvGT cycle of 300 MW, the cost of gas turbine cycle is around 66,000 k\$ and the cost of humidification tower is around 9500 k\$. However, for a combined cycle in the same size, the bottoming cycle may cost approximately half of the direct cost [45], which means about 85,000 k\$.

The influence of plant size on COE is shown in Fig. 7. The COE drops sharply when the plant size is increased from 13.78 to 100 MW for all of the studied three systems. Meanwhile, System III always has a slight higher COE than System II. Comparing with System I, the increments of COE caused by CO₂ capture are about 14 \$/MW h and 16 \$/MW h for System II and III respectively, which do not vary much along with the increase of plant size. In addition,

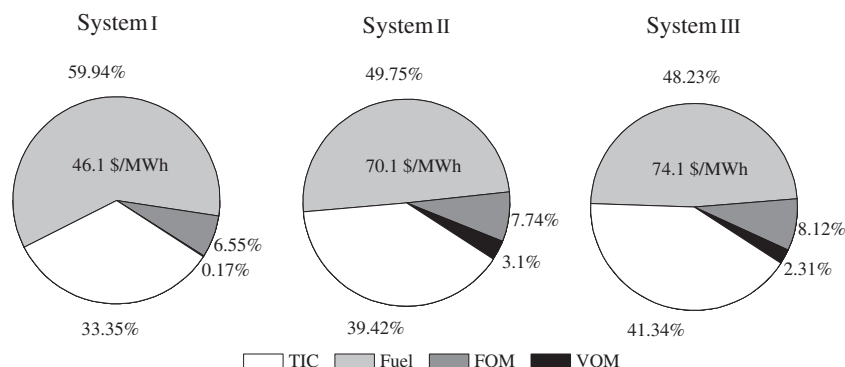
**Fig. 5.** Breakdown of the cost of CO₂ avoidance.

some data about COE from references are shown in Fig. 7 as well. The results of this work agree with them quite well.

The influence of plant size on COA is shown in Fig. 8. The variation of COA along with the increase of plant size is quite similar to that of COE. However, in contrast with COE, the COA of System III becomes less than that of System II as plant size is larger than 60 MW. This can be explained as that the proportion of TIC and FOM in the COA of System III is more than that in the COA of System II, as shown in Fig. 5. Consequently, System III is more sensitive to plant size than System II.

5.3.3. Comparison of results (400 MW gross power output) with others studies

There are some studies evaluating the cost of natural gas combined cycle (NGCC) plants with CO₂ capture [47,50]. Table 8 compares the results from references and the results presented in this paper. First of all, the specific investment costs (SIC) of the system with chemical absorption capture in both studies are less expensive than those with oxyfuel combustion capture, which is consistent with other results from Simbeck [51] and Singh et al. [42]. In addition, the SIC of the EvGT system is significantly lower than the NGCC system for integrated with the same CO₂ capture technique because no bottoming cycle is involved. As a result, the EvGT systems have lower COE than the NGCC system when integrated with the same CO₂ capture technology, even though the NGCC system has a higher electrical efficiency. Moreover, this study concludes that at big plant size, the cost of CO₂ avoidance of the system with chemical absorption capture is more expensive than that of the system with oxyfuel combustion capture. This is also consistent

**Fig. 4.** Composition diagram of COE for three systems.

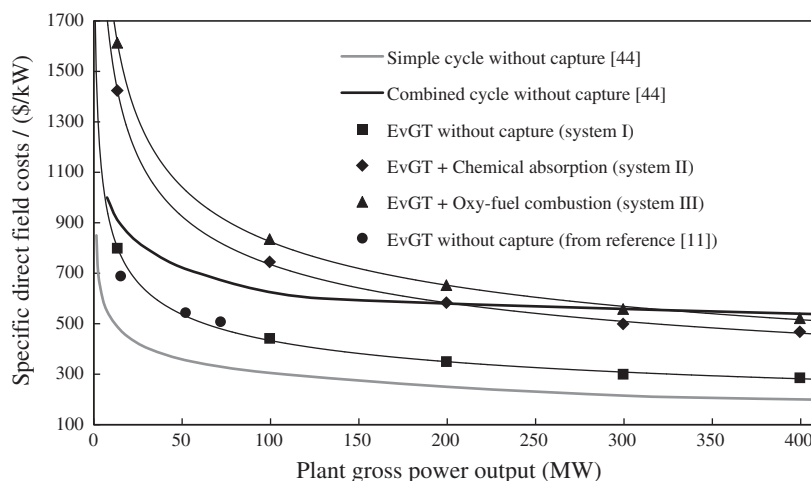


Fig. 6. Effects of plant size on direct costs in \$/kW price.

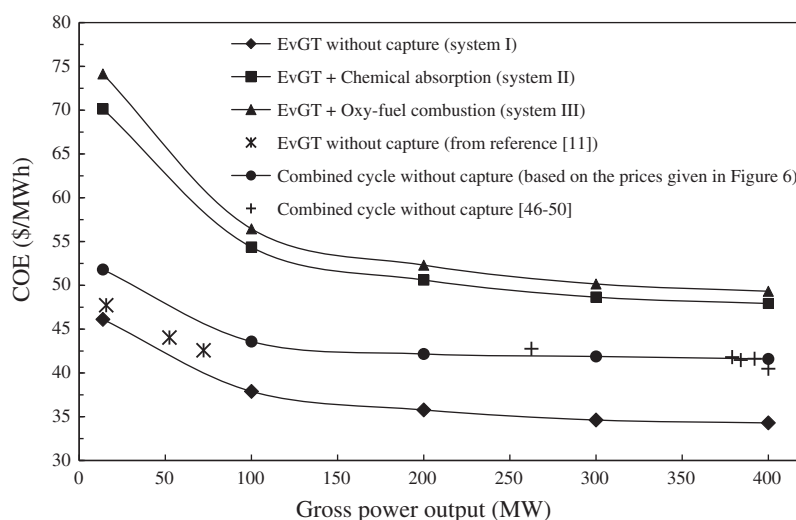


Fig. 7. Effects of plant size on cost of electricity. (See above-mentioned references for further information.)

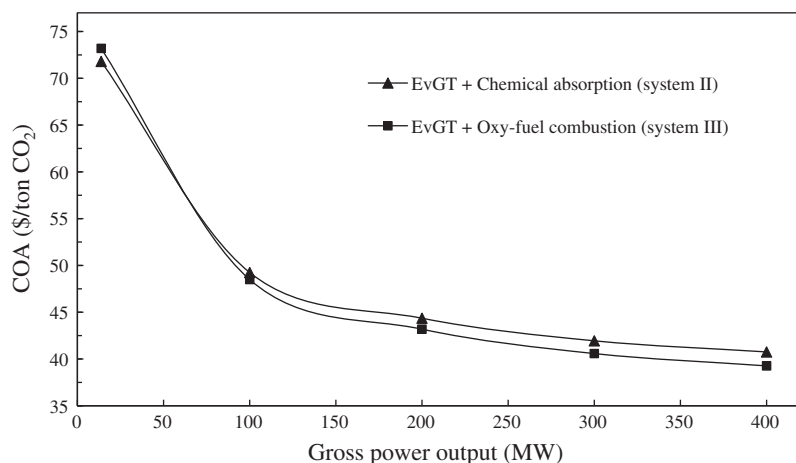


Fig. 8. Effects of plant size on cost of CO₂ avoidance.

to the results from Simbeck [51] and Singh et al. [42], but inverse to the NGCC cases listed in Table 8. Further studies are required to find out the problems.

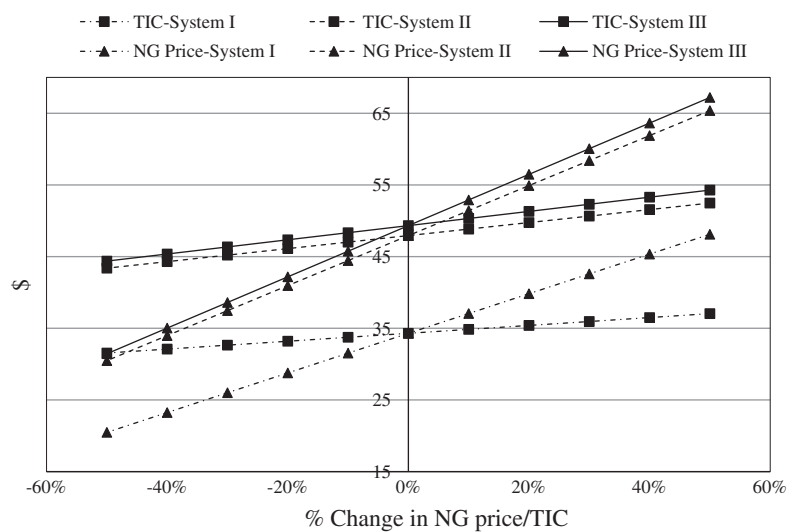
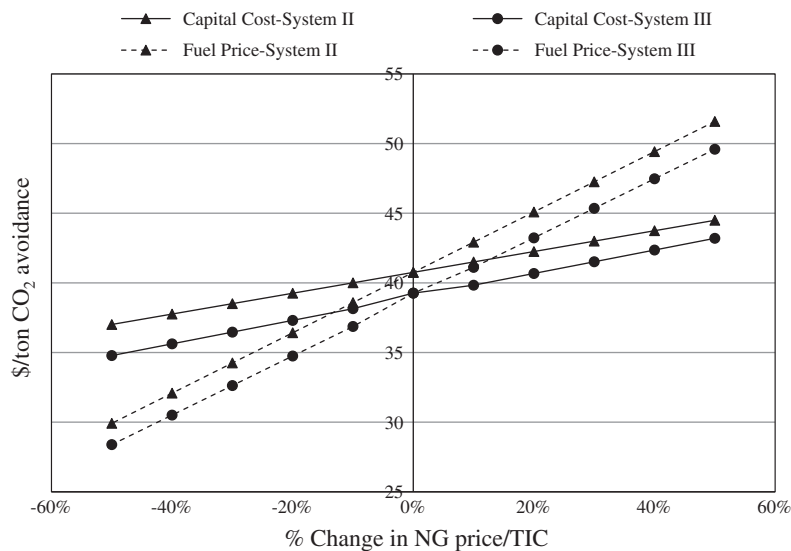
5.3.4. Sensitivity analysis

The sensitivity analyses were carried out for the plants size of 400 MW gross power output to identify the effects of natural gas

Table 8

Comparison on system parameters and economic parameters of different systems.

	Chemical absorption		Oxyfuel combustion	
	EvGT This study	NGCC NETL [47]	EvGT This study	NGCC Dillon et al. [50]
Plant capacity factor, %	87	85	87	85
Fuel price, LHV (\$/GJ)	4.42	3.55	4.42	3.00
<i>Reference plant without CO₂ capture</i>				
Plant net size, MW	400	379	400	388
Electrical efficiency, %	52.1	57.9	52.1	56
COE, \$/MWh	34.3	34.7	34.3	33.5
<i>Plant with CO₂ capture</i>				
Plant net size, MW	317	327	309	440
Electrical efficiency, %	41.6	49.9	40.3	44.7
SIC, \$/kW	575	911	642	1034
COE, \$/MWh	47.9	48.3	49.3	50.3
COA, \$/tonne CO ₂	41	45	39	47

**Fig. 9.** Sensitivity of cost of electricity to natural gas price and total investment costs.**Fig. 10.** Sensitivity of cost of CO₂ avoidance to natural gas price and total investment costs.

price, total investment costs, reboiler duty of stripper and energy consumption of ASU.

5.3.4.1. Effects of natural gas (NG) prices and total investment costs. Figs. 9 and 10 show the sensitivity study results about COE

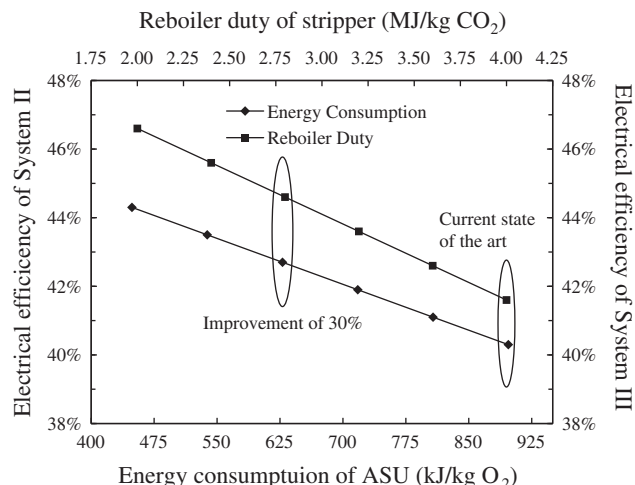


Fig. 11. Sensitivity of electrical efficiency to the specific reboiler duty of stripper and energy consumption of ASU.

and COA at different natural gas prices and total investment costs. The horizontal axis represents the change of the economic variable for natural gas price and TIC estimates in percentage. Regarding the variations ($\pm 50\%$) of TIC and fuel price respectively, for the EvGT system without CO₂ capture (System I), COE varies $\pm 8\%$ and $\pm 40\%$; for the EvGT system combined with chemical absorption (System II), COE varies $\pm 9\%$ and $\pm 36\%$ while COA varies $\pm 9\%$ and $\pm 27\%$; for the EvGT system combined with oxyfuel combustion (System III), COE varies $\pm 10\%$ and $\pm 36\%$ while COA varies $\pm 11\%$ and $\pm 27\%$. It can be easily found that both of COE and COA are more sensitive to the fuel price than to the total investment costs for all of systems.

5.3.4.2. Reboiler duty of stripper and energy consumption of ASU. As discussed above, the efficiency penalties caused by CO₂ capture are the high thermal energy demand of stripper reboiler in System II and the high energy consumption of air separation unit in System III. If some technology breakthroughs could be achieved to reduce those energy consumptions, the performances of systems with CO₂ capture could be improved. It can further decline the cost of elec-

tricity and the cost of CO₂ avoidance. Fig. 11 shows the variation of electrical efficiencies of System II and III along with the change of energy consumptions of specific reboiler duty and ASU. For the current state of the art, the specific reboiler duty is 4.0 MJ/kg CO₂ under conditions as MEA: 30 wt.%; Lean loading: 0.3 [39]; Stripper pressure: 2 bar; and the energy consumption of ASU is 897 kJ/kg O₂ with a purity of 97 mol%). But both of them could be improved as much as 30% [50,52], which implies the specific reboiler duty and energy consumption could be reduced to 2.8 MJ/kg CO₂ and 628 kJ/kg O₂ respectively. As a result, the electrical efficiency of System II is improved by 7.2% and the one of System III is improved by 6.0%.

The variations of COE and COA of System II and III along with the change of energy consumptions of specific reboiler duty and ASU were displayed in Fig. 12. It is clear that COE of both systems reduce parallel, which means the energy consumption of specific reboiler duty influences COE of System II in the same degree as the energy consumption of ASU influences COE of System III. However, comparatively the impact of energy consumptions of specific reboiler duty on COA of System II is more significant than that of energy consumption of ASU on COA of system III.

6. Conclusions

The techno-economic evaluation of the evaporative gas turbine (EvGT) system combined with two CO₂ capture options has been carried out. By compared with a reference system: the EvGT system without CO₂ capture (System I), the electrical efficiency, energy penalty due to the CO₂ capture, and costs of electricity and CO₂ avoidance have been evaluated for the EvGT system with chemical absorption capture (System II), and the EvGT system with oxyfuel combustion capture (System III). Based on the results, it is concluded that:

- (1) The electrical efficiencies of the EvGT integrated with mono ethanol amine (MEA)-based chemical absorption and oxyfuel combustion can reach 41.6% and 40.3% of NG LHV respectively. Compared with the EvGT cycle without CO₂ capture, the efficiency penalties caused by CO₂ capture are 10.5% and 11.8%, respectively.
- (2) Based on the prototype gas turbine, LM1600PD, which has a gross power output of 13.78 MW, the total investment costs

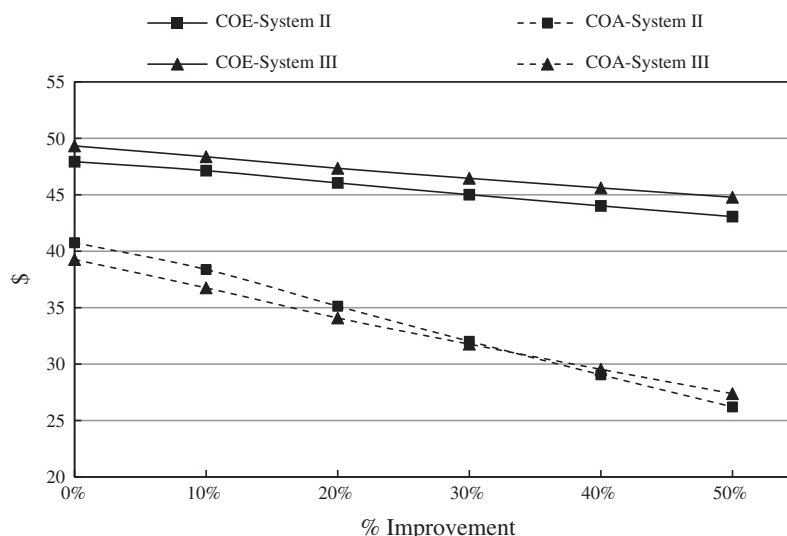


Fig. 12. Sensitivity of COE and COA to improvements of the specific reboiler duty of stripper and energy consumption of ASU.

(TIC) were estimated for all of three systems. Compared with the system without CO₂ capture, the total investment cost increments caused by CO₂ capture are 42% and 54% for the options of chemical absorption and oxyfuel combustion respectively. The increases of TIC will further cause the increases of cost of electricity (COE), which are 52.0% for System II and 60.7% for System III. Correspondingly, the costs of CO₂ avoidance (CoA) are 71.8 \$/MWh and 73.2 \$/MWh for Systems II, and III.

- (3) The direct costs of the EvGT locate between simple cycle prices and combined cycle prices; and the direct costs of System III are a little higher than the direct costs of System II. Compared with the direct costs of a combined cycle, the direct costs of the EvGT system integrated with CO₂ capture are still lower as long as the plant size is larger than 300 MW. The major reason is due to the absence of the bottoming cycle.
- (4) Compared with others studies about the natural gas combined cycle (NGCC), the EvGT system has lower COE and COA than the NGCC system no matter which CO₂ capture technology is integrated.
- (5) Sensitivity study results about COE and COA show that both of them are more sensitive to the natural gas price than total investment costs for all of the studied systems. And comparatively the impact of energy consumptions of specific reboiler duty on COA of System II is more significant than that of energy consumption of air separation unit on COA of System III. Moreover, as plant size is larger than 60 MW, even though System II has a lower COE than System III because of the higher electrical efficiency of System II, System III has a lower COA than System II, which is due to the higher CO₂ capture ratio of System III.

Acknowledgements

The financial supports by China Scholarship Council (CSC) and Royal Institute of Technology (KTH), Sweden are appreciated.

References

- [1] IPCC special report on carbon dioxide capture and storage. Cambridge, United Kingdom and New York, NY, USA: Cambridge University Press; 2005. 442 pp.
- [2] Key World Energy Statistics. Paris: OECD/IEA; 2008.
- [3] EIA Annual Energy Outlook 2009 with Projections to 2030. DOE/EIA-0383(2008); March 2009.
- [4] Bolland O, Mathieu P. Comparison of two CO₂ removal options in combined cycle power plants. *Energy Convers Manage* 1998;39(16–18):1653–63.
- [5] Bolland O, Undrum H. A novel methodology for comparing CO₂ capture options for natural gas-fired combined cycle plants. *Adv Environ Res* 2003;7:901–11.
- [6] Kvamsdal HM, Jordal K, Bolland O. A quantitative comparison of gas turbine cycles with CO₂ capture. *Energy* 2007;32:10–24.
- [7] Rao AD. Process for producing power. US Patent No. 4829763; 1989.
- [8] Jonsson M, Yan J. Humidified gas turbines—a review of proposed and implemented cycles. *Energy* 2005;30:1013–78.
- [9] Rao AD, Day WH. Mitigation of greenhouse gases from gas turbine power plants. *Energy Convers Manage* 1996;37:909–14.
- [10] Jonsson M, Yan J. Gas turbine with kalina bottoming cycle versus evaporative gas turbine cycle. ASME Paper JPGC2001/PWR-19005. In: International joint power generation conference, New Orleans, United States; 2001.
- [11] Jonsson M, Yan J. Economic assessment of evaporative gas turbine cycles with optimized part flow humidification systems. In: Proceedings of ASME turbo expo, power for land, sea, and air, Atlanta, Georgia, USA; June 16–19, 2003.
- [12] Jonsson M, Yan J. Exergy analysis of part flow evaporative gas turbine cycles, Part I – assumption and methods (GT2002-30125). In: Proceedings of ASME turbo expo, Amsterdam, Netherlands; 2002.
- [13] Jonsson M, Yan J. Exergy analysis of part flow evaporative gas turbine cycles, Part II – results and discussion (GT2002-30126). In: Proceedings of ASME turbo expo, Amsterdam, Netherlands; 2002.
- [14] Yan J, Eidensten L, Svedberg G. Simulation of externally fired evaporative gas turbine cycle. Internal report project of new processes for power and heat generation; 1993.
- [15] Yan J, Eidensten L. Status and perspective of externally fired gas turbines. *J Propul Power* 2000;16:572–6.
- [16] Cleeton JPE, Kavanagh RM, Parks GT. Blade cooling optimisation in humid-air and steam-injected gas turbines. *Appl Therm Eng* 2009;29:3274–83.
- [17] Bidini G, Desideri U, Di Maria F. Thermodynamic analysis of injected water recovery systems for the humid air turbine (HAT) cycle. In: Proceedings, 1996 ASME international mechanical engineering congress and exposition, Atlanta, Georgia; November 17–22 1996.
- [18] Desideri U, Di Maria F. Humid air turbine cycles with water recovery: how to dispose heat in an efficient way. ASME Paper 98-GT-60, presented at the 43rd ASME international gas turbine and aeroengine congress and exposition, Stockholm, Sweden; June 2–5 1998.
- [19] Desideri U, Di Maria F. Water recovery from HAT cycle exhaust gas: a possible solution for reducing stack temperature problems. *Int J Energy Res* 1998;21(9):809–22.
- [20] Dalili F. Humidification in evaporative power cycles. Doctoral Thesis, Department of Chemical Engineering and Technology, Energy Processes, Royal Institute of Technology, Stockholm, Sweden; 2003.
- [21] Nishida K, Takagi T, Kinoshita S. Regenerative steam-injection gas-turbine systems. *Appl Energy* 2005;81:231–46.
- [22] Wang Y, Li Y, Weng S, Su M. Experimental investigation on humidifying performance of counter flow spray saturator for humid air turbine cycle. *Energy Convers Manage* 2007;48:756–63.
- [23] Wang Y, Li Y, Weng S, Wang Y. Numerical simulation of counter-flow spray saturator for humid air turbine cycle. *Energy* 2007;32:852–60.
- [24] Pedemonte AA, Traverso A, Massardo AF. Experimental analysis of pressurised humidification tower for humid air gas turbine cycles. Part A: experimental campaign. *Appl Therm Eng* 2008;28:1711–25.
- [25] Pedemonte AA, Traverso A, Massardo AF. Experimental analysis of pressurised humidification tower for humid air gas turbine cycles. Part B: correlation of experimental data. *Appl Therm Eng* 2008;28:1623–9.
- [26] Ji X, Lu X, Yan J. Survey of experimental data and assessment of calculation methods of properties for the air–water mixture. *Appl Therm Eng* 2003;23:2213–28.
- [27] Ji X, Lu X, Yan J. Saturated humidity, entropy and enthalpy for the nitrogen–water system at elevated temperature and pressure. *Int J Thermophys* 2003;24(6):1681–96.
- [28] Ji X, Yan J. Saturated thermodynamic properties for the air–water system at elevated temperature and pressure. *Chem Eng Sci* 2003;58(22):5069–77.
- [29] Ji X, Lu X, Yan J. Phase equilibria for the oxygen–water system at elevated temperatures and pressures. *Fluid Phase Equilib* 2004;222–223:39–47.
- [30] Ji X, Yan J. Thermodynamic properties for humid gases from 298 to 573 K and up to 200 bar. *Appl Therm Eng* 2006;26(2–3):251–8.
- [31] Carbon capture & storage: assessing the economics. McKinsey & Company; 2008.
- [32] Croiset E, Thambimuthu KV. Coal combustion O₂/CO₂ mixtures. *Can J Chem Eng* 2000;78(2):402–7.
- [33] Li H, Yan J. Performance comparison on the evaporative gas turbine cycles combined with different CO₂ capture options. *Int J Green Energy* 2009;6:512–26.
- [34] Li H, Flores S, Hu Y, Yan J. Simulation and optimization of evaporative gas turbine with chemical absorption for carbon dioxide capture. *Int J Green Energy* 2009;6:527–39.
- [35] Hu Y, Li H, Yan J. Integration of evaporative gas turbine with oxy-fuel combustion for carbon dioxide capture. *Int J Green Energy* 2010;7:615–31.
- [36] Gas Turbine World, GTW Handbook. Pequet Publishing Inc.; 2004.
- [37] Turton R, Bailie RC, Whiting WB, Shaeiwitz JA. Analysis, synthesis, and design of chemical processes, 2nd ed. Prentice Hall PTR; 2003.
- [38] Yan J, Eidensten L, Svedberg G. An investigation of the heat recovery system in externally fired evaporative gas turbines. In: Proceedings of ASME international gas turbine and aeroengine congress and exposition. Houston, Texas, USA; 1995.
- [39] Li H, Ditaranto M, Berstad D. Technologies for increasing CO₂ concentration in exhaust gas from natural gas-fired power production with post combustion, amine-based CO₂ capture. *Energy* 2011;36:1124–33.
- [40] Natural gas weekly update. <<http://www.eia.doe.gov/oog/info/ngw/ngupdate.asp>> (accessed 02.06.10).
- [41] Abu-Zahra M, Niederer J, Feron P, Versteeg G. CO₂ capture from power plants, Part II. A parametric study of the economical performance based on mono-ethanolamine. *Int J Greenhouse Gas Control* 2007;1:135–42.
- [42] Singh D, Croiset E, Douglas PL, Douglas MA. Techno-economic study of CO₂ capture from an existing coal-fired power plant: MEA scrubbing vs. O₂/CO₂ recycle combustion. *Energy Convers Manage* 2003;44:3073–91.
- [43] TEG price. <<http://www.ics.com/Articles/2004/08/06/602645/deg-and-teg-prices-surge.html>> (accessed 02.06.10).
- [44] Gas Turbine World, GTW Handbook. Pequet Publishing Inc.; 2009.
- [45] Kehlhofer R. Combined-cycle gas & steam turbine power plants. The Fairmont Press, Inc.; 1991.
- [46] IEA, cost and performance of retrofitting existing NGCC units for carbon capture. DOE/NETL-401/080610; October 1, 2010.
- [47] Parsons EL, Shelton WW, Lyons JL. Advanced fossil power systems comparison study. Final report prepared for NETL; December, 2002.
- [48] Parsons Infrastructure and Technology Group, Inc. Updated cost and performance estimates for fossil fuel power plants with CO₂ removal. Report under Contract No. DE-AM26-99FT40465 to U.S.DOE/NETL, Pittsburgh, PA, and EPRI, Palo, CA; December 2002.

- [49] CCP. Economic and cost analysis for CO₂ capture costs in the CO₂ capture project, scenarios. In: Thomas DC, editor. Capture and separation of carbon dioxide from combustion sources, vol. 1. Oxford (UK): Elsevier Science; 2005.
- [50] Dillon DJ, Panesar RS, Wall RA, Allam RJ, White V, Gibbins J, et al. Oxy-combustion processes for CO₂ capture from advanced supercritical PF and NGCC power plant. *Greenhouse Gas Control Technol* 2005;7:211–20.
- [51] Simbeck DR. CO₂ mitigation economics for existing coal-fired power plants. In: First conference on carbon sequestration, Washington, DC, United States; 2001.
- [52] Chakma A. CO₂ capture processes-opportunities for improved energy efficiencies. *Energy Convers Manage* 1997;38(S-1):51–4.

Analysis of Gas-Steam Combined Cycles With Natural Gas Reforming and CO₂ Capture

Alessandro Corradetti

Umberto Desideri

e-mail: umberto.desideri@unipg.it

Dipartimento di Ingegneria Industriale,
Università di Perugia,
Via G. Duranti 93,
06125 Perugia, Italy

In the last several years greenhouse gas emissions, and, in particular, carbon dioxide emissions, have become a major concern in the power generation industry and a large amount of research work has been dedicated to this subject. Among the possible technologies to reduce CO₂ emissions from power plants, the pretreatment of fossil fuels to separate carbon from hydrogen before the combustion process is one of the least energy-consuming ways to facilitate CO₂ capture and removal from the power plant. In this paper several power plant schemes with reduced CO₂ emissions were simulated. All the configurations were based on the following characteristics: (i) syngas production via natural gas reforming; (ii) two reactors for CO-shift; (iii) "precombustion" decarbonization of the fuel by CO₂ absorption with amine solutions; (iv) combustion of hydrogen-rich fuel in a commercially available gas turbine; and (v) combined cycle with three pressure levels, to achieve a net power output in the range of 400 MW. The base reactor employed for syngas generation is the ATR (auto thermal reformer). The attention was focused on the optimization of the main parameters of this reactor and its interaction with the power section. In particular the simulation evaluated the benefits deriving from the postcombustion of exhaust gas and from the introduction of a gas-gas heat exchanger. All the components of the plants were simulated using ASPEN PLUS software, and fixing a reduction of CO₂ emissions of at least 90%. The best configuration showed a thermal efficiency of approximately 48% and CO₂ specific emissions of 0.04 kg/kWh.
[DOI: 10.1115/1.1850941]

Introduction

Since the second half of eighteenth century anthropogenic emissions have increased atmospheric concentration of greenhouse gases. The radiative forcing (i.e., the increase in the total downward flux of infrared, emitted by the atmosphere, due to the additional amount of gas) is estimated at 2.43 W/m². The carbon dioxide alone is responsible for 60% of this radiative forcing because CO₂ has always been the main gas emitted by human activities. As a result CO₂ atmospheric concentration has reached 373 ppm in 2002 [1] while preindustrial value was approximately 280 ppm [2].

The main source of carbon dioxide derives from the combustion of fossil fuels, which generates 90% of globally emitted CO₂. Fossil fuels are used in three fundamental fields: transportation, heating, and power generation. The latter is probably the one in which measures to decrease carbon dioxide emissions could be more effective. In recent years several studies have investigated the performances of innovative power cycles with low CO₂ emissions. These cycles are usually grouped into three different alternatives: (i) postcombustion decarbonization, (ii) oxy-fuel power cycles, (iii) precombustion decarbonization.

Postcombustion decarbonization consists in the removal of carbon dioxide from exhaust gases. This scheme requires minimum modifications to power cycle, as CO₂ separation involves only exhaust gas treatment. Among CO₂ capture technologies (chemical and physical absorption, adsorption, membranes, cryogenic separation), the most promising one for postcombustion decarbonization is chemical absorption because it is the least energy requiring when CO₂ partial pressure is very low, as in exhaust gases

[3,4]. Anyway this technology has not been optimized for power generation applications, and further developments in solvent composition is needed to improve the absorption process [5].

The second scheme (oxy-fuel combustion) requires the production of pure oxygen to be used as oxidizer in a close-to-stoichiometric combustion, which produces only CO₂ and H₂O. In these plants an air-separation unit is needed for the production of O₂. An example of these cycles can be found in Bolland and Mathieu [6]. They investigated a semi-closed combined cycle, in which the gas turbine uses carbon dioxide as working fluid; therefore, CO₂ capture is accomplished without the need of highly energy-requiring devices. The cycle showed a global efficiency of approximately 47%.

The third option to reduce CO₂ emissions from power plant is known as precombustion decarbonization. In this case fossil fuels are converted to syngas (i.e., a mix of CO and H₂). Syngas is the raw material for several chemical syntheses, such as methanol and ammonia. Both solid and gaseous fuels can be used for this purpose; gasification and reforming are, respectively, the technologies adopted to produce syngas from coal and natural gas. The integration of a gasifier with a combined cycle is nowadays regarded as the most promising way to generate power from coal because integrated gasification combined cycle (IGCC) plants are characterized by higher efficiencies than conventional pulverized coal-fired plant (PCFP). Various IGCC plants are operating worldwide, but CO₂ removal has never been attempted in these cases. However, several studies on the subject have been carried out in the last several years, showing that CO₂ can be easily captured in plants with conventional gas-sweetening processes, based on physical absorption (such as Selexol or Rectisol [7]). One or two "shift" reactors have to be introduced before CO₂ absorber, in order to convert CO to CO₂, so that the gas to be treated contains only hydrogen and carbon dioxide. IGCC net efficiency decreases from 44% to 46% to 37% to 40% if CO₂ is removed following this option [8,9].

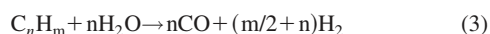
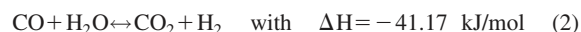
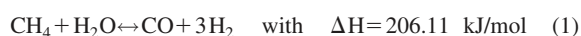
For natural gas-fired plants, precombustion decarbonization

Contributed by the International Gas Turbine Institute (IGTI) of THE AMERICAN SOCIETY OF MECHANICAL ENGINEERS for publication in the ASME JOURNAL OF ENGINEERING FOR GAS TURBINES AND POWER. Paper presented at the International Gas Turbine and Aeroengine Congress and Exhibition, Vienna, Austria, June 13–17, 2004, Paper No. 2004-GT-54091. Manuscript received by IGTI, October 1, 2003; final revision, March 1, 2004. IGTI Review Chair: A. J. Strazisar.

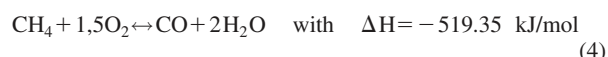
[10–13] implies the adoption of either a steam reformer or partial oxidizer. These reactors generate a blend of CO and H₂ (plus nitrogen, if air is used as oxidizer), just as gasifiers do. Of course syngas composition varies with the technology utilized and with operating parameters, but the basic principle is the same. In fact at reformer outlet syngas must be shifted and CO₂ removed in order to feed a gas turbine with a carbon-free fuel. In this case the chemical absorption process is preferred over physical absorption, as the pressure of produced syngas is lower. This option is very interesting because it requires components that have a commercially proven technology and can be operated under the same work conditions as usual. In this paper we have analyzed the thermodynamic performances of a combined cycle, which is fed by the fuel generated by the reforming process and deprived of CO₂. Particular attention was focused on the integration of the power plant with both the syngas production section and CO₂ removal plant. All the components investigated reflect the state of the art.

1 The Reforming Process

The reforming process involves the following reactions:



Both (1) and (2) can be considered at equilibrium conditions in commercially available reformers. The first is the methane reforming reaction, which requires steam and must be carried out at 700–950°C, as it is endothermic, and methane conversion is enhanced by the excess of steam and the high temperatures. Reaction (2) is known as the “CO-shift reaction” and also occurs during reforming process, thus determining CO and H₂ concentration at equilibrium. Reaction (3) constitutes the reforming of heavier hydrocarbons, which can be considered irreversible. The reforming process usually takes place in a tubular reactor, called steam methane reformer, where the heat of reaction is supplied externally by a flame fed with methane, too. Auto thermal reformers (ATR) carry out both reforming and combustion in a unique reactor, which supplies itself the energy for reforming reaction and for increasing gas temperature. Air (or pure oxygen) is also introduced into the ATR as oxidizer. In the upper part of the ATR several combustion reactions take place, but in a simplified model the molecular reaction which best represents the whole process is the combustion of methane to carbon monoxide and water [14]:



Therefore, a fraction of methane entering the ATR is not reformed because it works as fuel, supplying heat for endothermic reactions.

If air is used as oxidizer, then the gas leaving the ATR contains a large amount of nitrogen. In industrial practice oxygen is more often used instead of air, in order to reduce plant size and costs. Air is preferred over O₂ in ammonia plants, where it feeds a secondary reformer (substantially an ATR placed after SMR), and supplies the nitrogen necessary for ammonia synthesis. Previous studies [7,8] showed that air-blown reactors are perfectly suitable for integration with a combined cycle, for two reasons:

1. Air entering the ATR can be extracted directly from the gas turbine (GT) compressor.
2. Final fuel is diluted with nitrogen, therefore, NO_x emissions are reduced to acceptable values as stoichiometric flame temperature is lower.

In particular, NO_x emission control is a relevant problem when hydrogen is burned in a gas turbine because it is not possible to prevent thermal NO_x formation adopting dry-low-NO_x technologies. In fact hydrogen has a faster flame speed and a shorter au-

toignition delay time, so premixed combustion is not achievable at present time [15]. Even if more experimental work on this subject is needed, many theoretical studies [15–17] agree that fuel dilution with 50% nitrogen could be sufficient to limit NO_x emissions in the range of 25–50 ppmv.

2 Power Plant Schemes With ATR

Three power plant schemes have been investigated. They differ from each other substantially in the preheating of the streams entering reformer. For this goal, the “Reference Case” is provided with only one heat exchanger, in which GT exhaust gases are used to preheat natural gas and steam. In the supplementary firing (SF) configuration, exhaust gas temperature is increased by supplementary firing, and two heat exchangers are employed. In the GAS-GAS configuration the heat exchangers utilize the hot syngas leaving the reformer, instead of the exhaust gas, for natural gas and steam preheating.

The Reference Case configuration is shown in Fig. 1. Natural gas is mixed with the steam extracted from a medium-pressure level (MP) turbine at 18 bar. The reactants are heated to 480°C by GT exhaust gases in HE-IN-PRE. The mixed streams (2) enter PRE-REF, which provides for the reforming of heavier hydrocarbons. After pre-reforming, the gas (3) goes directly into the ATR, which uses a fraction of the air (Fig. 1(b)), leaving the GT compressor as an oxidizer. The pressure of this reactor is therefore imposed by GT pressure ratio. Two different temperatures (850°C and 950°C) have been chosen for ATR operating conditions. In any case the hot syngas leaving the ATR must be cooled down to 400°C, in order to be shifted in high-temperature shift (HTS). A waste heat boiler provides for this cooling, together with the production of high-pressure steam (E), which is sent to the heat recovery steam generator (HRSG) for superheating. CO concentration by volume is reduced from 9% to 3.5% by the shift reaction accomplished in the HTS. The gas (6) is further cooled in two convective heat exchangers (HEs): the first one (HE1) is used to preheat the water that feeds the waste heat boiler (WHB); the second one (fuel regenerator (REG)) is a gas-gas exchanger, which brings GT fuel to 280°C. The syngas (8) enters the low-temperature shift (LTS) at 160°C and exits at temperatures in the range of 200°C.

In order to be appropriately treated in the CO₂ capture plant, the gas leaving the shift reactor is cooled down to 35°C. Successively most of the water is removed, thus decreasing the volumetric flow of the gas to be treated and increasing CO₂ concentration. Carbon dioxide is separated in a typical plant based on chemical absorption. CO₂ is then compressed to 140 bar for liquefaction and transportation. The gas leaving the top of the absorber is poor in carbon and can feed the gas turbine; before entering the combustion chamber, the fuel is compressed to 20 bar and heated in the REG. The exhaust gases (c) from the turbine enter HE-IN-PRE approximately at 590°C, and the HRSG at 557°C. This determines the maximum temperature of the steam, having set the approach point ΔT at 20°C. The HRSG has three pressure levels. Syngas production and decarbonization decrease power produced by the steam turbine because medium pressure steam is extracted from the steam turbine (ST) for the reforming, while low-pressure steam is extracted for solvent regeneration. The interaction between syngas production and the power section has also a positive feature: from syngas cooling it is possible to preheat water and to generate saturated steam, thus increasing the power generated by the ST.

The Reference Case configuration has been slightly modified in order to decrease methane consumption in the ATR. Supplementary firing of the GT exhaust gases has been studied in SF configuration, whose main features are depicted in Fig. 2. Exhaust gas temperature rises to 646°C and the ATR inlet stream (3) can be heated to 600°C in HE-IN-ATR. In GAS-GAS configuration (Fig. 3) two gas-gas heat exchangers have been introduced to recover heat from syngas leaving the ATR. This equipment has to resist

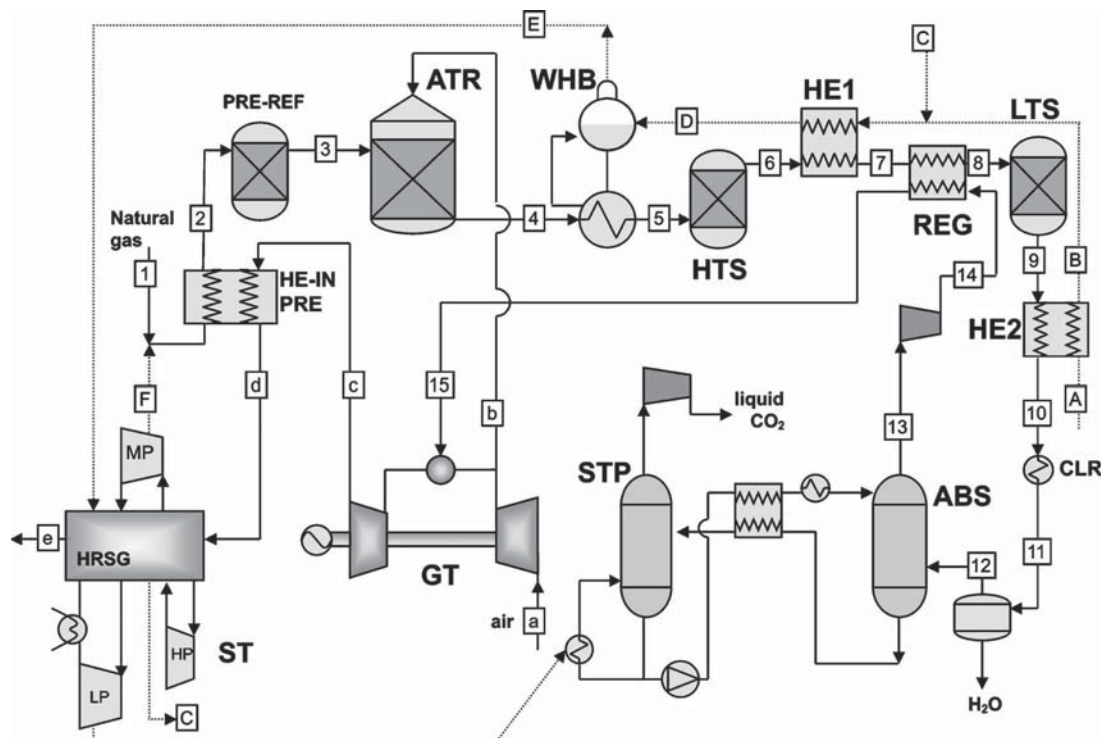


Fig. 1 Reference Case process flowsheet

high temperatures, and it has not been commercially proven. At the reformer outlet, syngas is cooled in HE-IN-ATR, which increases ATR inlet streams to 600°C. Syngas is further cooled in HE-IN-PRE, where natural gas and process steam are heated to 500°C. In this configuration the GT exhaust gases go directly into the HRSG.

3 Assumptions and Results

3.1 Syngas Production Section. The whole power plant has been studied with the ASPEN PLUS software [18–20]. The principal reactors (PRE, ATR, HTS, LTS) have been simulated by the Gibbs Reactor, a model available in the ASPEN+ library, which determines equilibrium conditions by minimizing Gibbs energy. The Pre-reformer is an adiabatic reactor, which operates with an

inlet stream temperature in the range of 470–550°C, depending on the configuration considered. In the Reference Case, the temperature of stream 2 is the lowest (481°C for T-ATR=850°C, 467°C for T-ATR=950°C), as the parameter fixed in HE-IN-PRE is the outlet temperature of stream *d* (557°C). For the SF configuration this temperature is set at 580°C, so pre-reformer inlet temperature rises to 542°C and 500°C, respectively for T-ATR=850°C and T-ATR=950°C. In GAS-GAS configuration, the pre-reformer inlet temperature is fixed at 500°C. Temperature drop in the pre-reformer is caused by the reforming of heavier hydrocarbons, which is strongly endothermic.

The gas leaving pre-reformer (PRE-REF) contains small amounts of ethane and propane: it enters ATR without preheating in the Reference Case, so ATR inlet temperature (418°C, 410°C) is given by temperature drop in the PRE-REF. In the other configurations, syngas is heated to 600°C before entering ATR (the choice

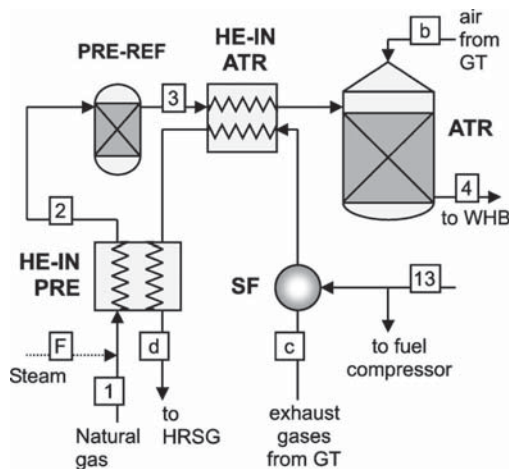


Fig. 2 Variations introduced in SF configuration

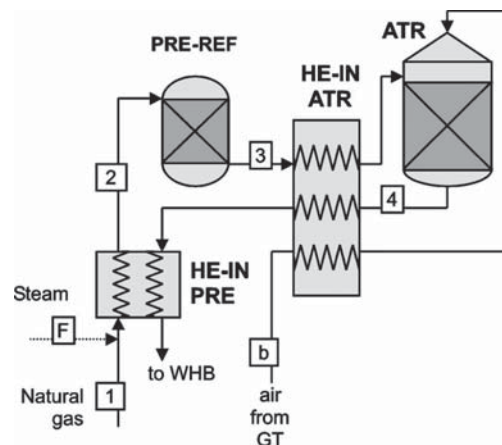


Fig. 3 Variations introduced in GAS-GAS configuration

Table 1 Gas composition in reference case

Stream	1	2	3	4	6	9	12	13
T [°C]	25.0	481.0	417.8	850	459.8	201.2	34.9	281.5
m [kg/s]	17.21	44.94	44.94	125.8	125.8	125.8	111.4	71.96
	composition [% by vol]							
CH ₄	91.2	35.9	35.6	0.6	0.6	0.6	0.7	0.8
C ₂ H ₆	4.4	1.7
C ₃ H ₈	0.1	0.04
CO	8.9	3.5	0.2	0.2	0.3
CO ₂	2.2	5.6	10.9	14.2	16.1	0.9
H ₂	7.0	30.6	35.9	39.2	44.5	52.4
N ₂ + AR	4.3	1.7	1.6	33.5	33.5	33.5	37.9	44.7
H ₂ O	...	60.6	53.6	20.9	15.6	12.3	0.4	0.8

of this value derives from the state of the art of heat exchangers preceding the ATR). In the GAS-GAS configuration air stream entering the ATR is heated to 600°C too, while in the other cases, the temperature of air is influenced only by isentropic efficiency of GT compressor (0.89).

The shift reaction, which converts CO to CO₂, is exothermic, so it takes advantage from low temperatures. The HTS inlet temperature is fixed at 400°C by the WHB, while outlet temperature varies in the range of 460–470°C, as also this component is adiabatic and the reaction accomplished is exothermic. Syngas is further cooled in HE1: temperature of stream 7 (290°C) has been determined by imposing a minimum ΔT of 10°C on the hot side of the REG. Syngas goes into the LTS at 160°C and exits at 200–210°C (this reactor is adiabatic, too). Then it is cooled down to 100°C by HE2 and finally to 35°C. Table 1 shows the composition of most significant streams for the Reference Case (with T-ATR = 850°C). The pressure of the entire circuit is imposed by GT pressure ratio ($\beta=17$) and by pressure losses, which are shown in Table 2.

S/C is the ratio between steam and carbon mole flow at the pre-reformer inlet. Methane conversion and hydrogen production in ATR are enhanced by high values of S/C, but power generation decreases as S/C rises because process steam is extracted from the MP turbine. In this work S/C has been fixed at 1.5, in order to minimize steam extraction. Lower values have not been considered because they have negative effects on carbon deposits formation, which is counteracted by H₂O in excess respect to the stoichiometric minimum. More precisely, since steam extraction is the same for all the cases and natural gas mass flow is variable, S/C is slightly different from a configuration to another. The ATR temperature influences methane conversion too: if *T* is increased, methane slip is lower. For example in the Reference Case the percentage of unreacted CH₄ decreases from 4.6% to 0.5% if the ATR operating temperature is raised from 850°C to 950°C. This is perfectly in agreement with the chemical equilibrium of reforming reaction, which is endothermic, thus enhanced by higher temperature. Table 3 shows the percentage of unreacted methane in the various configurations.

Methane reacted in the ATR is not completely reformed in accordance with reaction (1) because a fraction of CH₄ is burned to supply the heat of reforming and to increase reactants temperature. The burned fraction increases with higher ATR temperatures

and with larger mass flows of reactants because in these cases more energy is required. If the fraction of burned CH₄ is bigger, the low heating value (LHV) of produced syngas is lower. We have introduced the “Cold syngas efficiency,” which represents the ratio between chemical energy of produced syngas and natural gas LHV input. This parameter is used in IGCC performance analysis to express the fraction of coal chemical energy, which is transferred to the produced gas; thus, it does not take into account heat recovery from hot gas, which produces significant amounts of steam, but constitutes the degradation of heat available at high temperature. Cold syngas efficiencies of the studied configurations are shown in Table 4.

The oxygen introduced in ATR is completely consumed by partial and total combustion reactions. Therefore air extraction from the GT compressor is not constant, as it is a function of burned methane fraction. Table 4 shows air mass flow needed by the ATR and the composition of syngas entering CO₂ absorber (stream 12).

H₂/CH₄ is the ratio between the molar flow of hydrogen in stream 12 and CH₄ input molar flow. According to reactions (1) and (2) this ratio has to be 4, if all methane molecules are converted to H₂. Instead H₂/CH₄ is less than 4, thus confirming that a fraction of methane does not take part in reforming, as it is burned. Furthermore, this ratio expresses how much hydrogen can be produced by the same amount of natural gas. By increasing the ATR temperature, H₂/CH₄ increases in SF and GAS-GAS configurations, but it decreases in the Reference Case. This is substantially a consequence of the variation of ATR inlet streams temperature.

3.2 CO₂ Removal Plant. CO₂ removal is accomplished in an absorption/stripping plant, commonly used for synthesis gas sweetening. Figure 4 illustrates the process flowsheet simulated with ASPEN PLUS. The solvent used in this simulation is a blend of water and two amines: MDEA (30% by weight) and DEA (5%). CO₂ is captured by this solvent in the absorber column (ABS) and it is desorbed in a second column [stripper (STP)] by stripping. The stripping agent is the vapor of the solvent itself, which is produced in a Kettle reboiler. The choice of this mix allows a reduction of reboiler heat duty, as the MDEA requires less heat for regeneration than other amines, like MEA and DEA. Unfortunately the MDEA reaction with CO₂ is very slow and activators

Table 2 Pressure losses in syngas circuit

Component	Outlet pressure [bar]	Δp/p [%]
PRE+HE-IN-ATR	17.22	5
ATR	16.36	5
WHB	15.87	3
HTS	15.24	4
HE1+REG	14.78	3
LTS	14.34	3
HE2+cooler	14.06	2

Table 3 S/C and unreacted methane

Configuration	Actual S/C	Unreacted CH ₄ [% input]
Ref. case (T-ATR=850°C)	1.53	4.59
Ref. case (T-ATR=950°C)	1.46	0.54
SF (T-ATR=850°C)	1.50	6.17
SF (T-ATR=950°C)	1.43	0.74
Gas-Gas (T-ATR=850°C)	1.63	6.16
Gas-Gas (T-ATR=950°C)	1.56	0.78

Table 4 Main results of syngas production section

	Ref 850°C	Ref 950°C	SF 850°C	SF 950°C	Gas Gas 850°C	Gas Gas 950°C
Air mass flow to ATR [kg/s]	80.8	96.9	73.1	90.1	64.5	78.0
Stream “12” mass flow [kg/s]	111.4	127.3	106.2	123.3	95.9	109.6
Stream “12” composition [% by vol]						
CH ₄	0.71	0.08	0.99	0.11	0.99	0.12
CO	0.23	0.22	0.35	0.35	0.28	0.30
CO ₂	16.11	15.94	16.26	16.10	16.43	16.30
H ₂	44.54	42.19	47.16	44.73	48.35	46.28
N ₂ + AR	37.97	41.12	34.81	38.26	33.51	36.56
H ₂ O	0.44	0.44	0.44	0.44	0.44	0.44
H ₂ /CH ₄ input	2.87	2.86	2.95	2.97	3.00	3.05
Cold syngas efficiency [%]	84.3	80.1	88.0	83.7	89.4	85.7

are usually added in order to accelerate the absorption process in proprietary solvents. In this simulation, DEA is used as the activator; this device is often adopted commercially.

Table 5 illustrates the main differences characterizing the CO₂ removal plant, together with fuel mass flow and composition. Both absorber and stripper have been simulated as seven-stage columns, using the RadFrac model, available in the ASPEN PLUS library.

Since the reactions between CO₂ and amines are exothermic, both gas and liquid increase their temperature in the absorber (ABS): the gas exits from top of the absorber at 45–51°C, while the solvent loaded with CO₂ is at 62–63°C at the bottom of the ABS. The absorber works at 13.3 bar, while the stripper at 1.8 bar. Therefore, a flash separator has been put after the ABS, for partially regenerating the solvent by pressure reduction. The rich solvent is preheated to 80°C in H-EX by the lean solution coming from the stripper, which leaves the Kettle reboiler at 101.5°C.

Minimum ΔT between solution and steam condensing in the reboiler is about 10°C. In the stripper, condenser cooling duty is the same (5 MW) for all the configurations. On the contrary, reboiler heat duty changes because the following conditions have been imposed:

1. Same ΔT on H-EX cold side (7.35°C \pm 0.2).
2. Same composition of the solution entering ABS.

The latter has been verified by checking the MDEA+/MDEA ratio of the solution, which represents the percentage of the not-regenerated amine in the stripper. For all the configurations this ratio is in the range 0.210–0.215. CO₂ leaving the top of the stripper is compressed to 140 bar and liquefied for transportation in pipelines. The CO₂ compressor has been modeled by a four-stage intercooled compressor. Isentropic efficiency of the single stage is 0.85, mechanical efficiency is 0.95.

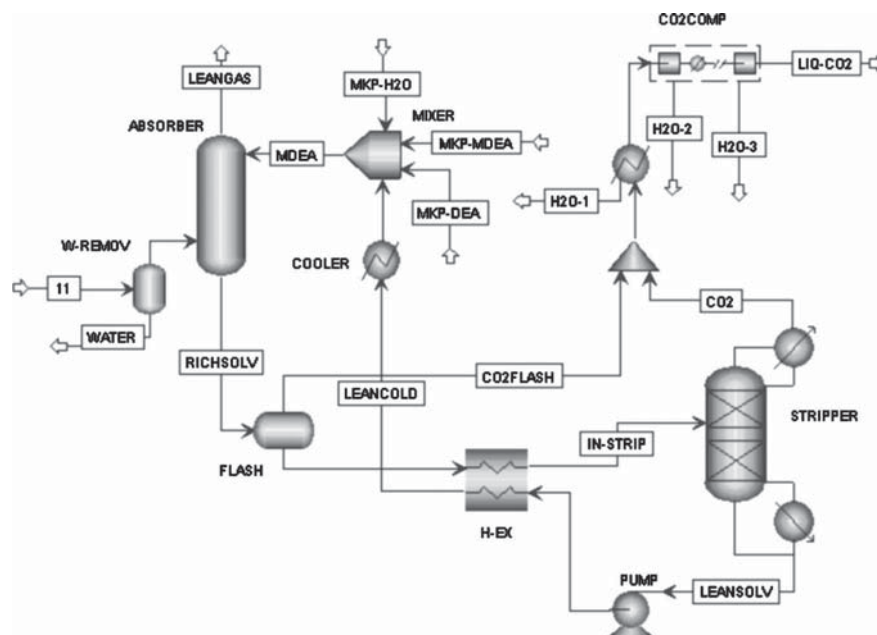


Fig. 4 CO₂ removal and liquefaction plant

Table 5 Main results of CO₂ removal plant and fuel composition

Configuration	REF 850°C	REF 950°C	SF 850°C	SF 950°C	GAS GAS 850°C	GAS GAS 950°C
Solvent mass flow [kg/s]	556.9	582.1	570.9	594.6	526.0	542.7
Q reboiler [MWt]	85.0	89.0	87.0	90.5	80.0	83.3
Steam [kg/s]	36.1	37.8	36.6	38.1	33.7	35.0
CO ₂ in ABS [kg/s]	41.72	45.58	41.66	46.09	38.61	42.33
Removed CO ₂ [kg/s]	39.74	41.79	40.57	42.67	37.45	39.11
Removed CO ₂ [%]	95.3	91.7	97.4	92.6	96.7	92.4
Fuel (stream "13") mass flow [kg/s]	71.96	85.97	65.78	81.0	58.61	70.90
Fuel composition [% by vol]						
CH ₄	0.84	0.09	1.17	0.13	1.18	0.14
CO	0.27	0.26	0.41	0.41	0.34	0.35
CO ₂	0.90	1.55	0.50	1.40	0.59	1.46
H ₂	52.45	49.19	55.92	52.35	57.38	54.25
N ₂ + AR	44.72	47.95	41.29	44.78	39.78	42.86
H ₂ O	0.83	0.96	0.70	0.93	0.73	0.94
Fuel LHV [MJ/kg]	9.32	7.80	10.87	8.83	11.44	9.46

The rate of carbon dioxide removal in the ABS is different for the various configurations. In fact a design specification has been created to set at 10% the percentage of all the carbon not removed from syngas. In this way it is possible to take into account CO and CH₄ fractions, which generate CO₂ while burning in GT. Thus, in every configuration CO₂ final emissions are 90% of emissions generated by a gas turbine combined cycle (GTCC) with the same natural gas input. The percentage of removed CO₂ is greater whenever CH₄ and CO conversion is lower; for example, in the Reference Case absorbed CO₂ is 95.3% of the total entering the ABS if T-ATR=850°C. If T-ATR is increased to 950°C, then removed CO₂ decreases to 91.7% because the CH₄ concentration in syngas to be treated is lower (see Table 4). However this variation does not deeply affect power and heat consumption in the CO₂ capture plant, which on the contrary greatly depends on the total mass flow of removed CO₂. In all the configurations if the T-ATR is increased, then the mass flow of carbon dioxide entering the ABS grows, thus increasing the reboiler heat duty needed for solvent regeneration. GAS-GAS (with T-ATR=850°C) is the configuration that requires the least heat duty (80 MW), even though the percentage of absorbed CO₂ is rather high (96.7%). Solvent mass flow has the same behavior of reboiler heat duty, as it depends above all on the total mass flow of CO₂ to be captured. After all GAS-GAS configurations generate less CO₂ than other cases, thus giving the following advantages:

1. Steam extraction from the ST for stripping is lower, as reboiler heat duty decreases.
2. CO₂ to be captured is less, so power consumption for solvent pump and CO₂ compressor is lower.

3.3 Power Generation. Power generation is accomplished by a gas-steam combined cycle. The gas turbine is a heavy-duty machine, corresponding to technology known as FA, characterized by a TIT of approximately 1350°C. The turbine modeled in the simulation matches the main parameters of a real machine, SIEMENS V94.3A ($\beta=17-TIT=1350^\circ\text{C}$). In particular, air mass flow rate at the compressor inlet is the same as the real machine (634 kg/s); the net efficiency and the net power output are, respectively, 38.2% and 256 MW, TOT is 590°C. The net power output generated by the GT is determined by a calculator block, which

uses fuel mass flow and composition and the fixed efficiency as input parameters to calculate the produced power. In any configuration, the natural gas mass flow rate has been changed to match the real machine net power. The HRSG is three pressure levels: 4/35/140 bar, with reheat and condenser at 0.04 bar. Heat recovery has been optimized by setting at 10°C, the minimum pinch point ΔT for all the pressure levels.

In the Reference Case and in the SF configuration, the approach point ΔT has been fixed at 20°C, which corresponds to a superheating (and reheating) steam temperature, respectively, of 537°C and 560°C. In the GAS-GAS configuration, maximum steam temperature is also 560°C, not to exceed the limit connected with corrosion. The ATR requires a significant amount of steam: 27.7 kg/s, needed to achieve a S/C ratio of 1.5, are extracted from MP steam turbine at 18.13 bar. Solvent regeneration also requires steam. A mass flow of 33.7–38.1 kg/s is extracted from the LP steam turbine at 2 bar. The main assumptions made for the power generation section are summarized in Table 6.

Table 6 Assumptions made for power generation section

Gas turbine cycle	
Gas turbine	SIEMENS V94.3A
Pressure ratio	17
TIT [°C]	1350
Inlet air flow rate [kg/s]	634
Thermodynamic efficiency [%]	38.2
Fuel compressor η_{is}	0.9
Steam cycle	
Pressure levels [bar]	140/35/4
Condenser pressure [bar]	0.04
Steam turbine η_{is}	0.9
Steam turbine η_{mec}	0.95
Pump efficiencies	0.9
ΔT pinch point [°C]	10
ΔT approach point [°C]	20
ΔT subcooling [°C]	10

Table 7 Overall performances of the various plants

	Reference 850°C	Reference 950°C	SF 850°C	SF 950°C	Gas Gas 850°C	Gas Gas 950°C
GT net power [MW]	256.27	256.21	256.34	256.30	256.23	256.14
Steam cycle net power [MW]	141.35	158.27	148.79	166.11	122.97	136.97
Fuel compressor [MW]	6.51	7.33	5.90	6.80	5.81	6.61
Solvent pump power [MW]	0.77	0.80	0.78	0.82	0.72	0.75
CO ₂ compressor [MW]	12.97	13.64	13.24	13.93	11.84	12.76
Plant net power [MW]	377.37	392.71	385.21	400.87	360.82	372.98
Natural gas LHV input [MW]	797	838	813	855	751	783
Net efficiency [%]	47.37	46.87	47.36	46.88	48.06	47.62
CO ₂ emissions [kg/s]	4.38	4.61	4.48	4.70	4.13	4.27
CO ₂ specific emissions [g/kWh]	41.8	42.2	41.8	42.2	41.2	41.2
Actual CO ₂ reduction [%]	88.3	88.1	88.3	88.2	88.4	88.4

4 Comparison of the Performance

Table 7 shows overall performances of the various plants. For a given configuration, the power generated by the steam cycle increases if the T-ATR is higher, as syngas cooling produces more steam (for example in the Reference Case, waste heat boiler generates 74.1 kg/s of the HP steam if T-ATR=850°C, 94.5 kg/s if T-ATR=950°C). Anyway net efficiency is 47.37% and 46.87% for a reactor temperature, respectively, of 850°C and 950°C. This is a consequence of the decrease in cold syngas efficiency, which forces to burn a greater fraction of natural gas in the ATR and to increase natural gas consumption. Furthermore, CO₂ to remove is 5% higher when T-ATR=950°C, so CO₂ compression work and steam extraction from the ST are greater. For T-ATR=950°C fuel compressor work rises, too, because the fuel flow rate is 19.5% greater than for T-ATR=850°C. This is due to the different fuel composition, which depends above all on air mass flow needed by ATR, as it determines nitrogen concentration in the fuel and its LHV.

For a given ATR temperature, in SF configurations the ST power is higher than in the Reference Case because maximum steam temperature is 560°C versus 537°C. SF configurations require also less power for fuel compression, as the LHV is higher than in the Reference Case. However, net efficiencies are quite similar for the Reference Case and SF configuration. In fact, even if cold syngas efficiencies are higher in SF configuration, a significant fraction of produced fuel is used for supplementary firing (6.2% of the total). This causes an increase by 2% in natural gas consumption. Furthermore, for a given ATR temperature, removed CO₂ is more in SF configurations than in the Reference Case, therefore, compressor work needed is higher.

In the GAS-GAS configuration all the parameters discussed above seem to be better than in other configurations. In particular, Table 7 clearly shows that:

- CO₂ compressor work is much lower, as carbon dioxide to remove decreases (see also Table 5).
- Fuel compressor work decreases, too, because fuel has the highest LHV.
- Cold syngas efficiency is higher. Therefore natural gas consumption is lower; for example for T-ATR=850°C, the Reference Case shows a cold syngas efficiency of 84.3%, while in the GAS-GAS configuration this parameter is 89.4% (see Table 4). This reduces natural gas input from 17.21 kg/s to 16.22 kg/s.
- Stripping requires less steam extracted from the LP for solvent regeneration because CO₂ absorption requires a lower solvent mass flow (see also Table 5).
- The net power is lower because of the reduction of the steam generated by the waste heat boiler, where syngas enters at a lower temperature.

- However, cycle net efficiency is higher. This is due not only to the reduction of auxiliaries consumption, but also to the increase in cold syngas efficiencies. For T-ATR=850°C net efficiency is 48.06%, for T-ATR=950°C net efficiency is 47.62%.

Since carbon removal has been fixed at 90%, both absolute and specific CO₂ emissions are similar for all the configurations. More precisely, specific emissions are lower in GAS-GAS configuration, where the best efficiency implies an increased power generation relative to natural gas input. However, specific emissions are all in the range 41–42 g/kWh.

The last row in Table 7 shows actual CO₂ reduction; this parameter takes into account the decrease in plant thermodynamic efficiency. In fact, if we assume that a conventional GTCC has a global efficiency of 56%, the cycles analyzed in this paper do not reduce CO₂ emissions by 90%, as they need supplementary natural gas to generate same power as GTCC. Therefore actual CO₂ reduction is the ratio between CO₂ specific emissions of the cycle considered and of GTCC characterized by a thermodynamic efficiency of 56% (approximately 356 g/kWh).

Conclusions

In this paper a gas-steam combined cycle with natural gas reforming and CO₂ capture is presented. An Auto Thermal Reformer has been simulated to generate syngas, whose concentration in hydrogen is increased by two CO-shift reactors in series that follow the ATR. Carbon dioxide is removed in an absorption column, using a blend of most common amines (MDEA, 30% by weight, and DEA, 5%). Lean gas leaving the absorber is characterized by a carbon concentration reduced by 90%. It feeds a commercially available gas turbine and the bottoming steam cycle. Power plant and syngas production plant were coupled and investigated in three main configurations. Among them the most promising scheme is the one with a high-temperature gas-gas heat exchanger, which heats the streams entering ATR and cools syngas at ATR outlet. This configuration showed a global thermal efficiency of 48.06% and CO₂ specific emissions of 41.2 g/kWh.

Acknowledgment

The software ASPEN PLUS® Version 11.1 used in this paper is under license of Aspen Technology, Inc.

Nomenclature

ABS = absorber
 ASU = air separation unit
 ATR = auto thermal reformer
 DEA = di-ethanol-amine
 GT = gas turbine

GTCC = gas turbine combined cycle
 HE = heat exchanger
 HP, LP, MP = high, low, medium pressure level
 HRSG = heat recovery steam generator
 HTS = high-temperature shift
 IGCC = integrated gasification combined cycle
 LHV = low heating value
 LTS = low-temperature shift
 MDEA = methyl-di-ethanol-amine
 MEA = mono-ethanol-amine
 PCFP = pulverized coal-fired plant
 PRE-REF = prereformer
 REF = reference case
 REG = fuel regenerator
 SF = supplementary firing
 SMR = steam methane reformer
 ST = steam turbine
 STP = stripper
 TIT = turbine inlet temperature
 TOT = turbine outlet temperature
 WHB = waste heat boiler
 β = pressure ratio

References

- [1] Keeling, C. D., and Whorf, T. P., 2003, Atmospheric CO₂ Records From Sites in the SIO Air Sampling Network, *Trends: a Compendium of Data on Global Change*, Carbon Dioxide Information Analysis Center, Oak Ridge National Laboratory, U.S. Department of Energy, Oak Ridge, TN.
- [2] IPCC Third Assessment Report: "Climate Change 2001: The Scientific Basis—Contribution of Working Group I to the Third Assessment Report of the Intergovernmental Panel on Climate Change (IPCC)," J. T. Houghton, Y. Ding, D. J. Griggs, M. Noguer, P. J. van der Linden, and D. Xiaosu, eds., Cambridge University Press, UK.
- [3] Desideri, U., and Paolucci, A., 1999, "Performance Modelling of a Carbon Dioxide Removal System for Power Plants," *Energy Convers. Manage.*, **40**(18), pp. 1899–1915.
- [4] Desideri, U., and Proietti, S., 2002, "CO₂ Capture and Removal System for a Gas-Steam Combined Cycle," *Proc. of Int. Mechanical Engineering Congress and Exposition*, November 17–22, New Orleans, LA.
- [5] Chapel, D. G., Mariz, C. L., and Ernest, J., 1999, "Recovery of CO₂ From Flue Gases: Commercial Trends," Originally presented at the Canadian Society of Chemical Engineers Annual Meeting, October 4–6, 1999, Saskatoon, Saskatchewan, Canada.
- [6] Bolland, O., and Mathieu, P., 1998, "Comparison of Two CO₂ Removal Options in Combined Cycle Power Plants," *Energy Convers. Manage.*, **39**(16–18), pp. 1653–1663.
- [7] Korens, N., Simbeck, D. R., and Wilhelm, D. J., 2002, "Process Screening Analysis of Alternative Gas Treating and Sulphur Removal for Gasification," Final Revised Report prepared for US Department of Energy, SFA Pacific, December.
- [8] Pruscek, R., Oeljeklaus, G., Brand, V., Haupt, G., and Zimmermann, G., 1994, GUD Power Plant With Integrated Coal Gasification, CO Shift and CO₂ Washing, POWER-GEN EUROPE '94, Conference Papers, 6, Köln/D, 17–19 May, 1994, pp. 205–225.
- [9] Lozza, G., and Chiesa, P., 2002, "CO₂ Sequestration Techniques for IGCC and Natural Gas Power Plants: A Comparative Estimation of Their Thermodynamic and Economic Performance," *Proc. of the Int. Conference on Clean Coal Technologies*, (CCT2002), Chia Laguna, Italy.
- [10] Audus, H., Kaarstad, O., and Skinner, G., 1998, "CO₂ Capture by Pre-Combustion Decarbonisation of Natural Gas," *Proc. of 4th Int. Conference on Greenhouse Gas Control Technologies*, Interlaken, Switzerland, Aug. 30–Sep. 2, 1998.
- [11] Andersen, T., Kvamsdal, H. M., and Bolland, O., 2000, "Gas Turbine Combined Cycle With CO₂ Capture Using Auto-Thermal Reforming of Natural Gas," ASME Paper 2000-GT-162.
- [12] Kvamsdal, H. M., Ertesvåg, I. S., Bolland, O., and Tolstad, T., 2002, "Exergy Analysis of Gas-Turbine Combined Cycle With CO₂ Capture Using Pre-Combustion Decarbonization of Natural Gas," ASME Paper GT-2002-30411.
- [13] Lozza, G., and Chiesa, P., 2001, "Low CO₂ Emission Combined Cycles With Natural Gas Reforming, Including NO_x Suppression," ASME Paper 2001-GT-0561.
- [14] Dybkjær, Ib., 1995, "Tubular Reforming and Autothermal Reforming of Natural Gas—An Overview of Available Processes," *Fuel Process. Technol.*, **42**, pp. 85–107.
- [15] Audus, H., and Jackson, A. J. B., 2000, "CO₂ Abatement by the Combustion of H₂-Rich Fuels in Gas Turbines," *Fifth Int. Conference on Greenhouse Gas Control Technologies*, Cairns, Australia, August, 13–16.
- [16] Chiesa, P., Lozza, G., and Mazzocchi, L., 2003, "Using Hydrogen as Gas Turbine Fuel," ASME Paper GT-2003-38205.
- [17] Todd, D. M., and Battista, R. A., 2000, "Demonstrated Applicability of Hydrogen Fuel for Gas Turbines," *Proc. of IchemE Gasification 4 Conference*, Noordwijk, Netherlands.
- [18] Aspen Technology Inc., 2000, "Aspen Plus—User Guide. Version 10.2."
- [19] Aspen Technology Inc., 2000, "Aspen Plus—Unit Operation Models. Version 10.2."
- [20] Aspen Technology Inc., 2000, "Aspen Plus—Physical Property Methods and Models. Version 10.2."

CO₂ Emission Abatement in IGCC Power Plants by Semiclosed Cycles: Part A—With Oxygen-Blown Combustion

P. Chiesa

G. Lozza

Dipartimento di Energetica,
Politecnico di Milano,
Piazza Leonardo da Vinci 32,
Milan, 20133, Italy

This paper analyzes the fundamentals of IGCC power plants where carbon dioxide produced by syngas combustion can be removed, liquefied and eventually disposed, to limit the environmental problems due to the "greenhouse effect." To achieve this goal, a semiclosed-loop gas turbine cycle using an highly-enriched CO₂ mixture as working fluid was adopted. As the oxidizer, syngas combustion utilizes oxygen produced by an air separation unit. Combustion gases mainly consist of CO₂ and H₂O: after expansion, heat recovery and water condensation, a part of the exhausts, highly concentrated in CO₂, can be easily extracted, compressed and liquefied for storage or disposal. A detailed discussion about the configuration and the thermodynamic performance of these plants is the aim of the paper. Proper attention was paid to: (i) the modelization of the gasification section and of its integration with the power cycle, (ii) the optimization of the pressure ratio due the change of the cycle working fluid, (iii) the calculation of the power consumption of the "auxiliary" equipment, including the compression train of the separated CO₂ and the air separation unit. The resulting overall efficiency is in the 38–39 percent range, with status-of-the-art gas turbine technology, but resorting to a substantially higher pressure ratio. The extent of modifications to the gas turbine engine, with respect to commercial units, was therefore discussed. Relevant modifications are needed, but not involving changes in the technology. A second plant scheme will be considered in the second part of the paper, using air for syngas combustion and a physical absorption process to separate CO₂ from nitrogen-rich exhausts. A comparison between the two options will be addressed there.

1 Introduction

The increasing concern about climatic changes, due the dispersion in the atmosphere of "greenhouse" gases produced by human activities, poses a formidable challenge to the power industry. Fossil fuels will remain the largest source of primary energy for many decades, according to any reasonable long-term projection. Therefore, carbon dioxide will be largely produced in the future, but its dispersion to the atmosphere can be avoided, provided that it is separated from other combustion products, collected and then ducted to underground storage or to deep sea for absorption. This objective can be pursued by various processes, all requiring a substantial amount of energy (thus reducing the conversion efficiency) and of additional equipment (thus increasing costs). Most studies (including the present paper) were devoted to coal-fired power stations, because coal is (i) the most widely used fossil fuel for power generation, (ii) the most abundant in terms of worldwide resources, (iii) a large CO₂ producer, if compared to natural gas.¹ Three methodologies have been proposed up to now:

- removal of CO₂ from exhausts of conventional power stations, for instance by means of ammine chemical absorption (Smelser et al., 1991), cryogenic distillation (U.S. Department

of Energy, 1993), membrane separation (Van der Sluijs et al., 1992)

- coal gasification followed by catalytic shift, producing CO₂ and H₂ from CO and H₂O: therefore, CO₂ can be separated by relatively low-cost physical absorption systems before being ducted to the gas turbine, which essentially uses hydrogen as fuel (Schütz et al., 1992; Chiesa and Consonni, 1999)
- cycles using enriched CO₂ mixtures as working fluid, usually employing pure oxygen as oxidizer: in this case, after condensation of water produced by combustion, the remaining working fluid is essentially carbon dioxide which can be easily removed and disposed (De Ruycck, 1992; Mathieu and DeRuycck, 1993; Ulizar and Pilidis, 1996, 1997; Chiesa and Lozza, 1997b). Oxygen combustion can be also applied to conventional boilers (Nakayama et al., 1992)

At present, little information is available to fully understand the merits and the drawbacks of each solution. However, according to McMullan et al. (1995), solutions based on gasification and gas turbine-derived cycles are of particular interest. This paper, divided into two parts, will consider two plant configurations: the first one (part A) fully belongs to the third group exposed above, while the second one (part B), using air as oxidizer rather than oxygen and including a physical absorption system to remove CO₂ from moderately enriched exhausts, represents a connection point between the two latter concepts.

The latter plant scheme represents a novel proposal, the former has already been addresses by some of the authors quoted above. We will consider here the power cycle, the complete gasification process, the oxygen production, and the CO₂ separation and compression as a whole, accounting for their interactions. Therefore, we will be able to assess the overall coal-to-electricity conversion

¹ Coal produces about 0.35 kg of CO₂ per kWh of thermal energy (a correct value depends on its actual composition), a figure 70 percent higher than natural gas. In terms of electricity the difference is larger due the higher conversion efficiency obtainable by combined cycles versus steam plants.

Contributed by the International Gas Turbine Institute (IGTI) of THE AMERICAN SOCIETY OF MECHANICAL ENGINEERS for publication in the ASME JOURNAL OF ENGINEERING FOR GAS TURBINES AND POWER. Paper presented at the International Gas Turbine and Aeroengine Congress and Exhibition, Stockholm, Sweden, June 2–5, 1998; ASME Paper 98-GT-384.

Manuscript received by IGTI March 23, 1998; final revision received by the ASME Headquarters June 23, 1999. Associate Technical Editor: R. Kielb.

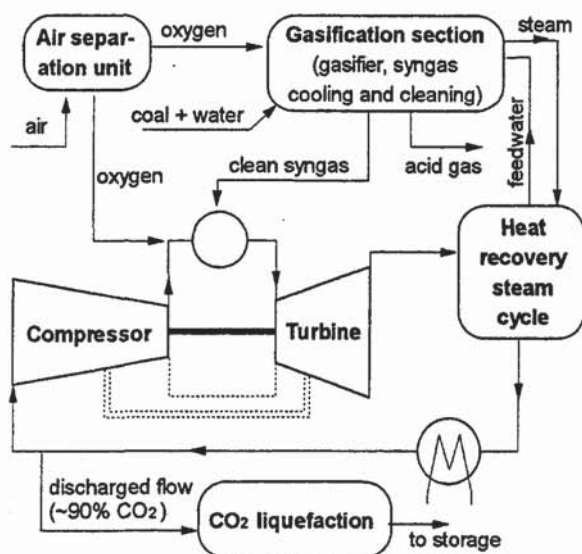


Fig. 1 Conceptual overview of the semiclosed cycle here analyzed, with oxygen combustion

efficiency, in power plants producing CO_2 as a separated stream, available for disposal without further energy expenses.

2 Conceptual Plant Configuration

To better understand the cycle concept here referred (semiclosed cycle with oxygen combustion), let's first consider Fig. 1, showing a very simplified scheme. The blocks of the figure perform the following tasks:

- a complete coal gasification section produces clean syngas from coal under the "usual" conditions of an IGCC plant: therefore, this block consists of a coal treatment plant, a gasifier, a syngas cooling system, and various syngas filtering devices (wet scrubbing, acid gas removal, sulfur plant)
- syngas is burned into the gas turbine combustor using oxygen as the oxidizer: combustion products mainly consist of CO_2 and H_2O
- after turbine expansion and heat recovery steam generator (feeding the steam cycle), combustion gases are cooled to remove H_2O by condensation: the remaining stream is almost pure CO_2 (about 90 percent mass fraction)
- part of this stream, such to conserve the mass balance of the cycle, exits the power cycle; the remainder is recycled, after compression, as a diluting agent to gas turbine combustion
- the stream removed from the cycle is compressed up to liquefaction of CO_2 , rendering it available for storage or disposal
- oxygen necessary to gasification and to syngas combustion is produced by a double-column air-separation-unit (ASU)

Carbon dioxide is the main component of the cycle working medium: the virtual absence of nitrogen in the combustion process leads to negligible NO_x formation, while sulfur is very efficiently captured in the IGCC process. Therefore, being CO_2 sequestered, the plant is virtually free of any kind of air pollution.

Before addressing with more detail the plant configuration, let us recall briefly the main features of the method of calculation used for predicting the on-design overall performance and the energy balance of the plant. It was described in previous papers, with reference to the gas turbine model (Macchi et al., 1991; Consonni, 1992), the steam plant model (Lozza, 1990), and the system used to analyze gasification processes (Lozza et al., 1996). Its main features are (i) capability of reproducing very complex plant schemes by assembling basic modules, such

as turbine, compressor, combustor, steam section, chemical reactor, heat exchanger, etc., (ii) built-in correlations for efficiency prediction of turbomachines, as a function of their operating conditions, (iii) built-in correlations for predicting cooling flows of the gas turbine, and (iv) calculation of gas composition at chemical equilibrium. A peculiarity of the present method is its ability to reproduce a whole IGCC process in a single computer run, without any need of "matching" results coming from different computational tools: it enables the possibility of studying heavily integrated processes and of performing a complete second law analysis of the entire plant. To preserve this peculiarity, a new module was added to consider the compression of a gas mixture in which CO_2 is treated as a real gas (including phase change). Therefore, ideal gas behaviour is assumed for all gaseous species, with the exceptions of water/steam in the steam cycle module and of carbon dioxide during its final compression and liquefaction. More details are given in 3.4.

The assumptions used for calculating the performance of the various components are fully reported in a recent paper (Chiesa and Lozza, 1997a). During the next chapter, we will recall and discuss the most important assumptions for each plant section.

3 Detailed Plant Description and Assumptions

Once discussed the basics, a deeper understanding of the plant configuration is necessary to perform a comprehensive thermodynamic analysis. Figure 2 provides a complete overview of the various plant sections and of their interaction. Let us now discuss the arrangement of the various blocks, by outlining the main assumptions necessary to calculate their performance.

3.1 Air Separation Unit. We will refer to conventional ASU processes, consisting of an air intercooled compressor (exit pressure was assumed as 4.8 bar, according to Rao (1993), compatible with a 95 percent oxygen purity in large plants) and of a double separation column providing gaseous nitrogen (dispersed to the ambient) and gaseous oxygen at near-atmospheric pressure. Oxygen must be compressed before being used: we stipulated a maximum oxygen temperature of 340°C ,² so the compression has to be partly intercooled. Due to the large oxygen requirement, the air compressor is directly driven by the gas turbine, to save expensive electric machinery and related power losses. Other ASU arrangements, sometimes found in IGCC plants (Smith et al., 1996), making use of compressed air from the gas turbine compressor, are not feasible here, due to the lack of oxygen in the cycle working fluid. The air compressor efficiency is relevant to the overall power balance: being its volume flow compatible with axial multi-stage machines, the general correlation for compressor polytropic efficiency estimation developed by the authors (Chiesa et al., 1995) was used.

3.2 Gasification Section. In this paper we will refer to an entrained-flow slurry-feed gasifier, reproducing the Texaco technology. Coal used is Illinois #6, with 3.4 percent sulfur content. The thermal input to the plant was set to $900 \text{ MW}_{\text{th}}$ (36.25 kg/s of coal with $\text{LHV} = 24.826 \text{ MJ/kg}$). Gasification pressure and temperature were assumed of 60 bar and 1600 K. Oxygen supply was calculated to actually obtain such a temperature with a gas composition imposed by the chemical equilibrium, considering a water/coal ratio in the slurry of 0.323. Raw syngas is cooled by radiative-convective syngas coolers, producing high pressure saturated steam and high temperature feedwater, the latter partly used to rise the temperature of clean syngas before combustion. Raw syngas is therefore cleaned by a wet scrubber. Low temperature

² The higher the temperature of oxygen for both combustion or gasification, the lower the fuel consumption to obtain the same combustion products. This overrides the larger compression work, increasing the cycle efficiency. However, a conservative value of oxygen temperature was stipulated to reduce hazards and risks of material corrosion.

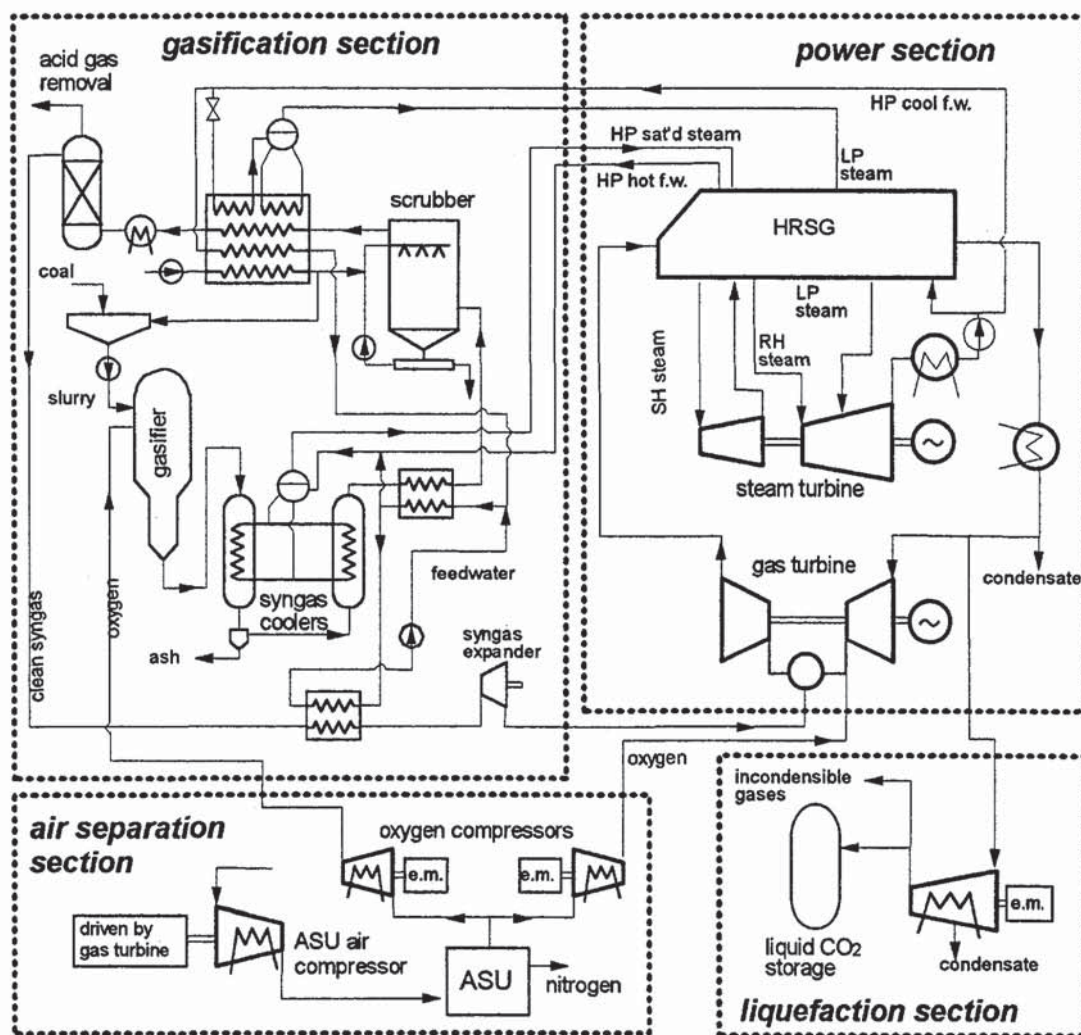


Fig. 2 Complete plant configuration of the semiclosed cycle with oxygen combustion here discussed

heat is recovered from syngas for various purposes (feedwater heating, make-up water heating, low pressure steam generation). Acid gases are removed from near-ambient temperature syngas and then treated to produce sulphur by means of processes well known in the IGCC practice. Clean syngas is preheated by the above quoted feedwater supply and therefore expanded, depending on the combustion pressure. Details on the calculation method and on the assumptions (heat exchangers effectiveness, pressure and thermal losses, etc.) have been quoted in previous papers (Lozza et al., 1996; Chiesa and Lozza, 1997a).

For this application, we did not consider any fuel dilution strategy for NO_x abatement (i.e., by moisturization or by nitrogen addition) due to the very low nitrogen concentration in the combustion region.

3.3 Power Plant. A semiclosed-cycle gas turbine is the key machine. Assumptions regarding its performance prediction (i.e., compressor and turbine polytropic efficiency, coolant requirement and cooled expansion modelization, pressure losses, etc.) have been calibrated during previous works (Macchi et al., 1991; Chiesa et al., 1995; Chiesa and Lozza, 1997a) to accurately reproduce the performance of modern gas turbines. We will make here reference to the today's proven technology of "F" industrial gas turbines: in particular, a TIT of 1280°C was stipulated for all considered solutions. In those conditions, a comparison between manufacturers' data and our predictions (with natural gas as fuel) shows a

very close agreement,³ confirming the reliability of the correlations when applied to open cycles.

We supposed here that the change of the working fluid will not affect the validity of the correlations used for calculating turbomachinery polytropic efficiency and cooling requirements of the hot parts of the turbine (Consonni, 1992; Chiesa et al., 1995). To be more clear, this does not mean that cooling flows and efficiencies remain constant between open and semiclosed cycle: the parameters governing the correlations are recalculated according to the actual values of volumetric flow, transport properties, etc.

However, the change of the working fluid claims for a novel optimization of the cycle. The most important parameter to be considered is the pressure ratio: the higher molecular mass and complexity of CO_2 mixtures versus air results in a lower temperature rise at the same pressure ratio. Since cycle performance mainly depends on the temperature history of the fluid, an higher pressure ratio will be required to obtain the same efficiency. To discuss this issue, the pressure ratio will be varied during the analysis from the basic value of 15, typical of large industrial "F" machines.

A possible variation to the scheme shown in Fig. 2 consists of

³ For instance, calculations of the GE Fr.9FA with a TIT of 1288°C (Miller, 1996) show an error as low as 0.3 percent on power output, 0.3 points on efficiency, 2°C on turbine outlet temperature.

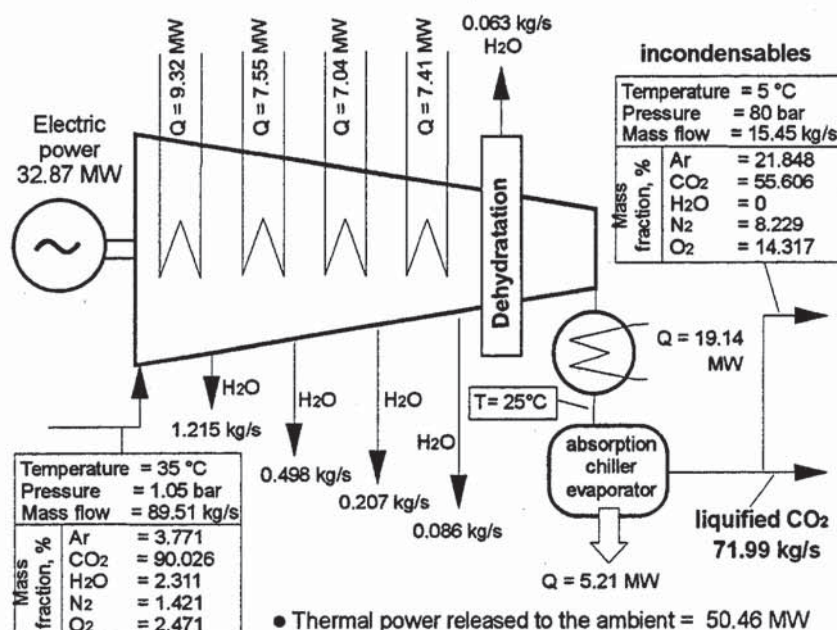


Fig. 3 Energy and mass balance of the carbon-dioxide compression/liquefaction train used for scheme A. Data are referred to a cycle pressure ratio of 30, with a thermal input of 900 MW (coal LHV).

moving the oxygen injection point from the compressor outlet to the compressor suction. In this mode, oxygen compression is performed by the same gas turbine compressor, rather than by a separated unit, with higher efficiency and lower plant complexity. However, the cooling flows, retrieved from the compressor, are enriched in oxygen, providing a lower CO₂ concentration in the exhausts: this increases the energy requirement for both air separation and CO₂ liquefaction. This issue was discussed in a previous paper (Chiesa and Lozza, 1997), showing a negligible influence on the overall efficiency, and will not be addressed further here.

The heat recovery steam cycle is a conventional combined cycle unit, based on a three-pressure reheat cycle. The method of calculation of the bottoming cycle and its optimization have been addressed by Lozza (1990 and 1993). Steam conditions here assumed are rather conservative: the maximum pressure is 110 bar, with SH and RH at 538/538 °C and a condensing pressure of 0.05 bar. A somewhat better efficiency may be obtained by resorting to more elevated steam conditions (for instance, slightly supercritical pressure and 565 or 580 °C, according to the above quoted papers and to the better steam technology): we decided here not to stress the technological issues in an already complicated and risky plant configuration. It must be also considered that the here adopted values are rather common even in the more advanced natural gas and coal gasification combined cycle presented up to now.

3.4 Carbon Dioxide Liquefaction. We will assume here that separated carbon dioxide must be available at the plant boundaries at a pressure of at least 80 bar and in liquid phase. This is necessary to allow for deep sea disposal without further energy expenses. The exhaust stream retrieved from the cycle can be simply compressed to achieve this goal. However, incondensable species (N₂, O₂, Ar) are present in this stream, increasing the compression power. Their amount depends on various parameters: (i) the above quoted position of the oxygen injection point, (ii) the oxygen purity, and (iii) the oxygen exceeding the stoichiometric combustion to ensure complete fuel oxidation. According to our calculations, an increase of the oxygen purity (beyond the assumed value of 95 percent) will require an higher ASU consumption, vanishing the savings in the liquefaction process. A 3 percent oxygen concentration by volume after combustion was stipulated,

believing it sufficient to make CO production negligible. In addition to incondensables, water vapour is also present: its initial amount depends on the water partial pressure in the exiting stream, and particularly on its temperature, here assumed as 35 °C after cooling of the entire exhaust flow. Under those assumptions, the exhaust composition is fixed and reported in Fig. 3, showing the energy and mass balance of the liquefaction system. Water is separated by condensation and by dehydration.

To improve CO₂ removal efficiency, the gaseous CO₂ fraction in the incondensables (wasted to the ambient) should be minimized. To achieve this goal, two ways are possible: (i) increasing the final pressure, thus the energy consumption; (ii) cooling down the stream. The compression train shown in Fig. 3 includes an absorption refrigerating unit, to obtain a final temperature of 5 °C: the same removal efficiency (89.4 percent) would have required a final pressure of 132 bar (rather than 80) at 25 °C, with a 10 percent higher power consumption. Low temperature heat needed by the absorption chiller (about 8 MW_{th}) can be easily retrieved from the compression train intercoolers without significant energy expenses. A further improvement of removal efficiency is possible: for instance, 96 percent can be achieved with a final pressure of 145 bar, requiring about 37 rather than 33 MW_e (approximately a 1 percent reduction of the plant net output).

About thermodynamic properties, the ideal gas assumption used for the power cycle cannot be realistic here. CO₂ properties were calculated by the corresponding state law (acentric factor = 0.239, Reid et al., 1988) with saturation curve from Casci et al. (1972). H₂O properties from Schmidt, 1982 (as used for the steam cycle). We assumed (i) ideal mixtures (i.e., mixing does not alter volumetric properties), (ii) Ar, N₂, O₂ as ideal gases, (iii) negligible liquid solubility in gases, and (iv) H₂O and CO₂ condensation rates according to the Raoult law.

4 Overall Plant Performance

4.1 General Overview. The results of the performance prediction are shown in Fig. 4 for various cycle pressure ratios. In the figure, two efficiency curves are shown: the upper dotted curve does not consider the power expenses for compression-

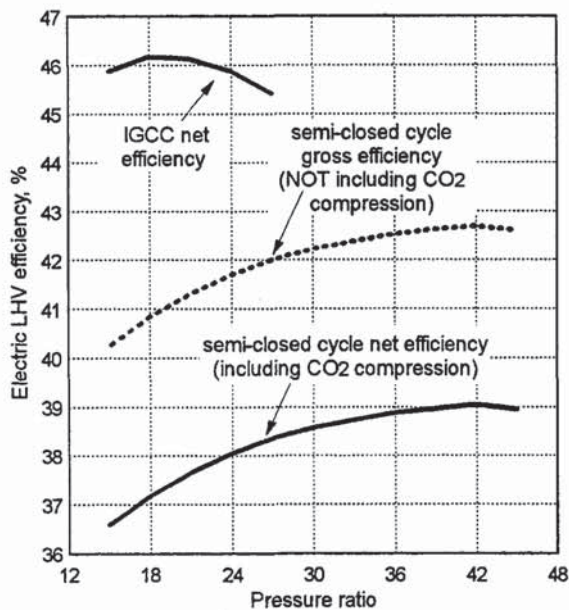


Fig. 4 Influence of the cycle pressure ratio on the efficiency of IGCC and semiclosed cycles

liquefaction of carbon dioxide, the lower curve represents the overall net plant efficiency. In addition, Fig. 4 quotes, as a reference, the performance of IGCC cycles based on the same gasification and power cycle technology, but not including any CO_2 removal strategy.

The loss of efficiency resulting from the adoption of CO_2 capture systems is severe, from about 46 percent of IGCC to about 39 percent at optimum pressure ratio. We can justify the efficiency decay by the following three considerations:

(i) CO_2 separation itself yields to a power loss, even if carried out by a reversible process and even if the separated gases would be available at ambient pressure, rather than pressurized. The production of separated species is, as a matter of facts, another "thermodynamic asset" (in addition to electricity) generated by the cycle. Its value corresponds to the mechanical work required by the reversible separation (isothermal compression from the partial to the total pressure). Referring to the IGCC exhausts ($\beta = 15$), this work is 196.4 kJ/kg of CO_2 (90 percent removal efficiency), yielding to 14.1 MW consumption: this brings the efficiency of an IGCC with ideal separation to 44.3 percent versus the original 45.9 percent.

(ii) CO_2 is compressed up to 80 bar, by means of a real machine: therefore, ideal isothermal compression work plus losses due to irreversibilities during the process are to be considered. This power consumption corresponds, in terms of efficiency loss, to the "distance" between the continuous and the dotted line of Fig. 4.

(iii) Another relevant source is related to the large oxygen consumption, here about 2.6 times the one of an IGCC. Irreversibilities of the ASU process are therefore much more detrimental to the overall efficiency. In fact, the air separation unit requires 868 kJ/kg of oxygen produced (under our assumptions), rather than 197 needed by a reversible process.

4.2 Influence of the Cycle Pressure Ratio. The above mentioned losses are largely independent on the power cycle thermodynamics. As far as this issue is concerned, the most important parameter is the pressure ratio (β) of the gas turbine cycle. Its influence is clearly shown in Fig. 4. The best performance of an IGCC plant is obtained at $\beta = 18$: the use of a lower pressure ratio of 15 (often found in large commercial heavy-duties) does not impair the plant efficiency in a significant way. On the contrary, the present scheme requires a much larger pressure ratio: the best

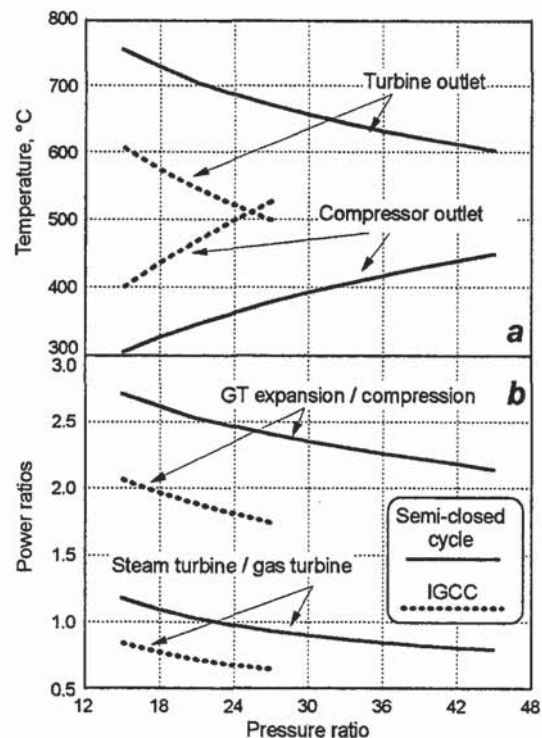


Fig. 5 Turbine and compressor outlet temperatures, expansion/compression and steam/gas turbine power ratios for IGCC and semiclosed cycles, as a function of the pressure ratio

value is 42, while 2.4 points of efficiency would be lost at $\beta = 15$. The reason of this discrepancy is the change of the working fluid composition, i.e., the increase of the molecular mass due to higher CO_2 content. In fact, Fig. 5(a) shows that, at the same pressure ratio, the CO_2 cycle presents consistently lower compressor outlet temperature and higher turbine outlet temperature: higher pressure ratios are therefore required to optimize the cycle, obtaining the same temperature levels found in IGCC and gas turbine practice. More information is given by Fig. 5(b): the power ratios between plant components indicate that, at the same β , more percentage power is produced by the steam turbine and less percentage power is consumed by the compressor. This is not favourable: for instance, at $\beta = 15$ a turbine outlet temperature of about 750°C would lead to substantial heat transfer irreversibilities in feeding heat to the steam plant, unable to operate efficiently at high temperatures, while a low compressor outlet temperature of 300°C, even if reducing compressor power consumption, improves combustion irreversibilities. At the optimum pressure ratio, both temperature and power ratios are similar to the ones of IGCCs.

In this discussion, the minimum cycle pressure was kept at near-atmospheric values, but it can be subject of optimization in a semiclosed cycle. We will address this issue in the second part of the paper, together with the cycle proposal discussed there.

4.3 Discussion of the "Reference" Scheme. In the following we will make reference to a pressure ratio of 30, as a compromise between performance and utilization of existing technologies ($\beta = 30$ is already used by aero-derived engines and by a modern reheat industrial unit). A pressure ratio of 15 was assumed for the IGCC case used for comparisons. The main characteristics of the selected plant are shown in Fig. 6. Together with information provided by Fig. 3 and by Table 1, reporting the electric power balance, we can comment that:

— the ASU air compressor has an inlet volume flow of 267 m³/s, versus 328 of the cycle compressor: the two machines have a comparable size, justifying their single-shaft arrangement

Table 2 Specifications involved in turbomachinery design, for the reference IGCC and semi-closed cycle

Plant type (input = 900 MW by coal LHV)	Open IGCC, $\beta=15$	Semi- closed, $\beta=30$
Gas turbine compressor		
Inlet volume flow, m ³ /s	507.9	328.3
Inlet/outlet volume flow ratio	7.262	15.975
Isentropic enthalpy rise, kJ/kg	337.9	305.5
ASU air compressor		
Inlet volume flow, m ³ /s	103.2	266.9
Real compression work, kJ/kg	176.7	169.4
CO₂ compressor		
Inlet volume flow, m ³ /s	-	52.34
Real compression work, kJ/kg	-	335.6
Gas turbine		
Outlet volume flow, m ³ /s	1633.9	1182.5
Turbine outlet / compressor inlet volume flow	3.217	3.602
First nozzle throat area, m ²	0.4433	0.1817
Turbine inlet / compressor inlet volume flow	0.351	0.1827
Isentropic enthalpy drop (cooled expansion), kJ/kg	1062	974.2
First nozzle cooling flow / gas flow (volume)	0.0256	0.0309
First rotor cooling flow / gas flow (volume)	0.0243	0.0265

it is a very conventional unit. The CO₂ compressor is an unconventional machine, but its development should not present particular technological issues.

6 Conclusions

The discussion here developed outlines the negative impact of CO₂ removal on the conversion efficiency and on the plant complexity, compared to the already capital-intensive and complicated IGCC stations. On another side, a virtually emission-free power production from coal can be realized, resorting to well-known technologies, with an efficiency very similar to the one of conventional steam power stations. A realistic economic study cannot be drawn at present, due to the difficulties of estimating the investment costs of components not available in the market. Among them, critical issues are the modified gas turbine, operating with an enriched CO₂ mixture, and the unusually large air separation unit. The necessity of adopting such components can be eliminated by using air rather than oxygen for syngas combustion and by introducing a separation process. The second part of the paper will discuss this concept and a comparison between the two plants, together with some final considerations, will be addressed.

References

Casati, C., Macchi, E., and Angelino, G., 1972, "Thermodynamic Properties of Carbon Dioxide," Tamburini Editore, Milan, Italy, (in Italian).

Chiesa, P., Lozza, G., Macchi, E., and Consonni, S., 1995, "An Assessment of the Thermodynamic Performance of Mixed Gas-Steam Cycles. Part A: Intercooled and Steam-Injected Cycles. Part B: Water-Injected and HAT Cycles," ASME JOURNAL OF ENGINEERING FOR GAS TURBINES AND POWER, Vol. 117, pp. 489-508.

Chiesa, P., and Lozza, G., 1997a, "Intercooled Advanced Gas Turbines in Coal Gasification Plants, with Combined or "HAT" Power Cycle," ASME Paper 97-GT-039.

Chiesa, P., and Lozza, G., 1997b, "Coal Power Plants with Semi-Closed Combined Cycle for CO₂ Removal: A Preliminary Study," Proceedings IX National Congress *Tecnologie e Sistemi Energetici Complessi—Sergio Stecco*, Milan, Italy, pp. 165-181, (in Italian).

Chiesa, P., and Consonni, S., 1999, "Shift Reactors and Physical Absorption for Low-CO₂ Emission IGCCs," ASME JOURNAL OF ENGINEERING FOR GAS TURBINES AND POWER, Vol. 121, pp. 295-305.

Consonni, S., 1992, "Performance Prediction of Gas/Steam Cycles for Power Generation," Ph.D. thesis n. 1893-T, MAE Dept., Princeton University, Princeton, NJ. De Ruick, J., 1992, "Efficient CO₂ Capture Through a Combined Steam and CO₂ Gas Turbine Cycle," *Energy Convers. Mgmt.*, Vol. 33, pp. 397-404.

Lozza, G., 1990, "Bottoming Steam Cycles for Combined Gas-Steam Power Plants: A Theoretical Estimation of Steam Turbine Performance and Cycle Analysis," Proceedings, 4th ASME Cogen-Turbo, New Orleans, LA, pp. 83-92.

Lozza, G., 1993, "Steam Cycles for Large-Size High-Gas-Temperature Combined Cycles," Proceedings, 1993 ASME Cogen-Turbo Power Symposium, Bournemouth, UK, pp. 435-444.

Lozza, G., Chiesa, P., and DeVita, L., 1996, "Combined Cycle Power Stations Using Clean-Coal-Technologies: Thermodynamic Analysis of Full Gasification versus Fluidized Bed Combustion With Partial Gasification," ASME JOURNAL OF ENGINEERING FOR GAS TURBINES AND POWER, Vol. 118, pp. 737-748.

Macchi, E., Bombarda, P., Chiesa, P., Consonni, S., and Lozza, G., 1991, "Gas-Turbine-Based Advanced Cycles for Power Generation. Part A: Calculation Model. Part B: Performance Analysis of Selected Configurations," Proceedings, 1991 Yokohama Int'l Gas Turbine Congress, Vol. III, Yokohama, Japan, pp. 201-219.

Mathieu, P., and De Ruick, J., 1993, "CO₂ Capture in CC and IGCC Power Plants Using a CO₂ Gas Turbine," IGTT-Vol. 8 ASME Cogen-Turbo, ASME, New York.

McMullan, J. T., Williams, B. C., Campbell, P., Mellvee-Wright, D., and Berntgen, J. M., 1995, "Techno-Economic Assessment Studies of Fossil Fuel and Fuel Wood Power Generation Technologies," in "R&D in Clean Coal Technology," Report to the European Commission, Bruxelles, Belgium.

Miller, H. E., 1996, "F" Technology—the First Half-Million Operating Hours," GE Company Report GER-3950, Schenectady, NY.

Nakayama, S., Noguchi, Y., Kiga, T., Miyamae, S., Maeda, U., Kawai, M., Tanaka, T., Koyata, K., and Makino, H., 1992, "Pulverized Coal Combustion in O₂/CO₂ Mixtures on a Power Plant for CO₂ Recovery," *Energy Convers. Mgmt.*, Vol. 33, pp. 379-386.

Rao, A. D., et al., 1993, "HP Integrated versus Non-Integrated ASU in Destec IGCC," Proceedings, Twelfth EPRI Conference on Gasification Power Plants, San Francisco, CA.

Reid, R. C., Prausnitz, J. M., and Poling, B. E., 1988, *The Properties of Gases and Liquids*, 4th ed., McGraw-Hill, New York.

Schmidt, E., 1982, *Properties of Water and Steam in S.I. Units*, Springer-Verlag, Berlin.

Schütz, M., Daun, M., Weinspach, P. M., Krumbeck, M., and Hein, K. R. G., 1992, "Study on the CO₂-Recovery From an IGCC Plant," *Energy Convers. Mgmt.*, Vol. 33, pp. 357-364.

Smelser, S. C., Stock, R. M., and McCleary, G. J., 1991, "Engineering and Economic Evaluation of CO₂ Removal From Fossil-Fuel-Fired Power Plants—Volume 1 Pulverized-Coal-Fired Power Plants," EPRI Report IE-7365.

Smith, A. R., Klosek, J., and Woodward, D. W., 1996, "Next-Generation Integration Concepts for Air Separation Units and Gas Turbines," ASME Paper 96-GT-144.

Ulizar, I., and Pilidis, P., 1996, "A Semiclosed Cycle Turbine with Carbon Dioxide-Argon as Working Fluid," ASME Paper 96-GT-345.

Ulizar, I., and Pilidis, P., 1997, "Design of a Semiclosed Cycle Gas Turbine with Carbon Dioxide—Argon as Working Fluid," ASME Paper 97-GT-125.

U.S. Department of Energy, 1993, "The Capture, Utilization and Disposal of Carbon Dioxide from Fossil Fuel-Fired Power Plants," U.S. Department of Energy Report, Contract DE-FG02-92ER30194.

Van der Sluijs, J. P., Hendriks, C. A., and Blok, K., 1992, "Feasibility of Polymer Membranes for Carbon Dioxide Recovery from Flue Gases," *Energy Convers. Mgmt.*, Vol. 33, pp. 429-436.

CO₂ Emission Abatement in IGCC Power Plants by Semiclosed Cycles: Part B—With Air-Blown Combustion and CO₂ Physical Absorption

P. Chiesa

G. Lozza

Dipartimento di Energetica,
Politecnico di Milano,
Piazza Leonardo da Vinci 32,
Milan, 20133, Italy

This paper analyzes the fundamentals of IGCC power plants with carbon dioxide removal systems, by a cycle configuration alternative to the one discussed in Part A (with oxygen-blown combustion). The idea behind this proposal is to overcome the major drawbacks of the previous solution (large oxygen consumption and re-design of the gas turbine unit), by means of a semiclosed cycle using air as the oxidizer. Consequently, combustion gases are largely diluted by nitrogen and cannot be simply compressed to produce liquefied CO₂ for storage or disposal. However, CO₂ concentration remains high enough to make separation possible by a physical absorption process. It requires a re-pressurization of the flow subtracted from the cycle, with relevant consequences on the plant energy balance. The configuration and the thermodynamic performance of this plant concept are extensively addressed in the paper. As in the first part, the influence of the pressure ratio is discussed, but values similar to the ones adopted in commercial heavy-duty machines provide here acceptable performance. Proper attention was paid to the impact of the absorption process on the energy consumption. The resulting net overall efficiency is again in the 38–39 percent range, with assumptions fully comparable to the ones of Part A. Finally, we demonstrated that the present scheme enables the use of unmodified machines, but large additional equipment is required for exhausts treatment and CO₂ separation. A final comparison between the two semiclosed cycle concepts was therefore addressed.

1 Introduction

The separation of carbon dioxide from exhausts of power plants, followed by its disposal into underground cavities or by deep sea dispersion, can represent a significant contribution to reduce the concerns about climatic changes, due to the dispersion in the atmosphere of “greenhouse” gases produced by human activities. However, carbon dioxide concentration is rather poor in combustion products: from 4 percent in a natural gas-fired gas turbine, to 8 percent in an IGCC plant, to 12 percent in a conventional coal-fired boiler (all values, expressed by volume, are indicative). Therefore, to avoid processing huge gas flows with large energy consumption, carbon dioxide removal claims for measures to improve its concentration. The most radical solution is to use CO₂ as the main component of the working fluid in a semiclosed gas turbine cycle. It was the subject of the Part A of this paper and, as we discussed, such a solution requires pure oxygen for combustion and substantial modifications to the existing gas turbine engines. Now we will consider semiclosed cycles in which air is used as the oxidizer, characterized by a moderate CO₂ enrichment (about 20 percent by volume) and thus requiring a separation process.

The basic concept of the cycle is reported in Fig. 1. It includes a complete coal gasification section and a combined cycle power plant, similarly to the scheme discussed in part A (in the followings, we will shortly address the oxygen-blown plant of part A as

“scheme A” and the present air-blown plant as “scheme B”). Differently from scheme A, oxygen, produced by an air separation unit (ASU), is supplied to the gasification section only. Ambient air enters the cycle to provide the minimum amount of oxidizer necessary to the syngas combustion process. Part of exhaust gases are recycled to the compressor, acting as diluting agent to obtain the desired turbine inlet conditions, rather than excess air as in open cycle gas turbines. As anticipated, exhausts are moderately enriched by carbon dioxide: the fraction exiting the cycle can be treated to remove CO₂ by a physical absorption process. Eventually, CO₂ is compressed and liquefied for disposal, while the remaining components of exhausts (mainly nitrogen) are dispersed toward the ambient.

The paper will firstly address the plant arrangement and the solutions found for the physical separation process. Then we will discuss its performance prediction, based on the same calculation method and assumptions reported in Part A, and we will finally address a comparison between the solutions presented in the two parts of this paper.

2 Detailed Plant Configuration

2.1 IGCC Sections. Figure 2 provides a complete overview of the various plant sections and of their interactions. The sections typical of IGCC plants are rather similar to the ones described in chapter 3 of Part A, and the assumptions used during the calculation are unchanged. In particular:

Air Separation Unit. As for scheme A, we will refer to a conventional ASU process, consisting of an intercooled air compressor and of a double separation column. The only difference is size, since the oxygen consumption of scheme A is 2.6 times the

Contributed by the International Gas Turbine Institute (IGTI) of THE AMERICAN SOCIETY OF MECHANICAL ENGINEERS for publication in the ASME JOURNAL OF ENGINEERING FOR GAS TURBINES AND POWER. Paper presented at the International Gas Turbine and Aeroengine Congress and Exhibition, Stockholm, Sweden, June 2–5, 1998; ASME Paper 98-GT-385.

Manuscript received by IGTI March 23, 1998; final revision received by the ASME Headquarters June 23, 1999. Associate Technical Editor: R. Kielb.

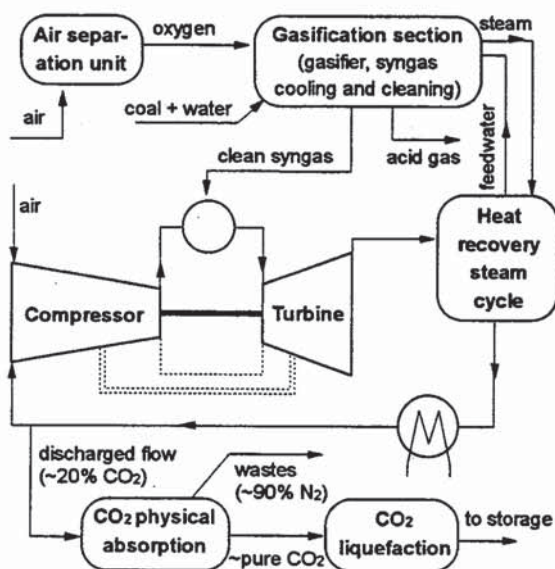


Fig. 1 Conceptual overview of the air-blown semiclosed cycles here analyzed, with physical absorption of CO₂

one of the present scheme. The reduced power consumption of the air compressor allows for an electric motor drive rather than direct drive by the gas turbine.

Gasification Section. We will refer again to an entrained-flow slurry-feed gasifier, reproducing the Texaco technology, with the same coal feedstock (Illinois #6) and gasification pressure and temperature (60 bar, 1600 K). The gasification section is mostly unchanged between scheme A and B. However, comparing Figs. 2 of part A and part B, two important differences can be outlined: (i) in scheme B, the convective syngas cooler, in addition to rising saturated HP steam, provides heat to the nitrogen stream exiting the absorption unit, before its expansion (see 2.2); (ii) a syngas saturator was introduced into scheme B, to contribute to NO_x abatement by fuel moisturization: warm water for saturation is produced from low temperature syngas cooling, substituting low pressure steam generation of scheme A. The adoption of NO_x control strategies requires some comment. It was unnecessary in scheme A, due to the virtual absence of nitrogen in the gas turbine combustion chamber. Here, nitrogen is abundantly present and fuel dilution by inert agents is advisable, even if not strictly necessary. Water saturation is a very effective method, not really affecting the efficiency, because of the correct thermodynamics of the process. On the contrary, the use of nitrogen as an inert diluent (available in the plant at sufficient pressure after the separation process) is not convenient, since it reduces the carbon dioxide fraction in the exhausts, increasing the CO₂ separation duty.

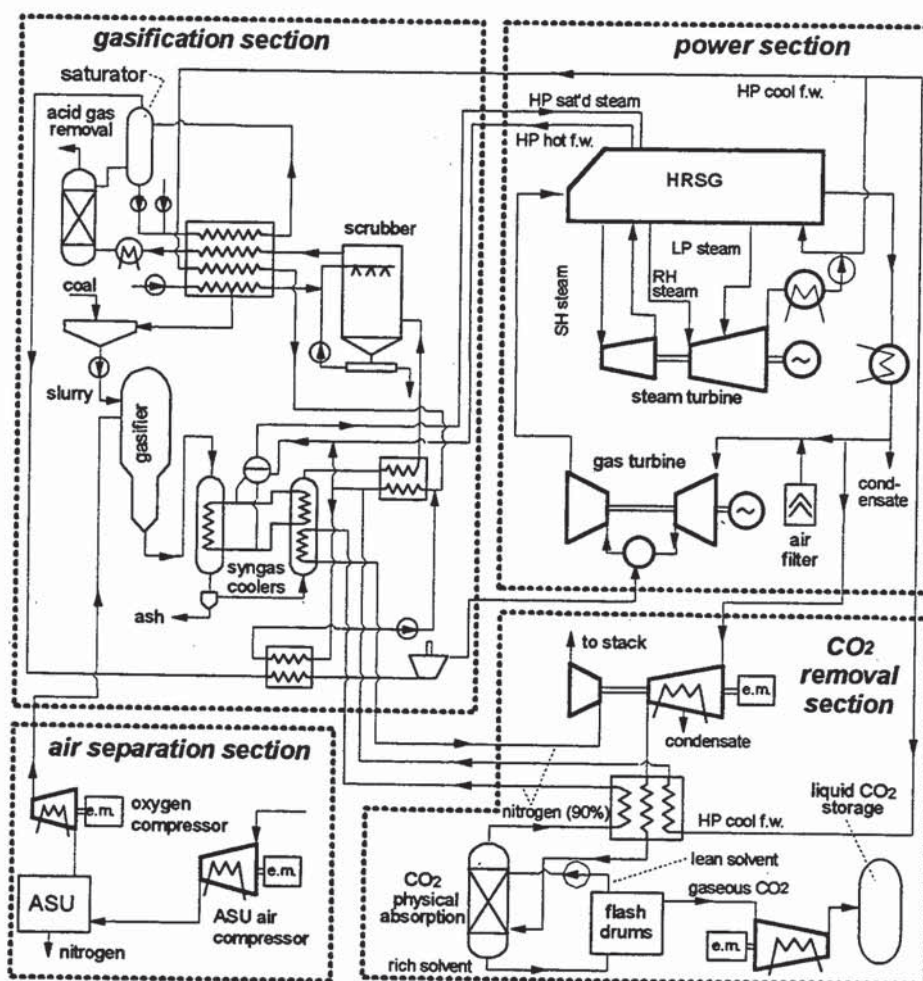


Fig. 2 Plant configuration of the semiclosed cycle with air-blow combustion (scheme B)

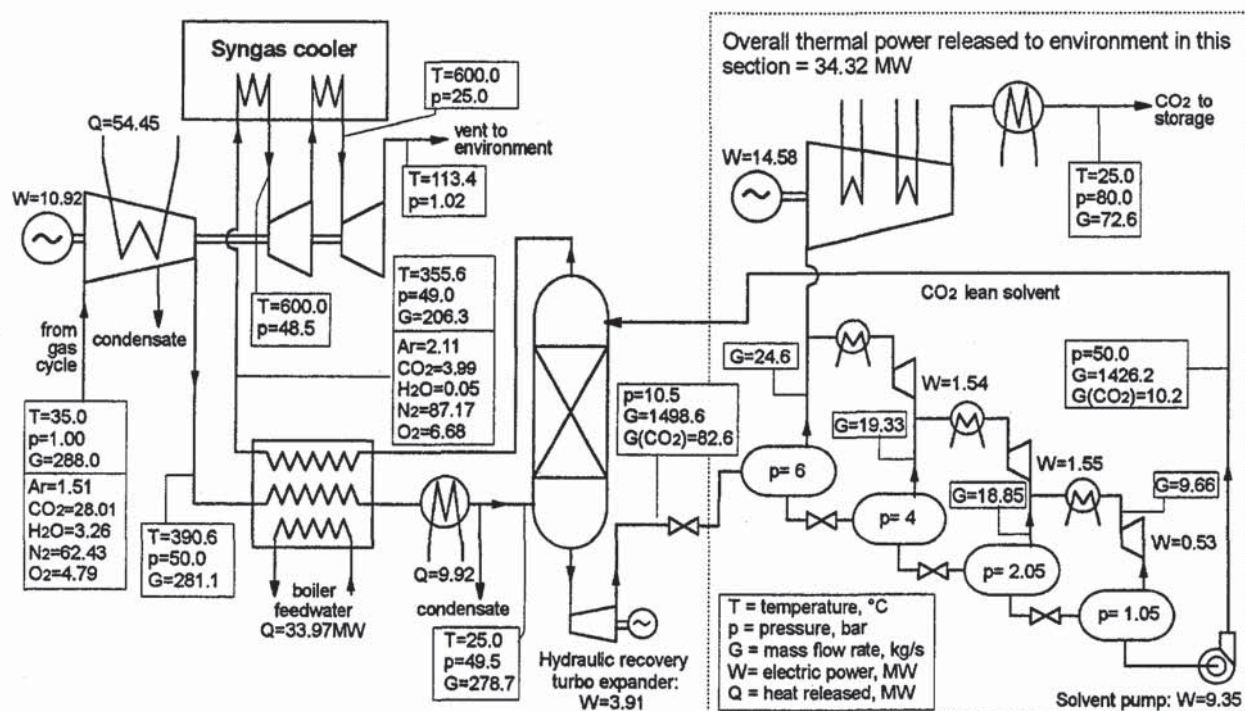


Fig. 3 Energy and mass balance of the carbon-dioxide physical separation process, including the compression/liquefaction train, for a cycle pressure ratio of 15 and a thermal input of 900 MW (LHV). Gas compositions in mass percentage fraction.

Power Plant. Apart from the change of the working fluid composition, no conceptual modifications are introduced from scheme A, both for the gas turbine technology (adopting a TIT of 1280°C as in "F" industrial machines) and for the heat recovery steam cycle. It can be anticipated that, in the present case, the composition of the fluid evolving within the semiclosed cycle is much more similar to the one of open cycle gas turbines: as we will discuss later, this allows for minimal modifications to the engine with respect to market-available units.

2.2 Carbon Dioxide Separation. The major differences between scheme A and B are concentrated in the treatment of the stream retrieved from the gas turbine. For scheme A a simple mechanical compression process was sufficient to make CO₂ available at the liquid state and at a pressure necessary for disposal without further energy expenses (here stipulated as 80 bar). For scheme B, the situation is much more complicated, since carbon dioxide must be separated from nitrogen-diluted exhausts.

CO₂ separation from gaseous mixtures can be carried out by means of different processes: among them, the most common ones are chemical and physical absorption (Kohl and Riesenfeld, 1985). In the first process capture of CO₂ is mainly due to chemical bonds created in the adsorber between CO₂ and solvent (usually aqueous solutions of ethanol-ammines). CO₂ is then stripped from solvent by breaking the chemical bonds and, since this operation is endothermic, large amounts of thermal energy are required for its accomplishment. On the contrary physical absorption relies upon the selective solubility of gases into a solvent and upon its variation with pressure: CO₂ is absorbed in the solvent at high pressure within a counter-current packed tower and then released by reducing the pressure of the CO₂-rich solvent stream. In this case, since CO₂ is removed from a mixture largely diluted with N₂, the solvent has to present a much larger solubility for the former substance compared to the latter one. The Selexol solvent, commercialized by Union Carbide, results very suitable for the purpose since, for the same partial pressure and temperature, about 0.01 mols of N₂ are captured for each mol of CO₂ (Bucklin and Schendel, 1984).

The theoretical energy requirement is relatively low (power for

pumping the solvent stream and for recompression of the separated gas), compared to the large low temperature heat requirement of chemical absorption processes. This does not imply any evaluation of chemical versus physical absorption, being the thermodynamic value of power and heat very different: chemical absorption can be the subject of future works.

Figure 3 shows the complete plant arrangement of the physical separation section (quoted values refer to the "reference" case described later). The operating pressure of the absorption tower depends on pressure selected for the last flash drum and on CO₂ concentration in the exhausted gaseous stream (i.e., CO₂ removal efficiency). In fact the former parameter brings about the purity of the solvent introduced at the top of the column; according to this purity, a minimum pressure can be determined to achieve the required CO₂ absorption, corresponding to an infinite tower height. In the scheme of Fig. 3, the last flash drum pressure has been assumed as 1.05 bar to operate the whole system above the atmospheric pressure. To achieve a 90 percent removal efficiency, 0.237 kmols of CO₂ per kmol of diluting gas must be captured. According with the solubility curves of CO₂ within Selexol (Bucklin and Schendel, 1984), a minimum operating pressure of 41 bar is needed. To obtain a reasonable driving force for mass transfer, absorption pressure was increased to 50 bar (see also Chiesa and Consonni, 1999, appendix A).

To achieve this pressure, a compressor processes the stream vented from the cycle at near-ambient pressure. The compression is partly intercooled, to limit the high pressure stage temperature within 400°C (similarly to gas turbine compressors). The pressurized stream is therefore cooled to near-ambient temperature, by a recuperative heat exchanger, and ducted to the absorption column. Within the column, CO₂ is captured by Selexol. The nitrogen-rich, CO₂-free stream, exiting the absorption column at high pressure (50 bar), must be heated and expanded, to recover its pressure content improving the energy balance. Heating is necessary to (i) keep the stream temperature above ambient at the expander cold end, to avoid freezing problems, and (ii) provide an enthalpy drop as high as possible, to drive the compressor. Heat is largely

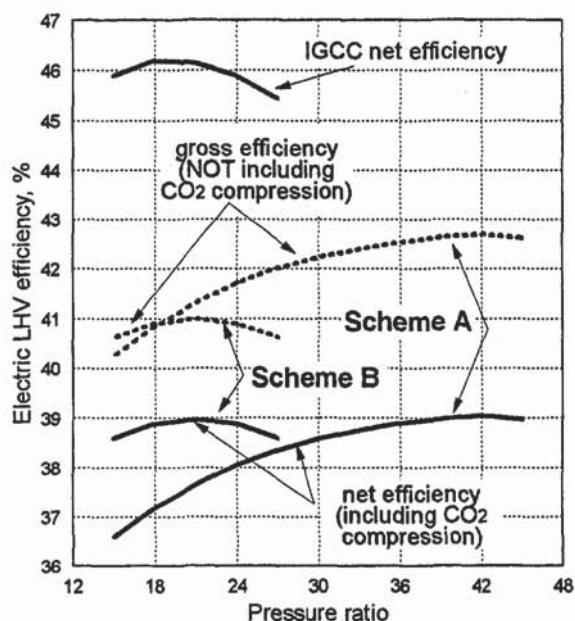


Fig. 4 Influence of the cycle pressure ratio on the efficiency of IGCC and of semiclosed cycles A and B. The dotted curves do not take into account the power consumption of the carbon dioxide compression/liquefaction train.

available from cooling of the compressed stream before absorption (in fact, hot feedwater is produced in the heat exchanger to achieve a complete heat recovery), but at a temperature not sufficient for those duties. Therefore, following the recuperative heat transfer, an additional heating is required. The only available heat sources are the convective syngas cooler and, to a lesser degree, the HRSG. We will discuss this issue later (section 3.2); Fig. 3 shows the "reference" solution in which a double expansion with reheat was adopted (unfortunately increasing the plant complexity) with heat extracted from the syngas cooler at a maximum temperature of 600°C. Turbines and intercooled compressor are arranged on the same shaft; an electric motor provides the extra power needed to balance this shaft.

On the Selexol side, Fig. 3 shows that the rich solution, after absorption of CO₂, is flashed within sequential chambers, where CO₂ is gradually released as pressure decreases, in order to reduce the power required for re-compression of the separated CO₂. From the last flash chamber, at near-atmospheric pressure, lean Selexol is pumped back to the absorber. The pump consumption is rather large (2.7 percent of the net total output), due to huge flow of Selexol (1426 kg/s); an hydraulic expander improves the energy balance, making use of the pressure drop between the absorption column and the first flash chamber. Carbon dioxide, released at various pressures, is re-compressed to the pressure of the first chamber and then ducted to a compression-liquefaction train similar to the one described in 3.4 (part A). Its power requirement is substantially reduced because (i) CO₂ is already pressurized (6 bar), and (ii) CO₂ is almost pure, because nitrogen, oxygen, and argon solubilities within Selexol are negligible compared to the one of CO₂.

3 Overall Plant Performance

3.1 Influence of the Cycle Pressure Ratio. The results of the cycle calculations are shown in Fig. 4, reporting the efficiency versus pressure ratio (β) of the present scheme (B, air-blown) and of the ones addressed in part A (i.e., scheme A, oxygen-blown, and the reference IGCC not including any CO₂ removal strategy). In the figure, two efficiency curves are shown for plant schemes A and B: the upper dotted curves do not consider the power expenses

for compression-liquefaction of carbon dioxide, the lower curves represent the overall net plant efficiency. Two basic considerations can be drawn:

- (1) The optimum pressure ratio range is very similar between IGCC and scheme B, and substantially different from scheme A. In fact, the working fluid composition and molecular mass of the air-blown cycle are rather similar to the ones of an open cycle, due to the large nitrogen concentration (Fig. 5). The best performance of scheme B is obtained at $\beta = 21$, versus an optimum β of 18 for IGCC, while a β as large as 42 was required to optimize the efficiency of scheme A. For the former two plants the use of a lower pressure ratio of 15 (often found in large commercial heavy-duty) does not impair the plant efficiency in a significant way. This represents an important confirmation about the possibility of using these machines with a limited amount of modifications.
- (2) At optimum pressure ratio, the overall efficiencies of schemes A and B are very similar (about 39 percent) and, thus, substantially lower from the IGCC one. However, reasons justifying the loss of efficiency are rather different from the ones outlined in part A. The gap between the continuous and the dotted lines represents the power consumption due to the need of providing pressurized CO₂ at the plant boundaries, rather than at atmospheric pressure. In scheme B, it includes the power requirement of the various CO₂ compressors represented in Fig. 3: the multiple flash chambers (together with the absence of incondensables) reduce their duty with respect to the unique compressor of scheme A. The major drawback of the present cycle is due to the necessity of compressing the exhaust stream up to the required absorption pressure of 50 bar. Even if a recovery of the pressure content of the separated gas is carried out, those processes (compression, expansion, heat transfer) are highly irreversible. Being the mass flow involved almost one half of the one of the power cycle, the associated exergy destruction is largely relevant to the whole energy balance. In fact, an additional power of 11 MW is needed to drive the turbo-compressor, and, mostly, a large amount of high temperature heat (82.8 MW) is subtracted from the syngas cooler, which in turn produces less steam, reducing the steam turbine power output. Those effects are mostly independent on the pressure ratio, because the separation process, at equal carbon input to the plant, involves the same CO₂ mass flow to be processed. We will therefore provide some more detail by addressing the reference scheme at $\beta = 15$.

3.2 Discussion of the "Reference" Scheme. In this section we will focus our discussion on the "reference" case with a pressure ratio of 15, selected to maintain the same value of the IGCC case. Its main characteristics are shown in Fig. 5: together with information provided by Fig. 3 and Table 1, a rather complete plant balance can be drawn. We can comment that

- about 45 percent of the gas turbine exhausts are ducted to the separation plant (the CO₂ fraction is 20 percent by volume—28 percent by mass): the size and cost of the turbo-compressor shown in Fig. 3, compared to the main gas turbine, is therefore of high relevance
- to better understand the above point let's say that (i) the compressor power is 141.8 MW (versus 222.5 of the one of the main engine), (ii) the reheat turbine power is 131.1 MW, and (iii) the thermal power coming from the syngas cooler is 82.8 MW, as already stated

To confirm the impact of this process on the power balance, let us consider the content of Table 1. Together with figures for open-cycle IGCC and "reference" scheme B, it addresses (last column) a semiclosed cycle at $\beta = 15$, similar to the one here discussed but deprived of the CO₂ removal section (therefore, producing full steam from the syngas cooler and directly venting to the ambient

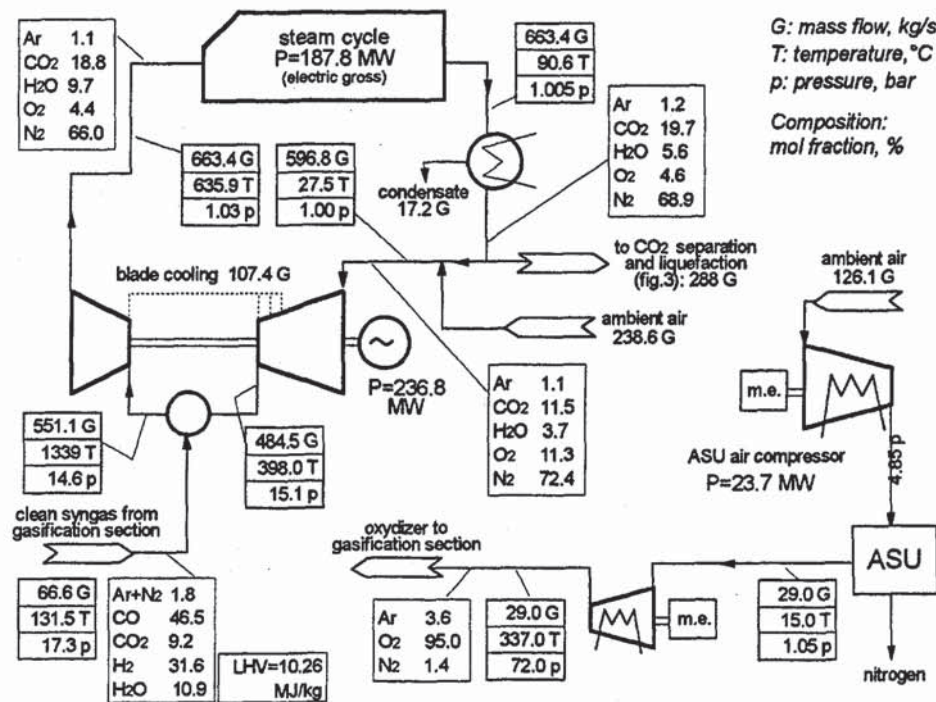


Fig. 5 Energy and mass balance of the power cycle and air separation components of the air-blown semiclosed cycle (scheme B) at a pressure ratio of 15

the stream extracted from the gas cycle). It can be noticed that the efficiency of this latter cycle is very close to the one of the IGCC. In fact, the differences on a thermodynamic point of view are rather limited: an higher turbine exit temperature (636°C versus 609°C, due to higher fluid molecular mass) provides a lower gas turbine output, recovered by the steam cycle; on the compressor side of the gas turbine, differences are negligible because the working fluid is largely diluted with air. Comparing this cycle to the one with CO₂ removal, a loss of steam turbine output of 33 MW, due to the vent stream heating, is clearly shown: together with the power consumption of the various devices reported in Fig. 3 (totaling 36.5 MW), the loss of overall efficiency (7 percentage points) is fully justified. The figures discussed up to now are based on a preheating of the vent stream up to 600°C by means of heat recovered from the convective syngas cooler. This temperature level was assumed in order to limit the thermal stresses in the heat

exchanger to values comparable to the ones of reheaters in steam boilers. Being this assumption relevant to the cycle performance and being rather questionable (no references can be found relatively to the demanding environment of a syngas cooler), a sensitivity analysis was performed, whose results are shown in Table 2. By decreasing this temperature a rather relevant loss of efficiency is found, because of the higher power consumption of the electric motor driving the turbo-expander (partly balanced by the lower thermal power retrieved by the syngas cooler). The last row shows the temperature at which the vent stream should be heated to balance the turbo-expander (789°C): it is not realistically achievable by available metallic materials for heat exchangers.

Alternatively, preheating of the vent stream can make use of heat recovered by the HRSG (by using a clean gas stream at a moderate temperature) rather than by the syngas cooler (with higher erosion-corrosion and high-temperature stresses). In this case, larger heat transfer surfaces would be needed, due to the much lower temperature difference, complicating the HRSG design (parallel tube bundles for the vent stream heater and the steam superheater and reheater). However, at equal maximum temperature, the heat source (HRSG or syngas cooler) does not influence the thermodynamic performance, because in both cases the heat subtracted by vent stream heating would have been used to generate the same amount of HP steam.

Table 1 Electric power balance of the various plant components for the open-cycle IGCC, the reference air-blown semiclosed cycle (scheme B) and a semiclosed air-blown cycle not including the CO₂ removal section. Thermal input of 900 MW by coal LHV for all cycles.

Type of cycle ($\beta=15$)	Open	Semiclosed	
		CO ₂ removal	
	IGCC	yes	no
Electric power, MW			
Gas turbine gross output	247.8	236.8	236.8
Steam turbine gross output	209.5	187.8	220.7
Syngas expander	11.4	11.4	11.4
ASU air/oxygen compressors	-40.6	-40.6	-40.6
Auxiliaries	-15.2	-13.6	-14.9
Exhausts compressor/expander	-	-10.9	-
Selexol pump/expander	-	-5.4	-
CO ₂ compression/liquefaction	-	-18.2	-
Net power output	412.9	347.3	413.4
Net LHV efficiency, %	45.88	38.59	45.93

Table 2 Influence of the vent stream temperature after heating in the syngas cooler (T_{rh}) for a semiclosed air-blown cycle with $\beta = 15$. Legend: η = overall LHV efficiency, P_{em} = power of the electric motor driving the turbo-expander, Q_{sc} = thermal power retrieved from the syngas cooler, p_{rh} = optimized reheat pressure of the vent stream, T_{st} = stack temperature. Results of the first three lines also apply to the case of heating in the HRSG.

T_{rh} , °C	η , %	P_{em} , MW	Q_{sc} , MW	p_{rh} , bar	T_{st} , °C
400	37.66	36.4	46.7	15	61.6
500	38.17	24.7	61.6	22	77.3
600	38.59	10.9	82.8	25	113.4
789	39.04	0.0	97.2	-	130.8

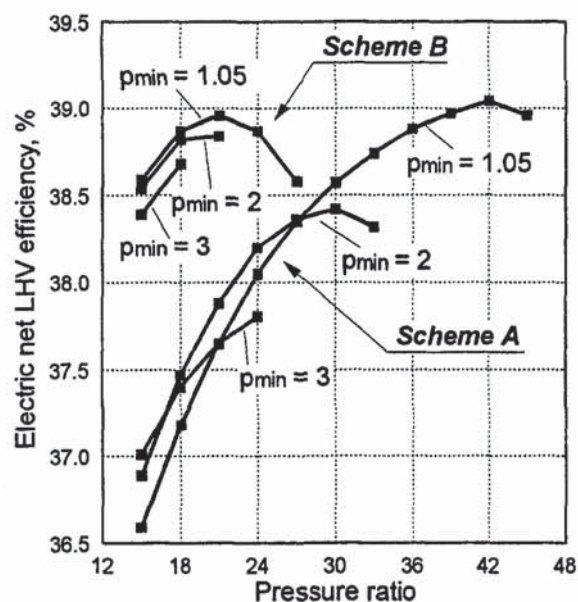


Fig. 6 Influence of the pressurization (p_{\min} is the minimum cycle pressure) on the efficiency of semiclosed cycles A and B, at various pressure ratios

3.3 Influence of the Cycle Pressurization. Up to now, the minimum cycle pressure was kept close to the atmosphere, mainly for compatibility with open-cycle machines. In closed cycles this pressure can be freely selected. In semiclosed cycles, like the ones here considered (including part A), the influence of pressurization can be discussed by separating its effects on auxiliaries consumption and on cycle thermodynamics.

In scheme A (oxygen-blown), pressurizing the cycle obviously brings about a pressure increase at the O_2 compressor outlet, needing more power compared to the atmospheric option. In case that the available syngas pressure is not enough to inject the fuel in the combustor, an additional compressor (rather than an expander) is required and its electric consumption has to be considered. With a syngas pressure of 51 bar (before the syngas expander), cycle pressurization at $2 \div 3$ bar necessarily requires this component for pressure ratios maximizing the efficiency. Similar considerations hold for cycle B where pressurization requires a large compressor to introduce fresh air into the cycle. In change of this additional work, the stream ducted to CO_2 absorption process is available at higher pressure decreasing the compression power requirements.

Nevertheless a restricted analysis, only considering the variation in consumption of the auxiliaries, leads to erroneous results because pressurization also has a significant influence upon the power cycle. As a first point, the turbomachines efficiency is influenced by "size," according to our correlations. Pressurization reduces the volumetric flow and negatively influences the efficiency. For large machines, this effect is rather limited (for instance, the compressor polytropic efficiency decreases of about 0.5 points at a minimum cycle pressure of 3 bar), but it is not negligible. In addition, pressurization has a great importance on the factors which control heat transfer in the hottest rows of the turbine. On the one side, increasing the operating pressure reduces volume flow and hence surfaces to be cooled. On the other side it increases the heat transfer coefficients on both sides of the cooling channels and hence the heat flux through the blade walls. It brings about an increase in the temperature drop due to conduction along the wall thickness which reduces the temperature rise available to the coolant in the inner blade channels. Therefore, larger coolant flows are required to remove the same thermal load. All these effects are taken into account by the cooling model here adopted, described by Consonni (1992).

Figure 6 depicts the overall effects of pressurization on the plant

efficiency. In scheme A, at low pressure ratio where blade cooling is less demanding due to a lower coolant temperature, pressurization is beneficial to performance. On the contrary, pressurization becomes noxious at higher β , where cycle efficiency approaches its peak. The critical condition reached by the cooling system is attested by the curves' breaks which occur for pressure ratio lower and lower as pressurization increases, thus impairing the achievement of the best efficiency. Curves referred to scheme B follow the same trend, but the cooling system results critical even at low β : in fact, compressor outlet (i.e., coolant) temperatures are higher than for scheme A, due to the lower molecular mass of the working fluid (see Fig. 5 of Part A, keeping into account that compressor outlet temperatures of scheme B are very similar to the ones of IGCC). Hence, pressurization penalizes efficiency of scheme B in the whole pressure ratio range reported in Fig. 6.

Apart from efficiency, pressurization could give some benefits in the practice. It reduces the size of gas cycle turbomachinery and enhances heat transfer in the recovery steam generator. In scheme A, requiring some changes in gas turbine design, a moderate pressurization could allow some advantage on the economic viewpoint. With regard to scheme B, pressurization does not have the same appeal since it introduces a supplementary air compressor and modifies the gas turbine operating conditions, conflicting with the rationale supporting this configuration: the adoption of an unchanged current engine.

4 Turbomachinery Design and Development

In the previous discussion, we often stated that the present configuration (with air-blown combustion) may result attractive if it makes feasible the adoption of unmodified gas turbines, with respect to the one available in the market. Now, this statement can be confirmed by looking at Table 3, in which some relevant turbomachinery specifications are compared for the IGCC machine and for a semi-closed cycle having (i) the same compressor inlet volume flow, and (ii) the same turbine nozzle throat area. The first assumption brings about a thermal input of 917 MW rather than 900, the second one can be accomplished by selecting a pressure ratio of 14.8 rather than 15, with negligible consequences on the plant efficiency. These conditions were stipulated to verify if the same gas turbine unit can operate safely under the new conditions imposed by the change of the working fluid, without any need of blade design or blade height modification. The results shown in Table 3 indicate that (i) the volume flow rate at the last compressor stage is less than 1 percent lower than the one of the IGCC machine, eliminating any risk of stall-surge at HP stages, (ii) the compressor work variation is minimal, (iii) variations on the turbine side are very limited and cannot influence its performance, and (iv) improvements in cooling flows are minimal. Considering

Table 3 Specifications involved in turbomachinery design, for an IGCC and a semiclosed air-blown cycle characterized by the same compressor inlet volume flow and turbine nozzle area

Common design parameters	Open IGCC, $\beta=15$	Semi-closed, $\beta=14.8$
Inlet volume flow = 507.9 m ³ /s		
First nozzle throat area = 0.4433 m ²		
Thermal input by coal LHV, MW	900	917
Gas turbine gross output, MW _e	247.8	243.0
Gas turbine compressor		
Inlet mass flow, kg/s	613.6	612.5
Inlet / outlet volume flow ratio	7.262	7.221
Isentropic enthalpy rise, kJ/kg	337.9	329.4
Gas turbine		
Outlet volume flow, m ³ /s	1633.9	1645.5
Outlet / inlet volume flow ratio	9.165	9.495
Isentropic enthalpy drop (cooled expansion), kJ/kg	1062	1046
First nozzle cooling flow / gas flow (vol.)	0.0256	0.0260
First rotor cooling flow / gas flow (vol.)	0.0243	0.0249

that problems cannot be expected on the mechanical standpoint, due to a slightly reduced power output, it can be concluded, beyond any reasonable doubt, that the very same machine of open cycles can be used with the moderately CO₂ enriched fluid here addressed. Regarding other turbomachines included in the cycle, the ASU compressors are unchanged with respect to the IGCC, while the duty of the CO₂ liquefaction compressor is much reduced if compared to the one of scheme A (14.6 versus 32.9 MW, with an inlet volume flow of 6.82 versus 52.34 m³/s). The real drawback of scheme B comes from the machines involved in the exhaust treatment and separation, especially as far as the main exhausts turbo-expander, pressurizing the absorption process, is concerned. This machine is about one-half the size of the main gas turbine, with an higher loading (larger stage number), intercoolers and reheat. It is a novel machine, resembling the characteristics of large process units. Its impact on the plant cost may represent a serious obstacle to the development of this class of plants. In addition, a polytropic efficiency lower than here estimated (on the basis of the same correlations used for gas turbine components) may seriously affect the cycle performance.

Other components to be considered are the absorption column, the flash chambers, the heat exchangers (the recuperative one shown in Fig. 3 and the gas heaters placed inside the convective syngas cooler), the Selexol turbo-pump and the minor CO₂ compressors connecting the flash chambers: they represent large pieces of additional equipment. The impact on the overall investment cost of the separation plant can therefore result prohibitive. A reliable cost prediction cannot be drawn at present, but a very rough estimation, based on limited data available to the authors, suggests a rise of 50–55 percent with respect to the already elevated plant costs of an IGCC having the same gasification capacity. It is authors' opinion that the proposal described in part A (oxygen blown) can be realized with lower costs (about 35 percent rise), assuming that the gas turbine development costs are scattered on a reasonable number of machines, to limit the cost rise of this component to a 30 percent. Considering the lower net output of these plants versus an IGCC (about 18 percent less), the estimated specific cost rise is substantially higher (in the range of 60 percent for scheme A and of 80 percent for scheme B, according to a very preliminary evaluation).

6 Final Comparisons and Conclusions

Figure 7 shows the efficiency decay of various plant types as a function of the specific CO₂ emission, for (i) the two schemes here discussed (including part A), (ii) the most efficient solution studied by Chiesa and Consonni (1999), based on syngas catalytic shift reaction, physical absorption of CO₂ and hydrogen-fueled gas turbine, (iii) a mix of conventional IGCC with a semiclosed CO₂ cycle (reference scheme A). The points representative of an IGCC, a coal-fired steam plant and a natural gas combined cycle are also reported. The figure shows that some improvements in the plant conversion efficiency can be achieved by reducing the CO₂ removal rate. For scheme A the final CO₂ pressure determines the amount of CO₂ condensed and therefore removed (see pressures quoted in Fig. 7). A pressure reduction brings about a very limited power saving, clearly demonstrating that such a scheme makes sense only if a very high removal rate is achieved. For scheme B, the efficiency of the CO₂ separation depends on the pressure drop between the absorber and the last flash chamber (see again pressures in Fig. 7): by operating the physical absorption at a lower pressure some efficiency gain may be obtained, but at a rather slow rate. The proposal from Chiesa and Consonni, being calculated under the same assumptions used in this paper and then fully comparable, shows about the same efficiency of our schemes at high removal rates (90 percent or higher) but achieves a substantially better efficiency at medium removal rate (50–70 percent), due to a lower consumption of high pressure steam needed by the shift reaction. At this intermediate rates, their performance is slightly better than the one achieved by a mix of IGCC + scheme

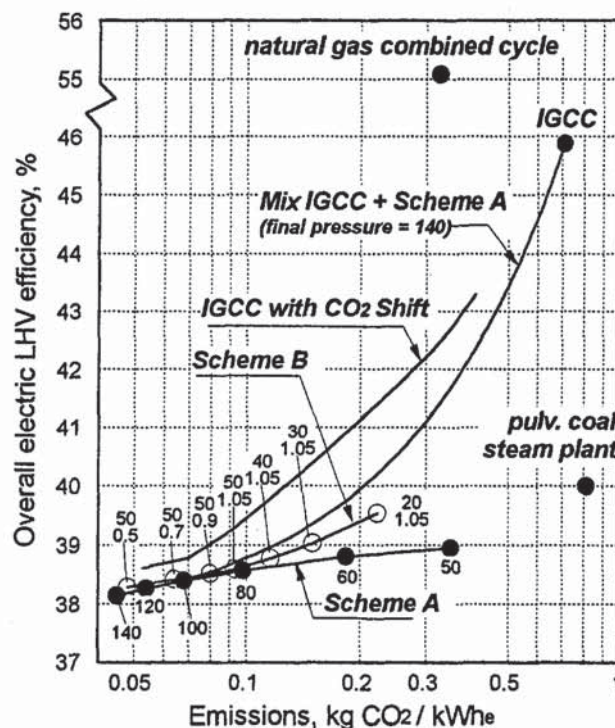


Fig. 7 Specific carbon dioxide emissions versus efficiency of various plant types. The numbers quoted for scheme A represent the final CO₂ delivery pressure (bar); for scheme B, they represent the pressure of the absorption column and of the last flash chamber.

A, with the additional advantage of the use of unmodified gas turbines and the disadvantage of unmodified NO_x emission (remember that scheme A is virtually NO_x free). A curve very similar to the one "IGCC + scheme A" can be also obtained by scheme B alone, if only a part of the stream exiting the power cycle is submitted to CO₂ separation (with the remainder vented to the atmosphere), due to the fact that IGCC and scheme B, without separation process, show the same net efficiency (see Table 1).

The selection of the best strategy of CO₂ removal, keeping into account its progressive penetration into the market, is beyond the scope of the paper and would anticipate the necessary research and development studies. In fact, the discussion here developed outlines the negative impact of CO₂ removal on the conversion efficiency and on the plant complexity, compared to the already high capital-intensive and complicated IGCC stations, but demonstrates that a drastic abatement of CO₂ emissions is within today's technological capabilities. A realistic economic study cannot be drawn at present, due to the difficulties of estimating the investment costs when novel components are introduced. In addition, any cost estimation should take into account the avoided costs of "externalities," i.e., the social cost connected to pollutant emission (mainly CO₂ and NO_x). Nevertheless, we believe that the present analysis can be useful to provide the necessary basic information to develop such estimations and to assess the possibility of success of emission-free fossil-fueled power plants in a competitive energy market constrained by increasingly stringent global emission regulations.

References

- Bucklin, R. W., and Schendel, R. L., 1984, "Comparison of Fluor Solvent and Selexol Processes," *Energy Progress*, Vol. 4, No. 3, pp. 137–142.
- Chiesa, P., and Consonni, S., 1999, "Shift Reactors and Physical Absorption for Low-CO₂ Emission IGCCs," *ASME JOURNAL OF ENGINEERING FOR GAS TURBINES AND POWER*, Vol. 121, pp. 295–305.
- Consonni, S., 1992, "Performance Prediction of Gas/Steam Cycles for Power Generation," Ph.D. thesis n. 1893-T, Princeton University, Princeton, NJ.
- Kohl, A., and Riesenfeld, F., 1985, *Gas Purification*, 4th ed., Gulf Publishing Co., Houston, TX.

Thermodynamic Performance of IGCC with Oxy-Combustion CO₂ Capture

G. Lozza, M. Romano, A. Giuffrida

Dipartimento di Energia, Politecnico di Milano, Via Lambruschini 4, 20156 Milano

giovanni.lozza@polimi.it

Milan - ITALY

ABSTRACT

This paper discusses the relevant thermodynamic aspects of IGCC plants with CO₂ capture, mainly focusing on oxy-combustion techniques. The following plant configurations were considered here, all based on a dry-feed oxygen-blown entrained-flow gasifier with syngas quench (Shell type) and a FB class gas turbine: (i) two reference cases, one without CO₂ capture and one with 'conventional' pre-combustion capture, (ii) three oxy-combustion cases, the first one with today's technology and the other two with advanced technology, including CO₂/SO₂ co-sequestration or, alternatively, Hot Gas Desulfurization.

It is concluded that oxy-combustion techniques in IGCC cycles may deserve some attention in the near future, because they have the potential of achieving better thermodynamic and environmental performance, in comparison with more conventional capture concepts: in the best case, 45% net efficiency and near-zero emissions were predicted. However, some technological challenges are an obstacle to their development, especially as far as the re-design of the gas turbine is concerned.

INTRODUCTION

CO₂ capture from fossil fuel power plants is increasingly proposed for greenhouse gases emission mitigation. However, when applied to conventional coal power stations, by means of post-combustion amine capture or by means of boiler oxy-combustion, severe loss of efficiency and larger investment costs can be predicted. To mitigate these drawbacks, CO₂ capture coupled to IGCC can be considered. Up to now, the most appealing solution, often quoted by the literature as the one showing the lowest possible cost of avoided CO₂, is based on the syngas decarbonization concept: CO is converted into CO₂ (water-gas shift) and CO₂ is removed from syngas before its combustion by means of physical or chemical solvents. This concept brings to an hydrogen-rich syngas (typically 90% H₂), then burned in a rather conventional gas turbine. The carbon capture cannot exceed 90% and some NO_x emission problems may be encountered due to elevated flame temperature.

An alternative concept for IGCC plants, providing better environmental performance, is represented by the oxy-combustion technique: the CO-rich syngas is basically burned by high purity oxygen in a semi-closed Joule cycle, exhausting a high purity CO₂ stream after water condensation. To moderate the combustor outlet temperature, combustion products are diluted by CO₂ re-circulated by a CO₂ compressor, in a semi-closed Joule cycle. The CO₂ stream exiting the power cycle, after water condensation, is compressed and liquefied for final storage: any release to the ambient of combustion gases, including any type of pollutant, is virtually eliminated, approaching 'zero-emission'. Such an approach requires deep modifications to existing gas turbine machines, not requiring unproven technologies but calling for a large development effort, whose extent will be discussed in the paper.

PLANT CONFIGURATIONS

To understand the potential of IGCC with oxy-combustion capture, we theoretically estimated the performance of some optimized plant configurations, including two reference cases (without CO₂ capture and with ‘conventional’ pre-combustion capture) and three oxy-fuel configurations, the first one with today’s technology and the other two with advanced technology, including CO₂/SO₂ co-sequestration or, alternatively, Hot Gas Desulfurization. With more detail, fig.1 shows the plant configuration of the reference case with pre-combustion capture by means of water-gas shift (WGS) and physical absorption of CO₂. The scheme for the no-capture plant is strictly similar, of course not showing WGS and CO₂ separation/compression.

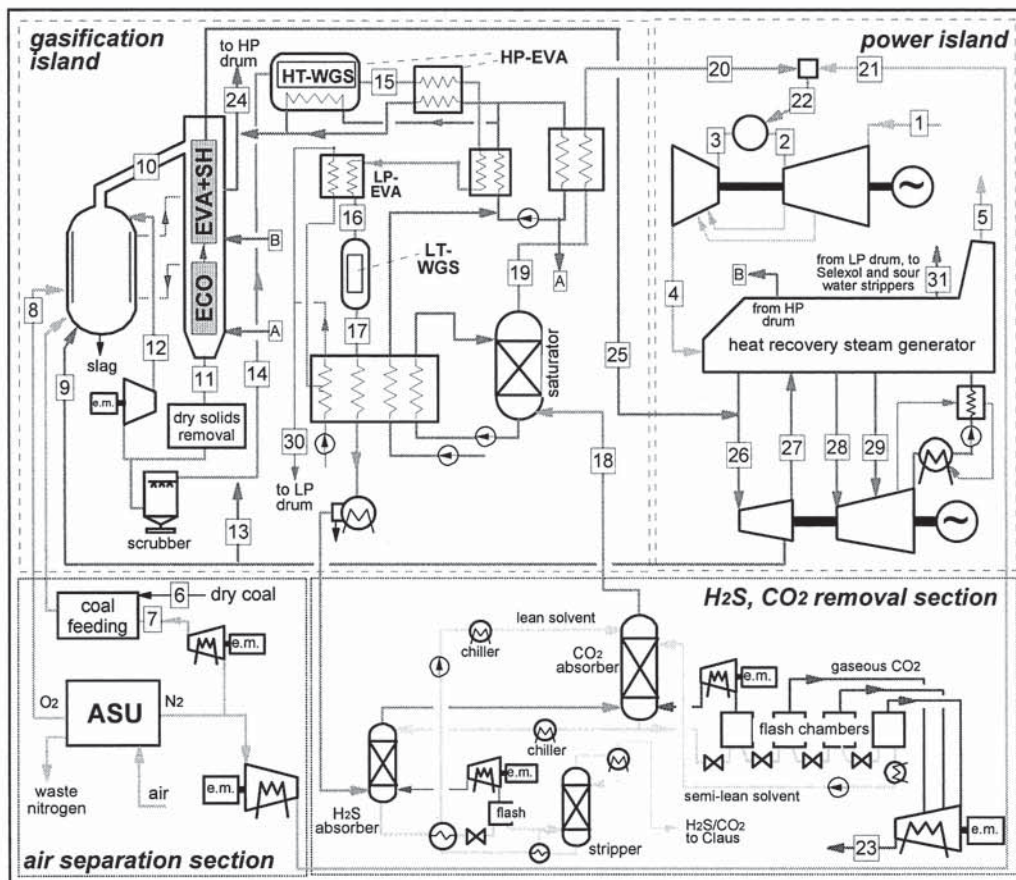


Figure 1 – Configuration of the IGCC plant with pre-combustion capture.

The plant scheme includes an oxygen-blown dry-feed entrained flow gasifier, resembling the Shell gasification process: the raw syngas at 1550°C is quenched by cooled syngas to produce HP steam in a convective syngas cooler, after slag removal. Two WGS reactors are used: an high temperature one for bulk removal (heat of reaction can be recovered to produce HP steam again) and a low temperature one to achieve a very elevated CO conversion. CO₂ is separated by means of a Selexol process with two separate absorbers: the first one, mainly removing H₂S, is fed by a semi-lean solvent regenerated in a low pressure stripper releasing H₂S to the Claus unit; the second one, using lean solvent at the top of the column, is devoted to CO₂ removal: the largest solvent fraction is regenerated by pressure-swing, within different flash chambers connected to the CO₂ compressor. The final syngas is low-purity hydrogen, with about a 10% of: (i) N₂ and Ar from oxygen impurities, (ii) CH₄ from gasifier, (iii) unconverted CO, (iv) CO₂ not separated. It is saturated by steam and then mixed with nitrogen from ASU to limit the NO formation in the combustor.

The same gasification process of the no-capture case is shared by the first oxy-combustion configuration, only modified to use CO_2 rather than N_2 for lock-hoppers pressurization, in order to avoid the presence of incondensable N_2 in the final stream exiting the cycle. The power cycle consists of a novel gas turbine machine: syngas (made of CO and H_2) is burnt in a oxy-fuel combustor and diluted by recycled pressurized CO_2 to limit the turbine inlet temperature to the typical values of today's machines. As we will discuss later, the different working fluid (mostly CO_2 with some water in the expansion) involves the selection of an higher pressure ratio and larger blade cooling flows; the excess oxygen for combustion is to be strictly controlled to limit the presence of incondensable gases in the final CO_2 stream.

The second oxy-fuel plant configuration, shown in fig.2, is more interesting, being based on advanced technologies and on some novel concept, due to the mid-long term time frame for its realization. The gasification process is similar, but a larger pressure was selected to join the larger cycle pressure ratio. An hot gas filtration by means of ceramic filters, operating at 550°C, was supposed to be available. H₂S is not removed from syngas: it is burnt in the GT combustor, eliminating the power and heat requirements of the desulfurization systems and making use of the H₂S heating value; SO₂ produced is co-sequestered together with CO₂. At present, it is not clear if co-sequestration is a viable practice: however, the thermodynamic benefits are quite relevant and they will be predicted here.

In the advanced configuration, some attention was deserved to optimize the blade cooling system, to obtain an elevated turbine inlet temperature. The CO₂ coolant for the first three rows is taken from the compressor outlet and then cooled to 250°C to limit the coolant needs.

Fig.2 also shows the CO₂ compression/liquefaction section, common to all the oxy-fuel plants here considered. It includes a separation process of the inert incondensable gases (O₂, N₂, Ar). The low purity CO₂ stream is liquefied at an intermediate pressure of 23 bar, where gases are separated from liquid CO₂. Liquefaction is obtained by evaporation of purified CO₂, after a flash at 16 bar to obtain a suitable ΔT in the heat exchanger. The CO₂ stream is compressed and liquefied at 90 bar, and then pumped to the final pressure of 150 bar. The last oxy-fuel configuration is very similar to the one of fig.2, but it includes an hot-gas-desulfurization process (HGD), following the hot gas filtration. This

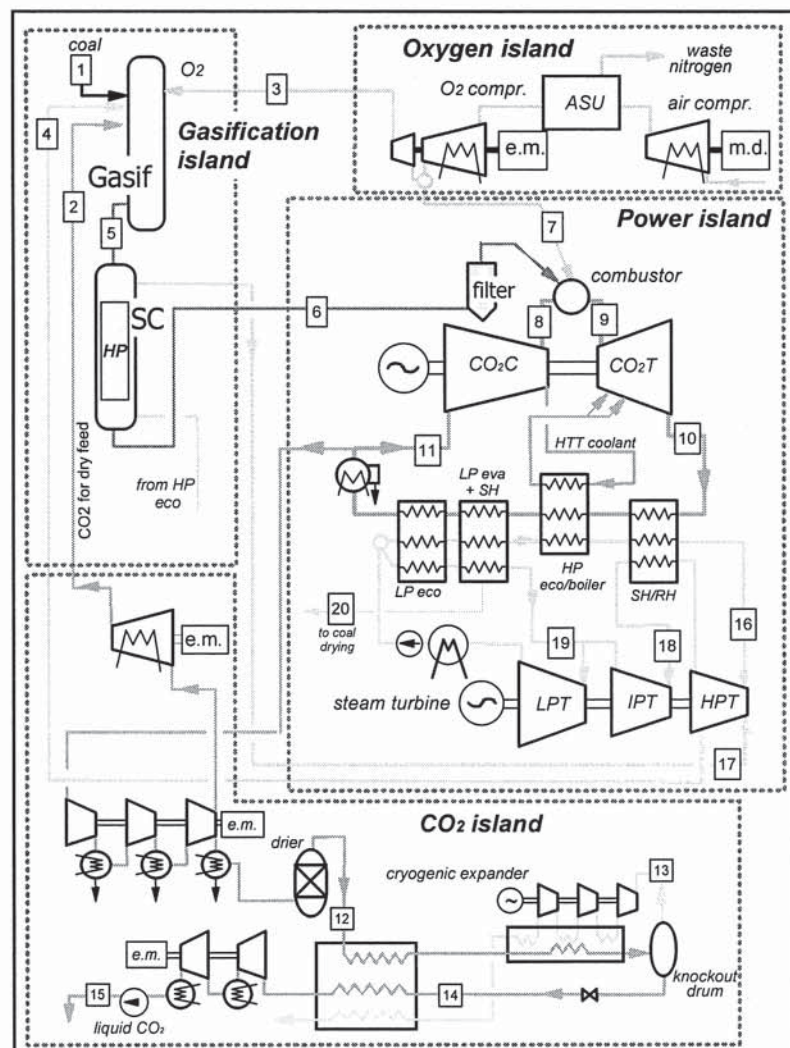


Figure 2 – IGCC plant with advanced oxy-fuel capture

is intend to avoid the need of co-sequestration of CO₂ and SO₂. The HGD block is shown in fig.3: it includes two circulating beds of zinc titanate where the following reactions take place:



Since the process operates at the gasification pressure, the mixture of air and nitrogen needed for regeneration must be compressed and therefore expanded for a proper management. It must be noted that the regeneration process cannot be carried out with air, to minimize the formation of zinc sulfate (ZnSO₄), deteriorating the system performance. An oxygen content as low as 2% in the regeneration agent was here used. The regeneration reaction is strongly exothermic: the reactor is kept at 750°C with a proper control of the circulating solid mass flow rate. A more detailed description of the process will be given in an upcoming authors' paper.

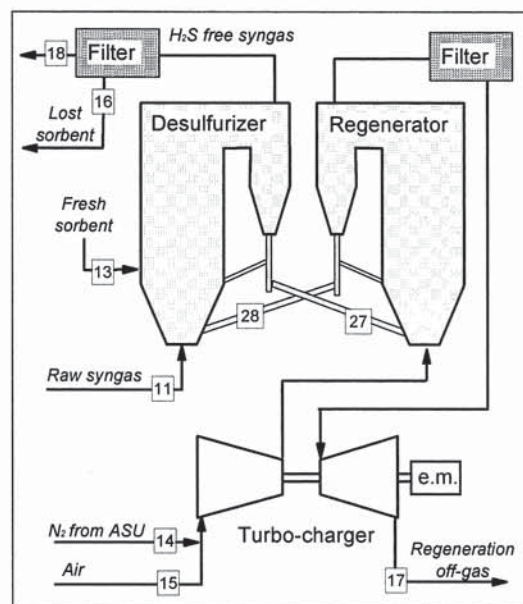


Figure 3 – Hot Gas Desulfurization

METHOD OF CALCULATION AND ASSUMPTIONS

The thermodynamic performance of the power plants here discussed were calculated by means of GS, which is an in-house computer code developed in the past years at the Department of Energy of Politecnico di Milano. The code is a powerful and flexible tool that can be used to accurately predict the performance of a very wide variety of chemical processes and systems for electricity production. GS was originally designed to assess the performance of gas-steam cycles for power production and has been progressively developed and improved to calculate complex systems including coal gasification, chemical reactors, fuel cells and essentially all the processes present in advanced plants for power generation from fossil fuels. As a brief reminder, the main features of the code are: (i) capability of reproducing very complex plant schemes by assembling basic modules, such as turbine, compressor, combustor, steam section, chemical reactor, heat exchanger, etc., (ii) built-in correlations to predict turbomachines efficiency (gas and steam turbine stages and compressors) as a function of their operating conditions, (iii) built-in correlations to predict gas turbine cooling flows, (iv) gas composition at reactors' outlet can be determined by assuming chemical equilibrium. The calculated plant performance are dependent on a large number of assumption, defining the various processes and qualifying the characteristics of the components (i.e. efficiency of turbomachines, ΔT and pressure losses in heat exchangers and so on). The main assumptions are reported in Tables 1-5, derived from the analysis of a large number of power plants, carried out in the last two decades, both from literature and from industrial practice. More details can be found in authors' previous papers¹.

For all cases, the coal considered has the following composition (% by weight): 64.4 C, 3.95 H, 7.40 O, 1.49 N, 0.85 S, 9.20 humidity, 12.67 ash, with lower and higher heating values of 24.62 and 25.71 MJ/kg.

¹ See for instance references quoted in: (1) Chiesa P., Kreutz T., Lozza G. "CO₂ Sequestration from IGCC Power Plants by Means of Metallic Membranes", J.Eng. for Gas Turbines and Power, Vol.129, pp.123-134, Jan.2007, or in (2) Chiesa, P., Macchi, E. "A Thermodynamic Analysis of Different Options to Break 60% Electric Efficiency in Combined Cycle Power Plants", J.Eng. for Gas Turbine and Power, Vol.126, No.4, pp. 770-785, 2004.

<i>Gasification and ASU</i>		<i>Gas turbine and steam cycle</i>	
Gasification pressure, bar	44	Fuel temperature, °C	250
Gasification temperature, °C	1550	GT turbine inlet temperature, °C	1335
Heat losses, % LHV	0.7	GT pressure ratio	17
Carbon conversion	99.0	Pressure levels, bar	130/36
Temperature of O ₂ to gasifier, °C	15	SH/RH temperature, °C	565
Moderator steam, kg _{H₂O} /kg _{coal}	0.06	Pinch point/sub-cooling ΔT, °C	10/5
N ₂ to lock hoppers, kg/kg _{dry-coal}	0.22	Condensing pressure, bar	0.04
Quenched syngas temperature, °C	900	Minimum stack temperature, °C	115
Cold recycle syngas temperature, °C	200	<i>CO₂ compression</i>	
Min. ΔT in syngas coolers, °C	20	Number of inter-cooled stages	5
Oxygen purity, % mol.	95	Inter-cooling temperature, °C	25
ASU electric consumption, kWh/tO ₂	325	Inter-coolers pressure loss, %	1
		Compressors isentropic efficiency, %	82

Table 1 – Assumptions for the reference IGCC plants, present technology.

<i>Water Gas Shift Reactors</i>		<i>Selexol Plant</i>	
Steam to carbon at first reactor inlet	1.5	L/G ratio (wt. basis) in H ₂ S/CO ₂	
HT reactor outlet temperature, °C	400	absorption columns	1.1/11.6
LT reactor outlet temperature, °C	210	CO ₂ flash tanks pressures, bar	15/8/3.5/1.5
		Reboiler heat duty, MW _{th}	27

Table 2 – Additional assumptions for the IGCC plant with pre-combustion capture.

CO ₂ to gasifier lock hoppers, kg/kg _{coal}	0.35	Fuel side pressure loss at combustor, %	20
GT pressure ratio	40	O ₂ content at combustor outlet, % mol.	2

Table 3 – Varied assumptions for the oxy-fuel IGCC plant, present technology.

Gasification temperature, °C	1427	Syngas temperature to GT, °C	550
Gasification pressure, bar	50	Steam pressures HP/RH, bar	247/58
Carbon conversion	99.5	LP evaporation pressure, bar	4
Temperature of O ₂ to gasifier, °C	200	SH/RH steam temperature, °C	600/600

Table 4 – Varied assumptions for the oxy-fuel IGCC plant, advanced technology.

ZnO to TiO ₂ mol.ratio in fresh sorbent	1	O ₂ mol.fraction in regeneration mixture	2%
System pressure, MPa	≈ 5	Regeneration temperature, °C	750
Desulphurization temperature, °C	550	ZnS to ZnO mol.ratio in regen.sorbent	0.1
Sorbent loss, % in wt.	0.1	Pressure loss at the hot gas filter, %	3

Table 5 – Assumptions for Hot Gas Desulfurization.

DISCUSSION OF THE RESULTS

The calculated performance of the above described plants are reported in Table 6, showing the power breakdown, the efficiency and the carbon emission. The reference IGCC plant without capture shows an elevated efficiency (47.6%), consistently higher than the one of the plants now in operation. However this is obtained by a very efficient configuration, based on a dry-feed gasifier, a state-of-the-art gas turbine, an optimized heat recovery: it is representative of the performance obtained by a ‘mature’ IGCC market, rather than by ‘demonstration’ plants. The loss of efficiency due to pre-combustion capture is severe: 9 percentage points are lost due a number of factors: (i) loss of syngas heating value, due to the exothermic shift reaction (see the lower CGE – Cold Gas Efficiency), (ii) the loss of steam turbine power, caused by the steam extraction needed to achieve the required S/C ratio in the WGS reactors, (iii) the energy consumptions (pumps and LP steam) of the gas separation plant, (iv) the power re-

quirement of the CO₂ compressor. Lower loss of efficiency were encountered in other pre-combustion configurations, but starting from intrinsically lower performance: for instance with a full water quench gasification process, syngas is largely diluted with steam and a turbine extraction is not needed. However, a 38% net efficiency is a pretty elevated figure for a coal plant with CO₂ capture, compared to other solutions.

Case	Reference IGCC	Pre-combus-tion IGCC	Oxy-IGCC	Advanced oxy-IGCC	Advanced oxy-IGCC + HGD
TIT, °C	1335	1335	1335	1400	1400
Sulfur co-sequestration	-	no	no	yes	no
Electric/mechanical power MW					
Gas turbine (2 units)	659.4	597.7	609.6	656.5	653.2
GT auxiliaries	-2.34	-2.12	-2.16	-2.30	-2.32
Steam Turbine	420.6	354.0	454.7	510.8	513.6
Steam cycle pumps	-6.53	-6.92	-6.51	-11.60	-11.01
ASU	-72.15	-72.17	-178.17	-188.2	-187.0
Lock hoppers N ₂ compress.	-9.11	-9.11	-	-	-
Syngas recycle fan	-2.4	-2.41	-2.42	-	-
Syngas compressor	-	-	-10.79	-	-
N ₂ compressor for fuel dilution	-69.13	-51.34	-	-	-
Aux. for H ₂ S / CO ₂ removal	-0.69	-26.16	-0.69	-	-3.40
CO ₂ compression	-	-40.80	-83.05	-83.30	-83.30
Auxiliaries for heat rejection	-5.86	-5.18	-8.88	-11.03	-11.03
Miscellaneous BOP	-7.40	-7.38	-7.40	-7.47	-7.45
Net power output, MW _{el}	904.4	728.2	764.2	863.5	861.3
Fuel input LHV, MW _{th}	1897.6	1897.6	1897.6	1897.6	1897.6
Cold Gas Efficiency, %	78.14	69.63	77.36	83.85	83.31
Net LHV efficiency, %	47.66	38.38	40.27	45.50	45.39
CO ₂ captured, %	0	90.76	97.38	97.38	97.38
CO ₂ specific emissions, g/kWh	732.1	82.3	25.1	22.2	22.3

Table 6 –Performance of the plants considered in the paper.

The oxy-fuel IGCC with present technology shows a somewhat better efficiency (40.3%) and a much better carbon capture, compared to the previous case. The CGE efficiency is not varied from the no-capture case, but, as easily predictable, the consumption of the ASU is largely improved: as much as 180 MWe out of 1060 gross produced are required for oxygen production and compression. Any variation of the ASU performance will largely affect the overall plant balance. Also the CO₂ compression power is much higher than for pre-combustion, even for similar CO₂ mass flow, due to many reasons: (i) CO₂ impurities increases the mass flow to be compressed, (ii) compression begins at near-atmospheric pressure for the whole stream, (iii) the separation of incondensable gas brings about a significant pressure loss. The power cycle has been optimized, as a consequence of the different fluid composition (mainly CO₂) and molecular complexity: a much larger pressure ratio (40 rather than 17) is required to have a similar temperature history of the Joule cycle, in order to optimize the cycle efficiency. This calls for a re-design of the axial compressor and expander, but the performance are rather brilliant.

The advanced oxy-fuel case, intended to predict the performance of a mid-term configurations, is very efficient (45.5%). In particular, the hot-gas-cleaning simplifies the plant scheme and eliminates the losses connected to cooling and re-heating of the syngas. Into addition, the heating value of the H₂S is here used in the gas turbine for power production. The cycle performance was improved: a turbine inlet temperature of 1400°C was adopted with comparable or lower cooling flows, thanks to some foreseeable technological improvements, mainly con-

sisting in the cooling of the coolant flow. A better insight of this configuration is given by Table 7, showing the main characteristics of the relevant streams in the process.

However, co-sequestration of CO₂ and SO₂ poses some big question marks, mainly related to the compatibility of sulfur compounds with the selected long-term storage strategy, but also regarding the possibility of acid corrosion in the transport pipeline and in the low temperature components of the power plant. Sulfur can be removed by a limestone wet scrubbing process applied to the final CO₂ stream or, in a more innovative fashion, by means of HGD. The last column of Table 6 shows that the loss of efficiency due to HGD is very limited: the turbo-charger shown in fig.3 just requires 3.4 MWe to be driven and it is the only relevant difference. It must be reminded that, even if H₂S is no longer burnt in the gas turbine, its heating value is not wasted: both desulfurization and regeneration reactions are exothermic, improving the heat available from the gaseous streams involved in the process.

Point	G kg/s	T °C	p bar	Composition, %mol.									
				CH ₄	CO	CO ₂	H ₂	H ₂ O	Ar	N ₂	O ₂	H ₂ S	SO ₂
1	36.83	15.0		dry coal (%wt.: 67.4 C, 4.2 H, 7.7 O, 1.6 N, 0.8 S, 5.0 H ₂ O, 13.3 ash)									
2	17.24	150.0	68.87	0.00	0.00	93.48	0.00	0.20	3.33	0.96	1.57	0.00	0.46
3	26.43	200.0	61.22	0.00	0.00	0.00	0.00	0.00	2.97	0.03	97.00	0.00	0.00
4	4.45	416.2	61.22	0.00	0.00	0.00	0.00	100	0.00	0.00	0.00	0.00	0.00
5	75.72	1426.8	51.00	0.02	65.45	5.19	21.16	5.98	1.13	0.72	0.00	0.35	0.00
6	75.72	550.0	48.00	0.02	65.45	5.19	21.16	5.98	1.13	0.72	0.00	0.35	0.00
7	49.51	200.0	40.00	0.00	0.00	0.00	0.00	0.00	2.97	0.03	97.00	0.00	0.00
8	441.6	406.9	40.00	0.00	0.00	88.51	0.00	5.51	3.15	0.91	1.48	0.00	0.44
9	566.8	1483.7	38.80	0.00	0.00	83.62	0.00	10.73	2.98	0.86	1.40	0.00	0.41
10	696.0	690.8	1.05	0.00	0.00	84.50	0.00	9.78	3.01	0.87	1.42	0.00	0.42
11	570.8	35.0	1.02	0.00	0.00	88.51	0.00	5.51	3.15	0.91	1.48	0.00	0.44
12	91.59	35.0	22.77	0.00	0.00	93.67	0.00	0.00	3.33	0.97	1.57	0.00	0.46
13	4.91	-37.0	22.09	0.00	0.00	54.88	0.00	0.00	24.20	9.86	11.04	0.00	0.02
14	86.68	-41.0	16.00	0.00	0.00	96.06	0.00	0.00	2.04	0.42	0.99	0.00	0.49
15	86.68	25.0	150.0	0.00	0.00	96.06	0.00	0.00	2.04	0.42	0.99	0.00	0.49
16	97.81	600.0	247.0	0	0	0	0	100	0	0	0	0	0
17	52.68	600.0	247.0	0	0	0	0	100	0	0	0	0	0
18	144.4	600.0	53.18	0	0	0	0	100	0	0	0	0	0
19	3.92	250.0	3.68	0	0	0	0	100	0	0	0	0	0
20	1.52	143.6	4.00	0	0	0	0	100	0	0	0	0	0

Table 7 – Mass flow, pressure, temperature and chemical composition of the relevant point of the advanced oxy-fuel IGCC (point numbers are visible on fig.2).

CONCLUSIONS

The results obtained for IGCC plants with oxy-combustion are very interesting. Better environmental performance, compared to any other realistic technology, can be obtained: (i) NO_x or SO_x are not released to the ambient, but are almost entirely solved within the CO₂ stream to be sequestered; (ii) the only carbon release to the ambient is the CO₂ contained in the in-condensable gases, here estimated as a 3% of the carbon input: these low figure can be further reduced to negligible values by treating this small and concentrated gas stream.

An elevated efficiency (above 45% net) can be achieved by advanced configurations. Advancements consists of: (i) some refinement in the gasification system and in the blade cooling technology, which is fully realistic in a time frame of one decade, (ii) the adoption of an Hot Gas Clean-up system, (iii) the development of a novel gas turbine unit. The last two statements require some comments. The major obstacle is the realization of an oxy-fuel gas turbine, which must be re-designed with very large modification to existing units. However, the design of an axial compressor or turbine for a semi-closed CO₂ cycle does not require any new methodology and therefore involves costs, but not risks. An oxy-combustor is a more sensitive and novel component, but it does not pose unsurpassable barriers.

The Hot Gas Filtration is today a quite risky practice, not fully demonstrated in terms of industrial acceptability and costs. However, the oxy-fuel IGCC concept offers the possibility of obtaining the full benefits from this technology: for pre-combustion, HGF is simply not useful, because the syngas has to be cooled for CO₂ separation. Supposing that CO₂-SO₂ co-sequestration or Hot Gas Desulfuration will be viable, oxy-fuel is again the solution for taking advantage from these practices.

We can therefore conclude that oxy-combustion IGCC techniques may deserve some more attention in the R&D programs for clean power production systems in a near-mid term perspective, because they have a potential to improve the efficiency and the environmental characteristics of coal power plants.

Keywords: IGCC, CO₂, Capture, Oxyfuel, HGCU.

GHGT-9

RWE's 450 MW IGCC/CCS Project – Status and Outlook

Werner Renzenbrink^a, Johannes Ewers^a, Dietmar Keller^a, Karl Josef Wolf^a
Wolfgang Apel^b

^a RWE Power AG, Huyssenallee 2, 45128 Essen, Germany

^b RWE DEA, Überseering 40, 22297 Hamburg, Germany

Elsevier use only: Received date here; revised date here; accepted date here

Abstract

Since mid-2006, RWE Power has been planning the construction of a coal-based demonstration power plant with carbon capture, transport and storage. A combined-cycle gas turbine plant with integrated coal gasification (IGCC) was chosen as the power plant technology to be used. The use of a modern gas turbine of the F class enables the plant to achieve a gross electric capacity of approx. 450MW. The separated CO₂ is to be stored safely over the long term in deep saline aquifers. The first grid connection is due to take place at the end of 2014/start of 2015.

As regards the power plant, a feasibility study was conducted to analyze and evaluate the technologies available in the process chain, decide on a technical concept, and establish the technical and economic parameters of the process. As far as CO₂ transport & storage is concerned, regional screening is about to be completed and the potential storage sites are being evaluated in-depth with respect to seismic data interpretation, lithology, and structure.

This presentation will outline key findings and results of this phase for both the power plant and transport & storage and present the next steps to be taken in the execution of the project. In light of a market situation characterized by high capacity utilization of potential contractors and an extraordinary rise in investment costs this aspect is currently very important. Another basic prerequisite needed for the project to proceed according to schedule is the establishment of a European and national regulatory framework for carbon transport and storage by mid-2009.

Keywords: Gasification, Coal, Electricity Generation, IGCC, Combined Cycle, CCS

1. Introduction

Innovative coal technologies are as indispensable to preventive climate protection as coal is to satisfying the world's thirst for energy. With its Clean Coal Power strategy, RWE faces the challenge of preventing climate change and is now introducing further elements of this strategy. In this respect, carbon capture and storage (CCS) play a key role if CO₂ reductions more substantial than is possible by merely increasing efficiencies are to be achieved.

* Corresponding author. Tel.: +49 201 12 24041; fax: +49 201 12 27408

E-mail address: werner.Renzenbrink@rwe.com

If this vision is to become reality, expertise, great commitment and a high willingness to take risks are required to implement a technological quantum leap.

The development of coal-fired power plants with CCS strengthens Germany's position as a technology leader, secures export potential for manufacturers and jobs in industry. The 450 MW IGCC/CCS project is part of RWE's overall strategy aimed at developing and implementing Clean Coal Power (Fig. 1).

RWE's Clean Coal Power Strategy

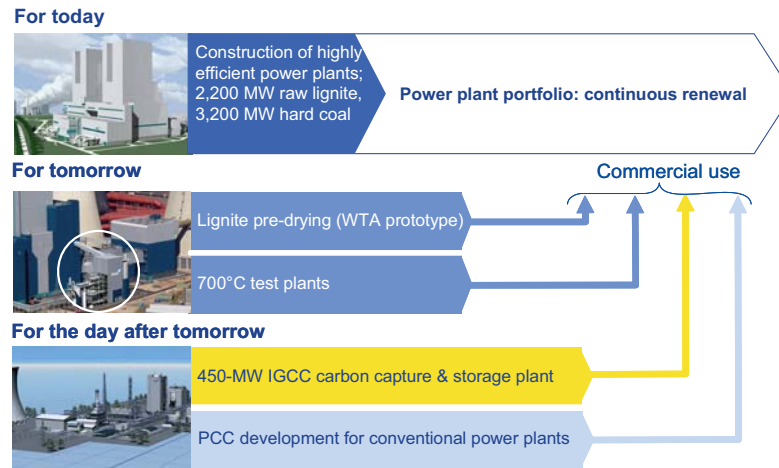


Figure 1: RWE's clean coal power strategy

On a broad basis – in line with the energy mix in the generation portfolio – innovation lines with different horizons are being pursued both for lignite and hard coal.

RWE has recently launched a large-scale renewal programme for coal- and natural gas-based power plants that involves using cutting-edge technology to increase efficiency for the sake of climate protection. Examples for the use of coal are the BoA 2/3 new-build projects at the Neurath power plant and the two hard coal-fired twin units at the Westfalen power plant and in Eemshaven in the Netherlands. The total new-build capacity based on coal amounts to 5,400 MW with corresponding capital costs of €6 bn. Each year, carbon emissions are reduced by 15 mill. t in these projects alone.

In a second horizon, RWE is developing technologies in collaboration with partners that permit efficiencies to be further increased beyond today's high level. The focus is on demonstrating the WTA (lignite pre-drying) technology, which was developed by RWE to dry moist lignite on the prototype plant at BoA 1 in Niederaussem and on the test plant for the 700°C technology; both lines of development allow a further efficiency increase of approx. 4% points. For these projects, RWE Power will expend approx. €60 million.

The 450-MW IGCC/CCS project, which will be described in the following, is the most outstanding endeavour of the third horizon, focusing on the capture and storage of the CO₂ emitted by fossil-fired power plants. In parallel, we will develop CO₂ scrubbing technologies for conventional power plants in pilot plants with the primary goal of retrofitting advanced power plants to achieve a substantial cut in carbon emissions.

The overall aim of RWE's Clean Coal Power Strategy is the continuous renewal of the power plant fleet using state-of-the-art technology that ensures both competitiveness and security of supply while protecting the climate, thus making RWE's generation business fit for the future.

2. Project Status

Following the project announcement in 2006, its concept was developed and specified in all process areas and its viability verified. RWE Power – which is responsible in the Group for electricity generation in continental Europe – was in charge of power plant matters, while RWE Dea, which is responsible for the exploration and production of crude oil and natural gas, worked on the CO₂ pipeline and storage facility. This work went hand in hand with our

intensive efforts to establish the necessary underlying conditions, such as a regulatory framework for the treatment of CO₂ and a communication concept for informing authorities and the public. In the following, the current status will be presented.

2.1. Power Plant

Figure 2 shows the key components of the power plant based on the IGCC (Integrated Gasification Combined Cycle) technology.

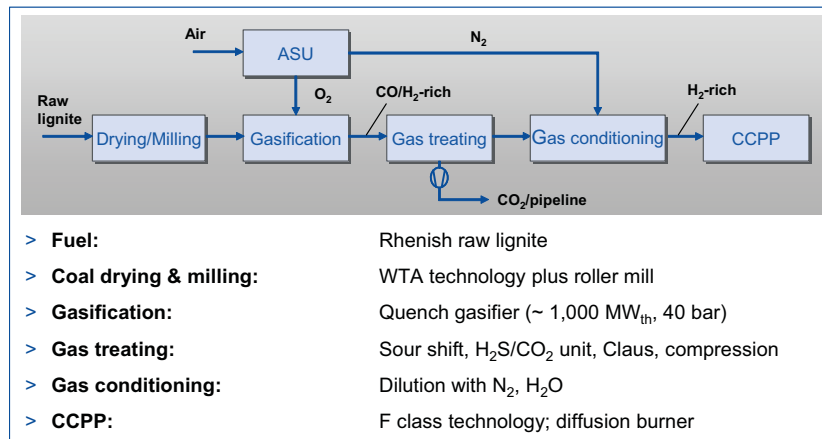


Figure 2: Main process features of the IGCC demonstration plant

Rhenish lignite from our own opencast mines serves as the fuel. In a first process step, its moisture content is reduced from approx. 55% to 12% using RWE's own WTA drying technology. Subsequently, the lignite is ground by roller mills according to gasification requirements. An entrained-flow gasifier with a dry lignite inlet and a thermal capacity of approx. 1,000 MW, operated at a pressure of approx. 40 bar, is employed for gasification. The hot, CO/H₂-rich raw gas is quenched to approx. 200°C using water. The resulting high portion of steam is used in the subsequent shift stage to convert the CO into more hydrogen and CO₂.

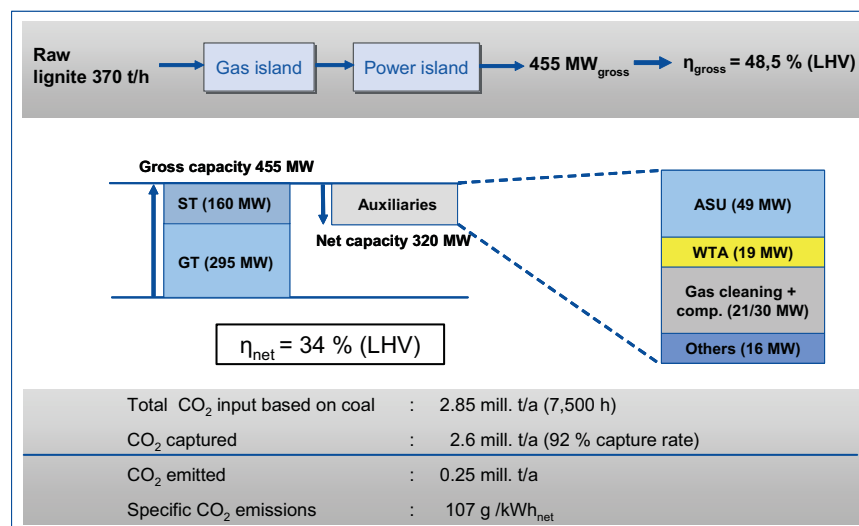


Figure 3: Key performance data of the 450 MW IGCC/CCS plant

The hydrogen-rich gas left over after the H_2S/CO_2 separation process is conditioned with N_2 from the air separation unit and if necessary with steam to create moderate combustion conditions and meet the legal requirements for NO_x values. The conditioned fuel gas is used to generate electricity in the CCPP unit. The capacity of the gas turbine (F class), which has a share of approx. 300 MW in the total electricity generation capacity of 450 MW, determines the capacity of the overall process. Thus, the process design largely corresponds to the concept of the HTW (high-temperature Winkler) demonstration plant that RWE already operated on an industrial scale from 1986 – 1997 to produce synthesis gas/methanol from lignite. The essential technical challenges of the new project consist in demonstrating the interaction of all individual processes and achieving normal power plant availability.

The gross efficiency of the overall plant (Fig 3) is 48.5% (LHV) and thus lower than that of a conventional IGCC plant. This is mainly due to conversion losses caused by the CO shift and the separation of CO_2 otherwise used as an additional working medium in the gas turbine. Taking into account auxiliary electric power requirements, the plant has a net capacity of 320 MW and a net efficiency of 34% (LHV). The carbon capture rate is calculated at 92%. We have decided to erect the IGCC/CCS power plant at the Goldenberg power plant location near Cologne (Fig 4).



Figure 4: Plant site Goldenberg/Cologne

The location thus resumes of RWE/Rheinbraun's earlier gasification activities in connection with the development of HTW gasification and it is already connected with our large lignite opencast mines via railway.

2.2. CO_2 Pipeline and Storage

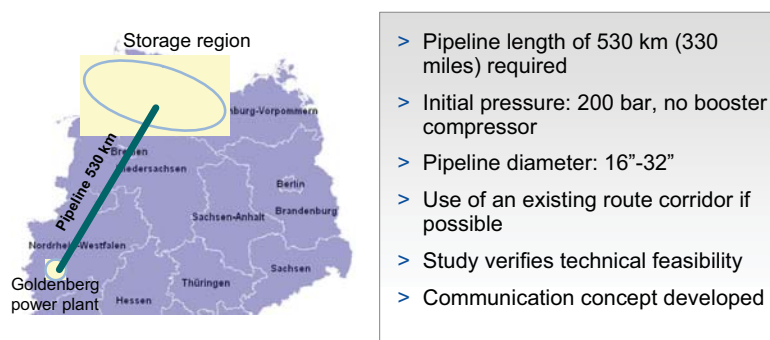


Figure 5: CO_2 Pipeline

As a result of our feasibility study regarding transport of CO_2 , pipeline is the best and most secure way to transport CO_2 , delivered from a continuous industrial process. Due to the fact that the nearest feasible storage

options are located in the northernmost Federal States, one of our challenges within this project, is the length of this pipeline. The pipeline will have a total length of approximately 530 km and will start at the power plant located in Goldenberg, cross three Federal States – NRW, Niedersachsen and Schleswig-Holstein – and will end in the northern part onshore (Fig. 5). Though, it is not planned to install a booster station. This means the pipeline will transport CO₂ in a high pressure regime. Inlet pressure will be approximately 200 bar – decreasing to 90 bar at the storage location. The diameter of the pipeline depends on pressure regime and flow rate of CO₂. By using a 16 inch diameter, we are able to transport 2.8 MM tons per year. Regarding the basic principles of spatial planning, we try to use existing pipeline routes to reduce influences through industry to public space.

Another major challenge in the pipeline project is the public acceptance. So the project has to watch carefully the public outreach and observe trends and discussions in the public. Also it is important to act proactive towards the public. A concept for communications is already developed, even in this early state.

2.3. CO₂ Storage

To find a suitable location for save storage of CO₂, RWE Dea investigated the geology of the northern part of Germany (yellow marked area in the picture of Figure 6). Criteria for suitable storage locations were:

- Depth between 1000m and 4000m to keep CO₂ in specific pressure and temperature conditions.
- Area with low tectonic impacts
- Sufficient seal, injectivity and capacity of the storage reservoir
- Preferred trapping system: Anticline/Syncline combination
- Salt structures shown as blue spots in the picture

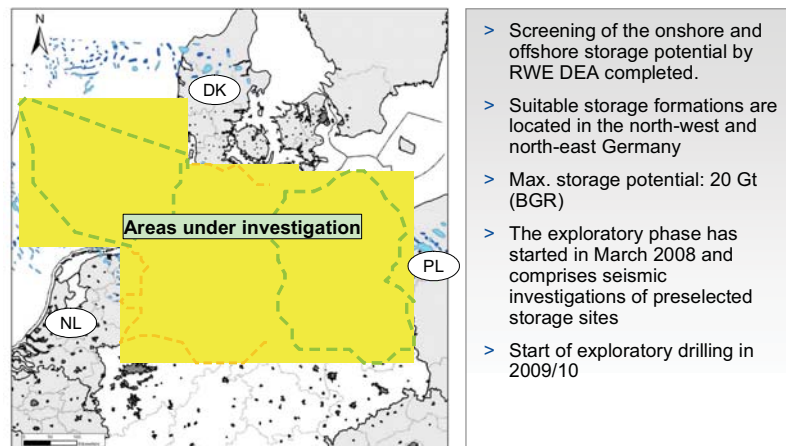


Figure 6: CO₂ Storage sites

Adequate reservoirs closest to the Rhenish Revier were found especially in northern Federal States. The technical accessible storage potential of the mentioned (yellow) study area in total is approximately 20 Gt. This means that a considerably infrastructure, including pipelines and injectors has to be installed to access this total amount of potential.

2.4. Regulatory framework

The CCS draft directive, issued by the EU at the start of 2008, in our opinion constitutes an important and positive basis for the next steps to be taken. The draft is due to be adopted at the end of 2008. Subsequently the directive has to be transposed into national law. We rely on this transposition to be completed within the current legislative period by mid-2009 to be able to keep to the project schedule. The following important requirements

have to be fulfilled by a regulatory framework from the point of view of operators:

- The experience gained from demonstration projects has to be taken account of in the regulatory framework
- Accelerated planning and building law for CO₂ pipelines
- Financial guarantees for stored CO₂ have to be adequate, risk-dependent and time-limited
- Financial support of the Federal Government in constructing a pipeline infrastructure

2.5. Important steps for implementation

With regard to the power plant, which we divide into the two main working sections ‘gas island’ and ‘power island’, work currently focuses on the selection of contractors for the PDP and FEED phase including approval planning. After the power plant, the pipeline and the storage facility have been approved – which is a prerequisite for taking the final investment decision – we will invite tenders for and award the EPC contracts.

With regard to the pipeline, the first important step in the approval procedure – namely the regional planning procedure – has just begun. After the second essential process, i.e. the formal public planning procedure, has been completed, construction can begin. As far as the storage facility is concerned, the exploratory phase comprising planned seismic investigations of preselected storage sites started in March 2008. Exploratory drilling is planned for 2009/2010.

Provided that a regulatory framework is developed in time and that the approval procedure duration is appropriate, commissioning of the project can start at the end of 2014/the start of 2015.

3. Costs and Commercial Perspective

3.1. Capital Costs

Figure 7 shows the absolute amount and structure of the capital costs of the overall project following the completion of the feasibility studies conducted in mid-2008.

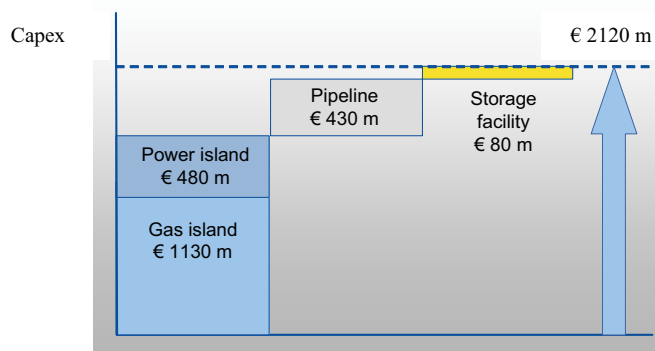


Figure 7: Capital Costs of the Demonstration Plant

The calculated costs are based on budgetary estimates provided by manufacturers for important plant units and on our own estimates for the balance of plant. The costs have been calculated on the basis of prices in 2008 in nominal terms, with an estimate accuracy of $\pm 25\%$. The total capital costs of €2,120 mill. are thus far above the €1,000 mill. mentioned in the initial project announcement.

This considerable increase in cost may be attributed mainly to the following causes:

- A longer pipeline (approx. €200 mill.)
- The general development of capital costs in the energy industry

3.2. Electricity Generation Costs

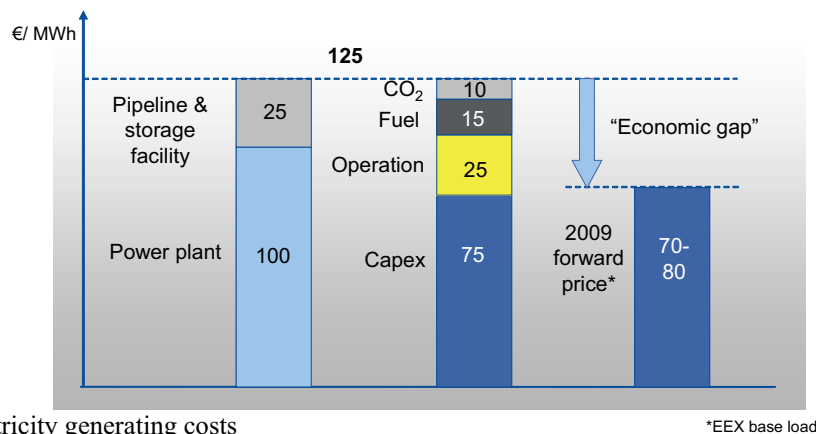


Figure 8: Electricity generating costs

The high capital costs have a corresponding effect on the electricity production costs of the demonstration plant. Figure 8 explains the structure and cost shares, which amount to a total of €125/MWh.

The power plant accounts for about 80% of the total costs. The pipeline and storage facility are estimated to constitute about 20%. At 60%, the capital costs make up the largest share of the total costs; hence the most important field for reducing the costs of future large-scale plants has been identified.

The costs have been calculated on the basis of an annual operating period of 7,500 h taking account of a learning curve in the first three years of operation, the use of Rhenish lignite, and the aforementioned technical performance of the plant. To be better able to estimate profitability, these figures are juxtaposed with the electricity prices for forwards (base load, 2009), which are currently traded for €70 - 80/MWh.

These figures confirm the typical “economic gap” of demonstration plants compared with commercial power plants.

A key driver of this effect are the high specific costs caused by the relatively low capacity of a demonstration plant, the plant concept that has yet to be optimized on the basis of the operational experience gained, and limited availability in particular during the start-up phase due to the unavoidable occurrence of “teething troubles” that have to be dealt with. Hence, an economic operation of the plant is not possible.

On the other hand, widespread commercial use before the suitability of this technology has been proven is irresponsible. For us to commit ourselves to a costly demonstration project given this situation, the following requirements must be met:

- Prospect of bridging the economic gap in future large scale plants
- Financial support by cooperations with industrial partners and/or research funding

The economic viability of the IGCC/CCS route was investigated by RWE Power as part of a separate study of large-scale plants. In addition to scale-up options for the various units in the process chain, cost reduction leverage is provided in particular by the future plant size and the implementation of learning effects gained in demonstration operation. Large-scale plants will presumably have even higher individual train capacities and be designed as a modular system based on a multi-train concept. This results especially in engineering savings, which today makes up some 20% of the capital costs of a demonstration power plant. In addition, we expect extensive optimizations and standardizations, and improvements regarding reliability, availability and maintainability (RAM) as a result of the experience gained in demonstration operation.

The widespread commercial use of CCS technology will require the construction of a pipeline infrastructure and lead to a further significant reduction in specific costs. The capex level of large-scale plants constructed after 2020 remains unpredictable. The large-scale plant study conducted by us assumed that the capital cost level remains unchanged compared with 2008.

Tapping the above-mentioned cost reduction potentials has a decisive effect on electricity generation costs. Fig. 9 shows that future large-scale IGCC/CCS plants will reach a level of €80/MWh.

By comparison, a conventional steam power plant equipped with cutting-edge technology has to buy a larger amount of emission allowances since it is operated without CCS. The electricity generation costs of this power plant are at the same level as those for the IGCC/CCS, resulting in avoidance costs of €46/t (See calculation shown in Fig. 9).

In case of higher allowance prices, the CCS technology is economically superior to conventional technology. The assumptions regarding expected carbon prices are understandably very uncertain. According to [1], for instance, a range of €35-50/MWh is specified for early full commercial-scale CCS projects, while prices in the mature commercial phase are expected to be in the range of €30-45/MWh.

This indicates that large-scale IGCC/CCS plants are basically viable, which justifies their further development. The high costs and risks of the demonstration plant nevertheless have to be dealt with. Thus, RWE Power is seeking financial support by cooperations with industrial partners and/or by research funding.

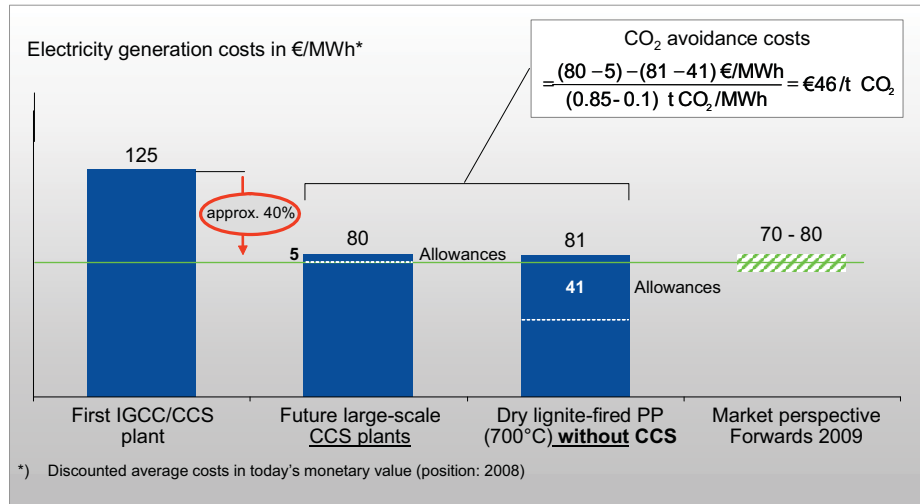


Figure 9: Commercial perspectives of future large-scale powerplants

4. Conclusion

RWE is working hard to promote the project in all fields. The key factors for successful implementation are:

Costs and profitability:

- Commercial large-scale IGCC/CCS plants can be economically self-sustaining.
- The high costs and risks of the demonstration plant require financial support.

Regulatory framework:

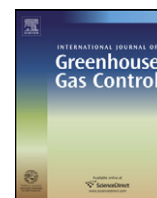
- Viable regulations must be developed as quickly as possible

Acceptance:

- Public awareness and support require a comprehensive communication concept and political support.

We rely on the commitment of all those involved to demonstrate the climate-friendly use of coal.

[1] Carbon Capture & Storage: Assessing the Economics, McKinsey Company, 2008



Overall environmental impacts of CCS technologies—A life cycle approach

Petra Zapp^{a,*}, Andrea Schreiber^a, Josefine Marx^a, Mike Haines^b, Jürgen-Friedrich Hake^a, John Gale^b

^a Forschungszentrum Jülich, Institute of Energy and Climate Research – Systems Analysis and Technology Evaluation (IEK-STE), D-52425 Jülich, Germany

^b IEA Greenhouse Gas R&D Programme, Stoke Orchard, Cheltenham, Glos. GL52 7RZ, UK

ARTICLE INFO

Article history:

Received 15 August 2011

Received in revised form 23 January 2012

Accepted 26 January 2012

Available online 24 February 2012

Keywords:

Carbon dioxide capture and storage

Life Cycle Assessment

Methodology approach

Technology evaluation

Study comparison

ABSTRACT

In the last decade the environmental performance of climate effective carbon dioxide capture and storage (CCS) considering also other environmental effects has become focus of several studies. With various technological CCS options under development, the field of possible technical solutions is hardly covered yet. This paper identifies technologies whose environmental effects have been analysed from a life cycle perspective.

Life Cycle Assessment (LCA) has proved to be a helpful tool to investigate the environmental consequences associated with the introduction of CCS. Even though, big differences in underlying assumptions of existing studies make comparison difficult, some general effects can be described.

In general the intended reduction in GWP by introducing CO₂ capture (up to – 85% hard coal oxy-fuel, – 95% lignite oxyfuel, – 80% natural gas post-combustion) is combined with an increase of other environmental effects, regardless of capture technology, time horizon or fuel considered. Performing the normalisation step shows that acidification and human toxicity potential have to be watched as well.

Additionally, three parameter sets have been identified, which have a significant impact on the effects: (a) development of plant efficiencies and energy penalties; (b) capture efficiency; (c) fuel origin and composition.

© 2012 Elsevier Ltd. All rights reserved.

1. Introduction

Main environmental focus of carbon dioxide capture and storage (CCS) technology is the extensive reduction of CO₂ emissions into the atmosphere at large point sources in order to protect our climate. This clearly essential goal, however, can only be reached by losing some of the efficiency. Furthermore, some technologies induce other environmental impacts which have to be recognised. A life cycle approach, including into the analysis upstream processes like additional fuel and operation material supply as well as downstream processes such as waste treatment, provides a basis for an extensive assessment of environmental impacts of commercial CCS adoption.

In the last years, several studies have addressed environmental consequences associated with the introduction of CCS in power plants beyond CO₂ reduction using Life Cycle Assessment (LCA) as a tool. Basis for the environmental assessment in this paper is a study on behalf of the IEA Greenhouse Gas R&D Programme (IEAGHG) finalised spring 2010 (Marx et al., 2010) in which the results of different studies were systematically compared considering the different approaches, site and time specific differences, and

methodological variations. Moreover, two recent studies are added to this analysis (Nie et al., 2011; Singh et al., 2011). In total the environmental assessment of this report is based on seventeen studies which have been undertaken after 2000, not including CCS studies dealing with enhanced oil and gas recovery (EOR, EGR) to maintain comparability. Many studies (9) have a European focus, three consider the US situation, one looks at the Japanese situation and four have a global approach. Even though basic assumptions differ in the studies as a matter of course, this paper tries to draw some general conclusions regarding environmental effects by combining the findings of the studies.

2. Systematic comparison of study parameters

A comparison of competing energy technologies requires a thorough understanding of each system and its boundaries. Assumptions regarding functions of the systems, their boundaries and generic data are especially important. Additionally, the wide range of performance possibilities and methodological challenges of LCA make a close investigation of the studies and their results necessary.

The functional unit of all investigated systems is 1 kWh of electricity generation. Other assumptions differ more widely within the studies, due to the varying focuses. In the following, the impacts on the results are described.

* Corresponding author. Tel.: +49 2461 615942; fax: +49 2461 612540.

E-mail address: p.zapp@fz-juelich.de (P. Zapp).

2.1. Technology driven differentiation

Some studies compare different CCS technologies against each other, while other studies concentrate on one specific CCS technology and/or compare CCS routes against alternative low CO₂ emission technologies such as energy production by renewable energy sources. A comparison with renewable systems is quite complex, due to different availability of 1 kWh of electricity produced by some renewable technologies (e.g. wind, photovoltaic) compared to fossil fuel technology. Furthermore renewable technologies have clearly lower global warming potential (GWP) but induce other impacts such as change of biocoenosis for wind or impairment of habitat for solar power (Viebahn et al., 2007). Additionally a couple of studies have a clear focus on the comparison of CCS and renewable energy generation (Spath and Mann, 2004; Viebahn et al., 2007). However, a detailed comparison between CCS-enabled electric power systems and renewable energy systems is not the focus of the work presented here.

2.1.1. Capture technology

The three capture technology routes, post-combustion, oxy-fuel and pre-combustion constitute the first differentiation criteria. Post-combustion capture technology as one possible future CCS system is examined in nearly every study. CO₂ capture systems that utilize Mono-ethanolamine (MEA) scrubbing are common to all papers analysed here. As several demonstration plants using MEA scrubbing already exist, some operation data should be available. However, most studies rely on modelled data.

Only two studies investigate other post-combustion technologies (Khoo, 2006; D'Addario et al., 2003). While Muramatsu and Iijima (2002) examined the performance of MHI's proprietary amines for CO₂ capture. The oxyfuel process route is described only in five of the newer studies (NEEDS et al., 2008; Nie et al., 2011; Pehnt and Henkel, 2008; Singh et al., 2011; Viebahn et al., 2007). The IGCC/NGCC technology with integrated pre-combustion technology is the objective of 9 studies (D'Addario et al., 2003; Doctor et al., 2001; IEA, 2006; NEEDS et al., 2008; Lombardi, 2003; Odeh and Cockerill, 2008; Pehnt and Henkel, 2008; Singh et al., 2011; Viebahn et al., 2007) (Table 1).

As fuel hard coal is considered in 14 studies. In four studies (NEEDS et al., 2008; Pehnt and Henkel, 2008; Schreiber et al., 2009; Viebahn et al., 2007) lignite as a local fuel is assumed. Looking at a European or even global level, natural gas is investigated as well (9 studies) (D'Addario et al., 2003; IEA, 2006; Modahl et al., 2009; NEEDS et al., 2008; Lombardi, 2003; Odeh and Cockerill, 2008; Singh et al., 2011; Spath and Mann, 2004; Viebahn et al., 2007) (Table 1).

As CCS is a future technology, the technological representation varies considerably across these studies. The used power plant information is either gathered by own modelling (often using Aspen) or by literature study. Typical literature which is quoted regularly is (Göttlicher, 1999; Rao and Rubin, 2002; Rubin et al., 2007; Thitakamol et al., 2007; Tzimas et al., 2007). As several of the studies focus on Europe the Ecoinvent database (Ecoinvent Centre, 2007) is often used for background data (IEA, 2006; Koornneef et al., 2008; NEEDS et al., 2008; Odeh and Cockerill, 2008; Pehnt and Henkel, 2008; Schreiber et al., 2009; Viebahn et al., 2007; Wildbolz, 2007).

No common understanding of future efficiency development for commercial power production exists, let alone of energy penalties due to capture. Often it is not clear which detailed technical assumptions, e.g. technological representation or emission reduction efficiencies are used for the analysis. In Fig. 1 the net efficiencies and the assumed energy penalties of the different studies are presented with respect to the fuels used.

For hard coal post-combustion efficiency values between 29.6% (2010 retrofit, Schreiber et al., 2009) and 49% (values for 2050,

Table 1
Scope of LCA studies.

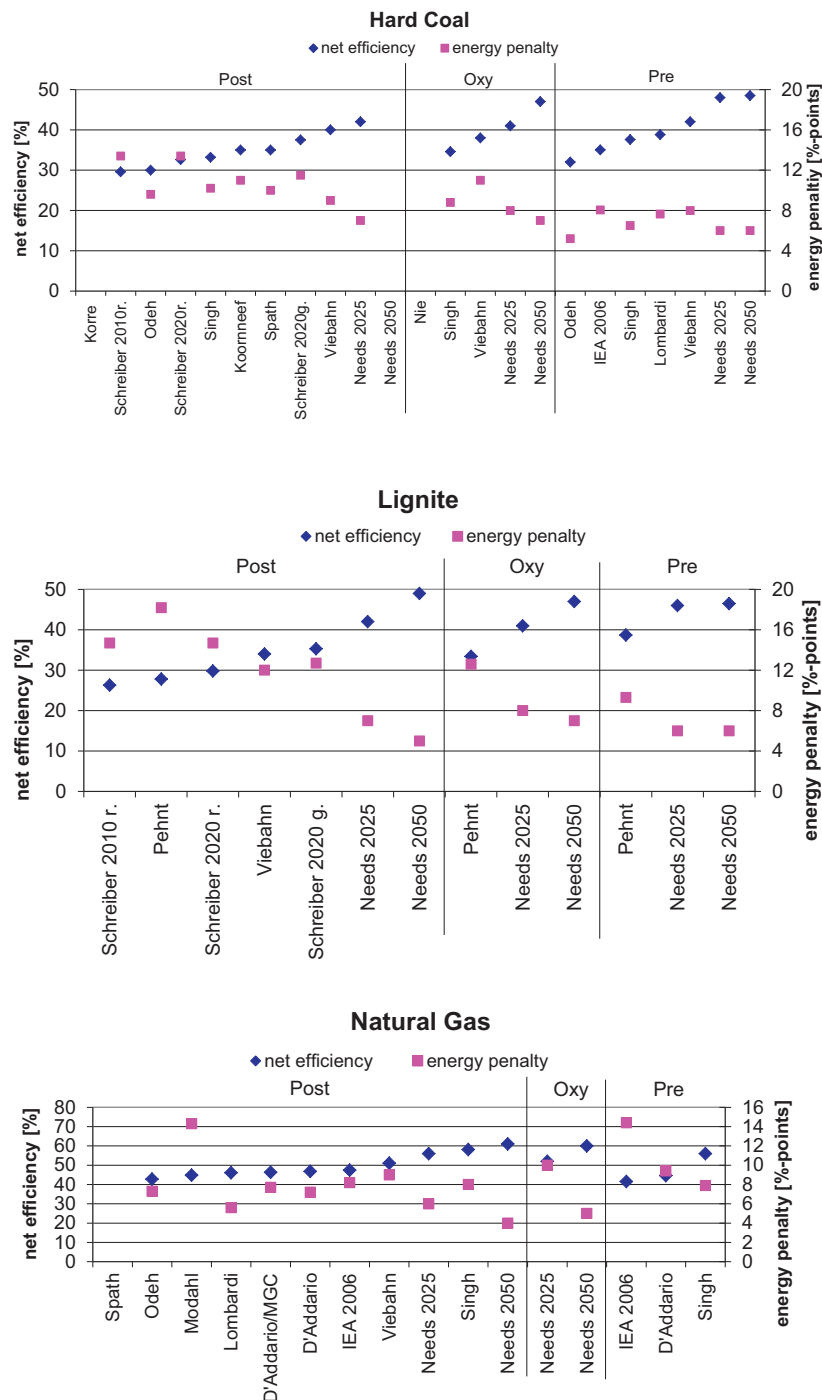
Study/year	Region	Time horizon	Capture		Fuel			Coverage		Outcomes			Normal. step	Aggregation
			Post-comb.	Pre-comb.	Oxy-fuel	Hard coal	Lignite	Gas	Trans. & storage	Emissions	GWP	Other impacts		
D'Addario et al. (2003)	Middle Italy	Present	X	X				X		X	X	X		
Doctor et al. (2001)	US	Present	X	X		X			Only T		X	X		
IEA (2006)	Global	Present–2050	X	X		X		X		X	X	X		
Khoo (2006)	US	Present	X			X			X ^{b,c}	X	X	X		X
Koornneef et al. (2008)	Netherlands	2000/2020	X			X			X ^c	X	X	X	X	
Korre et al. (2009)	Global	n.a.	X			X				X	X	X		
Nie et al. (2011)	Global	n.a.	X		X	X			X ^c	X	X	X		
Lombardi (2003)	Hypothetic (Italian costs)	n.a.	X	X		X		X		X	X	X		
Modahl et al. (2009)	Norway	n.a.	X					X	X ^b		X	X	X	X
Muramatsu and Iijima (2002)	Japan	Present	X			X			X ^b	X	X	X		
NEEDS et al. (2008)	Europe	Present, 2025, 2050	X	X		X	X	X	X ^c	X	X	X ^a		
Odeh and Cockerill (2008)	UK	2005	X	X		X		X	X ^b	X	X	X		
Pehnt and Henkel (2008)	Germany	2020	X	X		X	X	X	X ^c	X	X	X		
Schreiber et al. (2009)	Germany	2020	X	X		X	X	X	X ^c	X	X	X	X	
Singh et al. (2011)	Global	n.a.	X	X		X	X	X	X ^c	X	X	X		
Spath and Mann (2004)	US	Present	X	X		X		X	X ^c	X	X	X		
Viebahn et al. (2007)	Germany	2020	X	X		X	X	X	X ^c	X	X	X	X	

n.a., not available.

^a Personal communication (Bauer, 2009) based on NEEDS inventory.

^b Offshore.

^c Onshore.



Values for (Korre et al, 2009; Nie et al, 2011; Spath and Mann, 2004) are not available; r = retrofit, g = greenfield

Fig. 1. Net efficiency and energy penalty.

NEEDS et al., 2008) can be found. For lignite the difference between the lowest (26.3%, 2010 retrofit, Schreiber et al., 2009) and the highest efficiency (49%, values for 2050, NEEDS et al., 2008) is even higher. For the oxyfuel process a high share of energy is needed for the oxygen production. The specific demand is still very unclear, figures ranging from 160 kWh/tO₂ in Doosan Babcock (2009) up to 320 kWh/tO₂ in Pehnt and Henkel (2008). The significant difference originates from the underlying time perspective and the future technological representation of the studies. As expected NEEDS et al. (2008), the study with the furthest time horizon 2050, assesses the highest net efficiencies. In general, energy penalties for

pre-combustion processes are the lowest and for post-combustion the highest. The energy penalty of lignite fuelled post-combustion power plants differs mostly (from 7%-points up to 18.2%-points) due to different states of technology. The capture technology can be retrofitted to an existing power plant leading in higher energy penalties or being integrated into an optimised greenfield power plant, as explicitly analysed in Schreiber et al. (2009).

2.1.2. Transport and storage

All studies which include CO₂ transportation and storage into their analysis describe the share of these processes on the

Table 2
Impact categories considered.

Impact category	Abbreviation	Short description	Example of relevant LCI data	Characterisation factor (Guinée et al., 2002)
Global warming potential	GWP	Impact of human emissions on radiative forcing of atmosphere, causing a temperature rise	CO ₂ , N ₂ O, CH ₄ , SF ₆ , CHCl ₃ , CF ₄ , CFCs, HCFCs, CH ₃ Br	kg CO ₂ -equiv.
Acidification potential	AP	Emission of acid-forming substances	SO _x , NO _x , HCl, HF, NH ₃ , HNO ₃ , H ₂ SO ₄ , H ₃ O ₄ P	kg SO ₂ -equiv.
Eutrophication potential	EP	Excessive supply of nutrients	PO ₄ ³⁻ , N ₂ , NO ₂ , HNO ₃ , NH ₃ , H ₃ PO ₄ , COD	kg PO ₄ ³⁻ equiv.
Photochemical oxidation potential	POCP	Summer smog; formation of reactive chemical compounds by action of sunlight on primary pollutants	PAH, NO _x , NMVOC, CH ₄	kg ethylene-equiv.
Human toxicity potential	HTP	Impacts on human health of toxic substances	PM10, SO ₂ , NO _x , CH ₄ , CH ₂ O, C ₆ H ₆ PAH, As, Cd, dioxin	kg 1,4-DCB-equiv.
Fresh water aquatic ecotoxicity potential	FAETP	Effects of toxic substances on fresh water	Heavy metals	kg 1,4-DCB-equiv.
Terrestrial ecotoxicity potential	TETP	Effects of toxic substances on soil	Heavy metals	kg 1,4-DCB-equiv.
Cumulative energy demand	CED	Quantity of energy used	Energy resources	MJ

environmental effects of the overall system as relatively small, though in a wide range (approx. 1–10%), depending on the capture performance and fuel used. The lower the efficiency of the power plant (e.g. old-fashioned lignite-fuel power plants) or the higher the capture rate, the more CO₂ emissions have to be captured resulting in higher efforts for CO₂ transport and storage. Also, transport distance, number of recompression steps along the pipeline, type of storage (gas field, saline aquifer), and depth of injection affect the results, but to a smaller degree. Wildbolz (2007) stated a threefold higher energy demand for CO₂ injection and storage in a depleted gas field (2500 m deep) than in a saline aquifer (800 m deep). The length of the pipeline has the smallest effect. Spath and Mann (2004) received a share of transport on total GWP rising from 0.1% for 300 km to 1% for 1800 km pipeline length. However, as the different studies often do not describe the underlying parameters, it is not always possible to assess the share of transport and storage to the specific matters in detail.

2.2. LCA methodology driven differentiation

Although a standard defines the procedure of an LCA (ISO 14040/14044, 2006), the margin of flexibility in how to perform an LCA is still wide. As a consequence, some choices have a high impact on the overall results.

2.2.1. Impact categories

In the life cycle impact assessment (LCIA) the environmental effects of the investigated system are described by allocating the comprehended inputs and outputs to impact categories. For some impact categories there are several characterisation models and category indicators suggested. So it might be possible that studies, although addressing the same impact category, cannot be compared directly, because they use different category indicators. The NEEDS et al. (2008) study considers only inventory data (e.g. materials, energy, emissions). On basis of these data Bauer (2009) provided (for the 2025 systems) impact data (such as global warming potential) also, to allow comparison with the other studies.

Here results are presented for those categories for which a sufficient number of studies use the same impact indicator. The considered categories are: global warming potential GWP, acidification potential AP, eutrophication potential EP, photochemical oxidation potential POCP, human toxicity potential HTP, fresh water aquatic ecotoxicity potential (FAETP), terrestrial ecotoxicity potential (TETP) and cumulated energy demand CED. Table 2 describes briefly the different impact categories, names typical

emissions contributing to this effect and state the category indicator by which the effects are expressed.

The impact assessment is completed by applying a normalisation step in order to gain a better understanding of the relative importance of an effect on the environment (see also Section 2.2.3). As different impacts do not correspond directly to perceptible problems or prevailing threats it is sometimes difficult to interpret these absolute values. Therefore, each effect is benchmarked against the known total effect for this class of a specific region, e.g. Europe, global, to better understand the relative importance of this environmental effect.

2.2.2. Time horizon

The time horizon has an impact on the future technical parameters which are selected for CCS but also those selected for competing technologies. Almost all studies consider present and future power plant and CCS systems up to the year 2020. IEA (2006) and NEEDS et al. (2008) extrapolate the power plants up to 2030 and even to 2050, resulting primarily in different technology descriptions (see also Section 2.1.1).

The choice of time horizon plays also an important role evaluating the storage process and especially possible leakage. In LCAs, long-term emissions are implicitly cut off. Beyond this it is not clear, how far the long-term CO₂ emissions from possible storage leakage (occurring after 100 years or more) will have a negative environmental effect in the remote future. Apparently, LCA is not the appropriate tool to integrate long-term aspects. Nevertheless, Khoo (2006) and Viebahn et al. (2007) consider different leakage rates, to get an idea of long-term impact and not to underestimate the storage phase by ignoring it at all.

2.2.3. Spatial representation

In the CCS chain especially the storage sites are highly site specific. However, in those studies where storage is included, no site specific information beside CO₂ transport distances and in some studies number of wells as well as the energy demand for recompression and injection is used to describe the process.

Additionally, many products of second order processes, such as fuel supply or electricity mix are very site specific. Especially hard coal supply has a high impact on the results. Also different coal compositions yield to different power plant emissions even when the same technology is used. However, only a few studies explicitly address this topic (Korre et al., 2009; Odeh and Cockerill, 2008; Schreiber et al., 2009). Underlying site specific assumptions are hardly addressed, so that it is difficult to determine the effects on the results.

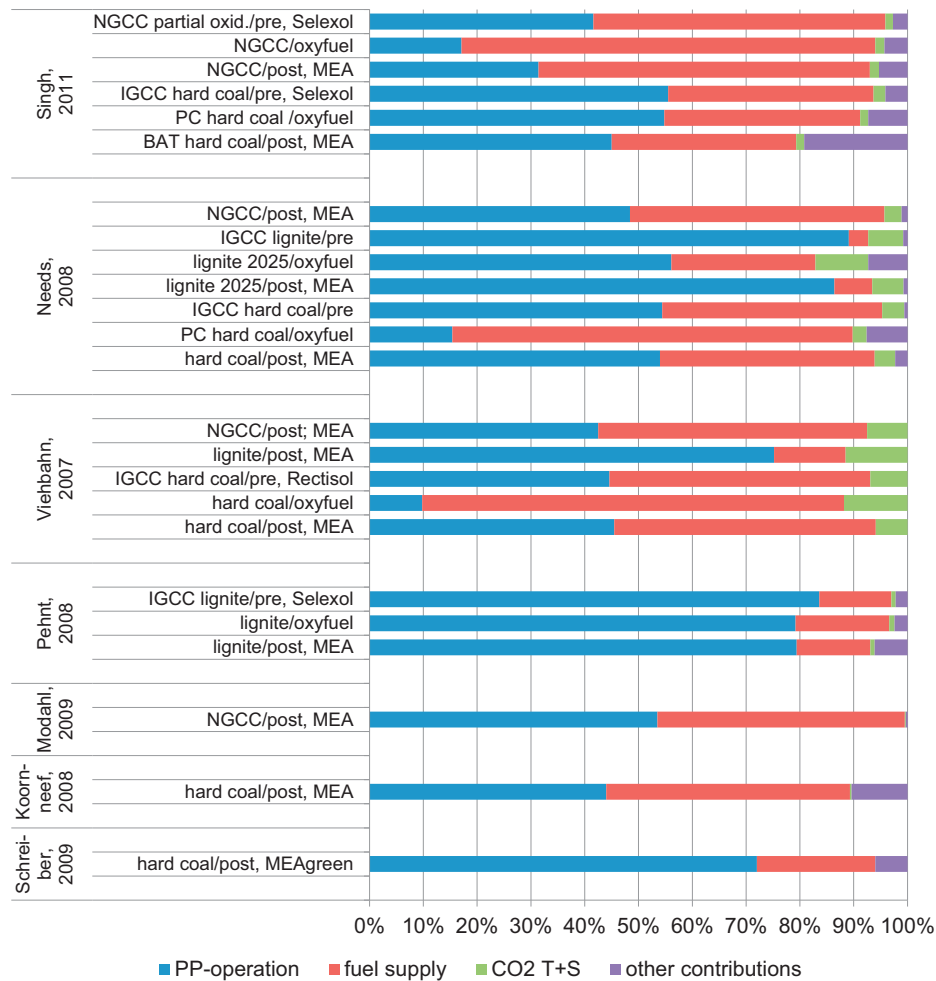


Fig. 2. Fractions of life cycle phases on GWP for different studies.

The different environmental impacts contribute on global (climate change, stratospheric ozone depletion), regional or even local scales (acidification, eutrophication). Related to the geographical location the impacts for regionally or locally scaled emissions can vary widely, depending on the ecosystem sensitivity. Although there are some approaches for including regionally different environmental impacts under discussion (Posch et al., 2008; Seppälä et al., 2006) no study uses site or region dependent impact factors. A marginal approach to consider regional references is the normalisation step, where each effect is benchmarked against the known total effect for this class of a specific region. Those studies (Koornneef et al., 2008; Modahl et al., 2009; Schreiber et al., 2009) including the normalisation step use the same approach of CML 2001 (Guinée et al., 2002) but different country specific data to set the relation.

2.2.4. Upstream and downstream processes

The analysis of the studies clearly shows the significant influence of upstream and downstream processes on the overall emissions and their impacts. The different studies approach the topic of upstream and downstream processes on different levels of detail. Along different impact categories the share can vary considerably. For power plants with CCS it is in general higher than for power plants without CCS, due to losses in efficiency associated with additional demand of fuel. For GWP the share of the different life cycle stage are described exemplarily for some studies in Fig. 2, distinguishing between emissions from power plant operation, fuel supply, CO₂ transport and storage, and other contributions. This last

category combines solvent supply, construction and dismantling of power plants which cannot be identified separately for all studies.

The variations between the different studies become obvious. The share of upstream and downstream processes varies from 90% for a hard coal oxyfuel plant in Viebahn et al. (2007) to 10% for an IGCC lignite pre-combustion plant in NEEDS et al. (2008). Also the differences in CO₂ transport and storage relevance can be seen (see also Section 2.1.2). However some trends can be identified. Within one fuel type the oxyfuel technology shows the least emissions by far at the power plant itself, followed mostly by post-combustion and then pre-combustion, which are often close by. Comparing within one technology route, the gas supply chain has the highest share and the lignite supply chain the clearly smallest (note that this order must not be the same for the absolute values). Consequentially, for lignite fuelled plants a performance improvement at the power plant itself is most promising, while for the other fuels a revision of the supply chain is interesting as well. Especially for the oxyfuel concept fuelled by gas or hard coal, contribution to GWP is dominated by the fuel supply chain.

The hard coal supply chain also contributes strongly to other impact categories, such as AP, EP and POCP. Especially ocean coal transport via ship fuelled by heavy oil is the major contributor (above 30%) to the AP. Furthermore, the MEA production chain accounts for an extreme increase in the HTP score due to the emission of ethylene oxide to air and water. In contrast to that the direct MEA emissions and the disposal of reclaimers bottoms from the capture process contribute only to a very small extent (0.005%) to HTP (Koornneef et al., 2008).

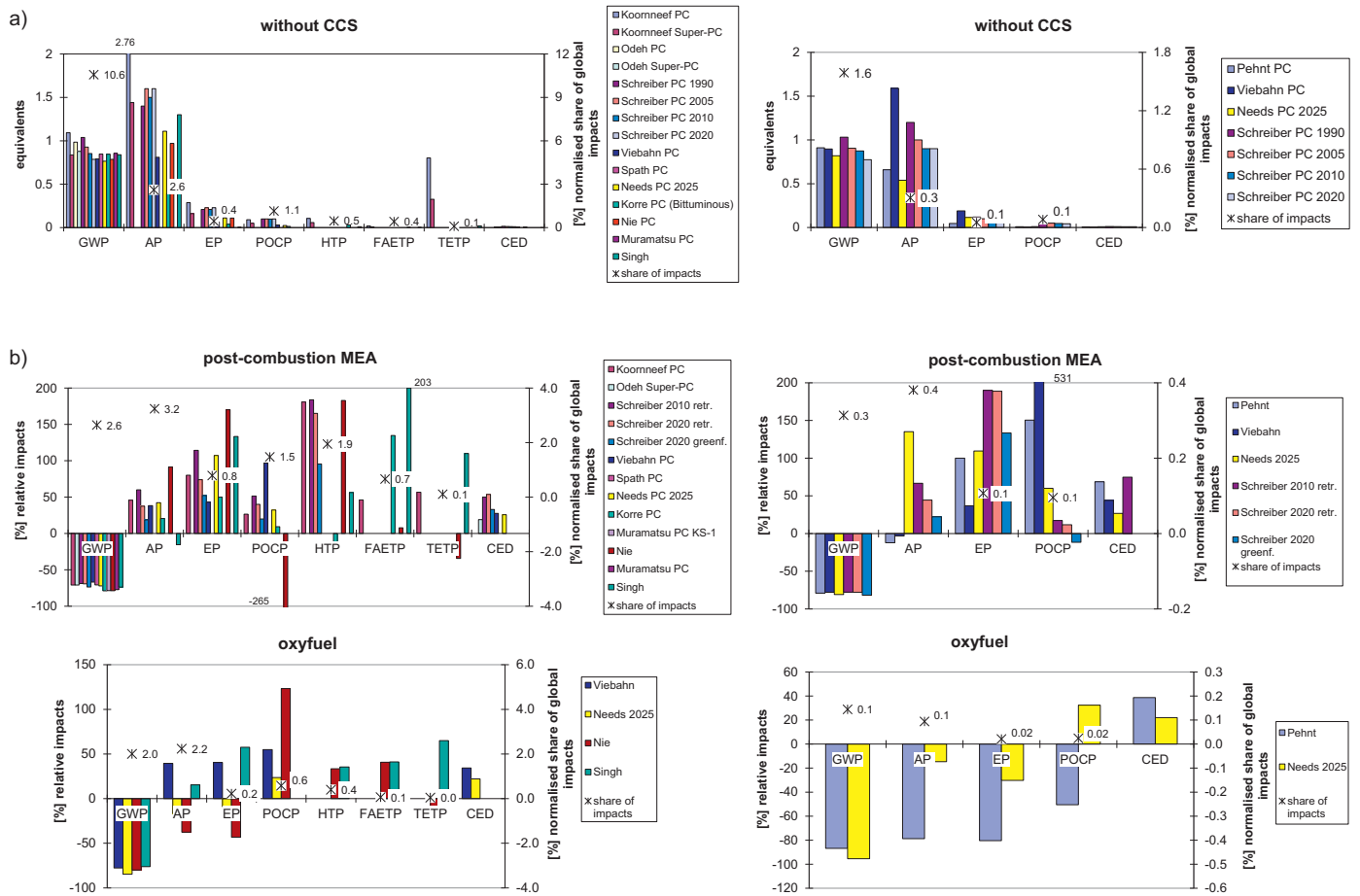


Fig. 3. Environmental impacts of hard coal (left column) and lignite (right column) fired pulverised coal combustion technology (a) without capture and (b) relative impacts for plants with post-combustion/MEA or oxyfuel capture and normalised values related to global emissions in 2000.

For conventional power systems it has often been proved, that construction and dismantling of power plants can be neglected. Koornneef et al. (2008) and Pehnt and Henkel (2008) consider a share of less than 0.2% on the total GWP connected to those life cycle phases. While for CCS systems the absolute GWP emissions during power plant operation are reduced, the values for construction and dismantling are constant, resulting in an increasing proportion of the construction and dismantling path. The studies differ in their estimation between 0.34% in Lombardi (2003) for a hard coal based IGCC and 4.9% in NEEDS et al. (2008) for a lignite fuelled oxyfuel system. In contrast, Singh et al. (2011) points out, that especially for other inputs such as EP but also toxicities (human, ecosystem, fresh water, marine), the influence of additional infrastructure increases significantly due to heavy metal emissions associated with the material production (mainly steel).

The upstream and downstream process chains are often not represented with the same quality as the main processes. For example, the score for HTP is highly uncertain due to possible inaccurate data on the production of MEA (Koornneef et al., 2008; Schreiber et al., 2009). This data should be verified because they have a major influence on the outcome.

3. CCS technologies and their impacts

The environmental impacts of CCS technologies are compared considering different capture techniques and types of fuel (Figs. 3–5). Therefore, the absolute impact equivalents for each fuel and technology are presented in the first diagram of a figure (a). The subsequent graphs always show the relative difference due to CO₂

capture (b). As discussed before, a presentation of relative changes in one diagram without further reflection might overvalue impact categories with big changes but still small contribution to the total environment. Therefore, a yearly contribution to a specific region is given as evidence (normalisation step). As the different studies cover different regions global emissions are chosen for the reference system. In an extensive study Sleeswijk et al. (2008) have gathered worldwide emissions for all impact categories for the year 2000 and calculated subsequent global normalisation values. Table 3 shows these global values for the different impact categories as the latest available figures.

For the CCS systems arithmetic average impact data were calculated from the studies for each capture technology. According to a specific capture route and fuel global power generation with this average impact data is assumed. For consistency, electricity generation figures for the different energy sources for the same year 2000 (hard coal: 5136 TWh, lignite: 749 TWh, natural gas: 2677 TWh; OECD/IEA, 2002) are chosen. Hence, in each figure (Figs. 3–5) the share of an assumed global power generation using exclusively one specific technology is given to display the importance of the various impact categories, by relating it to the total global emissions for the year 2000.

3.1. Hard coal and lignite

The absolute GWP of pulverised hard coal combustion technology without capture varies between 765 g CO₂-equiv./kWh (a future 2025 plant in NEEDS, 2008) and 1092 g CO₂-equiv./kWh (old PC plant 2000 in Koornneef et al., 2008), depending on the

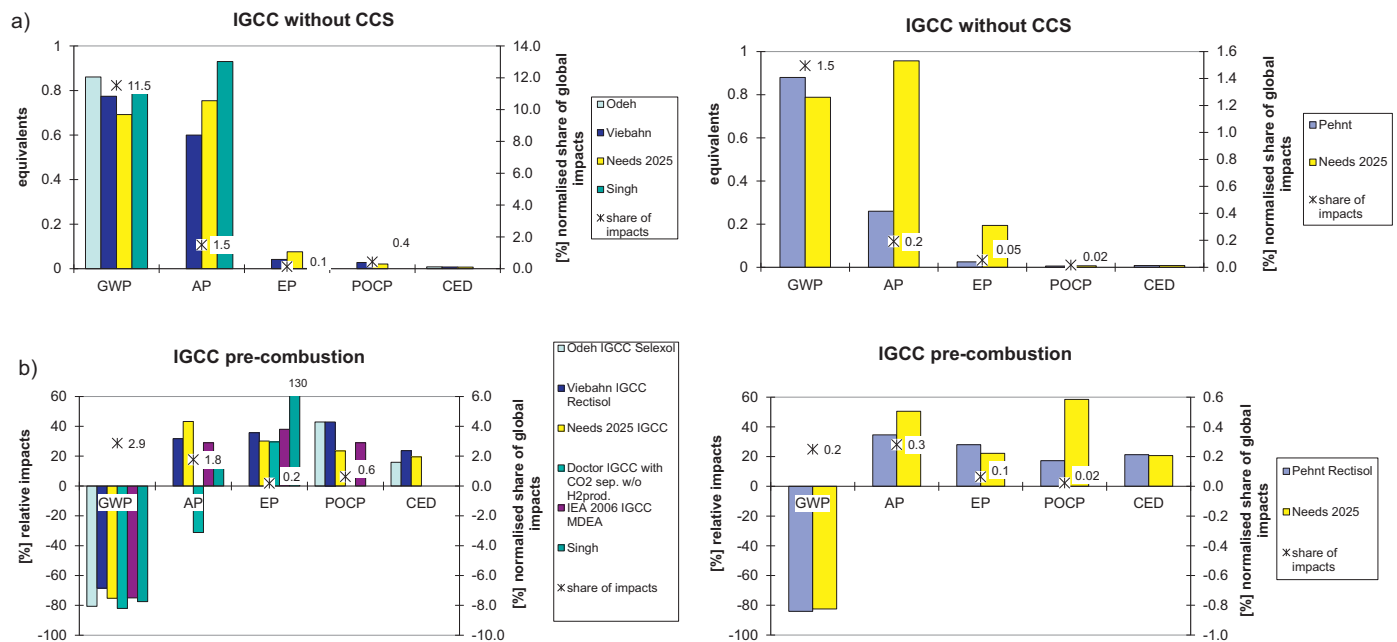


Fig. 4. Environmental impacts of an IGCC hard coal (left column) and lignite (right column) gasification system (a) without capture and (b) relative impacts of systems with pre-combustion capture and normalised values related to global emissions in 2000.

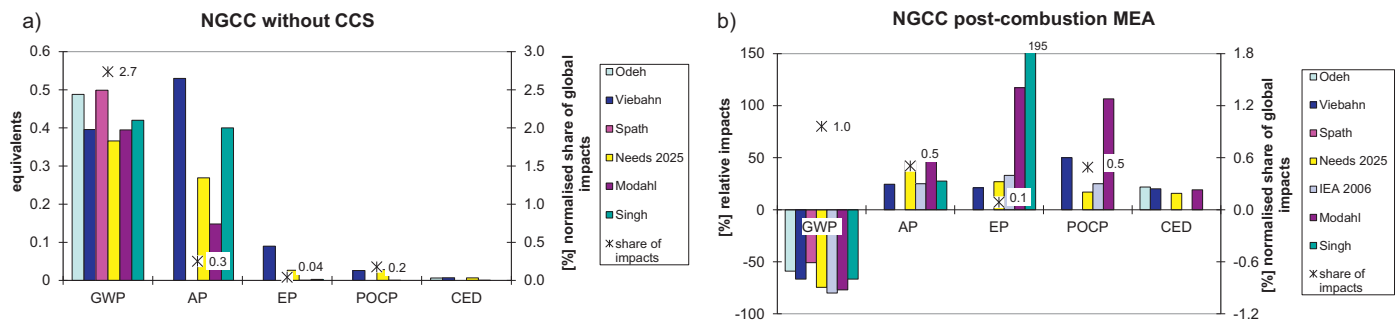


Fig. 5. Environmental impacts of a natural gas combined cycle (a) without capture and (b) relative impacts of systems with post-combustion MEA-capture and normalised values related to global emissions in 2000. No absolute figures for IEA (2006) available.

estimated efficiency and, to a lower extent on the type of coal used (Fig. 3a, left). The acidification potential values scatter much more. Koornneef et al. (2008) assume a very high value (2.8 g SO₂-equiv./kWh) for an old average PC plant from 2000, while the lowest value is 0.39 g SO₂-equiv./kWh (Korre et al., 2009). Most important here is the assumed flue gas treatment, but also again the coal composition. EP, POCP, CED as well as the toxic effects (HTP, FAETP and TETP) vary corresponding to the efficiencies assumed.

As expected the GWP for a lignite base plant without CCS (Fig. 3a, right) is slightly higher compared to hard coal. The AP varies between 0.66 and 1.59 g SO₂-equiv./kWh. In contrast to hard coal supply the local lignite mining requires no long distance transport

Table 3
Normalisation factors world 2000 (Sleeswijk et al., 2008).

Impact category	World 2000
Global warming potential (GWP 100 years)	4.18E+13 kg CO ₂ equiv.
Acidification potential (AP)	2.39E+11 kg SO ₂ equiv.
Eutrophication potential (EP)	1.58E+11 kg phosphate equiv.
Photochemical oxidation potential (POCP)	2.90E+10 kg ethane equiv.
Human toxicity potential (HTP)	3.63E+12 kg DCB equiv.
Fresh water aquatic ecotoxicity potential (FAETP)	3.47E+12 kg DCB equiv.
Terrestrial ecotoxicity potential (TETP)	1.09E+12 kg DCB equiv.

systems which are associated with NO_x and SO₂ emissions causing AP. Consequentially, lignite shows lower AP values.

The normalisation shows, that global hard coal based power generation (5136 TWh) without CCS contributes considerably to global GWP, with a share of 10.6%, assuming the power production by an average hard coal power plant gathered from the information of the studies. The share on the world's AP is 2.6%. Even smaller are the other effects (EP, POCP, HTP, FAETP and TETP). Due to the much smaller amount of power generation by lignite fired plants worldwide (749 TWh), the share of all environmental impacts on the global impact is much smaller, than for hard coal. For GWP it is maximum 1.6% without CCS and all other categories are negligible.

As expected, the results for hard coal and lignite power generation with CCS clearly indicate a substantial reduction in GWP. However, the reduction is less than the considered CO₂ capture rate (in most studies 90%). One reason is the efficiency loss and subsequently additional coal demand resulting in a higher amount of CO₂ emissions which have to be captured. Additionally, this higher coal demand results in an increase of methane emissions during mining and transport of the hard coal.

Furthermore, the LCAs show an increase in all the other considered impact categories (AP, EP, POCP, HTP, FAETP, TETP and CED) for post-combustion. The AP and EP of a MEA post-combustion system increases in almost all studies even though further reductions

of SO₂ and of NO_x at the power plant by improved flue gas desulphurisation (FGD) and denitrification, respectively, are assumed. Beside minor emissions from MEA processes main reason for this effect are the assumed higher SO₂ and NO_x emitted during heavy-oil freighter transport according to additional coal demand. This transport is also reason for the increase in POCP together with higher methane emissions by increased coal mining and ethylene oxide formation during the production of MEA.

Here, LCA shows clearly, that impacts are shifted between life cycle phases and by doing so probably also to other regions. While SO₂ and NO_x decreases at the power plant itself, the regional effects of AP and EP decreases as well (for example in Europe). Nonetheless, SO₂ and NO_x are increased during transport and associated AP and EP effects occur somewhere else (e.g. South America, oceans). The increasing CED is directly connected to the estimated efficiency loss. Impact categories describing toxicological effects are significantly affected by post-combustion technology. Especially recent studies, including these categories, often show an increase of up to 200% for post-combustion systems. This follows from two aspects: firstly, organic emissions (mainly ethylene oxide emissions from MEA supply) into air and water and secondly, heavy metals and some phosphate emissions into water from landfilling of hazardous waste and coal ash. Waste treatment of residues is still an open question for large scale MEA plants. An optimised waste management system might diminish the effect.

The normalisation still shows a relatively low importance of FAETP and TETP (0.7% and 0.1%) even with this high increase of absolute figures. However, the impact of HTP increases considerably (from 0.5% to 1.9%).

The share in the world AP for hard coal increases slightly from 2.6% to 3.2%. For EP and POCP the shares are 0.8% and 1.5%.

The impact assessments of the four studies analysing hard coal oxyfuel power plants present no consistent results, except for GWP. The relative values for AP and EP relating to the power plants without CO₂ capture lie between –38% and 40% and –43% and 58%, respectively, for POCP between 23% and 123%. The toxicity effects are considered in two studies and show the same tendency for HTP (approx. 34%) and FAETP (approx. 41%) but diverge for TETP (20–65%). Reason for the heterogeneous perspectives might be the differences in efficiency, energy penalty, flue gas treatment, or the distribution of SO₂ and NO_x in the compressed CO₂ stream versus in flue gas emissions. However, this cannot be deduced clearly from the studies. This implies, that no general conclusions can be drawn for the environmental assessment of oxyfuel power plants from existing studies so far. For the lignite oxyfuel system all other categories decrease as well. Only the CED increases due to the energy penalty. The two LCAs for oxyfuel demonstrate values for AP (–15% up to –80%) and EP (30 up to 80%). The obvious decrease of AP and EP compared to hard coal is again related to the absence of considerable transport distances. If the ratio of global lignite power production remains small the impacts will stay negligible. Even an increase of more than 500% for POCP using CCS will not have a noticeable effect on the total worldwide impacts.

The absolute figures for the IGCC system without CCS are smaller than for conventional pulverised combustion and more balanced. IGCC with CCS shows the same tendency as post-combustion technology, but on a lower level. Although all studies consider different solvents, the increase of AP, EP, POCP and CED in general is smaller than 40% and remain rather low compared to the global EP and POCP (Fig. 4). The share of AP on the world impact increases slightly from 1.5% to 1.8%, GWP decreases from 11.5% to 2.9%.

3.2. Natural gas

For natural gas mostly post-combustion systems are investigated. According to the efficiency of natural gas power plants

without CCS the absolute GWP is much lower as for coal plants. While power generation amounts to nearly half of the hard coal plants the share on the global GWP is less than a quarter (2.7%). With CCS it comes down to 1.0%. The results for GWP are again the most uniform. Within the studies no coherent picture concerning the other impact categories is visible. The increase for AP, EP, POCP and CED is mostly in the range between 15% and 50%. All normalised impacts are well below 1% of the world total, even with the considered increase within the different categories.

In summary for all fuel types and capture systems only GWP is a very robust impact parameter. For a reliable statement about other environmental impacts more, well documented LCAs are necessary including well described assumptions, parameters and uncertainties to explain the effects on the results clearly. For example, assumptions about transocean shipment of coal in a study, or solvent production in another study can all have a significant impact on various LCA categories of interest.

4. Conclusions and outlook

A comprehensive analysis of environmental consequences associated with the introduction of CCS has become subject of several studies in the last decade. Synergies and trade-offs on the environmental impacts are revealed to widen the discussion. As expected, it is difficult to obtain homogeneous information about environmental impacts of CCS technologies by comparing studies with diverging backgrounds. Nevertheless, overall effects and trends are recognisable and sensitive parameters can be identified.

In general the studies show an increase in other environmental impacts when the global warming potential is substantially reduced by introducing CCS, regardless of capture options or fuel used. This is most often related to the loss in efficiency and the corresponding additional demand for fuel, operating materials (e.g. solvents) and increasing wastes. Looking closer at the origin of these effects, it becomes obvious, that an exclusively optimisation of power plant performance alone is not sufficient to decrease the effects considerably. Especially for hard coal and gas fuelled power production the fuel supply has a high share in the varying impacts.

When scrubbing solvents are used in the process, typically toxicological impacts on humans and the environment increase. This is caused by the release of organic emissions, mostly ethylene oxide emissions from MEA supply, into air and water. Also AP and EP increase because of ammonia emissions during MEA production.

For hard coal plants heavy metals released into air and water and also, heavy metals and some phosphate emissions into water from landfilling of hazardous waste and coal ash are also causing toxicological effects. They are higher for CCS plants due to the energy penalty and relating additional coal demand. During fuel transport SO₂ and NO_x emissions occur, causing additional AP and EP. Here, LCA reveals a shift from emissions at power plants to regions of fuel extraction and transport.

By comparing the studies it has become obvious that process chains of operation material and waste treatment are often less well investigated compared to the process chain of power generation and capture. However, for many environmental impacts they are the main driver of the increase in impacts. Therefore, a more detailed look into these process chains is recommended.

For hard coal and lignite post-combustion systems the impacts except GWP can increase 100% and more. For oxyfuel and pre-combustion the increase is smaller, but still visible. However, a

relation to total global emissions shows clearly, that crucial impacts associated with power generation are the GWP which decreases drastically by using CCS technology and AP which increases slightly. For post-combustion HTP must be kept track. This normalisation step helps to rank the environmental effects and prevent overestimations and therefore should be included in every LCA.

A detailed look into the studies reveals parameters which have a considerable impact on the outcome. One significant aspect is the assumption of power plant efficiencies today and in the future. As it turns out, no common perception about future technology parameters with or even without CCS exists. The efficiencies vary from 37% to 54% for a hard coal system without CCS, representing different stages of technology. For lignite systems without CCS efficiencies of 41–54% and for natural gas systems of 50–66% are described. Energy penalty ranges from 6%-points to 18%-points can be found looking across all capture technologies.

Other parameters, with considerable impact on the results are capture efficiency and quality of CO₂ captured. Odeh and Cockerill (2008) show a GWP increase up to 25% if the capture efficiency decreases by 5%. Koornneef et al. (2008) state, that CO₂ removal efficiencies included in the IPCC report of $\pm 5\%$ translate to a change in GWP of $\pm 20\%$, in relation to a 90% efficiency basis. The influence of CO₂ quality requirements on the process performance has not been investigated in an LCA context yet. Although different CO₂ qualities do not hinder a comparison from a life cycle perspective, deeper knowledge about the effect on the results are desirable.

The parameters with the highest impact on the results, fuel composition and origin, differ for every study. Same technologies using different fuels have different emissions and subsequent different impacts. Though, without background data it is not possible to determine, which part of the result is related to the technology and which is related to the fuel. As it cannot be expected, that the practitioners of LCA studies use the same coal or gas input, it would be helpful to present the underlying fuel parameters, such as composition, heating value and transport distances.

Typically CO₂ transport and storage as well as construction and dismantling of the power plants and CCS systems have only a minor impact on the overall effects.

In summary, the analysis of existing studies has shown several open questions for further investigations. Especially for the oxy-fuel process, but also for the pre-combustion route, it is essential that more LCAs include well documented parameters and describe uncertainties and assumptions precisely. So far it is difficult to draw robust conclusions about environmental performances of oxyfuel processes. Also investigations about oxyfuel and pre-combustion technologies in natural gas power plants are missing. In addition, new, second generation capture technologies, such as chilled ammonia, membranes or others, should be covered also. A comparison of CCS with other GHG emission mitigation measures, particularly renewable energies, will follow.

However widening the portfolio of technologies will cause additional demand for new studies. To encourage an easier general interpretation of the results, it is helpful to have a set of background or benchmark information about technologies or fuel supply. A list of impacts to be considered as well as regional normalisation factors to rank the effects completes the basic requirements.

This study has shown, that LCA is a helpful tool to support the discussion about environmental effects associated with CCS technology. Beside the striving goal of CO₂ reduction also other environmental effects are considered. Additionally, the life cycle perspective helps to identify shifts in occurrence of effects along the life cycle or to other regions. Finally, the valuation of different environmental effects against each other is facilitated by the normalisation step, showing that GWP is reduced considerably while only the increase of AP and HTP (for hard coal post-combustion) have to be watched closely.

References

- Bauer, C., 2009. Personal communication concerning impact figures based on NEEDS results.
- Doosan Babcock Energy, 2009. Oxyfuel combustion R&D activities. In: APGTF Workshop on Carbon Abatement Technologies—Development and Implementation of Future UK Strategy, London, UK, February 2009.
- D'Addario, E., Clerici, G., Musicanti, M., Pulvirenti, G., Serenellini, S., Valdiserri, M.G., 2003. Environmental analysis of different options of CO₂ capture in power generation from natural gas. In: Gale, J., Kaya, Y. (Eds.), *Greenhouse Gas Control Technologies*, vol. 1. Elsevier Science Ltd., pp. 63–68.
- Doctor, R.D., Molburg, J.C., Brockmeier, N.F., Lynn, M., Victor, G., Massood, R., Gary, J.S., 2001. Life-cycle analysis of a shell gasification-based multi-product system with CO₂ recovery. In: *Proceedings of the First National Conference on Carbon Sequestration*, Washington, DC, USA.
- Ecoinvent Centre, 2007. Ecoinvent data v2.0, 2007. Swiss Centre for Life Cycle Inventories. www.ecoinvent.ch.
- Göttlicher, G., 1999. *Energetik der Kohlendioxidrückhaltung in Kraftwerken*. VDI Verlag, Düsseldorf.
- Guinée, J., Gorée, M., Heijungs, R., Huppes, G., Kleijn, R., Koning, A. de, Oers, L. van, Wegener Sleswijk, A., Suh, S., Udo de Haes, H.A., Bruijn, H. de, Duin, R. van, Huijbregts, M.A.J., 2002. *Handbook on Life Cycle Assessment. Operational Guide to the ISO Standards*. Kluwer Academic Publishers, Dordrecht, ISBN 1-4020-0228-9.
- IEA Greenhouse Gas R&D Programme (Gijlswijk van, R., Feron, P., Onk, H., Brouwer, J.P.), 2006. *Environmental Impact of Solvent Scrubbing of CO₂*. IEA GHG R&D Programme, 2006/14.
- ISO 14040/14044, 2006. *Environmental Management – Life Cycle Assessment – Principles and Framework, – Requirements and Guidelines*. Deutsches Institut für Normung e. V.
- Khoo, H.H., 2006. Life cycle investigation of CO₂ recovery and sequestration. *Environmental science and technology* 40/12, 4016–4024.
- Koornneef, J., van Keulen, T., Faaij, A., Turkenburg, W., 2008. Life cycle assessment of a pulverized coal power plant with post-combustion capture, transport and storage of CO₂. *International Journal of Greenhouse Gas Control* 2/4, 448–467.
- Korre, A., Nie, Z., Durucan, S., 2009. Life cycle modelling of fossil fuel power generation with post combustion. *Energy Procedia* 1, 3771–3778.
- Lombardi, L., 2003. Life cycle assessment comparison of technical solutions for CO₂ emission reduction in power generation. *Energy Conversion and Management* 44/1, 93–108.
- Marx, J., Schreiber, A., Zapp, P., Haines, M., Hake, J.-Fr., Gale, J., 2010. Environmental evaluation of CCS using life cycle assessment (LCA). IEA Greenhouse Gas R&D Programme, Technical Report number 2010/TR2.
- Modahl, I.S., Nyland, C.A., Raadal, H.L., Karstad, O., Torp, T.A., Hagemann, R., 2009. LCA as an ecodesign tool for production of electricity, including carbon capture and storage—a study of a gas power plant case with post-combustion CO₂ capture at Tjeldbergodden. In: *Proceedings of the Conference: Joint Actions on Climate Change*, Aalborg, Den, June 2009.
- Muramatsu, E., Iijima, M., 2002. Life cycle assessment for CO₂ capture technology from exhaust gas of coal power plant. In: *The 6th Greenhouse Gas Control Technologies*, Kyoto, Japan, October 1–4, 2002.
- NEEDS, Bauer, C., Heck, T., Dones, R., Mayer-Spohn, O., Blesl, M., NEEDS (New Energy Externalities Developments for Sustainability), 2008. Final report on technical data, costs, and life cycle inventories of advanced fossil power generation systems. Paul Scherrer Institut (PSI) und Institut für Energiewirtschaft und Rationelle Energieanwendung, Univ. Stuttgart (IER).
- Nie, Z., Korre, A., Durucan, S., 2011. Life cycle modelling and comparative assessment of the environmental impacts of oxy-fuel and post-combustion CO₂ capture, transport and injection processes. *Energy Procedia* 4, 2510–2517.
- Odeh, N.A., Cockerill, T.T., 2008. Life cycle GHG assessment of fossil fuel power plants with carbon capture and storage. *Energy Policy* 36 (1), 367–380.
- OECD/IEA, 2002. *Electricity Information*. OECD/IEA, Paris.
- Pehnt, M., Henkel, J., 2008. Life cycle assessment of carbon dioxide capture and storage from lignite power plants. *International Journal of Greenhouse Gas Control* 3 (1), 49–66.
- Posch, M., Seppälä, J., Hetterlingh, J.P., Johansson, M., Margni, M., Joliet, O., 2008. The role of atmospheric dispersion models and ecosystem sensitivity in the determination of characterisation factors for acidifying and eutrophying emissions in LCIA. *International Journal of Life Cycle Assessment* 13, 477–486.
- Rao, A.B., Rubin, E.S., 2002. A technical, economic, and environmental assessment of amine-based CO₂ capture technology for power plant greenhouse gas control. *Environmental Science & Technology* 36/21, 4467–4475.
- Rubin, E.S., Chen, C., Rao, A.B., 2007. Cost and performance of fossil fuel power plants with CO₂ capture and storage. *Energy Policy* 35/9, 4444–4454.
- Schreiber, A., Zapp, P., Kuckshinrichs, W., 2009. Environmental assessment of German electricity production from coal-fired power plants with amine-based carbon capture. *International Journal of Life Cycle Assessment* 14, 547–559.
- Seppälä, J., Posch, M., Johansson, M., Hetterlingh, J.-P., 2006. Country-dependent characterisation factors for acidification and terrestrial eutrophication based on accumulated exceedance as an impact category indicator. *International Journal of Life Cycle Assessment* 11, 403–446.
- Singh, B., Strømman, A., Hertwich, E., 2011. Comparative life cycle environmental assessment of CCS technologies. *International Journal of Greenhouse Gas Control* 5, 911–921.

- Sleeswijk, A.W., van Oers, L.F.C.M., Guinée, J.B., Struijs, J., Huijbregts, M.A.J., 2008. Normalisation in product life cycle assessment: an LCA of the global and European economic systems in the year 2000. *Science of the Total Environment* 390, 227–240.
- Spath, P., Mann, M., 2004. Biomass power and conventional fossil systems with and without CO₂ sequestration comparing the energy balance, greenhouse gas emissions and economics. National Renewable Energy Laboratory, Golden, CO. Report no. BB04.4010.
- Thitakamol, B., Veawab, A., Aroonwilas, A., 2007. Environmental impacts of absorption-based CO₂ capture unit from post-combustion treatment of flue gas from coal-fired power plant. *International Journal of Greenhouse Gas Control* 1/4, 318–342.
- Tzimas, E., Mercier, A., Cormos, C., Peteves, S.D., 2007. Trade-off in emissions of acid gas pollutants and of carbon dioxide in fossil fuel power plants with carbon capture. *Energy Policy* 35/8, 3991–3998.
- Viebahn, P., Nitsch, J., Fishedick, M., Esken, A., Pastowski, A., Schuwer, D., Supersberger, N., Bandi, A., Zuberbühler, U., Edenhofer, O., 2007. RECCS Strukturell-ökonomisch-ökologischer Vergleich regenerativer Energietechnologien (RE) mit Carbon Capture and Storage (CCS). Langfassung, Bundesministerium für Umwelt, Naturschutz und Reaktorsicherheit (BMU), December 2007.
- Wildbolz, C., 2007. Life cycle assessment of selected technologies for CO₂ transport and sequestration. Diploma Thesis No. 2007MS05, Swiss Federal Institute of Technology, Zurich.

Ökobilanz und Externe Kosten zukünftiger fossiler Stromerzeugungstechnologien mit CO₂-Abscheidung und Speicherung

Christian Bauer(*)¹, Roberto Dones¹, Thomas Heck¹,
Oliver Mayer-Spohn², Markus Blesl²

¹ Labor für Energiesystemanalysen, Paul Scherrer Institut, 5232 Villigen PSI, Schweiz, Tel.: +41 (0)56 310 2391, christian.bauer@psi.ch, <http://gabe.web.psi.ch/>

² Institut für Energiewirtschaft und Rationelle Energieanwendung, Universität Stuttgart, Hessbrühlstrasse 49a, 70565 Stuttgart, Deutschland, Tel.: +49 (0)711 685 87848, Oliver.Mayer-Spohn@ier.uni-stuttgart.de

Kurzfassung: Im Rahmen des Projekts NEEDS (New Energy Externalities Development for Sustainability) der Europäischen Kommission (2004 - 2008) wird eine Vielzahl von heutigen und zukünftigen Optionen zur Stromproduktion in Europa mit Hilfe von Lebenszyklusanalysen (LCA) auf ihre Umweltauswirkungen hin analysiert. Der vorliegende Beitrag präsentiert Umweltinventare und kumulierte Gesamtergebnisse dieser Ökobilanzen bzw. externe Kosten ausgewählter, repräsentativer fossiler Kraftwerkstechnologien mit und ohne CO₂-Abscheidung und den zugehörigen Brennstoffketten. Verschiedene Szenarien bis zum Jahr 2050 werden untersucht. Die Technologieauswahl beinhaltet konventionelle superkritische Kohlekraftwerke und Kombikraftwerke mit integrierter Kohlevergasung (IGCC), jeweils mit Braun- und Steinkohle befeuert. Die Analyse umfasst die drei wichtigsten Verfahren zur CO₂-Abscheidung, nämlich nach der Verbrennung, vor der Verbrennung und die Verbrennung in Sauerstoffumgebung. Die Modellierung beinhaltet den CO₂-Transport per Pipeline über verschiedene Distanzen sowie dessen Injektion und Speicherung in salinen Aquiferen und erschöpften Gaslagerstätten unterschiedlicher Tiefe. Für die Bilanzierung werden jeweils die vollständigen Energieketten, d.h. die Förderung der Ressourcen, der Transport von Brennstoffen und Materialien, der Betrieb der Kraftwerke bis hin zur Entsorgung der Abfälle, analysiert. Die Hintergrunddaten für die Ökobilanzen stammen aus der LCA-Datenbank ecoinvent.

Die LCA-Ergebnisse zeigen für die Stromerzeugung in fossilen Kraftwerken mit CO₂-Abscheidung und -Speicherung eine deutliche Reduktion der Treibhausgasemissionen. Der Strom kann allerdings nicht als CO₂-frei bezeichnet werden, da die Berücksichtigung der gesamten Energieketten stets zu nicht vernachlässigbaren Treibhausgasemissionen führt. Die in Folge der CO₂-Abscheidung reduzierten Nettowirkungsgrade der Kraftwerke verursachen im Vergleich zu fossilen Kraftwerken ohne CO₂-Abscheidung einen erhöhten Verbrauch an fossilen Ressourcen. Die Gesamtbetrachtung der Umweltauswirkungen mit unterschiedlichen Aggregationsmethoden ergibt für den Vergleich der einzelnen Optionen zur Stromproduktion ein differenzierteres Bild als die reine Fokussierung auf CO₂ bzw. Treibhausgase.

Keywords: Zukünftige Stromerzeugung, Carbon Capture and Storage (CCS), Lebenszyklusanalyse (LCA), Ökologische Bewertung.

1 Einleitung

Der vom Menschen verursachte Klimawandel verlangt dringend technologische Lösungen zur Reduktion der Treibhausgasemissionen. Der Bereich der Stromerzeugung spielt dabei eine wichtige Rolle, da weltweit rund 40% der im Zusammenhang mit der Energieversorgung verursachten CO₂-Emissionen aus diesem Bereich stammt [1]. Der globale Trend der letzten Jahre und die aktuellen Entwicklungen lassen nicht erwarten, dass die sich rasant entwickelnden, grossen Volkswirtschaften wie China und Indien auf fossile Stromerzeugung verzichten können, um den schnell wachsenden Strombedarf zu decken. Deshalb kommt der Weiterentwicklung der fossilen Kraftwerkstechnologien zur Treibhausgasreduktion eine entscheidende Rolle zu. Strategien zur Verringerung der Emissionen, die in den kommenden Jahren in grösserem Massstab umgesetzt werden können, reichen von der Modernisierung bestehender Kraftwerke über die Errichtung von neuen Anlagen auf dem aktuellen Stand der Technik als Ersatz für alte Einheiten bis zur Einführung von CO₂-Abscheide- und Speichertechnologien. Kurz- bis mittelfristig erscheinen auf globaler Skala die Alternativen – substanzieller Ausbau im Bereich der erneuerbaren Energien oder der Kernenergie – weniger realistisch. Im Rahmen des Projekts NEEDS (New Energy Externalities Development for Sustainability) der Europäischen Kommission (2004 - 2008) wird eine grosse Zahl von heutigen und zukünftigen Optionen zur Elektrizitätsproduktion in Europa mit Hilfe von Ökobilanzen auf ihre Umweltauswirkungen hin untersucht. Das Gesamtprojekt hat das Ziel, Lebenszyklusanalyse und die teilweise darauf basierende Berechnung externer Kosten der Stromerzeugung sowie die energieökonomische Modellierung der europäischen Volkswirtschaften zu verbessern und zu integrieren. Eine Multi-Kriterien-Analyse zur Nachhaltigkeitsbewertung unterschiedlicher Stromerzeugungstechnologien und energiepolitischer Strategien, basierend auf ökologischen, ökonomischen und sozialen Indikatoren, wird die Festlegung einer „Technology Roadmap“ der EU bis zum Jahr 2050 unterstützen [2].

Der vorliegende Beitrag präsentiert Umweltinventare und kumulierte Gesamtergebnisse der Lebenszyklusanalysen bzw. externe Kosten ausgewählter, repräsentativer fossiler Kraftwerkstechnologien mit und ohne CO₂-Abscheidung und der zugehörigen Brennstoffketten. Dabei werden verschiedene Szenarien bis zum Jahr 2050 analysiert. Die detaillierte Analyse der Energieketten beschränkt sich in diesem Beitrag auf Kohlekraftwerke.

2 Methodologie

Kern der vorliegenden Analyse sind Lebenszyklusanalysen oder Ökobilanzen verschiedener Optionen zur fossilen Stromproduktion. Das bedeutet, dass jeweils die vollständigen Energieketten – von der Förderung der Ressourcen, dem Transport und der Verarbeitung von Rohstoffen und Materialien über den Kraftwerksbetrieb mit all den damit verbundenen Stoffflüssen bis zur Entsorgung sämtlicher Abfälle – modelliert und bilanziert werden. Die Ökobilanzen liefern so genannt Umweltinventare, welche die Umweltauswirkungen pro Kilowattstunde Elektrizität ab Kraftwerksklemme beinhalten. In diesen ökologischen Profilen werden neben Luftschadstoffen auch Emissionen in Boden und Wasser sowie Ressourcen- und Landverbrauch erfasst.

Um die Potenziale der zukünftigen Technologieentwicklung in die Bilanzierung mit einbeziehen zu können, werden neben den heute als „best available technologies“ ange-

sehenen Kraftwerkstechnologien auch Kraftwerke in den Jahren 2025 und 2050 bilanziert. In diesem Zeitrahmen wird, ausgehend von den heutigen „state-of-the-art“ Anlagen, eine evolutionäre Technologieentwicklung angenommen. Eine derartige Bilanzierung von zukünftigen Technologien ist mittel- bis längerfristig natürlich bis zu einem gewissen Grad spekulativ und der Detaillierungsgrad daher beschränkt. Allerdings sollten diese näherungsweise Modellierung und die vorliegenden Ergebnisse aussagekräftig genug sein, um die verschiedenen Technologien mit Blick auf deren ökologische Auswirkungen vergleichen zu können und Schlüsse für zukünftige Optionen einer nachhaltigen Energiepolitik zu ziehen.

Für den gesamten LCA-Teil des Projekts NEEDS sind drei verschiedene Szenarien für die Zeit bis 2050 definiert, die mit „pessimistisch“ (PE), „realistisch-optimistisch“ (RO) und „sehr optimistisch“ (VO) bezeichnet werden. Diese Spezifizierungen beziehen sich auf den Grad des angenommenen Optimismus in der technologischen Entwicklung der einzelnen Stromerzeugungstechnologien und deren erfolgreiche Verbreitung auf dem Markt. Die drei Zukunftsszenarien ermöglichen die Illustration der möglichen Bandbreite für die Umweltauswirkungen der Stromerzeugung bis 2050. Im Gesamtprojekt werden neben der Palette an verschiedenen Kraftwerkstechnologien, die fossile und erneuerbare Energien sowie die Kernenergie umfasst, auch ausgewählte Wirtschaftssektoren wie etwa die Stahlproduktion oder der Transportsektor für zukünftige Verhältnisse bilanziert. All diese Daten werden in einem energieökonomischen Modell (Markal-Times) zu einem szenarienabhängigen Strommix kombiniert und dieser wiederum, ergänzt durch die in Zukunft als ökologischer angenommene Herstellung einzelner Grundstoffe, in der Berechnung der Ökobilanzen verwendet. Die in diesem Beitrag präsentierten Resultate beinhalten diese Gesamtmodellierung jedoch nicht, da die Daten nicht rechtzeitig zur Verfügung standen. Die illustrierten Ergebnisse – ausschließlich für Kohlekraftwerke – basieren auf einer vereinfachten LCA-Berechnung mit der Ökobilanzsoftware SimaPro und der LCA-Hintergrunddatenbank ecoinvent, Datenbestand v1.3 [3]. Diese Einschränkungen sollten einen vernachlässigbaren Einfluss auf die Gültigkeit und Anwendbarkeit der Ergebnisse haben, da bei der fossilen Stromerzeugung generell die Umwelteinwirkungen aus dem Kraftwerksbetrieb und den zugehörigen Brennstoffketten die kumulierten LCA-Gesamtergebnisse dominieren. Material- und Stromeinsatz sowie Transport spielen in der Regel eine untergeordnete Rolle [4].

2.1 Modellierte Kraftwerkstechnologien

Die Analyse beinhaltet Stein- und Braunkohlekraftwerke sowie Erdgas-Kombikraftwerke (NGCC) für die Jahre 2025 und 2050 jeweils mit und ohne CO₂-Abscheidung, -Transport und -Einlagerung („Carbon Capture and Storage“, CCS). Die im Detail untersuchten Kohlekraftwerkstechnologien sind konventionelle superkritische Kraftwerke (PC - „pulverized coal“) und Kombikraftwerke mit integrierter Kohlevergasung (IGCC). Um die technologische Weiterentwicklung in den kommenden Jahrzehnten gegenüber den derzeit anlaufenden Pilotanlagen mit CO₂-Abscheidung abzubilden, werden auch PC-Kraftwerke mit CO₂-Abscheidung für das Jahr 2010 bilanziert. Bei Kohlekraftwerken wird zwischen den drei wichtigsten Verfahren zur CO₂-Abscheidung unterschieden, nämlich nach der Verbrennung („post combustion“), vor der Verbrennung („pre combustion“) und die Verbrennung in Sauerstoffumgebung („oxyfuel combustion“). Bei Gaskraftwerken werden die „post combustion“- und „oxyfuel combustion“-Verfahren bilanziert.

Entscheidende Einflussfaktoren auf das ökologische Profil der Stromerzeugung mit CCS sind einerseits der **Energieaufwand für die CO₂-Abscheidung** im Kraftwerk und andererseits die **Effizienz der CO₂-Abscheidung**, d.h. der Anteil des zurückgehaltenen CO₂. Diese Faktoren sind abhängig vom Abscheidungsverfahren, vom Brennstoff und vom betrachteten Zukunftsszenario. Es wird angenommen, dass die Energie, die für die CO₂-Abscheidung und dessen Kompression vor dem Transport zur Einlagerung aus dem Kraftwerk selbst stammt, d.h. die Kraftwerksnettowirkungsgrade werden in der Bilanzierung entsprechend reduziert. **Tabelle 1** fasst diese Parameter für die verschiedenen Energieketten, Zeitpunkte und Szenarien zusammen.

Tabelle 1 **Schlüsselparameter** für die Modellierung der Kraftwerke mit und ohne CO₂-Abscheidung [5].

Brennstoff	Kraftwerkstechnologie	CO ₂ -Abscheidungsverfahren	Jahr	Szenario ¹	El. Nettowirkungsgrad ohne CCS	El. Nettowirkungsgrad mit CCS	Reduktion Wirkungsgrad ²	Effizienz CO ₂ -Abscheidung
					%	%	%	%
Erdgas	NGCC	Post Combustion	2025	PE	61	53	8	90
				RO	62	56	6	90
				VO	63	57	6	90
			2050	PE	62	56	6	90
				RO	65	61	4	90
				VO	66	62	4	90
		Oxyfuel Combustion	2025	PE	61	51	10	100
				RO	62	52	10	100
				VO	63	53	10	100
			2050	PE	62	52	10	100
				RO	65	60	5	100
				VO	66	61	5	100
Kohle	PC	Post Combustion	2010		43/45 ³	33/35 ³	10	90
			2025	PE	47	37	10	90
				RO	49	42	7	90
				VO	52	45	7	90
			2050	PE	50	43	7	90
				RO	54	49	5	90
				VO	57	52	5	90
		Oxyfuel Combustion	2010		43/45 ³	33/35 ³	10	99.5
			2025	PE	47	37	10	99.5
				RO	49	41	8	99.5
				VO	52	44	8	99.5
			2050	PE	50	42	8	100
				RO	54	47	7	100
				VO	57	50	7	100
	IGCC	Pre Combustion (Steinkohle)	2010		45	-	-	-
			2025	PE	53	47	6	90
				RO	54	48	6	90
				VO	55	49	6	90
			2050	PE	53.5	47.5	6	90
				RO	54.5	48.5	6	90
				VO	55.5	49.5	6	90
		Pre Combustion (Braunkohle)	2010		44	-	-	-
			2025	PE	51	45	6	90
				RO	52	46	6	90
				VO	53	47	6	90
			2050	PE	51.5	45.5	6	90
				RO	52.5	46.5	6	90
				VO	53.5	47.5	6	90

¹ Technologie-Szenario: PE = pessimistisch; RO = realistisch-optimistisch; VO = sehr optimistisch.

² Reduktion des Nettowirkungsgrades durch den Energieaufwand zur CO₂-Abscheidung und -Kompression im Kraftwerk.

³ Braunkohle/Steinkohle.

Aus Konsistenzgründen und um einen ausgewogenen Vergleich zwischen den verschiedenen Kohlekraftwerkstypen (PC und IGCC) zu ermöglichen wird angenommen, dass Kohle mit übereinstimmenden Charakteristika verfeuert wird. Es wird von einem unteren Heizwert von 26 MJ/kg für Steinkohle bzw. 8.8 MJ/kg für Braunkohle ausgegangen. Die CO₂-Emissionen betragen für Steinkohle 92.2 g/MJ bzw. 108.3 g/MJ für Braunkohle.

Als Referenzen für die die heutigen „best available technology“-Kohlekraftwerke dienen das Steinkohlekraftwerk Rostock (Deutschland), das Braunkohlekraftwerk „Niederaußem K“ (Bergheim, Deutschland) und ein verbessertes IGCC-Kraftwerk Puertollano (Spanien; modelliert mit Stein- und Braunkohle) [5, 6]. Die Betriebsdaten dieser Anlagen (Emissionsdaten, Wirkungsgrade, etc.) dienen als Basis für die generische Modellierung der heutigen und zukünftigen Referenztechnologien:

- PC-Kraftwerk, Steinkohle, Nettoleistung 600 MW_{el}, $\eta_{el} = 45\%$
- PC-Kraftwerk, Braunkohle, Nettoleistung 950 MW_{el}, $\eta_{el} = 43\%$
- IGCC-Kraftwerk, Steinkohle, Nettoleistung 450 MW_{el}, $\eta_{el} = 45\%$
- IGCC-Kraftwerk, Braunkohle, Nettoleistung 450 MW_{el}, $\eta_{el} = 44\%$

Während für die Kraftwerke bis 2050 eine evolutionäre Technologieentwicklung mit Verbesserungen vor allem bei den Wirkungsgraden angenommen wird, werden die dem Kraftwerk vorgelagerten Teile der Kohleketten (Kohleförderung, -Aufbereitung und -Transport) nicht verändert und wie in [7] modelliert. Weitere Hintergrunddaten für die Lebenszyklusanalysen wie etwa Betriebsstoffe zur CO₂-Abscheidung stammen aus der LCA-Datenbank ecoinvent, Datenbestand v1.3 [3].

Die CO₂-Abscheidung nach der Kohleverbrennung wird mit einem Aminwäscheprozess modelliert. Neben Monoethanolamin wird dazu Natronlauge und Aktivkohle eingesetzt, die verwendeten Mengen orientieren sich am oberen Bereich der in [8] angegebenen Bandbreite. Zusätzlich werden organische Chemikalien nach [9] bilanziert. Der Verbrauch dieser Betriebsstoffe wird in den verschiedenen Zukunftsszenarien nicht variiert, da über etwaige Prozessverbesserungen keine ausreichenden Informationen vorliegen. Beim „oxyfuel combustion“-Verfahren wird lediglich der Energieverbrauch zur Sauerstoffbereitstellung bilanziert. Zum Materialverbrauch dieses Abscheidungsprozesses sind keine belastbaren Daten verfügbar. Im Vergleich zu den PC-Kraftwerken ohne CO₂-Abscheidung sind die SO₂- und NO_x-Emissionen bei PC-Kraftwerken mit CO₂-Abscheidung reduziert [9, 10]. Für SO₂ ergeben sich Emissionswerte von etwa 0.1 g/kWh, bei der Verbrennung in Sauerstoffumgebung für NO_x Werte von weniger als 0.2 g/kWh.

2.2 CO₂-Transport und -Lagerung

Die Modellierung des CO₂-Transports und dessen Injektion in geologische Lagerstätten in superkritischem Zustand basiert auf einem technischen „bottom-up“-Ansatz [11, 12, 13]. Mit sämtlichen modellierten Kohlekraftwerken werden CO₂-Transport per Pipeline über zwei verschiedene Distanzen (200 km bzw. 400 km) und CO₂-Lagerung in zwei unterschiedlichen Lagerstätten (saliner Aquifer in 800 m Tiefe und erschöpfte Gaslagerstätte in 2500 m Tiefe) kombiniert. Damit sind zwar nicht sämtliche Praxisoptionen in dieser Analyse berücksichtigt, die Ergebnisse lassen aber eine Abschätzung der Einflüsse von CO₂-Transport und -Lagerung auf die gesamte Ökobilanz der Stromerzeugung zu. Der CO₂-Massenfluss wird

mit 250 kg/s angenommen, was etwa der abgeschiedenen CO₂-Menge von drei Kohlekraftwerken mit CCS der 500 MW-Klasse entspricht. Der CO₂-Transport über 200 km erfolgt ohne Zwischenkompression, über 400 km wird eine Zwischenkompression nach 200 km angenommen (mit etwa 30 bar). Die CO₂-Injektion in beide Lagerstätten wird mit je zwei Injektionsbohrungen modelliert mit einer Injektionsrate von jeweils 125 kg CO₂ pro Sekunde. Der Überdruck für die Injektion wird jeweils mit 30 bar angenommen. Die genannten Parameter basieren auf Informationen zu existierenden Testprojekten [11] und sollten durchschnittliche Rahmenbedingungen für die CO₂-Lagerung in Europa entsprechen. Die Verteilung von möglichen Lagerstätten und potenziellen Standorten fossiler CCS-Kraftwerke wurde nicht näher untersucht. Denkbare Langzeitemissionen an CO₂ aus den geologischen Lagerstätten werden in der Modellierung der Ökobilanzen nicht berücksichtigt. Es kann davon ausgegangen werden, dass vor einem Einsatz der CCS-Technologie in großem Maßstab die langfristige Dichtheit der Lager nachgewiesen werden muss.

3 Resultate

Die im Folgenden illustrierten kumulierten Ergebnisse der Ökobilanzen für Kohlekraftwerke mit und ohne CCS beinhalten drei verschiedene Methoden zur Aggregation der Umweltauswirkungen der Stromproduktion (ab Kraftwerksklemme):

1. Treibhausgasemissionen, gemessen in kg(CO₂-Äquivalent)/kWh, basierend auf den Treibhausgaspotenzialen der einzelnen klimawirksamen Emissionen nach IPCC [14]. Damit wird das zu erwartende Treibhausgas-Reduktionspotenzial für die einzelnen Elektrizitätsketten aufgezeigt.
2. Die ökologische Bewertungsmethode („Life Cycle Impact Assessment“, LCIA) Eco-Indicator'99(H,A) [15], gemessen in Punkten pro kWh. Weniger Punkte entsprechen einem besseren Resultat. LCIA-Methoden wie diese erlauben anhand der Quantifizierung von potenziellen Umweltschäden durch einzelne Schadstoffe, durch Land- und Ressourcenverbrauch und die anschließende Gewichtung aller Auswirkungen eine Aggregation sämtlicher erfasster Umweltschäden zu einem einzigen Indikator und damit einen anschaulichen Vergleich verschiedener Optionen. Der Schritt der Gewichtung bringt stets ein gewisses Maß an Subjektivität mit sich, die Resultate erfordern eine eingehende Interpretation. Hier wird die so genannte hierarchische Perspektive („H“) der Methode mit durchschnittlicher Gewichtung („A“) verwendet.
3. Externe Kosten, gemessen in €cents/kWh, basierend auf durchschnittlichen europäischen Schadensfaktoren aus ExternE [16]. Die Berechnung externer Kosten erlaubt die monetäre Quantifizierung von Gesundheitsschäden und Ernteinbussen als Auswirkung der Emission von Luftschadstoffen. Dazu werden Schadensfaktoren für zahlreiche Luftschadstoffe mit den LCA-Ergebnissen der Stromproduktion kombiniert. Die Anwendung von durchschnittlichen heutigen Schadensfaktoren und die daraus resultierende Vernachlässigung standortspezifischer Effekte – Emissionen verursachen je nach Ort der Freisetzung unterschiedliche Schäden – sowie möglicher Änderungen der zukünftigen Schadenswirkungen bringt zwar eine gewisse Unschärfe mit sich, die Ergebnisse erlauben aber dennoch aussagekräftige Vergleiche der untersuchten Elektrizitätsketten.

Abbildung 1 zeigt anhand der drei aggregierten Indikatoren die kumulierten LCA-Ergebnisse für eine Kilowattstunde Strom aus den PC-Elektrizitätsketten, Steinkohle- links und Braunkohle- kraftwerke rechts.

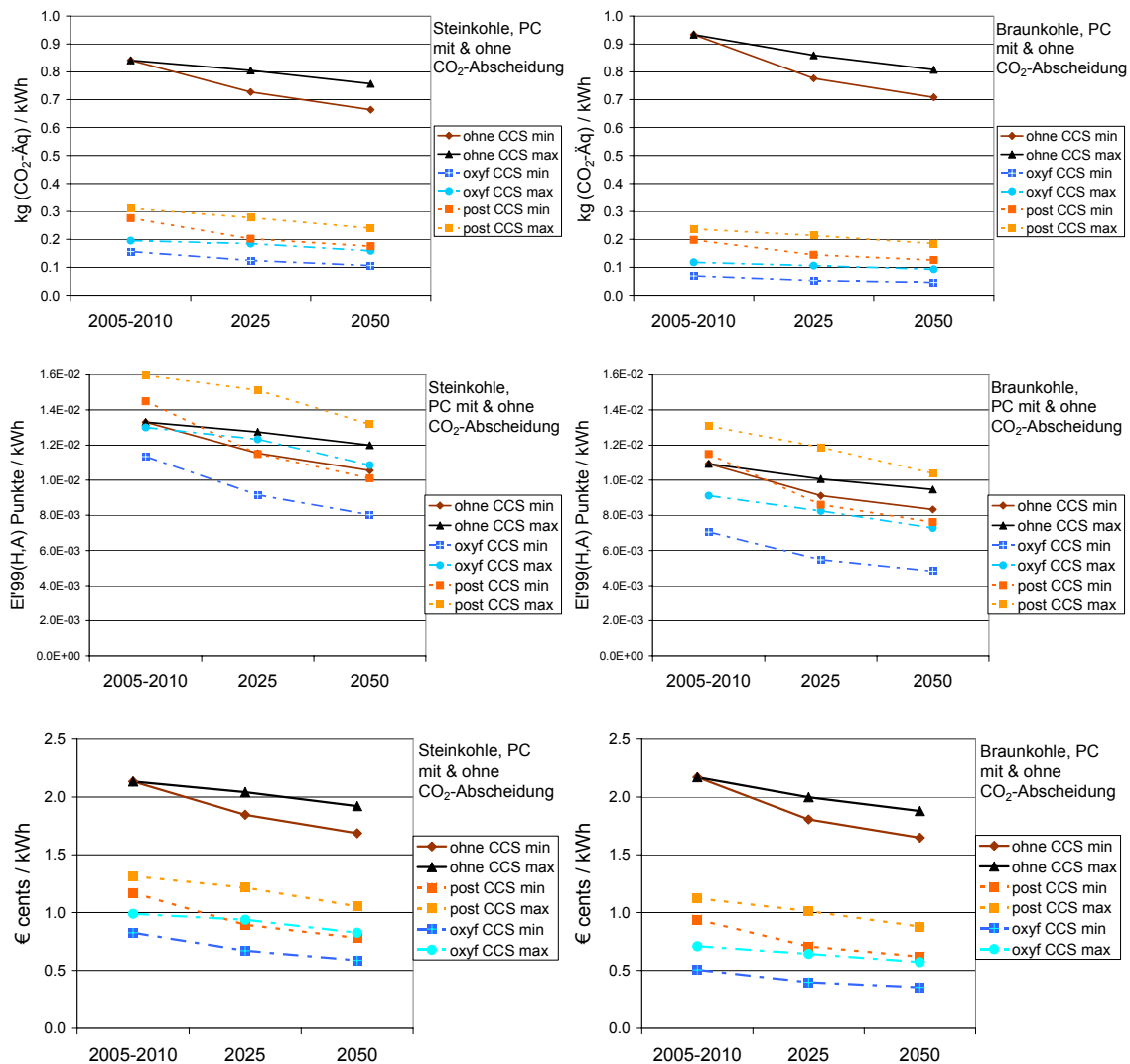


Abbildung 1 Treibhausgasemissionen, Eco-Indicator'99(H,A)-Punkte und Externe Kosten (von oben nach unten) für den Strom ab konventionellen (PC) Stein- und Braunkohlekraftwerken (links bzw. rechts), ohne bzw. mit „post combustion“ und „oxyfuel“ CO₂-Abscheidung und -Einlagerung (in jeder Grafik). Das Minimum („min“) der untersuchten Fälle stellt der CO₂-Transport über 200 km mit anschließender Injektion in den salinen Aquifer (800 m Tiefe) im sehr optimistischen Szenario dar; das Maximum („max“) der CO₂-Transport über 400 km mit anschließender Injektion in die erschöpfte Gaslagerstätte (2500 km Tiefe) im pessimistischen Szenario.

Sämtliche Indikatoren verbessern sich für alle Kraftwerke und in allen Szenarien bis 2050. Hauptverantwortlich dafür sind die steigenden Kraftwerkswirkungsgrade bzw. der sinkende Energieaufwand bei der CO₂-Abscheidung. Die Indikatorwerte für die Braunkohleketten mit CCS sind etwas besser als jene aus den Steinkohleketten mit CCS, da bei Förderung und Transport der Braunkohle weniger Emissionen anfallen (vgl. auch Tabelle 2). Mit dem

„oxyfuel“-Abscheideverfahren können die Treibhausgasemissionen stärker gesenkt werden, da der Abscheidegrad höher ist als beim „post combustion“-Verfahren. Bei der Aggregation mit Eco-Indicator'99(H,A) schneidet der Strom aus den Kraftwerken mit CCS nicht in jedem Fall besser ab als ohne CCS. Das liegt daran, dass die CO₂-Abscheidung die Nettowirkungsgrade der Kraftwerke um bis zu einem knappen Viertel verringert und deshalb alle Umweltauswirkungen mit Ausnahme der direkten CO₂-, NO_x- und SO₂-Emissionen der Kraftwerke entsprechend zunehmen (vgl. auch Abbildung 2). Besonders ins Gewicht fällt der steigende fossile Ressourcenverbrauch. Die externen Kosten werden bei der Berechnung hier mit einem Schadensfaktor von 19 €/t(CO₂-Äq.) bei den Kraftwerken ohne CO₂-Abscheidung von den Beiträgen der Treibhausgasemissionen dominiert (vgl. auch Abbildung 3). Aus der deutlichen Reduktion dieser Emissionen dank CCS folgt, dass Strom aus Kraftwerken mit CCS geringere externe Kosten aufweist. Die Kostenreduktionen liegen im Bereich von 40-65%.

Tabelle 2 zeigt eine Beitragsanalyse für die Treibhausgasemissionen, d.h. die Gesamtemissionen werden aufgeschlüsselt auf verschiedene Abschnitte der gesamten Stromerzeugungsketten (Brennstoffförderung & -verarbeitung; Kraftwerksbau & -entsorgung; Kraftwerksbetrieb; CO₂-Transport & -speicherung) für die verschiedenen Jahre und Szenarien.

Tabelle 2 Kumulative Treibhausgasemissionen der Stromerzeugung mit den untersuchten Kohleketten, aufgeschlüsselt als Beiträge aus verschiedenen Teilen der gesamten Energieketten [5].

Treibhausgasemissionen [g(CO ₂ -Äq.) pro kWh]	Brennstoffförderung & -verarbeitung		Kraftwerksbau & -entsorgung		Kraftwerksbetrieb (incl. CO ₂ -Abscheidung & -Kompression)		CO ₂ -Transport & Speicherung		GESAMT		Jahr
	min	max	min	max	min	max	min	max	min	max	
Braunkohle, PC	16	16	2	2	916	916	0	0	934	934	2010
	13	15	2	2	762	843	0	0	777	859	2025
	12	14	2	2	695	792	0	0	708	808	2050
Braunkohle, PC, CCS	21	21	3	3	23	150	20	71	69	237	2010
	15	19	3	3	18	135	15	63	53	214	2025
	13	16	2	3	16	117	13	56	46	185	2050
Steinkohle, PC	84	87	2	2	737	753	0	0	823	842	2010
	75	83	2	2	651	720	0	0	727	805	2025
	68	78	2	2	594	677	0	0	664	757	2050
Steinkohle, PC, CCS	111	111	4	4	24	146	16	57	156	311	2010
	86	105	3	4	19	120	13	54	125	277	2025
	75	93	3	3	13	104	11	48	106	240	2050
Braunkohle, IGCC	16	16	1	1	903	903	0	0	920	920	2010
	13	13	1	1	750	779	0	0	764	793	2025
	13	13	1	1	743	772	0	0	757	786	2050
Braunkohle, IGCC, CCS	na		na		na		na		na		2010
	15	15	1	2	99	104	14	47	129	168	2025
	14	15	1	1	98	103	14	47	128	166	2050
Steinkohle, IGCC	87	87	1	1	749	749	0	0	837	837	2010
	71	74	1	1	613	636	0	0	685	711	2025
	70	73	1	1	608	630	0	0	679	704	2050
Steinkohle, IGCC, CCS	na		na		na		na		na		2010
	80	83	1	1	79	83	11	38	172	206	2025
	79	82	1	1	79	82	11	38	170	203	2050

Die Treibhausgasemissionen der Stromerzeugung insgesamt nehmen – je nach Abscheidungstechnologie, Betrachtungszeitpunkt und Szenario – dank CCS gegenüber Kraftwerken ohne CCS für Steinkohle zwischen 63% und 84% ab, für Braunkohle zwischen 75%

und 94%. Bei der Stromerzeugung ohne CCS stammt der Grossteil der Emissionen aus dem Kraftwerksbetrieb. Wird direkt im Kraftwerk entstehendes CO₂ abgeschieden, so nehmen die indirekten Beiträge der Energieketten proportional zum sinkenden Kraftwerksnettowirkungsgrad zu. Die größten Beiträge bei der Steinkohlekette mit CCS stammen aus der Kohleförderung und -Aufbereitung. Dieser Bereich fällt bei Braunkohle mit CCS weniger ins Gewicht. Die durch CO₂-Abscheidung und -Kompression sowie CO₂-Transport und -Speicherung verursachten Emissionen hängen stark vom Abscheidungsverfahren, der Transportdistanz und der Injektionstiefe ab. Mit wachsender Distanz und Lagertiefe steigen der Energieverbrauch und damit die Emissionen. Die Beiträge der Kraftwerksinfrastruktur sind vernachlässigbar. Zwischen den beiden modellierten Technologien, PC- und IGCC-Kraftwerken, gibt es keine aussagekräftigen Unterschiede.

Wird die LCIA-Methode Eco-Indicator'99(H,A) [15] für den Vergleich der Stromerzeugung mit und ohne CCS verwendet, so zeigt sich, dass der Strom aus Kraftwerken mit CCS teilweise schlechter bewertet wird als ohne CCS (Abbildung 2, auch Abbildung 1, Mitte). Dank CCS sinken zwar die CO₂-Emissionen und damit die Beiträge zum Klimawandel („Climate Change“), diese Reduktion wird aber vor allem durch den steigenden Verbrauch an Kohle und anderen fossilen Energieträgern („Fossil Fuels“) sowie Gesundheitsschäden im Bereich Atemwegserkrankungen („Respiratory inorganics“) kompensiert. Auch bei den restlichen Schadenskategorien schneiden die Kraftwerke mit CCS schlechter ab, diese Kategorien haben jedoch vergleichsweise geringen Einfluss auf die aggregierten Gesamtergebnisse.

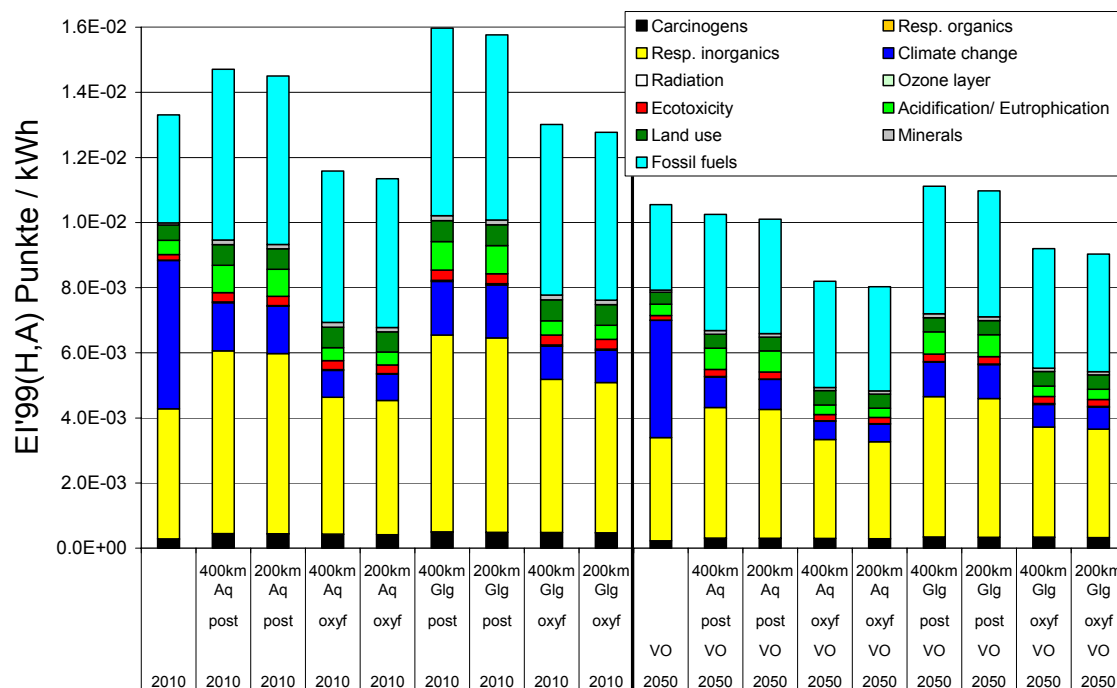


Abbildung 2 Bewertung der Stromerzeugung in Steinkohlekraftwerken (PC) mit und ohne CCS („post“ bzw. „oxyfuel combustion“) mit Eco-Indicator'99(H,A) [15], aufgeschlüsselt in einzelne Schadenskategorien; CO₂-Transportdistanz 200/400km, CO₂-Speicher Aquifer (Aq, 800 m Tiefe) oder erschöpfte Gaslagerstätte (Glg, 2500 m Tiefe). Zur Illustration werden nur zwei Fälle gezeigt: Jahr 2010 bzw. Jahr 2050 im sehr optimistischen Szenario.

Abbildung 3 zeigt, dass bei einer Berechnung der externen Kosten nach [16] mit einem Schadensfaktor von 19 €/t(CO₂-Äq.) die Beiträge der Treibhausgasemissionen das Resultat prägen und Strom aus Kraftwerken mit CCS geringere externe Kosten aufweist (siehe auch Abbildung 1, unten). Das „oxyfuel“-Verfahren zur CO₂-Abscheidung schneidet besser ab als das „post combustion“-Verfahren, da nicht nur direkten CO₂-Emissionen des Kraftwerks stärker reduziert werden, sondern auch die direkten NO_x-Emissionen, deren Wirkung im Bereich „Andere Luftemissionen“ quantifiziert wird. Die durch „Andere Luftemissionen“ verursachten externen Kosten liegen mit CCS teilweise höher als ohne, da die indirekten Luftschadstoffemissionen aus den Energieketten bei CCS-Kraftwerken zunehmen und diese Zunahme nicht immer von den Reduktionen der direkten NO_x und SO₂-Emissionen kompensiert wird. Die in der Literatur vorhandenen Schadensfaktoren für Treibhausgasemissionen weisen zwar eine hohe Bandbreite von –3 \$/t(CO₂-Äq.) bis +95 \$/t(CO₂-Äq.) auf und sind mit entsprechenden Unsicherheiten verbunden [17], aber nur eine Berechnung der externen Kosten mit Werten im untersten Bereich dieses Intervalls lässt insgesamt die Kraftwerke ohne CCS teilweise besser abschneiden als jene mit CCS.

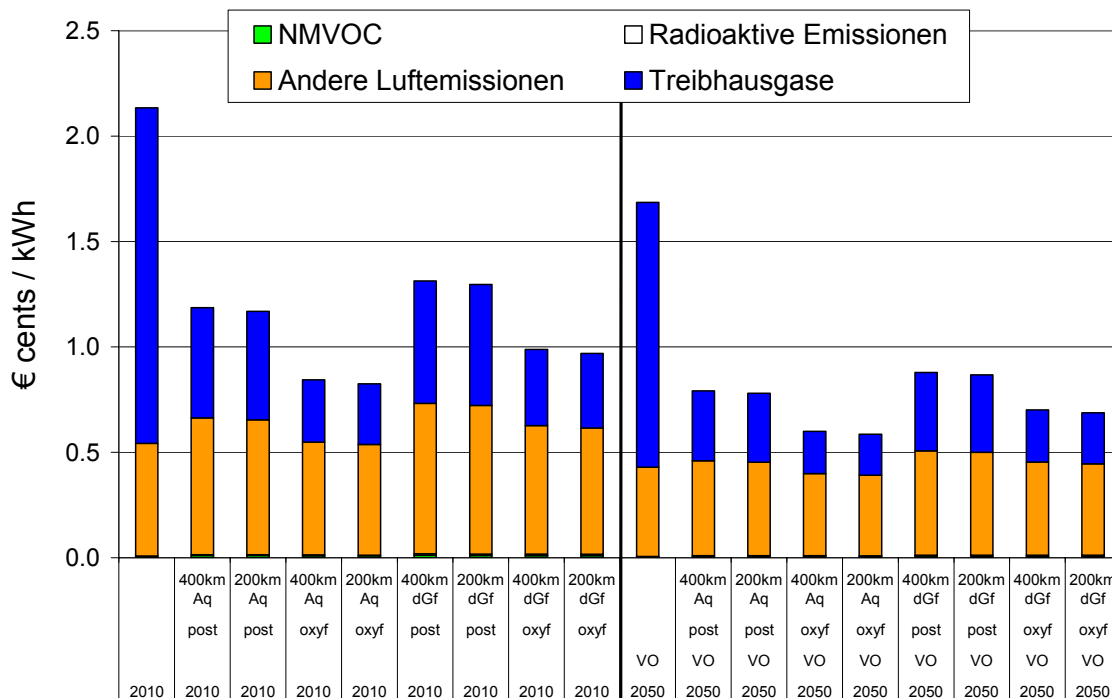


Abbildung 3 Externe Kosten der Stromerzeugung in Steinkohlekraftwerken (PC) mit und ohne CCS („post“ bzw. „oxyfuel combustion“); CO₂-Transportdistanz 200/400km, CO₂-Speicher Aquifer (Aq, 800 m Tiefe) oder erschöpfte Gaslagerstätte (Glg, 2500 m Tiefe). Zur Illustration werden nur zwei Fälle gezeigt: Jahr 2010 bzw. Jahr 2050 im sehr optimistischen Szenario.

4 Schlussfolgerungen

Die Ökobilanzen der Stromerzeugung in fossilen Kraftwerken mit und ohne CO₂-Abscheidung und -Lagerung zeigen eine deutliche Reduktion der Treibhausgasemissionen pro Kilowattstunde Elektrizität. Allerdings werden durch Energie- und Materialverbrauch für die CO₂-Abscheidung, dessen Transport und Einlagerung nicht vernachlässigbare Emissionen an Treibhausgasen und anderen Schadstoffen verursacht. Die CO₂-Abscheidung erhöht auch den Verbrauch an fossilen Ressourcen und damit die mit der Brennstoffförderung und -aufbereitung verbundenen, indirekten Emissionen. Insgesamt kann dies – abhängig von der Bewertungsmethode – dazu führen, dass Strom aus fossilen Kraftwerken mit CCS aus ökologischer Sicht schlechter abschneidet als Strom aus Anlagen ohne CCS.

Die hier errechneten Resultate sollten nicht als abschließende Antworten aufgefasst werden, da noch viele Unsicherheiten in der bestehenden Modellierung der Ökobilanzen existieren, die mit Sensitivitätsanalysen tiefer untersucht werden sollten. Abweichungen von den hier getroffenen Annahmen sind speziell für den Energieaufwand und die Effizienz der verschiedenen Verfahren zur CO₂-Abscheidung, die Verbrauchsraten für die Betriebsstoffe sowie für deren Art und Herstellungsweise denkbar. Auch die Modellierung der CO₂-Lagerstätten muss in Zukunft anhand von in der Praxis realisierten Systemen überprüft werden.

5 Verdankung

Das Projekt NEEDS (New Energy Externalities Development for Sustainability) wird im Rahmen des 6. RTD (Research, Technology Development and Demonstration) Rahmenprogramms der Europäischen Union finanziert.

6 Referenzen

- [1] OECD/IEA (2007) „World Energy Outlook 2006.“ International Energy Agency (IEA), Head of Publications Service, 9 rue de la Fédération, 75739 Paris Cedex 15, Frankreich.
- [2] NEEDS Project, European Commission, <http://www.needs-project.org>.
- [3] www.ecoinvent.ch
- [4] R. Frischknecht, H.-J. Althaus, C. Bauer, G. Doka, T. Heck, N. Jungbluth, D. Kellenberger, T. Nemecek (2007) „The Environmental Relevance of Capital Goods in Life Cycle Assessments of Products and Services.“ In: The International Journal of LCA Special Issue 1/07, pp. 7-17. DOI: <http://dx.doi.org/10.1065/lca2007.02.309>
- [5] R. Dones, C. Bauer, T. Heck, O. Mayer-Spohn, M. Blesl (2008) „Final technical paper on technical data, costs and life cycle inventories of advanced fossil fuels.“ Europäische Kommission, Veröffentlichung 2008.
- [6] European Commission (2000) „Improvement of Integrated Gasification Combined Cycles Starting from State of the Art – Development of Improved Solid Gasification Systems for Cost Effective Power Generation with Low Environmental Impact.“ JOULE III Programme, Clean Coal Technology R&D. Volume III, EC, Directorate-General for Science, Research and Development, Brüssel. ISBN 3-00-004658-5.

- [7] A. Röder, C. Bauer, R. Dones (2004) „Kohle.“ In: R. Dones (Ed.) et al., Sachbilanzen von Energiesystemen: Grundlagen für den ökologischen Vergleich von Energiesystemen und den Einbezug von Energiesystemen in Ökobilanzen für die Schweiz. Final report ecoinvent 2000 No. 6-VI, Paul Scherrer Institut Villigen, Swiss Centre for Life Cycle Inventories, Dübendorf, Schweiz.
- [8] IPCC (2005) „Carbon Dioxide Capture and Storage.“ Cambridge University Press, New York, USA.
- [9] E.S. Rubin, C. Chen, A.B. Rao (2007) „Cost and performance of fossil fuel power plants with CO₂ capture and storage.“ In: Energy Policy 35, p. 4444-4454.
- [10] K. Andersson, F. Johnsson (2006) „Process evaluation of an 865 MW_e lignite fired O₂/CO₂ power plant.“ In: Energy Conversion and Management (47), p. 3487-3498.
- [11] C. Wildbolz (2007) „Life Cycle Assessment of Selected Technologies for CO₂ Transport and Sequestration.“ Diplomarbeit No. 2007MS05, Department Bau, Umwelt und Geomatik, Institute of Environmental Engineering (IfU), ETHZ, Zürich, Schweiz.
- [12] G. Doka (2007) „Critical Review of Life Cycle Assessment of Selected Technologies for CO₂ Transport and Sequestration.“ Diplomarbeit No. 2007MS05 von C. Wildbolz, Zürich, Schweiz.
- [13] C. Hendriks, W. Graus, F. van Bergen (2004) „Global Carbon Dioxide Storage Potential and Costs.“ ECOFYS and TNO, Niederlande.
- [14] IPCC (2001) „Climate Change 2001: The Scientific Basis.“ In: Third Assessment Report of the Intergovernmental Panel on Climate Change (IPCC) (ed. J. T. Houghton, Y. Ding, D. J. Griggs, M. Noguer, P. J. van der Linden, D. Xiaosu). IPCC, Intergovernmental Panel on Climate Change, Cambridge University Press, The Edinburgh Building Shaftesbury Road, Cambridge, UK.
- [15] M. Goedkoop, R. Spriensma (2000) „The Eco-indicator 99: A damage oriented method for life cycle impact assessment.“ PRé Consultants, Amersfoort, Niederlande.
- [16] European Commission (2004) „Externalities of Energy: Extension of accounting framework and Policy Applications (ExternE-Pol).“ Vol. Final Report, Contract ENG1-CT2002-00609. European Commission, DG Research, Technological Development and Demonstration (RTD), Brüssel, Belgien.
- [17] R.J.T. Klein, S. Huq, F. Denton, T.E. Downing, R.G. Richels, J.B. Robinson, F.L. Toth (2007) „Inter-relationships between adaptation and mitigation.“ In: Climate Change 2007: Impacts, Adaptation and Vulnerability. Contribution of Working Group II to the Fourth Assessment Report of the Intergovernmental Panel on Climate Change (ed. M.L. Parry, O.F. Canziani, J.P. Palutikof, P.J. van der Linden, C.E. Hanson). Cambridge University Press, Cambridge, UK.